World Meteorological Organization
Global Ozone Research and Monitoring Project — Report No. 37

SCIENTIFIC ASSESSMENT OF OZONE DEPLETION: 1994

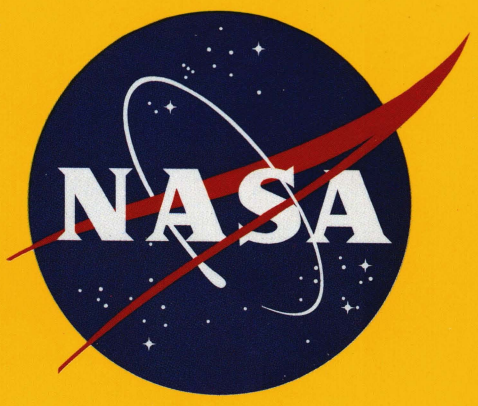

National Oceanic and Atmospheric Administration
National Aeronautics and Space Administration
United Nations Environment Programme
World Meteorological Organization

World Meteorological Organization
Global Ozone Observing System (GO_3OS)
41 Avenue Giuseppe Motta
P.O. Box 2300
Geneva 2, CH 1211
Switzerland

United Nations Environment Programme
United Nations Headquarters
Ozone Secretariat
P.O. Box 30552
Nairobi
Kenya

U.S. Department of Commerce
National Oceanic and Atmospheric Administration
14th Street and Constitution Avenue NW
Herbert C. Hoover Building, Room 5128
Washington, D.C. 20230
USA

National Aeronautics and Space Administration
Office of the Mission to Planet Earth
Two Independence Square
300 E Street SW
Washington D.C. 20546
USA

Published in February 1995.

ISBN 92-807-1449-X

Requests for extra copies by scientific users should be directed to:
WORLD METEOROLOGICAL ORGANIZATION
attn. Dr. Rumen Bojkov
P.O. Box 2300
1211-Geneva, Switzerland

World Meteorological Organization
Global Ozone Research and Monitoring Project — Report No. 37

SCIENTIFIC ASSESSMENT OF OZONE DEPLETION: 1994

National Oceanic and Atmospheric Administration
National Aeronautics and Space Administration
United Nations Environment Programme
World Meteorological Organization

List of International Authors, Contributors, and Reviewers

Assessment Co-chairs

Daniel L. Albritton, Robert T. Watson, and Piet J. Aucamp

Chapter Lead Authors

1: Neil R.P. Harris
2: Eugenio Sanhueza
3: David W. Fahey
4: Roderic L. Jones
5: Andreas Volz-Thomas and Brian A. Ridley
6: Malcolm K.W. Ko
7: Frode Stordal
8: Keith P. Shine
9: Richard L. McKenzie
10: Stuart A. Penkett
11: Andreas Wahner and Marvin A. Geller
12: R.A. Cox
13: Susan Solomon and Donald J. Wuebbles

Coordinating Editor

Christine A. Ennis

Authors, Contributors, and Reviewers

Daniel L. Albritton	US	Byron Boville	US
Marc Allaart	The Netherlands	Kenneth P. Bowman	US
Fred N. Alyea	US	Geir Braathen	Norway
Gerard Ancellet	France	Guy P. Brasseur	US
Meinrat O. Andreae	Germany	Carl Brenninkmeijer	New Zealand
James K. Angell	US	Christoph Brühl	Germany
Frank Arnold	Germany	William H. Brune	US
Roger Atkinson	US	James H. Butler	US
Elliot Atlas	US	Sergio Cabrera	Chile
Piet J. Aucamp	South Africa	Bruce A. Callander	UK
L. Avallone	US	Daniel Cariolle	France
Helmuth Bauer	Germany	R. Cebula	US
Slimane Bekki	UK	William L. Chameides	US
Tibor Bérces	Hungary	S. Chandra	US
T. Berntsen	Norway	Marie-Lise Chanin	France
Lane Bishop	US	J. Christy	US
Donald R. Blake	US	Ralph J. Cicerone	US
N.J. Blake	US	G.J.R. Coetzee	South Africa
Mario Blumthaler	Austria	Peter S. Connell	US
Greg E. Bodeker	South Africa	D. Considine	US
Rumen D. Bojkov	Switzerland	R.A. Cox	UK
Charles R. Booth	US	Paul J. Crutzen	Germany

AUTHORS, CONTRIBUTORS, AND REVIEWERS

Derek N. Cunnold	US
John Daniel	US
Malgorzata Degórska	Poland
John J. DeLuisi	US
Dirk De Muer	Belgium
Frank Dentener	The Netherlands
Richard G. Derwent	UK
Terry Deshler	US
Susana B. Diaz	Argentina
Russell Dickerson	US
J. Dignon	US
Ed Dlugokencky	US
Anne R. Douglass	US
Tom Duafala	US
James E. Dye	US
Dieter H. Ehhalt	Germany
James W. Elkins	US
Christine Ennis	US
D. Etheridge	Australia
David W. Fahey	US
T. Duncan A. Fairlie	US
Donald A. Fisher	US
Jack Fishman	US
Eric L. Fleming	US
Frank Flocke	Germany
L. Flynn	US
P.M. de F. Forster	UK
James Franklin	Belgium
Paul J. Fraser	Australia
John E. Frederick	US
Lucien Froidevaux	US
J.S. Fuglestvedt	Norway
Reinhard Furrer	Germany
Ian E. Galbally	Australia
Brian G. Gardiner	UK
Marvin A. Geller	US
Hartwig Gernandt	Germany
James F. Gleason	US
S. Godin	France
Amram Golombek	Israel
Ulrich Görsdorf	Germany
Thomas E. Graedel	US
Claire Granier	US
William B. Grant	US
L. Gray	UK
William L. Grose	US
J. Gross	Germany
A. Grossman	US
Alexander Gruzdev	Russia
James E. Hansen	US
Neil R.P. Harris	UK
Shiro Hatakeyama	Japan
D.A. Hauglustaine	France
Sachiko Hayashida	Japan
G.D. Hayman	UK
Kjell Henriksen	Norway
Ernest Hilsenrath	US
David J. Hofmann	US
Stacey M. Hollandsworth	US
James R. Holton	US
Lon L. Hood	US
Øystein Hov	Norway
Carleton J. Howard	US
Robert D. Hudson	US
D. Hufford	US
Linda Hunt	US
Abdel M. Ibrahim	Egypt
Mohammad Ilyas	Malaysia
Ivar Isaksen	Norway
Tomoyuki Ito	Japan
Charles H. Jackman	US
Daniel J. Jacob	US
Colin E. Johnson	UK
Harold S. Johnston	US
Paul V. Johnston	New Zealand
Roderic L. Jones	UK
Torben S. Jørgensen	Denmark
M. Kanakidou	France
Igor L. Karol	Russia
Prasad Kasibhatla	US
Jack A. Kaye	US
Hennie Kelder	The Netherlands
James B. Kerr	Canada
M.A.K. Khalil	US
Vyacheslav Khattatov	Russia
J.T. Kiehl	US
S. Kinne	Germany
D. Kinnison	US
Volker Kirchhoff	Brazil
Malcolm K.W. Ko	US
Ulf Köhler	Germany
Walter D. Komhyr	US
Yutaka Kondo	Japan
Janusz W. Krzyścin	Poland

Antti Kulmala	Switzerland
Michael J. Kurylo	US
K. Labitzke	Germany
Murari Lal	India
K.S. Law	UK
G. LeBras	France
Yuan-Pern Lee	Taiwan
Frank Lefèvre	France
Jos Lelieveld	The Netherlands
Robert Lesclaux	France
J.S. Levine	US
Joel Levy	US
J. Ben Liley	New Zealand
Peter Liss	UK
David H. Lister	UK
Zenobia Lityńska	Poland
Shaw C. Liu	US
Jennifer A. Logan	US
Nicole Louisnard	France
Pak Sum Low	Kenya
Daniel Lubin	US
Sasha Madronich	US
Jerry Mahlman	US
Gloria L. Manney	US
Huiting Mao	US
W. Andrew Matthews	New Zealand
Konrad Mauersberger	Germany
Archie McCulloch	UK
Mack McFarland	US
M.E. McIntyre	UK
Richard L. McKenzie	New Zealand
Richard D. McPeters	US
Gérard Mégie	France
Paulette Middleton	US
A.J. Miller	US
Igor Mokhov	Russia
Mario Molina	US
G.K. Moortgat	Germany
Hideaki Nakane	Japan
Paul A. Newman	US
Paul C. Novelli	US
Samuel J. Oltmans	US
Alan O'Neill	UK
Michael Oppenheimer	US
S. Palermi	Italy
K. Patten	US
Juan Carlos Pelaez	Cuba
Stuart A. Penkett	UK
J. Penner	US
Thomas Peter	Germany
Leon F. Phillips	New Zealand
Ken Pickering	US
R.B. Pierce	US
S. Pinnock	UK
Michel Pirre	France
Giovanni Pitari	Italy
Walter G. Planet	US
R.A. Plumb	US
Jean-Pierre Pommereau	France
Lamont R. Poole	US
Michael J. Prather	US
Margarita Préndez	Chile
Ronald G. Prinn	US
Joseph M. Prospero	US
John A. Pyle	UK
Lian Xiong Qiu	China
Richard Ramaroson	France
V. Ramaswamy	US
William Randel	US
Philip J. Rasch	US
A.R. Ravishankara	US
William S. Reeburgh	US
C.E. Reeves	UK
J. Richardson	US
Brian A. Ridley	US
David Rind	US
Curtis P. Rinsland	US
Aidan E. Roche	US
Michael O. Rodgers	US
Henning Rodhe	Sweden
Jose M. Rodriguez	US
M. Roemer	The Netherlands
Franz Rohrer	Germany
Richard B. Rood	US
F. Sherwood Rowland	US
C.E. Roy	Australia
Jochen Rudolph	Germany
James M. Russell III	US
Nelson Sabogal	Kenya
Karen Sage	US
Ross Salawitch	US
Eugenio Sanhueza	Venezuela
K.M. Sarma	Kenya
T. Sasaki	Japan

AUTHORS, CONTRIBUTORS, AND REVIEWERS

Sue M. Schauffler	US
Hans Eckhart Scheel	Germany
Ulrich Schmidt	Germany
Rainer Schmitt	Germany
Ulrich Schumann	Germany
M.D. Schwarzkopf	US
Gunther Seckmeyer	Germany
Jonathan D. Shanklin	UK
Keith P. Shine	UK
H. Sidebottom	Ireland
P. Simmonds	UK
Paul C. Simon	Belgium
H. Singh	US
Paula Skřivánková	Czech Republic
Herman Smit	Germany
Susan Solomon	US
Johannes Staehelin	Switzerland
Knut Stamnes	US
L. Paul Steele	Australia
Leopoldo Stefanutti	Italy
Richard S. Stolarski	US
Frode Stordal	Norway
A. Strand	Norway
B.H. Subbaraya	India
N.-D. Sze	US
Anne M. Thompson	US
Xue X. Tie	US
Margaret A. Tolbert	US
Darin W. Toohey	US
Ralf Toumi	UK
Michael Trainer	US
Charles R. Trepte	US
Adrian Tuck	US
R. Van Dorland	The Netherlands
Karel Vanicek	Czech Republic
Geraint Vaughan	UK
G. Visconti	Italy
Andreas Volz-Thomas	Germany
Andreas Wahner	Germany
W.-C. Wang	US
D.I. Wardle	Canada
David A. Warrilow	UK
Joe W. Waters	US
Robert T. Watson	US
E.C. Weatherhead	US
Christopher R. Webster	US
D. Weisenstein	US
Ray F. Weiss	US
Paul Wennberg	US
Howard Wesoky	US
Thomas M.L. Wigley	US
Oliver Wild	UK
Paul H. Wine	US
Peter Winkler	Germany
Steven C. Wofsy	US
Donald J. Wuebbles	US
Vladimir Yushkov	Russia
Ahmed Zand	Iran
Rudi J. Zander	Belgium
Joseph M. Zawodny	US
Reinhard Zellner	Germany
Christos Zerefos	Greece
Xiu Ji Zhou	China

TABLE OF CONTENTS

SCIENTIFIC ASSESSMENT OF OZONE DEPLETION: 1994

TABLE OF CONTENTS

PART 4. CONSEQUENCES OF OZONE CHANGE

PART 5. SCIENTIFIC INFORMATION FOR FUTURE DECISIONS

TABLE OF CONTENTS

PREFACE

The present document is a scientific assessment that will be part of the information upon which the Parties to the Montreal Protocol will base their future decisions regarding protection of the stratospheric ozone layer.

Specifically, the Montreal Protocol on Substances That Deplete the Ozone Layer states (Article 6): ". . . the Parties shall assess the control measures . . . on the basis of available scientific, environmental, technical, and economic information." To provide the mechanisms whereby these assessments are conducted, the Protocol further states: ". . . the Parties shall convene appropriate panels of experts" and "the panels will report their conclusions . . . to the Parties."

Three assessment reports have been prepared during 1994 to be available to the Parties in advance of their meeting in 1995, at which they will consider the need to amend or adjust the Protocol. The two companion reports to the present scientific assessment focus on the environmental and health effects of ozone layer depletion and on the technology and economic implications of mitigation approaches.

The present report is the latest in a series of seven scientific assessments prepared by the world's leading experts in the atmospheric sciences and under the international auspices of the World Meteorological Organization (WMO) and the United Nations Environment Programme (UNEP). The chronology of those scientific assessments and the relation to the international policy process are summarized as follows:

Year	Policy Process	Scientific Assessment
1981		*The Stratosphere 1981 Theory and Measurements.* WMO No. 11.
1985	Vienna Convention	*Atmospheric Ozone 1985.* 3 vol. WMO No. 16.
1987	Montreal Protocol	
1988		*International Ozone Trends Panel Report 1988.* 2 vol. WMO No. 18.
1989		*Scientific Assessment of Stratospheric Ozone:* 1989. 2 vol. WMO No. 20.
1990	London Amendment	
1991		*Scientific Assessment of Ozone Depletion: 1991.* WMO No. 25.
1992		*Methyl Bromide: Its Atmospheric Science, Technology, and Economics* (Assessment Supplement). UNEP (1992).
1992	Copenhagen Amendment	
1994		*Scientific Assessment of Ozone Depletion: 1994.* WMO No. 37 (This report.)
(1995)	Vienna Amendment (?)	

The genesis of *Scientific Assessment of Ozone Depletion: 1994* occurred at the 4th meeting of the Conference of the Parties to the Montreal Protocol in Copenhagen, Denmark, in November 1992, at which the scope of the scientific needs of the Parties was defined. The formal planning of the present report was a workshop that was held on 11 June 1993 in

Virginia Beach, Virginia, at which an international steering group crafted the outline and suggested scientists from the world community to serve as authors. The first drafts of the chapters were examined at a meeting that occurred on 2 - 4 March 1994 in Washington, D.C., at which the authors and a small number of international experts improved the coordination of the text of the chapters.

The second draft was sent out to 123 scientists worldwide for a mail peer review. These anonymous comments were considered by the authors. At a Panel Review Meeting in Les Diablerets, Switzerland, held on 18 - 21 July 1994, the responses to these mail review comments were proposed by the authors and discussed by the 80 participants. Final changes to the chapters were decided upon, and the Executive Summary was prepared by the participants.

The final result is this document. It is the product of 295 scientists from the developed and developing world[1] who contributed to its preparation and review (230 scientists prepared the report and 147 scientists participated in the peer review process).

What follows is a summary of their current understanding of the stratospheric ozone layer and its relation to humankind.

[1] Participating were Argentina, Australia, Austria, Belgium, Brazil, Canada, Chile, Cuba, Czech Republic, Denmark, Egypt, France, Germany, Greece, Hungary, India, Iran, Ireland, Israel, Italy, Japan, Kenya, Malaysia, New Zealand, Norway, Poland, Russia, South Africa, Sweden, Switzerland, Taiwan, The Netherlands, The People's Republic of China, United Kingdom, United States of America, and Venezuela.

EXECUTIVE SUMMARY

Recent Major Scientific Findings and Observations

The laboratory investigations, atmospheric observations, and theoretical and modeling studies of the past few years have provided a deeper understanding of the human-influenced and natural chemical changes in the atmosphere and their relation to the Earth's stratospheric ozone layer and radiative balance of the climate system. Since the last international scientific assessment of the state of understanding, there have been several key ozone-related findings, observations, and conclusions:

- **The atmospheric growth rates of several major ozone-depleting substances have slowed, demonstrating the expected impact of the Montreal Protocol and its Amendments and Adjustments.** The abundances of the chlorofluorocarbons (CFCs), carbon tetrachloride, methyl chloroform, and halons in the atmosphere have been monitored at global ground-based sites since about 1978. Over much of that period, the annual growth rates of these gases have been positive. However, the data of recent years clearly show that the growth rates of CFC-11, CFC-12, halon-1301, and halon-1211 are slowing down. In particular, total tropospheric organic chlorine increased by only about 60 ppt/year (1.6%) in 1992, compared to 110 ppt/year (2.9%) in 1989. Furthermore, tropospheric bromine in halons increased by only about 0.25 ppt/year in 1992, compared to about 0.85 ppt/year in 1989. The abundance of carbon tetrachloride is actually decreasing. The observed trends in total tropospheric organic chlorine are consistent with reported production data, suggesting less emission than the maximum allowed under the Montreal Protocol and its Amendments and Adjustments. Peak total chlorine/bromine loading in the troposphere is expected to occur in 1994, but the stratospheric peak will lag by about 3 - 5 years. Since the stratospheric abundances of chlorine and bromine are expected to continue to grow for a few more years, increasing global ozone losses are predicted (other things being equal) for the remainder of the decade, with gradual recovery in the 21st century.

- **The atmospheric abundances of several of the CFC substitutes are increasing, as anticipated.** With phase-out dates for the CFCs and other ozone-depleting substances now fixed by international agreements, several hydrochlorofluorocarbons (HCFCs) and hydrofluorocarbons (HFCs) are being manufactured and used as substitutes. The atmospheric growth of some of these compounds (*e.g.*, HCFC-22) has been observed for several years, and the growth rates of others (*e.g.*, HCFC-142b and HCFC-141b) are now being monitored. Tropospheric chlorine in HCFCs increased by 5 ppt/year in 1989 and about 10 ppt/year in 1992.

- **Record low global ozone levels were measured over the past two years.** Anomalous ozone decreases were observed in the midlatitudes of both hemispheres in 1992 and 1993. The Northern Hemispheric decreases were larger than those in the Southern Hemisphere. Globally, ozone values were 1 - 2% lower than would be expected from an extrapolation of the trend prior to 1991, allowing for solar-cycle and quasi-biennial-oscillation (QBO) effects. The 1994 global ozone levels are returning to values closer to those expected from the longer-term downward trend.

- **The stratosphere was perturbed by a major volcanic eruption.** The eruption of Mt. Pinatubo in 1991 led to a large increase in sulfate aerosol in the lower stratosphere throughout the globe. Reactions on sulfate aerosols resulted in significant, but temporary, changes in the chemical partitioning that accelerated the photochemical ozone loss associated with reactive hydrogen (HO_x), chlorine, and bromine compounds in the lower stratosphere in midlatitudes and polar regions. Absorption of terrestrial and solar radiation by the Mt. Pinatubo aerosol resulted in a transitory rise of 1°C (globally averaged) in the lower-stratospheric temperature and also affected the distribution of ozone through circulation changes. The observed 1994 recovery of global ozone is qualitatively consistent with observed gradual reductions of the abundances of these volcanic particles in the stratosphere.

- **Downward trends in total-column ozone continue to be observed over much of the globe, but their magnitudes are underestimated by numerical models.** Decreases in ozone abundances of about 4 - 5% per decade at midlatitudes in the Northern and Southern Hemispheres continue to be observed by both ground-based and satellite-borne monitoring instruments. At midlatitudes, the losses continue to be much larger during winter/spring than during summer/fall in both hemispheres, and the depletion increases with latitude, particularly in the Southern Hemisphere. Little or no downward trends are observed in the tropics (20°N - 20°S). While the current two-dimensional stratospheric models simulate the observed trends quite well during some seasons and latitudes, they underestimate the trends by factors of up to three in winter/spring at mid- and high latitudes. Several known atmospheric processes that involve chlorine and bromine and that affect ozone in the lower stratosphere are difficult to model and have not been adequately incorporated into these models.

- **Observations have demonstrated that halogen chemistry plays a larger role in the chemical destruction of ozone in the midlatitude lower stratosphere than expected from gas phase chemistry.** Direct *in situ* measurements of radical species in the lower stratosphere, coupled with model calculations, have quantitatively shown that the *in situ* photochemical loss of ozone due to (largely natural) reactive nitrogen (NO_x) compounds is smaller than that predicted from gas phase chemistry, while that due to (largely natural) HO_x compounds and (largely anthropogenic) chlorine and bromine compounds is larger than that predicted from gas phase chemistry. This confirms the key role of chemical reactions on sulfate aerosols in controlling the chemical balance of the lower stratosphere. These and other recent scientific findings strengthen the conclusion of the previous assessment that the weight of scientific evidence suggests that the observed middle- and high-latitude ozone losses are largely due to anthropogenic chlorine and bromine compounds.

- **The conclusion that anthropogenic chlorine and bromine compounds, coupled with surface chemistry on natural polar stratospheric particles, are the cause of polar ozone depletion has been further strengthened.** Laboratory studies have provided a greatly improved understanding of how the chemistry on the surfaces of ice, nitrate, and sulfate particles can increase the abundance of ozone-depleting forms of chlorine in the polar stratospheres. Furthermore, satellite and *in situ* observations of the abundances of reactive nitrogen and chlorine compounds have improved the explanation of the different ozone-altering properties of the Antarctic and Arctic.

- **The Antarctic ozone "holes" of 1992 and 1993 were the most severe on record.** The Antarctic ozone "hole" has continued to occur seasonally every year since its advent in the late-1970s, with the occurrences over the last several years being particularly pronounced. Satellite, balloon-borne, and ground-based monitoring instruments revealed that the Antarctic ozone "holes" of 1992 and 1993 were the biggest (areal extent) and deepest (minimum amounts of ozone overhead), with ozone being locally depleted by more than 99% between about 14 - 19 km in October, 1992 and 1993. It is likely that these larger-than-usual ozone depletions could be attributed, at least in part, to sulfate aerosols from Mt. Pinatubo increasing the effectiveness of chlorine- and bromine-catalyzed ozone destruction. A substantial Antarctic ozone "hole" is expected to occur each austral spring for many more decades because stratospheric chlorine and bromine abundances will approach the pre-Antarctic-ozone-"hole" levels (late-1970s) very slowly during the next century.

- **Ozone losses have been detected in the Arctic winter stratosphere, and their links to halogen chemistry have been established.** Studies in the Arctic lower stratosphere have been expanded to include more widespread observations of ozone and key reactive species. In the late-winter/early-spring period, additional chemical losses of ozone up to 15 - 20% at some altitudes are deduced from these observations, particularly in the winters of 1991/2 and 1992/3. Model calculations constrained by the observations are also consistent with these losses, increasing the confidence in the role of chlorine and bromine in ozone destruction. The interannual variability in the photochemical and dynamical conditions of the Arctic polar vortex continues to limit the ability to predict ozone changes in future years.

- **The link between a decrease in stratospheric ozone and an increase in surface ultraviolet (UV) radiation has been further strengthened.** Measurements of UV radiation at the surface under clear-sky conditions show that low overhead ozone yields high UV radiation and in the amount predicted by radiative-transfer theory. Large increases of surface UV are observed in Antarctica and the southern part of South America during the period of the seasonal ozone "hole." Furthermore, elevated surface UV levels at mid-to-high latitudes were observed in the Northern Hemisphere in 1992 and 1993, corresponding to the low ozone levels of those years. However, the lack of a decadal (or longer) record of accurate monitoring of surface UV levels and the variation introduced by clouds and other factors have precluded the unequivocal identification of a long-term trend in surface UV radiation.

- **Methyl bromide continues to be viewed as a significant ozone-depleting compound.** Increased attention has been focused upon the ozone-depleting role of methyl bromide. Three potentially major anthropogenic sources of atmospheric methyl bromide have been identified (soil fumigation, biomass burning, and the exhaust of automobiles using leaded gasoline), in addition to the natural oceanic source. Recent laboratory studies have confirmed the fast rate for the $BrO + HO_2$ reaction and established a negligible reaction pathway producing HBr, both of which imply greater ozone losses due to emissions of compounds containing bromine. While the magnitude of the atmospheric photochemical removal is well understood, there are significant uncertainties in quantifying the oceanic sink for atmospheric methyl bromide. The best estimate for the overall lifetime of atmospheric methyl bromide is 1.3 years, with a range of 0.8 - 1.7 years. The Ozone Depletion Potential (ODP) for methyl bromide is calculated to be about 0.6 (relative to an ODP of 1 for CFC-11).

- **Stratospheric ozone losses cause a global-mean negative radiative forcing.** In the 1991 scientific assessment, it was pointed out that the global ozone losses that were occurring in the lower stratosphere caused this region to cool and result in less radiation reaching the surface-troposphere system. Recent model studies have strengthened this picture. A long-term global-mean cooling of the lower stratosphere of between 0.25 and 0.4°C/decade has been observed over the last three decades. Calculations indicate that, on a global mean, the ozone losses between 1980 and 1990 offset about 20% of the radiative forcing due to the well-mixed greenhouse-gas increases during that period (*i.e.*, carbon dioxide, methane, nitrous oxide, and halocarbons).

- **Tropospheric ozone, which is a greenhouse gas, appears to have increased in many regions of the Northern Hemisphere.** Observations show that tropospheric ozone, which is formed by chemical reactions involving pollutants, has increased above many locations in the Northern Hemisphere over the last 30 years. However, in the 1980s, the trends were variable, being small or nonexistent. In the Southern Hemisphere, there are insufficient data to draw strong inferences. At the South Pole, a decrease has been observed since the mid-1980s. Model simulations and limited observations suggest that tropospheric ozone has increased in the Northern Hemisphere since pre-industrial times. Such changes would augment the radiative forcing from all other greenhouse gases by about 20% over the same time period.

- **The atmospheric residence times of the important ozone-depleting gases, CFC-11 and methyl chloroform, and the greenhouse gas, methane, are now better known.** A reconciliation of observed concentrations with known emissions using an atmospheric model has led to a best-estimate lifetime of 50 years for CFC-11 and 5.4 years for methyl chloroform, with uncertainties of about 10%. These lifetimes provide an accurate standard for gases destroyed only in the stratosphere (such as CFCs and nitrous oxide) and for those also reacting with tropospheric hydroxyl radical, OH (such as HCFCs and HFCs), respectively. Recent model simulations of methane perturbations and a theoretical analysis of the tropospheric chemical system that couples methane, carbon monoxide, and OH have demonstrated that methane perturbations decay with a lengthened time scale in a range of about 12 - 17 years, as compared with the 10-year lifetime derived from the total abundance and losses. This longer response time and other indirect effects increase the estimate of the effectiveness of emissions of methane as a greenhouse gas by a factor of about two compared to the direct-effect-only values given in the 1991 assessment.

Supporting Scientific Evidence and Related Issues

Ozone Changes in the Tropics and Midlatitudes and Their Interpretation

- Analysis of global total-column ozone data through early 1994 shows substantial decreases of ozone in all seasons at midlatitudes (30° - 60°) of both hemispheres. For example, in the middle latitudes of the Northern Hemisphere, downward trends of about 6% per decade over 1979 - 1994 were observed in winter and spring and about 3% per decade were observed in summer and fall. In the Southern Hemisphere, the seasonal difference was somewhat less, but the midlatitude trends averaged a similar 4% to 5% per decade. There are no statistically significant trends in the tropics (20°S - 20°N). Trends through 1994 are about 1% per decade more negative in the Northern Hemisphere (2% per decade in the midlatitude winter/spring in the Northern Hemisphere) compared to those calculated without using data after May 1991. At Northern midlatitudes, the downward trend in ozone between 1981 - 1991 was about 2% per decade greater compared to that of the period 1970 - 1980.

- Satellite and ozonesonde data show that much of the downward trend in ozone occurs below 25 km (*i.e.*, in the lower stratosphere). For the region 20 - 25 km, there is good agreement between the trends from the Stratospheric Aerosol and Gas Experiment (SAGE I/II) satellite instrument data and those from ozonesondes, with an observed annual-average decrease of 7 ± 4% per decade from 1979 to 1991 at 30° - 50°N latitude. Below 20 km, SAGE yields negative trends as large as 20 ± 8% per decade at 16 - 17 km, while the average of available midlatitude ozonesonde data shows smaller negative trends of 7 ± 3% per decade. Integration of the ozonesonde data yields total-ozone trends consistent with total-ozone measurements. In the 1980s, upper-stratospheric (35 - 45 km) ozone trends determined by the data from SAGE I/II, Solar Backscatter Ultraviolet satellite spectrometer (SBUV), and the Umkehr method agree well at midlatitudes, but less so in the tropics. Ozone declined 5 - 10% per decade at 35 - 45 km between 30°- 50°N and slightly more at southern midlatitudes. In the tropics at 45 km, SAGE I/II and SBUV yield downward trends of 10 and 5% per decade, respectively.

- Simultaneous *in situ* measurements of a suite of reactive chemical species have directly confirmed modeling studies implying that the chemical destruction of ozone in the midlatitude lower stratosphere is more strongly influenced by HO_x and halogen chemistry than NO_x chemistry. The seasonal cycle of ClO in the lower stratosphere at midlatitudes in both hemispheres supports a role for *in situ* heterogeneous perturbations (*i.e.*, on sulfate aerosols), but does not appear consistent with the timing of vortex processing or dilution. These studies provide key support for the view that sulfate aerosol chemistry plays an important role in determining midlatitude chemical ozone destruction rates.

- The model-calculated ozone depletions in the upper stratosphere for 1980 - 1990 are in broad agreement with the measurements. Although these model-calculated ozone depletions did not consider radiative feedbacks and temperature trends, including these effects is not likely to reduce the predicted ozone changes by more than 20%.

- Models including the chemistry involving sulfate aerosols and polar stratospheric clouds (PSCs) better simulate the observed total ozone depletions of the past decade than models that include only gas phase reactions. However, they still underestimate the ozone loss by factors ranging from 1.3 to 3.0.

- Some unresolved discrepancies between observations and models exist for the partitioning of inorganic chlorine species, which could impact model predictions of ozone trends. These occur for the ClO/HCl ratio in the upper stratosphere and the fraction of HCl to total inorganic chlorine in the lower stratosphere.

- The transport of ozone-depleted air from polar regions has the potential to influence ozone concentrations at middle latitudes. While there are uncertainties about the importance of this process relative to *in situ* chemistry for midlatitude ozone loss, both directly involve ozone destruction by chlorine- and bromine-catalyzed reactions.

- Radiosonde and satellite data continue to show a long-term cooling trend in globally annual-average lower-stratospheric temperatures of about 0.3 - 0.4°C per decade over the last three decades. Models suggest that ozone depletion is the major contributor to this trend.

- Anomalously large downward ozone trends have been observed in midlatitudes of both hemispheres in 1992 and 1993 (*i.e.*, the first two years after the eruption of Mt. Pinatubo), with Northern-Hemispheric decreases larger than those of the Southern Hemisphere. Global-average total-ozone levels in early 1993 were about 1% to 2% below that expected from the long-term trend and the particular phase of the solar and QBO cycles, while peak decreases of about 6 - 8% from expected ozone levels were seen over 45 - 60°N. In the first half of 1994, ozone levels returned to values closer to those expected from the long-term trend.

- The sulfur gases injected by Mt. Pinatubo led to large enhancements in stratospheric sulfate aerosol surface areas (by a maximum factor of about 30 - 40 at northern midlatitudes within a year after the eruption), which have subsequently declined.

- Anomalously low ozone was measured at altitudes below 25 km at a Northern-Hemispheric midlatitude station in 1992 and 1993 and was correlated with observed enhancements in sulfate-aerosol surface areas, pointing towards a causal link.

- Observations indicate that the eruption of Mt. Pinatubo did not significantly increase the HCl content of the stratosphere.

- The recent large ozone changes at midlatitudes are highly likely to have been due, at least in part, to the greatly increased sulfate aerosol in the lower stratosphere following Mt. Pinatubo. Observations and laboratory studies have demonstrated the importance of heterogeneous hydrolysis of N_2O_5 on sulfate aerosols in the atmosphere. Evidence suggests that $ClONO_2$ hydrolysis also occurs on sulfate aerosols under cold conditions. Both processes perturb the chemistry in such a way as to increase ozone loss through coupling with the anthropogenic chlorine and bromine loading of the stratosphere.

- Global mean lower stratospheric temperatures showed a marked transitory rise of about 1°C following the eruption of Mt. Pinatubo in 1991, consistent with model calculations. The warming is likely due to absorption of radiation by the aerosols.

Polar Ozone Depletion

- In 1992 and 1993, the biggest-ever (areal extent) and deepest-ever (minimum ozone below 100 Dobson units) ozone "holes" were observed in the Antarctic. These extreme ozone depletions may have been due to the chemical perturbations caused by sulfate aerosols from Mt. Pinatubo, acting in addition to the well-recognized chlorine and bromine reactions on polar stratospheric clouds.

- Recent results of observational and modeling studies reaffirm the role of anthropogenic halocarbon species in Antarctic ozone depletion. Satellite observations show a strong spatial and temporal correlation of ClO abundances with ozone depletion in the Antarctic vortex. In the Arctic winter, a much smaller ozone loss has been observed. These losses are both consistent with photochemical model calculations constrained with observations from *in situ* and satellite instruments.

- Extensive new measurements of HCl, ClO, and $ClONO_2$ from satellites and *in situ* techniques have confirmed the picture of the chemical processes responsible for chlorine activation in polar regions and the recovery from those processes, strengthening current understanding of the seasonal cycle of ozone depletion in both polar regions.

- New laboratory and field studies strengthen the confidence that reactions on sulfate aerosols can activate chlorine under cold conditions, particularly those in the polar regions. Under volcanically perturbed conditions when aerosols are enhanced, these processes also likely contribute to ozone losses at the edges of PSC formation regions (both vertical and horizontal) just outside of the southern vortex and in the Arctic.

- Satellite measurements have confirmed that the Arctic vortex is much less denitrified than the Antarctic, which is likely to be an important factor in determining the interhemispheric differences in polar ozone loss.

- Interannual variability in the photochemical and dynamical conditions of the vortices limits reliable predictions of future ozone changes in the polar regions, particularly in the Arctic.

Coupling Between Polar Regions and Midlatitudes

- Recent satellite observations of long-lived tracers and modeling studies confirm that, above 16 km, air near the center of the polar vortex is substantially isolated from lower latitudes, especially in the Antarctic.

- Erosion of the vortex by planetary-wave activity transports air from the vortex-edge region to lower latitudes. Nearly all observational and modeling studies are consistent with a time scale of 3 - 4 months to replace a substantial fraction of Antarctic vortex air. The importance of this transport to *in situ* chemical effects for midlatitude ozone loss remains poorly known.

- Air is readily transported between polar regions and midlatitudes below 16 km. The influence of this transport on midlatitude ozone loss has not been quantified.

Tropospheric Ozone

- There is observational evidence that tropospheric ozone (about 10% of the total-column ozone) has increased in the Northern Hemisphere (north of 20°N) over the past three decades. The upward trends are highly regional. They are smaller in the 1980s than in the 1970s and may be slightly negative at some locations. European measurements at surface sites also indicate a doubling in the lower-tropospheric ozone concentrations since earlier this century. At the South Pole, a decrease has been observed since the mid-1980s. Elsewhere in the Southern Hemisphere, there are insufficient data to draw strong inferences.

- There is strong evidence that ozone levels in the boundary layer over the populated regions of the Northern Hemisphere are enhanced by more than 50% due to photochemical production from anthropogenic precursors, and that export of ozone from North America is a significant source for the North Atlantic region during summer. It has also been shown that biomass burning is a significant source of ozone (and carbon monoxide) in the tropics during the dry season.

- An increase in UV-B radiation (*e.g.*, from stratospheric ozone loss) is expected to decrease tropospheric ozone in the background atmosphere, but, in some cases, it will increase production of ozone in the more polluted regions.

- Model calculations predict that a 20% increase in methane concentrations would result in tropospheric ozone increases ranging from 0.5 to 2.5 ppb in the tropics and the northern midlatitude summer, and an increase in the methane residence time to about 14 years (a range of 12 - 17 years). Although there is a high degree of consistency in the global transport of short-lived tracers within three-dimensional chemical-transport models, and a general agreement in the computation of photochemical rates affecting tropospheric ozone, many processes controlling tropospheric ozone are not adequately represented or tested in the models, hence limiting the accuracy of these results.

Trends in Source Gases Relating to Ozone Changes

- CFCs, carbon tetrachloride, methyl chloroform, and the halons are major anthropogenic source gases for stratospheric chlorine and bromine, and hence stratospheric ozone destruction. Observations from several monitoring networks worldwide have demonstrated slowdowns in growth rates of these species that are consistent (except for carbon tetrachloride) with expectations based upon recent decreases in emissions. In addition, observations from several sites have revealed accelerating growth rates of the CFC substitutes, HCFC-22, HCFC-141b, and HCFC-142b, as expected from their increasing use.

- Methane levels in the atmosphere affect tropospheric and stratospheric ozone levels. Global methane increased by 7% over about the past decade. However, the 1980s were characterized by slower growth rates, dropping from approximately 20 ppb per year in 1980 to about 10 ppb per year by the end of the decade. Methane growth rates slowed dramatically in 1991 and 1992, but the very recent data suggest that they have started to increase in late 1993. The cause(s) of this behavior are not known, but it is probably due to changes in methane sources rather than sinks.

- Despite the increased methane levels, the total amount of carbon monoxide in today's atmosphere is less than it was a decade ago. Recent analyses of global carbon monoxide data show that tropospheric levels grew from the early 1980s to about 1987 and have declined from the late 1980s to the present. The cause(s) of this behavior have not been identified.

EXECUTIVE SUMMARY

Consequences of Ozone Changes

- The only general circulation model (GCM) simulation to investigate the climatic impacts of observed ozone depletions between 1970 and 1990 supports earlier suggestions that these depletions reduced the model-predicted warming due to well-mixed greenhouse gases by about 20%. This is consistent with radiative forcing calculations.

- Model simulations suggest that increases in tropospheric ozone since pre-industrial times may have made significant contributions to the greenhouse forcing of the Earth's climate system, enhancing the current total forcing by about 20% compared to that arising from the changes in the well-mixed greenhouses gases over that period.

- Large increases in ultraviolet (UV) radiation have been observed in association with the ozone hole at high southern latitudes. The measured UV enhancements agree well with model calculations.

- Clear-sky UV measurements at midlatitude locations in the Southern Hemisphere are significantly larger than at a corresponding site in the Northern Hemisphere, in agreement with expected differences due to ozone column and Sun-Earth separation.

- Local increases in UV-B were measured in 1992/93 at mid- and high latitudes in the Northern Hemisphere. The spectral signatures of the enhancements clearly implicate the anomalously low ozone observed in those years, rather than variability of cloud cover or tropospheric pollution. Such correlations add confidence to the ability to link ozone changes to UV-B changes over relatively long time scales.

- Increases in clear-sky UV over the period 1979 to 1993 due to observed ozone changes are calculated to be greatest at short wavelengths and at high latitudes. Poleward of 45°, the increases are greatest in the Southern Hemisphere.

- Uncertainties in calibration, influence of tropospheric pollution, and difficulties of interpreting data from broadband instruments continue to preclude the unequivocal identification of long-term UV trends. However, data from two relatively unpolluted sites do appear to show UV increases consistent with observed ozone trends. Given the uncertainties of these studies, it now appears that quantification of the natural (*i.e.*, pre-ozone-reduction) UV baseline has been irrevocably lost at mid- and high latitudes.

- Scattering of UV radiation by stratospheric aerosols from the Mt. Pinatubo eruption did not alter total surface-UV levels appreciably.

Related Phenomena and Issues

Methyl Bromide

- Three potentially major anthropogenic sources of methyl bromide have been identified: (i) soil fumigation: 20 to 60 ktons per year, where new measurements reaffirm that about 50% (ranging from 20 - 90%) of the methyl bromide used as a soil fumigant is released into the atmosphere; (ii) biomass burning: 10 to 50 ktons per year; and (iii) the exhaust of automobiles using leaded gasoline: 0.5 to 1.5 ktons per year or 9 to 22 ktons per year (the two studies report emission factors that differ by a factor of more than 10). In addition, the one known major natural source of methyl bromide is oceanic, with emissions of 60 to 160 ktons per year.

- Recent measurements have confirmed that there is more methyl bromide in the Northern Hemisphere than in the Southern Hemisphere, with an interhemispheric ratio of 1.3.

- There are two known sinks for atmospheric methyl bromide: (i) atmospheric, with a lifetime of 2.0 years (1.5 to 2.5 years); and (ii) oceanic, with an estimated lifetime of 3.7 years (1.5 to 10 years). The overall best estimate for the lifetime of atmospheric methyl bromide is 1.3 years, with a range of 0.8 to 1.7 years. An overall lifetime of less than 0.6 years is thought to be highly unlikely because of constraints imposed by the observed interhemispheric ratio and total known emissions.

- The chemistry of bromine-induced stratospheric ozone destruction is now better understood. Laboratory measurements have confirmed the fast rate for the BrO + HO_2 reaction and have established a negligible reaction pathway producing HBr, both of which imply greater ozone losses due to emissions of compounds containing bromine. Stratospheric measurements show that the abundance of HBr is less than 1 ppt.

- Bromine is estimated to be about 50 times more efficient than chlorine in destroying stratospheric ozone on a per-atom basis. The ODP for methyl bromide is calculated to be about 0.6, based on an overall lifetime of 1.3 years. An uncertainty analysis suggests that the ODP is unlikely to be less than 0.3.

Aircraft

- Subsonics: Estimates indicate that present subsonic aircraft operations may be significantly increasing trace species (primarily NO_x, sulfur dioxide, and soot) at upper-tropospheric altitudes in the North-Atlantic flight corridor. Models indicate that the NO_x emissions from the current subsonic fleet produce upper-tropospheric ozone increases as much as several percent, maximizing at northern midlatitudes. Since the results of these rather complex models depend critically on NO_x chemistry and since the tropospheric NO_x budget is uncertain, little confidence should be put in these quantitative model results at the present time.

- Supersonics: Atmospheric effects of supersonic aircraft depend on the number of aircraft, the altitude of operation, the exhaust emissions, and the background chlorine and aerosol loadings. Projected fleets of supersonic transports would lead to significant changes in trace-species concentrations, especially in the North-Atlantic flight corridor. Two-dimensional model calculations of the impact of a projected fleet (500 aircraft, each emitting 15 grams of NO_x per kilogram of fuel burned at Mach 2.4) in a stratosphere with a chlorine loading of 3.7 ppb, imply additional (*i.e.*, beyond those from halocarbon losses) annual-average ozone column decreases of 0.3 - 1.8% for the Northern Hemisphere. There are, however, important uncertainties in these model results, especially in the stratosphere below 25 km. The same models fail to reproduce the observed ozone trends in the stratosphere below 25 km between 1980 and 1990. Thus, these models may not be properly including mechanisms that are important in this crucial altitude range.

- Climate Effects: Reliable quantitative estimates of the effects of aviation emissions on climate are not yet available. Some initial estimates indicate that the climate effects of ozone changes resulting from subsonic aircraft emissions may be comparable to those resulting from their CO_2 emissions.

Ozone Depletion Potentials (ODPs)

- If a substance containing chlorine or bromine decomposes in the stratosphere, it will destroy some ozone. HCFCs have short tropospheric lifetimes, which tends to reduce their impact on stratospheric ozone as compared to CFCs and halons. However, there are substantial differences in ODPs among various substitutes. The steady-state ODPs of substitute compounds considered in the present assessment range from about 0.01 - 0.1.

- Tropospheric degradation products of CFC substitutes will not lead to significant ozone loss in the stratosphere. Those products will not accumulate in the atmosphere and will not significantly influence the ODPs and Global Warming Potentials (GWPs) of the substitutes.

- Trifluoroacetic acid, formed in the atmospheric degradation of HFC-134a, HCFC-123, and HCFC-124, will enter into the aqueous environment, where biological, rather than physico-chemical, removal processes may be effective.

- It is known that atomic fluorine (F) itself is not an efficient catalyst for ozone loss, and it is concluded that the F-containing fragments from the substitutes (such as CF_3O_x) also have negligible impact on ozone. Therefore, ODPs of HFCs containing the CF_3 group (such as HFC-134a, HFC-23, and HFC-125) are likely to be much less than 0.001.

- New laboratory measurements and associated modeling studies have confirmed that perfluorocarbons and sulfur hexafluoride are long-lived in the atmosphere and act as greenhouse gases.

- The ODPs for several new compounds, such as HCFC-225ca, HCFC-225cb, and CF_3I, have been evaluated using both semi-empirical and modeling approaches, and are found to be 0.03 or less.

Global Warming Potentials (GWPs)

- Both the direct and indirect components of the GWP of methane have been estimated using model calculations. Methane's influence on the hydroxyl radical and the resulting effect on the methane response time lead to substantially longer response times for decay of emissions than OH removal alone, thereby increasing the GWP. In addition, indirect effects including production of tropospheric ozone and stratospheric water vapor were considered and are estimated to range from about 15 to 45% of the total GWP (direct plus indirect) for methane.

- GWPs, including indirect effects of ozone depletion, have been estimated for a variety of halocarbons, clarifying the relative radiative roles of ozone-depleting compounds (*i.e.*, CFCs and halons). The net GWPs of halocarbons depend strongly upon the effectiveness of each compound for ozone destruction; the halons are highly likely to have negative net GWPs, while those of the CFCs are likely to be positive over both 20- and 100-year time horizons.

Implications for Policy Formulation

The research findings of the past few years that are summarized above have several major implications as scientific input to governmental, industrial, and other policy decisions regarding human-influenced substances that lead to depletion of the stratospheric ozone layer and to changes of the radiative forcing of the climate system:

- **The Montreal Protocol and its Amendments and Adjustments are reducing the impact of anthropogenic halocarbons on the ozone layer and should eventually eliminate this ozone depletion.** Based on assumed compliance with the amended Montreal Protocol *(Copenhagen, 1992)* by all nations, the stratospheric chlorine abundances will continue to grow from their current levels (3.6 ppb) to a peak of about 3.8 ppb around the turn of the century. The future total bromine loading will depend upon choices made regarding future human production and emissions of methyl bromide. After around the turn of the century, the levels of stratospheric chlorine and bromine will begin a decrease that will continue into the 21st and 22nd centuries. The rate of decline is dictated by the long residence times of the CFCs, carbon tetrachloride, and halons. Global ozone losses and the Antarctic ozone "hole" were first discernible in the late 1970s and are predicted to recover in about the year 2045, other things being equal. The recovery of the ozone layer would have been impossible without the Amendments and Adjustments to the original Protocol *(Montreal, 1987)*.

- **Peak global ozone losses are expected to occur during the next several years.** The ozone layer will be most affected by human-influenced perturbations and susceptible to natural variations in the period around the year 1998, since the peak stratospheric chlorine and bromine abundances are expected to occur then. Based on extrapolation of current trends, observations suggest that the maximum ozone loss, relative to the late 1960s, will likely be:

  (i) about 12 - 13% at Northern midlatitudes in winter/spring (*i.e.*, about 2.5% above current levels);
  (ii) about 6 - 7% at Northern midlatitudes in summer/fall (*i.e.*, about 1.5% above current levels); and
  (iii) about 11% (with less certainty) at Southern midlatitudes on a year-round basis (*i.e.*, about 2.5% above current levels).

  Such changes would be accompanied by 15%, 8%, and 13% increases, respectively, in surface erythemal radiation, if other influences such as clouds remain constant. Moreover, if there were to be a major volcanic eruption like that of Mt. Pinatubo, or if an extremely cold and persistent Arctic winter were to occur, then the ozone losses and UV increases could be larger in individual years.

- **Approaches to lowering stratospheric chlorine and bromine abundances are limited.** Further controls on ozone-depleting substances would not be expected to significantly change the timing or the magnitude of the peak stratospheric halocarbon abundances and hence peak ozone loss. However, there are four approaches that would steepen the initial fall from the peak halocarbon levels in the early decades of the next century:

  (i) If emissions of methyl bromide from agricultural, structural, and industrial activities were to be eliminated in the year 2001, then the integrated effective future chlorine loading above the 1980 level (which is related to the cumulative future loss of ozone) is predicted to be 13% less over the next 50 years relative to full compliance to the Amendments and Adjustments to the Protocol.
  (ii) If emissions of HCFCs were to be totally eliminated by the year 2004, then the integrated effective future chlorine loading above the 1980 level is predicted to be 5% less over the next 50 years relative to full compliance with the Amendments and Adjustments to the Protocol.
  (iii) If halons presently contained in existing equipment were never released to the atmosphere, then the integrated effective future chlorine loading above the 1980 level is predicted to be 10% less over the next 50 years relative to full compliance with the Amendments and Adjustments to the Protocol.
  (iv) If CFCs presently contained in existing equipment were never released to the atmosphere, then the integrated effective future chlorine loading above the 1980 level is predicted to be 3% less over the next 50 years relative to full compliance with the Amendments and Adjustments to the Protocol.

- **Failure to adhere to the international agreements will delay recovery of the ozone layer.** If there were to be additional production of CFCs at 20% of 1992 levels for each year through 2002 and ramped to zero by 2005 (beyond that allowed for countries operating under Article 5 of the Montreal Protocol), then the integrated effective future chlorine loading above the 1980 level is predicted to be 9% more over the next 50 years relative to full compliance to the Amendments and Adjustments to the Protocol.

- **Many of the substitutes for the CFCs and halons are also notable greenhouse gases.** Several CFC and halon substitutes are not addressed under the Montreal Protocol (because they do not deplete ozone), but, because they are greenhouse gases, fall under the purview of the Framework Convention on Climate Change. There is a wide range of values for the Global Warming Potentials (GWPs) of the HFCs (150 - 10000), with about half of them having values comparable to the ozone-depleting compounds they replace. The perfluorinated compounds, some of which are being considered as substitutes, have very large GWPs (*e.g.*, 5000 - 10000). These are examples of compounds whose current atmospheric abundances are relatively small, but are increasing or could increase in the future.

- **Consideration of the ozone change will be one necessary ingredient in understanding climate change.** The extent of our ability to attribute any climate change to specific causes will likely prove to be important scientific input to decisions regarding predicted human-induced influences on the climate system. Changes in ozone since pre-industrial times as a result of human activity are believed to have been a significant influence on radiative forcing; this human influence is expected to continue into the foreseeable future.

COMMON QUESTIONS ABOUT OZONE

Ozone is exceedingly rare in our atmosphere, averaging about 3 molecules of ozone for every ten million air molecules. Nonetheless, atmospheric ozone plays vital roles that belie its small numbers. This Appendix to the *World Meteorological Organization/United Nations Environment Programme (WMO/UNEP) Scientific Assessment of Ozone Depletion: 1994* answers some of the questions that are most commonly asked about ozone and the changes that have been occurring in recent years. These common questions and their answers were discussed by the 80 scientists from 26 countries who participated in the Panel Review Meeting of the *Scientific Assessment of Ozone Depletion: 1994*. Therefore, this information is presented by a large group of experts from the international scientific community.

Ozone is mainly found in two regions of the Earth's atmosphere. Most ozone (about 90%) resides in a layer between approximately 10 and 50 kilometers (about 6 to 30 miles) above the Earth's surface, in the region of the atmosphere called the stratosphere. This stratospheric ozone is commonly known as the "ozone layer." The remaining ozone is in the lower region of the atmosphere, the troposphere, which extends from the Earth's surface up to about 10 kilometers. The figure below shows this distribution of ozone in the atmosphere.

While the ozone in these two regions is chemically identical (both consist of three oxygen atoms and have the chemical formula "O_3"), the ozone molecules have very different effects on humans and other living things depending upon their location.

Stratospheric ozone plays a beneficial role by absorbing most of the biologically damaging ultraviolet sunlight called UV-B, allowing only a small amount to reach the Earth's surface. The absorption of UV radiation by ozone creates a source of heat, which actually forms the stratosphere itself (a region in which the temperature rises as one goes to higher altitudes). Ozone thus plays a key role in the temperature structure of the Earth's atmosphere. Furthermore, without the filtering action of the ozone layer, more of the Sun's UV-B radiation would penetrate the atmosphere and would reach the Earth's surface in greater amounts. Many experimental studies of plants and animals, and clinical studies of humans, have shown the harmful effects of excessive exposure to UV-B radiation (these are discussed in the WMO/UNEP reports on impacts of ozone depletion, which are companion documents to the WMO/UNEP scientific assessments of ozone depletion).

At the planet's surface, ozone comes into direct contact with life-forms and displays its destructive side. Because ozone reacts strongly with other molecules, high levels are toxic to living systems and can severely damage the tissues of plants and animals. Many studies have documented the harmful effects of ozone on crop production, forest growth, and human health. The substantial negative effects of surface-level tropospheric ozone from this direct toxicity contrast with the benefits of the additional filtering of UV-B radiation that it provides.

With these dual aspects of ozone come two separate environmental issues, controlled by different forces in the atmosphere. In the troposphere, there is concern about *increases* in ozone. Low-lying ozone is a key component of smog, a familiar problem in the atmosphere of many cities around the world. Higher than usual amounts of surface-level ozone are now increasingly being observed in rural areas as well. However, the ground-level ozone concentrations in the smoggiest cities are very much smaller than the concentrations routinely found in the stratosphere.

There is widespread scientific and public interest and concern about *losses* of stratospheric ozone. Ground-based and satellite instruments have measured decreases in the amount of stratospheric ozone in our atmosphere. Over some parts of Antarctica, up to 60% of the total overhead amount of ozone (known as the "column ozone") is depleted during September and October. This phenomenon has come to be known as the Antarctic "ozone hole." Smaller, but still significant, stratospheric decreases have been seen at other, more-populated regions of the Earth. Increases in surface UV-B radiation have been observed in association with decreases in stratospheric ozone.

The scientific evidence, accumulated over more than two decades of study by the international research community, has shown that human-made chemicals are responsible for the observed depletions of the ozone layer over Antarctica and likely play a major role in global ozone losses. The ozone-depleting compounds contain various combinations of the chemical elements chlorine, fluorine, bromine, carbon, and hydrogen, and are often described by the general term *halocarbons*. The com-

pounds that contain only carbon, chlorine, and fluorine are called *chlorofluorocarbons*, usually abbreviated as *CFCs*. CFCs, carbon tetrachloride, and methyl chloroform are important human-made ozone-depleting gases that have been used in many applications including refrigeration, air conditioning, foam blowing, cleaning of electronics components, and as solvents. Another important group of human-made halocarbons is the *halons*, which contain carbon, bromine, fluorine, and (in some cases) chlorine, and have been mainly used as fire extinguishants. Governments have decided to discontinue production of CFCs, halons, carbon tetrachloride, and methyl chloroform, and industry has developed more "ozone-friendly" substitutes.

Two responses are natural when a new problem has been identified: cure and prevention. When the problem is the destruction of the stratospheric ozone layer, the corresponding questions are: Can we repair the damage already done? How can we prevent further destruction? Remedies have been investigated that could (i) remove CFCs selectively from our atmosphere, (ii) intercept ozone-depleting chlorine before much depletion has taken place, or (iii) replace the ozone lost in the stratosphere (perhaps by shipping the ozone from cities that have too much smog or by making new ozone). Because ozone reacts strongly with other molecules, as noted above, it is too unstable to be made elsewhere (e.g., in the smog of cities) and transported to the stratosphere. When the huge volume of the Earth's atmosphere and the magnitude of global stratospheric ozone depletion are carefully considered, approaches to cures quickly become much too expensive, impractical, and potentially damaging to the global environment. Prevention involves the internationally agreed-upon Montreal Protocol and its Amendments and Adjustments, which call for elimination of the production and use of the CFCs and other ozone-damaging compounds within the next few years. As a result, the ozone layer is expected to recover over the next fifty years or so as the atmospheric concentrations of CFCs and other ozone-depleting compounds slowly decay.

The current understanding of ozone depletion and its relation to humankind is discussed in detail by the leading scientists in the world's ozone research community in the *Scientific Assessment of Ozone Depletion: 1994*. The answers to the common questions posed below are based upon that understanding and on the information given in earlier WMO/UNEP reports.

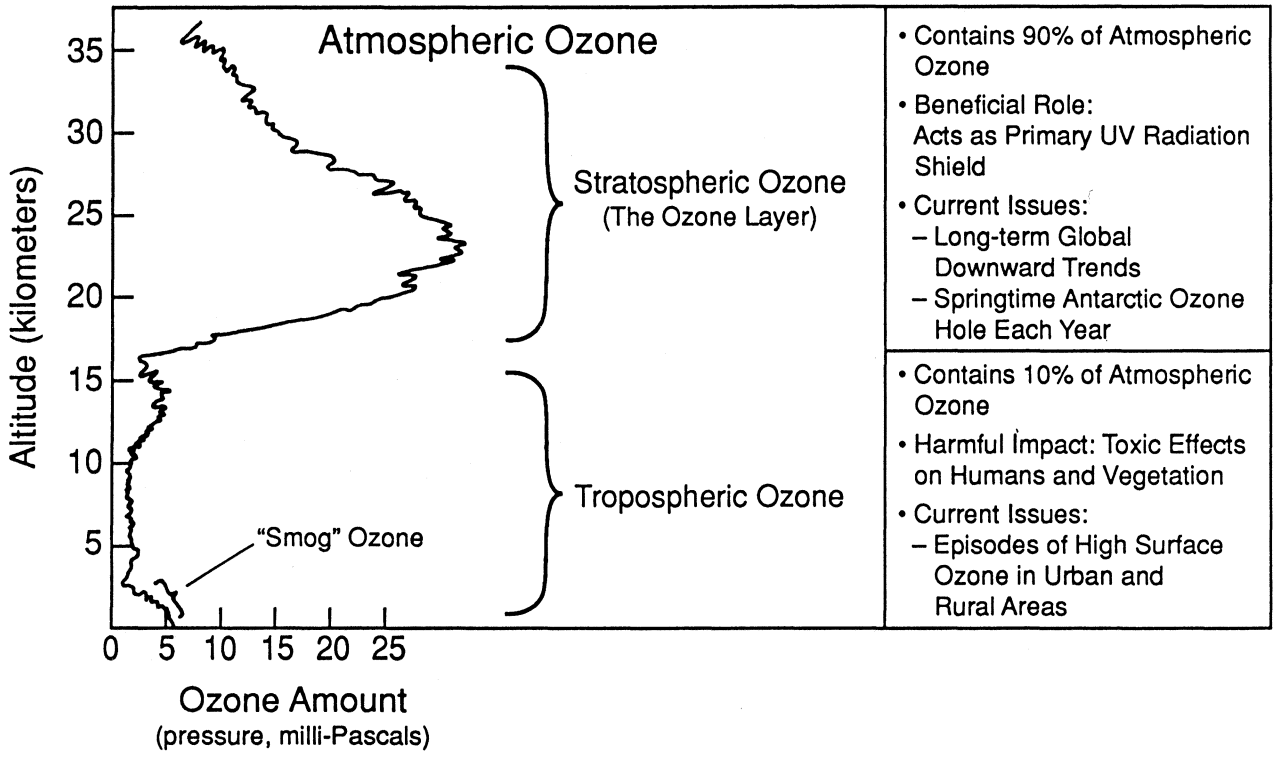

How Can Chlorofluorocarbons (CFCs) Get to the Stratosphere If They're Heavier than Air?

Although the CFC molecules are indeed several times heavier than air, thousands of measurements have been made from balloons, aircraft, and satellites demonstrating that the CFCs are actually present in the stratosphere. The atmosphere is not stagnant. Winds mix the atmosphere to altitudes far above the top of the stratosphere much faster than molecules can settle according to their weight. Gases such as CFCs that are insoluble in water and relatively unreactive in the lower atmosphere (below about 10 km) are quickly mixed and therefore reach the stratosphere regardless of their weight.

Much can be learned about the atmospheric fate of compounds from the measured changes in concentration versus altitude. For example, the two gases carbon tetrafluoride (CF_4, produced mainly as a by-product of the manufacture of aluminum) and CFC-11 (CCl_3F, used in a variety of human activities) are both much heavier than air. Carbon tetrafluoride is completely unreactive in the lower 99.9% of the atmosphere, and measurements show it to be nearly uniformly distributed throughout the atmosphere as shown in the figure. There have also been measurements over the past two decades of several other completely unreactive gases, one lighter than air (neon) and some heavier than air (argon, krypton), which show that they also mix upward uniformly through the stratosphere regardless of their weight, just as observed with carbon tetrafluoride. CFC-11 is unreactive in the lower atmosphere (below about 15 km) and is similarly uniformly mixed there, as shown. The abundance of CFC-11 decreases as the gas reaches higher altitudes, where it is broken down by high energy solar ultraviolet radiation. Chlorine released from this breakdown of CFC-11 and other CFCs remains in the stratosphere for several years, where it destroys many thousands of molecules of ozone.

Measurements of CFC-11 and CF_4

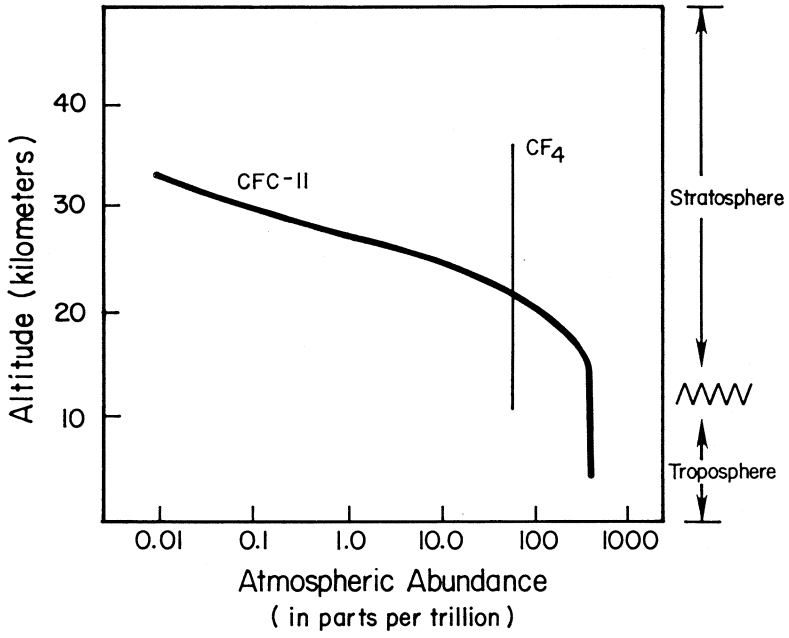

What is the Evidence that Stratospheric Ozone is Destroyed by Chlorine and Bromine?

Laboratory studies show that chlorine (Cl) reacts very rapidly with ozone. They also show that the reactive chemical chlorine oxide (ClO) formed in that reaction can undergo further processes which regenerate the original chlorine, allowing the sequence to be repeated very many times (a "chain reaction"). Similar reactions also take place between bromine and ozone.

But do these ozone-destroying reactions occur in the real world? All of our accumulated scientific experience demonstrates that if the conditions of temperature and pressure are like those in the laboratory studies, the same chemical reactions will take place in nature. However, many other reactions including those of other chemical species are often also taking place simultaneously in the stratosphere, making the connections among the changes difficult to untangle. Nevertheless, whenever chlorine (or bromine) and ozone are found together in the stratosphere, the ozone-destroying reactions must be taking place.

Sometimes a small number of chemical reactions is so important in the natural circumstance that the connections are almost as clear as in laboratory experiments. Such a situation occurs in the Antarctic stratosphere during the springtime formation of the ozone hole. During August and September 1987 – the end of winter and beginning of spring in the Southern Hemisphere – aircraft equipped with many different instruments for measuring a large number of chemical species were flown repeatedly over Antarctica. Among the chemicals measured were ozone and chlorine oxide, the reactive chemical identified in the laboratory as one of the participants in the ozone-destroying chain reactions. On the first flights southward from the southern tip of South America, relatively high concentrations of ozone were measured everywhere over Antarctica. By mid-September, however, the instruments recorded low concentrations of ozone in regions where there were high concentrations of chlorine oxide and vice versa, as shown in the figure. Flights later in September showed even less ozone over Antarctica, as the chlorine continued to react with the stratospheric ozone.

Independent measurements made by these and other instruments on this and other airplanes, from the ground, from balloons, and from satellites have provided a detailed understanding of the chemical reactions going on in the Antarctic stratosphere. Regions with high concentrations of reactive chlorine reach temperatures so cold (less than approximately -80°C, or -112°F) that stratospheric clouds form, a rare occurrence except during the polar winters. These clouds facilitate other chemical reactions that allow the release of chlorine in sunlight. The chemical reactions related to the clouds are now well understood through study under laboratory conditions mimicking those found naturally. Scientists are working to understand the role of such reactions of chlorine and bromine at other latitudes, and the involvement of particles of sulfuric acid from volcanoes or other sources.

Measurements of Ozone and Reactive Chlorine from a Flight into the Antarctic Ozone Hole

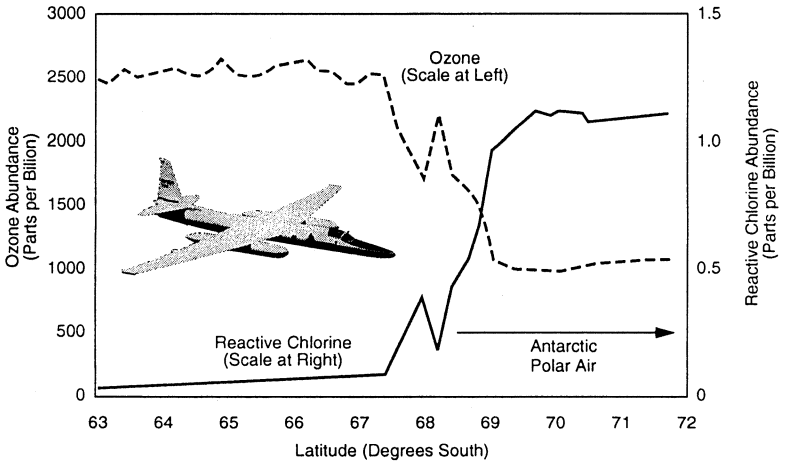

Does Most of the Chlorine in the Stratosphere Come from Human or Natural Sources?

Most of the chlorine in the stratosphere is there as a result of human activities.

Many compounds containing chlorine are released at the ground, but those that dissolve in water cannot reach stratospheric altitudes. Large quantities of chlorine are released from evaporated ocean spray as sea salt (sodium chloride) aerosol. However, because sea salt dissolves in water, this chlorine quickly is taken up in clouds or in ice, snow, or rain droplets and does not reach the stratosphere. Another ground-level source of chlorine is its use in swimming pools and as household bleach. When released, this chlorine is rapidly converted to forms that dissolve in water and therefore are removed from the lower atmosphere, never reaching the stratosphere in significant amounts. Volcanoes can emit large quantities of hydrogen chloride, but this gas is rapidly converted to hydrochloric acid in rain water, ice, and snow and does not reach the stratosphere. Even in explosive volcanic plumes that rise high in the atmosphere, nearly all of the hydrogen chloride is scrubbed out in precipitation before reaching stratospheric altitudes.

In contrast, human-made halocarbons – such as CFCs, carbon tetrachloride (CCl_4) and methyl chloroform (CH_3CCl_3) – are not soluble in water, do not react with snow or other natural surfaces, and are not broken down chemically in the lower atmosphere. While the exhaust from the Space Shuttle and from some rockets does inject some chlorine directly into the stratosphere, this input is very small (less than one percent of the annual input from halocarbons in the present stratosphere, assuming nine Space Shuttle and six Titan IV rocket launches per year).

Several pieces of evidence combine to establish human-made halocarbons as the primary source of stratospheric chlorine. First, measurements (see the figure below) have shown that the chlorinated species that rise to the stratosphere are primarily manufactured compounds (mainly CFCs, carbon tetrachloride, methyl chloroform, and the HCFC substitutes for CFCs), together with small amounts of hydrochloric acid (HCl) and methyl chloride (CH_3Cl) which are partly natural in origin. The natural contribution now is much smaller than that from human activities, as shown in the figure below. Second, in 1985 and 1992 researchers measured nearly all known gases containing chlorine in the stratosphere. They found that human emissions of halocarbons plus the much smaller contribution from natural sources could account for all of the stratospheric chlorine compounds. Third, the *increase* in total stratospheric chlorine measured between 1985 and 1992 corresponds with the known increases in concentrations of human-made halocarbons during that time.

Primary Sources of Chlorine Entering the Stratosphere

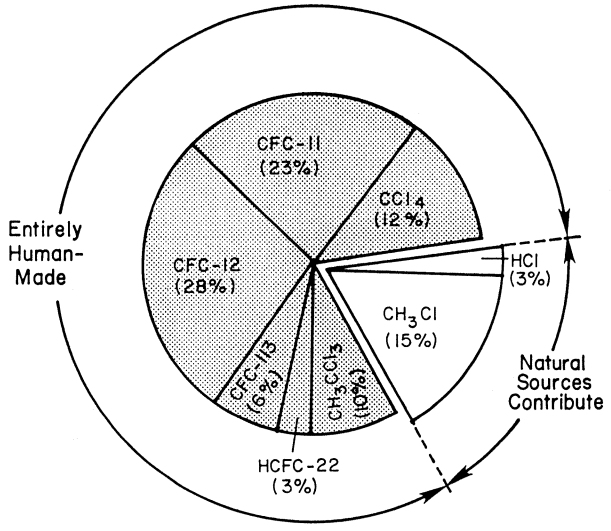

Can Changes in the Sun's Output Be Responsible for the Observed Changes in Ozone?

Stratospheric ozone is primarily created by ultraviolet (UV) light coming from the Sun, so the Sun's output affects the rate at which ozone is produced. The Sun's energy release (both as UV light and as charged particles such as electrons and protons) does vary, especially over the well-known 11-year sunspot cycle. Observations over several solar cycles (since the 1960s) show that total global ozone levels decrease by 1-2% from the maximum to the minimum of a typical cycle. Changes in the Sun's output cannot be responsible for the observed long-term changes in ozone, because these downward trends are much larger than 1-2%. Further, during the period since 1979, the Sun's energy output has gone from a maximum to a minimum in 1985 and back through another maximum in 1991, but the trend in ozone was downward throughout that time. The ozone trends presented in this and previous international scientific assessments have been obtained by evaluating the long-term changes in ozone concentrations after accounting for the solar influence (as has been done in the figure below).

Global Ozone Trend (60°S–60°N)

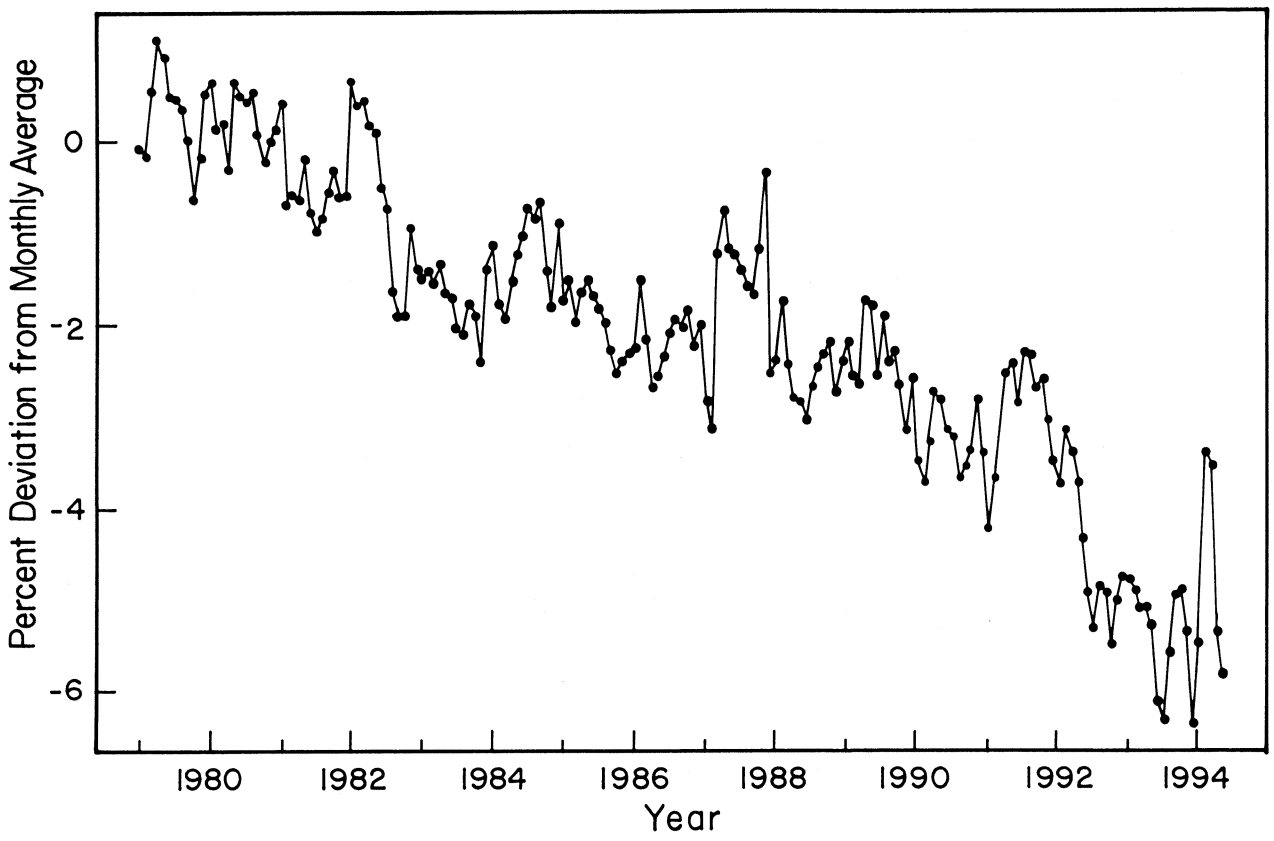

When Did the Antarctic Ozone Hole First Appear?

The Antarctic ozone hole is a new phenomenon. The figure shows that observed ozone over the British Antarctic Survey station at Halley Bay, Antarctica first revealed obvious decreases in the early 1980s compared to data obtained since 1957. The ozone hole is formed each year when there is a sharp decline (currently up to 60%) in the total ozone over most of Antarctica for a period of about two months during Southern Hemisphere spring (September and October). Observations from three other stations in Antarctica, also covering several decades, reveal similar progressive, recent decreases in springtime ozone. The ozone hole has been shown to result from destruction of stratospheric ozone by gases containing chlorine and bromine, whose sources are mainly human-made halocarbon gases.

Before the stratosphere was affected by human-made chlorine and bromine, the naturally occurring springtime ozone levels over Antarctica were about 30-40% lower than springtime ozone levels over the Arctic. This natural difference between Antarctic and Arctic conditions was first observed in the late 1950s by Dobson. It stems from the exceptionally cold temperatures and different winter wind patterns within the Antarctic stratosphere as compared to the Arctic. This is not at all the same phenomenon as the marked downward trend in total ozone in recent years referred to as the ozone hole and shown in the figure below.

Changes in stratospheric meteorology cannot explain the ozone hole. Measurements show that wintertime Antarctic stratospheric temperatures of past decades have not changed prior to the development of the hole each September. Ground, aircraft, and satellite measurements have provided, in contrast, clear evidence of the importance of the chemistry of chlorine and bromine originating from human-made compounds in depleting Antarctic ozone in recent years.

A single report of extremely low Antarctic winter ozone in one location in 1958 by an unproven technique has been shown to be completely inconsistent with the measurements depicted here and with all credible measurements of total ozone.

Historical Springtime Total Ozone Record for Halley Bay, Antarctica (76°S)

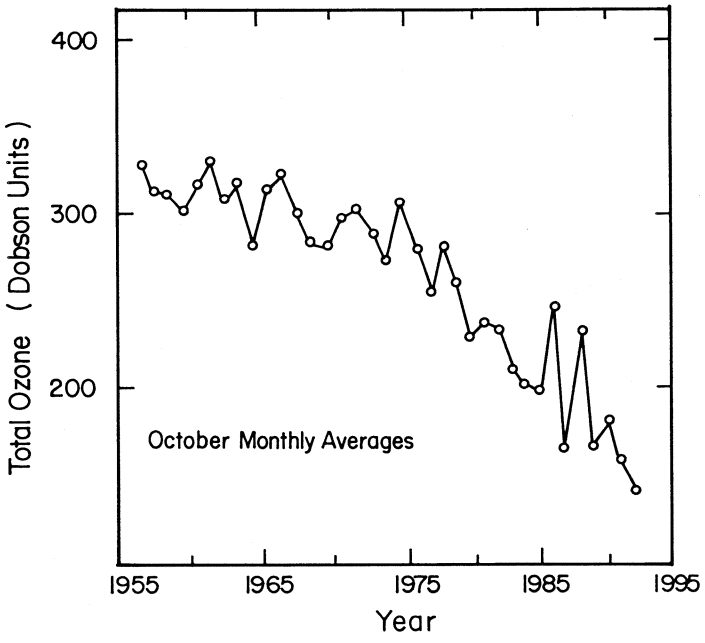

Why is the Ozone Hole Observed over Antarctica When CFCs Are Released Mainly in the Northern Hemisphere?

Human emissions of CFCs do occur mainly in the Northern Hemisphere, with about 90% released in the latitudes corresponding to Europe, Russia, Japan, and North America. Gases such as CFCs that are insoluble in water and relatively unreactive are mixed within a year or two throughout the lower atmosphere (below about 10 km). The CFCs in this well-mixed air rise from the lower atmosphere into the stratosphere mainly in tropical latitudes. Winds then move this air poleward – both north and south – from the tropics, so that air throughout the stratosphere contains nearly the same amount of chlorine. However, the meteorologies of the two polar regions are very different from each other because of major differences at the Earth's surface. The South Pole is part of a very large land mass (Antarctica) that is completely surrounded by ocean. These conditions produce very low stratospheric temperatures which in turn lead to formation of clouds (polar stratospheric clouds). The clouds that form at low temperatures lead to chemical changes that promote rapid ozone loss during September and October of each year, resulting in the ozone hole.

In contrast, the Earth's surface in the northern polar region lacks the land/ocean symmetry characteristic of the southern polar area. As a consequence, Arctic stratospheric air is generally much warmer than in the Antarctic, and fewer clouds form there. Therefore, the ozone depletion in the Arctic is much less than in the Antarctic.

Schematic of Antarctic Ozone Hole

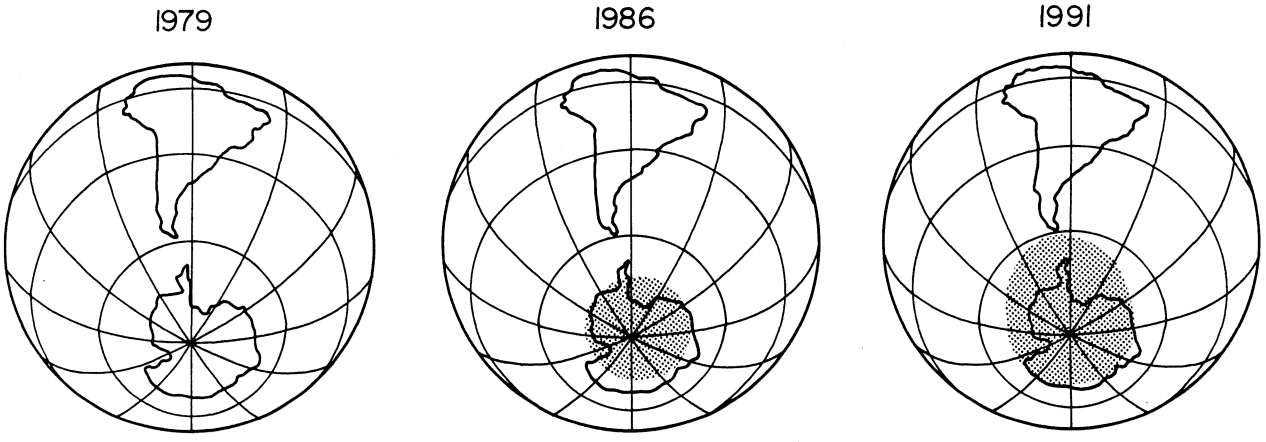

Is the Depletion of the Ozone Layer Leading to an Increase in Ground-Level Ultraviolet Radiation?

The Sun emits light over a wide range of energies, with about two percent given off in the form of high-energy, ultraviolet (UV) radiation. Some of this UV radiation (UV-B) is especially effective in causing damage to living things, including sunburn, skin cancer, and eye damage for humans. The amount of solar UV radiation received at any particular location on the Earth's surface depends upon the position of the Sun above the horizon, on the amount of ozone in the atmosphere, and upon local cloudiness and pollution. Scientists agree that in the absence of changes in clouds or pollution, decreases in atmospheric ozone will increase ground-level UV radiation.

The largest decreases in ozone during the last decade have been observed over Antarctica, especially during each September and October when the "ozone hole" forms. During the last several years, simultaneous measurements of UV radiation and total ozone have been made at several Antarctic stations. As shown in the figure below, when the ozone amounts decrease, UV-B increases. Because of the ozone hole, the UV-B intensity at Palmer Station, Antarctica, in late October, 1993, was more intense than found at San Diego, California, at any time during all of 1993.

In areas where small ozone depletion has been observed, UV-B increases are more difficult to detect. Detection of UV trends associated with ozone decreases can also be complicated by changes in cloudiness or by local pollution, as well as by difficulties in keeping the detection instrument in precisely the same condition over many years. Prior to the late 1980s, instruments with the necessary accuracy and stability for measurement of small long-term trends in ground-level UV-B were not employed. Recently, however, such instruments have been used in the Antarctic because of the very large changes in ozone being observed there. When high-quality measurements have been made in other areas far from major cities and their associated air pollution, decreases in ozone have regularly been accompanied by increases in UV-B. The data from urban locations with older, less specialized instruments provide much less reliable information, especially because good simultaneous measurements are not available for any changes in cloudiness or local pollution.

Increases in Erythemal (Sunburning) UV Radiation Due to Ozone Reductions

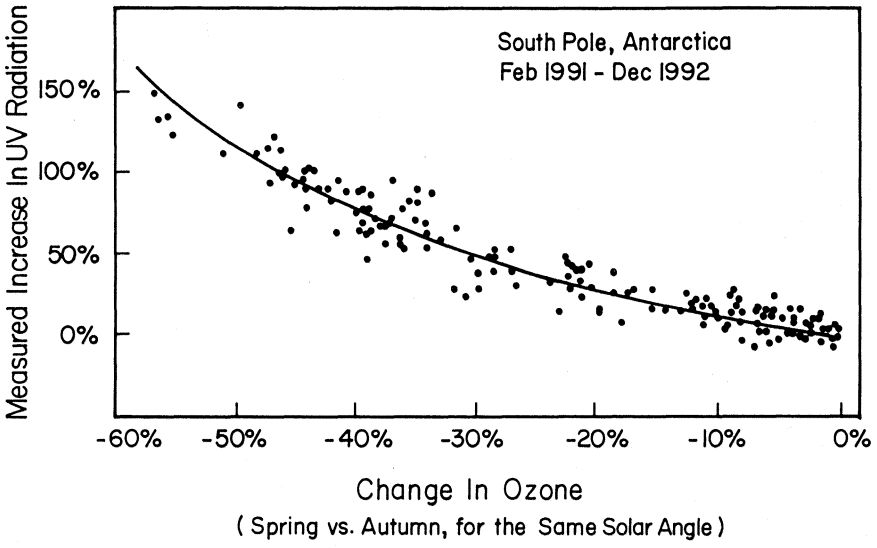

How Severe Is the Ozone Depletion Now, and Is It Expected to Get Worse?

Scientific evidence shows that ozone depletion caused by human-made chemicals is continuing and is expected to persist until chlorine and bromine levels are reduced. Worldwide monitoring has shown that stratospheric ozone has been decreasing for the past two decades or more. Globally averaged losses have totaled about 5% since the mid-1960s, with cumulative losses of about 10% in the winter and spring and 5% in the summer and autumn over locations such as Europe, North America, and Australia. Since the late-1970s, an ozone "hole" has formed in Antarctica each Southern Hemisphere spring (September / October), in which up to 60% of the total ozone is depleted. The large increase in atmospheric concentrations of human-made chlorine and bromine compounds is responsible for the formation of the Antarctic ozone hole, and the weight of evidence indicates that it also plays a major role in midlatitude ozone depletion.

During 1992 and 1993 ozone in many locations dropped to record low values: springtime depletions exceeded 20% in some populated northern midlatitude regions, and the levels in the Antarctic ozone hole fell to the lowest values ever recorded. The unusually large ozone decreases of 1992 and 1993 are believed to be related, in part, to the volcanic eruption of Mount Pinatubo in the Philippines during 1991. This eruption produced large amounts of stratospheric sulfate aerosols that temporarily increased the ozone depletion caused by human-made chlorine and bromine compounds. Recent observations have shown that as those aerosols have been swept out of the stratosphere, ozone concentrations have returned to the depleted levels consistent with the downward trend observed before the Mount Pinatubo eruption.

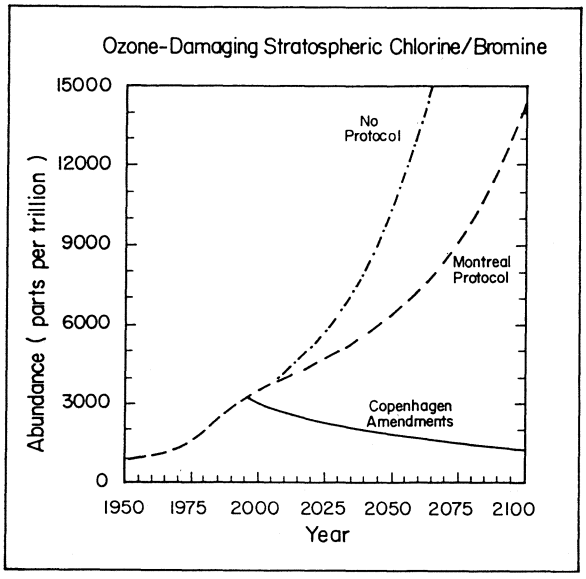

In 1987 the recognition of the potential for chlorine and bromine to destroy stratospheric ozone led to an international agreement (The United Nations Montreal Protocol on Substances that Deplete the Ozone Layer) to reduce the global production of ozone-depleting substances. Since then, new global observations of significant ozone depletion have prompted amendments to strengthen the treaty. The 1992 Copenhagen Amendments call for a ban on production of the most damaging compounds by 1996. The figure shows past and projected future stratospheric abundances of chlorine and bromine: (a) without the Protocol; (b) under the Protocol's original provisions; and (c) under the Copenhagen Amendments now in force. Without the Montreal Protocol and its Amendments, continuing human use of CFCs and other compounds would have tripled the stratospheric abundances of chlorine and bromine by about the year 2050. Current scientific understanding indicates that such increases would have led to global ozone depletion very much larger than observed today. In contrast, under current international agreements, which are now reducing and will eventually eliminate human emissions of ozone-depleting gases, the stratospheric abundances of chlorine and bromine are expected to reach their maximum within a few years and then slowly decline. All other things being equal, the ozone layer is expected to return to normal by the middle of the next century.

In summary, record low ozone levels have been observed in recent years, and substantially larger future global depletions in ozone would have been highly likely without reductions in human emissions of ozone-depleting gases. However, worldwide compliance with current international agreements is rapidly reducing the yearly emissions of these compounds. As these emissions cease, the ozone layer will gradually improve over the next several decades. The recovery of the ozone layer will be gradual because of the long times required for CFCs to be removed from the atmosphere.

PART 1

OBSERVED CHANGES IN OZONE AND SOURCE GASES

Chapter 1
Ozone Measurements

Chapter 2
Source Gases:
Trends and Budgets

CHAPTER 1

Ozone Measurements

Lead Author:
N.R.P. Harris

Co-authors:
G. Ancellet
L. Bishop
D.J. Hofmann
J.B. Kerr
R.D. McPeters
M. Préndez
W. Randel
J. Staehelin
B.H. Subbaraya
A. Volz-Thomas
J.M. Zawodny
C.S. Zerefos

Contributors:
M. Allaart
J.K. Angell
R.D. Bojkov
K.P. Bowman
G.J.R. Coetzee
M. Degórska
J.J. DeLuisi
D. De Muer
T. Deshler
L. Froidevaux
R. Furrer
B.G. Gardiner
H. Gernandt
J.F. Gleason
U. Görsdorf
K. Henriksen
E. Hilsenrath
S.M. Hollandsworth
Ø. Hov
H. Kelder
V. Kirchhoff
U. Köhler
W.D. Komhyr
J.W. Krzyścin
Z. Lityńska
J.A. Logan
P.S. Low
A.J. Miller
S.J. Oltmans
W.G. Planet
J.-P. Pommereau
H.-E. Scheel
J.D. Shanklin
P. Skřivánková
H. Smit
J. Waters
P. Winkler

CHAPTER 1

OZONE MEASUREMENTS

Contents

SCIENTIFIC SUMMARY

The quality of the total ozone measurements made by ground-based and satellite systems has been assessed and trends calculated where appropriate.

- Trends in total ozone since 1979 have been updated through early 1994:
  - Northern Hemisphere middle latitude trends are significantly negative in all seasons, but are much larger in winter/spring (about 6%/decade), than in summer/fall (about 3%/decade).
  - Tropical (approx. 20°S – 20°N) trends are slightly negative, but not statistically significant when suspected drift in the satellite data is incorporated into the uncertainty.
  - Southern midlatitude trends are significantly negative in all seasons, and increase in magnitude for high latitudes.

- Representative trends (annual averages, in % per decade) for north and south midlatitudes and the tropics are as follows.

		Latitude		
		Mid South	Equatorial	Mid North
Recent:				
1/79 to 5/94	SBUV+SBUV/2	-4.9 ± 1.5	-1.8 ± 1.4	-4.6 ± 1.8
1/79 to 2/94	Dobson network	-3.2 ± 1.3	-1.1 ± 0.6	-4.8 ± 0.8
1/79 to 2/94	Ozonometer (former USSR)	na	na	-4.9 ± 0.8
Pre-Pinatubo:				
1/79 to 5/91	SBUV+SBUV/2	-4.9 ± 2.3	-0.8 ± 2.1	-3.3 ± 2.4
1/79 to 5/91	TOMS	-4.5 ± 2.1	+0.4 ± 2.1	-4.0 ± 2.1
1/79 to 5/91	Dobson network	-3.8 ± 1.3	+0.2 ± 1.2	-3.9 ± 0.7
1/79 to 5/91	Ozonometer (former USSR)	na	na	-3.8 ± 1.0

Note: Uncertainties (±) are expressed at the 95% confidence limits (2 standard errors).

- The corresponding ozone loss (in %) accumulated over 15.3 years for trends calculated through 1994 are:

	Latitude		
	Mid South	Equatorial	Mid North
SBUV+SBUV/2	-7.4 ± 2.3	-2.7 ± 2.2	-7.0 ± 2.7
Dobson network	-4.8 ± 2.1	-1.7 ± 0.9	-7.3 ± 1.3
Ozonometer (former USSR)	na	na	-7.5 ± 1.3

OZONE MEASUREMENTS

- There was a statistically significant increase (about 2%/decade) in the average rate of ozone depletion at the Dobson stations north of 25°N in the period 1981-1991 compared to the period 1970-1980.

- We have confidence in the trends deduced from the ground-based network, particularly in the Northern Hemisphere. The record is longer than for the satellite instruments, although the geographic coverage is patchy, with most stations situated in the Northern Hemisphere midlatitudes. The absolute calibration of the International Standard Dobson spectrophotometer has been maintained at ± 1%/decade. The quality of the data from the ground-based network has improved since the last assessment, partly as a result of improvements to the existing records and partly as a result of the improving quality control in the ground-based network.

- An extensive revision and reanalysis of the measurements made using the filter ozonometer data from the vast area of the former USSR has recently been performed. Trend estimates from these revised data substantiate those made at similar latitudes by Dobson and satellite instruments.

- During the 1980s, the Total Ozone Mapping Spectrometer (TOMS) total ozone calibration drifted by 1-2% relative to the Dobson instruments, depending on latitude. In addition, a systematic bias of 1-2%/decade may be present in measurements made at high solar zenith angles (and so is most important at high latitudes in winter). Our confidence in the trends presented in the 1991 Ozone Assessment, which covered the period through March 1991, is unchanged.

- However after this time, a problem developed in the TOMS instrument that lasted until the instrument became inoperative in May 1993. This problem resulted in systematic errors dependent on both season and latitude, and caused, on average, a drift of 1-2% between 1991 and 1993. TOMS satellite measurements made after May 1991 were, therefore, not used for trend analyses. A TOMS instrument was launched on the Meteor-3 satellite in August 1991. The satellite orbit is not ideal and the measurements from this instrument have not yet been sufficiently assessed to allow use in trend analyses.

- The drift in the calibration of total ozone by the Solar Backscatter Ultraviolet (SBUV) instrument from January 1979 to June 1990 was 1% or less relative to Dobson instruments, and any seasonal differences in the Northern Hemisphere were less than 1%. The SBUV/2 instrument on board the NOAA-11 satellite has measurements available from January 1989. The drift relative to Dobson instruments in the Northern Hemisphere has been less than 1%. However, there is an apparent seasonal cycle in the differences of about 1-2% (minimum to maximum).

- Nearly all ground-based instruments are now on the calibration scale of the World Standard Dobson Instrument #83. The quality of the measurements made at individual stations is tested using satellite data; any revision of the data is based on available instrumental records. Satellite measurements are independently calibrated by checking the internal consistency. However, the satellite record is tested for possible drift by comparison with the collection of station data. Thus, the ground-based and satellite records are not completely independent from one another.

Trends in the Vertical Distribution of Ozone

The state of knowledge about the trends in the vertical distribution of ozone is not as good as that about the total ozone trends. The quality of the available data varies considerably with altitude.

- At altitudes of 35-45 km, there is reasonable agreement between the Stratospheric Aerosol and Gas Experiment I/II (SAGE I/II), SBUV, and Umkehr, that during 1979-1991, ozone declined 5-10% per decade at 30-50°N and slightly more at southern midlatitudes. In the tropics, SAGE I/II gives larger trends (ca. -10% per decade) than SBUV (ca. -5% per decade) at these altitudes.

- At altitudes between 25 and 30 km, there is reasonable agreement between SAGE I/II, SBUV, Umkehr, and ozonesondes that, during the 1979-1991 period, there was no significant ozone depletion at any latitude. The agreement continues down to about 20 km, where statistically significant reductions of 7 ± 4% per decade were observed between 30 and 50°N by both ozonesondes and SAGE I/II. Over the longer period from 1968-1991, the ozonesonde record indicates a trend of -4 ± 2% per decade at 20 km at northern midlatitudes.

- There appear to have been sizeable ozone reductions during the 1979-1991 period in the 15-20 km region in midlatitudes. There is disagreement on the magnitude of the reduction, with SAGE indicating trends as large as -20 ± 8% per decade at 16-17 km and the ozonesondes indicating an average trend of -7 ± 3% per decade in the Northern Hemisphere. The trend in the integrated ozone column for SAGE is larger than those found from SBUV, TOMS, and the ground-based network, but the uncertainties are too large to evaluate the consistency between the data sets properly. For 1968-1991 the ozonesonde record indicates a trend of -7 ± 3% per decade at 16 km at northern midlatitudes.

- In the tropics, trend determination at altitudes between 15 and 20 km is made difficult by the small ozone amounts. In addition, the large vertical ozone gradients make the trends very sensitive to small vertical displacements of the profile. The SAGE I/II record indicates large (-20 to -30% (± 18%) per decade) trends in the 16-17 km region (-10% (± 8%) at 20 km). Limited tropical ozonesonde data sets at Natal, 6°S and Hilo, 20°N do not indicate significant trends between 16 and 17 km or at any other altitude for this time period. With currently available information it is difficult to evaluate the trends below 20 km in the tropics, as the related uncertainties are large. The effect on the trend in the total column from any changes at these altitudes would be small.

- In the free troposphere, only limited data (all from ozonesondes) are available for trend determination. In the Northern Hemisphere, trends are highly variable between regions. Upward trends in the 1970s over Europe have declined significantly in the 1980s, have been small or non-existent over North America, and continue upward over Japan. The determination of the size of the change over North America requires a proper treatment of the relative tropospheric sensitivities for the type of sondes used during different time periods.

- Surface measurements indicate that ozone levels at the surface in Europe have doubled since the 1950s. Over the last two decades there has been a downward trend at the South Pole, and positive trends are observed at high altitude sites in the Northern Hemisphere. When considering the latter conclusion, the regional nature of trends in the Northern Hemisphere must be borne in mind.

Observations of Ozone and Aerosols in 1991-1994

- Global total ozone values in 1992/93 were 3-4% lower than the 1980s average. If the trend, solar cycle, and quasi-biennial oscillation (QBO) effects inferred from the 1980s record are extrapolated, an additional global anomaly of between -1 and -2% remains.

- The most negative anomalies were observed in the Northern Hemisphere springs in 1992 and 1993, with peak deviations of 6-10% in February-April 1993.

OZONE MEASUREMENTS

- A reduction of 3-4% occurred in the tropics in the six months following the eruption of Mt. Pinatubo.

- Overall the smallest effects were observed in the extra-tropical Southern Hemisphere, where total ozone amounts were at the low end of the range observed in the 1980s, as would be expected from the long-term downward trend observed in that region.

- In 1994, global ozone levels are also at the low end of the 1980s range, again in line with expectations of a continuation of the observed long-term trend.

- Following the June 1991 eruption of Mt. Pinatubo, stratospheric aerosol levels increased globally, with northern midlatitude peak particle surface areas increasing by factors of 30-40 above pre-eruption values about one year after the eruption. Since that time, they have been decreasing.

- Several mechanisms have been suggested as causes of the total ozone anomalies, though the relative importance is not yet clear. The possible influences include: radiative, dynamical, and chemical perturbations resulting from the Mt. Pinatubo volcanic aerosol; and global and regional dynamical perturbations, including the El Niño-Southern Oscillation.

Antarctic Ozone Depletion

- Record low mean values for October were observed at three Antarctic ground-based stations with continuous records since the late 1950s and early 1960s. There is no evidence of major springtime ozone depletion in Antarctica at any of the four Dobson stations prior to 1980.

- In early October 1993, a record low daily value of total ozone of 91 $\pm$ 5 Dobson units was observed with an ozonesonde at the South Pole. During this flight (and in several others), no detectable ozone (less than 1%) was found over a 5 km range from 14 to 19 km, implying that complete chemical destruction of ozone had occurred. The geographical extents of the ozone holes in 1992 and 1993 were the two largest on record.

- A comparison of ozonesonde measurements made at the South Pole from 1967-1971 with those made between 1986 and 1991 reaffirms that the Antarctic depletion that has developed since the early period occurs at altitudes between 14 and 20 km, and that the largest changes occur in September, October, and November.

1.1 INTRODUCTION

Ozone in the atmosphere is easy to detect. Several techniques have been successfully used: most are optical, using absorption or emission of light in many regions of the spectrum; others are chemical; and some are a mixture of the two. However, while it is relatively easy to detect ozone in the atmosphere, it has proved difficult to make sufficiently precise and numerous measurements to determine credible changes of a few percent on a decadal time scale. Difficulties include: knowing what the absolute calibrations of the instruments are and how they change with time; assessing how much variability in any set of measurements is caused by the instrument and how much by the natural variability in the atmosphere; and making meaningful comparisons of measurements made by different instruments, especially when different techniques are used. Detailed descriptions of the major techniques and instruments were given in the report of the International Ozone Trends Panel (IOTP) (WMO, 1990a) and are not repeated here.

We first consider the quality of total ozone measurements, particularly those made by the ground-based observing network, the Total Ozone Mapping Spectrometer (TOMS), and the Solar Backscatter Ultraviolet spectrometers (SBUV). The ground-based and satellite instruments have proven invaluable in assessing each others' data quality. Nearly all ground-based instruments are now on the calibration scale of the World Standard Dobson Instrument #83. The quality of the measurements made at individual stations is tested using satellite data; any revision of the data is based on available instrumental records. Satellite measurements are independently calibrated by checking the internal consistency. However, the satellite record is tested for possible drift by comparison with the collection of station data. Thus, the ground-based and satellite records are not completely independent from one another.

Given this perspective, we next present the trends in total ozone calculated to May 1994. Special attention is paid to how the trends are affected by the record low ozone values that were observed in 1992 and 1993. This theme is taken up again later, in Section 1.4, where we describe the ozone changes seen in this period. The evolution of stratospheric aerosol following the eruptions of Mt. Pinatubo in June 1991 and Volcán Hudson in August 1991, and possible links with the low ozone values, are briefly discussed, along with other potentially important influences on ozone at this time.

In Section 1.3 we discuss the quality of the various techniques (remote and *in situ*) that measure the vertical distribution of ozone in the atmosphere. Although progress has been made, a good deal of work remains before a clear picture can emerge, especially in the region near the tropopause, which is so important in determining the impact of ozone changes on climate.

Last, the development of the Antarctic ozone hole in 1992 and 1993 is described in Section 1.5, together with some new analyses of some old measurements.

1.2 TOTAL OZONE

1.2.1 Total Ozone Data Quality

Total column ozone has been measured using Dobson instruments since the 1920s. The number of monitoring stations has increased through the years, and since the 1960s a large enough network has existed to monitor ozone over most of the world with particularly good coverage in the northern midlatitudes and in Antarctica. Truly global monitoring has been possible only since the introduction of satellite-based instruments. The 1988 IOTP (WMO, 1990a) examined the quality of ozone measurements from both ground-based systems (Dobson, M83, M124) and satellite systems. They reported great variability in the quality of the data from ground-based instruments and found large calibration drifts in the SBUV and TOMS instruments caused by imperfectly corrected degradation of the on-board diffuser plates. When the 1991 assessment of ozone trends was made (WMO, 1992a), improvements in the quality of ozone data were noted. The re-evaluation of historical Dobson data records initiated by Bojkov *et al.* (1990) had been carried out at a small number of stations. Similarly, the quality of the satellite data had improved, though unresolved problems were still apparent. The entire TOMS ozone data record had been reprocessed using the version 6 algorithm, which improved the instrument calibration through the requirement that ozone amounts measured by different wavelength pairs maintain relative stability (Herman *et al.*, 1991). Comparison with the World Standard Dobson instrument number 83

(I83) at Mauna Loa indicated that good, long-term precision had been achieved (McPeters and Komhyr, 1991).

1.2.1.1 Ground-Based Observations

Since January 1992, all ground-based measurements have been reported using the Bass and Paur (1985) ozone cross sections. This change should increase the accuracy of the ozone record for direct comparison with other measurement systems, but should have no effect on the core time series of observations made with the AD wavelength pairs since the conversion from the old Vigroux (1953) scale is defined (Komhyr *et al.*, 1993). Since the last assessment the number of Dobson stations at which the historical records have been reanalyzed by the responsible personnel has increased to over 25, with many more in the process of reanalysis.

In a full re-evaluation, the station log books and lamp calibration records are carefully examined and corrections are made where appropriate (WMO, 1992b). Measurements are treated on an individual basis, in contrast to the "provisionally revised" data described and used in IOTP and subsequent assessments where monthly averages are treated. Comparisons with external data sets (total ozone records in the same synoptic region, meteorological data and, since 1978, satellite overpass data) are made to identify periods where special attention should be paid. The data are only corrected if a cause is found based on the station records. The goal of re-evaluation is to produce a high quality, long-term total ozone record. Increasingly frequent international intercomparisons of ground-based instruments bring more consistency to the global network. Recent intercomparisons were made at Arosa (Switzerland) in 1990, at Hradec Kralove (Czech Republic) in 1993, and at Izaña (Canary Islands) in 1994. In addition, the practice of using traveling standard lamps to check the calibration of individual instruments has become more frequent in recent years, with a consequent reduction in the observed scatter (Grass and Komhyr, 1989; WMO, 1994a).

Several important concerns about the quality of the ground-based data remain – in particular, how reliable are trends determined from Dobson data in the 1960-1980 period? While the program to reanalyze Dobson records is important, there are limits to what can be achieved. Not only is sufficient information not available in many cases, particularly in the early years, but, even in recent TOMS overpass comparisons, apparent calibration shifts are identified for which no cause has been found. Another issue of concern is whether uniform data quality can be maintained when a Dobson instrument is replaced by a Brewer. Brewer instruments replaced Dobsons at 4 Canadian sites (Churchill, Edmonton, Goose Bay, and Resolute) in the mid-1980s. During the changeover at each site, both instruments were operated for a period of at least 3 years in order to quantify possible biases and differences in seasonal response. In order to ensure continuity, a simulated Dobson AD direct sun measurement is reported for these sites (Kerr *et al.*, 1988). The data records for these sites must be monitored for possible biases and differences in seasonal response that might affect trend analyses.

In Section 1.2.2, trend analyses of the measurements from 43 stations are reported. The records from many more were examined for possible inclusion, but were not used for a variety of reasons. First, only records starting before 1980 were considered sufficiently long for meaningful analyses to be made. Second, a minimum of 12 days of observation were required for a monthly mean to be included. In the case of three high latitude stations, all midwinter monthly means were missing, a situation that cannot be handled by the current, well-documented statistical technique, at least as far as computation of seasonal average trends is concerned. For this assessment, no analysis of data from such stations is made. Third, some station records show large variations against nearby stations or satellite overpasses that cannot be explained in terms of any natural phenomena. These records are few and were not used. A number of points requiring corrections have been identified in the measurements submitted to the World Ozone Data Center. The re-evaluations used in the records used here for trend analysis will be documented in WMO Report No. 35 (appendix by Bojkov). About half of these corrections result from the WMO intercomparison program and individual instrument's calibration procedures, and most of the remainder are made from information made available from the instrument log books by the operating agency (Bojkov, private communication). A few obvious calibration shifts for which no instrumentally derived correction can be found are treated in the statistical analysis (see Section 1.2.2). An empirical technique has been used to correct the air mass dependencies at a few stations, as insufficient instrumental information

exists in these cases (see appendix by Bojkov in WMO, 1994b).

The chief instrument used in the former USSR was a filter ozonometer. Various improvements have been made over the years, and the record of the M-83 and M-124 versions since 1973 has been assessed by Bojkov *et al.* (1994) using recently available information on the individual instruments' performance and calibration histories. The errors associated with these instruments are larger than those of Dobson or Brewer instruments, and Bojkov *et al.* combine the individual station data into regional averages.

Sulfur dioxide (SO_2) absorbs ultraviolet at the wavelengths used by Dobson and Brewer instruments to measure total ozone. The presence of SO_2 causes a false increase of total ozone measured by Dobson instruments for both the AD and CD wavelengths. As part of a detailed revision of the total ozone record at Uccle, Belgium, De Muer and De Backer (1992) considered the effect of the locally measured reduction in surface SO_2 on the total ozone record from 1972 to 1991. Over this period, surface SO_2 levels dropped by a factor of about 5. The size of the downward correction to the observed total ozone was found to be 3-4% in 1972 and just under 1% in 1990, a change of similar size to the trend calculated in IOTP (WMO, 1990a). The trends calculated using the revised data for 1978-1991 are in reasonable agreement with TOMS version 6 overpass measurements (WMO, 1992).

This analysis clearly raises the question as to how many records might be similarly affected (De Muer and De Backer, 1993). Most North American stations are in unpolluted areas and measurements made there will not have been influenced by tropospheric SO_2. In Canada, surface SO_2 measurements made since 1974 are reported by Environment Canada in the National Air Pollution Surveillance Series for sites in Toronto, the worst affected station in Canada. In 1974 the average surface SO_2 concentration in Toronto was 42 $\mu g\ m^{-3}$, about 40% that measured near Uccle in the same year. A review of these data indicates that about 1% (3-4 Dobson units, DU) false total ozone may have occurred at Toronto in the early part of the record. This dropped to 0.3% (1.2 DU false ozone) in the early to mid-1980s and has remained level since then, in good agreement with Kerr *et al.* (1985, 1988). There is greater uncertainty in the earlier data made by wet chemical instruments (which may be sensitive to other pollutants besides SO_2) than there is in the later data made by pulse fluorescence techniques. Similar measurements made at Edmonton indicate that interference due to SO_2 is less than 0.2% throughout the record (in good agreement with Kerr *et al.*, 1989). The effects of SO_2 on the three other non-urban sites in Canada are thought to be negligible. In the United States, anthropogenic emissions of SO_2 decreased by 27-29% from 1970 to 1988 (Placet, 1991). None of the U.S. stations is in as heavily populated a region as Uccle and so should not have been as affected.

A model study of SO_2 concentrations in Europe, based on emission estimates, indicated that the largest changes in SO_2 concentrations since 1970 have occurred over Belgium, Holland, and Northern France, and that in 1960 the SO_2 concentrations calculated for Belgium were among the highest in Europe (Mylona, 1993). Decreases by a factor of 50-75% were calculated for this region, while elsewhere in Europe and Scandinavia the reductions since 1970 seem to have been 50% at most and are often less. Thus while some Dobson measurements in Europe were affected by the decreasing SO_2 concentrations, it is likely that Uccle is one of the most heavily influenced.

Elsewhere, stations are in polluted regions where the SO_2 trends are different from those in Europe and parts of North America. Work still needs to be done to assess the impact of SO_2 on O_3 measurements at many individual stations.

In June of 1991 the eruption of Mt. Pinatubo resulted in the injection of large amounts of material into the stratosphere. The plume included large amounts of SO_2, but this had decreased to low levels by the end of July (Bluth *et al.*, 1992). Of greater concern is the high level of stratospheric aerosol that spread over the globe and produced large aerosol optical depths for more than a year. But Komhyr (private communication) notes that the data record from the World Standard Dobson instrument I-83 shows little apparent disturbance when the initial, dense aerosol cloud passed over Mauna Loa Observatory in early July. The initial error appeared to be only a tenth of a percent or so. A small change (<1%) in the calibration of I-83 was seen in June 1992. In June 1993, when the stratosphere over Mauna Loa was much cleaner, the calibration of I-83 was the same as in 1991. Thus ozone measurement errors due to Mt. Pinatubo aerosols most likely did not exceed ±1%, for direct sun

observations made by a well-maintained Dobson instrument using the fundamental AD wavelength pairs. This result should be expected, as the wavelength pairs were originally chosen to minimize the effect of aerosol on the measurement (Dobson, 1957).

1.2.1.2 Satellite-Based Observations

Total ozone data are now available from a number of satellite systems. The Nimbus 7 TOMS produced global ozone maps (except in polar night) on nearly every day from November 1978 until May 6, 1993, when the instrument failed. Another TOMS instrument was launched on the Russian Meteor 3 spacecraft in August of 1991 and continues to operate, so a continuous TOMS data record has been maintained, although, because of its drifting orbit, the geographic coverage of the Meteor 3 TOMS is not as extensive as that of Nimbus 7 TOMS.

TOMS has been used as the "most reliable" satellite-based monitor of total ozone because it gives daily global coverage and has a 14.5-year record of observations. The version 6 TOMS data were produced using a calibration based on data up through May 1990, and there is concern that its calibration may have drifted since then. This issue will be addressed through comparisons with other instruments. There is a known error at large solar zenith angles (>70°) demonstrated by comparison with Système d'Analyse par Observation Zénithale (SAOZ) spectrometers (Pommereau and Goutail, 1988), which make zenith sky measurements of ozone at sunset and sunrise and thus avoid the concerns about airmass or temperature dependencies that arise with the shorter wavelengths used in the Dobson, Brewer, TOMS, and SBUV instruments. This error in TOMS is caused by a dependence on the shape of the ozone profile when the ultraviolet light, used to measure the ozone, no longer penetrates well to the ground. For the Nimbus 7 TOMS, this problem is only important at high latitudes in the winter hemisphere. Wellemeyer *et al.* (1993) estimate that the 60° latitude winter trend will be in error by less than 1-2% per decade; errors at lower latitudes should be insignificant.

The sensitivity of TOMS to volcanic aerosol has been analyzed in detail (Bhartia *et al.*, 1993). There are systematic errors depending on scan angle, but on a zonal mean basis the errors largely cancel. Aerosol-related effects on the TOMS observation were only observed in the tropics for a few months, so there should not be a significant effect on trends.

Data from Meteor 3 TOMS have been available since its launch in August 1991, but the consistency of the data from the two TOMS instruments (Nimbus 7 TOMS and Meteor 3 TOMS) has not been properly assessed yet. The comparison is complicated by the orbit of Meteor 3, which drifts from near-noon observations to near-terminator observations every 53 days. Periodically, all data from Meteor 3 TOMS are collected at very large solar zenith angles, so that the problems connected with high latitude measurements occur at all latitudes. In the light of these problems and the lack of a more detailed assessment of the data quality, no use is made of the Meteor 3 TOMS measurements for the trends presented in this assessment.

The SBUV instruments also measure total ozone, viewing directly below the orbital track of the spacecraft. The SBUV instrument on Nimbus 7 operated from November 1978 to June 1990. While SBUV and TOMS were separate instruments, they shared the diffuser plate measuring the extraterrestrial solar flux and so did not have completely independent calibrations. The same basic algorithm is used to calculate both the TOMS and the SBUV total ozone measurements. Data are also available from the NOAA-11 SBUV/2 beginning in January 1989 through May 1994. The SBUV/2, which has suffered much less degradation than SBUV, maintains calibration using on-board calibration lamps and comparison with periodic flights of the Shuttle SBUV instrument (Hilsenrath *et al.*, 1994), and so its data record is truly independent of the other systems. There is a concern that, as the NOAA-11 orbit has drifted from an initial 1:30 PM equator crossing time to a 4:30 PM equator crossing time in 1994, zenith angle dependent errors could be aliased into the ozone trend from SBUV/2.

The TOVS (TIROS Operational Vertical Sounder) instruments (flown on a number of platforms) monitor total ozone using the 9.6 μm channel, which makes them most sensitive to ozone near the ozone maximum. This fact and the unresolved problem of possible calibration differences between the series of TOVS instruments limit the current usefulness of TOVS for trend analysis.

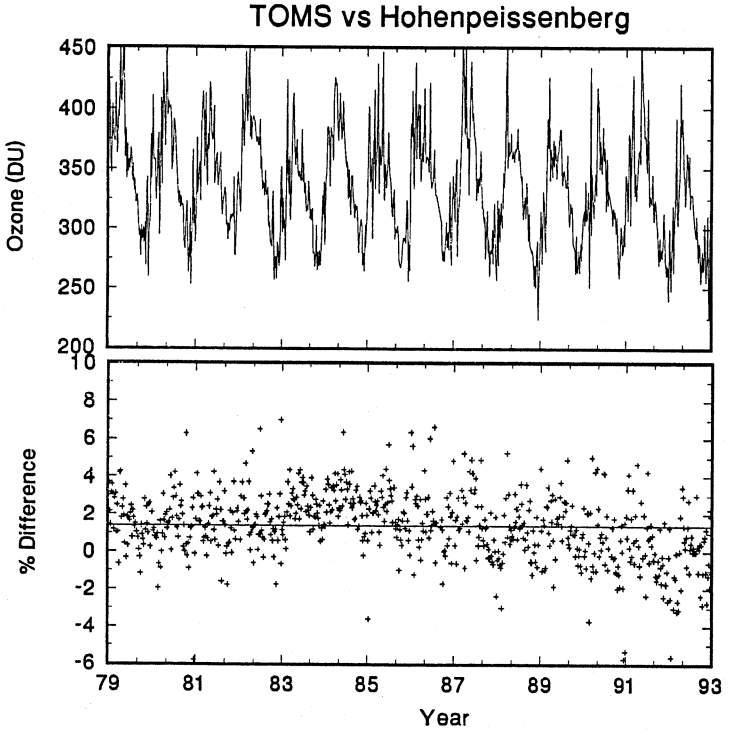

Figure 1-1. Time series of weekly average TOMS ozone overpasses at Hohenpeissenberg (top) and of the percent difference between TOMS and Hohenpeissenberg total ozone amounts (bottom). (The Hohenpeissenberg data were taken from the World Ozone Data Center in December 1993; some minor revisions have since been made.)

1.2.1.3 Data Quality Evaluation

The large natural variations in ozone complicate the evaluation of the quality of total ozone measurements. The comparison of simultaneous measurements of the same quantity by independent instruments is an effective means of checking the quality of the individual instruments. For the early Dobson record there are no independent, simultaneous measurements of total ozone except during rare intercomparisons. (An exception occurred at Arosa, where two instruments have been operated simultaneously since 1968). The quality of the early record thus depends on how well the individual instruments and their calibrations were maintained. Evaluations of the early Dobson records are based on comparisons with data from other stations in the same synoptic region, with meteorological data such as the 100 hPa temperature series, and critical examination of available log books. Such methods were discussed at length in the IOTP (WMO, 1990a) and have been described further in WMO Report No. 29 (1992b). Details of the calibration histories at individual stations will be published in WMO Report No. 35 (1994b).

Since the launch of TOMS in 1978, a total ozone measurement has been made almost daily from space within 1° of every Dobson station. Figure 1-1 shows an example of a TOMS-Dobson comparison for Hohenpeissenberg, Germany. Similar comparisons have been made for each of 142 ground-based stations (Dobson, Brewer, and M-124) with relatively complete records over the life of TOMS (Ozone Data for the World, 1993). A single such comparison shows the relative differences between the two measurement systems; examination of many such plots can reveal the cause for differences between the systems. Changes relative to TOMS that occur at one station but not at other nearby stations can be presumed to be caused by that one station, but a change that is seen at most stations can be presumed to be caused by TOMS. Two simple indicators of data

quality that can be derived from these plots are the average bias and drift relative to TOMS. Figure 1-2 shows the first-year bias and trend relative to TOMS of 18 Dobson stations, including I83 in its measurements at Mauna Loa each summer. The average offset of TOMS relative to Dobson of 3-4% is almost certainly due to small prelaunch calibration errors in TOMS. The scatter in this diagram is noticeably less now that revised total ozone records are used, indicating an improvement in the quality of these measurements. The average drift of TOMS relative to the Dobson network of about -2% per decade is discussed below.

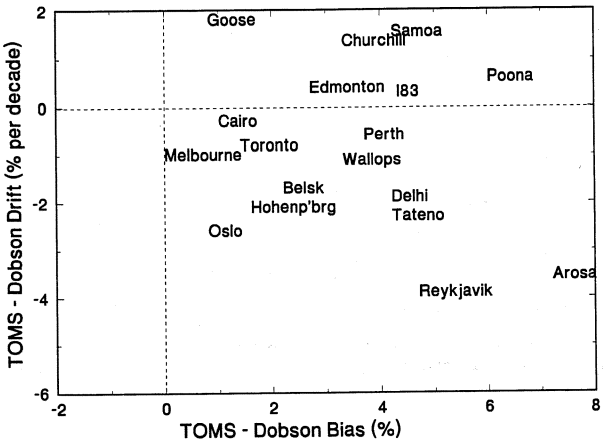

Figure 1-2. The average bias relative to TOMS in the first year (usually 1979) and the drift relative to TOMS over 14 years for a sample of 18 Dobson stations. The Dobson station data were taken from the World Ozone Data Center in December 1993. I83 at Mauna Loa and the regular Mauna Loa record are shown separately.

Despite the variability of individual Dobson stations, random errors should largely cancel in a network of Dobson stations, so that conclusions can be made about the performance of TOMS. Figure 1-3 shows comparisons of TOMS with ground-based measurements, including I83 both at Mauna Loa and at Boulder, a network of 30 Northern Hemisphere (25-60°N) Dobson stations that have complete data records through May 6, 1993, and summer-only averages for the same stations. TOMS is stable relative to I83 over its life. The error bars shown for the I83 comparisons are statistical uncertainties (95% confidence limits) for each summer's

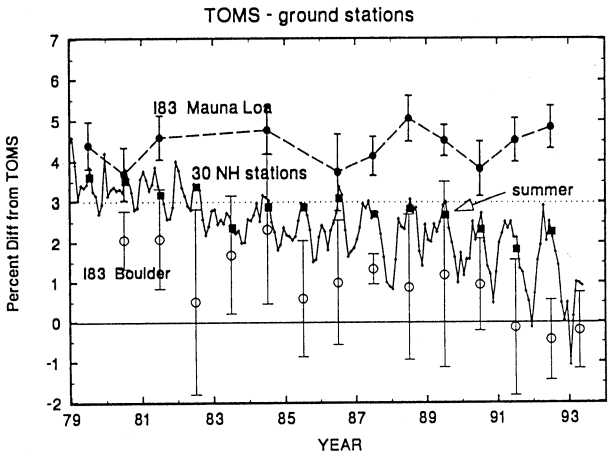

Figure 1-3. Percent difference between TOMS and World Standard Dobson #83, at both Mauna Loa (solid circles) and at Boulder (empty circles); monthly average differences for an average of 30 Northern Hemisphere Dobson stations; and summer only (JJA) differences for the same stations (squares). The uncertainties shown are 95% confidence limits for the mean value.

set of match-ups; the ±0.5% or so year-to-year variation represents the limit of accuracy for a single site comparison, since many errors are systematic and not random as the statistical error calculation assumes. A preliminary comparison of I83 observations made in Boulder, where fewer measurements were made with I83, shows a drift relative to TOMS that is very similar to that seen in the 30-stations average, which implies a TOMS latitude (or zenith angle) dependent drift. The comparison with the ensemble of 30 Northern Hemisphere Dobson stations was made using monthly averages. There is a seasonal cycle in the TOMS-Dobson difference of about 1% amplitude in 1985 and increasing thereafter.

An initial decline of TOMS ozone relative to Dobson (or increase in Dobson ozone relative to TOMS) between 1979 and 1984 is followed by a period of apparent lesser drift between 1984 and 1990 and, after 1990, a significant decline of about $2^1/2$%. Evidence of this decline beginning in about 1989 can also be seen in Figure 1-1, the comparison with Hohenpeissenberg. The initial decline of TOMS relative to Dobson could be caused by an error in TOMS not resolved by the internal calibration method or, possibly, it could be partly due to a change in the average calibration of the Dobson network in the

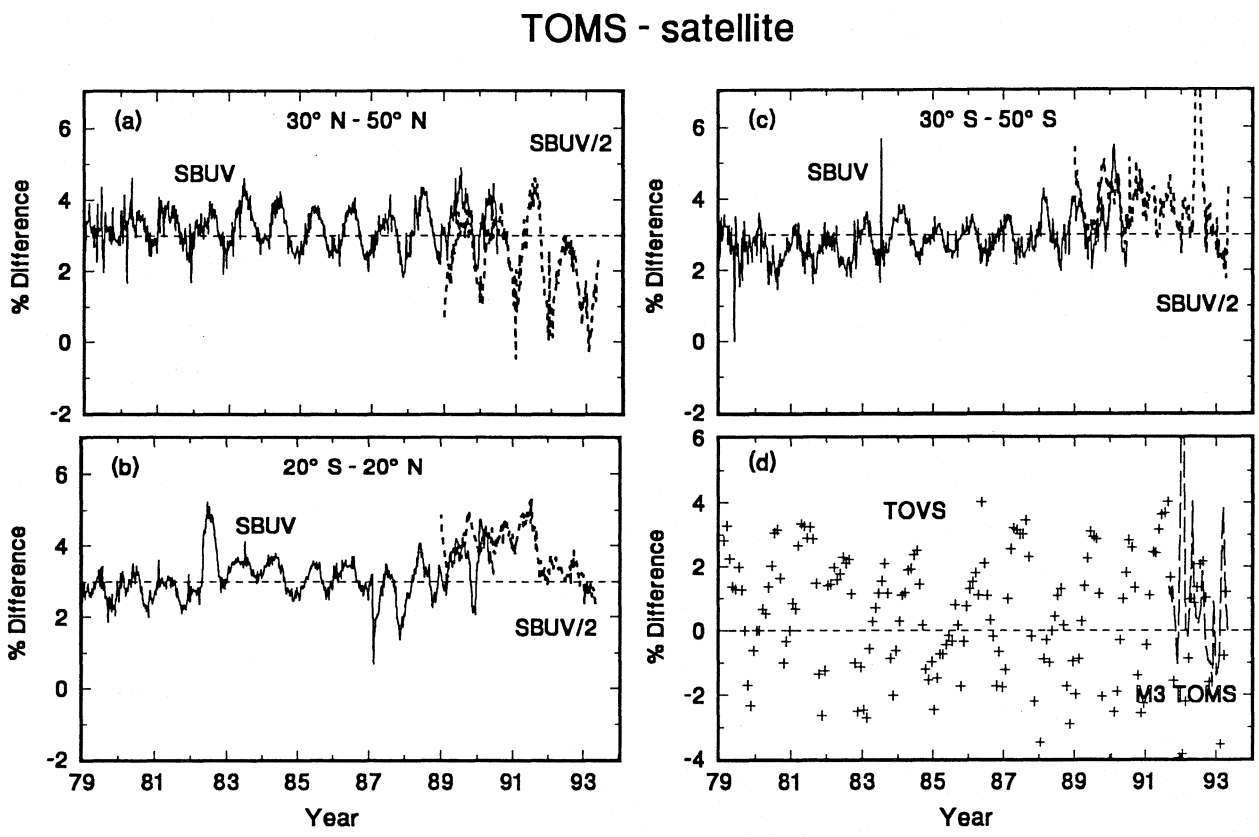

Figure 1-4. Weekly average differences between TOMS and SBUV, NOAA-11 SBUV/2, and Meteor 3 TOMS, and monthly average differences between TOMS and TOVS.

early 1980s before the strong program of intercomparison was extended. Figure 1-3 shows that such a decline is common to the Dobson records for most stations. Possible solar zenith angle dependent errors (in either Dobson or TOMS) can be minimized by comparing summer average values (where summer is defined as June-July-August). There is a similar time dependence, though of lesser magnitude (1-1.5%). Most of the seasonal cycle must then be due to TOMS. The decline of TOMS relative to I83 at Boulder, coupled with the stability relative to I83 at Mauna Loa, indicates a TOMS error that depends on the signal level, because UV signal levels are generally lower at Boulder (more ozone) than at Hilo. It is most likely that the TOMS photomultiplier has developed a small nonlinearity in its response that has increased with time. If true, the equatorial and summer midlatitude trends from TOMS should be accurate, but the high and winter midlatitude trends could be too large by 1-2% per decade.

Comparisons with TOMS have been done with an average of 9 Brewer stations (not shown). The data record is simply not long enough for definitive comparisons, but the seasonal dependence is larger, probably because the Brewers tend to be at high latitude sites. There is a decline between 1990 and 1992 that is consistent with the Dobson results.

Figure 1-4 is a comparison of Nimbus 7 TOMS with other satellite instruments: Nimbus-7 SBUV, NOAA-11 SBUV/2, TOVS, and Meteor 3 TOMS. Comparisons have been done of weekly zonal mean ozone, except for TOVS, where monthly means are used. The comparisons for the 30°-50°N, 30°-50°S, and 20°S-20°N zones are shown. Although 3% higher than SBUV, TOMS is quite stable relative to SBUV, not surprising since both were recalibrated using similar techniques and the two instruments use the same diffuser plate, albeit with different viewing geometries. There is a seasonal variation of about 1% magnitude that again is

likely caused by nonlinearity in the TOMS photomultiplier. There is no evidence for nonlinearity in the SBUV photomultiplier. The NOAA-11 SBUV/2 calibration is completely independent and is maintained through use of on-board calibration lamps. There is a decline of TOMS relative to SBUV/2 of 1% or so between 1989 and 1993. A comparison of SBUV/2 with an ensemble of ground-based stations between 20° and 60°N indicates that there has been little drift and that there is an apparent seasonal cycle of about 1-2% (minimum to maximum).

Finally, comparisons with monthly average TOVS zonal means for 30°-50°N are shown (Figure 1-4). The TOVS data show significant variance, presumably resulting from the sensitivity to stratospheric temperatures, and cannot currently be used for trend analysis.

1.2.2 Trends in Total Ozone

Trends in total ozone were reported in the last assessment (WMO, 1992a; see also Stolarski *et al.*, 1992), using TOMS satellite data from November 1978 through March 1991, and ground-based data through March 1991 where available. A number of recent studies have examined the available records, either on large scales (Krzyścin, 1992, 1994a; Reinsel *et al.*, 1994a) or at individual stations (Degórska *et al.*, 1992; Henriksen *et al.*, 1992, 1993; Kundu and Jain, 1993; Lehmann, 1994). In addition, a number of studies investigated the effects of interannual variability, and its various causes, on total ozone trends (Hood and McCormack, 1992; Shiotani, 1992; Marko and Fissel, 1993; Krzyścin, 1994b, c; Randel and Cobb, 1994; Zerefos *et al.*, 1992, 1994). In general, the conclusions of these studies agree well with those presented in WMO (1992a) and here. One exception is the analysis by Henriksen *et al.* (1992, 1993) of the total ozone record from Tromsø (70°N). Measurements have been made there using a Dobson spectrophotometer that show no long-term change from 1939 to 1989. Two difficulties arise in the interpretation of this record. First, there is a gap between 1969 and 1984 during which the instrument was overhauled. Unfortunately the amount of adjustment caused by this overhaul cannot be given (Henriksen *et al.*, 1992). Second, the natural variability of ozone is such that there are geographic differences in the trends (WMO, 1992a), so that one would expect the trends measured at some individual stations to be zero.

For this assessment, trends have been updated through the most recent available data. The trend update is complicated by the failure of the Nimbus 7 TOMS instrument on May 6, 1993, and concerns about the correction of its calibration after 1990 (see Section 1.2.1.3). However, SBUV data have been re-evaluated since the 1991 assessment, and are now suitable for trend analysis when combined with the SBUV/2 data from the NOAA-11 satellite. In the following section, trend analyses of SBUV data extended with SBUV/2 after 1988, abbreviated SBUV(/2), are updated through May 1994.

Trends from the Dobson network are updated through February 1994 at the majority of stations, and several new stations have been added. In addition, since the 1991 assessment, a number of Dobson stations have revised data for part or all of their historical records based on detailed re-evaluations. These data have been used if submitted to the World Ozone Data Center or directly to the chapter authors. In addition, at some stations, revisions were made by R. Bojkov (private communication) from the WMO intercomparison program results or from information in the station log books (see Section 1.2.1.1). Furthermore, data from 45 filter ozonometer stations in the former USSR have been thoroughly assessed and revised by Bojkov *et al.* (1994). Regional average data for the four regions discussed in that paper have been obtained from the authors and trends calculated using the same statistical fit as for the Dobson stations; the trends calculated for this report are close to those tabulated by the authors.

As discussed in detail in Section 1.4, ozone levels declined a few months after the eruption of Mt. Pinatubo in June 1991, and at northern midlatitudes they remained abnormally low through the fall of 1993 (Gleason *et al.*, 1993; Herman and Larko, 1994; Bojkov *et al.*, 1993; Kerr *et al.*, 1993; Komhyr *et al.*, 1994a). Whatever the cause of these low values, the calculation of trends with abnormally low data at the end of the time period may lead to substantially more negative values for the calculated trend. This presents difficulties in interpretation of the results, since the use of the word "trend" implies a generally consistent, continuing change over a given period. By the inclusion of very recent data in late 1993 and the first half of 1994, this effect is lessened, except in the Jun-Jul-Aug season where the very low 1993 data are at the end of the series. Section 1.2.2.3 compares SBUV(/2) trends through May 1991 versus trends

through May 1994 as an analysis of the effect of including this period of anomalous ozone.

1.2.2.1 Statistical Models for Trends

As discussed in previous reports (WMO 1990a; WMO 1990b; WMO 1992a), proper trend analysis of ozone series uses a statistical regression model that fits terms for seasonal variation in mean ozone, seasonal variation in ozone trends, and the effects of other identifiable variables such as the 11-year solar cycle, quasi-biennial oscillation (QBO), and atmospheric nuclear tests (if data from the early 1960s are used). The residuals from the model are autocorrelated, and this autocorrelation should be fitted as part of the statistical estimation procedure to ensure reliable standard errors for the calculated trends (see, for example, Reinsel *et al.*, 1987; 1994a; Bojkov *et al.*, 1990). Also, proper error analysis requires a weighted regression technique, since ozone levels are much more variable in winter months than in summer. For the long-term Dobson analyses, the trend fitted for each month was a "hockey stick," with a level baseline prior to December 1969 and a linear trend after 1970. For series beginning after 1970, including all satellite data, the trend is a simple linear monthly trend. As in previous reports, the other explanatory variables used are: 10.7cm radio flux for the effect of the solar cycle; and 50 mbar winds in the tropics (average of Ascension, Balboa, and Singapore) for the QBO with an appropriate latitude-dependent lag. For a given monthly ozone series, individual monthly means in Dobson units (DU) are calculated from the model for the beginning of the time period, and monthly trends are calculated in DU/year. For compactness in presentation, these are averaged over four seasons, DJF, MAM, JJA, SON (December-January-February, etc.), together with a summary year-round trend. The trends are expressed in % per decade, with the average DU/decade trends given as a percent of the seasonal mean ozone in DU. Note that the seasonal definitions are slightly different from those used in previous assessments (DJFM, MJJA, SON, with April not reported).

Mean level shifts ("intervention terms") can be used in the statistical model to account for instrument calibrations or changes, and other sudden shifts in observed mean ozone, for which the calibration information necessary for direct adjustment is not available. Reinsel *et al.* (1994a) describe the methodology and give the dates at each station where intervention terms are necessary if the publicly available data from the World Ozone Data Center are used. In most cases in this report, direct adjustment using known calibration information was used, except in the sensitivity analysis presented in Section 1.2.2. An additional intervention term not used in Reinsel *et al.* was calculated in the analysis here for Mauna Loa at June 1976 to adjust for an unexplained but clear drop in mean ozone of several percent.

It is necessary to ensure correct intercalibration between the SBUV and SBUV/2 satellite records, and the following procedure was used to estimate a possible shift between records for each latitude zone. The standard statistical model was fit to the combined records beginning 1/79, and ending in 5/91 to avoid the anomalous ozone period after that time. There is an overlap of eighteen months in the SBUV and SBUV/2 satellite records (1/89 to 6/90), and each series was given one-half weight in the overlap period. Intervention terms were fit to estimate any difference in calibration between the satellites, and these were typically found to be less than 1% (in two zones, $1\frac{1}{2}$%). These same shifts were used to adjust SBUV/2 data to the level of SBUV for analyses through 1994, the fit then being done giving each series one-half weight in the overlap period, but without further intervention terms.

1.2.2.2 Total Ozone Trends Updated through 1994

This section presents a comparison of trends from ground-based data through February 1994 and SBUV(/2) satellite data through May 1994. The analysis of ground-based data gives both long-term (using data from 1/64) and short-term (1/79 to 2/94) trends for direct comparison to SBUV(/2) results. As noted in the 1991 assessment, the short-term, more recent trends are more negative than the long-term trends; an analysis of this apparent trend acceleration is presented in Section 1.2.2.4.

The ground-based trend analysis uses a set of 43 Dobson stations, the majority of which are in Northern Hemisphere mid- to high latitudes. The station set is a subset (see Section 1.2.1.1) of the 56 stations used in Reinsel *et al.* (1994a), together with the addition of Lisbon, now with revised data. The trends at individual stations are tabulated only in one case (Table 1-1); otherwise the individual station trends have been averaged

Table 1-1. Set of 43 Dobson stations used for the trend analyses, with dates of usable data (although the earliest analysis in this report begins at 1/64). Stations are grouped by the latitude zones used in Figures 1-5 through 1-9. Seasonal trend estimates by station are shown for the period 1/79 through 2/94; these are plotted in Figure 1-5 (zonal averages in Figure 1-6). The columns labeled "2se" give 95% uncertainty limits (two standard errors). The "Src" column indicates the source of the data used here, with codes: WODC = data from World Ozone Data Center, Sta = data supplied by the station authorities, Rev = revised as discussed in Section 1.2.1.1.

				Dec-Feb		Mar-May		Jun-Aug		Sep-Nov		Year		
Station	Latitude	First	Last	est	2se	est	2se	est	2se	est	2se	est	2se	Src
St. Petersburg	60.0 N	68-08	94-02	-7.4	5.5	-7.4	4.2	-4.7	2.7	-3.8	3.1	-6.0	2.3	Sta
Churchill	58.8 N	65-01	93-10	-5.7	4.2	-6.9	3.4	-4.5	2.3	-2.4	3.2	-5.0	1.8	Sta
Edmonton	53.6 N	58-03	94-02	-5.6	4.7	-7.6	3.3	-5.5	2.2	-3.4	3.2	-5.6	1.9	Sta
Goose	53.3 N	62-01	94-02	-2.8	5.4	-5.7	4.4	-7.6	3.0	-3.4	2.8	-4.9	2.4	Sta
Belsk	51.8 N	63-04	93-12	-9.1	5.4	-6.7	4.0	-4.0	2.4	-1.4	3.2	-5.5	2.3	Rev
Uccle	50.8 N	71-07	94-02	-5.9	5.4	-7.4	3.8	-1.3	2.4	-0.3	3.4	-4.0	2.2	WODC
Hradec Kralove	50.2 N	62-03	94-02	-7.3	5.3	-6.4	3.8	-4.4	2.4	-0.8	2.9	-4.9	2.2	WODC
Hohenpeissenberg	47.8 N	68-05	94-02	-8.4	4.7	-6.1	4.6	-3.6	2.6	-2.0	3.1	-5.2	2.4	Sta
Caribou	46.9 N	62-09	94-02	-5.3	4.4	-6.5	2.7	-2.6	2.2	-3.1	3.3	-4.5	1.8	Sta
Arosa	46.8 N	57-07	94-02	-5.9	4.7	-4.5	3.8	-2.2	2.0	-1.1	2.6	-3.6	2.1	Sta
Bismarck	46.8 N	62-12	94-02	-1.9	3.5	-6.8	2.9	-2.1	2.3	-1.8	2.1	-3.3	1.5	Sta
Sestola	44.2 N	76-11	94-02	-5.4	4.7	-6.8	4.0	-4.3	2.2	-0.9	3.0	-4.6	2.0	Rev
Toronto	43.8 N	60-01	94-02	-4.5	3.7	-5.9	2.8	-2.7	1.8	-0.5	3.1	-3.6	1.6	Sta
Sapporo	43.1 N	58-02	94-02	-6.8	3.7	-5.6	3.1	-4.0	2.6	-2.2	2.6	-4.8	1.8	WODC
Vigna Di Valle	42.1 N	57-07	94-02	-8.0	4.3	-5.5	5.1	-3.8	2.4	-4.8	2.7	-5.6	2.4	Rev
Boulder	40.0 N	76-09	94-02	-2.5	3.2	-7.5	3.2	-1.7	1.6	-1.7	2.6	-3.6	1.6	Sta
Shiangher	39.8 N	79-01	93-08	-5.1	3.2	-3.8	3.6	-0.4	2.7	-1.0	2.8	-2.7	1.8	WODC
Lisbon	38.8 N	67-08	94-02	-1.3	3.4	-6.7	2.8	-4.1	1.7	-1.5	2.7	-3.6	1.4	Sta
Wallops Island	37.9 N	57-07	94-02	-6.5	3.5	-5.4	3.5	-4.4	2.2	-3.0	3.3	-4.9	1.9	Sta
Nashville	36.3 N	62-08	94-02	-5.0	3.3	-4.4	3.9	-2.9	2.6	-1.3	3.1	-3.5	1.9	Sta
Tateno	36.1 N	57-07	94-02	-3.6	3.7	-1.2	3.3	-0.8	2.2	0.5	2.3	-1.3	1.7	Sta
Kagoshima	31.6 N	63-02	94-02	-2.6	3.1	-1.8	3.1	-0.6	1.9	0.3	2.0	-1.2	1.6	Sta
Quetta	30.2 N	69-08	93-02	-5.3	4.3	-1.6	4.2	0.7	2.7	-0.2	2.5	-1.6	2.5	Rev
Cairo	30.1 N	74-11	94-02	-1.7	4.0	-3.1	3.0	-0.2	1.6	-0.9	1.6	-1.5	1.7	Sta
New Delhi	28.7 N	75-01	94-02	-2.2	3.3	-2.0	3.2	0.3	2.9	-0.4	1.5	-1.1	1.9	WODC
Naha	26.2 N	74-04	94-02	-2.3	3.0	-2.0	2.9	-0.3	1.7	-1.0	2.0	-1.4	1.5	WODC
Varanasi	25.3 N	75-01	94-02	-2.2	2.4	-1.4	2.5	-0.2	2.5	-1.2	1.9	-1.2	1.5	Rev
Kunming	25.0 N	80-01	94-02	-0.5	2.6	-1.8	3.5	0.2	1.8	-1.2	1.7	-0.8	1.6	Rev
Ahmedabad	23.0 N	59-01	92-12	-1.1	2.7	-1.6	3.4	-4.3	1.7	1.2	2.5	-1.5	1.7	Rev
Mauna Loa	19.5 N	64-01	94-02	-0.6	3.4	0.2	3.1	-0.1	2.3	-0.4	1.9	-0.2	1.8	Sta
Kodaikanal	10.2 N	76-08	94-02	1.1	2.6	0.2	2.6	-0.8	2.8	-1.0	2.9	-0.2	2.1	WODC
Singapore	1.3 N	79-02	93-10	1.0	3.1	-0.4	4.0	-1.1	3.0	-1.1	3.3	-0.4	2.9	Rev
Mahe	4.7 S	75-11	93-10	-0.7	1.8	-1.0	2.4	-2.0	2.5	-1.7	2.3	-1.4	1.6	Rev
Natal	5.8 S	78-12	94-02	-0.3	2.5	1.6	2.0	-1.6	2.4	-1.1	2.4	-0.4	1.6	Rev
Huancayo	12.1 S	64-02	92-12	-0.7	1.7	-1.4	2.0	-3.4	2.8	-0.5	2.1	-1.5	1.5	Rev
Samoa	14.3 S	75-12	94-02	-1.6	1.9	-2.5	1.8	-1.3	3.1	-1.9	2.5	-1.8	1.7	Sta
Brisbane	27.4 S	57-07	93-07	-2.2	1.8	-2.1	1.7	-1.8	3.6	-1.9	2.4	-2.0	1.5	Rev
Perth	31.9 S	69-03	94-02	-0.4	1.4	-1.7	2.0	-1.4	3.4	-0.9	2.0	-1.1	1.3	Rev
Buenos Aires	34.6 S	65-10	94-02	-2.1	1.5	-1.4	2.4	-4.2	3.3	-2.0	3.4	-2.5	1.6	Sta
Aspendale	38.0 S	57-07	93-07	-2.9	1.6	-3.5	1.6	-3.2	2.8	-2.1	2.4	-2.9	1.2	Rev
Hobart	42.8 S	67-07	92-04	-4.4	2.1	-5.2	2.7	-5.2	3.4	-2.7	2.7	-4.3	1.6	Rev
Invercargill	46.4 S	70-07	94-02	-5.2	1.6	-2.0	2.1	-1.2	2.6	-3.2	2.6	-2.9	1.2	Rev
MacQuarie Island	54.5 S	63-03	93-06	-6.8	2.6	-3.4	3.0	-6.5	4.8	-6.0	3.2	-5.7	1.9	Rev

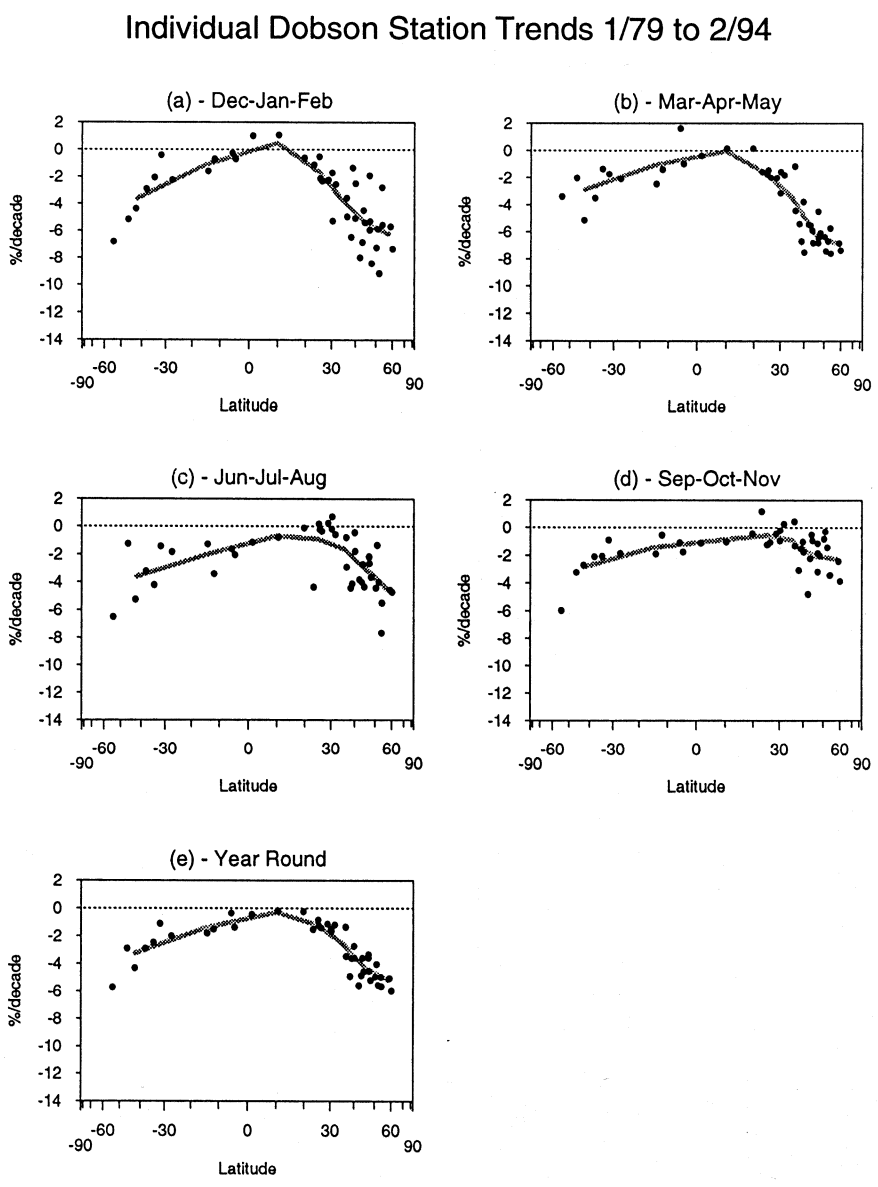

Figure 1-5. Individual Dobson station seasonal trends in total ozone in %/decade against latitude, over the period 1/79 through 2/94 (where data are available). The gray curves are the averages of the individual stations' trends in the following latitudinal zones: 55-30°S, 30°S-0, 0-20°N, 20-30°N, 30-40°N, 40-50°N, and 50-60°N. These averages (plus standard errors) are tabulated in Table 1-3.

within the following latitudinal zones: 55°S-30°S, 30°S-0, 0-20°N, 20-30°N, 30°N-40°N, 40°N-50°N, and 50°N-65°N. Figure 1-5 shows the individual station trends together with the zonal averages for the period 1/79 through 2/94. Although there is substantial scatter among individual stations, the latitudinal pattern is clearly represented by the zonal averages, which will be used in the following analyses for comparison to satellite trends. Seasonal trends from the reassessed filter ozonometer in four large regions of the former USSR are plotted as separate points in Figure 1-6; they are consistent with and support the Dobson data analysis.

SBUV(/2) trends through May 1994 are given by season and latitudinal zone in Table 1-2. Ground-based

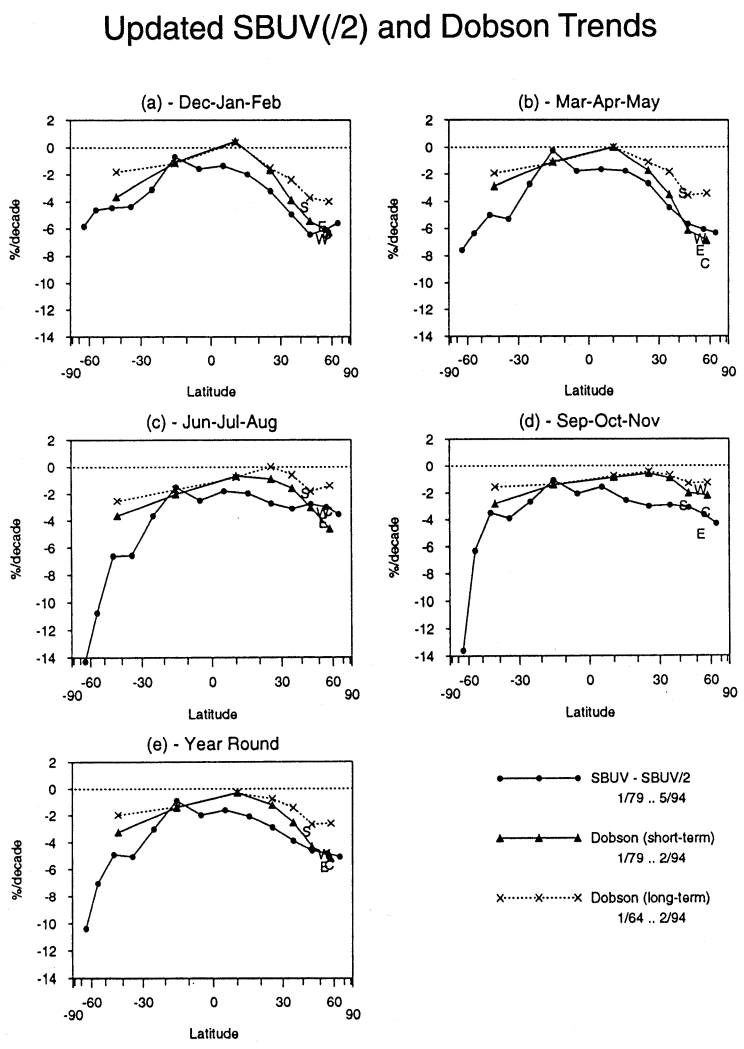

Figure 1-6. Updated SBUV(/2) and Dobson seasonal total ozone trends in percent per decade by latitude. Solid circles are SBUV(/2) trends in 10 degree zones over 1/79 to 5/94; solid triangles are short-term Dobson trends over 1/79 to 2/94; X's are long-term Dobson trends fitted using data over 1/64 to 2/94, with trend calculated over 1/70 to 2/94. The Dobson trends are averages within latitudinal zones of individual trends at 43 Dobson stations. The coverage of SBUV-2 is incomplete at high southern latitudes in southern winter, and the uncertainties associated with the high latitude southern winter trends probably underestimate the true uncertainty. Trends over 1/79 through 2/94 in regional average ozone from filter ozonometer data re-evaluated by Bojkov *et al.* (1994) are shown by the following symbols: W (West) = European region, S (South) = Central Asia, C (Central) = Western Siberia, E (East) = Far East and Eastern Siberia. The horizontal axis is scaled in terms of sin(latitude) so that equal spacings on the axis represent equal areas on the globe.

trends through February 1994 are given in Tables 1-3 (from January 1979) and 1-4 (from January 1964). The three sets of trends are plotted together for comparison in Figure 1-6.

The most obvious features of the total ozone trends have been commented upon in previous assessments and are confirmed in this updated analysis. Statistically significant negative trends are seen at mid- and high latitudes in both hemispheres in all seasons. The largest negative ozone trends at mid- and high latitudes in the Northern Hemisphere are seen in winter (Dec-Feb) and spring (Mar-May); these trends are about -4 to

Table 1-2. SBUV(/2) trends in %/decade by season and latitudinal zone over the period 1/79 to 5/94, with 95% uncertainty limits (two standard errors, labeled 2se).

Zone	Dec-Feb	2se	Mar-May	2se	Jun-Aug	2se	Sep-Nov	2se	Year	2se
65N	-5.6	4.2	-6.3	2.9	-3.5	1.4	-4.3	1.6	-5.0	2.0
55N	-6.0	3.4	-6.1	2.6	-3.0	1.6	-3.7	1.5	-4.8	1.9
45N	-6.4	2.9	-5.7	2.3	-2.8	1.5	-3.1	1.5	-4.6	1.8
35N	-4.9	2.4	-4.5	2.5	-3.1	1.5	-2.9	1.5	-3.9	1.8
25N	-3.2	2.0	-2.7	2.5	-2.7	1.6	-3.0	1.3	-2.9	1.6
15N	-2.0	1.6	-1.8	1.8	-2.0	1.9	-2.6	1.4	-2.1	1.4
5N	-1.3	1.8	-1.7	2.2	-1.8	1.5	-1.6	1.8	-1.6	1.6
5S	-1.5	1.3	-1.8	1.7	-2.5	1.3	-2.1	1.5	-2.0	1.2
15S	-0.7	1.1	-0.3	1.1	-1.5	1.8	-1.0	1.5	-0.9	1.1
25S	-3.1	0.9	-2.7	1.3	-3.6	2.6	-2.7	1.8	-3.0	1.4
35S	-4.4	1.0	-5.3	1.8	-6.5	2.6	-3.9	2.0	-5.0	1.5
45S	-4.4	1.4	-5.0	1.7	-6.6	2.5	-3.5	2.2	-4.9	1.5
55S	-4.6	1.6	-6.3	1.9	-10.7	3.0	-6.3	3.3	-7.0	2.1
65S	-5.8	1.4	-7.6	2.1	-14.3	3.8	-13.6	5.2	-10.4	2.4

Table 1-3. Short-term Dobson trends in %/decade using data from 1/79 to 2/94. Tabled numbers are averages of individual trends within latitude zones, with 95% uncertainty limits (two standard errors, labeled 2se).

Zone	N	Dec-Feb	2se	Mar-May	2se	Jun-Aug	2se	Sep-Nov	2se	Year	2se
50-65 N	7	-6.2	1.5	-6.9	0.5	-4.6	1.4	-2.2	1.1	-5.2	0.5
40-50 N	9	-5.4	1.5	-6.1	0.6	-3.0	0.6	-2.0	0.9	-4.3	0.5
30-40 N	8	-3.9	1.3	-3.5	1.4	-1.6	1.4	-0.9	0.8	-2.5	1.0
20-30 N	5	-1.7	0.7	-1.8	0.2	-0.9	1.7	-0.5	0.9	-1.2	0.2
0-20 N	3	0.5	1.1	-0.0	0.4	-0.7	0.6	-0.8	0.4	-0.3	0.2
30- 0 S	5	-1.1	0.7	-1.1	1.4	-2.0	0.7	-1.4	0.5	-1.4	0.6
55-30 S	6	-3.6	1.9	-2.9	1.2	-3.6	1.7	-2.8	1.4	-3.2	1.3

Table 1-4. Long-term Dobson trends in %/decade using data from 1/64 to 2/94 (trends from 1/70). Tabled numbers are averages of individual trends within latitude zones, with 95% uncertainty limits (two standard errors, labeled 2se).

Zone	N	Dec-Feb	2se	Mar-May	2se	Jun-Aug	2se	Sep-Nov	2se	Year	2se
50-65 N	7	-4.0	1.0	-3.4	0.5	-1.4	0.4	-1.2	0.5	-2.6	0.4
40-50 N	9	-3.7	0.8	-3.6	0.9	-1.8	0.6	-1.3	0.4	-2.7	0.5
30-40 N	8	-2.4	1.0	-1.8	0.7	-0.6	0.5	-0.7	0.5	-1.4	0.6
20-30 N	5	-1.5	0.8	-1.1	0.5	0.0	0.3	-0.4	0.7	-0.7	0.4
0-20 N	3	0.4	0.8	-0.0	0.4	-0.8	0.7	-0.7	0.9	-0.3	0.3
30- 0 S	5	-1.2	0.7	-1.2	1.5	-1.7	0.3	-1.4	0.7	-1.4	0.7
55-30 S	6	-1.8	1.0	-1.9	0.8	-2.5	0.6	-1.6	0.8	-2.0	0.7

-7%/decade. In the Southern Hemisphere, extremely large ozone depletion is seen in the southern winter (Jun-Aug) and spring (Sep-Nov).

The agreement between SBUV(/2) satellite and Dobson ground-based trends is not as good as seen in the 1991 assessment between TOMS satellite and ground-based trends. In the 1991 assessment, TOMS trends averaged slightly more negative than the Dobson trends, but only by 1%/decade or less. As seen in Figure 1-6, the SBUV(/2) trends average 1 to 2%/decade more negative than the short-term Dobson trends in all seasons and at all latitudes except mid- to high northern latitudes. In the case of the mid- to high northern latitudes, the agreement is much better. In the equatorial regions, while the Dobson network shows essentially no trend in total ozone in concurrence with previous assessments, the SBUV(/2) analysis indicates a seasonally independent trend of about -2%/decade; these are just statistically significant in many cases, since two standard errors of the trend estimates are about 2%/decade in low latitudes. This is particularly so in the Jun-Jul-Aug period; however, due to the timing of this assessment, we cannot update trends in that period beyond the extremely low 1993 values discussed in Section 1.2.2.4.

In order to check the consistency of the SBUV(/2) trends versus both Dobson and TOMS, Figure 1-7 shows seasonal trends in total ozone using data through May 1991 for all three. The TOMS trends through May 1991 are similar to those reported in the 1991 assessment (only an additional two months of data are used), although the seasonal definitions were different in the 1991 assessment (Dec-Jan-Feb-Mar, May-Jun-Jul-Aug, Sep-Oct-Nov, with April not reported). The Dobson and TOMS curves in Figure 1-7 are close to those given in Reinsel *et al.* (1994a) for the period 11/78 through 12/91; slight differences in the recent Dobson results are primarily due to use of Dobson station revisions.

Over the same time period, SBUV(/2) trends tend to be consistently more negative than both TOMS and Dobson at low latitudes, say 30°S to 30°N. TOMS trends are also slightly more negative than Dobson trends on the average, as noted above and in the previous assessment. SBUV(/2) trends average close to -2%/decade in the tropics, even when data from the low 1992-1993 period are excluded.

Reinsel *et al.* (1994a) used a set of 56 Dobson station records, publicly available from the World Ozone Data Center, to analyze trends through 1991. Figure 1-8 shows the year-round trends calculated for this report as discussed above compared to the year-round trends from the 56 Reinsel *et al.* stations records, updated with publicly available data. The data used for the comparison analysis were obtained from the World Ozone Data Center, except that newly revised data for the U.S. stations and Arosa were used as obtained directly from the stations. The same statistical interventions as used in Reinsel *et al.* were also used in the comparison analysis, with an additional one at Mauna Loa as discussed above. The results from the larger Reinsel *et al.* set of stations, using in many cases data that have not yet been processed using current quality control procedures (WMO, 1992b), show much more variation in the trends; however the average across stations within each latitude zone is close to the analogous average for the 43-station analysis discussed here.

1.2.2.3 The Effect of the 1992-1994 Data

As discussed in the preamble to Section 1.2.2, it is desirable to update trend estimates through the most recently available data. However, interpretation of these trends that include the recent period must be made with caution, since global total ozone was low over the period late 1991 through late 1993.

Figure 1-9 shows the effect of using data over the period 1992-1994, compared to stopping the trend analyses at December 1991, for SBUV(/2) and Dobson data. The comparison is not made for TOMS, because of the concerns about the TOMS calibration in the last couple of years of the instrument's life, and because of difficulties in extending the TOMS data beyond May 1993.

The effect of excluding the 1992-1994 data from the trend calculations is less than one might expect, given the size of the 1992-1993 anomaly, although certainly on the average the updated trends are slightly more negative. The largest consistent effects are in the Jun-Jul-Aug period in the tropics (note the latest Jun-Jul-Aug data in this analysis are from 1993) seen in both SBUV and Dobson analyses; the effect is to make the trends about 1%/decade more negative. The Dobson data show about a 2%/decade effect in winter and spring in the mid- to high north latitudes, which is not so clear from SBUV except in the high northern latitudes. In other seasons/latitudes, the effects are typically less than about 1%/decade.

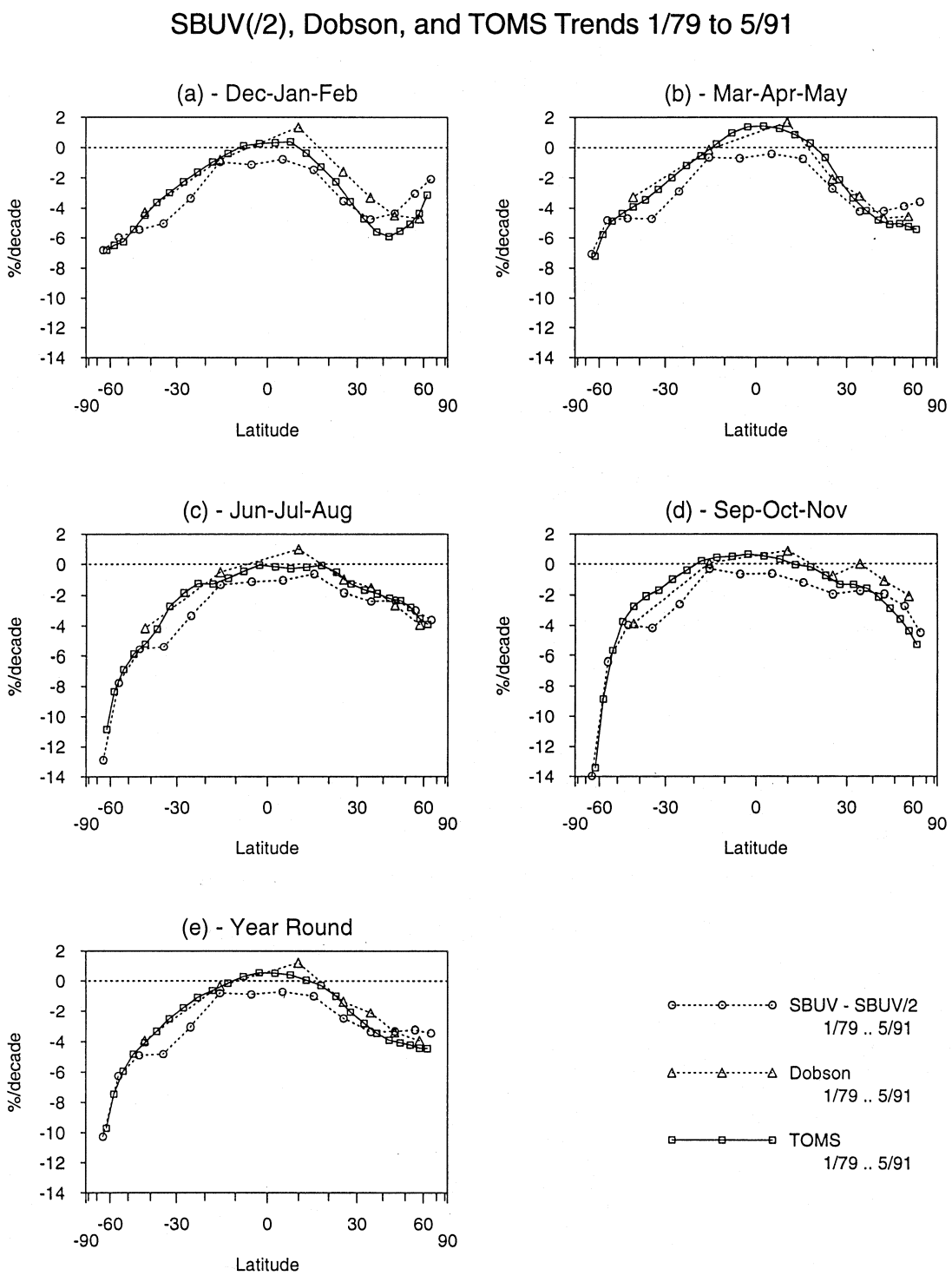

Figure 1-7. SBUV(/2), Dobson, and TOMS seasonal total ozone trends in percent per decade by latitude through 5/91. Open circles are SBUV(/2) trends over 1/79 to 5/91; open triangles are Dobson trends over 1/79 to 5/91; open squares are TOMS trends over 1/79 through 5/91. The Dobson trends are averages within latitudinal zones of individual trends at 59 Dobson stations.

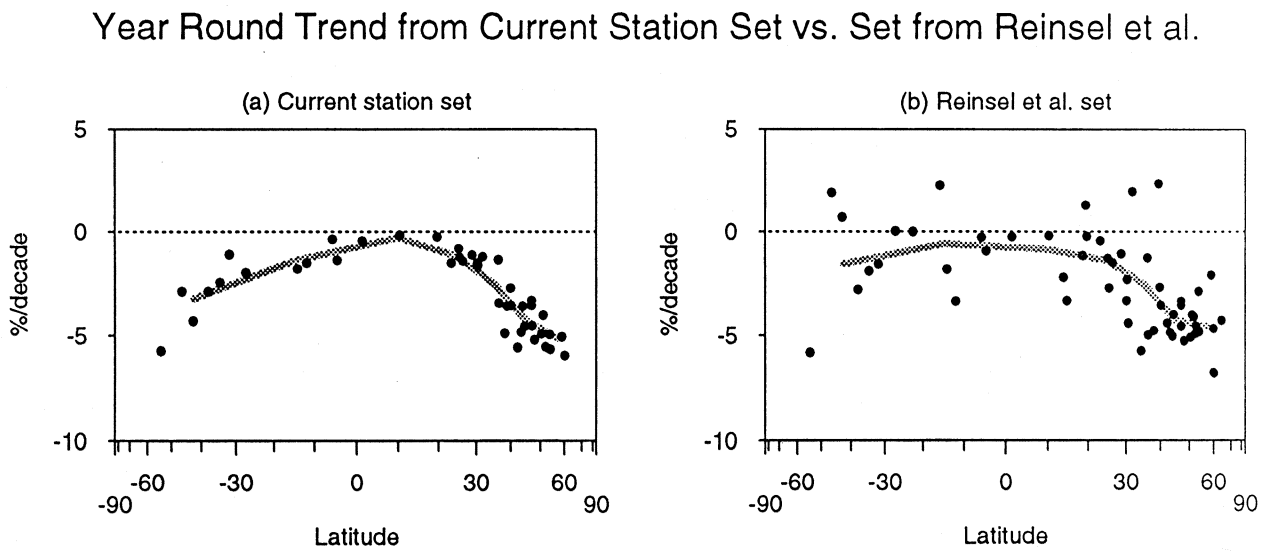

Figure 1-8. Comparison of year-round trends 1/79 through 2/94 from the 43-station set of revised data used in this report (plot (a)) with trends from the station set of Reinsel *et al.* (1994a) using data from the World Ozone Data Center together with updates for the U.S.A. stations and Arosa obtained from the stations (plot (b)). The gray curves are averages within latitudinal zones as in Figure 1-5.

1.2.2.4 Acceleration of Ozone Trends

It was commented upon in the 1991 assessment (WMO, 1992a) that trends in the 1979-1991 period from the Dobson network tended to be larger (more negative) than trends calculated over the longer period 1970-1991. This is also seen in Figure 1-6, comparing the short-term (1/79 to 2/94) trends with the long-term (1/70 to 2/94) trends. This phenomenon has led to speculation that ozone trends have accelerated in recent years compared to the trends in the 1970s.

To test this, a double trends model was used to analyze data from 34 Dobson stations whose records begin by January 1975, but utilizing data from January 1964 where available, as for the long-term trend analysis in Table 1-4. The time trend fitted was a "double jointed hockey stick," with a level base before 1970, a trend beginning in January 1970, and a possibly different trend from January 1981 through December 1991 (the date of the trend change was chosen for convenience to divide the 22-year period 1970-1991 into two equal 11-year segments). Interest focuses on the difference in the trends over 1981-1991 vs. 1970-1980. This model was fitted to the 34 Dobson stations, and the trend difference calculated at each station for each season. The year-round average differences are shown in Figure 1-10.

There is an indication of an acceleration in the annual trends in northern mid- to high latitudes and in all seasons except Sep-Oct-Nov (seasonal results not shown in plot). The largest number of Dobson stations are in mid- to high north latitudes where trends, especially in winter and spring, are large. Table 1-5 shows the mean trend difference for the 24 Dobson stations in this analysis north of 25° north latitude, together with the standard error of the mean. The largest trend acceleration appears in the spring, followed by the winter and summer seasons. The average trend differences are statistically significant in the spring, summer, and year-round average, and very nearly so in winter.

1.2.3 Discussion

As a result of efforts to reanalyze the historical ground-based data record and of a continuing program of instrument intercomparisons relative to the World Standard Instrument, the quality of the Dobson (and M-124) record has improved since the last report (WMO, 1992a). We can thus have greater confidence in the derived trends. There is still a great deal of station-

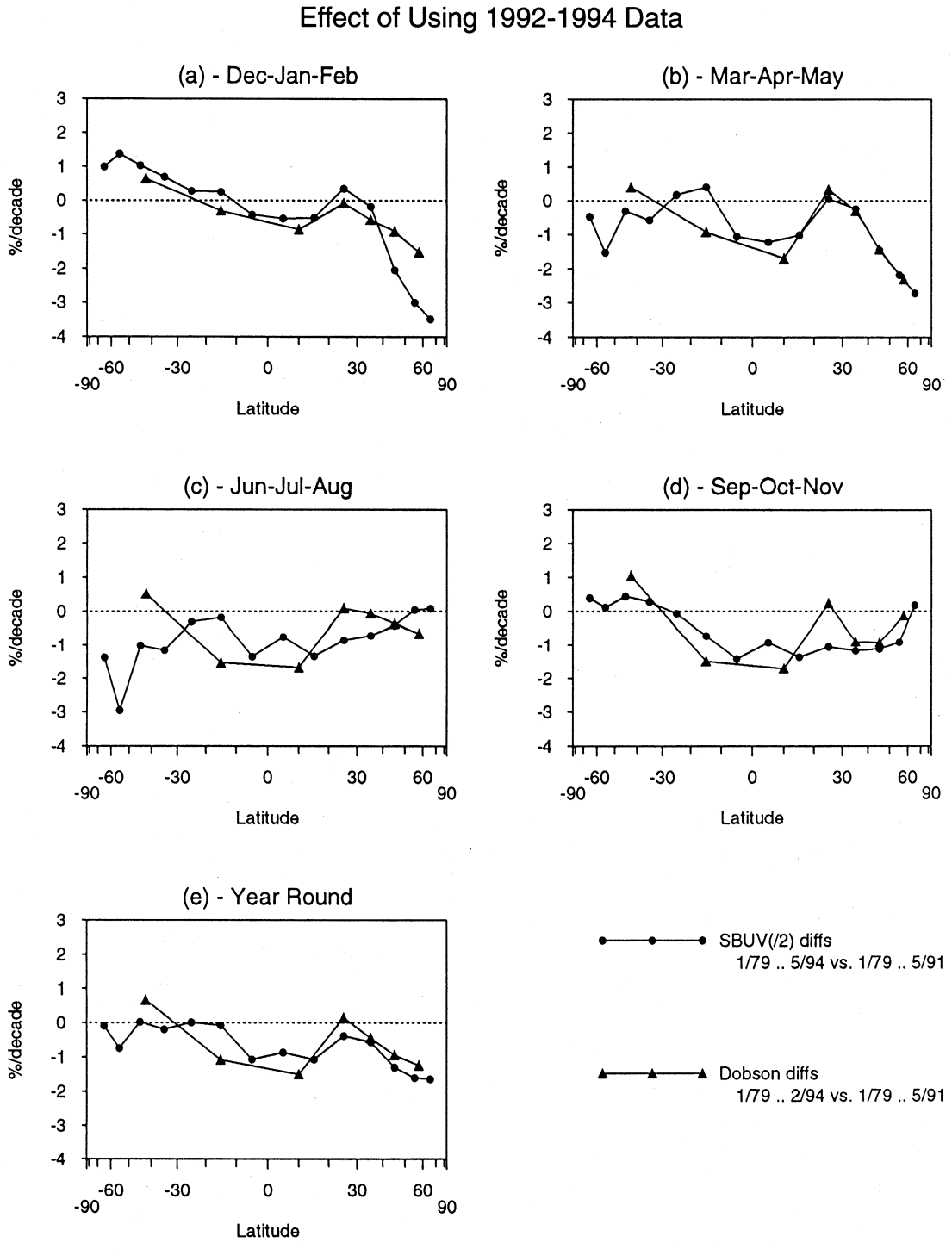

Figure 1-9. Effect on trends of using 1992-1994 data. Triangles denote the difference in the trends calculated from Dobson data (1/79 to 2/94 minus 1/79 to 5/91). Circles denote the difference in the trends (1/79 to 5/94 minus 1/79 to 5/91) calculated from SBUV(/2) data.

Table 1-5. Difference in trends 1981-1991 vs. 1970-1980 from the double trends model, averaged over 24 Dobson stations north of 25°N. The column labeled 2se represents 95% uncertainty limits (two standard errors) for the difference in trend.

Season	Average Trend Difference	2se
Dec-Jan-Feb	-2.0	1.5
Mar-Apr-May	-2.8	1.1
Jun-Jul-Aug	-1.9	1.5
Sep-Oct-Nov	-0.4	1.2
Year round	-1.8	0.7

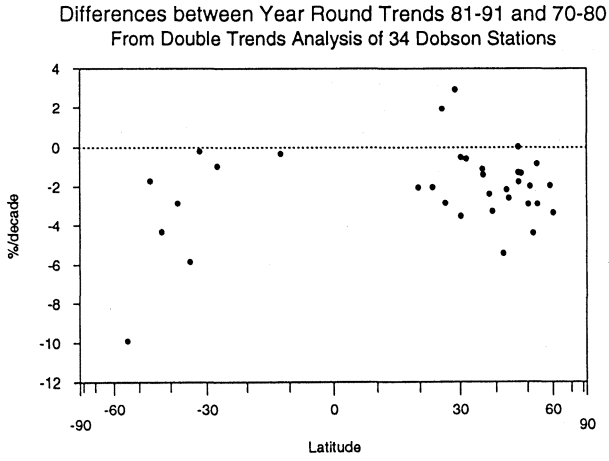

Figure 1-10. Differences between trends 1981-1991 and 1970-1980 at 34 Dobson stations from double trends analysis.

to-station variability as determined when TOMS is used as a transfer standard to look for short-term shifts. It is important that stations' records continue to be maintained and improved.

When the TOMS trends through May 1990 were evaluated (Stolarski *et al.*, 1991) the trend error was estimated to be 1.3% per decade (two sigma error). As a result of a recent evaluation it appears that the Nimbus 7 TOMS calibration has drifted by 1-2% since 1990. The changing seasonal cycle in the TOMS-Dobson and TOMS-SBUV differences appears to be caused by changing nonlinearity in the TOMS photomultiplier response. While the previous error estimate may be appropriate for equatorial and midlatitude summer data, the photomultiplier nonlinearity may be introducing as much as 2% per decade error into midlatitude winter trends.

The SBUV record has benefited greatly from the work done on the TOMS measurements (the same basic algorithm is used; the diffuser plate correction is the same). The drift in the calibration of total ozone by the SBUV instrument from January 1979 to June 1990 was 1% or less, and any seasonal differences relative to Dobson instruments in the Northern Hemisphere were less than 1%. The SBUV2 instrument has the on-board calibration lamps and has been compared with the Shuttle Solar Backscatter Ultraviolet (SSBUV) flights since 1989. There was good agreement during the 18 months that both SBUV and SBUV2 made measurements. The main problems with the combined SBUV/SBUV2 record are the possible aliasing of trends resulting from the changing orbit of the NOAA-11 satellite and the possibly linked seasonal difference of 1-2% (minimum to maximum) relative to the ground-based network in the Northern Hemisphere. The TOMS non-winter measurements agree well with those from SBUV and SBUV/2. Given these factors, and the extra year of data in the combined SBUV(/2) record, it is best at this time to focus on trends derived from the SBUV(/2) measurements.

The most obvious features of the total ozone trends have been commented upon in previous assessments. Statistically significant negative trends are seen at mid- and high latitudes in all seasons. The largest negative ozone trends at mid- and high latitudes in the northern Hemisphere are seen in winter (Dec-Feb) and spring (Mar-May); these trends are about -4 to -7%/decade. In the Southern Hemisphere, the annual variation in the trends at midlatitudes is smaller, though the average trend is similar to the Northern Hemisphere average.

The effect of including the 1992-1994 data in the trend calculations is less than one might expect, given the size of the 1992-1993 anomaly, although certainly on the average the updated trends are slightly more negative. The largest consistent effects are in the Jun-Jul-Aug period in the tropics (note the latest Jun-Jul-Aug data in this analysis are from 1993) seen in both SBUV and Dobson analyses; the effect is to make the trends about 1%/decade more negative. The Dobson data show about a 2%/decade effect in winter and spring in the mid- to high north latitudes, which is not so clear from SBUV except in the high north. In other seasons/latitudes, the effects are typically less than about 1%/decade.

Analysis of TOMS, SBUV(/2), Dobson, and ozonometer data through 5/91 reconfirms the results in the 1991 assessment (WMO, 1992), which were based on TOMS and Dobson analyses through 3/91. The SBUV(/2) trends tend to be slightly more negative than either TOMS or Dobson trends, particularly in the tropics, while as pointed out in the 1991 report, TOMS trends are also slightly more negative than Dobson. However, the differences between the instrument systems are within the 95% confidence limits.

SBUV(/2) trends in the tropics over the period 1/79 through 5/94 are estimated to be about -2%/decade in all seasons, with formal 95% confidence limits in the tropics of 1.5 to 2%/decade. This appears to be due to a combination of two effects: (1) SBUV/2 trends are about 1%/decade more negative than TOMS and Dobson in the tropics, raising suspicions of an instrumental drift; and (2) the inclusion of the low 1992-1994 data makes the trends an additional 1%/decade more negative in the tropics.

There was a statistically significant increase (about 2%/decade) at the Dobson stations north of 25°N in the average rate of ozone depletion in the period 1981-1991 compared to the period 1970-1980.

1.3 OZONE PROFILES

1.3.1 Ozone Profile Data Quality

Various techniques have been used to measure ozone profiles. However only a few of these have produced data sets that are long enough, and of sufficient quality, to be considered for trends. In this section we consider two ground-based methods that have been in use since the 1960s (Umkehr and ozonesondes) and two satellite instruments (SBUV and the Stratospheric Aerosol and Gas Experiment, SAGE).

1.3.1.1 Umkehr

The long-term records of Umkehr observations are made using Dobson spectrophotometers at high solar zenith angles using zenith sky observations (*e.g.*, Götz, 1931; Dobson, 1968). A new inversion algorithm has been developed (Mateer and DeLuisi, 1992), and all the Umkehr records submitted to the World Data Center have been recalculated. The new algorithm uses new temperature-dependent ozone absorption coefficients (Bass and Paur, 1985) and revised initial estimates of the ozone profiles. The correction for the presence of aerosols is still calculated after the ozone retrieval (DeLuisi *et al.*, 1989), and the aerosol corrections needed for the new and old retrievals are similar (Reinsel *et al.*, 1994b). Mateer and DeLuisi concluded that reliable ozone trends can only be found for Umkehr layers 4-8 (19-43 km). Lacoste *et al.* (1992) compared the lidar and Umkehr measurements made at Observatoire de Haute-Provence from 1985-1988. They found good agreement between these two measurements systems from layers 4-7 (the lidar was not sensitive below layer 4) and attributed the poor agreement in layer 8 to the low return signals in the lidar system from this high altitude at that time.

Some information is available below layer 4 because total ozone must be balanced within the complete profile. DeLuisi *et al.* (1994) have compared Umkehr observations (calculated using the old algorithms) with SBUV ozone profile data in the 30-50°N latitude band for 1979-1990 and showed that there is good agreement in layer 4 and above. The agreement in the SBUV and Umkehr profiles is not so good lower down, but useful trend information may be present, a situation that could improve when the new algorithm is used. For now, as in recent assessments, only the trends in layers 4 and above will be considered.

1.3.1.2 Ozonesondes

Ozonesondes are electrochemical cells sensitive to the presence of ozone that are carried on small balloons to altitudes above 30 km. Several versions have been used, and the important ones for ozone trend determination are the Brewer-Mast (BM), the electrochemical

concentration cell (ECC), and the OSE (used principally in Eastern Europe). The principle on which they work is that the current produced in the cell from the reaction of ozone with potassium iodide solution is proportional to the amount of ozone passing through the cell. This is not true if other sources of current exist. Two such cases are discussed here: the zero-ozone current output possibly caused by chemicals other than O_3; and the interfering gas, SO_2. Changes in operational procedures can also strongly influence the ozonesonde data quality. Two ways by which the quality of the ozonesondes can be assessed are also discussed: intercomparisons and correction factors.

The ozonesonde network is geographically uneven, with the large majority of stations in Europe and North America. The highest density of stations is in Europe, where they are all located between 44 and 52°N and between 5 and 21°E. The long-term records in Europe all involve BM sondes or OSE sondes. With the exception of Wallops Island, the North American stations do not have continuous records longer than 15 years, as Brewer Mast sondes were used at Canadian stations until about 1980, when there was a switch to ECC sondes. The frequency of launches at the Japanese stations has been quite low at times, which has the effect of increasing the uncertainties associated with the long-term trends. However, the most obvious shortage of data is in the Southern Hemisphere, where the only long-term, non-Antarctic records are at Natal (6°S) and Melbourne (38°S: Aspendale/Laverton). Unfortunately, the launch frequency at these sites has been irregular as well. Last, it should be noted that many stations have ongoing programs to assess and improve the quality of the measurements.

1.3.1.2a Background Current

The presence of a background (zero ozone) current has long been recognized in the ECC sonde and the standard operating procedures include a method for correction (Komhyr, 1969). For most ECC sondes that have been flown, a correction has been applied that assumes that the background current decreases with altitude (Komhyr and Harris, 1971). Measurements are sensitive to errors in the correction for the background current in regions where the ozone concentration is low, *i.e.,* at or near the tropopause. Such errors have the potential to be large as the background current can become similar in magnitude to the ozone-generated current, for example, in the tropical upper troposphere. In the stratosphere, where ozone concentrations are much higher, the errors associated with background current corrections are small.

The response time of the ECC sonde to ozone is about 20 seconds. Laboratory studies indicate that there is an additional component of the background current with a response time of 20-30 minutes (Hofmann, Smit, private communications). For this component there is a memory effect as the balloon rises and the background current would vary through the flight. Earlier studies (Thornton and Niazy, 1983; Barnes *et al.*, 1985) concluded that the background current remained constant in the troposphere. No correction is made for the zero current in BM sondes, although some stations measure it before launch. For BM sondes, the procedure is to reduce this zero current to a very low value by adjusting the sonde output, possibly at the expense of the sonde sensitivity. Any changes in the magnitude of the background current over the last 20-30 years will most strongly affect the trends calculated for the free troposphere. More work is needed to assess the size and impact of any changes in the background current in the different ozonesondes.

1.3.1.2b SO_2

The presence of SO_2 lowers the ozonesonde readings (one SO_2 molecule roughly offsets one O_3 molecule), an effect that can linger in the BM sonde because the SO_2 can accumulate in the bubbler (Schenkel and Broder, 1982). The SO_2 contamination is a problem at Uccle, where the measured SO_2 concentrations were high in the 1970s and have dropped by a factor of about 5 over the last 20 years. A procedure has been developed to correct for the SO_2 effect at Uccle, and the influence is found to be greatest in the lower troposphere (De Muer and De Backer, 1994). Logan (1994) argues that the Hohenpeissenberg, Tateno, and Sapporo ozonesonde measurements in the lower troposphere may have been affected by SO_2. This interference is worst in winter when the highest concentrations of SO_2 occur. Staehelin *et al.* (1994; personal communication) have found that SO_2 levels in Switzerland were too low to have a noticeable effect at Payerne. Other stations are also likely to have been less affected.

1.3.1.2c Operational Changes

Changes in operational procedures at an ozonesonde station can have dramatic effects on the ozone measurements, particularly in the troposphere. Two clear examples are: (a) the change from BM to ECC sondes at the Canadian stations that took place in the early 1980s, when there was an apparent jump in the amount of tropospheric ozone measured at most of these stations; and (b) the change in launch time at Payerne in 1982, which affected the measurements in the lowest layer of the troposphere (Staehelin and Schmid, 1991). Logan (1994) argues that there is a jump in lower and mid-tropospheric ozone values in the combined Berlin/ Lindenberg record, corresponding to the change in ozonesonde launch site from Berlin to Lindenberg and to the simultaneous change in sonde type from BM to OSE. Alterations in the manufacture of the sensors and in the pre-launch procedures can also have an effect.

Another possible cause of error is a change in the efficiency of the pump. The air flow through the ozone sensor is not measured, but is calculated from laboratory tests performed at a number of pressures (Görsdorf *et al.*, 1994; Komhyr *et al.*, 1994b, and references therein). It is possible that there have been some changes in the design of the pump that may have changed its efficiency over time and that primarily affect measurements made at altitudes above 25-28 km.

1.3.1.2d Intercomparisons

A series of campaigns have been mounted in which different ozonesondes have been compared to see whether the quality of any type of ozonesonde has changed over time and to find out what systematic differences exist between different types of sonde and between the sondes and other instruments (lidar, UV photometer). In each campaign good agreement was found between the various ECC sondes flown simultaneously. However in the most recent WMO campaign held at Vanscoy, Canada, in May 1991, the BM gave results 15% higher than the ECC in the troposphere, whereas in the previous campaigns (1970, 1978, 1984) the BM was reported as measuring 12% less tropospheric ozone than the ECC (Kerr *et al.*, 1994, and references therein). This result may indicate a change in the sensitivity of the BM to ozone. This conclusion is supported to some extent by the findings of a study at Observatoire de Haute Provence, where comparisons involving BM and ECC sondes, lidars, and UV photometers made in 1989 and 1991 showed a change in the BM sensitivity relative to ECC in the troposphere. However, operational practices maintained during campaigns can be different from those used at home, and it is hard to assess how representative the measurements made under campaign conditions are. The implications of such findings on trends in tropospheric ozone are discussed in Section 1.3.2.3. The measurements in the stratosphere show good agreement in all the comparisons.

Although one must be careful in the comparison of the regular Brewer-Mast sondes with the GDR sondes manufactured in the former East Germany, results of two intercomparison campaigns in Germany (Attmannspacher and Dütsch, 1970, 1981) showed similar differences between BM and OSE of 3 and 5 nbar, respectively, in the free troposphere (a difference of about 5% of the measured ozone concentration) and no differences in the stratosphere. This may be a good indication that OSE sonde quality remained the same, at least over the time period 1970-1978; and therefore differences between trend estimates obtained at various stations need not be strongly dependent on the type of sondes used, unless changes in sonde type occurred.

1.3.1.2e Correction Factors

Ozonesonde readings are normalized so that the integrated ozone of the sonde (corrected for the residual ozone at altitudes above the balloon burst level) agrees with the total ozone amount given by a nearby Dobson (or other ground-based) instrument. This is a good way to assess the overall sounding quality – an unusually high or low correction factor indicates that something might be wrong with a particular sounding. A correction factor of 1 is not a guarantee that the profile is correct.

However, care is needed in using correction factors, as new errors can be generated. First, the process relies on the quality of the local total ozone measurement. For instance, errors can be introduced either by a single, erroneous reading or through changes in the calibration of the ground-based instrument. It is important to ensure that the ozonesonde records are updated in line with the ground-based revisions. Second, errors in the pressure and ozone reading at the burst level will affect the value of the residual ozone, which in turn influences the rest of the profile through an inaccurate correction

factor. Third, any variation of the sonde sensitivity to ozone changes with altitude leads to an incorrectly shaped profile, which the use of a correction factor (based only on total column amounts) cannot adjust. ECC sondes are thought to have a more constant response with altitude than the BM sondes which tend to underestimate tropospheric ozone amounts.

No significant long-term trend in the correction factor has been seen at Hohenpeissenberg, Payerne, and Uccle, a fact which suggests that there has not been a change in sensitivity of the BM sonde, possibly indicating that the result of the intercomparisons arose from the different operational conditions used in the intercomparisons. Changes in correction factor over shorter times have occurred, *e.g.,* at Payerne in the early 1970s and since 1990 (Logan, 1994). Logan (1994) has compared the trends estimated using measurements calculated with and without correction factors and found only small changes in the ozone trends in all but 3 of the 15 ozonesonde records.

1.3.1.3 Satellite Measurements of the Ozone Profile

The SAGE I and SAGE II instruments were described in detail in the IOTP (WMO, 1990a). SAGE I operated from February 1979 to November 1981 and SAGE II from October 1984 to the present day. They are solar occultation instruments measuring ozone absorption at 600 nm. Correction is made for attenuation by molecular and aerosol scattering and NO_2 absorption along the line of sight by using the observations made at other wavelengths. Comparisons of SAGE II number density profiles with near-coincident balloon and rocket measurements have shown agreement on average to within ± 5-10% (Attmannspacher *et al.*, 1989; Chu *et al.*, 1989; Cunnold *et al.*, 1989; De Muer *et al.* 1990; Barnes *et al.*, 1991).

The SAGE I and SAGE II instruments are different in some respects, but, in principle, there are few reasons for calibration differences between the two instruments. One reason is the altitude measurements of the two instruments, which are now thought to be offset by 300 m. The effects of such an offset would be felt most at altitudes between 15 and 20 km, where the ozone concentrations vary rapidly with altitude. Two independent investigations have found a potential error in the altitude registration of the SAGE I data set. From a detailed intercomparison with sondes and lidars, Cunnold (private communication) has found that agreement between SAGE I and these other measurements can be significantly improved if the SAGE I profiles are shifted up in altitude by approximately 300 meters. The prelaunch calibration archives for SAGE I have been reexamined, and together these data show that the spectral location of the shortest wavelength channel may be in error by 3 nm (382 nm instead of 385 nm). Since this channel is used to correct the altitude registration via the slant path Rayleigh optical depth, a shift of 3 nm to shorter wavelengths would result in an upward altitude shift of about 300 ± 100 m. The full impact of this wavelength error is being studied and a preliminary version of the shifted SAGE I ozone data set is used in this assessment.

The presence of aerosols increases the errors associated with the measurement, as the aerosols are effective scatterers of light at 600 nm. Comparisons of SAGE II ozone measurements with those made by Microwave Limb Sounder (MLS) (which should be unaffected by aerosol) indicate that errors become appreciable when the aerosol extinction at 600 nm is larger than 0.003 km^{-1}, which corresponds to about 8 times the background aerosol at 18 km. Only measurements made with an aerosol extinction less than 0.001 km^{-1} are used in the trend analyses presented in the next section. Using the 0.001 per km extinction value as a screening criterion, the following general observations follow. The SAGE II ozone measurements were interrupted for a period of one year following the eruption of Mt. Pinatubo at 22 km near 40°N and 40°S. At the equator the gap in the series was two years at the same altitude. Extratropical measurements were uninterrupted at altitudes of 26 km and above (30 km and above at the equator). By early 1994, SAGE II was making measurements at all latitudes down to the tropopause.

SBUV operated from November 1978 to June 1990. The total ozone measurements are described in Section 1.2.1. Ozone profiles are found by measuring the backscatter from the atmosphere at wavelengths between 252 and 306 nm. The wavelengths most strongly absorbed by ozone give information about the higher altitudes. There is little sensitivity to the shape of the profile at or below the ozone maximum. As with the Umkehr measurements, some information is available below the ozone maximum because the complete profile must be balanced with the total ozone. Hood *et al.*

(1993) considered the partial column from the ground to 32 mbar (26 km) as the most useful quantity in this region.

Corrections have been made for the diffuser plate degradation using the pair justification method (Herman *et al.*, 1991; Taylor *et al.*, 1994), so the quality of the SBUV profile measurements has improved since the IOTP (WMO, 1990). The shorter wavelengths were corrected using a form of the Langley technique: near the summer pole, ozone measurements are made at each latitude with two solar zenith angles. If the zonal mean ozone values are constrained to be the same, the wavelength dependence of the correction to the diffuser plate degradation can be determined. The accuracy of any derived trend in the ozone profile is no better than 2-3% per decade. Above 25 km, the vertical resolution of SBUV is about 8 km, and this increases below 25 km to about 15 km. A limit on the independence of the SBUV ozone profile data in trend determination is that the retrieval algorithm requires further information on the shape of the ozone profile within these layers. It is thus possible that a trend in the shape of the profile within a given layer could induce a trend in the retrieved layer amount, even though the actual layer amount remains unchanged.

A problem with the synchronization of the chopper in the SBUV instrument occurred after February 1987. After corrections are made, there is no evidence of bias at the 1-2% level between the data collected before and after this date, although the latter data are somewhat noisier (Gleason *et al.*, 1993; Hood *et al.*, 1993).

McPeters *et al.* (1994) have compared the SAGE II and SBUV measurements from 1984 to 1990, the period when both instruments were in operation. Co-located data were sorted into 3 latitude bands (20°S-20°N, 30-50°N, and 30-50°S). Agreement is usually better than 5% (Figure 1-11, 20°S-20°N not shown). The main exceptions are near and below 20 km, where SBUV has reduced vertical resolution, and above 50 km, where the sampling of the diurnal variation of ozone is not accounted for in the comparison. A discrepancy between the SAGE sunrise and sunset data was found in the upper stratosphere near the equator. This may be related to the SAGE measurements made at sun angles, which causes the measurements to be of long duration so that the spacecraft motion during the event can be on the order of 10 great circle degrees.

The drift from 1984-1990 between the two measurements above 32 mb is less than 5% and is statistically insignificant (Figure 1-12). Below this, the drift is 10% per decade in the tropics and becomes smaller (4-6%) at midlatitudes. These are roughly consistent with the difference in the ozone trends from the two instruments. Some, or all, of this apparent drift may be caused by the requirement of information about the shape of the ozone profile in the SBUV retrievals (McPeters *et al.*, 1994). In contrast, the relative drift between SBUV and the Umkehr measurements (all between 30 and 50°N) is less than 2%. However, below the ozone maximum the average ozone amounts from SBUV and Umkehr differ by as much as 20% (DeLuisi *et al.*, 1994).

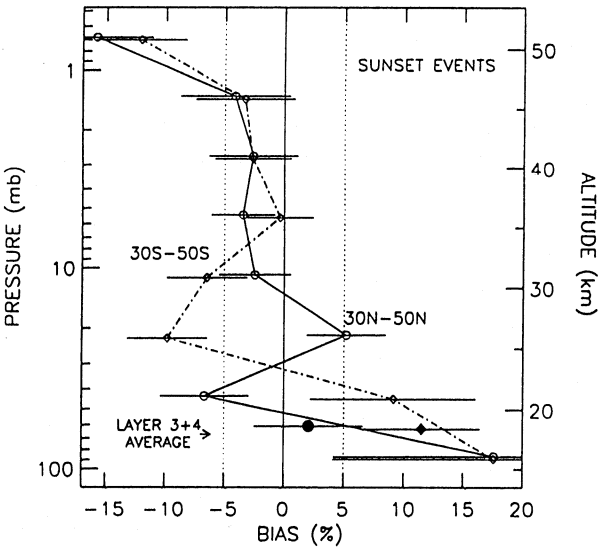

Figure 1-11. Ozone profile bias of SBUV relative to SAGE sunset data in northern midlatitudes (o) and southern midlatitudes (◊) for 1984-1990. The solid symbols are for layers 3+4 combined to represent the low SBUV resolution in the lower stratosphere. Standard deviations of the appropriate daily values used in calculating the average biases are also plotted. (McPeters *et al.*, 1994.)

1.3.2 Trends in the Ozone Profile

Ozone trends in three altitude ranges received special attention in the 1991 report. In the upper stratosphere (35 km and above) the ozone losses reported from two observational systems (Umkehr and SAGE) were

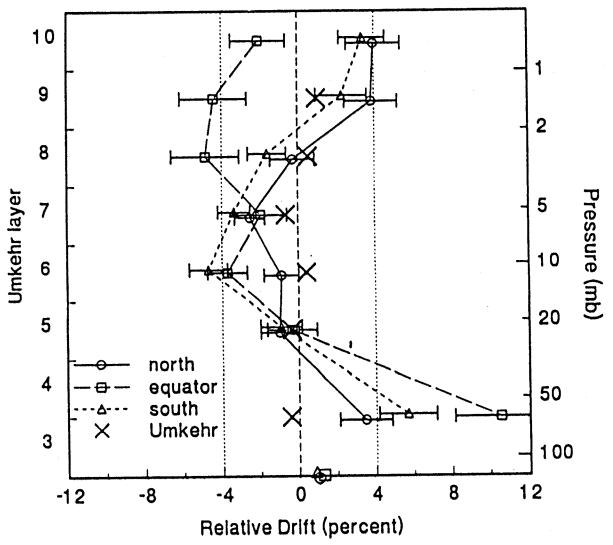

Figure 1-12. Linear drift of SBUV relative to SAGE II over the 1984-1990 time interval for layers 5-10 and for layer 3+4 combined, derived from a linear fit applied to percent difference data. (SBUV-SAGE)/SAGE in percent is plotted. Symbols on X axis give drift of layer 3-10 integrated ozone amounts. For comparison, drift relative to an average of five Umkehr stations (1984-1990) is also shown. The 1σ errors from the standard regression analysis are given. (McPeters *et al.*, 1994).

qualitatively similar but quantitatively different. These high altitude decreases have long been calculated in atmospheric models and are caused by gas phase chlorine-catalyzed ozone loss. Ozone losses were also reported below 25 km, though there were discrepancies between the values inferred from ozonesonde and SAGE measurements, especially below 20 km. In the free troposphere, long-term ozone increases were reported at three European ozonesondes sites. Ozone is an important radiative component of the free troposphere and a better understanding of ozone changes on a global scale is important. No significant ozone losses were reported around 30 km altitude or near the tropopause, where the lower stratospheric decrease switched to an upper tropospheric increase.

In this assessment the same altitude ranges are examined (starting in the upper stratosphere and working down) in the light of some new analyses of both the data quality (see Section 1.3.1) and of the data themselves. In addition, there is discussion of some ground-level measurements from which inferences can be drawn regarding changes in free tropospheric ozone.

McCormick *et al.* (1992) calculated trends using the combined SAGE I/II data set. The SAGE data used here are slightly different, as the altitude correction has been applied to the SAGE I data. Also, the base year used to calculate percentage changes is 1979 here (not 1988, used by McCormick *et al.*), so that the percentage changes in the lower stratosphere, where SAGE reports the largest decreases, are smaller. Hood *et al.* (1993) used the Nimbus 7 SBUV data from 1978 to 1990 to estimate trends. In this assessment we use the combined SBUV/SBUV2 data to extend the record, but the calculated trends are similar.

1.3.2.1 Trends in the Upper Stratosphere

In Section 1.3.1, we described an intercomparison of the various ozone data sets over a limited time interval. Upper stratospheric trends in ozone have been estimated from Umkehr, SAGE, and SBUV measurements using the full data sets. While the periods of time represented by each differ, they all represent, to first order, the changes observed from 1980 through 1990. Figure 1-13 shows the observed decadal trends as a function of altitude and latitude from the SBUV and SAGE I/II data sets. The two are now in reasonable agreement in the upper stratosphere. The altitude of the maximum percentage ozone loss is around 45 km and relatively independent of latitude. The magnitude of this peak decrease is smallest at the equator (about 5%/decade) and increases towards the poles in both hemispheres, reaching values in excess of 10% per decade poleward of 55 degrees latitude.

Figure 1-14 shows the ozone trend profile as a function of altitude in the latitude band from 30 to 50°N from SBUV and SAGE, along with the average Umkehr and ozonesonde trend profiles. SBUV, SAGE, and Umkehr all show a statistically significant loss of 5-10% per decade at 40-45 km, although there is some uncertainty as to its exact magnitude. Below 40 km the trends become smaller and are indistinguishable from zero near 25 km.

The seasonal dependence of the trends in the upper stratosphere has been investigated using the SBUV and Umkehr data (Hood *et al.*, 1993; DeLuisi *et al.*, 1994; Miller *et al.*, 1994). The Umkehr records between 19°N

and 54°N have been examined and their combined data do not show a significant seasonal variation in the trend. This is slightly at odds with the analysis of the SBUV measurements, which shows that the largest ozone decreases have occurred in winter at high latitudes in both hemispheres, though this difference may not be significant given the problems associated with measurements made at high solar zenith angles.

1.3.2.2 Trends in the Lower Stratosphere

As discussed in Section 1.3.1, we rely on SAGE and ozonesondes for information on ozone trends in the lower stratosphere, as the SBUV and Umkehr capabilities are limited at these altitudes. SAGE measures ozone from high altitudes to below 20 km. Ozonesondes operate from the ground up to about 30 km.

In the 1991 assessment, the SAGE I/II midlatitude trends below 20 km were reported as greater than 20% per decade, twice as large as were measured at two ozonesonde stations or than found from an average of five Umkehr records in the Northern Hemisphere. The size of the SAGE trends at these altitudes has provoked a great amount of discussion, partly because of the sensitivity of climate to changes in ozone in this region. As mentioned earlier, the SAGE I/II trends shown here differ in two respects from those reported previously. First, an altitude correction of 300 m has been applied to the SAGE I measurements. Second, the year used to calculate the percentage change is now 1979, not 1988. Below 20 km the effect of both these changes is to reduce the SAGE I/II trends because ozone changes rapidly with altitude and because the largest losses are observed at these altitudes so that the change in the base value is greatest. Two other factors complicate the SAGE measurement below 20 km: (i) ozone concentrations are smaller than at the maximum, so that the signal is lower; and (ii) the amount of aerosol is greater, which attenuates the signal and acts as an additional interference. These are well-recognized difficulties for which allowance is made in the calculation of the ozone amount and which contribute to the size of the uncertainties in SAGE ozone trends in the lower stratosphere.

Figures 1-13 and 1-14 show the lower stratospheric ozone trends in the 1980s from SBUV, SAGE, and the non-satellite systems. At altitudes between 25 and 30 km, there is reasonable agreement between SAGE I/II, SBUV, Umkehr, and ozonesondes that there was no significant ozone depletion at any latitude. The agreement continues down to about 20 km, where statistically significant reductions of 7 ± 4% per decade were observed between 30 and 50°N by both ozonesondes and SAGE I/II. In the equatorial region, the combined SAGE I/II record (1979-1991) shows decreases of more than 20% per decade in a region just above the tropopause between about 30°N and 30°S, although in absolute terms this loss in the tropics is quite small as there is not much ozone at these altitudes. The height of the peak decrease in ozone is about 16 km, and the region of decrease becomes broader away from the equator. At northern midlatitudes (Figure 1-14) the SAGE I/II trend at 16-17 km is -20 ± 8% per decade, compared with an average trend from the ozonesondes of -7 ± 3% per decade.

The SAGE I/II trends in the column above 15 km have been compared with the total ozone trends found from TOMS, SBUV(/2), and the ground-based network for 1979-1991. This comparison implicitly assumes little or no change in the ozone amount below 15 km. The SAGE I/II trends are larger than those found with the other data sets, peaking at -6% per decade in the northern midlatitudes, but the associated uncertainties are too large for firmer conclusions to be drawn. Hood *et al.* (1993) compared the tropical trend from SBUV for the partial column from the ground to 26 km with the SAGE I/II trends reported by McCormick *et al.* (1992). They decided that no conclusive comparison could be made, although they found trends of about +3 ± 4% per decade for SBUV for 1979-1990 (see Figure 1-13(a) for an updated version), while McCormick *et al.* found trends similar to the ones shown in Figure 1-13(b) for 1979-1991. While not shown here, comparisons of SBUV with SAGE II have recently been completed (McPeters *et al.*, 1994). Comparisons of the sum of ozone in Umkehr layers 3-10 (15 km-55 km) show that SBUV increased relative to SAGE (or SAGE decreased relative to SBUV) by 1.1% between 1984 and 1990.

Logan (1994), London and Liu (1992), and Miller *et al.* (1994) have reviewed the global long-term ozonesonde data records. Furrer *et al.* (1992, 1993) and Lityńska (private communication) have analyzed the records at Lindenberg, Germany, and Legionowo, Poland, respectively. These studies handled data quality issues differently and used different statistical models, but they gave broadly similar results in the lower stratosphere. The large natural variability of ozone concen-

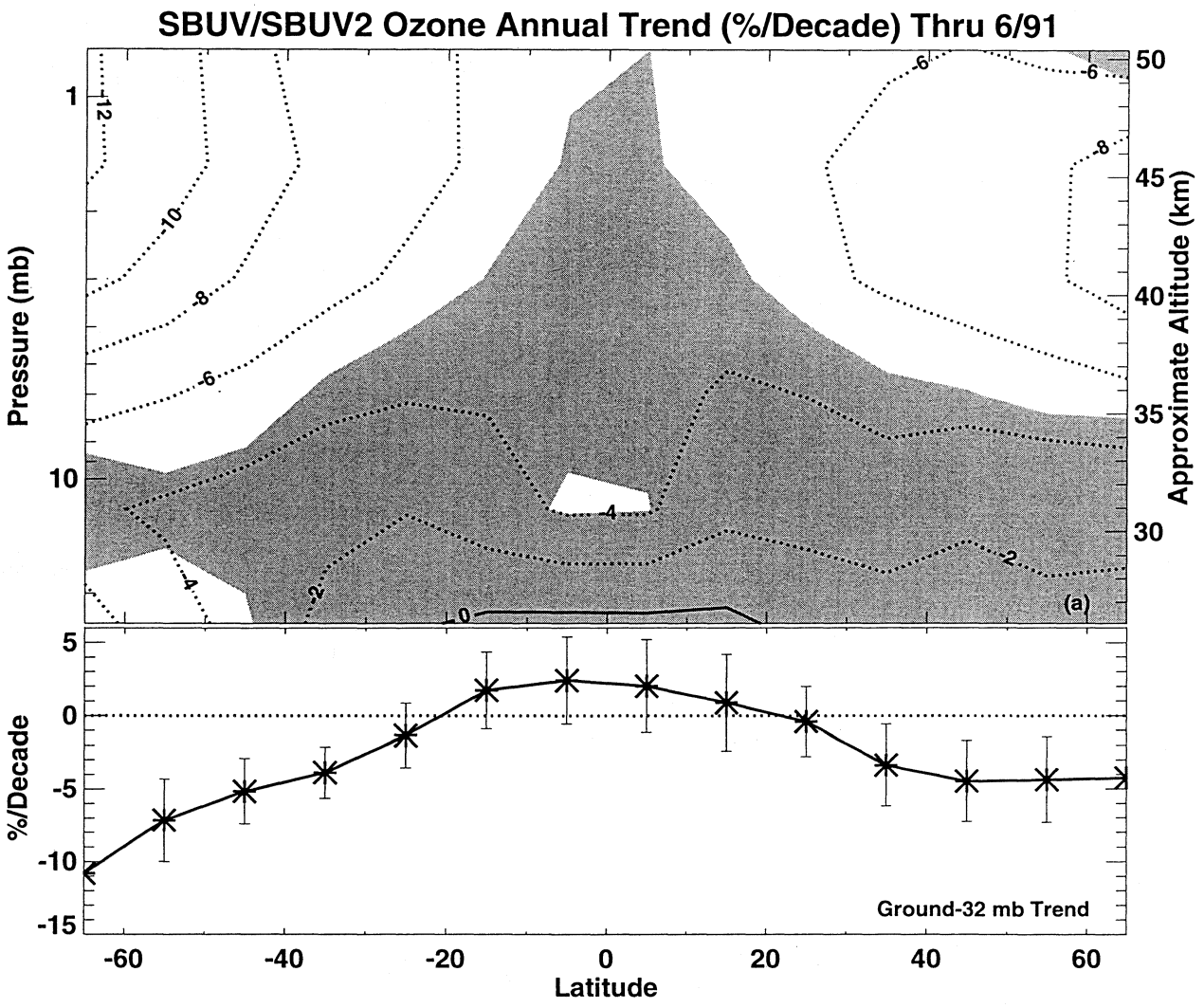

Figure 1-13. (a) Trends calculated for the combined SBUV/SBUV2 data set for 1/79 to 6/91. Hatched areas in the upper panel indicate that the trends are not significant (95% confidence limits). The lower panel shows the trends in the partial column between the ground and 32 mbar. Error bars in the lower panel represent 95% confidence levels.

trations is compounded at some stations by a low sampling frequency. It is hard to draw firm conclusions about seasonal effects. The following results are thus general and not true for all stations.

Figure 1-15 shows the ozone trends calculated from the ozonesonde records for the period 1970-1991. In the northern midlatitudes, a maximum trend of -8 to -12%/decade was found near 90 mbar from the early 1970s to 1991. Decreases extend from about 30 mbar down to near the troposphere. Significant ozone loss certainly appears to have occurred between 90 and 250 mbar. Few conclusions about the seasonal nature of the trends are statistically significant. A possible difference exists between the Canadian ozonesonde records where the summer trends are similar to, and possibly even greater than, the winter trends. At Wallops Island, U.S., and at the European stations, the winter loss is greater than the summer loss. These features are also seen in the total ozone record from 1978-1991 observed at these stations.

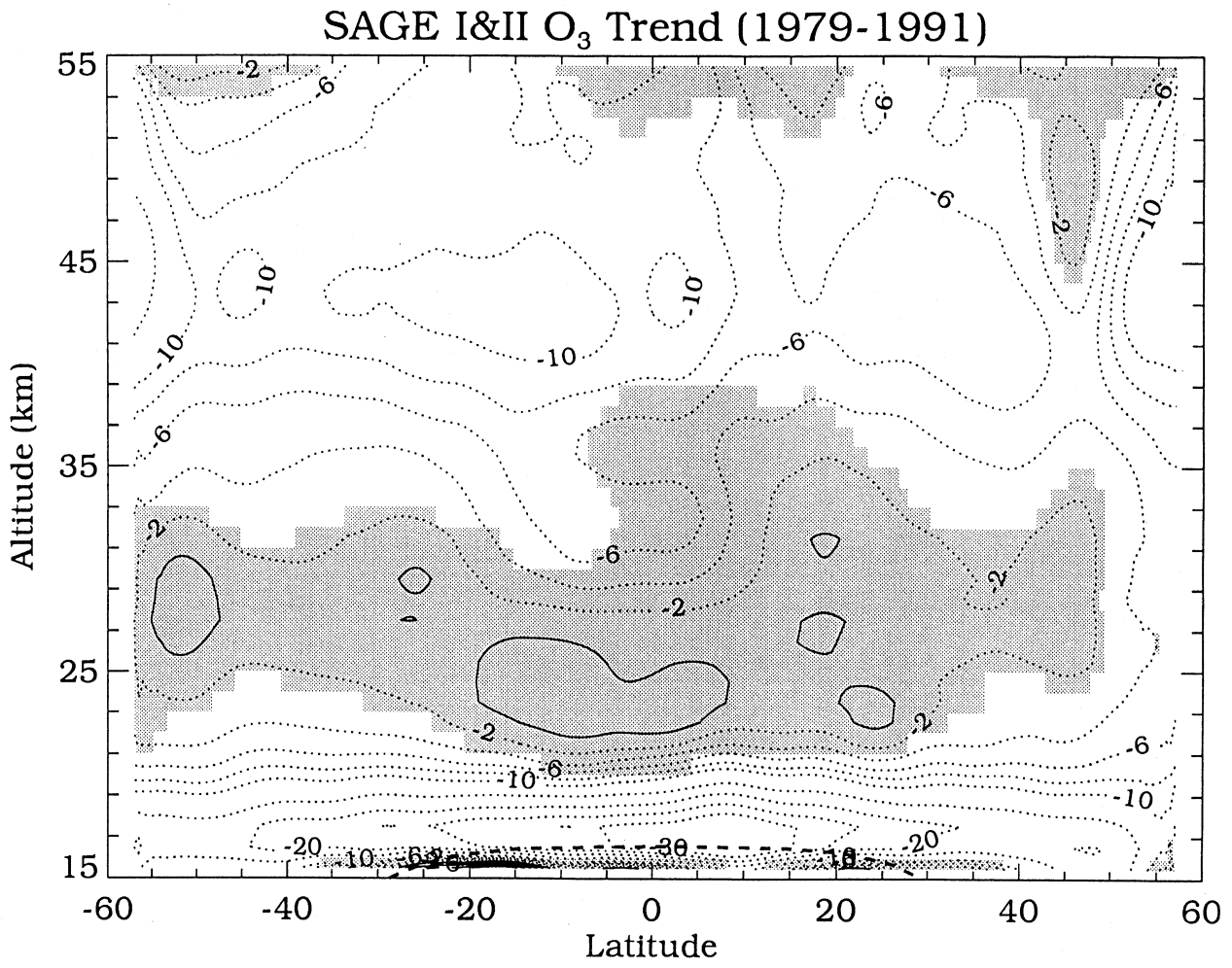

Figure 1-13. (b) Trends calculated for SAGE I/II for 1979-91. Hatched areas indicate trends calculated to be insignificant at the 95% confidence level. The dashed line indicates the tropopause. The altitudes of the SAGE I measurements have been adjusted by 300 meters.

In the tropics, only Natal (6°S) has an ozonesonde record longer than 10 years. The trend found by Logan at 70-90 mbar is -10 (± 15)%/decade. At Hilo, Hawaii (20°N), ozonesondes from 1982 to 1994 indicate insignificant trends of -12 ± 15% per decade near the tropopause (17-18 km) and -0.7 ± 6% per decade in the lower stratosphere at 20 km (Oltmans and Hofmann, 1994). Trends from both ozonesonde records are smaller than the calculated SAGE tropical trends, but the large uncertainties mean that the two trends are not inconsistent. In the Southern Hemisphere, the only long-running station outside Antarctica is at Melbourne, Australia, where a trend of about -10% per decade is observed in the lower stratosphere.

1.3.2.3 Trends in the Free Troposphere

Only ozonesonde data are available for ozone trend analyses in the free troposphere. As discussed in Section 1.3.1, the quality of the ozonesonde data in the troposphere is worse than in the stratosphere. The strong likelihood of regional differences in trends further confuses attempts to assess the consistency of a limited number of ozonesonde records. In the last report, ozone in the free troposphere at Payerne was shown to have

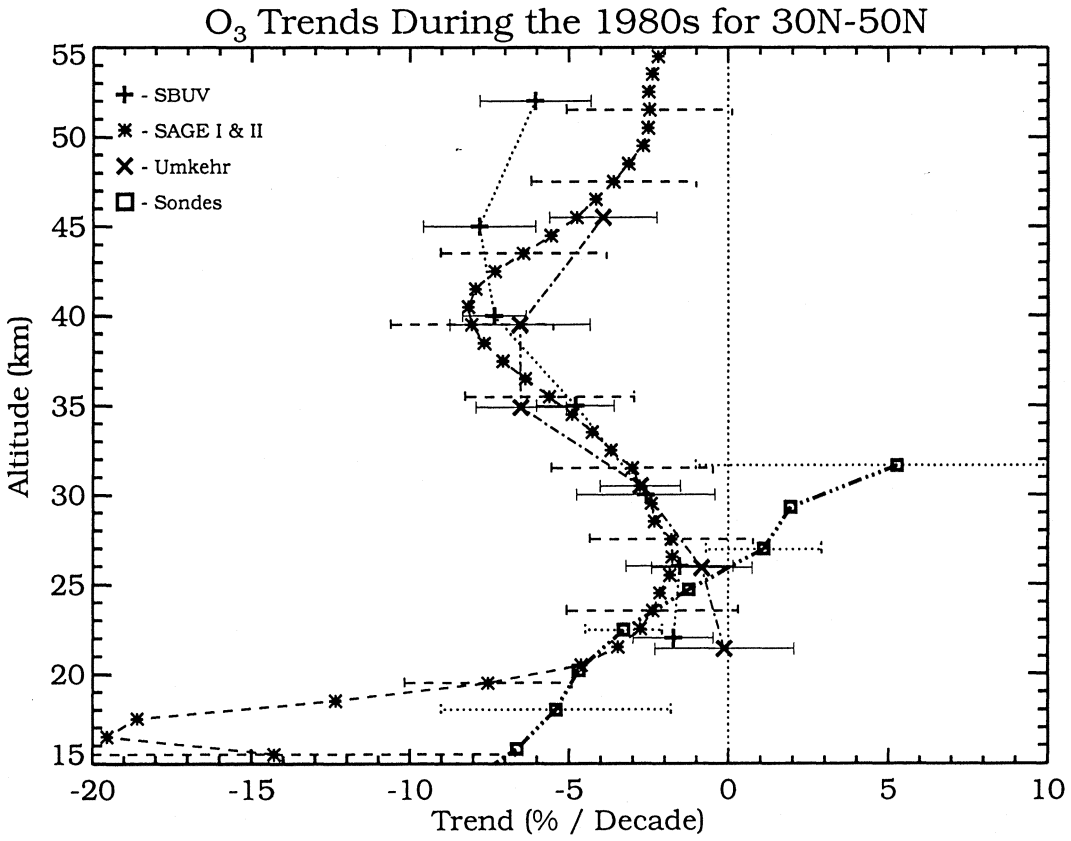

Figure 1-14. Comparison of trends in the vertical distribution of ozone during the 1980s. Ozonesonde and Umkehr trends are those from Miller *et al.* (1994). 95% confidence limits are shown.

increased by 30-50% since 1969. An assessment of data from several stations through 1986 was made (WMO, 1990b) that showed regional effects with increases at the European and Japanese stations. A tropospheric increase was also reported at Resolute (75°N), but decreases were found at the three midlatitude Canadian sites.

Since then, Logan (1994) and Miller *et al.* (1994) have analyzed the global ozonesonde record, paying particular attention to inhomogeneities in the data. A similar study by London and Liu (1992) did not account for instrumental changes at some sites. There is now evidence that the upward trend over Europe is smaller since about 1980 than before. The Hohenpeissenberg ozone measurements show no increase since the early to mid-1980s. The Payerne record shows a somewhat similar behavior until 1990. This conclusion is supported by the recent analyses of the Berlin/Lindenberg record (Furrer *et al.*, 1992, 1993) and of the Legionowo record (Lityńska and Kois, private communication). Furrer *et al.* found a large tropospheric trend from 1967-1988 of about +15%/decade, but this seems to have been at least partly caused by a jump in the measured ozone levels at the change of station in the early 1970s. Logan (1994) finds no significant trend at 500 mbar for 1980-1991 and points out that this trend is sensitive to changes in the correction factor over this period and could be negative. At Legionowo, an upper tropospheric trend of -10 (± 4.4)%/decade is reported for 1979-1993, a trend that is dominated by changes in spring.

Some of the trends, particularly those in Europe, might be influenced by changes in SO_2 levels. De Muer and De Backer (1994) have corrected the Uccle data set allowing for all known instrumental effects, including SO_2. The ozone trend in the upper troposphere was only slightly reduced (10-15%/decade, 1969-1991) and re-

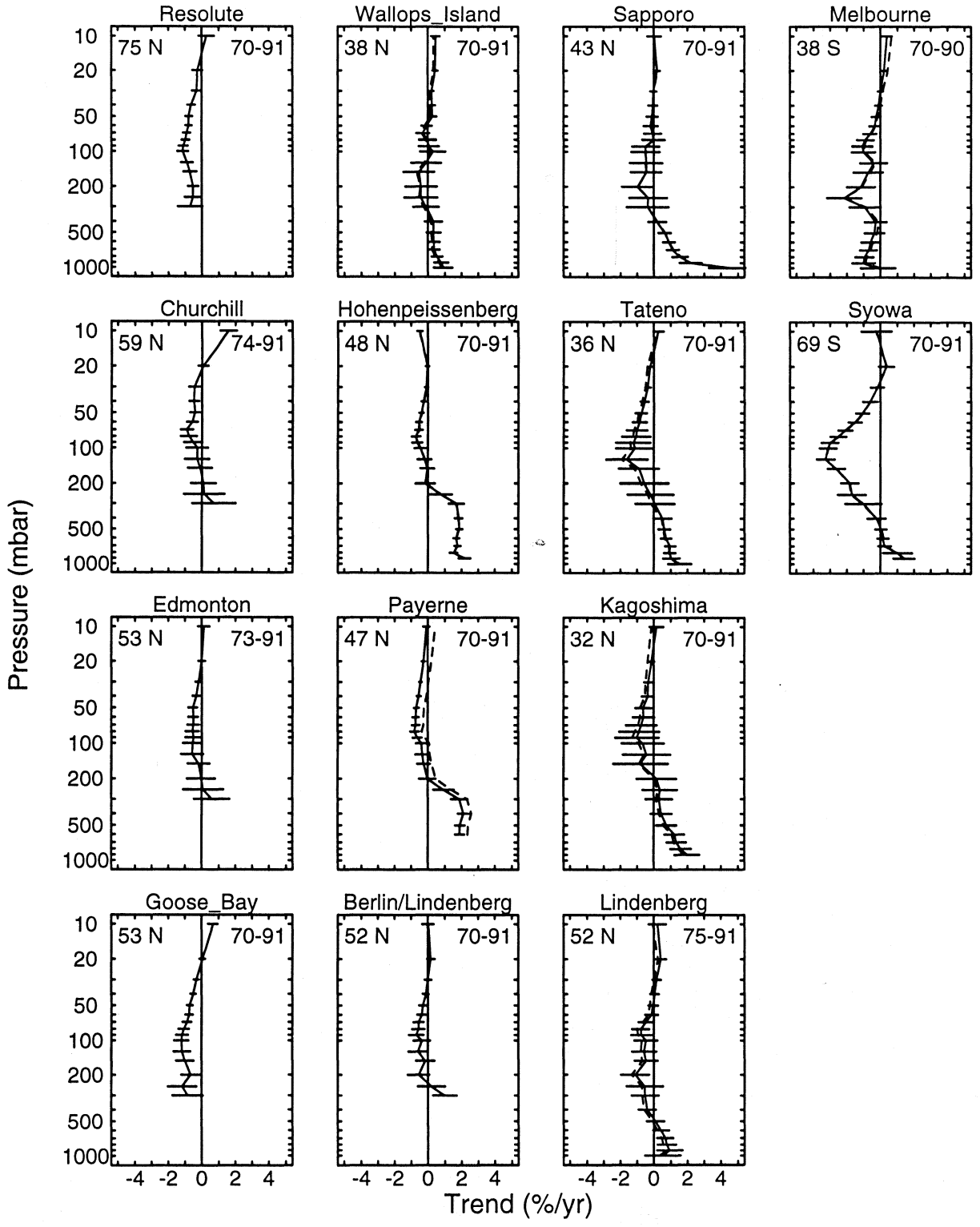

Figure 1-15. Trends for the periods shown in the ozonesonde measurements at different altitudes. 95% confidence limits are shown. (Adapted from Logan, 1994.)

mained statistically significant. However, below 5 km, the trend was reduced and became statistically insignificant, going from around +20%/decade to +10%/decade. Logan (1994) argues, using SO_2 emission figures and nearby surface measurements of ozone and SO_2, that measurements made at Hohenpeissenberg, Lindenberg, and possibly other European stations might be influenced by SO_2 and points out that any such effect would be largest in winter. In polluted areas, local titration of ozone by NO_x can also influence measurements of ozone at low altitude. However neither of these effects should have much influence except in the lower troposphere (<4 km).

Tropospheric ozone over Canada decreased between 1980 and 1993 at about -1 ± 0.5%/year (Tarasick *et al.*, 1994). The positive trend observed at Wallops Island has diminished and from 1980-1991 was close to zero (Logan, 1994). Prior to 1980 the situation is more confused. Wallops Island is the only station in North America with a homogeneous record from 1970 to 1991, and a trend of just under +10% per decade was observed (Figure 1-15). In two cases, the critical factor needed to deduce the long-term tropospheric ozone changes over North America is the ratio of the tropospheric ozone measured by BM and ECC sondes. First, the Canadian stations changed from BM to ECC sondes around 1980, and a conversion factor is needed if the two parts of the record are to be combined into one. Second, BM ozonesonde measurements were made at Boulder in 1963-1966 (Dütsch *et al.*, 1970), while ECC sondes have been used in the soundings made since 1985 (Oltmans *et al.*, 1989). Logan (1994) has compared the Boulder data by multiplying the BM data at 500 and 700 mbar by 1.15 and concluded that (a) no increase has occurred in the middle or upper troposphere, and (b) a 10-15% increase occurred in the lower troposphere caused by local pollution. The factor of 1.15 was based on a reanalysis of the intercomparisons in 1970, 1978, and 1984 (see Section 1.3.1.2d). Bojkov (1988; private communication) compared the concurrent measurements made by several hundred ECC sondes at Garmisch-Partenkirchen and BM sondes at Hohenpeissenberg, and concluded that the ratio should be between 1.04 and 1.12 depending on altitude. This approach would produce a larger change at Boulder in the lower troposphere and would indicate a small increase at 500 mbar. However, it is possible that the differences depend on the pre-launch procedures in use at the different sites, in which case no single factor can be used: this possibility is supported by the apparently different jumps seen at the changeovers at the four Canadian stations. Anyway, there is no sign that ozone concentrations over Boulder rose by the 50% observed at Hohenpeissenberg or Payerne since 1967; at most a 10-15% increase has occurred, similar to the increase observed at Wallops Island.

A reanalysis of the ozonesonde records from the three Japanese stations from 1969-1990 (Akimoto *et al.*, 1994) found annual trends of 25 ± 5%/decade and 12 ± 3%/decade for the 0-2 km and 2-5 km layers, respectively. Between 5-10 km the trend is 5 ± 6%/year. There is no evidence for a slowing of trends in the 1980s.

In the tropics, Logan (1994) reports that Natal shows an increase between 400 and 700 mbar, but which is only significant at 600 mbar. The Melbourne record shows a decrease in tropospheric ozone that is just significant between 600 and 800 mbar and is largest in summer.

1.3.2.4 Trends Inferred from Surface Observations

Some information about free tropospheric ozone is contained in measurements of ozone at the Earth's surface, although care has to be taken in the interpretation of these data as they are not directly representative of free tropospheric levels.

Ground-based measurements were made during the last century, mostly with the Schoenbein method (*e.g.* Anfossi *et al.*, 1991; Sandroni *et al.*, 1992; Marenco *et al.*, 1994), which is subject to interferences from wind speed (Fox, 1873) and humidity (Linvill *et al.*, 1980). Kley *et al.* (1988) concluded that these data are only semi-quantitative in nature and should not be used for trend estimates. Recent improvements in the analysis are still insufficient to allow simple interpretation of such data. A quantitative method was used continuously from 1876 until 1911 at the Observatoire de Montsouris, Paris (Albert-Levy, 1878; Bojkov, 1986; Volz and Kley, 1988). The average ozone concentration was around 10 ppbv, about a factor of 3-4 smaller than is found today in many areas of Europe and North America. However, the measurements at Montsouris were made close to the ground and, hence, are not representative of free tropospheric ozone concentrations during the last century.

Staehelin *et al.* (1994) reviewed occasional measurements by optical and chemical techniques at a num-

ber of European locations in the 1930s and measurements made at Arosa in the 1950s (Götz and Volz, 1951; Perl, 1965). Figure 1-16 shows a comparison of the ozone concentrations found in the 1930s and 1950s with measurements made at Arosa and other European locations in the late 1980s. On average, ozone concentrations in the troposphere over Europe (0-4 km) today seem to be a factor of two larger than in the earlier period. The Arosa data also suggest that the relative trends are largest in winter. The measurements in the 1950s were made by iodometry and are potentially biased low from SO_2 interferences caused by local sources, although Staehelin *et al.* (1994) argue that SO_2 at Arosa was probably less than a few ppbv.

Figure 1-16 also shows that, because of the variance between the different sites, little can be inferred about a possible increase in tropospheric ozone before 1950. In this context, it is interesting to note that the data from Montsouris (1876-1911; 40 m ASL) and those from Arosa (1950-1956; 1860 m ASL) do not show a single day with ozone concentrations above 40 ppb (Volz-Thomas, 1993; Staehelin *et al.*, 1994).

"Modern" ozone measurements, *e.g.*, using UV-absorption, were started in the 1970s at several remote coastal and high altitude sites (Scheel *et al.*, 1990, 1993; Kley *et al.*, 1994; Oltmans and Levy, 1994; Wege *et al.*, 1989). The records for Mauna Loa, Hawaii, and Zugspitze, Southern Germany, are shown in Figure 1-17. A summary of the trends observed at the remote sites is presented in Figure 1-18. All stations north of about 20°N exhibit a positive trend in ozone that is statistically significant. On the other hand, a statistically significant negative trend of about -7%/decade is observed at the South Pole. For the most part, the trends increase from -7%/decade at 90°S to +7%/decade at 70°N. Somewhat anomalous are the large positive trends observed at the high elevation sites in Southern Germany (10-20%/decade); these large trends presumably reflect a regional influence (Volz-Thomas, 1993). It must be noted, however, that the average positive trends observed at the high altitude sites of the Northern Hemisphere are largely due to the relatively rapid ozone increase that occurred in the seventies. If the measurements had started in the 1980s when the ozone concentrations tended to be at their peak (Figure 1-17), no significant ozone increase would have been found.

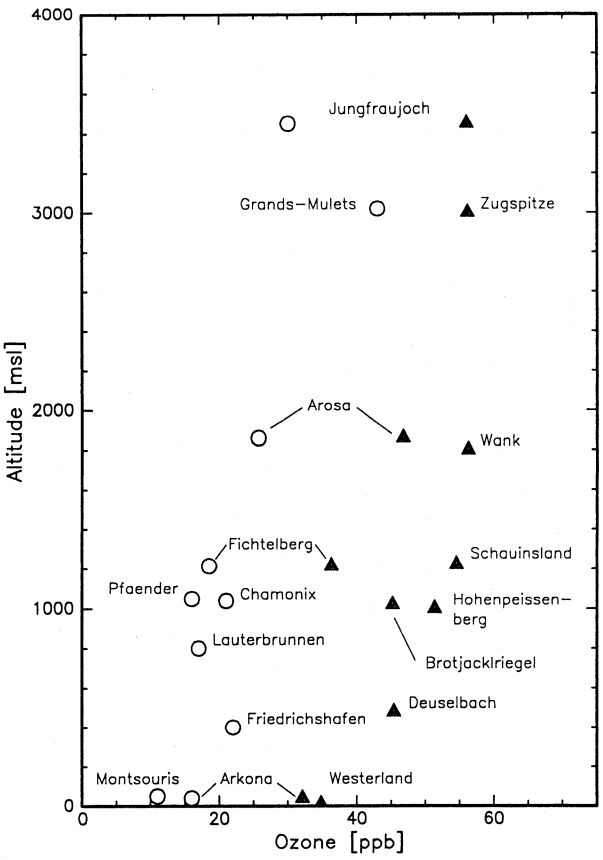

Figure 1-16. Measurements of surface ozone concentrations from different locations in Europe performed before the end of the 1950s (circles) and in recent years (1990-1991; triangles) during August and September, as function of altitude. (Reprinted from *Atmospheric Environment, 28,* Staehelin *et al.*, Trends in surface ozone concentrations at Arosa [Switzerland], 75-87, 1994, with kind permission from Elsevier Science Ltd., The Boulevard, Langford Lane, Kidlington OX5 1GB, UK.)

Unlike ozonesondes, and sites such as Mauna Loa and Zugspitze, where data are specifically identified as free tropospheric or otherwise (Oltmans and Levy, 1994; Sladkovic *et al.*, 1994), the ground-based instruments do not often sample free tropospheric air. However, the marine boundary layer sites like Samoa, Cape Point, and Barrow are representative of large geographical regions, and although the absolute concentrations may be different from those in the free troposphere, this fact should exhibit only a second-order influence on the trends.

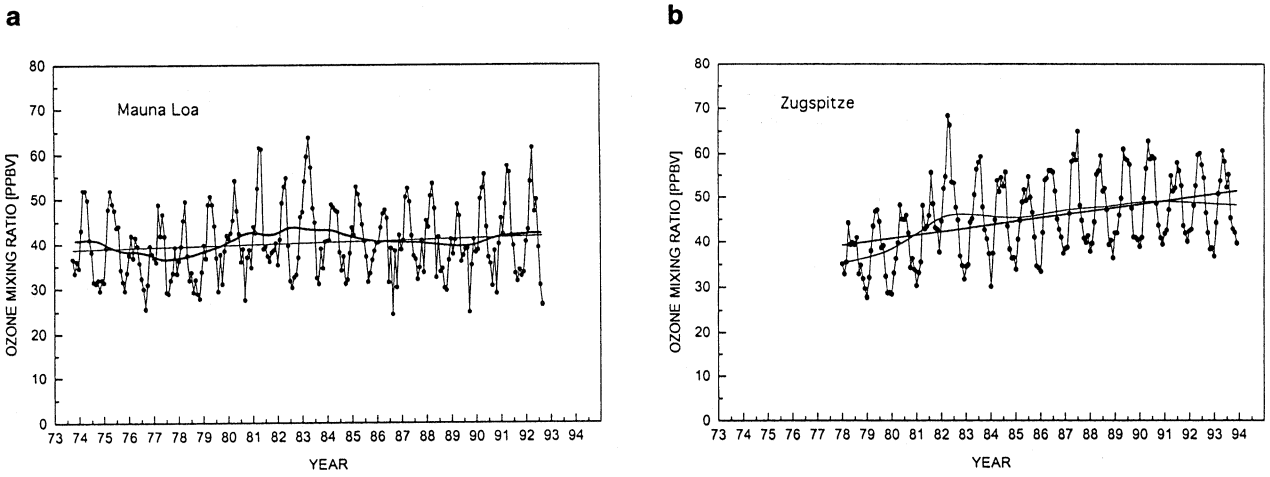

Figure 1-17. Surface ozone concentrations observed during the past two decades at Mauna Loa (Hawaii, 20°N, 3400m) (adapted from Oltmans and Levy, 1994) and Zugspitze (Germany, 47°N, 3000 m) (Sladkovic *et al.*, 1994).

Whether this is the case for Barrow is open to some question, as Jaffe (1991) has suggested it may be influenced by local ozone production associated with the nearby oil fields.

1.3.3 Discussion

The state of knowledge about the trends in the vertical distribution of ozone is not as good as that about the total ozone trends. The quality of the available data varies considerably with altitude.

The global decreases in total ozone are mainly due to decreases in the lower stratosphere, where the uncertainties in the available data sets are largest. SBUV and Umkehr measurements are most reliable around and above the ozone maximum. Information at lower altitudes is available from these techniques, but it is not clear at the present time whether much can be learned about trends in these regions. Ozonesondes make reliable measurements in the lower stratosphere, but the natural variability is such that the uncertainties associated with trends calculated for individual stations are large. Only in the northern midlatitudes do enough ozonesonde records exist for trends to be calculated with uncertainties smaller than 5%/decade. SAGE can measure ozone down to 15 km altitude. Two factors complicate the SAGE measurement below 20 km: (i) ozone concentrations are smaller than at the maximum,

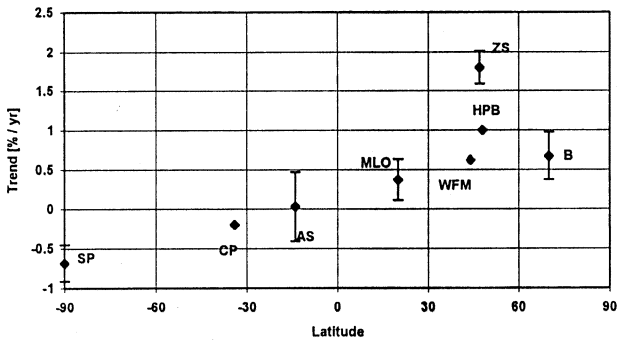

Figure 1-18. Trends in tropospheric ozone observed at different latitudes, including only coastal and high-altitude sites (after Volz-Thomas, 1993). CP: Cape Point, 34°S (Scheel *et al.*, 1990); SP: South Pole, 90°S, 2800m ASL; AS: American Samoa, 14°S; MLO: Mauna Loa, 20°N, 3400m; B: Barrow, 70°N (Oltmans and Levy, 1994); WFM: Whiteface Mountain, 43°N, 1600m (Kley *et al.*, 1994); ZS: Zugspitze, 47°N, 3000m; HPB: Hohenpeissenberg, 48°N, 1000m (Wege *et al.*, 1989).

so that the signal is lower; and (ii) the amount of aerosol is greater, so that there is an additional interference. These are well recognized difficulties for which allowance is made in the calculation of the ozone amount.

At altitudes of 35-45 km, there is reasonable agreement between SAGE I/II, SBUV(/2), and Umkehr

that, during 1979-1991, ozone declined 5-10% per decade at 30-50°N and slightly more at southern midlatitudes. In the tropics, SAGE I/II gives larger trends (ca. -10% per decade) than SBUV (ca. -5% per decade) at these altitudes.

At altitudes between 25 and 30 km, there is reasonable agreement between SAGE I/II, SBUV(/2), Umkehr, and ozonesondes that, during the 1979-1991 period, there was no significant ozone depletion at any latitude. The agreement continues down to about 20 km, where statistically significant reductions of 7 ± 4% per decade were observed between 30 and 50°N by both ozonesondes and SAGE I/II. Over the longer period from 1968 to 1991, the ozonesonde record indicates a trend of -4 ± 2% per decade at 20 km at northern midlatitudes.

There appear to have been sizeable ozone reductions during the 1979-1991 period in the 15-20 km region in midlatitudes. There is disagreement on the magnitude of the reduction, with SAGE indicating trends as large as -20 ± 8% per decade at 16-17 km and the ozonesondes indicating an average trend of -7 ± 3% per decade in the Northern Hemisphere. The trend in the integrated ozone column for SAGE is larger than those found from SBUV, TOMS, and the ground-based network, but the uncertainties are too large to evaluate the consistency between the data sets properly. Over the longer period from 1968 to 1991, the ozonesonde record indicates a trend of -7 ± 3% per decade at 16 km at northern midlatitudes.

In the tropics, trend determination at altitudes between 15 and 20 km is made difficult by the small ozone amounts. In addition, the large vertical ozone gradients make the trends very sensitive to small vertical displacements of the profile. The SAGE I/II record indicates large (-20 to -30% (±18%) per decade) trends in the 16-17 km region (-10% ±8% at 20 km). Limited tropical ozonesonde data sets at Natal, 6°S and Hilo, 20°N do not indicate significant trends between 16 and 17 km or at any other altitude for this time period. With currently available information it is difficult to evaluate the trends below 20 km in the tropics, as the related uncertainties are large. The effect on the trend in the total column from any changes at these altitudes would be small.

In the free troposphere, only limited data (all from ozonesondes) are available for trend determination. In the Northern Hemisphere, trends are highly variable between regions. Upward trends in the 1970s over Europe have declined significantly in the 1980s, have been small or non-existent over North America, and continue upward over Japan. The determination of the size of the change over North America requires a proper treatment of the relative tropospheric sensitivities for the type of sondes used during different time periods.

Surface measurements indicate that ozone levels at the surface in Europe have doubled since the 1950s. Over the last two decades there has been a downward trend at the South Pole and positive trends are observed at high altitude sites in the Northern Hemisphere. When considering the latter conclusion, the regional nature of trends in the Northern Hemisphere must be borne in mind.

1.4 OZONE AND AEROSOL SINCE 1991

Since the last report, record low ozone values have been observed. This section describes the ozone measurements in this period to allow the updated trends given in Section 1.2.2 to be put into perspective. There is also a brief discussion of a variety of possible causes, including the aftermath of the eruption of Mt. Pinatubo, aspects of which will be discussed at greater length in later chapters.

1.4.1 Total Ozone Anomalies

Figure 1-19(a) shows the daily global average (50°N-50°S) ozone amount during 1992-1994, together with the envelope of 1979-1990 observations. Persistent low ozone levels are observed beginning in late 1991 (not shown), with values completely below the 1979-1990 envelope from March 1992–January 1994. During 1993 total ozone was about 10-20 DU (3-6%) below the 1980s average. Total ozone in early 1994 recovered somewhat and was at the bottom end of the range observed in the 1980s.

Figure 1-19(b)-(d) shows similar plots for the latitude bands 30-50°S, 20°S-20°N, and 30-50°N. The largest and longest-lived anomalies are seen at the northern midlatitudes (15-50 DU lower in 1993), with 1980s values reached again in January 1994. Ground-based measurements made at sites with long records show that the anomalies in the northern midlatitudes were the largest since measurements began, and that values in early

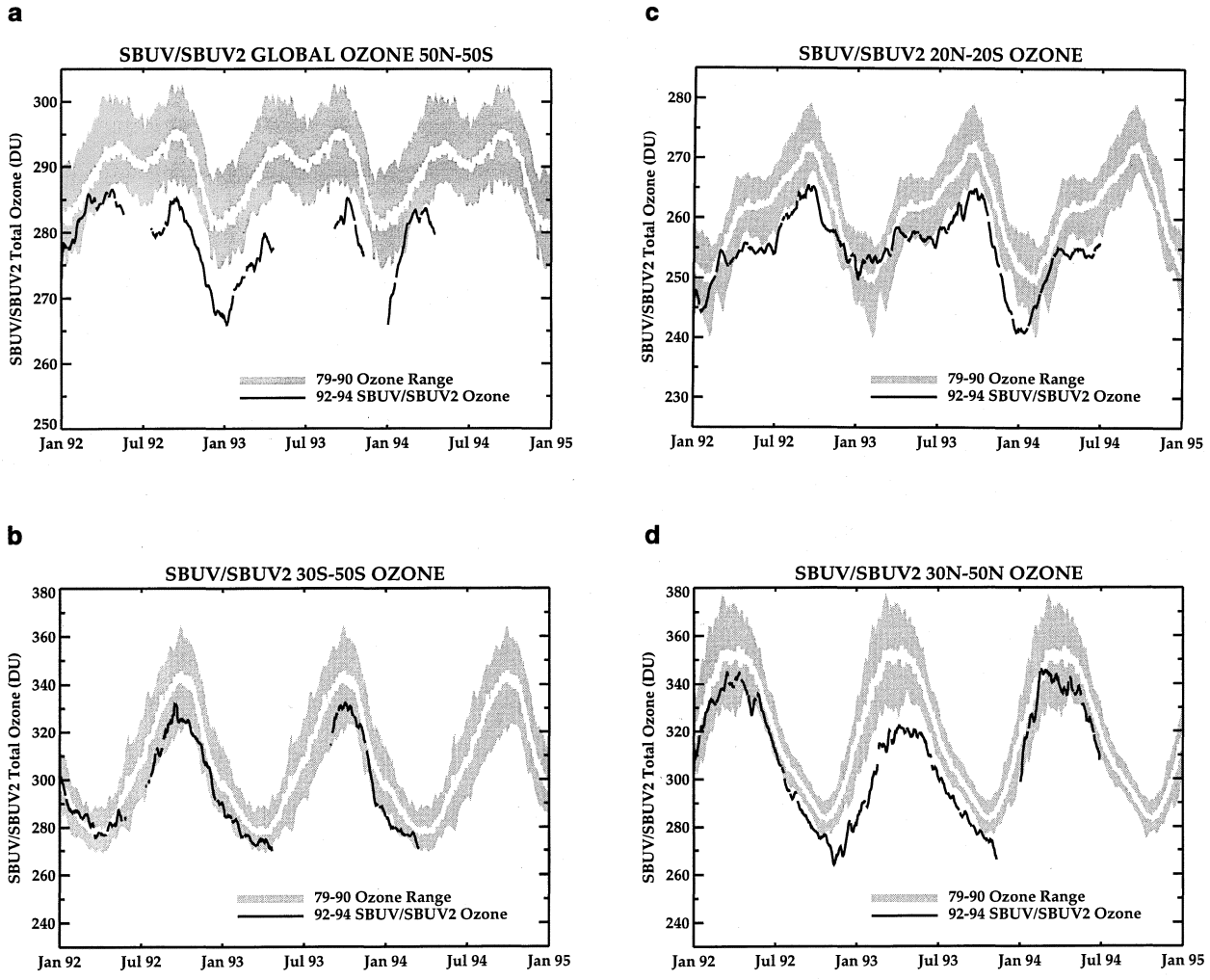

Figure 1-19. Total ozone measured by SBUV and SBUV(/2) since January 1992 compared with the 1980s range and average: (a) 50°N-50°S, Global ozone; (b) 30°-50°S; (c) 20°N-20°S; (d) 30°-50°N.

1993 were about 15% lower than the average values observed before 1970 (Bojkov *et al.*, 1993; Kerr *et al.*, 1993; Komhyr *et al.*, 1994a). The largest ozone losses occurred at higher latitudes in early 1993; deviations were in excess of 60 DU (15% lower than the 1980s mean). Total ozone values over North America in 1994 were in line with the long-term decline, but no longer below it (Hofmann, 1994).

In southern midlatitudes, total ozone values during 1993 were about 15-20 DU below the 1980s mean and were close to the low end of the 1980s range. In the tropics, the maximum negative anomaly was about 10 DU, and from late 1992 to early 1993 total ozone was slightly higher than the 1980s average. Locally, larger anomalies were seen, with negative ozone anomalies of about 15 DU (6%) occurring near the equator in September-November 1991 and in the southern tropics in mid-1992.

The solar cycle and the quasi-biennial oscillation (QBO) affect total ozone levels by a few percent and it is thus useful to remove these influences. Figure 1-20(a) shows the 60°S-60°N average total ozone from SBUV(/2) after these effects (and the annual cycle) have been removed by the statistical analysis described in Section 1.2.2. The most obvious remaining feature is the long-term decrease in total ozone, which has been fitted with a

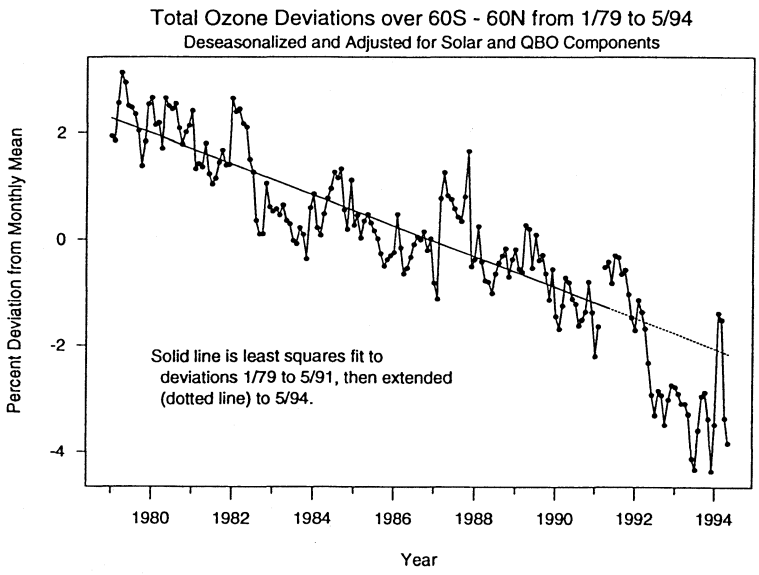

Figure 1-20. (a) Total ozone (60°N-60°S) from 1/79 to 5/94 measured by SBUV(/2). The annual cycle and the effects of the solar cycle and QBO have been removed. The solid line shown is a simple least squares fit to the data through 5/91. The dashed line is an extrapolation through 5/94.

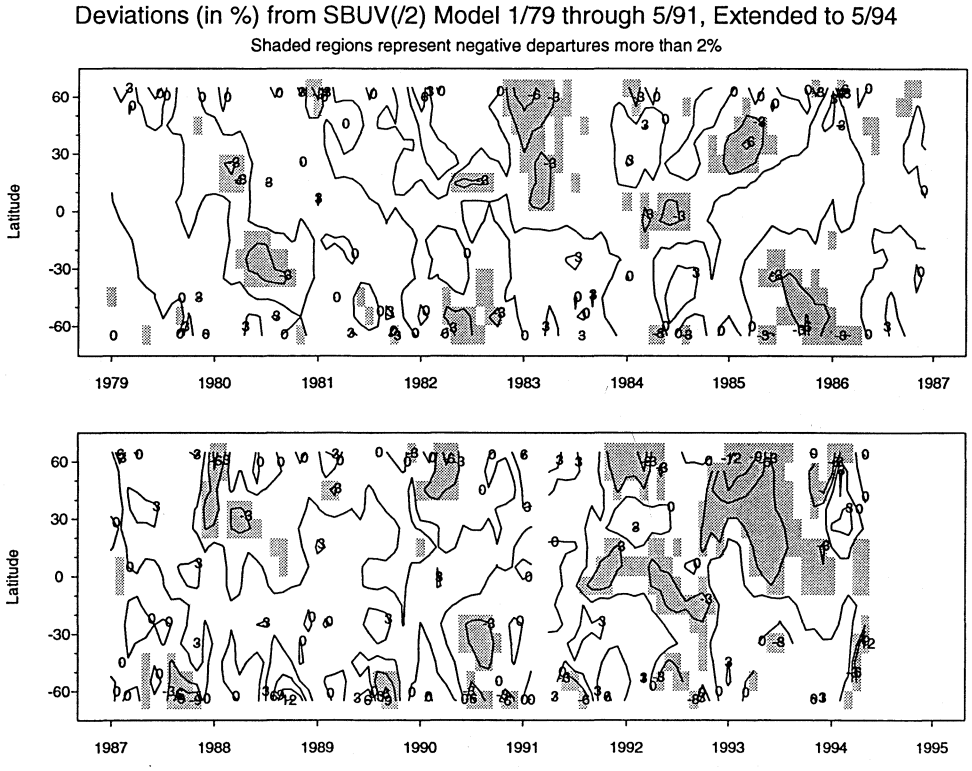

Figure 1-20. (b) Contour plots of total ozone residuals as a function of latitude and time from the statistical fit to the SBUV(/2) satellite data over the period 1/79 to 5/91. The fitted model was extrapolated through 5/94 to calculate the residuals over the extended period 1/79-5/94. The total ozone data have the seasonal, trend, solar, and QBO components removed, and the resulting deviations are expressed as percentages of the mean ozone level at the beginning of the series. Shown are contours of constant deviations at intervals of 3%, and the shaded areas indicate negative departures of at least 2%. The 1992-1993 low ozone values are prominent, as well as other periods of very low values in 1982-1983 and 1985.

linear trend (-2.9% per decade) from January 1979 to May 1991 (pre-Pinatubo). The recent (1992-1993) global anomaly is about 2% below the trend line and about 1% less than previous negative anomalies. The 1992-1993 anomaly also stands out as the most persistent, spanning nearly 2 years. The only other negative anomaly lasting more than one year followed the El Chichón eruption in 1982. Figure 1-20(b) shows the time evolution at all latitudes (60°S-60°N) of the total ozone deviations found after the removal of the trend found for 1/79 to 5/91 (extrapolated to 5/94), the annual cycle, and the effects of the solar cycle and the QBO. The strong regional nature of the deviations is again obvious, with the largest (6-10%) occurring in northern midlatitudes in January to April 1993. The Southern Hemisphere, by contrast, was hardly affected.

1.4.2 Vertical Profile Information

Figure 1-21(a) shows the ozonesonde measurements at Edmonton made in January-April in 1980/1982, 1988/1991, and 1993 (Kerr *et al.*, 1993). Similar results were found at Resolute, Goose Bay, and Churchill. These indicate that the decrease in early 1993 occurred in the same altitude region as the decline during the 1980s. The standard deviations are ±8 nbar (1980-1982 and 1988-1991 profiles) and ±9 nbar (1993 profiles) where the maximum ozone difference is found (100 mbar). The differences between the 1993 and 1980-1982 profiles are statistically significant (2 standard deviations) between 200 and 40 mbar. Ozone levels were depleted by about 25% over approximately 14-23 km (at and below the profile maximum), spatially coincident with the observed aerosol maximum, as shown in Figure 1-21(b) (Hofmann *et al.*, 1994a). Notably, there is substantial ozone increase above the profile maximum (above 25 km) at Boulder, of about 15% of background levels, which is also seen at Hilo, Hawaii (Hofmann *et al.*, 1993).

1.4.3 Stratospheric Aerosol after the Eruption of Mt. Pinatubo

The eruption in the Philippines of Mt. Pinatubo (15°N, 120°E) in June 1991 injected approximately 20 Tg of sulfur dioxide (SO_2) directly into the lower stratosphere at altitudes as high as 30 km. Within a month or so, this SO_2 was oxidized to sulfuric acid, which rapidly condensed as aerosol. In August 1991, Volcán Hudson (46°S, 73°W) erupted and deposited about 2 Tg of SO_2 into the lower stratosphere, mostly below 14 km. Several studies of the SO_2 and aerosol observations have been published (*e.g.*, Bluth *et al.*, 1992; Lambert *et al.*, 1993; Read *et al.*, 1993; Trepte *et al.*, 1993; Deshler *et al.*, 1993; Hofmann *et al.*, 1994b), which are now briefly discussed. The latitudinal variation of optical depth from 1991 to 1994 is shown in Figure 1-22 as measured by SAGE II and the Stratospheric Aerosol Measurement (SAM II) instrument.

The initial aerosol cloud from Mt. Pinatubo dispersed zonally but was confined mostly within the tropics below 30 km for the first several months. By September 1991 the Mt. Pinatubo aerosol had moved into the midlatitude Southern Hemisphere at altitudes between 15 and 30 km. It did not enter into the Antarctic vortex in 1991, unlike the aerosol from Volcán Hudson, which was observed at altitudes of 10-13 km over McMurdo station, 78°S (Deshler *et al.*, 1992). In the tropics the Mt. Pinatubo plume rose to altitudes of 30 km during December 1991-March 1992. Strong dispersal from the tropics into northern middle-high latitudes was observed during the 1991-1992 winter, and enhanced aerosol levels have been detected over 15-25 km in the Northern Hemisphere since that time.

The total mass of the stratospheric aerosol maximized several months after the eruption at about 30 Tg and thereafter remained fairly constant until mid-1992, since when it has been declining with an approximate e-folding time of one year. The total aerosol loading in January 1994 was about 5 Tg, still 5-10 times higher than the background levels observed before the Mt. Pinatubo eruption.

The size distribution of the aerosol particles evolved significantly over time, increasing in effective radius from approximately 0.2 μm just after the eruption to a peak of some 0.6-0.8 μm a year or so later, since when it has slowly decreased (Deshler *et al.*, 1993). At northern midlatitudes, the aerosol surface area peaked at about 40 $\mu m^2\ cm^{-3}$ (Figure 1-23). The altitude of the maximum surface area has episodically decreased since early 1992.

Negative total ozone anomalies of about 15 DU, 6%, occurred near the equator in September-November 1991 (Schoeberl *et al.*, 1993; Chandra, 1993), at the same time that the maximum temperature increase,

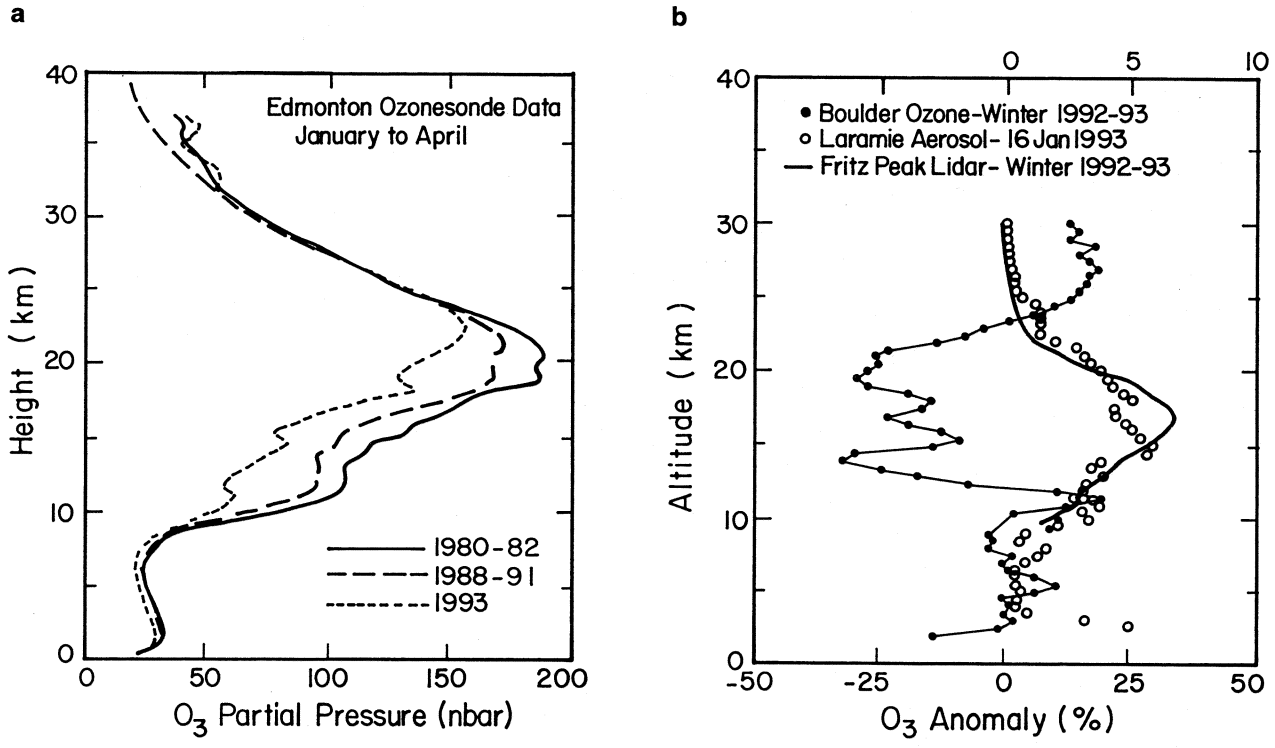

Figure 1-21. (a) Average ozone profiles found from ozonesonde measurements at Edmonton in spring (January to April) for 1980-1982 (46 sondes), 1988-1991 (42 sondes), and 1993 (13 sondes). Adapted from Kerr *et al.*, 1993. (b) Percentage differences (bottom axis) in the ozonesonde measurements at Boulder in 1992-1993 relative to 1985-1989. Also shown are the aerosol data from the Fritz Peak lidar (bottom axis: backscatter in 10^8 ST^{-1} m^{-1}) and the University of Wyoming particle counter (top axis: aerosol concentration in cm^{-3}) for winter 1992-1993. Adapted from Hofmann *et al.*, 1994a.

about 2-3K at 30-50 mbar, was observed (Labitske and McCormick, 1992). These early tropical ozone anomalies are probably related to enhanced vertical motions induced by the aerosol heating (Brasseur and Granier, 1992; Young *et al.*, 1994), but gas phase perturbations to the gas phase photochemistry by the initially high concentrations of SO_2 may also have played a part (Bekki *et al.*, 1993).

In addition to radiative and dynamical influences, the Mt. Pinatubo aerosol provides a surface on which chemical reactions can occur, possibly leading to chemical ozone loss, as discussed in Chapters 3 and 4. These reactions tend to proceed faster at lower temperatures and the ozone depletion process is more effective at low light levels. In this context it is worth noting that both the 1991/1992 and 1992/1993 northern winters were cold with later-than-average final warmings (*e.g.*, Naujokat *et al.*, 1993), and that the cold temperatures occurred both within and on the edge of the Arctic vortex, so that there was the opportunity for large areas to be affected.

For comparison, the maximum aerosol surface area and its peak altitude following the eruption of El Chichón in early 1982 are shown in Figure 1-23. The Mt. Pinatubo eruption provided twice the aerosol surface area as that from El Chichón. The total ozone anomalies in 1982/1983 (as compared with 1980, 1981, 1985, 1986 TOMS values) are now thought to have been smaller than the earlier initial estimates, about 3-4% in the 1982/1983 winter rather than 10% (Stolarski and Krueger, 1988).

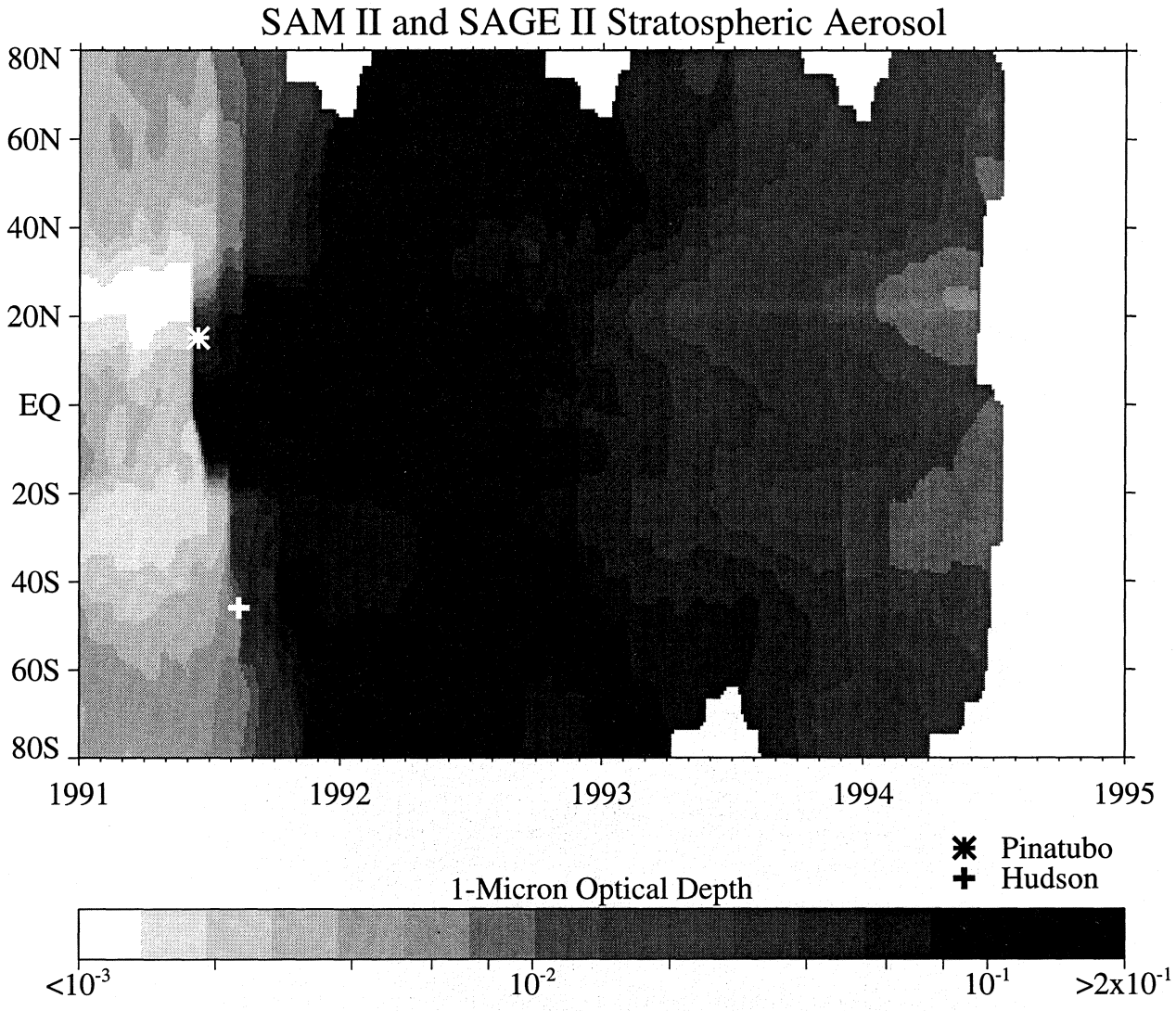

Figure 1-22. Aerosol optical depths from 1991-1994 measured by SAM II and SAGE II showing the effects of the Mt. Pinatubo (*) and Volcán Hudson (+) volcanic eruptions. (Updated by L. Thomason from data shown in Trepte *et al.*, 1993.)

1.4.4 Dynamical Influences

Natural variations in ozone are induced by meteorological phenomena such as the El Niño-Southern Oscillation (ENSO), in addition to the QBO (*e.g.*, Zerefos, 1983; Bojkov, 1987; Komhyr *et al.*, 1991; Zerefos *et al.*, 1992). Thus the observed ozone anomalies since 1991 will have been affected to some degree by the prolonged El Niño event that lasted throughout 1992/1993. The amplitude of the El Niño effect in total ozone is 2-6%, but such anomalies are highly localized. While ENSO effects for zonal or large-area means were about 1%, ozone in specific areas may have been reduced by an additional 2-3% in 1992-1993 (Zerefos *et al.*, 1992; Shiotani, 1992; Zerefos *et al.*, 1994; Randel and Cobb, 1994). Other dynamical influences can strongly affect total ozone on a regional basis; one clear example was the persistent blocking anti-cyclone in the northeast Atlantic from December 1991 to February 1992 (Farman *et al.*, 1994).

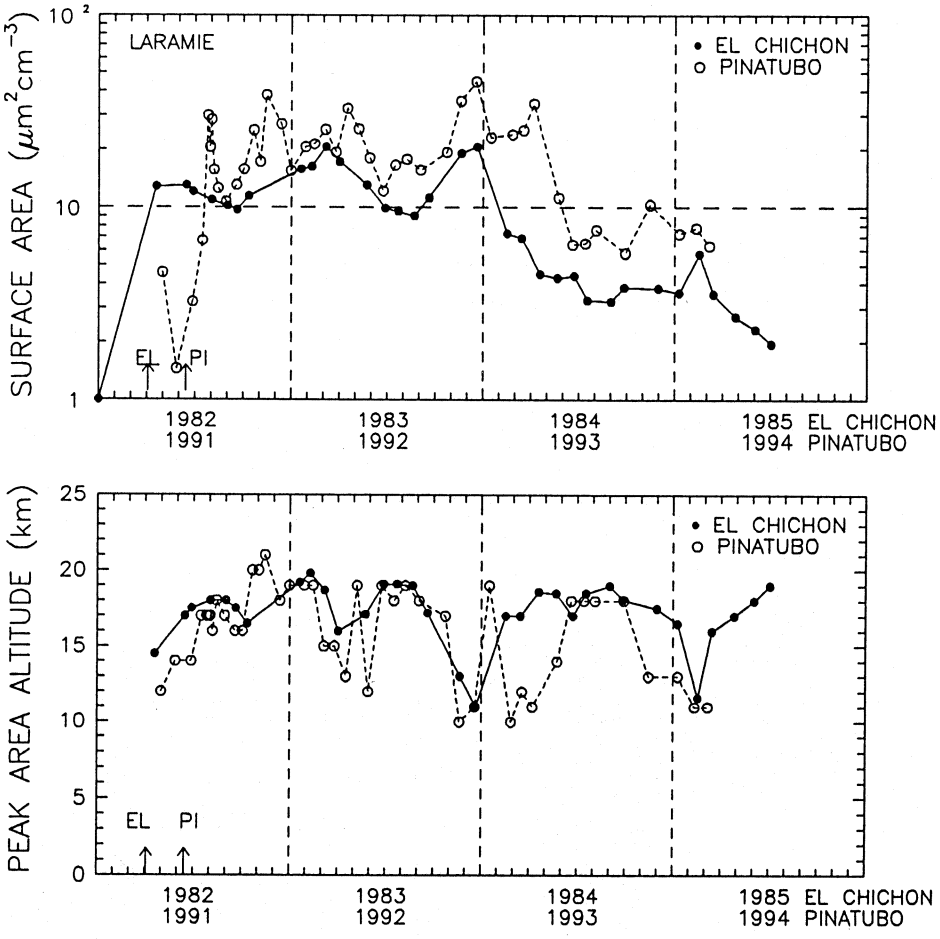

Figure 1-23. The maximum surface area and its altitude observed at Laramie, Wyoming, in the years following the El Chichón and Mt. Pinatubo eruptions (Deshler *et al.*, 1993).

1.5 ANTARCTIC OZONE DEPLETION

1.5.1 Introduction and Historical Data

Total ozone records obtained with Dobson spectrophotometers with a traceable calibration are available for Antarctica from 1957 at the British stations Halley (76°S, formerly Halley Bay) and Faraday (65°S, formerly Argentine Islands). They are available from the American station at the South Pole (Amundsen-Scott, 90°S) since 1962 and at the Japanese station Syowa (69°S) since 1966, although measurements had been obtained at Syowa in 1961. Figure 1-24 shows October monthly means for these four stations. In the case of the South Pole station, the average is for October 15-31 since inadequate sunlight precludes accurate total ozone measurements from the surface before about October 12.

Halley and Amundsen-Scott show similar long-term total ozone declines in October, presumably reflecting the fact that the region of most severe ozone depletion is generally shifted off the pole towards east Antarctica. The decline in ozone above these stations began in the late 1960s, accelerated around 1980, and after 1985 remained relatively constant at a total ozone value of about 160 DU. In 1993, record low values (about 116 DU) were recorded at Halley and Amundsen-Scott.

The decline in total ozone at Faraday and Syowa in October was more subtle, if existent at all, prior to 1980. The major decline occurred between 1980 and 1985, lev-

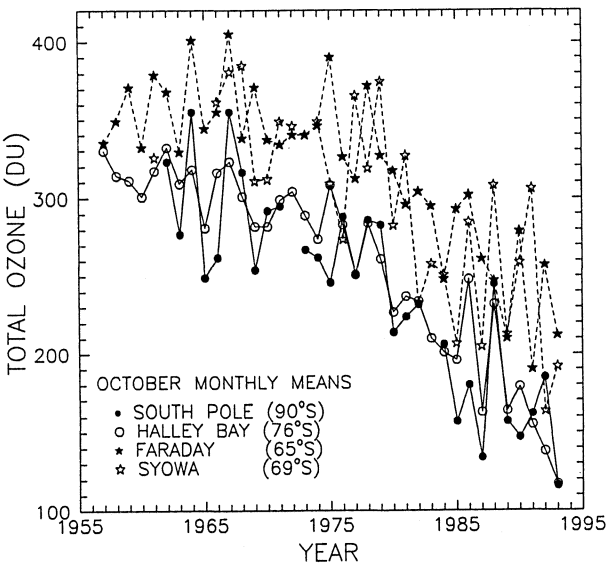

Figure 1-24. The historical springtime total ozone record for Antarctica as measured by Dobson spectrophotometers during October at Halley Bay, Syowa, and Faraday and from 15-31 October at South Pole. (Data courtesy J. Shanklin, T. Ito, and D. Hofmann.)

elling off with a value of total ozone of about 260 DU thereafter. An unusually low value of about 160 DU was observed at Syowa in 1992, a feature not seen at Faraday.

Although the earliest ozone vertical profiles showing the 1980 rapid ozone hole onset were obtained at Syowa in 1983 (Chubachi, 1984), the most extensive set of ozone profile data for trend studies has been obtained at the South Pole using ECC ozonesondes throughout (Oltmans *et al.*, 1994). This data set includes the approximately 500 year-round profiles measured between 1986 and 1993, and a series of about 85 profiles made between 1967 and 1971. Winter data for the earlier period do not extend to as high an altitude because rubber balloons were used. Figure 1-25 shows a comparison of smoothed monthly average ozone mixing ratio values at pressure levels 400 hPa (~6.5 km), 200 hPa (~10.5 km), 100 hPa (~14.5 km), 70 hPa (~16.5 km), 40 hPa (~19.5 km) and 25 hPa (~22.5 km) for these two periods. The major springtime ozone depletion has occurred in the 14-22 km region at the South Pole between the 1967-1971 and 1986-1991 periods, and it has worsened since 1992. The 1967-1971 data indicate a weak minimum in the spring in the 40-100 hPa (14-19 km) region. This feature might result from heterogeneous ozone loss related to considerably lower stratospheric chlorine levels, consistent with the weak downward trend in total ozone at South Pole for this period shown in Figure 1-24. In 1992 and 1993, ozone was almost completely destroyed in the 70-100 hPa range (14-17 km).

Summer (December to February) ozone levels in 1986-1991 are lower in the 70-200 hPa (10-17 km) region than they were in 1967-1971. The ozone that is transported to the South Pole following vortex breakdown at these altitudes now replenishes the ozone lost during the previous spring, rather than causing the marked late spring maximum which existed in 1967-1971. At all altitudes, ozone values from March to August are similar (to within about 10%) in the two periods.

Rigaud and Leroy (1990) reanalyzed measurements taken at Dumont d'Urville (67°S) in 1958 using a double monochromator with spectrographic plates (Fabry and Buisson, 1930; Chalonge and Vassey, 1934). They calculated some very low total ozone values (as low as 110 DU) that are only observed nowadays in the ozone hole. De Muer (1990) and Newman (1994) have examined the available 1958 meteorological and total ozone data. They find that the early Dumont d'Urville data are inconsistent with any other source of data from 1958: (a) the variability was greater throughout the year than that measured with any Dobson spectrophotometer in Antarctica that year (Figure 1-24); (b) Dumont d'Urville was not under the vortex that year (see also Alt *et al.*, 1959), but under the warm belt where ozone values are high; and (c) while the climatologies of measurements taken by Dobson instruments that year are fully consistent with those derived from TOMS measurements in the last decade, there is little or no consistency between the TOMS climatologies and that from Dumont d'Urville in 1958. Some doubts concerning a number of experimental aspects of the spectrographic plate instrument are also raised. These reported values thus appear to be a good example of being able to detect ozone without necessarily being able to measure it well.

1.5.2 Recent Observations

Figure 1-26 shows monthly average total column ozone measured at the South Pole by balloon-borne

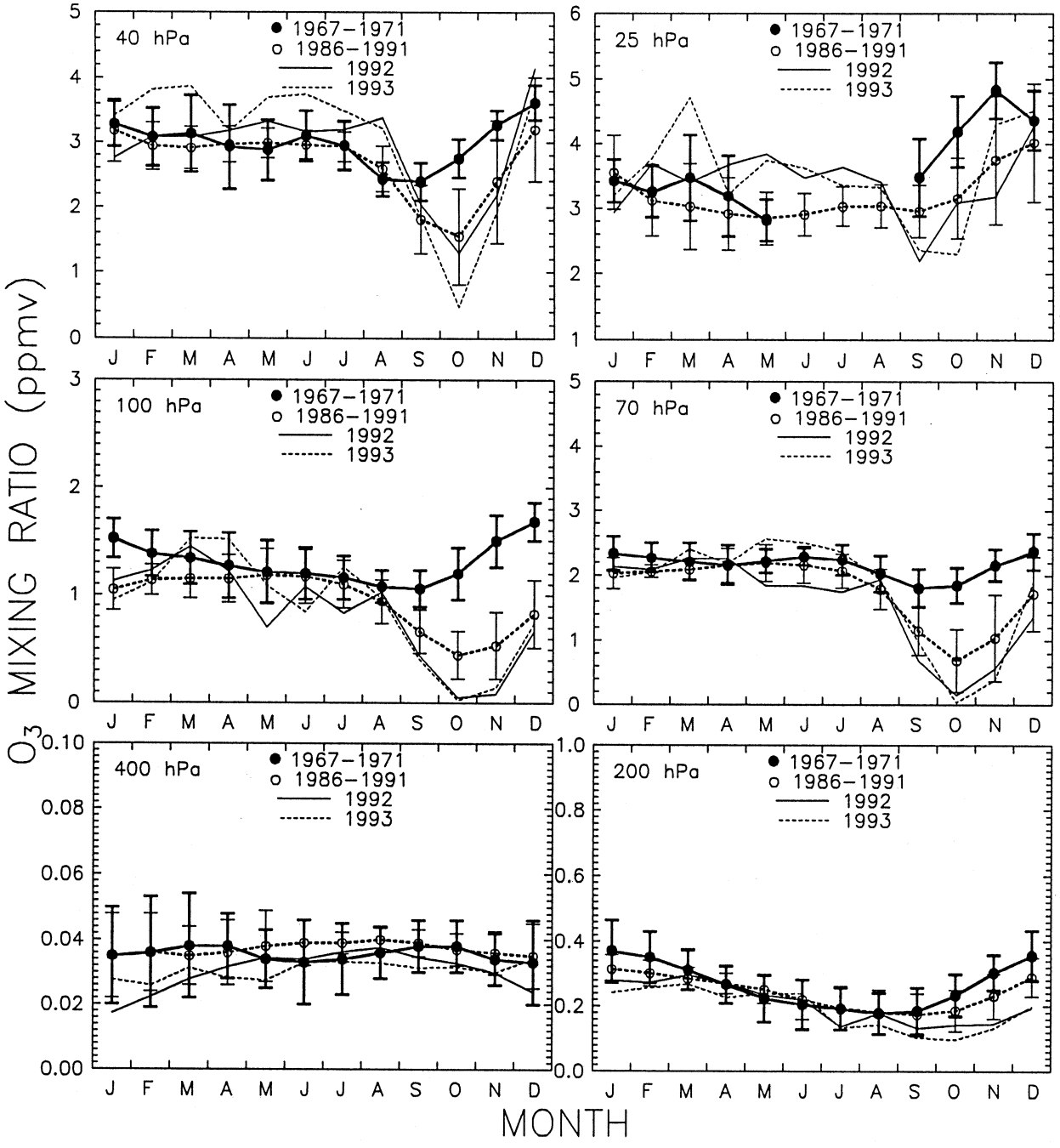

Figure 1-25. Comparison of smoothed monthly average ozone mixing ratios at 6 pressure levels for the 1967-1971 period (filled points and full lines), the 1986-1991 period (open points and dashed lines), and for 1992 and 1993 (straight and dashed lines, respectively). The error bars represent ±1 standard deviation. (Adapted from Oltmans *et al.*, 1994.)

ozonesondes since 1986 (Hofmann *et al.*, 1994b). (Total ozone is obtained by assuming that the ozone mixing ratio is constant above the highest altitude attained, a procedure that has an estimated uncertainty of about 2-3 DU.) These data are independent of the Dobson spectrophotometer data shown in Figure 1-24 and corroborate the fact that the major springtime depletion started between the 1967-1971 and 1986-1991 periods.

On 12 October 1993, total ozone at the South Pole fell to a new low of 91 DU, well below the previous low of 105 DU measured there in October 1992. Sub-100 DU readings were observed on 4 occasions and readings in the 90-105 DU range were measured on 8 consecutive soundings from 25 September to 18 October 1993.

Ozone levels in austral winter prior to the depletion period show no systematic variation, with values of 250 ± 30 DU. Similarly, coming out of the depletion period, January values show no systematic variation since 1986, but are lower than the 1967-1971 values.

At the South Pole, both Dobson spectrophotometer and Meteor TOMS measurements showed record low total ozone levels after the return of adequate sunlight in mid-October. Similarly, NOAA-11 SBUV2 measurements indicate new record lows for the 70°S-80°S region in 1993 (NOAA, 1993). Thus, since 1991, the September total ozone decline has continued/worsened.

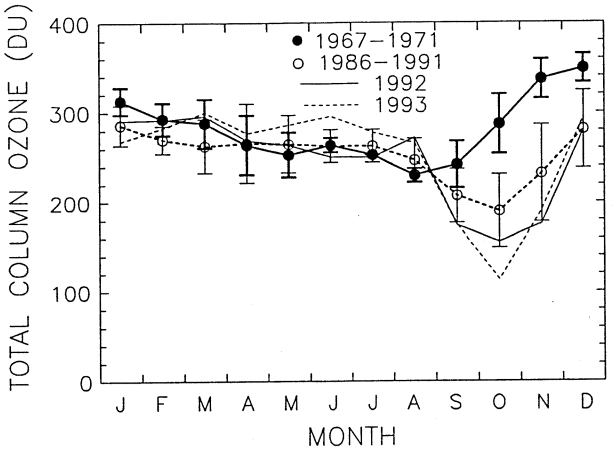

Figure 1-26. Monthly averaged total column ozone by month measured in balloon flights at South Pole for the 1967-1971 and 1986-1993 periods, and for 1992 and 1993 (straight and dashed lines, respectively). (Adapted from Oltmans *et al.*, 1994.)

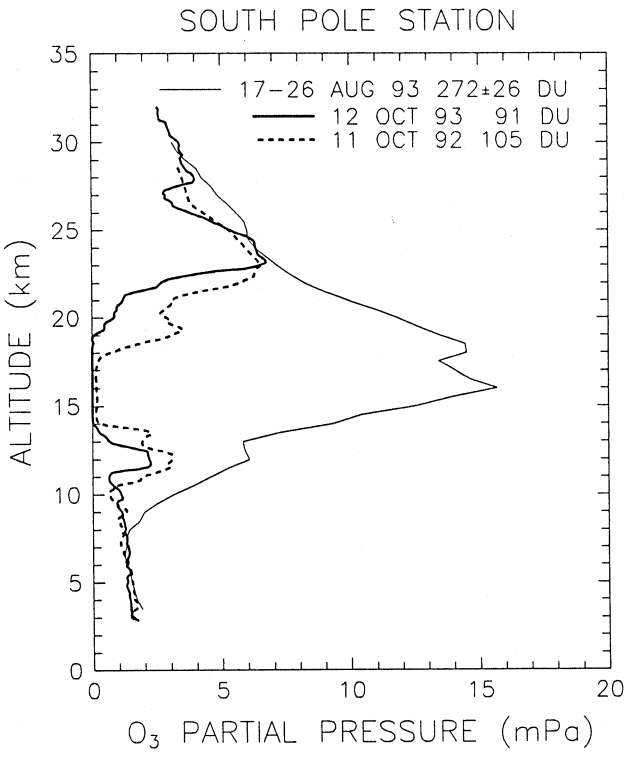

Figure 1-27. Comparison of the South Pole pre-depletion ozone profile in 1993 (average of 4 soundings) with the profile observed when total ozone reached a minimum in 1992 and 1993. (Adapted from Hofmann *et al.*, 1994b.)

In Figure 1-27 the average of four ozone profiles before depletion began in August 1993 is compared with the profiles at the time of minimum ozone in 1992 and 1993 (Hofmann *et al.*, 1994b). Total destruction (>99%) of ozone was observed from 14 to 19 km in 1993, a 1 km upward extension of the zero-ozone region from the previously most severe year, 1992. Unusually cold temperatures in the 20 km region are believed to be the main cause of lower-than-normal ozone in the 18-23 km range. These lower temperatures prolong the presence of polar stratospheric clouds (PSCs), in particular nitric acid trihydrate (NAT), thought to be the dominant component of PSCs. This tends to enhance the production and lifetime of reactive chlorine and concomitant ozone depletion at the upper boundary of the ozone hole, because chlorine in this region is not totally activated in years with normal temperatures. Temperatures at 20 km in September 1993 were similar to those of 1987 and

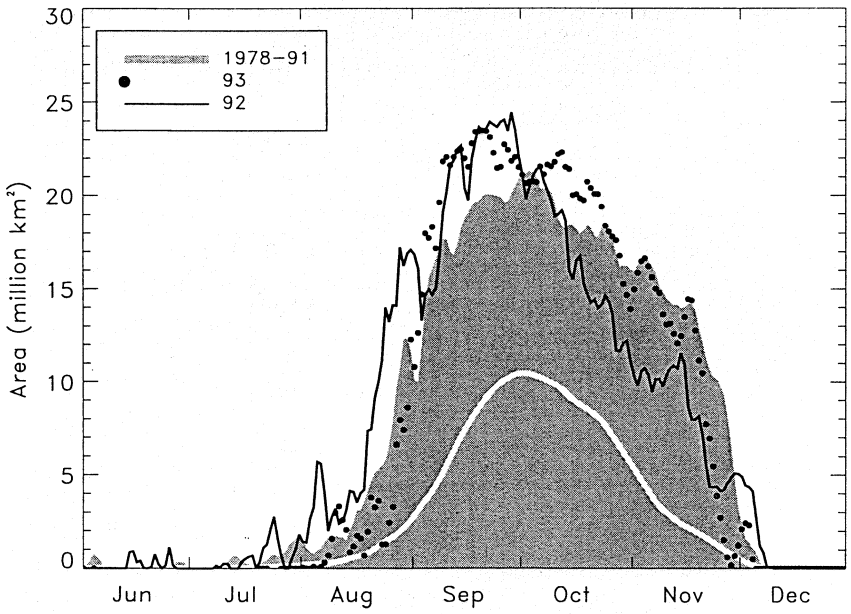

Figure 1-28. Area of the region enclosed by the 220 DU total ozone contour in the Southern Hemisphere. The white line represents the 1978-1991 average with the shaded area representing the extremes for this period. The 1992 and 1993 areas are represented by the continuous line and points, respectively. 12 million square kilometers is about 5% of the surface area of the Southern Hemisphere, so that the maximum extent of the region in 1992 or 1993 with total ozone less than 220 DU, if circular, was about 65°S. Data for 1978-1992 are from Nimbus 7 TOMS; data for 1993 are from Meteor TOMS. Only measurements made south of 40°S were considered, to avoid including any low tropical values recorded. (Courtesy of the Ozone Processing Team, NASA Goddard.)

1989, other very cold years at this altitude. Cold sulfate aerosol from Mt. Pinatubo, present at altitudes between 10 and 16 km, probably contributed to the low ozone through heterogeneous conversion of chlorine species (see Chapters 3 and 4).

Figure 1-28 shows the horizontal extent of the Antarctic ozone hole in terms of the area contained within the 220 DU total ozone contour from Nimbus TOMS (1978-1991 shaded region and 1992 curve) and from Meteor TOMS (1993 points). These data indicate that the 1992 and 1993 ozone hole areas were the largest on record and that the development of the depleted region began about 1-2 weeks earlier, a fact also apparent in the total ozone data in Figure 1-26.

Since 1991, springtime ozone depletion at the South Pole has worsened in the 12-16 km region, with total ozone destruction at 15-16 km in 1992 and 1993. Similar observations were made in 1992 at McMurdo, 78°S (Johnson *et al.*, 1994), Syowa, 69°S (T. Ito, private communication), and Georg Forster stations (71°S) (H. Gernandt, private communication), indicating that this depletion at lower altitudes was widespread. In addition, the 1993 springtime ozone loss was very severe in the 18-22 km region, effectively extending the ozone depletion region upward by about 1-2 km (Figure 1-27). This occurred in spite of ozone being considerably higher than normal during the preceding winter (Figure 1-26). Complete ozone destruction from 14 to 19 km was peculiar to 1993 and, combined with lower-than-normal ozone at 20-22 km, resulted in the record low total ozone recorded in early October 1993.

The decrease in summer ozone levels at 10-17 km since the late 1960s is not apparent in the 1986-1993 data, possibly because the record is too short.

REFERENCES

Akimoto, H., N. Nakane, and Y. Matsumoto, The chemistry of oxidant generation: Tropospheric ozone increase in Japan, in *The Chemistry of the Atmosphere: Its Impact on Global Change*, edited by J.G. Calvert, Blackwell Sci. Publ., Oxford, 261-273, 1994.

Albert-Levy, Analyse de l'air, *Annulaire de l'Obser. de Montsouris*, Gauthier-Villars, Paris, 495-505, 1878.

Alt, J., P. Astapenko, and N.J. Roper, Some aspects of the Antarctic atmospheric circulation in 1958, *IGY General Report Series, 4,* 1-28, 1959.

Anfossi, D., S. Sandroni, and S. Viarengo, Tropospheric ozone in the nineteenth century: The Montalieri series, *J. Geophys. Res., 96,* 17349-17352, 1991.

Attmannspacher, W., and H. Dütsch, International ozone sonde intercomparison at the Observatory of Hohenpeissenberg, *Berichte des Deutschen Wetterdienstes, 120,* 85 pp., 1970.

Attmannspacher, W., and H. Dütsch, 2nd International ozone sonde intercomparison at the Observatory of Hohenpeissenberg, *Berichte des Deutschen Wetterdienstes, 157,* 65 pp., 1981.

Attmannspacher, W., J. de la Noé, D. De Muer, J. Lenoble, G. Mégie, J. Pelon, P. Pruvost, and R. Reiter, European validation of SAGE II ozone profiles, *J. Geophys. Res., 94,* 8461-8466, 1989.

Barnes, R.A., A.R. Bandy, and A.L. Torres, Electrochemical concentration cell ozonesonde accuracy and precision, *J. Geophys. Res., 90,* 7881-7887, 1985.

Barnes, R.A., L.R. McMaster, W.P. Chu, M.P. McCormick, and M.E. Gelman, Stratospheric Aerosol and Gas Experiment II and ROCOZ-A ozone profiles at Natal, Brazil: A basis for comparison with other satellite instruments, *J. Geophys. Res., 96,* 7515-7530, 1991.

Bass, A.M., and R.J. Paur, The ultraviolet cross-sections of ozone: I. The measurements, in *Atmospheric Ozone*, edited by C.S. Zerefos and A.M. Ghazi, Reidel, Dordrecht, The Netherlands, 606-610, 1985.

Bekki, S., R. Toumi, and J.A. Pyle, Role of sulphur photochemistry in tropical ozone changes after the eruption of Mount Pinatubo, *Nature, 362,* 331-333, 1993.

Bhartia, P.K., J. Herman, R.D. McPeters, and O. Torres, Effect of Mt. Pinatubo aerosols on total ozone measurements from backscatter ultraviolet (BUV) experiments, *J. Geophys. Res., 98,* 18547-18554, 1993.

Bluth, G.J.S., S.D. Doiron, C.C. Schnetzler, A.J. Krueger, and L.S. Walter, Global tracking of the SO_2 clouds from the June 1991 Mount Pinatubo eruptions, *Geophys. Res. Lett., 19,* 151-154, 1992.

Bojkov, R.D., Surface ozone during the second half of the nineteenth century, *J. Clim. Appl. Meteorol., 25,* 343-352, 1986.

Bojkov, R.D., The 1983 and 1985 anomalies in ozone distribution in perspective, *Mon. Wea. Rev., 115,* 2187-2201, 1987.

Bojkov, R.D., Ozone changes at the surface and in the free troposphere, in *Tropospheric Ozone, Regional and Global Scale Interactions,* edited by I.S.A. Isaksen, NATO ASI Series C, 227, 83-96, Reidel, Dordrecht, The Netherlands, 1988.

Bojkov, R.D., L. Bishop, W.J. Hill, G.C. Reinsel, and G.C. Tiao, A statistical trend analysis of revised Dobson total ozone data over the Northern Hemisphere, *J. Geophys. Res., 95,* 9785-9807, 1990.

Bojkov, R.D., C.S. Zerefos, D.S. Balis, I.C. Ziomas, and A.F. Bais, Record low total ozone during northern winters of 1992 and 1993, *Geophys. Res. Lett., 20,* 1351-1354, 1993.

Bojkov, R.D., V.E. Fioletov, and A.M. Shalamjansky, Total ozone changes over Eurasia since 1973 based on reevaluated filter ozonometer data, *J. Geophys. Res., 99,* 22985-22999, 1994.

Brasseur, G., and C. Granier, Mount Pinatubo aerosols, chlorofluorocarbons and ozone depletion, *Science, 257,* 1239-1242, 1992.

Chalonge, D., and E. Vassy, Spectrographic astigmatique à prisme objectif, *Rev. Opt. Theor. Instrum., 13,* 113-126, 1934.

Chandra, S., Changes in stratospheric ozone and temperature due to the eruption of Mt. Pinatubo, *Geophys. Res. Lett., 20,* 33-36, 1993.

Chu, W.P., M.P. McCormick, J. Lenoble, C. Brogniez, and P. Pruvost, SAGE II inversion algorithm, *J. Geophys. Res., 94,* 8339-8351, 1989.

Chubachi, S., Preliminary result of ozone observations at Syowa Stations from February, 1982 to January 1983, *Mem. Natl. Inst. Polar. Res., Spec. Iss., 34,* 13-18, 1984.

Cunnold, D.M., W.P. Chu, R.A. Barnes, M.P. McCormick, and R.E. Veiga, Validation of SAGE II ozone measurements, *J. Geophys. Res., 94,* 8447-8460, 1989.

De Muer, D., Comment on "Presumptive Evidence for a Low Value of the Total Ozone Content above Antarctica in September, 1958" by P. Rigaud and B. Leroy, *Annales Geophysicae, 11,* 795-796, 1990.

De Muer, D., H. De Backer, R.E. Veiga, and J.M. Zawodny, Comparison of SAGE II ozone measurements and ozone soundings at Uccle (Belgium) during the period February 1985 to January 1986, *J. Geophys. Res., 95,* 11903-11911, 1990.

De Muer, D., and H. De Backer, Revision of 20 years of Dobson total ozone data at Uccle (Belgium): Fictitious Dobson total ozone trends induced by sulfur dioxide trends, *J. Geophys. Res., 97,* 5921-5937, 1992.

De Muer, D., and H. De Backer, Influence of sulphur dioxide trends on Dobson measurements and on electrochemical ozone soundings, in *Proceedings of the Society of Photo-Optical Instrumentation Engineers, 2047, 33,* 18-26, 1993.

De Muer, D., and H. De Backer, Trend analysis of 25 years of regular ozone soundings at Uccle (Belgium), Abstract, EUROTRAC meeting, Garmisch-Partenkirchen, April 1994.

Degórska, M., B. Rajewska-Wiech, and R.B. Rybka, Total ozone over Belsk: Updating of trends through 1991 and comparison of the Dobson data with those from TOMS in 1978-1991, *Publs. Inst. Geophys. Pol. Acad. Soc., 252,* 53-58, 1992.

DeLuisi, J.J., D.A. Londenecker, C.L. Mateer, and D.J. Wuebbles, An analysis of Northern middle latitude Umkehr measurements corrected for stratospheric aerosols for 1979-1986, *J. Geophys. Res., 94,* 9837-9846, 1989.

DeLuisi, J.J., C.L. Mateer, D. Theisen, P.K. Bhartia, D. Longenecker, and B. Chu, Northern middle-latitude ozone profile features and trends observed by SBUV and Umkehr, 1979-1990, *J. Geophys. Res., 99,* 18901-18908, 1994.

Deshler, T., A. Adriani, G.P. Gobbi, D.J. Hofmann, G. Di Donfrancesco, and B.J. Johnson, Volcanic aerosol and ozone depletion within the Antarctic polar vortex during the austral spring of 1991, *Geophys. Res. Lett., 19,* 1819-1822, 1992.

Deshler, T., B.J. Johnson, and W.R. Rozier, Balloonborne measurements of Pinatubo aerosol during 1991 and 1992 at 41°N: Vertical profiles, size distribution and volatility, *Geophys. Res. Lett., 20,* 1435-1438, 1993.

Dobson, G.M.B., Observers handbook for the ozone spectrophotometer, *Ann. IGY, 5,* 46-89, 1957.

Dobson, G.M.B., Forty years' research on atmospheric ozone at Oxford: A history, *Applied Optics, 7,* 401, 1968.

Dütsch, H.U., W. Zuliz, and C.C. Ling, Regular ozone observations at Thalwill, Switzerland and at Boulder, Colorado, *Rep. LAPETH 1,* Lab. Atmosphärenphys. Edigenöss., Tech. Hochsch., Zurich, 1970.

Fabry, C., and H. Buisson, L'absorption des radiations dans la haute atmosphere, *Memorial Sc. Phys., 11,* 1-64, 1930.

Farman, J.C., A. O'Neill, and R. Swinbank, The dynamics of the arctic polar vortex during the EASOE campaign, *Geophys. Res. Lett., 21,* 1195-1198, 1994.

Feister, U., and W. Warmbt, Long-term measurements of surface ozone in the German Democratic Republic, *J. Atmos. Chem., 5,* 1-21, 1987.

Fox, C.B., *Ozone and Antozone*, Churchill Publ., London, 1873.

Furrer, R., W. Döhler, H. Kirsch, P. Plessing, and U. Görsdorf, Evidence for vertical ozone redistribution since 1967, *J. Atmos. Terr. Phys., 11,* 1423-1445, 1992.

Furrer, R., W. Döhler, H. Kirsch, P. Plessing, and U. Görsdorf, Evidence for vertical ozone redistribution since 1967, *Surveys in Geophysics, 14,* 197-222, 1993.

Gleason, J.F., P.K. Bhartia, J.R. Herman, R. McPeters, P. Newman, R.S. Stolarski, L. Flynn, G. Labow, D. Larko, C. Seftor, C. Wellemeyer, W.D. Komhyr, A.J. Miller, and W. Planet, Record low global ozone in 1992, *Science, 260,* 523-526, 1993.

Görsdorf, U., H. Steinhagen, and H. Gernandt, Bestimmung der Forderleistung von Ozonsondenpumpen bei veränderlichen Messbedingungen, *Z. Meteoro.*, in press, 1994.

Götz, F.W.P., Zum Strahlungsklima des Spitzbergensommers. Strahlungs- und Ozonmessungen in der Königsbucht 1929, *Gerlands Beitr. Geophys., 31,* 119, 1931.

Götz, F.W.P., and F. Volz, Aroser Messungen des Ozonegehaltes in der unteren Troposphäre und sein Jahresgang, *Z. Naturforsch., 6a,* 634-639, 1951.

Grass, R.D., and W.D. Komhyr, Traveling standard lamp calibration checks of Dobson ozone spectrophotometers during 1985-1987, in *Ozone in the Atmosphere*, edited by R.D. Bojkov and P. Fabian, A. Deepak Publ., Hampton, Virginia, 144-146, 1989.

Henriksen, K., T. Svenøe, and S.H.H. Larsen, On the stability of the ozone layer at Tromsø, *J. Atmos. Terr. Phys., 54,* 1113-1117, 1992.

Henriksen, K., E.I. Terez, G.A. Terez, V. Roldugin, T. Svenøe, and S.H.H. Larsen, On the stationarity of the ozone layer in Norway and U.S.S.R., *J. Atmos. Terr. Phys., 55,* 145-154, 1993.

Herman, J.R., R.D. Hudson, R.D. McPeters, R.S. Stolarski, Z. Ahmad, X-Y. Gu, S.L. Taylor, and C.G. Wellemeyer, A new self-calibration method applied to TOMS and SBUV backscattered data to determine long-term global ozone change, *J. Geophys. Res., 96,* 7531-7545, 1991.

Herman, J.R., and D. Larko, Low ozone amounts during 1992-1993 from Nimbus 7 and Meteor 3 Total Ozone Mapping Spectrometers, *J. Geophys. Res., 99,* 3483-3496, 1994.

Hilsenrath, E., D.E. Williams, R.T. Caffrey, R.P. Cebula, and S.J. Hynes, Calibration and radiometric stability of the Shuttle Solar Backscattered Ultra-Violet (SSBUV) experiment, *Metrologia*, in press, 1994.

Hofmann, D.J., S.J. Oltmans, J.M. Harris, W.D. Komhyr, J.A. Lathrop, T. DeFoor, and D. Kuniyuki, Ozonesonde measurements at Hilo, Hawaii following the eruption of Pinatubo, *Geophys. Res. Lett., 20,* 1555-1558, 1993.

Hofmann, D.J., S.J. Oltmans, W.D. Komhyr, J.M. Harris, J.A. Lathrop, A.O. Langford, T. Deshler, B.J. Johnson, A. Torres, and W.A. Matthews, Ozone loss in the lower stratosphere over the United States in 1992-1993: Evidence for heterogeneous chemistry on the Pinatubo aerosol, *Geophys. Res. Lett., 21,* 65-68, 1994a.

Hofmann, D.J., S.J. Oltmans, J.A. Lathrop, J.M. Harris, and H. Voemel, Record low ozone at the South Pole in the spring of 1993, *Geophys. Res. Lett., 21,* 421-424, 1994b.

Hofmann, D.J., Recovery of stratospheric ozone over the U.S. in the winter of 1993-1994, *Geophys. Res. Lett., 21,* 1779-1782, 1994.

Hood, L.L., and J.P. McCormack, Components of interannual ozone change based on Nimbus 7 TOMS data, *Geophys. Res. Lett., 19,* 2309-2312, 1992.

Hood, L.L., R.D. McPeters, J.P. McCormack, L.E. Flynn, S.M. Hollandsworth, and J.F. Gleason, Altitude dependence of stratospheric ozone trends based on Nimbus 7 SBUV data, *Geophys. Res. Lett., 20,* 2667-2670, 1993.

Jaffe, D.A., Local sources of pollution in the Arctic: From Prudhoe Bay to the Taz Peninsula, *Pollution of the Arctic Atmosphere*, edited by W.T. Sturges, Elsevier, New York, 255-287, 1991.

Johnson, B.J., T. Deshler, and W.R. Rozier, Ozone profiles at McMurdo station, Antarctica during the austral spring of 1992, *Geophys. Res. Lett., 21,* 269-272, 1994.

Kerr, J.B., C.T. McElroy, D.I. Wardle, R.A. Olafson, and W.F.J. Evans, The automated Brewer spectrophotometer, in *Proceedings 1984 Quadrennial Ozone Symposium*, edited by C.S. Zerefos and A. Ghazi, Reidel Publ., Dodrecht, The Netherlands, 396, 1985.

Kerr, J.B., I.A. Asbridge, and W.F.J. Evans, Intercomparison of total ozone measured by the Brewer and Dobson spectrophotometers at Toronto, *J. Geophys. Res., 93,* 11129-11140, 1988.

Kerr, J.B., I.A. Asbridge, and W.F.J. Evans, Long-term intercomparison between the Brewer and Dobson spectrophotometers at Edmonton, in *Ozone in the Atmosphere*, edited by R.D. Bojkov and P. Fabian, A. Deepak Publ., Hampton, Virginia, 105, 1989.

Kerr, J.B., D.I. Wardle, and D.W. Tarasick, Record low ozone values over Canada in early 1993, *Geophys. Res. Lett., 20,* 1979-1982, 1993.

Kerr, J.B., H. Fast, C.T. McElroy, S.J. Oltmans, J.A. Lathrop, E. Kyro, A. Paukkunen, H. Claude, U. Köhler, C.R. Sreedharan, T. Takao, and Y. Tsukagoshi, The 1991 WMO international ozonesonde intercomparison at Vanscoy, Canada, *Atmosphere-Ocean*, in press, 1994.

Kley, D., A. Volz, and F. Mülhiems, Ozone measurements in historic perspective, in *Tropospheric Ozone, Regional and Global Scale Interactions,* edited by I.S.A. Isaksen, *NATO ASI Series C, 227,* 63-72, Reidel Publ., Dordrecht, The Netherlands, 1988.

Kley, D., H. Geiss, and V.A. Mohnen, Concentrations and trends of tropospheric ozone and precursor emissions in the USA and Europe, in *The Chemistry of the Atmosphere: Its Impact on Global Change*, edited by J.G. Calvert, Blackwell Sci. Publ., Oxford, 245-259, 1994.

Komhyr, W., and T.B. Harris, Note on flow rate measurements made on Brewer-Mast ozone sensor pumps, *Mon. Wea.. Rev., 93,* 267-268, 1965.

Komhyr, W.D., Electrochemical concentration cells for gas analysis, *Ann. Geophys., 25,* 203-210, 1969.

Komhyr, W.D., and T.B. Harris, Development of the ECC ozonesonde, *NOAA Technical Report* ERL 200-APCL 18, U.S. Department of Commerce, NOAA Environmental Research Laboratories, Boulder, Colorado, 54 pp., 1971.

Komhyr, W.D., S.J. Oltmans, R.D. Grass, and R.K. Leonard, Possible influence of long-term sea surface temperature anomalies in the tropical Pacific on global ozone, *Canadian. J. Phys., 65,* 1093-1102, 1991.

Komhyr, W.D., C.L. Mateer, and R.D. Hudson, Effective Bass-Paur 1985 ozone absorption coefficients for use with Dobson ozone spectrophotometers, *J. Geophys. Res., 98,* 451-465, 1993.

Komhyr, W.D., R.D. Grass, R.D. Evans, R.K. Leonard, D.M. Quincy, D.J. Hofmann, and G.L. Koenig, Unprecedented 1993 ozone decrease over the United States from Dobson spectrophotometer observations, *Geophys. Res. Lett., 21,* 210-214, 1994a.

Komhyr, W.D., J.A. Lathrop, D.P. Opperman, R.A. Barnes, and G.B. Brothers, ECC ozonesonde performance evaluation during STOIC 1989, *J. Geophys. Res.*, in press, 1994b.

Krzyścin, J.W., Interannual changes in the atmospheric ozone derived from ground-based measurements, *Papers in Met. and Geophys., 43,* 133-164, 1992.

Krzyścin, J.W., Total ozone changes in the Northern Hemisphere mid-latitudinal belt (30-60°N) derived from Dobson spectrophotometer measurements, 1964-1988, *J. Atmos. Terr. Phys., 56,* 1051-1056, 1994a.

Krzyścin, J.W., Long-term changes in the statistical distribution of Dobson total ozone in selected Northern Hemisphere geographical regions, in *Proceedings of the Quadrennial Ozone Symposium 1992*, Charlottesville, Virginia, NASA CP-3266, 207-210, 1994b.

Krzyścin, J.W., Statistic analysis of annual total ozone extremes for the period 1964-1988, in *Proceedings of the Quadrennial Ozone Symposium 1992*, Charlottesville, Virginia, NASA CP-3266, 203-206, 1994c.

Kundu, N., and M. Jain, Total ozone trends over low latitude Indian stations, *Geophys. Res. Lett., 20,* 2881-2883, 1993.

Labitske, K., and M.P. McCormick, Stratospheric temperature increases due to Pinatubo aerosols, *Geophys. Res. Lett., 19,* 207-210, 1992.

Lacoste, A.M., S. Godin, and G. Mégie, Lidar measurements and Umkehr observations of the ozone vertical distribution at the Observatoire de Haute-Provence, *J. Atmos. Terr. Phys., 54,* 571-582, 1992.

Lambert, A., R.G. Grainger, J.J. Remedios, D.C. Rodgers, M. Corney, and F.W. Taylor, Measurements of the evolution of the Mt. Pinatubo aerosol clouds by ISAMS, *Geophys. Res. Lett., 20,* 1287-1290, 1993.

Lehmann, P., A statistical seasonal analysis of winter decreases in ozone at Macquarie Island, *Geophys. Res. Lett., 21,* 381-384, 1994.

Linvill, D.E., W.J. Hooken, and B. Olson, Ozone in Michigan's environment (1876-1880), *Mon. Wea. Rev., 108,* 1883-1891, 1980.

Logan, J.A., Trends in the vertical distribution of ozone: An analysis of ozonesonde data, *J. Geophys. Res.*, in press, 1994.

London, J., and S. Liu, Long-term tropospheric and lower stratospheric ozone variations from ozonesondes observations, *J. Atmos. Terr. Phys., 5,* 599-625, 1992.

Marenco, A., H. Gouget, P. Nédélec, J.-P. Pagés, and F. Karcher, Evidence of a long-term increase in tropospheric ozone from Pic du Midi data series —Consequences: Positive radiative forcing, *J. Geophys. Res., 99,* 16617-16632, 1994.

Marko, J.R., and D.B. Fissel, Empirical linkages between Arctic sea ice extents and Northern Hemisphere mid-latitude column ozone levels, *Geophys. Res. Lett., 20,* 37-40, 1993.

Mateer, C.L., and J.J. DeLuisi, A new Umkehr inversion algorithm, *J. Atmos. Terr. Phys., 54,* 537-556, 1992.

McCormick, M.P., R.E. Veiga, and W.P. Chu, Stratospheric ozone profile and total ozone trends derived from the SAGE I and SAGE II data, *Geophys. Res. Lett., 19,* 269-272, 1992.

McPeters, R.D., and W.D. Komhyr, Long-term changes in TOMS relative to World Primary Standard Dobson Spectrometer 83, *J. Geophys. Res., 96,* 2987-2993, 1991.

McPeters, R.D., T. Miles, L.E. Flynn, C.G. Wellemeyer, and J.M. Zawodny, Comparison of SBUV and SAGE II ozone profiles: Implications for ozone trends, *J. Geophys. Res., 99,* 20513-20524, 1994.

Miller, A.J., G.C. Tiao, G.C. Reinsel, D. Wuebbles, L. Bishop, J. Kerr, R.M. Nagatani, and J.J. DeLuisi, Comparisons of observed ozone trends in the stratosphere through examination of Umkehr and balloon ozonesonde data, in preparation, 1994.

Mylona, S., Trends of sulphur dioxide emissions, air concentrations and depositions of sulphur in Europe since 1880, in *European Monitoring and Evaluation Program/Meteorological Synthesis Center-West Report 2/93,* August 1993.

Naujokat, B., K. Petzoldt, K. Labitzke, R. Lenschow, B. Rajewski, M. Wiesner, and R-C. Wohlfart, The stratospheric winter 1992/1993: A cold winter with a minor warming and a late final warming, *Beilage zur Berliner Wetterkarte, SO 21/93,* 1993.

Newman, P.A., Antarctic ozone hole in 1958, *Science, 264,* 543-546, 1994.

NOAA (National Oceanic and Atmospheric Administration), Southern Hemisphere Winter Summary, Selected indicators of stratospheric climate, Climate Analysis Center, 1993.

Oltmans, S.J., W.D. Komhyr, P.R. Franchois, and W.A. Matthews, Tropospheric ozone: Variations from surface and ECC ozonesonde observations, in *Ozone in the Atmosphere*, edited by R.D. Bojkov and P. Fabian, A. Deepak Publ., Hampton, Virginia, 539-543, 1989.

Oltmans, S.J., D.J. Hofmann, W.D. Komhyr, and J.A. Lathrop, Ozone vertical profile changes over South Pole, in *Proceedings of the Quadrennial Ozone Symposium 1992,* Charlottesville, Virginia, 13 June 1992, NASA CP-3266, 578-581, 1994.

Oltmans, S.J., and H. Levy II, Surface ozone measurements from a global network, *Atmos. Environ., 28,* 9-24, 1994.

Oltmans, S.J., and D.J. Hofmann, Trends in the vertical profile of ozone at Hilo, Hawaii, from 1982 to 1994, in preparation, 1994.

Ozone Data for the World, Atmospheric Environment Service, Department of the Environment in cooperation with the World Meteorological Organization, Downsview, Ontario, Canada, *34,* 3, 1993.

Paur, R.J., and A.M. Bass, The ultraviolet cross-sections of ozone: II. Results and temperature dependence, in *Atmospheric Ozone*, edited by C.S. Zerefos and A.M. Ghazi, Reidel Publ., Dordrecht, The Netherlands, 611-616, 1985.

Perl, G., Das bodennahe Ozon in Arosa, seine regelmässigen und unregelmässigen Schwankungen, *Arch. Met. Geophys. Bioklimat., 14,* 449-458, 1965.

Placet, M., Emissions involved in acidic deposition processes, in *Acidic Deposition: State of Science and Technology*, Summary report of the U.S. National Acid Precipitation Assessment Program, edited by P.M. Irving, 1991.

Pommereau, J.-P., and F. Goutail, O_3 and NO_2 ground-based measurements by visible spectrometry during Arctic winter and spring 1988, *Geophys. Res. Lett., 15,* 891-895, 1988.

Randel, W.J., and J.B. Cobb, Coherent variations of monthly mean total ozone and lower stratospheric temperature, *J. Geophys. Res., 99,* 5433-5447, 1994.

Read, W.G., L. Froidevaux, and J.W. Waters, Microwave Limb Sounder measurement of stratospheric SO_2 from the Mt. Pinatubo volcano, *Geophys. Res. Lett., 20,* 1299-1302, 1993.

Reinsel, G.C., G.C. Tiao, A.J. Miller, D.J. Wuebbles, P.S. Connell, C.L. Mateer, and J. DeLuisi, Statistical analysis of total ozone and stratospheric Umkehr data for trends and solar cycle relationship, *J. Geophys. Res., 92,* 2201-2209, 1987.

Reinsel, G.C., G.C. Tiao, D.J. Wuebbles, J.B. Kerr, A.J. Miller, R.M. Nagatani, L. Bishop, and L.H. Ying, Seasonal trend analysis of published ground-based and TOMS total ozone data through 1991, *J. Geophys. Res., 99,* 5449-5464, 1994a.

Reinsel, G.C., W.-K. Tam, and L.H. Ying, Comparison of trend analyses for Umkehr data using new and previous inversion algorithms, *Geophys. Res. Lett., 21,* 1007-1010, 1994b.

Rigaud, P., and B. Leroy, Presumptive evidence for a low value of the total ozone content above Antarctica in September 1958, *Annales Geophysicae, 11,* 791-794, 1990.

Sandroni, D., D. Anfossi, and S. Viarengo, Surface ozone levels at the end of the nineteenth century in South America, *J. Geophys. Res., 97,* 2535-2540, 1992.

Scheel, H.E., E.G. Brunke, and W. Seiler, Trace gas measurements at the monitoring station Cape Point, South Africa, between 1978 and 1988, *J. Atm. Chem., 11,* 197-210, 1990.

Scheel, H.E., R. Sladovic, and W. Seiler, Ozone related species at the stations Wank and Zugspitze: Trends, short-term variations and correlations with other parameters, in *Photo-Oxidants: Precursors and Products*, Proc. EUROTRAC Symp. 1992, edited by P.M. Borell, P. Borell, T. Cvitas, and W. Seiler, Acad. Publ., The Hague, The Netherlands, 104-108, 1993.

Schenkel, A., and B. Broder, Interference of some trace gases with ozone measurements by the KI-method, *Atmos. Environ., 16,* 2187-2190, 1982.

Schoeberl, M.R., P.K. Bhartia, and E. Hilsenrath, Tropical ozone loss following the eruption of Mt. Pinatubo, *Geophys. Res. Lett., 20,* 29-32, 1993.

Shiotani, M., Annual, quasi-biennial and El Niño-Southern Oscillation (ENSO) time scale variations in equatorial total ozone, *J. Geophys. Res., 97,* 7625-7633, 1992.

Sladkovic, R., H.E. Scheel, and W. Seiler, Ozone climatology of the mountain sites, Wank and Zugspitze, in *Transport and Transformation of Pollutants in the Troposphere*, Proc. EUROTRAC Symp. April 1994, edited by P.M. Borrell, P. Borrell, P. Cvitas, and W. Seiler, in press, 1994.

Staehelin, J., and W. Schmid, Trend analysis of tropospheric ozone concentrations utilizing the 20-year data set of ozone balloon soundings over Payerne, *Atmos. Environ., 9,* 1739-1749, 1991.

Staehelin, J., J. Thudium, R. Bühler, A. Volz-Thomas, and W. Graber, Trends in surface ozone concentrations at Arosa (Switzerland), *Atmos. Environ., 28,* 75-87, 1994.

Stolarski, R.S., and A.J. Krueger, Variations of total ozone in the North Polar region as seen by TOMS, paper presented at the Polar Ozone Workshop, NASA/NOAA/NSF/CMA, Snowmass, Colorado, May 9-13, 1988.

Stolarski R.S., P. Bloomfield, R. McPeters, and J. Herman, Total ozone trends deduced from Nimbus 7 TOMS Data, *Geophys. Res. Lett., 18,* 1015-1018, 1991.

Stolarski, R., R. Bojkov, L. Bishop, C. Zerefos, J. Staehelin, and J. Zawodny, Measured trends in stratospheric ozone, *Science, 256,* 342-349, 1992.

Tarasick, D.W., D.I. Wardle, J.B. Kerr, J.J. Bellefleur, and J. Davies, Tropospheric ozone trends over Canada: 1980-1993, submitted to *Geophys. Res. Lett.*, 1994.

Taylor, S.L., R.D. McPeters, and P.K. Bhartia, Procedures to validate/correct calibration error in solar backscattered ultraviolet instruments, in *Proceedings of the Quadrennial Ozone Symposium 1992*, Charlottesville, Virginia, NASA CP-3266, 923-926, 1994.

Thornton, D., and N. Niazy, Effects of solution mass transport on the ECC ozonesonde background current, *Geophys. Res. Lett., 10,* 148-151, 1983.

Trepte, C.R., R.E. Veiga, and M.P. McCormick, The poleward dispersal of Mount Pinatubo volcanic aerosol, *J. Geophys. Res., 98,* 18563-18573, 1993.

Vigroux, E., Determination des coefficients moyen d'absorption de l'ozone, *Ann. Phys., 8,* 709-762, 1953.

Volz, A., and D. Kley, Evaluation of the Montsouris series of ozone measurements made in the nineteenth century, *Nature, 332,* 240-242, 1988.

Volz-Thomas, A., Trends in photo-oxidant concentrations, in *Photo-Oxidants: Precursors and Products, Proc. EUROTRAC Symp. 1992*, edited by P.M. Borrell, P. Borrell, T. Cvitas, and W. Seiler, Acad. Publ., The Hague, The Netherlands, 59-64, 1993.

Wege, K., H. Claude, and R. Hartmannsgruber, Several results from the 20 years of ozone observations at Hohenpeissenberg, in *Ozone in the Atmosphere*, edited by R.D. Bojkov and P. Fabian, A. Deepak Publ., Hampton, Virginia, 109-112, 1989.

Wellemeyer, C.G., S.L. Taylor, C.J. Seftor, and R.D. McPeters, TOMS profile shape errors estimates at high latitude, in *Proceedings of the Symposium on High Latitude Optics*, Tromsø, Norway, 1993.

WMO, *Report of the International Ozone Trends Panel: 1988*, World Meteorological Organization Global Ozone Research and Monitoring Project—Report No. 18, Geneva, 1990a.

WMO, *Scientific Assessment of Stratospheric Ozone: 1989*, World Meteorological Organization Global Ozone Research and Monitoring Project—Report No. 20, Geneva, 1990b.

WMO, *Scientific Assessment of Ozone Depletion: 1991*, World Meteorological Organization Global Ozone Research and Monitoring Project—Report No. 25, Geneva, 1992a.

WMO, *Handbook for Dobson Ozone Data Re-evaluation*, World Meteorological Organization Global Ozone Research and Monitoring Project—Report No. 29, Geneva, 1992b.

WMO, *Proceedings of the Fourth WMO/NOAA Workshop on Ozone Data Re-evaluation*, World Meteorological Organization Global Ozone Research and Monitoring Project—Report No. 36, Geneva, in preparation, 1994a.

WMO, *Proceedings of a Workshop on Homogenizing Total Ozone Records for Use in Ozone Assessments and Early Warning of Ozone Changes*, World Meteorological Organization Global Ozone Research and Monitoring Project—Report No. 35, Saloniki 1993, in preparation, 1994b.

Young, R.E., H. Houben, and O.B. Toon, Radiatively forced dispersion of the Mt. Pinatubo volcanic cloud and induced temperature perturbations in the stratosphere during the first few months following the eruption, *Geophys. Res. Lett., 21,* 369-372, 1994.

Zerefos, C.S., On the quasi-biennial oscillation in equatorial stratospheric temperatures and total ozone, *Adv. Space. Res., 2,* 177-181, 1983.

Zerefos, C.S., A.F. Bais, I.C. Ziomass, and R.D. Bojkov, On the relative importance of quasi-biennial oscillation and El Niño-Southern Oscillation in the revised Dobson total ozone records, *J. Geophys. Res., 97,* 10135-10144, 1992.

Zerefos, C., K. Tourpali, and A. Bais, Further studies on possible volcanic signal in total ozone, *J. Geophys. Res.*, in press, 1994.

CHAPTER 2

Source Gases: Trends and Budgets

Lead Author:
E. Sanhueza

Co-authors:
P.J. Fraser
R.J. Zander

Contributors:
F.N. Alyea
M.O. Andreae
J.H. Butler
D.N. Cunnold
J. Dignon
E. Dlugokencky
D.H. Ehhalt
J.W. Elkins
D. Etheridge
D.W. Fahey
D.A. Fisher
J.A. Kaye
M.A.K. Khalil
P. Middleton
P.C. Novelli
J. Penner
M.J. Prather
R.G. Prinn
W.S. Reeburgh
J. Rudolph
P. Simmonds
L.P. Steele
M. Trainer
R.F. Weiss
D.J. Wuebbles

CHAPTER 2

SOURCE GASES: TRENDS AND BUDGETS

Contents

SCIENTIFIC SUMMARY

Tropospheric growth rates of the major anthropogenic source species for stratospheric chlorine and bromine (chlorofluorocarbons (CFCs), carbon tetrachloride, methyl chloroform, halons) have slowed significantly, in response to substantially reduced emissions required by the Montreal Protocol. Total tropospheric chlorine grew by about 60 pptv (1.6%) in 1992 compared to 110 pptv (2.9%) in 1989. Tropospheric bromine in the form of halons grew by 0.2-0.3 pptv in 1992, compared to 0.6-1.1 pptv in 1989.

Hydrochlorofluorocarbon (HCFC) growth rates are accelerating, as they are being used increasingly as CFC substitutes. Tropospheric chlorine as HCFCs increased in 1992 by about 10 pptv, thus accounting for about 15% of total tropospheric chlorine growth, compared to 5 pptv in 1989 (5% of tropospheric chlorine growth).

The atmospheric residence times of CFC-11 and methyl chloroform are now better known. Model studies simulating atmospheric abundances using more realistic emission amounts have led to best-estimated lifetimes of 50 years for CFC-11 and 5.4 years for methyl chloroform, with uncertainties of about 10%. These models, calibrated against CFC-11 and methyl chloroform, are used to calculate the lifetimes, and hence ODPs (Ozone Depletion Potentials), of other gases destroyed only in the stratosphere (other CFCs and nitrous oxide) and those reacting significantly with tropospheric hydroxyl radicals (HCFCs and hydrofluorocarbons (HFCs)).

Methyl chloride, released from the oceans (natural) and biomass burning (anthropogenic), is a significant source of tropospheric chlorine, contributing about 15% of the total tropospheric chlorine abundance in 1992 (3.8 ppbv). Data collected from the late 1970s to the mid-1980s showed no long-term trend. A paucity of published observational data since means that the likely existence of a global trend in this important species cannot be assessed further.

The total abundance of organic halocarbons in the lower stratosphere is well characterized by *in situ* and remote observations of individual species. Observed totals are consistent with abundances of primary species in the troposphere, suggesting that other source species are not important in the stratosphere. Loss of halocarbons is found as their residence time in the stratosphere increases, consistent with destruction by known photochemical processes. Since the loss of halocarbons produces inorganic chlorine and bromine species associated with ozone loss processes, these observations also constrain the abundance of these organic species in the lower stratosphere.

Volcanoes are an insignificant source of stratospheric chlorine. Satellite and aircraft observations of upper and lower stratospheric hydrochloric acid (HCl) are consistent with stratospheric chlorine being organic, largely anthropogenic, in origin. No significant increase in HCl was found in the stratosphere following the intense eruption of Mt. Pinatubo in 1991. Elevated HCl levels were detected in the eruption cloud of the El Chichón volcano in 1982, but no related change in global stratospheric HCl was observed.

The 1980s were characterized by declining global methane growth rates, being approximately 20 ppbv per year in 1980 declining approximately monotonically to 10 ppbv per year by the end of the decade. Methane growth rates slowed dramatically in 1991-1992, but probably started to increase in late 1993. During 1992 global methane levels grew by only 5 ppbv. The causes of this global anomaly (which manifested predominantly at high latitudes in the Northern Hemisphere) are not known with certainty, but are probably due to changes in methane sources rather than in methane sinks. Global growth rate anomalies have been observed in methane records in the 1920s and 1970s from air trapped in Antarctic ice.

Despite the increased methane levels, the total amount of carbon monoxide (CO) in today's atmosphere is less than it was a decade ago. Recent analyses of global CO data show that tropospheric levels grew from the early 1980s to about 1987 and have declined from the late 1980s to the present. The causes of this behavior have not been identified.

TABLE 2-1. Current atmospheric levels, changes in abundance (1992 minus 1990) and lifetimes of long-lived trace gases. (Adapted from IPCC, 1994a.)

Species	Chem. Formula	mixing ratios (1992) ppbv	growth (1992-1990) ppbv	burden (Tg)	lifetime[a] (years)
CFC-11	CCl_3F	0.268	0.005	6.2	50 (±5)
CFC-12	CCl_2F_2	0.503	0.026	10.3	102
CFC-113	CCl_2FCClF_2	0.082	0.005	2.6	85
CFC-114	$CClF_2CClF_2$	0.020	0.001		300
CCl_4		0.132	-0.002	3.4	42
CH_3CCl_3		0.160	0.007	3.5	5.4 (±0.4)
CH_3Cl		0.600	?	5.0	1.5
HCFC-22	$CHClF_2$	0.102	0.014	1.5	13.3
HCFC-141b	CH_3CCl_2F	0.0003			9.4
HCFC-142b	CH_3CClF_2	0.0035			19.5
CH_3Br	(see Chapter 10)				
H-1211	$CBrClF_2$	0.0025	0.0001	0.08	20
H-1301	$CBrF_3$	0.0020	0.0003	0.05	65
CF_4		0.070		0.9	50000
C_2F_6		0.004			10000
SF_6		[0.002-0.003]			3200
N_2O (N)		310	1.4	1480	120
CH_4		1714	14	4850	10[b]
CO_2 (C)		356000	2000	760000	(50-200)[c]

[a] Lifetimes of additional halocarbons are given in Chapter 13.

[b] The adjustment time is 12 to 17 years; this takes into account the indirect effect of methane on its own lifetime (IPCC, 1994a).

[c] No single lifetime can be defined because of the different rates of uptake by different sink processes (IPCC, 1994b).

TABLE 2-2. Recent halocarbon trends compared with the values given in the 1991 assessment.

Compound	Period	This Assessment[a] pptv/yr	This Assessment[a] %/yr	1991 Assessment[b] pptv/yr	1991 Assessment[b] %/yr
CFC-11	90-92	2.5	0.9	9.3-10.1	3.7-3.8
CFC-12	90-92	13	2.6	16.9-18.2	3.7-4.0
CFC-113	90-92	2.5	3.1	5.4- 6.2	9.1
CCl_4	90-92	-1	-0.8	1- 1.5	1.2
CH_3CCl_3	90-92	3.5	2.2	4.8- 5.1	3.7
HCFC-22	92	7.0	6.9	5- 6	6-7
HCFC-142b	92	~1	~30	n.d.	n.d.
HCFC-141b	93	~0.75	~200	n.d.	n.d.
H-1211	90-92	0.075	3	0.2-0.4	15
H-1301	90-92	0.16	8	0.4-0.7	20
Total Cl		~60		~110	
Total Br[c]		0.2-0.3		0.6-1.1	

[a] see text for references

[b] 1989 increase (WMO, 1992)

[c] bromine in the form of halons

growth rate observed in 1990 has continued, presumably due to reduced emissions in 1991-92 as compared to 1990 and in part to increasing OH levels (1 ± 0.8 %/yr; Prinn *et al.*, 1992). The methyl chloroform calibration problems detailed in Fraser *et al.* (1994a) have yet to be resolved.

Recent global HCFC-22 data (Montzka *et al.*, 1993) indicate a global mixing ratio in 1992 of 102 ± 1 pptv, an interhemispheric difference of 13 ± 1 pptv, and a globally averaged growth rate of 7.3 ± 0.3 %/yr, or 7.4 ± 0.3 pptv/yr, from mid-1987 to 1992. Based on the latest industry estimates of HCFC-22 emissions (Midgley and Fisher, 1993) the data indicate an atmospheric lifetime for HCFC-22 of 13.3 (15.5-12.1) years. Regular vertical column abundances measured by infrared solar absorption spectroscopy in Arizona (32°N), Switzerland (46.6°N) (Zander *et al.*, 1994a), and California (34.4°N) (Irion *et al.*, 1994) have revealed rates of increase of 7.0 ± 0.2%/yr (1981-1992), 7.0 ± 0.5%/yr (1981-1992), and 6.5 ± 0.5%/yr (1985-1990), respectively. Using the HCFC-22 column abundances obtained at McMurdo, Antarctica (78°S), Irion *et al.* (1994) derived a south-north interhemispheric growth rate ratio of 0.85, in good agreement with the ratio of 0.88 obtained by Montzka *et al.* (1993) from *in situ* surface measurements. The latest 1993 HCFC-22 data indicate that the near-linear trend observed in earlier data has continued (J. Elkins, NOAA; R. Zander, I.A., Univ. of Liege, personal communications to E.S.).

CH_3CClF_2 (HCFC-142b) and CH_3CCl_2F (HCFC-141b) have been recently introduced as CFC substitutes. For HCFC-142b the National Oceanic and Atmospheric Administration (NOAA) flask network results indicate an atmospheric concentration of 3.1 pptv for 1992, with a growth rate of ~1 pptv/yr (~30%/yr) (Swanson *et al.*, 1993). The concentration of HCFC-141b for the last quarter of 1992 was 0.36 pptv and 1.12 pptv at the end of 1993 (~0.75 pptv/yr or ~200%/yr) (Montzka *et al.*, 1994). Pollock *et al.* (1992) detected upper tropospheric levels of HCFC-142b at about 1.1 pptv in 1989, growing at 7%/yr.

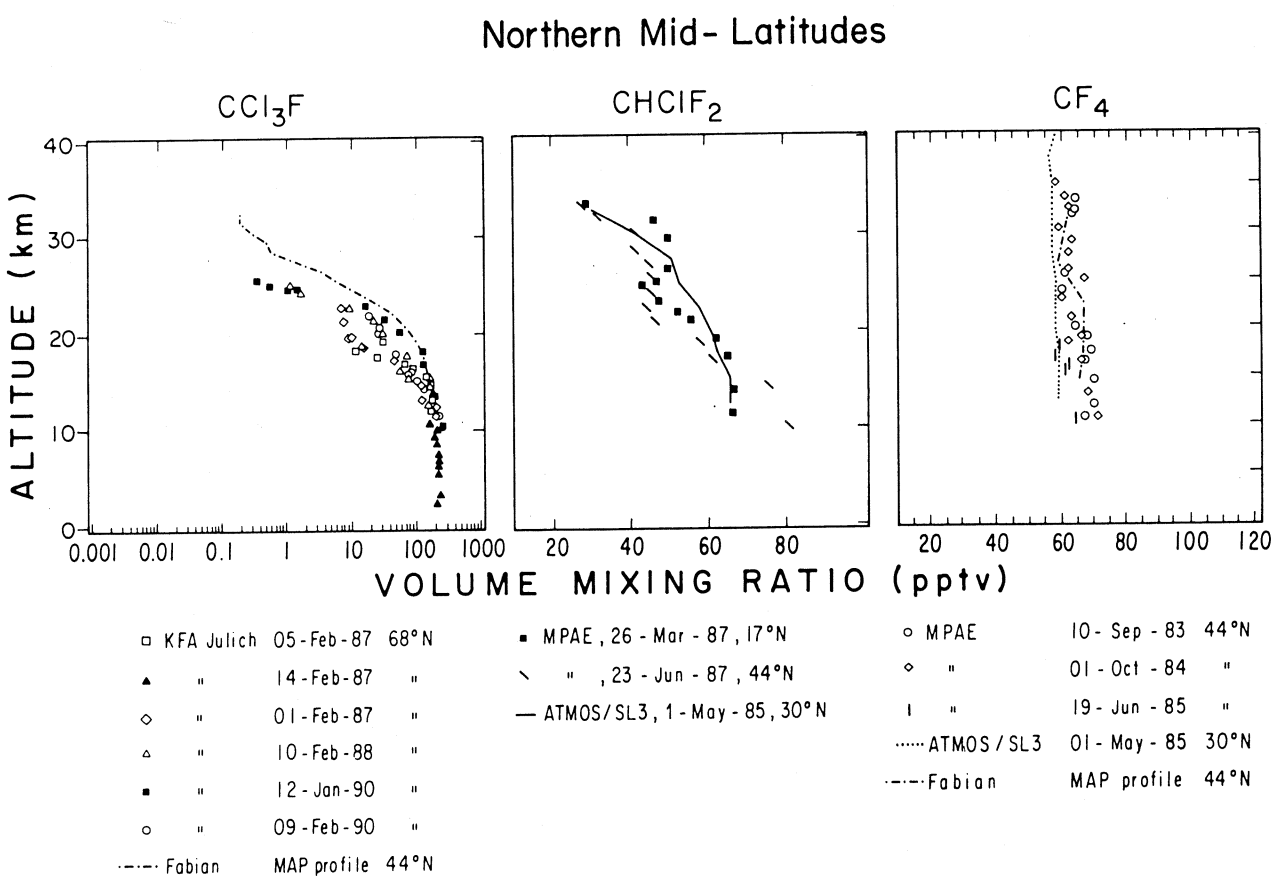

Figure 2-3. Vertical distributions of CCl_3F, $CHClF_2$, and CF_4 volume mixing ratios. Source: Adapted from Fraser *et al.*, 1994a.

2.2.2 Stratospheric Observations

When investigating the concentrations of halocarbons in the stratosphere, the main objectives are to determine partitioning among chlorine and bromine "families," their total loading and their time variations. It is therefore important to measure simultaneously and regularly the largest possible number of halocarbons in order to meet these objectives. For obvious technical reasons, such combined stratospheric measurements have been much sparser during the last decade than tropospheric investigations. The measurements are generally performed using *in situ* air sampling techniques aboard airplane and balloons, and through infrared remote observations made from airplane, balloon, and orbiting platforms.

A recent thorough review dealing with measurements of the stratospheric abundance and distribution of halocarbons can be found in Chapter 1 of the NASA Report (Fraser *et al.*, 1994a). The review is a compilation of measured concentrations expressed as volume mixing ratios versus altitude for CCl_3F, CCl_2F_2, CCl_4, $CHClF_2$, CH_3Cl, CH_3CCl_3, $C_2Cl_3F_3$, $C_2Cl_4F_2$, C_2ClF_5, C_2F_6, $CClF_3$, CF_4, CH_3Br, $CBrF_3$, and $CBrClF_2$, gathered between 1984 and 1990. As an example the concentration profiles for three halogenated methanes at northern midlatitudes are shown in Figure 2-3. The relative changes in stratospheric concentrations are due to different photochemical destruction rates of these compounds in the stratosphere: $CCl_3F > CHClF_2 >> CF_4$.

The *in situ* measurements at sub-tropical, mid- and high northern latitudes of the long-lived chlorinated halocarbons indicate that (i) the concentrations observed in the sub-tropics decline less rapidly with altitude than at midlatitudes, because of increased upward motion at

such latitudes (*i.e.*, Kaye *et al.*, 1991), thus allowing for photodissociation to occur at higher altitudes; (ii) the concentrations of both the halocarbons and the long-lived "reference" gases observed in the Arctic show a much more rapid decline with altitude than at midlatitudes, in particular within the winter vortex where subsidence is often present (Schmidt *et al.*, 1991; Toon *et al.*, 1992a, b, c). Thus, surfaces of constant mixing ratio of long-lived chlorinated halocarbons slope poleward and downward in the lower stratosphere.

During recent years, a few investigations dealing with simultaneous measurements of many chlorine- and/or bromine-bearing gases and related inventories have been reported. One of these concerns the budget of Cl (sources, sinks, and reservoirs) between 12.5 and 55 km altitude, near 30° north latitude, based on the 1985 ATMOS (Atmospheric Trace Molecule Spectroscopy Experiment)/Spacelab 3 measurements of HCl, CH_3Cl, $ClONO_2$, CCl_4, CCl_2F_2, CCl_3F, and $CHClF_2$, complemented by results for CH_3CCl_3, $C_2Cl_3F_3$, ClO, HOCl, and COClF obtained by other techniques (Zander *et al.*, 1992 and references therein). The main conclusions of this work indicate that (i) within the observed uncertainty, partitioning among chlorinated source, sink, and reservoir species is consistent with the conservation of Cl throughout the stratosphere; (ii) the mean 1985 concentration of stratospheric Cl was found equal to 2.55 ± 0.28 ppbv; (iii) above 50 km altitude, the inorganic chlorine burden is predominantly contained in the form of HCl, thus making this measurement a unique and simple way of assessing the effective stratospheric chlorine loading.

Based on historical emissions for the main chlorinated source gases, Weisenstein *et al.* (1992) used a time-dependent model to calculate the atmospheric total chlorine as a function of time, latitude, and altitude. Their results indicate that the total Cl mixing ratio for 1985 reaches an asymptotic value of 2.35 ppbv in the upper stratosphere. Considering that the source input fluxes to the model are probably too low by about 15% because they do not include emission from China, the former Soviet Union, and Eastern Europe, it can be concluded that the result found by Weisenstein *et al.* (1992) for 1985 is in good agreement with the stratospheric Cl budget derived from the 1985 ATMOS observations (Zander *et al.*, 1992).

The ATMOS instrument was flown again in 1992 (Gunson, 1992) and 1993 as part of the Atmospheric Laboratory for Applications and Science (ATLAS) 1 and 2 Missions to Planet Earth. HCl mixing ratios in the range 3.4 ± 0.3 ppbv were measured above 50 km altitude at different latitudes (30°N to 55°S) during March-April 1992, as compared to the measured value of 2.55 ± 0.28 ppbv in April-May 1985 (Gunson *et al.*, 1994). This corresponds to an increase of 35% over the 7 years between both measurements and is in excellent agreement with model-predicted increases of about 0.11 to 0.13 ppbv per year (Prather and Watson, 1990; WMO, 1992; Weisenstein *et al.*, 1992).

During the 1991/92 Airborne Arctic Stratospheric Expedition II (AASE II), a whole air sampler developed by NCAR-NASA/Ames (Heidt *et al.*, 1989) was operated on board the NASA ER-2 aircraft, which attempted to determine the amounts of organic chlorine and bromine entering the stratosphere. Over 600 air samples were collected during AASE II. Twelve of these that were sampled in the latitude/altitude range of the tropical tropopause, between 23.8°N and 25.3°N, have been analyzed by Schauffler *et al.* (1993) for the mixing ratios of 12 chlorinated species (CCl_3F, CCl_2F_2, $C_2Cl_3F_3$, $C_2Cl_2F_4$, C_2ClF_5, $CHClF_2$, CH_3CClF_2, CH_3Cl, CH_2Cl_2, $CHCl_3$, CH_3CCl_3, and CCl_4) and 5 brominated compounds ($CBrF_3$, $CBrClF_2$, $C_2Br_2F_4$, CH_3Br, and CH_2Br_2). From this extensive suite of measurements, Schauffler *et al.* (1993) derived average total mixing ratios of 3.50 ± 0.06 ppbv for Cl and 21.1 ± 0.8 pptv for Br. The natural source of chlorine is ~0.5 ppbv of the total. Since inorganic chlorine species are negligible at the tropopause, total chlorine at this level is dominated by the anthropogenic release of chlorinated halocarbons at the surface. The stratospheric Cl concentrations derived from the March-April 1992 ATMOS measurements and the January-March 1992 burdens found by Schauffler *et al.* (1993) near the tropopause provide a further confirmation of the conservation of chlorine throughout the stratosphere. The individual contributions to the total organic budget of bromine near the tropical tropopause were found equal to 54% for CH_3Br, ~7% for CH_2Br_2, and the remaining 39% nearly evenly distributed among the halons $CBrF_3$, $CBrClF_2$, and $C_2Br_2F_4$.

On the NASA DC-8 aircraft that also participated in the AASE II campaign, Toon *et al.* (1993) operated a

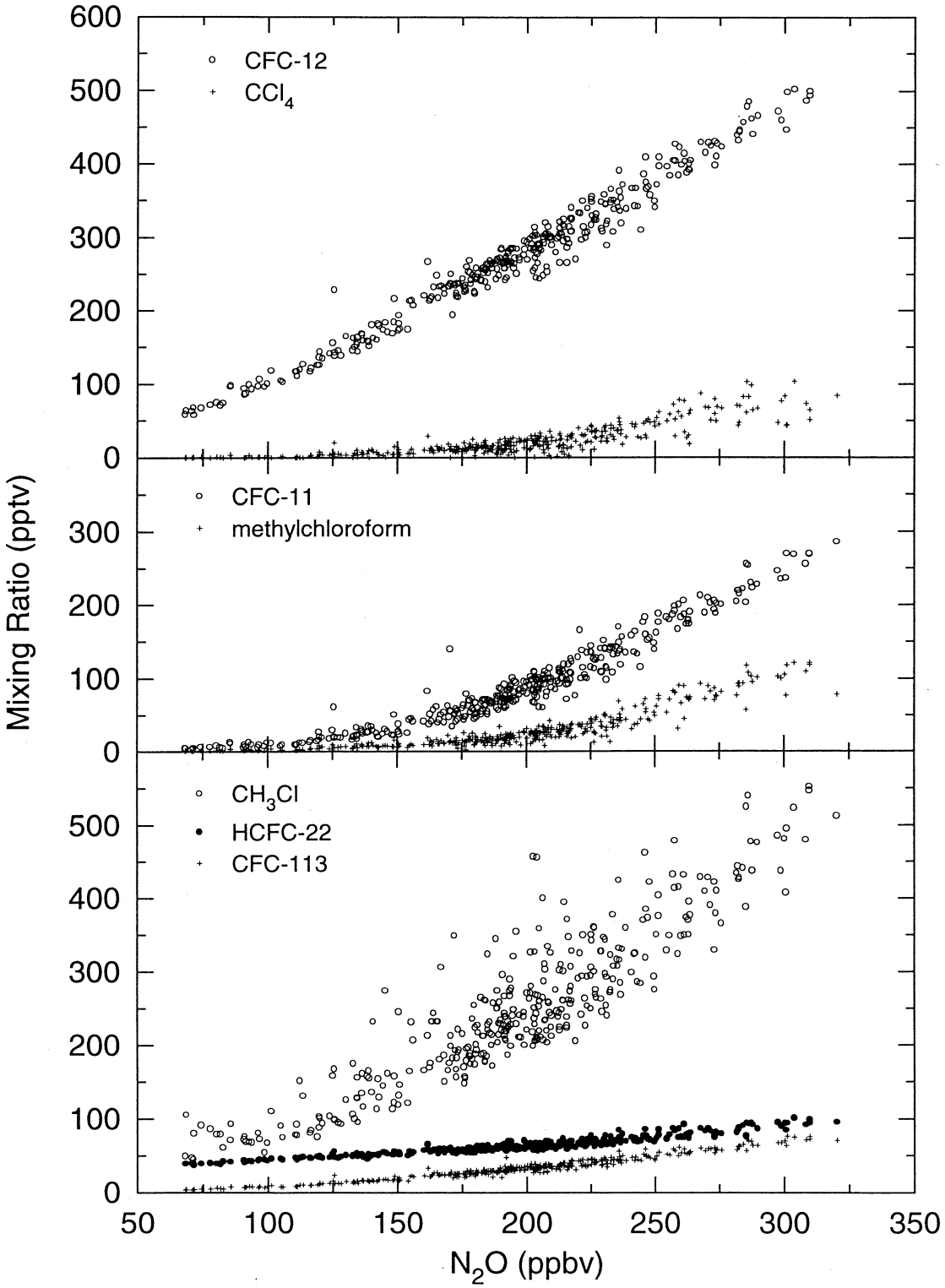

Figure 2-4. Concentrations of halocarbons in the lower stratosphere from NCAR/NASA Ames Whole Air Sampler plotter vs. ATLAS N_2O. Source: Woodbridge *et al.*, 1994.

high-resolution Fourier transform infrared (FTIR) spectrometer to determine the stratospheric columns above about 11 km cruising altitude of a number of trace gases, including CCl_2F_2 and CCl_3F. Based on these and other long-lived gases (*e.g.*, N_2O, CH_4), they found considerably more uplifting (~4 km) near the equator than in the sub-tropics.

Above the tropopause, the AASE II data set can be used to describe the depletion of chlorinated halocarbons in the lower stratosphere. As residence time in the stratosphere increases, destruction primarily by UV photolysis liberates Cl and Br from individual halocarbon species, thereby forming the inorganic halocarbon reservoir species HCl and $ClONO_2$. Nitrous oxide can be used as an index to examine changes in halocarbon abundances (Kawa *et al.*, 1992). N_2O has a near-uniform abundance in the troposphere of approximately 310 ppbv and is destroyed in the mid-stratosphere with a lifetime near 120 years. Figure 2-4 shows the correlation of several chlorinated halocarbon species with simultaneous measurements of N_2O within the AASE II data set (Woodbridge *et al.*, 1994). The seven species shown represent approximately 99 percent of organic halocarbon species with lifetimes over a year. For each species a distinct correlation is found, with the halocarbon species decreasing with decreasing N_2O. In each case, the decrease begins at upper tropospheric altitudes as reported by Schauffler *et al.* (1993). The slope of each correlation near tropospheric values is related to the ratio of the lifetime of the halocarbons species to that of N_2O (Plumb and Ko, 1992). The compact nature of ranges of these correlations demonstrates the systematic degradation of the chlorinated halocarbons in the stratosphere. The net loss of these organic species over a range of N_2O bounds the available inorganic chlorine reservoir in the lower stratosphere (see Chapter 3). Inorganic species participate in the principal catalytic loss cycles that destroy stratospheric ozone.

The emission of HCl from volcanoes can exceed the annual anthropogenic emissions of total organic chlorine (*e.g.*, CFCs, HCFCs) to the atmosphere. However, emitted HCl is largely removed in the troposphere before it can enter the stratosphere. For the recent Mt. Pinatubo eruption, column measurements of HCl before and after the eruption confirmed that the increase of HCl in the stratosphere was negligible (Wallace and Livingston, 1992; Mankin *et al.*, 1992). Elevated HCl levels were detected in the eruption cloud of the El Chichón volcano in 1982 (Mankin and Coffey, 1984), but significant changes in the global stratospheric HCl were not observed. The removal of HCl and H_2O is expected to result from scavenging on liquid water droplets formed in the volcanic plume (Tabazadeh and Turco, 1993).

Additional material of relevance to this section can be found in Chapter 3 (Polar Ozone), which also deals with stratospheric abundances of both total organic chlorine and total available chlorine during the Arctic winter; these data may be compared with the mixing ratios of total chlorine quoted here before.

2.2.3 Sources of Halocarbons

CFCs, halons, HCFCs, and hydrofluorocarbons (HFCs) are exclusively of industrial origin, as are methyl chloroform and carbon tetrachloride. Their primary uses are as refrigerants (CFCs-11, 12, and -114; HCFC-22; HFC-134a), foam blowing agents (HCFCs-22 and -142b; CFCs-11 and -12), solvents and feedstocks (CFC-113, carbon tetrachloride, and methyl chloroform), and fire retardants (halons-1211 and -1301). Worldwide emissions of individual halocarbons have fallen significantly following enactment of the Montreal Protocol (Figure 2-5; AFEAS, 1993, 1994; Fisher *et al.*, 1994). From 1988 to 1992 annual emissions of CFCs into the atmosphere have decreased by approximately 34%. Emission levels of methyl chloroform have also declined over this period, with a very large emission reduction (~50%) from 1992 to 1993 (P. Midgley, personal communication to P.F.). HCFC-22 has shown a continued rise (Midgley and Fisher, 1993); it has replaced CFCs in many applications as its use has not been restricted by the Protocol. HCFC-142b release began in the early 1980s and is growing rapidly (35%/yr since 1987). Emissions in 1992 were 10.8×10^6 kg (AFEAS, 1994). Emissions are difficult to estimate accurately as the bulk of the production (90%) is used in closed cell foams with residence times greater than 10 years. Between 1987 and 1990, emissions of halons have dropped substantially (McCulloch, 1992) (no data are available yet for 1991 and 1992). No emission data are available for carbon tetrachloride as its production and use has not been surveyed. A detailed update of the anthropogenic emissions of methyl bromide is given in Chapter 10.

Recently, using the atmospheric data and the equilibrium lifetimes, Cunnold *et al.* (1994) estimated the

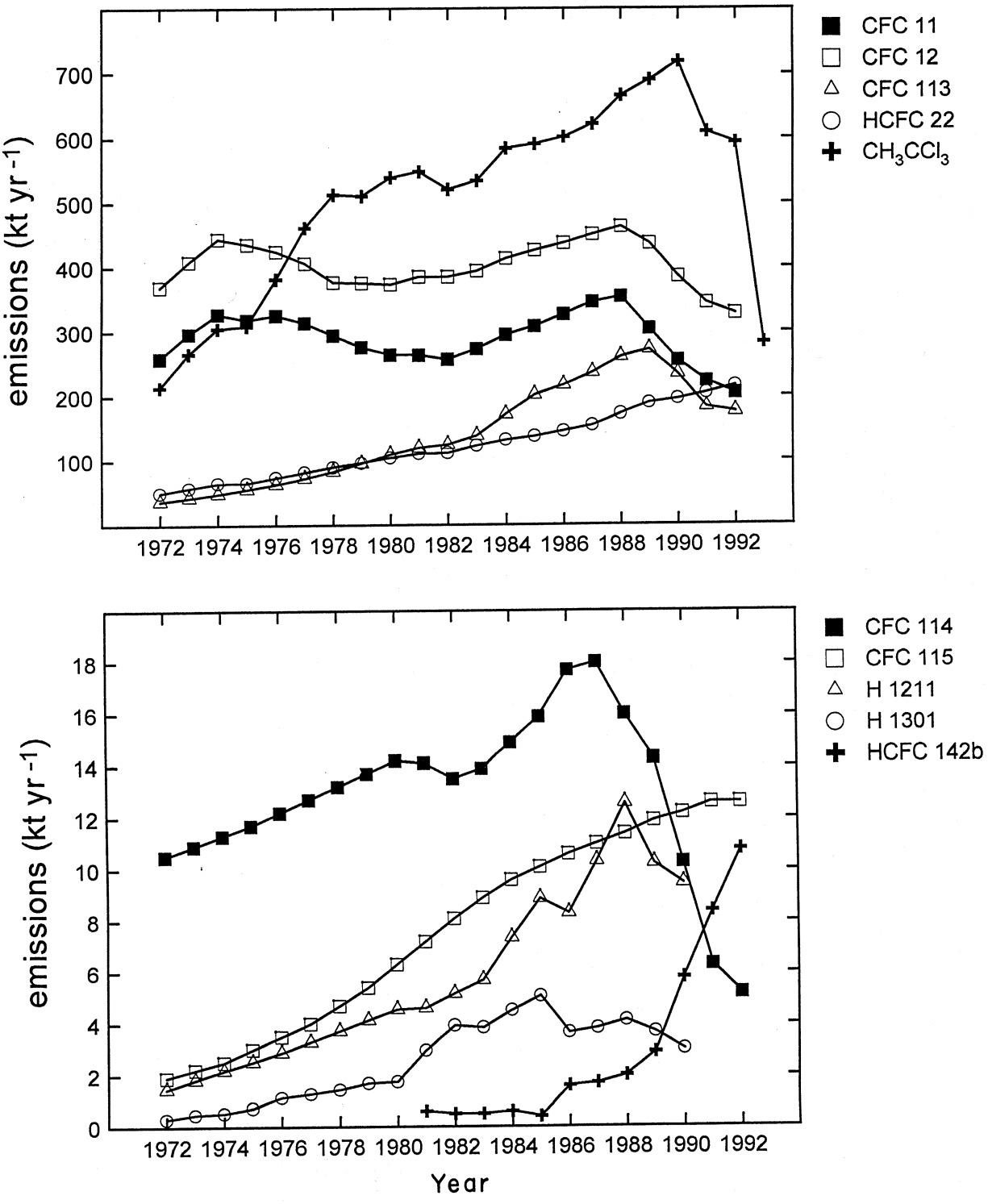

Figure 2-5. Annual emissions of halocarbons in kt/yr. The CFC-11, -12 and -113 data are estimates of global emissions, whereas the remaining estimates are based on data only from reporting companies. Source: AFEAS, 1993; Fisher *et al.*, 1994; D. Fisher, Du Pont, personal communication to P.F.; P. Midgley, M&D Consulting, personal communication to P.F.

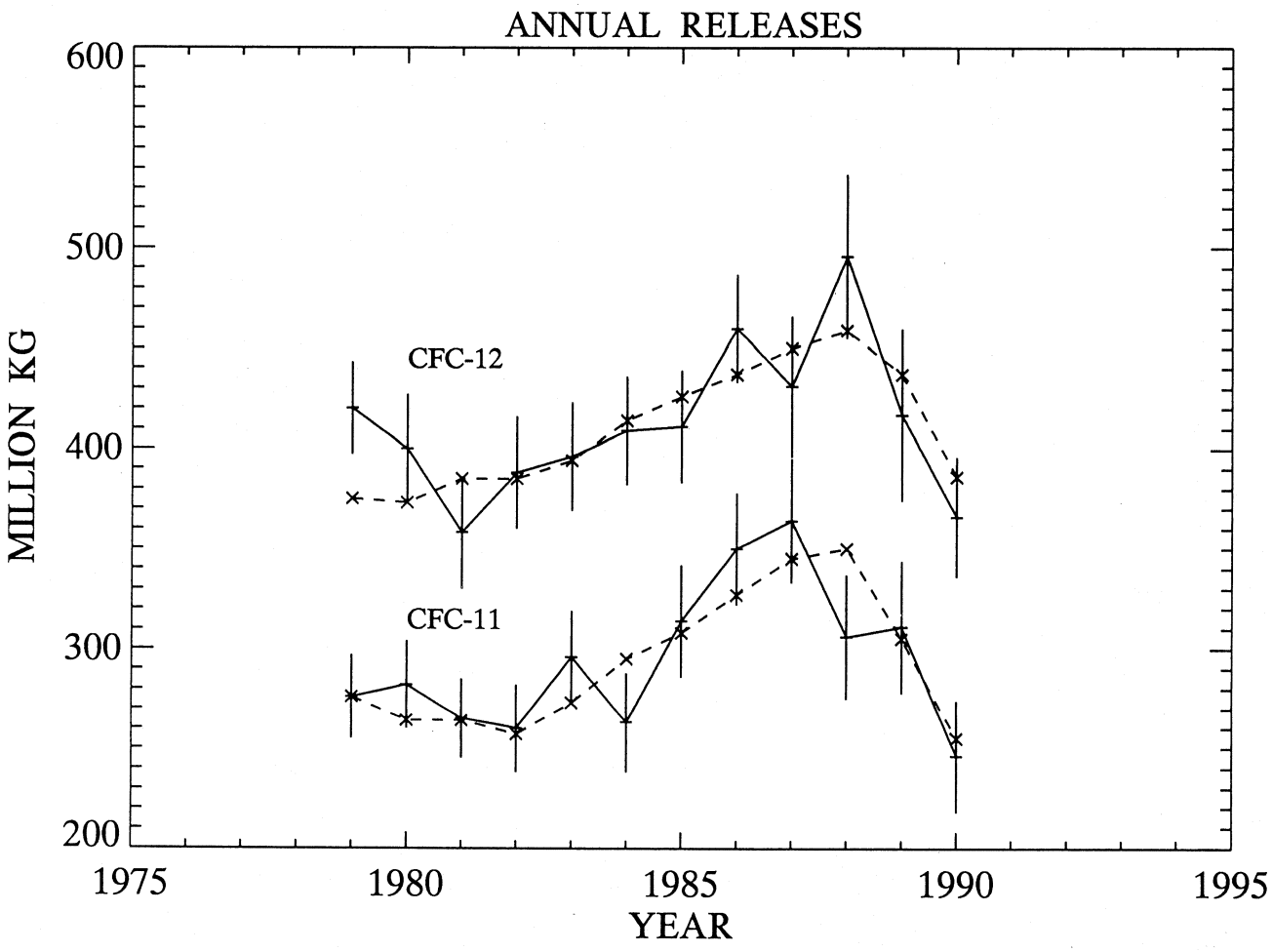

Figure 2-6. Annual releases of CCl_3F and CCl_2F_2 estimated from 13 years of ALE/GAGE data (points are joined by a full line), and most recent estimates of world releases of these compounds (Fisher *et al.*, 1994). Source: Cunnold *et al.*, 1994.

1990 CFC-11 and CFC-12 releases to be 249 ± 28 kton and 366 ± 30 kton, respectively. These values are comparable to the global emissions assembled by Fisher *et al.* (1994) (CFC-11: 255.2 kton and CFC-12: 385.6 kton) (Figure 2-6).

CH_2Cl_2 and $CHClCCl_2$ are used as industrial cleaning solvents. Sources of 0.9 and 0.6 Tg/yr have been recently estimated from observed atmospheric abundances (Koppmann *et al.*, 1993). Industry estimates of 1992 emissions for CCl_2CCl_2, $CHClCCl_2$, and CH_2Cl_2 were 0.24, 0.16, and 0.39 Tg, respectively. Total emissions for these species have declined by 40% since 1982 (P. Midgley, personal communication to P.F.). The aluminum refining industry produces CF_4 (0.018 Tg/yr) and C_2F_6 (0.001 Tg/yr), however, there are no estimates of other potential sources (Cicerone, 1979). 80% of SF_6 production (0.005 Tg in 1989) is used for insulation of electrical equipment, 5-10% for degassing molted reactive metals, and a small amount as an atmospheric tracer (Ko *et al.*, 1993). The rate of increase of SF_6 in the atmosphere (Zander *et al.*, 1991a; Rinsland *et al.*, 1993; Maiss and Levin, 1994) implies that its sources are increasing.

Methyl halides are produced during biomass burning. Annual emissions of 1.5-1.8 Tg/yr (Lobert *et al.*, 1991; Andreae, 1993) and 30 Gg/yr (Manö and Andreae, 1994) have been estimated for CH_3Cl and CH_3Br, respectively.

A major source of methyl halides appears to be the marine/aquatic environment, likely associated with algal growth (Sturges *et al.*, 1993; Moore and Tokarczyk, 1993a). Methyl chloride, present in the troposphere at about 600 pptv, is the most prevalent halogenated methane in the atmosphere. Maintaining this steady-state mixing ratio with an atmospheric lifetime of the order of two years requires a production of around 3.5 Tg/yr, most of which comes from the ocean and biomass burning. The atmospheric budget of methyl bromide is discussed in Chapter 10. Other halogenated methanes, such as $CHBr_3$, $CHBr_2Cl$, and CH_2CBr_2, are produced by macrophytic algae (seaweeds) in coastal regions (Manley *et al.*, 1992) and possibly by open ocean phytoplankton (Tokarczyk and Moore, 1994), but they do not accumulate significantly in the atmosphere.

2.2.4 Halocarbon Sinks

Fully halogenated halocarbons are destroyed primarily by photodissociation in the mid-to-upper stratosphere. These gases have atmospheric lifetimes of decades to centuries (Table 2-1).

Halocarbons containing at least one hydrogen atom, such as HCFC-22, chloroform, methyl chloroform, the methyl halides, and other HCFCs and HFCs are removed from the troposphere mainly by reaction with OH. The atmospheric lifetimes of these gases range from years to decades, except for iodinated compounds such as methyl iodide, which have lifetimes of the order of days to months. However, some of these gases also react with seawater. About 5-10% of the methyl chloroform in the atmosphere is lost to the oceans, presumably by hydrolysis (Butler *et al.*, 1991). About 2% of atmospheric HCFC-22 is apparently destroyed in the ocean, mainly in tropical surface waters (Lobert *et al.*, 1993). Methyl bromide sinks are discussed in Chapter 10.

Recent studies show that carbon tetrachloride may be destroyed in the ocean. Widespread, negative saturation anomalies (-6 to -8%) of carbon tetrachloride, consistent with a subsurface sink (Lobert *et al.*, 1993), have been reported in both the Pacific and Atlantic oceans (Butler *et al.*, 1993; Wallace *et al.*, 1994). Published hydrolysis rates for carbon tetrachloride are not sufficient to support these observed saturation anomalies (Jeffers *et al.*, 1989) which, nevertheless, indicate that about 20% of the carbon tetrachloride in the atmosphere is lost in the oceans.

Recent investigation of the atmospheric lifetimes of perfluorinated species CF_4, CF_3CF_3, and SF_6 indicates lifetimes of >50,000, >10,000, and 3200 years (Ravishankara *et al.*, 1993). Loss processes considered include photolysis, reaction with $O(^1D)$, combustion, reaction with halons, and removal by lightning.

2.2.5 Lifetimes

Lifetimes are given in Table 2-1. An assessment and re-evaluation of the empirical models used to derive the atmospheric residence lifetime of two major industrial halocarbons, CH_3CCl_3 and CFC-11, have been made recently (Bloomfield, 1994). The analysis uses four components: observed concentrations, history of emissions, a predictive atmospheric model, and an estimation procedure for describing an optimal model. An optimal fit to the observed concentrations at the five Atmospheric Lifetime Experiment/Global Atmospheric Gases Experiment (ALE/GAGE) surface sites over the period 1978-1990 was done with two statistical/atmospheric models: the ALE/GAGE 12-box atmospheric model with optimal inversion (Prinn *et al.*, 1992) and the North Carolina State University/University of California-Irvine 3D-Goddard Institute for Space Studies (NCSU/UCI 3D-GISS) model with autoregression statistics (Bloomfield, 1994). There are well-defined differences in these atmospheric models, which contribute to the uncertainty of derived lifetimes.

The lifetime deduced for CH_3CCl_3 is 5.4 years with an uncertainty range of ±0.4 yr (IPCC, 1994a). From this total atmospheric lifetime, the losses to the ocean and the stratosphere are used to derive a tropospheric lifetime for reaction with OH radicals of 6.6 yr (±25%); this value is used to scale the lifetimes of HCFCs and HFCs (*e.g.*, Prather and Spivakousky, 1990). On the other hand, the semi-empirical lifetime for CFC-11 of 50 ± 5 years (IPCC, 1994a) provides an important transfer standard for species that are mainly removed in the stratosphere, *i.e.*, the relative modeled lifetimes given in Table 2-1 for CFCs, H-1301, and N_2O are scaled to a CFC-11 lifetime of 50 yr.

A more recent analysis of the ALE/GAGE data (1978-1991) using the ALE/GAGE model and a revised CFC-11 calibration scale (SIO 93) gives an equilibrium lifetime for CFC-11 of 44 (+17/-10) years (Cunnold *et al.*, 1994).

2.3 STRATOSPHERIC INPUTS OF CHLORINE AND PARTICULATES FROM ROCKETS

Solid-fuel rocket motors of launch vehicles release chemicals in the stratosphere, including chlorine (mainly HCl), nitrogen, and hydrogen compounds that, directly or indirectly, can contribute to the catalytic destruction of ozone. Chapter 10 of the WMO-Report No. 25 covers this subject (Harwood *et al.*, 1992). Since that report, which summarized model studies that evaluated the chlorine buildup in the stratosphere and its impact on the ozone layer, based on the projected launches of the larger rocket types (Space Shuttle and Titan IV by Prather *et al.*, 1990, and by Karol *et al.*, 1991; Ariane 5 by Pyle and Jones, 1991), no additional studies have been released. The main conclusions arrived at by Harwood *et al.* (1992) were: i) within the expanding exhaust trail of a large rocket, stratospheric ozone can be reduced substantially, up to >80% at some heights and up to 3 hours after launch; ii) because of the slant layout of the trajectory, column ozone is probably reduced by less than 10% over an area of a few hundred square kilometers; iii) the local plume ozone reductions decrease to near zero within 24 hours and the regional effects are too small to be detected by satellite observations; iv) steady-state model calculations for realistic launch scenarios of large rockets by NASA and ESA (European Space Agency) show that for both scenarios, ozone decreases are less than 0.2% locally in the region of maximum chlorine increase, with corresponding changes in ozone column of much less than 0.1%.

2.3.1 Stratospheric Chlorine Input

The specific chlorine (Cl) input to the stratosphere (above 15 km altitude) from rocket exhausts can be estimated if the Cl amount and its time-dependent release along the ascent are known. Such evaluations were reported by Prather *et al.* (1990) regarding the Space Shuttle (68 tons Cl) and the Titan IV launcher (32 tons Cl), and by Pyle and Jones (1991) for Ariane 5 (57 tons Cl). Assuming a projection of 10 launches per year for each of these chlorine-releasing rocket types, a total of 1570 tons of Cl is then deposited in the stratosphere each year. This corresponds to only 0.064% of the present-day stratospheric burden of chlorine (based on a Cl volume mixing ratio of 3.5 ppbv, or a total of 2.45×10^6 tons of Cl above 15 km altitude). However, at the rate of increase of the stratospheric chlorine loading measured between 1985 and 1992, *i.e.*, 0.13 ppbv per year (see Section 2.2.2) caused by the release of 30×10^4 tons/yr of Cl from the photodissociation of CFCs in the stratosphere (Prather *et al.*, 1990), the scenario of large rocket launches envisaged here corresponds to an additional injection of Cl above 15 km equal to about 0.6% per year. This percentage will increase as CFCs are phased out. No similar Cl input to the stratosphere can be evaluated for a large number of smaller rockets, because their exhaust characteristics as well as their number of launches worldwide (maybe some 100, all types combined; Harwood *et al.*, 1992) are poorly documented or inaccessible.

2.3.2 Particulates from Solid-Fuel Rockets

Besides gases, solid-fuel rocket motors release particulates in the form of aluminum oxide (Al_2O_3), soot, and ice. Attempts to determine the distribution of exhausted aluminum oxide particles in the rocket exhausts are limited, with only one Shuttle-related set of measurements made some 10 years ago (Cofer *et al.*, 1985) indicating a distribution of particles with significantly more particles below 1 μm than above 1 μm in size. The lack of satisfactory information on rocket particulate releases significantly hampers the quantification of impacts that heterogeneous chemistry (Hofmann and Solomon, 1989; Granier and Brasseur, 1992) may have on ozone depletion by rockets.

The only research programs that have provided some indication about the recent evolution of particulates and aerosols in the stratosphere are by Zolensky *et al.* (1989) and by Hofmann (1990, 1991). From impaction collections sampled in 1978 and 1984, Zolensky *et al.* (1989) found an order of magnitude increase in aluminum-rich particles of >0.5 μm diameter at 17-19 km altitude; they suggested that this rise is likely due to the influx of solid rocket motor exhaust and ablating rocket and satellite debris into the stratosphere in increasingly larger amounts, with the latter predominating. Hofmann (1990) observed an increase by about 80% of the background (non-volcanic) stratospheric sulfate burden at northern midlatitudes between 1979 and 1990. He speculated (Hofmann, 1991) that it may be partially caused by the increase in air traffic during that same period, basing his evaluation on a representative fleet and engine

emission index of sulfur dioxide (SO_2), as well as on a realistic lifetime for the stratospheric aerosol. However, Bekki and Pyle (1992) concluded that the increase in aerosol mass between 1979 and 1990 due to the rise of air traffic is largely insufficient to account for the observed mass trend and suggest that a rise in submicrometer particles due to the influx of solid rocket exhaust and ablating spacecraft material merits further investigations. Clearly, particulates from solid-fuel rockets deserve careful attention, especially as their stratospheric abundance may increase in the near future.

2.4 METHANE (CH_4)

Methane is an important greenhouse gas that is also a reactive gas that participates in establishing the oxidizing capacity of the troposphere, and therefore affects the lifetime of many other trace gases. In the stratosphere it is a source of hydrogen and water vapor, and a sink of atomic chlorine. It is mainly produced from a wide variety of anaerobic processes and removed by the hydroxyl radical. Its abundance in the atmosphere has been rising since the Industrial Revolution with its global 1992 tropospheric mixing ratio being equal to 1.714 ppmv. A large fraction of methane is released to the atmosphere from anthropogenic sources (~2/3) and is therefore susceptible to possible emission controls. A reduction of about 10% of anthropogenic emissions would stabilize the concentration at today's level (IPCC, 1994a).

2.4.1 Atmospheric Distribution and Trends

Due to the distribution of CH_4 sources, there is an excess Northern Hemispheric source of about 280 Tg/yr, and atmospheric concentrations in the Southern Hemisphere are ~6% lower. Recent modeling (Law and Pyle, 1993) and isotopic (Lassey *et al.*, 1993) studies confirm that the seasonal cycle of methane (±1.2% at midlatitudes) in the Southern Hemisphere is mainly controlled by the seasonality of methane oxidation by OH radicals in the lower troposphere and the transport of air from tropical regions that are affected by biomass burning.

During the past decade, global methane has increased on average by about 7% (Dlugokencky *et al.*, 1994a). The declining atmospheric methane growth identified in the previous assessment has continued. Measurements from two global observing networks show a steady decline in the globally averaged growth rate since the early 1980s (Steele *et al.*, 1992; Khalil and Rasmussen, 1993b; Khalil *et al.*, 1993a; Dlugokencky *et al.*, 1994c), being approximately 20 ppbv/yr in 1979-1980, 13 ppbv/yr in 1983, 10 ppbv/yr in 1990, and about 5 ppbv/yr in 1992 (Dlugokencky *et al.*, 1994c). The decline of the growth rate in the 30°-90°N semi-hemisphere was 2-3 times more rapid than in the other semi-hemisphere. The 1992 increase in the Northern Hemisphere was only 1.8 ± 1.6 ppbv (Dlugokencky *et al.*, 1994c). The cause of this global decline in methane growth is not entirely clear, but could be related to changes in emissions from fossil fuel (particularly natural gas) in the former Soviet Union (Dlugokencky *et al.*, 1994c) and from biomass burning in the tropics (Lowe *et al.*, 1994). Observed methane levels in the high Arctic (Alert, 83°N) in 1993 were actually lower than those observed in 1992 (Worthy *et al.*, 1994). Data reported for Antarctica (Aoki *et al.*, 1992) show the same trend observed by the NOAA-CMDL station in the same region. Vertical column abundance measurements above the Jungfraujoch station, Switzerland, between February 1985 and May 1994 indicate a rate of increase in the atmospheric burden of CH_4 equal to 0.73 ± 0.13 %/yr over the period 1985-1989, which slowed to 0.46 ± 0.11 %/yr between 1990 and May 1994 (Zander *et al.*, 1994c; R. Zander, personal communication to E.S.).

A significant decrease in $^{13}CH_4$ has been observed in the Southern Hemisphere since mid-1991, coincident with significant changes in the CH_4 growth rate (15 ppb/yr in 1991; 5 ppb/yr in 1992) (Lowe *et al.*, 1994). The isotopic data imply that the change in CH_4 growth rate is due to: i) decreasing sources rather than increasing sinks, and ii) a combination of decreased tropical biomass burning and a lower release of fossil CH_4 in the Northern Hemisphere.

Global measurements of CH_4 between 100 and 0.1 mb pressure levels have been performed by various instruments aboard the Upper Atmosphere Research Satellite (UARS). Since October 1991, the UARS Halogen Occultation Experiment (HALOE) has made routine measurements of methane concentrations at latitudes ranging from ~80°N to ~80°S. These measurements have been used in conjunction with other HALOE observations to evaluate vertical subsidence in the Antarctic spring polar vortex (Russell *et al.*, 1993); they have un-

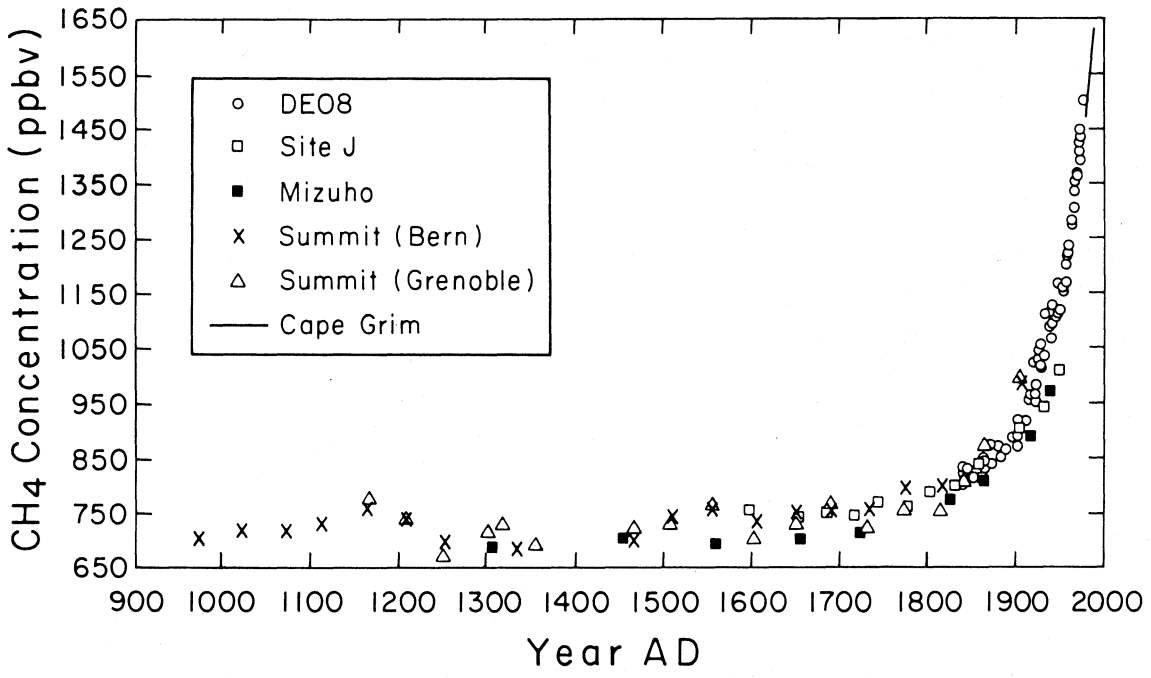

Figure 2-7. Methane mixing ratios observed in ice cores from Antarctica (Law Dome: Etheridge *et al.*, 1992; Mizuho: Nakazawa *et al.*, 1993) and Greenland (Site J: Nakazawa *et al.*, 1993; Summit: Blunier *et al.*, 1993) over the past 1000 years. Atmospheric data from Cape Grim, Tasmania, are included to demonstrate the smooth transition from ice core to atmospheric measurements. Source: IPCC, 1994a.

dergone intercomparison with ER-2 airplane observations (Tuck *et al.*, 1993), as part of validation exercises. The Cryogenic Limb Array Etalon Spectrometer (CLAES) UARS experiment also measured CH_4 concentrations globally, but results have only been reported so far as sample cases, as additional validation is required prior to releasing this data base (Kumer *et al.*, 1993). Although limited in time and in global coverage, the high spectral-resolution, multiple-species (over two dozen gases) observations made by the shuttle-based Atmospheric Trace Molecule Spectroscopy Experiment (ATMOS) instrument during the Spacelab 3 (April-May, 1985), ATLAS 1 (March-April, 1992) and ATLAS 2 (April, 1993) missions (Farmer, 1987; Gunson *et al.*, 1990; Gunson, 1992) are unique "benchmarks" for trends evaluations and for validation exercises.

The paleo record of atmospheric methane concentration has been improved by the analysis of new ice cores (Etheridge *et al.*, 1992; Nakazawa *et al.*, 1993; Blunier *et al.*, 1993; Jouzel *et al.*, 1993; Chappellaz *et al.*, 1993). Antarctic ice core data (Law Dome), which overlap the direct atmospheric measurements, indicate that the growth rate was not always monotonic, with apparent stabilization periods around the 1920s and again during the 1970s (see Figure 2-7; Etheridge *et al.*, 1992; Dlugokencky *et al.*, 1994a). From Greenland and Antarctic ice cores, Nakazawa *et al.* (1993) conclude that the pre-industrial natural sources in the Northern Hemisphere were larger than those in the Southern Hemisphere. New data from Antarctic Vostok ice core have extended the methane record from 160 thousand year BP (kaBP) through the penultimate glaciation to the end of the previous interglacial, about 220 kaBP (Jouzel *et al.*, 1993). Recent analyses of Greenland ice cores have provided additional climatic and atmospheric composition records (Chappellaz *et al.*, 1993). The methane concentration through the deglaciation is observed to be in phase with temperature. Warm periods, each lasting hundreds of years, are associated with methane peaks of about 100 ppbv. These variations have not been observed in the Antarctic ice cores, likely due to the coarse sampling interval and the slower pore close-off of the Antarctic sites.

2.4.2 Sources

A detailed discussion of the natural and anthropogenic sources of methane has been given in previous assessments (WMO, 1992; IPCC, 1990, 1992) and only an update is presented here. Methane sources are listed in Table 2-3.

Wetlands. Natural wetlands are the major source of methane and in recent years considerable new data on methane flux from these ecosystems have been published. Recent flux data from the Amazon region suggest that a large fraction of CH_4 is emitted from tropical wetlands (20°N-30°S), with a global estimate of ~60 Tg/yr (Bartlett *et al.*, 1990; Bartlett and Harris, 1993). High northern latitude studies indicate emissions ranging from 20 to 60 Tg/yr (Whalen and Reeburgh, 1992; Reeburgh *et al.*, 1994). Information from large areas of the world is lacking, particularly in the tropics and the Siberian Lowland (Bartlett and Harris, 1993). Recently, atmospheric data have been used to constrain emission estimates from wetlands in the former Soviet Union (Dlugokencky *et al.*, 1994b).

Ocean and Freshwater Ecosystems. A re-evaluation of the ocean source was performed by Lambert and Schmidt (1993). According to these authors only ~3.5 Tg/yr are emitted by the open oceans, but emissions from methane-rich areas could be considerably more important, producing a total oceanic source of the order of 50 Tg/yr. There is no new information about the contribution of freshwater ecosystems.

Termites. A recent estimate made by Martius *et al.* (1993) for the contribution of termites to the global CH_4 budget agrees well with the central value of 20 Tg/y given in the 1992 IPCC Supplement.

Other Natural Sources. New estimates have been made for volcanoes (3.5 ± 2.7 Tg/yr), hydrothermal emissions (2.3 ± 2.7 Tg/yr), and hydrates (~3 Tg/yr) (Judd *et al.*, 1993; Lacroix, 1993).

Fossil Carbon Related Sources. From studies of the carbon-14 content of atmospheric CH_4 it was established that about 20% (~100 Tg) of total annual CH_4 emission is from fossil carbon sources (IPCC, 1992). However, there are large uncertainties in the contribution of the various related sources: coal mines, natural gas and petroleum industry. New global estimates from coal mines are: 25 Tg/yr (CIAB, 1992), 17 Tg/yr (Müller, 1992), 43 Tg/yr (Beck, 1993), 49 Tg/yr (Subak *et al.*, 1993), and 45.6 Tg/yr (Kirchgessner *et al.*, 1993). Müller (1992) gives an emission from natural gas activities of 65 Tg/yr, which is much higher than the values given in the IPCC (1992) (25-42 Tg/yr). Khalil *et al.* (1993b) proposed that low-temperature combustion of coal (not included previously) could be a significant source of methane, with a global emission of ~16 Tg/yr. However, the emission factor derived by Khalil *et al.* is higher than the values obtained by Fynes *et al.* (1993) from coal-fired plants and the one quoted for handfired coal units by the Air Pollution Engineering Manual (Air and Waste Management Assn., USA, 1992); further research is clearly required to refine this estimate.

Waste Management Systems. Landfills, animal waste, and domestic sewage are significant global sources of methane, with a total emission estimate of ~80 Tg/yr (IPCC, 1992). New global estimates from landfills are 40 Tg/yr (Müller, 1992), 36 Tg/yr (Subak *et al.*, 1993), and 22 Tg/yr (Thorneloe *et al.*, 1993), in good agreement with the mean value (30Tg/yr) given previously (IPPC, 1992). No additional information has been published for animal waste and domestic sewage.

Enteric Fermentation. Anastasi and Simpson (1993) estimated for 1990 an emission of 84 Tg/yr from enteric fermentation in cattle, sheep, and buffalo. This result suggests that the strength of enteric fermentation be in the upper part of the range given in 1992 (65-100 Tg/yr). Furthermore, Minson (1993) in a re-evaluation of this source in Australia found values 43% higher than previous estimates for this country. Johnson *et al.* (1993) estimated a global emission of 79 Tg/yr.

Biomass Burning. New global estimates of this source are: 30.5 Tg/yr (Hao and Ward, 1993), 36 Tg/yr (Subak *et al.*, 1993), and 43 Tg/yr (Andreae and Warnek, 1994). These values are within the range of data reported previously (IPCC, 1992).

Rice Paddies. There is a very large uncertainty associated with the emissions estimate from rice paddies (IPCC, 1992). Three-dimensional (3-D) model calculations constrain estimates of methane emission from rice cultivation to ~100 Tg/yr (Fung *et al.*, 1991; Dlugokencky *et al.*, 1994b). The results reported earlier (IPCC, 1990, 1992) and recent estimates (*i.e.*, Wassman *et al.*, 1993; Delwiche and Cicerone, 1993; Bachelet and Neue, 1993; Subak *et al.*, 1993; Lal *et al.*, 1993; Shearer and Khalil, 1993; Neue and Roger, 1993) suggest an emis-

TABLE 2-3. Estimated sources and sinks of methane (Tg CH_4 per year).

	Range	Likely	Totals
Sources			
Natural			
Wetlands[a]			
Tropics	30-80	~60	
Northern Latitudes	20-60	40	
Others	5-10	10	
Termites	10-50	20	
Ocean	5-50[a]	10	
Freshwater	1-25	5	
Others[a]	8-13	10	
Total Natural			155
Anthropogenic			
Fossil Fuel Related		100[b]	
Coal Mines	15-45[a]		
Natural Gas	25-50[a]		
Petroleum Industry	5-30		
Coal Combustion	7-30[a]		
Waste Management System			
Landfills	20-70	30	
Animal Waste	20-30	25	
Domestic Sewage Treatment	?	25	
Enteric Fermentation	65-100	80	
Biomass Burning	20-80	40	
Rice Paddies[a]	20-100	60	
Total Anthropogenic			360
Total Source			515
Sinks			
Reaction with OH[a]	330-560	445	
Removal in Stratosphere[a]	25-55	40	
Removal by Soils	15-45	30	
Atmospheric Increase	30-40	37	
Total Sink			552

[a] indicates revised estimates since previous assessments

[b] from carbon-14 studies (IPCC, 1992)

sion range of 20-100 Tg/yr with a most likely value of 60 Tg/yr.

2.4.3 Sinks

CH_4 is mainly removed through chemical reactions in the troposphere and stratosphere (485 Tg/yr). A growing number of studies (reviewed by Reeburgh *et al.*, 1994) show that methane is consumed by soil microbial communities in the range between 20 and 60 Tg/yr. Methane oxidation is expected to be particularly important in modulating methane emissions from rice paddies, wetlands, and landfills. Ojima *et al.* (1993) estimate that ~20 Tg of methane is consumed annually by temperate soil, and that this sink has decreased by ~30% due to soil disturbance.

2.4.4 Potential Feedbacks from a Changed Climate

There are several potential climate feedbacks that could affect the atmospheric methane budget (IPCC, 1990). At present, however, the attention has focused on northern wetlands and on permafrost.

High-Latitude Wetlands. Changes in surface temperature and rainfall are predicted by general circulation models (GCMs) to occur in high-latitude regions. When changes in temperature are considered alone, an increase in the emission of CH_4 is predicted (Hameed and Cess, 1983; Lashoff, 1989). Recent calculations suggest only a moderate increase in CH_4 emissions in a $2\times CO_2$ scenario (Harris and Frolking, 1992). On the other hand, using a hydro-thermal model, Roulet *et al.* (1992) estimated a significant decrease in moisture storage that resulted in an 80% decrease in CH_4 fluxes (negative feedback); the corresponding increase due to temperature changes is only 15%. These estimates have been confirmed by measurements indicating a reduced CH_4 flux from drained northern peatlands (Roulet *et al.*, 1993). It seems that northern wetlands are more sensitive to changes in moisture than temperature; however, the biospheric feedback mechanisms are poorly understood (Reeburgh *et al.*, 1994).

Permafrost. The methane content of permafrost in Fairbanks (Kvenvolden and Lorenson, 1993) and northern Alaska (Rasmussen *et al.*, 1993) was recently evaluated at 2-3 mg/kg. Using these concentrations and the changes in temperature predicted by various scenarios, Kvenvolden and Lorensen (1993) predict that in 100 years the maximum methane release rate will be ~27 Tg/yr and that during the first 30 years no significant release will occur. The heat transfer and gas diffusion model of Moraes and Khalil (1993) indicates that in the future, permafrost is likely to contribute less than 10 Tg of methane per year.

2.5 NITROUS OXIDE (N_2O)

Nitrous oxide has a long atmospheric lifetime. It is the major source of stratospheric nitrogen oxides, which are important in regulating stratospheric ozone. N_2O is also a greenhouse gas. It is emitted by several small sources, which have large uncertainties, and its atmospheric budget is difficult to reconcile. It is removed by photolysis and oxidation in the stratosphere and microbial oxidation in soils. A reduction of more than 50% of anthropogenic sources would stabilize its concentration at today's level of about 310 ppbv (IPCC, 1994a).

2.5.1 Atmospheric Distribution and Trends

The available global nitrous oxide data indicate that the trend over the past decade is very variable, ranging from 0.5 to 1.2 ppbv/yr (WMO, 1992; Khalil and Rasmussen, 1992). A recent analysis of seventeen years of data collected on oceanic expeditions as well as in Alaska, Hawaii, and Antarctica (Weiss, 1994) and sixteen years of data from the NOAA global network (Swanson *et al.*, 1993) shows that the global average abundance at the beginning of 1976 was 299 ppbv, which has risen to 310 ppbv at the beginning of 1993. During 1976-82 the growth rate was about 0.5-0.6 ppbv/yr, which increased to a maximum of 0.8-1 ppbv/yr in 1988-89, declining to the current rate of 0.5-0.6 ppbv/yr.

An analysis of IR solar absorption spectra recorded at the Jungfraujoch Station (46.6°N) in 1950-51 and from 1984 to 1992 has been recently performed by Zander *et al.* (1994b). The results indicate that the rate of increase of the column of N_2O was 0.23 ± 0.04 for the period 1951 to 1984, and 0.36 ± 0.06 %/yr from 1984 to 1992. The corresponding volume mixing ratios at the levels of the site (3.58 km altitude) increased from 275 ppbv to 305 ppbv between 1951 and 1992. The 1951 concentration is quite similar to the pre-industrial values obtained from ice cores (285 ppbv; IPCC, 1990), sug-

TABLE 2-4. Estimated sources and sinks of N_2O (Tg N per year).

Sources	
A. Natural	
Oceans	1.4-5.2*
Tropical Soils	
Wet forests	2.2-3.7
Dry savannas	0.5-2.0
Temperate Soils	
Forests	0.05-2.0
Grasslands	?
B. Anthropogenic	
Cultivated Soils	1-3
Animal Waste*	0.2-0.5
Biomass Burning	0.2-1.0
Stationary Combustion	0.1-0.3
Mobile Sources*	0.1-0.6
Adipic Acid Production	0.4-0.6
Nitric Acid Production	0.1-0.3
Sinks	
Removal by Soils	?
Photolysis in the Stratosphere*	12.3 (9-17)
Atmospheric increase*	3.1-4.7

* indicates revised estimates since previous assessment

gesting that the pre-industrial level was lower (see below), or that it persisted until the middle of this century and that the increase occurred thereafter.

Satellite global measurements of N_2O have been made by CLAES and ISAMS (Improved Stratospheric and Mesospheric Sounder) aboard UARS (Kumer *et al.*, 1993; Taylor *et al.*, 1993), but no validated results have been released so far.

Ice core records of N_2O show an increase of about 8% over the industrial period (IPCC, 1990). New records covering the last 45 ka were obtained from Antarctica and Greenland (Leuenberger and Siegenthaler, 1992). The Greenland record suggests a pre-industrial level of about 260 ppbv, 10 to 25 ppbv lower than previous records (IPCC, 1990). The Antarctic core shows that N_2O was lower during glacial periods, consistent with the hypothesis that soils are a major natural source of nitrous oxide.

2.5.2 Sources

A detailed presentation of N_2O sources was made in IPCC (1990) and a revised budget was given in the 1991 ozone assessment (WMO, 1992). N_2O is emitted by a large number of small sources, most of them difficult to evaluate and the estimates are very uncertain. Here we will only present new information not included in previous assessments. The updated budget is presented in Table 2-4. The overall uncertainty in the N_2O budget suggests that it could be balanced with the currently identified sources.

N_2O fluxes from an upwelling area of the Indian Ocean (Law and Owen, 1990) and the Peruvian upwelling region (Codispoti *et al.*, 1992) indicate that the oceans may be a larger source of this gas. Weiss (1994) calculated that the total pre-industrial source of N_2O was ~9 TgN/yr, of which ~3 TgN/yr was oceanic. An isotopic study (nitrogen-15 and oxygen-18) of atmospheric N_2O suggests a large gross ocean-atmosphere flux (Kim and Craig, 1993). Therefore, the upper range for that source has been extended to 5.2 TgN/yr in this assessment.

Recent emission estimates from some anthropogenic sources made by Subak *et al.* (1993) agree well with previous values. The increasing use of catalytic converters in cars stimulated the evaluation of the global contribution of this source: from tailpipe emission measurements, Dasch (1992) derived a global emission of 0.13 Tg N/yr; Khalil and Rasmussen (1992) from measurements in crowded highways in California estimate a global emission of 0.06-0.6 TgN/yr; Berges *et al.* (1993) from measurements in two tunnels (Stockholm and Hamburg) estimate a global emission of 0.24 ± 0.14 TgN/yr. This new information on N_2O emissions from catalytic converters, together with previous estimates (WMO, 1992) results in a revised emission range of 0.1-0.6 TgN/yr.

Important emissions are produced by agricultural activities. Recent global estimates from fertilized soils are 0.9 TgN/yr (Kreileman and Bouwman, 1994) and 2 TgN/yr (Pepper *et al.*, 1992). A source that was not included in the 1992 Report is cattle and feed lots. Based on the ratios of excess N_2O to excess CH_4 in barn studies, Khalil and Rasmussen (1992) estimate a source of 0.2-0.5 TgN/yr from cattle. Kreileman and Bouwman (1994) estimate for 1990 a global emission of 0.6 TgN/yr for the animal waste source. New information in tropical land use change indicates that the flux of N_2O depends on the age of the pasture, with young pastures (<10 years) emitting 3-10 times more N_2O than tropical forests, whereas older pastures emit less (Keller *et al.*, 1993). A rather low source of 0.2 TgN/yr was estimated by Kreileman and Bouwman (1994) due to enhanced soil N_2O emission following deforestation. More research on tropical agricultural systems is required before conclusions can be reached concerning the relative importance of tropical agricultural systems as a growing N_2O source (Keller and Matson, 1994).

2.5.3 Sinks

The major sink of N_2O is photodissociation in the stratosphere; a secondary loss of about 10% occurs through reaction with $O(^1D)$. The lifetime is 120 ± 30 yr (Prather and Remsberg, 1992). Important evidence of N_2O consumption by soils was reported by Donoso *et al.* (1993), but there are insufficient data to determine whether soil provides a significant global N_2O sink. Based on recent data (Swanson *et al.*, 1993; Weiss, 1994) the atmospheric increase is estimated to be 3.1-4.7 TgN/yr. The estimated sinks (including the atmospheric increase) range from ~12 to ~21 TgN/yr; therefore, to balance the N_2O atmospheric budget, all sources should be near their upper limits. This is in agreement with calculations based on ice core records and atmospheric concentrations that suggest a total anthropogenic emission of ~4.5 TgN/yr and ~9.5 TgN/yr for the natural sources (Khalil and Rasmussen, 1992).

2.6 SHORT-LIVED OZONE PRECURSOR GASES

Tropospheric ozone is a greenhouse gas, of particular importance in the upper troposphere. It also plays a significant role in the oxidizing capacity of the atmosphere. A detailed evaluation of tropospheric ozone is made in Chapter 5. Since the concentration of O_3 depends on the levels of its precursors (*i.e.*, NO_x, CO, CH_4, NMHC), we assess their sources, sinks and atmospheric distributions in the following sub-sections.

2.6.1 Nitrogen Oxides (NO_x = NO + NO_2)

2.6.1.1 Tropospheric Distribution

Because of its complex geographical source pattern and its short lifetime, the spatial and temporal distribution of tropospheric NO_x is complex and highly variable, over 3 orders of magnitude in non urban areas (Carroll and Thompson, 1994). A detailed discussion of the tropospheric distribution of NO_x is presented in Chapter 5.

2.6.1.2 Sources

Estimated NO_x source strengths are summarized in Table 2-5.

TABLE 2-5. Estimated sources of NO_x (TgN/yr).

	Range	Likely
Natural Soils	5-12	7
Lightning	3-20	7
Biomass Burning	3-13	8
Subsonic Aircraft	0.2-1	0.4
Fossil Fuel	21-25	24
Agricultural Soils	?	?

Soils. Soil microbial activity is an important natural source of NO_x, but a very large uncertainty affects its estimate (IPCC, 1992). Recently, Williams *et al.* (1992) derived an emission of only ~0.1 TgN/yr from natural soils (grassland, forest, and wetlands) within the U.S. From studies in Venezuela, Sanhueza (1992) estimated an emission of ~4 TgN/yr for the global savannah region. Tropical forest soils produce large amounts of NO; however, due to removal processes inside the forest itself, most of the NO never reaches the "open" atmosphere (Bakwin *et al.*, 1990). Recent global estimates of this source include: Davidson (1991), 13 TgN/yr; Müller (1992), 4.7 TgN/yr; and Dignon *et al.* (1992), 5 TgN/yr.

Agricultural soils could be an important source of NO_x, but no reliable global budgets exist. Cultivated soils from the U.S. emit 0.2 TgN/yr (Williams *et al.*, 1992); plowing of tropical savannah soil produces a large increase of NO emissions (Sanhueza *et al.*, 1994), but the impact to the global budget has not been estimated.

Lightning. The global estimates of NO_x production by lightning show a very large uncertainty (Liaw *et al.*, 1990). Using a global chemistry, transport, and deposition model, Atherton *et al.* (1993) found that a lightning source of 5-10 TgN/yr (with an upper limit of 20 TgN/yr) is compatible with the NO_y levels in remote locations. This is in agreement with Logan (1983), who indicates that the distribution of nitric acid (HNO_3) in the remote troposphere is consistent with a lightning NO_x source of <10 TgN/yr.

Biomass burning. Tropical biomass burning is an important source of NO_x (Crutzen and Andreae, 1990; Lobert *et al.*, 1991; Andreae, 1991; Penner *et al.*, 1991; Müller, 1992), ranging from 2 to 8 TgN/yr. Estimates including extratropical burning indicate global production of 9.6 TgN/yr (Andreae, 1993) and 13 TgN/yr (Dignon and Penner, 1991).

Aircraft. Emissions from aircraft are a relatively small source of NO. However, since a large fraction of the NO_x is released at altitudes between 9-13 km, this has a large impact on the photochemistry of the free troposphere (Johnson *et al.*, 1992; Beck *et al.*, 1992), and is likely responsible for a large fraction of the NO_x found at those altitudes at northern midlatitudes (Ehhalt *et al.*, 1992). Estimates of the global source from aircraft range from 0.23 to 1.0 TgN/yr (Egli, 1990; Johnson *et al.*, 1992; Beck *et al.*, 1992; Penner *et al.*, 1994). A very detailed evaluation of this source has been recently completed (Baughcum *et al.*, 1993). This study includes emissions from scheduled airliner and cargo, scheduled turboprop, charter, military, and former Soviet Union aircraft. The results indicate a global emission of 0.44 TgN/yr, with 7% of the emission occurring in the Southern Hemisphere. A detailed geographical distribution of this source is given in Chapter 11.

Fossil Fuel Combustion. This is the largest source of NO_x (24 TgN/yr) and its global distribution is relatively well known (Dignon and Hameed, 1989; Hameed and Dignon, 1991; Müller, 1992; Dignon, 1992). According to Hameed and Dignon (1991), the emission of NO_x increased from 18.1 TgN/yr in 1970 to 24.3 TgN/yr in 1986 (25% increase).

2.6.1.3 Sinks

The removal processes of NO_x (atmospheric oxidation of NO_x and dry deposition of NO_2) are reasonably well known. However, it is not possible to make a direct estimate of the global NO_x sink since the global distribution of NO_x is too poorly known.

TABLE 2-6. Estimated sources of NMHC (TgC/yr).

	Range	Likely
Vegetation*	230-800	500
Oceans	20-150	?
Biomass Burning	30-90	40
Technological	60-100	70

* mainly isoprene and terpenes

2.6.2 Non-Methane Hydrocarbons (NMHCs)

2.6.2.1 Atmospheric Distribution

Most NMHCs (heavier alkanes, alkenes, alkyl benzenes, isoprene, terpenes) have atmospheric lifetimes of less than a week (sometimes less than a day). In this case the atmospheric distributions reflect the source pattern and the regional transport situation, and the mixing ratios generally range from several ppbv in the boundary layer near the sources to a few pptv or less in the background atmosphere. NMHCs with predominantly anthropogenic sources exhibit a maximum in winter, reflecting the seasonality of the removal by OH radicals. Biogenic NMHCs (*i.e.*, isoprene, terpenes) present very low mixing ratios in winter and highest abundance in summer, a consequence of the seasonality of the emission rate (Fehsenfeld *et al.*, 1992).

For NMHCs with lifetimes of few weeks or more (*i.e.*, ethane, acetylene, propane) there is a better understanding of their atmospheric distributions (Ehhalt, 1992; Rudolph *et al.*, 1992). Seasonal cycles and long-term trends in the vertical column abundances of ethane and acetylene above the Jungfraujoch station, Switzerland, have been investigated by Ehhalt *et al.* (1991) and Zander *et al.* (1991b).

2.6.2.2 Sources

Estimated source strengths of NMHCs are reported in Table 2-6.

Vegetation. Foliar emissions are, by far, the most important sources of NMHC. Rasmussen (1972) estimated a global emission ranging from 230 to 440 TgC/yr. Zimmerman *et al.* (1978) found that vegetation emits 350 TgC/yr of isoprene and 480 TgC/yr of terpenes. Recently, Müller (1992) reported the following values (in TgC/yr): isoprene 250, terpenes 147, aromatics 42, and paraffins 52 (total 491 TgC/yr); Allwine *et al.* (1994) estimate a total NMHC emission of 827 Tg/yr.

Oceans. Ehhalt and Rudolph (1984) estimate a global rate from the ocean of 21 TgC/yr (C_2-C_6 hydrocarbons), whereas Bonsang *et al.* (1988) report a much larger rate of 52 TgC/yr. Based on the results of Donahue and Prinn (1990), Müller (1992) indicates that there is a large uncertainty in marine emissions and gives a range of 30-300 TgC/yr.

Biomass burning. Emissions of NMHC from biomass burning range from 36 to 90 TgC/yr (Lobert *et al.* 1991; Müller, 1992; Andreae, 1993). Ethane, ethene, propene, acetylene, and benzene are emitted with a rate >2 TgC/yr (Lobert *et al.*, 1991; Bonsang *et al.*, 1991).

Technological sources. These include gasoline handling, natural gas, refuse disposal, and chemical manufacturing, and produce a global emission ranging between 60 and 140 TgC/yr (Warneck, 1988; Müller, 1992; Piccot *et al.*, 1992; Bouwman, 1993).

2.6.2.3 Sinks

NMHCs react rapidly with the OH radical (unsaturated compounds also react with O_3) and with the exception of ethane (lifetime 2-3 months), their atmospheric lifetimes are shorter than one month; isoprene and terpenes have lifetimes of only a few hours.

2.6.3 Carbon Monoxide (CO)

2.6.3.1 Atmospheric Distribution and Trends

The atmospheric distribution and trends of CO were reviewed previously (WMO, 1992; IPCC, 1992). CO mixing ratios in the troposphere present systematic latitudinal and seasonal variations, ranging from around

TABLE 2-7. Estimated sources and sinks of CO (Tg/yr)

	Range	Likely
Sources		
Technological	300-900	500
Biomass Burning	400-700	600
Biogenics	60-160	100
Oceans	20-190	?
Methane Oxidation	400-1000	600
NMHC Oxidation	300-1300	600
Sinks		
OH Reaction	1400-2600	2100
Soil Uptake	250-640	250
Stratospheric Remotion	~100	100

40 to 200 ppbv. Annual mean CO levels in the high latitudes of the Northern Hemisphere are about a factor of 3 greater than those at similar latitudes in the Southern Hemisphere.

During the 1980s there was evidence that atmospheric CO was increasing at ~1%/year in the Northern Hemisphere, whereas no significant trend was observed in the Southern Hemisphere (WMO, 1992). Recent measurements indicate that global CO levels have fallen sharply from the late 1980s. Novelli *et al.* (1994) found that in the Northern Hemisphere, CO decreased at a spatially and temporally average rate of 7.3 ± 0.9 ppbv/yr (6.1 %/yr) (June 1990 to June 1993), whereas in the Southern Hemisphere it decreased at 4.2 ± 0.5 ppbv/yr (7.0 %/yr). Khalil and Rasmussen (1994) for the period 1987 to 1992 reported a decrease of 1.4 ± 0.9 %/yr in the Northern Hemisphere and 5.2 ± 0.7 %/yr in the Southern Hemisphere. While the above results concern surface levels of CO, total vertical column abundances of CO above the Jungfraujoch station, Switzerland, also show a mean rate of decrease equal to 1.15 ± 0.32 %/yr between 1985 and 1993 (Zander *et al.*, 1994c). The causes of this behavior have not been identified, but decreases in tropical biomass burning and Northern Hemisphere urban emissions have been suggested. The total amount of CO in today's atmosphere is less than it was a decade ago.

Preliminary global and seasonal variations of CO between 30 and 90 km altitude have been reported by Lopez-Valverde *et al.* (1993), based on ISAMS/UARS infrared limb emission measurements. These are the first global measurements of CO in the middle atmosphere, with data validation being still in progress.

2.6.3.2 Sources

Estimated strengths of sources and sinks of CO are summarized in Table 2-7.

Technological sources. Technological sources include transportation, combustion, industrial processes, and refuse incineration. There are several evaluations (Jaffe, 1973; Logan, 1980; Seiler and Conrad, 1987; Cullis and Hirshler, 1989; Khalil and Rasmussen, 1990; Müller, 1992; Subak, *et al.*, 1993) ranging from 300 to 900 TgCO/yr.

Biomass burning. Recent estimates for the tropics range from 400-700 TgCO/yr (Lobert *et al.*, 1991; Müller, 1992; Andreae, 1993; Subak *et al.*, 1993). Including extratropical burning, Andreae (1993) derives a global source equal to 621 TgCO/yr.

Terrestrial biogenic sources. These include vegetation, soils, and animals (*i.e.*, termites). Based on the emission rates found on higher plants of the temperate region, Seiler and Conrad (1987) estimated a global source of 75 ± 15 TgCO/yr. Assuming CO emissions proportional to net primary productivity (NPP) and using the flux reported by Kirchhoff and Marinho (1990) for tropical forests, Müller (1992) evaluated a global

biogenic source at 165 TgCO/yr. Photoproduction of CO from dead plant matter has been reported (Valentine and Zepp, 1993; Tarr *et al.*, 1994), however, no global evaluation of this source has been made.

Oceans. Early estimates of CO emissions from the oceans (IPCC, 1992) range from 20 to 190 TgCO/yr. Using an atmospheric general circulation model, Erickson (1989) calculated a global ocean source equal to 165 ± 80 TgCO/yr.

Hydrocarbon oxidation. This is the most important source of atmospheric CO. The production of CO from methane oxidation ranges from 400 to 1000 TgCO/yr, and 300 to 1300 TgCO/yr from NMHC (Zimmerman *et al.*, 1978; Logan, 1980; Khalil and Rasmussen, 1990; Crutzen and Zimmerman, 1991).

2.6.3.3 Sinks

Reaction with the OH radical is the major sink for CO. Soil uptake and removal in the stratosphere are minor sinks. In principle, the atmospheric removal rates for CO can be calculated from the atmospheric CO distribution, the distribution of the OH radical concentration, and the related reaction rate. Model calculations predict a removal rate of about 2000 Tg(CO)/yr (WMO, 1986; Seiler and Conrad, 1987; Khalil and Rasmussen 1990; Crutzen and Zimmerman, 1991).

2.7 CARBON DIOXIDE (CO_2)

The change in atmospheric concentration of CO_2, from 280 ppmv pre-industrial to ~360 ppmv in 1993, is the major contributor to the calculated increase in radiative forcing since the pre-industrial period (*i.e.*, 1.5 W m^{-2}). An updated review of the CO_2 budget has been made in the 1994 IPCC report (IPCC, 1994b).

Observations of CO_2 since the 1950s show systematic upward trends, in both concentration and rate of concentration increase, albeit with substantial variation in the rate of increase from year to year. During the period 1991 to 1993, the rate of increase of CO_2 per year slowed substantially (to as low as 0.5 ppmv/yr from the long-term average of 1.5 ppmv/yr). There are numerous examples in the record of short periods where growth rates are higher or lower than the long-term mean. The most recent observations indicate that growth rates are now increasing again (IPCC, 1994b).

CO_2 emission from industrial processes (mainly fossil fuel combustion and cement production) in 1991 is estimated at 6.2 GtC/yr (Andres *et al.*, 1994), compared with 6.0 ± 0.5 GtC in 1990 (IPCC, 1992). The cumulative input since the pre-industrial period is estimated at 230 GtC (Andres *et al.*, 1994). Recent satellite remote sensing measurements of land clearing rates in the Brazilian Amazon have resulted in substantially reduced estimates (by ~50%) for this area (INPE, 1992; Skole and Tucker, 1993). However, deforestation rates for the rest of the tropics remain poorly quantified. Current net flux estimates (in GtC/yr) that include regrowth after deforestation are: 0.6 for Latin America, 0.7 for South and Southeast Asia, 0.3 for Africa, and -0.3 to -1.1 for mid/high latitudes, producing a global mean for the 1980s of 1.1 ± 1.2 GtC/yr (IPCC, 1994b). The oceans represent a significant sink of atmospheric CO_2, averaging 2.0 ± 0.8 GtC/yr over the decade 1980-89.

The imbalance between atmospheric concentration changes, estimated emissions, and estimated ocean uptake, as well as the discrepancies between the observed and calculated inter-hemispheric gradients of CO_2, indicate the existence of an unaccounted-for terrestrial sink of 1.2 ± 1.6 GtC/yr, probably attributable to a combination of CO_2-induced plant growth (0.5-2.0 Gt/yr), nitrogen fertilization (0.2-1.0 Gt/yr), and possible climatic effects (0-1.0 Gt/yr) (IPCC, 1994b).

Climatic feedback appears to be positive, amplifying the effect of anthropogenic emissions, although this amplification may be reduced due to feedbacks and compensating processes within the marine and terrestrial systems. It is likely that the effect of CO_2 fertilization on plant production will be substantially smaller than the 20-40% observed in most agricultural plants. An important body of data supports the view that responses of plant production to elevated CO_2 are restricted in nutrient-limited ecosystems (*e.g.*, Díaz *et al.*, 1993); however, it is possible that N deposition arising from the use of fertilizers and fossil fuel combustion will reduce the intensity or spatial distribution of nitrogen limitation.

Carbon cycle modeling studies of CO_2 concentrations, under a range of emissions scenarios and for a range of stabilized CO_2 concentrations up to 750 ppmv, yield the following results (IPCC, 1994b): i) because of the long residence time for carbon dioxide, stabilization of anthropogenic emissions at projected 2000 levels (from IS92a scenario) leads to a nearly constant rate of

increase in atmospheric concentrations for at least two centuries; modeled concentrations reach 480-540 ppbv by 2100; ii) stable CO_2 concentration at values up to 750 ppmv can be maintained only with anthropogenic emissions that eventually drop below 1990 levels; iii) there is a close relationship between the eventual stabilized concentration and the integrated CO_2 emission from now until the time of stabilization. Integrated emissions for stabilization at levels lower than 750 ppmv are less than those calculated for the IS92 a, b, e, and f scenarios.

REFERENCES

AFEAS, *Production, Sales and Atmospheric Release of Fluorocarbons through 1992,* Alternative Fluorocarbons Environmental Acceptability Study, SPA-AFEAS, Inc., Washington, D.C., USA, 1993.

AFEAS, *Historic Production, Sales and Atmospheric Release of HCFC-142b,* Alternative Fluorocarbons Environmental Acceptability Study, SPA-AFEAS, Inc., Washington, D.C., USA, 1994.

Albritton, D., and R. Watson, Methyl bromide and the ozone layer: A summary of current understanding, in *Methyl Bromide: Its Atmospheric Science, Technology, and Economics*, Montreal Protocol Assessment Supplement, edited by R. Watson, D. Albritton, S. Anderson and S. Lee-Bapty, United Nations Environment Programme, Nairobi, Kenya, 1992.

Allwine, *et al.*, An initial global inventory of biogenic VOC emitted from terrestrial sources, submitted to *J. Geophys. Res.*, 1994.

Anastasi, C., and V.J. Simpson, Future methane emissions from animals, *J. Geophys. Res., 98,* 7181-7186, 1993.

Andreae, M.O., Biomass burning: Its history, use, and distribution and its impact on environmental quality and global climate, in *Global Biomass Burning: Atmospheric, Climatic and Biospheric Implications*, edited by J.S. Levine, MIT Press, 3-21, 1991.

Andreae, M.O., The influence of tropical biomass burning on climate and the atmospheric chemistry, in *Biogeochemistry of Global Change: Radiatively Active Trace Gases*, edited by R.S. Oreland, Chapman and Hall, New York, 113-150, 1993.

Andreae, M.O., and P. Warneck, Global methane emissions from biomass burning and comparison with other sources, *Pure and Appl. Chem., 66,* 162-169, 1994.

Andres, T.J., G. Marland, T. Boden, and S. Bischoff, Carbon dioxide emissions from fossil fuel combustion and cement manufacture 1751-1991 and an estimate for their isotopic composition and latitudinal distribution, Global Change Institute, Snowmass, Colorado, USA, 1994.

Aoki, S., T. Nakazawa, S. Murayama, and S. Kawaguchi, Measurements of atmospheric methane at the Japanese Antarctic Station, Syowa, *Tellus, 44B,* 273-281, 1992.

Atherton, C.S., J.E. Penner, and J.J. Walton, The role of lightning in the tropospheric nitrogen budget: model investigations, in preparation, 1993.

Atlas, E., W. Pollock, J. Greenberg, L. Heidt, and A.M. Thompson, Alkyl nitrates, nonmethane hydrocarbons, and halocarbon gases over the equatorial Pacific Ocean during SAGA 3, *J. Geophys. Res., 98D,* 16933-16947, 1993.

Bachelet, D., and H.U. Neue, Methane emissions from wetland rice areas of Asia, *Chemosphere, 26,* 219-237, 1993.

Bakwin, P.S., S.C. Wofsy, S.M. Fan, M. Keller, S.E. Trumbore, and J.M. da Costa, Emissions of nitric oxide (NO) from tropical forest soils and exchange of NO between the forest canopy and atmospheric boundary layers, *J. Geophys. Res., 95,* 16765-16774, 1990.

Bartlett, K.B., and R.C. Harris, Review and assessment of methane emissions from wetlands, *Chemosphere, 26,* 261-320, 1993.

Bartlett, K.B., P.M. Crill, J.A. Bonassi, J.E. Richey, and R.C. Harris, Methane flux from the Amazon River floodplain: Emissions during rising water, *J. Geophys. Res., 95,* 16773-16788, 1990.

Baughcum, S.L., M. Metwally, R.K. Seals, and D.J. Wuebbles, Emissions scenarios development: Complete scenario database (Subchapter 3-4), in *The Atmospheric Effects of Stratospheric Aircraft: A Third Program Report*, edited by R.S. Stolarski and H.L. Wesoky, NASA Ref. Publ. 1313, 185-208, 1993.

Beck, J.P., C.E. Reeves, F.A.A.M. de Leeuw, and S.A. Penkett, The effect of aircraft emissions on tropospheric ozone in the northern hemisphere, *Atmos. Environ., 26A,* 17-29, 1992.

Beck, L.L., A global methane emissions program for landfills, coal mines, and natural gas systems, *Chemosphere, 26,* 447-452, 1993.

Bekki, S., and J.A. Pyle, Two-dimensional assessment of the impact of aircraft sulphur emissions on the stratospheric sulphate aerosol layer, *J. Geophys. Res., 97,* 15839-15847, 1992.

Berges, M.G.M., R.M. Hofmann, D. Scharffe, and P.J. Crutzen, Nitrous oxide emissions from motor vehicles in tunnels and their global extrapolation, *J. Geophys. Res., 98D,* 18527-18531, 1993.

Bloomfield, P., Inferred lifetimes, Chapter 3 in *NASA Report on Concentrations, Lifetimes and Trends of CFCs, Halons and Related Species*, edited by J. Kaye, S. Penkett and F. Osmond, NASA Reference Publication 1339, Washington D.C., 3.1-3.23, 1994.

Blunier, T., J. Chappellaz, J. Schwander, J. Barnola, T. Desperts, B. Stauffer, and D. Raynaud, Atmospheric methane record from a Greenland ice core over the past 1000 years, *Geophys. Res. Lett., 20,* 2219-2222, 1993.

Bonsang, B., M. Kanakidou, G. Lambert, and P. Monfray, The marine source of C_2-C_6 aliphatic hydrocarbons, *J. Atmos. Chem., 6,* 3-20, 1988.

Bonsang, B., G. Lambert, and C. Boissard, Light hydrocarbons emissions from African savannah burning, in *Global Biomass Burning; Atmospheric, Climatic and Biospheric Implications*, edited by J.S. Levine, MIT Press, 155-161, 1991.

Bouwman, A.F., Report of the third workshop of the Global Emission Inventory Activity (GEIA). RIVM Report 481507002, RIVM, Bilthoven, The Netherlands, 1993.

Butler, J.H., J.W. Elkins, T.M. Thompson, B.D. Hall, and V. Koropalov, Oceanic consumption of CH_3CCl_3: Implications for tropospheric OH, *J. Geophys. Res., 96,* 22347-22355, 1991.

Butler, J.H., J.W. Elkins, B.D. Hall, S.O. Cummings, and S.A. Montzka, A decrease in the growth rates of atmospheric halon concentrations, *Nature, 359,* 403-405, 1992.

Butler J.H., J.W. Elkins, T.M. Thompson, B.D. Hall, J.M. Lobert, T.H. Swanson, and V. Koropalov, A significant oceanic sink for atmospheric CCl_4, The Oceanography Society, Third Scientific Meeting, April 13-16, Seattle, USA. Abstracts, p.55, 1993.

Butler, J., J. Elkins, B. Hall, S. Montzka, S. Cummings, P. Fraser, and L. Porter, Recent trends in the global atmospheric mixing ratios of halon-1301 and halon-1211, in *Baseline 91*, edited by C. Dick and J. Gras, Bureau of Meteorology—Commonwealth Science and Industrial Research Organization (CSIRO), in press, 1994.

Carroll, M.A., and A.M. Thompson, NO_x in the non-urban troposphere, in *Current Problems and Progress in Atmospheric Chemistry*, edited by J.R. Barker, Advances in Physical Chemistry, in press, 1994.

Chappellaz, J., T. Blunier, D. Raynaud, J.M. Barnola, J. Schwander, and B. Stauffer, Synchronous changes in atmospheric CH_4 and Greenland climate between 40 and 8 kyr BP, *Nature, 366,* 443-445, 1993.

CIAB, *Global Methane Emissions from the Coal Industry,* Coal Industry Advisory Board, Global Climate Committee, October, 1992.

Cicerone, R.J., Atmospheric carbon tetrafluoride: A nearly inert gas, *Science, 206,* 59-61, 1979.

Codispoti, L., J. Elkins, T. Yoshinari, G. Frederich, C. Sakamoto, and T. Packard, On the nitrous oxide flux from productive regions that contain low oxygen waters, in *Oceanography of the Indian Ocean*, edited by B. Desai, 271-284, Oxford & IBH Publishing Co., New Delhi, India, 1992.

Cofer, W.R., III, R.J. Bendura, D.I. Sebacher, G.L. Pellet, G.L. Gregory, and G.L. Maddrea, Jr., Airborne measurements of Space Shuttle exhaust constituents, *AIAA J., 23,* 283-287, 1985.

Crutzen, P.J., and M.O. Andreae, Biomass burning in the tropics: Impact on atmospheric chemistry and biogeochemical cycles, *Science, 250,* 1669-1679, 1990.

Crutzen, P.J., and P.H. Zimmerman, The changing photochemistry of the troposphere, *Tellus, 43AB,* 136-151, 1991.

Cullis, C.F., and M.M. Hirschler, Man's emissions of carbon monoxide and hydrocarbons into the atmosphere, *Atmos. Environ., 23,* 1195-1203, 1989.

Cunnold, D., P. Fraser, R. Weiss, R. Prinn, P. Simmonds, B. Miller, F. Alyea, and A. Crawford, Global trends and annual releases of CCl_3F and CCl_2F_2 estimated from ALE/GAGE and other measurements from July 1978 to June 1991, *J. Geophys. Res., 99,* 1107-1126, 1994.

Dasch, J.M., Nitrous oxide emissions from vehicles, *J. Air Waste Manage. Assoc., 42,* 63-67, 1992.

Davidson, E.A., Fluxes of nitrous oxide and nitric oxide from terrestrial ecosystems, in *Microbial Production and Consumption of Greenhouse Gases: Methane, Nitrogen Oxides, and Halomethanes*, edited by J.E. Rogers and W.B. Whitman, Washington, D.C., 219-235, 1991.

Delwiche, C.C., and R.J. Cicerone, Factors affecting methane production under rice, *Global Biogeochem. Cycles, 7,* 143-155, 1993.

Díaz, S., J.P. Grime, J. Harris, and E. McPherson, Evidence of a feedback mechanism limiting plant response to elevated carbon dioxide, *Nature, 364,* 616-617, 1993.

Dignon, J., NO_x and SO_x emissions from fossil fuels: A global distribution, *Atmos. Environ., 26A,* 1157-1163, 1992.

Dignon, J., C.S. Atherton, J.E. Penner, and J.J. Walton, NO_x pollution from biomass burning: A global study, *Proceedings of the 11th Conference on Fire and Forest Meteorology*, Missoula, Montana. April 16-19, 1991.

Dignon, J., and S. Hameed, Global emission of nitrogen and sulfur oxides from 1960 to 1980, *J. Air Poll. Control Assoc., 39,* 180-186, 1989.

Dignon, J., and J.E. Penner, Biomass burning: A source of nitrogen oxides in the atmosphere, in *Global Biomass Burning: Atmospheric, Climatic and Biospheric Implications*, edited by J.S. Levine, MIT Press, 370-375, 1991.

Dignon, J., J.E. Penner, C.S. Atherton, and J.J. Walton, Atmospheric reactive nitrogen: A model study of natural and anthropogenic sources and the role of microbial soil emissions, in *Proceedings of CHEMRAWN VII World Conference on the Chemistry of the Atmosphere: Its Impact on Global Change*, Baltimore, Maryland, December 2-6, 1992.

Dlugokencky, E.J., L.P. Steele, P.M. Lang, and K.A. Masarie, The growth rate and distribution of atmospheric methane, *J. Geophys. Res., 99D,* 17021-17043, 1994a.

Dlugokencky, E.J., J.M. Harris, Y.S. Chung, P.P. Tans, and I. Fung, The relationship between the methane seasonal cycle and regional sources and sinks at Tae-ahn Peninsula, Korea, *Atmos. Environ., 27A,* 2115-2120, 1994b.

Dlugokencky, E.J., K.A. Masarie, P.M. Lang, P.P. Tans, L.P. Steele, and E.G. Nisbet, A dramatic decrease in the growth rate of atmospheric methane in the northern hemisphere during 1992, *Geophys. Res. Lett., 21,* 45-48, 1994c.

Donahue, N.M., and R.G. Prinn, Non-methane hydrocarbon chemistry in the remote marine boundary layer, *J. Geophys. Res., 95,* 18387-18411, 1990.

Donoso, L., R. Santana, and E. Sanhueza, Seasonal variation of N_2O fluxes at a tropical savannah site: Soil consumption of N_2O during the dry season, *Geophys. Res. Lett., 20,* 1379-1382, 1993.

Egli, R.A., Nitrogen oxide emissions from air traffic, *Chimia, 44,* 369-371, 1990.

Ehhalt, D.H., Concentrations and distributions of atmospheric trace gases, *Ber. Bunsenges, Phys. Chem., 96,* 229-240, 1992.

Ehhalt, D.H., and J. Rudolph, On the importance of light hydrocarbons in multiphase atmospheric systems, *Berichte der Kernforschungsanlage Jülich, No 1942*, Institut für Chemie 3, Atmosphärische Chemie, Eds., 1-43, 1984.

Ehhalt, D.H., U. Schmidt, R. Zander, P. Demoulin, and C.P. Rinsland, Seasonal cycle and secular trend of the total and tropospheric column abundance of ethane above the Jungfraujoch, *J. Geophys. Res., 96,* 4985-4994, 1991.

Ehhalt, D.H., F. Rohrer, and A. Wahner, Sources and distribution of NO_x in the upper troposphere at northern mid-latitudes, *J. Geophys. Res., 97,* 3725-3738, 1992.

Elkins, J., T. Thompson, T. Swanson, J. Butler, B. Hall, S. Cummings, D. Fisher, and A. Raffo, Decrease in the growth rates of atmospheric chlorofluorocarbons-11 and -12, *Nature, 364,* 780-783, 1993.

Erickson, D.J., Ocean to atmosphere carbon monoxide flux: global inventory and climate implications, *Global Biogeochem. Cycles, 3,* 305-314, 1989.

Etheridge, D.M., Pearman, G.I., and Fraser, P.J., Changes in tropospheric methane between 1841 and 1978 from a high accumulation rate Antarctic ice core, *Tellus, 44B,* 282-294, 1992.

Fabian, P. Borcher, B.C. Kruger, and S. Lal, CF_4 and C_2F_6 in the atmosphere, *J. Geophys. Res., 92,* 9831-9835, 1987.

Farmer, C.B., High resolution infrared spectroscopy of the sun and earth's atmosphere from space, *Microchim. Acta* (Wien) III, 198-214, 1987.

Fehsenfeld, F., J. Calvert, R. Fall, P. Goldan, A. Guenther, C.N. Hewitt, B. Lamb, S. Liu, M. Trainer, H. Westberg, and P. Zimmerman, Emissions of volatile organic compounds from vegetation and the implications for atmospheric chemistry, *Global Biogeochem. Cycles, 6,* 389-430, 1992.

Fisher, D., T. Duafala, P. Midgley, and C. Niemi, Production and emissions of CFCs, halons and related molecules, Chapter 2 in *NASA Report on Concentrations, Lifetimes and Trends of CFCs, Halons and Related Species*, edited by J. Kaye, S. Penkett, and F. Osmond, NASA Reference Publication 1339, Washington, D.C., 2.1-2.35, 1994.

Fraser, P., and N. Derek, Halocarbons, nitrous oxide, methane and carbon monoxide—the GAGE program, in *Baseline 91*, edited by C. Dick and J. Gras, Bureau of Meteorology–Commonwealth Science and Industrial Research Organization, in press, 1994.

Fraser, P., S. Penkett, M. Gunson, R. Weiss, and F.S. Rowland, Measurements, Chapter 1 in *NASA Report on Concentrations, Lifetimes and Trends of CFCs, Halons and Related Species* edited by J. Kaye, S. Penkett, and F. Ormond, NASA Reference Publication 1339, Washington, D.C., 1.1-1.68, 1994a.

Fraser, P., N. Derek, L. Porter, D. Cunnold, F. Alyea, R. Prinn, P. Simmonds, and R. Weiss, Atmospheric chlorocarbons: Trends, lifetimes and emissions from ALE/GAGE global observations, in *Fourth International Conference on Southern Hemisphere Meteorology and Oceanography*, preprints, Hobart, March 1993, American Meteorology Society, 426-428, 1994b.

Fraser, P., D. Cunnold, F. Alyea, R. Prinn, P. Simonds, R. Weiss, B. Miller, and A. Crawford, Lifetime and emission estimates of 1,1,2 trichlorotrifluoroethane (CFC-113) from ALE/GAGE and other measurements, 1978-1992, in preparation, 1994c.

Fung, I., J. John, J. Lerner, E. Matthews, M. Prather, L.P. Steele, and P.J. Fraser, Three-dimensional model synthesis of the global methane cycle, *J. Geophys. Res., 96,* 13033-13065, 1991.

Fynes, G., I.S.C. Hughes, and P.W. Sage, The contribution of coal combustion to non-CO_2 greenhouse gas emissions inventories, *International Symposium on Non-CO_2 Greenhouse Gases, Why and How to Control?,* Maastricht, December, 1993.

Granier, C., and G. Brasseur, Impact of heterogeneous chemistry on model predictions of ozone changes, *J. Geophys. Res., 97,* 18015-18033, 1992.

Gunson, M.R., The atmospheric trace molecule spectroscopy (ATMOS) experiment—the Atlas-1 mission, SPIE vol. 1715, *Optical Methods in Atmospheric Chemistry,* 513-521, 1992.

Gunson, M.R., C.B. Farmer, R.H. Norton, R. Zander, C.P. Rinsland, J.H. Shaw, and B. C. Gao, Measurements of CH_4, N_2O, CO, H_2O and O_3 in the middle atmosphere by the Atmospheric Trace Molecule Spectroscopy Experiment on Spacelab 3, *J. Geophys. Res., 95,* 13867-13882, 1990.

Gunson, M.R., M.C. Abrams, L.L. Lowes, E. Mahieu, R. Zander, C.P. Rinsland, M.K.W. Ko, N.D. Sze, and D.K. Weisenstein, Increase in levels of stratospheric chlorine and fluorine loading between 1985 and 1992, *Geophys. Res. Lett.*, in press, 1994.

Hameed, S., and R. Cess, Impact of global warming on biospheric sources of methane and its climate consequences, *Tellus, 35B,* 1-7, 1983.

Hameed, S., and J. Dignon, Global emissions of nitrogen and sulfur oxides in fossil fuel combustion 1970-1986, *J. Air Waste Manage. Assoc., 42,* 159-163, 1991.

Hao, W.M., and D.E. Ward, Methane production from global biomass burning, *J. Geophys. Res., 98,* 20657-20661, 1993.

Harris, R.C., and S. Frolking, The sensitivity of methane emissions from northern freshwater wetlands to global change, in *Global Warming and Freshwater Ecosystems*, edited by P. Firth and S. Fisher, in press, 1992.

Harwood, R.S., C.H. Jackman, I.L. Karol, and L.X. Qiu, Predicted rocket and shuttle effects on stratospheric ozone, Chapter 10 in *Scientific Assessment of Ozone Depletion: 1991,* WMO Global Ozone Research and Monitoring Project—Report No. 25, pp. 10.1-10.12, World Meteorological Organization, Geneva, Switzerland, 1992.

Heidt, L.E., J.F. Vedder, W.H. Pollock, R.A. Lueb, and B.E. Henry, Trace gases in the Antarctic atmosphere, *J. Geophys. Res., 94,* 11599-11611, 1989.

Hofmann, D.J., and S. Solomon, Ozone destruction through heterogeneous chemistry following the eruption of El Chichón, *J. Geophys. Res., 94,* 5029-5041, 1989.

Hofmann, D.J., Increase in the stratospheric background sulfuric acid aerosol mass in the past 10 years, *Science, 248,* 996-1000, 1990.

Hofmann, D.J., Aircraft sulfur emissions, *Nature, 349,* 659, 1991.

INPE, *Deforestation in Brazilian Amazonia,* Instituto Nacional de Pesquisas Espaciais, Sao Paulo, Brazil, 1992.

IPCC, Intergovernmental Panel on Climate Change, R. Watson, H. Rodhe, H. Oeschger, and U. Siegenthaler, Greenhouse gases and aerosols, Chapter 1 in *Climate Change, The IPCC Scientific Assessment,* edited by J.T. Houghton, G.J. Jenkins, and J.J. Ephroums, Cambridge University Press, Cambridge, 1-40, 1990.

IPCC, Intergovernmental Panel on Climate Change, R. Watson, L.G. Meira-Filho, E. Sanhueza, and A. Janetos, Greenhouse gases: sources and sinks, Chapter A1 in *Climate Change 1992, The Supplementary Report to the IPCC Scientific Assessment,* edited by J.T. Houghton, B.A. Callander, and S.K. Varney, Cambridge University Press, Cambridge, 28-46, 1992.

IPCC, Intergovernmental Panel on Climate Change, M. Prather, R. Derwent, D. Ehhalt, P. Fraser, E. Sanhueza, and X. Zhou, Other trace gases and atmospheric chemistry, Chapter 2 in *1994 IPCC Interim Report, Radiative Forcing of Climate Change 1994,* in preparation, 1994a.

IPCC, Intergovernmental Panel on Climate Change, D. Schimel, I. Enting, M. Heimann, T. Wigley, D. Raynaud, D. Alves, and U. Siegenthaler, The carbon cycle, Chapter 1, in *1994 IPCC Interim Report, Radiative Forcing of Climate Change 1994,* in preparation, 1994b.

IPCC, Intergovernmental Panel on Climate Change, P.R. Jonas, R.J. Charlson, and H. Rodhe, Aerosols, Chapter 3, in *1994 IPCC Interim Report, Radiative Forcing of Climate Change 1994,* in preparation, 1994c.

Irion, F.W., M. Brown, G.C. Toon, and M.R. Gunson, Increase in atmospheric $CHClF_2$ (HCFC-22) over southern California from 1985 to 1990, *Geophys. Res. Lett., 21,* 1723-1726, 1994.

Jaffe, L.S., Carbon monoxide in the biosphere: Sources, distribution, and concentrations, *J. Geophys. Res., 78,* 5293-5305, 1973.

Jeffers, P.M., L.M. Ward, L.M. Woytowitch, and N.L. Wolfe, Homogenous hydrolysis rate constants for selected chlorinated methanes, ethanes, ethenes, and propanes, *Environ. Sci. Technol., 23,* 965-969, 1989.

Johnson, C., J. Henshaw, and G. McInnes, Impact of aircraft and surface emissions of nitrogen oxides on tropospheric ozone and global warming, *Nature, 355,* 69-71, 1992.

Johnson D.E., T.M. Hill, G.M. Ward, K.A. Johnson, M.E. Branine, B.R. Carmean, and D.W. Lodman, Ruminant and other animals, in *Atmospheric Methane: Sources, Sinks, and Role in Global Change,* edited by M.A.K. Khalil, Springer-Verlag, Berlin, 199-229, 1993.

Jouzel, J., N.I. Barkov, J.M. Barnola, M. Bender, J. Chappellaz, C. Genthon, V.M. Kotlyakov, V. Lipenkov, C. Lorius, J.R. Petit, D. Raynaud, G. Raisbeck, C. Ritz, T. Sowers, M. Stievenard, F. Yiou, and P. Yiou, Extending the Vostok ice-core record of paleoclimate to the penultimate glacial period, *Nature, 364,* 407-412, 1993.

Judd, A.G., R.H. Chalier, A. Lacroix, G. Lambert, and C. Rowland, Minor sources of methane, in *Atmospheric Methane: Sources, Sinks, and Role in Global Change,* edited by M.A.K. Khalil, Springer-Verlag, Berlin, 432-456, 1993.

Karol, I.L., Y.E. Ozolin, and E.V. Rozanov, Effect of space rocket launches on ozone and other atmospheric gases, paper presented at the European Geophys. Assoc. Conference, Wiesbaden, 1991.

Kawa, S.R., D.W. Fahey, L.E. Heidt, W.H. Pollock, S. Solomon, D.E. Anderson, M. Loewenstein, M.H. Proffitt, J.J. Margitan and K.R. Chan, Photochemical partitioning of the reactive nitrogen and chlorine reservoirs in the high-latitude stratosphere, *J. Geophys. Res., 97,* 7905-7923, 1992.

Kaye, J., S. Penkett and F. Ormond (Eds.), *Report on Concentrations, Lifetimes and Trends of CFCs, Halons, and Related Species*, NASA Reference Publication 1339, Washington, D.C., 1994.

Kaye, J.A., A.R. Douglass, C.H. Jackman, R.S. Stolarski, R. Zander and G. Roland, Two-dimensional model calculation of fluorine-containing reservoir species in the stratosphere, *J. Geophys. Res, 96,* 12865-12881, 1991.

Keller, M., and P. Matson, Biosphere-atmosphere exchange of trace gases in the tropics: Evaluating the effects of land use change, in *Global Atmospheric-Biospheric Chemistry: The First IGAC Scientific Conference,* edited by R.G. Prinn, 103-117, 1994.

Keller, M., E. Veldkamp, A.M. Weis, and W.A. Reiners, Pasture age effect on soil-atmosphere trace gas exchange in a deforested area of Costa Rica, *Nature, 365,* 244-246, 1993.

Khalil, M.A.K., and R.A. Rasmussen, Atmospheric carbon tetrafluoride (CF_4): Sources and trends, *Geophys. Res. Lett., 12,* 671-672, 1985.

Khalil, M.A.K., and R.A. Rasmussen, The global cycle of carbon monoxide: Trends and mass balance, *Chemosphere, 20,* 227-242, 1990.

Khalil, M.A.K., and R.A. Rasmussen, The global sources of nitrous oxide, *J. Geophys. Res., 97,* 14651-14660, 1992.

Khalil, M.A.K., and R.A. Rasmussen, The environmental history and probable future of fluorocarbon 11, *J. Geophys. Res., 98,* 23091-23106, 1993a.

Khalil, M.A.K., and R.A. Rasmussen, Decreasing trend of methane: Unpredictability of future concentrations, *Chemosphere, 26,* 803-814, 1993b.

Khalil, M.A.K., and R.A. Rasmussen, Global decrease of atmospheric carbon monoxide, *Nature, 370,* 639-641, 1994.

Khalil, M.A.K., R.A. Rasmussen, and F. Moraes, Atmospheric methane at Cape Meares: Analysis of a high resolution data base and its environmental implications, *J. Geophys. Res., 98,* 14753-14770, 1993a.

Khalil, M.A.K., R.A. Rasmussen, M.J. Shearer, S. Ge, and J.A. Rau, Methane from coal burning, *Chemosphere, 26,* 473-477, 1993b.

Kim, K.R. and H. Craig, Nitrogen-15 and oxygen-18 characteristics of nitrous oxide: A global perspective, *Science, 262,* 1855-1857, 1993.

Kirchgessner, D.A., S.D. Piccot, and J.D. Winkler, Estimate of global methane emissions from coal mines, *Chemosphere, 26,* 453-472, 1993.

Kirchhoff, V.W.J.H., and E.V.A. Marinho, Surface carbon monoxide measurements in Amazonia, *J. Geophys. Res., 95,* 16933-16943, 1990.

Ko, M., N. Sze, W.-C. Wang, G. Shia, A. Goldman, F. Murcray, D. Murcray, and C. Rinsland, Atmospheric sulfur hexafluoride: Sources, sinks and greenhouse warming, *J. Geophys. Res., 98,* 10499-10507, 1993.

Koppmann, R., F.J. Johnen, C. Plass-Dülmer, and J. Rudolph, Distribution of methylchloride, dichloromethane, trichloroethene and tetrachloroethene over the North and South Atlantic, *J. Geophys. Res., 98,* 20517-20526, 1993.

Kreileman, G.J.J., and A.F. Bouwman, Computing land use emissions of greenhouse gases, *Water, Air and Soil Poll., 76,* 231-258, 1994.

Kumer, J.B., J.L. Mergenthaler, and A.E. Roche, CLAES CH_4, N_2O and CCl_2F_2 (F12) global data, *Geophys. Res. Lett., 20,* 1239-1242, 1993.

Kvenvolden, K.A., and T.D. Lorenson, Methane in permafrost: Preliminary results from coring at Fairbanks, Alaska, *Chemosphere, 26,* 609-616, 1993.

Lacroix, A.V., Unaccounted-for sources of fossil and isotopically-enriched methane and their contribution to the emissions inventory, *Chemosphere, 26,* 507-557, 1993.

Lal, S., S. Venkataramani, and B.H. Subbaraya, Methane flux measurements from paddy fields in the tropical Indian region, *Atmos. Environ., 27A,* 1691-1694, 1993.

Lambert, G., and S. Schmidt, Reevaluation of the oceanic flux of methane: Uncertainties and long term variations, *Chemosphere, 26,* 579-589, 1993.

Lashoff, D.A., The dynamic greenhouse: Feedback processes that may influence future concentrations of atmospheric trace gases and climate change, *Clim. Change, 14,* 213-242, 1989.

Lassey, K.R., D.C. Lowe, C.A.M. Brenninkmeijer, and A.J. Gómez, Atmospheric methane and its carbon isotopes in the southern hemisphere: Their time series and an instructive model, *Chemosphere, 26,* 95-109, 1993.

Law, C.S., and N.J.P. Owen, Significant flux of atmospheric nitrous oxide from the northwest Indian Ocean, *Nature, 346,* 826-828, 1990.

Law, K.S., and J.A. Pyle, Modeling trace gas budgets in the troposphere, 2: CH_4 and CO, *J. Geophys. Res., 98,* 18401-18412, 1993.

Leuenberger, M., and U. Siegenthaler, Ice-age atmospheric concentration of nitrous oxide from an Antarctic ice core, *Nature, 360,* 449-451, 1992.

Liaw, Y.P., D.L. Sisterson, and N.L. Miller, Comparison of field, laboratory, and theoretical estimates of global nitrogen fixation by lightning, *J. Geophys. Res., 95,* 22489-22494, 1990.

Lobert, J.M., D.H. Scharffe, W.M. Hao, T.A. Kuhlbusch, R. Seuwen, P. Warneck, and P.J. Crutzen, Biomass burning: Experimental evaluation of biomass burning emissions: Nitrogen and carbon containing compounds, in *Global Biomass Burning: Atmospheric, Climatic and Biospheric Implications*, edited by J.S. Levine, MIT Press, 289-304, 1991.

Lobert, J.M., T.J. Baring, J.H. Butler, S.A. Montzka, R.C. Myers, and J.W. Elkins, Ocean-atmosphere exchange of trace compounds, 1992. Final report to AFEAS on oceanic measurements of HCFC-22, methylchloroform, and other selected halocarbons. National Oceanic and Atmospheric Administration/Climate Monitoring and Diagnostics Laboratory, Boulder, Colorado, USA, 1993.

Logan, J.A., Nitrogen oxides in the troposphere: Global and regional budgets, *J. Geophys. Res., 88,* 10785-10807, 1983.

Logan, J.A., Sources and sinks for carbon monoxide, in *Proceedings of the NATO Advanced Study Institute on Atmospheric Ozone: Its Variation and Human Influences*, Aldeia Las Acoteias, Algarre, Portugal. October 1-13, 323-342, 1980.

López-Valverde, M.A., M. López-Puertas, C.J. Marks, and F.W. Taylor, Global and seasonal variations in middle atmosphere CO from UARS/ISAMS, *Geophys. Res. Lett., 20,* 1247-1250, 1993.

Lowe, D., C.A.M. Brenninkmeijer, G. Brailsford, K. Lassey, and A. Gomez, Concentration and ^{13}C records of atmospheric methane in New Zealand and Antarctica: Evidence for changes in methane sources, *J. Geophys. Res., 99D,* 16913-16925, 1994.

Maiss, M., and I. Levin, Global increase of SF_6 observed in the atmosphere, *Geophys. Res. Lett., 21,* 569-573, 1994.

Makide, Y., L. Chen, and T. Toninaga, Accurate measurements and changing trends of atmospheric concentrations of CFC-11, CFC-12, CFC-113, CFC-114, CH_3CCl_3, CCl_4, halon-1301 and halon-1211, *Proc. International Symposium on Global Cycles of Atmospheric Greenhouse Gases*, Sendai, Japan, March, 38-51, 1994.

Mankin, W.G., and M.T. Coffey, Increased stratospheric hydrogen chloride in the El Chichón cloud, *Nature, 226,* 170-174, 1984.

Mankin, W.G., M.T. Coffey, and A. Goldman, Airborne observation of SO_2, HCl, and O_3 in the stratospheric plume of the Pinatubo volcano in July 1991, *Geophys. Res. Lett., 19,* 179-182, 1992.

Manley, S.L., K. Goodwin, and W.J. North, Laboratory production of bromoform, methylene bromide, and methyl iodide by macroalgae and distribution in nearshore southern California waters, *Limnol. Oceanogr., 37,* 1652-1659, 1992.

Manö, S., and M.O. Andreae, Emission of methyl bromide from biomass burning, *Science, 263,* 1255-1257, 1994.

Martius, C., R. Wassmann, U. Thein, A. Bandeira, H. Rennenberg, W. Junk, and W. Seiler, Methane emission from wood-feeding termites in Amazonia, *Chemosphere, 26,* 623-632, 1993.

McCulloch, A., Global production and emissions of bromochloro-difluoromethane and bromotrifluoromethane (halons 1211 and 1301), *Atmos. Environ., 26A,* 1325-1329, 1992.

Midgley, P., and D. Fisher, The production and release to the atmosphere of chlorodifluoromethane (HCFC-22), *Atmos. Environ., 27A,* 2215-2223, 1993.

Minson, D.J., Methane production by sheep and cattle in Australia, *Tellus, 45B,* 86-88, 1993.

Montzka, S.A., R.C. Myers, J.H. Butler, and J.W. Elkins, Global tropospheric distribution and calibration scale of HCFC-22, *Geophys. Res. Lett., 20,* 703-706, 1993.

Montzka, S.A., R.C. Myers, J.W Elkins, J.H. Butler, and S.O. Cummings, Measurements of HCFC-141b (1,1-dichloro-1-fluoroethane) and HCFC-142b (1-chloro-1,1-difluoroethane) in ambient air samples from the NOAA/CMDL global flask network, manuscript in preparation, 1994.

Moore, R.M., and R. Tokarczyk, Volatile biogenic halocarbons in the northwest Atlantic, *Global Biogeochem. Cycles, 7(1),* 195-210, 1993a.

Moore, R.M., and R. Tokarczyk, Chloro-iodomethane in N. Atlantic waters: A potentially significant source of atmospheric iodine, *Geophys. Res. Lett., 19,* 1779-1782, 1993b.

Moraes, F., and M.A.K. Khalil, Permafrost methane content: 2. Modelling theory and results, *Chemosphere, 26,* 595-607, 1993.

Müller, J.F., Geographical distribution and seasonal variation of surface emissions and deposition velocities of atmospheric trace gases, *J. Geophys. Res., 97,* 3787-3804, 1992.

Nakazawa, T., T. Machida, M. Tanaka, Y. Fujii, S. Aoki, and O. Watanabe, Differences of the atmospheric CH_4 concentration between the Arctic and Antarctic regions in preindustrial/agricultural era, *Geophys. Res. Lett., 20,* 943-946, 1993.

Neue, H.U. and P.A. Roger, Rice agriculture: Factor controlling emissions, in *Atmospheric Methane: Sources, Sinks, and Role in Global Change,* edited by M.A.K. Khalil, Springer-Verlag, Berlin, 254-298, 1993.

Novelli, P.C., K.A. Masarie, P.P. Tans, and P.M. Lang, Recent changes in atmospheric carbon monoxide, *Science, 263,* 1587-1590, 1994.

Ojima, D.S., D.W. Valentine, A.R. Mosier, W.J. Parton, and D.S. Schimel, Effect of land use change on methane oxidation in temperate forest and grassland soils, *Chemosphere, 26,* 675-685, 1993.

Penkett S.A., J.D. Prosser, R.A. Rasmussen, and M.A.K. Khalil, Atmospheric measurements of CF_4 and other fluorocarbons containing the CF_3 grouping, *J. Geophys. Res., 86,* 5172-5178, 1981.

Penner, J.E., C.S. Atherton, J. Dignon, S.J. Ghan, J.J. Walton, and S. Hameed, Tropospheric nitrogen: A three-dimensional study of sources, distributions, and deposition, *J. Geophys. Res., 96,* 959-990, 1991.

Penner, J.E., C.S. Atherton, and T.E. Graedel, Global emissions and models of photochemically active compounds, in *Global Atmospheric-Biospheric Chemistry: The First IGAC Scientific Conference,* edited by R.G. Prinn, in press, 1994.

Pepper, W., J. Legger, R. Swart, J. Watson, J. Edmonds, and I. Mintzer, *Emission Scenarios for the IPCC: An Update. Assumptions, Methodology and Results,* prepared for IPCC WG I, May 1992, 115 pp., 1992.

Piccot, S.D., J.J. Watson, and J.W. Jones, A global inventory of volatile organic compound emissions from anthropogenic sources, *J. Geophys. Res., 97,* 9897-9912, 1992.

Plumb, R.A., and M.K.W. Ko, Interrelationships between mixing ratios of long-lived stratospheric constituents, *J. Geophys. Res., 97,* 10145-10156, 1992.

Pollock, W.H., L.E. Heidt, R.A. Lueb, J.F. Vedder, M.J. Mills, and S. Solomon, On the age of stratospheric air and ozone depletion potentials in polar regions, *J. Geophys. Res., 97,* 12993-12999, 1992.

Prather, M.J., and R.T. Watson, Stratospheric ozone depletion and future levels of atmospheric chlorine and bromine, *Nature, 344,* 729-734, 1990.

Prather, M.J., and C.M. Spivakovsky, Tropospheric OH and the lifetime of hydrochlorofluorocarbons (HCFCs), *J. Geophys. Res., 95,* 18723-18729, 1990.

Prather, M.J., and E.E. Remsberg, Eds., *The Atmospheric Effects of Stratospheric Aircraft: Report of the 1992 Model and Measurements Workshop*, NASA Reference Publication 1292, 1992.

Prather, M.J., M.M. Garcia, A.R. Douglas, C.H. Jackman, M.K.W. Ko and N.D. Sze, The space shuttle's impact on the stratosphere, *J. Geophys. Res., 95,* 18583-18590, 1990.

Prinn, R., D. Cunnold, P. Simmonds, F. Alyea, R. Boldi, A. Crawford, P. Fraser, D. Gutzler, D. Hartley, R. Rosen, and R. Rasmussen, Global average concentration and trend for hydroxyl radicals deduced from ALE/GAGE trichloroethane (methyl chloroform) data for 1978-1990, *J. Geophys. Res., 97,* 2445-2461, 1992.

Pyle, J.A., and A.E. Jones, An investigation of the impact of the Ariane-5 launches on stratospheric ozone. Report to the European Space Agency, 1991.

Rasmussen, R.A., Isoprene: Identification as a forest type emission to the atmosphere, *Environ. Sci. Technol., 4,* 667-671, 1972.

Rasmussen, R.A., M.A.K. Khalil, and F. Moraes, Permafrost methane content: 1. Experimental data from sites in Northern Alaska, *Chemosphere, 26,* 591-594, 1993.

Ravishankara, A.R., S. Solomon, A.A. Turnipseed, and R.F. Warren, Atmospheric lifetimes of long-lived halogenated species, *Science, 259,* 194-199, 1993.

Reeburgh, W.S., N.T. Roulet, and B.H. Svensson, Terrestrial biosphere-atmosphere exchange in high latitudes, in *Global Atmospheric-Biospheric Chemistry: The First IGAC Scientific Conference*, edited by R.G. Prinn, 165-178, 1994.

Rinsland, C.P., M.R. Gunson, M.C. Abrams, L.L. Lowes, R. Zander, and E. Mahieu, ATMOS/ATLAS 1 measurements of sulphur hexafluoride (SF_6) in the lower stratosphere and upper troposphere, *J. Geophys. Res., 98,* 20491-20494, 1993.

Roulet, N., T. Moore, J. Bubier, and P. Lafleur, Northern fens: Methane flux and climatic change, *Tellus, 44B,* 100-105, 1992.

Roulet, N.T., R. Ash, W. Quinton, and T. Moore, Methane flux from drained northern peatlands: Effect of a persistent water table lowering on flux, *Biogeochem. Cycles, 7,* 749-769, 1993.

Rowland, F.S., C. Warg, and D. Blake, Reduction in the rates of growth of global atmospheric concentrations for CCl_3F (CFC-11) and CCl_2F_2 (CFC-12), in *Proceedings International Symposium on Global Cycles of Atmospheric Greenhouse Gases*, Sendai, Japan, 7-10 March, 38-51, 1994.

Rudolph, J., A. Khedim, T. Clarkson, and D. Wagenbach, Long term measurements of light alkanes and acetylene in the Antarctic troposphere, *Tellus, 44B,* 252-261, 1992.

Russell, J.M. III, A.F. Tuck, L.L. Gordley, J.H. Park, S.R. Drayson, J.E. Harries, R.J. Cicerone, and P.J. Crutzen, HALOE Antarctic observations in the spring of 1991, *Geophys. Res. Lett., 20,* 718-721, 1993.

Sanhueza, E., Biogenic emissions of NO and N_2O from tropical savanna soils, in *Proceedings International Symposium on Global Change (IGBP)*, Tokyo, Japan, March 27-29, 24-34, 1992.

Sanhueza, E., L. Cárdenas, L. Donoso and M. Santana, 1994: Effect of plowing on CO_2, CO, CH_4, N_2O and NO fluxes from tropical savannah soils. *J. Geophys. Res., 99D,* 16429-16434, 1994.

Schauffler, S.M., L.E. Heidt, W.L. Pollock, T.M. Gilpin, J.F. Vedder, S. Solomon, R.A. Lueb, and E.L. Atlas, Measurements of halogenated organic compounds near the tropical tropopause, *Geophys. Res. Lett., 20,* 2567-2570, 1993.

Schmidt, U., R. Bauer, A. Khedim, G. Kulessa, and C. Schiller, Profile observations of long-lived trace gases in the Arctic vortex, *Geophys. Res. Lett., 18,* 767-770, 1991.

Seiler, W., and R. Conrad, Contribution of tropical ecosystems to the global budgets of trace gases, especially CH_4, H_2, CO, and N_2O, in *The Geophysiology of Amazonia*, edited by R. Dickenson, Wiley, New York, 133-160, 1987.

Shearer, M.J., and M.A.K. Khalil, Rice agriculture: Emissions, in *Atmospheric Methane: Sources, Sinks, and Role in Global Change,* edited by M.A.K. Khalil, Springer-Verlag, Berlin, 230-253, 1993.

Simmonds, P., D. Cunnold, G. Dolland, T. Davies, A. McCulloch, and R. Derwent, Evidence of the phase out of CFC use over Europe over the period 1987-1990, *Atmos. Environ., 27A,* 1397-1407, 1993.

Skole, D., and C. Tucker, Tropical deforestation and habitat fragmentation in the Amazon: Satellite data from 1978 to 1988, *Science, 260,* 1905-1910, 1993.

Steele, L.P., E.J. Dlugokencky, P.M. Lang, P.P. Tans, R.C. Martin, and K.A. Masarie, Slowing down of the global accumulation of atmospheric methane during the 1980's, *Nature, 358,* 313-316, 1992.

Sturges, W.T., C.W. Sullivan, R.C. Schnell, L.E. Heidt, W.H. Pollock, and C.E. Quincy, Bromoalkane production by Antarctic ice algae: A possible link to surface ozone loss, *Tellus, 45B,* 120-126, 1993.

Subak, S., P. Raskin, and D.V. Hippel, National greenhouse gases accounts: Current anthropogenic sources and sinks, *Climate Change, 25,* 15-58, 1993.

Swanson, T., J.W. Elkins, J.H. Butler, S.A. Montzka, R.C. Myers, T.M. Thompson, T.J. Baring, S.O. Cumming, G.S. Dutton, A.H. Hayden, J.M. Lobert, G.A. Holcomb, W.T. Sturges, and T.M. Gilpin, Nitrous Oxide and Halocarbons Division, Section 5 of CMDL No. 21 Summary Report 1992, edited by J.T. Peterson and R.M. Rosson, 59-75, 1993.

Tabazadeh, A., and R.P. Turco, Stratospheric chlorine injection by volcanic eruptions: HCl scavenging and implications for ozone, *Science, 260,* 1082-1086, 1993.

Tarr, M.A., W.L. Miller, and R.G. Zepp, Direct photoproduction of carbon monoxide from plant matter, *J. Geophys. Res.*, submitted, 1994.

Taylor, F.W., *et al.*, Remote sensing of atmospheric structure and composition by pressure modulator radiometer from space: The ISAMS experiment on UARS, *J. Geophys. Res., 98,* 10799-10814, 1993.

Thorneloe, S.A., M.A. Barlaz, R. Peer, L.C. Huff, L. Davis, and J. Mangino, Waste management, in *Atmospheric Methane: Source, Sinks, and Role in Global Change*, edited by M.A.K. Khalil, Springer-Verlag, Berlin, 362-398, 1993.

Tokarczyk, R., and R.M. Moore, Production of volatile organohalogens by phytoplankton cultures, *Geophys. Res. Lett., 21,* 285-288, 1994.

Toon, G.C., C.B. Farmer, P.W. Schaper, L.L. Lowes, and R.H. Norton, Composition measurements of the 1989 Arctic winter stratosphere by airborne infrared solar absorption spectroscopy, *J. Geophys. Res., 97,* 7939-7961, 1992a.

Toon, G.C., C.B. Farmer, P.W. Schaper, L.L. Lowes, and R.H. Norton, Evidence for subsidence in the 1989 Arctic winter stratosphere from airborne infrared composition measurements, *J. Geophys. Res., 97,* 7963-7970, 1992b.

Toon, G.C., J.F. Blavier, J.N. Solario, and J.T. Szeto, Airborne observations of the 1992 Arctic winter stratosphere by FTIR solar absorption spectroscopy, in *Optical Methods in Atmospheric Chemistry*, SPIE Vol.1715, 457-467, 1992c.

Toon, G.C., J.F. Blavier, J.N. Solario, and J.T. Szeto, Airborne observations of the composition of the 1992 tropical stratosphere by FTIR solar absorption spectrometry, *Geophys. Res. Lett., 20,* 2503-2506, 1993.

Tuck, A.F., S.J. Hovde, K.K. Kelly, J.M. Russell III, C.R. Webster, and R.D. May, Intercomparison of HALOE and ER-2 aircraft H_2O and CH_4 observations collected during the second Airborne Arctic Stratospheric Experiment (AASE-II), *Geophys. Res. Lett., 20,* 1243-1246, 1993.

Valentine, R.L., and R.G. Zepp, Formation of carbon monoxide from photodegradation of terrestrial dissolved organic carbon in natural waters, *Environ. Sci. Technol., 27,* 409-412, 1993.

Wallace, L., and W. Livingston, The effect of the Pinatubo cloud on hydrogen chloride and hydrogen fluoride, *Geophys. Res. Lett., 19,* 1209-1212, 1992.

Wallace, D.W.R., P. Beinung and A. Putzka, Carbon tetrachloride and chlorofluorocarbons in the South Atlantic Ocean, 19°S, submitted to *J. Geophys. Res.*, 1994.

Warneck, P., Chemistry of the natural atmosphere, *Int. Geophys. Ser., 41,* Academic, San Diego, California, 1988.

Wassmann, R., H. Papen, and H. Rennenberg, Methane emission from rice paddies and possible mitigation strategies, *Chemosphere, 26,* 201-217, 1993.

Weisenstein, D.K., M.K.W. Ko, and N.D. Sze, The chlorine budget of the present-day atmosphere: A modeling study, *J. Geophys. Res., 97,* 2547-2559, 1992.

Weiss, R., Changing global concentration of atmospheric nitrous oxide, in *Proceedings International Symposium on Global Cycles of Atmospheric Greenhouse Gases*, Sendai, Japan, 7-10 March, 1994.

Whalen, S.C., and W. Reeburgh, Interannual variations in tundra methane emission: A 4-year time series at fixed sites, *Global Biogeochem. Cycles, 6,* 139-159, 1992.

Williams, E.J., A. Guenther, and F.C. Fehsenfeld, An inventory of nitric oxide emissions from soils in the United States, *J. Geophys. Res., 97,* 7511-7519, 1992.

WMO, *Atmospheric Ozone 1985: Assessment of Our Understanding of the Processes Controlling Its Present Distribution and Change,* World Meteorological Organization, Global Ozone Research and Monitoring Project – Report No. 16, Geneva, Switzerland, 1986.

WMO, *Scientific Assessment of Ozone Depletion: 1991,* World Meteorological Organization, Global Ozone Research and Monitoring Project – Report No. 25, Geneva, Switzerland, 1992.

Woodbridge *et al.*, Estimates of total organic and inorganic chlorine in the lower stratosphere from *in situ* measurements during AASE II, submitted to *J. Geophys. Res.*, 1994.

Worthy, D., N. Trivett, K. Higuchi, J. Hopper, E. Dlugokencky, M. Ernst, and M. Glumpak, Six years of in situ atmospheric methane measurements at Alert, N.W.T., Canada, 1988-1993: Seasonal variations, decreasing growth rate and long range transport, in *Proceedings International Symposium on Global Cycles of Atmospheric Greenhouse Gases*, Sendai, Japan, 7-10 March, 130-133, 1994.

Zander, R., C.P. Rinsland, and P. Demoulin, Infrared spectroscopic measurements of the vertical column abundance of sulphur hexafluoride, SF_6, from the ground, *J. Geophys. Res., 96,* 15447-15454, 1991a.

Zander, R., C.P. Rinsland, D.H. Ehhalt, J. Rudolph, and Ph. Demoulin, Vertical column abundances and seasonal cycle of acetylene, C_2H_2, above the Jungfraujoch station, derived from IR solar observations, *J. Atmos. Chem., 13,* 359-372, 1991b.

Zander, R., M.R. Gunson, C.B. Farmer, C.P. Rinsland, F.W. Irion, and E. Mahieu, The 1985 chlorine and fluorine inventories in the stratosphere based on ATMOS at 30° north latitude, *J. Atmos. Chem., 15,* 171-186, 1992.

Zander, R., E. Mahieu, P. Demoulin, C.P. Rinsland, D.K. Weisenstein, M.K.W. Ko, N.D. Sze, and M.R. Gunson, Secular evolution of the vertical column abundances of $CHClF_2$ (HCFC-22) in the Earth's atmosphere inferred from ground-based IR solar observations at Jungfraujoch and at Kitt Peak, and comparison with model calculations, *J. Atmos. Chem., 18,* 129-148, 1994a.

Zander, R., D.H. Ehhalt, C.P. Rinsland, U. Schmidt, E. Mahieu, J. Rudolph, P. Demoulin, G. Roland, L. Delbouille, and A.J. Sauval, Secular trend and seasonal variability of the column abundance of N_2O above the Jungfraujoch station determined from IR solar spectra, *J. Geophys. Res., 99D,* 16745-16756, 1994b.

Zander, R., Ph. Demoulin, and E. Mahieu, Monitoring of the atmospheric burdens of CH_4, N_2O, CO, $CHClF_2$ and CF_2Cl_2 above central Europe during the last decade, in *Proceedings of International Symposium on Non-CO_2 Greenhouse Gases—Why and How to Control?*, Maastricht, Dec. 13-15, 1993, to appear in *Environmental Monitoring and Assessment,* Kluwer Academic Pub., 1994c.

Zimmerman, P.R., R.B. Chatfield, J. Fishman, P.J. Crutzen, and P.L. Hanst, Estimates on the production of CO and H_2 from the oxidation of hydrocarbon emissions from vegetation, *Geophys. Res. Lett., 5,* 679-682, 1978.

Zolensky, M.E., D.S. McKay, and L.A. Kaczor, A tenfold increase in the abundance of large solid particles in the stratosphere, as measured over the period 1976-1984, *J. Geophys. Res., 94,* 1047-1056, 1989.

PART 2

Atmospheric Processes Responsible for the Observed Changes in Ozone

CHAPTER 3

Polar Ozone

Lead Author:
D.W. Fahey

Co-authors:
G. Braathen
D. Cariolle
Y. Kondo
W.A. Matthews
M.J. Molina
J.A. Pyle
R.B. Rood
J.M. Russell III
U. Schmidt
D.W. Toohey
J.W. Waters
C.R. Webster
S.C. Wofsy

Contributors:
T. Deshler
J.E. Dye
T.D.A. Fairlie
W.L. Grose
G.L. Manney
P.A. Newman
A. O'Neill
R.B. Pierce
W. Randel
A.E. Roche
C.R. Trepte

CHAPTER 3

POLAR OZONE

Contents

SCIENTIFIC SUMMARY

Substantial new results have been obtained since the last assessment in the areas of observations, laboratory measurements, and modeling. These new results reaffirm the key role of anthropogenic halocarbons as the cause of ozone loss in polar regions and increase confidence in the processes associated with this loss: the formation of a polar vortex in high-latitude winter, the growth of aerosol surfaces at low temperatures characteristic of the vortex, the conversion of inactive chlorine to active forms on these surfaces, the subsequent chlorine-catalyzed loss of ozone, the return of chlorine to inactive forms in the polar regions in spring, and the breakup of the vortex and its dispersal to lower latitudes.

Ozone

- Results of observational and modeling studies since the last assessment reaffirm the role of anthropogenic halocarbon species in Antarctic ozone depletion. Satellite observations show a strong spatial and temporal correlation of chlorine monoxide (ClO) abundances with ozone depletion in the Antarctic vortex. Photochemical model calculations of ozone depletion are consistent with observed losses in the Antarctic.

- Chlorine- and bromine-catalyzed ozone loss has been confirmed in the Arctic winter. Consistent with expectations, these losses are smaller than those observed over Antarctica. Photochemical model calculations constrained with *in situ* and satellite observations yield results consistent with the observed ozone loss.

- Interannual variability in the photochemical and dynamical conditions of the vortices continues to limit reliable predictions of future ozone changes in polar regions, particularly in the Northern Hemisphere.

Chlorine species

- Satellite measurements show that elevated ClO concentrations cover most of both polar vortex regions during much of the winter. This is consistent with the picture that virtually all available chlorine becomes fully activated in both winter vortices through heterogeneous reactions that occur on aerosol particles formed at low temperatures.

- *In situ* and remote measurements show that hydrochloric acid (HCl) and chlorine nitrate ($ClONO_2$) concentrations are markedly reduced in the vicinity of the elevated ClO concentrations. This anticorrelation is quantitatively consistent with the picture that HCl and $ClONO_2$ are converted to reactive chlorine. Chlorine in the stratosphere originates largely from anthropogenic halocarbons.

Aerosols

- Laboratory studies reaffirm that surface reactions on aerosol particles efficiently produce active chlorine from inactive forms. The rate of the principal reaction of HCl with $ClONO_2$ is a strong function of temperature and relative humidity, and depends to a lesser extent on bulk aerosol composition.

- Sulfate aerosol from the Mt. Pinatubo eruption reached high latitudes in the stratosphere, enhancing reactions involving aerosol particles in and near the polar vortices. This led to chlorine activation over larger regions in the high latitude stratosphere, especially near the vortex boundaries, and extended the spatial extent of halogen-related ozone loss.

- The formation and reactivity of aerosol particles within the vortex can be simulated, in part, by microphysical models. Two- and three-dimensional photochemical transport models confirm observations that chlorine can be activated efficiently throughout the entire vortex within days.

POLAR PROCESSES

- Aerosol particles in the polar stratosphere are known ternary condensates of nitric acid (HNO_3), sulfuric acid (H_2SO_4), and water (H_2O). Important progress has been made in the characterization of these condensates in theoretical and laboratory studies.

- Satellite measurements confirm that the sequestering and removal of HNO_3 by aerosol particles is a predominant feature of the Antarctic vortex for much of the winter, whereas removal in the Arctic is generally less intense and more localized.

- Despite extensive observational evidence for dehydration and denitrification, the underlying microphysical mechanisms and necessary atmospheric conditions that control particle formation and sedimentation have not been adequately described. This is an important limitation for reliably predicting ozone loss in polar regions, particularly in the Northern Hemisphere.

Vortex

- New satellite observations of long-lived tracers and modeling studies confirm that air within the center of the polar winter vortices is substantially isolated from extravortical air, especially in the Antarctic.

- Nearly all observational and modeling studies are consistent with a time scale of three to four months to replace a substantial fraction of inner Antarctic vortex air.

- Models show that most mass transport out of the vortex in the lower stratosphere occurs below about 16 km altitude.

- Erosion by planetary and synoptic wave activity transports air from the vortex edge region to lower latitudes. Data and model studies provide conflicting interpretations of the magnitude of this transport and its effect on lower latitudes. There is little evidence of significant lateral mixing into the vortex except during strong wave events in the Arctic.

- Observed correlations of nitrous oxide abundances with those of inactive chlorine species, reactive nitrogen, and ozone over broad regions at high latitudes in the lower stratosphere have proved useful for diagnosing ozone destruction throughout the vortex.

3.1 INTRODUCTION

Depletion of polar ozone in the winter seasons continues to be an important scientific issue for both hemispheres. While the "ozone hole" has become an annual feature in the Southern Hemisphere, increased losses have been noted in the Northern Hemisphere in recent years. Increased losses at midlatitudes may be connected to the more intense loss processes occurring in polar regions. The World Meteorological Organization (WMO) *Scientific Assessment of Ozone Depletion: 1991* reaffirmed halogen chemistry as the cause of severe ozone depletion in the Antarctic as well as of smaller losses in the Arctic (WMO, 1992). The causes for the observed year-to-year variability of such losses and effects at midlatitudes were left as uncertain. For this assessment, a wide variety of new evidence is available to confirm the basic paradigm of ozone loss in polar regions. This new evidence, which follows from a high level of activity involving observational, laboratory, and modeling studies that took place in the period 1991-1994, has better defined a number of the photochemical and dynamical aspects of polar ozone depletion.

The principal cause of ozone loss in the polar regions is photochemistry involving the halogen species, chlorine and bromine. Long-lived halogens species, primarily chlorofluorocarbons, are released in the troposphere from human activities. The photochemical degradation of these organic source molecules in the stratosphere leads to the formation of inorganic halogen species, of which chlorine monoxide (ClO), chlorine nitrate ($ClONO_2$), hydrochloric acid (HCl), bromine monoxide (BrO), and bromine nitrate ($BrONO_2$) are most important. The release of chlorine from the more stable reservoirs occurs in high-latitude winter in reactions on surfaces of stratospheric aerosol particles. The formation and reactivity of these particles are enhanced at the low temperatures characteristic of the interior of the polar vortices. This reactive processing maintains high levels of active chlorine species that, along with BrO, catalytically destroy ozone as this air encounters sunlight. With sufficient insolation and warmer temperatures, chlorine is returned to its reservoir forms during a photochemical recovery period and ozone destruction slows. The removal of reactive nitrogen by aerosol particle sedimentation in the vortex, a process defined as denitrification, strongly regulates the rate of recovery by controlling the availability of active chlorine. This paradigm, illustrated in Figure 3-1, has been broadly supported by a wide variety of data and interpretation in previous WMO assessments and has been strengthened substantially in this assessment period.

This assessment period was marked by the launch of the National Aeronautics and Space Administration (NASA) Upper Atmosphere Research Satellite (UARS) in late 1991, after more than a decade of preparation (Reber, 1990; Reber *et al.*, 1993). The satellite contains four instruments for the measurement of trace species in the stratosphere (Barath *et al.*, 1993; Russell *et al.*, 1993a; Roche *et al.*, 1993a; Taylor *et al.*, 1993) and other instruments for wind, solar radiation, and energetic particles. From an orbit of 600 km inclined 57° to the equator, UARS provides broad coverage in both hemispheres with a maximum latitude of 80°. The precession of the orbit with respect to the Sun provides measurements during all local solar times over a month-long period. Of particular importance for this assessment are the UARS observations at high latitudes of the chlorine reservoir species $ClONO_2$ and HCl, active chlorine in the form of ClO, the reactive nitrogen species nitric acid (HNO_3), water vapor, aerosol extinction, and the long-lived tracers nitrous oxide (N_2O), methane (CH_4), and hydrofluoric acid (HF). In addition, ozone measurements show the distribution and evolution of ozone loss in the polar regions. New aspects of the transport of air in and near the vortex are evident from the observations of long-lived tracers. The interpretation of UARS data will remain an active research area as the data set continues to grow.

The body of *in situ* observations in the stratosphere was greatly increased with aircraft and balloon measurements made during the European Arctic Stratospheric Ozone Experiment (EASOE) (Pyle *et al.*, 1994) and the NASA Airborne Arctic Stratospheric Expedition II (AASE II) (Anderson and Toon, 1993), which were both held during the Northern Hemisphere winter of 1991/92. Each included measurements of reactive nitrogen and chlorine species, long-lived tracers and reservoir species, and aerosols, combined with modeling studies of observed photochemical and dynamical changes. The observation period extended from pre-vortex conditions in fall, through the lowest temperature conditions marked by chlorine activation, and into the photochemical recovery period in early spring. The breadth of

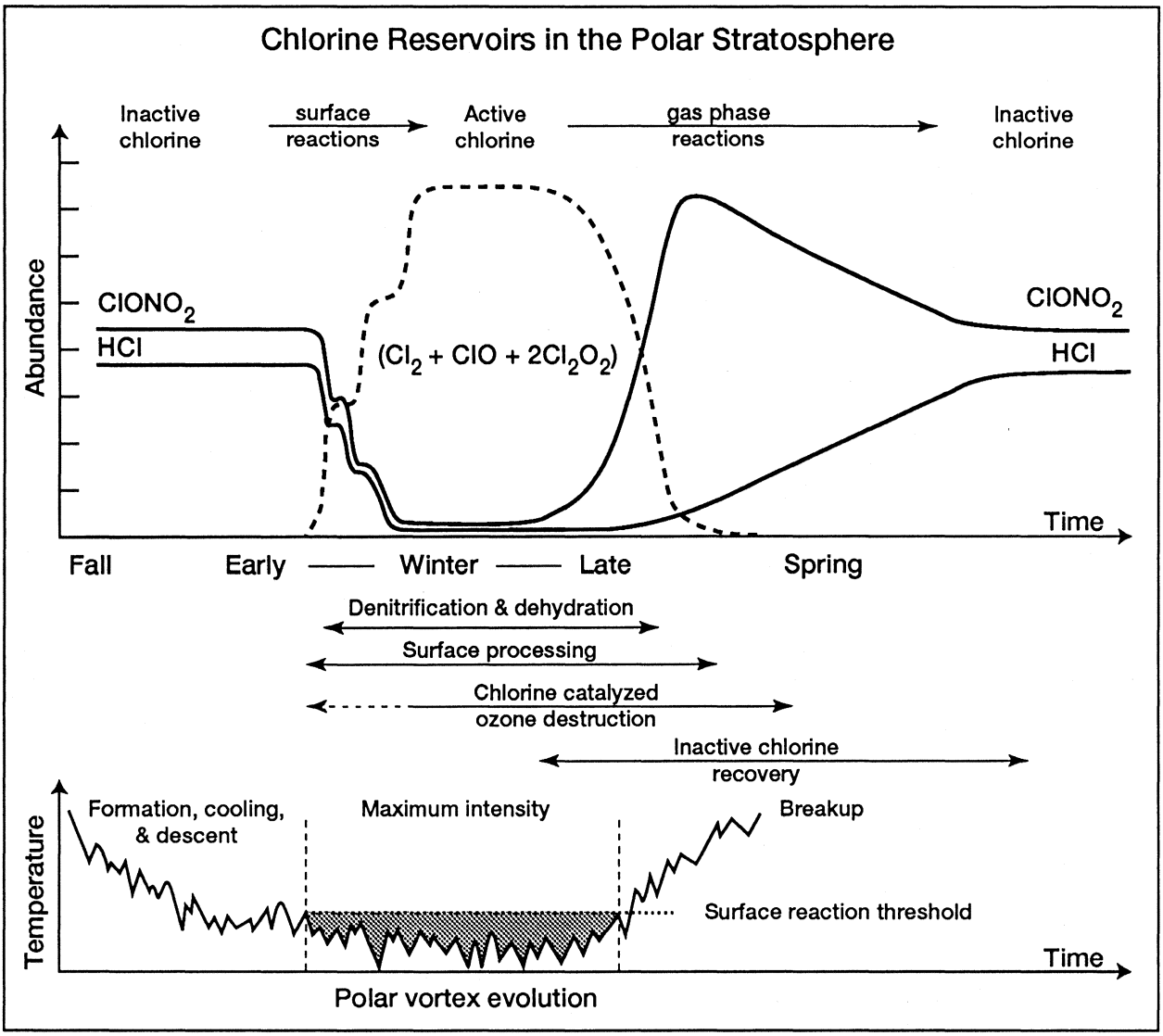

Figure 3-1. Schematic of the photochemical and dynamical features of the polar regions related to ozone depletion. The upper panel represents the conversion of chlorine from inactive to active forms in winter in the lower stratosphere and the reformation of inactive forms in spring. The partitioning between the active chlorine species Cl_2, ClO, and Cl_2O_2 depends on exposure to sunlight after polar stratospheric cloud (PSC) processing. The corresponding stages of the polar vortex are indicated in the lower panel, where the temperature scale represents changes in the minimum polar temperatures in the lower stratosphere (see Figure 3-3) (adapted from Webster *et al.*, 1993a).

instrumentation and period of measurements have resulted in a unique data set for the examination of the paradigm in Figure 3-1. In addition, ground-based observations during EASOE and separate efforts in Antarctica have also yielded important insights into the evolution of reactive chlorine and nitrogen during the winter season.

Modeling studies continue to advance with improvements in computational facilities and algorithms and with new atmospheric data. Specifically, photochemical models that incorporate observations of long-lived tracers, reservoir species, new kinetic data, and meteorological conditions are now able to make more representative calculations of ozone loss in the polar vortex. Studies of the fluid dynamics near the vortex now provide more detailed descriptions of air parcel motion in regions of high potential vorticity (PV) gradients, improving estimates of the transport into and out of the vortex interior. The continued refinement of such models is an essential component for future predictions of ozone loss and its variability.

New laboratory studies have examined aspects of the homogeneous and heterogeneous chemistry underlying the kinetics of ozone loss. Specifically, new photolysis cross section measurements have been made for HNO_3 and $ClONO_2$ under stratospheric conditions. Photolysis of HNO_3 is a limiting step for photochemical recovery in early spring in the vortex. Significant advances have been made in the understanding of the formation and growth of aerosols and the reactivity of aerosol surfaces in polar regions. These advances build on the extensive effort expended in recent years to develop new laboratory techniques to characterize multiphase surface growth under stratospheric conditions. At the same time, the understanding of the thermodynamics of aerosol growth has progressed to explain laboratory and atmospheric observations.

Finally, the assessment period was marked by the eruption of Mt. Pinatubo in the Philippines in June 1991, months before the launch of the UARS satellite and the start of the EASOE and AASE II campaigns. The increased loading of stratospheric aerosol was predicted to cause significant changes in ozone at midlatitudes as a result of increased heterogeneous reactivity (Brasseur and Granier, 1992; Prather, 1992; Hofmann and Solomon, 1989) (see Chapter 4). The aerosol did not reach polar regions in abundance until the southern winter of 1992 and the northern winter of 1992-93. Observational and modeling evidence suggests the enhancement of volcanic aerosol near the vortex will increase ozone loss associated with heterogeneous processes in that region. Studies have continued as the volcanic aerosol in the stratosphere gradually diminished over a period of several years following the eruption.

3.2 VORTEX FORMATION AND TRACER RELATIONS

The vortex that forms in each winter hemisphere in the polar region sets the context of ozone depletion (see Figures 3-1 and 3-2). The temporal as well as the

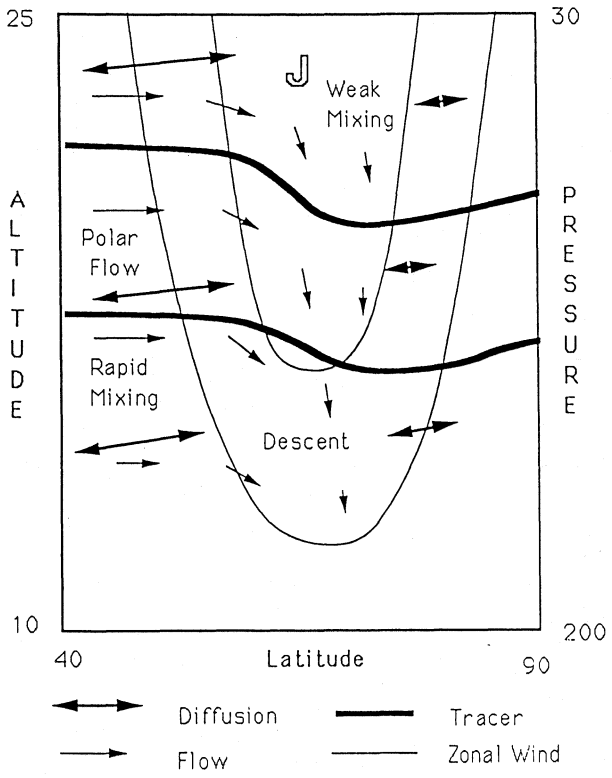

Figure 3-2. Schematic of the circulation and mixing associated with the polar vortex in the Arctic midwinter or Antarctic early spring periods. The vertical scale is shown in altitude (km) and pressure (mb) units. The horizontal scale is latitude in degrees. Arrows indicate mixing (double) and flow (single), with longer arrows representing larger rates. Other features are zonal wind contours (thin lines), jet core (J), and long-lived tracer isopleths (thick lines) (Schoeberl *et al.*, 1992).

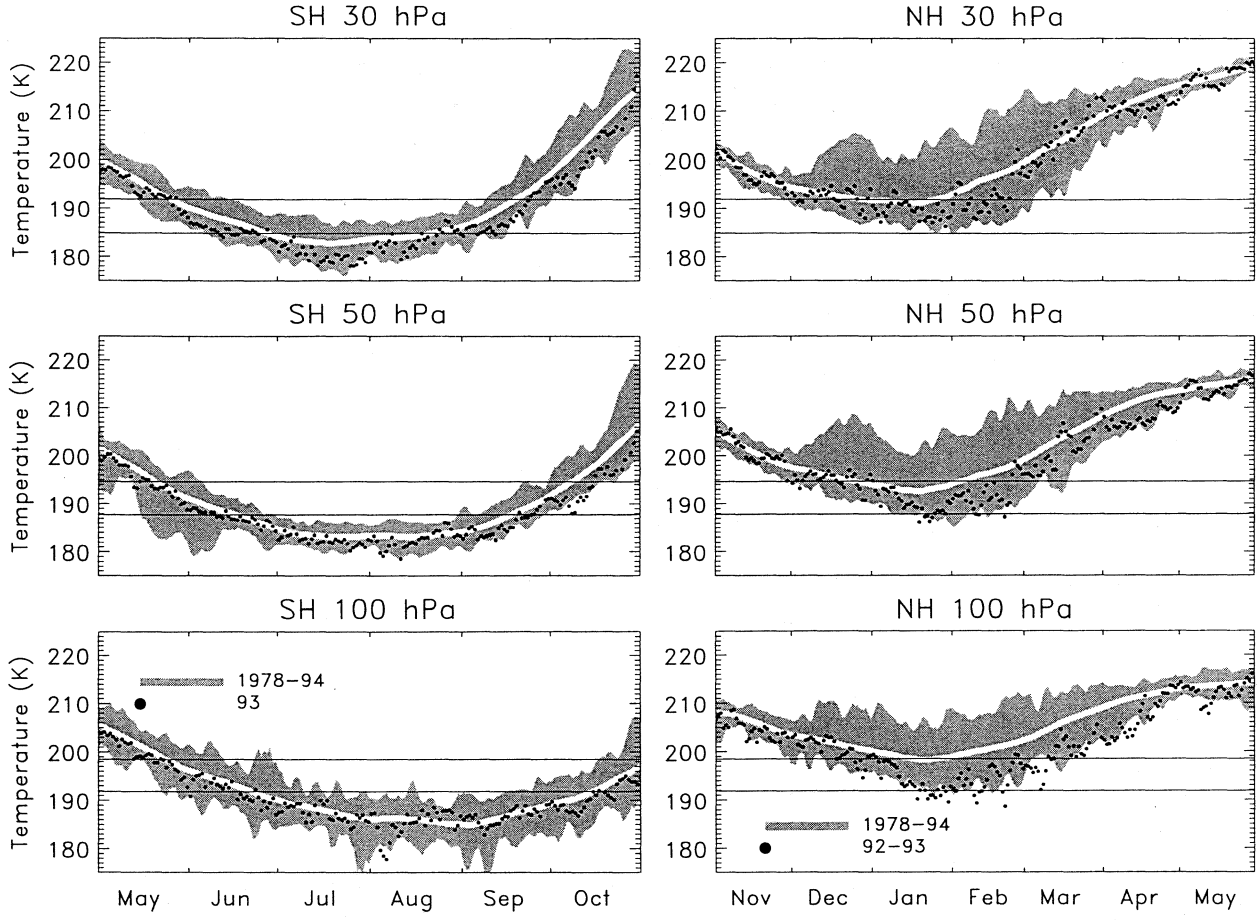

Figure 3-3. A summary of the minimum polar vortex temperatures in the period 1978 to 1994 at 30 hPa, 50 hPa, and 100 hPa (1 hPa = 1 mb) in the lower stratosphere in the Northern (NH) and Southern (SH) hemispheres (National Meteorological Center analysis). The range of observations between 1978 and 1992 is given by the shaded region. The narrow white band is the average of the data set. The black dots represent data for 1993 in the Antarctic and 1992-93 in the Arctic winter. Lines indicate approximate temperature thresholds for Type I (upper) and Type II (lower) PSC formation (adapted from Nagatani *et al.*, 1990).

spatial scale of the activation of chlorine that catalytically destroys ozone is associated with the extent of low temperatures inside the vortex. In addition, the dynamical features of the vortex determine the distribution of air from the vortex to lower latitudes and the incorporation of lower latitude air into the vortex. Many features of vortex formation are understood from observational and modeling studies (Schoeberl and Hartmann, 1991; Schoeberl *et al.*, 1992; Dritschel and Legras, 1993; Manney and Zurek, 1993; Strahan and Mahlman, 1994a, b). After autumn equinox, increasing polar darkness and radiative cooling of polar air lead to the formation of a circumpolar wind belt. This westerly wind belt, or polar night jet, defines the polar vortex in each hemisphere (see Figure 3-2). The vortex edge region is characterized by large gradients in PV and mixing and transport properties. Large differences in the wind and temperature fields of the vortex exist between hemispheres (see Figure 3-3) (Manney and Zurek, 1993). The vortex in the Southern Hemisphere is stronger, develops lower temperatures, and persists longer than the northern vortex. The cause is related to differences in planetary wave activity that modifies the temperature and dynamical structure of the vortex. Wave activity is more frequent and of larger amplitude in the north, owing to more dominant orographic features and the greater land/sea

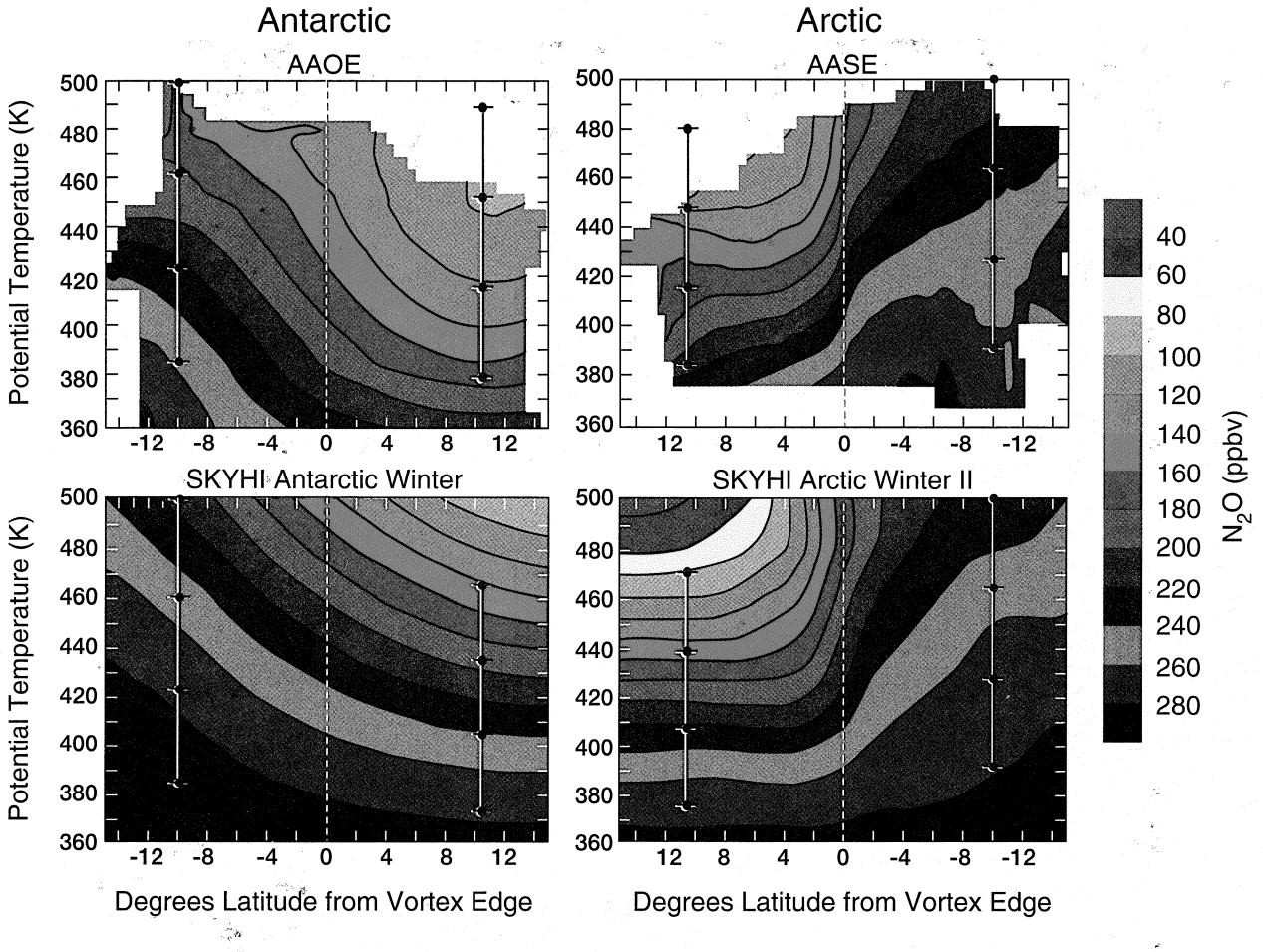

Figure 3-4. Top panels: Mean N_2O mixing ratios on potential temperature surfaces calculated from aircraft flight data in high-latitude winter. Bottom panels: Same, except using the Geophysical Fluid Dynamics Laboratory SKYHI model results from 24 days covering the same spatial and temporal region. Positive values on the abscissa represent degrees of latitude poleward of the vortex edge. The internal four-point vertical scales in each panel represent approximate pressure altitudes inside and outside the vortex. From top to bottom, the points correspond to altitudes of 20, 18, 16, and 14 km, respectively (adapted from Strahan and Mahlman, 1994a). (See Garcia *et al.* [1992] for two-dimensional model results.)

contrast. Because ozone depletion depends on the interaction of the vortex wind field with local regions of low temperatures and the resultant chemical processing, the temperature differences represented in Figure 3-3 underlie the large differences in ozone depletion observed between the hemispheres (see Section 3.4). Thus, predictions of future ozone losses and the role of climate change in polar processes depend directly on factors that change the temperature and wind fields during the winter seasons.

An important diagnostic for the formation of the polar vortices and subsequent ozone loss is the high-latitude distribution of long-lived trace species such as N_2O, CH_4, and the chlorofluorocarbons CFC-11 and CFC-113. All have large gradients in the stratosphere (decreasing with altitude) resulting from photochemical loss and transport. Air descending into the center of the vortex reduces values of these traces species, thereby creating horizontal gradients inside the vortex (see Figure 3-4). Balloon and aircraft measurements of N_2O beginning before vortex formation serve as a baseline for documenting the temporal variation of the vertical structure within the vortex (Bauer *et al.*, 1994; Podolske *et al.*, 1993). A comparison of the location of high PV from

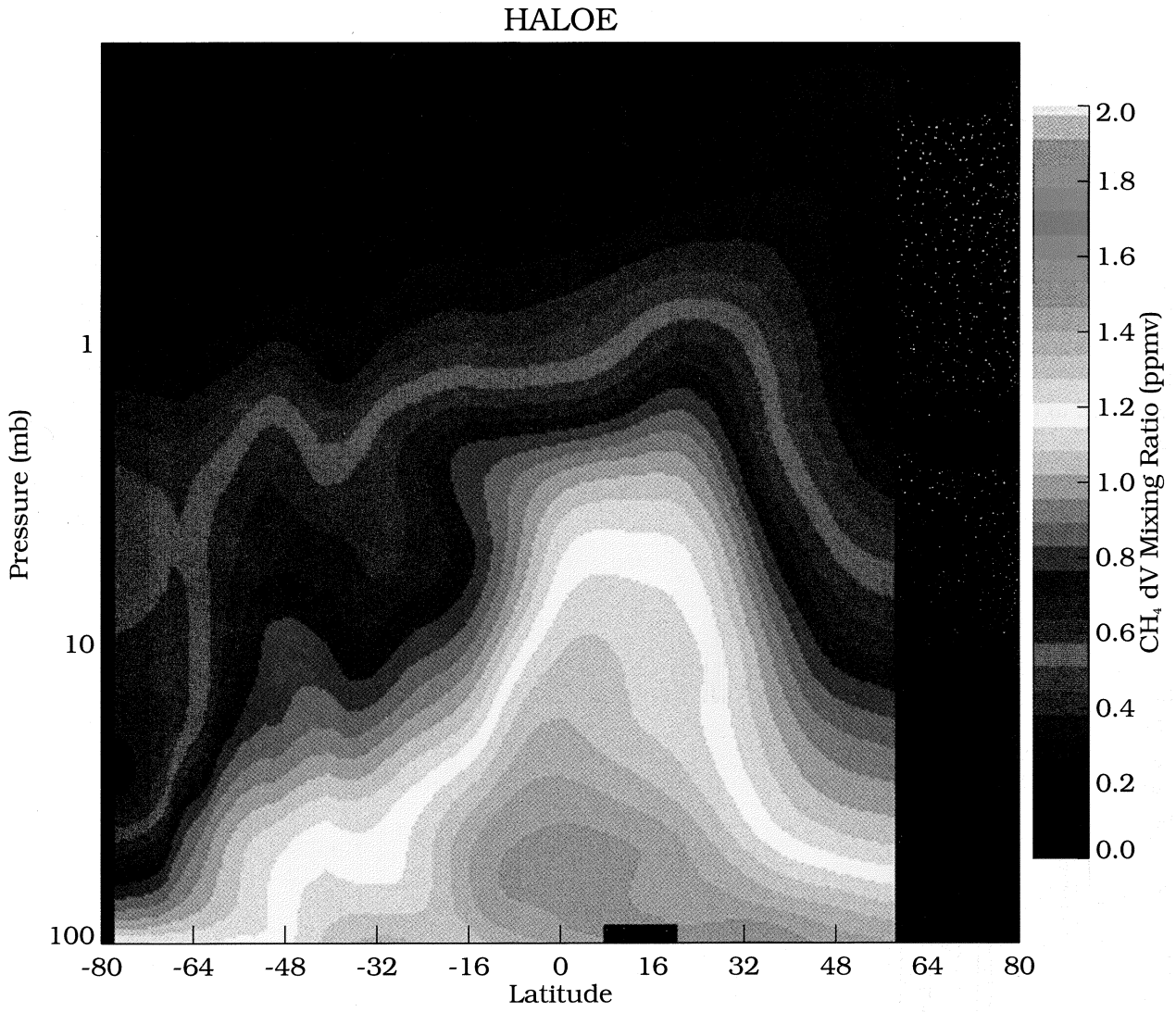

Figure 3-5. Pressure versus latitude cross section of CH_4 from the UARS Halogen Occultation Experiment (HALOE) satellite instrument. Data are from sunset scans over the period 21 September to 15 October 1992 analyzed with the version-17 algorithm. The pressure range corresponds to altitudes between about 16 and 65 km. Latitude is expressed in degrees, with negative latitude values corresponding to the Southern Hemisphere (adapted from Russell *et al.*, 1993b).

meteorological analyses and low N_2O from satellite fields shows excellent correspondence in the Arctic, thereby increasing confidence in the analysis of vortex structure (Manney *et al.*, 1994a). Simulations using a general circulation model and an improved two-dimensional model successfully reproduce important features of the observed N_2O distributions in and near the northern vortex (see Figure 3-4 and Section 3.5.5) (Strahan and Mahlman, 1994a; Garcia *et al.*, 1992).

Satellite observations of CH_4 and HF reveal unmixed vertical descent taking place at the center of the vortex in the Antarctic (see Figure 3-5) (Russell *et al.*, 1993b). The lack of vertical gradient indicates that air at lower altitudes containing larger CH_4 values has not been mixed with the descending air. Although not observed before, the strong descent implied by the observations matches earlier predictions (Danielsen and Houben, 1988). The observations are qualitatively simu-

lated with a mechanistic three-dimensional (3-D) model (see Section 3.5.5), following many atmospheric air parcels as they undergo transport from the mesosphere as a result of radiative cooling in winter and early spring (Fisher *et al.*, 1993). These results augment the depiction of the vortex in Figure 3-2, further clarifying its dynamical evolution.

Observations have established that simple, compact relationships exist in the lower stratosphere between N_2O and other long-lived species that also are photochemically destroyed in the stratosphere. These relationships result when photochemical lifetimes are long compared to transport and mixing times between low- and high-latitude regions (Plumb and Ko, 1992; Mahlman *et al.*, 1980). The compactness of the relationship allows one of the species to be predicted confidently from a measurement of the other. The distribution of N_2O in and near the vortex is often related to the distribution of PV and potential temperature (Strahan and Mahlman, 1994a, b). Thus, these relationships are useful in predicting conditions throughout the vortex relevant to the specific reactive processes that control ozone. However, since the knowledge of these relationships is based on limited data sets, assimilation of further data must continue in order to establish the range of applicability.

The first of three important examples of these relationships is that of N_2O to organic and inorganic chlorine reservoirs (see Figure 3-6) (Woodbridge *et al.*, 1994; Schmidt *et al.*, 1991, 1994; Schauffler *et al.*, 1993; Kawa *et al.*, 1992a). The principal species in the organic chlorine reservoir, CCl_y,

$$CCl_y = CCl_2F_2 \text{ (CFC-12)} + CCl_3F \text{ (CFC-11)} + CCl_2FCClF_2 \text{ (CFC-113)} + CCl_4 \text{ (carbon tetrachloride)} + CH_3CCl_3 \text{ (CFC-140a)} + CHClF_2 \text{ (CFC-22)} + CH_3Cl \text{ (methyl chloride)} \quad (3\text{-}1a)$$

include those species that comprise over 95 percent of the available organic chlorine in the stratosphere. Each species displays a compact correlation with N_2O, where the slope is related to the ratio of lifetimes in the stratosphere (see Chapter 2). As a consequence, CCl_y, as the sum over organic species, also shows a compact relation with N_2O. The inorganic chlorine reservoir, Cl_y,

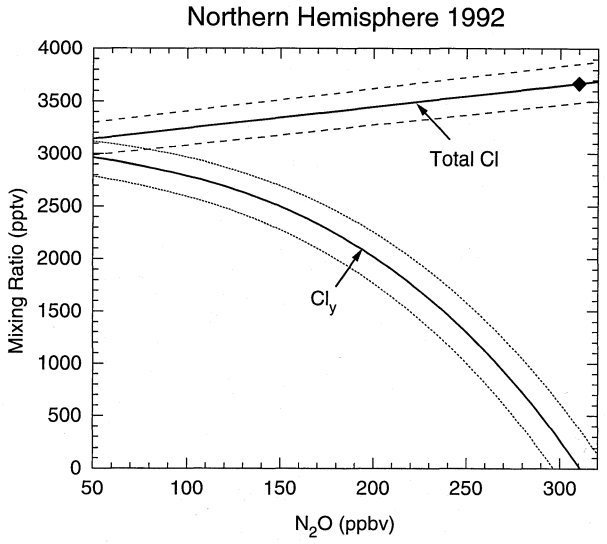

Figure 3-6. Total available chlorine (upper line) and total inorganic chlorine (Cl_y) (lower line) plotted versus N_2O from aircraft observations in the Arctic winter of 1991/92. The vertical scale is in parts per trillion by volume (pptv). Total organic chlorine (CCl_y) is the difference between total available chlorine and Cl_y. As the residence time of air increases in the stratosphere, photochemical reactions decrease N_2O values in an air parcel and convert CCl_y species to Cl_y species. The diamond symbol represents the reference point for tropospheric chlorine in 1991/92 of 3.67 ppbv. The dashed lines represent estimated uncertainties (Woodbridge *et al.*, 1994).

$$Cl_y = Cl + 2Cl_2 + ClO + OClO + 2Cl_2O_2 + HOCl + HCl + BrCl + ClONO_2 \quad (3\text{-}1b)$$

is produced as CCl_y and N_2O are destroyed in the stratosphere. Since Cl_y contains ClO, an effective reactant in ozone destruction, the distribution of Cl_y in polar regions is of great interest. The combination of the distribution of N_2O at high latitudes in Figure 3-4 and the compact relations in Figure 3-6 indicates how CCl_y and Cl_y are distributed throughout both vortices. Modeling of ozone loss throughout the vortex can be usefully constrained by knowledge of these distributions (Salawitch *et al.*, 1993).

The second example is the linear relationship between N_2O and the reactive nitrogen reservoir, NO_y (Fahey *et al.*, 1990a; Loewenstein *et al.*, 1993; Kondo *et al.*, 1994a). The primary source of NO_y,

$$NO_y = NO + NO_2 + NO_3 + 2N_2O_5 + HONO + HO_2NO_2 + HNO_3 + CH_3C(O)OONO_2 + ClONO_2 + BrONO_2 + \text{aerosol nitrate} + ..., \quad (3\text{-}2)$$

is the photochemical destruction of N_2O in the middle stratosphere. In the polar lower stratosphere in winter, the sequestering of active chlorine in the form of $ClONO_2$ moderates ozone destruction. The NO_y/N_2O correlation has been observed to be linear before vortex formation in the Northern Hemisphere and outside the vortex boundary in both hemispheres. Departures from linearity at low N_2O values have been observed as expected from the photochemical destruction of NO_y in the upper stratosphere. Departures from linearity at higher N_2O values demonstrate the irreversible removal of NO_y as a result of the sedimentation of aerosol particles containing NO_y species. This removal of NO_y greatly enhances the potential for ozone destruction in an air parcel located in the polar vortex in spring (Brune *et al.*, 1991; Salawitch *et al.*, 1993).

The third example is the correlation of ozone with N_2O that primarily follows from the production of ozone in regions where N_2O is photochemically destroyed. *In situ* aircraft measurements, satellite observations, and photochemical model simulations show linear correlations during winter months at mid- and high latitudes in the absence of significant polar ozone loss (Proffitt *et al.*, 1990, 1992, 1993; Weaver *et al.*, 1993). Since ozone also has loss processes in the stratosphere at other latitudes and during other seasons, deviations from a constant linear correlation cannot be attributed solely to vortex chemistry, particularly during summer and early fall at high latitudes (Perliski *et al.*, 1989; Proffitt *et al.*, 1992). However, during the vortex lifetime, changes in the correlation may be used to bound photochemical ozone loss in air parcels inside or near the vortex boundary (see Figure 3-7). This is especially useful inside and outside the Arctic vortex or outside the Antarctic vortex, where ozone changes are generally small in comparison to the natural variability.

3.3 PROCESSING ON AEROSOL SURFACES

3.3.1 Polar Stratospheric Cloud Formation and Reactivity

As shown in Figure 3-1, reservoir chlorine species are converted beginning in early winter to form the active chlorine species such as molecular chlorine (Cl_2) and, ultimately, ClO and its dimer Cl_2O_2. The conversion is attributed to processing of polar air by surface reactions involving both HCl and $ClONO_2$. The reactions occur on sulfate aerosol particles and polar stratospheric cloud (PSC) particles that form at the low temperatures and constituent concentrations characteristic of the interior of the winter vortices. The body of laboratory data on the formation thermodynamics and reactivities of these surfaces and the body of atmospheric observations of stratospheric aerosols and their constituents have continued to grow in this assessment period.

The basic features of the ternary condensation of nitric acid (HNO_3), sulfuric acid (H_2SO_4), and water (H_2O) in the stratosphere are illustrated in Figure 3-8. With an abundance ratio in the high-latitude lower stratosphere of these species of approximately 10 ppbv/1 ppbm/4 ppmv, respectively, H_2O is always the predominant constituent (ppbv = parts per billion by volume, ppbm = parts per billion by mass, ppmv = parts per million by volume). For volcanically perturbed conditions, the range of H_2SO_4 abundance can reach 100 ppbm. Volcanic activity over the past 25 years has increased the average H_2SO_4 abundance in the stratosphere to near 5 ppbm. Confidence in the features of the ternary system has been established in a wide variety of laboratory experiments and with the use of thermodynamical constraints (Molina *et al.*, 1993; Kolb *et al.*, 1994). At the highest temperatures, liquid aerosol particles composed primarily of H_2SO_4 and H_2O are present in the lower stratosphere at all latitudes. At lower temperatures (< 200 K), the H_2SO_4/H_2O liquid increasingly takes up HNO_3. If the particles undergo freezing, HNO_3 hydrates become stable: nitric acid dihydrate ($HNO_3 \cdot 2H_2O$ = NAD) and nitric acid trihydrate ($HNO_3 \cdot 3H_2O$ = NAT). Liquid or frozen particles that contain appreciable HNO_3 at temperatures above the frost point are termed Type I PSC particles. In the absence of HNO_3, the H_2SO_4/H_2O liquid aerosol can freeze to form sulfuric acid tetrahydrate (SAT) or other sulfate hydrates. Below

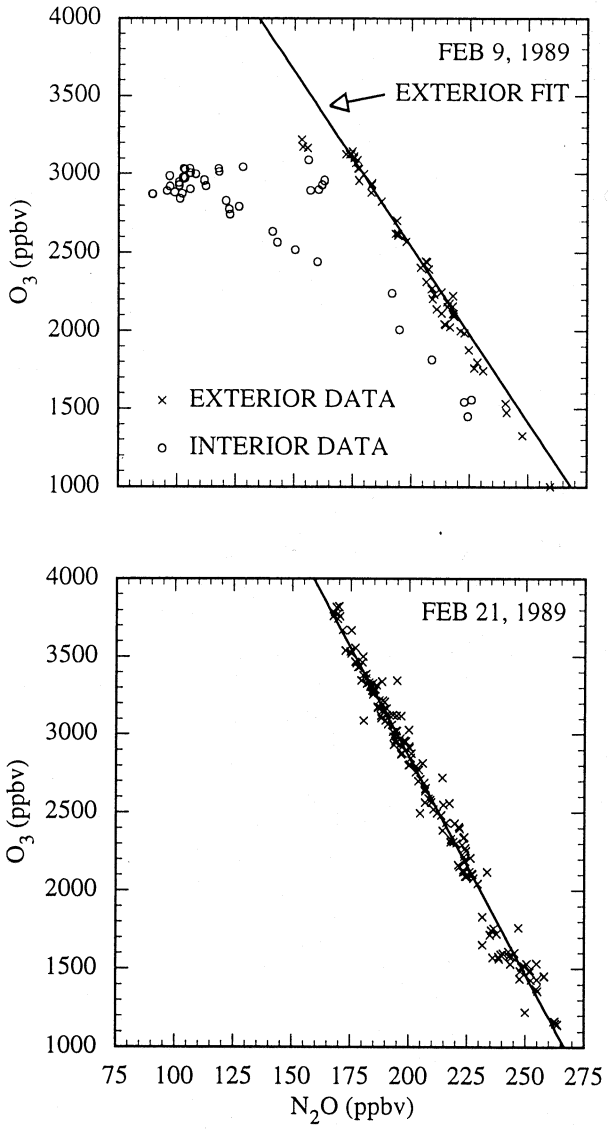

Figure 3-7. Average ozone and N_2O values from aircraft observations. Top: Data from the Arctic polar vortex (60°N to 80°N) on 9 February 1989. Bottom: Data from the continental United States (37°N to 39°N) on 21 February 1989. Data taken inside and outside the vortex are denoted as interior and exterior data, respectively (adapted from Proffitt *et al.*, 1992).

the frost point, Type II PSCs are formed as the condensation of H_2O predominates in the continued growth of the particles, with condensation of HNO_3 playing a lesser role. Recent laboratory results that underlie the PSC formation features in Figure 3-8 are the following:

- HNO_3 is soluble in liquid H_2SO_4/H_2O aerosols as temperatures approach the frost point where the aerosol composition becomes 8 to 12 weight percent (wt%) HNO_3 and 35 to 40 wt% H_2SO_4 (Molina *et al.*, 1993; Reihs *et al.*, 1990; Zhang *et al.*, 1993a, b). Thermodynamic models suggest that dramatic changes take place when the frost point is approached, rendering the aerosol into a binary HNO_3/H_2O solution (Carslaw *et al.*, 1994; Tabazadeh *et al.*, 1994).
- As temperatures are reduced in $HNO_3/H_2SO_4/H_2O$ mixtures, NAD nucleates from the vapor phase before NAT under some conditions (Middlebrook *et al.*, 1992; Worsnop *et al.*, 1993).
- $HNO_3/H_2SO_4/H_2O$ solutions with compositions similar to those estimated for the high-latitude stratospheric aerosols yield NAT, SAT, and possibly other hydrates upon freezing (Molina *et al.*, 1993).
- Solutions containing only H_2SO_4 and H_2O crystallize with difficulty for compositions corresponding to stratospheric abundances and temperatures greater than but near the frost point (Molina *et al.*, 1993; Ohtake, 1993; Luo *et al.*, 1994a).
- NAT crystallizes readily from $HNO_3/H_2SO_4/H_2O$ solutions at temperatures for which HNO_3 is supersaturated (> 10) with respect to NAT formation. Typically, this occurs several degrees above the frost point in the lower stratosphere (Molina *et al.*, 1993). The relationship of bulk solution properties to those of stratospheric aerosols has not been determined (Carslaw *et al.*, 1994).
- SAT melts at 220 to 230 K when exposed to partial pressures of H_2O that are typical of the lower stratosphere (Middlebrook *et al.*, 1994; Zhang *et al.*, 1993a).

Both NAT and NAD may play a role in Type I PSC formation when saturation ratios for HNO_3 are greater than unity. However, the phase of Type I PSCs is not certain in this temperature range, as illustrated in Figure 3-8 (Dye *et al.*, 1992). Once frozen, SAT within the particles may remain a solid well above the initial freezing tempera-

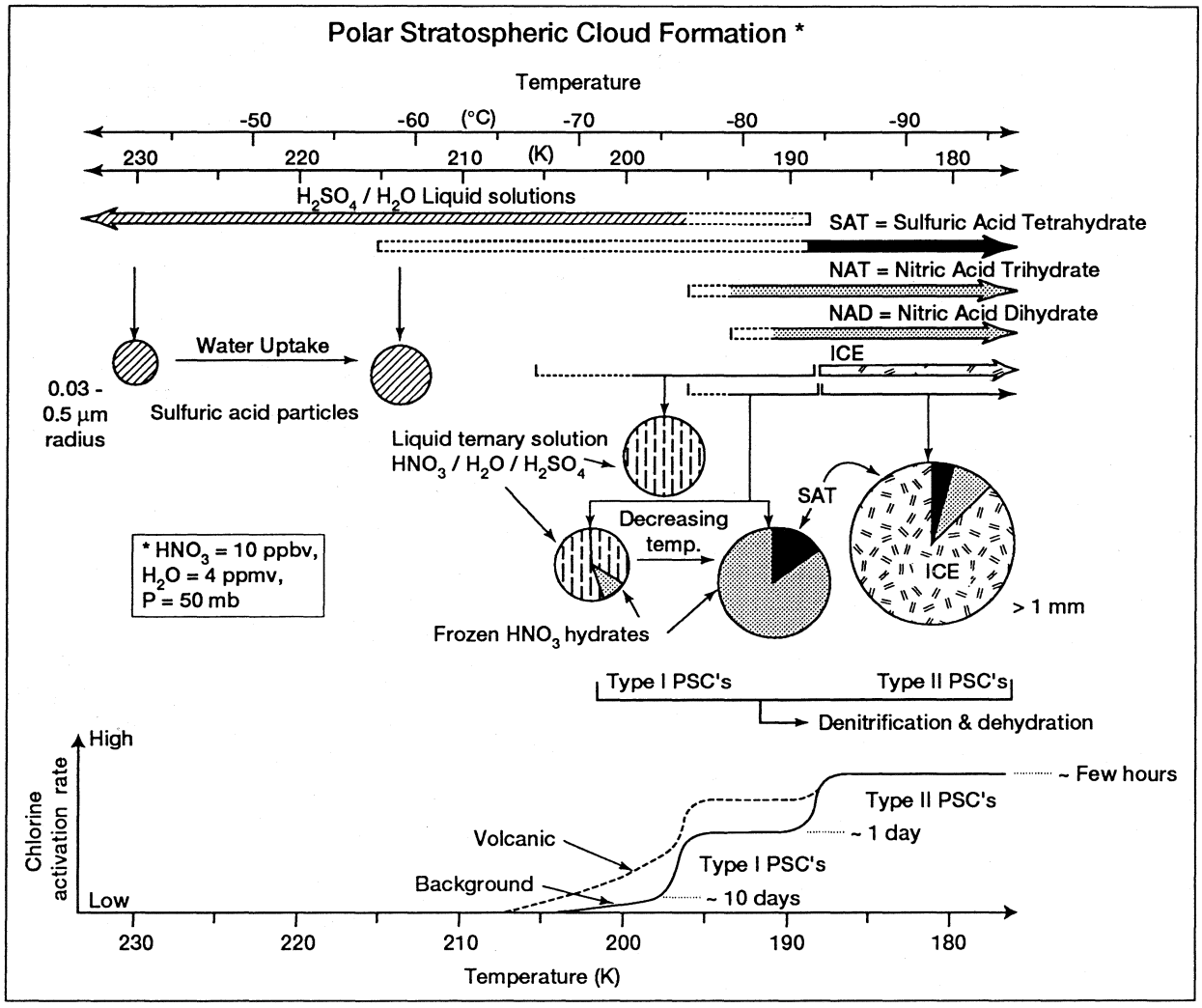

Figure 3-8. Schematic representation of the ternary condensation system for nitric acid (HNO_3), sulfuric acid (H_2SO_4), and water (H_2O) over a range of temperatures where growth of aerosols occurs to form Type I and II PSC particles in the stratosphere. The changes are represented for nominal abundances of condensing species in the lower polar stratosphere as indicated. The shading in the horizontal arrows and circular particle diagrams represents various binary and ternary compositions as indicated. In the lower part, the chlorine activation rate on PSCs is represented as a function of temperature (adapted from J. E. Dye, private communication, 1994).

ture. The phase of the particles above the frost point affects the rate of surface conversion for reactive nitrogen and chlorine species (see Table 3-1).

The principal heterogeneous reactions of H_2SO_4/HNO_3/H_2O aerosols in Figure 3-8 are listed in Table 3-1. Reaction rates are considered fast if reaction probabilities are in the range 0.01-0.1 for temperatures and reactant abundances characteristic of the stratosphere. Reactions involving H_2O are influenced by its ubiquitous presence in aerosol particles throughout the stratospheric temperature range. Reactions with HCl depend on the solubility of HCl in an aerosol particle. Laboratory studies of Reaction (3-3) reveal that the reaction probability depends strongly on relative humidity and, to a lesser extent, on aerosol composition. Specifically, the reaction probabilities for Reaction (3-3) are similar on Type I PSCs, SAT, and liquid sulfuric acid over a wide temperature range at stratospheric relative humidity (see Figure 3-9) (Molina *et al.*, 1993; Hanson and Ravishankara, 1994). The probability for Reaction (3-5) increases exponentially as the sulfate aerosol dilutes with H_2O near 200 K and below (Cox *et al.*, 1994), as does the probability of Reaction (3-4) due to enhanced uptake of HCl (Hanson and Ravishankara, 1993; Luo *et al.*, 1994b). The increase suggests that Reactions (3-4) and (3-5) may play a significant role in chlorine processing when temperatures are low but do not reach Type I or Type II temperatures (Solomon *et al.*, 1993; Hanson *et al.*, 1994).

The growth of the ternary aerosol system from sulfate aerosols to Type I and II PSCs and the surface reactions in Table 3-1 combine effectively to release active chlorine in the polar regions. In Figure 3-8, the rate of chlorine activation is qualitatively noted as a function of temperature. Some activation occurs on background aerosol particles prior to temperatures decreasing to Type I formation temperatures. The rate increases significantly as more surface area containing HNO_3 hydrates and ice forms. Inside the polar vortices, full activation within an air parcel is estimated to occur within a day or perhaps a few hours. Thus, the initial activation of the entire vortex can occur in a matter of days (Newman *et al.*, 1993). When aerosol particle size and surface area are increased by volcanic eruptions, the rate of activation can be significantly enhanced at temperatures above Type I formation.

Table 3-1. Rates of heterogeneous reactions on polar stratospheric cloud particles and sulfate aerosol particles.

	PSCs		Sulfate Aerosols		
	Ice (Type II)	HNO_3 hydrates[a] (Type I)	Supercooled	Frozen	
$ClONO_2 + HCl \rightarrow Cl_2 + HNO_3$	Fast f(RH)[b]	Fast f(RH)[b]	f(wt% H_2SO_4)[b]	Fast f(RH)[b]	(3-3)
$HOCl + HCl \rightarrow Cl_2 + H_2O$	Fast f(RH)[b]	Fast f(RH)[b]	f(wt% H_2SO_4)[b]	Fast f(RH)[b]	(3-4)
$ClONO_2 + H_2O \rightarrow HOCl + HNO_3$	Fast	Slow	f(wt% H_2SO_4)[b]	Slow	(3-5)
$N_2O_5 + H_2O \rightarrow 2HNO_3$	Fast	Slow	Fast	Slow	(3-6)
$N_2O_5 + HCl \rightarrow ClNO_2 + HNO_3$	c	c	c	c	(3-7)

[a] Nitric acid trihydrate (NAT), nitric acid dihydrate (NAD)

[b] Rate is function of aerosol wt% H_2SO_4 or relative humidity (RH).

[c] Unlikely to be fast, but not well studied

References: Abbatt and Molina, 1992a, b; Chu *et al.*, 1994; Fried *et al.*, 1994; Hanson and Ravishankara, 1991, 1992, 1994; Kolb *et al.*, 1994; Middlebrook *et al.*, 1992, 1994; Molina *et al.*, 1993; Van Doren *et al.*, 1991; Zhang *et al.*, 1994

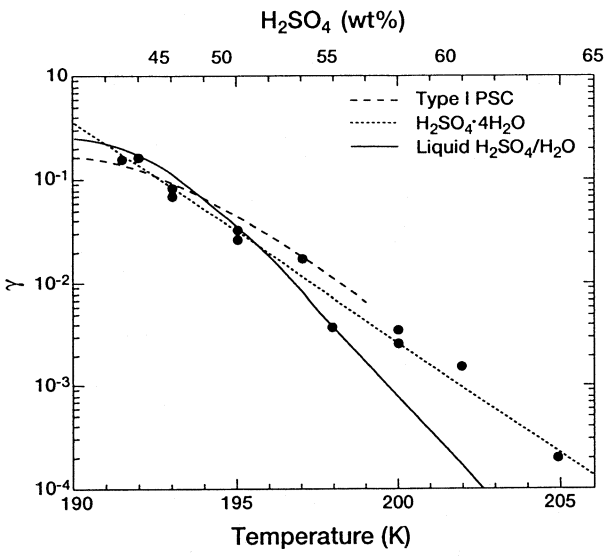

Figure 3-9. Temperature dependence of the reaction probability γ for Reaction (3-3), $ClONO_2$ + HCl, occurring on surfaces of sulfuric acid tetrahydrate ($H_2SO_4 \cdot 4H_2O$ = SAT), nitric acid trihydrate (NAT) or Type I PSCs, and liquid sulfuric acid and water solutions, H_2SO_4/H_2O. The measurements are made at a constant partial pressure of water vapor of 0.2 mTorr. Thus, relative humidity increases as temperature decreases. The weight percent (wt%) of the corresponding sulfuric acid/water solution is indicated on the top axis (adapted from Hanson and Ravishankara, 1994).

3.3.2 Atmospheric Observations

3.3.2.1 Aerosol Measurements

The threshold formation and growth of PSC aerosol particles have been observed *in situ* over a wide range of conditions in both polar regions (Hofmann *et al.*, 1989, 1990; Hofmann and Deshler, 1989). Satellites have made global aerosol observations using the extinction of solar illumination (Osborn *et al.*, 1990). The data show a persistent increase in aerosol extinction in polar regions when temperatures fall to the range below where Type I PSCs are expected (see Figure 3-10) (Poole and Pitts, 1994). The observations do not allow the phase of the aerosol to be determined. Lidar measurements in both polar regions also detect aerosol layers where temperatures reach estimated PSC thresholds (Gobbi and Adriani, 1993; Browell *et al.*, 1990). Lidar polarization measurements indicate that both spherical and non-spherical particles are present in cloud events (Kent *et al.*, 1990; Adriani *et al.*, 1994; Toon *et al.*, 1990a). *In situ* measurements with balloons show enhancements in the size distribution for larger particles (Deshler *et al.*, 1994). Distinct growth begins on some particles near the threshold for HNO_3 hydrates (Dye *et al.*, 1992) and involves all pre-existing particles before decreasing temperatures reach the frost point (Hofmann *et al.*, 1990). Other measurements near the edges of PSCs have been made with simultaneous constituent measurements of reactive nitrogen and water (Kawa *et al.*, 1992b). These measurements show definitively that the condensed phase includes reactive nitrogen species in the form of HNO_3, but that significant aerosol growth above background values often requires a large supersaturation of HNO_3 over the stable hydrate phases.

The systematic formation of aerosol containing HNO_3 is well documented. However, aerosol measurements of concentration, size, phase, and composition correlated with the gas phase abundance of the principal condensing species H_2SO_4, HNO_3, and H_2O are critically absent in observational studies. In addition, observations are not available to constrain important features of the nucleation and early growth stages in an aerosol. Without such measurements, the ability to predict the distribution of aerosol particles and their chemical reactivity remains limited.

3.3.2.2 Release of Active Chlorine

Active chlorine is produced as a result of the heterogeneous reactions in Table 3-1. The photolysis of the Cl_2 and hypochlorous acid (HOCl) reaction products forms Cl, which in turn reacts with ozone to produce ClO. ClO participates in catalytic reaction cycles that destroy ozone (see Section 3.4.1). The activation of chlorine over the winter poles has been clearly demonstrated by *in situ* and remote measurements of ClO (Anderson *et al.*, 1991; WMO, 1992; Toohey *et al.*, 1993; deZafra *et al.*, 1987). The spatial and temporal scale of ClO observations has been significantly extended by the UARS satellite (Waters *et al.*, 1993a, b; Manney *et al.*, 1994b). Observations are available in both polar regions from vortex formation to photochemical recovery in the 1991/92 northern winter and the 1992 southern winter (see Figure 3-11). In early northern winter (14 December), infrequent PSCs keep ClO values low inside the vortex

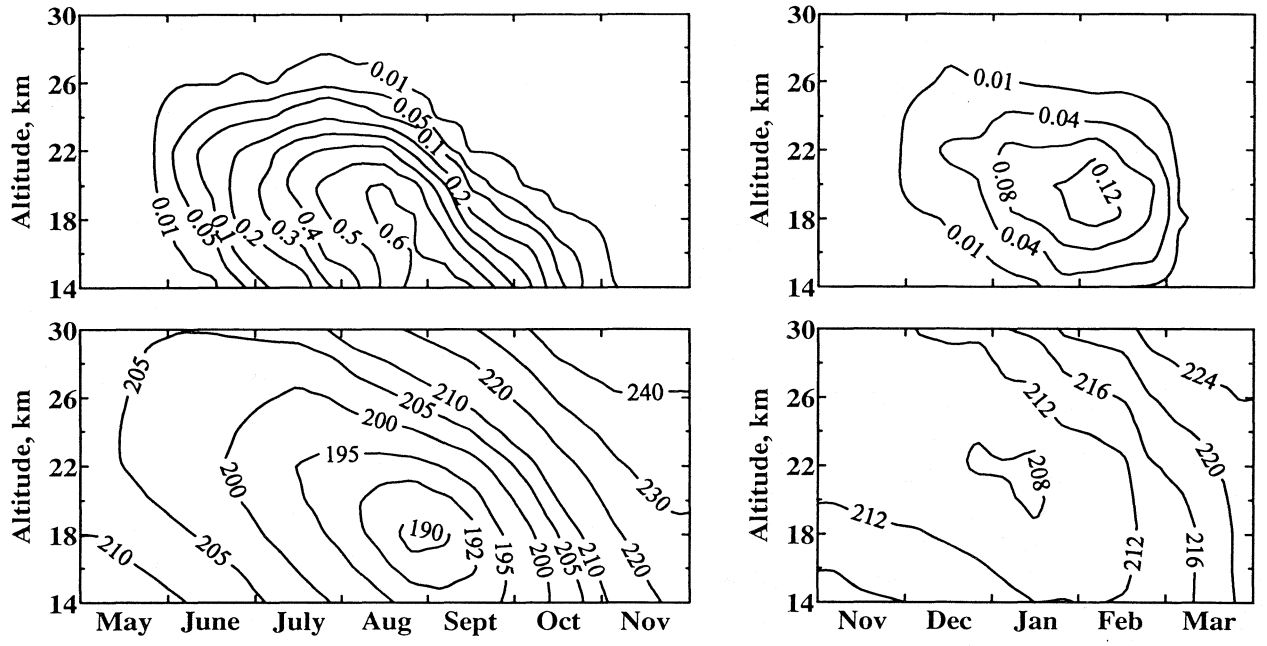

Figure 3-10. PSC sighting probabilities (top panels) as a function of altitude in the lower stratosphere during the winter months in the Antarctic (left) and in the Arctic (right). Data are zonal averages of the Stratospheric Aerosol Measurement II (SAM II) satellite data set for the years 1978 to 1989. The bottom panels represent the analyzed temperatures in Kelvin from the National Oceanic and Atmospheric Administration coinciding with the PSC observations in the upper panels. A PSC is identified as an extinction ratio significantly larger than that of the local background aerosol. The analysis is confined to the inside of the respective vortex defined by a maximum in the geopotential height gradient (Poole and Pitts, 1994).

near 18 km (465 K). In early southern winter (1 June), lower temperatures activate sulfate aerosol and begin the formation of PSCs, increasing ClO accordingly. In areas of darkness inside the vortex, active chlorine is in the form of Cl_2, Cl_2O_2, or HOCl. When air parcels make excursions to sunlit lower latitudes within the vortex flow, ClO values increase directly from the photolysis of Cl_2O_2 or indirectly from the photolysis of Cl_2. As the geographic area and frequency of PSCs continue to increase due to lower temperatures (2 January/11 July), ClO values and their extent increase substantially in both vortices. In some areas over both poles, ClO values indicate that essentially all available chlorine is in the active form. Outside the vortex, little ClO is formed. When PSCs cease to exist (17 February), ClO values fall as reservoir chlorine is photochemically reformed. In the southern vortex, high ClO values persist in September because gas phase HNO_3 is suppressed either due to temperatures below the PSC threshold, which sequester HNO_3 in aerosols, or to the removal of HNO_3 in denitrification (see Section 3.3.2.5). This sequence for the distribution of ClO is qualitatively and quantitatively consistent with other *in situ* and remote measurements (Toohey *et al.*, 1993; Crewell *et al.*, 1994; Gerber and Kämpfer, 1994).

Features of the ClO temporal and spatial distribution are consistent with the theoretical determination of PSC activity associated with low temperatures (Waters *et al.*, 1993a). The dependence of ClO on PSC activity and, hence, temperatures within the vortex, is demonstrated by contrasting ClO observations on 15 February in late northern winter for two consecutive years (see Figure 3-12). In 1993, the vortex contained temperatures below 195 K, significantly lower than found in 1992. Changes in available chlorine (Cl_y) cannot explain increased active chlorine found in 1993. Instead, the changes are attributed to increased formation and reactivity of aerosols at the lower stratospheric temperatures

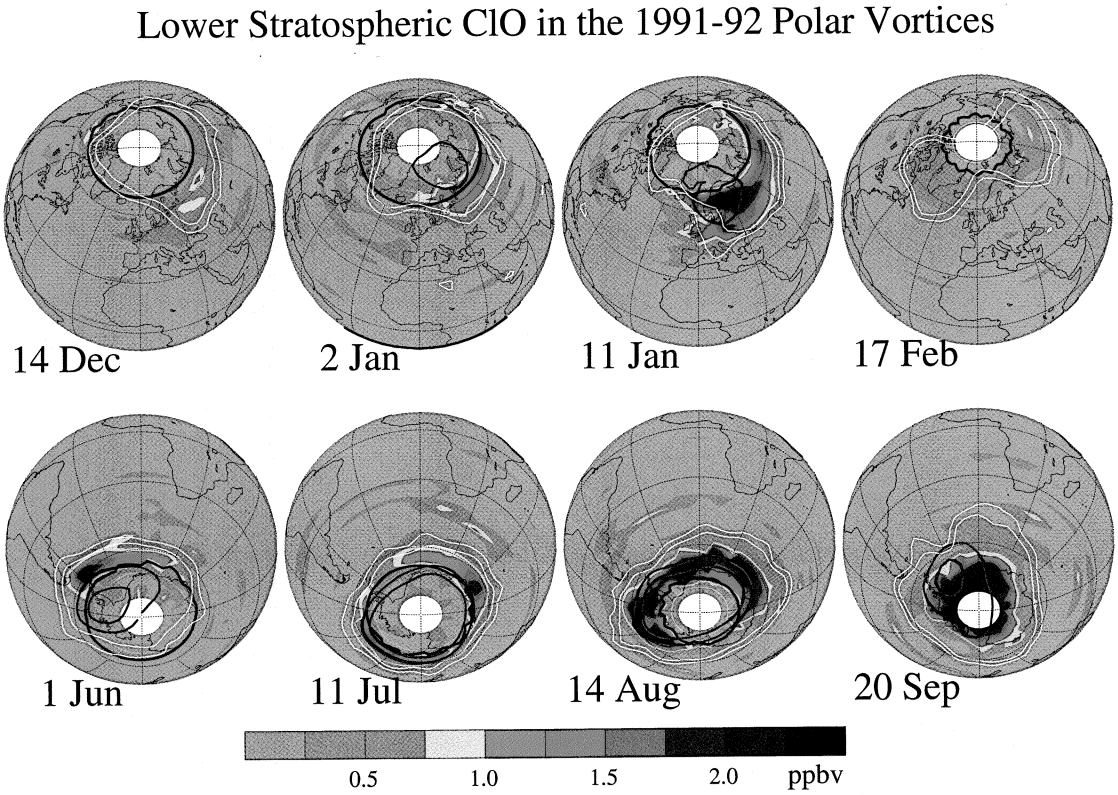

Figure 3-11. (a) Observations of lower stratospheric ClO in the 1991/92 northern winter (top row) and 1992 southern winter (bottom row) from the Microwave Limb Sounder (MLS) on UARS. The color bar gives ClO abundances in parts per billion by volume (ppbv) interpolated to the 465 K isentropic surface in the lower stratosphere (see Figure 3-4 for altitude reference). The irregular white lines are contours of potential vorticity (2.5 and 3.0 x 10^{-5} K $m^2kg^{-1}s^{-1}$) indicating the polar vortex boundary. Measurements poleward of the black contour were made for solar zenith angles greater than 91° (in darkness or edge of daylight). The edge of polar night is shown by the thin white circle concentric with the pole. No measurements are available in the white area poleward of 80° latitude. The green contours indicate temperatures of 190 K (inner) and 195 K (outer) (Waters *et al.*, 1993a, b).

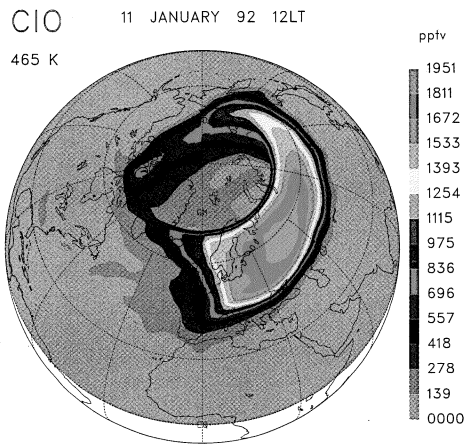

Figure 3-11. (b) ClO distribution calculated with a three-dimensional chemistry and transport model of the stratosphere. The ClO field for 11 January 1992 on the 465 K potential temperature surface was mapped at all locations for local noon to achieve better temporal coincidence with UARS satellite measurements in (a) (note discontinuity on both sides of date line) (Lefèvre *et al.*, 1994).

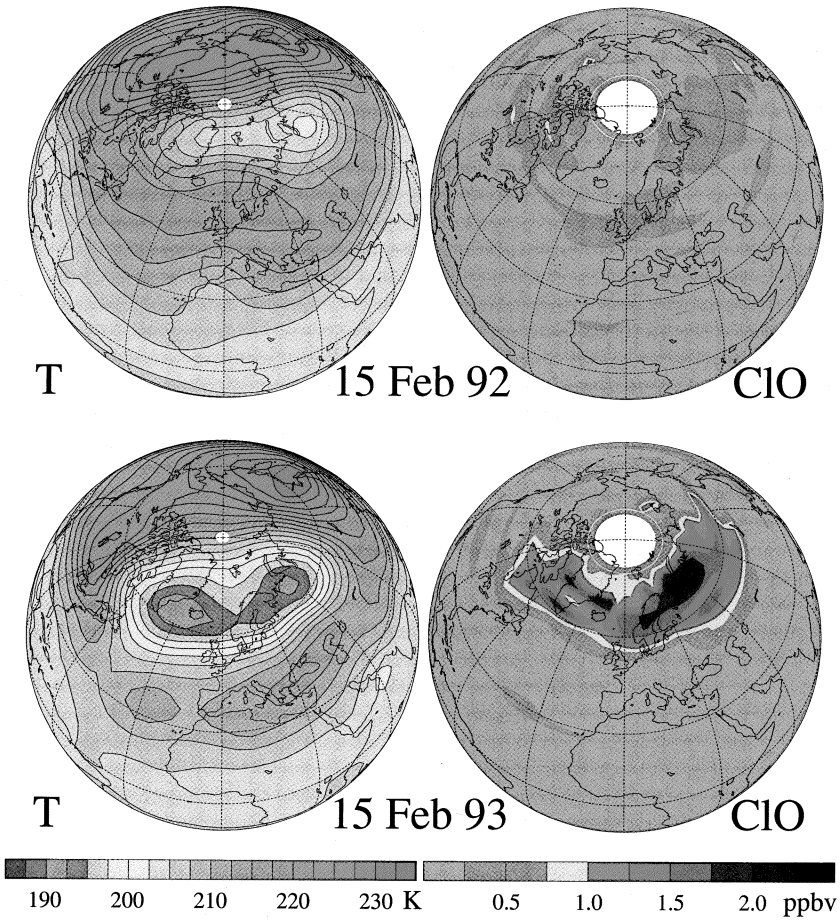

Figure 3-12. Observations of ClO from the UARS MLS satellite instrument and NMC temperatures in the lower stratosphere at 465 K potential temperature in the Northern Hemisphere on 15 February 1992 and 1993 (see Figure 3-4 for altitude reference). No measurements are available in the white area poleward of 80° latitude (Waters *et al.*, 1993a).

in 1993 as demonstrated in a 3-D model simulation (Chipperfield, 1994a). The 15 February data sets are representative of the systematic differences in ClO and temperature between 1992 and 1993 and, hence, also demonstrate interannual variability characteristic of the Northern Hemisphere vortex (see Section 3.4.2).

Observed changes in ClO are also consistent with changes within the reactive nitrogen reservoir. Activation of a large fraction of available chlorine to ClO sets an upper limit on NO_x (= NO + NO_2) that can be present in the NO_y reservoir (see Equation (3-2)) to form $ClONO_2$. From *in situ* observations near the vortex edge, nitric oxide (NO) is suppressed wherever ClO is enhanced (Toohey *et al.*, 1993; Kawa *et al.*, 1992a). The same reactions that activate chlorine (see Table 3-1) reduce NO and NO_x through the formation of HNO_3, a longer-lived species. In addition, NO_x is reduced indirectly through denitrification, the irreversible removal of NO_y (see Section 3.3.2.5). Column measurements of nitrogen dioxide (NO_2) and HNO_3 are generally consistent with expected changes in NO_y partitioning (Solomon and Keys, 1992; Keys *et al.*, 1993; Wahner *et al.*, 1990a; Koike *et al.*, 1994).

Activation of chlorine is also indicated by increases in OClO, formed in the reaction ClO + BrO (Solomon *et al.*, 1989; Tung *et al.*, 1986; Sanders *et al.*, 1993). OClO has been observed in both vortices, with the largest column abundances found in the Antarctic vortex

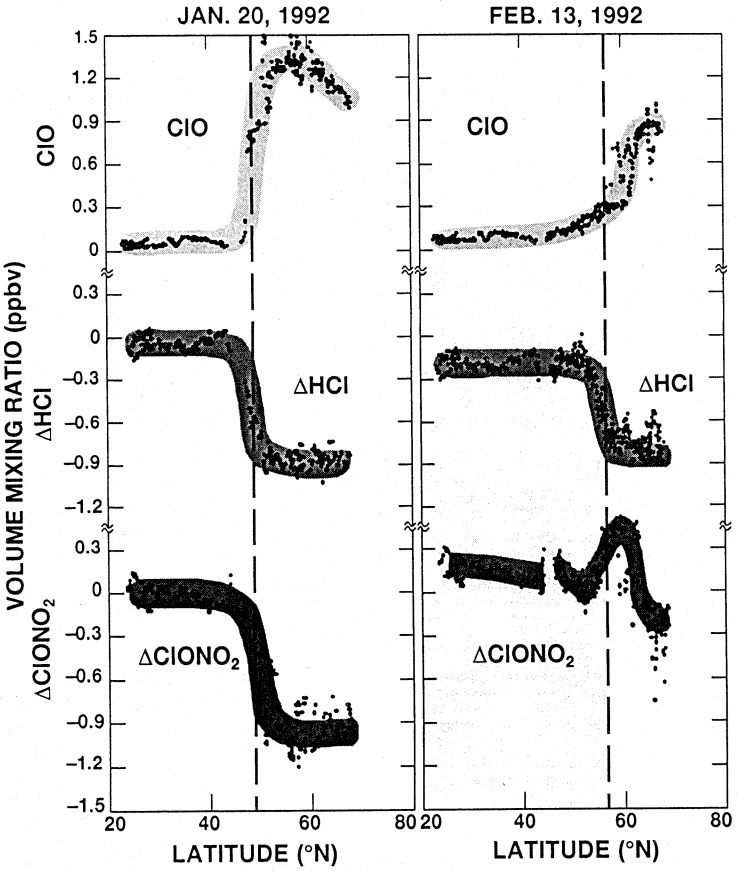

Figure 3-13. Aircraft data from 20 January and 13 February in the 1992 Arctic winter. Values for the changes in HCl and $ClONO_2$ are noted as ΔHCl and $\Delta ClONO_2$, respectively, where negative values indicate depletion. Values of ΔHCl are determined using the observed correlation with N_2O as a reference. Values for $\Delta ClONO_2$ are derived in three steps. First, total inorganic chlorine is estimated along the flight track from the correlation of total organic chlorine with N_2O (see Figure 3-6) (Kawa *et al.*, 1992a). Second, $ClONO_2$ is assumed to be the balance in the inorganic chlorine reservoir after account is made for measured HCl, ClO, and calculated Cl_2O_2. Third, changes in $ClONO_2$ from that calculated using the reference value of HCl are designated as $\Delta ClONO_2$. The dotted vertical line indicates the vortex edge determined from the maximum zonal wind measured on board the aircraft (Webster *et al.*, 1993a).

(Schiller *et al.*, 1990; Sanders *et al.*, 1993; Brandtjen *et al.*, 1994). The abundances are broadly consistent with expectations from model simulations. In the Arctic and Antarctic vortex regions following the eruption of Mt. Pinatubo, increases in OClO were observed before PSC temperatures were noted in the lower stratosphere (Solomon *et al.*, 1993; Perner *et al.*, 1994). Such measurements are a sensitive indicator of changes in active chlorine, especially for the low Sun conditions characteristic of high-latitude winter. The activation, attributed to enhancements in the rate of Reaction (3-5) on volcanic sulfate aerosols, implies additional ozone destruction at high latitudes during periods of enhanced aerosol.

3.3.2.3 Changes in Reservoir Chlorine

The selective conversion of the inactive chlorine reservoirs HCl and $ClONO_2$ in surface reactions occurring in the polar vortices is a fundamental aspect of the ozone depletion process depicted in Figure 3-1. In previous assessments, polar observations of these reservoir species were limited to remote soundings from the ground and aircraft *in situ* measurements. However, the

general feature of the winter conversion of the reservoirs and their subsequent formation in spring can be found in these observations. New observations include simultaneous *in situ* measurements of HCl and ClO in the Arctic region (see Figure 3-13) (Webster *et al.*, 1993a, b). In addition, $ClONO_2$ is deduced as the residual in the Cl_y reservoir after account is made for HCl, ClO, and estimated Cl_2O_2 (see Figure 3-6). Near-complete removal of HCl was observed in some air masses at 20 km in the vortex. Changes at the vortex edge show losses in the reservoir species that correlate with increased ClO. Losses in the reservoir species are comparable and equate well with the sum of observed ClO and calculated Cl_2O_2, indicating stoichiometric conversion of HCl and $ClONO_2$ in Reaction (3-3). Before PSC processing, *in situ* HCl values are somewhat less than those of estimated $ClONO_2$ at mid- to high northern latitudes, conflicting with standard photochemical models which find HCl to be in excess. At lower latitudes away from PSC processing, the sum of the inorganic and organic chlorine species is constant throughout the lower and upper stratosphere, indicating that chlorine is conserved in the conversion of chlorine to inorganic forms (Zander *et al.*, 1992).

In remote ground-based measurements, the column abundance of HCl over northern Sweden was observed throughout midwinter 1991/92 (Bell *et al.*, 1994). The anticorrelation with column ClO clearly shows the conversion of HCl to active forms (see Figure 3-14). Earlier column measurements from aircraft showed the complete conversion of HCl and $ClONO_2$ deep inside the northern vortex in January and early February 1989 (Toon *et al.*, 1992). The measurements are consistent with complete removal of HCl up to 27 km. Profile measurements of $ClONO_2$ show that the midwinter depletion extends throughout a broad vertical region in the Arctic stratosphere (see Figure 3-15) (von Clarmann *et al.*, 1993).

The UARS remote measurements of HCl and $ClONO_2$ significantly extend the spatial and temporal scale of previous observations. Inside the edge of the Antarctic vortex in late September, significant depletion of HCl is found around a latitude circle near the vortex edge (see Figure 3-16) when HCl values are compared with those of the long-lived tracer species CH_4 and HF. These data sets confirm the large-scale depletion of HCl in low-temperature regions in the Antarctic vortex. Sat-

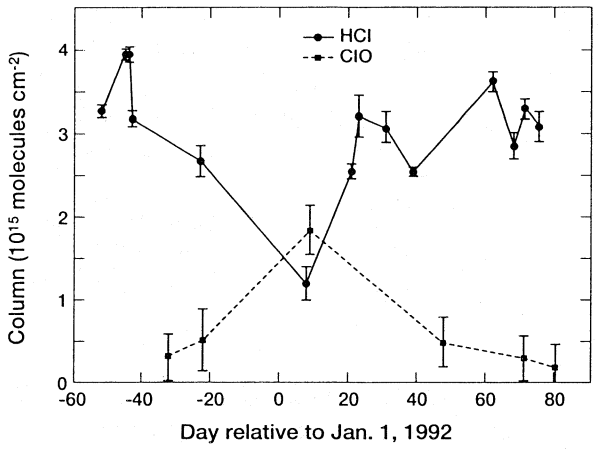

Figure 3-14. HCl and ClO column abundances over Åre, Sweden (63.4°N) during the EASOE campaign in 1992. The HCl column is measured by ground-based, infrared solar absorption spectroscopy. The ClO column is the amount above 100 mb (~16 km) at the same location as measured by the UARS MLS satellite instrument (Bell *et al.*, 1994).

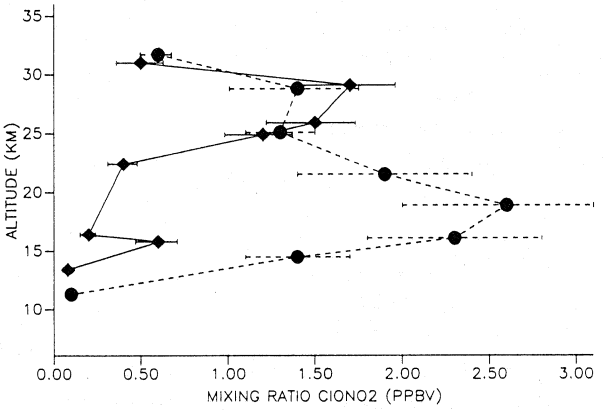

Figure 3-15. Retrieved Michelson Interferometric Passive Atmosphere Sounder-B (MIPAS-B) $ClONO_2$ profiles from balloon flights near Kiruna, Sweden (68°N) during the EASOE campaign in 1992. The peak of the 13 January mixing ratio profile (solid curve) is at a higher altitude than the peak of the 14/15 March profile (dashed curve). Similar values are obtained above 25 km, but large differences between the profiles appear in the lower stratosphere (von Clarmann *et al.*, 1993).

ellite measurements also show low abundances of $ClONO_2$ and HNO_3 inside the Antarctic vortex as early as mid-June (early winter), suggesting substantial PSC processing (see Figure 3-17) (Santee *et al.*, 1994; Roche *et al.*, 1993b, 1994). In addition, a region of high $ClONO_2$ surrounding the vortex is noted in late winter. $ClONO_2$ values will be enhanced in areas where processing is limited or infrequent, and where sunlight is available to produce NO_2 in the photolysis of HNO_3 and, thereby, reform $ClONO_2$ in advance of HCl (see Figures 3-1 and 3-17 and Section 3.4). This region, termed the "collar" region as first noted in remote soundings from aircraft (Toon *et al.*, 1989a), is also identifiable in estimates of $ClONO_2$ based on *in situ* observations near the vortex edge (see Figure 3-13). In late winter, the "collar" region extends into the sunlit vortex, as noted in Arctic soundings which show recovery of the vertical profile of $ClONO_2$ (see Figure 3-15). Although the early UARS observations are made in years of high volcanic aerosol loading, these observations and estimates of $ClONO_2$ add confidence to the role reservoir species play in the activation of chlorine.

3.3.2.4 Active Bromine

Although the bromine source gases in the stratosphere are less than one percent the size of chlorine source gases, active bromine in the form of BrO plays an important role in photochemical ozone destruction. *In situ* and remote observations establish the abundance of BrO in the range of 4 to 10 parts per trillion by volume (pptv), corresponding to approximately half of total available bromine (Toohey *et al.*, 1990; Wahner *et al.*, 1990b; Carroll *et al.*, 1989). Observations of high levels of OClO also confirm the presence of BrO since OClO is formed in the reaction ClO + BrO (see Section 3.3.2.2) (Salawitch *et al.*, 1988). Since gas phase photochemistry rapidly couples BrO with the inactive reservoirs ($BrONO_2$, HBr), BrO is readily available to participate in catalytic reaction cycles as described in detail in Chapter 10. Calculations based on observed abundances estimate that, depending on temperature, between 25 and 50 percent of ozone loss in the polar vortices is due to the ClO + BrO catalytic cycle (see Section 3.4.1) (Salawitch *et al.*, 1993). The fractional contribution to total ozone loss is estimated to be greater in the Arctic, where higher temperatures reduce the effectiveness of the ClO + ClO cycle.

3.3.2.5 Denitrification and Dehydration

PSC particles formed at low temperatures inside the polar vortices become large enough to sediment appreciable distances in the lower stratosphere over time periods much shorter than the winter season. As a result, up to 90 percent of available reactive nitrogen has been observed to be irreversibly removed from air parcels sampled *in situ* in both polar vortices (Fahey *et al.*, 1990a, b; Schlager and Arnold, 1990; Kondo *et al.*, 1992, 1994a; Arnold *et al.*, 1992). This irreversible removal defines denitrification. Removal of reactive nitrogen in the form of HNO_3 helps sustain active chlorine in an air parcel (see Section 3.4.3). Denitrification is quantified by using the NO_y/N_2O correlation observed at high latitudes in the absence of PSCs (see Section 3.2). *In situ* measurements indicate that the temporal and spatial extent of denitrification is substantially greater in the Antarctic, consistent with observed lower temperatures (see Figure 3-3). In the Arctic, at altitudes below particle formation, the evaporation of sedimenting aerosols enhances NO_y values (Hübler *et al.*, 1990). Another example of this redistribution is provided by the comparison of HNO_3 profile measurements and estimates of the unperturbed NO_y reservoir from the N_2O tracer correlation (Murcray *et al.*, 1994; Bauer *et al.*, 1994).

Satellite observations of HNO_3 at high latitudes now confirm the temporal and spatial scale of HNO_3 removal and the contrast between the two polar regions (Santee *et al.*, 1994; Roche *et al.*, 1994). In the Southern Hemisphere (see Figure 3-17), removal or sequestering of HNO_3 in aerosol particles is observed in late fall. Sequestering occurs when HNO_3 is reversibly incorporated into particles that do not undergo sedimentation. By midwinter, HNO_3 values less than 0.5 ppbv fill a large fraction of the vortex where ClO values are above 1 ppbv in the sunlit portion (see Figure 3-11a). Values of HNO_3 comparable to those expected from tracer correlations with NO_y (about 10 ppbv) surround the vortex at lower latitudes. By late winter, after PSC temperatures cease to occur, low HNO_3 values persist in the vortex, indicating denitrification. In the Northern Hemisphere (see Figure 3-17), higher average temperatures than in the Antarctic (see Figure 3-3) generally limit the removal or sequestering of HNO_3. An example is the local minimum in HNO_3 near Iceland in observations on 22 February 1993 (see Figure 3-17). Thus, sequestering and removal of HNO_3 is a predominant feature of the Antarctic vortex

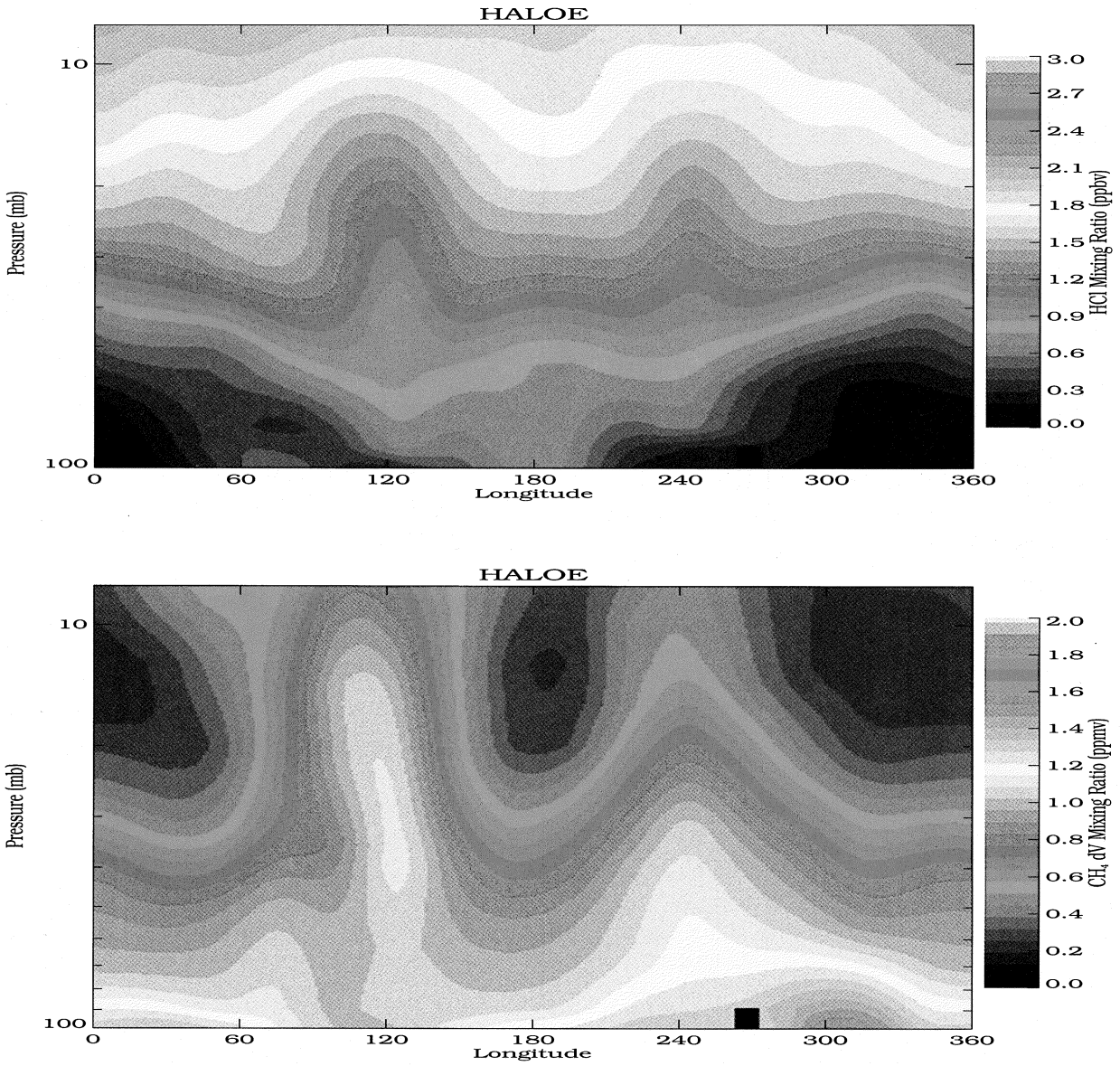

Figure 3-16. UARS HALOE satellite observations of HCl (top) and CH_4 (bottom) on 27 September 1992 in the Southern Hemisphere at 66°S latitude. The data are from sunrise scans analyzed with the version-16 algorithm. The pressure range corresponds to altitudes between 16 and 30 km. At low and high longitude values, the spatial gradients and low absolute values of HCl relative to CH_4 indicate depletion of HCl (adapted from Russell *et al.*, 1993b).

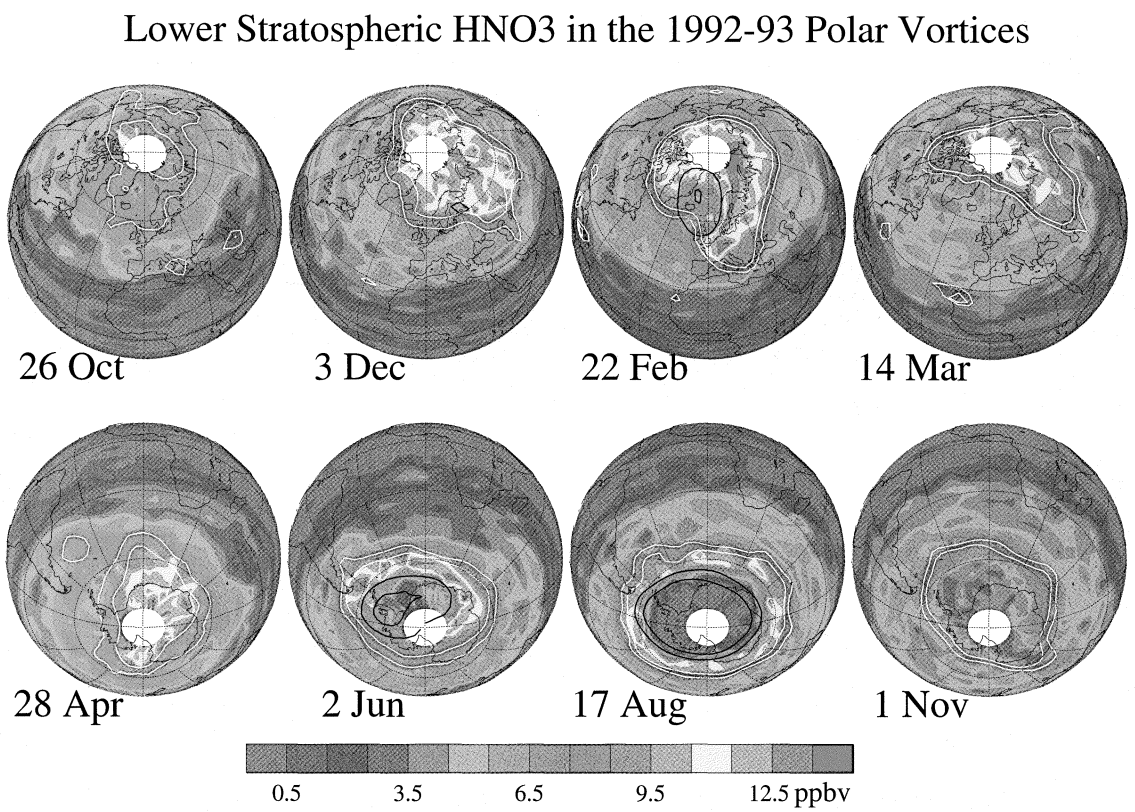

Figure 3-17a. Observations of lower stratospheric HNO_3 in the 1992/93 northern winter (top row) and 1992 southern winter (bottom row) from the UARS MLS satellite instrument. The color bar gives HNO_3 abundances in ppbv interpolated to the 465 K isentropic surface (see Figure 3-4 for altitude reference). The irregular white lines are contours of potential vorticity (2.5 and 3.0 x 10^{-5} K $m^2kg^{-1}s^{-1}$) indicating the polar vortex boundary. No measurements are available in the white area poleward of 80° latitude. Black contours indicate temperatures of 190 K (inner) and 195 K (outer). The days were chosen to illustrate periods (1) before temperatures fell low enough for PSC formation (26 October and 3 December in the north, 28 April in the south), (2) when temperatures were low enough for PSC formation (22 February in the north, 2 June and 17 August in the south), and (3) after temperatures had increased above the PSC threshold (14 March in the north, 1 November in the south) (Santee *et al.*, 1994).

for much of the winter, whereas removal in the Arctic is much less intense and more localized.

The irreversible removal of water, or dehydration, accompanies denitrification in the Antarctic but not in the Arctic (Fahey *et al.*, 1990b). Dehydration requires the sedimentation of Type II PSCs in order to effect the removal of 50 percent of available water as observed in the Antarctic region. Water vapor profiles in the winter vortices show interhemispheric differences, with lower values in the Antarctic. The differences reflect the more frequent occurrence of low temperatures in the Antarctic that facilitate Type II PSC formation (Kelly *et al.*, 1989; 1990). Balloon and satellite observations of H_2O and CH_4 in the Southern Hemisphere confirm extensive dehydration in the vortex and its near environment (Hofmann and Oltmans, 1992; Tuck *et al.*, 1993; Rind *et al.*, 1993). Because H_2O and molecular hydrogen (H_2) are produced in the oxidation of CH_4 in the stratosphere and mesosphere, changes in the quantity [$2CH_4 + H_2O$] are a more sensitive indicator of dehydration than changes in H_2O alone (see Figure 3-18 and Section 3.5.2). The large spatial and temporal scales of dehydration observed over the Antarctic are not observed anywhere else in the atmosphere (Tuck *et al.*, 1993). The combined re-

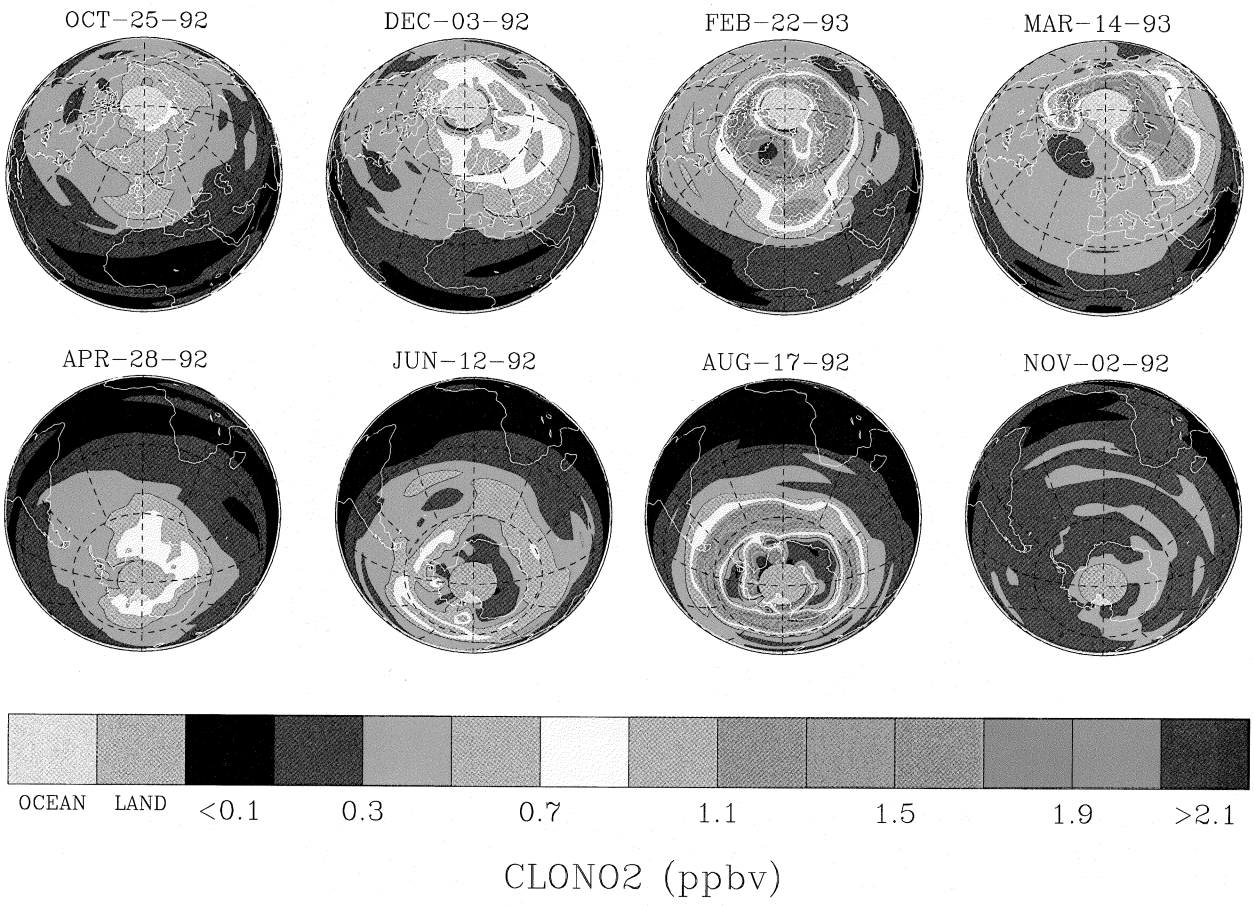

Figure 3-17b. Observations of lower stratospheric $ClONO_2$ in the 1992/93 northern winter (top row) and in the 1993 southern winter (bottom row) from the UARS Cryogenic Limb Array Etalon Spectrometer (CLAES) satellite instrument. The color bar gives $ClONO_2$ abundances in ppbv interpolated to the 465 K isentropic surface (see Figure 3-4 for altitude reference). The instrument does not see poleward of 80° latitude. The days were chosen to illustrate periods (1) before temperatures fell low enough for PSC formation (25 October and 3 December in the north, 28 April in the south), (2) when temperatures were low enough for PSC formation (22 February in the north, 12 June and 17 August in the south), and (3) after temperatures had increased above the PSC threshold (14 March in the north, 2 November in the south) (adapted from Roche *et al.*, 1994).

moval of H_2O and HNO_3 reduces the available condensable material for the formation of PSCs and, hence, lowers the minimum formation temperature. This feature is most notable in the Antarctic between the early and late winter periods (see Figure 3-10) (Poole and Pitts, 1994).

Despite extensive observational evidence for dehydration and denitrification, all of the underlying microphysical mechanisms and atmospheric conditions that control particle formation and sedimentation have not been completely confirmed in observational or laboratory studies. The overall process is complicated by the potential roles of air parcel cooling rates and barriers to nucleation of aerosol particles (Toon *et al.*, 1989b; Wofsy *et al.*, 1990a, b). The sedimentation process is generally better understood (Müller and Peter, 1992). The combined *in situ* data from both vortices show that intense denitrification (about 90-percent removal) oc-

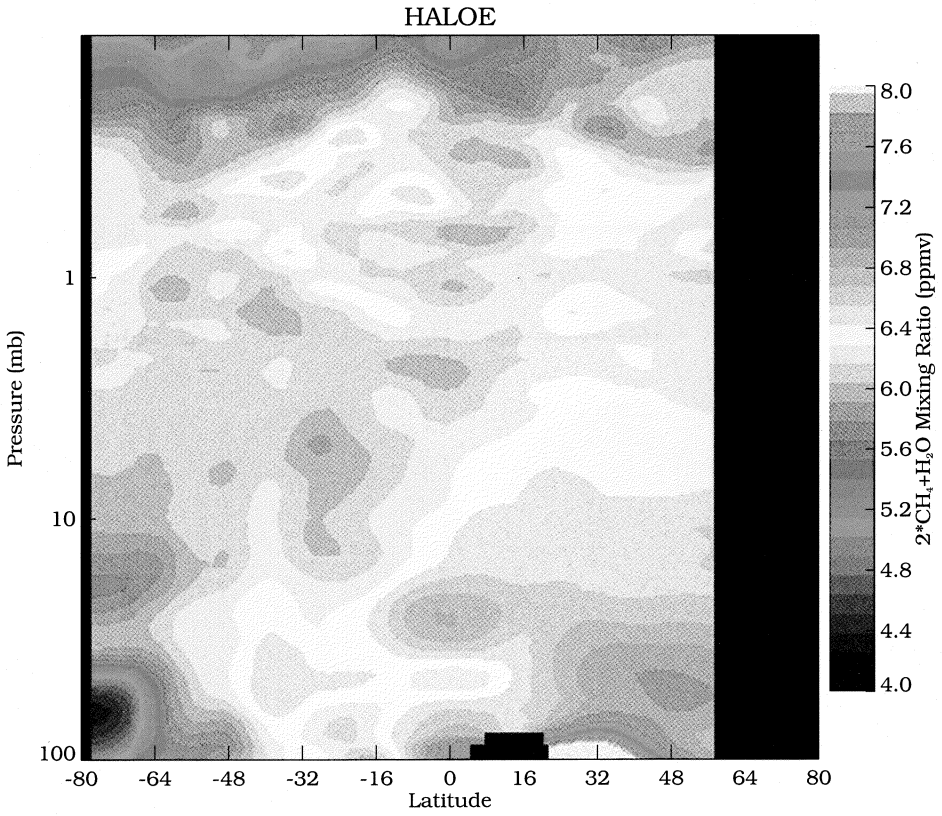

Figure 3-18. Latitude-altitude cross section of UARS HALOE satellite data for the period 21 September to 15 October 1992 for values of [$2CH_4 + H_2O$]. The data are from sunset scans analyzed with the version-17 algorithm. The progression of viewing latitude with date is shown above the panel, and the pressure range corresponds approximately to the 16 to 65 km altitude range. Latitude is expressed in degrees, with negative latitude values corresponding to the Southern Hemisphere (adapted from Tuck *et al.*, 1993).

curs with and without intense dehydration (about 50-percent removal). However, intense dehydration has not been observed without intense denitrification (Fahey *et al.*, 1990b). Observations do not preclude independent processes for intense denitrification and dehydration, as discussed in theoretical studies (Toon *et al.*, 1990b; Salawitch *et al.*, 1989; Wofsy *et al.*, 1990a, b). Water vapor plays a role in denitrification due to its presence in condensed hydrates of HNO_3 (see Figure 3-8). However, since gas phase abundances of water vapor exceed those of HNO_3 by large factors, changes in water vapor are negligible as denitrification occurs. In addition, the analysis of the export of denitrified and dehydrated air from the Antarctic vortex reveals a quantitative inconsistency that may be explained by independent removal processes (Tuck *et al.*, 1994).

3.3.3 Role of Mt. Pinatubo Aerosol

Volcanic eruptions are potentially important sources of sulfur dioxide (SO_2), HCl, and H_2O for the lower stratosphere (GRL, 1992). The eruption of Mt. Pinatubo in the Philippines in June 1991 is a recent large event that affected stratospheric measurements during this assessment period. The injection of SO_2 into the lower stratosphere in the tropics exceeded that of the El Chichón eruption in 1982 by three times (McCormick and Veiga, 1992). The SO_2 cloud rapidly forms H_2SO_4, which augments the formation and growth of sulfate aerosol particles in the stratosphere (Wilson *et al.*, 1993; Borrmann *et al.*, 1993). Figure 3-19 shows the evolution of aerosol extinction from near-background conditions before the 1991 eruption to one year later. Surface area

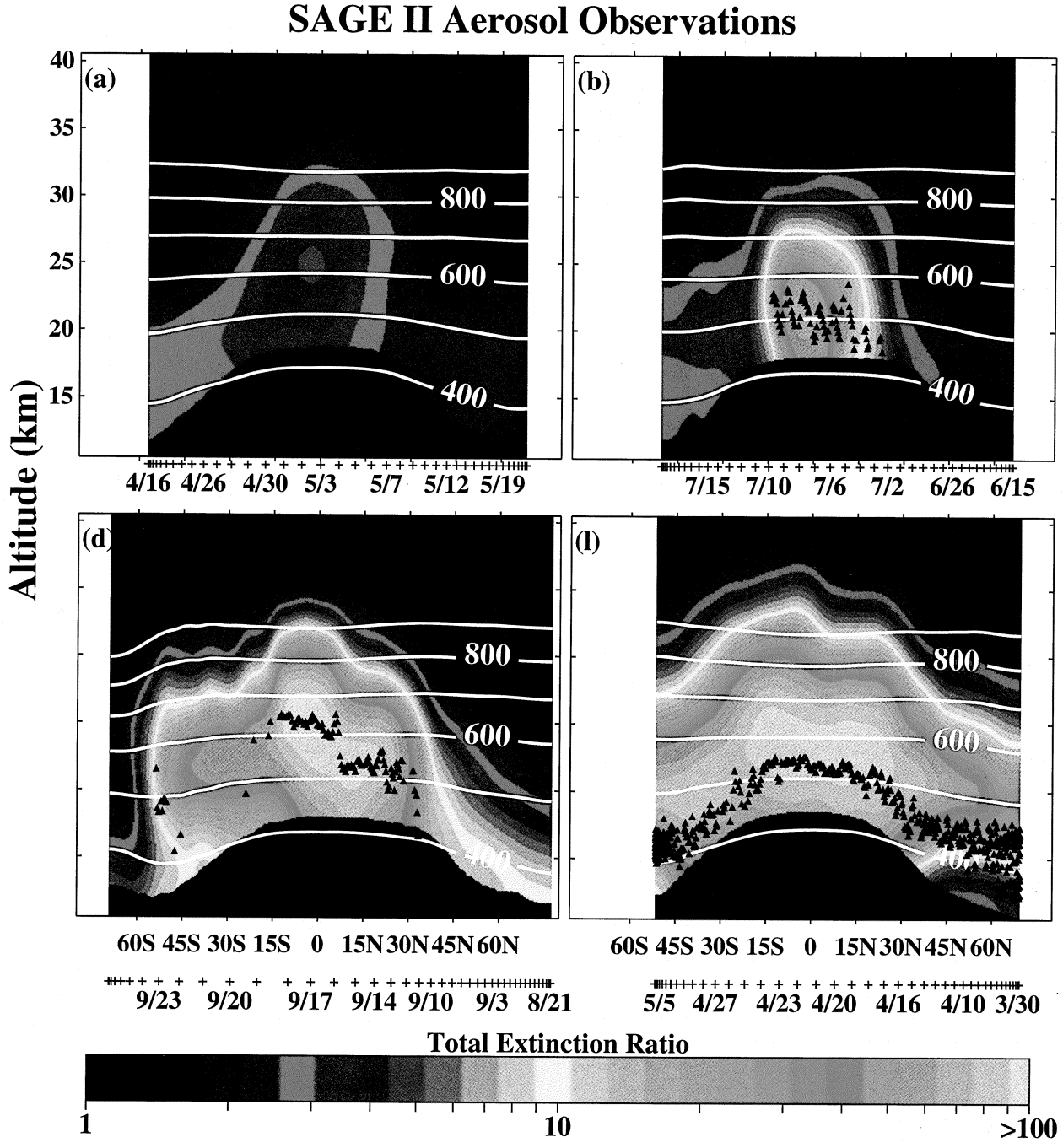

Figure 3-19. Latitude-altitude cross sections of the Stratospheric Aerosol and Gas Experiment II (SAGE II) 1-μm extinction ratio measurements that show the effect of the eruption of Mt. Pinatubo in June 1991 on aerosol abundance in the lower atmosphere. The specific dates of observation are indicated with crosses below each panel for the periods: (a) 15 April to 25 May 1991 (pre-eruption); (b) 14 June to 26 July 1991 (early austral winter); (d) 20 August to 30 September 1991 (late austral winter); and (l) 29 March to 9 May 1992 (full dispersal). No data were used 2 km below the tropopause (blacked out). Small triangles indicate truncation altitude for the SAGE II data. Lidar data were used below this altitude. Isentropes (constant potential temperature in K) appear as white contour lines (adapted from Trepte *et al.*, 1993).

values are increased by factors up to 100 over much of both hemispheres within the year. Since the residual circulation in the stratosphere is upward in the tropics and poleward and downward at higher latitudes, volcanic aerosol is transported to the polar regions, where it is incorporated into the polar vortices. Mt. Pinatubo aerosol did not appear in the Antarctic vortex during the austral winter of 1991 (see Figure 3-19d) but was present at the South Pole following vortex breakup (Cacciani *et al.*, 1993) and was present in the vortex during the following austral winter (Deshler *et al.*, 1994). In the 1991/92 boreal winter, some enhanced levels were observed in the vortex (Wilson *et al.*, 1993). The decay of volcanic aerosol in the lower stratosphere occurs with a time constant that varies with latitude and particle size, but generally averages about one year for an integral parameter such as particle surface area.

Although the emission of HCl from volcanoes can exceed the annual anthropogenic emissions of chlorine to the atmosphere, emitted HCl is largely removed in the troposphere before appreciable amounts can enter the stratosphere. For the Mt. Pinatubo eruption, column measurements of HCl before and after the eruption confirmed that the increase of HCl in the stratosphere was negligible (Wallace and Livingston, 1992; Mankin *et al.*, 1992). The removal of HCl and H_2O is expected to result from scavenging on liquid water droplets formed in the volcanic plume (Tabazadeh and Turco, 1993). These and other dissolution processes reduce HCl abundances by several orders of magnitude, thereby limiting the availability of HCl for transport to the stratosphere. In contrast, only 0.5 to 1.5 percent of SO_2 in the plume is removed by dissolution, thereby facilitating the transport of SO_2 to the stratosphere, where it is oxidized to form H_2SO_4.

The principal consequence of volcanic eruptions for the stratosphere is the enhancement of sulfate aerosol over the globe, thereby affecting the rates of heterogeneous reactions that convert reactive chlorine and nitrogen species (see Table 3-1). In midlatitudes, volcanic aerosol drives the conversion of dinitrogen pentoxide (N_2O_5) to HNO_3 (see Reaction (3-6)) to saturation (Prather, 1992; Fahey *et al.*, 1993; Koike *et al.*, 1994). Volcanic aerosol in the Antarctic is associated with an increased frequency of PSCs and a reduction in large particle formation within the cloud (Deshler *et al.*, 1994). Aerosol surface area densities found in the vortex following the eruption of Mt. Pinatubo are comparable to those in a Type I PSC formed in the absence of volcanic influence. Thus, increased rates of chlorine activation above Type I PSC temperatures are expected in 1992 and 1993 (see Figure 3-8). However, Type II PSC surface areas are still predominant at lower temperatures. In the center of the ozone depletion region (14-18 km), chlorine is fully activated in both vortices in most years and the presence of volcanic aerosol here will not increase the intensity of chlorine activation. However, in the 10 to 14 km region and the region above 18 km where chlorine is usually not fully activated, additional surface area provided by volcanic aerosol can result in increased chemical processing. Furthermore, because the sulfate aerosol is active at temperatures above the PSC formation threshold, the spatial and temporal extent of chlorine activation will be increased, especially in the vortex edge region. Chlorine activation there has been observed to be greater than that in non-volcanic periods and is associated with enhanced ozone loss (Solomon *et al.*, 1993; Hofmann *et al.*, 1992; Hofmann and Oltmans, 1993). Since the scale of this near-vortex region can be comparable to or larger than the vortex interior, enhanced processing outside the vortex edge may be especially important in ozone balance throughout the hemispheres (see Chapter 4).

3.3.4 Model Simulations

Model simulations of the formation of PSCs in the vortex require detailed knowledge of both the thermodynamics inherent in Figure 3-8 and of the nucleation and growth features of the various aerosol particles. Several studies have met with success in simulating the general features of a PSC (Peter *et al.*, 1992; Drdla and Turco, 1991; Toon *et al.*, 1989b, 1990b). However, significant uncertainties remain in the prediction of PSC formation conditions and other characteristics (Dye *et al.*, 1992; Kawa *et al.*, 1992b). Specifically, the threshold temperature for the appearance of Type I aerosols is well below the saturation temperature in Arctic observations. Various explanations are possible, but remain unconfirmed at present. In addition, details of the PSC sedimentation process causing denitrification and dehydration are uncertain. Specifically, uncertainty in the coupling of denitrification and dehydration affects model simulations of PSC activity as well as ozone depletion.

As a result of these uncertainties, model simulations adopt a simplified parameterization of PSC formation and sedimentation processes. These studies confirm the effectiveness of the heterogeneous reactions listed in Table 3-1 for the conversion of inactive to active chlorine (Brasseur and Granier, 1992; Cariolle *et al.*, 1990; Eckman *et al.*, 1993; Lutman *et al.*, 1994a; Chipperfield *et al.*, 1994b, c; Newman *et al.*, 1993; Lefèvre *et al.*, 1994). PSCs formed in localized low-temperature regions in the strong zonal flow of the vortex can fully activate the vortex in the lower stratosphere in a matter of days. Thus, predicting intense activation of chlorine in the vortex seems not to require detailed knowledge of PSC events. Using a 3-D transport and chemistry model, a comparison of modeled and satellite observations of ClO in Arctic winter shows excellent agreement (see Figure 3-11b). In a similar study, the comparison reveals differences in the dynamic structures that force PSC activity at high latitudes (Douglass *et al.*, 1993). In addition, *in situ* and satellite observations of vortex ClO over a wide range of values can be simulated with trajectory models that account for exposure to PSCs as well as the recovery of inactive chlorine in sunlight following a PSC event (Lutman *et al.*, 1994a, b; Schoeberl *et al.*, 1993a, b; Toohey *et al.*, 1993).

Other model simulations are used to evaluate ground-based measurements of OClO in Antarctica that were made when volcanic aerosol was present (Solomon *et al.*, 1993; Hanson *et al.*, 1994). In matching the observed activation of chlorine, the simulations demonstrate the importance of regions that have temperatures close to, but above those required for PSC formation and modest solar illumination. In these regions, chlorine activation on sulfate aerosols (see Table 3-1) effectively competes with the photolysis of HNO_3 which drives the recovery of the inactive $ClONO_2$ reservoir. The activation of chlorine has the potential to enhance ozone depletion in these regions, especially when volcanic aerosols are present.

3.4 DESTRUCTION OF OZONE

3.4.1 Ozone Loss: Observations and Calculations

Significant ozone loss in polar regions requires the activation of chlorine and exposure to sunlight (see Figure 3-1). This association has been substantiated in previous assessments using active chlorine observations over limited regions of the vortex and limited time periods (Anderson *et al.*, 1991; Brune *et al.*, 1991). Photochemical loss of ozone is attributed to catalytic reaction cycles involving enhanced ClO, namely

$$\begin{aligned} ClO + ClO + M &\rightarrow (ClO)_2 + M && (3\text{-}8)\\ (ClO)_2 + h\nu &\rightarrow ClOO + Cl && (3\text{-}8a)\\ ClOO &\rightarrow Cl + O_2\\ 2(Cl + O_3 &\rightarrow ClO + O_2)\\ \text{Net: } 2O_3 &\rightarrow 3O_2 \end{aligned}$$

$$\begin{aligned} ClO + BrO &\rightarrow Cl + Br + O_2 && (3\text{-}9)\\ &\rightarrow Br + OClO && (3\text{-}9a)\\ &\rightarrow BrCl + O_2\\ BrCl + h\nu &\rightarrow Br + Cl\\ Br + O_3 &\rightarrow BrO + O_2\\ Cl + O_3 &\rightarrow ClO + O_2\\ \text{Net: } 2O_3 &\rightarrow 3O_2 \end{aligned}$$

$$\begin{aligned} ClO + O &\rightarrow Cl + O_2 && (3\text{-}10)\\ Cl + O_3 &\rightarrow ClO + O_2\\ \text{Net: } O + O_3 &\rightarrow 2O_2 \end{aligned}$$

where reaction steps (3-8a) and (3-9a) do not result in ozone destruction and where the cycles are listed in order of importance for ozone destruction inside the vortex (Salawitch *et al.*, 1993; Lutman *et al.*, 1994b; Molina and Molina, 1987; McElroy *et al.*, 1986; Solomon *et al.*, 1986; Tung *et al.*, 1986). The rates of the homogeneous photochemical reactions involved in chlorine catalytic cycles follow from a wide variety of laboratory investigations and are generally well understood (JPL, 1992). However, studies continue to improve the precision of earlier results. For example, the temperature dependence of HNO_3 and $ClONO_2$ photolysis cross sections have been remeasured. Those of $ClONO_2$ were found to be in good agreement with previous recommendations for temperatures characteristic of the lower stratosphere, whereas those of HNO_3 were reduced somewhat at stratospheric temperatures (Burkholder *et al.*, 1994a, b).

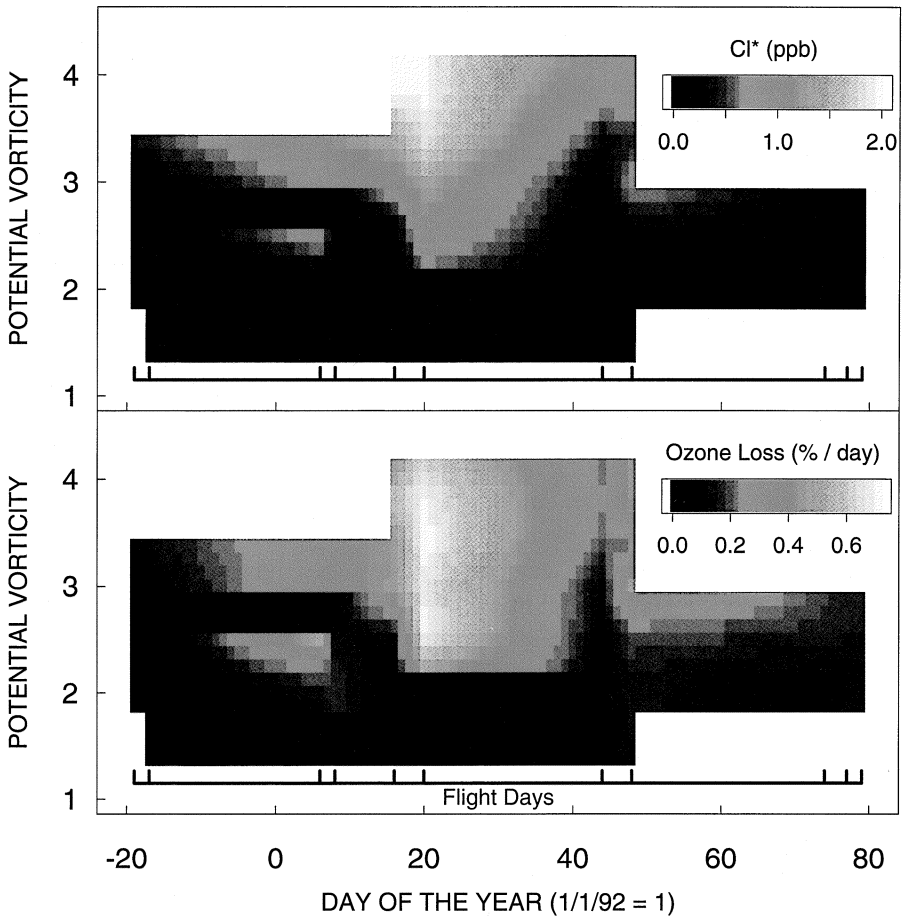

Figure 3-20. Calculation of Cl^* (= ClO + $2Cl_2O_2$) (top) and the 24-hour mean loss rate for ozone on the 470 K potential temperature surface (bottom) from a full diurnal photochemical model calculation. Both are plotted as a function of potential vorticity (PV), in units of (10^{-5} K $m^2kg^{-1}s^{-1}$), and day of the year for the Arctic vortex in 1991/92 (day 1 = 1 January 1992). The approximate mean latitudes of parcels with PV of 2 and 4 are 40° and 65°N, respectively, for this period (Salawitch *et al.*, 1993).

A cycle involving $ClONO_2$ has also been recognized to contribute to ozone depletion. After PSCs are no longer present and the recovery period begins (see Section 3.4.3), active chlorine forms elevated amounts of $ClONO_2$. The production of Cl from $ClONO_2$ photolysis initiates a catalytic cycle similar to Reaction (3-8) (Toumi *et al.*, 1993; Minton *et al.*, 1992). In full models of ozone destruction, $ClONO_2$ photolysis and associated reactions are typically included, but the associated ozone loss is often not distinguished from the primary catalytic loss cycles represented in Reactions (3-8, 3-9, and 3-10).

Quantitative evaluation of ozone destruction rates, constrained by observed ClO, provides reasonable agreement with the measured decay of ozone over the Antarctic where ozone loss is rapid and the vortex is assumed to be isolated over the measurement period (see Chapter 1) (Anderson *et al.*, 1989; Solomon, 1990; Anderson *et al.*, 1991). Loss rates of about one percent per day are found there when chlorine is fully activated in sunlight. Recent model calculations for the Arctic show a detailed relationship between active chlorine abundance and ozone loss rates in the lower stratosphere in early 1992 (see Figure 3-20) (Salawitch *et al.*, 1993). The model represents vortex photochemistry more comprehensively than in previous studies because of the use of extensive *in situ* and satellite observations of reactive

and trace species, meteorological analyses, and recent laboratory results for gas phase and heterogeneous reactions. After parameterization, ozone loss rates are estimated using a full-diurnal photochemical calculation. The maximum loss rates are similar to the Antarctic, but the rates are sustained for a shorter period, resulting in smaller total losses. For a given chlorine level, loss rates on an isentropic surface are greater at lower latitude (or lower PV) values where solar illumination is greater. Cumulative losses of 15 to 20 percent in the Arctic implied by Figure 3-20 are corroborated by estimates made using *in situ* observations of ozone (Browell *et al.*, 1993) and changes in the relationship between ozone and the long-lived tracer N_2O (Proffitt *et al.*, 1993) (see Section 3.2). Corroboration is also provided by model simulations that utilize the extensive ozonesonde data available in the 1991/92 northern winter. The data are analyzed by using estimates of descent of polar air over winter months and by using trajectories to identify air parcels sampled twice in sonde measurements separated in time and space (Lucic *et al.*, 1994; von der Gathen *et al.*, 1994). These recent results increase confidence in earlier estimates of ozone loss in the Arctic vortex (Schoeberl *et al.*, 1990; McKenna *et al.*, 1990; Salawitch *et al.*, 1990).

With extensive observations of ClO and ozone, the UARS satellite substantially increases the evidence that ozone loss occurs in both polar regions and that reactions involving ClO are the cause of this depletion (Waters *et al.*, 1993a; Manney *et al.*, 1994b). Total column amounts of ClO correlate well with regions depleted in column ozone in two consecutive years in the Antarctic (see Figure 3-21). In addition, this correlation has been observed in mid-August in the Antarctic (Waters *et al.*, 1993b), in agreement with the interpretation of *in situ* observations (Proffitt *et al.*, 1989a). In the Arctic, variability in column ozone abundances tends to obscure the smaller Arctic losses. However, averages of ClO and ozone in the Arctic show a negative correlation during peak ClO values, with ozone loss rates in reasonable agreement with calculations. Satellite N_2O observations or PV analyses are used to account for ozone changes resulting from the transport of ozone. These results suggest that conclusions and interpretation derived from the highly localized *in situ* and ground-based data sets have relevance on the vortex scale.

A new perspective of ozone loss comes from satellite observations of late-winter changes in ozone averaged around PV contours (see Figure 3-22) (Manney *et al.*, 1993, 1994b). This approach can detect significant changes in the 3-D distribution of ozone without *a priori* assumptions about the specific role of photochemistry or transport of ozone. With PV generally increasing poleward, poleward transport of ozone-rich air at upper levels and ozone loss at lower levels are both evident in the Antarctic vortex region in each year. In contrast, ozone increases are expected to extend to the lowest potential temperatures in these regions without localized, *in situ* photochemical loss. In the Arctic, ozone increases are found in both 1992 and 1993, but significant ozone loss in the February-to-March time period is found only in 1993 in the lower stratosphere. The loss is consistent with enhanced ClO values in 1993 that resulted from more extensive low temperatures (see Figures 3-11 and 3-12).

3.4.2 Variability

Perhaps the greatest difficulty in increasing the accuracy of predictions of ozone loss in polar regions is the interannual and intra-annual variability of the conditions that determine loss rates. Large variability in meteorological and photochemical parameters featured in Figure 3-1 increases the difficulty of the interpretation of limited data sets and reduces their value for predicting future changes in ozone. Variability largely follows from the fluid mechanical features of the vortex and its environment, and the stochastic nature of the forces that act to change the vortex and its environment. Of greatest concern are changes in the spatial and temporal extent of low temperatures and the duration of the vortex into the spring season (Austin *et al.*, 1992; Austin and Butchart, 1994; Salawitch *et al.*, 1993). Lower temperatures promote activation of chlorine, and a long-lived vortex promotes the photochemical destruction of ozone by active chlorine. The northern winters of 1991/92 and 1992/93 present a striking example of interannual variability in ClO and ozone (see Figures 3-12 and 3-22) (Larsen *et al.*, 1994). In general, variability in the Arctic vortex is greater than in the Antarctic, particularly for minimum temperatures (see Figure 3-3). Because the formation of PSCs requires temperatures below a certain threshold, fluctuations of a few degrees will substantially change

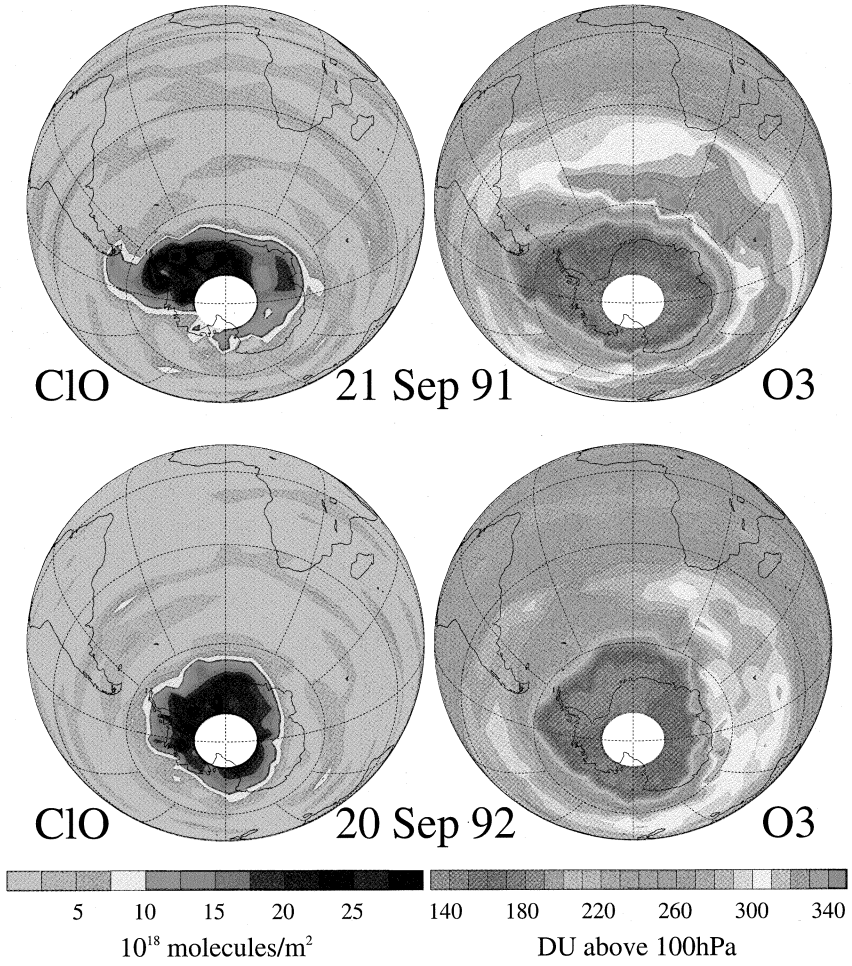

Figure 3-21. Observations of column abundances of ClO (10^{18} molecules m^{-2}) and ozone (Dobson units) above 100 hPa (about 16 km) in the Antarctic in September 1991 and 1992 from the UARS MLS satellite instrument (Waters *et al.*, 1993a).

the extent of processing inside the vortex and the extent of denitrification as sunlight returns to the vortex in spring. Ozone destruction rates in the late vortex strongly depend on the extent of denitrification (see Figure 3-23) (Brune *et al.*, 1991; Salawitch *et al.*, 1993). Reduced values of reactive nitrogen slow the formation of the $ClONO_2$ reservoir and thereby maintain active chlorine levels as sunlight returns to high latitudes.

The variability in both polar regions follows from wave activity near the vortex and the interaction of waves with tropospheric weather systems. These wave perturbations can change the chemical evolution of the vortex through the associated temperature changes (Farman *et al.*, 1994; Gobbi and Adriani, 1993; Rood *et al.*, 1992) or the transport into and out of the vortex, especially for the weaker Arctic vortex (Dahlberg and Bowman, 1994; Manney *et al.*, 1994c). Regions cooled to PSC temperatures can process a large fraction of vortex air in a relatively short period of time, contributing significantly to the total amount of vortex processing (MacKenzie *et al.*, 1994; Newman *et al.*, 1993; Lefèvre *et al.*, 1994). When these low-temperature regions are near the vortex edge, the resultant processing may influence midlatitude ozone destruction (see Chapter 4). Wave activity also distorts the vortex from a symmetric polar flow, thereby transporting processed air into sunlight at lower latitudes. Because ozone loss rates increase substantially in sunlight when chlorine is acti-

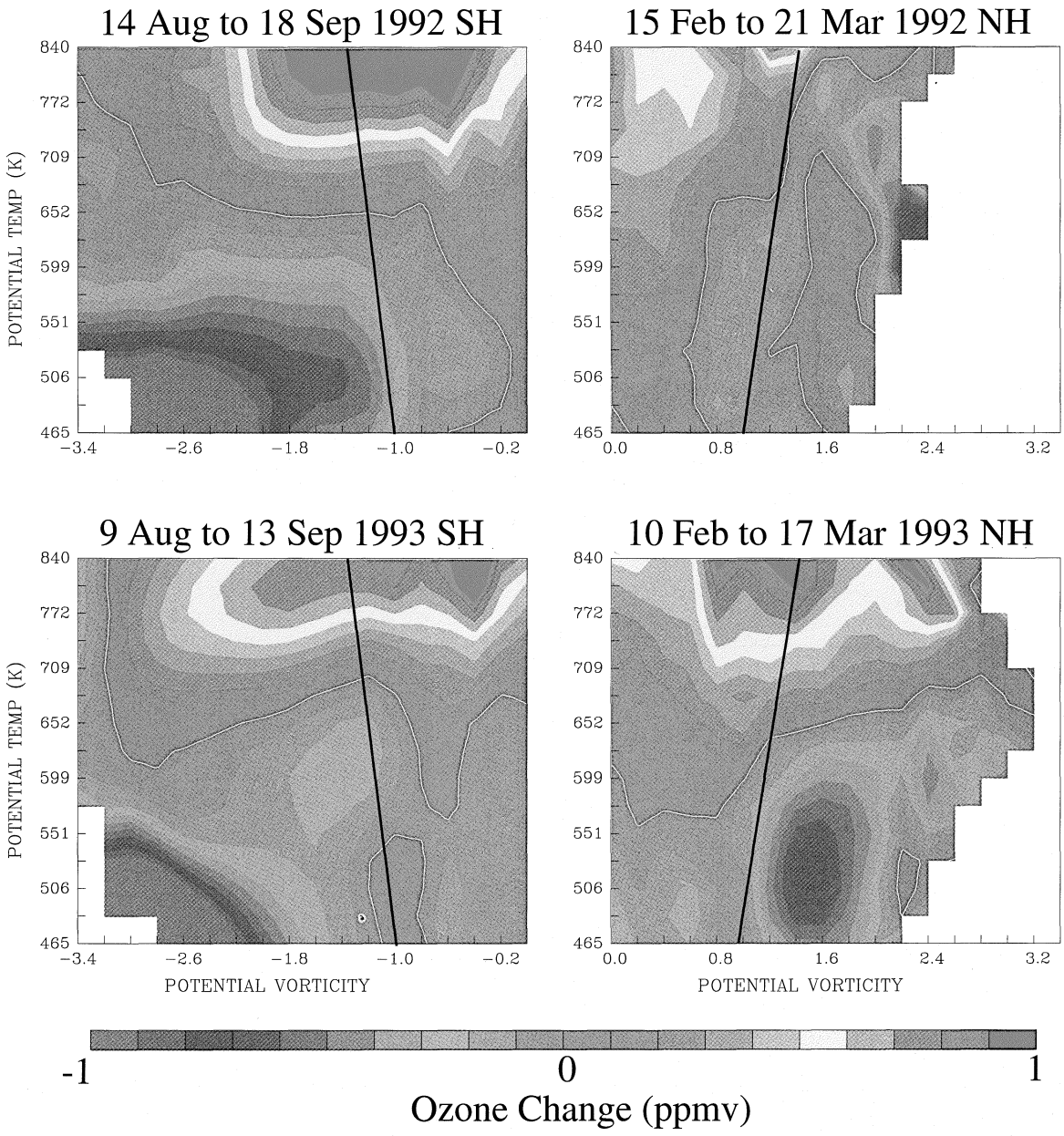

Figure 3-22. Observations of late winter ozone changes for 1992 (top) and 1993 (bottom) in the Arctic (right) and Antarctic (left) from the UARS MLS instrument. The horizontal coordinate is scaled PV. PV is a surrogate for latitude, with values increasing with increasing latitude. The vertical coordinate is potential temperature, a surrogate for altitude, covering the range of approximately 15 to 30 km (see Figure 3-4). These coordinates help separate chemical and diabatic effects from adiabatic and transport effects occurring at constant potential temperature. Measurements shown here are the difference in ozone averaged around contours of PV between the two dates indicated in each panel. The black line gives the approximate edge of the vortex, with the interior to the right in the Northern Hemisphere (NH) and to the left in the Southern Hemisphere (SH). During the periods shown here, the vortex edge extended as far equatorward as 40° latitude in the Northern Hemisphere and 50° latitude in the Southern Hemisphere (see Figures 3-11 and 3-17). The zero-change contour is indicated in white (Manney *et al.*, 1994b).

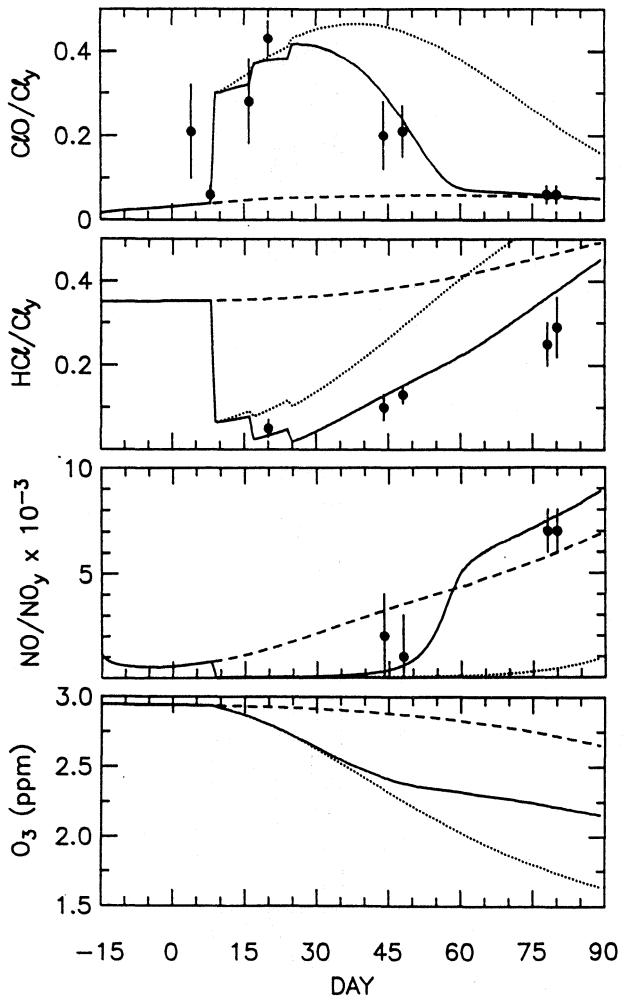

Figure 3-23. Calculated seasonal evolution (day 1 = 1 January 1992) of ClO, HCl, NO, and ozone at noon for an air parcel at 18 km altitude, 65°N latitude, processed periodically by PSCs. Case A: No denitrification (solid line). Case B: 90-percent denitrification following the first PSC event (dotted line). Case C: No PSC processing (dashed line). Reduction in ozone during March in the absence of PSC processing occurs because of reactions involving NO_x. Data points represent mean and standard deviation of aircraft observations during AASE II for the 470 K potential temperature surface and potential vorticity values greater than 2.8 x 10^{-5} K $m^2kg^{-1}s^{-1}$. Data used for ClO and NO are restricted to daytime observations (solar zenith angle < 86°). Concentrations of ClO, HCl, and NO have been normalized to their respective reservoirs to remove the influence of small-scale atmospheric gradients (Salawitch *et al.*, 1993).

vated, total ozone loss may increase significantly (Brune *et al.*, 1991; Solomon, 1990).

Wave activity in polar regions is also thought to be influenced by phenomena occurring at lower latitudes. The strongest of these is the quasi-biennial oscillation (QBO) (van Loon and Labitzke, 1993; Angell, 1993; Labitzke, 1992; Poole *et al.*, 1989). The QBO refers to changes in the direction and magnitude of stratospheric winds above the equator that occur with a period of about 27 months. In years when the winds in the equatorial lower stratosphere are from the east, the northern vortex is comparatively weak and warm, thereby minimizing the potential for ozone depletion. In westerly years, the vortex is colder and more intense in both hemispheres. El Niño/Southern Oscillation (ENSO) effects, referring to changes in sea surface temperature and associated shifts in atmospheric mass in the South Pacific Ocean, represent a much weaker influence (Angell, 1993; Baldwin and O'Sullivan, 1994).

Wave activity plays a more important role in subseasonal variability in the Northern Hemisphere than in the Southern Hemisphere. Specifically, major midwinter warming events often result in the Northern Hemisphere from strong wave activity in the troposphere associated with cyclones and anticyclones (Labitzke, 1992; Manney *et al.*, 1994a). In the middle stratosphere, the polar vortex may break apart or split during a warming, causing large amounts of lower latitude air to be transported to high latitudes and reversing the meridional temperature gradient. Such warmings eventually mark the end of PSC temperatures throughout the vortex and change the effectiveness of ozone catalytic loss cycles. Wave activity also creates variability in column ozone by changing tropopause heights and temperatures in localized regions (Farman *et al.*, 1994; Petzoldt *et al.*, 1994). Ozone column amounts are reduced by convergence of ozone-poor air below and divergence of ozone-rich air above, and by rapid advection of low-latitude air in the case of persistent ridge formation in the upper troposphere/lower stratosphere (Orsolini *et al.*, 1994). These changes do much to obscure ozone changes due to photochemical loss.

Volcanic eruptions are also a source of variability in the stratosphere. In addition to chemical effects (see Section 3.3.3), increases in stratospheric aerosol that follow an eruption have direct and indirect effects on temperature and circulation in both the stratosphere and

troposphere (Rind *et al.*, 1992). The direct effect in the lower stratosphere is a warming in the tropics (Kinne *et al.*, 1992; Labitzke and McCormick, 1992) and a cooling in polar regions. These and other changes may influence the vortex and the formation of PSCs.

As a final consideration, trends in source gas emissions in the troposphere may eventually affect polar ozone loss and its variability. Of greatest interest are changes in H_2O, CH_4, carbon dioxide (CO_2), N_2O, and halogen-containing species (see Chapter 2), which all participate in establishing the meteorological and photochemical context of the depletion process. Increases in CO_2 are expected to decrease temperatures in the lower stratosphere, thereby increasing the frequency and extent of PSCs (Austin and Butchart, 1994; Austin *et al.*, 1992). With additional cooling caused by the subsequent destruction of ozone, total ozone loss in the Arctic could become comparable to that in the Antarctic. More directly, a doubling of inorganic chlorine species in the stratosphere would likely result in Arctic ozone losses that are comparable to those in the Antarctic (Salawitch *et al.*, 1993). PSC frequency would also increase in response to growth in atmospheric CH_4 and to an increase in the amount of H_2O entering the stratosphere in the tropics. A more direct source is the emission of H_2O and NO_y species from aircraft operating in the upper troposphere and lower stratosphere (Peter *et al.*, 1991).

3.4.3 Photochemical Recovery

After the cessation of PSC formation inside the vortex, the conversion rate of inactive reservoir chlorine to active chlorine is reduced to pre-winter values (see Figure 3-1). Accordingly, ClO values fall from their midwinter peak values throughout the vortex (see Figures 3-20 and 3-23) (Waters *et al.*, 1993a, b; Toohey *et al.*, 1993; Salawitch *et al.*, 1993). In this recovery period, changes caused by PSCs are reversed as photochemistry restores reservoir chlorine to pre-winter values. In the Northern Hemisphere, air usually experiences PSC temperatures on only a few occasions and for only a small fraction of time throughout midwinter (Newman *et al.*, 1993). Thus, recovery is ongoing throughout the winter, in contrast to the Southern Hemisphere. Recovery proceeds with reactions involving active chlorine and reactive nitrogen species:

$$ClO + NO_2 + M \rightarrow ClONO_2 + M \quad (3\text{-}11)$$

$$ClO + NO \rightarrow Cl + NO_2 \quad (3\text{-}12)$$

$$Cl + CH_4 \rightarrow HCl + CH_3 \quad (3\text{-}13)$$

$$HNO_3 + h\nu \rightarrow NO_2 + OH \quad (3\text{-}14)$$

where hν is solar radiation and OH is the hydroxyl radical. Reaction (3-14) is key to maintaining the partitioning within the NO_y reservoir in Equation (3-2). Reaction (3-11) is predominant in the early recovery phase because of the availability of NO_2 from Reaction (3-14). NO_2 increases dramatically with the return of sunlight to the poles when HNO_3 is available (Keys *et al.*, 1993; Solomon and Keys, 1992). Changes in reservoir chlorine have been confirmed with *in situ* measurements of HCl and remote soundings of $ClONO_2$ near the vortex edge and inside the vortex in the Arctic when denitrification is low (see Figures 3-13, 3-14, 3-15, 3-16, and 3-17) (Lutman *et al.*, 1994b; Roche *et al.*, 1993b, 1994). Specifically, the enhancement of $ClONO_2$ estimates in the early recovery phase is evident in aircraft measurements in the Arctic in February 1992 (see Figure 3-13). As recovery progresses, more reservoir chlorine shifts from $ClONO_2$ to HCl, until values present in late fall are restored (Liu *et al.*, 1992). When denitrification is significant entering the recovery phase, $ClONO_2$ may not be formed as readily as indicated in Figure 3-1. Instead, Reaction (3-13) dominates, restoring HCl rapidly and causing HCl to exceed $ClONO_2$ temporarily. As reactive nitrogen is mixed back into the air parcel, more $ClONO_2$ is formed and $ClONO_2$ and HCl return to unperturbed values.

Ozone loss during the recovery phase depends strongly on the extent of denitrification. With extensive denitrification, the abundance of NO_2 produced by Reaction (3-14) is limited, thereby enhancing ozone loss rates (see Figure 3-23) (Salawitch *et al.*, 1993; Kondo *et al.*, 1994b; Brune *et al.*, 1991). Full recovery must then wait until breakup of the vortex facilitates mixing with lower latitude air that has not been denitrified. The enhancement of $ClONO_2$ values during recovery and elevated temperatures mean that catalytic cycles other than ClO + ClO contribute to ozone loss during this period (Toumi *et al.*, 1993).

Ultimately, the importance of the recovery phase for ozone depletion depends on details of vortex breakup. Planetary wave activity in the spring breaks apart the

vortex weakened by the reduction in radiative forcing. In the Antarctic, variability is lower, but significant interannual differences still occur in the lifetime of the vortex (see Figure 3-3). As the area covered by PSC temperatures lessens, the distortion of the vortex in a wave event can typically lead to a rapid breakup of the vortex (Krueger *et al.*, 1992). In any year, an early breakup phase minimizes ozone depletion. However, in the breakup process, the vortex may distort to reach lower latitudes, significantly increasing local ozone loss rates (Solomon, 1990; Brune *et al.*, 1991). After breakup, the transport of lower latitude air to the poles displaces air parcels depleted in ozone. At the same time, processed air that is low in ozone, contains active chlorine, or is potentially denitrified and dehydrated is transported to lower latitudes (Atkinson *et al.*, 1989; Harwood *et al.*, 1993). As ozone loss continues in these air parcels, midlatitude ozone may be significantly impacted (see Chapter 4).

3.5 VORTEX ISOLATION AND EXPORT TO MIDLATITUDES

Understanding the isolation of the winter polar vortex is a key factor in understanding the budgets of ozone and other trace constituents at high latitudes. If a large flow exists through the region of processed air inside the vortex (see Figure 3-2), then photochemical loss rates of ozone must be substantially larger than in an isolated vortex to cause observed ozone depletion (Anderson *et al.*, 1991). In addition, export of processed air to lower latitudes and lower altitudes may enhance ozone depletion in those regions (see Chapter 4) (Brune *et al.*, 1991). However, even if highly isolated during winter, processed air in the vortex has the potential to influence lower latitudes following vortex breakup in late winter/early spring. Significant progress has occurred in this assessment period in the modeling and interpretation of data related to the transport of air in and near the vortex. Trace constituent observations, radiative balance arguments, and various fluid mechanical models of the vortex have all provided valuable insights into vortex motion. In addition, the identification of a vortex edge region and a range of definitions for the vortex boundary have become important concepts. A large body of those results supports a substantial isolation in winter of an inner vortex region that is surrounded by an edge region in which stronger mixing to midlatitudes occurs.

3.5.1 Vortex Boundaries

The motion of mass into the winter polar vortex is poleward and downward from the upper stratosphere and mesosphere (see Figure 3-2) (Schoeberl and Hartmann, 1991; Schoeberl *et al.*, 1992). Flow out of the vortex in the lower stratosphere must cross through the outer boundary or edge region or through a lower boundary or bottom of the vortex. Since pressure increases with depth into the vortex from above, the velocities associated with such mass flow decrease accordingly. The edge region is denoted by the location of strong horizontal gradients in parameters associated with the vortex. These gradients provide definitions for a boundary of the vortex. Choices include the maximum in the speed of the polar wind jet, the maximum latitude gradient in PV, a large change in one or more trace constituents with latitude, and a kinematic barrier as identified in transport model simulations. Because of the convergence of the meridians at high latitudes, the vortex edge region represents most of the mass of the vortex and, hence, is crucial for the evaluation of outflow and its influence at midlatitudes.

The maximum wind speed in the circumpolar flow of the polar jet provides the most accessible definition of the boundary (see Figure 3-2). PV gradients, though obtained from highly derived quantities, are more directly related to dynamical barriers within the flow (Schoeberl *et al.*, 1992). PV combines the absolute vorticity of an air parcel with static stability expressed as the vertical gradient of potential temperature (Hoskins *et al.*, 1985). In isentropic and frictionless flow, PV is conserved, making it a useful diagnostic for air motion over limited periods. Large meridional gradients of PV (generally increasing poleward) form in the polar regions as a result of diabatic cooling and Rossby wave breaking in the winter season. The polar jet is a response to the temperature gradient formed by the cooling at high latitudes in winter. A boundary defined with a change in a trace constituent is often associated with processing of polar air by PSCs formed at the low vortex temperatures (Proffitt *et al.*, 1989b, c). As discussed above, processing results in chlorine activation, dehydration, denitrification, and, ultimately, ozone loss on the scale of the vortex. Finally,

a kinematic barrier to large-scale isentropic flow is revealed in the Lagrangian evolution of air masses on isentropic surfaces (Pierce and Fairlie, 1993). The approach uses assimilated wind fields to move material lines initialized on closed streamlines encircling the Antarctic vortex. In some instances, a particular material line is found which shows no irreversible deformation for periods of days to weeks. This "separating material line" defines a kinematic boundary to large-scale isentropic transport in the polar region. Material poleward of this separating material line remains highly isolated from the surrounding circulation.

These boundary definitions are interrelated since each is derived from or caused by features of the wind and temperature fields in the winter season. The kinematic barrier, the maximum PV gradient, and the jet maximum are generally located within a few degrees of latitude of each other within the polar jet core. However, transient distortions of the vortex caused in the lower stratosphere by tropospheric weather systems cause an interweaving and distortion of these boundaries within the edge region. While circumnavigating the vortex in the jet, an air parcel may cross the PV or jet maximum boundary while remaining inside the kinematic barrier and/or outside the chemical boundary. Thus, an evaluation of the vortex export of air that resides near a boundary will, in general, be dependent on the chosen boundary.

In the quantification of outflow, the choice of a vortex edge is complicated by the fact that much of the air "outside" of the vortex remains close to the edge and varies with the large-scale fluctuations of the vortex (Figure 15 in Rood *et al.*, 1992; Manney *et al.*, 1994c; Waugh *et al.*, 1994). For changes in midlatitude ozone, the important factors are the extent to which air undergoes horizontal transport away from the center of the vortex or away from the edge region to lower latitudes and the extent to which this air has undergone processing and, perhaps, loss of ozone. A substantial amount of processing can occur within the vortex edge region, particularly in the Antarctic vortex (Tao and Tuck, 1994). As a result, transport within the edge region, perhaps across a particular boundary, is of considerably less importance. In the evaluation of ozone loss photochemistry within the vortex, the total loss of processed air from the center of the vortex and edge region is the quantity of interest.

At the lower boundary of the vortex region, a transition is noted below which there is a much weaker barrier to transport out of the vortex region to lower latitudes (Tuck, 1989; Loewenstein *et al.*, 1989; Manney *et al.*, 1994c). The transition is clearly noted in the vertical distribution of long-lived stratospheric tracers. At these low altitudes (< 15 km), the polar jet is considerably weaker, consequently weakening the identification of vortex boundaries as defined above. Transport through the bottom of the vortex is driven by diabatic descent throughout the vortex lifetime as air cools, approaching radiative equilibrium over the Antarctic (Rosenfield *et al.*, 1994; Proffitt *et al.*, 1989b, 1990, 1993). The rate of cooling varies with time during the winter season, with the largest cooling rates occurring early when air is farthest from radiative equilibrium. Without strong barriers to horizontal transport, air that is transported through the lower vortex boundary is readily transported and mixed to lower latitudes. Processed air that leaves the vortex through the lower boundary rather than through the edge region has relatively less influence on midlatitude ozone because of the higher altitude of the ozone layer in midlatitudes.

3.5.2 Constituent Observations

Constituent observations from aircraft and satellites have been used as a diagnostic for vortex outflow in the winter from both vortices. In the Antarctic, the intense dehydration that occurs inside the vortex is of particular importance (see Section 3.3.2.5). Significant export of this dehydrated air to midlatitudes is considered to be a source of low values of $[2CH_4 + H_2O]$ above 400 K (about 15 km) outside the Antarctic vortex in September and October (Tuck, 1989; Kelly *et al.*, 1989; Tuck *et al.*, 1993). The value of CH_4 is included in the sum in order to account for H_2O produced in CH_4 oxidation in the stratosphere. Values of $[2CH_4 + H_2O]$ in the range 6.4 to 6.7 ppmv are characteristic of air that has passed through the tropical tropopause. The dehydration signal, defined as values below this range, extended to the subtropical jet in the early interpretation of satellite data sets, suggesting significant outflow in the 15 to 20 km altitude range from the vortex (Tuck *et al.*, 1993). Using the relative mass of the vortex in the Southern Hemisphere, a residence time of 30 days (e-folding time) is required to lower $[2CH_4 + H_2O]$ to the reported values

at midlatitudes. This corresponds to replacing the air in the vortex in approximately 90 days. Subsequent revisions of the satellite H_2O data set (version 17) significantly reduce the vertical and horizontal extent of the dehydration signature at midlatitudes (see Figure 3-18) (Russell, private communication, 1994), increasing the vortex replacement time to about 120 days. With a replacement time in this range, processed air inside the dehydrated Antarctic vortex can be characterized as largely isolated from influencing midlatitudes.

Further study of satellite observations of H_2O and CH_4 confirms the isolated character of the inner vortex (Pierce *et al.*, 1994). The distribution of these species over the winter reveals sustained diabatic descent accompanied by dehydration in the middle of the vortex. A gradient in dehydration is established between the center of the vortex and the jet core region where both normal and dehydrated air are found. Trajectory calculations that follow air parcels sampled by satellite for 25 days in early spring show no evidence for large-scale transport of significantly dehydrated jet core air into midlatitudes on either the 425 K (16 km) or 700 K (28 km) potential temperature surfaces. However, some irreversible transport from the edge region to lower latitudes does take place. In addition, the observations also show descent in the jet core region bringing down air with higher values of $[2CH_4 + H_2O]$.

In the Arctic, the absence of intense and widespread dehydration within the vortex makes the use of H_2O and CH_4 observations to detect vortex outflow more difficult. However, using PV as a substitute tracer in meteorological analyses, significant outflow of processed air from the vortex edge region was deduced for the vortex near 18 km (475 K) (Tuck *et al.*, 1992). This result is not inconsistent with an isolated center of the vortex because the outflow is from the vortex edge region. Analysis of aircraft observations shows that the residual motion in regions of high active chlorine inside the vortex is poleward and downward (Proffitt *et al.*, 1989c, 1990, 1993). The descent rates imply significant flow through the vortex lower boundary and large diabatic cooling rates. The Arctic region has also been used as a reference state to show the existence of denitrification and dehydration outside the Antarctic vortex (Tuck *et al.*, 1994). However, a quantitative inconsistency remains between the amount of denitrification and dehydration observed outside and inside the vortex, suggesting that the understanding of the respective removal processes or vortex export processes remains incomplete (see Section 3.3.2.5).

Apart from the effort to evaluate vortex outflow with the signature of dehydration, the basic observation of a large hemispheric asymmetry in water vapor in the lower stratosphere remains (Kelly *et al.*, 1990). After account is made for CH_4 oxidation in mid- to late-winter observations, water vapor in the Northern Hemisphere is larger by about 1.5 ppmv. The export of dehydrated air from the Antarctic is one explanation of the difference. Other explanations include the role of the tropics in removing water upon entry of air into the stratosphere (Tuck, 1989; Tuck *et al.*, 1993; Kelly *et al.*, 1989).

3.5.3 Radiative Cooling

To provide continuity for a substantial material flux outward through the Antarctic vortex, either a strong vertical transport between the middle and lower stratosphere or compensating inward horizontal transport is required. To exchange the mass of the vortex between 16 to 24 km with a 30-day time scale requires a vertical velocity of -0.1 cm s^{-1} at 16 km, which is equivalent to a potential temperature change near 1.3 K per day. However, both N_2O trends (Hartmann *et al.*, 1989; Loewenstein *et al.*, 1989; Schoeberl *et al.*, 1992) and radiative calculations (Shine, 1989; Rosenfield *et al.*, 1987; Schoeberl *et al.*, 1992; Manney *et al.*, 1994c; Strahan *et al.*, 1994) give much smaller values for this velocity, near -0.02 cm s^{-1} (0.2 K per day). Hence, a substantial body of interpretation supports a small net flux through the Antarctic vortex on sub-seasonal time scales.

Using more recent satellite observations of CH_4 and HF, rapid and deep descent into the Antarctic vortex has been observed (Russell *et al.*, 1993b; Schoeberl *et al.*, 1994; Fischer *et al.*, 1993). The descent rate is consistent with expected cooling rates in the upper stratosphere (Rosenfield *et al.*, 1994). Lower in the stratosphere, the descent rate slows, with an upper limit of 0.07 cm s^{-1}, corresponding to a replacement time of vortex air of about 120 days (Schoeberl *et al.*, 1994). This is consistent with the estimates made from the appearance of dehydrated air at midlatitudes in the satellite observations as noted above (see Section 3.5.2)

Consistent with the enhanced wave activity, the vertical flux between the middle and lower stratosphere in the Arctic is much larger than that found in the Antarctic; mean vertical velocities in the Arctic lower stratosphere are near -0.06 cm s^{-1}, or 0.6 K per day (Schoeberl *et al.*, 1992; Strahan *et al.*, 1994; Bauer *et al.*, 1994; Manney *et al.*, 1994c). Interannual variability in the wave disturbances in the Arctic also creates variability in the vortex transport. In isentropic trajectory studies examining 14 years of meteorological data, interannual differences were found in the predominance of inward and outward transport across the vortex boundary (Dahlberg and Bowman, 1994). Thus, quantification and prediction of interannual variability are fundamentally more difficult in the Arctic than in the Antarctic, impacting prediction of ozone changes both in the vortex and at midlatitudes.

3.5.4 Trajectory Models

In trajectory models, transport is examined by calculating the dispersion of an ensemble of notional air parcels over a typical one-month period, where the initial position of each parcel is specified. Studies are based on National Meteorological Center (NMC)-derived winds (Bowman, 1993) or on United Kingdom Meteorological Office-analyzed or modeled wind fields (Chen *et al.*, 1994; Manney *et al.*, 1994c; Pierce *et al.*, 1994; Pierce and Fairlie, 1993). Approaches include following individual parcels or ensembles of parcels forming material lines around vortex streamlines. In each case, large-scale horizontal transport through the vortex edge region in the Antarctic is small near 20 km (450 K isentropic level) (see Figure 3-24). In the figure, parcels that are initiated inside the vortex, as defined by column ozone values, remain in the vortex after 30 days. Similarly, the evolution of material lines in the vortex region reveals a kinematic barrier to large-scale isentropic flow out of the vortex (Pierce and Fairlie, 1993). However, substantial mixing and transport does occur across the lower vortex boundary (16 to 20 km, or 375 to 425 K). This transport is consistent with transport deduced from constituent observations (Tuck, 1989; Proffitt *et al.*, 1989b, 1990, 1993). However, omission of diabatic effects and inertial gravity waves in such isentropic trajectory studies may significantly underestimate transport and mixing processes at the vortex boundary (Pierce *et al.*, 1994).

In the Arctic vortex, large episodic disruptions occur as a result of planetary and synoptic wave disturbances. These events, which are less frequent in the Antarctic, are associated with transport of vortex air to midlatitudes in the lower stratosphere in the form of narrow tongues, or filaments, that are pulled from the edge of the vortex (Juckes and McIntyre, 1987; Norton, 1993; Pierce and Fairlie, 1993; Waugh *et al.*, 1994; Manney *et al.*, 1994c). These features are simulated in contour advection modeling in which high spatial resolution is maintained in the advection of material contours. The result is that approximately 5 to 10 percent of the vortex area is typically transported outward, with up to 20 percent during exceptionally large events (Waugh *et al.*, 1994). As an example, the total export from the vortex in January 1992 represents only nine percent of the area between 30°N and the vortex edge. There is also evidence that low-latitude air is entrained into the vortex during large disruptions, although the volume of air involved is probably small (Plumb *et al.*, 1994). At the rate of one to two planetary-scale events per month, the e-folding time for vortex exchange to midlatitudes by this mechanism is on the order of three to six months in the lower stratosphere, depending on the intensity and number of such events.

3.5.5 Three-Dimensional Models

In addition to trajectory models, three-dimensional (3-D) chemistry transport models (CTMs), 3-D mechanistic models, and 3-D general circulation models (GCMs) driven by winds from meteorological data assimilation systems support relatively limited flow through the vortex in winter. Three-dimensional models improve the evaluation of vortex outflow because they include both the horizontal transport through the vortex edge and the vertical transport connecting the lower stratosphere with the upper stratosphere and the mesosphere. For example, satellite data clearly show the descent of mesospheric air deep into the stratosphere sometime during the winter (see Figure 3-5) (Russell *et al.*, 1993b). Furthermore, since outflow will likely result from zonally asymmetric mechanisms driving transport at the vortex edge, both planetary-scale events and synoptic-scale events in the lower stratosphere can be considered in 3-D models.

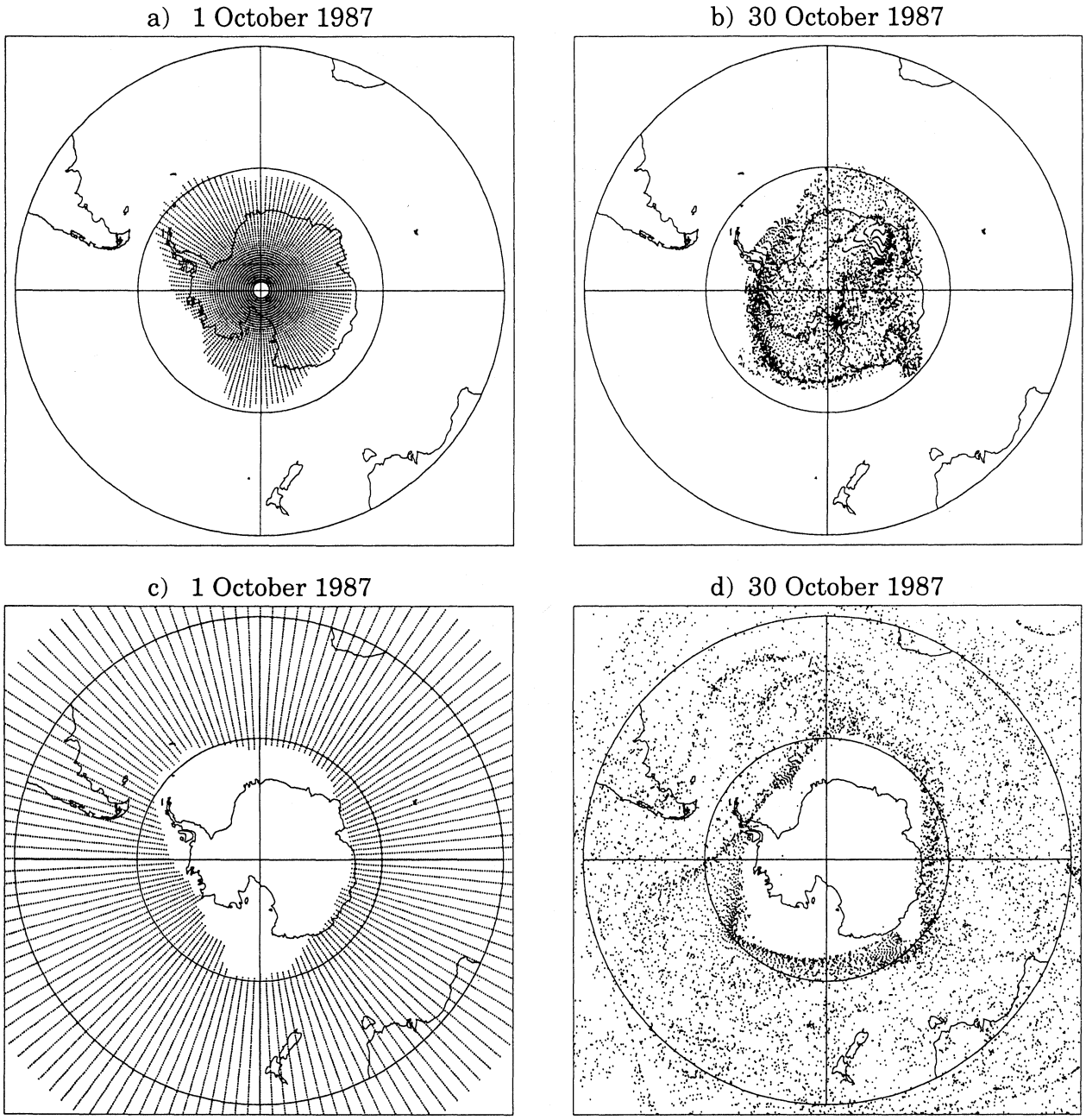

Figure 3-24. Evolution of air parcels on the 450 K (19 to 20 km) surface in the lower stratosphere over the period 1-30 October 1987 in the Antarctic. Initial locations for approximately 16,000 parcels on 1 October are indicated in (a) and (c) for interior and exterior vortex parcels, respectively. Final locations on 30 October are shown in (b) and (d) for the same groups, respectively. In each panel, the vertical line is the Greenwich meridian and the large and small circles correspond to 30° and 60° latitude, respectively. The 250 Dobson unit (DU) contour from the TOMS satellite observations of total ozone is used to separate the two parcel groups. Parcel motion is determined by trajectory calculations using winds derived from National Meteorological Center-analyzed height fields (Bowman, 1993).

In results from 3-D CTMs using winds from data assimilation systems, relatively little flow is found from within the vortex to midlatitudes (Rood *et al.*, 1992). These models incorporate diabatic and mixing effects that have not been considered in all trajectory and contour surgery models. In evaluations using aircraft, balloon, and satellite measurements, these models have been shown to represent synoptic- and planetary-scale variability on seasonal time scales. These models can simulate satellite ozone observations (*e.g.*, Limb Infrared Monitor of the Stratosphere [LIMS] and Total Ozone Mapping Spectrometer [TOMS]) for the entire winter season equally well in vortical and non-vortical air, suggesting that the transport mechanisms are at least qualitatively correct. These CTMs also show material peeling off the edge of the vortex into subpolar latitudes. This transport is wave-driven, with the planetary scales dominating the synoptic scales at altitudes above 20 mb. The results of Rood *et al.* (1992) in the Northern Hemisphere found that typically five percent of the air poleward of the subtropical jet stream and outside of the vortex had been processed by PSCs. During extreme events, this fraction could increase to 20 percent, in broad agreement with others (Plumb *et al.*, 1994; Tuck *et al.*, 1992).

A significant uncertainty in 3-D CTMs is whether or not the spatial resolution is adequate to simulate vortex processes. For instance, in Douglass *et al.* (1991), the general characteristics of aircraft ClO measurements were well simulated, but the detailed structure close to the vortex edge was not matched. Waugh *et al.* (1994) have shown that winds from the relatively coarse NMC analyses indeed contain enough information that, through differential advection, detailed structure can be meaningfully simulated. Therefore, in 3-D models and contour advection, the problem becomes one of choosing the appropriate mixing scale. The ability of carefully formulated 3-D models to perform seasonal integrations while maintaining realistic contrast between the vortex and midlatitudes suggests that they are reasonably mixed. Hence, the results suggest that it is not necessary to simulate the details of the fine structure, but it is necessary to simulate a self-consistent advective cascade with subscale mixing. Furthermore, transport studies driven by winds from assimilation analyses are likely to be of sufficient quality that transport across the vortex edge can be properly evaluated. High resolution may still be required for a quantitative evaluation of ozone depletion that occurs as processed air originating in the vortex is transported and mixed with lower latitude air.

Plumb *et al.* (1994) have also identified a discrete event of air being transported on horizontal surfaces into the lower vortex. Dahlberg and Bowman (1994) have performed a systematic evaluation of Arctic winters and find only limited transport into the vortex, with most of the activity remaining on the edge. Occasional inward transport is associated with planetary-scale blocking patterns and concomitant synoptic-scale lows that are associated with meteorological conditions in the troposphere. These studies all suggest only limited horizontal transport of extravortex air into the vortex throughout the winter.

Mechanistic 3-D models are a good tool for studying descent. They are forced from observations at some lower boundary (*e.g.*, 100 mb), with the stratosphere allowed to evolve self-consistently in balance with this forcing (*e.g.*, Fisher *et al.*, 1993). Because of the proximity of the forcing to the lower boundary, this approach has limited utility in the lower stratosphere. However, mechanistic models do provide an effective way to address the cold-pole problem (Mahlman and Umscheid, 1987) and other biases present in GCMs. Specifically, forcing from observations raises the polar temperature closer to observations, affording a more accurate representation of diabatic descent. Recent studies (*e.g.*, Jackman *et al.*, 1993; Nielsen *et al.*, 1994) show that mechanistic models can reproduce the descent of mesospheric ozone depletion and NO_2 enhancement that occurs during solar proton events (SPEs). This wintertime descent occurs across all stratospheric and mesospheric altitudes and requires consistent representation of mean-meridional flow in the mesosphere. The models do, in fact, represent the cross-equatorial transport of long-lived tracers observed in the mesosphere by satellite. Mechanistic models show unmixed descent consistent with satellite observations (Russell *et al.*, 1993b; Fisher *et al.*, 1993). Satellite data also indicate descent with little or no large-scale mixing across the vortex edge in the mid-stratosphere (Lahoz *et al.*, 1993). During midwinter, very little of the mesospheric air leaves the vortex in the lower stratosphere. This is consistent with the Stratospheric Aerosol and Gas Experiment (SAGE) NO_2 enhancements observed during an SPE. Mixing of mesospheric air that has

undergone descent occurs dramatically during vortex breakdown in the winter-to-spring seasonal transition, as has been observed in satellite data (Harwood *et al.*, 1993; Lahoz *et al.*, 1993). However, this is one-time mixing of air that was contained in the vortex, and does not provide a continual flow of air through the vortex. The mechanistic models establish that, given a realistic temperature distribution, radiative models calculate descent rates that are fundamentally in agreement with observed constituent behavior in the mid- to upper stratosphere. In the lower stratosphere, some uncertainty remains in modeling the relative effects of dynamical mixing and diabatic descent. However, Schoeberl *et al.* (1994) and Strahan *et al.* (1994) have shown that the aircraft N_2O data are in agreement with calculated radiative descent. The uncertainty that remains in the 3-D models will not substantially alter the arguments presented here.

GCMs provide an internally consistent, deterministic simulation of the atmosphere, although they cannot be used to simulate specific events for more than a few days, inhibiting direct day-to-day comparisons with constituent observations. Traditionally, GCMs underestimate polar temperatures (cold-pole), apparently due to a lack of dynamic activity (Mahlman and Umscheid, 1987). This leaves the model atmosphere too close to radiative equilibrium and, subsequently, leads to weak estimates of wintertime descent. The current generation of GCMs that extend up to the mesosphere (Strahan and Mahlman, 1994a, b; Boville, 1991; Cariolle *et al.*, 1992) has now been integrated for several seasonal cycles. In the Northern Hemisphere, the models can produce a disturbed flow in winter with the development of stratospheric warmings associated with the amplification of planetary waves. The model vortex is about 20 K warmer in the Northern Hemisphere than in the Southern Hemisphere, reasonably consistent with atmospheric observations. Comparisons with N_2O data show that the fall-to-winter descent can be simulated with considerable accuracy, and that the wintertime descent is maintained at a level comparable to observations (Strahan *et al.*, 1994). Transport of vortex edge air is simulated with mixing in the midlatitudes. Deep vortical air remains relatively isolated.

N_2O distributions from a GCM have also been compared with aircraft measurements (Strahan and Mahlman, 1994a, b). These studies show that, within the resolution constraints of the model, the processes that produce shredding from the vortex edge are consistent with observations. In addition, the mesoscale component of the variance, which is linked to planetary wave breaking processes, is also consistent in the Northern Hemisphere. A separate study of the N_2O aircraft observations supports only a limited outward flow near the vortex edge (Bacmeister *et al.*, 1992). These observations, when combined with theory and modeling results, provide a very powerful statement about transport through the vortex and model fidelity.

GCM simulations of the troposphere and stratosphere in the Antarctic are not as good as those in the Arctic, because the cold-pole problem is still significant and synoptic-scale activity is poorly represented in the southern ocean. In data assimilation approaches, the observations in the Southern Hemisphere are not sufficient to define many of the important waves. With less wave activity, the model atmosphere is closer to radiative equilibrium, resulting in less wintertime polar-night descent and a more isolated vortex. The observations of the Antarctic vortex strongly indicate that it is closer to radiative equilibrium than the Arctic vortex. The Antarctic temperatures are lower, the vortex is larger, and there is significantly less wave activity perturbing the flow, further suggesting that the Antarctic vortex is more isolated than the Arctic vortex.

These 3-D model approaches provide a consistent picture of dynamical processes of the polar vortex. The mechanisms in the 3-D global models are consistent with the barotropic models (*e.g.*, Juckes and McIntyre, 1987) and the contour advection models (*e.g.*, Waugh *et al.*, 1994) that have been used to isolate transport mechanisms. Most of the transport into and out of the vortex occurs along the edges, and deep vortical air is largely isolated throughout the winter. The material that is shred out of the vortex is spread broadly in midlatitudes, but satellite observations and model studies (Rood *et al.*, 1992, 1993) suggest that the midlatitudes are not homogeneously mixed. There is one-time mixing of the deep vortex air during the winter-to-spring transition, with processed air reaching mid- to low latitudes. There is continual circulation of midlatitude air towards the poles at high altitudes, followed by descent as the air enters polar night and cools. This circulation is largely on the edge of the vortex and should not see the full impact of polar processing. There can be substantial local mixing at low altitudes associated with dissipating synoptic

scales. Given the local nature of this transport, it does not require compensation by transport from above. In summary, given the seasonal lifetime of the vortex, the mixing times inferred from observations and models, the confinement of mixing to the edges, and the mixing in the winter-to-spring transition, it seems unlikely that the total volume of air that experiences polar chemical processing can exceed two times the volume of the midwinter vortex.

REFERENCES

Abbatt, J. P. D., and M. J. Molina, Heterogeneous interactions of $ClONO_2$ and HCl on nitric acid trihydrate at 202 K, *J. Phys. Chem., 96,* 7674-7679, 1992a.

Abbatt, J. P. D., and M. J. Molina, The heterogeneous reaction HOCl + HCl $\rightarrow$ Cl_2 + H_2O on ice and nitric acid trihydrate: Reaction probabilities and stratospheric implications, *Geophys. Res. Lett., 19,* 461-464, 1992b.

Adriani, A., T. Deshler, G. P. Gobbi, and G. Di Donfrancesco, Polar stratospheric clouds and volcanic aerosol during 1992 spring over McMurdo Station, Antarctica: Lidar and particle counter comparisons, *J. Geophys. Res.,* in press, 1994.

Anderson, J. G., W. H. Brune, S. A. Lloyd, D. W. Toohey, S. P. Sander, W. L. Starr, M. Loewenstein, and J. R. Podolske, Kinetics of O_3 destruction by ClO and BrO within the Antarctic vortex: An analysis based on *in situ* ER-2 data, *J. Geophys. Res., 94,* 11480-11520, 1989.

Anderson, J. G., D. W. Toohey, and W. H. Brune, Free radicals within the Antarctic vortex: The role of CFCs in Antarctic ozone loss, *Science, 251,* 39-46, 1991.

Anderson, J. G., and O. B. Toon, Airborne Arctic Stratospheric Expedition II: An overview, *Geophys. Res. Lett., 20,* 2499-2502, 1993.

Angell, J., Reexamination of the relation between depth of the Antarctic ozone hole, and equatorial QBO and SST, 1962-1992, *Geophys. Res. Lett., 20,* 1559-1562, 1993.

Arnold, F., K. Petzoldt, and E. Reimer, On the formation and sedimentation of stratospheric nitric acid aerosols—Implications for polar ozone destruction, *Geophys. Res. Lett., 19,* 677-680, 1992.

Atkinson, R. J., W. A. Matthews, P. A. Newman, and R. A. Plumb, Evidence of the mid-latitude impact of Antarctic ozone depletion, *Nature, 340,* 290-294, 1989.

Austin, J. N., N. Butchart, and K. P. Shine, Possibility of an Arctic ozone hole in a doubled-CO_2 climate, *Nature, 360,* 221-225, 1992.

Austin, J. N., and N. Butchart, The influence of climate change and the timing of stratospheric warmings on Arctic ozone depletion, *J. Geophys. Res., 99,* 1127-1145, 1994.

Bacmeister, J. T., M. R. Schoeberl, M. Loewenstein, J. R. Podolske, S. E. Strahan, and K. R. Chan, An estimate of the relative magnitude of small-scale tracer fluxes, *Geophys. Res. Lett., 19,* 1101-1104, 1992.

Baldwin, M. P., and D. O'Sullivan, Stratospheric effects of ENSO-related tropospheric circulation anomalies, *J. Climate,* in press, 1994.

Barath, F. T., M. C. Chavez, R. E. Cofield, D. A. Flower, M. A. Frerking, M. B. Gram, W. M. Harris, J. R. Holden, R. F. Jarnot, W. G. Kloezeman, G. J. Klose, G. K. Lau, M. S. Loo, B. J. Maddison, R. J. Mattauch, R. P. McKinney, G. E. Peckham, H. M. Pickett, G. Siebes, F. S. Soltis, R. A. Suttie, J. A. Tarsala, J. W. Waters, and W. J. Wilson, The Upper Atmosphere Research Satellite Microwave Limb Sounder Experiment, *J. Geophys. Res., 98,* 10751-10762, 1993.

Bauer, R., A. Engel, H. Franken, E. Klein, G. Kulessa, C. Schiller, U. Schmidt, R. Borchers, and J. Lee, Monitoring the vertical structure of the Arctic polar vortex over northern Scandinavia during EASOE: Regular N_2O profile observations, *Geophys. Res. Lett., 21,* 1211-1214, 1994.

Bell, W., N. A. Martin, T. D. Gardiner, N. R. Swann, P. T. Woods, P. F. Fogal, and J. W. Waters, Column measurements of stratospheric trace species over Åre, Sweden in the winter of 1991-92, *Geophys. Res. Lett., 21,* 1347-1350, 1994.

Borrmann, S., J. E. Dye, D. Baumgardner, J. C. Wilson, H. H. Jonsson, C. A. Brock, M. Loewenstein, J. R. Podolske, G. V. Ferry, and K. S. Barr, *In-situ* measurements of changes in stratospheric aerosol and the N_2O-aerosol relationship inside and outside of the polar vortex, *Geophys. Res. Lett., 20,* 2559-2562, 1993.

Boville, B., Sensitivity of simulated climate to model resolution, *J. Climate, 4,* 469-485, 1991.

Bowman, K. P., Large-scale isentropic mixing properties of the Antarctic polar vortex from analyzed winds, *J. Geophys. Res., 98,* 23013-23027, 1993.

Brandtjen, R., T. Klüpfel, D. Perner, and B. M. Knudsen, Airborne measurements during the European Arctic Stratospheric Ozone Experiment: Observation of OClO, *Geophys. Res. Lett., 21,* 1363-1366, 1994.

Brasseur, G. P., and C. Granier, Mount Pinatubo aerosols, chlorofluorocarbons, and ozone depletion, *Science, 257,* 1239-1242, 1992.

Browell, E. V., C. F. Butler, S. Ismail, P. A. Robinette, A. F. Carter, N. S. Higdon, O. B. Toon, M. R. Schoeberl, and A. F. Tuck, Airborne lidar observations in the wintertime Arctic stratosphere: Polar stratospheric clouds, *Geophys. Res. Lett., 17,* 385-388, 1990.

Browell, E. V., C. F. Butler, M. A. Fenn, W. B. Grant, S. Ismail, M. R. Schoeberl, O. B. Toon, M. Loewenstein, and J. R. Podolske, Ozone and aerosol changes during the 1991-1992 Airborne Arctic Stratospheric Expedition, *Science, 261,* 1155-1158, 1993.

Brune, W. H., J. G. Anderson, D. W. Toohey, D. W. Fahey, S. R. Kawa, R. L. Jones, D. S. McKenna, and L. R. Poole, The potential for ozone depletion in the Arctic polar stratosphere, *Science, 252,* 1260-1266, 1991.

Burkholder, J. B., R. K. Talukdar, A. R. Ravishankara, and S. Solomon, Temperature dependence of the HNO_3 UV absorption cross sections, *J. Geophys. Res., 98,* 22937-22948, 1994a.

Burkholder, J. B., R. K. Talukdar, and A. R. Ravishankara, Temperature dependence of the $ClONO_2$ UV absorption spectrum, *Geophys. Res. Lett., 21,* 585-588, 1994b.

Cacciani, M., P. Di Girolamo, A. di Sarra, G. Fiocco, and D. Fuà, Volcanic aerosol layers observed by lidar at South Pole, September 1991-June 1992, *Geophys. Res. Lett., 20,* 807-810, 1993.

Cariolle, D., A. Lasserre-Bigorry, and J. F. Boyer, A general circulation model simulation of the springtime Antarctic ozone decrease and its impact on midlatitudes, *J. Geophys. Res., 95,* 1883-1898, 1990.

Cariolle, D., M. Amodei, and P. Simon, Dynamics and the ozone distribution in the winter stratosphere: Modelling the inter-hemispheric differences, *J. Atmos. Terr. Phys., 54,* 627-640, 1992.

Carroll, M. A., R. W. Sanders, S. Solomon, and A. L. Schmeltekopf, Visible and near-ultraviolet spectroscopy at McMurdo Station, Antarctica 6. Observations of BrO, *J. Geophys. Res., 94,* 16633-16638, 1989.

Carslaw, K., B. P. Luo, S. L. Clegg, Th. Peter, P. Brimblecombe, and P. J. Crutzen, Stratospheric aerosol growth and HNO_3 gas phase depletion from coupled HNO_3 and water uptake by liquid particles, *Geophys. Res. Lett.,* in press, 1994.

Chen, P., J. R. Holton, A. O'Neill, and R. Swinbank, Quasi-horizontal transport and mixing in the Antarctic stratosphere, *J. Geophys. Res., 99,* 16851-16866, 1994.

Chipperfield, M. P., A 3-D model comparison of PSC processing during the Arctic winters of 1991/92 and 1992/93, *Annales Geophysicae, 12,* 342-354, 1994a.

Chipperfield, M. P., D. Cariolle, and P. Simon, A 3D transport model study of chlorine activation during EASOE, *Geophys. Res. Lett., 21,* 1467-1470, 1994b.

Chipperfield, M. P., D. Cariolle, and P. Simon, A three-dimensional transport model study of PSC processing during EASOE, *Geophys. Res. Lett., 21,* 1463-1466, 1994c.

Chu, L. T., M.-T. Leu, and L. F. Keyser, Heterogeneous reactions of $HOCl + HCl \rightarrow Cl_2 + H_2O$ and $ClONO_2 + HCl \rightarrow Cl_2 + HNO_3$ on ice surfaces at polar stratospheric conditions, *J. Phys. Chem.,* in press, 1994.

Cox, R. A., A. R. MacKenzie, R. H. Müller, Th. Peter, and P. J. Crutzen, Activation of stratospheric chlorine by reactions in liquid sulfuric acid, *Geophys. Res. Lett., 21,* 1439-1442, 1994.

Crewell, S., K. Künzi, H. Nett, T. Wehr, and P. Hartogh, Aircraft measurements of ClO and HCl during EASOE 1991/92, *Geophys. Res. Lett., 21,* 1267-1270, 1994.

Dahlberg, S. P., and K. P. Bowman, Climatology of large-scale isentropic mixing in the Arctic winter stratosphere from analyzed winds, *J. Geophys. Res., 99,* 20585-20599, 1994.

Danielsen, E. F., and H. Houben, Dynamics of the Antarctic stratosphere and implications for the ozone hole, *Anthropogene Beeinflussung der Ozonschicht,* 191-242, DECHEMA, Frankfurt-am-Main, 1988.

Deshler, T., B. J. Johnson, and W. R. Rozier, Changes in the character of polar stratospheric clouds over Antarctica in 1992 due to the Pinatubo volcanic aerosol, *Geophys. Res. Lett., 21,* 273-276, 1994.

deZafra, R. L., M. Jaramillo, A. Parrish, P. Solomon, R. Connor, and J. Barrett, High concentrations of chlorine monoxide at low altitudes in the Antarctic spring stratosphere: Diurnal variation, *Nature, 328,* 408-411, 1987.

Douglass, A. R., R. B. Rood, J. A. Kaye, R. S. Stolarski, D. J. Allen, and E. M. Larson, The influence of polar heterogeneous processes on reactive chlorine at middle latitudes: Three-dimensional model implications, *Geophys. Res. Lett., 18,* 25-28, 1991.

Douglass, A. R., R. B. Rood, J. W. Waters, L. Froidevaux, W. Read, L. S. Elson, M. Geller, Y. Chi, M. C. Cerniglia, and S. Steenrod, A 3D simulation of the early winter distribution of reactive chlorine in the north polar vortex, *Geophys. Res. Lett., 20,* 1271-1274, 1993.

Drdla, K., and R. P. Turco, Denitrification through PSC formation: A 1-D model incorporating temperature oscillations, *J. Atmos. Chem., 12,* 319, 1991.

Dritschel, D. G., and B. Legras, Modeling oceanic and atmospheric vortices, *Phys. Today,* 44-51, March 1993.

Dye, J. E., D. Baumgardner, B. W. Gandrud, S. R. Kawa, K. K. Kelly, M. Loewenstein, G. V. Ferry, K. R. Chan, and B. L. Gary, Particle size distributions in Arctic polar stratospheric clouds, growth and freezing of sulfuric acid droplets, and implications for cloud formation, *J. Geophys. Res., 97,* 8015-8034, 1992.

Eckman, R. S., R. E. Turner, W. T. Blackshear, T. D. A. Fairlie, and W. L. Grose, Some aspects of the interaction between chemical and dynamic processes relating to the Antarctic ozone hole, *Adv. Space Res., 13,* 311-319, 1993.

Fahey, D. W., S. Solomon, S. R. Kawa, M. Loewenstein, J. R. Podolske, S. E. Strahan, and K. R. Chan, A diagnostic for denitrification in the winter polar stratospheres, *Nature, 345,* 698-702, 1990a.

Fahey, D. W., K. K. Kelly, S. R. Kawa, A. F. Tuck, M. Loewenstein, K. R. Chan, and L. E. Heidt, Observations of denitrification and dehydration in the winter polar stratospheres, *Nature, 344,* 321-324, 1990b.

Fahey, D. W., S. R. Kawa, E. L. Woodbridge, P. Tin, J. C. Wilson, H. H. Jonsson, J. E. Dye, D. Baumgardner, S. Borrmann, D. W. Toohey, L. M. Avallone, M. H. Proffitt, J. J. Margitan, M. Loewenstein, J. R. Podolske, R. J. Salawitch, S. C. Wofsy, M. K. W. Ko, D. E. Anderson, M. R. Schoeberl, and K. R. Chan, *In situ* measurements constraining the role of sulfate aerosols in mid-latitude ozone depletion, *Nature, 363,* 509-514, 1993.

Farman, J. C., A. O'Neill, and R. Swinbank, The dynamics of the Arctic polar vortex during the EASOE campaign, *Geophys. Res. Lett., 21,* 1195-1198, 1994.

Fisher, M. A., A. O'Neill, and R. Sutton, Rapid descent of mesospheric air into the stratospheric polar vortex, *Geophys. Res. Lett., 20,* 1267-1270, 1993.

Fried, A., B. E. Henry, J. G. Calvert, and M. Mozurkewich, The reaction probability of N_2O_5 with sulfuric acid aerosols at stratospheric temperatures and compositions, *J. Geophys. Res., 99,* 3517-3532, 1994.

Garcia, R. R., F. Stordal, S. Solomon, and J. T. Kiehl, A new numerical model of the middle atmosphere 1. Dynamics and transport of tropospheric source gases, *J. Geophys. Res., 97,* 12967-12991, 1992.

Gerber, L., and N. Kämpfer, Millimeter-wave measurements of chlorine monoxide at the Jungfraujoch Alpine Station, *Geophys. Res. Lett., 21,* 1279-1282, 1994.

Gobbi, G. P., and A. Adriani, Mechanisms of formation of stratospheric clouds observed during the Antarctic late winter of 1992, *Geophys. Res. Lett., 20,* 1427-1430, 1993.

GRL, Special Section, The stratospheric and climatic effects of the 1991 Mt. Pinatubo eruption: An initial assessment, *Geophys. Res. Lett., 19,* 149-218, 1992.

Hanson, D. R., and A. R. Ravishankara, The reaction probabilities of $ClONO_2$ and N_2O_5 on 40 to 75 percent sulfuric acid solutions, *J. Geophys. Res., 96,* 17307-17314, 1991.

Hanson, D. R., and A. R. Ravishankara, Investigation of the reactive and nonreactive processes involving $ClONO_2$ and HCl on water and nitric acid doped ice, *J. Phys. Chem., 96,* 2682-2691, 1992.

Hanson, D. R., and A. R. Ravishankara, Uptake of HCl and HOCl onto sulfuric acid: Solubilities, diffusivities, and reaction, *J. Phys. Chem., 97,* 12309-12319, 1993.

Hanson, D. R., and A. R. Ravishankara, The reaction $ClONO_2$ + HCl on NAT, NAD, and frozen sulfuric acid and the hydrolysis of N_2O_5 and $ClONO_2$ on frozen sulfuric acid, *J. Geophys. Res., 98,* 22931-22936, 1994.

Hanson, D. R., A. R. Ravishankara, and S. Solomon, Heterogeneous reactions in sulfuric acid aerosols: A framework for model calculations, *J. Geophys. Res., 99,* 3615-3629, 1994.

Hartmann, D. L., L. E. Heidt, M. Loewenstein, J. R. Podolske, J. F. Vedder, W. L. Starr, and S. E. Strahan, Transport into the south polar vortex in early spring, *J. Geophys. Res., 94,* 16779-16795, 1989.

Harwood, R. S., E. S. Carr, L. Froidevaux, R. F. Jarnot, W. A. Lahoz, C. L. Lau, G. E. Peckham, W. G. Read, P. D. Ricaud, R. A. Suttie, and J. W. Waters, Springtime stratospheric water vapour in the Southern Hemisphere as measured by MLS, *Geophys. Res. Lett., 20,* 1235-1238, 1993.

Hofmann, D. J., and T. Deshler, Comparison of stratospheric clouds in the Antarctic and Arctic, *Geophys. Res. Lett., 16,* 1429-1432, 1989.

Hofmann, D. J., and S. Solomon, Ozone destruction through heterogeneous chemistry following the eruption of El Chichón, *J. Geophys. Res., 94,* 5029-5041, 1989.

Hofmann, D. J., J. M. Rosen, J. W. Harder, and J. V. Hereford, Balloon-borne measurements of aerosol, condensation nuclei, and cloud particles in the stratosphere at McMurdo Station, Antarctica, during the spring of 1987, *J. Geophys. Res., 94,* 11253-11269, 1989.

Hofmann, D. J., T. Deshler, F. Arnold, and H. Schlager, Balloon observations of nitric acid aerosol formation in the Arctic stratosphere: II. Aerosol, *Geophys. Res. Lett., 17,* 1279-1282, 1990.

Hofmann, D. J., and S. J. Oltmans, The effect of stratospheric water vapor on the heterogeneous reaction rate of $ClONO_2$ and H_2O for sulfuric acid aerosol, *Geophys Res. Lett., 19,* 2211-2214, 1992.

Hofmann, D. J., S. J. Oltmans, J. M. Harris, S. Solomon, T. Deshler, and B. J. Johnson, Observation and possible causes of new ozone depletion in Antarctica in 1991, *Nature, 359,* 283-287, 1992.

Hofmann, D. J., and S. J. Oltmans, Anomalous Antarctic ozone during 1992: Evidence for Pinatubo volcanic aerosol effects, *J. Geophys. Res., 98,* 18555-18561, 1993.

Hoskins, B. J., M. E. McIntyre, and A. W. Robertson, On the use and significance of isentropic potential vorticity maps, *Quart. J. Roy. Meteorol. Soc., 111,* 877-946, 1985.

Hübler, G., D. W. Fahey, K. K. Kelly, D. D. Montzka, M. A. Carroll, A. F. Tuck, L. E. Heidt, W. H. Pollock, G. L. Gregory, and J. F. Vedder, Redistribution of reactive odd nitrogen in the lower Arctic stratosphere, *Geophys. Res. Lett., 17,* 453-456, 1990.

Jackman, C. H., R. D. McPeters, A. R. Douglass, J. E. Nielsen, D. J. Allen, M. C. Cerniglia, R. B. Rood, and J. M. Zawodny, Polar stratospheric downward transport during northern winter observed by SAGE II and simulated using a three-dimensional model after the October 1989 solar proton events, *EOS Transactions, 74,* 178, 1993.

JPL, *Chemical Kinetics and Photochemical Data for Use in Stratospheric Modeling*, Evaluation No. 10, Jet Propulsion Laboratory, JPL Publication 92-20, 1992.

Juckes, M. N., and M. E. McIntyre, A high resolution one-layer model of breaking planetary waves in the stratosphere, *Nature, 328,* 590-596, 1987.

Kawa, S. R., D. W. Fahey, L. E. Heidt, W. H. Pollock, S. Solomon, D. E. Anderson, M. Loewenstein, M. H. Proffitt, J. J. Margitan, and K. R. Chan, Photochemical partitioning of the reactive nitrogen and chlorine reservoirs in the high-latitude stratosphere, *J. Geophys. Res., 97,* 7905-7923, 1992a.

Kawa, S. R., D. W. Fahey, K. K. Kelly, J. E. Dye, D. Baumgardner, B. W. Gandrud, M. Loewenstein, G. V. Ferry, and K. R. Chan, The Arctic polar stratospheric cloud aerosol: Aircraft measurements of reactive nitrogen, total water, and particles, *J. Geophys. Res., 97,* 7925-7938, 1992b.

Kelly, K. K., A. F. Tuck, D. M. Murphy, M. H. Proffitt, D. W. Fahey, R. L. Jones, D. S. McKenna, M. Loewenstein, J. R. Podolske, S. E. Strahan, G. V. Ferry, K. R. Chan, J. F. Vedder, G. L. Gregory, W. D. Hypes, M. P. McCormick, E. V. Browell, and L. E. Heidt, Dehydration in the lower Antarctic stratosphere during late winter and early spring, 1987, *J. Geophys. Res., 94,* 11317-11357, 1989.

Kelly, K. K., A. F. Tuck, L. E. Heidt, M. Loewenstein, J. R. Podolske, S. E. Strahan, and J. F. Vedder, A comparison of ER-2 measurements of stratospheric water vapor between the 1987 Antarctic and 1989 Arctic Airborne Missions, *Geophys. Res. Lett., 17,* 465-468, 1990.

Kent, G. S., L. R. Poole, M. P. McCormick, S. F. Schaffner, W. H. Hunt, and M. T. Osborn, Optical backscatter characteristics of Arctic polar stratospheric clouds, *Geophys. Res. Lett., 17,* 377-380, 1990.

Keys, J. G., P. V. Johnston, R. D. Blatherwick, and F. J. Murcray, Evidence for heterogeneous reactions in the Antarctic autumn stratosphere, *Nature, 361,* 49-51, 1993.

Kinne, S., O. B. Toon, and M. J. Prather, Buffering of stratospheric circulation by changing amounts of tropical ozone: A Pinatubo case study, *Geophys. Res. Lett., 19,* 1927-1930, 1992.

Koike, M., N. B. Jones, W. A. Matthews, P. V. Johnston, R. L. McKenzie, D. Kinnison, and J. Rodriguez, Impact of Pinatubo aerosols on the partitioning between NO_2 and HNO_3, *Geophys. Res. Lett., 21,* 597-600, 1994.

Kolb, C. E., D. R. Worsnop, M. S. Zahniser, P. Davidovits, L. F. Keyser, M.-T. Leu, M. J. Molina, D. R. Hanson, A. R. Ravishankara, L. R. Williams, and M. R. Tolbert, Laboratory studies of atmospheric heterogeneous chemistry, in *Current Problems in Atmospheric Chemistry*, edited by J. R. Barker, in press, 1994.

Kondo, Y., P. Aimedieu, M. Koike, Y. Iwasaka, P. A. Newman, U. Schmidt, W. A. Matthews, M. Hayashi, and W. R. Sheldon, Reactive nitrogen, ozone, and nitrate aerosols observed in the Arctic stratosphere in January 1990, *J. Geophys. Res., 97,* 13025-13038, 1992.

Kondo, Y., U. Schmidt, T. Sugita, P. Aimedieu, M. Koike, H. Ziereis, and Y. Iwasaka, Total reactive nitrogen, N_2O, and ozone in the winter Arctic stratosphere, *Geophys. Res. Lett., 21,* 1247-1250, 1994a.

Kondo, Y., W. A. Matthews, S. Solomon, M. Koike, M. Hayashi, K. Yamazaki, H. Nakajima, and K. Tsukui, Ground based measurements of column amounts of NO_2 over Syowa Station, Antarctica, *J. Geophys. Res., 99,* 14535-14548, 1994b.

Krueger, A., M. R. Schoeberl, P. A. Newman, and R. S. Stolarski, The 1991 Antarctic ozone hole: TOMS observations, *Geophys. Res. Lett., 19,* 1215-1218, 1992.

Labitzke, K., On the variability of the stratosphere in the Arctic regions in winter, *Ber. Bunsenges. Phys. Chem., 96,* 496-501, 1992.

Labitzke, K., and M. P. McCormick, Stratospheric temperature increases due to Pinatubo aerosols, *Geophys. Res. Lett., 19,* 207-210, 1992.

Lahoz, W. A., E. S. Carr, L. Froidevaux, R. S. Harwood, J. B. Kumer, J. L. Mergenthaler, G. E. Peckham, W. G. Read, P. D. Ricaud, A. E. Roche, and J. W. Waters, Northern Hemisphere mid-stratosphere vortex processes diagnosed from H_2O, N_2O, and potential vorticity, *Geophys. Res. Lett., 20,* 2671-2674, 1993.

Larsen, N., B. Knudsen, I. S. Mikkelsen, T. S. Jørgensen, and P. Eriksen, Ozone depletion in the Arctic stratosphere in early 1993, *Geophys. Res. Lett., 21,* 1611-1614, 1994.

Lefèvre, F., G. P. Brasseur, I. Folkins, A. K. Smith, and P. Simon, The chemistry of the 1991-92 stratospheric winter: Three-dimensional model simulations, *J. Geophys. Res., 99,* 8183-8195, 1994.

Liu, X., R. D. Blatherwick, F. J. Murcray, J. G. Keys, and S. Solomon, Measurements and model calculations of HCl column amounts and related parameters over McMurdo during the Austral spring in 1989, *J. Geophys. Res., 97,* 20795-20804, 1992.

Loewenstein, M., J. R. Podolske, K. R. Chan, and S. E. Strahan, Nitrous oxide as a dynamical tracer in the 1987 Airborne Antarctic Ozone Experiment, *J. Geophys. Res., 94,* 11589-11598, 1989.

Loewenstein, M., J. R. Podolske, D. W. Fahey, E. L. Woodbridge, P. Tin, A. Weaver, P. A. Newman, S. E. Strahan, S. R. Kawa, M. R. Schoeberl, and L. R. Lait, New observations of the NO_y/N_2O correlation in the lower stratosphere, *Geophys. Res. Lett., 20,* 2531-2534, 1993.

Lucic, D., N. R. P. Harris, J. A. Pyle, and R. L. Jones, Diagnosing ozone loss in the Northern Hemisphere for the 1991/92 winter, *J. Geophys. Res.*, in press, 1994.

Luo, B. P., Th. Peter, and P. J. Crutzen, Freezing of stratospheric aerosol droplets, *Geophys. Res. Lett., 21,* 1447-1450, 1994a.

Luo, B. P., Th. Peter, and P. J. Crutzen, HCl solubility and liquid diffusion in aqueous sulfuric acid under stratospheric conditions, *Geophys. Res. Lett., 21,* 49-52, 1994b.

Lutman, E. R., J. A. Pyle, R. L. Jones, D. J. Lary, A. R. MacKenzie, I. Kilbane-Dawe, N. Larsen, and B. M. Knudsen, Trajectory model studies of ClO_x activation during the 1991/92 Northern Hemispheric winter, *Geophys. Res. Lett., 21,* 1419-1422, 1994a.

Lutman, E. R., R. Toumi, R. L. Jones, D. J. Lary, and J. A. Pyle, Box model studies of ClO_x deactivation and ozone loss during the 1991/92 Northern Hemispheric winter, *Geophys. Res. Lett., 21,* 1415-1418, 1994b.

MacKenzie, A. R., B. M. Knudsen, R. L. Jones, and E. R. Lutman, The spatial and temporal extent of chlorine activation by polar stratospheric clouds in the Northern Hemisphere winters of 1988/89 and 1991/92, *Geophys. Res., Lett., 21,* 1423-1426, 1994.

Mahlman, J. D., H. Levy II, and W. J. Moxim, Three-dimensional tracer structure and behavior as simulated in two ozone precursor experiments, *J. Atmos. Sci., 37,* 655-685, 1980.

Mahlman, J. D., and L. Umscheid, Comprehensive modeling of the middle atmosphere: The influence of horizontal resolution, in *Transport Processes in the Middle Atmosphere*, edited by G. Visconti and R. Garcia, D. Reidel, Hingham, Massachusetts, 251-266, 1987.

Mankin, M. G., M. T. Coffey, and A. Goldman, Airborne observations of SO_2, HCl, and O_3 in the stratospheric plume of the Pinatubo volcano in July 1991, *Geophys. Res. Lett., 19,* 179-182, 1992.

Manney, G. L., and R. W. Zurek, Interhemispheric comparison of the development of the stratospheric polar vortex during fall: A 3-dimensional perspective for 1991-1992, *Geophys. Res. Lett., 20,* 1275-1278, 1993.

Manney, G. L., L. Froidevaux, J. W. Waters, L. S. Elson, E. F. Fishbein, R. W. Zurek, R. S. Harwood, and W. A. Lahoz, The evolution of ozone observed by UARS MLS in the 1992 late winter southern polar vortex, *Geophys. Res. Lett., 20,* 1279-1282, 1993.

Manney, G. L., R. W. Zurek, A. O'Neill, R. Swinbank, J. B. Kumer, J. L. Mergenthaler, and A. E. Roche, Stratospheric warmings during February and March 1993, *Geophys. Res. Lett., 21,* 813-816, 1994a.

Manney, G. L., L. Froidevaux, J. W. Waters, R. W. Zurek, W. G. Read, L. S. Elson, J. B. Kumer, J. L. Mergenthaler, A. E. Roche, A. O'Neill, R. S. Harwood, I. MacKenzie, and R. Swinbank, Chemical depletion of lower stratospheric ozone in the 1992-1993 northern winter vortex, *Nature, 370,* 429-434, 1994b.

Manney, G. L., R. W. Zurek, A. O'Neill, and R. Swinbank, On the motion of air through the stratospheric polar vortex, *J. Atmos. Sci., 51,* 2973-2994, 1994c.

McCormick, M. P., and R. E. Veiga, SAGE II measurements of early Pinatubo aerosols, *Geophys. Res. Lett., 19,* 155-158, 1992.

McElroy, M. B., R. J. Salawitch, S. C. Wofsy, and J. A. Logan, Reduction of Antarctic ozone due to synergistic interactions of chlorine and bromine, *Nature, 321,* 759-762, 1986.

McKenna, D. S., R. L. Jones, L. R. Poole, S. Solomon, D. W. Fahey, K. K. Kelly, M. H. Proffitt, W. H. Brune, M. Loewenstein, and K. R. Chan, Calculations of ozone destruction during the 1988/89 Arctic winter, *Geophys. Res. Lett., 17,* 553-556, 1990.

Middlebrook, A. M., B. G. Koehler, L. S. McNeill, and M. A. Tolbert, Formation of model polar stratospheric cloud films, *Geophys. Res. Lett., 24,* 2417-2420, 1992.

Middlebrook, A. M., L. T. Iraci, L. S. McNeill, B. G. Koehler, O. W. Saastad, and M. A. Tolbert, FTIR studies of thin H_2SO_4/H_2O films: Formation, water uptake, and solid-liquid phase changes, *J. Geophys. Res.*, in press, 1994.

Minton, T. K., C. M. Nelson, T. A. Moore, and M. Okamura, Direct observation of ClO from chlorine nitrate photolysis, *Nature, 328,* 1342-1345, 1992.

Molina, L. T., and M. J. Molina, Production of Cl_2O_2 from the self-reaction of the ClO radical, *J. Phys. Chem., 91,* 433-436, 1987.

Molina, M. J., R. Zhang, P. J. Wooldridge, J. R. McMahon, J. E. Kim., H. Y. Chang, and K. Beyer, Physical chemistry of the $H_2SO_4/HNO_3/H_2O$ system: Implications for the formation of polar stratospheric clouds and heterogeneous chemistry, *Science, 261,* 1418-1423, 1993.

Müller, R., and T. Peter, The numerical modeling of the sedimentation of polar stratospheric cloud particles, *Ber. Bunsenges. Phys. Chem., 96,* 353-361, 1992.

Murcray, F. J., J. R. Starkey, W. J. Williams, W. A. Matthews, U. Schmidt, P. Aimedieu, and C. Camy-Peyret, HNO_3 profiles obtained during the EASOE campaign, *Geophys. Res. Lett., 21,* 1223-1226, 1994.

Nagatani, R. M., A. J. Miller, M. E. Gelman, and P. A. Newman, A comparison of Arctic lower stratospheric winter temperatures for 1988-89 with temperatures since 1964, *Geophys. Res. Lett., 17,* 333-336, 1990.

Newman, P. A., L. R. Lait, M. R. Schoeberl, E. R. Nash, K. K. Kelly, D. W. Fahey, R. M. Nagatani, D. W. Toohey, L. M. Avallone, and J. G. Anderson, Stratospheric meteorological conditions in the Arctic polar vortex, 1991 to 1992, *Science, 261,* 1143-1146, 1993.

Nielsen, J. E., R. B. Rood, A. R. Douglass, M. C. Cerniglia, D. J. Allen, and J. E. Rosenfield, Tracer evolution in winds generated by a global spectral mechanistic model, *J. Geophys. Res., 99,* 5399-5420, 1994.

Norton, W. A., Breaking Rossby waves in a model stratosphere diagnosed by a vortex following system and contour advection technique, *J. Atmos. Sci., 51,* 654-673, 1993.

Ohtake, T., Freezing points of H_2SO_4 aqueous solutions and formation of stratospheric ice clouds, *Tellus, 45B,* 138-144, 1993.

Orsolini, Y. D., D. Cariolle, and M. Déqué, A GCM study of the late January 1992 'mini-hole' event observed during EASOE, *Geophys Res. Lett., 21,* 1459-1462, 1994.

Osborn, M. T., M. C. Pitts, K. A. Powell, and M. P. McCormick, SAM II aerosol measurements during the 1989 AASE, *Geophys. Res. Lett., 17,* 397-400, 1990.

Perliski, L. M., S. Solomon, and J. London, On the interpretation of the seasonal variations of stratospheric ozone, *Planet. Space Sci., 37,* 1527-1538, 1989.

Perner, D., A. Roth, and T. Klüpfel, Groundbased measurements of stratospheric OClO, NO_2, and O_3 at Søndre Strømfjord in winter 1991/92, *Geophys. Res. Lett., 21,* 1367-1370, 1994.

Peter, Th., C. Brühl, and P. J. Crutzen, Increase in the PSC-formation probability caused by high-flying aircraft, *Geophys. Res. Lett., 18,* 1465-1468, 1991.

Peter, Th., R. Müller, K. Drdla, K. Petzoldt, and E. Reimer, A micro-physical box model for EASOE: Preliminary results for the January/February 1990 PSC event over Kiruna, *Ber. Bunsenges. Phys. Chem., 96,* 362-367, 1992.

Petzoldt, K., B. Naujokat, and K. Neugebohren, Correlation between stratospheric temperature, total ozone, and tropospheric weather systems, *Geophys. Res. Lett., 21,* 1203-1206, 1994.

Pierce, R. B., and T. D. A. Fairlie, Chaotic advection in the stratosphere: Implications for the dispersal of chemically perturbed air from the polar vortex, *J. Geophys. Res., 98,* 18589-18595, 1993.

Pierce, R. B., W. L. Grose, J. M. Russell III, and A. F. Tuck, Spring dehydration in the Antarctic vortex observed by HALOE, *J. Atmos. Sci., 51,* 2931-2941, 1994.

Plumb, R. A., and M. K. W. Ko, Interrelationships between mixing ratios of long-lived stratospheric constituents, *J. Geophys. Res., 97,* 10145-10156, 1992.

Plumb, R. A., D. W. Waugh, R. J. Atkinson, P. A. Newman, L. R. Lait, M. R. Schoeberl, E. V. Browell, A. J. Simmons, and M. Loewenstein, Intrusions into the lower stratospheric Arctic vortex during the winter of 1991/92, *J. Geophys. Res., 99,* 1089-1105, 1994.

Podolske, J. R., M. Loewenstein, A. Weaver, S. E. Strahan, and K. R. Chan, Northern Hemisphere nitrous oxide morphology during the 1989 AASE and the 1991-92 AASE II campaigns, *Geophys. Res. Lett., 20,* 2535-2538, 1993.

Poole, L. R., S. Solomon, M. P. McCormick, and M. C. Pitts, The interannual variability of polar stratospheric clouds and related parameters in Antarctica during September and October, *Geophys. Res. Lett., 16,* 1157-1160, 1989.

Poole, L. R., and M. C. Pitts, Polar stratospheric cloud climatology based on Stratospheric Aerosol Measurement II observations from 1978 to 1989, *J. Geophys. Res., 99,* 13083-13089, 1994.

Prather, M. J., Catastrophic loss of ozone in dense volcanic clouds, *J. Geophys. Res., 97,* 10187-10191, 1992.

Proffitt, M. H., D. W. Fahey, K. K. Kelly, and A. F. Tuck, High-latitude ozone loss outside the Antarctic ozone hole, *Nature, 342,* 233-237, 1989a.

Proffitt, M. H., K. K. Kelly, J. A. Powell, B. L. Gary, M. Loewenstein, J. R. Podolske, S. E. Strahan, and K. R. Chan, Evidence for diabatic cooling and poleward transport within and around the 1987 Antarctic ozone hole, *J. Geophys. Res., 94,* 16797-16813, 1989b.

Proffitt, M. H., J. A. Powell, A. F. Tuck, D. W. Fahey, K. K. Kelly, A. J. Krueger, M. R. Schoeberl, B. L. Gary, J. J. Margitan, K. R. Chan, M. Loewenstein, and J. R. Podolske, A chemical definition of the boundary of the Antarctic ozone hole, *J. Geophys. Res., 94,* 11437-11448, 1989c.

Proffitt, M. H., J. J. Margitan, K. K. Kelly, M. Loewenstein, J. R. Podolske, and K. R. Chan, Ozone loss in the Arctic polar vortex inferred from high-altitude aircraft measurements, *Nature, 347,* 31-36, 1990.

Proffitt, M. H., S. Solomon, and M. Loewenstein, Comparison of 2-D model simulations of ozone and nitrous oxide at high latitudes with stratospheric measurements, *J. Geophys. Res., 97,* 939-944, 1992.

Proffitt, M. H., K. Aikin, J. J. Margitan, M. Loewenstein, J. R. Podolske, S. E. Strahan, and A. Weaver, Ozone loss inside the northern polar vortex during the 1991-1992 winter, *Science, 261,* 1150-1154, 1993.

Pyle, J. A., N. R. P. Harris, J. C. Farman, F. Arnold, G. Braathen, R. A. Cox, P. Faucon, R. L. Jones, G. Mégie, A. O'Neill, U. Platt, J.-P. Pommereau, U. Schmidt, and F. Stordal, An overview of the EASOE campaign, *Geophys. Res. Lett., 21,* 1191-1194, 1994.

Reber, C. A., The Upper Atmosphere Research Satellite, *EOS Transactions, 71,* 1867-1878, 1990.

Reber, C. A., C. E. Trevathan, R. J. McNeal, and M. R. Luther, The Upper Atmosphere Research Satellite (UARS) mission, *J. Geophys. Res., 98,* 10643-10647, 1993.

Reihs, C. M., D. M. Golden, and M. A. Tolbert, Nitric acid uptake by sulfuric acid solutions under stratospheric conditions: Determination of Henry's law solubility, *J. Geophys. Res., 95,* 16545-16550, 1990.

Rind, D., N. K. Balachandran, and R. Suozzo, Climate change and the middle atmosphere. Part II: The impact of volcanic aerosols, *J. Climate, 5,* 189-208, 1992.

Rind, D., E.-W. Chiou, W. Chu, S. Oltmans, J. Lerner, J. Larsen, M. P. McCormick, and L. McMaster, Overview of the Stratospheric Aerosol and Gas Experiment II water vapor observations: Method, validation, and data characteristics, *J. Geophys. Res., 98,* 4835-4856, 1993.

Roche, A. E., J. B. Kumer, J. L. Mergenthaler, G. A. Ely, W. G. Uplinger, J. F. Potter, T. C. James, and L. W. Sterritt, The Cryogenic Limb Array Etalon Spectrometer (CLAES) on UARS: Experiment description and performance, *J. Geophys. Res., 98,* 10763-10775, 1993a.

Roche, A. E., J. B. Kumer, and J. L. Mergenthaler, CLAES observations of $ClONO_2$ and HNO_3 in the Antarctic stratosphere, between June 15 and September 17, 1992, *Geophys. Res. Lett., 20,* 1223-1226, 1993b.

Roche, A. E., J. B. Kumer, J. L. Mergenthaler, R. W. Nightingale, W. G. Uplinger, G. A. Ely, J. F. Potter, D. J. Wuebbles, P. S. Connell, and D. E. Kinnison, Observations of lower stratospheric $ClONO_2$, HNO_3, and aerosol by the UARS CLAES experiment between January 1992 and April 1993, *J. Atmos. Sci., 51,* 2877-2902, 1994.

Rood, R. B., J. E. Nelson, R. S. Stolarski, A. R. Douglass, J. A. Kaye, and D. J. Allen, Episodic total ozone minima and associated effects on heterogeneous chemistry and lower stratospheric transport, *J. Geophys. Res., 97,* 7979-7996, 1992.

Rood, R. B., A. R. Douglass, J. A. Kaye, and D. B. Considine, Characteristics of wintertime and autumn nitric acid chemistry as defined by Limb Infrared Monitor of the Stratosphere (LIMS) data, *J. Geophys. Res., 98,* 18533-18545, 1993.

Rosenfield, J. E., M. R. Schoeberl, and M. A. Geller, A computation of the stratospheric diabatic circulation using an accurate radiative transfer model, *J. Atmos. Sci., 44,* 859-876, 1987.

Rosenfield, J. E., P. A. Newman, and M. R. Schoeberl, Computations of diabatic descent in the stratospheric polar vortex, *J. Geophys. Res., 99,* 16677-16689, 1994.

Russell, J. M., III, L. L. Gordley, J. H. Park, S. R. Drayson, W. D. Hesketh, R. J. Cicerone, A. F. Tuck, J. E. Frederick, J. E. Harries, and P. J. Crutzen, The Halogen Occultation Experiment, *J. Geophys. Res., 98,* 10777-10797, 1993a.

Russell, J. M., III, A. F. Tuck, L. L. Gordley, J. H. Park, S. R. Drayson, J. E. Harries, R. J. Cicerone, and P. J. Crutzen, HALOE Antarctic observations in the spring of 1991, *Geophys. Res. Lett., 20,* 719-722, 1993b.

Salawitch, R. J., S. C. Wofsy, M. B. McElroy, Chemistry of OClO in the Antarctic stratosphere: Implications for bromine, *Planet. Space Sci., 36,* 213-224, 1988.

Salawitch, R. J., G. P. Gobbi, S. C. Wofsy, and M. B. McElroy, Denitrification in the Antarctic stratosphere, *Nature, 339,* 525-527, 1989.

Salawitch, R. J., M. B. McElroy, J. H. Yatteau, S. C. Wofsy, M. R. Schoeberl, L. R. Lait, P. A. Newman, K. R. Chan, M. Loewenstein, J. R. Podolske, S. E. Strahan, and M. H. Proffitt, Loss of ozone in the Arctic vortex for the winter of 1989, *Geophys. Res. Lett., 17,* 561-564, 1990.

Salawitch, R. J., S. C. Wofsy, E. Gottlieb, L. R. Lait, P. A. Newman, M. R. Schoeberl, M. Loewenstein, J. R. Podolske, S. E. Strahan, M. H. Proffitt, C. R. Webster, R. D. May, D. W. Fahey, D. Baumgardner, J. E. Dye, J. C. Wilson, K. K. Kelly, J. W. Elkins, K. R. Chan, and J. G. Anderson, Chemical loss of ozone in the Arctic polar vortex in the winter of 1991-1992, *Science, 261,* 1146-1149, 1993.

Sanders, R. W., S. Solomon, J. P. Smith, L. Perliski, H. L. Miller, G. H. Mount, J. G. Keys, and A. L. Schmeltekopf, Visible and near-ultraviolet spectroscopy at McMurdo Station, Antarctica 9. Observations of OClO from April to October 1991, *J. Geophys. Res., 98,* 7219-7228, 1993.

Santee, M. L., W. G. Read, J. W. Waters, L. Froidevaux, G. L. Manney, D. A. Flower, R. F. Jarnot, R. S. Harwood, and G. E. Peckham, Interhemispheric differences in polar stratospheric HNO_3, H_2O, ClO, and O_3 from UARS MLS, submitted to *Science,* 1994.

Schauffler, S. M., L. E. Heidt, W. H. Pollock, T. M. Gilpin, J. F. Vedder, S. Solomon, R. A. Lueb, and E. L. Atlas, Measurements of halogenated organic compounds near the tropical tropopause, *Geophys. Res. Lett., 20,* 2567-2570, 1993.

Schiller, C., A. Wahner, U. Platt, H.-P. Dorn, J. Callies, and D. H. Ehhalt, Near UV atmospheric absorption measurements of column abundances during Airborne Arctic Stratospheric Expedition, January-February 1989: 2. OClO observations, *Geophys. Res. Lett., 17,* 501-504, 1990.

Schlager, H., and F. Arnold, Measurements of stratospheric gaseous nitric acid in the winter Arctic vortex using a novel rocket-borne mass spectrometric method, *Geophys. Res. Lett., 17,* 433-436, 1990.

Schmidt, U., R. Bauer, A. Khedim, E. Klein, G. Kulessa, and C. Schiller, Profile observations of long-lived trace gases in the Arctic vortex, *Geophys. Res. Lett., 18,* 767-770, 1991.

Schmidt, U., R. Bauer, A. Engel, R. Borchers, and J. Lee, The variation of available chlorine, Cl_y, in the Arctic polar vortex during EASOE, *Geophys. Res. Lett., 21,* 1215-1218, 1994.

Schoeberl, M. R., M. H. Proffitt, K. K. Kelly, L. R. Lait, P. A. Newman, J. E. Rosenfield, M. Loewenstein, J. R. Podolske, S. E. Strahan, and K. R. Chan, Stratospheric constituent trends from ER-2 profile data, *Geophys. Res. Lett., 17,* 469-472, 1990.

Schoeberl, M. R., and D. L. Hartmann, The dynamics of the stratospheric polar vortex and its relation to springtime ozone depletions, *Science, 251,* 46-52, 1991.

Schoeberl, M. R., L. R. Lait, P. A. Newman, and J. E. Rosenfield, The structure of the polar vortex, *J. Geophys. Res., 97,* 7859-7882, 1992.

Schoeberl, M. R., A. R. Douglass, R. S. Stolarski, P. A. Newman, L. R. Lait, D. W. Toohey, L. M. Avallone, J. G. Anderson, W. H. Brune, D. W. Fahey, and K. K. Kelly, The evolution of ClO and NO along air parcel trajectories, *Geophys. Res. Lett., 20,* 2511-2514, 1993a.

Schoeberl, M. R., R. S. Stolarski, A. R. Douglass, P. A. Newman, L. R. Lait, J. W. Waters, L. Froidevaux, and W. G. Read, MLS ClO observations and Arctic polar vortex temperatures, *Geophys. Res. Lett., 20,* 2861-2864, 1993b.

Schoeberl, M. R., M. Luo, and J. E. Rosenfield, An analysis of the Antarctic HALOE trace gas observations, *J. Geophys. Res.,* in press, 1994.

Shine, K. P., Sources and sinks of zonal momentum in the middle atmosphere diagnosed using the diabatic circulation, *Quart. J. Roy. Meteorol. Soc., 115,* 265-292, 1989.

Solomon, S., Progress towards a quantitative understanding of Antarctic ozone depletion, *Nature, 347,* 347-354, 1990.

Solomon, S., R. R. Garcia, F. S. Rowland, and D. J. Wuebbles, On the depletion of Antarctic ozone, *Nature, 321,* 755-758, 1986.

Solomon, S., R. W. Sanders, M. A. Carroll, and A. L. Schmeltekopf, Visible and near-ultraviolet spectroscopy at McMurdo Station, Antarctica 5. Observations of the diurnal variations of BrO and OClO, *J. Geophys. Res., 94,* 11393-11403, 1989.

Solomon, S., and J. G. Keys, Seasonal variations in Antarctic NO_x chemistry, *J. Geophys. Res., 97,* 7971-7978, 1992.

Solomon, S., R. W. Sanders, R. R. Garcia, and J. G. Keys, Increased chlorine dioxide over Antarctica caused by volcanic aerosols from Mount Pinatubo, *Nature, 363,* 245-248, 1993.

Strahan, S. E., and J. D. Mahlman, Evaluation of the SKYHI general circulation model using aircraft N_2O measurements: 1. Polar winter stratospheric meteorology and tracer morphology, *J. Geophys. Res., 99,* 10305-10318, 1994a.

Strahan, S. E., and J. D. Mahlman, Evaluation of the SKYHI general circulation model using aircraft N_2O measurements: 2. Tracer variability and diabatic meridional circulation, *J. Geophys. Res., 99,* 10319-10332, 1994b.

Strahan, S. E., J. E. Rosenfield, M. Loewenstein, J. R. Podolske, and A. Weaver, Evolution of the 1991-1992 Arctic vortex and comparison with the GFDL SKYHI general circulation model, *J. Geophys. Res., 99,* 20713-20723, 1994.

Tabazadeh, A., and R. P. Turco, Stratospheric chlorine injection by volcanic eruptions: HCl scavenging and implications for ozone, *Science, 260,* 1082-1086, 1993.

Tabazadeh, A., R. P. Turco, and M. Z. Jacobson, A model for studying the composition and chemical effects of stratospheric aerosols, *J. Geophys. Res., 99,* 12897-12914, 1994.

Tao, X., and A. F. Tuck, On the distribution of cold air near the vortex edge in the lower stratosphere, *J. Geophys. Res., 99,* 3431-3450, 1994.

Taylor, F. W., C. D. Rodgers, J. G. Whitney, S. T. Werrett, J. J. Barnett, G. D. Peskett, P. Venters, J. Ballard, C. W. P. Palmer, R. J. Knight, P. Morris, T. Nightingale, and A. Dudhia, Remote sensing of atmospheric structure and composition by pressure modulator radiometry from space: The ISAMS experiment on UARS, *J. Geophys. Res., 98,* 10799-10814, 1993.

Toohey, D. W., J. G. Anderson, W. H. Brune, and K. R. Chan, *In situ* measurements of BrO in the Arctic stratosphere, *Geophys. Res. Lett., 17,* 513-516, 1990.

Toohey, D. W., L. M. Avallone, L. R. Lait, P. A. Newman, M. R. Schoeberl, D. W. Fahey, E. L. Woodbridge, and J. G. Anderson, The seasonal evolution of reactive chlorine in the Northern Hemisphere stratosphere, *Science, 261,* 1134-1136, 1993.

Toon, G. C., C. B. Farmer, L. L. Lowes, P. W. Schaper, J.-F. Blavier, and R. H. Norton, Infrared aircraft measurements of stratospheric composition over Antarctica during September 1987, *J. Geophys. Res., 94,* 16571-16596, 1989a.

Toon, G. C., C. B. Farmer, P. W. Schaper, L. L. Lowes, and R. H. Norton, Composition measurements of the 1989 Arctic winter stratosphere by airborne infrared solar absorption spectroscopy, *J. Geophys. Res., 97,* 7939-7962, 1992.

Toon, O. B., R. P. Turco, J. Jordan, J. Goodman, and G. Ferry, Physical processes in polar stratospheric ice clouds, *J. Geophys. Res., 94,* 11359-11380, 1989b.

Toon, O. B., E. V. Browell, S. Kinne, and J. Jordan, An analysis of lidar observations of polar stratospheric clouds, *Geophys. Res., Lett., 17,* 393-396, 1990a.

Toon, O. B., R. P. Turco, and P. Hamill, Denitrification mechanisms in the polar stratospheres, *Geophys. Res., Lett., 17,* 445-448, 1990b.

Toumi, R., R. L. Jones, and J. A. Pyle, Stratospheric ozone depletion by $ClONO_2$ photolysis, *Nature, 365,* 37-39, 1993.

Trepte, C. R., R. E. Veiga, and M. P. McCormick, The poleward dispersal of Mount Pinatubo volcanic aerosol, *J. Geophys. Res., 98,* 18563-18573, 1993.

Tuck, A. F., Synoptic and chemical evolution of the Antarctic vortex in late winter and early spring, 1987, *J. Geophys. Res., 94,* 11687-11737, 1989.

Tuck, A. F., T. Davies, S. J. Hovde, M. Noguer-Alba, D. W. Fahey, S. R. Kawa, K. K. Kelly, D. M. Murphy, M. H. Proffitt, J. J. Margitan, M. Loewenstein, J. R. Podolske, S. E. Strahan, and K. R. Chan, Polar stratospheric cloud processed air and potential vorticity in the Northern Hemisphere lower stratosphere at mid-latitudes during winter, *J. Geophys. Res., 97,* 7883-7904, 1992.

Tuck, A. F., J. M. Russell III, and J. E. Harries, Stratospheric dryness: Antiphased desiccation over Micronesia and Antarctica, *Geophys. Res. Lett., 20,* 1227-1230, 1993.

Tuck, A. F., D. W. Fahey, M. Loewenstein, J. R. Podolske, K. K. Kelly, S. J. Hovde, D. M. Murphy, and J. W. Elkins, Spread of denitrification from 1987 Antarctic and 1988-1989 Arctic stratospheric vortices, *J. Geophys. Res., 99,* 20573-20583, 1994.

Tung, K. K., M. K. W. Ko, J. M. Rodriguez, and N.-D. Sze, Are Antarctic ozone variations a manifestation of dynamics or chemistry?, *Nature, 322,* 811-814, 1986.

Van Doren, J. M., L. R. Watson, P. Davidovits, D. R. Worsnop, M. S. Zahniser, and C. E. Kolb, Uptake of N_2O_5 and HNO_3 by aqueous sulfuric acid droplets, *J. Phys. Chem., 95,* 1684-1689, 1991.

van Loon, H., and K. Labitzke, Interannual variations in the stratosphere of the Northern Hemisphere: A description of some probable influences, in *Interactions between Global Climate Subsystems, The Legacy of Hann, Geophysical Monograph, 75,* IUGG Volume 15, 111-122, 1993.

von Clarmann, T., H. Fischer, F. Friedl-Valoon, A. Linden, H. Oelhaf, C. Piesch, M. Seefeldner, and W. Völker, Retrieval of stratospheric O_3, HNO_3, and $ClONO_2$ profiles from 1992 MIPAS-B limb emission spectra: Method, results, and error analysis, *J. Geophys. Res., 98,* 20495-20506, 1993.

von der Gathen, P., M. Rex, N. R. P. Harris, D. Lucic, B. Knudsen, R. Fabian, H. Fast, I. B. Mikkelsen, M. Rummukainen, J. Staehelin, and C. Varotsos, Chemical depletion of ozone observed during the 1991/1992 winter, submitted to *J. Geophys. Res.*, 1994.

Wahner, A., J. Callies, H.-P. Dorn, U. Platt, and C. Schiller, Near UV atmospheric absorption measurements of column abundances during Airborne Arctic Stratospheric Expedition, January-February 1989: 1. Technique and NO_2 observations, *Geophys. Res. Lett., 17,* 497-500, 1990a.

Wahner, A., J. Callies, H.-P. Dorn, U. Platt, and C. Schiller, Near UV atmospheric absorption measurements of column abundances during Airborne Arctic Stratospheric Expedition, January-February 1989: 3. BrO observations, *Geophys. Res. Lett., 17,* 517-520, 1990b.

CHAPTER 4

TROPICAL AND MIDLATITUDE OZONE

Contents

SCIENTIFIC SUMMARY

Since the last Assessment, much new information has been obtained about the photochemical and dynamical processes that influence ozone concentrations at middle latitudes. Measurements in the lower stratosphere have significantly increased our confidence in the basic gas phase and heterogeneous processes affecting ozone at middle latitudes, although some discrepancies still exist. Laboratory studies have provided data that have led to an improved quantification of the photochemical processes that affect ozone at middle latitudes. Understanding of the dynamical factors influencing middle latitudes has improved, although significant uncertainties remain. The relative contributions of these different processes to the ozone trends observed middle latitude are still poorly understood and important uncertainties are still outstanding.

The major new findings are:

Photochemical Processes

- Observations, coupled with photochemical model calculations, have established with little doubt the role of the heterogeneous hydrolysis of N_2O_5 on the sulfate aerosol layer. However, there are instances where discrepancies still arise, and it is unclear whether these reflect deficiencies in modeling known chemistry (*e.g.*, imperfect knowledge of aerosol surface areas, photolysis rates, etc.) or, more profoundly, missing chemical processes.

- Measurements of radical species in the low stratosphere have provided direct confirmation that *in situ* photochemical ozone loss in the lower stratosphere at midlatitudes is dominated by HO_x and (man-made) halogen chemistry, and not by (largely natural) NO_x chemistry. Nevertheless, NO_x chemistry exerts an important control on the effectiveness of the halogen loss cycles. Current photochemical models can reproduce observed radical concentration changes and coupling between different chemical families, provided that heterogeneous reactions are incorporated and that the source gases are suitably constrained by observations.

- Satellite and *in situ* measurements of chlorine monoxide (ClO) concentrations in the low stratosphere at middle latitudes in both hemispheres show the existence of a seasonal cycle with maximum ClO during winter months. This variation appears to be broadly consistent with changes in NO_x due to *in situ* heterogeneous processes but does not appear consistent with the timing of springtime vortex dilution or wintertime flow through the vortex.

- There is evidence that the hydrolysis of chlorine nitrate ($ClONO_2$) on sulfate aerosols can occur at low temperatures and may be important in middle latitudes under high aerosol loading conditions.

- There are unresolved discrepancies between models and observations regarding the partitioning between reservoir and reactive species, notably the ratio of ClO_x to HCl. Even when constrained by observed source gas fields and radical species, photochemical models in the low stratosphere significantly overestimate observed HCl amounts. In the upper stratosphere models overestimate the ClO/HCl ratio.

Laboratory Studies

- Recent studies have confirmed that N_2O_5 hydrolysis on sulfate aerosol surfaces is fast and occurs readily under most stratospheric conditions, while reactions that lead directly to chlorine activation depend strongly on atmospheric temperature and humidity.

- The rate of the reaction of BrO with HO_2 has been revised upwards by a factor of 6, implying a much larger bromine-catalyzed ozone loss in the low stratosphere.

TROPICAL/MIDLATITUDE PROCESSES

- Quenching rates for vibrationally excited O_2 appear to be faster than previously thought, reducing the likely importance of the photolysis of vibrationally excited O_2 as a source of ozone in the upper stratosphere. The discrepancy between observed and modeled ozone in this region still persists.

Dynamical Processes

- The transport of air from polar regions has the potential to influence ozone concentrations at middle latitudes. While there are uncertainties about the relative contributions of transport and *in situ* chemistry for midlatitude ozone loss, both processes directly involve ozone destruction by bromine- and chlorine-catalyzed reactions.

- Observations and models indicate that, above about 16 km in winter, air at midlatitudes is mixed relatively efficiently and that influx of air from the tropics and from the interior of the polar vortex is weak. However, the importance of the erosion of air from the edge of the polar vortex relative to *in situ* chemical effects for midlatitude ozone loss is poorly known.

- Below 16 km, air is more readily transported between polar regions and midlatitudes. The influence of this transport on midlatitude ozone loss has not been quantified.

Eruption of the Mt. Pinatubo Volcano

- The eruption of Mt. Pinatubo in 1991 led to a massive increase in sulfate aerosol in the lower stratosphere. There is compelling evidence that this led to significant, but temporary, changes in the partitioning of NO_x, reactive halogen compounds, and abundances of HO_x in the low and mid-stratosphere at middle latitudes in such a way as to accelerate photochemical ozone loss. However, there is also evidence that circulation changes associated with heating on Mt. Pinatubo aerosols led to significant changes in the distribution of ozone in the tropics and middle latitudes. Changes in photolysis rates arising directly from the presence of volcanic aerosols are also thought to have affected ozone amounts.

4.1 GENERAL INTRODUCTION

In the light of the observed trends in ozone away from polar regions, a wide range of observational and modeling studies have been focused on the midlatitude lower stratosphere. A large number of dynamical and photochemical mechanisms that can influence the concentrations of stratospheric ozone have been identified. Those processes that are now thought to be the more important for midlatitude ozone loss are shown schematically in Figure 4-1. Assessments of the importance of chemical and dynamical processes are given in Sections I and II respectively.

I. Chemical Processes influencing Middle Latitude and Tropical Ozone

4.2 INTRODUCTION

The main photochemical processes that are thought to be important in midlatitude ozone photochemistry are shown schematically in Figure 4-1. The diagram is intended to show the winter months when the polar vortex is well established.

Ozone is produced by the photolysis of O_2 at wavelengths shorter than 242 nm to give oxygen atoms, followed by recombination **(1)**. Variations in the solar output, for example during the 11-year solar cycle, lead directly to small changes in the photolysis of O_2 and thus to a correlated change in ozone amounts **(2)**. Catalytic ozone loss occurs through a range of gas phase chemical cycles **(3)**, those currently thought to be most important in the low stratosphere at midlatitudes being shown in the figure. It is known that at middle latitudes the hydrolysis of N_2O_5 **(4)** can proceed effectively on sulfate aerosols, reducing the available NO_x and indirectly increasing the degree of chlorine activation. At the lower temperatures present at higher latitudes, the hydrolysis of chlorine nitrate ($ClONO_2$) can occur **(5)**, leading directly to increased chlorine activation. In the colder polar regions, chlorine activation on polar stratospheric clouds may also occur **(6)**. Processes **(4)** and **(5)** are dependent on the aerosol loading in the stratosphere, and thus on the level of volcanic activity.

Processes **(4)** and **(5)** have the effect of altering the balance of photochemical ozone loss by the different chemical cycles shown, reducing the effectiveness of the NO_x-only cycles in the low stratosphere in favor of the HO_x-only and coupled HO_x-halogen cycles. Information leading to this picture is discussed below.

4.2.1 Laboratory Studies of Photochemistry and Gas Phase Kinetics

Several new laboratory measurements of rate parameters and absorption cross sections (DeMore *et al.*, 1992) are of direct consequence for understanding ozone loss in the tropics and midlatitudes.

The photolysis of nitric acid (HNO_3) in the atmosphere is important because it affects NO_x concentrations and thus, indirectly, ClO_x amounts. The temperature dependence of the HNO_3 absorption cross section (Rattigan *et al.*, 1992; Burkholder *et al.*, 1993) and the wavelength dependence of the hydroxyl radical (OH) quantum yield from HNO_3 photolysis (Turnipseed *et al.*, 1992; Schiffman *et al.*, 1993) have now been measured. The OH yield was confirmed to be nearly unity at long wavelengths, but other products, such as HONO, become more important at wavelengths shorter than 250 nm. The absorption cross section shows a temperature dependence (smaller at lower temperatures) that is strongest at wavelengths longer than 300 nm. As a result, the greatest effect on the calculated photolysis rate occurs at altitudes below about 28 km (Burkholder *et al.*, 1993). These new data will yield more accurate calculations of the HNO_3 photolysis rate in photochemical models, but the magnitude of the effect will depend on the prior formulation used by each model.

The product yield from $ClONO_2$ photolysis at 193 and 248 nm has also been investigated (Minton *et al.*, 1992), indicating that the products are split roughly evenly between $ClO + NO_2$ and $Cl + NO_3$. In contrast to prior measurements, no evidence was found for O-atom formation. However, it must be recognized that most $ClONO_2$ photolysis takes place at wavelengths longer than ~280 nm, where different products may form. If a similar effect were to be present at longer wavelengths, the result would be a reduction in the efficiency of ozone destruction from $ClONO_2$ photolysis (Toumi *et al.*, 1993c). In addition, the quantum yields for NO_3 photolysis between 570 and 635 nm have recently been remeasured (Orlando *et al.*, 1993) and give photolysis rates in reasonable agreement with the currently recom-

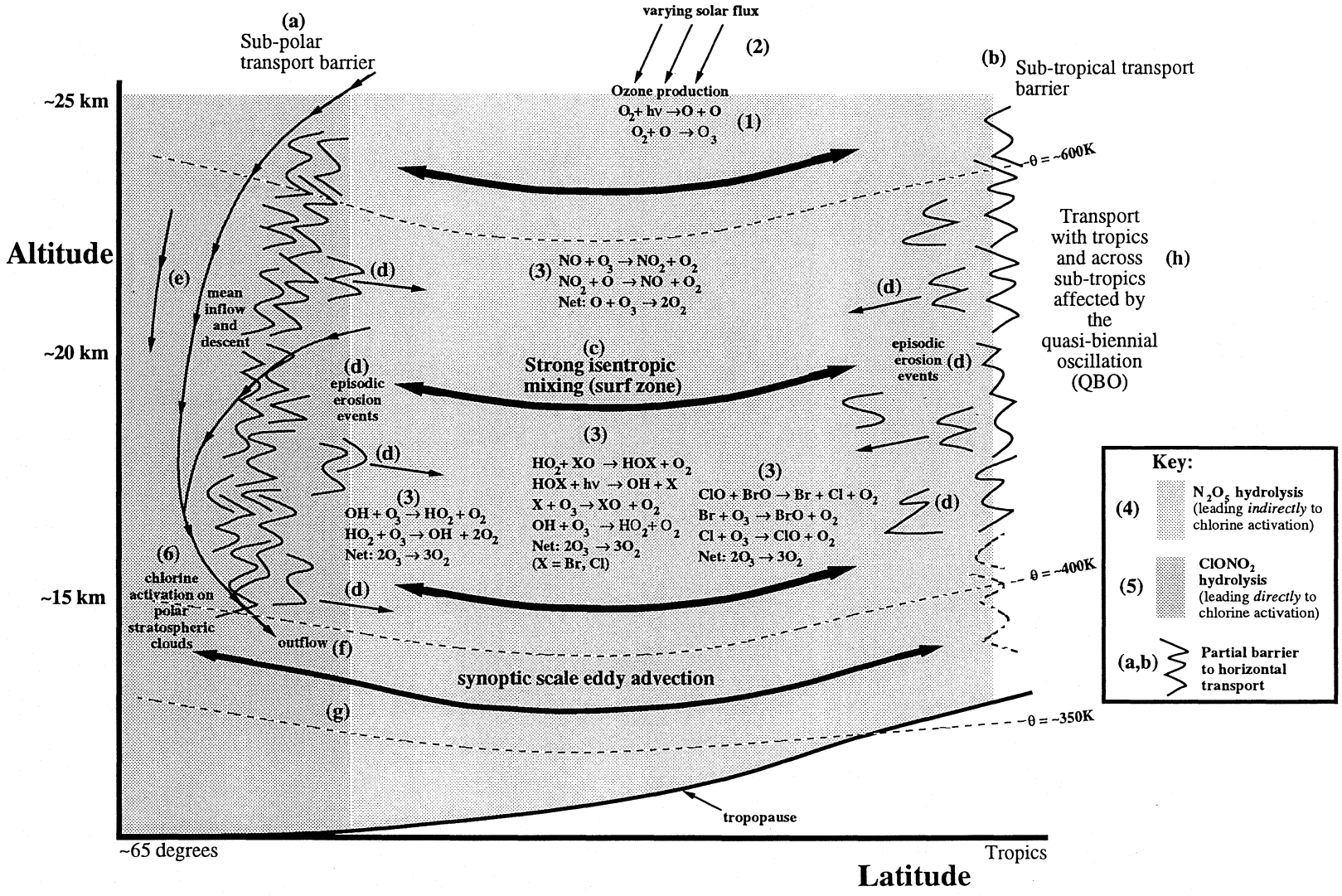

Figure 4-1. A schematic illustrating the dynamical and photochemical processes thought to play roles in controlling midlatitude ozone amounts. The various processes are discussed in the text (see Section 4.2 and following for a discussion of processes **1 - 6**, and Section 4.6 for a discussion of processes **a - h**).

mended values (DeMore *et al.*, 1992) but that are probably temperature dependent.

Increases in calculated photolysis rates and, hence, reductions in calculated lifetimes for species such as chlorofluorocarbons (CFCs) and nitrous oxide (N_2O) may be expected following adoption of more accurate cross sections for oxygen in the Schumann-Runge bands calculated using line-by-line methods (Minschwaner *et al.*, 1992; Toumi and Bekki, 1994). Recent estimates for N_2O, CF_2Cl_2 (CFC-12), and $CFCl_3$ (CFC-11) are 123, 116, and 44 years, respectively (Minschwaner *et al.*, 1993).

A recent measurement has shown that the room-temperature rate constant for the reaction of BrO with HO_2 is a factor of 6 larger than previously determined (Poulet *et al.*, 1992). Combined with an estimated temperature dependence based on the HO_2 + ClO reaction (DeMore *et al.*, 1992), this new determination dramatically increases the importance of bromine-catalyzed ozone loss, particularly in the 15 to 20 km region. The magnitude of possible HBr production from this reaction is currently under scrutiny. However, atmospheric HBr observations by Traub *et al.* (1992) suggest that only 2 ± 2 pptv of HBr is present at 32 km, implying that this channel must be slow.

Some unresolved discrepancies between observations and models exist for the partitioning of inorganic chlorine species in the stratosphere that could impact model predictions of ozone trends.

In the upper stratosphere there are uncertainties regarding the ClO/HCl ratio. The first simultaneous measurements of these species were reported by Stachnik *et al.* (1992) and supported the earlier assertion (McElroy and Salawitch, 1989) that models overestimate this ratio in the upper stratosphere. Calculations of the ClO/HCl ratio can be considerably improved by including a minor channel (approximately 5%) for the reaction of OH with ClO to give HCl. This reaction channel is unobserved to date, however, a channel of this magnitude would be within the upper limit suggested by laboratory studies (DeMore *et al.*, 1992). Addition of this channel to photochemical model calculations improves agreement with Atmospheric Trace Molecule Spectroscopy (ATMOS) data (Natarajan and Callis, 1991), with the annual amplitude of O_3 changes (Chandra *et al.*, 1993), and with the ozone trend in the upper stratosphere (Toumi and Bekki, 1993a).

In the lower stratosphere, there are indications of outstanding problems in the ratio of HCl to Cl_y (see Section 4.2.3.2).

The underestimation of upper stratospheric ozone remains unresolved (Minschwaner *et al.*, 1993), although the deficit now appears to be less than 20%. Calculations that incorporate the photolysis of vibrationally excited oxygen as a potential additional source of ozone gave promising results (Toumi *et al.*, 1991; Toumi, 1992; Minschwaner *et al.*, 1993; Eluszkiewicz and Allen, 1993), but recent laboratory measurements of the quenching rates for vibrationally excited O_2 imply they are more rapid than previously thought (Price *et al.*, 1993), suggesting that this mechanism is unlikely to be important.

4.2.2 Heterogeneous Processes

Five heterogeneous reactions on stratospheric sulfuric acid aerosols have been identified that could play important roles in the midlatitude ozone balance:

$$N_2O_5 + H_2O \rightarrow 2HNO_3 \quad (1)$$

$$ClONO_2 + H_2O \rightarrow HOCl + HNO_3 \quad (2)$$

$$ClONO_2 + HCl \rightarrow Cl_2 + HNO_3 \quad (3)$$

$$HOCl + HCl \rightarrow Cl_2 + H_2O \quad (4)$$

$$N_2O_5 + HCl \rightarrow ClNO_2 + HNO_3 \quad (5)$$

These reactions all activate chlorine, either directly by converting reservoir species to photochemically active forms (2-5), or indirectly by reducing NO_x, which regulates ClO via formation of $ClONO_2$ (reaction 1).

Recent laboratory results suggest that the rates of heterogeneous reactions (1-5) on stratospheric sulfuric acid aerosol particles (SSAs) depend strongly on the chemical composition and phase of the aerosols. SSAs are thought to be composed primarily of sulfuric acid and water, but at temperatures lower than about 205 K they may take up significant amounts of HNO_3 (Molina *et al.*, 1993; Zhang *et al.*, 1993; Tabazadeh *et al.*, 1993) and may eventually freeze, with uncertain effects on the rates of heterogeneous reactions.

The hydrolysis of N_2O_5 (reaction 1) occurs rapidly on all liquid SSAs, with very little temperature dependence (see Tolbert, 1993, for a review of these results). In contrast, the hydrolysis of $ClONO_2$ (reaction 2) is a strong function of aerosol composition, occurring faster

for more dilute aerosols (Hanson *et al.*, 1994, and references therein). In the stratosphere, this property manifests itself as a strong temperature dependence, with an increasing reaction rate at low temperatures at which SSAs are most dilute.

At present, it is difficult to assess the importance of reactions 3-5, as there are few relevant measurements; values for HCl solubility vary by an order of magnitude (Zhang *et al.*, 1993; Williams and Golden, 1993; Hanson and Ravishankara, 1993b; Luo *et al.*, 1994). There are no direct measurements of diffusion coefficients and very few second-order rate constants have been determined. In general, however, these reactions appear to be limited by the availability of HCl in solution. Because HCl solubility increases rapidly with decreasing temperature and decreasing H_2SO_4 concentration, the rates of reactions 3-5 should behave similarly with temperature to that of reaction 2.

A reactive uptake model has been used to investigate the differences between reaction probabilities in small particles and in the bulk liquid (Hanson *et al.*, 1994). The differences are illustrated in Figure 4-2, which shows calculated reaction probabilities (γ) as functions of weight percent sulfuric acid (and temperature) for reactions 2 and 3 on 0.5 μm particles, together with the measured bulk rate for reaction 2.

At very low temperatures, possibly after the formation of polar stratospheric clouds (PSCs), sulfuric acid aerosol particles are likely to freeze as sulfuric acid tetrahydrate (SAT). Once frozen, SAT are expected to remain solid until they warm to above 210 to 215 K (Middlebrook *et al.*, 1993). Although there are relatively few studies of heterogeneous reactions on frozen SSAs, some results are available. Reaction 1, fast on all liquid SSAs, appears to be quite slow on SAT, even at high relative humidity (Hanson and Ravishankara, 1993a). Reaction 2 also appears to be slower on SAT than on liquid SSAs, although there is uncertainty in the measured value of γ (Hanson and Ravishankara, 1993a; Zhang *et al.*, 1994). In contrast, reaction 3 occurs readily on SAT surfaces at high relative humidity. Like its counterpart on type I PSCs, the rate of reaction 3 on SAT decreases as the relative humidity decreases. Reactions 4 and 5 have not yet been studied on SAT surfaces.

Laboratory work also shows that several species in the HO_x family, for example, OH and HO_2 (Hanson *et al.*, 1992) and CH_2O (Tolbert *et al.*, 1993), are readily taken up by SSAs. The competing gas phase reactions of OH and HO_2 are so rapid that heterogeneous loss does not significantly perturb the HO_x budget or partitioning (Hanson *et al.*, 1994). However, condensed phase reactions of OH or HO_2 and uptake of HO_x reservoirs such as CH_2O may impact the chemistry of other radical families.

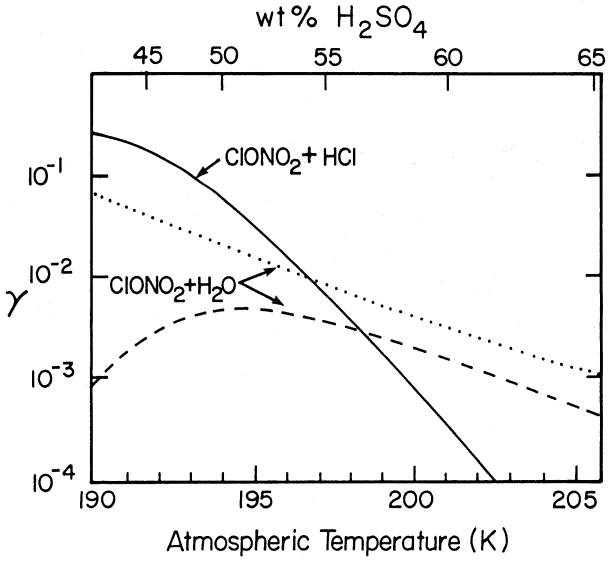

Figure 4-2. The uptake coefficients (γ) for $ClONO_2$ onto small liquid sulfuric acid droplets due to reaction with HCl (solid curve) and with H_2O (dashed curve) are shown here. These values are calculated with parameters obtained from laboratory measurements over bulk liquid surfaces using the methodology presented in Hanson *et al.* (1994). The calculation was made for a partial pressure of water equal to 2×10^{-4} mTorr, equivalent to 5 ppmv at 50 hpa. The approximate H_2SO_4 content of the droplets is shown at the top of the figure. The dotted curve is the laboratory measured γ for $ClONO_2$ with H_2O in the absence of HCl. The reaction probability for HOCl + HCl is similar to that for $ClONO_2$ + HCl. The reactive loss coefficient for N_2O_5 on 60 wt% H_2SO_4 at low temperatures is ~0.1, and probably does not vary greatly from this value over the range of acid content shown in this figure. (Adapted from Hanson *et al.*, 1994.)

A number of studies (Abbatt, 1994; Hanson and Ravishankara, 1994) have shown that heterogeneous reactions of bromine compounds (HBr, HOBr, and $BrONO_2$) occur on sulfate aerosol and may be important sources of halogen atoms.

Finally it should be noted that heterogeneous reactions also occur very readily on polar stratospheric clouds. These processes, which may have an impact on midlatitude chemistry (see Section 4.7), are discussed in Chapter 3.

4.2.3 Atmospheric Observations

Since the last Assessment, measurements from a variety of sources including the Stratospheric Photochemistry, Aerosols and Dynamics Expedition (SPADE) and the second Airborne Arctic Stratospheric Expedition (AASE II) campaigns, from the Upper Atmosphere Research Satellite (UARS) and ATMOS instruments, and from ground-based instruments have all provided new information that bears directly on the issue of midlatitude ozone loss. Details of these advances are given below.

4.2.3.1 NO_x/NO_y Ratio

Many new measurements indicate that incorporation of reaction 1 (see above) into photochemical models results in better agreement between theory and measurements. A variety of observations of nitrogen oxide species show a lower-than-gas-phase NO_x/NO_y ratio including *in situ* (Fahey *et al.*, 1993; Webster *et al.*, 1994a), column measurements (Keys *et al.*, 1993; Koike *et al.*, 1993), and ATMOS data (McElroy *et al.*, 1992; Toumi *et al.*, 1993b). Indirect measurements (*e.g.,* the balloon-borne ClO profiles measured by Avallone *et al.*, 1993a) also support inclusion of N_2O_5 hydrolysis in models, in order to more accurately reproduce observations. Figure 4-3 illustrates a comparison between data and models from that study.

Observations obtained during the SPADE campaign showed that models that neglect heterogeneous chemistry provide a completely inadequate description of the observed radicals, but that inclusion of the heterogeneous hydrolysis of N_2O_5 and $ClONO_2$ at the recommended rates resulted in better agreement between observation and theory. The modeled partitioning between NO_x and NO_y generally shows good (30 percent) agreement with the measured ratio when the hydrolysis of N_2O_5 and the temperature dependence of the nitric acid cross sections (Burkholder *et al.*, 1993) are used (*e.g.,* Salawitch *et al.*, 1994a, b; Wennberg *et al.*, 1994).

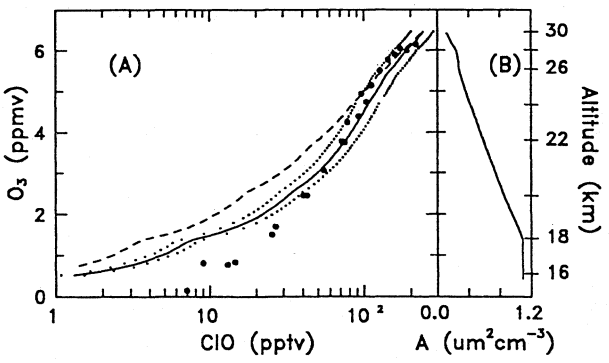

Figure 4-3. Curve A: A 0.5-km average of measured ClO, shown as solid circles. The dashed line represents gas-phase-only model results and the heavy solid line shows the calculation with addition of N_2O_5 hydrolysis. The dotted lines depict the range of uncertainty in calculated ClO for the heterogeneous model resulting from the reported uncertainty in ozone, which was used to initialize the trace gases in the model. The model is unable to reproduce ClO at the lowest altitudes, possibly due to inaccurate partitioning of HCl and $ClONO_2$. **Curve B:** Surface area density used for the heterogeneous model calculations. (From Avallone *et al.*, 1993a.)

Systematic differences between model and observations suggest, however, that our knowledge of N_2O_5 chemistry may still be incomplete. For example, Toumi *et al.* (1993c) conclude that the currently recommended γ for N_2O_5 hydrolysis is too fast to be consistent with the ATMOS observations. Other specific anomalies remain, for example anomalous NO_x/NO_y ratios (Fahey *et al.*, 1994). However, it is unclear whether these reflect deficiencies in modeling known chemistry (*e.g.,* imperfect knowledge of aerosol surface areas, photolysis rates, etc.), or more profoundly, missing chemical or transport processes.

4.2.3.2 Partitioning of Radical Species

During the SPADE campaign (November 1992 to April/May 1993), measurements of the concentrations of the free radicals NO_2, NO, ClO, HO_2, and OH were obtained, together with those of ozone and a number of tracers and reservoir species (CO_2, H_2O, N_2O, CH_4, HCl). The main results from this campaign that have implications for ozone photochemistry are summarized in the following paragraphs.

Modeled OH and HO_2 concentrations are in reasonable agreement with the measurements, although usually systematically lower by 10-20% (Salawitch *et al.*, 1994a, b; Wennberg *et al.*, 1994). While this is well within the uncertainty of the measurements, there were at times more serious discrepancies: OH and HO_2 concentrations at high solar zenith angles are much higher (as much as 10 times at 90° SZA) than expected. This is most pronounced in the sunrise data (Wennberg *et al.*, 1994). It is unclear what process is responsible for this HO_x production (Michelsen *et al.*, 1994), although, since there is a simultaneous increase in NO, the photolysis of HONO formed by the heterogeneous decomposition of HNO_4 has been suggested (Wennberg *et al.*, 1994).

The partitioning between OH and HO_2 agrees well (15 percent) with that expected based on a simple steady state model using the measured concentrations of NO and O_3 (Cohen *et al.*, 1994). This result is a confirmation of our understanding of the coupling between the HO_x and NO_x families and the ozone reaction chemistry with OH and HO_2.

The measured partitioning between NO_2 and NO is usually in reasonable (30%) agreement with the expected steady-state relationship:

$$NO_2/NO = \{k_{NO+O_3}(O_3) + k_{NO+ClO}(ClO)\} / J_{NO_2}$$

although disagreements of more than a factor of two are occasionally observed (Jaeglé *et al.*, 1994).

In combination with the earlier AASE II observations (King *et al.*, 1991; Avallone *et al.*, 1993b), the SPADE measurements demonstrate the role that aerosols play in enhancing ClO (Salawitch *et al.*, 1994a, b). The ratio of ClO to the available inorganic chlorine was observed to be strongly anticorrelated with the available NO_x (Wennberg *et al.*, 1994; Stimpfle *et al.*, 1994), and it was observed that ClO concentrations dropped between the fall and spring flights, consistent with a direct response to observed NO_x enhancements.

However, balancing the chlorine budget in the lower stratosphere remains problematic. Calculations of the ClO/HCl ratio from ER-2-based measurements (Webster *et al.*, 1993) show that this ratio is not accurately represented by a model that includes the heterogeneous hydrolysis of N_2O_5, as shown in Figure 4-4. This conclusion was also drawn in the work of Avallone *et al.* (1993a), in which the model was unable to reproduce the measured values of ClO below about 18 km altitude. However, as discussed below, provided the ratio of NO_x to NO_y is modeled correctly, accurate simulations of observed ClO are obtained, implying that the modeled HCl concentrations are in error, but not the modeled ClO concentrations. Models predict much higher (1.5 to 3 times) HCl than was measured (Webster *et al.* 1994b; Salawitch *et al.*, 1994b). While the disagreement observed during SPADE was smaller than that during the AASE II campaign, large differences remain.

If, however, the inorganic chlorine unaccounted for is taken to be chlorine nitrate, the observed ClO and NO concentrations would imply that the photolysis rate of chlorine nitrate must be approximately 1/3 of the recommended value (Webster *et al.*, 1994b). While simultaneous measurements of chlorine nitrate are a prerequisite to resolving this problem, the reasons for this discrepancy, and the implication for ozone loss, remain unclear.

Figure 4-5 shows measurements of the diurnal dependencies of stratospheric free radicals obtained on the flights of May 11 (sunrise) and May 12 (sunset) at 37°N and 63 hPa (18.8 km). Making certain assumptions (see caption), Salawitch *et al.* (1994a), using a data-assimilation photochemical model constrained by the observed source gas fields, obtained very good agreement with the observations (see Figure 4-5), implying a good understanding of the basic controlling processes.

Further confirmation of our generally good understanding of fast photochemistry over a range of conditions in the low stratosphere was provided by the SPADE survey flights, which were made from 15-60°N with altitude profiles (15-21 km) made approximately every 10 degrees of latitude. Figure 4-6 shows data obtained during the SPADE ER-2 flights of May 14 and May 18, 1993, compared with the data-assimilation model of Salawitch *et al.* (1994b) constrained by observed source gas fields. Observed changes in aerosol surface area along the flight track of between ~5 and ~15 $\mu m^2 cm^{-3}$ are also included in the calculations. Details of the model calculations are given in the figure caption. Salawitch *et al.* conclude that inclusion of heterogeneous processes is essential if radical concentrations are to be modeled correctly, although discrepancies remain, notably in the modeled OH/HO_2 and NO/NO_2 ratios.

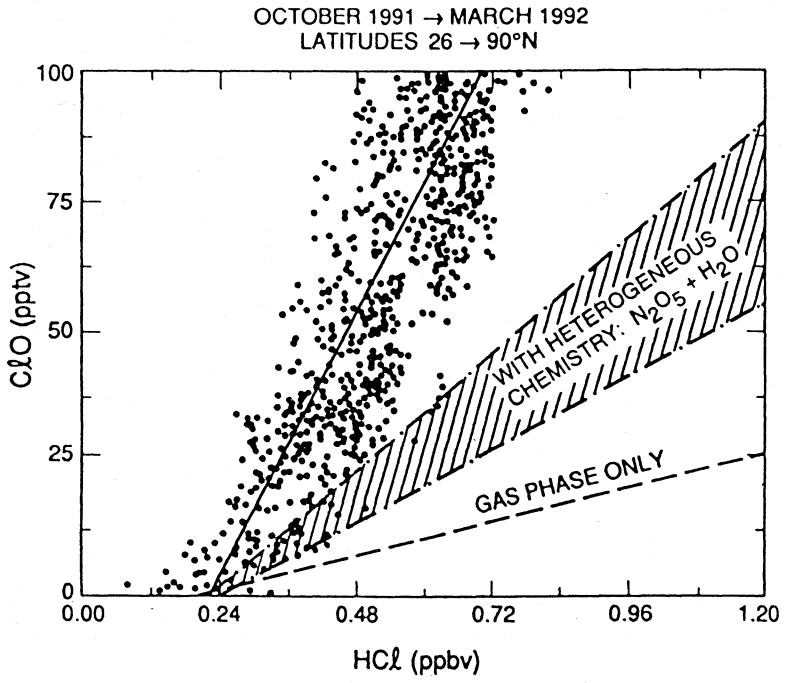

Figure 4-4. Scatter plot of ClO versus HCl data from instruments aboard the NASA ER-2, taken on the flights of Oct. 14, 1991, Feb. 13, 1992, and Mar. 15 and 22, 1992, covering latitudes between 26° and 90°N. The data included are limited to ClO mixing ratios less than 100 pptv, and to solar zenith angles less than or equal to 80°. Also plotted are results from the 2-D model of Solomon and Garcia using either gas-phase-only photochemistry, or including the heterogeneous hydrolysis of N_2O_5 on two levels of sulfate aerosol surface area that bracketed the ER-2 observations. The figure illustrates that observed HCl concentrations for a given ClO amount are approximately a factor of 2 lower than model calculations including heterogeneous chemistry would imply. (From Webster *et al.*, 1993.)

These discrepancies can be reduced, but not eliminated, with further refinements.

Measurements from the Microwave Limb Sounder (MLS) have allowed the global behavior of ClO concentrations in the low stratosphere to be determined. In Figures 4-7 (left and right panels) (Froidevaux *et al.*, 1994) are shown monthly mean zonal average ClO mixing ratios at 22 hPa, 46 hPa, and 100 hPa averaged over 30°N-50°N and 30°S-50°S, respectively. The data extend from September 1991 through to the end of 1993.

The MLS data reveal a distinct seasonal cycle in both hemispheres, with maximum ClO mixing ratios seen during midwinter months. This variation appears to be qualitatively consistent with expected changes in NO_x as discussed above. In agreement with studies mentioned above, lower stratospheric midlatitude ClO values of 0.1 to 0.2 ppbv, as measured by MLS, cannot be explained with gas phase chemistry alone (Froidevaux *et al.*, 1994). The MLS data show that ClO mixing ratios at 46 hPa and 22 hPa are closely comparable in the respective seasons in the two hemispheres.

Differences would be expected in the extent of air exposed to heterogeneous processes in the polar regions of the Southern and Northern Hemispheres, and indeed interannual differences would be present, particularly in the North (Jones and Kilbane-Dawe, 1994). Thus, the consistent phasing of the observed ClO maxima and, after adjustment for season, the comparable ClO amounts in the two hemispheres, suggest that *in situ* chemistry rather than the processing of air from the polar vortex is the main factor controlling these midlatitude ClO concentrations (Froidevaux *et al.*, 1994). However, it should be noted that the MLS instrument has very limited sensitivity in the lowest region of the strato-

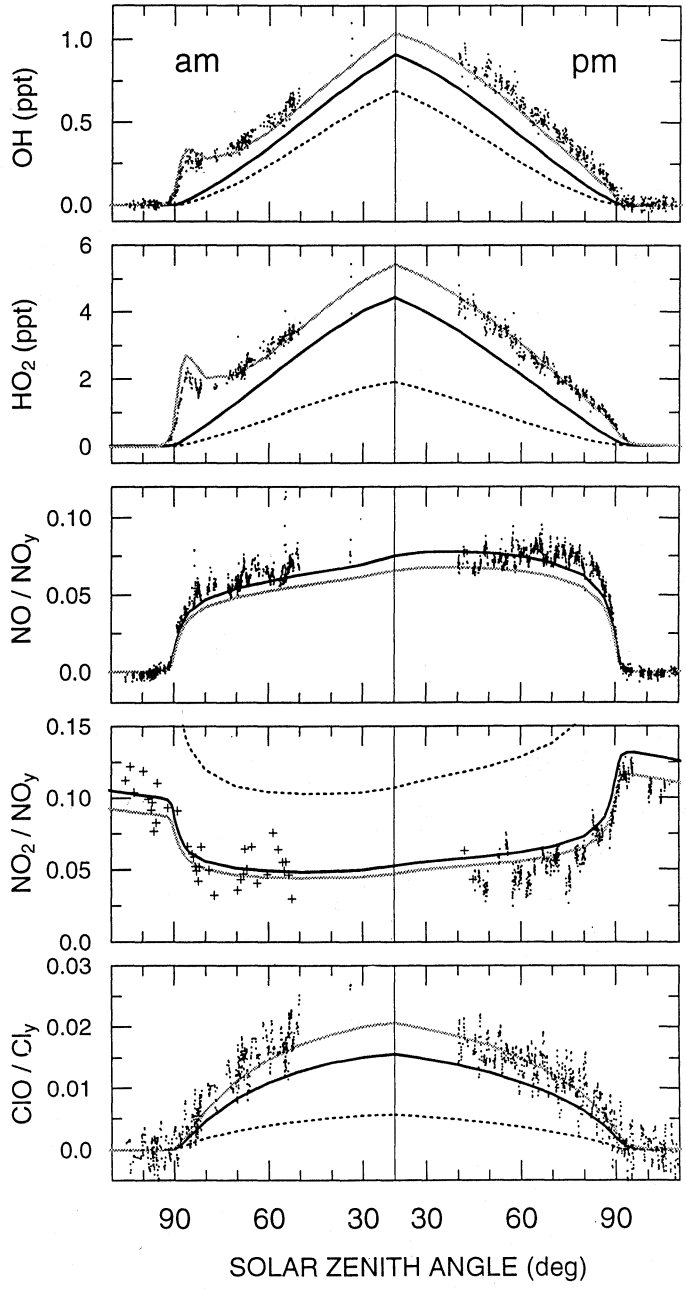

Figure 4-5. Measurements (dots) of the diurnal variations of stratospheric free radicals NO_2, NO, HO_2, OH (crosses and dots represent data from the JPL and NOAA instruments, respectively), and ClO from two ER-2 flights of May 11 (sunrise) and May 12 (sunset), both near 37°N and 63 hPa and [N_2O] between 240 and 260 ppbv, plotted as a function of solar zenith angle. Also shown are results from a constrained data assimilation model (Salawitch *et al.*, 1994a). Three calculations are shown. Dark dotted curve: gas phase reactions only, using rate constants and cross sections of DeMore *et al.* (1992). Curve 1, dark solid line: as for above, except including also the heterogeneous hydrolysis of N_2O_5 and $ClONO_2$. Curve 2, gray line: as for curve 1, except including the heterogeneous decomposition of HNO_4 to form HONO, the $O(^1D)$ quantum yield of Michelsen *et al.* (1994), and the temperature-dependent cross sections of HNO_3 from Burkholder *et al.* (1993). (From Salawitch *et al.*, 1994a.)

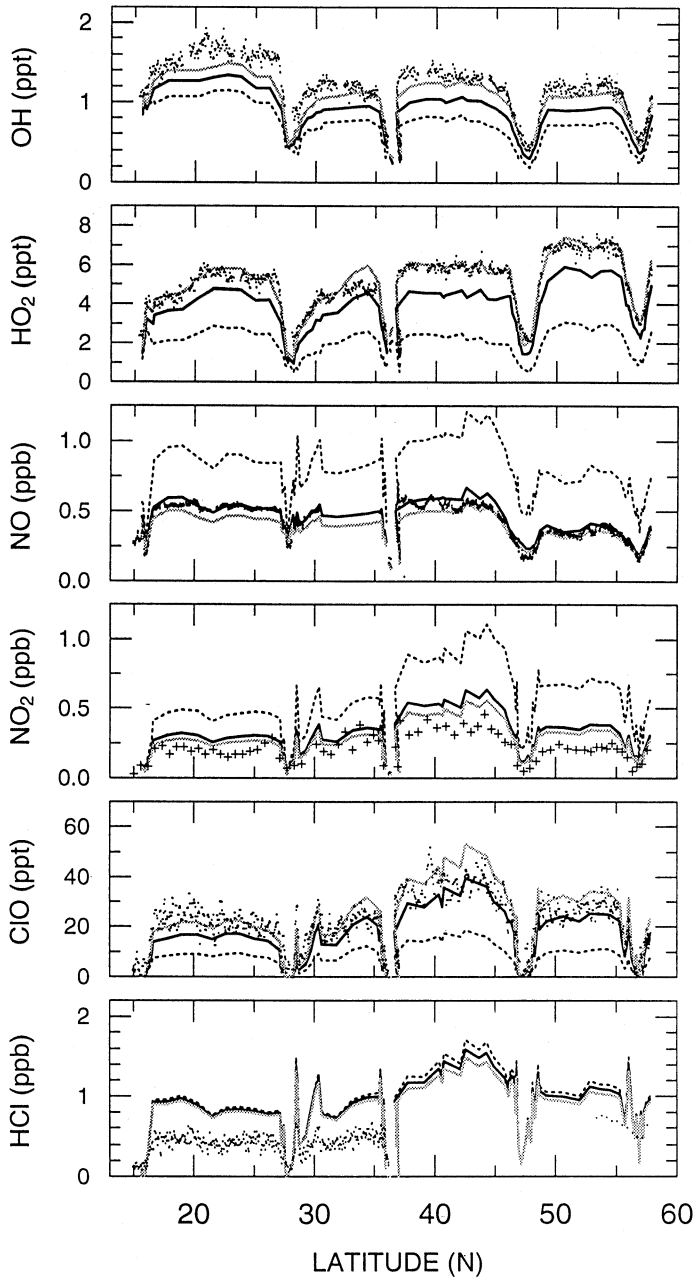

Figure 4-6. Measurements (points) of NO_2, NO, ClO, HO_2, OH, and HCl obtained on May 14 and 18, 1993, during which the ER-2 flew from 15 - 55°N. Also shown are calculations from the data assimilation model of Salawitch *et al.,* 1994b. The individual calculations are as for Figure 4-5. As can be seen, all three calculations significantly overestimate HCl concentrations. (From Salawitch *et al.*, 1994b.)

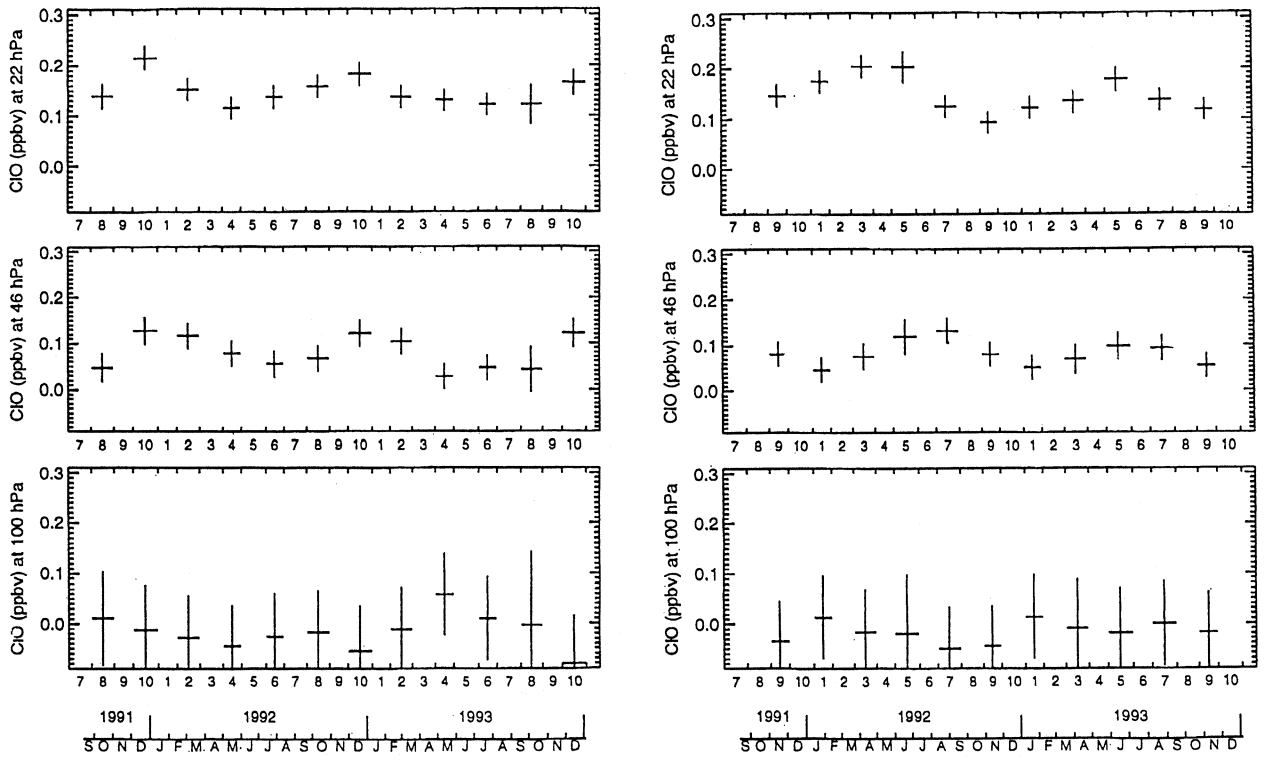

Figure 4-7. (left panels) Monthly zonal mean lower stratospheric ClO mixing ratio from 30°N - 50°N from the UARS MLS instrument. The figure shows monthly zonal mean ClO between September 1991 and December 1993. Results are given for pressures of 22 hPa (approximately 25 km, upper), 46 hPa (approximately 20 km, center) and 100 hPa (approximately 15 km, lower). In order to remove small biases, day (solar zenith angles < 90°) minus night (SZA > 95°) differences have been taken. Error bars are ± 2.8 σ. (Adapted from Froidevaux *et al.*, 1994.) **(right panels)** As Figure 4-7a) except for 30°S - 50°S. (Adapted from Froidevaux *et al.*, 1994.)

sphere (~100 hPa). This is an important limitation because the bulk of the ozone column at midlatitudes resides in this region, and any hemispheric differences in ClO at these low altitudes might not be detected.

Detailed comparisons of HCl data from the NASA ER-2 instrument of Webster *et al.* (*e.g.,* 1993) and the Halogen Occultation Experiment (HALOE) (Russell *et al.*, 1993b) are ongoing. $ClONO_2$ measurements from the Cryogenic Array Etalon Spectrometer (CLAES) (Roche *et al.*, 1993) will also augment this data set to provide a nearly complete inorganic chlorine budget for the lower stratosphere.

4.3 ERUPTION OF MT. PINATUBO

The eruption of Mt. Pinatubo, located in the Philippines (15°N, 120°E), culminated in an enormous explosion on June 14-15, 1991. The plume reached altitudes in excess of 30 km, depositing 15 to 20 Mt of sulfur dioxide (SO_2) into the stratosphere (Bluth *et al.*, 1992; McPeters, 1993; Read *et al.*, 1993), nearly 3 times as much as the El Chichón eruption in 1982. Conversion of SO_2 into sulfuric acid (H_2SO_4) occurred rapidly, resulting in sulfate aerosol surface areas as large as 85 $\mu m^2 cm^{-3}$ over Northern midlatitudes (Deshler *et al.*, 1992, 1993) at some altitudes. This huge perturbation has allowed a test of many aspects of our understanding of heterogeneous chemical processes in the stratosphere, building on the earlier work of Hofmann and Solomon (1989).

4.3.1 Effects on Chemical Composition

In the first few months following the Mt. Pinatubo eruption, low ozone amounts were detected in the tropics, roughly coincident with the region of largest aerosol loading (*e.g.*, Grant *et al.*, 1992, 1994; Schoeberl *et al.*, 1993a). On a longer time scale, ozone reductions were observed at midlatitudes by satellite (Gleason *et al.*, 1993; Waters *et al.*, 1993), ground-based (Bojkov *et al.*, 1993; Kerr *et al.*, 1993), and *in situ* instrumentation (Weaver *et al.*, 1993; Hofmann *et al.*, 1994). Details of this anomalous ozone behavior are given in Chapter 1.

The short-term tropical ozone decline has been attributed both to dynamical effects (see Section 4.6.3), and to a reduction of O_2 photolysis, and hence ozone production, due to absorption of solar ultraviolet radiation by SO_2 (Bekki *et al.*, 1993). SO_2 has also been shown to be capable of catalyzing ozone production via the following mechanism (Crutzen and Schmailzl, 1983; Bekki *et al.*, 1993):

$$SO_2 + h\nu \rightarrow SO + O \ (\lambda > 220 \text{ nm})$$
$$SO + O_2 \rightarrow SO_2 + O$$
$$2(O + O_2 + M \rightarrow O_3 + M)$$
$$\text{net: } 3O_2 \rightarrow 2O_3$$

The longer-term ozone decrease is likely to be the result of a combination of enhanced heterogeneous chemistry resulting from the large increase in sulfate aerosol surface area, changes in the radiation field, and altered stratospheric dynamics (see, for example, Brasseur and Granier, 1992; Michelangeli *et al.*, 1992; Pitari and Rizi, 1993; Tie *et al.*, 1994).

Once the initial SO_2 plume is converted to aerosol particles, enhanced absorption of terrestrial emission and backscattering of solar radiation is expected especially in the tropics, leading to changed photolysis rates. The enhanced backscatter reduces the photolysis of all molecules below the cloud, but for molecules that absorb radiation at wavelengths longer than 300 nm, which can penetrate to the low stratosphere (for example, O_3 and NO_2), photolysis rates are enhanced above the cloud-top. The net effect is to accelerate photochemical ozone loss, leading to reductions in column ozone of several percent in the vicinity of the cloud (Pitari and Rizi, 1993; Tie *et al.*, 1994).

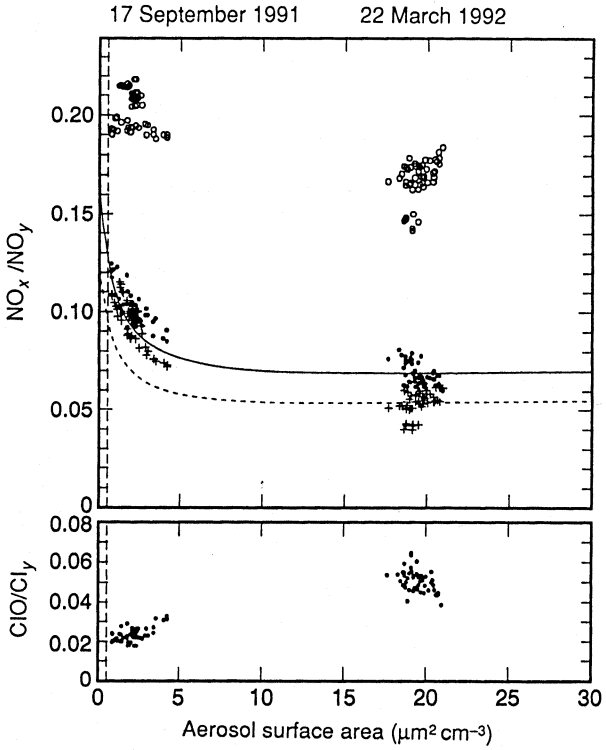

Figure 4-8. Scatter plot of NO_x/NO_y and ClO/Cl_y data from the NASA ER-2 with observed aerosol surface area (solid circles) in high and low aerosol conditions. Gas phase only (open circles) and heterogeneous case (crosses) model calculations are included (using observed aerosol surface areas with reaction 1). The surface area scale has no meaning for the gas phase case, except to separate data from the two flights. The vertical dashed line represents background aerosol surface area. The curved lines represent the dependence on surface area in the model heterogeneous case for the average conditions in September (solid) and March (dashed) data sets. Also shown are the corresponding ClO/Cl_y observations. (From Fahey *et al.*, 1993.)

A variety of chemical changes thought to be the results of heterogeneous reactions on the Mt. Pinatubo aerosol cloud have been observed. Fahey *et al.* (1993) and Kawa *et al.* (1993) showed dramatic reductions in the NO_x/NO_y ratio as sulfate surface area increased (see Figure 4-8). In response to this change, the amount of active chlorine (ClO/Cl_y) was observed to increase, as expected (Wilson *et al.*, 1993; Avallone *et al.*, 1993b;

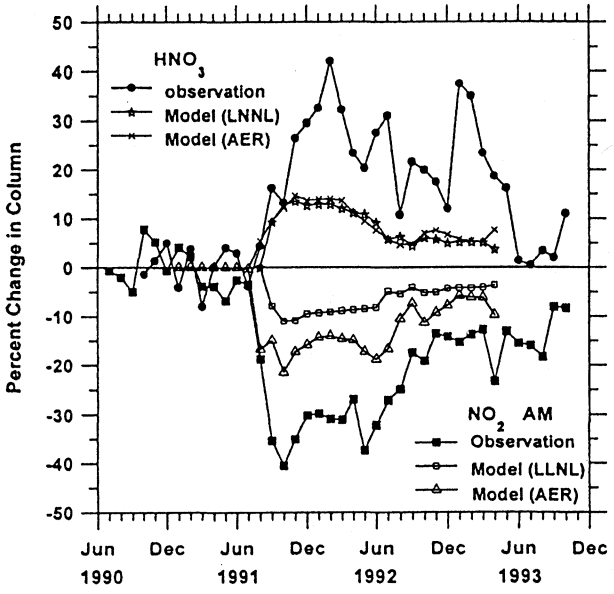

Figure 4-9. Percentage changes in HNO_3 and NO_2 column amounts above Lauder, New Zealand, (45°S) following the arrival of the Mt. Pinatubo aerosol. The Lawrence Livermore National Laboratory (LLNL) results are for 42.5°S and the Atmospheric Environmental Research, Inc. (AER) results are for 47°S. Heterogeneous chemistry is included in the calculations based on the observed aerosol field from SAGE II. (From Koike *et al.*, 1994.)

and Wennberg *et al.*, 1994). In addition, several measurements of column NO_2 at middle and high latitudes showed substantial decreases (25 to 50%) in comparison to previous years (Johnston *et al.*, 1992; Koike *et al.*, 1994; Mills *et al.*, 1993; Coffey and Mankin, 1993; Solomon *et al.*, 1994a).

The hydrolysis of N_2O_5 is expected to saturate at moderate values of surface area (Prather, 1992), but the hydrolysis of $ClONO_2$ may become increasingly important as surface area grows, as in the case of the Mt. Pinatubo aerosol. This saturation effect is evident in the NO_x/NO_y measurements of Fahey *et al.* (1993) (Figure 4-8) and further confirmed by the lack of major ClO enhancements at mid- to high Northern latitudes (Avallone *et al.*, 1993a; Dessler *et al.*, 1993) and seen in the MLS data shown in Figure 4-7. Further qualitative support for N_2O_5 hydrolysis comes from Koike *et al.* (1994), who have observed the effects of Mt. Pinatubo aerosol on NO_2 and HNO_3 over New Zealand. In Figure 4-9 are shown percent changes in HNO_3 and NO_2 columns over Lauder (45°S) from June 1990 to December 1993. The data show a reduction in NO_2 columns as the Mt. Pinatubo cloud reached Lauder, and a simultaneous increase in column HNO_3. Model calculations using the observed aerosol field from SAGE II (Stratospheric Aerosol and Gas Experiment II) (Kent and McCormick, 1993) as input show good qualitative agreement with the observations, although the magnitude of the changes is underestimated in the models.

A number of studies have provided evidence for the heterogeneous hydrolysis of $ClONO_2$ on sulfate aerosols, particularly during periods of volcanic activity. Solomon *et al.* (1993) argue that the observation of enhancements to the OClO column in the austral fall of 1992 are due to the hydrolysis of $ClONO_2$ on sulfate aerosols. The formation of substantial OClO amounts requires enhanced ClO in addition to moderate BrO concentrations, and had in the past only been detected following the appearance of PSCs. However, in 1992, OClO was detected earlier and in larger quantities than in previous years, suggesting that chlorine had been activated to some degree on sulfate aerosols. This conclusion is predicated on the absence of PSC processing prior to the observation of OClO.

Column reductions of $ClONO_2$, HCl, and HNO_3 were also observed from the NASA DC-8 during transit below a very cold region of volcanically enhanced aerosol (O. Toon *et al.*, 1993). The heterogeneous reaction probability γ for $ClONO_2$ hydrolysis calculated from these observations, taking into account the history of the air parcels, is very close to laboratory values. Dessler *et al.* (1993) attempt a similar calculation based on balloon observations of ClO and NO and determine a value of γ again consistent with laboratory experiments. However, the possible influence of PSC processing at some earlier time cannot be entirely ruled out as influencing the observed concentrations of ClO and OClO.

Calculations using 2- and 3-dimensional models suggest that once the aerosol cloud is dispersed from the tropics and the aerosol loading begins to increase at mid- and high latitudes, significant (several percent) column ozone reductions arising from accelerated heterogeneous chemistry are likely to be widespread, with maximum reductions (up to ~10%) at midlatitudes in winter where the photolysis of HNO_3 is slow (Pitari and Rizi, 1993; Tie *et al.*, 1994). This is discussed further in

Section 4.6.3. However, there are several outstanding anomalies. For example, despite the more rapid movement of the Mt. Pinatubo aerosol cloud to the Southern Hemisphere (Trepte *et al.*, 1993), ozone trends were apparently smaller in the South compared to the North following the Mt. Pinatubo eruption. This is discussed further in Section 4.4.

4.3.2 Implications for the Normal State of the Atmosphere

Observations of chemical constituents in the presence of enhanced sulfate aerosol surface area and over a wide temperature range have shown that the heterogeneous hydrolysis of $ClONO_2$ should be considered in addition to the hydrolysis of N_2O_5 to more accurately simulate ozone loss in the stratosphere. The area of largest debate regarding heterogeneous chemistry is an accurate quantification of the actual rates of reaction in the stratosphere. Laboratory determination of rate parameters and uptake coefficients for a variety of species is essential, but improved understanding of the composition and physical characteristics of the stratospheric aerosol layer at temperatures less than about 210 K when ternary ($H_2O/HNO_3/H_2SO_4$) solutions may exist is equally important. Understanding of the potential role of heterogeneous processes other than the hydrolysis of N_2O_5 and $ClONO_2$ is expected to improve as a result of measurements made during periods of highly perturbed surface area, as reaction rates are expected to be large enough to cause an observable effect (Hanson *et al.*, 1994). It is unlikely that all of these processes will be important under "background" surface area conditions, but the possible continued emission of sulfur from current subsonic aircraft and a proposed supersonic fleet may significantly increase the sulfate aerosol loading of the stratosphere (Bekki and Pyle, 1992). Under such a scenario, heterogeneous reduction of NO_x and subsequent enhancement of active chlorine may have a serious effect on the ozone balance in the tropical and midlatitude stratosphere.

4.4 PHOTOCHEMICAL OZONE LOSS PROCESSES AT MIDLATITUDES

There is now a much clearer understanding of the relative importance of different photochemical destruction cycles to ozone loss in the low stratosphere, supported, as discussed above, by a comprehensive range of atmospheric measurements, laboratory studies, and model calculations. However, knowledge of the absolute rate of photochemical ozone loss still remains uncertain, primarily because of limitations in our ability to model accurately the distributions of source gases, but also because of uncertainties in heterogeneous chemistry.

A number of recent studies have provided a relatively consistent picture of the relative importance of different ozone destruction cycles (*e.g.*, Avallone *et al.*, 1993a; Rodriguez *et al.*, 1994; Garcia and Solomon, 1994; Wennberg *et al.*, 1994). In Figure 4-10 are shown calculations of the contributions of different photochemical cycles to ozone loss between 13 and 23 km, for 32°-63°N (from Rodriguez *et al.*, 1994). Panels show: a) background aerosol conditions, b) volcanically enhanced aerosol with hydrolysis of N_2O_5 only, and c) volcanically enhanced aerosol with hydrolysis of both N_2O_5 and $ClONO_2$. The broad picture is of reactions involving HO_2 being responsible for over half the photochemical destruction of ozone in the low stratosphere, while halogen (chlorine and bromine) chemistry accounts for a further third. Although catalytic destruction by NO_x accounts for less than 20% of the photochemical ozone loss, NO and NO_2 are vital in regulating the abundance of hydrogen and halogen radicals and thus the total photochemical ozone destruction rate. The effect of increased aerosol loading is to enhance the HO_x and halogen destruction cycles at the expense of the NO_x, with a net increase of ~20% in the ozone loss rate at peak aerosol loading. Figure 4-11 shows loss rates as a function of altitude from the model of Garcia and Solomon (1994) for 40°N in March for background aerosol loading. Below 22 km, reactions involving HO_x dominate, while between 23 and 40 km, NO_x cycles dominate. Bromine and chlorine loss cycles are important in the low stratosphere and chlorine becomes dominant near 40 km. Reductions in NO_x above about 22 km, where it represents the dominant photochemical loss mechanism, would therefore result in local ozone increases (Tie *et al.*, 1994).

This provides a possible explanation of the apparent absence of an ozone reduction in the Southern Hemisphere following Mt. Pinatubo (Hofmann *et al.*, 1994). The altitudes at which the Mt. Pinatubo cloud

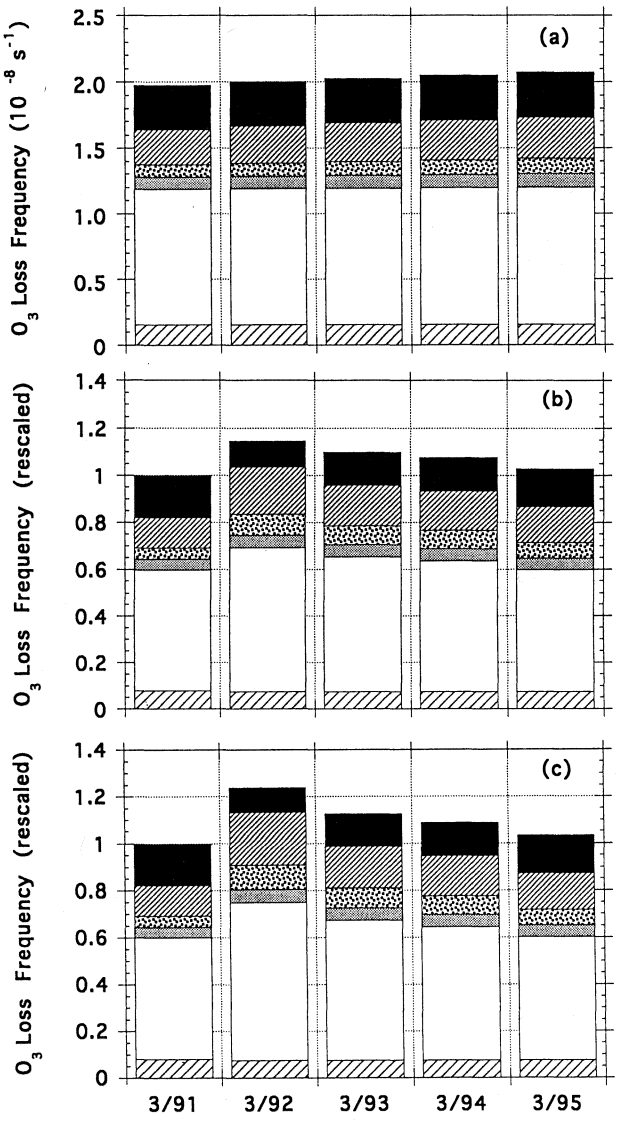

Figure 4-10. Calculated total average loss frequencies and relative contributions of different catalytic loss cycles from March 1991 to March 1995 showing the estimated effect of the Mt. Pinatubo eruption. Average loss frequencies are defined as the total loss rate of ozone between 13 and 23 km, and 32° and 63°N, divided by the total ozone content in this region. The relative contribution of each catalytic cycle is indicated by the different shadings: solid (NO_x cycles); dense diagonal (Cl_x cycles); large dot (Cl_x-Br_x); shaded (Br_x); white (HO_x); and diagonal (O + O_3). Panel a) shows loss frequencies for a background aerosol case; panels b) and c) are for volcanically enhanced aerosol and show, respectively, the effect of N_2O_5 hydrolysis alone, and the effects of both N_2O_5 and $ClONO_2$ hydrolysis. (From Rodriguez *et al.*, 1994.)

penetrated the two hemispheres differed markedly, with peak concentrations near or above 22 km in the South, but at lower altitudes in the North (Trepte *et al.*, 1993). In the Southern Hemisphere, ozone losses below 22 km would have been compensated for by slowed destruction above, leading to little net change in the ozone column. However, in the North, the absence of aerosol at higher altitudes meant that little or no compensating slowing of the ozone destruction occurred at the higher altitude, leading to significant overall declines in the column.

Finally, the suggestion has been made that iodine compounds (primarily CH_3I) can reach the low stratosphere in sufficient quantities to perturb significantly the ozone photochemical balance (Solomon *et al.*, 1994b). The relevant reactive iodine compounds have yet to be detected in the stratosphere. However, if confirmed, this process would have a significant impact on our understanding of photochemical ozone loss in the low stratosphere at midlatitudes.

4.5 THE SOLAR CYCLE AND QUASI-BIENNIAL OSCILLATION (QBO) EFFECTS ON TOTAL OZONE

The largest depletions of ozone noted in Chapter 1 of this document have occurred in the lowest part of the stratosphere and are systematic from year to year. While such changes are qualitatively consistent with either local chemical removal by HO_x and halogen cycles (Section 4.4) or the transport of ozone-depleted air from polar regions (Section 4.7), they are not, according to our best understanding, compatible with either changes in solar output or QBO effects. Nevertheless, solar cycle and QBO influences on total ozone must be removed if ozone trends are to be quantified reliably.

4.5.1 Solar Ultraviolet Variability and Total Ozone

Although solar radiation at wavelengths less than 300 nm accounts for only about 1% of the total radiative output of the sun, it is the principal energy source at altitudes between the tropopause and the lower thermosphere. It both drives the photochemistry of the upper atmosphere and is a source of heating, thus affecting the circulation of the upper atmosphere. Variations of the solar ultraviolet (UV) flux can affect column ozone

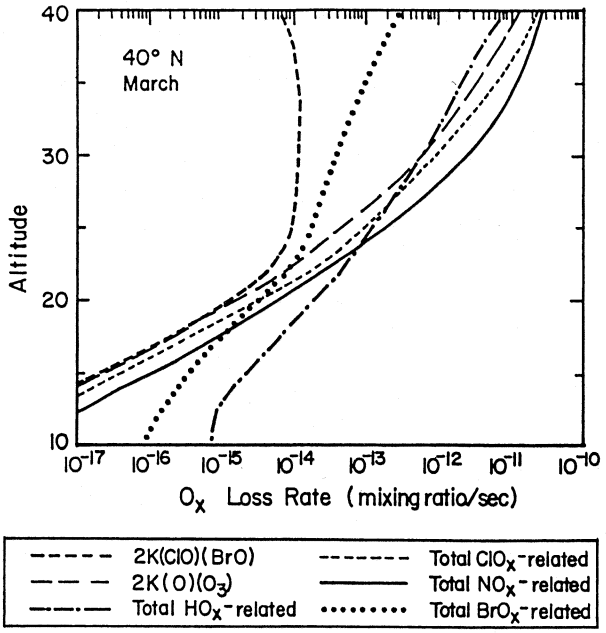

Figure 4-11. Calculated 24-hour averaged O_x loss rates (mixing ratio/sec) from various chemical cycles for 40°N in March for low (*i.e.,* non-volcanic) sulfate aerosol loading. In these circumstances the dominant ozone loss below 22 km is due to reactions involving OH and HO_2, with NO_x dominating between 23 and 40 km. Under higher aerosol loading conditions, coupled HO_x - halogen cycles become more significant. (From Garcia and Solomon, 1994.)

amounts and profiles, with the largest changes occurring in the upper stratosphere (Hood *et al.*, 1993; Brasseur, 1993; Fleming *et al.*, 1994).

Most solar UV variation occurs with time scales of about 11 years (*e.g.,* Cebula *et al.*, 1992) and 27 days. Over the 11-year cycle, Lyman alpha (121.6 nm) radiation varies by about a factor of two (Lean, 1991). The mid-UV (200 - 300 nm) strength varied by about 9% between the 1986 solar minimum and the 1990 solar maximum. Figure 4-12 displays the F10.7 index (a measure of the solar UV flux [*e.g.,* Donnelly, 1988]) superposed on the SBUV/SBUV2 (Solar Backscatter Ultraviolet spectrometer) total ozone that has had the QBO signal, the seasonal signal, and the trend removed by statistical methods (see Stolarski *et al.*, 1991, and Section 4.5.2 below). The figure shows that global average total ozone (40°S to 40°N) changes are correlated with UV flux variations, changing by about 1.5% (4.5 Dobson units, DU) from solar maximum to solar minimum. These changes are in reasonable agreement with calculations using 2-D models (Fleming *et al.*, 1994; Garcia *et al.*, 1984; Brasseur, 1993; Huang and Brasseur, 1993; Wuebbles *et al.*, 1991).

4.5.2 The Quasi-Biennial Oscillation and Total Ozone

Variability in the equatorial lower stratosphere is dominated by the presence of an oscillation in equatorial winds, with a period of approximately 27 months, known as the quasi-biennial oscillation (QBO). The oscillation affects not only the winds but also the thermal structure and the distribution of ozone and other minor constituents at all latitudes (*e.g.,* Chipperfield *et al.*, 1994a, and references therein). Despite the magnitude of the ozone QBO being relatively small (approx. 5-10 DU at the equator; up to about 20 DU at high latitudes) it is nevertheless significant in ozone trend studies and must be characterized and removed. Ozone trend analy-

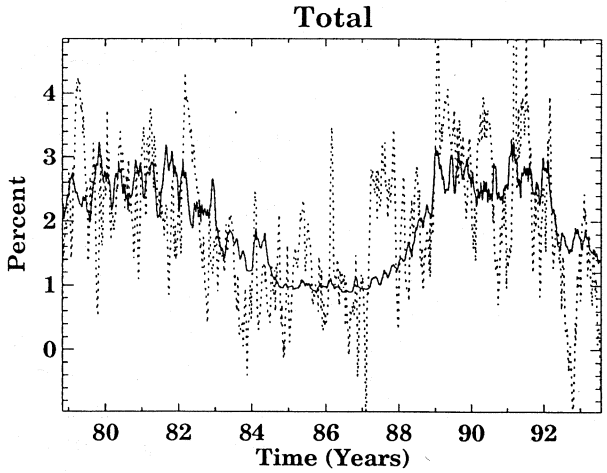

Figure 4-12. Response of SBUV/SBUV2 40°N-40°S average column ozone to the solar cycle as determined by a linear regression model after subtraction of the seasonal cycle, trend, and QBO (dashed curve). Also shown is the 10.7 cm radio flux (solid curve), which is a proxy for the solar output. The figure shows that changes in global column ozone of the order of 1.5% (4.5 DU) are to be expected during the 11-year cycle in solar output, mostly at higher altitudes. (From P. Newman, personal communication, 1994.)

ses (*e.g.*, Stolarski *et al.*, 1991) use linear regression techniques to isolate and remove the QBO signal. Observed equatorial wind data (*e.g.*, at 30 hPa) are employed as the reference time series, with the possibility of a time lag to take into account the observed variations of the QBO signal with latitude. However, observations of the ozone QBO show a strong seasonal and hemispheric asymmetry and the period of the observed ozone QBO at mid- and high latitudes is also not identical to that at the equator, often being closer to two years (Gray and Dunkerton, 1990). The use of equatorial wind data in ozone trend analyses to characterize the QBO signal at all latitudes is therefore not ideal.

II. Transport Processes Linking the Tropics, Middle, and High Latitudes

4.6 INTRODUCTION

The structure of the lower stratosphere in winter, the period when observed declines in ozone at middle latitudes are largest, is shown schematically in Figure 4-1. The diagram is intended to show the winter hemisphere when the polar vortex is well established. While the processes described below are known to occur to some extent at least, their magnitudes and relative contributions to the observed ozone declines have in many cases not been quantified reliably. While different in detail, both hemispheres correspond broadly to this picture.

In an altitude or log(pressure) framework, isentropes rise both in the tropics and in polar regions, indicative of the lower temperatures in both regions. Mixing along these isentropes can be rapid, on a time scale of days to weeks, except where potential vorticity (PV) gradients exist. In these regions, mixing is inhibited by a combination of horizontal wind shearing and dynamical "Rossby wave elasticity." The midlatitude region is bounded by a flexible PV barrier on its poleward side **(a)**, and a similar but less distinct tropical barrier to transport **(b)** at ~20 degrees. Mixing along isentropes is relatively rapid in middle latitudes in the so called "surf zone" **(c)**. Both barriers undergo episodic erosion events **(d)** when at times substantial volumes of air are transported irreversibly to middle latitudes. Evidence is accumulating that larger volumes of air come from the sub-tropical than the sub-polar barrier. However, the transport of polar air, containing high active chlorine and low ozone amounts, to midlatitudes has potentially a major influence on middle latitude composition. A mean inflow of air into the polar vortex is thought to occur **(e)** which, when coupled to descent and outflow into the more disturbed region below a potential temperature (θ) of 400 K (~16 km), allows possibly chlorine-activated ozone-depleted polar air to reach middle latitudes **(f)**. As a result of tropospheric weather features, air flow in the region below θ ~400 K is less zonal than at higher altitudes, and synoptic-scale eddy advection exchanges air between midlatitudes and polar regions.

At these low altitudes, chlorine activation may occur either on sulfate aerosols or, in the colder polar regions, on polar stratospheric clouds, again possibly influencing midlatitude ozone amounts in the very low stratosphere **(g)**. Finally, transport of air from the tropics is highly dependent on the phase of the quasi-biennial oscillation and the degree of distortion of the polar vortex **(h)**.

The extent of our understanding of these different processes is discussed below.

4.6.1 Transport of Air from the Tropics to Middle Latitudes

The tropics remain the most poorly documented and understood region of the stratosphere. Limitations in knowledge of its meteorology stem from sparse *in situ* data coverage and the breakdown of the balance approximations by which winds can be calculated from satellite-based temperature retrievals. There have also been fewer tracer measurements in the tropics than in middle latitudes. It is known that, overall, there is mean upwelling through the tropics and that this is where tropospheric source gases enter the stratosphere.

Evidence has been accumulating to support the notion that the tropical stratosphere is to some degree isolated from the active mixing present at midlatitudes in winter. Following injection into the tropical stratosphere of material from nuclear bomb tests (Feely and Spar, 1960) and the eruption of tropical volcanoes (*e.g.*, Mt. Agung; Dyer and Hicks, 1968), a decaying equatorial maximum seemed to persist as a tropical "reservoir" for up to two years. This effect has also been seen more

recently following the El Chichón and Mt. Pinatubo eruptions (Trepte *et al.*, 1993; Hofmann *et al.*, 1994). The existence of at least a partial subtropical transport barrier, at the equatorward edge of the winter midlatitude "surf zone," has also been deduced from theoretical arguments and numerical models (McIntyre 1990; Norton 1994; Polvani *et al.*, 1994). Recent observations of the tracers N_2O and CO_2 in the low stratosphere (Boering *et al.*, 1994) provide direct observational support for the relatively short mixing times in the "surf zone" region.

Analyses of data from the Limb Infrared Monitor of the Stratosphere (LIMS) instrument on Nimbus 7, from *in situ* aircraft data, and from instruments on the Upper Atmosphere Research Satellite (UARS) have all shown strong gradients of tracers and of potential vorticity in the sub-tropics, with occasional filaments of tropical material being entrained poleward (Leovy *et al.*, 1985; Murphy *et al.*, 1993; Randel *et al.*, 1993); this behavior is also reproduced in dynamical models (Boville *et al.*, 1991; Norton, 1994; Pierce *et al.*, 1993; Rood *et al.*, 1992; Waugh, 1993a; Chen and Holton, 1994; Polvani *et al.*, 1994; Bithell *et al.*, 1994).

The tropical lower stratosphere is also strongly influenced by the quasi-biennial oscillation (QBO), which has a significant impact on the meridional circulation (Plumb and Bell, 1982). The QBO affects meridional transport of ozone and other trace species by a modulation of planetary (Rossby) wave transport. When the Rossby wave amplitude increases sufficiently, the waves "break," resulting in irreversible transport in midlatitudes. The latitudinal region in which the waves break (the "surf zone") is affected by the background winds in equatorial regions, particularly in the case of strongly nonlinear waves (O'Sullivan and Young, 1992). Easterly equatorial winds confine the Rossby waves further polewards than westerly winds, resulting in enhanced meridional exchange of air between the subtropical and higher latitudes (see, *e.g.*, Baldwin and Dunkerton, 1990; Garcia, 1991; Dunkerton and Baldwin, 1992).

Extensive observations — ground-based, *in situ*, and satellite-based — of the formation, dispersion, and decay of stratospheric aerosol produced by the eruption of Mt. Pinatubo (15°N) in June 1991 have provided much insight into the processes of transport out of the tropics. These observations and their implications are described in the following.

4.6.2 The Mt. Pinatubo Eruption: Implications for Understanding of Transport Processes

Prior to the June 1991 eruption, the total stratospheric aerosol mass (as inferred using SAGE observations) was approximately 1 Mt, but by the end of 1991 the estimated mass had increased to ~30 Mt. The total mass has since decreased to approximately 10 Mt by mid-1993 and to around 3 Mt by mid-1994 (see Figure 4-13). The formation of the Mt. Pinatubo aerosol cloud in the stratosphere and its subsequent dispersal around the globe, monitored from the ground and satellites, have provided useful tests of our understanding of transport processes.

4.6.2.1 Tropical Latitudes

In many respects, the temporal development of the Mt. Pinatubo aerosol distribution was similar to that observed following other high altitude tropical injections. A distinguishing characteristic of this eruption was the rapid movement of volcanic material across the equator within two weeks of the eruption (Bluth *et al.*, 1992; McCormick and Veiga, 1992). Young *et al.* (1993) re-

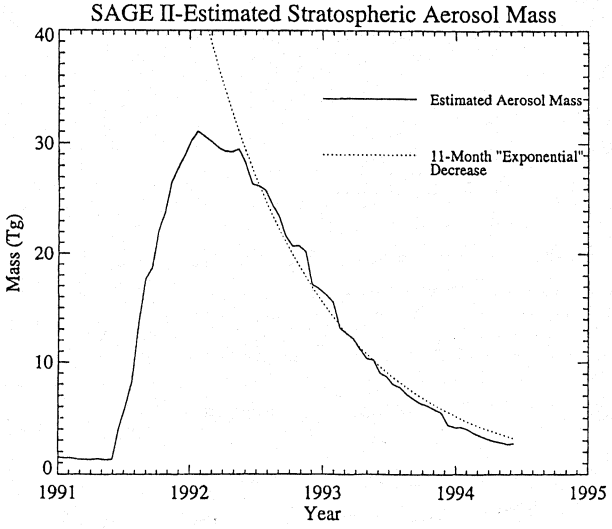

Figure 4-13. SAGE II estimated stratospheric aerosol mass, showing the near exponential decay on a time scale of ~11 months following the eruption in mid-1991. (Thomason and Poole, private communication.)

ported that this drift was induced by local aerosol heating. The heating was also sufficient to cause large increases in tropical stratospheric temperatures (Labitzke and McCormick, 1992) and may have contributed to the upward transport of aerosols to above 35 km by October 1991 (Trepte *et al.*, 1993). The tropical aerosol reservoir has gradually diminished in magnitude since the eruption as aerosols became dispersed poleward and were removed by sedimentation.

It is now appreciated that the detrainment of tropical air to midlatitudes occurs in episodic events when the polar vortex becomes displaced from the pole and interacts with the subtropical flow (*e.g.,* Randel *et al.*, 1993; Trepte *et al.*, 1993; Waugh, 1993a).

Transport from the tropics takes place in two regimes, at different altitudes. In the lower transport regime (about a scale height above the tropopause) air moves rapidly poleward and downward (Fujiwara *et al.*, 1982; Kent and McCormick, 1984). This transport is most effective during winter, especially in the Northern Hemisphere. Poleward spreading of aerosols is also observed during summer associated with tropospheric monsoon circulations. Early appearances of aerosol above Japan and Germany, amongst other places, were associated with this circulation (Hayashida, 1991; Jaeger, 1992). The dispersion rate of the main aerosol cloud was estimated from shipboard lidar measurements to be around 5 degrees latitude per month in the region 8°N to 22°N, during the period July 11 to September 21 (Nardi *et al.*, 1993).

In the upper regime (above 22 km), aerosols are redistributed by motions associated with the QBO (Trepte and Hitchmann, 1992). During the descending QBO westerly wind shear, anomalous subsidence (relative to the climatological upwelling) takes place over the equator, transporting aerosols downward and poleward below the shear layer. However, during the descending QBO easterly shear, enhanced lofting of aerosol occurs over the equator, with poleward flow above the shear layer.

Consistent with this picture, within the upper regime at altitudes where zonal mean westerlies existed, strong meridional gradients of volcanic aerosol, indicative of rapid poleward mixing, were present near 20°N and S (Browell *et al.*, 1993; Trepte *et al.*, 1993), while at heights where easterlies lay over the equator, the subtropical gradients were diminished or absent, with greater mixing taking place at higher altitudes.

4.6.2.2 Middle and High Latitudes

Some aerosol spread rapidly to middle and high Northern latitudes in the low stratosphere, being first observed two weeks after the eruption in midlatitudes (Jaeger, 1992), in early August at Andoya (69°N) and on August 11 at Ny-Alesund (79°N) (Neuber *et al.*, 1994). However, the main part of the cloud did not reach Haute-Provence and Garmisch-Partenkirchen (48°N) until mid-October, with the highest backscatter ratios being observed in December 1992. In the Arctic, values of integrated backscatter at Spitzbergen were generally lower than at midlatitudes (Jaeger, 1993). In addition to satellite observations, extensive aerosol measurements from ground-based lidars in middle and high latitudes, and from airborne lidar and *in situ* instruments were performed during the European Arctic Stratospheric Ozone Experiment (EASOE) and NASA Airborne Arctic Stratospheric Expedition (AASE II) campaigns of winter 1991-92. Together, these data indicate efficient latitudinal transport below about 400-450K (15-19 km) but a largely isolated vortex, with little aerosol penetration, at higher altitudes (Tuck, 1989; Brock *et al.*, 1993; Browell *et al.*, 1993; Neuber *et al.*, 1994; Pitts and Thomason, 1993), although the differences in aerosol characteristics between inside and outside the vortex are less apparent when referenced to N_2O (Borrmann *et al.*, 1993; Proffitt *et al.*, 1993). Also, occasional intrusions of aerosol-rich midlatitude air into polar regions have been documented (Rosen *et al.*, 1992; Plumb *et al.*, 1994). Lidar measurements performed during the same period of time at Dumont d'Urville (68°S) showed that the aerosol did not penetrate the Antarctic vortex in 1991 (Godin *et al.*, 1992). In contrast, the smaller volcanic cloud of Cerro Hudson (46°S), which was injected into the lower stratosphere (around 12 km) in August 1991, spread rapidly into polar regions, again revealing efficient transport beneath the vortex (Godin *et al.*, 1992; Pitts and Thomason, 1993; Schoeberl *et al.*, 1993b). (Refer to Figure 4-14.)

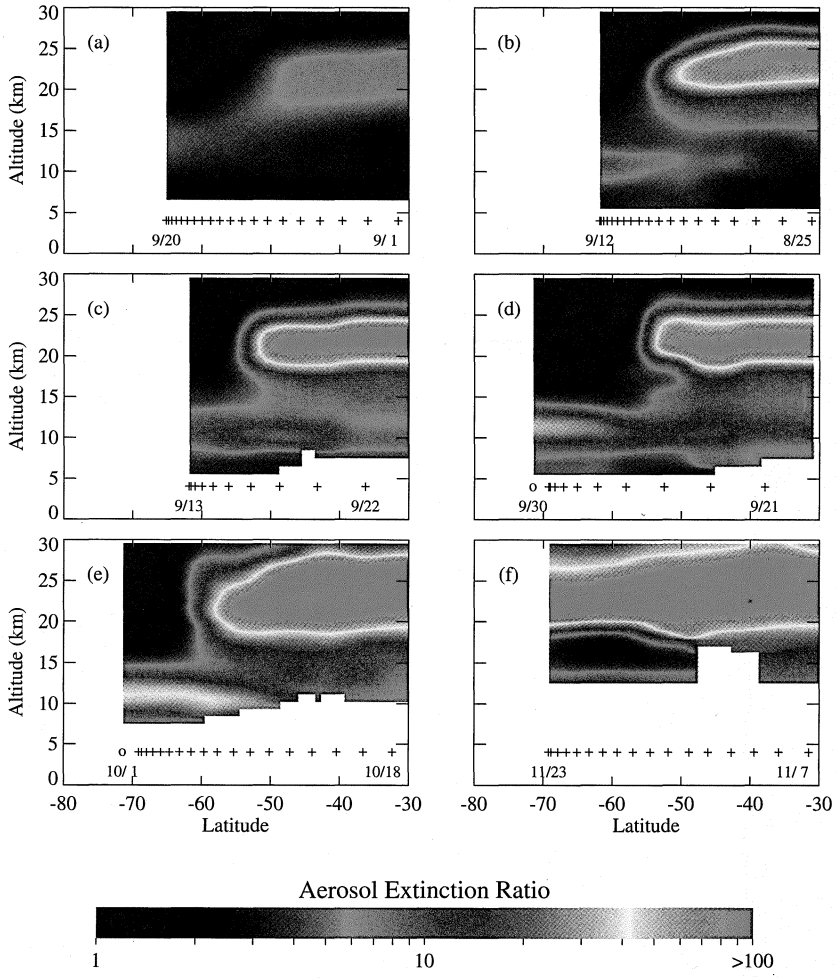

Figure 4-14. Latitude-altitude median cross sections of SAGE II and Stratospheric Aerosol Measurement (SAM II) 1-μm aerosol extinction ratio for six periods shown in each panel. The crosses and circles indicate the daily mean latitudes of the SAGE II and SAM II observations, respectively. The main region of high extinction ratio at 20 - 25 km is due to the Mt. Pinatubo aerosol cloud, while the band at 10 km originates from the Mt. Cerro Hudson eruption. The higher altitude cloud does not penetrate the established polar vortex, while that at lower altitudes progresses poleward more readily. (From Pitts and Thomason, 1993.)

4.6.3 Circulation-Induced Ozone Changes Resulting from the Mt. Pinatubo Eruption

4.6.3.1 Radiative Effects of Stratospheric Aerosol

Changes in stratospheric aerosol loading alter the radiative properties of the atmosphere, and so have the potential to not only modify local temperatures but also to alter the stratospheric circulation. In general, changes both to the absorption and emission of infrared radiation and to the solar heating rate must be considered.

In the infrared, the effects of small aerosol particles (radius less than ~0.1 μm) can generally be neglected, as their extinction is insignificant. Infrared absorption and emission become increasingly important at larger aerosol sizes. The strength of infrared heating also depends on the difference between the aerosol temperature and the radiative temperature of the troposphere below. Thus, the largest differential infrared heating by

aerosol particles of a given size would occur over warm surfaces, such as are found in the tropical troposphere.

The absorption of solar radiation by sulfuric acid particles (of any size) is small. This contrasts with, for example, ash particles, which would be expected to absorb solar radiation strongly.

4.6.3.2 Heating by Mt. Pinatubo Aerosols

The Mt. Pinatubo eruption injected huge amounts of SO_2 into the stratosphere. Ash particles also injected may have caused transitory local heating before falling back into the troposphere. The subsequent conversion of SO_2 into H_2SO_4/H_2O particles (~75% sulfuric acid solution droplets at normal stratospheric temperatures, *e.g.*, Sheridan *et al.*, 1992) generated, within several weeks, sharp increases not only in aerosol abundance and but also aerosol size (*e.g.*, Valero and Pilewskie, 1992).

Infrared radiative effects dominated in the presence of the sulfuric acid aerosols particles, which were transparent to solar radiation. Heating in the stratospheric aerosol layer was strongest over tropical latitudes, not only because most of the aerosol was initially confined to that region, but also because there, the tropospheric radiative temperatures were highest.

Reductions in aerosol optical depth occurred in the tropics as aerosol was transported to higher latitudes and sedimentation took place (Stowe *et al.*, 1992; Mergenthaler *et al.*, 1993). The resulting reduction in differential infrared heating was partially compensated by growth of aerosols to larger sizes (Dutton *et al.*, 1994). Thus, calculated infrared heating anomalies in the tropical lower stratosphere, which reached a maximum of about 0.4 K/day immediately following the eruption (*e.g.*, Brasseur and Granier, 1992), remained at above 0.2 K/day for at least another year.

4.6.3.3 Aerosol Heating and Induced Response

The relationship between aerosol heating and the induced circulation is complex. Locally, temperatures are determined both by local heating and by the remotely-forced meridional circulation. The stratospheric meridional circulation is, in turn, controlled not only by radiation but also by midlatitude wave driving (Haynes *et al.*, 1991), although the control by the latter may be less complete in the tropics than in midlatitudes. Modeling studies (Pitari, 1993) established that changes in the Brewer-Dobson circulation and in planetary wave behavior would occur in response to tropical temperature changes resulting from the increased aerosol loading.

There are also a number of feedback effects, many of which are negative, implying that the actual response would be weaker than radiative calculations alone would suggest. For example, there is a negative ozone feedback effect: enhanced upward motion in the tropical lower stratosphere would reduce ozone concentrations, resulting in smaller (mainly solar but also infrared) ozone heating in the aerosol layer. Also, local warming would be expected to reduce directly the infrared radiative heating rate.

Following the eruption, temperature anomalies of 2-3 K were observed in the tropical lower stratosphere (Labitzke and McCormick, 1992). Brasseur and Granier (1992) and Pitari (1993), using 2-D and 3-D models, respectively, have calculated radiative heating anomalies of around 0.2 K/day in that region and anomalous upwelling of around 0.05 mm/s through much of the tropical stratosphere during the Northern winter. Kinne *et al.* (1992) deduced a stronger circulation response in a calculation that did not include dynamical feedbacks. Tracer observations confirmed this picture, indicating enhanced upward motion over the central tropics (*e.g.*, G. Toon *et al.*, 1993).

Ozone concentrations in the tropical lower stratosphere were reduced well into the second year after the Mt. Pinatubo eruption (Grant *et al.*, 1992). The ozone reductions immediately following the eruption may be explained almost entirely by aerosol-induced upwelling (Kinne *et al.*, 1992). For longer-term changes, chemical as well as dynamical effects must be considered. Calculations of ozone reduction arising from circulation changes have been made in 2-D (Brasseur and Granier, 1992; Tie *et al.*, 1994) and 3-D (Pitari, 1993; Pitari and Rizi, 1993) models.

In the tropics, models calculate column ozone reductions of the order of 5%. In the model of Pitari and Rizi (1993), this reduction was attributed largely to changes in photolysis rates, with the direct effect of circulation changes being small (0-2%). However, Brasseur and Granier (1992) and Tie *et al.* (1994) suggest that circulation changes led to somewhat larger reductions (up to ~5%) in column ozone in the months immediately following the eruption. Loss of tropical

ozone in the tropics by heterogeneous chemical processes was, in all instances, found to be small.

At midlatitudes, circulation changes were found to lead to generally small reductions in ozone in the Southern (summer) Hemisphere, but to significant increases (2-8%) at middle and high latitudes in the Northern (winter) Hemisphere in the year following the eruption. However, in the winter hemisphere, the column ozone increases due to transport were more than offset by large (>10%) losses due to heterogeneous chemistry that was more effective largely because of reduced winter photolysis rates, leaving widespread net ozone reductions of 5-10%.

Overall, the calculations suggest that as a result of the Mt. Pinatubo eruption, chemical effects, through heterogeneous reactions and changes in photolysis rates, appear to be the major factors leading to ozone changes globally; changes in atmospheric transport are likely to have produced significant regional effects.

4.7 TRANSPORT OF AIR FROM POLAR REGIONS TO MIDDLE LATITUDES

4.7.1 Transport of Air from High Latitudes: Possible Influence on Midlatitude Ozone Loss

There are differences of view regarding the importance of the transport of air through polar regions to middle latitudes and its impact on midlatitude ozone loss. One view is that containment of air within the polar vortex is, to a good approximation, complete during winter, and that virtually all transport occurs as the polar vortex breaks down during spring. During this process, air from within the polar vortex, in which ozone may have been depleted, mixes with low-latitude air and reduces the midlatitude ozone column purely by dilution. There is then a clear upper limit on ozone loss: no more ozone can be destroyed than the amount contained within the polar vortex when it first forms in early winter.

An alternative view is that expressed as the "flowing processor hypothesis," namely, that the air in polar regions is not well contained and that a substantial volume of air passes through those regions to middle latitudes throughout the winter months. If vortex temperatures are low enough, then polar stratospheric clouds (PSCs) will form within the vortex and heterogeneous chemistry will cause reactive chlorine concentrations to rise. Denitrification, which allows active chlorine compounds to persist for longer, may also occur (as may dehydration). Large amounts of air passing through the vortex to middle latitudes could thus be chemically primed for ozone loss. In such a situation, although temperatures in middle latitudes may never have reached the threshold for PSC formation, the effects of heterogeneous PSC chemistry (and dehydration) would still be apparent. Midlatitude ozone loss could then proceed, initiated by the polar air. Because the volume of lower-stratospheric air exposed to PSC chemistry could be substantially greater than the instantaneous volume of the polar vortex, the potential for ozone loss would be significantly enhanced over simple dilution. Two main transport pathways have been proposed: that air from the polar vortex spreads outwards throughout the hemisphere during the winter at altitudes up to ~35 km (10 hpa); or that air descends rapidly through the lower boundary of the vortex at about θ = 400 K to the sub-vortex region, where it can be transported to lower latitudes.

It is also possible that chlorine activation is not confined to the polar vortex, but could occur on PSCs or on sulfate aerosol outside the vortex, either in the region surrounding the vortex edge or in the very low stratosphere below about θ = 400 K where the polar vortex is less well defined. PSC formation in both regions is certainly possible, and indeed is likely at the temperatures observed in winter.

These different scenarios have very different implications for understanding and predicting midlatitude ozone loss.

4.7.2 Fluid-Dynamical Considerations

The present perception of polar-vortex dynamics is that the vortex, above a "transition isentrope" at about 400K, is very likely to behave in a manner similar to that of idealized polar vortices in single-layer, high-resolution models (*e.g.,* Legras and Dritschel, 1993; Norton, 1994 and references therein), in laboratory experiments (*e.g.,* Sommeria *et al.*, 1989), and in the multi-layer, low-resolution models now being run by several groups. From these studies, it appears that the edge of the vortex acts as a flexible barrier, strongly inhibiting the large-scale, quasi-horizontal eddy transport. However, none of the models suggests that this inhibition is complete.

Fluid-dynamical evidence points not to mean outflow but to weak mean inflow. It is just such inflow that creates the vortex on the seasonal time scale. Total poleward parcel displacements of a few degrees in latitude are enough to create the vortex; these displacements are of the same order as would be given by a simplistic angular momentum budget for a frictionless, exactly circular vortex.

Some additional inflow, of a similar order of magnitude, is required to maintain the vortex against Rossby and gravity wave drag. Conversely, if a strong mean outflow were to exist in the real wintertime polar lower stratosphere, then a strong eastward force of unknown origin would have to be acting to maintain the vortex. An outflow strong enough to conform to the flowing processor hypothesis in its extreme form, *i.e.*, an outflow strong enough to export, say, three vortex masses per winter, would, in the absence of an eastward force, obliterate the vortex on a short time scale of the order of 5 days (McIntyre, 1994).

Eddy-induced erosion of the vortex can act against the mean inflow. Outward eddy transport is limited by the rate at which the vortex edge can be eroded by episodic disturbances and associated midlatitude stirring. There is remarkable consistency with which strong eddy-transport inhibition is predicted over a big range of artificial model diffusivities, and of numerical resolutions from effective grid sizes from about 10 degrees of latitude (Pierce and Fairlie, 1993) through 1 degree of latitude (Juckes and McIntyre, 1987) to effectively infinite resolution obtained via adaptive Lagrangian numerics (*e.g.*, Legras and Dritschel, 1993; Dritschel and Saravanan, 1994). Model studies that use either Eulerian techniques or high-resolution Lagrangian advection techniques (contour advection or many-particle) on model-generated wind fields or on meteorologically analyzed wind fields have also been performed (*e.g.*, Pierce and Fairlie, 1993; Manney *et al.*, 1994; Norton, 1994; Rood *et al.*, 1992; Fisher *et al.*, 1993; Waugh, 1994b; Waugh *et al.*, 1994; Chen *et al.*, 1994). All give weak erosion rates, in the sense that the mass transported is, conservatively, no more than about a third of a vortex mass per month on average, regardless of the ambiguity in defining the vortex edge (due to its filamentary fine structure) and regardless of the very wide range of model resolutions and artificial model eddy diffusivities.

However, the possible roles of unresolvable motions such as breaking inertia-gravity waves in the lower stratospheric vortex edge have yet to be quantified.

Several other transport mechanisms should be considered. For example, if there is significant descent of vortex air into the sub-vortex region, this could be rapidly dispersed throughout the hemisphere. However, in order to sustain a large enough transport through the vortex, diabatic descent rates within the lower-stratospheric vortex would need to be much greater than seems compatible with observed temperatures and with very extensive studies in atmospheric radiation, whose physics is fundamentally well understood (*e.g.*, Schoeberl *et al.*, 1992).

Another possibility is that the sub-vortex region below the transition isentrope around 400-425 K could itself act as a "flowing processor." The transition isentrope exists because of stirring by anticyclones and other synoptic-scale meteorological disturbances underneath the vortex and the upward-evanescent character of the relevant waves. There is less inhibition of quasi-horizontal eddy transport at these lower levels: large eddy exchanges of midlatitude air with the sub-vortex region are thus expected (Tuck, 1989; McIntyre, 1994). The sub-vortex region is also cold enough, in the late Antarctic winter at least, to produce chlorine activation, dehydration, and denitrification (Jones and Kilbane-Dawe, 1994).

It is also possible that chlorine activation can take place in air parcels that are above the transition isentrope but are outside the vortex (see for example, Jones *et al.*, 1990; MacKenzie *et al.*, 1994; and Pyle *et al.*, 1994).

There is evidence that all three mechanisms (shown schematically in Figure 4-1) are realized to some degree, and presumably in different proportions in the South and North. Large transport rates of air from within the vortex seem likely to occur only when the vortex breaks down. However, the above arguments suggest that while transport due to vortex erosion may play a noticeable role in midlatitude ozone loss, it would not appear to be the dominant one.

4.7.3 Observational Studies Relating to Transport through the Vortex

4.7.3.1 Exchange of Air across the Vortex Boundary

The appearance near the vortex edge of filamentary structure in many species (see, *e.g.,* Murphy *et al.,* 1989; Tuck *et al.*, 1992; and below), and features such as laminae in ozone profiles (Reid *et al.*, 1993), is highly suggestive that some irreversible exchange of air is occurring across the boundary of the vortex. A number of studies have attempted to quantify outflow rates.

Using data from the Halogen Occultation Experiment (HALOE), Russell *et al.* (1993a) deduced a time constant for the replacement of air between 15 and 20 km by horizontal transfer of less than a month in October 1991. Tuck *et al.* (1993), using HALOE data, have also suggested that dehydration originating from within the Antarctic polar vortex spread over the entire Southern Hemisphere up to the 10-20 hPa region. The extent of the dehydration implied, they argued, that vortex air was being flushed out "several times" during the winter months. However, subsequent revisions of these satellite data based on an improved retrieval (Chapter 3; Figure 3-18) have markedly reduced the vertical and latitudinal extents of the dehydration apparent in the data, implying significantly lower outflow rates than these early studies suggested.

Several other studies have suggested relatively rapid exchange. Tao and Tuck (1994) examined the distribution of temperatures with respect to the vortex edge in the Southern winter of 1987 and the Northern winter of 1988-1989. They find that there is evidence of air chemically unprocessed by PSCs being dynamically resupplied to the vortex, they argue by mixing and descent. Tuck *et al.* (1994) used ER-2 observations of NO_y from the airborne missions in 1987, 1988-1989, and 1991-1992 to attempt to quantify vortex outflow rates. From the appearance of hemispheric and interannual differences in midlatitude NO_y, they concluded that the vortex must have been flushed more than once during the period of denitrification and dehydration.

The latter study is hard to reconcile with a number of other studies. Proffitt *et al.* (1989) argue that NO_y and N_2O observations obtained during the 1987 airborne mission point rather to significant inflow and descent (see Section 4.7.3.2). However, the extent of inflow proposed by Proffitt *et al.* is probably inconsistent with the angular momentum budget (*e.g.,* Plumb, 1990). Jones and MacKenzie (1994) also used the observed relationship between NO_y and N_2O concentrations to attempt to quantify the transport of air from the polar regions to midlatitudes. In that study some instances when recently denitrified air was found outside the vortex were observed, arguing against complete containment, but these features were small in scale. However, they found no evidence of large-scale outflow of air from the polar vortices above $\theta = 400$ K.

4.7.3.2 Descent of Air through the Lower Boundary of the Vortex

Proffitt *et al.* (1989, 1990, 1993) and Tuck (1989) have argued that the descent of ozone-depleted air through the lower boundary of the polar vortex, where it can be dispersed to lower latitudes, can significantly reduce midlatitude ozone amounts. Using statistical relationships between O_3 and N_2O, Proffitt *et al.* (1993) deduced altitude-dependent changes in ozone during the Northern winter of 1991-1992, with decreases at the bottom of the vortex and increases at the highest altitudes accessible to the ER-2 aircraft. The increase aloft was attributed to ozone-rich air entering the vortex from above, while the reduction lower down was taken to be the result of chlorine-catalyzed loss during descent through the region of PSC formation. Basing the rate of downward motion of air on a cooling rate of 1 K/day (in θ), ozone-depleted air released from the bottom of the vortex in 1991-1992 was, they argued, sufficient to reduce significantly the ozone column in middle latitudes. Using the same methodology, Collins *et al.* (1993) made measurements of the N_2O-O_3 correlation from the DC-8, which they interpret as showing descent of vortex air over the Arctic to levels just above the tropopause during the winter of 1991-1992; they also show 20% ozone reductions in March relative to January and February.

However, there is considerable debate about the importance of the descent of air through the vortex lower boundary for midlatitude ozone. The efficacy of such a process will depend on the rate of descent of air, and thus on diabatic cooling rates. For example, the cooling rate used in Proffitt *et al.*, 1993, (1 K/day) is a factor of 2-10 larger than other published estimates of diabatic cooling rates (*e.g.,* Schoeberl *et al.*, 1992).

4.7.3.3 Transport in the Sub-Vortex Region

There is less inhibition of quasi-horizontal eddy transport at the levels below the vortex (θ = 400-425 K) and large eddy exchanges of midlatitude air with the sub-vortex region are thus expected (Tuck, 1989; McIntyre, 1994). Jones and Kilbane-Dawe (1994) have investigated the extent to which ozone can be reduced in this region by *in situ* chemical processes rather than by transport of ozone-depleted air from the vortex above. They pointed out that temperatures in this region fall significantly below the threshold for polar stratospheric cloud formation, and thus for chlorine activation, for much of the Southern winter and, although more variable, the same is frequently seen in the North. Using ozonesonde measurements made during the 1987 Southern winter, Jones and Kilbane-Dawe (1994) identified significant reductions of ozone in the sub-vortex region (~350K) extending to ~55°S. As these reductions occurred at a time when temperatures were cold enough for chlorine activation, and when the ozone vertical gradient was such that diabatic descent would have increased ozone mixing ratios, they attributed these reductions to *in situ* photochemical loss. The total *in situ* ozone loss in the sub-vortex region was, in 1987, a significant fraction of the overall hemispheric reduction. They also argue that in the Northern Hemisphere in some winters (*e.g.*, the winter of 1993-4) the sub-vortex region may allow a significant fraction of lower latitude air to become chlorine-activated, and may, in some years, be more important than at higher altitudes.

4.7.4 Model Studies Relating to Transport through the Vortex

Since the last WMO/UNEP assessment, a number of new modeling studies have been carried out to investigate the extent to which air is mixed between the polar vortex and middle latitudes. Many of these have concentrated on the Arctic vortex, studied extensively in the two polar campaigns, EASOE and AASE II, in the winters of 1991/92. Studies using UARS data have also appeared.

The studies all show mixing, to a greater or lesser extent, but most support the idea of only limited flow through the polar vortex. However, it should be pointed out that chemical tracer measurements suggest that structure exists on scales so far unresolved by even the highest resolution analyses but, as indicated above, whether this represents a fatal flaw in model studies is not clear.

In separate studies of the AASE and Airborne Antarctic Ozone Experiment (AAOE) data, involving the reconstruction of the chemical constituent fields in PV-θ space followed by an estimation of the meridional circulation and eddy diffusivities, Schoeberl *et al.* (1992) reached similar conclusions to the earlier study of Hartmann *et al.* (1989): that the center of the vortex is highly isolated but that exchange of trace gases does occur, principally at the vortex edge, by erosional wave activity. Consistent with earlier studies, Rood *et al.* (1992) conclude that intense cyclonic activity close to the vortex edge and large planetary-scale events are the major mechanisms of extra-vortex transport. Nevertheless, in their study of a disturbed period in January and February 1989, only a small amount of vortex air was found at lower latitudes.

Erosion at the vortex edge has been demonstrated in greater detail in a number of new studies using the technique of contour advection with surgery (Norton, 1994; Waugh, 1994b; Plumb *et al.*, 1994; Waugh *et al.*, 1994). Results from these studies show thin filaments being dragged around the vortex edge and being carried into middle latitudes. An example during a disturbed period in January 1992 is shown in Figure 4-15. The fine structure evident in the figure is consistent with potential vorticity, but reveals structure on scales not resolvable in the PV maps. Estimates of the outflow of vortex air to midlatitudes by Waugh *et al.*, 1994 (see Table 4-1) suggest, however, that while major erosion events do occur (*e.g.*, Jan. 16-28), the net outflow of air from the vortex appears small, at least above 400 K. Similar conclusions are drawn by Pierce and Fairlie (1993) in a study of the evolution of material lines; by Strahan and Mahlman (1994), who compared high resolution general circulation model results with N_2O observations near the vortex edge; and by Dahlberg and Bowman (1994), who carried out isentropic trajectory studies for nine Northern Hemisphere winters.

A number of studies have attempted to model the chemical effects relating to ozone loss. Chipperfield *et al.* (1994b) and Chipperfield (1994) studied the Arctic winters of 1991/92 and 1922/93. Figure 4-16 shows the distribution of a tracer indicating that air has experienced the conditions (low temperatures and sunlight) necessary for rapid ozone loss. Most of the tracer is well

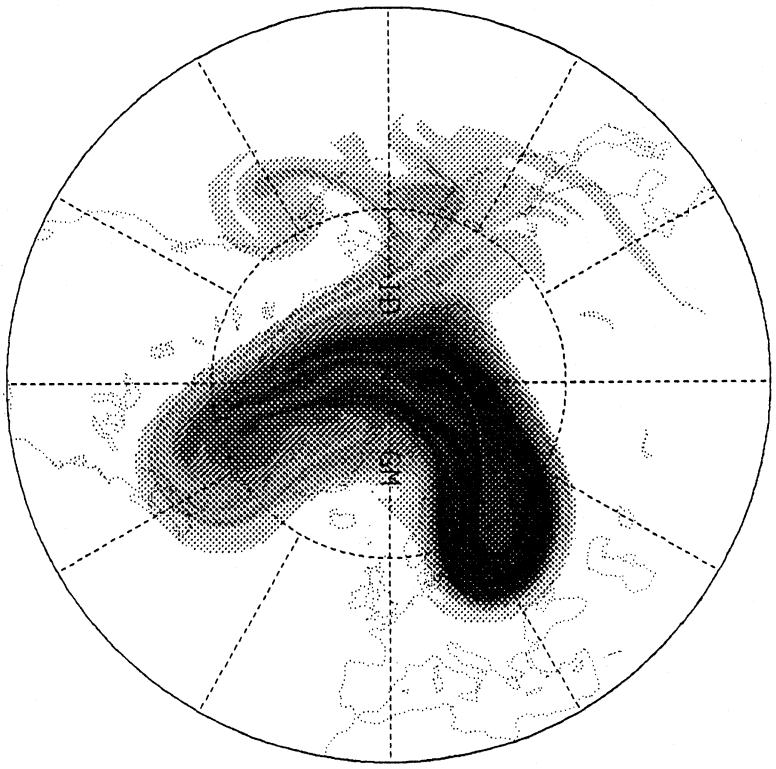

Figure 4-15. High resolution evolution of the vortex on the 450 K isentropic surface, 16-28 January 1992, as determined using contour advection with surgery. Model contours were initialized on 16 January on potential vorticity contours from the NMC analysis. Subsequently the contours were advected with the daily analyzed 450 K balanced winds. Note the transport of a significant volume of air to midlatitudes near 165°E. (From Plumb *et al.*, 1994.)

Table 4-1. Area of air transported out of the vortex expressed as a percentage of the vortex area (P_1) or as a percentage of the area between the vortex and 30°N (P_2) during selected periods during the Northern winter of 1991/2. (From Waugh *et al.*, 1994.)

Period	P_1	P_2
Dec. 6 - 18, 1991	1	0
Dec. 16 - 26, 1991	1	0
Dec. 23, 1991 to Jan. 2, 1992	5	1
Jan. 1 - 11, 1992	7	2
Jan. 7 - 17, 1992	3	1
Jan. 16 - 28, 1992	31	7
Feb. 2 - 11, 1992	2	0
Feb. 9 - 19, 1992	0	0
Feb. 19 - 28, 1992	5	3

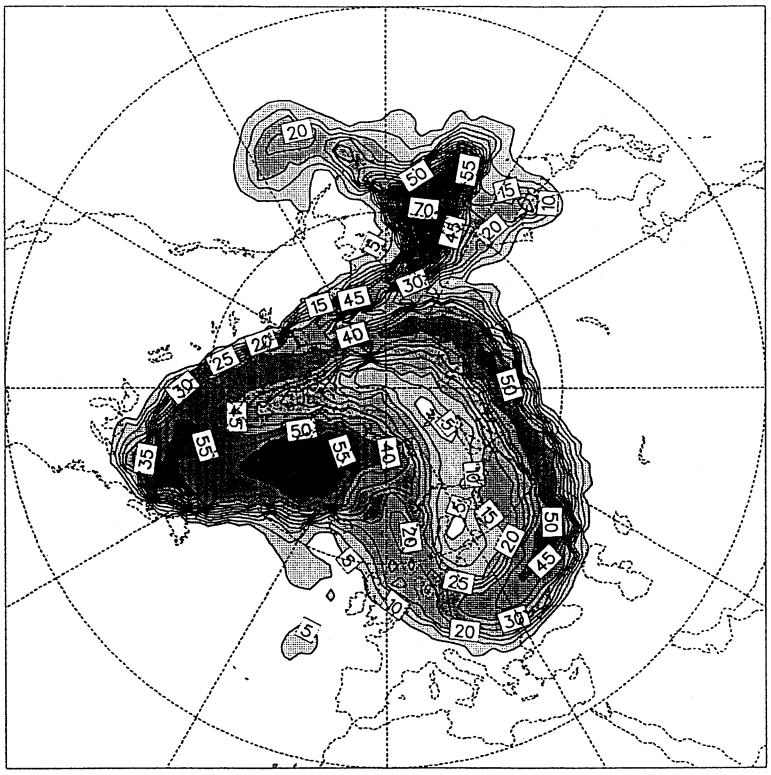

Figure 4-16. Modeled distribution of a tracer showing chlorine activation and exposure to sunlight on the 475 K potential temperature surface for January 20, 1992. In this case, the tracer is the number of hours of ozone destruction. As in Figure 4-15, significant transport outside the vortex is seen near 165°E. High ClO_x concentrations are calculated to be present in the same region. (From Chipperfield *et al.*, 1994b.)

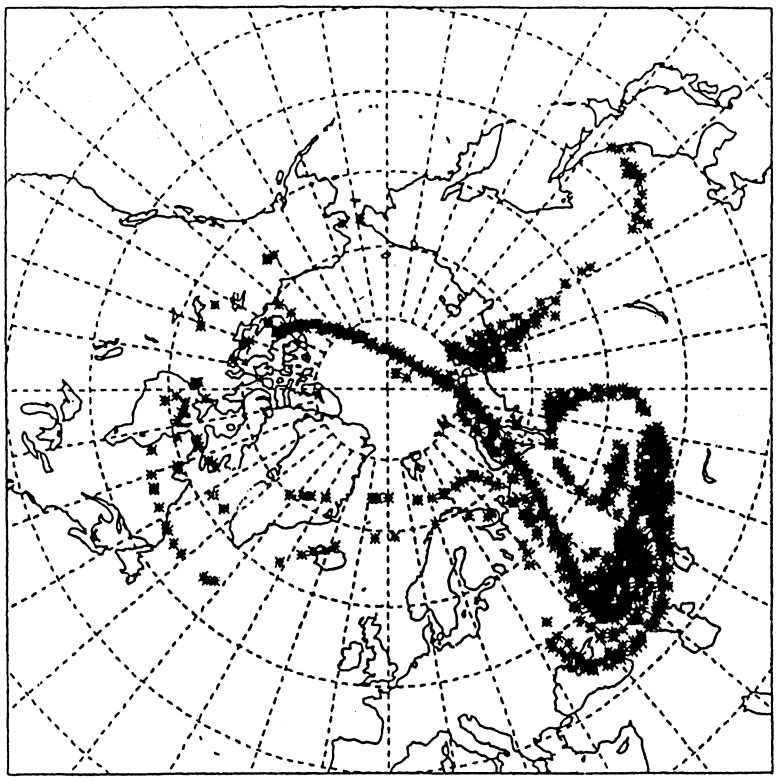

Figure 4-17. Trajectory endpoints for 28 January 1992. The trajectories were initialized on the 475 K potential temperature surface 10 days earlier close to the edge of the polar vortex in a region favorable for PSC formation and in which chlorine activation was expected to have occurred. While the majority of the trajectories remained on the vortex edge, a significant number became detached from the vortex. In the latter group (shown near the Black Sea) O_3 losses of ~1% per day were calculated. (From Pyle *et al.*, 1994.)

within the polar vortex, but there is an activated region moving away from the vortex edge at 165°E. The level of consistency between these results and the contour advection results of Plumb *et al.* (1994) for the same period (Figure 4-15) is striking, particularly given their differences of approach.

A number of recent studies using trajectories confirm the notion that chlorine activation can occur at the vortex edge (see, *e.g.*, Jones *et al.*, 1990). MacKenzie *et al.* (1994), using ensembles of isentropic trajectories, found examples of air that had been chlorine-activated by PSCs outside the vortex. However, in these cases the relevant low temperatures had been encountered at PV values characteristic of the vortex edge. Such a conclusion is consistent with the work of Tao and Tuck (1994). However, MacKenzie *et al.* (1994) found no evidence of air having been ejected from the center of the vortex. Broadly similar results were obtained by Pierce *et al.* (1994), who performed trajectory studies to analyze the HALOE data in the Southern Hemisphere. In an explicit calculation of photochemical ozone loss, Pyle *et al.* (1994) used trajectories to show that a region of high PV chlorine-activated air had been eroded from the vortex to 45°N in January 1992 (see Figure 4-17). Ozone depletions of around 0.1% per day were calculated for those trajectories staying close to the vortex edge. However, for the trajectories that moved to lower latitudes, a depletion of the order of 1% per day was calculated.

Thus, while it appears that the processes discussed in Section 4.7.1 are indeed affecting midlatitude ozone amounts, these modeling studies suggest that their impact is modest.

REFERENCES

Abbatt, J.P.D., Heterogeneous reaction of HOBr with HBr and HCl on ice surfaces at 228 K, *Geophys. Res. Lett., 21*, 665-668, 1994.

Avallone, L.M., D.W. Toohey, W.H. Brune, R.J. Salawitch, A.E. Dessler, and J.G. Anderson, Balloon-borne in situ measurements of ClO and ozone: Implications for heterogeneous chemistry and mid-latitude ozone loss, *Geophys. Res. Lett., 20*, 1794-1797, 1993a.

Avallone, L.M., D.W. Toohey, M.H. Proffitt, J.J. Margitan, K.R. Chan, and J.G. Anderson, In situ measurements of ClO at mid-latitudes: Is there an effect from Mt. Pinatubo?, *Geophys. Res. Lett., 20*, 2519-2522, 1993b.

Baldwin, M.P., and T.J. Dunkerton, Quasi-biennial oscillation above 10 mb, *Geophys. Res. Lett., 18*, 1205-1208, 1990.

Bekki, S., and J.A. Pyle, 2-D assessment of the impact of aircraft sulphur emissions on the stratospheric sulphate aerosol layer, *J. Geophys. Res., 97*, 15839-15847, 1992.

Bekki, S., R. Toumi, and J.A. Pyle, Role of sulphur photochemistry in tropical ozone changes after the eruption of Mt. Pinatubo, *Nature, 362*, 331-333, 1993.

Bithel, M., L.J. Gray, J.E. Harries, J.M. Russell, and A.F. Tuck, Synoptic interpretation of measurements from HALOE, *J. Atmos. Sci., 51*, 2942-2956, 1994.

Bluth, G.J.S., S.D. Doiron, A.J. Krueger, I.S. Walter, and C.C. Schnetzler, Global tracking of the SO_2 cloud from the June 1991 Mt. Pinatubo eruptions, *Geophys. Res. Lett., 19*, 151-154, 1992.

Boering, K.A., B.C. Daub, S.C. Wofsy, M. Loewenstein, J.R. Podolske, and E.R. Keim, Tracer-tracer relationships and lower stratospheric dynamics: CO_2 and N_2O correlations during SPADE, *Geophys. Res. Lett., 21*, 2567-2570, 1994.

Bojkov, R.D., C.S. Zerefos, D.S. Balis, I.C. Ziomas, and A.F. Bais, Record low total ozone during Northern winters of 1992 and 1993, *Geophys. Res. Lett., 20*, 1351-1354, 1993.

Borrmann, S., *et al.*, In situ measurements of changes in stratospheric aerosol and the N_2O-aerosol relationship inside and outside of the polar vortex, *Geophys. Res. Lett., 20*, 2559-2562, 1993.

Boville, B.A., J.R. Holton, and P.W. Mote, Simulation of the Pinatubo aerosol cloud in general circulation model, *Geophys. Res. Lett., 18*, 2281-2284, 1991.

Brasseur, G.P., The response of the middle atmosphere to long-term and short-term solar variability: A two-dimensional model, *J. Geophys. Res., 98*, 23079-23090, 1993.

Brasseur, G.P., and C. Granier, Mt. Pinatubo aerosols, chlorofluorocarbons, and ozone depletion, *Science, 257*, 1239-1242, 1992.

Brock, C.A., H.H. Johnson, J.C. Wilson, J.E. Dye, D. Baumgardner, S. Borrmann, M.C. Pitts, M.T. Osborn, D.J. DeCoursy, and D.C. Woods, Relationships between optical extinction, backscatter and aerosol surface and volume in the stratosphere following the eruption of Mt. Pinatubo, *Geophys. Res. Lett., 20,* 2555-2558, 1993.

Browell, E.V., C.F. Butler, M.A. Fenn, W.B. Grant, S. Ismail, M.R. Schoeberl, O.B. Toon, M. Loewenstein, and J.R. Podolske, Ozone and aerosol changes during the 1991-1992 Airborne Arctic Stratosphere Expedition, *Science, 261*, 1155-1158, 1993.

Burkholder, J.B., R.K. Talukdar, A.R. Ravishankara, and S. Solomon, Temperature dependence of the HNO_3 UV absorption cross sections, *J. Geophys. Res., 98*, 22937-22948, 1993.

Cebula, R., and E. Hilsenrath, Ultraviolet solar irradiance measurements from the SSBUV-1 and SSBUV-2 missions, in *Proceedings of the Workshop of the Solar Electromagnetic Radiation Study for Solar Cycle 22*, edited by R.F. Donnelly, NOAA Environmental Research Laboratories, Boulder, Colorado, 1992.

Chandra, S., C.H. Jackman, A.R. Douglass, E.L. Fleming, and D.B. Considine, Chlorine-catalyzed destruction of ozone: Implications for ozone variability in the upper stratosphere, *Geophys. Res. Lett., 20*, 351-354, 1993.

Chen, P., and J.R. Holton, Mass exchange between the tropics and extratropics in the stratosphere, *J. Atmos. Sci.*, submitted, 1994.

Chen, P., J.R. Holton, A. O'Neill, and R. Swinbank, Quasi-horizontal transport and mixing in the Antarctic stratosphere, *J. Geophys. Res., 99*, 16851-16866, 1994.

Chipperfield, M.P., A 3-D model comparison of PSC processing during the Arctic winters of 1991/92 and 1992/93, *Ann. Geophys., 12*, 342-354, 1994.

Chipperfield, M.P., L.J. Gray, J.S. Kinnersley, and J. Zawodny, A two-dimensional model study of the QBO signal in SAGE II NO_2 and O_3, *Geophys. Res. Lett.*, in press, 1994a.

Chipperfield, M.P., D. Cariolle, and P. Simon, A three-dimensional transport model study of PSC processing during EASOE, *Geophys. Res. Lett., 21*, 1463-1466, 1994b.

Coffey, M.T., and W.G. Mankin, Observations of the loss of stratospheric NO_2 following volcanic eruptions, *Geophys. Res. Lett., 20*, 2873-2876, 1993.

Cohen, R.C., *et al.*, Odd nitrogen in the lower stratosphere: New constraints from the in situ measurement of hydroxyl radicals, submitted to *Geophys. Res. Lett.*, 1994.

Collins, J.E., G.W. Sachse, B.E. Anderson, A.J. Weinheimer, J.G. Walega, and B.A. Ridley, AASE-II *in-situ* tracer correlations of methane, nitrous-oxide, and ozone as observed aboard the DC-8, *Geophys. Res. Lett., 20*, 2543-2546, 1993.

Crutzen, P.J., and U. Schmailzl, Chemical budgets of the stratosphere, *Planet. Space Sci., 31,* 1009-1032, 1983.

Dahlberg, S.P., and K.P. Bowman, Climatology of large scale isentropic mixing in the Arctic winter stratosphere, submitted to *J. Geophys. Res.*, 1994.

DeMore, W.B., S.P. Sander, D.M. Golden, R.F. Hampson, M.J. Kurylo, C.J. Howard, A.R. Ravishankara, C.E. Kolb, and M.J. Molina, *Chemical Kinetics and Photochemical Data for Use in Stratospheric Modeling, Evaluation No. 9,* NASA JPL Publication 92-20, Jet Propulsion Laboratory, Pasadena, California, 1992.

Deshler, T., D.J. Hofmann, B.J. Johnson, and W.R. Rozier, Balloonborne measurements of the Pinatubo aerosol size distribution and volatility at Laramie, Wyoming during the summer of 1991, *Geophys. Res. Lett., 19*, 199-202, 1992.

Deshler, T., B.J. Johnson, and W.R. Rozier, Balloonborne measurements of Pinatubo aerosol during 1991 and 1992 at 41°N: Vertical profiles, size distribution and volatility, *Geophys. Res. Lett., 20*, 1435-1438, 1993.

Dessler, A.E., R.M. Stimpfle, B.C. Daube, R.J. Salawitch, E.M. Weinstock, D.M. Judah, J.D. Burley, J.W. Munger, S.C. Wofsy, J.G. Anderson, M.P. McCormick, and W.P. Chu, Balloonborne measurements of ClO, NO and O_3 in a volcanic cloud: An analysis of heterogeneous chemistry between 20 and 30 km, *Geophys. Res. Lett., 20*, 2527-2530, 1993.

Donnelly, R.F., Uniformity in solar UV flux variations important to the stratosphere, *Ann. Geophys., 6*, 417-424, 1988.

Dritschel, D.G., and R. Saravanan, Three-dimensional quasi-geostrophic contour dynamics, with an application to stratospheric vortex dynamics, *Quart. J. Roy. Meteorol. Soc.*, in press, 1994.

Dunkerton, T.J., and M.P. Baldwin, Modes of interannual variability in the stratosphere, *Geophys. Res. Lett., 19*, 49-52, 1992.

Dutton, E.G., P. Ready, S. Ryan, and J.J. DeLuisi, Features and effects of aerosol optical depth observed at Mauna Loa, Hawaii: 1982-1992, *J. Geophys. Res., 99*, 8295-8301, 1994.

Dyer, A.J., and B.B. Hicks, Global spread of the volcanic dust from the Bali eruption of 1963, *Quart. J. Roy. Meteorol. Soc., 94,* 545-554, 1968.

Eluszkiewicz, J., and M. Allen, A global analysis of the ozone deficit in the upper stratosphere and mesosphere, *J. Geophys. Res., 98*, 1069-1081, 1993.

Fahey, D.W., S.R. Kawa, E.L. Woodbridge, P. Tin, J.C. Wilson, H.H. Jonsson, J.E. Dye, D. Baumgardner, S. Borrmann, D.W. Toohey, L.M. Avallone, M.H. Proffitt, J. Margitan, M. Loewenstein, J.R. Podolske, R.J. Salawitch, S.C. Wofsy, M.K.W. Ko, D.E. Anderson, M.R. Schoeberl, and K.R. Chan, In situ measurements constraining the role of sulphate aerosols in mid-latitude ozone depletion, *Nature, 363*, 509-514, 1993.

Fahey, D.W., *et al.*, The removal of NO near the tropopause at mid-latitudes: A photochemical anomaly, NASA High Speed Research Program, Annual Meeting, Virginia Beach, Virginia, 1994.

Feely, H.W., and H. Spar, Tungsten-185 from nuclear bomb tests as a tracer for stratospheric meteorology, *Nature, 188*, 1062-1064, 1960.

Fisher, M., A. O'Neill, and R. Sutton, Rapid descent of mesospheric air into the stratospheric polar vortex, *Geophys. Res. Lett., 20*, 1267-1270, 1993.

Fleming, E., S. Chandra, C. Jackman, D. Considine, and A. Douglass, The middle atmospheric response to short- and long-term solar UV variations: Analysis of observations and 2-D model results, *J. Atmos. Terr. Phys.*, in press, 1994.

Froidevaux, L., J.W. Waters, W.G. Read, L.S. Elson, D.A. Flower, and R.F. Jarnot, Global ozone observations from the UARS MLS: An overview of zonal-mean results, *J. Atmos. Sci., 51,* 2846-2866, 1994.

Fujiwara, M., T. Shibata, and M. Hirono, Lidar observations of a sudden increase of aerosols in the stratosphere caused by volcanic injections, II. Sierra Negra event, *J. Atmos. Terr. Phys., 44*, 811-818, 1982.

Garcia, R.R., Parameterization of planetary wave breaking in the middle atmosphere, *J. Atmos. Sci., 48*, 1405-1419, 1991.

Garcia, R.R., S. Solomon, R.G. Roble, and D.W. Rusch, A numerical study of the response of the middle atmosphere to the 11-year solar cycle, *Planet. Space Sci., 32,* 411-423, 1984.

Garcia, R.R., and S. Solomon, A new numerical model of the middle atmosphere 2. Ozone and related species, *J. Geophys. Res., 99,* 12937-12951, 1994.

Gleason, J.F., P.K. Bhartia, J.R. Herman, R. McPeters, P. Newman, R.S. Stolarski, L. Flynn, G. Labow, D. Larko, C. Seftor, C. Wellemeyer, W.D. Komhyr, A.J. Miller, and W. Planet, Record low global ozone in 1992, *Science, 260*, 523-526, 1993.

Godin, S., C. David, A. Sarkissian, F. Goutal, P. Aimedieu, and E. Le Bouar, Systematic measurements at the Antarctic station of Dumont d'Urville, in *Proceedings of the Quadrennial Ozone Conference*, Charlottesville, Virginia, 1992.

Grant, W.B., J. Fishman, E.V. Browell, V.G. Brackett, D. Nganga, A. Minga, B. Cros, R.E. Veiga, C.F. Butler, M.A. Fenn, and G.D. Nowicki, Observations of reduced ozone concentrations in the tropical stratosphere after the eruption of Mt. Pinatubo, *Geophys. Res. Lett., 19*, 1109-1112, 1992.

Grant, W.B., E.V. Browell, J. Fishman, V.G. Brackett, R.E. Veiga, D. Nganga, A. Minga, B. Cros, C.F. Butler, M.A. Fenn, C.S. Long, and L.L. Stowe, Aerosol-associated changes in tropical stratospheric ozone following the eruption of Mt. Pinatubo, *J. Geophys. Res.*, in press, 1994.

Gray, L.J., and T.J. Dunkerton, The role of the seasonal cycle in the quasi-biennial oscillation in ozone, *J. Atmos. Sci., 47*, 2429-2451, 1990.

Hanson, D.R., J.B. Burkholder, C.J. Howard, and A.R. Ravishankara, Measurement of OH and HO_2 radical uptake coefficients on water and sulfuric acid surfaces, *J. Phys. Chem., 96,* 4979-4985, 1992.

Hanson, D.R., and A.R. Ravishankara, The reaction $ClONO_2$ + HCl on NAT, NAD and frozen sulfuric acid and the hydrolysis of N_2O_5 and $ClONO_2$ on frozen sulfuric acid, *J. Geophys. Res., 98*, 22931-22936, 1993a.

Hanson, D.R., and A.R. Ravishankara, Uptake of HCl and HOCl onto sulfuric acid — Solubilities, diffusivities and reaction, *J. Phys. Chem., 97*, 12309-12319, 1993b.

Hanson, D.R., A.R. Ravishankara, and S. Solomon, Heterogeneous reactions in sulfuric acid aerosols: A framework for model calculations, *J. Geophys. Res., 99*, 3615-3629, 1994.

Hanson, D.R., and A.R. Ravishankara, Heterogeneous chemistry of bromine species in sulfuric acid under stratospheric conditions, *Geophys. Res. Lett.*, in press, 1994.

Hartmann, D.L., L.E. Heidt, M. Loewenstein, J.R. Podolske, J. Vedder, W.L. Starr, and S.E. Strahan, Transport into the south polar vortex in early Spring, *J. Geophys. Res., 94*, 16779-16795, 1989.

Hayashida, S., Atmospheric effects, in *Global Volcanism Network Bull., 16*, 1991.

Haynes, P.H., C.J. Marks, M.E. McIntyre, T.G. Shepherd, and K.P. Shine, On the downward control of extratropical diabatic circulations by eddy-induced mean zonal forces, *J. Atmos. Sci., 48*, 651-679, 1991.

Hofmann, D.J., and S. Solomon, Ozone destruction through heterogeneous chemistry following the eruption of El Chichón, *J. Geophys. Res., 94*, 5029-5041, 1989.

Hofmann, D.J., S.J. Oltmans, W.D. Komhyr, J.M. Harris, J.A. Lathrop, A.O. Langford, T. Deshler, B.J. Johnson, A. Torres, and W.A. Matthews, Ozone loss in the lower stratosphere over the United States in 1992-1993: Evidence for heterogeneous chemistry on the Pinatubo aerosol, *Geophys. Res. Lett., 21*, 65-68, 1994.

Hood, L.L., R.D. McPeters, J.P. McCormack, L.E. Flynn, S.M. Hollandsworth, and J.F. Gleason, Altitude dependence of stratospheric ozone trends based on Nimbus-7 SBUV data, *Geophys. Res. Lett., 20*, 2667-2670, 1993.

Huang, T.Y.W., and G.P. Brasseur, The effect of long-term solar variability in a two-dimensional interactive model of the middle atmosphere, *J. Geophys. Res., 98*, 20413-20427, 1993.

Jaeger, H., The Pinatubo eruption cloud observed by lidar at Garmisch-Partenkirchen, *Geophys. Res. Lett., 19*, 191-194, 1992.

Jaeger, H., *ESMOS II Final Report*, CEC, DG XII, 1993.

Jaeglé, L., *et al.*, In situ measurements of the NO_2/NO ratio for testing atmospheric photochemical models, *Geophys. Res. Lett., 21*, 2555-2558, 1994.

Johnston, P.V., R.L. MacKenzie, J.G. Keys, and W.A. Matthews, Observations of depleted stratospheric NO_2 following the Pinatubo volcanic eruption, *Geophys. Res. Lett., 19*, 211-213, 1992.

Jones, R.L., D.S. McKenna, L.R. Poole, and S. Solomon, On the influence of polar stratospheric cloud formation on chemical composition during the 1988/89 Arctic winter, *Geophys. Res. Lett., 17*, 545-548, 1990.

Jones, R.L., and I. Kilbane-Dawe, The influence of the stratospheric sub-vortex region on mid-latitude composition, submitted to *Geophys. Res. Lett.*, 1994.

Jones, R.L., and A.R. MacKenzie, Observational studies of the role of polar regions in mid-latitude ozone loss, submitted to *Geophys. Res. Lett.*, 1994.

Juckes, M.N., and M.E. McIntyre, A high resolution, one-layer model of breaking planetary waves in the stratosphere, *Nature, 328*, 590-596, 1987.

Kawa, S.R., D.W. Fahey, J.C. Wilson, M.R. Schoeberl, A.R. Douglass, R.S. Stolarski, E.L. Woodbridge, H. Jonsson, L.R. Lait, P.A. Newman, M.H. Proffitt, D.E. Anderson, M. Loewenstein, K.R. Chan, C.R. Webster, R.D. May, and K.K. Kelly, Interpretation of NO_x/NO_y observations from AASE-II using a model of chemistry along trajectories, *Geophys. Res. Lett.*, 20, 2507-2510, 1993.

Kent, G.S., and M.P. McCormick, SAGE and SAM II measurements of global stratospheric aerosol optical depth and mass loading, *J. Geophys. Res., 89*, 5303-5314, 1984.

Kent, G.S., and M.P. McCormick, SAGE and SAM II measurements of global stratospheric aerosol optical depth and mass loading, *J. Geophys. Res., 98*, 5303-5314, 1993.

Kerr, J.B., D.I. Wardle, and D.W. Tarrasick, Record low ozone values over Canada in early 1993, *Geophys. Res. Lett., 20*, 1979-1982, 1993.

Keys, J.G., P.V. Johnston, R.D. Blatherwick, and F.J. Murcray, Evidence for heterogeneous reactions in the Antarctic autumn stratosphere, *Nature, 361*, 49-51, 1993.

King, J.C., *et al.*, Measurements of ClO and O_3 from 21°N to 61°N in the lower stratosphere during February 1988: Implications for heterogeneous chemistry, *Geophys. Res. Lett., 18*, 2273-2276, 1991.

Kinne, S., O.B. Toon, and M.J. Prather, Buffering of stratospheric circulation by changing amounts of tropical ozone—a Pinatubo case study, *Geophys. Res. Lett., 19*, 1927-1930, 1992.

Koike, M, Y. Kondo, W.A. Matthews, P.V. Johnston, and K. Yamazaki, Decrease of stratospheric NO_2 at 44°N caused by Pinatubo volcanic aerosols, *Geophys. Res. Lett., 20*, 1975-1978, 1993.

Koike, M.Y., N.B. Jones, W.A. Matthews, P.V. Johnston, R.L. MacKenzie, D. Kinnison, and J. Rodriguez, Impact of Pinatubo aerosols on the partitioning between NO_2 and HNO_3, *Geophys. Res. Lett., 21*, 597-600, 1994.

Labitzke, K., and M.P. McCormick, Stratospheric temperature increases due to Pinatubo aerosols, *Geophys. Res. Lett., 19*, 207-210, 1992.

Lean, J., Variations in the sun's radiative output, *Rev. Geophys., 29*, 505-535, 1991.

Legras, B., and D. Dritschel, Vortex stripping and the generation of high vorticity gradients in two-dimensional flows, in *Advances in Turbulence IV, Applied Scientific Research Vol. 51*, edited by F.T.M. Nieuwstadt, Kluwer, Dordrecht, The Netherlands, 445-455, 1993.

Leovy, C.B., C.R. Sun, M.H. Hitchmann, E.E. Remsberg, J.M. Russell III, L.L. Gordely, J.C. Gille, and L.V. Lyjak, Transport of ozone in the middle atmosphere: Evidence for planetary wave breaking, *J. Atmos. Sci., 42*, 230-244, 1985.

Luo, B.P., S.L. Clegg, T. Peter, R. Mueller, and P.J. Crutzen, HCl solubility and liquid diffusion in aqueous sulfuric acid under stratospheric conditions, *Geophys. Res. Lett., 21*, 49-52, 1994.

MacKenzie, A.R., B. Knudsen, R.L. Jones, and E.R. Lutman, The spatial and temporal extent of chlorine activation by polar stratospheric clouds in the Northern-Hemisphere winters of 1988/89 and 1991/92, *Geophys. Res. Lett., 21*, 1423-1426, 1994.

Manney, G.L., J.D. Farrara, and C.R. Mechoso, Simulations of the February 1979 stratospheric sudden warming: Model comparisons and three-dimensional evolution, *Monthly Weather Rev.*, in press, 1994.

McCormick, M.P., and R.E. Veiga, SAGE II measurements of early Pinatubo aerosols, *Geophys. Res. Lett., 19*, 155-158, 1992.

McElroy, M.B., and R.J. Salawitch, Changing composition of the global stratosphere, *Science, 243*, 763-770, 1989.

McElroy, M.B., R.J. Salawitch, and K. Minschwaner, The changing stratosphere, *Planet. Space Sci., 40*, 373-401, 1992.

McIntyre, M.E., Middle atmospheric dynamics and transport: Some current challenges to our understanding, in *Dynamics, Transport and Photochemistry in the Middle Atmosphere of the Southern Hemisphere,* San Francisco NATO Workshop, edited by A. O'Neill, Kluwer, Dordrecht, The Netherlands, 1-18, 1990.

McIntyre, M.E., The stratospheric polar vortex and subvortex: Fluid dynamics and midlatitude ozone loss, to be submitted to *Phil. Trans. Roy. Soc. London*, 1994.

McPeters, R.D., The atmospheric SO_2 budget for Pinatubo derived from NOAA-11 SBUV/2 spectral data, *Geophys. Res. Lett., 20*, 1971-1974, 1993.

Mergenthaler, J.L., J.B. Kumer, and A.E. Roche, CLAES south-looking aerosol observations for 1992, *Geophys. Res. Lett., 20,* 1295-1298, 1993.

Michelangeli, D.V., M. Allen, Y.L. Yung, R.L. Shia, D. Crisp, and J. Eluszkiewicz, Enhancement of atmospheric radiation by an aerosol layer, *J. Geophys. Res., 97*, 865-874, 1992.

Michelsen, H.A., R.J. Salawitch, P.O. Wennberg, and J.G. Anderson, Production of $O(^1D)$ from photolysis of O_3, *Geophys. Res. Lett., 21,* 2227-2230, 1994.

Middlebrook, A.M., L.T. Iraci, L.S. McNeill, B.G. Koehler, O.W. Saastad, M.A. Tolbert, and D.R. Hanson, FTIR studies of thin H_2SO_4/H_2O films: Formation, water uptake and solid-liquid phase changes, *J. Geophys. Res., 98*, 20473-20481, 1993.

Mills, M.J., A.O. Langford, T.J. O'Leary, K. Arpag, H.L. Miller, M.H. Proffitt, R.W. Sanders, and S. Solomon, On the relationship between stratospheric aerosols and nitrogen dioxide, *Geophys. Res. Lett., 20*, 1187-1190, 1993.

Minschwaner, K., G.P. Anderson, L.A. Hall, and K. Yoshino, Polynomial coefficients for calculating O_2 Schumann-Runge cross sections at 0.5 cm^{-1} resolution, *J. Geophys. Res., 97*, 10103-10108, 1992.

Minschwaner, K., R.J. Salawitch, and M.B. McElroy, Absorption of solar radiation by O_2: Implications for O_3 and lifetimes of N_2O, $CFCl_3$ and CF_2Cl_2, *J. Geophys. Res., 98*, 10543-10561, 1993.

Minton, T.K., C.M. Nelson, T.A. Moore, and M. Okumura, Direct observation of ClO from chlorine nitrate photolysis, *Science, 258*, 1342-1345, 1992.

Molina, M.J., R. Zhang, P.J. Wooldridge, J.R. McMahon, J.E. Kim, H.Y. Chang, and K.D. Beyer, Physical chemistry of the $H_2SO_4/HNO_3/H_2O$ system: Implications for polar stratospheric clouds, *Science, 261*, 1418-1423, 1993.

Murphy, D.M., A.F. Tuck, K.K. Kelly, K.R. Chan, M. Loewenstein, J.R. Podolske, M.H. Proffitt, and S.E. Strahan, Indicators of transport and vertical motion from correlations between in situ measurements in the Airborne Antarctic Ozone Experiment, *J. Geophys. Res., 94*, 11669-11685, 1989.

Murphy, D.M., *et al.*, Reactive nitrogen and its correlation with ozone in the lower stratosphere and upper troposphere, *J. Geophys. Res., 98*, 8751-8773, 1993.

Nardi, B., M.-L. Chanin, A. Hauchecorne, S.I. Avdyushin, G.F. Tulinov, B.N. Kuzmenko, and I.R. Mezhuev, Morphology and dynamics of the Pinatubo aerosol layer in the northern hemisphere as detected from a ship-borne lidar, *Geophys. Res. Lett., 18*, 1967-1970, 1993.

Natarajan, M., and L.B. Callis, Stratospheric photochemical studies with Atmospheric Trace Molecule Spectroscopy (ATMOS) measurements, *J. Geophys. Res., 96*, 9361-9370, 1991.

Neuber, R., G. Beyerle, G. Fiocco, A. di Sarra, K.H. Fricke, C. David, S. Godin, B.M. Knusden, L. Stefanutti, G. Vaughan, and J.-P. Wolf, Latitudinal distribution of stratospheric aerosols during the EASOE winter 1991/92, *Geophys. Res. Lett., 21*, 1283-1286, 1994.

Norton, W.A., Breaking Rossby waves in a model stratosphere diagnosed by a vortex-following coordinate system and a technique for advecting material contours, *J. Atmos. Sci., 51*, 654-673, 1994.

O'Sullivan, D., and R.E. Young, Modeling the quasi-biennial oscillation's effect on the winter stratospheric circulation, *J. Atmos. Sci., 49*, 2437-2448, 1992.

Orlando, J.J., G.S. Tyndall, G.K. Moortgat and J.G. Calvert, Quantum yields for NO_3 photolysis between 570 and 635 nm, *J. Phys. Chem., 97*, 10996-11000, 1993.

Pierce, B.R., and T.D.A. Fairlie, Chaotic advection in the stratosphere: Implications for the dispersal of chemically perturbed air from the polar vortex, *J. Geophys. Res., 98*, 18589-18595, 1993.

Pierce, R.B., W.L. Grose, J.M. Russell III, and A.F. Tuck, Evolution of southern hemisphere spring air masses observed by HALOE, *Geophys. Res. Lett., 21*, 213-216, 1994.

Pitari, G., A numerical study of the possible perturbation of stratospheric dynamics due to Pinatubo aerosols: Implications for tracer transport, *J. Atmos. Sci., 50*, 2443-2461, 1993.

Pitari, G., and V. Rizi, An estimate of the chemical and radiative perturbation of stratospheric ozone following the eruption of Mt. Pinatubo, *J. Atmos. Sci., 50*, 3260-3276, 1993.

Pitts, M.C., and L.W. Thomason, The impact of the eruptions of Mt. Pinatubo and Cerro Hudson on Antarctic aerosol levels during the 1991 austral spring, *Geophys. Res. Lett., 20*, 2451-2454, 1993.

Plumb, R.A., Atmospheric dynamics — ozone depletion in the Arctic, *Nature, 347*, 20-21, 1990.

Plumb, R.A., and R.C. Bell, A model of the quasi-biennial oscillation on an equatorial beta-plane, *Quart. J. Roy. Meteorol. Soc., 108*, 335-352, 1982.

Plumb, R.A., D.W. Waugh, R.J. Atkinson, M.R. Schoeberl, L.R. Lait, P.A. Newman, E.V. Browell, A.J. Simmons, and M. Loewenstein, Intrusions into the lower stratospheric Arctic vortex during the winter of 1991/92, *J. Geophys. Res., 99*, 1089-1106, 1994.

Polvani, L.M., D.W. Waugh, and R.A. Plumb, On the subtropical edge of the stratospheric surf zone, submitted to *J. Atmos. Sci.*, 1994.

Poulet, G., M. Pirre, F. Maguin, R. Ramaroson, and G. LeBras, Role of the BrO + HO_2 reaction in the stratospheric chemistry of bromine, *Geophys. Res. Lett., 19*, 2305-2308, 1992.

Prather, M., Catastrophic loss of stratospheric ozone in dense volcanic clouds, *J. Geophys. Res., 97*, 10187-10191, 1992.

Price, J.M., J.A. Mack, C.A. Rogaski, and A.M. Wodtke, Vibrational-state-specific self-relaxation rate constant—Measurements of highly vibrationally excited O_2 (v = 19-28), *J. Chem. Phys., 175*, 83-98, 1993.

Proffitt, M.H.,K.K. Kelly, J.A. Powell, B.L. Gary, M. Loewenstein, J.R. Podolske, S.E. Strahan, and K.R. Chan, Evidence for diabatic cooling and poleward transport within and around the 1987 Antarctic ozone hole, *J. Geophys. Res., 94*, 16797-16813, 1989.

Proffitt, M.H., J.J. Margitan, K.K. Kelly, M. Loewenstein, J.R. Podolske, and K.R. Chan, Ozone loss in the arctic polar vortex inferred from high-altitude aircraft measurements, *Nature, 347*, 31-36, 1990.

Proffitt, M.H., K. Aikin, J.J. Margitan, M. Loewenstein, J.R. Podolske, S.E. Strahan, and A. Weaver, Ozone loss inside the northern polar vortex during the 1991-1992 winter, *Science, 261*, 1150-1154, 1993.

Pyle, J.A., G.D. Carver, and U. Schmidt, Some case studies of chlorine activation during the EASOE campaign, *Geophys. Res. Lett., 21*, 1431-1434, 1994.

Randel, W.J., J.C. Gille, A.E. Roche, J.B. Kumer, J.L. Mergenthaler, J.W. Waters, E.F. Fishbein, and W.A. Lahoz, Stratospheric transport from the tropics to middle latitudes by planetary-wave mixing, *Nature, 365*, 533-535, 1993.

Rattigan, O., E.R. Lutman, R.L. Jones, and R.A. Cox, Temperature dependent absorption cross-sections and atmospheric photolysis rates of nitric acid, *Ber. Bunsenges. Phys. Chem., 96*, 399-404, 1992.

Read, W.G., L. Froidevaux, and J.W. Waters, Microwave Limb Sounder measurement of stratospheric SO_2 from the Mt. Pinatubo volcano, *Geophys. Res. Lett., 20,* 1299-1302, 1993.

Reid, S.J., G. Vaughan, and E. Kyro, Occurrence of ozone laminae near the boundary of the stratospheric polar vortex, *J. Geophys. Res., 98,* 8883-8890, 1993.

Roche, A.E., J.B. Kumer, and J.L. Mergenthaler, CLAES observations of $ClONO_2$ and HNO_3 in the Antarctic stratosphere, between June 15 and September 17, 1992, *Geophys. Res. Lett., 20*, 1223-1226, 1993.

Rodriguez, J., M.K.W. Ko, N.-D. Sze, and C.W. Heisey, Ozone response to enhanced heterogeneous processing after the eruption of Mt. Pinatubo, *Geophys. Res. Lett., 21*, 209-212, 1994.

Rood, R., A. Douglass, and C. Weaver, Tracer exchange between tropics and middle latitudes, *Geophys. Res. Lett., 19,* 805-808, 1992.

Rosen, L.M., N.T. Kjome, and H. Fast, Penetration of Mt. Pinatubo aerosols into the north polar vortex, *Geophys. Res. Lett., 19*, 1751-1754, 1992.

Russell, J.M., III, A.F. Tuck, L.L. Gordley, J.H. Park, S.R. Drayson, J.E. Harries, R.J. Cicerone, and P.J. Crutzen, HALOE Antarctic observations in the spring of 1991, *Geophys. Res. Lett., 20,* 719-722, 1993a.

Russell, J.M., III, L.L. Gordley, J.H. Park, S.R. Drayson, W.D. Hesketh, R.J. Cicerone, A.F. Tuck, J.E. Frederick, J.E. Harries, and P.J. Crutzen, The Halogen Occultation Experiment, *J. Geophys. Res., 98*, 10777-10797, 1993b.

Salawitch, R.J., *et al.*, The diurnal variation of hydrogen, nitrogen, and chlorine radicals: Implications for the heterogeneous production of HNO_2, *Geophys. Res. Lett., 21,* 2551-2554, 1994a.

Salawitch, R.J. *et al.*, The distribution of hydrogen, nitrogen, and chlorine radicals in the lower stratosphere: Implications for changes in O_3 due to emission of NO_y from supersonic aircraft, *Geophys. Res. Lett., 21,* 2547-2550, 1994b.

Webster, C.R., R.D. May, M. Allen, L. Jaeglé, and M.P. McCormick, Balloon profiles of stratospheric NO_2 and HNO_3 for testing the heterogeneous hydrolysis of N_2O_5 on sulfate aerosols, *Geophys. Res. Lett., 21*, 53-56, 1994a.

Webster, C.R., *et al.*, Hydrochloric acid and the chlorine budget of the lower stratosphere, *Geophys. Res. Lett., 21*, 2575-2578, 1994b.

Wennberg, P.O., *et al.*, The removal of stratospheric O_3 by radicals: In situ measurements of OH, HO_2, NO, NO_2, ClO, and BrO, *Science, 266*, 398-404, 1994.

Williams, L.R., and D.M. Golden, Solubility of HCl in sulfuric acid at stratospheric temperatures, *Geophys. Res. Lett., 20*, 2227-2230, 1993.

Wilson, J.C., H. Jonsson, C.A. Brock, D.W. Toohey, L.M. Avallone, D. Baumgardner, J.E. Dye, L.R. Poole, D.C. Woods, R.J. DeCoursey, M. Osborn, M.C. Pitts, K.K. Kelly, K.R. Chan, G.V. Ferry, M. Loewenstein, J.R. Podolske, and A. Weaver, In situ observations of aerosol and chlorine monoxide after the 1991 eruption of Mt. Pinatubo—Effect of reactions on sulfate aerosol, *Science, 261*, 1140-1143, 1993.

Wuebbles, D.J., D.E. Kinnison, K.E. Grant, and J. Lean, The effect of solar flux variations and trace gas emissions on recent trends in stratospheric ozone and temperature, *J. Geomagn. Geoelectr., 43*, 709-718, 1991.

Young, R.E, H. Houben, and O.B. Toon, Simulation of the dispersal of the Mt. Pinatubo volcanic aerosol cloud in the stratosphere immediately following the eruption, *Geophys. Res. Lett.*, to appear, 1993.

Zhang, R., P.J. Wooldridge, and M.J. Molina, Vapor pressure measurements for the $H_2SO_4/HNO_3/H_2O$ and $H_2SO_4/HCl/H_2O$ systems: Incorporation of stratospheric acids into background sulfate aerosols, *J. Phys. Chem., 97*, 8541-8548, 1993.

Zhang, R., J.T. Jayne, and M.J. Molina, Heterogeneous interactions of $ClONO_2$ and HCl with sulfuric acid tetrahydrate: Implications for the stratosphere, *J. Phys. Chem.*, in press, 1994.

CHAPTER 5

Tropospheric Ozone

Lead Authors:
A. Volz-Thomas
B.A. Ridley

Co-authors:
M.O. Andreae
W.L. Chameides
R.G. Derwent
I.E. Galbally
J. Lelieveld
S.A. Penkett
M.O. Rodgers
M. Trainer
G. Vaughan
X.J. Zhou

Contributors:
E. Atlas
C.A.M. Brenninkmeijer
D.H. Ehhalt
J. Fishman
F. Flocke
D. Jacob
J.M. Prospero
F. Rohrer
R. Schmitt
H.G.J. Smit
A.M. Thompson

CHAPTER 5

TROPOSPHERIC OZONE

Contents

SCIENTIFIC SUMMARY

Although representing only 10 percent of the total ozone column, tropospheric ozone is important because it can influence climate, as it is a greenhouse gas itself, and because its photolysis by UV radiation in the presence of water vapor is the primary source for hydroxyl radicals (OH). Hydroxyl radicals are responsible for the oxidative removal of many trace gases, such as methane (CH_4), hydrofluorocarbons (HFCs), and hydrochlorofluorocarbons (HCFCs), that influence climate and/or are important for the stratospheric ozone layer.

Tropospheric ozone arises from two processes: downward flux from the stratosphere; and *in situ* photochemical production from the oxidation of hydrocarbons and carbon monoxide (CO) in the presence of NO_x ($NO + NO_2$). Ozone is removed from the troposphere by *in situ* chemistry and by uptake at the Earth's surface. The role of photochemistry in the local ozone balance depends strongly on the concentration of NO_x. Human impact on tropospheric ozone and hydroxyl occurs through the emission of precursors, *e.g.*, NO_x, CO, and hydrocarbons. In the case of free tropospheric ozone, this is brought about by the export of both ozone and its precursors, in particular NO_x, from source regions.

While substantial uncertainties remain in assessing the global budget of tropospheric ozone, recent studies have led to significant advances in understanding the local balance of ozone in some regions of the atmosphere.

- Recent measurements of the NO_y/O_3 ratio have basically confirmed earlier estimates of the flux of ozone from the stratosphere to be in the range of 240-820 $Tg(O_3)/yr$, which is in reasonable agreement with results from general circulation models (GCMs).

- The observed correlation between ozone and alkyl nitrates suggests a natural ozone concentration of 20-30 ppb in the upper planetary boundary layer (at about 1 km altitude), which agrees well with the estimate from the few reliable historic data (cf. Figure 1-16, Chapter 1).

- Measurements of the gross ozone production rate yielded values as high as several tens of ppb per hour in the polluted troposphere over populated regions, in good agreement with theoretical predictions. Likewise, the efficiency of NO_x in ozone formation in moderately polluted air masses was found to be in reasonable agreement with theory.

- Direct measurements of hydroxyl and peroxy radicals have become available. While they do not serve to establish a global climatology of OH, they do provide a test of our understanding of the fast photochemistry. To date, theoretical predictions of OH concentrations (from measured trace gas concentrations and photolysis rates) tend to be higher than the measurements by up to a factor of two.

- Measurements of peroxy radical concentrations in the remote free troposphere are in reasonable agreement with theory; however, significant misunderstanding exists with regard to the partitioning of odd nitrogen and the budget of formaldehyde.

- Measurements have shown that export of ozone produced from anthropogenic precursors over North America is a significant source for the North Atlantic region during summer. It has also been shown that biomass burning is a significant source for ozone in the tropics during the dry season. These findings show the influence of human activities on the global ozone balance.

TROPOSPHERIC OZONE PROCESSES

- Photochemical net ozone destruction in the remote atmosphere has been identified in several experiments. It is likely to occur over large parts of the troposphere with rates of up to several ppb per day. Consequently, an increase in UV-B radiation (*e.g.*, from stratospheric ozone loss) is expected to decrease tropospheric ozone in the remote atmosphere but in some cases will increase production of ozone in and transport from the more polluted regions. The integrated effect on hydroxyl concentrations and climate is uncertain.

Uncertainties in the global tropospheric ozone budget, particularly in the free troposphere, are mainly associated with uncertainties in the global distribution of ozone itself and its photochemical precursors, especially CO and NO_x. These distributions are strongly affected by dynamics, by the magnitude and spatial/temporal distribution of sources, particularly those for NO_x to the middle and upper troposphere from the stratosphere, lightning, aircraft, and convective systems, and by the partitioning and removal of NO_y constituents. The role of heterogeneous processes including multiphase chemistry in the troposphere is not well characterized, and the catalytic efficiency of NO_x in catalyzing ozone formation in the free troposphere has not been confirmed by measurements.

5.1 INTRODUCTION

As is outlined in more detail in Chapter 1, there is some, albeit limited, evidence to suggest that ozone concentrations in the troposphere of the Northern Hemisphere have increased by a factor of two or more over the past 100 years, with most of the increase having occurred since 1950. This conclusion is consistent with ozone data gathered continuously since the 1970s at a series of remote and in some cases high altitude stations. It is interesting to note that all stations north of about 20°N exhibit a positive trend in ozone over the past two decades that is significant to the 95% confidence level. During the same time, a statistically significant negative trend of about 0.5%/yr is observed at the South Pole.

For the most part, the trends appear to fall more or less along a straight line that extends from -0.5%/yr at 90°S to +0.8%/yr at 70°N. Somewhat anomalous are the large positive trends observed at the high elevation sites in Southern Germany (1-2%/yr); these large trends perhaps reflect a regional influence above and beyond the smaller global trend (Volz-Thomas, 1993). It should be noted, however, that the average positive trends observed in the Northern Hemisphere are largely due to the relatively rapid ozone increase that occurred in the seventies. Over the last decade, no or little ozone increase has occurred in the free troposphere except over Southern Germany and Switzerland. Indeed, ozone concentrations at some locations in the polluted planetary boundary layer (PBL) over Europe have decreased over the last decade (Guicherit, 1988; Low *et al.*, 1992).

It is important that we understand the causes of the apparent increase in tropospheric ozone concentrations in the Northern Hemisphere because of ozone's central role in global biogeochemistry, its effectiveness as a greenhouse gas, especially in the upper troposphere, and its toxicity to living organisms. It is equally important, however, to understand the causes for the decrease observed at high latitudes in the Southern Hemisphere because of the influence of ozone on the concentration of hydroxyl radicals and, hence, the oxidizing capacity of the atmosphere, which controls the budgets of many long-lived greenhouse gases. This, in turn, requires a quantitative understanding of the chemical and meteorological processes that determine the budget of tropospheric ozone.

5.2 REVIEW OF FACTORS THAT INFLUENCE TROPOSPHERIC OZONE CONCENTRATIONS

The presence of ozone in the troposphere is understood to arise from two basic processes: (1) tropospheric/stratospheric exchange that causes the transport of stratospheric air, rich in ozone, into the troposphere, and (2) production of ozone from photochemical reactions occurring within the troposphere. Similarly, removal of tropospheric ozone is accomplished through two competing processes: (1) transport to and removal at the Earth's surface, and (2) *in situ* chemical destruction. For the past two decades, research on tropospheric ozone has largely focused on understanding the relative roles of these processes in controlling the abundance and distribution of ozone in the troposphere. The basic chemical mechanisms that control the local ozone budget are now reasonably well understood, except for the role of heterogeneous processes. The situation is not as good concerning our quantitative understanding of the natural sources of ozone and its precursors. Transport of ozone and NO_y (see Figure 5-1) from the stratosphere and production of NO_x (= NO + NO_2) through lightning must be known to a better degree in order to assess the role of anthropogenic influences, such as air traffic (see Chapter 11). Likewise, a better understanding is needed of the atmospheric transport processes that redistribute ozone and its precursors between the polluted continental regions and the remote atmosphere and between the planetary boundary layer and the free troposphere.

Boundary layer processes, including large-scale eddy mixing and smaller scale turbulence, control the rate at which sources of NO_x and hydrocarbon emissions can combine to begin ozone production chemistry. Because of the nonlinear dependence of photochemical ozone formation on the precursor concentrations, models that assume instantaneous mixing over large spatial grids may significantly overestimate ozone production rates. Vertical transport of ozone and its precursors between the boundary layer and higher altitudes (together with exchange of air with the stratosphere) has a strong influence on ozone distributions in the troposphere due to the longer lifetimes of ozone and precursors in the free troposphere. On the other hand, the upward flow in convective systems must be balanced by downward mesoscale flow, which then carries ozone and odd nitrogen species from the free troposphere into the planetary

boundary layer, where they are destroyed more rapidly (see Lelieveld and Crutzen, 1994). Observations of O_3 in convective systems suggest that both mechanisms are in effect (Dickerson *et al.*, 1987; Pickering *et al.*, 1992b), but their relative magnitude has not been evaluated experimentally. Lastly, long-range horizontal advection influences ozone distributions by transport of both ozone and its precursors from source areas into other regions, including the marine environment. This type of long-range transport has been shown to be an important factor in the generation of large regional-scale events of elevated ozone (see, for example, Fishman *et al.*, 1985; Vukovich *et al.*, 1985; Logan, 1989; Sillman *et al.*, 1990).

5.2.1 Stratosphere-Troposphere Exchange

Following the elucidation by Haynes *et al.* (1991) of the control exercised on the diabatic circulation in the stratosphere by waves propagating up from the troposphere (the so-called Downward Control Principle), a clearer picture of stratosphere-troposphere exchange processes has emerged. Trace species such as ozone and NO_y with sources in the middle stratosphere are fed into the lower stratosphere by the diabatic circulation at a rate determined by the dissipation of planetary and gravity wave fields in the stratosphere and mesosphere. The lower stratosphere (especially in midlatitudes) is subject to efficient isentropic mixing, which maintains a close correlation between trace species (Plumb and Ko, 1992). The lower levels of the stratosphere also exchange air with the troposphere.

Estimates of fluxes across the tropopause remain uncertain. For example, the net downward flux of air estimated by Holton (1990) and Rosenlof and Holton (1993), which was based on the concepts described above, is a factor of 2-3 larger than the lower limit of the upward flux derived by Follows (1992) from the growth of CFC-11 in the troposphere. Deriving an analogous estimate for the trace species is even more difficult because their distributions must be accurately known. However, the very close correlation between nitrous oxide (N_2O), NO_y, and ozone in the lower stratosphere (Fahey *et al.*, 1990; Murphy *et al.*, 1993) offers the possibility of deriving the flux of trace gases from the N_2O budget. Murphy and Fahey (1994) used an annual destruction rate of N_2O in the stratosphere of 8-17 Tg(N)/yr to infer a transport of 0.28-0.6 Tg(N)/yr of NO_y and 240-820 Tg/yr of ozone into the troposphere. This corresponds to a flux of $(2\text{-}6)\times10^{10}$ molecules cm^{-2} s^{-1} of ozone, which is slightly less than the earlier estimates made from observations of tropopause folding events (Danielsen and Mohnen, 1977) and is comparable to the fluxes derived from general circulation models (*e.g.*, Gidel and Shapiro, 1980; Levy *et al.*, 1985).

The most active regions of stratosphere-troposphere exchange are in cyclonic regions of the upper troposphere, near jet streams, troughs, and cut-off lows. The contribution of tropopause folds to the exchange has been well documented (*e.g.*, WMO, 1986) and has been confirmed by recent work (Ancellet *et al.*, 1991, 1994; Wakamatsu *et al.*, 1989). Potential vorticity (PV) analyses on isentropic surfaces near the tropopause show long streamers of elevated PV curving anticyclonically from high latitudes, corresponding to narrow streaks and a low tropopause. These streaks are clearly revealed by Meteosat water vapor images (Appenzeller and Davies, 1992), but their contribution to stratosphere-troposphere exchange has yet to be assessed. The contribution of cut-off lows, formed by cyclonically-curving PV streamers (Thorncroft *et al.*, 1993), is better understood. These are preferentially found in particular regions of the world, *e.g.*, Europe (Price and Vaughan, 1992), and can promote exchange by vigorous convective mixing as well as shear instabilities near jet streams (Price and Vaughan, 1993; Lamarque and Hess, 1994). Recently, the contribution of mesoscale convective systems to stratosphere-troposphere exchange was shown to be of potential importance (Poulida, 1993; Alaart *et al.*, 1994).

There have been no studies of trends in stratosphere-troposphere exchange, so the contribution of the stratospheric source to the observed trend in tropospheric ozone remains an open question. A better understanding is also required of transport between the lower stratosphere and the troposphere, and of links between the opposing ozone trends in these two regions of the atmosphere. Decreasing ozone concentrations in the lower stratosphere would, at first approximation, imply a decreasing flux into the troposphere. However, this effect could be offset by changes in the meridional circulation in the stratosphere. Following the Downward Control Principle and assuming the primary source of ozone in the stratosphere to have remained constant, changes in downward flux would have to be forced by changes in

gravity wave dissipation. Therefore, changes in climate could well have led to changes in the ozone flux from the stratosphere. As noted by WMO (1992), however, there have not been enough studies of trends in stratospheric temperatures and transport to deduce trends in the ozone flux into the troposphere.

5.2.2 The Photochemical Balance of Ozone in the Troposphere

The production of ozone in the troposphere is accomplished through a complex series of reactions referred to as the "photochemical smog mechanism." The basics of this mechanism were originally identified by Haagen-Smit (1952) as being responsible for the rise of air pollution in Los Angeles in the 1950s. As is outlined in Figure 5-1, this well-known mechanism (see NRC, 1991) involves the photo-oxidation of volatile organic compounds (VOC) and carbon monoxide (CO) in the presence of NO_x (= NO + NO_2). Typical of this mechanism are reactions (R5-1) through (R5-7):

(R5-1)	$RH + OH$	$\rightarrow$	$R + H_2O$
(R5-2)	$R + O_2 + M$	$\rightarrow$	$RO_2 + M$
(R5-3a)	$RO_2 + NO$	$\rightarrow$	$RO + NO_2$
(R5-4)	$RO + O_2$	$\rightarrow$	$HO_2 + R'CHO$
(R5-5)	$HO_2 + NO$	$\rightarrow$	$OH + NO_2$
2 × (R5-6)	$NO_2 + h\nu$	$\rightarrow$	$NO + O$
2 × (R5-7)	$O + O_2 + M$	$\rightarrow$	$O_3 + M$
Net:	$RH + 4\,O_2 + 2\,h\nu$	$\rightarrow$	$R'CHO + H_2O + 2O_3$

where an initial reaction between a hydrocarbon (RH) and a hydroxyl radical (OH) results in the production of two O_3 molecules and an aldehyde R'CHO or a ketone. Additional ozone molecules can then be produced from the degradation of R'CHO. In addition to the oxidation of hydrocarbons, ozone can be generated from CO oxidation via (R5-8) and (R5-9) followed by (R5-5), (R5-6), and (R5-7).

(R5-8)	$CO + OH$	$\rightarrow$	$CO_2 + H$
(R5-9)	$H + O_2 + M$	$\rightarrow$	$HO_2 + M$

Hydrocarbons and CO provide the fuel for the production of tropospheric ozone and are consumed in the process. In remote areas of the troposphere, CO and methane typically provide the fuel for ozone production (Seiler and Fishman, 1981). In urban locations, reactive olefinic and aromatic hydrocarbons (often but not exclusively of anthropogenic origin) are usually the dominant fuel, while in more rural environments reactive biogenic VOC such as isoprene often dominate (Trainer *et al.*, 1987; Chameides *et al.*, 1988).

In contrast to hydrocarbons and CO, NO_x is conserved in the process of ozone production and thus acts as a catalyst in ozone formation. The conversion of NO to NO_2 by peroxy radicals (HO_2 and RO_2) is the crucial step, since the rapid photolysis of NO_2 yields the oxygen atom required to produce ozone (R5-7). Indeed, the *in situ* rate of formation of ozone is given by

$$P(O_3) = [NO] \cdot \{k_5 \cdot [HO_2] + \Sigma k_{3ai} \cdot [RO_2]_i\}$$

As catalysis continues until NO_x is permanently removed by physical processes (deposition) or is transformed to other NO_y compounds that act as temporary or almost permanent reservoirs, the catalytic production efficiency of NO_x can, at first approximation, be defined as the ratio of the rate at which NO molecules are converted to NO_2 by reaction with peroxy radicals to the rate of transformation or removal of NO_x. The lifetime of NO_x varies from a few hours in the boundary layer to at least several days in the upper troposphere. Thus the catalytic production efficiency of NO_x can vary considerably and nonlinearly over the more than three orders of magnitude range of concentrations (see Figure 5-9) typically found between remote and polluted regions of the troposphere (Liu *et al.*, 1987; Lin *et al.*, 1988; Hov, 1989).

As is seen in Figure 5-1, the conversion of NO to NO_2 occurs to a large extent through reaction with O_3 itself:

(R5-10)	$NO + O_3$	$\rightarrow$	$NO_2 + O_2$

This process constitutes only a temporary loss, because O_3 (and NO) are regenerated in the photolysis of NO_2 (R5-6) followed by R5-7. The cycle adjusts the photostationary state between O_3, NO, and NO_2, and therefore, the NO/NO_2 ratio (Leighton, 1961). Through this, reaction R5-10 influences the catalytic efficiency of NO_x in ozone formation since it decreases the fraction of NO_x that is responsible for O_3 production via R5-3a and R5-5 and, at the same time, increases the fraction that is responsible for the loss of NO_x.

Because of the rapid interconversion between NO and NO_2 during daylight, the quantity NO_x = NO + NO_2 was defined. Similarly, it was found to be useful to

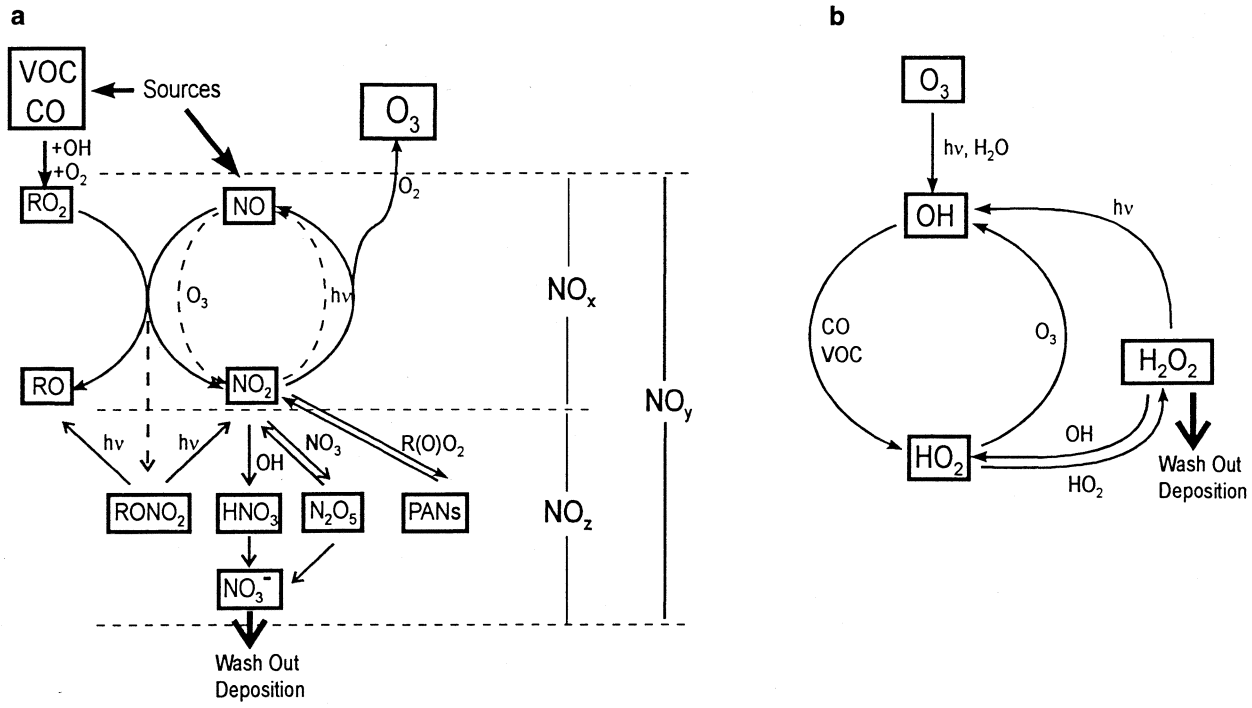

Figure 5-1a. Schematic view of the cycles of NO_x and NO_y and their relation to the chemical ozone balance. The quantity NO_z is defined as NO_y - NO_x and represents the sum of all oxidation products of NO_x.
Figure 5-1b. Primary formation of OH from O_3 photolysis and the HO_x cycle in the absence of NO_x. It leads to formation of hydrogen peroxide and net destruction of ozone.

define the quantity $O_x = O_3 + NO_2$, in order to account for temporary losses of O_3 in highly polluted environments (Guicherit, 1988; Kley *et al.*, 1994). It is a better measure of the time-integrated ozone production than ozone itself (Volz-Thomas *et al.*, 1993a).

Photochemical loss of tropospheric ozone is accomplished through photolysis followed by reaction of the $O(^1D)$ atom with water vapor, (R5-11) and (R5-12). Additional losses occur through reaction of the HO_2 radical formed in (R5-9) with O_3 via (R5-13) and (to a lesser extent) through reaction of OH with O_3 (R5-14):

(R5-11) $O_3 + h\nu \rightarrow O(^1D) + O_2$
(R5-12) $O(^1D) + H_2O \rightarrow 2\ OH$
(R5-13) $HO_2 + O_3 \rightarrow OH + 2\ O_2$
(R5-14) $OH + O_3 \rightarrow HO_2 + O_2$

The photochemical rate of ozone loss is approximated by

$$L(O_3) = [O_3] \cdot \{J_{11} \cdot F_{O^1D} + k_{13} \cdot [HO_2] + k_{14} \cdot [OH]\}$$

where F_{O^1D} is the fraction of excited oxygen atoms that react with water vapor. This expression is only approximate and is more appropriate to the remote free troposphere, since it neglects important loss processes that can occur in the continental boundary layer, such as dry deposition and reactions with unsaturated hydrocarbons. It also neglects potential losses that have been suggested to occur in cloud droplets and nighttime or wintertime losses through nitrate radical (NO_3) chemistry. As such, it is a lower limit for the loss rate.

Ultimately, the budget of ozone in a given region is governed by transport of ozone into or out of the region and the net rate of ozone formation, $P(O_3)$ - $L(O_3)$. Except for urban regions, where NO_2 is the predominant sink for OH radicals and, hence, limits the formation of RO_2 radicals, the rate of O_3 production is most often limited by the availability of NO_x even in the boundary layer over the European and North American continents. In the remote atmosphere, not only is the production rate of O_3 limited by the availability of NO_x, the concentration

of NO_x can be so small that $L(O_3)$ exceeds $P(O_3)$. These regions thus act as a buffer against any excess ozone imported from areas having higher production rates or from the stratosphere.

A coarse estimate for the "critical" NO concentration at which local O_3 production and loss rates are equivalent was given by Crutzen (1979) by simply equating the rate of R5-13 to the rate of R5-5. The critical daytime NO concentration thus derived is within a factor of two of 10 ppt, depending on the actual ozone concentration and other factors. However, this is a lower limit because other loss processes have been neglected and the term $J_{11} \cdot F_{O^1D}$ is the dominant contribution to $L(O_3)$ in the remote lower-to-middle troposphere. For example, from experimental observations made at 3.4 km in the mid-North Pacific Ocean region, this term accounted for nearly 50% of the total loss rate when averaged over 24 hours (Ridley *et al.*, 1992).

Nevertheless, any non-zero concentration of NO_x contributes to O_3 production, compensates the loss rate, and increases the lifetime of O_3. Since $P(O_3)$ is so sensitive to the NO_x abundance and $L(O_3)$ is, to first approximation, insensitive to NO_x in the remote atmosphere, possible trends in tropospheric O_3 are intimately dependent upon trends in NO_x concentrations. Clearly, assessing the contribution of photochemical processes to trends in global and regional ozone relies on a good knowledge of the distribution of O_3, the fuels (CO, CH_4, NMHC), and especially the distribution of NO_x. Reactions R5-11 and R5-12 not only constitute an important O_3 loss rate but also initiate the oxidation cycles via OH radicals (see Section 5.4) and therefore link stratospheric O_3 change to tropospheric photochemistry through the sensitive dependence of J_{11} on the overhead column of O_3.

The depletion of stratospheric ozone during the last decade has led to increased ultraviolet radiation of wavelength 290-320 nm penetrating to the troposphere (see Chapter 9). Liu and Trainer (1988) studied the influence of enhanced UV radiation on tropospheric ozone with a simple photochemical model and found that the net effect depended on ambient NO_x levels. To first order, an increase in the ultraviolet flux essentially accelerates the already-existing production and destruction processes. For this reason, a positive trend in UV radiation will, most likely, cause a negative trend in tropospheric ozone in regions where the net photochemical balance is negative, that is, over large areas of the Southern Hemisphere and the remote oceanic regions of the Northern Hemisphere (Section 5.3). The long-term observations at the South Pole (Schnell *et al.*, 1991; Thompson, 1991) indicate that some enhanced net destruction of tropospheric ozone may already be occurring in association with the large stratospheric ozone losses in that region. On the other hand, a long-term increase in UV radiation will likely contribute to an increase in photochemical ozone formation in the NO_x-rich continental regions and possibly in large-scale plumes downwind of these or areas of biomass burning.

Removal or conversion of NO_x to longer-lived reservoirs clearly decreases the local catalytic efficiency of O_3 production. During daytime, losses of NO_x proceed through the reaction of NO_2 with OH radicals (R5-15) and the formation of peroxyacetylnitrate (PAN) and its homologues (R5-16):

$$\text{(R5-15)} \qquad NO_2 + OH + M \rightarrow HNO_3 + M$$

$$\text{(R5-16)} \qquad NO_2 + RC(O)O_2 \leftrightarrow RC(O)O_2NO_2$$

While nitric acid (HNO_3), at least in the planetary boundary layer, provides an effective sink for NO_x, the thermally unstable compound PAN provides only a temporary reservoir for NO_2. Most important, the lifetime of PAN becomes long enough at the colder temperatures of the middle and upper troposphere that it can be transported over long distances and serve as a carrier of NO_x into remote regions. NO_x is also removed by the formation of alkyl nitrates ($RONO_2$) that are formed in the alternative reaction path of RO_2 with NO (R5-3b) (Atkinson *et al.*, 1982):

$$\text{(R5-3b)} \qquad RO_2 + NO \rightarrow RONO_2$$

Similar to PAN, alkyl nitrates could provide a source of NO_x to more remote regions via photolysis or through reaction with OH following transport (Atlas, 1988).

An important loss process for NO_x that was not included in earlier model studies (Liu *et al.*, 1987) is the oxidation of NO_2 by ozone itself. The NO_3 radical formed in reaction (R5-17) is extremely sensitive to photolysis but can build up at night to concentrations of several hundred ppt (Platt *et al.*, 1981; Wayne *et al.*, 1991). Because of the thermal equilibrium (R5-18) that is established between NO_3, NO_2, and N_2O_5, heterogeneous losses of N_2O_5 or NO_3 in addition to reactions of NO_3 with some hydrocarbons provide a sink for NO_x in

addition to the reaction with OH (R5-15). For example, (R5-19) constitutes a non-photochemical conversion of active NO_x to long-lived aerosol nitrate (or HNO_3 in case of evaporation of the droplets). According to model calculations, this mechanism could provide a significant sink for NO_x on a global scale (Dentener and Crutzen, 1993). Observations of the chemical lifetime of NO_3 (Platt *et al.*, 1984) indicate that in the boundary layer, the initial reaction R5-17 is often the rate-limiting step for the removal of NO_x by these processes.

(R5-17) $NO_2 + O_3 \rightarrow NO_3 + O_2$

(R5-18) $NO_2 + NO_3 \leftrightarrow N_2O_5$

(R5-19) $N_2O_5 + H_2O_{lq} \rightarrow 2\,H^+ + 2\,NO_3^-$

The occurrence of clouds changes the chemical processing in an air mass significantly (Chameides and Davis, 1982). Although the volume fraction of liquid water in clouds is only of the order of 10^{-6} or less, some gases are so soluble that they largely go into the aqueous phase. This has several consequences: (1) the soluble gases are concentrated in a relatively small volume, which can enhance reaction rates, and (2) soluble gases are separated from insoluble ones, so that some reaction rates are significantly reduced. An important example is reaction R5-5, which almost ceases within clouds because HO_2 is very soluble, whereas NO remains in the interstitial air. Furthermore, the dissociation of dissolved HO_2 yields O_2^-, which destroys O_3 in the aqueous phase. The production of HO_2 in the droplets results to a large extent from the oxidation of dissolved formaldehyde. A radical reaction cycle is thus initiated in which both formaldehyde and O_3 are destroyed.

The estimated effect of cloud chemistry is that the photochemical O_3 production rate in the lower troposphere (where most clouds occur) is reduced by 30-40%, while O_3 destruction reactions are enhanced by up to a factor 2 (Lelieveld and Crutzen, 1990). The net effect of cloud processes on the O_3 burden in the troposphere is estimated to be much smaller, however, since these processes compete with dry deposition (Dentener *et al.*, 1993). Model simulations suggest a 10-30% lower tropospheric ozone burden as compared to a cloud-free atmosphere (Johnson and Isaksen, 1993; Dentener *et al.*, 1993).

5.3 INSIGHTS FROM FIELD OBSERVATIONS: PHOTOCHEMISTRY AND TRANSPORT

During the summer months, elevated and potentially harmful levels of ozone are commonly observed in urban and rural areas of North America and Europe (Cox *et al.*, 1975; Logan, 1985). Slow-moving high pressure systems with predominantly clear skies and elevated temperatures set the stage for the photochemical formation and accumulation of ozone and other oxidants over wide regions during episodes that last several days (Guicherit and van Dop, 1977; Vukovich *et al.*, 1977). There is substantial evidence from field measurements and model calculations that most of this ozone is being produced photochemically from ozone precursors emitted within the region. The export of O_3 and its precursors from the urban to regional and global scales represents the greatest potential impact on trends in global ozone by anthropogenic activities.

5.3.1 Urban and Near-Urban Regions

High ozone levels in and downwind of urban regions remain an important air quality problem throughout the world. While most industrialized countries have made significant progress in lowering peak ozone concentrations over the last two decades, unhealthy levels of ozone persist in and around many larger cities. In particular, in many developing countries, the absence or ineffectiveness of emissions control efforts can result in extremely high ozone concentrations.

The limited atmospheric chemical measurements from urban areas in developing countries suggest that conditions in many of these areas essentially mimic conditions observed in the Organization for Economic Cooperation and Development (OECD) countries during the 1960s before implementation of large-scale emissions control programs. For example, observations of individual hydrocarbon ratios in Mexico City, Mexico, during 1992 (Seila *et al.*, 1993) were similar to those observed in Los Angeles, California, during the 1960s and are consistent with motor vehicles as the major source of hydrocarbon emissions in this area. Motor vehicle emissions have also been demonstrated to be the major source of hydrocarbons in Athens, Greece; Rio de Janeiro, Brazil; and Beijing, China (see Tang *et al.*, 1993; Xiuli *et al.*, 1994).

The impact of anthropogenic NO_x and VOC emissions on regional and global ozone levels depends on the rate of ozone formation, the amount of ozone that is formed per precursor, and the rate and the pathway of transport out of the source regions. Direct and indirect measurements of peroxy radical concentrations that were made at several rural sites indicate concentrations of up to several hundred ppt at noontime on clear summer days (Parrish *et al.*, 1986; Volz *et al.*, 1988; Mihelcic *et al.*, 1990; Mihelcic and Volz-Thomas, 1993; Cantrell *et al.*, 1993). When combined with concurrent NO measurements, these RO_2 radical concentrations indicate substantial *in situ* ozone production rates of several tens of ppb/h at rural locations in the vicinity of industrialized regions (Volz *et al.*, 1988; Trainer *et al.*, 1991; Cantrell *et al.*, 1993). Such measurements can be used to determine the relative roles of UV radiation, NO_x, and VOC for *in situ* ozone production. The observed ozone increase is usually much smaller than the gross production rate derived from the RO_2 measurements, which indicates that the losses through dry deposition or reactions with unsaturated VOCs such as terpenes and by dilution must be of similar magnitude as the production rate. This indicates that the characteristic lifetime of ozone in polluted air masses is rather small, *e.g.*, less than one day.

In photochemically aged air in summer, O_3 was found to increase with increasing NO_y concentration, from a background value of 30-40 ppb O_3 at NO_y mixing ratios below 1 ppb to values between 70 to 100 ppb at NO_y levels of 10-20 ppb (Fahey *et al.*, 1986). As is expected from photochemical theory, an even better correlation is observed between ozone and the products of the NO_x oxidation (Trainer *et al.*, 1993; Volz-Thomas *et al.*, 1993a). Figure 5-2 shows the results from measurements made during summertime at several rural locations in the U.S. and Canada, and at Schauinsland in Europe. The slope of the correlation provides, at first approximation, experimental information on the ozone production efficiency, *e.g.*, the number of ozone molecules produced by each NO_x molecule before oxidation to more stable products such as HNO_3 and peroxyacetyl nitrate (see Section 5.2.2). The increments in the individual data sets in Figure 5-2 range from 4 to 10 and suggest a somewhat smaller production efficiency than what has been predicted by models for NO_x levels typically encountered in rural regions of the industrialized countries (Liu *et al.*, 1987; Lin *et al.*, 1988; Hov, 1989).

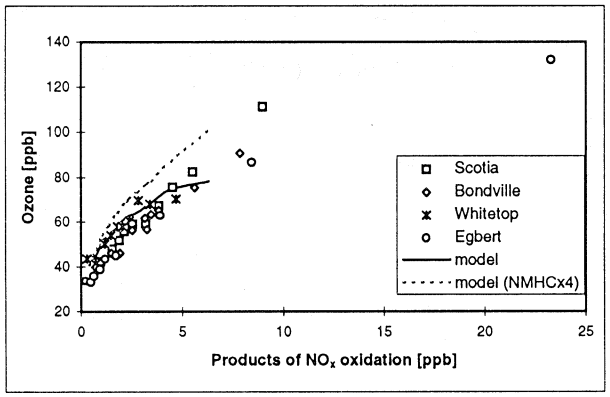

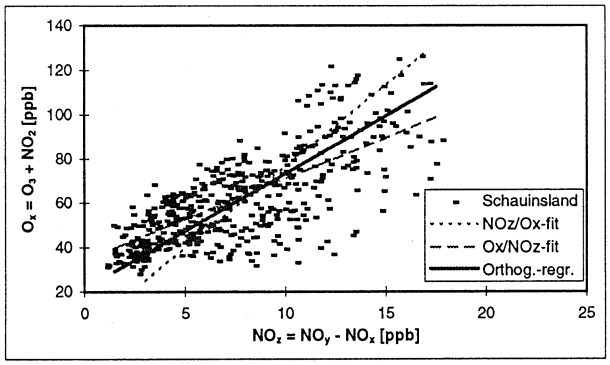

Figure 5-2a. Ozone versus the concentration of NO_x oxidation products (*e.g.*, NO_z in Figure 5-1), as measured at four sites in the eastern United States and Canada during summer 1988 and the results from a model calculation (based upon Trainer *et al.*, 1993).

Figure 5-2b. Same relation as 5-2a measured at Schauinsland, Germany, during summer 1990 in air masses advected from the Rhine Valley (based upon Volz-Thomas *et al.*, 1993a). The quantity $O_x = O_3 + NO_2$ is used to account for titration of O_3 under high NO_x conditions (R5-10 in Section 5.2.2).

The data also indicate a significantly lower production efficiency for the air masses encountered at Schauinsland in Europe.

The role of hydrocarbons and nitrogen oxides for ozone formation on the urban / sub-urban scale was studied by Hess *et al.*, (1992a, b, c) in an outdoor smog chamber using a synthetic gas blend that closely resembled that of automobile exhaust. The most important finding was that the initial rate of ozone formation depended on the mix of hydrocarbons used and, of course, on the availability of UV light. However, the final

amount of O_3 produced during one day depended mainly on the availability of NO_x. To some extent, the latter depends on the hydrocarbon mix, specifically on the existence of NO_x sinks in the chemistry through formation of organic nitrates (Carter and Atkinson, 1989).

Insight into the chemical breakdown of hydrocarbons and their role in ozone formation can be obtained from field measurements of alkyl nitrates ($RONO_2$), since these species are formed as a by-product in reaction (R5-3), which is rate-limiting in ozone formation. From an extensive series of measurements made at Schauinsland, a mountain site in Southern Germany, in summer, a linear relation was found between ozone and alkyl nitrate concentrations, which is shown in Figure 5-3 (Flocke *et al.*, 1991, 1993). The high degree of correlation found in air masses that originate in the Rhine Valley, and thus represent a relatively uniform mix of hydrocarbons, clearly points out that most of the ozone observed at Schauinsland in summer (70 ppb average and peak values of 130 ppb) is formed *in situ* from anthropogenic precursors emitted within the region. By extrapolation to $RONO_2$ concentrations of zero, an estimate of 20-30 ppb is obtained for today's non-photochemical background mixing ratio of ozone in the continental boundary layer in summer (Flocke, 1992; Flocke *et al.*, 1993; Volz-Thomas *et al.*, 1993b). This finding supports the conclusions drawn by Volz and Kley (1988) and by Staehelin *et al.*, (1994) from historic measurements (see Chapter 1) and proves the predominant anthropogenic influence on ozone levels in some rural areas today. Since alkyl nitrates are not removed by rainout, they are better suited for such an extrapolation than either NO_y or NO_z (= NO_y - NO_x), since the latter contain soluble HNO_3 as a major constituent.

The European studies also led to the conclusion that about one ozone molecule per carbon atom is formed from the oxidation of hydrocarbons in these air masses (Flocke, 1992). Furthermore, the relative abundance of the different alkyl nitrates indicates that most of the smaller RO_2 radicals are not formed from the oxidation of the respective parent hydrocarbons but by decomposition of larger alkoxy radicals. This finding is in agreement with results from laboratory studies (Atkinson *et al.*, 1992) and RO_2 production from the decomposition of RO radicals is now a common feature in detailed chemical mechanisms used in urban airshed models (Carter, 1990; Atkinson 1990). The finding is also

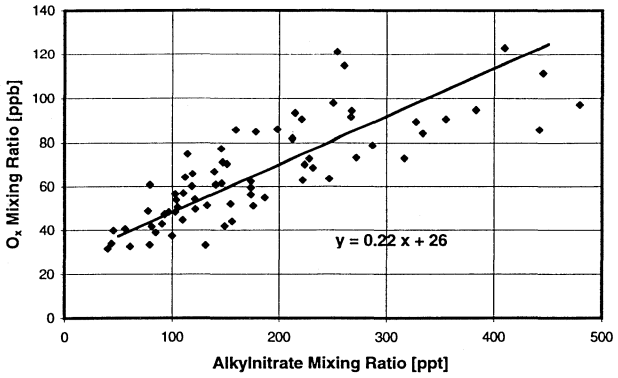

Figure 5-3. Correlation of $O_x = O_3 + NO_2$ concentrations with those of alkyl nitrates ($RONO_2$) as observed at Schauinsland, Germany, in summer under polluted conditions (based upon Flocke *et al.*, 1992). O_x and $RONO_2$ emerge from the same reaction (R5-3).

consistent with the fact that measured ratios of organic peroxy radicals to HO_2 are significantly larger than those predicted by models that do not include this mechanism (Mihelcic and Volz-Thomas, 1993). The conclusion is that the rate of production of RO_2 radicals is greater than originally assumed in these models.

Carbon monoxide is an anthropogenic pollutant that has a relatively long photochemical lifetime (1 month in summer) and is not affected by rainout. Thus, it is a suitable tracer of anthropogenic pollution on longer time scales (Fishman and Seiler, 1983). Parrish *et al.* (1993) observed a strong correlation between ozone and CO with a consistent slope $\Delta O_3/\Delta CO = 0.3$ at several island sites in eastern Canada (Figure 5-4). The sites were located at approximately 500-km intervals downwind of the northeastern urban corridor of the United States, and covered approximately one-third of the distance from Boston to Ireland. By scaling the observed slope to a CO emission inventory, they inferred a net export of 5 Tg anthropogenic O_3 out of the eastern U.S. in summer. Chin *et al.* (1994) successfully simulated the observed O_3-CO relationship in a continental-scale three-dimensional (3-D) model and concluded that the correlation slope of 0.3 is a general characteristic of aged polluted air in the U.S. The model allowed in particular to correct for the effect of O_3 deposition. From this calculation, Chin *et al.* (1994) estimated that export of eastern North American pollution contributes 7 Tg of O_3

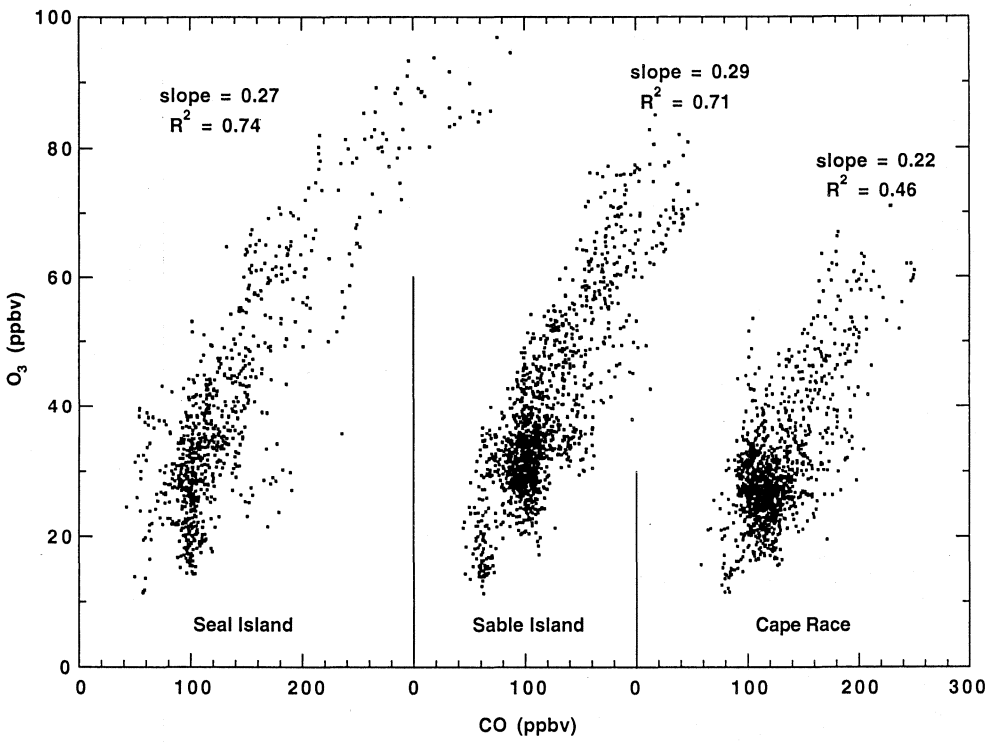

Figure 5-4. Relation between O_3 and CO observed at three island sites in the North Atlantic west of Canada during summer 1992 (based upon Parrish *et al.*, 1993).

in summer. Jacob *et al.* (1993) used the same model to estimate that pollution from all of North America contributes 30 Tg of O_3 to the Northern Hemisphere in summer, of which 15 Tg is due to direct export and 15 Tg is due to export of NO_x leading to O_3 production in the remote troposphere. This anthropogenic source of O_3 is about one-third of the estimated cross-tropopause transport of O_3 in the Northern Hemisphere in summer. Considering that the U.S. accounts for about 30% of fossil fuel NO_x emissions in the Northern Hemisphere, it can be concluded that anthropogenic sources make a major contribution to tropospheric ozone on the hemispheric scale, of magnitude comparable to influx from the stratosphere.

While the summertime measurements show a strong positive correlation of ozone with anthropogenic tracers such as NO_y and CO, a negative correlation was observed during winter. A decrease in the O_3 concentration with increasing CO concentration is observed at a number of locations in North America and Europe (Poulida *et al.*, 1991; Parrish *et al.*, 1993; Scheel *et al.*, 1993; Simmonds, 1993; Derwent *et al.*, 1994). Derwent *et al.* conclude from their analysis of the air masses that arrive at Mace Head, Ireland, that the European continent is a net source of ozone in summer, but is a net sink in winter. This estimate, however, is only valid for the planetary boundary layer and does not include the influence of NO_x export on the net photochemical balance of ozone.

A seasonal trend is also apparent in the correlation of ozone with NO_y and NO_z (Fahey *et al.*, 1986; Volz-Thomas *et al.*, 1993a). The wintertime measurements of O_3, NO_x, and NO_y at Schauinsland indicate a decrease of ozone with increasing concentrations of the products of the NO_x oxidation and, hence, support the importance of nighttime chemistry in the oxidation of NO_x at the expense of ozone in polluted air masses.

Since anthropogenic NO_x emissions do not have a strong seasonal variation, Calvert *et al.* (1985) argued that the absence of a seasonal cycle in nitrate deposition rates provided evidence for the importance of NO_3 chemistry in the removal of NO_x. However, more recent data from the National Acid Deposition Program and

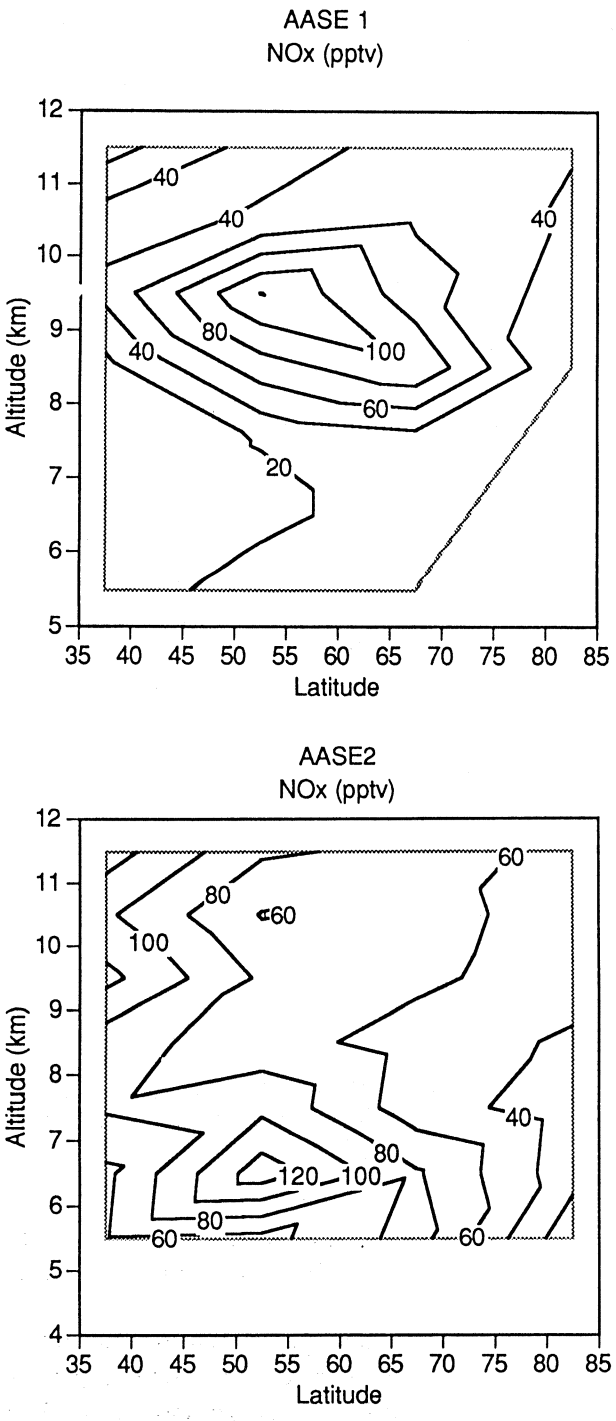

Figure 5-8. Summary of NO_x = NO + NO_2 concentrations in the free troposphere measured in the Northern Hemisphere during the AASE I and AASE II missions (based upon Carroll *et al.*, 1990a and Weinheimer *et al.*, 1994).

that this component is even more important at high latitudes. Evidence for stratospheric input to the Arctic troposphere was presented by Shapiro *et al.* (1987) and Oltmans *et al.* (1989). Furthermore, airborne lidar measurements made over the Arctic region in summer found that stratospheric intrusions dominated the ozone budget in the free troposphere (Browell *et al.*, 1992; Gregory *et al.*, 1992). There is also a suggestion in ozonesonde data from the South Pole (Gruzdev and Sitnov, 1993) that ozone depletion in the Antarctic polar vortex extends into the upper troposphere.

An example of progress in determining large-scale reactive nitrogen distributions over the complete tropospheric altitude regime is shown in Figure 5-7, which contrasts the seasonal distribution of NO from aircraft measurements made during the Tropospheric Ozone II (TROPOZ II) mission in January 1991 (Wahner *et al.*, 1994) and the Stratospheric Ozone III (STRATOZ III) mission in June 1984 (Drummond *et al.*, 1988; Ehhalt *et al.*, 1992). The mixing ratios are considerably higher in the Northern Hemisphere, particularly at high latitudes in winter, and at 20-50°N at high altitudes in summer. Vertical gradients are strongest in June north of 20°S. The high mixing ratios of NO at northern midlatitudes are attributed to stratospheric input, aircraft emissions, and convective transport from the "polluted" boundary layer (Ehhalt *et al.*, 1992).

The NO concentrations observed during TROPOZ II are much larger than what has been observed by other investigators at similar latitudes and seasons. Figure 5-8 shows NO_x concentrations observed during the Arctic Airborne Stratospheric Expedition (AASE) I and II missions (Carroll *et al.*, 1990a; Weinheimer *et al.*, 1994). While these flights were made during the same season as TROPOZ II and at overlapping latitudes, they show much lower NO_x (=NO+NO_2) concentrations than the NO concentrations alone that were observed during TROPOZ II. The AASE measurements are in general agreement although separated by a three-year period. The difference may be due to the shorter measurement period of the TROPOZ program, and an unusual synoptic event, compared to the longer-term AASE programs. Barring unexpected measurement uncertainty, the differences demonstrate the difficulty in ascertaining a climatology of a short-lived species like NO_x over larger scales.

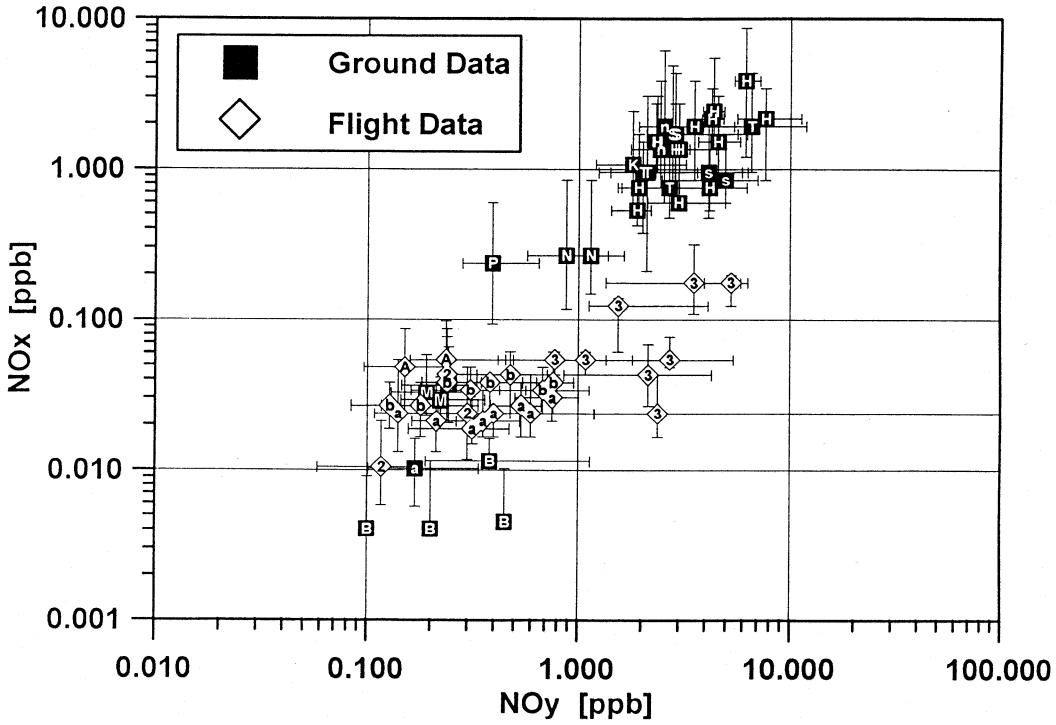

Figure 5-9. Summary of NO_x and NO_y concentrations in the PBL and free troposphere (from Prather *et al.*, 1994, based on Carroll and Thompson, 1994). The majority of the airborne measurements shows NO_x concentrations that are too small to sustain net ozone production. The letters and numbers within the symbols refer to the following measurement campaigns (see Appendix for acronym definitions): a = ABLE3a; A = AASE; b = ABLE3b; B = Barrow, Alaska; H = Harvard Forest; K = Kinterbush, Alabama; M = MLOPEX; n = NACNEMS; N = Niwot Ridge, Colorado; P = Point Arena, California; s = SOS/SONIA, S = Scotia, Pennsylvania; T = TOR; 2 = CITE2; 3 = CITE3.

Murphy *et al.* (1993) have measured vertical distributions of NO_y and O_3 into the stratosphere. Although a strong correlation between NO_y and O_3 was found in the stratosphere, they observed only weak to no correlation between these constituents in the troposphere, *i.e.*, the tropospheric NO_y/O_3 ratio can be larger and more variable, a reflection of the variety of sources, sinks, and transport processes of NO_y and O_3 in the troposphere. In contrast, Wofsy *et al.* (1992) and Hübler *et al.* (1992a, b) reported a significant positive correlation when the data are averaged over a large number of observations. The observed slope was much steeper than that derived from continental boundary layer studies (Section 5.3.2) and approached that found in the stratosphere. The large decrease in the NO_y/O_3 ratio between the continental surface studies and the remote free atmosphere is believed to largely reflect the shorter lifetime of NO_y compared to O_3 in the free troposphere, mixing, and input from the stratosphere.

A summary of tropospheric NO_x and NO_y concentrations from Prather *et al.* (1994) is shown in Figure 5-9. It is based on the compilation of Carroll and Thompson, (1994) of measurements made by various groups in the lower and middle troposphere over the U.S. and Europe. Although very high concentrations from urban areas are excluded, the concentrations of NO_x span a range of three orders of magnitude. On the average, a correlation between NO_x and NO_y is seen. However, the individual data sets clearly show that the shorter-lived NO_x can still vary over an order of magnitude for a given NO_y concentration. From this and the differences in NO_x observations in the upper troposphere at northern latitudes discussed above, it is clear that present measurements are insufficient to reasonably describe a meaningful climatology.

Aircraft programs have continued to strengthen the role of PAN as a reservoir for NO_x, at least in the 3-6 km altitude range over continental regions (Singh *et al.*, 1992, 1994), where PAN decomposition was able to account for much of the observed NO_x, a result that emphasizes the role of transport of odd nitrogen reservoirs. Very high PAN concentrations of up to 200 ppt were also observed in long-range transport events at Izana during spring, whereas PAN concentrations remained below 20 ppt at the higher temperatures of summer (Schmitt and Hanson, 1993). Other studies have shown that the importance of PAN as a NO_x reservoir is not global. Measurements made in the Northern Hemisphere upper troposphere mostly over the Atlantic Ocean have generally shown smaller mixing ratios than observed in the middle troposphere over continental regions, and Southern Hemisphere mixing ratios were very small throughout the troposphere (Rudolph *et al.*, 1987; Perros, 1994). Similarly, during studies at the Mauna Loa Observatory experiment, PAN was not a major constituent. HNO_3 was the dominant reservoir (median of 43% of NO_y), followed by NO_x (14%), particulate nitrate (5%), PAN (5%), and alkyl nitrates (2%) (Atlas *et al.*, 1992).

The role of the remote marine PBL as a strong net sink for ozone has been clearly identified in a large number of investigations, a finding first reported by Liu *et al.* (1983). For example, a clear anticorrelation in the diurnal and seasonal variation of O_3 and H_2O_2 was observed by Ayers *et al.* (1992) in marine air at Cape Grim, Tasmania (Figure 5-10). As is seen in Figure 5-1, HO_2 radical recombination leads to formation of H_2O_2, which can thus be utilized as a tracer for photochemical activity. The results are consistent with net photochemical destruction of O_3 in a very low NO_x atmosphere. Net photochemical destruction of O_3 in the tropical PBL of up to 25%/day was also inferred from the data gathered during several ship cruises (Thompson *et al.*, 1993; Smit *et al.*, 1989; Smit and Kley 1993; Harris *et al.*, 1992).

The photochemical buffer regions are not confined to the remote maritime lower atmosphere. Aircraft flights covering Alaska, northern Ontario and Quebec, and Labrador have concluded that the surface layer, especially the boreal forest, was an efficient sink for O_3 and NO_y (Gregory *et al.*, 1992; Jacob *et al.*, 1992; Bakwin *et al.*, 1992). In some regions of these flights, NO_x was nearly independent of altitude up to 6 km with a median mixing ratio of only 25 ppt, insufficient to overcome average net photochemical destruction of O_3 (Sandholm *et al.*, 1992). Earlier studies over the continental U.S. by Carroll *et al.* (1990b) found that air masses between the boundary layer and 5-6 km, were nearly equipartitioned between net loss, approximate balance, and net production of O_3.

An extremely interesting finding that yet awaits complete explanation is the occurrence of nearly complete O_3 depletion in the Arctic surface layer in spring (Barrie *et al.*, 1988; Bottenheim *et al.*, 1990; McConnell *et al.*, 1992; Fan and Jacob, 1992). A recent analysis of the ratios of different hydrocarbons provides evidence for bromine chemistry being responsible for the ozone removal (Jobson *et al.*, 1994), although Platt and Hausmann (1994) argue that the measured BrO concentrations were too small to explain the complete ozone depletion on the short time scales implied by the observations.

Net ozone loss of 0.5 ppb/day, or ~1%/day, was also found in the free troposphere near 3.4 km from observations at the Mauna Loa Observatory (Ridley *et al.*, 1992). The concentrations of peroxy radicals and the rate of ozone formation, $P(O_3)$, were derived from the photostationary state of NO_x (Figure 5-11) and the loss rate, $L(O_3)$, was inferred from model calculations based on the measured concentrations of all relevant parameters. It is noteworthy that both the total concentration of HO_2 and RO_2 determined during this study, as well as the modeled HO_2/RO_2 ratio, are in good agreement with recent direct measurements made by matrix isolation and ESR spectroscopy at Izana, Tenerife (D. Mihelcic, private communication).

The net destruction rate found in spring at Mauna Loa in the free troposphere is slow enough that vertical exchange with the marine boundary layer can overrule *in situ* chemistry. Vertical soundings made from a ship cruise in the Pacific clearly demonstrate the importance of convective transport for the ozone balance of the free troposphere. Extremely low ozone concentrations, that had their origin in the marine boundary layer, were found in the upper troposphere (Smit and Kley, 1993). These observations contrast those made or modeled over continental regions, where an emphasis has been on the role of convection of boundary layer precursors in augmenting O_3 production in the middle and upper troposphere (Dickerson *et al.*, 1987; Pickering *et al.*, 1992a, b; Thompson *et al.*, 1994). As was suggested by

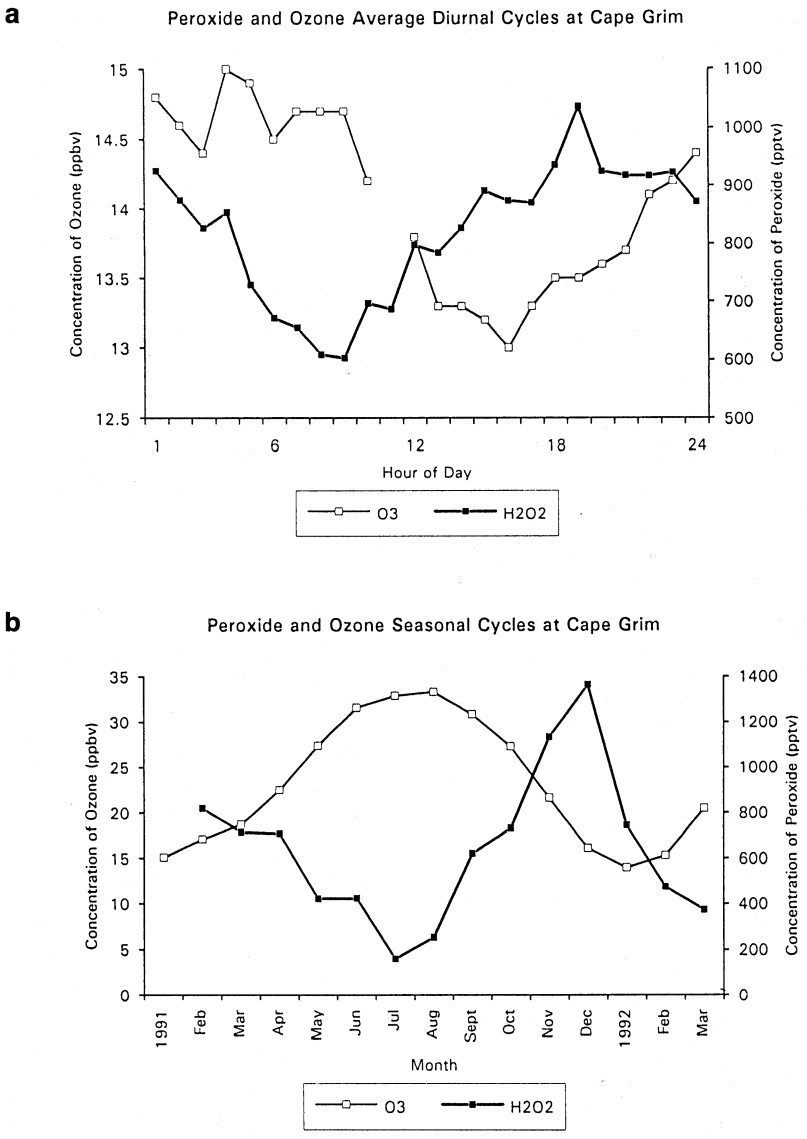

Figure 5-10a. Average diurnal cycles for peroxide and ozone in background air at Cape Grim for January 1992 (based upon Ayers *et al.*, 1992).
Figure 5-10b. Seasonal cycles of peroxide and ozone in background air at Cape Grim (based upon Ayers *et al.*, 1992).

modeling studies (Lelieveld and Crutzen, 1994), downward mesoscale flow in the cloud environment can carry O_3 to the Earth's surface, where it is destroyed more rapidly. Although these model studies yet await confirmation by experimental data, it is likely that deep convection tends to increase free tropospheric ozone levels downwind of continental source areas but may reduce tropospheric O_3 in regions that are removed from polluted areas.

Intensive studies at Mauna Loa have suggested some possible discrepancies in our understanding of the atmospheric oxidizing capacity. Programs completed more recently may help to determine whether these results are more universal in the remote troposphere. First, the abundance of formaldehyde (HCHO) predicted from

Doddridge, B.G., *et al.,* Trace gas concentrations and meteorology in rural Virginia 2. Reactive nitrogen compounds, *J. Geophys. Res., 97,* 20631-20646, 1992.

Dorn, H.-P., J. Callies, U. Platt, and D.H. Ehhalt, Measurement of tropospheric OH concentrations by laser long-path absorption spectroscopy, *Tellus, 40B,* 437-445, 1988.

Drummond, J., D.H. Ehhalt, and A. Volz, Measurements of nitric oxide between 0-12 km altitude and 67°N and 60°S latitude obtained during STRATOZ III, *J. Geophys. Res., 93,* 15831-15849, 1988.

Ehhalt, D.H., H.P. Dorn, and D. Poppe, The chemistry of the hydroxyl radical in the troposphere, *Proc. Roy. Soc. Edinburgh, 97B,* 17-34, 1991.

Ehhalt, D.H., F. Rohrer, and A. Wahner, Sources and distribution of NO_X in the upper troposphere at northern mid-latitudes, *J. Geophys. Res., 97,* 3725-3738, 1992.

Eisele, F.L., G.H. Mount, F.C. Fehsenfeld, J. Harder, E. Marovich, D.D. Parrish, J. Roberts, M. Trainer, and D. Tanner, Intercomparison of tropospheric OH and ancillary trace gas measurements at Fritz Peak Observatory, Colorado, *J. Geophys. Res., 99,* 18605-18626, 1994.

Fahey, D.W., *et al.,* Reactive nitrogen species in the troposphere: Measurements of NO, NO_2, HNO_3, particulate nitrate, peroxyacetyl nitrate (PAN), O_3, and total reactive odd nitrogen (NO_y) at Niwot Ridge, Colorado, *J. Geophys. Res., 91,* 9781-9793, 1986.

Fahey, D.W., S. Solomon, S.R. Kawa, M. Loewenstein, J.R. Podolske, S.E. Strahan, and K.R. Chan, A diagnostic for denitrification in the winter polar stratosphere, *Nature, 345,* 698-702, 1990.

Fan, S.-M., and D.J. Jacob, Surface ozone depletion in Arctic spring sustained by aerosol bromine reactions, *Nature, 359,* 522-524, 1992.

Felton, C.C., J.C. Sheppard, and M.J. Campbell, Measurements of the diurnal OH cycle by a ^{14}C-tracer method, *Nature, 335,* 53-55, 1988.

Finnlayson-Pitts, B.J., M.J. Ezell, and J.N. Pitts, Jr., Formation of chemically active chlorine compounds by reactions of atmospheric NaCl particles with gaseous N_2O_5 and $ClONO_2$, *Nature, 337,* 241-244, 1989.

Fishman, J., and W. Seiler, Correlative nature of ozone and carbon monoxide in the troposphere: Implications for the tropospheric ozone budget, *J. Geophys. Res., 88,* 3662-3670, 1983.

Fishman, J., F.M. Vukovich, and E.V. Browell, The photochemistry of synoptic-scale ozone synthesis: Implications for the global tropospheric ozone budget, *J. Atmos. Chem., 3,* 299-320, 1985.

Fishman, J., C.E. Watson, J.C. Larsen, and J.A. Logan, Distribution of tropospheric ozone determined from satellite data, *J. Geophys. Res., 95,* 3599-3617, 1990.

Fishman, J., K. Fakhruzzaman, B. Cros, and D. Nganga, Identification of widespread pollution in the southern hemisphere deduced from satellite analyses, *Science, 252,* 1693-1696, 1991.

Fishman, J., V.G. Brackett, and K. Fakhruzzaman, Distribution of tropospheric ozone in the tropics from satellite and ozonesonde measurements, *J. Atmos. Terrestrial Phys., 54,* 589-597, 1992.

Flocke, F., Messungen von Alkylnitraten (C_1-C_8) am Schauinsland im Schwarzwald. Ein Beitrag zur Bilanzierung der Photochemischen Ozonproduktion, Inaugural-Dissertation zur Erlangung des Doktorgrades des Fachbereichs Naturwissenschaften II der Bergischen Universität-Gesamthochschule Wuppertal, 1992.

Flocke, F., A. Volz-Thomas, and D. Kley, Measurements of alkyl nitrates in rural and polluted air masses, *Atmos. Environ., 25A(9),* 1951-1960, 1991.

Flocke, F., A. Volz-Thomas, and D. Kley, The use of alkyl nitrate measurements for the characterization of the ozone balance in southwestern Germany, *EOS 74 (43),* 180, 1993.

Follows, M.J., On the cross-tropopause exchange of air, *J. Atmos. Sci., 49,* 879-82, 1992.

Gidel, L.T., and M.A. Shapiro, General circulation model estimates of the net vertical flux of ozone in the lower stratosphere and the implications for the tropospheric ozone budget, *J. Geophys. Res., 85,* 4049-4058, 1980.

Greenberg, J.P., *et al.,* Diurnal variability of methane, nonmethane hydrocarbons, and carbon monoxide at Mauna Loa, *J. Geophys. Res., 97,* 10395, 1992.

Gregory, G.L., B.E. Anderson, L.S. Warren, E.V. Browell, D.R. Bagwell, and C.H. Hudgins, Tropospheric ozone and aerosol observations: The Alaskan Arctic, *J. Geophys. Res., 97*, 16451-16471, 1992.

Gruzdev, A.N., and S.A. Sitnov, Tropospheric ozone annual variation and possible troposphere-stratosphere coupling in the Arctic and Antarctic as derived from ozone soundings at Resolute and Amundsen-Scott stations, *Tellus, 45B*, 89-98, 1993.

Guicherit, R., and H. van Dop, Photochemical production in western Europe (1971-1975) and its relation to meteorology, *Atmos. Environ., 11*, 145-156, 1977.

Guicherit, R., Ozone on an urban and regional scale – with special reference to the situation in the Netherlands, in *Tropospheric Ozone—Regional and Global Scale Interactions*, edited by I.S.A. Isaksen, *NATO ASI Series C. Vol. 227*, D. Reidel Publ., Dordrecht, The Nederlands, 49-62, 1988.

Haagen-Smit, A.J., Chemistry and physiology of Los Angeles smog, *Indust. Eng. Chem., 44*, 1342-1346, 1952.

Hameed, S., J.P. Pinto, and R.W. Stewart, Sensitivity of the predicted CO-OH-CH_4 perturbation to tropospheric NO_x concentrations, *J. Geophys. Res., 84*, 763-768, 1979.

Harris, G.W., D. Klemp, T. Zenker, and J.P. Burrows, Tunable diode laser measurements of trace gases during the 1988 Polarstern cruise and intercomparisons with other methods, *J. Atmos. Chem., 15*, 315-326, 1992.

Haynes, P.H., C.J. Marks, M.E. McIntyre, T.G. Shepherd, and K.P. Shine, On the "downward control" of extratropical diabatic circulations by eddy-induced mean zonal forces, *J. Atmos. Sci., 48*, 651-78, 1991.

Heikes, B., Formaldehyde and hydroperoxides at Mauna Loa Observatory, *J. Geophys. Res., 97*, 18001-18013, 1992.

Hess, G.D., F. Carnovale, M.E. Cooper, and G.M. Johnson, The evaluation of some photochemical smog reaction mechanisms—I. Temperature and initial composition effects, *Atmos. Environ., 26*, 625-641, 1992a.

Hess, G.D., F. Carnovale, M.E. Cooper, and G.M. Johnson, The evaluation of some photochemical smog reaction mechanisms—II. Initial addition of alkanes and alkenes, *Atmos. Environ., 26*, 643-651, 1992b.

Hess, G.D., F. Carnovale, M.E. Cooper, and G.M. Johnson, The evaluation of some photochemical smog reaction mechanisms—III. Dilution and emissions effects, *Atmos. Environ., 26*, 653-659, 1992c.

Holton, J.R., On the global exchange of mass between the stratosphere and the troposphere, *Mon. Wea. Rev., 47*, 392-4, 1990.

Honrath, R.E., and D.A. Jaffe, The seasonal cycle of nitrogen oxides in the Arctic troposphere at Barrow, Alaska, *J. Geophys. Res., 97*, 20615-20630, 1992.

Hov, Ø., Changes in tropospheric ozone: A simple model experiment, in *Ozone in the Atmosphere*, Proceedings of the Quadrennial Ozone Symposium 1988 and Tropospheric Ozone Workshop, Göttingen, edited by R.D. Bojkov and P. Fabian, A. Deepak Publ., Hampton, Virginia, 557-560, 1989.

Hübler, G., *et al.*, Airborne measurements of total reactive odd nitrogen (NO_y), *J. Geophys. Res., 97*, 9833-9850, 1992a.

Hübler, G., *et al.*, Total reactive oxidized nitrogen (NO_y) in the remote Pacific troposphere and its correlation with O_3 and CO: Mauna Loa Observatory Photochemistry Experiment 1988, *J. Geophys. Res., 97*, 10427-10477, 1992b.

Huebert, B.J., *et al.*, Measurements of the nitric acid to NO_x ratio in the troposphere, *J. Geophys. Res., 95*, 10193-10198, 1990.

Jacob, D.J., S.-M. Fan, S.C. Wofsy, P.A. Spiro, P.S. Bakwin, J. Ritter, E.V. Browell, G.L. Gregory, D.R. Fitzjarrald, and K.E. Moore, Deposition of ozone to tundra, *J. Geophys. Res., 97*, 16473-16479, 1992.

Jacob, D., J.A. Logan, G.M. Gardener, R.M. Yevich, C.M. Spivakovsky, and S.C. Wofsy, Factors regulating ozone over the United States and its export to the global atmosphere, *J. Geophys. Res., 98*, 14817-14826, 1993.

Jobson, B.T., *et al.*, Measurements of C_2-C_6 hydrocarbons during the Polar Sunrise 92 experiment, *J. Geophys. Res.*, in press, 1994.

Johnson, J.E., and I.S.A. Isaksen, Tropospheric ozone chemistry: The impact of cloud chemistry, *J. Atmos. Chem., 16*, 99-122, 1993.

Kirchhoff, V.W.J.H., A.W. Setzer, and M.C. Pereira, Biomass burning in Amazonia: Seasonal effects on atmospheric O_3 and CO, *Geophys. Res. Lett., 16*, 469-472, 1989.

Kirchhoff, V.W.J.H., and E.V.A. Marinho, Layer enhancements of tropospheric ozone in regions of biomass burning, *Atmos. Environ., 28*, 69-74, 1994.

Kirchhoff, V.W.J.H., Z. Nakamura, E.V.A. Marinho, and M.M. Mariano, Excess ozone production in Amazonia from large scale burnings, *J. Atmos. Terrestrial Phys., 54*, 583-588, 1992.

Kley, D., H. Geiss, and V.A. Mohnen, Concentrations and trends of tropospheric ozone and precursor emissions in the USA and Europe, in *The Chemistry of the Atmosphere: Its Impact on Global Change*, edited by J.G. Calvert, Blackwell Sci. Publ., Oxford, 245-259, 1994.

Kley, D., A. Volz, and F. Mülheims, Ozone measurements in historic perspective, in *Tropospheric Ozone—Regional and Global Scale Interactions*, edited by I.S.A. Isaksen, *NATO ASI Series C. Vol. 227*, D. Reidel Publ., Dordrecht, The Netherlands, 63-72, 1988.

Lamarque, J.-F., and P.G. Hess, Cross-tropopause mass exchange and potential vorticity budget in a simulated tropopause folding, *J. Atmos. Sci., 51*, 2246-2269, 1994.

Leighton, P.A., *Photochemistry of Air Pollution*, Academic Press, San Diego, California, 1961.

Lelieveld, J., and P.J. Crutzen, Influences of cloud photochemical processes on tropospheric ozone, *Nature, 343*, 227-233, 1990.

Lelieveld, J., and P.J. Crutzen, Role of deep cloud convection in the ozone budget of the troposphere, *Science, 264*, 1759-1761, 1994.

Levy, H.B., J.D. Mahlman, W.J. Moxim, and S. Liu, Tropospheric ozone: The role of transport, *J. Geophys. Res., 90*, 3753-3771, 1985.

Lin, X., M. Trainer, and S.C. Liu, On the nonlinearity of the tropospheric ozone production, *J. Geophys. Res., 93*, 15879-15888, 1988.

Liu, S.C., M. McFarland, D. Kley, O. Zafiriou, and B. Huebert, Tropospheric NO_x and O_3 budgets in the equatorial Pacific, *J. Geophys. Res., 88*, 1349-1368, 1983.

Liu, S.C., M. Trainer, F.C. Fehsenfeld, D.D. Parrish, E.J. Williams, D.W. Fahey, G. Hübler, and P.C. Murphy, Ozone production in the rural troposphere and the implications for regional and global ozone distributions, *J. Geophys. Res., 92*, 4191-4207, 1987.

Liu, S.C., and M. Trainer, Response of tropospheric ozone and odd hydrogen radicals to column ozone change, *J. Atmos. Chem., 6*, 221-233, 1988.

Liu, S.C., *et al.*, A study of the photochemistry and ozone budget during the Mauna Loa Observatory Photochemistry Experiment, *J. Geophys. Res., 97*, 10463-10471, 1992.

Logan, J.A., M.J. Prather, C.S. Wofsy, and M.B. McElroy, Tropospheric chemistry: A global perspective, *J. Geophys. Res., 86*, 7210-7254, 1981.

Logan, J.A., Tropospheric ozone: Seasonal behaviour, trends, and anthropogenic influence, *J. Geophys. Res., 90*, 10463-10482, 1985.

Logan, J.A., Ozone in rural areas of the United States, *J. Geophys. Res., 94*, 8511-8532, 1989.

Low, P.S., P.S. Kelly, and T.D. Davies, Variations in surface ozone trends over Europe, *Geophys. Res. Lett., 19*, 1117-1120, 1992.

Marenco, A., J.C. Medale, and S. Prieur, Study of tropospheric ozone in the tropical belt (Africa, America) from STRATOZ and TROPOZ campaigns, *Atmos. Environ., 24A*, 2823-2834, 1990.

McConnell, J.C., G.S. Henderson, L. Barrie, J. Bottenheim, H. Niki, C.H. Langford, and E.M. Templeton, Photochemical bromine production implicated in Arctic boundary-layer ozone depletion, *Nature, 355*, 150-152, 1992.

Mihelcic, D., A. Volz-Thomas, H.W. Pätz, D. Kley, and M. Mihelcic, Numerical analysis of ESR spectra from atmospheric samples, *J. Atmos. Chem., 11*, 271-297, 1990.

Mihelcic, D., and A. Volz-Thomas, The ratio of hydroperoxy to organic peroxy radicals: Direct measurements by matrix isolation/ESR spectroscopy, *EOS 74 (43)*, 167, 1993.

Mount, G.H., and F.L. Eisele, An intercomparison of tropospheric OH measurements at Fritz Peak Observatory, Colorado, *Science, 256,* 1187-1190, 1992.

Murphy, D.M., D.W. Fahey, M.H. Proffitt, S.C. Liu, K.R. Chan, C.S. Eubank, S.R. Kawa, and K.K. Kelly, Reactive nitrogen and its correlation with ozone in the lower stratosphere and upper troposphere, *J. Geophys. Res., 98*, 8751-8774, 1993.

Murphy, D.M., and D.W. Fahey, An estimate of the flux of stratospheric reactive nitrogen and ozone into the troposphere, *J. Geophys. Res., 99*, 5325-5332, 1994.

NRC, *Rethinking the Ozone Problem in Urban and Regional Air Pollution,* National Research Council, National Academy Press, Washington, D.C., 1991.

Oltmans, S.J., W.E. Raatz, and W.D. Komhyr, On the transfer of stratospheric ozone into the troposphere near the North Pole, *J. Atmos. Chem., 9*, 245-53, 1989.

Oltmans, S.J., and H. Levy, II, Seasonal cycle of surface ozone over the western North Atlantic, *Nature, 358*, 392-394, 1992.

Oltmans, S.J., and H. Levy, II, Surface ozone measurements from a global network, *Atmos. Env., 28*, 9-24, 1994.

Parrish, D.D., M. Trainer, E.J. Williams, D.W. Fahey, G. Hübler, C.S. Eubank, S.C. Liu, P.C. Murphy, D.L. Albritton, and F.C. Fehsenfeld, Measurements of the NO_x-O_3 photostationary state at Niwot Ridge, Colorado, *J. Geophys. Res., 91*, 5361-5370, 1986.

Parrish, D.D., J.S. Holloway, M. Trainer, P.C. Murphy, G.L. Forbes, and F.C. Fehsenfeld, Export of North American ozone pollution to the North Atlantic Ocean, *Science, 259*, 1436-1439, 1993.

Penkett, S.A., N.J. Blake, P. Lightman, A.R.W. Marsh, P. Anwyl, and G. Butcher, The seasonal variation of nonmethane hydrocarbons in the free troposphere over the North Atlantic Ocean: Possible evidence for extensive reaction of hydrocarbons with the nitrate radical, *J. Geophys. Res., 98*, 2865-2885, 1993.

Perner, D., *et al.*, OH radicals in the lower troposphere, *Geophys. Res. Lett., 8*, 466-468, 1976.

Perner, D., *et al.*, Measurements of tropospheric OH concentrations: A comparison of field data with model prediction, *J. Atmos. Chem., 5*, 185-216, 1987.

Perros, P.E., Large scale distribution of peroxyacetylnitrate from aircraft measurements during the TROPOZ II experiment, *J. Geophys. Res., 99*, 8269-8280, 1994.

Pickering, K.E., A.M. Thompson, J.R. Scala, W.-K. Tao, and J. Simpson, Ozone production potential following convective redistribution of biomass burning emissions, *J. Atmos. Chem., 14*, 297-313, 1992a.

Pickering, K.E., A.M. Thompson, J.R. Scala, W.-K. Tao, R.R. Dickerson, and J. Simpson, Free tropospheric ozone production following entrainment of urban plumes into deep convection, *J. Geophys. Res., 97*, 17985-18000, 1992b.

Platt, U., D. Perner, J. Schröder, C. Kessler, and A. Toenissen, The diurnal variation of NO_3, *J. Geophys. Res., 86*, 11965-11970, 1981.

Platt, U., A.M. Winer, H.W. Biermann, R. Atkinson, and J.N. Pitts, Jr., Measurement of nitrate radical concentration in continental air, *Environ. Sci. Technol., 18*, 365-369, 1984.

Platt, U., M. Rateike, W. Junkermann, J. Rudolph, and D.H. Ehhalt, New tropospheric OH measurements, *J. Geophys. Res., 93*, 5159-5166, 1988.

Platt, U., and M. Hausmann, Spectroscopic measurement of the free radicals NO_3, BrO, IO, and OH in the troposphere, *Res. Chem. Intermed., 20,* 557-578, 1994.

Plumb, R.A., and M.K.W. Ko, Interrelationships between mixing ratios of long-lived stratospheric constituents, *J. Geophys. Res., 97*, 10145-10156, 1992.

Poppe, D., *et al.*, Comparison of measured OH concentrations with model calculations, *J. Geophys. Res., 99,* 16633-16642, 1994.

Poulida, O., *et al.*, Trace gas concentrations and meteorology in rural Virginia 1. Ozone and carbon monoxide, *J. Geophys. Res., 96*, 22461-22475, 1991.

Poulida, O., *Observations and Photochemistry of Reactive Trace Gases in the Atmosphere,* Dissertation at the Faculty of the Graduate School of the University of Maryland, 1993.

Prather, M., R.G. Derwent, D.H. Ehhalt, P. Fraser, E. Sanhueza, and X. Zhou, Chapter 2: Other trace gases and atmospheric chemistry, *Radiative Forcing of Climate Change 1994,* Report to IPCC, Intergovernmental Panel on Climate Change, in preparation, 1994.

Price, J.D., and G. Vaughan, Statistical studies of cut-off low systems, *Annales Geophysicae, 10,* 96-102, 1992.

Price, J.D., and G. Vaughan, On the potential for stratosphere-troposphere exchange in cut-off low systems, *Quart. J. Roy. Met. Soc., 119*, 343-365, 1993.

Prospero, J.M., R. Schmitt, E. Cuevas, D. Savoie, W. Graustein, K. Turekian, A. Volz-Thomas, S. Oltmans, H. Levy, and A. Diaz, Temporal variability of ozone and aerosols in the free troposphere over the Eastern North Atlantic, submitted to *Nature*, 1993.

Pszenny, A.A.P., W.C. Keene, D.J. Jacob, S. Fan, J.R. Maben, M.P. Zetwo, M. Springer-Young, and J.N. Galloway, Evidence of inorganic gases other than hydrogen chloride in marine surface air, *Geophys. Res. Lett., 20*, 699-702, 1993.

Ridley, B.A., S. Madronich, R.B. Chatfield, J.G. Walega, R.E. Shetter, M.A. Carroll, and D.D. Montzka, Measurements and model simulations of the photostationary state during the Mauna Loa Observatory Photochemistry Experiment: Implications for radical concentrations and ozone production and loss rates, *J. Geophys. Res., 97*, 10375-10388, 1992.

Rosenlof, K.H., and J.R. Holton, Estimates of the stratospheric residual circulation using the downward control principle, *J. Geophys. Res., 98*, 10465-10480, 1993.

Rudolph, J., B. Vierkorn-Rudolph, and F.X. Meixner, Large-scale distribution of peroxyacetylnitrate. Results from the STRATOZ III flights, *J. Geophys. Res., 92*, 6653-6661, 1987.

Sandholm, S.T., *et al.*, Summertime tropospheric observations related to N_xO_y distributions and partitioning over Alaska: Arctic Boundary Layer Expedition 3A, *J. Geophys. Res., 97*, 16481-16509, 1992.

Sandroni, S., D. Anfossi, and S. Viarengo, Surface ozone levels at the end of the nineteenth century in South America, *J. Geophys. Res., 97*, 2535-2540, 1992.

Savoie, D.L., J.M. Prospero, S.J. Oltmans, W.C. Graustein, K.K. Turekian, J.T. Merrill, and H. Levy II, Sources of nitrate and ozone in the marine boundary layer of the tropical North Atlantic, *J. Geophys. Res., 97*, 11575-11589, 1992.

Scheel, H.E., E.G. Brunke, and W. Seiler, Trace gas measurements at the monitoring station Cape Point, South Africa, between 1978 and 1988, *J. Atmos. Chem., 11*, 197-210, 1990.

Scheel, H.E., R. Sladkovic, and W. Seiler, Ground-based measurements of ozone and related precursors at 47°N, 11°E, in *Proceedings EUROTRAC Symposium '92,* edited by P.M. Borrell *et al.*, SPB Academic Publ., The Hague, The Netherlands, 104-108, 1993.

Schmitt, R., B. Schreiber, and I. Levin, Effects of long-range transport on atmospheric trace constituents at the Baseline Station Tenerife (Canary Islands), *J. Atmos. Chem., 7*, 335-351, 1988.

Schmitt, R., and L. Hanson, Ozone in the free troposphere over the North Atlantic: Production and long-range transport, *EUROTRAC Annual Report Part 9 (TOR)*, 112-118, 1993.

Schnell, R.C., S.C. Liu, S.J. Oltmans, R.S. Stone, D.J. Hofmann, E.G. Dutton, T. Deshler, W.T. Sturges, J.W. Harder, S.D. Sewell, M. Trainer, and J.M. Harris, Decrease of summer tropospheric ozone concentrations in Antarctica, *Nature, 35*, 726-729, 1991.

Seila, R.L., W.A. Lonneman, M.E.R. Santoyo, and J.T. Ruiz, VOCs in Mexico City ambient air, in *Proceedings of the International Symposium on Measurement of Toxic and Related Air Pollutants,* Air and Waste Management Association, Pittsburgh, Pennsylvania, 616-621, 1993.

Seiler, W., and J. Fishman, The distribution of carbon monoxide and ozone in the free troposphere, *J. Geophys. Res., 86*, 7255-7265, 1981.

Shapiro, M.A., T. Hampel, and A.J. Krueger, The Arctic tropopause fold, *Mon. Wea. Rev., 115*, 444-454, 1987.

Sillman, S., J.A. Logan, and S.C. Wofsy, A regional scale model for ozone in the United States with subgrid representation of urban and power plant plumes, *J. Geophys. Res., 95*, 5731-5748, 1990.

Simmonds, P.G., Tropospheric ozone research and global atmospheric gases experiment, Mace Head, Ireland, *EUROTRAC Annual Report Part 9 (TOR)*, 234-242, 1993.

Singh, H.B., *et al.*, Atmospheric measurements of PAN and other organic nitrates at high latitudes: Possible sources and sinks, *J. Geophys. Res., 97*, 16511-16522, 1992.

Singh, H.B., *et al.*, Summertime distribution of PAN and other reactive nitrogen species in the northern high latitude atmosphere of eastern Canada, *J. Geophys. Res., 99*, 1821-1836, 1994.

Smit, H.G.J., D. Kley, S. McKeen, A. Volz, and S. Gilge, The latitudinal and vertical distribution of tropospheric ozone over the Atlantic Ocean in the Southern and Northern Hemispheres, in *Ozone in the Atmosphere*, Proceedings of the Quadrennial Ozone Symposium 1988 and Tropospheric Ozone Workshop, Göttingen, edited by R.D. Bojkov and P. Fabian, A. Deepak Publ., Hampton, Virginia, 419-422, 1989.

Smit, H.G.J., D. Kley, H. Loup, and W. Sträter, Distribution of ozone and water vapor obtained from soundings over Jülich: Transport versus chemistry, in *Proceedings EUROTRAC Symposium '92,* edited by P. Borrell *et al.*, SBP Academic Publ., The Hague, The Netherlands, 145-148, 1993.

Smit, H.G.J., and D. Kley, Vertical distribution of tropospheric ozone and its correlation with water vapour over the equatorial Pacific Ocean between 160E and 160W, *EOS 74 (43)*, 115, 1993.

Staehelin, J., J. Thudium, R. Buehler, A. Volz-Thomas, and W. Graber, Trends in surface ozone concentrations at Arosa (Switzerland), *Atmos. Environ., 28*, 75-87, 1994.

Tang, X.Y., Air quality measurements in the People's Republic of China, MILOX (Mid-Latitude Ecosystems and Photochemical Oxidants) Committee Meeting, Atlanta, Georgia, September, 1993.

Thompson, A.M., and R.J. Cicerone, Possible perturbations to atmospheric CO, CH_4, and OH, *J. Geophys. Res., 91*, 10853-10864, 1986.

Thompson, A.M., New ozone hole phenomenon, *Nature, 352*, 282-283, 1991.

Thompson, A. M., *et al.*, Ozone observations and a model of the marine boundary layer photochemistry during SAGA 3, *J. Geophys. Res., 98*, 16955-16968, 1993.

Thompson, A.M., K.E. Pickering, R.R. Dickerson, W.G. Ellis, Jr., D.J. Jacob, J.R. Scala, W.-K. Tao, D.P. McNamara, and J. Simpson, Convective transport over the central United States and its role in regional CO and ozone budgets, *J. Geophys. Res., 99,* 18703-18711, 1994.

Thorncroft, C.D., B.J. Hoskins, and M.E. McIntyre, Two paradigms of baroclinic-wave life-cycle behaviour, *Quart. J. Roy. Met. Soc., 119*, 17-55, 1993.

Trainer, M., E.T. Williams, D.D. Parrish, M.P. Buhr, E.J. Allwine, H.H. Westberg, F.C. Fehsenfeld, and S.C. Liu, Models and observations of the impact of natural hydrocarbons in rural ozone, *Nature, 329*, 705-707, 1987.

Trainer, M., M.P. Buhr, C.M. Curran, F.C. Fehsenfeld, E.Y. Hsie, S.C. Liu, R.B. Norton, D.D. Parrish, E.J. Williams, B.W. Gandrud, B.A. Ridley, J.D. Shetter, E.J. Allwine, and H.H. Westberg, Observations and modeling of the reactive nitrogen photochemistry at a rural site, *J. Geophys. Res., 96*, 3045-3063, 1991.

Trainer, M., *et al.*, Correlation of ozone with NO_y in photochemically aged air, *J. Geophys. Res., 98*, 2917-2925, 1993.

Volz, A., and D. Kley, Evaluation of the Montsouris series of ozone measurements made in the nineteenth century, *Nature, 332*, 240, 1988.

Volz, A., *et al.*, Ozone production in the Black Forest: Direct measurements of RO_2, NO_x, and other relevant parameters, in *Tropospheric Ozone—Regional and Global Scale Interactions*, edited by I.S.A. Isaksen, *NATO ASI Series C. Vol. 227*, D. Reidel Publ., Dordrecht, The Netherlands, 293-302, 1988.

Volz-Thomas, A., Trends in photo-oxidant concentrations, in *Proceedings EUROTRAC Symposium '92,* edited by P.M. Borrell *et al.*, SPB Academic Publ., The Hague, The Netherlands, 59-64, 1993.

CHAPTER 6

Model Simulations of Stratospheric Ozone

Author:
M.K.W. Ko

Co-authors:
A. Ibrahim
I. Isaksen
C. Jackman
F. Lefèvre
M. Prather
P. Rasch
R. Toumi
G. Visconti

Contributors:
S. Bekki
G. Brasseur
C. Brühl
P. Connell
D. Considine
P.J. Crutzen
E. Fleming
J. Gross
L. Hunt
D. Kinnison
S. Palermi
Th. Peter
G. Pitari
K. Sage
T. Sasaki
X. Tie
D. Weisenstein
D.J. Wuebbles

CHAPTER 6

MODEL SIMULATIONS OF STRATOSPHERIC OZONE

Contents

SUMMARY

Model Simulations of Stratospheric Ozone

- Multi-dimensional models are designed to provide simulations of the large-scale transport in the stratosphere. This transport rate is combined with the local chemical production and removal rates of ozone to determine the distribution of ozone as a function of longitude, latitude, height, and season.

- There is strong observational evidence that heterogeneous chemistry (hydrolysis of N_2O_5 and $ClONO_2$) is operating on surfaces of the aerosol particles in the stratospheric sulfate layer. There is a general agreement on how this should be represented in the models. Models that include these reactions produce calculated ozone decreases (between 1980 and 1990) that are larger and in better agreement with the observed trend than those produced by models that include only gas-phase reactions. All model simulations reported here include these two reactions.

- Both three-dimensional and two-dimensional models have been used in simulating polar stratospheric cloud (PSC) chemistry in the vortex and how the equatorward transport of chemically perturbed polar air may affect ozone at midlatitudes. Our lack of understanding of the detailed mechanisms for denitrification, dehydration, and transport processes reduces our confidence in these model predictions.

- No multi-year simulation has been performed to date using three-dimensional models. Two-dimensional (latitude-altitude) models remain the primary tools for extensive diagnostic studies and multi-year simulations.

How well do models simulate the distributions and trends of ozone in the stratosphere?

Upper stratosphere

- The model-simulated ozone concentration in the upper stratosphere is typically 20% smaller than the observed values, a problem that has been identified previously. This suggests that there is a problem with our understanding of the photochemistry in that region.

- The model-calculated ozone trends above 25 km due to emission of halocarbons between 1980 and 1990 are in reasonable agreement with the trends (both in the altitude profile and latitudinal variation) derived from the satellite measurements. Most of the model results did not consider radiative feedback and temperature trends that are likely to reduce the predicted ozone decreases by about a factor of 0.8.

Lower stratosphere

- The models underestimate the amount of ozone in the lower stratosphere at high latitudes during winter and spring. This, coupled with the model-calculated behaviors of other trace gases, indicates that the models do not have a good representation of the transport processes in those seasons.

- The partitioning of the radical species in the lower stratosphere is influenced to a large extent by the hydrolysis rates of N_2O_5 and $ClONO_2$. This, in turn, affects the calculated ozone response in the lower stratosphere to increases in chlorine and bromine. The trend in the polar region is also affected by PSC chemistry in the vortex as well as heterogeneous conversion of HCl on sulfate particles at cold temperatures.

- Comparison with the local trend derived from observations indicates that models that include only hydrolysis of N_2O_5 and $ClONO_2$ on sulfate particles underestimate the trend between 15 and 20 km at all latitudes. Including PSC processing and the heterogeneous conversion of hydrochloric acid (HCl) on cold sulfate aerosol in model simulations gives larger trends at high latitudes.

STRATOSPHERIC MODELS

COLUMN ABUNDANCE

- The model-simulated ozone columns in the tropics are within 10% of the observed values. However, some models underestimate the spring maximum in the Northern Hemisphere by as much as 30%.

- The models calculate a trend in the tropics of about -1% per decade in the column abundance of ozone due to emissions of halocarbons between 1980 and 1990. This is consistent with the trend derived from the Dobson stations, the Solar Backscatter Ultraviolet (SBUV) instrument, and the Total Ozone Mapping Spectrometer (TOMS). The model-calculated trend in the tropics is largely a result of the calculated ozone decrease above 25 km.

- The decreases in column ozone at high latitudes calculated by models that include hydrolysis of N_2O_5 and $ClONO_2$ as the only heterogeneous reactions are between 2% to 3% per decade. This is smaller than the observed negative trends of 4%-8% per decade at the northern high latitudes, and 8%-14% at southern high latitudes outside the vortex.

- Models with PSC chemistry calculate a trend at high latitudes comparable to observation. However, the trend at midlatitudes is still small compared to the observed decrease of 4%-6% during winter and spring (Northern Hemisphere) and winter and summer (Southern Hemisphere).

- A larger trend can be obtained at midlatitudes by including the effects from export of chemically perturbed air from the polar region, by adjusting the transport, or by invoking additional chemical ozone removal cycles. The importance of the processes has not been resolved because of the lack of laboratory and field data.

- The increase in aerosol loading due to the eruption of Mt. Pinatubo was predicted to perturb the lower stratosphere. An idealized simulation was designed to isolate the effect of the photochemical response to a uniform thirty-fold increase in aerosol loading starting in June that decays with a time constant of 1 year. The model-calculated decreases range from 2% to 8% around 50°N in the spring after the prescribed increase, with the calculated decrease diminishing to zero over a five-year period.

Model Predictions of Future Trends

- Using an emission scenario that is designed to represent global compliance with the international agreements, the calculated chlorine loading in the stratosphere reaches its maximum value about 3-5 years after the prescribed tropospheric organic chlorine concentration achieves its maximum value. The maximum calculated chlorine and bromine concentrations and the lowest ozone values occur within 2 years of each other in this scenario.

- Comparison of the model results indicates that although there are significant differences among the model-calculated local photochemical rates and transport rates, the rates from each individual model combine to produce reasonable present-day ozone distributions and the 1980 to 1990 ozone trend. However, as the atmosphere is perturbed farther away from its present state (*e.g.*, large increase in aerosol loading, changes due to long-term trends of N_2O, CH_4, and halocarbons), the model-predicted responses differ by larger amounts. Current efforts aimed at direct validation of the transport process and photochemical process will help to resolve the differences and bolster our confidence in the model predictions.

6.1 INTRODUCTION

Ozone concentrations in the atmosphere are maintained by the balance between photochemical production (mainly the photolysis of O_2) and removal by photochemical reactions associated with the hydrogen (HO_x), nitrogen (NO_x), chlorine (ClO_x), and bromine (BrO_x) radicals. However, this balance is not always local because an ozone molecule created at one location can be transported to another location before it is photochemically destroyed. Ozone concentration in the lower stratosphere is maintained by a balance among the following processes: production in the tropics, transport to mid- and high latitudes, photochemical removal in the mid- and high latitudes, and removal from the stratosphere by stratosphere/troposphere (strat/trop) exchange. The magnitude of each term changes with seasons and their combined value determines the seasonal behavior of ozone. In the tropical upper stratosphere (above 30 km between 30°N and 30°S), the photochemical reactions are sufficiently fast that local balance holds and the local ozone concentration is determined by the local production and removal rates. However, transport still affects ozone indirectly by modulating the concentrations of the radical species.

The role of the radical species in the removal of ozone has been confirmed by process studies using *in situ* observations. The concentrations of the radical species are maintained by photodegradation of the corresponding source gases: H_2O and methane (CH_4) for HO_x, nitrous oxide (N_2O) for NO_x, and halogen source gases for ClO_x and BrO_x. The large-scale circulation that transports ozone is also responsible for the redistribution of source gases, radicals, and other trace gases that can affect the partitioning of the radical species. Increases in radical concentrations (*e.g.*, increases in ClO_x due to chlorofluorocarbons (CFCs) emitted at the Earth's surface, and increases in NO_x due to N_2O emitted at the ground and stratospheric injection of NO_x by aircraft) lead to changes in ozone.

In this chapter, we discuss modeling of the seasonal behavior of ozone in the stratosphere using multi-dimensional models. The amount of ozone in the atmosphere may be separated into three layers according to the processes controlling the concentrations: 1000 mb (ground) to 100 mb (16 km) in the tropics and 200 mb (11 km) in the extra tropics; from the first layer to 10 mb (30 km); and 10 mb to 1 mb (45 km) (see, *e.g.*, Jackman *et al.*, 1989). Ninety percent of the ozone resides in the upper two layers, with more than two-thirds in the middle layer. Although the models include a simple version of the troposphere, representation of many of the processes is incomplete (see Chapter 5 and Chapter 7 in this report for discussions of ozone in the troposphere). In the upper layer, where ozone is controlled by local production and removal, the ozone concentration can be simulated by box models if the concentrations of the radical species and overlying ozone column are known. The middle layer has received the most attention for several reasons. It is where the aerosol layer and the polar stratospheric clouds reside. The observations from the various aircraft campaigns and satellite observations (see Chapters 3 and 4, this report) have provided a wealth of data for studying this middle layer.

Because of limitations in computer resources, it is not practical to use three-dimensional models to perform multi-year simulations to study the response of stratospheric ozone to perturbations of the source gases and the radical species. These calculations have been done using two-dimensional (latitude-altitude) zonal-mean models. They incorporate processes that have been proven to be important. The same models are used to compute the atmospheric lifetimes of various trace gases (see Kaye *et al.*, 1994) and the ozone depletion potential indices for the halocarbons (see Chapter 13). While questions can be raised regarding some aspects of the formulation and representation of the processes in two-dimensional (2-D) models, model results from individual models that appeared in the literature are found to be in reasonable agreement with the present-day atmosphere (within 20% of the observed ozone column away from the polar region).

This chapter reviews the recent improvements in model formulation and discusses the strengths and weaknesses of these models. An open letter was sent to modeling groups to solicit results for a number of prescribed calculations. Different models have reported the results of their calculations in the scientific literature. More often than not, the results are not in agreement with each other. The purpose of the prescribed calculations is to ask each model to do the same calculations with the same input so that the model results can be compared. For this reason, the criterion for choosing the prescribed conditions is that they can be easily imple-

Table 6-1. Models providing results in this chapter.

Model Name	Institution	Investigators
AER	Atmospheric and Environmental Research Inc., USA	M. Ko and D. Weisenstein
CAMBRIDGE	University of Cambridge, United Kingdom	S. Bekki
GSFC	NASA Goddard Space Flight Center, USA	C. Jackman, D. Considine, E. Fleming
ITALY	Universita degli Studi L'Aquila, Italy	G. Pitari, S. Palermi, G. Visconti
LLNL	Lawrence Livermore Laboratory, USA	D. Kinnison, P. Connell
MPIC	Max Planck Institute for Chemistry, Germany	C. Brühl, J. Gross, P.J. Crutzen, Th. Peter
MRI	Meteorological Research Institute, Japan	T. Sasaki
NCAR	National Center for Atmospheric Research, USA	G. Brasseur, X. Tie
OSLO	University of Oslo, Norway	I. Isaksen

mented, rather than being faithful to what actually occurs in the atmosphere. For these calculations, it is more meaningful for the model results to be compared with each other rather than with observations. Clearly, comparison with observation still remains as the only real test on the reliability of model results.

Modeling groups that submitted results are listed in Table 6-1. They are all 2-D models. Most of these models (with the exception of the CAMBRIDGE model) have participated in one or more of the intercomparison exercises, the latest of which took place in 1991 and 1992 (see Prather and Remsberg, 1993). This intercomparison involved 14 different groups from 6 countries. The intercomparison was comprehensive and included: 1) source, radical, and reservoir gases important in ozone photochemistry; 2) radioactive tracers ^{14}C and ^{90}Sr and the Mt. Ruiz volcanic cloud, which tested the models' transport; and 3) a detailed model intercomparison of photodissociation rates, transport fluxes, and idealized tracers that highlighted some of the models' similarities and differences. One result of these exercises was to help eliminate simple coding errors in the models and give more confidence that the range of predictions is due to differences in formulations and approaches. The remaining differences will ultimately have to be resolved by comparison with observations. The results from these calculations will show that there are substantial differences among the model predictions, particularly when perturbations are large. Unfortunately, the schedule of this report does not allow enough time to resolve all the issues. It is hoped that this will be done soon.

6.2 COMPONENTS IN A MODEL SIMULATION

This section discusses how the models simulate the distributions of the source gases, the partitioning of the radical species, and the distribution of ozone in the stratosphere. To simulate the distribution of ozone, the models calculate the local production and removal rates for ozone, and combine them with the effect of transport to determine the ozone concentration as a function of longitude, latitude, altitude, and season. The local production and removal rates depend on the model-computed distributions of the source gases and the radical species, and the partitioning of the radicals (which in turn depends on the local temperature and solar insolation). One thing to note is that the photochemical removal rate for ozone in most of the lower stratosphere is about 10% per month in summer and 1% per month in winter. Thus, it is always necessary to consider the effect of transport and the combined cumulative effect over several years to assess the ozone response. This is to be contrasted with situations where activation of the chlorine radicals in the polar vortex leads to a rapid ozone removal rate of 1% per day.

6.2.1 Source Gases and Radical Species

The models simulate the following processes in the life cycle of a source gas released in the troposphere: the cycling of the source gas between the troposphere and the stratosphere via strat/trop exchange; the photochemical reactions that release the radical species; the subsequent redistribution of the radical species by the large-scale transport; and the partitioning of the radical species into the active and reservoir species. A molecule in the stratosphere can either be photochemically removed, or it will spend, on average, about three years before it is transported back to the troposphere (see *e.g.*, Holton, 1990). The three-year residence time corresponds to the average for all material in the stratosphere. Clearly, material introduced to the stratosphere near the tropopause will have a much shorter residence time. The exchange between the troposphere and stratosphere is simulated in the models in terms of the large-scale advection and eddy transport. This is probably adequate for source gases such as N_2O and the CFCs, and the radical families Cl_y, Br_y, and NO_y, whose distributions are relatively uniform. A more sophisticated treatment is needed for cases involving direct injection of radical species, such as injection of chlorine radicals by the space shuttle solid rocket engine and injection of NO_x by high-flying aircraft.

6.2.1.1 Halogen Species

The odd chlorine (Cl_y) and bromine (Br_y) species in the stratosphere come from degradation of the source gases. Among the source gases that have been measured in the atmosphere, the atmospheric burdens of methyl chloride (CH_3Cl), methyl bromide (CH_3Br), and other bromomethanes are thought to be maintained, in part, by natural sources. Other man-made sources include the chlorofluorocarbons (CFCs), the hydrochlorofluorocarbons (HCFCs), the bromomethanes (mainly methyl bromide), and the halons in the stratosphere. Photodegradation of the CFCs takes place almost exclusively in the stratosphere. The hydrogenated halogen species can be broken down by photochemical reactions in both the troposphere and stratosphere. The Cl_y and Br_y species released in the troposphere will be washed out relatively quickly and will not be transported to the stratosphere. Thus, source gases that react in the troposphere will deliver less of their chlorine or bromine to the stratosphere. The radical species released in the stratosphere are redistributed in the stratosphere and eventually removed from the stratosphere by the large-scale transport that parameterizes strat/trop exchange in the models. While in the stratosphere, they will be partitioned into the active species (Cl, ClO, Cl_2O_2, BrO) and the reservoir species (HCl, $ClONO_2$, HOCl, HBr, $BrONO_2$, HOBr). The active species participate directly in the ozone removal cycles. Observed concentrations of the reservoir species provide an important check for the model results.

Model calculations have been used to simulate the distribution of the chlorine radicals released by specific source gases in the present-day stratosphere (see Weisenstein *et al.*, 1992). This can be used to estimate the individual contribution of a specific source gas to chlorine loading and ozone depletion. A similar breakdown can also be obtained using observed concentrations of the source gases in the lower stratosphere (Kawa *et al.*, 1992; Woodbridge *et al.*, 1994).

Two other sources for chlorine radicals were discussed in Chapter 2. These are deposition of chlorine by solid-fuel rockets and injection of HCl into the stratosphere by violent volcanic eruptions. These sources are not included in the model simulations. The estimated input of 0.7 kiloton (Cl)/yr from solid-fuel rockets is small compared to the annual input of 300 kiloton (Cl)/yr from the current inventory of organic halocarbons in the atmosphere (Prather *et al.*, 1990a). Theoretical calculations discussed in Chapter 3 show that HCl will be scavenged in the volcanic plume (Tabazadeh and Turco, 1993). This, together with the lack of observed increase in HCl after eruptions (Wallace and Livingston, 1992; Mankin *et al.*, 1992), supports the conclusion that volcanic eruptions contribute little to stratospheric chlorine.

6.2.1.2 The Odd Nitrogen Species

The odd nitrogen species are introduced into the stratosphere by several sources. The major natural source of NO_y is from the reaction of N_2O with $O(^1D)$, producing two NO molecules (Crutzen, 1970; McElroy and McConnell, 1971). This is why changes in concentration of N_2O will affect the concentration of NO_y radicals and ozone. Reaction of N_2O with excited O_2 molecules has been suggested as a possible source (Toumi, 1993) but cannot be quantified because of lack of rate data. Other suggested continuous natural sources

Table 6-2. Comparison of sources and sinks for odd nitrogen species in the stratosphere.

SOURCES	Magnitude (kiloton(N)/yr)
Nitrous oxide oxidation $N_2O + O(^1D) \rightarrow 2NO$	600
Transport of NO_x produced by lightning in the troposphere	250
Galactic cosmic rays (solar minimum) (solar maximum)	86 63
Solar proton events (1972, solar maximum) (1975, solar minimum)	35 0.01
Input from mesosphere and thermosphere, relativistic electron precipitations, meteors	?
Nuclear explosions (1961 & 1962 nuclear tests)	550
Stratospheric-flying aircraft	depends on emission index, fleet size, and flight paths
Rocket launches	?
SINKS	
Reforming of molecular nitrogen $N + NO \rightarrow N_2 + O$	195
Rainout of HNO_3 transported to the troposphere	750

of stratospheric NO_y that have a regional impact are galactic cosmic rays for the polar lower stratosphere (Warneck, 1972; Nicolet, 1975; Legrand *et al.,* 1989), lightning for the lower equatorial stratosphere (Noxon, 1976; Tuck, 1976; Liu *et al.,* 1983; Ko *et al.,* 1986; Kotamarthi *et al.,* 1994), and the downward flux of odd nitrogen from the thermosphere (Strobel, 1971; McConnell and McElroy, 1973) especially in the polar region during winter (Solomon *et al.,* 1982; Garcia *et al.,* 1984; Russell *et al.,* 1984). Sporadic natural sources of stratospheric NO_x include meteors (Park and Menees, 1978), solar proton events (Zadorozhny *et al.,* 1992; Jackman, 1993), and precipitation by relativistic electrons (Callis *et al.,* 1991). The frequency and magnitude of these sporadic sources are not well quantified. Most models include the lightning source in addition to N_2O oxidation, but ignore other sources. Mankind also influences stratospheric NO_x production through atmospheric nuclear explosions (Johnston *et al.,* 1973; Foley and Ruderman, 1973), rocket launches (Karol *et al.,* 1992; Chapter 10 in WMO, 1992), and high-flying aircraft (CIAP, 1975; Albritton *et al.,* 1993).

The odd nitrogen species introduced into the stratosphere are redistributed by the large-scale transport. They are partitioned into N, NO, NO_2, NO_3, N_2O_5, HNO_3, HNO_4, $ClONO_2$, and $BrONO_2$. The active species ($NO_x = NO + NO_2$) are important in ozone control. Besides reacting with ozone, the NO_x constituents are also important in interference reactions with other families (HO_x, Cl_x, Br_x) involved in ozone regulation through reactions with OH (forming HNO_3), with ClO (forming $ClONO_2$), and with BrO (forming $BrONO_2$).

Photochemical removal occurs in the upper part of the stratosphere via the reaction of N with NO forming N_2. The rest of the production is balanced by transport removal. Table 6-2 (from Jackman *et al.,* 1980, 1990; Prather *et al.,* 1992) shows a comparison of the magnitude of some of these suggested sources and sinks of odd nitrogen. Nitrous oxide oxidation is believed to be the largest source, with lightning also contributing substantially in the lower equatorial stratosphere. The transport to the troposphere is thought to be the largest sink, with the reforming of N_2 also contributing significantly.

6.2.1.3 The HO_x Species

The HO_x species are produced from the reaction of $O(^1D)$ with H_2O and CH_4. Reaction of excited O_2 molecules with H_2 has been suggested as a source (Toumi, 1993) but cannot be quantified because of lack of rate

data. The reaction $N_2O_5 + H_2O \rightarrow 2HNO_3$ occurs on the surfaces of the aerosol particles. After the HNO_3 molecules are released to the atmosphere, they can either react with OH or be photolyzed to produce OH and NO_2. Thus, depending on the fate of the HNO_3 molecules, the reaction can be a source of OH. Model calculations show that there is a net increase in OH when the reaction is included (see discussion in Rodriguez *et al.*, 1991). Removal of the HO_x species in the stratosphere is dominated by reaction of OH with HO_2, HNO_3, HNO_4, and HCl. The species OH and HO_2 participate in the ozone removal reactions and modulate the partitioning of the NO_y, Cl_y, and Br_y species.

The H_2O concentration in the stratosphere is maintained by oxidation of CH_4 and import of H_2O from the troposphere. The exchange of H_2O across the tropopause is not well understood. Some models (ITALY, LLNL, MPIC, MRI, NCAR) parameterized this by imposing a boundary condition along the tropopause. Other models (AER and GSFC) keep the stratospheric H_2O concentration fixed at observed values (see section B in Prather and Remsberg, 1993) and make adjustments for future changes from CH_4 increase and from engine emissions of stratospheric aircraft.

6.2.2 Heterogeneous Reactions and Partitioning of the Radical Species

Studies of the Antarctic ozone hole pointed to the importance of heterogeneous reactions in affecting ozone in the lower stratosphere. These early modeling studies, laboratory experiments, and field measurements were summarized in a review paper by Solomon (1990). Subsequent studies were reviewed in WMO (1992). Chapters 3 and 4 presented more recent evidence that shows that heterogeneous reactions do occur on particles in the atmosphere at rates that are consistent with rate constants determined in the laboratory. These reactions are

$$N_2O_5 + H_2O(\text{on particles}) \rightarrow 2HNO_3 \quad (6\text{-}1)$$

$$ClONO_2 + H_2O(\text{on particles}) \rightarrow HOCl + HNO_3 \quad (6\text{-}2)$$

$$ClONO_2 + HCl(\text{on particles}) \rightarrow Cl_2 + HNO_3 \quad (6\text{-}3)$$

$$N_2O_5 + HCl(\text{on particles}) \rightarrow HNO_3 + ClNO_2 \quad (6\text{-}4)$$

$$HOCl + HCl(\text{on particles}) \rightarrow Cl_2 + H_2O \quad (6\text{-}5)$$

In each reaction, a gas molecule (*e.g.*, N_2O_5) is assumed to collide with a particle and proceed to react with another molecule (H_2O or HCl) already on the particle. As discussed in Chapter 3, these reactions occur on liquid or frozen sulfate particles and on polar stratospheric clouds (PSCs) at different rates. The effectiveness of each reaction in altering the partitioning of the radical species depends on how fast the heterogeneous conversion rate is compared to the gas-phase reactions that control the partitioning in specific regions of the atmosphere. Because HCl is much more soluble on PSCs, reactions (6-3) through (6-5) are more effective on PSCs than on liquid sulfate particles. A common effect of the first four reactions is to decrease the NO_x/NO_y ratio, with the net effect of reducing the ozone destruction due to the NO_x loss cycle. At the same time, the reduction in NO_x also inhibits the formation of $ClONO_2$, leaving more of the active chlorine in the form of ClO, and increases the ClO_x removal of ozone. The additional HNO_3 produced in the reaction also increases OH and the removal of ozone due to the HO_x cycle. The last three reactions involve direct activation of chlorine species by converting HCl to active chlorine. The inclusion of these reactions in the models has brought the model results in closer agreement with observations (see Chapters 3 and 4).

The information on the reaction rate constants indicates that reaction (6-1) has the dominant effect at normal stratospheric temperatures at midlatitudes (see discussion in Hanson *et al.*, 1994). Reaction (6-1) reduces the efficiency of the NO_x cycle, while both the HO_x and ClO_x cycles are enhanced. As a result, the HO_x cycle is the dominant ozone removal cycle in the lower stratosphere. This has been confirmed using direct observations of OH and HO_2 in the lower stratosphere (Wennberg *et al.*, 1994). The net effect on the local removal rate of ozone is small for normal aerosol loading, so that the present-day ozone abundances calculated with and without heterogeneous chemistry are within 10% of each other (Rodriguez *et al.*, 1991; Weisenstein *et al.*, 1991, 1993; McElroy *et al.* 1992). However, these same reactions make the model-calculated ozone more sensitive to increases in chlorine and less sensitive to added nitrogen-containing radicals.

Reaction (6-2) has a more noticeable impact on the partitioning of the radical species for temperatures less than 200 K and/or under enhanced aerosol loading

(Hanson *et al.*, 1994). Indirect evidence for this reaction was reported in Solomon *et al.* (1993) and Sanders *et al.* (1993), who detected enhanced OClO in the Antarctic, consistent with $ClONO_2$ hydrolysis on Mt. Pinatubo aerosols before the onset of PSCs. The effect of reactions (6-3) through (6-5) appears to be limited to ice surfaces, but could be important on sulfate particles at high latitudes under very cold temperatures (Hanson *et al.*, 1994). We discuss below how models attempt to simulate the effects of these reactions.

6.2.2.1 Heterogeneous Chemistry on the Sulfate Layer

Reactions (6-1) and (6-2) proceed on liquid sulfate aerosol particles that are present in the global sulfate layer throughout the lower stratosphere. Molina *et al.* (1993) reported experimental results that show that if the temperature is below 200 K, the activation may also take place on solid H_2SO_4 hydrates. The rates of the reactions depend on the surface area density and the water content of the aerosol, and possibly the phase of the aerosol particle. In the models, a first-order reaction rate constant is defined for each reaction as the product of the collision frequency of the gas-phase reactant with the aerosol particles in the sulfate layer and the sticking coefficient (γ), which is the reaction probability per collision. The collision frequency depends on the surface area density of the sulfate particles. The effect of the varying water content and phase of the aerosol is parameterized in the models by defining an effective γ in terms of the local temperature and concentration of water vapor. However, there is observational evidence that indicates that the phase of the aerosol particles may also depend on the history of the particles, and not just on local conditions. A final assumption made in the models is that the products of the reaction are released to the atmosphere. Thus, there is no sequestering of the reaction products.

Most model studies have assumed a γ value of 0.1 for reaction (6-1). Recent results reported by Fried *et al.* (1994) indicate that γ for (6-1) may vary between 0.077 to 0.15 at 230 K for H_2SO_4 weight percent between 64% to 81%. The extrapolated rate in the atmosphere based on their semi-empirical model ranges from 0.03 to 0.15. Other studies (Tolbert *et al.*, 1993; Fried *et al.*, 1994) discussed whether uptake of formaldehyde may change the composition of the aerosol and affect the γ values. The effect of such variation for reaction (6-1) has not been explored.

Hanson *et al.* (1994) recommended the following expression for γ for reaction (6-2) :

$$\gamma(ClONO_2 + H_2O) = 10^{(1.86-0.0747W)}$$

where W is the weight percent of acid, defined as

$$W = \frac{T(0.6246Z-14.458) + 3565}{T(-0.19988) + 1.3204Z + 44.777}$$

with Z = ln (partial pressure H_2O (mb)), T is the temperature in K. Hanson *et al.* (1994) also provided parameters for reactions (6-3) and (6-5). They concluded from their model calculation that the reactions should be included in simulating the ozone behavior at high latitude winter under enhanced aerosol conditions. The calculations in this chapter include reactions (6-1) and (6-2) as the only heterogeneous reactions on sulfate particles.

There are additional problems specific to simulating the effects of these reactions in a 2-D zonal-mean model. The model results presented in this chapter use a prescribed zonal-mean aerosol surface density specified as a function of altitude and latitude (Chapter 8, WMO, 1992) derived from the Stratospheric Aerosol and Gas Experiment (SAGE) observations. If we assume that the surface area density is constant in the zonal direction, a constant value for γ in (6-1) would mean that the conversion rate can be represented reasonably well as a zonal-mean rate. On the other hand, the parameterization for reaction (6-2) depends on local temperature and partial pressure of H_2O. As the dependence on these zonally varying quantities become more nonlinear, simulating the effect of the conversion as a zonal-mean quantity becomes more problematic (Murphy and Ravishankara, 1994; Considine *et al.*, 1994). The effects of longitudinal temperature fluctuation on the zonal-mean rate of reaction (6-2) has been studied by Pitari (1993a). The conversion rate experienced by an air parcel following the actual trajectory in the polar vortex was found to be as much as a factor of 10 larger than the rate calculated using the zonal-mean temperature.

6.2.2.2 Heterogeneous Chemistry on PSCs

Modeling the effects of polar stratospheric clouds (PSCs) involves two steps. The model must simulate the removal of H_2O and HNO_3 vapor when the particles are

formed, and the effects of heterogeneous conversions that occur on the surfaces. Inside the polar vortex, the conversion rates due to PSC chemistry are so fast that the amount converted is limited by the availability of the reactants (N_2O_5, $ClONO_2$, HOCl, HCl) once the particles are formed. As a result, the calculated repartitioning depends less on the details of how the reactions are parameterized.

Early 2-D model studies of the effects of polar heterogeneous processes parameterized the heterogeneous reactions as first-order conversion rates for the gas-phase reactants triggered by location and season (Chipperfield and Pyle, 1988; Isaksen *et al.,* 1990) or by the zonal-mean temperature falling below a threshold value (Granier and Brasseur, 1992). In the latter case, the threshold zonal mean temperature was picked to give a reasonable PSC frequency of occurrence. Denitrification was included in Isaksen *et al.* (1990) by ad hoc removal of 50% of the HNO_3 in the PSC regions. Granier and Brasseur (1992) included denitrification and dehydration for Type II PSCs by introducing a first-order removal rate for H_2O and HNO_3 with a time constant of 5 days when the zonal-mean temperature falls below the threshold value. Denitrification was included for Type I PSCs using a first-order removal rate for HNO_3 with a time constant of 30 days. To obtain the surface area density, a log-normal size distribution was assumed. In the 3-D model studies of Chipperfield *et al.* (1993) and Lefèvre *et al.* (1994), the amounts of H_2O, and HNO_3 condensed to form Type I and Type II PSCs were calculated assuming thermodynamic equilibrium using the local model temperature, H_2O, and HNO_3 concentrations. The surface area densities were calculated assuming that the particles have radii of 1 μm and 10 μm for Type I and Type II PSCs, respectively. Sedimentation was included for Type II particles in the transport of the condensed material. Pitari *et al.* (1993) developed a code in their 2-D model in which PSC occurrence and surface area were calculated rather than prescribed. They used a tracer continuity equation for condensed material with a production term that included terms parameterizing condensation, coagulation, sedimentation, and rainout. Different treatments for the uptake of HCl were used in the models. Pitari *et al.* (1993) ignored the uptake of HCl. Chipperfield *et al.* (1993) and Lefèvre *et al.* (1994) assumed that HCl is incorporated in the PSCs using the mole fractions given by Hanson and Mauersberger (1988). In all cases, it is assumed that the reaction rate can be represented by an effective γ.

Modeling such processes on PSCs in 2-D models presents special challenges. First, the motions of air-parcels are typically not zonally symmetric. The effectiveness of reactions (6-3) through (6-5) depends on the availability of sunlight to photolyze Cl_2 and $ClONO_2$ to form Cl and ClO. It is not clear whether a full air-trajectory calculation is needed to take into account the solar insolation experienced by the air parcel, or whether the situation can be approximated by an average exposure to PSCs over several trips around the globe. The problems will likely be most severe at the beginning and end of the polar winters, especially in the Arctic, which experiences large temperature fluctuations and azonal motions throughout the winter. The Southern Hemisphere vortex in the depth of the winter is more uniformly cold and zonally symmetric. Secondly, it is not clear that using the zonal-mean temperature alone can capture the complexity of the different temperatures experienced by an air parcel. Peter *et al.* (1991) developed a way to use climatological temperature statistics to derive probabilities for PSC formation as a function of latitude and altitude for both Type I and Type II PSCs. This formed the basis of methods that other studies used to predict surface area densities without relying solely on zonal mean temperatures (Pitari *et al.,* 1993; Grooss *et al.,* 1994; Considine *et al.,* 1994).

6.2.3 Transport and Ozone

If ozone is calculated assuming local photochemical equilibrium (*i.e.,* local production balanced by local removal), the calculated column abundance will have its maximum value of 700 Dobson units (DU) in the tropics, decreasing to about 200 DU in the summer high latitudes. The observed behavior of the column abundance of ozone (minimum at the tropics and maximum at high latitude) is a good indication that transport plays an important role in redistributing ozone from the production region in the tropics to high latitudes.

Transport of trace gases in three-dimensional chemistry-transport models (CTMs) is based on either three-dimensional winds from general circulation models (GCMs) or data-assimilated winds derived from observations. Because of the limitation in computational resources, it is not yet practical for 3-D CTMs to

predict evolution of chemical species over time periods much longer than a few years. The same limitation also precludes incorporating full chemistry into a GCM to calculate ozone and winds interactively. Thus, the GCM winds are calculated using prescribed ozone based on observation.

In 2-D models, transport is represented by advection from the zonal-mean velocities and eddy mixing coefficients. Most models used prescribed velocity and eddy coefficients with seasonal variations. The same circulation and temperature are used year after year to simulate the climatological mean state. However, previous studies (Tung and Yang, 1988; Schneider *et al.*, 1991; Jackman *et al.*, 1991; Yang *et al.*, 1991) have shown that the observed interannual variations in temperature would induce corresponding variations in the transport circulation leading to changes in ozone of about 3% to 4%. Variations in the circulation can also come from the quasi-biennial oscillation (QBO) in the equatorial winds. Gray and Pyle (1989) and Gray and Dunkerton (1990) produced a QBO in ozone in their 2-D model with interactive dynamics by parameterizing the QBO in the equatorial winds through specification of damping of waves. In Gray and Ruth (1993), a QBO in the equatorial winds was introduced into the model by relaxing the model winds toward the monthly mean observed winds. The calculated ozone QBO showed anomalies of ±6 Dobson units (±3%) at the tropics and ±12 DU (±2%) at midlatitudes. The broad patterns were shown to be in agreement with the anomalies derived from TOMS (Lait *et al.*, 1989), although the amplitude was larger in the model.

6.2.3.1 Relation to Observation

Most applications of 3-D CTMs are formulated as initial value problems where the concentrations of the trace gases are first initialized from observations, and the models are then used to simulate the evolution of the trace gases (typically for a season) for comparison with observations. Granier and Brasseur (1991) used a mechanistic 3-D model with rather detailed chemistry to investigate the mechanisms responsible for ozone depletion over the Antarctic and the Arctic. Kaye *et al.* (1991), Douglass *et al.* (1991), and Rood *et al.* (1991) used a simple parameterized chemistry to assess the importance of chemical processing in polar regions during the winters of 1979 and 1989. The transport of chemical tracers in those studies was driven by winds from the STRATAN assimilated system (Rood *et al.*, 1989). Chipperfield *et al.* (1993) and Lefèvre *et al.* (1994) simulated the behavior of chemical constituents in the Arctic lower stratosphere during the winters of 1989-1990, and 1991-1992, respectively. These models used analyzed winds and temperature from the European Centre for Medium-Range Weather Forecasts (ECMWF). The simulations reproduce successfully the activation of atmospheric chlorine in polar regions and predict the depletion of ozone in PSC-processed air. While the simulations cannot be used to predict the long-term behavior of the trace gases, they provide the opportunity to diagnose observations and to quantify the different processes that have led to the observed ozone depletion. Chipperfield *et al.* (1993), for example, quantified the respective contribution of the different catalytic cycles responsible for the destruction of ozone in the Arctic lower stratosphere during the 1989-1990 winter.

In 2-D models, the relation to observation is less straightforward. In models that use the residual mean formulation, the velocity and eddy mixing coefficient can be related to observed quantities as follows. The vertical velocity is related to the ratio of the local diabatic heating rate and the lapse rate. Comparison of the vertical velocity in the model with the diabatic heating rate calculated from observed ozone and temperature (Rosenfield *et al.*, 1987) and the lapse rate provides a reference point (see Prather and Remsberg, 1993). The values of the eddy diffusion coefficient K_{yy} can be compared with values derived using mixing rates for potential vorticity (Newman *et al.*, 1988). The interaction between the vertical velocity and the eddy mixing determines the shapes of the surfaces of constant mixing ratios in the lower stratosphere. Measured concentrations of different trace gases indicate that they share the same mixing surfaces in the lower stratosphere when the local photochemical time constant is longer than the transport time constant. This sharing of the mixing ratio surfaces is evident in that an x-y plot of the mixing ratios of two long-lived trace gases shows a compact curve (Plumb and Ko, 1992). This feature is present in both observations and model results (see section H in Prather and Remsberg, 1993). The mixing ratio surfaces in a model defined by the advection velocity and the eddy diffusion coefficient help to determine the latitudinal

gradient of the model-calculated column abundance of ozone.

Finally, the simulated distributions of the long-lived trace gases from 2-D models can be compared to observations. Simulations of source gases N_2O and CH_4 were reasonable when compared to SAMS (Stratospheric and Mesospheric Sounder), ATMOS (Atmospheric Trace Molecule Spectroscopy), and balloon measurements at mid- to high latitudes between 20 and 30 km; however, the variabilities near the winter poles were more difficult to simulate (see Prather and Remsberg, 1993). It was noted in Prather and Remsberg (1993) that direct comparison of model results for the sources gases or transient tracers (such as the radioisotopes ^{14}C and ^{90}Sr from nuclear weapons tests) with observation is difficult because the transport can vary significantly from year to year, with the quasi-biennial oscillation leading to two distinctly separate modes of stratospheric circulation. The transport as formulated in the 2-D models can, at best, represent the averaged transport on a seasonal time scale and does not provide any specific information on the transport of the trace gases on shorter time scales. Such information has to come from 3-D CTMs using three-dimensional winds from a data assimilation procedure or similar analysis using observations. Analysis of such results should provide the information necessary to assess the appropriateness of the transport parameterization in the 2-D models.

6.2.3.2 Transport Between the Polar Vortices and Midlatitudes

The representation of either a closed or a leaky vortex is a major challenge for models. This is particularly problematic for 2-D models, where the inherent dependence on diffusion coefficients does not allow for a completely satisfactory representation of either process. Previous attempts by 2-D models (Sze *et al.*, 1989; Chipperfield and Pyle, 1988) to simulate the effect of export of ozone-poor air from the breakdown of the Antarctic vortex suggest that the dilution process could have a large effect on the ozone behavior year-round in the southern midlatitudes. The results of Sze *et al.* (1989) showed that for an imposed ozone hole with 50% reduction in the column, the calculated ozone column at 30°S and in the tropics decreased year-round by 3% and 0.5%, respectively. In contrast, the results from Chipperfield and Pyle (1988) showed a decrease of less than 0.5% northward of 40°S. Prather *et al.* (1990b) used the Goddard Institute for Space Studies (GISS) 3-D CTM to assess the magnitude of the dispersion of ozone-depleted air over several months following the breakdown of the Antarctic polar vortex and obtained a 2% decrease in total ozone year-round at 30°S.

Prather and Jaffe (1990) used a 3-D CTM to look at the effects of the export of chemically perturbed air. Toumi *et al.* (1993) suggested that polar-processed air reaching midlatitudes is expected to contain large amounts of $ClONO_2$ and may also play a part in affecting the ozone trend. Cariolle *et al.* (1990) used the 3-D general circulation model of Meteo-France (Emeraude) to examine the evolution of the Antarctic polar vortex. They found ozone reduction (about 2%) at midlatitudes in September well before the vortex breakdown. More recently, Mahlman *et al.* (1994) used the Geophysical Fluid Dynamics Laboratory (GFDL) SKYHI GCM to show that, with the 25% depletion in total ozone calculated over Antarctica during the spring season, the ozone column abundance at the equator was reduced by 1% by the end of a 4.5-year model experiment, and the local ozone concentration in the lower stratosphere was reduced by 5%.

The studies of Kaye *et al.* (1991) and Douglass *et al.* (1991), in which the transport of chemical tracers was driven by assimilated winds, concluded that the transport of processed air in the Arctic to midlatitudes was limited. Lefèvre *et al.* (1994) reported the simulation of the behavior of the chemical constituents in the Arctic lower stratosphere during the winter of 1991-1992. The model used analyzed winds and temperature (from ECMWF) and included a comprehensive scheme for gas-phase reactions, as well as a parameterization of heterogeneous reactions occurring on the surface of nitric acid trihydrate (NAT) and ice particles in polar stratospheric clouds, and heterogeneous processes on the surface of sulfate aerosol particles. The model results showed that the combined effects of PSC processing in the vortex, vortex erosion, and aerosol processing at midlatitudes led to significant ozone reductions in the Northern Hemisphere during January 1992. However, chemical processes produced only a limited fraction of the ozone deficit observed at high latitudes during a period dominated by a strong blocking anticyclone over the North Atlantic.

6.2.3.3 Models with Interactive Dynamics

The results presented in this chapter are mostly from model simulations in which the temperature and circulation are kept fixed. It is clear that the thermal structure and the transport circulation will change as the trace gas concentrations change. Changes can be due to changes in ozone or changes in other greenhouse gases. Decrease of ozone in the stratosphere and increases in greenhouse gases will cause a cooling of the stratosphere. In addition, changes in ozone near the tropopause and increases in greenhouse gases will cause a warming of the troposphere. We will restrict the discussion in this section to the effect of the cooling in the stratosphere. The effects from changes in the troposphere will be discussed in Section 6.4.3.

First-order effects on the coupling of ozone, temperature, and wave feedback are relatively well understood, and much of the relevant work is summarized in earlier WMO publications. However, the thermal structure of the atmosphere is controlled by a delicate balance between radiative processes (which are related to ozone) and dynamical processes. At the same time, ozone is controlled by a delicate balance between chemical production and destruction (which depends on the thermal structure) and dynamical transport. Thus, processes that appear to be of secondary importance can act to tip the balance in perturbation studies.

Previous studies ignoring heterogeneous reactions (Nicoli and Visconti, 1982; Schneider *et al.*, 1993) suggested that the cooling of the middle atmosphere could be a mechanism for increasing ozone because the ozone-removing cycles are less efficient at lower temperatures. Thus, this temperature feedback is a negative feedback in that the model-calculated ozone decrease will be reduced. However, a cooler stratosphere could lead to an enhanced occurrence of PSCs (Peter *et al.*, 1991; Austin *et al.*, 1992) resulting in increased chlorine activation, giving rise to the possibility of a Northern Hemisphere ozone hole. Pitari *et al.* (1992) used results from a simple 3-D model to show that the ozone response to CO_2 doubling is distinctly different if PSCs are present and heterogeneous reactions on PSCs are included. They showed that the large stratospheric cooling caused by the CO_2 increase would induce a substantial polar ozone decrease despite the fact that the rates of homogeneous catalytic cycles are reduced.

The changes in local heating will also lead to changes in the circulation, and have an attendant effect on the transport of heat, momentum, and trace species. For example, latitudinal changes in the ozone distribution (*i.e.*, the ozone hole) can lead to substantial changes in the persistence and strength of the polar vortex, and thus enhance the chlorine-catalyzed ozone reduction in polar regions. Several GCM studies examined the coupling between temperature change and the ozone hole. Kiehl *et al.* (1988), using the National Center for Atmospheric Research (NCAR) Community Climate Model (CCM2), found that the introduction in the model of a prescribed Antarctic ozone hole produced in the polar stratosphere a cooling of approximately 5 K during the month of October, and introduced a possible delay in the timing of the final warming. A similar cooling was calculated by Cariolle *et al.* (1990) and Prather *et al.* (1990b) using the Meteo-France model and the GISS model, respectively. However, the results of Mahlman *et al.* (1994) show a larger sensitivity, where a 25% reduction in ozone produces a temperature reduction of 8 K.

While attempts to implement full chemistry schemes in GCMs are still limited by computational resources, there has been important progress in including interactive dynamics in 2-D models. Interactive models can be separated into groups according to the treatment of the forcing term for the zonal-momentum equation. The first group uses externally specified momentum fluxes (Harwood and Pyle, 1975; Vupputuri, 1978; Garcia and Solomon, 1983) or calculates the fluxes from the gradient of the zonal mean potential vorticity from externally specified K_{yy} (Ko *et al.*, 1993). Feedback in these models is limited to changes induced by changes in local heating rates. A second group of models calculates the forcing term explicitly from the zonal waves computed in the model. This latter approach can, in principle, account for the effect of the interaction between the waves and mean circulations. Examples in these groups are the models of Brasseur *et al.* (1990), Garcia *et al.* (1992), Garcia and Solomon (1994), and Kinnersly and Harwood (1993).

6.3 COMPARISON OF MODEL RESULTS WITH OBSERVATION

If the models are designed to simulate the behavior of ozone, an obvious question concerns how well they

simulate the ozone behavior in the present-day atmosphere and the observed changes in the past decades. Another question is to what extent we can trust the model predictions. Ironically, one cannot answer those questions by simply comparing the model-simulated ozone directly with the observations. The reasons are as follows. The winds and temperature in the global models represent climatological averaged states. It would not be appropriate to compare the model simulations with the observed behavior in any one particular year. The behavior of ozone is the net effect from many competing mechanisms. Thus, it is difficult to come to any definitive conclusion about the role of any specific mechanism by simply looking at whether the model-simulated ozone values agree with observations. The balance among these mechanisms in the future atmosphere could be very different from that in the present-day atmosphere. The important thing is not only whether we have the proper balance in the present-day atmosphere, but whether the correct physics has been included so that we can predict with confidence how changes in these terms will affect ozone.

Comparison of model results with observations has to be done indirectly after further processing of the observations and/or model-simulated results. One example is the process study that prescribes values for winds, temperature, and concentrations of some of the trace gases based on observations. A more restricted simulation is performed to calculate the remaining trace gases. A comparison is then made for the restricted set to test the few mechanisms that control the behavior of those species. Examples of these are the studies that use data-assimilated winds to isolate the short-term transport, and modeling studies associated with aircraft campaigns that test the mechanisms for the photochemical partitioning. Another example is the intercomparison exercise in Prather and Remsberg (1993) that calculates the relative abundance of the odd-nitrogen and chlorine species in the altitude range of 20 to 40 km, constrained by observed concentrations from ATMOS. Other methods have been developed specifically for ozone. In previous studies to obtain trends in the column abundance of ozone, analyses were performed to take out the quasi-biennial oscillations and the 11-year solar cycle effects to obtain an ozone trend that can be ascribed to changes in trace gases (see, *e.g.*, Bojkov 1987; Reinsel *et al.*, 1994; Stolarski *et al.*, 1992). The derived trend is then compared to a model simulation that examines the effect of changes in trace gases on ozone. We will discuss some of the model results in Section 6.3.2.

6.3.1 Present-Day Atmosphere

In the comparisons shown below, the University of Oslo (OSLO), NCAR, and Max Planck Institute for Chemistry (MPIC) modeling groups submitted results from calculations that include chemical reactions on PSC surfaces. The Goddard Space Flight Center (GSFC) group submitted two sets of results, one with and one without polar heterogeneous processes.

6.3.1.1 Ozone in the Upper Stratosphere

Several problems identified previously in the upper stratosphere have not been resolved. The Model & Measurement Intercomparison Workshop (Prather and Remsberg, 1993) confirmed previous findings that model-calculated O_3 around 40 km is 20% to 40% smaller than the values derived from the Solar Backscatter Ultraviolet (SBUV) measurement (see Figure 6-1). Recent analysis by Eluszkiewicz and Allen (1993) indicates a deficit of 8% to 20% even when observations are used to constrain the concentrations of the radical species.

Previous suggestions that vibrationally excited oxygen molecules may produce ozone in the upper stratosphere (Slanger *et al.*, 1988; Toumi *et al.*, 1991; Toumi, 1992) are found to be ineffective because of rapid quenching (Patten *et al.*, 1994). The values for the ClO/HCl ratio derived from measurements (Stachnik *et al.*, 1992) are found to be smaller than model-calculated values. Recent model simulations show that the effects of assuming a branching that produces HCl from the reaction of ClO with OH (McElroy and Salawitch, 1989; Natarajan and Callis, 1991) are to increase the calculated ozone concentration at 2 mb (Chandra *et al.*, 1993) and to decrease the calculated decadal ozone trend at the same altitude (Toumi and Bekki, 1993). However, the results from Chandra *et al.* (1993) show that even with the branching, the calculated ozone concentration is still 20% too small in the summer months.

Although the amount of ozone in the upper layer is relatively small and the error may not affect the model-calculated ozone column, the discrepancy may be an indication that there is missing chemistry in the models. There is a need to obtain simultaneous measurements of

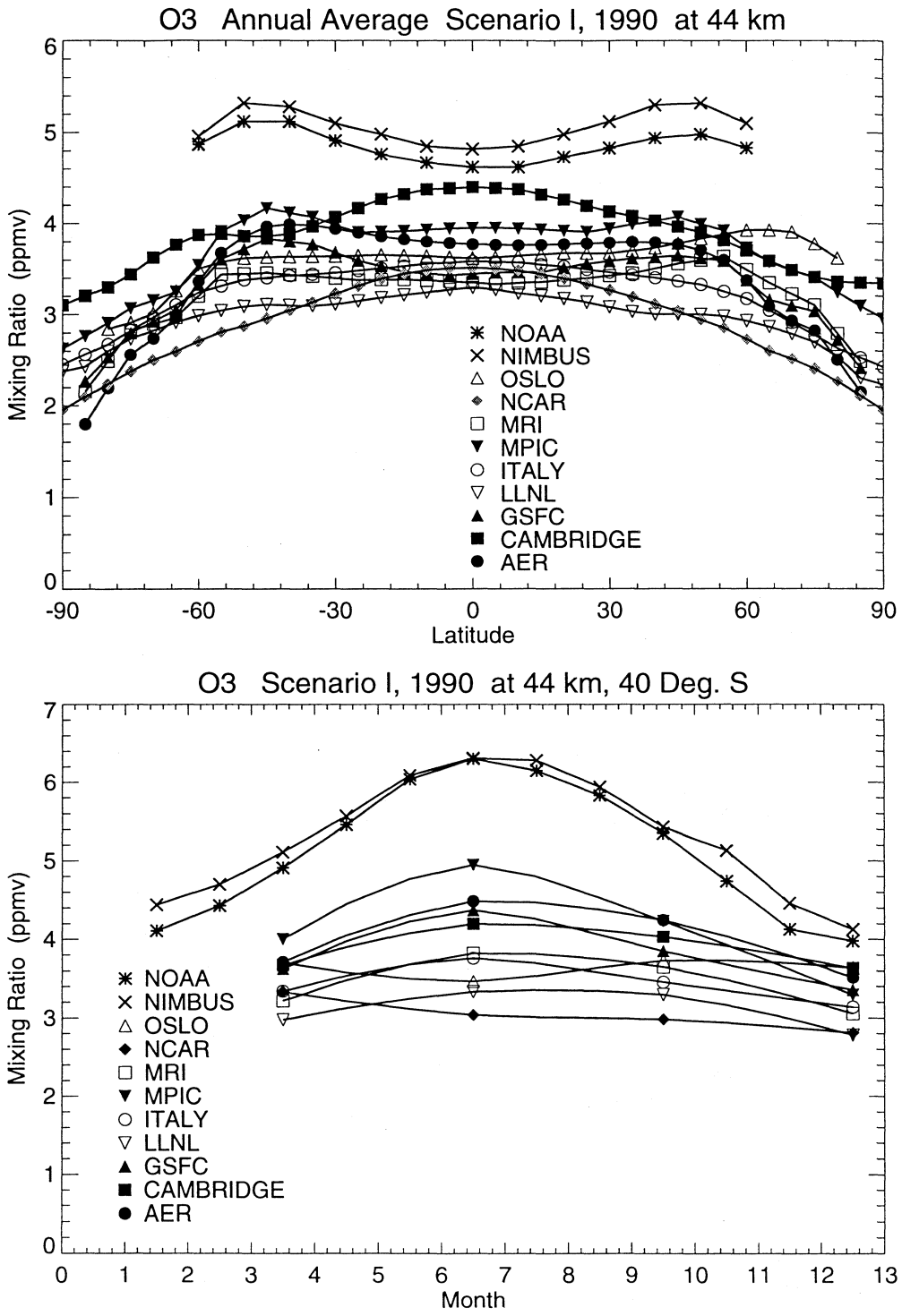

Figure 6-1. Comparison of the model-calculated ozone concentrations at 44 km (2 mb) for 1990 with observations. The observations are the 1989 and 1990 averages from the NOAA-11 SBUV/2 and the Nimbus-7 SBUV as compiled by Chandra *et al.* (1993). The upper panel shows the annual averaged concentrations as a function of latitude. The lower panel shows the calculated concentrations at 40°S for four seasons.

ozone, temperature, and radical species such as OH, HO_2, ClO, and NO_2 in the upper stratosphere to help resolve this.

6.3.1.2 Ozone column

Figure 6-2a shows the calculated column abundance of ozone for the 1990 condition. The model results are within 20% of the observations away from the polar region. The zonal-mean total ozone derived from the Total Ozone Mapping Spectrometer (TOMS) observation indicates that the spring maximum in the Northern Hemisphere extends all the way to the pole, while the Southern Hemisphere shows a sub-polar maximum, with the largest value occurring at about 60°S. This has been attributed to the different surface topographies in the two hemispheres inducing different circulations, resulting in a more stable vortex that encircles the pole in the Southern Hemisphere. By adjusting the circulation and the eddy diffusion coefficients, most models succeeded in producing these features. Hou *et al.* (1991) discussed the relative roles of the circulation and eddy diffusion coefficients in determining the result in the Atmospheric and Environmental Research, Inc. (AER) model. However, none of the models simulates the isolation of the air in the vortex. Thus, it is questionable whether the models produce the observed ozone behavior by simulating the actual mechanisms occurring in the atmosphere.

In Prather and Remsberg (1993), the model-calculated ozone distributions were compared with the average of the 1979 and 1980 observed distribution. This was done to minimize the ozone QBO in the observation. The difference (in Dobson units) between the model-calculated total ozone for 1980 and the averaged observed abundance is plotted in Figure 6-2b. The calculated total ozone values in most models are within 20 Dobson units (10%) of the observed value in the tropics. The models also calculate smaller column ozone than the observed values during the spring maxima in polar regions, up to 100 DU (30%) smaller in some cases.

6.3.2 Ozone Trends Between 1980 and 1990

6.3.2.1 Mechanisms that Can Affect the Ozone Trend

The distribution of ozone can be modified in many ways. The concentrations of the radical species can be increased by the introduction of additional source gases or direct introduction of radical species, such as injection of chlorine radicals by the space shuttle solid rocket engine (WMO, 1992) and injection of NO_x by high-flying aircraft (WMO, 1992; this report). The partitioning of the radical species can be affected by changes in temperature, which affect the reaction rate constants and the frequency of occurrence of the PSCs. Analyses of temperature records (see, *e.g.*, Spencer and Christy, 1993; Oort and Liu, 1993) suggested a cooling trend of about 0.4 K/decade. This cooling may be a result of the increase in CO_2 and ozone depletion that occurred in this period. The partitioning can also be affected by changes in surface areas of the sulfate layer that affect the rate of heterogeneous conversion. Observations (see Chapter 3, WMO [1992]) showed that the aerosol loading has been decreasing after the eruption of El Chichón in 1982. Other works suggested that aircraft emission of SO_2 from combustion of aviation fuel may have increased the sulfate loading in the past decade (see Hofmann, 1991; Bekki and Pyle, 1992).

Other mechanisms that can affect the ozone trend are the QBO in equatorial winds (which has a period of 2 years), the 11-year solar cycle, and the El Niño/Southern Oscillation (ENSO) with a period of about 4 years. Modeling of the ozone QBO was reviewed in Section 6.2.3. Previous studies using 2-D models (Brasseur and Simon, 1981; Garcia *et al.*, 1984; Callis *et al.*, 1985) provided quantitative estimates for the sensitivity of ozone to long-term variations in solar flux at ultraviolet (UV) wavelengths. Results from four 2-D models containing gas-phase chemistry only that were reported in WMO (1990) indicate that the global ozone content is 2% larger at solar maximum than at solar minimum. Results from models with heterogeneous chemistry are available from several recent studies. Unfortunately, it is difficult to compare the results because each work used different assumptions on the variation of the solar flux. Huang and Brasseur (1993) reported that total ozone at solar maximum is 0.5% smaller at winter high latitudes and 0.5% larger at the tropics compared to the values at solar minimum. Brasseur (1993) reported that total ozone is 1% larger at the tropics and 1.5% larger at high latitudes at solar maximum compared to solar minimum when a 3% change in solar flux between 208-265 nm is assumed. Fleming *et al.* (1994) estimated that annual averaged total ozone between 45°N and 45°S is about

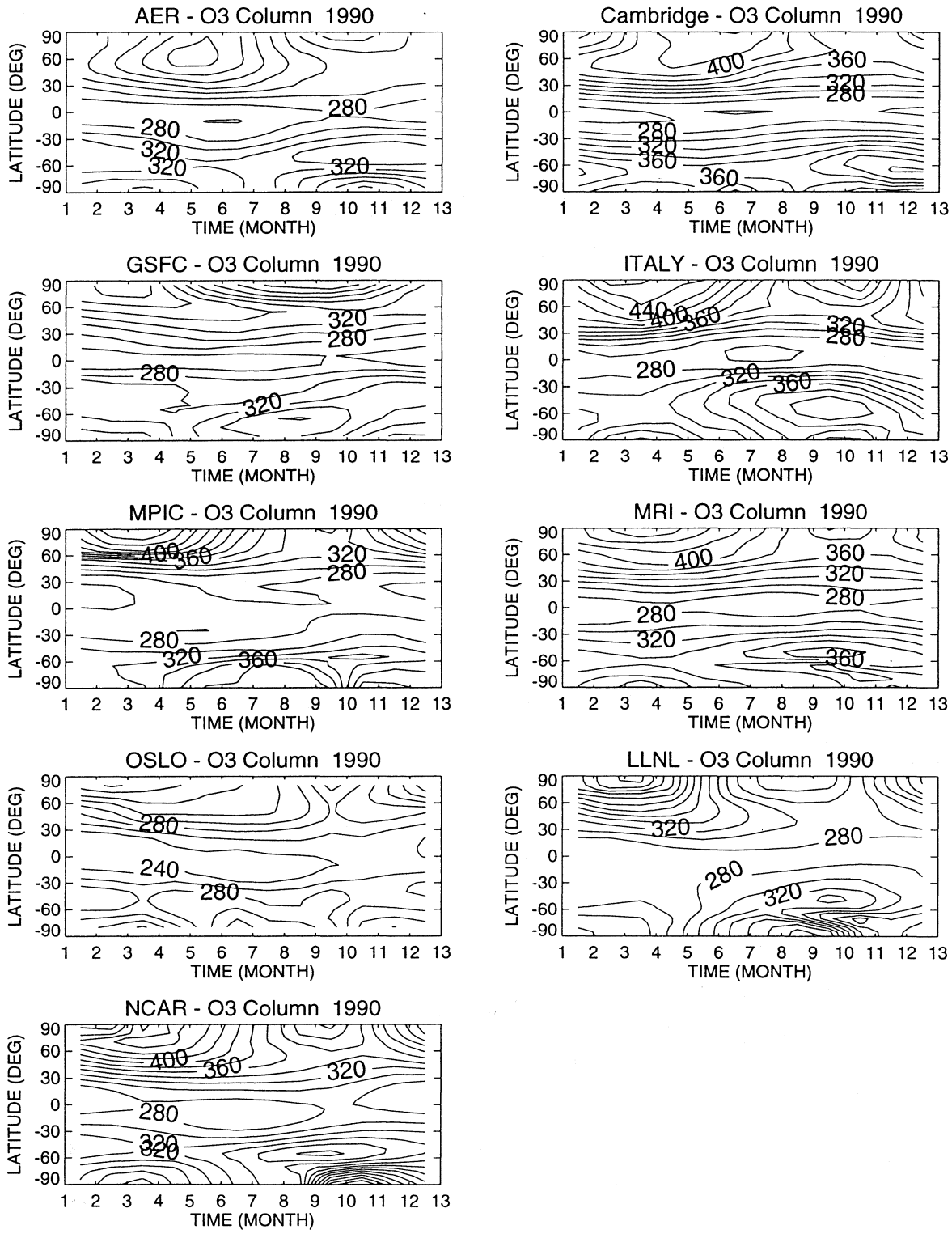

Figure 6-2a. Model-simulated column abundance of ozone for 1990 conditions. The contour levels are in steps of 20 Dobson units.

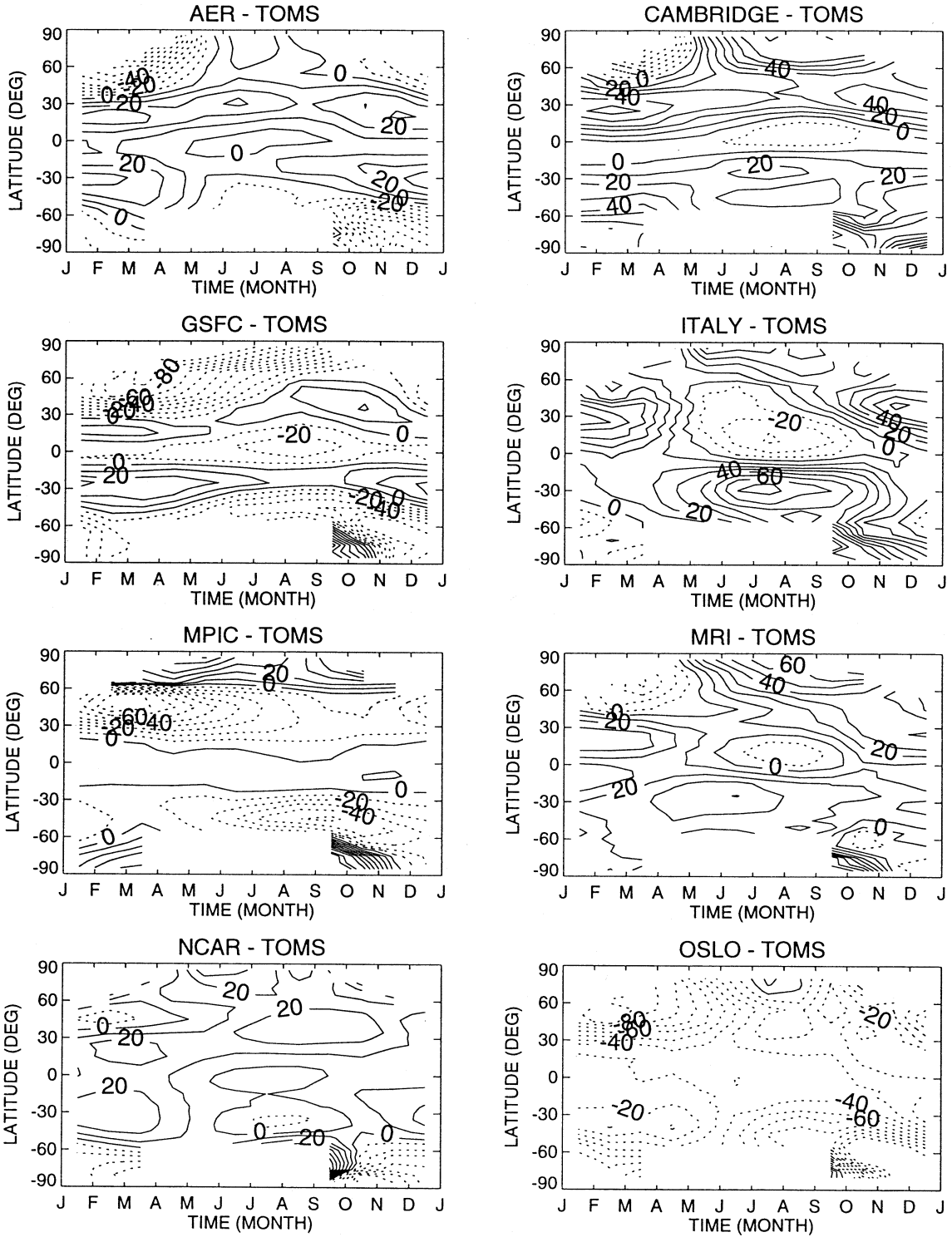

Figure 6-2b. The differences (in Dobson units) between the model-calculated column abundance of ozone for 1980 and the average of the 1979 and 1980 observed column from TOMS. The contour levels are in steps of 10 Dobson units.

Table 6-3. Surface concentrations for halocarbons (pptv), HCFCs (pptv), N_2O (ppbv), and CH_4 (ppbv) for Scenario I.

year	CFC-11	CFC-12	CFC-113	CCl_4	CH_3CCl_3	CH_3Br	H-1301	H-1211	HCFC-22	HCFC-141b	HCFC-142b	HCFC-123	HCFC-124	N_2O	CH_4
1970	59.5	119.8	0.0	85.7	6.5	10.9	0.0	0.1	8.1	0.0	0.0	0.0	0.0	295.0	1420.0
1975	116.1	204.3	10.7	92.0	44.0	11.3	0.1	0.4	30.7	0.0	0.0	0.0	0.0	298.0	1495.0
1980	169.1	286.0	22.1	97.5	93.9	11.9	0.4	0.9	51.1	0.0	0.0	0.0	0.0	302.0	1570.0
1985	216.1	370.6	40.3	102.4	123.1	12.7	1.1	1.7	74.6	0.0	0.0	0.0	0.0	306.0	1650.0
1990	270.1	465.3	70.5	108.2	153.2	13.6	1.7	2.9	105.8	0.3	0.0	0.0	0.2	310.0	1715.0
1995	278.5	502.7	86.0	110.5	148.6	14.5	1.9	3.0	138.5	2.7	3.1	0.2	1.6	313.9	1780.0
2000	257.4	496.9	81.9	98.1	59.1	14.2	1.8	2.4	176.5	10.2	10.3	0.7	4.2	317.8	1845.0
2005	236.2	478.6	77.3	87.1	23.4	14.2	1.7	1.8	214.8	13.8	17.0	1.1	6.9	321.8	1910.0
2010	216.2	457.5	73.0	77.3	9.3	14.2	1.5	1.4	248.2	14.2	21.8	1.6	9.3	325.9	1975.0
2015	197.6	436.3	68.9	68.7	3.7	14.2	1.4	1.1	258.5	14.6	18.7	2.0	9.3	330.0	2040.0
2020	180.4	415.8	64.9	61.0	1.5	14.2	1.3	0.9	263.6	15.0	16.4	1.8	4.2	334.1	2105.0
2025	164.5	396.1	61.3	54.1	0.6	14.2	1.2	0.7	248.1	17.6	14.8	1.6	2.0	338.3	2170.0
2030	149.9	377.2	57.8	48.0	0.2	14.2	1.1	0.5	221.5	21.0	13.8	1.5	1.1	342.6	2235.0
2035	136.5	359.2	54.5	42.6	0.1	14.2	1.0	0.4	152.1	12.3	10.7	0.0	0.5	346.9	2300.0
2040	124.3	342.1	51.4	37.9	0.0	14.2	1.0	0.3	104.4	7.2	8.3	0.0	0.2	351.2	2365.0
2045	113.0	325.7	48.4	33.6	0.0	14.2	0.9	0.3	71.7	4.3	6.4	0.0	0.1	355.6	2430.0
2050	102.8	310.2	45.7	29.8	0.0	14.2	0.8	0.2	49.2	2.5	5.0	0.0	0.0	360.1	2495.0

3.5% larger in 1985 and 1979 (solar maxima) than in 1985 (solar minimum). These values are to be compared with the value of 1.2% derived from the statistical analysis of the Dobson data on ozone and the $F_{10.7}$ solar flux through 1984 (Reinsel *et al.,* 1987), and the 1-2% value cited in Chapter 7 of WMO (1990). A review of the effects of ENSO on ozone can be found in Zerefos *et al.* (1992). Analyses of the observations indicate that there was a 2% ozone decrease in the tropics after the large ENSO event in 1982-1983. No modeling work has been done to simulate the suggested mechanisms to produce the ozone response.

6.3.2.2 Model Results

As discussed in the beginning of Section 6.3, the effects of the 11-year solar cycle and QBO are subtracted from the ozone trend using statistical techniques. Here, we compare this remaining trend to the model-calculated trend due to changes in other trace gases. The trends in the surface concentrations of the halocarbons, CH_4, and N_2O are discussed in Chapter 2 of this report. The modelers were asked to perform a calculation in which the changes in the surface concentrations of the source gases are as given in Table 6-3. With the exception of the CAMBRIDGE model, all models kept the temperature, circulation, and surface area of the sulfate particles constant in the calculation. The CAMBRIDGE model includes dynamics feedback in its calculation.

The model-calculated changes in ozone between 1980 and 1990 are shown in Figure 6-3a. The effect of PSC chemistry is included in the OSLO, NCAR, and MPIC models. The GSFC model results shown correspond to the case without PSC chemistry. Note that most models show a calculated decrease of about 1-2% in the tropics, increasing to 4% at the high latitudes. Compared to the derived trend reported in Stolarski *et al.* (1992), models without PSC chemistry fail to reproduce the following features: the over 6% decrease north of 50°N during March; the 6% decrease south of 40°S throughout the year; and the large decrease in the Antarctic polar vortex. Including PSC chemistry in the model will help to produce some of these features. The OSLO, NCAR and MPIC results all showed decreases of about 7% at northern high latitudes. The calculated decreases for the southern high latitudes range from 7% to 9%. The GSFC model with PSC chemistry shows calculated decreases of about 3% at northern high latitudes and up to 9% in the south. Figure 6-3b shows the calculated trend as a function of latitude compared to the derived trend between 1980 and 1990. The model results agree well with the derived trend in the tropics. Only models with PSC chemistry calculate the large trend at high latitudes. Around 40° latitudes, the observed ozone trend is between -4% to -8% per decade in winter, and -4% to -6% per decade in spring and fall. These are to be compared with the model-calculated values of -2% to -3% per decade year round. Thus, the model-calculated trends are a factor of 1.3 to 3 smaller than the observed trends, depending on season.

Figure 6-4 shows the calculated percentage change in the local concentration of ozone between 1980 and 1990. The model-calculated ozone trends for the past decade are typically 8% to 12% between 30°N and 50°N at 40 km. These values are too large compared to the trend derived from SAGE I and SAGE II (McCormick *et al.,* 1992) and that derived from the Umkehr data (see WMO, 1992). However, a recent study (Hood *et al.,* 1993) of the SBUV data indicates that the trend may be larger and somewhat closer to the model-calculated trends. As discussed in Section 6.3.1, a smaller trend can be obtained if a branching for production of HCl is assumed for the reaction of OH with ClO (Toumi and Bekki, 1993). The model-calculated trend would also be smaller if the feedback effects from the cooling of the stratosphere due to the ozone decrease were included in the models. This temperature feedback is included in the CAMBRIDGE model only. Calculations from models (Schneider *et al.,* 1993) indicate that the feedback will provide a 20% compensation in the calculated ozone decrease.

Results in Figure 6-4 show that none of the models reproduced the 5% to 10% per decade decrease in ozone in the midlatitude lower stratosphere derived from the SAGE data (McCormick *et al.,* 1992). There are suggestions as to how a larger decrease can be calculated in the models. One suggestion is that the transport parameterizations in the models fail to represent how ozone at high latitudes can affect the midlatitude region. A more realistic representation of the transport may give a larger ozone decrease. Another suggestion is that there may be missing photochemistry. Solomon *et al.* (1994a) showed that if IO is assumed to react with ClO and BrO at sufficiently fast rates, the calculated ozone decrease in the lower stratosphere will be larger.

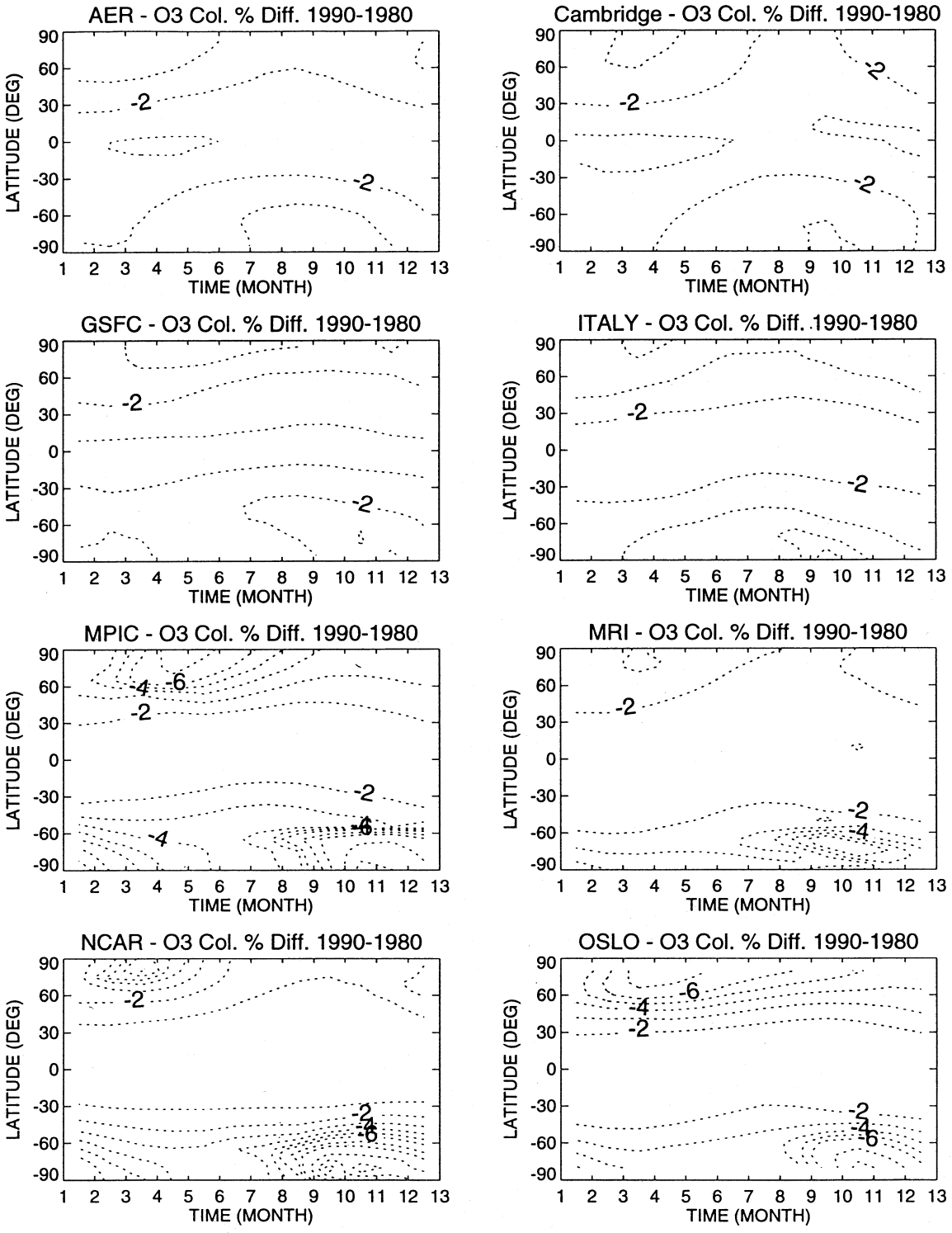

Figure 6-3a. Model-calculated changes in column ozone between 1980 and 1990. The models simulate the effect of chlorine increase with the aerosol kept at the background values. PSC chemistry is excluded except for the OSLO, MPIC, and NCAR models. Contour levels are in 1% steps.

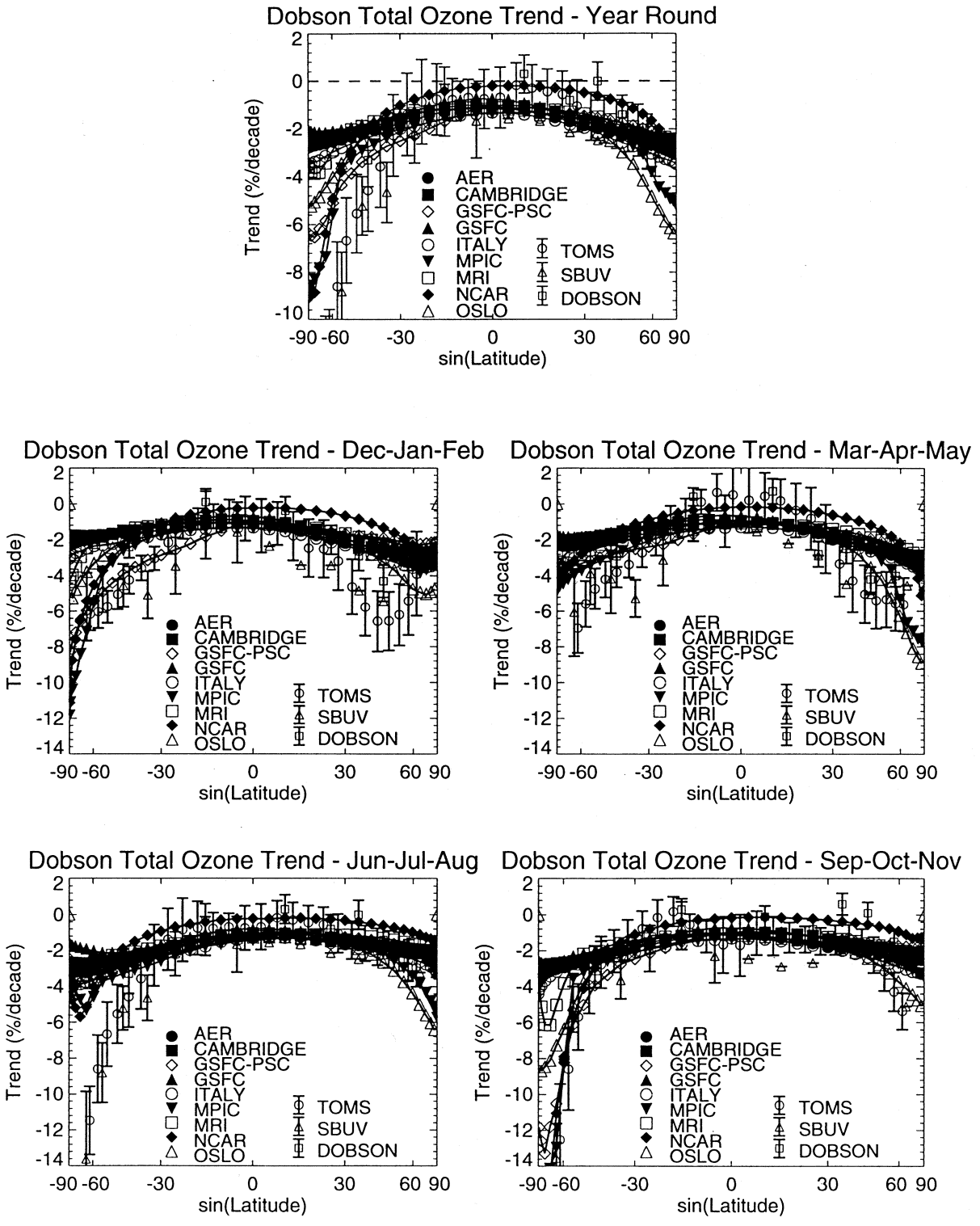

Figure 6-3b. Model-calculated changes in column ozone between 1980 and 1990 compared to derived trends.

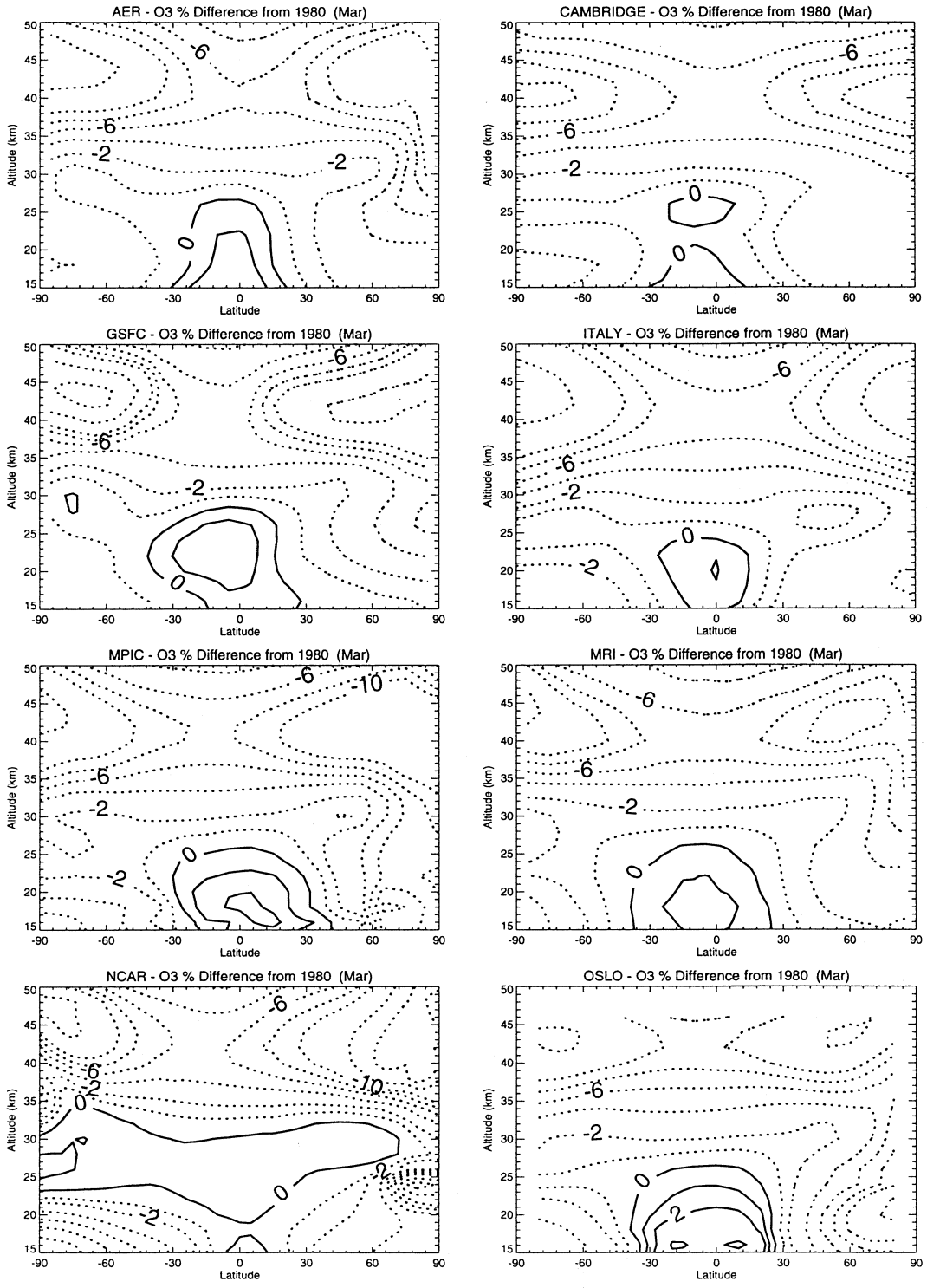

Figure 6-4. Model-calculated local change in ozone between 1980 and 1990 for March condition. PSC chemistry is excluded except for the OSLO, MPIC, and NCAR models. Contour levels are 2%, 1%, 0, -1%, -2%, and -4%, and in steps of 2% thereafter.

6.3.3 Effects of the Mt. Pinatubo Eruption

Volcanic eruptions introduce large amounts of SO_2 into the stratosphere that will be oxidized to form sulfate aerosol. Model simulations (Golombek and Prinn, 1993; Pitari *et al.*, 1993) have shown that the background stratospheric aerosol layer can be explained in terms of the present input of SO_2, and OCS (carbonyl sulfide). However, the lack of detailed knowledge on the microphysics of particle formation precludes a detailed prediction on how the surface area will change.

Prior to the formation of the volcanic aerosol, SO_2 chemistry can affect the photochemical removal rate of ozone in the tropics for the initial months after the eruption (Bekki *et al.*, 1993). The increase of the aerosol surface area available for heterogeneous processes is the most immediate effect of aerosol changes (Hofmann and Solomon, 1989). However, modeling studies (Michelangeli *et al.*, 1989; Brasseur and Granier, 1992; Kinne *et al.*, 1992; Pitari, 1993b; Pitari and Rizi, 1993; Schoeberl *et al.*, 1993) have shown that other effects may be as important. The UV flux is increased substantially above the aerosol layer and may decrease below, thus affecting the photolysis rates. Another effect is related to the heating of the aerosol layer due to the absorption of solar and terrestrial radiation. The additional heat source can modify the dynamics and affect the reaction rates of those catalytic cycles whose reaction rates depend on temperature.

6.3.3.1 Radical Species

The effects of the volcanic aerosol on several radical species were reviewed in Chapter 4. The observations and the accompanying modeling studies indicate that the behaviors of the radical species are in qualitative agreement with enhanced processing on the surface of the volcanic aerosols. These include observation of NO_x/NO_y ratios from aircraft (Fahey *et al.*, 1993; Kawa *et al.*, 1993), observation of N_2O_5 and HNO_3 from ATMOS (Rinsland *et al.*, 1994), measurement of ClO from aircraft (Avallone *et al.*, 1993; Wilson *et al.*, 1993), and measurement of ClO, NO, and O_3 (Dessler *et al.*, 1993) and NO_2 and HNO_3 (Webster *et al.*, 1994) from balloons. In addition, there are column measurements of $ClONO_2$, HCl, and HNO_3 from aircraft (Toon *et al.*, 1993) and ground-based measurements of NO_2 (Johnston *et al.*, 1992; Mills *et al.*, 1993; Coffey and Mankin, 1993; Koike *et al.*, 1994; Solomon *et al.*, 1994b) and HNO_3 (Koike *et al.*, 1994). Solomon *et al.* (1993) reported that the enhanced level of OClO observed over McMurdo Station during autumn of 1992 is consistent with expected effects from the enhanced conversion of $ClONO_2$ via reaction (6-2).

6.3.3.2 Ozone Behavior in the Tropics in Late 1991

Using satellite and lidar measurements, Labitzke and McCormick (1992) concluded that the monthly averaged zonal mean 30-mb (24 km) temperatures at 20°N in September and October 1991 are as much as 2.5 K warmer than the 26-year average. Warming in the equatorial region was measured to be as high as 4 K. DeFoor *et al.* (1992) deduced from lidar data that there was a total lift of 1.8 km in the tropics 100 days after the eruption. There are some disagreements on how the eruption has affected ozone because of the difficulty in isolating the effects of the QBO and other mechanisms that cause interannual variations of ozone. Using the Nimbus-7 TOMS and the NOAA-11 satellite Solar Backscatter Ultraviolet/2 (SBUV/2) spectrometer data, Chandra (1993) suggests that the maximum change in column ozone attributed to the Mt. Pinatubo eruption may not be greater than a 2-4% decrease at mid- and low latitudes a few months after the eruption after removing the effect of the QBO. Schoeberl *et al.* (1993) used a different method in analyzing the Nimbus 7 TOMS data and derived a decrease of 5-6% in column ozone between 12°N and 12°S between June and December 1991. Grant *et al.* (1992, 1994) compared the electrochemical concentration cell (ECC) sondes data and the airborne UV Differential Absorption Lidar (DIAL) data to Stratospheric Aerosol and Gas Experiment II (SAGE II) climatology and deduced a column ozone decrease in the tropics of $9\% \pm 4\%$ in September, 1991.

Bekki *et al.* (1993) investigated the role of gas-phase sulfur photochemistry on ozone in the first month following the eruption. Most other studies did not include this on the assumption that its effect is short-lived. Kinne *et al.* (1992), Brasseur and Granier (1992), Pitari and Rizi (1993), Kinnison *et al.* (1994), and Tie *et al.* (1994) investigated the coupled radiative-dynamical perturbation on ozone following the eruption and provided diagnostics to estimate the contributions from dynamics, radiation, and heterogeneous processing. All models estimated a net increase in heating of about 0.3 to 0.4 K/

day. However, different approaches were used to determine how this extra heating is to be partitioned into warming or enhanced vertical motion. The studies of Brasseur and Granier (1992), Tie *et al.* (1994), and Pitari and Rizi (1993) used the dynamics equations in their respective models to apportion the heating. The calculated decrease in tropical ozone in late 1991 is 9% in Pitari and Rizi (1993), which results from a 4% decrease from changes in photolysis rate, a 4% decrease from increased heterogeneous processing, and 1% decrease from temperature and circulation changes. The calculated decrease in Tie *et al.* (1994) is 2%, which results from a 2% decrease caused by changes in photolysis rates, a 2% decrease from changes in temperature and circulation, and a 2% increase from changes in heterogeneous processing. The studies of Kinnison *et al.* (1994) provided separate estimates under the assumption that all the heating is dissipated either by local warming or by enhanced upward motion. The calculated decrease is 2% (-1.5% from motion and -0.5% from heterogeneous processing) if it is assumed that the extra heating goes to enhanced upward motion, and 1% (-0.5% from temperature change and -0.5% from heterogeneous processing) if it is assumed that all the heating is balanced by warming. The work of Kinne *et al.* (1992) estimated an uplifting of 1.7 km after accounting for the warming using the observed temperature change. They used a simple 1-D mechanistic model to estimate an ozone decrease of 10%.

6.3.3.3 Ozone Behavior in 1992 and 1993

Gleason *et al.* (1993) reported that during 1992, TOMS on the Nimbus-7 satellite measured global average total ozone to be 1-2% lower than expected if ozone is assumed to be decreasing at the same linear trend in the past decade. These results are consistent with analysis of the TOMS and Meteor 3 data (Herman and Larko, 1994), which showed that the 1993 ozone amount is 12.5% below the historical mean (from 1979) at high latitude, 7% at midlatitude, and 4% at low latitude. Low ozone for the winter of 1992-1993 was also reported from the Microwave Limb Sounder (MLS) instrument on the Upper Atmosphere Research Satellite (UARS) (Froidevaux *et al.*, 1994) and the NOAA-11 SBUV/2 instrument (Planet *et al.*, 1994). Froidevaux *et al.* (1994) also emphasized examining the latitude and height behavior of the observed ozone decrease to try to identify the causes for the lower values.

In Pitari and Rizi (1993), the model calculated a decrease in ozone of about 12% at 60°N in March 1992. Diagnostic results showed that this is a combination of a 12% decrease due to heterogeneous chemistry, a 4% decrease due to changes in photolysis rate, and a 4% increase due to changes in transport. In contrast, the additional ozone (about 4%) transported into the region from the strengthening of the mean circulation in the Kinnison *et al.* (1994) study tends to cancel the reduction of ozone due to the increase in heterogeneous conversion rates, producing changes in ozone that do not agree well with observed data. Tie *et al.* (1994) showed that the changes in ozone at northern high latitudes are -10% in spring of 1992 and -8% in spring of 1993. Because so many different mechanisms can change ozone after the eruption, it is difficult to understand the ozone response by comparison of model-simulated ozone with observations alone. Additional diagnostics based on observations are needed to isolate the effects of the different mechanisms.

6.3.3.4 Isolating the Effects of Heterogeneous Processing

Results from Rodriguez *et al.* (1994) and Kinnison *et al.* (1994) showed that the effects of increased heterogeneous processing from the Mt. Pinatubo aerosol caused an additional 2-5% decrease in ozone at mid- to high latitudes in the winter of 1993. However, the results of Pitari and Rizi (1993) and Granier and Brasseur (1992) indicated that the change in aerosol would lead to a 10% decrease in ozone column due to heterogeneous chemistry alone. It is difficult to compare the model predictions because each model used a different set of parameters to describe the aerosol loading and its decay. In an attempt to see if the model predictions will agree better if the models use uniform input, we prescribed the following set of simulations. The first simulation calculates the behavior of ozone using the surface concentrations for trace gases as prescribed in Table 6-3 while keeping the aerosol surface area at the background value. The second calculation uses the same surface concentrations but assumes the aerosol surface area increases by a factor of 30 in June 1991. The excess surface area is assumed to decay with an exponential

Table 6-4. Mixing ratios for halocarbons (in pptv) for Scenario II.

year	CFC-11	CFC-12	CFC-113	CCl_4	CH_3CCl_3	CH_3Br
1992	281.8	487.6	79.1	110.5	178.1	14.1
1995	290.4	513.7	87.5	113.7	159.3	14.7
2000	284.6	528.6	85.5	118.5	75.8	15.4
2005	278.0	532.4	82.9	122.8	42.5	16.4
2010	264.3	526.9	79.6	117.7	22.0	17.6

time constant of 1 year. The simulation is to include only the effect of enhanced heterogeneous processing. The differences between the ozone in the two simulations (second simulation minus the first) are given in Figure 6-5.

Prather (1992) investigated the potential for a non-linear, catastrophic loss of stratospheric ozone if the aerosol density were greatly increased following a massive eruption. None of the models indicates that such a situation was reached in the Mt. Pinatubo case. Figure 6-5a shows the results for northern midlatitudes, indicating that the effect of enhanced processing is to decrease the ozone. The results fall into three groups: about -3% (AER and LLNL), about -5% (GSFC and MPIC), and about -8% (ITALY and NCAR). The results for the tropics are given in Figure 6-5b. The ozone decrease ranges from less than 0.5% to 2.5%.

It is unclear what the causes are for the differences in the model predictions. Possible explanations include the different treatments used in calculating the concentration of N_2O_5 and the different effects of reaction (6-2) in the models caused by different temperatures being used. The AER model and the LLNL model use an explicit diurnal variation in calculating N_2O_5, while other models use various methods to estimate the N_2O_5 concentration from an averaged sun condition.

6.4 RESULTS FROM SCENARIO CALCULATIONS

For the purpose of a model intercomparison, we have prescribed two scenarios for the source gases. The surface concentrations of the species are specified as functions of time as given in Tables 6-3 and 6-4. Values prior to 1990 are based on available observations. The growth rate for N_2O is based on previous estimates of 0.25% per year. Khalil and Rasmussen (1992) showed that the actual increase in the past decade has been very variable, ranging from 0.5 ppbv per year to 1.2 ppbv per year. For CH_4, a linear growth rate of 13 ppbv per year is assumed after 1992. Recent observations for CH_4 (Dlugokencky *et al.*, 1994; Khalil and Rasmussen, 1993) indicate that the CH_4 growth rate has slowed to as little as 2 ppbv per year.

The surface concentration for the CH_3Cl is set at 600 pptv. Surface concentrations for the CFCs, HCFCs, halons, and CH_3Br were calculated using a box model with assumed emissions and the reference lifetimes given in Chapter 13. In Scenario I (Table 6-3), the emissions for the halocarbons follow the guidelines in the Amendments to the Montreal Protocol. For CH_3Br, it is assumed that a background of 9 pptv is maintained by natural sources. Emission of anthropogenic CH_3Br assumes a schedule that maintains constant emission at the 1991 level. This, when combined with the natural sources, results in a surface concentration of 14.2 pptv after the year 2000. The substitute HCFCs are a combination of HCFC-22, HCFC-141b, HCFC-142b, HCFC-123, and HCFC-124. The Ozone Depletion Potential (ODP)-weighted annual production is taken to be 3.1% of the ODP-weighted emissions in 1990. In addition to the basic scenario, results are also presented for a second scenario (Table 6-4) where we assume partial compliance with the Protocol for CFC-11, CFC-12, CFC-113, CH_3CCl_3, and CCl_4. The emission for CH_3Br is also assumed to be larger, resulting in a surface concentration of 17.6 pptv in 2010. The Scenario II calculation extends only to 2010.

6.4.1 Chlorine and Bromine Loading

Figure 6-6a shows the model-calculated chlorine concentrations for 58 km at 50°N. The observed concentrations of HCl from the ATMOS instrument for 1985 (Zander *et al.*, 1990) and 1992 (Gunson *et al.*, 1994) are

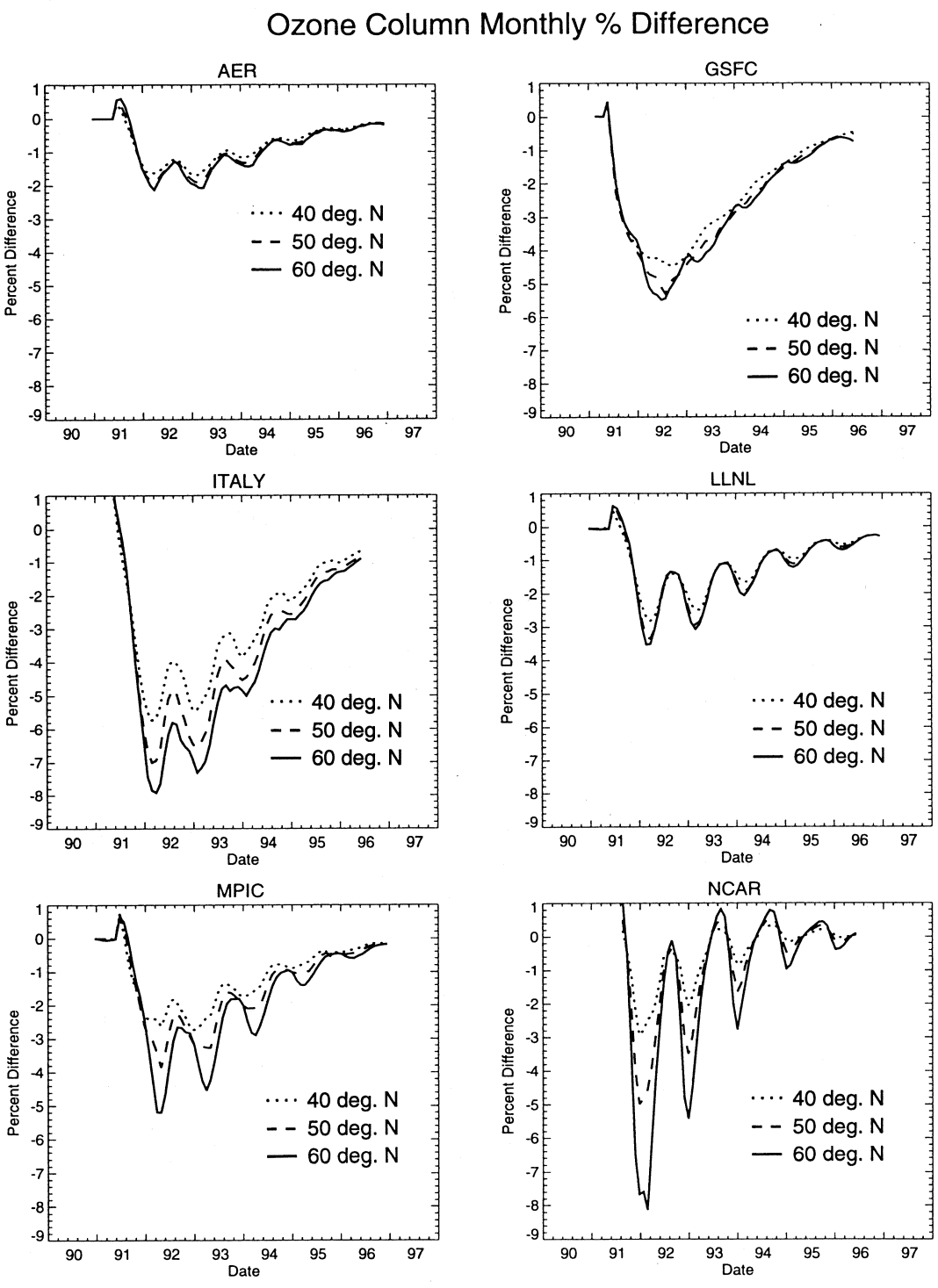

Figure 6-5a. Calculated percent change in ozone column at 40°N, 50°N, and 60°N for a thirty-fold increase in surface area. The values are obtained by comparing the column calculated using fixed background aerosol with the column calculated where there is a 30-fold increase in aerosol surface area in June 1991 with the excess aerosol decaying with a time constant of 1 year.

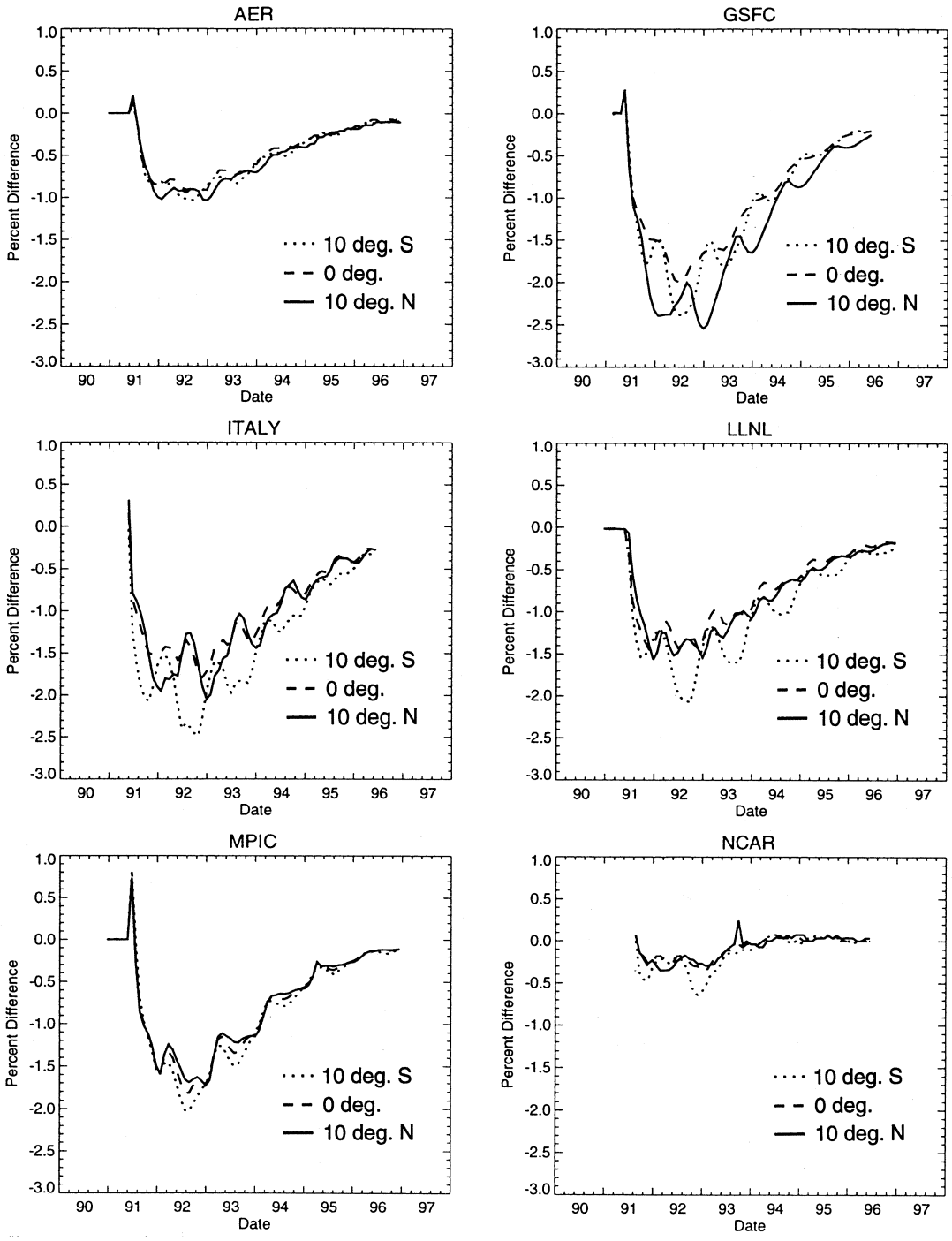

Figure 6-5b. Same as Figure 6-5a except for 10°S, Equator, and 10°N.

Bekki, S., and J.A. Pyle, Two-dimensional assessment of the impact of aircraft sulfur emissions on the stratospheric sulfate aerosol layer, *J. Geophys. Res.*, *97*, 15839-15847, 1992.

Bekki, S., R. Toumi, and J.A. Pyle, Role of sulfur photochemistry in tropical ozone changes after the eruption of Mount Pinatubo, *Nature*, *362*, 331-333, 1993.

Bojkov, R.D., The 1983 and 1985 anomalies in ozone distribution in perspective, *Mon. Wea. Rev.*, *115*, 2187-2201, 1987.

Boville, B.A., The influence of the polar night jet on the tropospheric circulation in a GCM, *J. Atmos. Sci.*, *41*, 1132-1142, 1984.

Brasseur, G., The response of the middle atmosphere to long-term and short-term solar variability: A two-dimensional model, *J. Geophys. Res.*, *98*, 23079-23090, 1993.

Brasseur, G., and P.C. Simon, Stratospheric chemical and thermal response to long-term variability in solar UV irradiance, *J. Geophys. Res.*, *86*, 7343-7362, 1981.

Brasseur, G., M.H. Hitchman, S. Walters, M. Dymek, E. Falise, and M. Pirre, An interactive chemical-dynamical radiative two-dimensional model of the middle atmosphere, *J. Geophys. Res.*, *95*, 5639-5655, 1990.

Brasseur, G.P., and C. Granier, Mount Pinatubo aerosols, chlorofluorocarbons, and ozone depletion, *Science*, *257*, 1239-1242, 1992.

Callis, L.B., J.C. Alpert, and M.A. Geller, An assessment of thermal, wind and planetary wave changes in the middle and lower atmosphere due to 11-year UV-flux variation, *J. Geophys. Res.*, *90*, 2237-2282, 1985.

Callis, L.B., *et al.*, Precipitating relativistic electrons: Their long-term effect on stratospheric odd nitrogen levels, *J. Geophys. Res.*, *96*, 2939-2976, 1991.

Cariolle, D., A. Lasserre-Bigorry, J.-F. Royer, and J.-F. Geleyn, A general circulation model simulation of the springtime Antarctic ozone decrease and its impact on mid-latitudes, *J. Geophys. Res.*, *95*, 1883-1898, 1990.

Chandra, S., Changes in stratospheric ozone and temperature after the eruption of Mt. Pinatubo, *Geophys. Res. Lett.*, *20*, 33-36, 1993.

Chandra, S., C.H. Jackman, A.R. Douglass, E.I. Fleming, and D.B. Considine, Chlorine catalyzed destruction of ozone: Implications for ozone variability in the upper stratosphere, *Geophys. Res. Lett.*, *20*, 351-354, 1993.

Chipperfield, M.P., and J.A. Pyle, Two-dimensional modeling of the Antarctic lower stratosphere, *Geophys. Res. Lett.*, *15*, 875-878, 1988.

Chipperfield, M.P., D. Cariolle, P. Simon, R. Ramoroson, and D.J. Lary, A three-dimensional modeling study of trace species in the Arctic lower stratosphere during winter 1989-1990, *J. Geophys. Res.*, *98*, 7199-7218, 1993.

CIAP Monograph 3, *The Stratosphere Perturbed by Propulsion Effluents*, DOT-TST-75-53, U.S. Department of Transportation, Washington, D.C., 1975.

Coffey M.T., and W.G. Mankin, Observations of the loss of stratospheric NO_2 following volcanic eruptions, *Geophys. Res. Lett.*, *20*, 2873-2876, 1993.

Considine, D.B., A.R. Douglass, and C.H. Jackman, Effects of a PSC parameterization on ozone depletion due to stratospheric aircraft in a 2D model, *J. Geophys. Res.*, *99*, 18879-18894, 1994.

Crutzen, P.J., The influence of nitrogen oxides on the atmospheric ozone content, *Quart. J. Roy. Meteorol. Soc.*, *96*, 320-325, 1970.

DeFoor, T.E., E. Robinson, and S. Ryan, Early lidar observations of the June 1991 Pinatubo eruption plume at Mauna Loa Observatory, Hawaii, *Geophys. Res. Lett.*, *19*, 187-190, 1992.

Dessler, A.E., *et al.*, Balloonborne measurements of ClO, NO and O_3 in volcanic cloud: An analysis of heterogeneous chemistry between 20 and 30 km, *Geophys. Res. Lett.*, *20*, 2527-2530, 1993.

Dlugokencky, E.J., K.A. Masarie, P.M. Lang, P.P. Tans, L.P. Steele, and E.G. Nisbet, A dramatic decrease in the growth rate of atmospheric methane in the northern hemisphere during 1992, *Geophys. Res. Lett.*, *21*, 43-48, 1994.

Douglass, A.R., R.B. Rood, J.A. Kaye, R.S. Stolarski, D.J. Allen, and E.M. Larsen, The influence of polar stratospheric heterogeneous processes on reactive chlorine at mid-latitudes: Three-dimensional model implications, *Geophys. Res. Lett.*, *18*, 25-28, 1991.

Eluszkiewicz J., and M. Allen, Global analysis of the ozone deficit, *J. Geophys. Res., 98*, 1069-1082, 1993.

Fahey, D.W., *et al.,* In situ measurements constraining the role of sulphate aerosols in mid-latitude ozone depletion, *Nature, 363*, 509-514, 1993.

Fleming, E.L., S. Chandra, C.H. Jackman, D.B. Considine, and A.R. Douglass, The middle atmospheric response to short and long term solar UV variations: Analysis of observations and 2D model results, *J. Atmos. and Terrestrial Phys.*, in press, 1994.

Foley, H.M., and M.A. Ruderman, Stratospheric NO production from past nuclear explosions, *J. Geophys. Res., 78*, 4441-4450, 1973.

Fried, A., B.E. Henry, J.G. Calvert, and M. Mozurkewich, The reaction probability of N_2O_5 with sulfuric acid aerosols at stratospheric temperatures and compositions, *J. Geophys. Res., 99*, 3517-3532, 1994.

Froidevaux, L., J.W. Waters, W.G. Read, L.S. Elson, D.A. Flower, and R.F. Jarnot, Global ozone observations from UARS MLS: An overview of zonal mean results, *J. Atmos. Sci.*, in press, 1994.

Garcia, R.R., and S. Solomon, A numerical model of the zonally averaged dynamical and chemical structure of the middle atmosphere, *J. Geophys. Res., 88*, 1379-1400, 1983.

Garcia, R.R., S. Solomon, R.G. Roble, and D.W. Rusch, A numerical response of the middle atmosphere to the 11-year solar cycle, *Planet. Space Sci., 32*, 411-423, 1984.

Garcia, R.R., F. Stordal, S. Solomon, and J.F. Kiehl, A new numerical model of the middle atmosphere 1. Dynamics and transport of tropospheric source gases, *J. Geophys. Res., 97*, 12967-12991, 1992.

Garcia, R.R., and S. Solomon, A new numerical model of the middle atmosphere 2. Ozone and related species, *J. Geophys. Res., 99*, 12937-12951, 1994.

Geller, M.A., and J.C. Alpert, Planetary wave coupling between the troposphere and the middle atmosphere as a possible sun-weather mechanism, *J. Atmos. Sci., 37*, 1197-1215, 1980.

Gleason, J.F., *et al.,* Record low global ozone in 1992, *Science, 260*, 523-526, 1993.

Golombek, A., and R.G. Prinn, A global 3-D model of the stratospheric acid layer, *J. Atmos. Chem., 16*, 179-199, 1993.

Granier, C., and G. Brasseur, Ozone and other trace gases in the Arctic and Antarctic regions: Three-dimensional model simulations, *J. Geophys. Res., 96*, 2995-3011, 1991.

Granier, C., and G. Brasseur, Impact of heterogeneous chemistry on model predictions of ozone changes, *J. Geophys. Res., 97*, 18015-10833, 1992.

Grant, W.B., *et al.,* Observations of reduced ozone concentrations in the tropical stratosphere after the eruption of Mt. Pinatubo, *Geophys. Res. Lett., 19,* 1109-1112, 1992.

Grant, W.B., *et al.,* Aerosol-associated changes in tropical stratospheric ozone following the eruption of Mt. Pinatubo, *J. Geophys. Res., 99*, 8197-8211, 1994.

Gray, L.J., and J.A. Pyle, A two-dimensional mean circulation model of the quasi-biennial oscillation of ozone, *J. Atmos. Sci., 46*, 203-220, 1989.

Gray, L.J., and T.J. Dunkerton, The role of the seasonal cycle in the quasi-biennial oscillation of ozone, *J. Atmos. Sci., 47*, 2429-2451, 1990.

Gray, L.J., and S. Ruth, The modeled latitudinal distribution of the ozone quasi-biennial oscillation using observed equatorial winds, *J. Atmos. Sci., 50*, 1033-1046, 1993.

Grooss, J.U., T. Peter, C. Brühl, and P.J. Crutzen, The influence of high flying aircraft on polar heterogeneous chemistry, in *Impact of Emissions from Aircraft and Spacecraft upon the Atmosphere: Proceedings of an International Scientific Colloquium,* edited by U. Schumann and D. Wurzel, DLR-Mitteilung 94-06, 229-234, 1994.

Gunson, M.R., *et al.,* Increase in levels of stratospheric chlorine and fluorine loading between 1985 and 1992, *Geophys. Res. Lett., 21,* 2223-2226, 1994.

Hansen, J.G., *et al.,* Efficient three-dimensional global models for climate studies: Models I and II, *Mon. Wea. Rev., 111*, 609-662, 1983.

Hanson, D., and K. Mauersberger, Solubility and equilibrium vapor pressures of HCl dissolved in polar stratospheric cloud material: Ice and the trihydrate of nitric acid, *Geophys. Res. Lett., 15*, 1507-1510, 1988.

Hanson, D.R., A.R. Ravishankara, and S. Solomon, Heterogeneous reactions in sulfuric acid aerosol: A framework for model calculations, *J. Geophys. Res.*, *99*, 3615-3629, 1994.

Harwood, R.S., and J.A. Pyle, A two-dimensional mean circulation model for the atmosphere below 80 km, *Quart. J. Roy. Meteorol. Soc.*, *101*, 723-748, 1975.

Herman, J.R., and D. Larko, Low ozone amounts during 1992-1993 from Nimbus 7 and Meteor 3 total ozone mapping spectrometers, *J. Geophys. Res.*, *99*, 3483-3496, 1994.

Hofmann, D.J., Aircraft sulphur emissions, *Nature*, *349*, 659, 1991.

Hofmann, D.J., and S. Solomon, Ozone destruction through heterogeneous chemistry following the eruption of El Chichón, *J. Geophys. Res.*, *94*, 5029-5041, 1989.

Holton, J.R., On the global exchange of mass between the stratosphere and troposphere, *J. Atmos. Sci.*, *47*, 392-395, 1990.

Hood, L.L., R.D. McPeters, J.P. McCormick, L.E. Flynn, S.M. Hollandsworth, and J.F. Gleason, Altitude dependence of stratospheric ozone trends based on Nimbus 7 SBUV data, *Geophys. Res. Lett.*, *20*, 2667-2670, 1993.

Hou, A.Y., H.R. Schneider, and M.K.W. Ko, A dynamical explanation for the asymmetry in zonally-averaged column abundances of ozone between northern and southern springs, *J. Atmos. Sci.*, *48*, 547-556, 1991.

Huang, T.Y.W., and G. Brasseur, The effect of long-term solar variability in a two-dimensional interactive model of the middle atmosphere, *J. Geophys. Res.*, *98*, 20413-20427, 1993.

Isaksen, I.S.A., B. Rognerud, F. Stordal, M.T. Coffey, and W.G. Mankin, Studies of Arctic stratospheric ozone in a 2-D model including some effects of zonal asymmetries, *Geophys. Res. Lett.*, *17*, 557-560, 1990.

Jackman, C.H., Energetic particle influences on NO_y and ozone in the middle atmosphere, *Geophysical Monograph 75*, IUGG vol. 15, 131-139, 1993.

Jackman, C.H., J.E. Frederick, and R.S. Stolarski, Production of odd nitrogen in the stratosphere and mesosphere: An intercomparison of source strengths, *J. Geophys. Res.*, *85*, 7495-7505, 1980.

Jackman, C.H., A.R. Douglass, P.D. Guthrie, and R.S. Stolarski, The sensitivity of total ozone and ozone perturbation scenarios in a two-dimensional model due to dynamical inputs, *J. Geophys. Res.*, *94*, 9873-9887, 1989.

Jackman, C.H., A.R. Douglass, R.B. Rood, R.D. McPeters, and P.E. Meade, Effect of solar proton events on the middle atmosphere during the past two solar cycles as computed using a two-dimensional model, *J. Geophys. Res.*, *96*, 7417-7428, 1990.

Jackman, C.H., A.R. Douglass, S. Chandra, R.S. Stolarski, J.E. Rosenfield, and J.A. Kaye, Impact of interannual variability (1979-1986) of transport and temperature on ozone as computed using a two-dimensional photochemical model, *J. Geophys. Res.*, *96*, 5073-5079, 1991.

Johnston, H., G. Whitten, and J. Birks, Effect of nuclear explosions on stratospheric nitric oxide and ozone, *J. Geophys. Res.*, *78*, 6107-6135, 1973.

Johnston, P.V., R.L. McKenzie, J.G. Keys, and W.A. Matthews, Observations of depleted stratospheric NO_2 following the Pinatubo volcanic eruption, *Geophys. Res. Lett.*, *19*, 211-213, 1992.

Karol, I.L., Y.E. Ozolin, and E.V. Rozanov, Effect of space rocket launches on ozone, *Annales Geophysicae, 10,* 1810-1814, 1992.

Kawa, S.R., *et al.*, Photochemical partitioning of the reactive nitrogen and chlorine reservoirs in the high-latitude stratosphere, *J. Geophys. Res.*, *97*, 7905-7923, 1992.

Kawa, S.R., *et al.*, Interpretation of NO_x/NO_y observations from AASE-II using a model of chemistry along trajectories, *Geophys. Res. Lett.*, *20*, 2507-2510, 1993.

Kaye, J.A., *et al.*, Spatial and temporal variability of the extent of chemically processed stratospheric air, *Geophys. Res. Lett.*, *18*, 29-32, 1991.

Kaye, J.A., S.A. Penkett, and F.M. Ormond, eds., *Report on Concentrations, Lifetimes, and Trends of CFCs, Halons, and Related Species*, NASA Reference Publication 1339, 1994.

Khalil, M.A.K., and R.A. Rasmussen, The global sources of nitrous oxide, *J. Geophys. Res.*, *97*, 14651-14660, 1992.

Khalil, M.A.K., and R.A. Rasmussen, Decreasing trend of methane: Unpredictability of future concentrations, *Chemosphere*, *26*, 803-814, 1993.

Kiehl, J.T., B.A. Boville, and B.P. Briegleb, Response of a general circulation model to a prescribed Antarctic ozone hole, *Nature*, *332*, 501-504, 1988.

Kinne, S., O.B. Toon, and M.J. Prather, Buffering of stratospheric circulation by changing amounts of tropical ozone: A Pinatubo case study, *Geophys. Res. Lett.*, *19*, 1927-1930, 1992.

Kinnersley, J.S., and R.S. Harwood, An isentropic 2-dimensional model with an interactive parameterization of dynamical and chemical planetary-wave fluxes, *Quart. J. Roy. Meteorol. Soc.*, *119*, 1167-1193, 1993.

Kinnison, D.E., K.E. Grant, P.S. Connell, D.J. Wuebbles, and D.A. Rotman, The chemical radiative effects of the Mt. Pinatubo eruption, *J. Geophys. Res.*, in press, 1994.

Ko, M.K.W., M.B. McElroy, D.K. Weisenstein, and N.-D. Sze, Lightning: A possible source of stratospheric odd nitrogen, *J. Geophys. Res.*, *91*, 5395-5404, 1986.

Ko, M.K.W., H.R. Schneider, R.-L. Shia, D.K. Weisenstein, and N.-D. Sze, A two-dimensional model with coupled dynamics, radiation, and photochemistry: 1. Simulation of the middle atmosphere, *J. Geophys. Res.*, *98*, 20429-20440, 1993.

Kodera, K., Influence of the stratospheric circulation change on the troposphere in the northern hemisphere winter, in *The Role of the Stratosphere in Global Change*, edited by M.-L. Chanin, Springer-Verlag, 227-243, 1993.

Kodera, K., M. Chiba, K. Yamazaki, and K. Shiba, A possible influence of the polar night stratospheric jet on the subtropical tropospheric jet, *J. Meteorol. Soc. Japan*, *69*, 715-721, 1991.

Koike, M., *et al.*, Impact of Pinatubo aerosols on the partitioning between NO_2 and HNO_3, *Geophys. Res. Lett.*, *21*, 597-600, 1994.

Kotamarthi, V.R., M.K.W. Ko, D.K. Weisenstein, and N.-D. Sze, The effect of lightning on the concentration of odd nitrogen species in the lower stratosphere: An update, *J. Geophys. Res.*, *99*, 8167-8173, 1994.

Labitzke, K., and M.P. McCormick, Stratospheric temperature increases due to Pinatubo aerosols, *Geophys. Res. Lett.*, *19*, 207-210, 1992.

Lait, L.R., M.R. Schoeberl, and P.A. Newman, Quasi-biennial modulation of the Antarctic ozone depletion, *J. Geophys. Res.*, *94*, 11559-11571, 1989.

Lefèvre, F., G.P. Brasseur, I. Folkins, A.K. Smith, and P. Simon, Chemistry of the 1991-1992 stratospheric winter: Three-dimensional model simulations, *J. Geophys. Res.*, *99*, 8183-8195, 1994.

Legrand, M.R., F. Stordal, I.S.A. Isaksen, and B. Rognerud, A model study of the stratospheric budget of odd nitrogen, including effects of solar cycle variations, *Tellus*, *41B*, 413-426, 1989.

Liu, S.C., M. McFarland, D. Kley, O. Zafirious, and B. Huebert, Tropospheric NO_x and O_3 budgets in the equatorial Pacific, *J. Geophys. Res.*, *88*, 1360-1368, 1983.

Mahlman, J.D., J.P. Pinto, and L.J. Umscheid, Transport, radiative, and dynamical effects of the Antarctic ozone hole: A GFDL "SKYHI" model experiment, *J. Atmos. Sci.*, *51*, 489-508, 1994.

Mankin, M.G., M.T. Coffey, and A. Goldman, Airborne observations of SO_2, HCl, and O_3 in the stratospheric plume of the Pinatubo volcano in July 1991, *Geophys. Res. Lett.*, *19*, 179-182, 1992.

McConnell, J.C., and M.B. McElroy, Odd nitrogen in the atmosphere, *J. Atmos. Sci.*, *30*, 1464-1480, 1973.

McCormick, M.P., R.E. Veiga, and W.P. Chu, Stratospheric ozone profile and total ozone trends derived from the SAGE I and SAGE II data, *Geophys. Res. Lett.*, *19*, 269-272, 1992.

McElroy, M.B., and J.C. McConnell, Nitrous oxide: A natural source of stratospheric NO, *J. Atmos. Sci.*, *28*, 1095-1098, 1971.

McElroy, M.B., and R.J. Salawitch, Changing composition of the global stratosphere, *Science*, *243*, 763-770, 1989.

McElroy, M.B., R.J. Salawitch, and K. Minschwaner, The changing stratosphere, *Planet. Space Sci.*, *40*, 373-401, 1992.

Michelangeli, D.V., M. Allen, and Y.L. Yung, El Chichón volcanic aerosols: Impact of radiative, thermal, and chemical perturbations, *J. Geophys. Res.*, *94*, 18429-18443, 1989.

Mills, M.J., *et al.,* On the relationship between stratospheric aerosols and nitrogen dioxide, *Geophys. Res. Lett., 20,* 1187-1190, 1993.

Molina M.J., *et al.,* Physical chemistry of the H_2SO_4/HNO_3/H_2O system: Implications for polar stratospheric clouds, *Science, 261,* 1418-1423, 1993.

Murphy, D.M., and A.R. Ravishankara, Temperature averages and rates of stratospheric reactions, *Geophys. Res. Lett.*, in press, 1994.

Natarajan, M., and L.B. Callis, Stratospheric photochemical studies with Atmospheric Trace Molecule Spectroscopy (ATMOS) measurements, *J. Geophys. Res., 96,* 9361-9370, 1991.

Newman, P.A., M.R. Schoeberl, R.A. Plumb, and J.E. Rosenfield, Mixing rates calculated from potential vorticity, *J. Geophys. Res., 93,* 5221-5240, 1988.

Nicolet, M., On the production of nitric oxide in the stratosphere by cosmic rays in the mesosphere and stratosphere, *Planet. Space Sci., 23,* 637-649, 1975.

Nicoli, M.P., and G. Visconti, Impact of coupled perturbations of atmospheric trace gases on earth's climate and ozone, *Pure Appl. Geophys., 120,* 626-641, 1982.

Noxon, J.F., Atmospheric nitrogen fixation by lightning, *Geophys. Res. Lett., 3,* 463-465, 1976.

Oort, A.H., and H. Liu, Upper-air temperature trends over the globe, 1958-1989, *J. Climate, 6,* 292-307, 1993.

Park, C., and G.P. Menees, Odd nitrogen production by meteoroids, *J. Geophys. Res., 83,* 4029-4035, 1978.

Patten, K.O., Jr., P.S. Connell, D.E. Kinnison, D.J. Wuebbles, T.G. Slanger, and L. Froidevaux, Effect of vibrationally excited oxygen on ozone production in the stratosphere, *J. Geophys. Res., 99,* 1211-1224, 1994.

Peter, T., C. Brühl, and P.J. Crutzen, Increase in the PSC formation probability caused by high-flying aircraft, *Geophys. Res. Lett., 18,* 1465-1468, 1991.

Pitari, G., Contribution to the ozone trend of heterogeneous reactions of $ClONO_2$ on the sulfate aerosol layer, *Geophys. Res. Lett., 20,* 2663-2666, 1993a.

Pitari, G., A numerical study of the possible perturbation of stratospheric dynamics due to Pinatubo aerosols: Implications for tracer transport, *J. Atmos. Sci., 50,* 2443-2461, 1993b.

Pitari, G., S. Palermi, G. Visconti, and R. Prinn, Ozone response to a CO_2 doubling: Results from a stratospheric circulation model with heterogeneous chemistry, *J. Geophys. Res., 97,* 5953-5962, 1992.

Pitari, G., and V. Rizi, An estimate of the chemical and radiative perturbation of stratospheric ozone following the eruption of Mt. Pinatubo, *J. Atmos. Sci., 50,* 3260-3276, 1993.

Pitari, G., V. Rizi, L. Ricciardulli, and G. Visconti, High speed civil transport impact: Role of sulfate, nitric acid trihydrate and ice aerosols studied with a two-dimensional model including aerosol physics, *J. Geophys. Res., 98,* 23141-23164, 1993.

Planet, W.G., *et al.,* Northern hemisphere total ozone values from 1989-1993 determined with the NOAA-11 Solar Backscatter Ultraviolet (SBUV/2) instrument, *Geophys. Res. Lett., 21,* 205-208, 1994.

Plumb, R.A., and M.K.W. Ko, Interrelationships between mixing ratios of long-lived stratospheric constituents, *J. Geophys. Res., 97,* 10145-10156, 1992.

Prather, M.J., Catastrophic loss of stratospheric ozone in dense volcanic clouds. *J. Geophys. Res., 97,*10187-10191, 1992.

Prather, M., and A.H. Jaffe, Global impact of the Antarctic ozone hole: Chemical propagation, *J. Geophys. Res., 95,* 3473-3492, 1990.

Prather, M.J., M.M. Garcia, A.R. Douglass, C.H. Jackman, M.K.W. Ko, and N.-D. Sze, The space shuttle's impact on the stratosphere, *J. Geophys. Res., 95,* 18583-18590, 1990a.

Prather, M., M.M. Garcia, R. Suozzo, and D. Rind, Global impact on the Antarctic ozone hole: Dynamical dilution with a three-dimensional chemical transport model, *J. Geophys. Res., 95,* 3449-3471, 1990b.

Prather, M.J., *et al., The Atmospheric Effects of Stratospheric Aircraft: A First Program Report,* NASA Reference Publication 1272, 46-50, January 1992.

Prather, M.J., and E.E. Remsburg, eds., *The Atmospheric Effects of Stratospheric Aircraft: Report of the 1992 Models and Measurements Workshop,* NASA Reference Publication 1292, Vol. 1, National Aeronautics and Space Administration, Washington, D.C., 1993.

Ramaswamy, V.M., D. Schwarzkopf, and K.P. Shine, Radiative forcing of climate from halocarbon-induced global stratospheric ozone loss, *Nature*, *355*, 810-812, 1992.

Reinsel, G.C., *et al.,* Statistical analysis of total ozone and stratospheric umkehr data for trends and solar cycle relationship, *J. Geophys. Res.*, *92*, 2201-2209, 1987.

Reinsel, G.C., *et al.,* Seasonal trend analysis of published ground-based and TOMS total ozone data through 1991, *J. Geophys. Res., 99,* 5449-5464, 1994.

Rind, D., R. Suozzo, N.K. Balachandran, and M.J. Prather, Climate change and the middle atmosphere. Part I: The doubled CO_2 climate, *J. Atmos. Sci.*, *47*, 475-494, 1990.

Rinsland, C.P., *et al.,* Heterogeneous conversion of N_2O_5 to HNO_3 in the post-Mt. Pinatubo eruption stratosphere, *J. Geophys. Res.*, *99*, 8213-8219, 1994.

Rodriguez J.M., M.K.W. Ko, and N.-D. Sze, The role of heterogeneous conversion of N_2O_5 on sulphate aerosols in global ozone losses, *Nature*, *352*, 134, 1991.

Rodriguez, J.M., M.K.W. Ko, N.-D. Sze, C.E. Heisey, G.K. Yue, and M.P. McCormick, Ozone response to enhanced heterogeneous processing after the eruption of Mt. Pinatubo, *Geophys. Res. Lett., 21*, 209-212, 1994.

Rood, R., D.J. Allen, W.E. Baker, D.J. Lamich, and J.A. Kaye, The use of assimilated stratospheric data in constituent transport calculations, *J. Atmos. Sci.*, *46*, 687-701, 1989.

Rood, R.B., *et al.,* Three-dimensional simulations of wintertime ozone variability in the lower stratosphere, *J. Geophys. Res.*, *96*, 5055-5071, 1991.

Rosenfield, J.E., M.R. Schoeberl, and M.A. Geller, A computation of the stratospheric diabatic circulation using an accurate radiative transfer model, *J. Atmos. Sci.*, *44*, 859-876, 1987.

Russell, J.M., III, S. Solomon, L.L. Gordley, E.E. Remsberg, and L.B. Callis, The variability of stratospheric and mesospheric NO_2 in the polar winter night observed by LIMS, *J. Geophys. Res.*, *89*, 7267-7275, 1984.

Sanders, R.W., *et al.,* Visible and near-ultraviolet spectroscopy at McMurdo Station, Antarctica, 9. Observations of OClO from April to October 1991, *J. Geophys. Res.*, *98*, 7219-7228, 1993.

Schneider, H.R., M.K.W. Ko, and C.A. Peterson, Interannual variations of ozone: Interpretation of 4 years of satellite observations of total ozone, *J. Geophys. Res.*, *96*, 2889-2896, 1991.

Schneider, H.R., M.K.W. Ko, R.-L. Shia, and N.-D. Sze, A two-dimensional model with coupled dynamics, radiative transfer, and photochemistry, 2. Assessment of the response of stratospheric ozone to increased levels of CO_2, N_2O, CH_4, and CFC, *J. Geophys. Res.*, *98*, 20441-20449, 1993.

Schoeberl, M.R., P.K. Bhartia, and E. Hilsenrath, Tropical ozone loss following the eruption of Mt. Pinatubo, *Geophys. Res. Lett.*, *20*, 29-32, 1993.

Slanger, T.G., L.E. Jusinski, G. Black, and G.E. Gadd, A new laboratory source of ozone and its potential atmospheric implications, *Science, 241*, 945-950, 1988.

Solomon, S., Antarctic ozone: Progress toward a quantitative understanding, *Nature*, *347*, 347-354, 1990.

Solomon, S., P.J. Crutzen, and R.G. Roble, Photochemical coupling between the thermosphere and the lower atmosphere, 1. Odd nitrogen from 50 to 120 km, *J. Geophys. Res.*, *87*, 7206-7220, 1982.

Solomon, S., R.W. Sanders, R.R. Garcia, and J.G. Keys, Increased chlorine dioxide over Antarctica caused by volcanic aerosols from Mt. Pinatubo, *Nature*, *363*, 245-248, 1993.

Solomon, S., R.R. Garcia, and A.R. Ravishankara, On the role of iodine in ozone depletion, *J. Geophys. Res., 99,* 20491-20500, 1994a.

Solomon, S., *et al.,* Visible and near-ultraviolet spectroscopy at McMurdo Station, Antarctica 10. Reductions of stratospheric NO_2 due to Pinatubo aerosols, *J. Geophys. Res.*, in press, 1994b.

Spencer, R.W., and J.R. Christy, Precision lower stratospheric temperature monitoring with the MSU: Technique, validation and results 1979-1991, *J. Climate, 6*, 1194-1204, 1993.

Stachnik, R.A., J.C. Hardy, J.A. Tarsala, J.W. Waters, and N.R. Erickson, Submillimeterwave heterodyne measurements of stratospheric ClO, HCl, O_3 and HO_2: First results, *Geophys. Res. Lett.*, *19*, 1931-1934, 1992.

Stolarski, R., R. Bojkov, L. Bishop, C. Zerefos, J. Staehelin, and J. Zawodny, Measured trends in stratospheric ozone, *Science*, *256*, 342-349, 1992.

Strobel, D.F., Odd nitrogen in the mesosphere, *J. Geophys. Res.*, *76*, 8384-8393, 1971.

Sze, N.-D., M.K.W. Ko, D.K. Weisenstein, J.M. Rodriguez, R.S. Stolarski, and M.R. Schoeberl, Antarctic ozone hole: Possible implications for ozone trends in the Southern Hemisphere, *J. Geophys. Res.*, *94*, 11521-11528, 1989.

Tabazadeh, A., and R.P. Turco, Stratospheric chlorine injection by volcanic eruptions: HCl scavenging and implications for ozone, *Science*, *260*, 1082-1086, 1993.

Tie, X., G.P. Brasseur, B. Briegleb, and C. Granier, Two-dimensional simulation of Pinatubo aerosol and its effect on stratospheric ozone, *J. Geophys. Res.*, *99*, 20545-20562, 1994.

Tolbert, M.A., J. Pfaff, I. Jayaweera, and M.J. Prather, Uptake of formaldehyde by sulfuric acid solutions: Impact on stratospheric ozone, *J. Geophys. Res.*, *98*, 2957-2962, 1993.

Toon, O., *et al.*, Heterogeneous reaction probabilities, solubilities and physical state of cold volcanic aerosols, *Science*, *261*, 1136-1140, 1993.

Toumi, R., An evaluation of autocatalytic ozone production from vibrationally excited oxygen in the middle atmosphere, *J. Atmos. Chem.*, *15*, 69-77, 1992.

Toumi, R., A potential new source of OH and odd-nitrogen in the atmosphere, *Geophys. Res. Lett.*, *20*, 25-28, 1993.

Toumi, R., and S. Bekki, The importance of the reactions between OH and ClO for stratospheric ozone, *Geophys. Res. Lett.*, *20*, 2447-2450, 1993.

Toumi, R., B.J. Kerridge, and J.A Pyle, Highly vibrationally excited oxygen as a potential source of ozone in the upper stratosphere and mesosphere, *Nature*, *351*, 217-219, 1991.

Toumi, R., R.L. Jones, and J.A. Pyle, Direct stratospheric ozone depletion by $ClONO_2$ photolysis, *Nature*, *365*, 37-39, 1993.

Tuck, A.F., Production of nitrogen oxides by lightning discharges, *Quart. J. Roy. Meteorol. Soc.*, *102*, 749-755, 1976.

Tung, K.K., and H. Yang, Dynamical component of seasonal and year-to-year changes in Antarctic and global ozone, *J. Geophys. Res.*, *93*, 12537-12559, 1988.

Vupputuri, R.K.R., The structure of the natural stratosphere and the impact of chlorofluoromethanes on the ozone layer investigated in a 2-D time dependent model, *Pure Appl. Geophys.*, *117*, 448-485, 1978.

Wallace, L., and W. Livingston, The effect of the Pinatubo cloud on hydrogen chloride and hydrogen fluoride, *Geophys. Res. Lett.*, *19*, 1209, 1992.

Wang, W.-C., Y.-C. Zhuang, and R.D. Bojkov, Climate implications of observed changes in ozone vertical distributions at middle and high latitudes of the northern hemisphere, *Geophys. Res. Lett.*, *20*, 1567-1570, 1993.

Warneck, P., Cosmic radiation as a source of odd nitrogen in the stratosphere, *J. Geophys. Res.*, *77*, 6589-6591, 1972.

Webster, C.R., R.D. May, M. Allen, L. Jaegle, and M.P. McCormick, Balloon profiles of stratospheric NO_2 and HNO_3 for testing the heterogeneous hydrolysis of N_2O_5 on sulfate aerosols, *Geophys. Res. Lett.*, *21*, 53-56, 1994.

Weisenstein, D., M.K.W. Ko, J.M. Rodriguez, and N.-D. Sze, Impact of heterogeneous chemistry on model-calculated ozone change due to high speed civil transport aircraft, *Geophys. Res. Lett.*, *18*, 1991-1994, 1991.

Weisenstein, D., M.K.W. Ko, and N.-D. Sze, The chlorine budget of the present-day atmosphere: A modeling study, *J. Geophys. Res.*, *97*, 2547-2559, 1992.

Weisenstein, D.K., M.K.W. Ko, J.M. Rodriguez, and N.-D. Sze, Effects on stratospheric ozone from high-speed civil transport: Sensitivity to stratospheric aerosol loading, *J. Geophys. Res.*, *98*, 23133-23140, 1993.

Wennberg, P.O., *et al.*, Removal of stratospheric O_3 by free radicals: In situ measurements of OH, HO_2, NO, NO_2, ClO and BrO, *Science*, *266*, 398-404, 1994.

Wilson, J.C., *et al.*, In situ observations of aerosol and chlorine monoxide after the 1991 eruption of Mt. Pinatubo: Effects of reactions on sulfate aerosol, *Science*, *261*, 1140-1143, 1993.

Woodbridge, E.L., *et al.,* Estimates of total organic and inorganic chlorine in the lower stratosphere from in situ measurements during AASE II, *J. Geophys. Res.*, in press, 1994.

WMO, *Report of the International Ozone Trends Panel: 1988,* World Meteorological Organization Global Ozone Research and Monitoring Project – Report No. 18, Washington, D.C., 1990.

WMO, *Scientific Assessment of Ozone Depletion: 1991*, World Meteorological Organization Global Ozone Research and Monitoring Project – Report No. 25, Geneva, 1992.

Yang, H., E. Olaguer, and K.K. Tung, Simulation of the present-day atmospheric ozone, odd nitrogen, chlorine and other species using a coupled 2-D model in isentropic coordinates, *J. Atmos. Sci., 48*, 442-471, 1991.

Zadorozhny, A.M., G.A. Tuchkov, V.N. Kikhtenko, J. Lastovicka, J. Boska, and A. Novak, Nitric oxide and lower ionosphere quantities during solar particle events of October 1989 after rocket and ground-based measurements, *J. Atmos. Terr. Phys., 54*, 183-192, 1992.

Zander, R., M.R. Gunson, J.C. Foster, C.P. Rinsland, and J. Namkung, Stratospheric $ClONO_2$, HCl and HF concentration profiles derived from Atmospheric Trace Molecule Spectroscopy experiment Spacelab 3 observations: An update, *J. Geophys. Res., 95*, 20519-20525, 1990.

Zerefos, C.S., A.F. Bais, I.C. Ziomas, and R.D. Bojkov, On the relative importance of quasi-biennial oscillation and El Niño/Southern Oscillation in the revised Dobson total ozone records, *J. Geophys. Res., 97*, 10135-10144, 1992.

CHAPTER 7

Model Simulations of Global Tropospheric Ozone

Lead Author:
F. Stordal

Co-authors:
R.G. Derwent
I.S.A. Isaksen
D. Jacob
M. Kanakidou
J.A. Logan
M.J. Prather

Contributors:
T. Berntsen
G.P. Brasseur
P.J. Crutzen
J.S. Fuglestvedt
D.A. Hauglustaine
C.E. Johnson
K.S. Law
J. Lelieveld
J. Richardson
M. Roemer
A. Strand
D.J. Wuebbles

CHAPTER 7

MODEL SIMULATIONS OF GLOBAL TROPOSPHERIC OZONE

Contents

SCIENTIFIC SUMMARY

Simulations of chemical tracers and comparison with observations indicate that global three-dimensional (3-D) models are able to describe gross features of atmospheric transport, such as boundary layer ventilation and long-range transport from continents to oceans. The broad distributions of the tropospheric ozone, such as altitudinal and seasonal variation, are captured to within about a factor 2. Important inaccuracies still remain: stratospheric/tropospheric exchange, natural emissions of precursors (*e.g.*, NO_x from lightning), reactions in aerosols and clouds, and representation of processes not resolved at the scale of models.

Three-dimensional simulations of O_3 over polluted continents have shown some success in reproducing observed distributions of ozone, NO_x, NO_y, and hydrocarbons under conditions where emissions and meteorology are well characterized.

Models and analyses of observations show evidence for a large anthropogenic contribution to tropospheric ozone in the Northern Hemisphere (NH). A few global model studies report that tropospheric ozone has increased by more than 50% since pre-industrial times over large regions of the NH lower and middle troposphere.

The global mean hydroxyl radical (OH) concentrations predicted by a variety of 2-D and 3-D models are within a factor 1.3 of the values that have been derived from budget studies of methyl chloroform (CH_3CCl_3) and hydrochlorofluorocarbons (HCFCs), and are also consistent with analysis of ^{14}CO.

Two model intercomparison exercises have been conducted to test the ability of models to simulate a) the transport of short-lived tracers and b) basic features of O_3 photochemistry. More than twenty models participated. A high degree of consistency was found in the global transport of a short-lived tracer within the 3-D chemistry transport models (CTMs). General agreement was also found in the computation of photochemical rates affecting tropospheric O_3. These are the first extensive intercomparisons of global tropospheric models.

2-D tropospheric chemistry models capture the coarse features of the ozone distribution and are useful for some analyses. Quantitative assessments based on these models will remain highly uncertain. The model intercomparison cited above showed that 2-D models cannot transport short-lived species in the same manner or magnitude as 3-D models.

A set of five 2-D and 3-D models predicted the O_3 change expected for a 20% increase in methane (CH_4) concentration. All models predicted small tropospheric O_3 increases, ranging from 0.5 to 2.5 ppb in the tropics and the midlatitude northern summer. The large range in the results demonstrates the large uncertainty in quantitative assessment. All models predicted an increase in the effective CH_4 lifetime.

These simulations and a theoretical analysis of the tropospheric chemical system coupling CH_4, CO, and OH have shown that CH_4 perturbations decay with a lengthened time scale, about 13.6 (11.3-16.0) yr, as compared with the lifetime derived from total abundance and losses, about 9.4 yr. This longer residence time describes the decay of any reasonably sized methane pulse, including all associated perturbations to tropospheric O_3 and stratospheric H_2O. It also increases our estimate of the greenhouse effectiveness of CH_4 emissions by a factor 1.45 as compared with previous assessments.

7.1 INTRODUCTION

Tropospheric models contain mathematical formulations of the life cycles of the major tropospheric source gases and the photochemistry, transport, and surface exchange processes that couple them together and to the life cycle of tropospheric ozone. They are used to quantify the importance of the various terms in the life cycles and budgets for ozone as well as for methane and other ozone precursors. They allow an estimation of the concentration distribution of the main tropospheric oxidant, the hydroxyl (OH) radical in the troposphere, and of the processes by which it is controlled. The strong chemical tie between ozone and several other climate gases causes tropospheric ozone to be very important in the regulation of the Earth's climate. This indirect climatic role of ozone comes in addition to the direct climate effect of ozone due to its radiative properties.

The processes governing the tropospheric ozone budget are described in Chapter 5 and summarized in Figure 7-1. A substantial amount of the tropospheric ozone is produced in the stratosphere and transported to the troposphere at high and middle latitudes. The *in situ* photochemical production is several times larger than the import from the stratosphere, but is to a large extent counteracted by chemical loss. The relative importance of these processes to the ozone budget remains a topic for future research. In the boundary layer, ozone is deposited at the surface and produced on urban and regional scales that are not adequately resolved in global models. Transport processes, especially vertical transport of O_3 and its shorter-lived precursors such as NO_x (=NO+NO_2) and non-methane hydrocarbons (NMHC), affect tropospheric chemistry and determine the level of change in O_3 concentration in the upper troposphere, thereby strongly influencing the global budget of tropospheric ozone.

The development of our understanding of the tropospheric chemistry of ozone has been driven forward

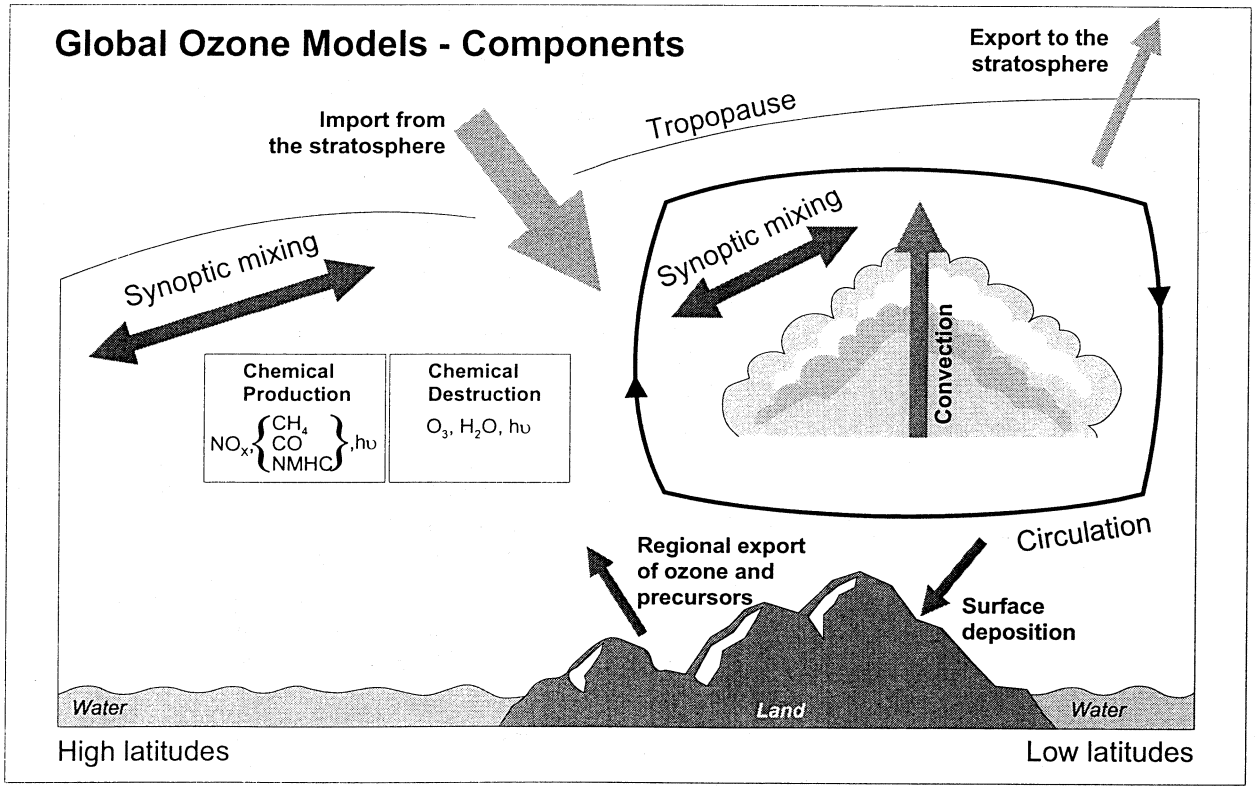

Figure 7-1. Processes governing the global tropospheric ozone budget. The major components are import of ozone from the stratosphere, chemical production and loss, deposition at the ground, and ozone production on the smaller urban and regional scales.

by a combination of careful field observation, laboratory investigation, and theoretical modeling. Modeling may point to hitherto undiscovered relationships between trace gases and processes, and observations can challenge our theoretical understanding, leading to the development of a more complete explanation of atmospheric systems.

Recently, theoretical modeling has been given heightened importance, particularly for ozone, through its role in explaining the relationship between atmospheric composition and the emissions of trace gases from human activities. Theoretical modeling offers the prospect of being able to unravel the cause of the trends and the possible role of human activities in them. This naturally leads to an important question as to whether any of these observed trends will continue in the foreseeable future. Furthermore, models offer the possibility to estimate future changes in ozone resulting from changes in emissions of ozone precursors.

Whether any of the conclusions derived from models concerning trends in ozone concentrations actually describe what happens in the real atmosphere depends on the adequacy and completeness of their formulation, which is tied to our understanding of physical and chemical processes in the troposphere, as well as on the accuracy of their input data. Testing of models involves comparison with observations, which are inevitably limited in their accuracy and coverage in space or time. In a complex model, it is difficult to explain the good agreement with observations often found in some atmospheric regions for some species and the rather poorer agreement sometimes found elsewhere. Tropospheric models are in their infancy at present; the global data sets required to validate them adequately are not yet available, nor is the computer capacity to handle all the processes that are believed to be important.

This chapter briefly surveys, in Section 7.2, the successes and problems revealed in recent 3-D model simulations of transport and chemistry in the troposphere. Most attention has been devoted to global models. In order to successfully model troposphere ozone globally, it is necessary to describe regional ozone, since the global picture is only a conjunction of regional parts. A few recent continental-scale model studies are therefore also assessed in Section 7.2.

A range of global-scale models have been used for studies of tropospheric ozone. Section 7.3 presents a short compilation of such 2-D and 3-D models. The section compares the zonally averaged ozone distribution and budget terms for stratosphere/troposphere exchange fluxes, chemical production and loss, and surface deposition in several of the models currently used for global ozone studies. A survey of the major limitations in current models is also included in Section 7.3, whereas Section 7.4 presents global model integration of some selected applications of key relevance for past, current, and future tropospheric ozone.

As a part of the IPCC (1994) assessment as well as this assessment (Section 7.5), a comparison of global chemical models, that were used to calculate the effects of changes in methane (CH_4) on chemistry and climate forcing, was performed. Two standard atmospheric simulations were specified as part of the model intercomparison: global transport of short-lived gases, and photodissociation and chemical tendencies in tropospheric air parcels.

A third model intercomparison on simulation of a methane increase in today's atmosphere (also a part of IPCC, 1994) is also included in Section 7.5. This serves as the only example in this chapter of possible future changes in tropospheric ozone due to changes in ozone precursors. The previous ozone assessment (WMO, 1992) includes a thorough discussion of future changes in ozone due to changes in several precursor gases.

7.2 3-D SIMULATIONS OF THE PRESENT-DAY ATMOSPHERE: EVALUATION WITH OBSERVATIONS

7.2.1 Atmospheric Transport

Transport of chemical species in global 3-D models includes terms from both the grid-resolved circulation (winds) and from parameterized subgrid processes (convection, small-scale eddies). A number of recent studies have used chemical tracers with well-known sources and sinks to test specific features of model transport: interhemispheric exchange with chlorofluorocarbons (CFCs) and ^{85}Kr (Prather *et al.*, 1987; Jacob *et al.*, 1987); convection over continents and long-range transport of continental air to the oceans with ^{222}Rn (Jacob and Prather, 1990; Feichter and Crutzen, 1990; Balkanski and Jacob, 1990; Balkanski *et al.*, 1992); transport and deposition of aerosols with ^{210}Pb and ^{7}Be

(Brost *et al.*, 1991; Feichter *et al.*, 1991; Balkanski *et al.*, 1993). These simulations show that global 3-D models can provide a credible representation of atmospheric transport on both global and regional scales. Some major difficulties remain in simulating subgrid processes involved in interhemispheric exchange, convective mass transport, and wet deposition of aerosols. Work is also needed to test the simulation of stratosphere-troposphere exchange; chemical tracers such as bomb-generated $^{14}CO_2$ can be used for that purpose.

7.2.2 Nitrogen Oxides

Global 3-D simulations of NO_x and nitric acid (HNO_3) including sources from combustion, lightning, soils, and stratospheric injection have been reported by Crutzen and Zimmerman (1991) and Penner *et al.* (1991). The Geophysical Fluid Dynamics Laboratory (GFDL) 3-D model with three transported species (NO_x, peroxyacetyl nitrate (PAN), and HNO_3) has been used to simulate the global distributions of NO_y and individual reactive nitrogen species resulting from stratospheric injection (Kasibhatla *et al.*, 1991), fossil fuel combustion (Kasibhatla *et al.*, 1993), and aircraft (Kasibhatla, 1993). The same model including all sources of NO_x has been used to simulate the pre-industrial, present, and future deposition of nitrate (Galloway *et al.*, 1994) and the impact of pollution-generated O_3 on the world's crop production (Chameides *et al.*, 1994). The Oslo 3-D model has been used to study the global distribution of NO_x and NO_y (Berntsen and Isaksen, 1994).

The models of NO_x and NO_y have been, in general, fairly successful at reproducing observations in polluted regions. Concentrations of NO_x in remote regions of the troposphere (*e.g.*, the south Pacific) tend to be underestimated, sometimes by more than an order of magnitude. Possible explanations include an underestimate of the lightning source (Penner *et al.*, 1991), and chemical cycling between NO_x and its oxidation products by mechanisms that are not yet well understood (Chatfield, 1994; Fan *et al.*, 1994).

7.2.3 Hydroxyl Radical

Estimates of the global OH distribution have been made in a number of 3-D model studies of long-lived gases removed from the atmosphere by reaction with OH (Spivakovsky *et al.*, 1990a, b; Crutzen and Zimmerman, 1991; Fung *et al.*, 1991; Tie *et al.*, 1992; Easter *et al.*, 1993; Berntsen and Isaksen, 1994). These estimates have generally been done by using climatological distributions for the principal chemical variables involved in OH production and loss (O_3, NO_x, CO, CH_4) and computing OH concentrations with a photochemical model. Exceptions are the works of Crutzen and Zimmerman (1991) and Berntsen and Isaksen (1994), where O_3 and NO_x concentrations were computed within the model in a manner consistent with the computation of OH concentrations. The accuracy of the global mean OH concentration obtained by the various models appears to be within 30%, as indicated by simulations of methyl chloroform, CH_3CCl_3 (Spivakovsky *et al.*, 1990a; Tie *et al.*, 1992). The seasonality of OH at midlatitudes appears to be well captured, as indicated by a recent simulation of ^{14}CO (Spivakovsky and Balkanski, 1994).

7.2.4 Continental-Scale Simulations of Ozone

The budget of ozone over the North American continent in summer was examined recently using the results of a 3-D model simulation (Jacob *et al.*, 1993a, b). The model was evaluated by comparison with measurements of ozone, NO_x, carbon monoxide (CO), and hydrocarbons. The model captures successfully the development of regional high-ozone episodes over the eastern U.S. on the back side of weak, warm, stagnant anticyclones. Ozone production over the U.S. is strongly NO_x-limited, reflecting the dominance of rural areas as sources of ozone on the regional scale. About 70% of the net ozone production in the U.S. boundary layer is exported, while the rest is deposited within the region. Only 6% of NO_x emitted in the U.S. is exported out of the boundary layer as NO_x or peroxy-acyl nitrates (*e.g.*, PAN), but this export contributes disproportionately to the U.S. influence on global tropospheric ozone because of the high ozone production efficiency per unit NO_x in remote air. Jacob *et al.* (1993b) estimate that export of U.S. pollution supplies 35 Tg ozone to the global troposphere in summer (90 days), half of which is produced downwind of the U.S., following export of NO_x. Recent comparison of O_3-CO correlation in the model and in the observations at sites in the United States and downwind lends support to the model estimate for export of O_3 pollution from North America (Chin *et al.*, 1994).

The ozone model of EMEP MSC-W (European Monitoring and Evaluation Programme, Meteorological

Synthesizing Centre-West) has been used to study photochemistry over Europe for two extended summer periods in 1985 and 1989 (Simpson, 1993), in combination with observations made in the EMEP program. The model describes the boundary layer, combining trajectories in a regular geographical grid over Europe. It is different from the models listed in Table 7-1, and is limited in the context of large-scale ozone modeling mainly by its neglect of explicit representation of free tropospheric processes. Significant differences in the concentrations of the photo-oxidants were observed and modeled between the two summer seasons that were studied. The modeled ozone concentrations compare satisfactorily with observations, particularly in 1989. The study showed that NO_x limits ozone formation in the European boundary layer in most locations, whereas NMHCs limit the production mostly in polluted areas.

Flatøy *et al.* (1994) present results from a set of simulations with a three-dimensional mesoscale chemistry transport model driven by meteorological data from a numerical weather prediction model with an extensive treatment of cloud physics and precipitation processes. New formulations for the vertical transport of chemical tracers in connection with convective plumes and the compensating sinking motion, and the calculation of photolysis rates in clouds, are employed. The chemistry transport model is used to calculate ozone and other chemical species over Europe over a 10-day period in July 1991, characterized by warm weather and frequent cumulus episodes. When modeled vertical ozone profiles are compared to ozone soundings, better correlation is found than for calculation without convection, indicating that physical processes, especially convection, can dominate in the vertical distribution of ozone in the free troposphere, and that sinking air that compensates for convective updrafts is important for the tropospheric ozone budget.

7.3 CURRENT TROPOSPHERIC OZONE MODELING

Modeling tropospheric ozone is probably one of the most difficult tasks in atmospheric chemistry. This is due not only to the large number of processes that control tropospheric ozone, but even more to interactions of processes occurring on different spatial and temporal scales (Section 7.1, Figure 7-1). The field of tropospheric ozone modeling is currently under rapid development.

To cover various spatial scales with limited computer resources, different types of models have been used. 2-D models have been widely used for several years to study tropospheric ozone on a global scale. 3-D models covering the global scale have only recently been developed. An accurate representation of the 3-D transport is needed in models, especially in order to describe distributions of species with a chemical lifetime of the order of days or weeks (like NO_x and ozone) in areas where the transport is efficient, as, *e.g.*, in convective cells.

7.3.1 Global and Continental-Scale Models

Categories of Models

Several chemistry transport models (CTMs) have been used to study ozone and precursor molecules in the troposphere and in general to understand processes and budgets of atmospheric constituents. A list of models is given in Table 7-1, where models have been grouped in four categories.

The first group is 2-D zonally averaged models. Such models have been used for several years to study global distributions of ozone and precursors in the current atmosphere. To represent the various processes explained in Figure 7-1, they contain detailed and relatively similar schemes of ozone photochemistry. The transport is described by a meridional circulation, and relatively large diffusion is included to account for transport due to wave activity. Only a few 2-D models represent convection explicitly. Most of the models have been used to study changes in ozone, some in the past and most of the models in the future, due to changes in emissions of ozone precursors (NO_x, CH_4, CO, NMHC; see Figure 7-1) and in physical variables such as temperature, water vapor, and UV radiation. With currently available computing resources, such models can, *e.g.*, be used to predict ozone changes over several decades for a range of trace gas emission scenarios.

The next three categories contain 3-D models. One group of 3-D models uses monthly averaged wind fields to transport tracers, and therefore also need relatively efficient diffusion to account for transport due to winds that change on a day-to-day basis. However, the

Table 7-1. Current 2-D (global) and 3-D (global and mesoscale) Chemistry-Transport Models.

Model	References
2-D models	
UK Met Office	Derwent (1994)
Harwell	Johnson (1993); Johnson *et al.* (1992)
Univ Cambridge	Law and Pyle (1993a, b)
Univ Oslo	Fuglestvedt *et al.* (1994a, b)
Univ Bergen	Strand and Hov (1993; 1994)
TNO	Roemer and van der Hout (1992)
NCAR/CNRS	Hauglustaine *et al.* (1994)
MPI-tropo	Singh and Kanakidou (1993); Kanakidou *et al.* (1991)
LLNL	Wuebbles *et al.* (1993); Patten *et al.* (1994)
3-D monthly average	
Moguntia	Lelieveld (1994)
Images	Müller and Brasseur (1994)
3-D synoptic global	
LLNL	Penner *et al.* (1991; 1994)
GFDL/GIT	Kasibhatla *et al.* (1991; 1993)
GISS/Harvard	Spivakovsky *et al.* (1990a, b)
Univ Oslo	Berntsen and Isaksen (1994)
3-D synoptic mesoscale	
GISS/Harvard	Jacob *et al.* (1993a, b)
Univ Bergen	Flatøy (1994); Flatøy *et al.* (1994)

TNO = Netherlands Organization for Applied Scientific Research; NCAR = National Center for Atmospheric Research; CNRS = Centre National de la Recherche Scientifique; MPI = Max-Planck Institute; LLNL = Lawrence Livermore National Laboratory; GFDL = Geophysical Fluid Dynamics Laboratory; GIT = Georgia Institute of Technology; GISS = Goddard Institute for Space Studies

models in this category include detailed photochemical schemes. In the last two categories, the models use daily varying windfields and describe either the global scale or mesoscales. Only recently, 3-D models of this category have been developed to include detailed ozone chemistry. Applications and further development of such models are expected in the near future. Some models included in Table 7-1 have been used to study other trace gases, *e.g.*, NO_y. Work is currently going on to include ozone chemistry in some of these models.

Modeled Ozone Distributions

Zonally averaged ozone distributions from several of the models listed in Table 7-1 are shown in Figure 7-2. The distributions that are shown are all for near-solstice conditions, for January and July. Although all model results represent the current atmosphere, there are differences between the models in the choices of boundary conditions and in the emissions of chemical ozone precursors.

The models agree on the general feature of the zonally averaged ozone distribution. The vertical distri-

bution, with maximum values in the upper troposphere and minimum values at the surface, reflects mainly the import of ozone from the stratosphere and deposition at the ground. It is also clear that current global tropospheric ozone models are able to reproduce gross features of observed ozone distributions (see Section 7.5.3 below).

The modeled mixing ratios in the tropics at the 10 km level are in the range 40-60 ppb and the boundary layer values about 10-30 ppb. Generally the models give higher ozone mixing ratios over the Northern Hemisphere (NH) than over the Southern Hemisphere (SH) during summertime. The modeled ozone levels in the lowest few kilometers at northern middle latitudes are in the range 30-50 ppb in July. In January the corresponding values are 10-30 ppb in the SH. Comparison and interpretation of the ozone levels in the region of largest importance for radiative forcing (upper troposphere/lower stratosphere) are difficult due to insufficient information about the tropopause levels in the models. The ozone levels in this region are to a high degree determined by processes in the lower stratosphere, where ozone mixing ratios or fluxes through the tropopause are fixed in most models. The latitudinal distribution varies considerably between the models, reflecting clearly the efficiency of the horizontal diffusion adopted in the model, as discussed below in Section 7.5.2, with the least latitudinal gradients in some of the 2-D models.

Global Ozone Budgets

From some of the models listed in Table 7-1, global budget numbers are available that can be used to explore the relative roles of the processes governing tropospheric ozone, as explained in Figure 7-1. Stratosphere/troposphere exchange, photochemical reactions, and surface deposition are identified as the three major classes of processes governing the tropospheric ozone budget. There are substantial differences between the relative importance of these processes, in the way they are represented in current models, as can be seen from Table 7-2.

There is a factor 3 spread in the stratosphere/troposphere exchange fluxes and the surface deposition values between the models. This merely reflects the large uncertainty in our knowledge of the efficiency of these processes. The models usually either fix the flux through the tropopause or fix the ozone mixing ratios in the lower stratosphere, strongly tying the flux to observations. The most recent estimate of the ozone flux across the tropopause is based on aircraft measurements (Murphy *et al.*, 1993; see discussion in Chapter 5), yielding values in the range 240-820 Tg (O_3)/yr, which are comparable with or slightly less than previous estimates (Danielsen and Mohnen, 1977; Gidel and Shapiro, 1980; Mahlman *et al.*, 1980; see also Chapter 5). The spread in values for surface deposition is presumably reflecting differences in, *e.g.*, vertical transport through the boundary layer. Observations that can narrow the uncertainty in its efficiency do not exist. There is currently therefore little basis for judging which models calculate the most realistic tropospheric ozone budget terms.

The even larger differences in the budgets for net photochemical production of ozone (more than a factor 6) do not necessarily imply that the photochemical schemes in the models are very different. The net production is a small difference between large production and sink terms. This is illustrated in Table 7-2, showing also globally integrated values for the most important individual source and loss mechanisms (see Chapter 5) in one 2-D model (Derwent, 1994). In this model the total production and the total loss is about 4 times larger than the flux from the stratosphere, whereas the net production comes out as a number that is much smaller than the stratospheric flux.

It is obvious that differences in the import and export terms also influence the net chemical production, since the budget balances in the models. A model that, *e.g.*, has a large import from the stratosphere or an inefficient deposition at the ground, estimates high ozone concentrations in the troposphere, thereby increasing the chemical loss, since the ozone (or excited atomic oxygen produced from ozone) participates itself in the loss reactions (see Chapter 5 and Table 7-2), and since the photolysis of ozone initiates oxidation processes influencing production as well as loss reactions for ozone.

Aspects of Zonal Asymmetries

Two-dimensional tropospheric chemistry models calculate zonally averaged trace gas distributions, and therefore neglect zonal asymmetries. Yet they capture the coarse features of the ozone distribution and they are useful tools for sensitivity studies and analyses. Howev-

Table 7-2. Examples of globally integrated budget terms for tropospheric ozone, for the current and pre-industrial atmospheres, as calculated in various models, in Tg (O_3)/yr.

Model/Investigator	Ref.	Present atmosphere			Pre-industrial atmosphere		
		Chem[a]	Strat[b]	Dep[c]	Chem	Strat	Dep
UOslo 3-D/Berntsen	(1)	295	846	-1178			
Moguntia 3-D/Lelieveld	(2)	427	528	-953	-87	552	-465
Cambridge 2-D/Law	(3)	1021	601	-1622			
UKMO 2-D/Derwent	(4)	343*	1077	-1420			
TNO 2-D/Roemer	(5)	728	962	-1690	-195	962	-767
CNRS/NCAR 2-D/ Hauglustaine	(6)	216	408	-612	-75	458	-424
UBergen 2-D/Strand	(7)	1404	533	-1937			
AER 2-D/Kotomarthi	(8)	416	610	-1026			

a) Chem: The numbers represent net photochemical production, which is a small difference between large production and loss terms (see text and the panel below). Since the budgets balance, net chemical production must respond to stratosphere/troposphere exchange and surface deposition by changing the ozone abundances.

b) Strat: Net flux from the stratosphere to the troposphere, fixed or parameterized in the models.

c) Dep: Surface deposition.

(1) Berntsen and Isaksen (1994)
(2) Lelieveld (1994)
(3) Law and Pyle (1993a, b) + personal communication
(4) Derwent (1994) + personal communication
(5) Roemer and van der Hout (1992)
(6) Hauglustaine *et al.* (1994)
(7) Strand and Hov (1994)
(8) Kotomarthi, personal communication. AER = Atmospheric and Environmental Research, Inc.

* Individual chemical terms are as follows:

Term	Strength	
$HO_2 + NO$	3117	
$CH_3O_2 + NO$	1006	
$RO_2 + NO$	462	
Total production		4585
$O(^1D) + H_2O$	-1704	
$O_3 + OH$	-410	
$O_3 + HO_2$	-1719	
O_3 + NMHC	-178	
O_3 + NO (net loss)	-177	
$O(^3P)$ (net loss)	-54	
Total loss		-4242
Net chemical production		343

er, quantitative assessments based on these models will remain uncertain, due to limitations in their ability to simulate realistically global transport of tracers (see Section 7.5.2), and due to the lack of possibility to resolve longitudinal variations in several species of key importance for the ozone chemistry, in particular in NO_x mixing ratios, observed between continental and oceanic regions. The errors resulting from the assumption of longitudinally uniform emissions have been evaluated by use of a 3-D global monthly averaged model (Kanakidou and Crutzen, 1993). Longitudinally varying NO, C_2H_6, and C_3H_8 emissions lead to significantly lower O_3 and OH concentrations, especially in the middle and low troposphere in the tropics and at northern midlatitudes, than when zonally averaged emissions were used. The computed discord varies with latitude and height and was locally as high as 80% for OH concentrations in the tropics and 60% at midlatitudes.

On the other hand, there is no guarantee that 3-dimensional models can simulate correctly the NO_x distributions and total nitrate observations in the troposphere and, in particular, in remote marine locations (Penner *et al.*, 1991; Kasibhatla *et al.*, 1993; Gallardo *et al.*, 1994). This can be due to limitations in knowledge of emissions, but also in the simulation of atmospheric chemistry and transport from source areas in the model. For example, Gallardo *et al.* (1994), testing various scenarios of distribution of NO_x emissions from lightning, found that a convection-related lightning distribution could improve considerably the agreement with observations of NO_x and total nitrate in remote oceanic areas.

The Role of Convection

Representation of convection in global models requires parameterization, due to the small scale of the process. It therefore needs special consideration. One consequence of convection is that ozone precursors (NO_x, CO, and NMHC), once they are transported to the free troposphere, have a longer chemical lifetime, allowing them to be transported over long distances and contribute to ozone formation downwind of the convective cell. This has been confirmed in a model study of deep tropical convection events observed during the Amazon Boundary Layer Experiment 2A (ABLE 2A), showing enhanced ozone formation in the middle and upper troposphere (Pickering *et al.*, 1992). Meteorological and trace gas observations from convective episodes were analyzed in the study with models of cumulus convection and photochemistry. The level of formation of free tropospheric ozone was shown to depend on the surface trace gas emissions entrained in the cumulus convective events.

On the other hand, boundary layer air poor in NO_x depresses the upper tropospheric ozone formation following convective events. This was found in a study based on aircraft data from the Stratosphere-Troposphere Exchange Project (STEP) and the Equatorial Mesoscale Experiment (EMEX) flights off northern Australia, again using cumulus cloud and photochemical models (Pickering *et al.*, 1993). A 15-20% reduction in the rate of O_3 production between 15 and 17 km was the largest perturbation calculated for these experiments due to convection events. The study also showed that O_3 production between 12 and 17 km would slow down by a factor of 2 to 3 in the absence of NO_x from lightning.

A secondary effect of deep cumulus convection is associated with downward transport of ozone and NO_x-rich air from the upper troposphere in the cumulus downdrafts. The downward transport of ozone and NO_x brings these components into regions where their lifetime is much shorter than in the upper troposphere. Lelieveld and Crutzen (1994) have used a 3-D global model to quantify this effect. Their calculations give a decrease in total tropospheric ozone concentrations of 20% when deep convection is included in the calculations. The results are partly due to a corresponding decrease in the global column of NO_x of about 30%. However, the decreased downward transport of ozone resulted in an increase in the oxidation capacity of the troposphere. Inclusion of convection increased methane destruction by about 20% and CO destruction by about 10%.

7.3.2 Limitations in Global Models

Modeling of ozone production in the troposphere is very sensitive to the assumed strengths and distribution of sources of ozone precursors. Estimates of emissions, in particular of natural NO_x (lightning and surface sources) and hydrocarbons (isoprene and terpenes), are associated with large uncertainties that yield uncertainties also in modeled ozone production. Accurate emission data of O_3 precursors are clearly needed to correctly simulate tropospheric chemistry.

A global CTM needs to represent the transport of trace gases from their source to their sink regions. The mass flux can be formulated as a function of the wind velocity. The spatial and temporal resolution of wind data, as provided by data assimilation or models, is limited. Advection in a CTM therefore captures only a fraction of the total transport, and sub-grid processes need to be parameterized, limiting the accuracy of transport of ozone and other trace gases in the CTM. Such sub-grid processes include transport within the boundary layer, exchange between the boundary layer and the free troposphere, convective transport, small-scale mixing processes, and tropopause exchange. Inaccuracies in model representation of sub-grid processes is of largest importance for trace gases with lifetimes of the order of days or weeks, like ozone and NO_x. This is of particular importance since NO_x influences ozone chemically in a nonlinear way.

A variety of heterogeneous chemical reactions can affect the tropospheric ozone budget. The accuracy of global ozone models is limited by the fact that the paths and rates of such reactions are uncertain and by the fact that such processes take place on spatial scales that are not resolved in global models. Such heterogeneous reactions include oxidation of N_2O_5 to nitrate, loss reactions for ozone, removal of formaldehyde, and the separation of chemical ozone precursors inside (HO_2) and outside (NO) cloud water droplets.

Gas phase chemical kinetics and photochemical parameters are reasonably well established. However, calculation of photodissociation rates is difficult in regions with clouds and aerosols, due to difficulties in model representation of optical properties, and the small spatial and temporal scale of clouds.

A wide range of hydrocarbons take part in ozone production in the troposphere in the presence of NO_x. The formulations of the degradation mechanisms of hydrocarbons can be important sources of uncertainty in tropospheric ozone models. The oxidation chains of the dominant natural hydrocarbons, isoprene and terpenes, are still not well known. Furthermore, the number of emitted hydrocarbons is so large that they can only be represented in models in groups (lumped species).

Finally, development of global ozone models is hampered by the lack of extensive data sets for observed species distributions. In order to test and validate models, measurements are needed for several key species on synoptic and even smaller scales.

7.4 APPLICATIONS

Numerical models offer the possibility to assess the role of certain processes on a global scale. This section presents some selected applications of models, when they have been used to perform global integration of key processes of importance for tropospheric chemistry and the ozone budget.

7.4.1 Global Tropospheric OH

The hydroxyl radical, OH, is produced from O_3 following photolysis to the excited state $O(^1D)$ and its reaction with H_2O. In turn, the HO_x family (OH, HO_2, H_2O_2) is involved in the production of tropospheric O_3 in reactions with NO_x ($NO + NO_2$). The reaction of OH with NO_2 also provides the terminating step in NO_x-catalyzed production of O_3 by converting NO_x into HNO_3. Furthermore, HO_x also removes ozone in NO_x-poor environments. Thus the tropospheric chemistry of O_3 and OH are intertwined, and any possible calibration of modeled OH adds confidence to the simulation of tropospheric O_3.

OH concentrations respond almost instantly to variations in sunlight, H_2O, O_3, NO and NO_2 (NO_x), CO, CH_4, and NMHC; and therefore the OH field varies by orders of magnitude in space and time. Observations of OH can be used to test the photochemical models under specific circumstances, but are not capable of measuring the global OH field. Therefore we must rely on numerical models and surrogates to provide the global and seasonal distribution of OH; these models need to simulate the variations in sunlight caused by clouds and time-of-day in addition to the chemical fields. These calculations of global tropospheric OH and the consequent derivations of lifetimes have not changed significantly and are still much the same as in the AFEAS (Alternative Fluorocarbons Environmental Acceptability Study) Report (WMO, 1990); we cannot expect such calculations to achieve an accuracy much better than ±30%.

We can derive some properties of the global OH distribution by observations of trace gases whose abundance is controlled by reactions with OH, in conjunction

with some model for their emissions and atmospheric mixing. For example, the trace gases methyl chloroform (CH_3CCl_3), ^{14}CO, and HCFC-22 have been used to derive empirical OH and thus test the modeled OH fields. These gases (1) are moderately well mixed, (2) have well calibrated and well measured atmospheric burdens, and (3) have small or well defined other losses. However, they primarily test only the globally, annually averaged OH concentration, and even this average quantity is weighted by the distribution and reaction rate coefficient of OH with the gas. Some model studies have used CH_3CCl_3 (Spivakovsky *et al.*, 1990a) and ^{14}CO (Derwent, 1994) to test their ab initio calculations of tropospheric OH. Such studies have argued that the observed seasonal distributions support the modeled seasonal distribution of OH, but such seasonality also results from transport and depends on the rate of mixing between the aseasonal tropics and the midlatitudes.

The lifetimes for many ozone-depleting and greenhouse gases depend on tropospheric OH, and at this stage of model development we rely on the empirical values. CH_3CCl_3 fulfills all of the above requirements for calibrating tropospheric OH. It has the further advantage that its tropospheric distribution and reaction rate are similar to many of the other gases in which we are interested. A recent assessment (Kaye *et al.*, 1994) has reviewed and re-evaluated the lifetimes of two major industrial halocarbons, methyl chloroform (CH_3CCl_3) and CFC-11. An optimal fit to the observed concentrations of CH_3CCl_3 from the five Atmospheric Lifetime Experiment/Global Atmospheric Gases Experiment (ALE/GAGE) surface sites over the period 1978-1990 was done with a pair of statistical/atmospheric models (see Chapter 3 in Kaye *et al.*, 1994). The largest uncertainty in the empirical CH_3CCl_3 lifetime, 5.4 ± 0.6 yr, lies currently with the absolute calibration. The implication of a trend in this lifetime, presumably due to a change in tropospheric OH (Prinn *et al.*, 1992), is sensitive to the choice of absolute calibration. Analyses of the tropospheric budgets of the radio-isotope ^{14}CO (Derwent, 1994) and HCFC-22 (Montzka *et al.*, 1993) complement this analysis and confirm the empirical estimate of tropospheric OH.

7.4.2 Budgets of NO_y

Concentrations of NO_x are critical for ozone production. A central difficulty in modeling global ozone is to predict the distribution of NO_y components including the large variability observed on small scales, the transport out of the boundary layer, and chemical recycling of nitrogen reservoir species. It is a problem that the relative roles of sources of tropospheric NO_x (surface emissions, lightning, transport from the stratosphere, and aircraft emissions) in generating observed levels are not quantitatively well known. This section describes a few recent model studies addressing the role of emissions, transport, and chemical conversion of reactive nitrogen compounds.

A 3-D global chemistry-transport model has been used to assess the impact of fossil fuel combustion emissions on the fate and distribution of NO_y components in various regions of the troposphere (Kasibhatla *et al.*, 1993). It was found that wet and dry deposition of NO_y in source regions remove 30% and 40-45% of the emissions, respectively, with the remainder being exported over the adjacent ocean basins. The fossil fuel source was found to account for a large fraction of the observed surface concentrations and wet deposition fluxes of HNO_3 in the extratropical North Atlantic, but to have a minor impact on NO_y levels in the remote tropics and in the Southern Hemisphere.

Another global 3-D model study has calculated the effect of organic nitrates, which can act as reservoirs for NO_x and therefore redistribute NO_x in the troposphere (Kanakidou *et al.*, 1992). During their chemical formation, the organic nitrates may capture NO_x that can be released after transport and subsequent decomposition away from source regions. The importance of hydrocarbons in the formation of peroxyacetyl nitrate (PAN), which is the most abundant nitrate measured in the troposphere, was demonstrated in the study, which also included comparison with observations. According to the model calculations, the efficiency of acetone in producing PAN in the middle and high troposphere of the NH ranges between 20 and 25%. This relationship between acetone and PAN concentrations has also been observed during the Arctic Boundary Layer Expedition (ABLE) 3B experiment. The observed concentrations of acetone and PAN were much higher than those calculated by the model, which takes into account ethane and propane photochemistry only. Consideration of the oxidation of higher hydrocarbons and of direct emissions of acetone is therefore needed to explain the observed concentrations (Singh *et al.*, 1994).

An analysis of data from ABLE-3A using a photochemical model has shown that PAN and other organic nitrates act as reservoir species at high latitudes for NO_x that is mainly of anthropogenic origin, with a minor component from NO_x of stratospheric origin (Jacob *et al.*, 1992). This tropospheric reservoir of nitrogen is counteracting O_3 photochemical loss over western Alaska relative to a NO_x-free environment. The concentrations of O_3 in the Arctic and sub-arctic troposphere have been found to be regulated mainly by input from the stratosphere and losses of comparable magnitude from photochemistry and deposition (Singh *et al.*, 1992; Jacob *et al.*, 1992).

Based on 2-D model calculations, the previous ozone assessment (WMO, 1992) showed that injection of NO_x directly into the upper troposphere from commercial aircraft is substantially more efficient in producing ozone than surface-emitted NO_x. Model tests that have been performed show that the ozone-forming potential of NO_x emitted from airplanes depends on, *e.g.*, transport formulation, injection height, and the removal rate. Furthermore, making reliable quantitative estimates of the ozone production due to the aircraft emission is also difficult, as it is nonlinear and it depends strongly on the natural emissions and the background concentrations of NO_x, which are not well characterized (see discussion in Chapter 11).

7.4.3 Changes in Tropospheric UV

Reductions in ozone column densities due to enhanced ozone loss in the stratosphere will lead to enhanced UV penetration to the troposphere, causing chemical changes. Such increased UV levels have been observed in connection with reduced ozone column densities during the last few years (WMO, 1992; Smith *et al.*, 1993; Kerr and McElroy, 1993; Gleason *et al.*, 1993). The significance for tropospheric chemistry of enhanced UV fluxes is that they affect the lifetimes of key atmospheric compounds like CO, CH_4, NMHC, hydrofluorocarbons (HFCs), and hydrochlorofluorocarbons (HCFCs) and the photochemical production and loss of tropospheric ozone (Liu and Trainer, 1988; Brühl and Crutzen, 1989; Madronich and Granier, 1992; Fuglestvedt *et al.*, 1994a). The main cause of this change is that enhanced UV radiation increases $O(^1D)$ production, which in turn will lead to enhanced tropospheric OH levels.

The atmospheric lifetimes of the above-mentioned chemical compounds will be reduced since reactions with OH represent the main sink. The reduced growth rate of CH_4 that has been observed during the last decade could, at least partly, be due to decreased lifetime resulting from enhanced UV fluxes. Fuglestvedt *et al.* (1994a) have estimated that approximately 1/3 of the observed reduction in growth rate during the 1980s is due to enhanced UV radiation resulting from reduced ozone column densities over the same time period. In the same study it was found that tropospheric ozone was reduced in most regions. It was only at middle and high northern latitudes during limited time periods in the spring where NO_x levels were sufficiently high, that ozone was increased due to enhanced UV radiation. There might also be significant changes in UV radiation, and thereby in chemical activity, due to changes in the reflecting cloud cover and due to backscatter by anthropogenic sulfate aerosols (Liu *et al.*, 1991). Marked changes in the ratio of scattered UV-B radiation to direct radiation have also been observed in New Zealand after the Mount Pinatubo eruption (see Chapter 9).

7.4.4 Changes Since Pre-industrial Times

Measurements of the chemical composition of air samples extracted from ice cores have been compared to measurements of the present atmosphere, revealing that methane volume mixing ratios have increased from about 800 ppb to about 1700 ppb since the pre-industrial period (see Chapter 2). The methane increase may have reduced the OH concentration and the oxidizing efficiency of the atmosphere. However, an increase in production of ozone and thus also OH will also accompany growing CH_4 levels. As a result of industrialization, extensive anthropogenic emissions of the ozone precursors CO, NO_x, and NMHC have also occurred, increasing ozone on a local and regional scale and, to a lesser extent, on a global scale.

The temporal trends in tropospheric ozone in the past are difficult to calculate particularly because of the critical role of surface NO_x emissions. A few model studies of impacts of anthropogenic emissions since pre-industrial times predict large increases in ozone (Roemer and van der Hout, 1992; Hauglustaine *et al.*, 1994; Lelieveld, 1994). The predicted changes in ozone during the time of industrialization are not inconsistent with observations (see Chapter 1). Predictions of ozone change

have, however, only been made with a limited number of models. It has been done with models describing in principle the main processes governing the ozone budget. However, more detailed models are needed to calculate quantitatively reliable temporal trends in ozone.

A few models have estimated globally averaged strengths of the various budget terms for ozone under pre-industrial conditions. The numbers are given in Table 7-2. Only changes in emissions of gases like CH_4, CO, NO_x, and NMHC have been considered in the model experiments, whereas the meteorology and the transport of atmospheric species have been assumed to be unchanged. Despite the wide spread in the strength of individual processes regulating global tropospheric ozone (Section 7.3.1), there is good agreement between the models in the changes in the ozone chemistry that may have occurred during the time of industrialization. According to the model calculations, both production and loss were weaker in pre-industrial times, and the chemistry has changed from being a net sink to a net source of ozone. The global burden of tropospheric ozone increased in these model studies by 55-70% over the time of industrialization, supporting the assumption that the observed marked increase in ozone over the last approximately 100 years has at least partly been due to anthropogenic emissions.

In a review paper on the oxidizing capacity of the atmosphere, Thompson (1992) compiled changes in global OH since pre-industrial times as calculated in several global models. There is consensus that OH has decreased globally since the pre-industrial times. However, there is a substantial spread in the estimates, which range from only a few to about 20%.

7.5 INTERCOMPARISON OF TROPOSPHERIC CHEMISTRY/TRANSPORT MODELS

The observed changes in the cycles of many atmospheric trace gases are expected, and often observed, to produce a chemical response. For example, we have accumulated evidence that tropospheric ozone in the northern midlatitudes has increased substantially, on the order of 25 ppb, since pre-industrial times. During this period, the global atmospheric concentration of CH_4 has increased regularly, and the emissions of NO_x and NMHC, at least over northern midlatitudes, have also increased greatly. An accounting of the cause of the O_3 increases, particularly to any specific emissions, requires a global tropospheric CTM, preferably a 3-D model. A CTM provides the framework for coupling different chemical perturbations that are, by definition, indirect and thus cannot be evaluated simply with linear, empirical analyses. We are placing an increasing responsibility on CTM simulations of the atmosphere (*e.g.*, the GWP calculation for CH_4 in IPCC 1994) and should therefore ask how much confidence we have in these models. Models of tropospheric chemistry and transport have not been adequately tested in comparison with those stratospheric models used to assess ozone depletion associated with CFCs (*e.g.*, WMO, 1990, 1992; Prather and Remsberg, 1992). In addition, the greater heterogeneity within the troposphere (*e.g.*, clouds, convection, continental versus marine boundary layer) makes modeling and diagnosing the important chemical processes more difficult. This section presents a beginning, objective evaluation of the global CTMs that simulate tropospheric ozone.

There are numerous published examples of individual model predictions of the changes in tropospheric O_3 and OH in response to a perturbation (*e.g.*, pre-industrial to present, doubling CH_4, aircraft or surface combustion NO_x, stratospheric O_3 depletion). Since these calculations in general used different assumptions about the perturbants or the background atmosphere, it is difficult to use these results to derive an assessment. Further, we need to evaluate how representative those models are with a more controlled set of simulations and diagnostics.

Thus, two model intercomparisons and one assessment are included as part of this report: (1) prescribed tropospheric photochemical calculations that test the modeling of O_3 production and loss; (2) transport of short-lived radon-222 that highlights differences in transport description between 2-D and 3-D global chemical tracer models in the troposphere; and (3) assessing the impact of a 20% increase in CH_4 on tropospheric O_3 and OH. All of these studies were initiated as blind intercomparisons, with model groups submitting results before seeing those of others. The call for participation in (1) and (3) and preliminary specifications went out in June 1993; the first collation of results was reported to the participants in January 1994; and the final deadline for submissions to this report was June 1994. In the transport study, no obvious mistakes in performing the

Table 7-3. Initial values used in PhotoComp.

ALTITUDE (km)	MARINE 0	LAND+BIO 0	FREE 8	PLUME/X + PLUME/HC 4
T (K)	288.15	288.15	236.21	262.17
p (mbar)	1013.25	1013.25	356.50	616.60
N (#/cm^3)	2.55E19	2.55E19	1.09E19	1.70E19
H_2O (% v/v)	1.0	1.0	0.05	0.25
O_3 (ppb)	30	30	100	50
NO_x (ppt)	10	200	100	10000
HNO_3 (ppt)	100	100	100	100
CO (ppb)	100	100	100	600
CH_4 (ppb)	1700	1700	1700	1700
NMHC	none	none	none	see footnote

H_2 = 0.5 ppm; H_2O_2 = 2 ppb for all cases. BIO case equals LAND but with 1 ppb isoprene.
PLUME without NMHCs (/X) and with NMHCs (/HC). Initial values of NMHC (ppb): C_2H_6 = 25, C_2H_4 = 40, C_2H_2 = 15, C_3H_8 = 15, C_3H_6 = 12.5, C_4H_{10} = 5, toluene = 2, isoprene = 0.5.
(Note: Integrations were performed for 5 days starting July 1, with solar zenith angle 22 degrees.)

case studies were found, and detailed results will be published as a WCRP (World Climate Research Programme) workshop report. In the photochemical study and methane assessment, about half of the results contained some obvious errors in the setup, diagnosis, or model formulation that were found in January 1994. Most participants identified these errors and chose to resubmit new results. Removal or correction of obvious errors did not eliminate discrepancies among the models, and significant differences still remain and are presented here. The current list of contributions is identical to the parallel IPCC Assessment. The combination of these intercomparisons provides an objective, first look at the consistency across current global tropospheric chemical models.

7.5.1 PhotoComp: Intercomparison of Tropospheric Photochemistry

An evaluation of the chemistry in the global CTMs is not easy. There are no clear observational tests of the rapid photochemistry of the troposphere that include the net chemical tendency of O_3 and are independent of transport. Furthermore, uncertainties in the kinetic parameters would probably encompass a wide range of observations. Thus, we chose an engineering test (PhotoComp) in which all chemical mechanisms and data, along with initial conditions, were specified exactly as in Table 7-3. Atmospheric conditions were prescribed (July 1, U.S. standard atmosphere with only molecular scattering and $O_2 + O_3$ absorption) and the air parcels with specified initial conditions were allowed to evolve in isolation for five days with diurnally varying photolysis rates (J's). PhotoComp becomes, then, a test of the photochemical solvers used by the different groups in which there is only one correct answer. For most of these results, many models give similar answers, resulting in a "band" of consensus, which we assume here to be the correct numerical solution. The 23 different model results submitted to PhotoComp are listed in Table 7-4.

The PhotoComp cases were selected as examples of different chemical environments in the troposphere. The wet boundary layer is the most extensive, chemically active region of the troposphere. Representative conditions for the low-NO_x oceans (case: MARINE) and the high-NO_x continents (case: LAND) were picked. In MARINE, ozone is lost rapidly (-1.4 ppb/ day), but in

Table 7-4. Models participating in the PhotoComp and delta-CH_4 intercomparisons.

Code	Affiliation	Contributor*	(e-mail)
A	U. Mich.	Sandy Sillman	(sillman@madlab.sprl.umich.edu)
B	UKMetO/UEAnglia	Dick Derwent	(rgderwent@email.meto.govt.uk)
B&	UEA-Harwell/2-D	Claire Reeves	(c.reeves@uea.ac.uk)
C	U. Iowa	Gregory Carmichael	(gcarmich@icaen.uiowa.edu)
D	UC Irvine	Michael Prather	(prather@halo.ps.uci.edu)
E	NASA Langley	Jennifer Richardson	(richard@sparkle.larc.nasa.gov)
F	AER (box)	Rao Kotamarthi	(rao@aer.com)
G	Harvard	Larry Horowitz	(lwh@hera.harvard.edu)
H	NASA Ames	Bob Chatfield	(chatfield@clio.arc.nasa.gov)
I	NYU-Albany	Shengxin Jin	(jin@mayfly.asrc.albany.edu)
J	Jülich	Michael Kuhn	(ICH304@zam001.zam.kfa-juelich.de)
K	GFDL	Lori Perliski	(lmp@gfdl.gov)
L	Ga. Tech.	Prasad Kasibhatla	(psk@gfdl.gov)
M&	U. Camb/2-D	Kathy Law	(kathy@atm.ch.cam.ac.uk)
N	U. Camb (box)	Oliver Wild	(oliver@atm.ch.cam.ac.uk)
O&	LLNL/2-D	Doug Kinnison	(dkin@cal-bears.llnl.gov
P	LLNL/3-D	Joyce Penner	(penner1@llnl.gov)
P&	"	Cynthia Atherton	(cyndi@tropos.llnl.gov)
Q	NASA Goddard	Anne Thompson	(thompson@gator1.gsfc.nasa.gov)
R&	AER/2-D	Rao Kotomarthi	(rao@aer.com)
S	Cen. Faible Rad.	Maria Kanakidou	(mariak@asterix.saclay.cea.fr)
T	U. Oslo/3-D	Terje Berntsen	(terje.berntsen@geofysikk.uio.no)
T&	"	Ivar Isaksen	(ivar.isaksen@geofysikk.uio.no))
U	NILU	Frode Stordal	(frode@nilu.no)
Y#	U. Wash.	Hu Yang	(yang@amath.washington.edu)
Z#	Ind. Inst. Tech.	Murari Lal	(mlal@netearth.iitd.ernet.in)

Notes:
* Only a single point-of-contact is given here; for other collaborators see appropriate references.
\# Results for photolysis rates only.
& Also did delta-CH_4 experiment in a 2-D or 3-D model.
NYU = New York University; NILU = Norwegian Institute for Air Research

LAND, the initial NO_x boosts O_3 levels. Over the continental boundary layer, NO_x loss is rapid and the high NO_x levels must be maintained by local emissions. In addition, these high-NO_x, ozone-producing regions have the capability of exporting significant amounts of O_3 (and its precursors) to the free troposphere (Pickering *et al.*, 1992; Jacob *et al.*, 1993a, b). Rapid O_3 formation has been observed to occur in biomass burning plumes, and the rate is predicted to depend critically on whether hydrocarbons are present (PLUME/HC) or not (PLUME/X). In the dry upper troposphere (FREE), O_3 evolves very slowly, less than 1%/day, even at NO_x levels of 100 ppt.

The photolysis of O_3 yielding $O(^1D)$ is the first step in generating OH, and it controls the net production of O_3. Tropospheric values peak at about 4-8 km because of molecular scattering. Model predictions for this J at noon, shown in Figure 7-3a, fall within a band, ±20%

of the mean value, if a few outliers are not considered. These differences are still large considering that all models purport to be making the same calculation. Another key photolysis rate, that of NO_2 in Figure 7-3b, shows a similar range of results but with a more distinct pattern: a majority clusters within 5% of one another, and the remaining results are systematically greater or smaller by about 15%. It appears likely that this discrepancy may be caused by the different treatments of scattering, because NO_2 photolysis peaks at about 380 nm, where the only significant cause of extinction is Rayleigh scattering. It is likely that such model differences could be reduced to the 5% level with some modest effort.

The photolysis of O_3 and subsequent reaction with H_2O (reaction 2) drives the major loss of O_3 in MARINE (0 km, 10 ppt NO_x), as shown in Figure 7-3c. The spread in results after 5 days, 21 to 23 ppb, or ±12% in O_3 loss, does not seem to correlate with the O_3 photolysis rates in Figure 7-3a. Also shown in Figure 7-3c is the evolution of O_3 in LAND (0 km, 200 ppt NO_x). The additional NO_x boosts O_3 for a day or two and doubles the discrepancy in the modeled ozone. The disagreement here is important since most tropospheric O_3 is destroyed under these conditions in the wet, lower troposphere.

In the cold, dry upper troposphere, the net tendency of O_3 is for slow loss, even with initially 100 ppt of NO_x, as shown for FREE in Figure 7-3d. The divergence of results is disturbing but limited to a few models (*i.e.*, losses after 5 days range from 2 to 4 ppb). These differences are not likely to affect the ozone budget for the majority of models. In contrast, the production of O_3 in a NO_x-rich PLUME (4 km, 10 ppb NO_x) without non-methane hydrocarbons is rapid and continues over 5 days, as shown in Figure 7-3e. Model agreement is excellent on the initial increases from 30 to 60 ppb O_3 in 48 hours, but starts to diverge as NO_x levels fall. When large amounts of NMHC are included in PLUME+HC (also Figure 7-3e), ozone is produced and NO_x depleted rapidly, in less than one day. Differences among models become much greater, in part because different chemical mechanisms for NMHC oxidation were used. (The reaction pathways and rate coefficients for chemistry with CH_4 as the only hydrocarbon have become standardized, but different approaches are used for non-methane hydrocarbons.) Some of these differences become even more obvious in the NO_x predicted for PLUME+HC as shown in Figure 7-3f. By day 3, NO_x levels in individual models are nearly constant but with a large range, from 0 to 50 ppt.

The 24-hour averaged OH concentrations are shown for LAND and MARINE in Figure 7-3g. Values are high for LAND during the first day and demonstrate the dependence of OH on NO_x, which begins at 200 ppt and decays rapidly to about 10 ppt by day 4. The divergence among LAND results is greater than MARINE, in part due to the larger differences in the residual NO_x left from the initial value. Modeled OH values generally fall within a ±20% band. This variation in OH between models, however, does not correlate obviously as expected with any other model differences such as the photolysis rate of O_3 or the abundance of NO_x.

While O_3 and OH may seem only moderately sensitive to numerical treatment of the photochemistry, some minor species appear to be less constrained. The MARINE results for noontime formaldehyde (CH_2O), shown in Figure 7-3h, reach an approximate steady state by day 5, but the range in model results is large, about a factor of 2.

These results show that basic model-to-model differences of 30% or more exist in the calculations of O_3 change and OH concentrations. This spread is not a true scientific uncertainty, but presumably a result of different numerical methods that could be resolved given some effort, although no single fix, such as O_3 photolysis rates, would appear to reduce the spread. A more significant uncertainty in the current calculations of O_3 tendencies is highlighted by the parallel experiments with and without NMHC: the sources, transport and oxidation, and in particular the correlation of NO_x emissions and NMHC emissions on a fine scale, may control the rate at which NO_x produces O_3.

7.5.2 Intercomparison of Transport: A Case Study of Radon

A critical element in calculating tropospheric ozone is the transport of short-lived tracers such as NO_x and O_3. The model comparison that tested atmospheric transport was carried out primarily as a WCRP Workshop on short-range transport of greenhouse gases as a follow up to a similar workshop on long-range transport of CFC-11 (December 1991). A detailed description is being prepared as a WCRP Report. The basic intercomparison examined the global distribution and variability predicted for ^{222}Rn emitted ubiquitously by decay of ra-

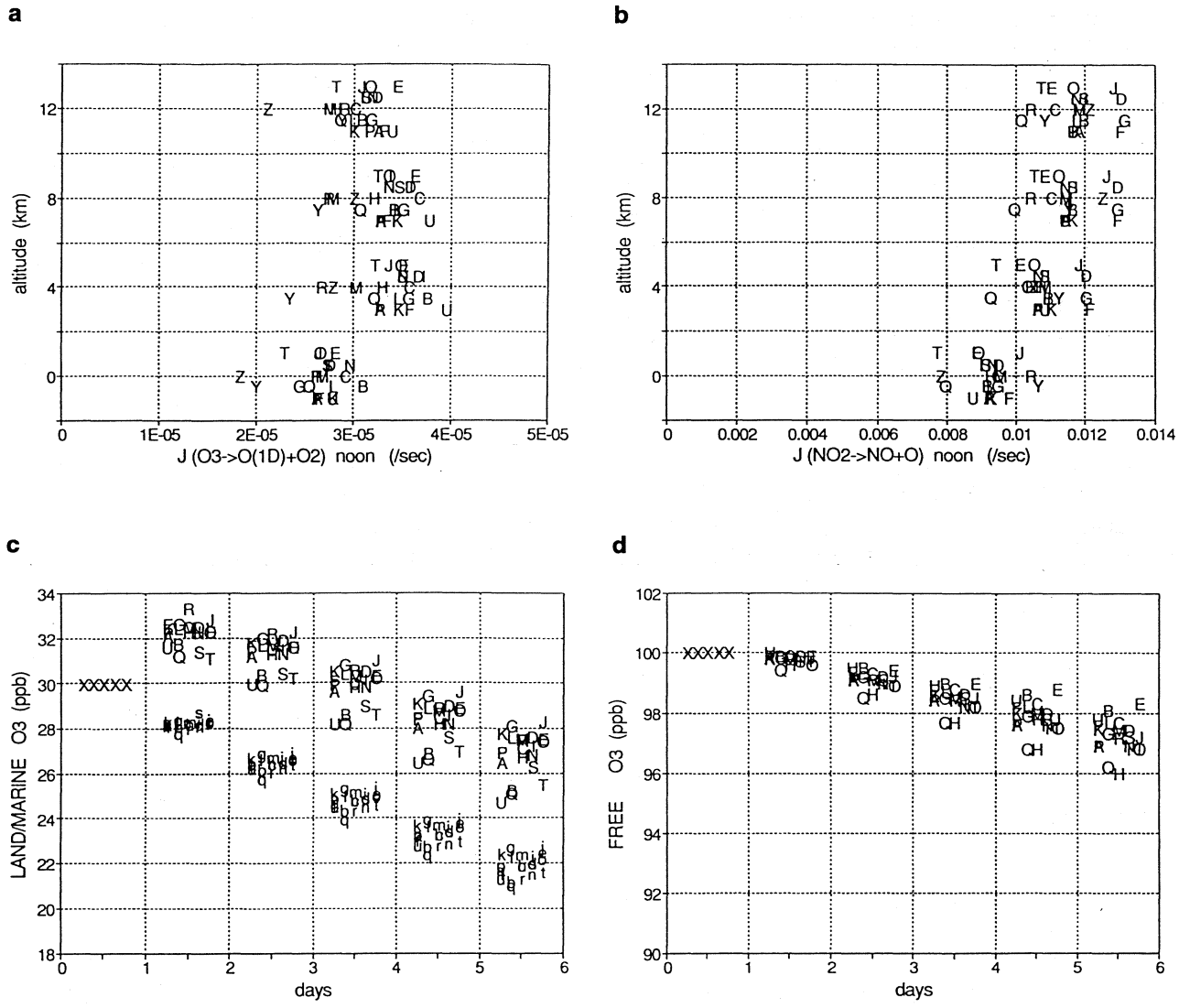

Figure 7-3. Results from the PhotoComp model intercomparison of 23 models (2 with only J-values); see Table 7-4 for the key letters and Table 7-3 for the initial conditions. Photolysis (J) rates for O_3 to $O(^1D)$ (a) and for NO_2 (b) are for local noon, July 1, 45°N, U.S. Standard Atmosphere. Results are reported for altitudes of 0, 4, 8, and 12 km. For clarity, the letter codes have been offset in altitude here, and in time-of-day in subsequent panels. Ozone mixing ratios are shown for noon in the boundary layer LAND (c, upper case codes) and MARINE (c, lower case) cases, for the FREE troposphere (d) case, and finally for the biomass

(continued on page 7.21)

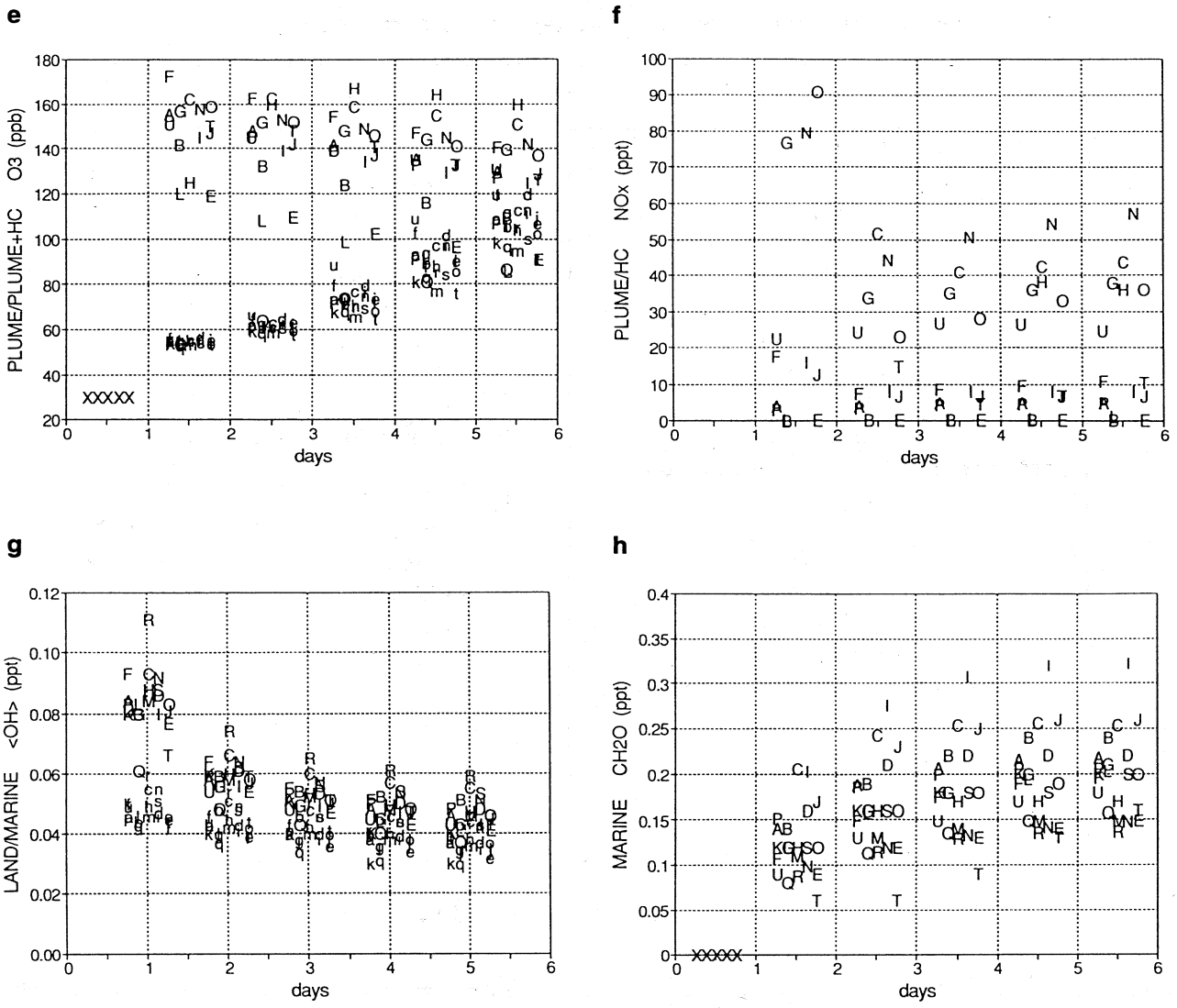

Figure 7-3, continued.
burning PLUME, without (e, lower case codes) and with NMHC (e, upper case). O_3 was initialized at the 'X'. Noontime NO_x mixing ratios are shown for the PLUME case with NMHC (f); whereas 24-hour average values of OH (from noon to noon) are shown for the 5-day integration of LAND (g). Noontime mixing ratios for CH_2O are finally given for the MARINE case (h).

Table 7-5. Models participating in the Rn/Pb transport intercomparison.

	Model	Code	Contributor
CTMs established: 3-D synoptic			
	CCM2	1	Rasch
	ECHAM3	2	Feichter/Koehler
	GFDL	3	Kasibhatla
	GISS/H/I	4	Jacob/Prather
	KNMI	5	Verver
	LLNL/Lagrange	6	Penner/Dignon
	LLNL/Euler	7	Bergman
	LMD	8	Genthon/Balkanski
	TM2/Z	9	Ramone/Balkanski/Monfray
CTMs under development: 3-D synoptic			
	CCC	10	Beagley
	LaRC	11	Grose
	LLNL/Impact	12	Rotman
	MRI	13	Chiba
	TOMCAT	14	Chipperfield
	UGAMP	15	P. Brown
CTMs used in assessments: 3-D/2-D monthly average			
	Moguntia/3-D	16	Zimmermann/Feichter
	AER/2-D	17	Shia
	UCamb/2-D	18	Law
	Harwell/2-D	19	Reeves
	UWash/2-D	20	M. Brown

KNMI = Koninklijk Nederlands Meteorologisch Instituut; LaRC = NASA Langley Research Center

dium in soils. The radon is treated as an ideal gas with constant residence time of 5.5 days. Although NO_x would seem a more relevant choice for these model comparisons, the large variations in the residence time for NO_x (*e.g.*, <1 day in the boundary layer and 10 days in the upper troposphere) make it difficult to prescribe a meaningful experiment without running realistic chemistry, a task beyond the capability of most of the participating models. Furthermore, the nonlinearity of the NO_x-OH chemistry would require that all major sources be included (see Chapter 5), which again is too difficult for this model comparison.

Twenty atmospheric models (both 3-D and 2-D) participated in the radon/lead intercomparison for CTMs (see Table 7-5). Most of the participants were using established (*i.e.*, published), synoptically varying (*i.e.*, with daily weather) 3-D CTMs; several presented results from new models under development. Among these synoptic CTMs, the circulation patterns represented the entire range: grid-point and spectral, first generation climate models (*e.g.*, GFDL and GISS), newly developed climate models (*e.g.*, CCM2 and ECHAM3), and analyzed wind fields from ECMWF (European Centre for Medium-Range Weather Forecasts) (*e.g.*, TM2Z and KNMI). One monthly averaged 3-D CTM and four longitudinally and monthly averaged 2-D models also participated.

We have a limited record of measurements of ^{222}Rn with which to test the model simulations. Some of these data are for the surface above the continental sources (*e.g.*, Cincinnati, Ohio), and some are from islands far from land sources (*e.g.*, Crozet I.). The former

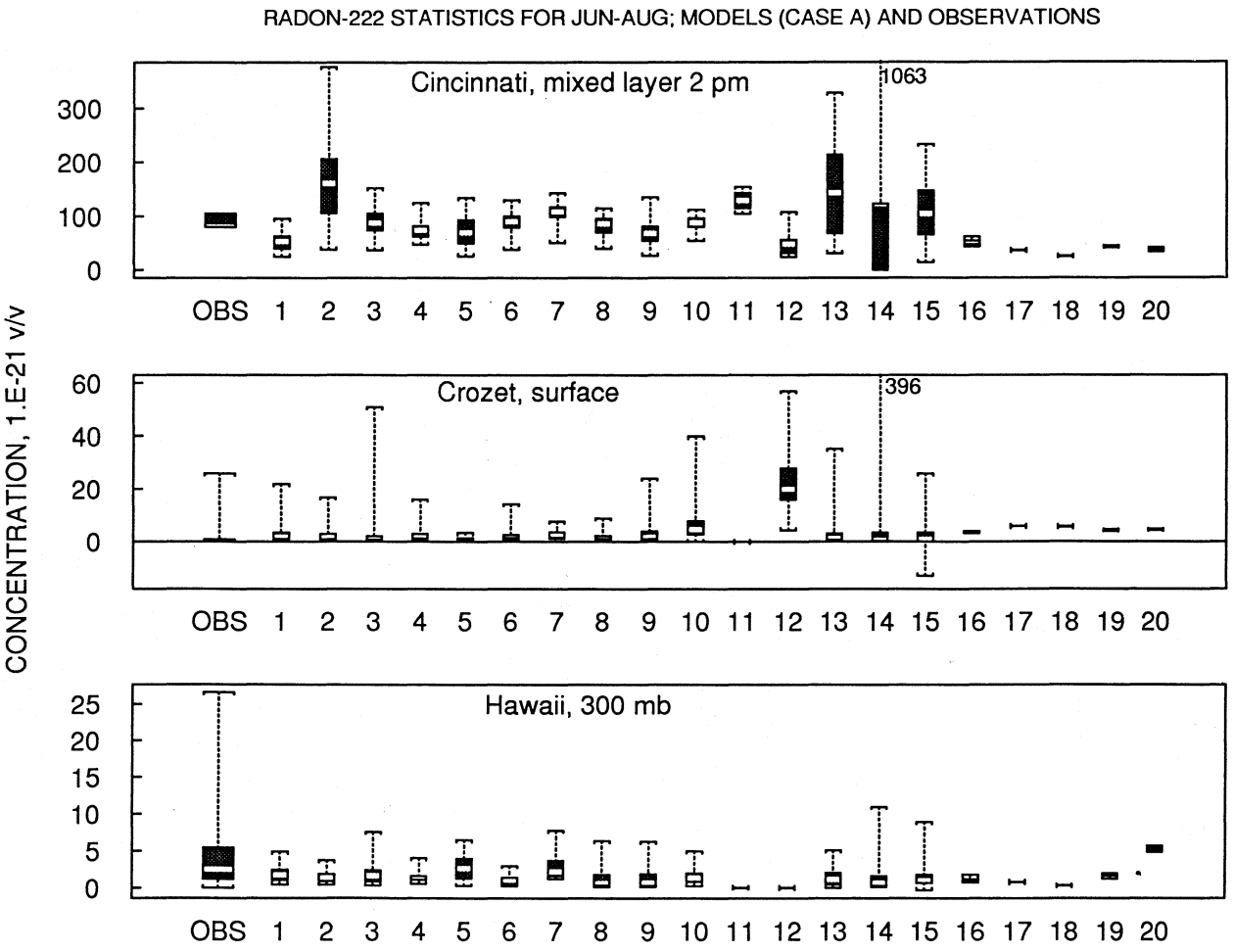

Figure 7-4. Radon-222 concentration statistics for Jun-Jul-Aug at Cincinnati, Ohio (40N 84W, mixed layer at 2 p.m.), Crozet I, (46S 51E, surface), and over Hawaii (20N 155W, 300 mbar). Modeled time series show minima and maxima, quartiles (shaded box), and medians (white band). Identification codes are given in Table 7-5. Observations at Hawaii (Balkanski *et al.*, 1992) show the same statistics; but for Cincinnati (Gold *et al.*, 1964) the shaded box gives the interannual range of June-August means; and for Crozet (Polian *et al.*, 1986) the shaded box gives typical background concentrations with the top of the vertical bar, a typical summer maximum.

sites show a diurnal cycle, with large values at the surface at night when vertical mixing is suppressed. The latter sites show a very low-level background, with large events lasting as long as a few days. An even more limited set of observations from aircraft over the Pacific (*e.g.*, 300 mbar over Hawaii) shows large variations with small layers containing very high levels of radon, obviously of recent continental origin. A set of box plots in Figure 7-4 summarizes the observations of radon at each of these three sites and compares with model predictions (see Table 7-5 for model codes). At Cincinnati, the synoptic 3-D CTMs generally reproduce the mean afternoon concentrations in the boundary layer, although some have clear problems with excessive variability, possibly with sampling the boundary layer in the afternoon. At Crozet, most of the synoptic models can reproduce the low background with occasional radon "storms." In the upper troposphere over Hawaii, the one set of aircraft observations shows occasional, extremely high values, unmatched by any model; but the median

value is successfully simulated by several of the synoptic 3-D CTMs. The monthly averaged models could not, of course, simulate any of the time-varying observations.

The remarkable similarity of results from the synoptic CTMs for the free-tropospheric concentrations of Rn in all three experiments was a surprise to most participants. All of the established CTMs produced patterns and amplitudes that agreed within a factor of two over a dynamic range of more than 100. As an example, the zonal mean Rn from case (i) for Dec-Jan-Feb is shown for the CCM2 and ECHAM3 models in Figure 7-5a-b. The two toothlike structures result from major tropical convergence and convective uplift south of the equator and the uplift over the Sahara in the north. This basic pattern is reproduced by all the other synoptic CTMs. In Jun-Jul-Aug (not shown) the 5-contour shifts north of the equator, and again, the models produce similar patterns. In contrast, the 2-D model results, shown for the AER model in Figure 7-5c, have much smoother latitudinal structures, do not show the same seasonality, and, of course, cannot predict the large longitudinal gradients expected for Rn (similar arguments hold for NO_x; see Kanakidou and Crutzen, 1993). Results from the Moguntia CTM (monthly average 3-D winds) fell in between these two extremes and could not represent much of the structures and variations predicted by the synoptic CTMs.

Such differences in transport are critical to this assessment. Both NO_x and O_3 in the upper troposphere have chemical time scales comparable to the rate of vertical mixing, and the stratified layering seen in the monthly averaged models is likely to distort the importance of the relatively slow chemistry near the tropopause. Compared with the synoptic models, it is also obvious that the monthly averaged models would transport surface-emitted NO_x into the free troposphere very differently, which may lead to inaccurate simulation of total NO_x concentrations. The 2-D models appear to have a clear systematic bias favoring high-altitude sources (*e.g.*, stratosphere and aircraft) over surface sources (*e.g.*, combustion) and may also calculate a very different ozone response to the same NO_x perturbations.

The participating synoptic CTMs are derived from such a diverse range of circulation patterns and tracer models that the universal agreement is not likely to be fortuitous. It is unfortunate that we lack the observations to test these predictions. Nevertheless, it is clear that the currently tested 2-D models, and to a much lesser extent the monthly averaged 3-D models, have a fundamental flaw in transporting tracers predominantly by diffusion, and they cannot simulate the global distribution of short-lived species accurately. The currently tested synoptic 3-D CTMs are the only models that have the capability of simulating the global-scale transport of NO_x and O_3; however, this capability will not be realized until these models include better simulations of the boundary layer, clouds, and chemical processes.

7.5.3 Assessing the Impact of Methane Increases

The impacts of methane perturbations are felt throughout all of atmospheric chemistry from the surface to the exosphere, and most of these mechanisms are well understood. Quantification of these effects, however, is one of the classic problems in modeling atmospheric chemistry. Similar to the ozone studies noted above, the published methane-change studies have examined scenarios that range from 700 ppb (pre-industrial) to 1700 ppb (current) to a doubling by the year 2050 (*e.g.*, WMO, 1992), but these scenarios are not consistent across models. This delta-CH_4 study was designed to provide a common framework for evaluating the multitude of indirect effects, especially changes in O_3 and OH, that are associated with an increase in CH_4. The study centers on today's atmosphere: use each model's best simulation of the current atmosphere and then increase the CH_4 concentration (not fluxes) in the troposphere by 20%, from 1715 ppb to 2058 ppb (expected in about 30 years based on observed 1980-1990 trend). This increase is small enough so that perturbations to current atmospheric chemistry should be approximately linear. The history and protocol of the delta-CH_4 assessment is the same as that of PhotoComp described above, and the six participating research groups are also denoted in Table 7-4.

The Current Atmosphere

Important diagnostics from delta-CH_4 include O_3 and NO_x profiles for the current atmosphere, providing a test of the realism of each model's simulation. Typical profiles observed for O_3 in the tropics and in northern midlatitudes over America and Europe are shown in Figure 7-6. The corresponding calculated O_3 profiles,

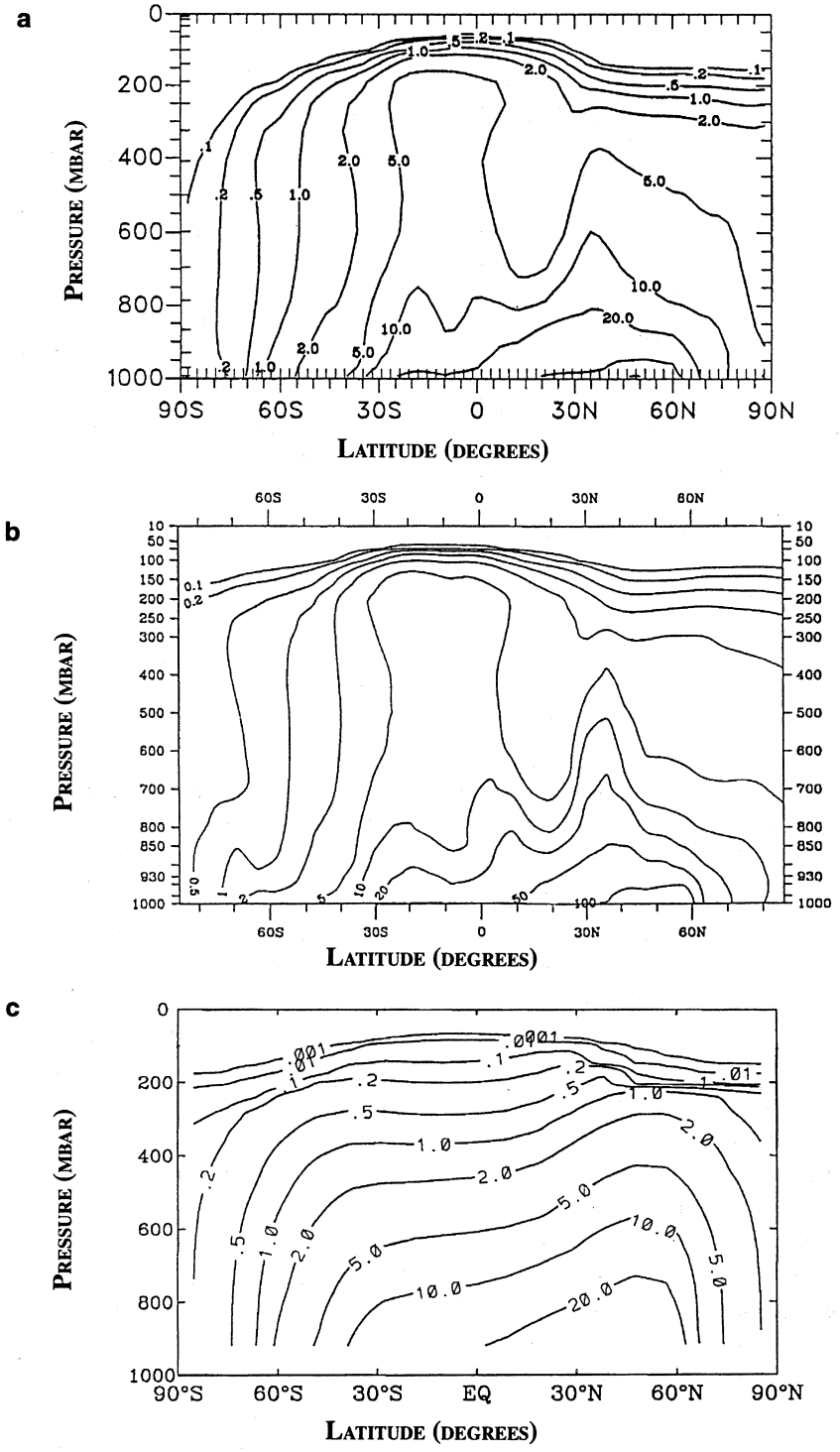

Figure 7-5. Latitude by altitude contours of chemical transport model simulations of a continental source of radon-222. Units are 1E-21 v/v. Zonal means for the period Dec-Jan-Feb are shown for two 3-D models, (a) CCM2 and (b) ECHAM3, and for (c) the AER 2-D model. These results are examples form a WCRP workshop on tracer transport.

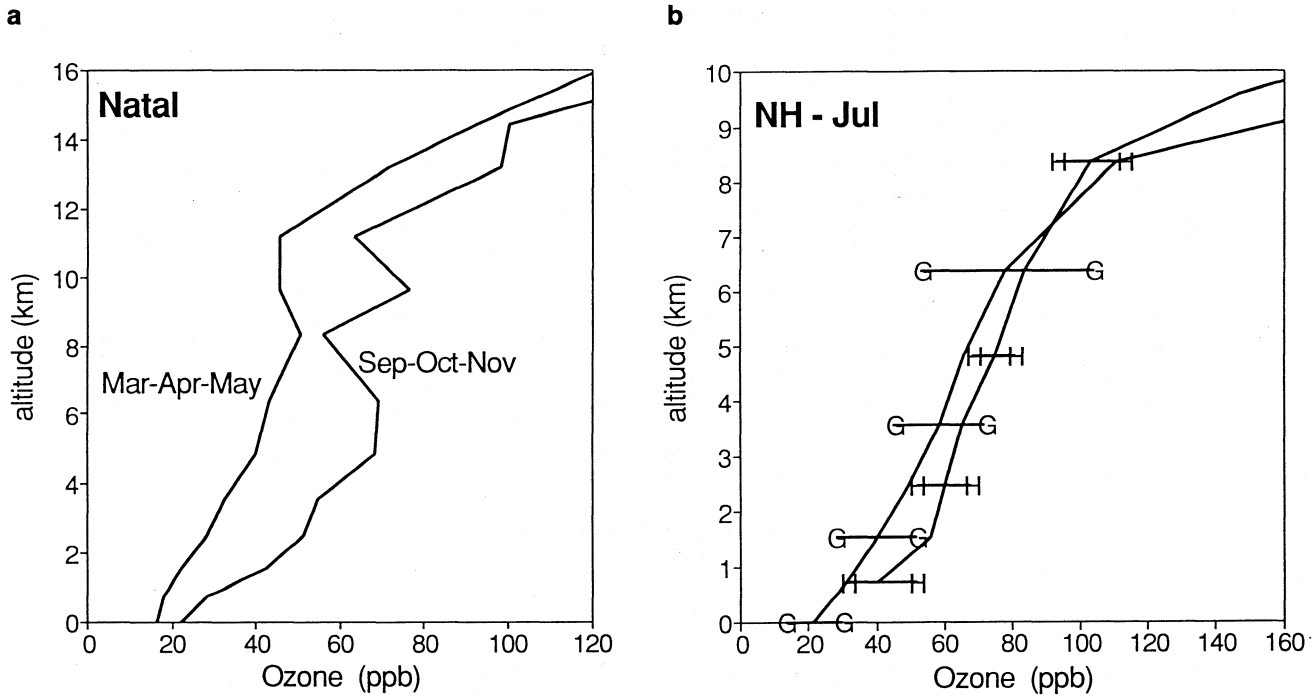

Figure 7-6. Observed mean profiles of O_3 in the tropics (Natal, panel a) and at northern midlatitudes in July (G = Goose Bay and H = Hohenpeissenberg, panel b). Data from northern stations were averaged over 1980-1991. Tropical station shows seasons of minimum (Mar-Apr-May) and maximum (Sep-Oct-Nov) ozone. Source: Logan, 1994; Kirchhoff *et al.*, 1990.

shown in Figure 7-7a-b, differ by almost a factor of two, but encompass the observations. Clear divergence of results above 10 km altitude illustrates difficulties in determining the transition between troposphere and stratosphere. This exercise is only the beginning of an objective evaluation of tropospheric ozone models through comparison with measurements.

The modeled zonal-mean NO_x profiles, shown in Figure 7-7c, differ by up to almost a factor of 10. Comparisons in the lowest 2 km altitude are not meaningful since the CTMs average regions of high urban pollution with clean marine boundary layer. The range of modeled NO_x values in the free troposphere often falls outside the range of typical observations, about 20 to 100 ppt (see Chapter 5).

O_3 Perturbations

The predicted changes in tropospheric O_3 for Jun-Jul-Aug in northern midlatitudes and the tropics are shown in Figure 7-8a and 7-8b for the delta-CH_4 study. Ozone increases everywhere in the troposphere, by values ranging from about 0.5 ppb to more than 5 ppb. (The extremely high values for model P in the upper troposphere must be considered cautiously since this recent submission has not yet been scrutinized as much as the other results.) In general the increase is larger at midlatitudes, but not for all models. Results for the southern midlatitudes in summer (Dec-Jan-Feb) (not shown) are similar to the northern.

The large spread in these results shows that our ability to predict changes in tropospheric O_3 induced by CH_4 perturbations is not very good. This conclusion is not unexpected given the large range in modeled NO_x (Figure 7-7c), but the differences in O_3 perturbations do not seem to correlate with the NO_x distribution in the models. Nevertheless, a consistent pattern of increases in tropospheric O_3, ranging from 0.5 to 2.5 ppb, occurs throughout most of the troposphere. Our best estimate is that a 20% increase in CH_4 would lead to an increase in ozone of about 1.5 ppb throughout most of the tropo-

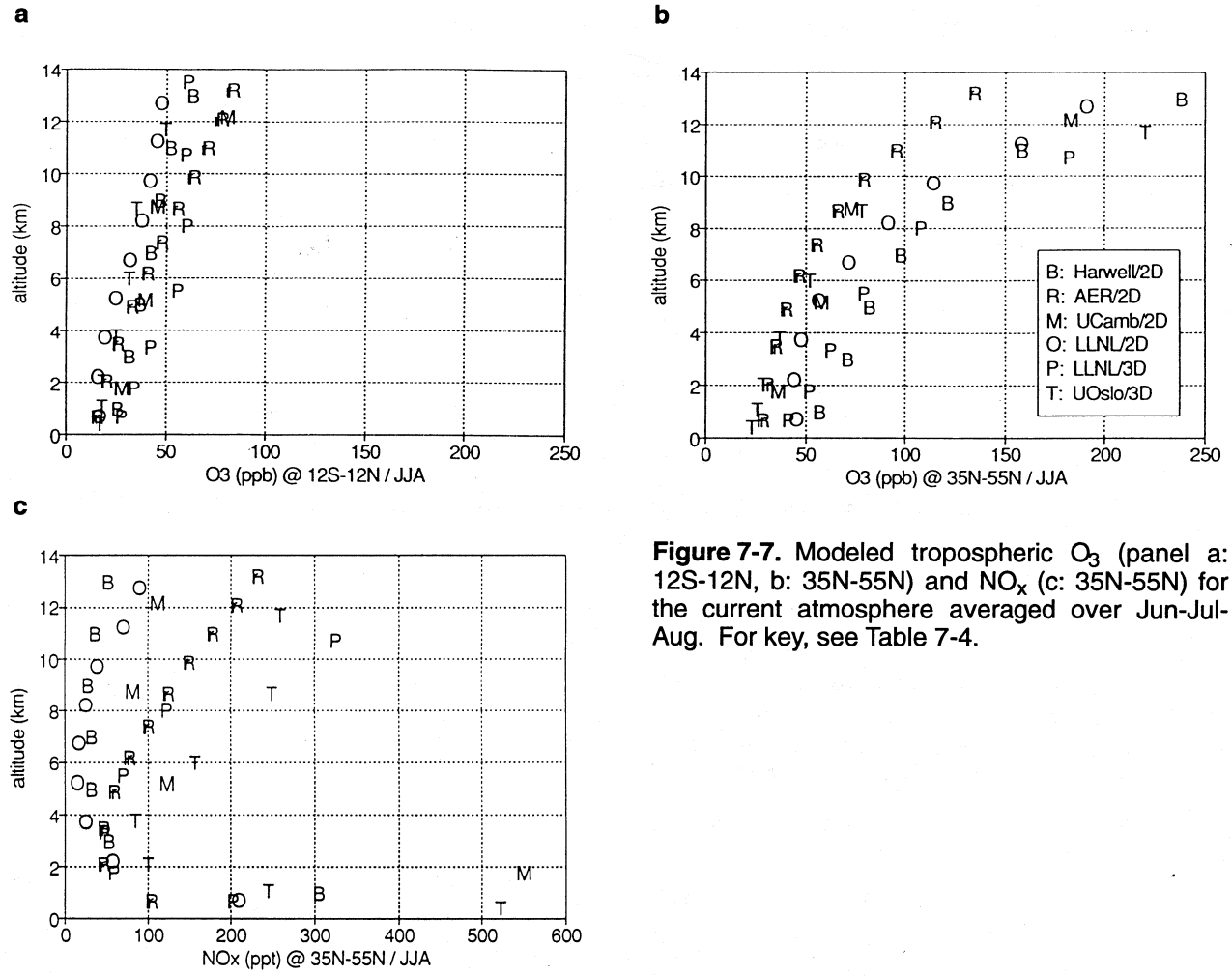

Figure 7-7. Modeled tropospheric O_3 (panel a: 12S-12N, b: 35N-55N) and NO_x (c: 35N-55N) for the current atmosphere averaged over Jun-Jul-Aug. For key, see Table 7-4.

Figure 7-8. (Below). Modeled change in O_3 for a 20% increase in CH_4, averaged over Jun-Jul-Aug (panel a: 12S-12N, b: 35N-55N). For key, see Table 7-4.

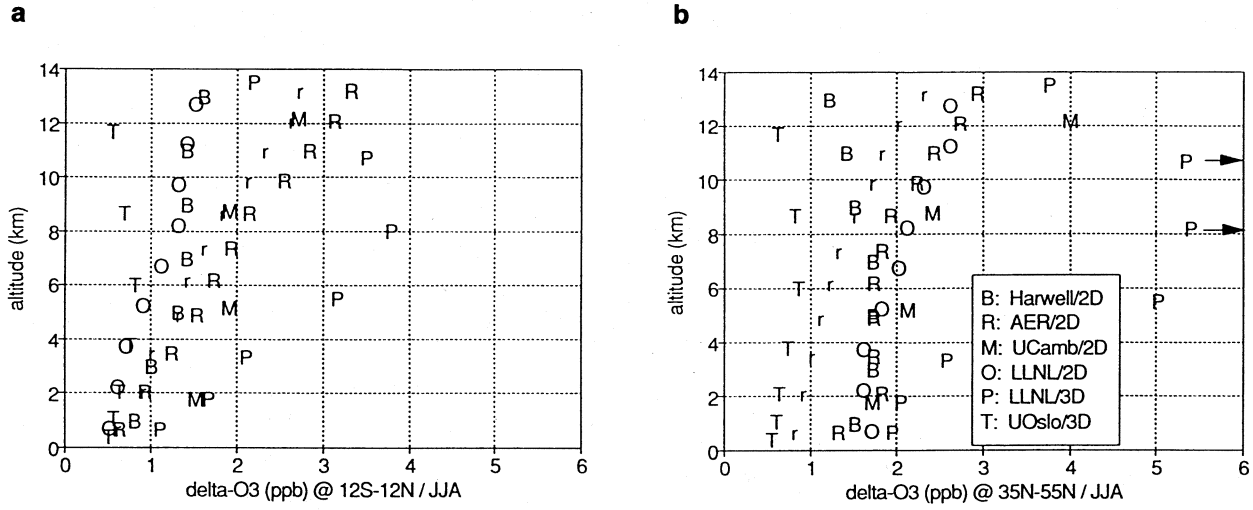

Table 7-6. Inferred CH_4 response time from delta-CH_4 simulations.

Model code	FF*	RT/LT**
B	-0.20%	1.29
M	-0.17%	1.23#
O	-0.35%	1.62
P	-0.22%	1.32
R	-0.26%	1.39
(R)	-0.18%	1.26#
T	-0.34%	1.61

Notes:

* FF = feedback factor, relative change (%) in the globally averaged CH_4 loss frequency (*i.e.*, (OH)) for a +1% increase in CH_4 concentrations

** RT = residence time and LT = lifetime

\# Uses fixed CO concentrations, underestimates this ratio.

sphere in both tropics and summertime midlatitudes. This indirect impact on the radiative forcing is about 25% ± 15% of that due to the 343 ppb increase in CH_4 alone.

Residence Time of CH_4 Emissions

Methane is the only long-lived gas that has a clearly identified, important chemical feedback: increases in atmospheric CH_4 reduce tropospheric OH, increase the CH_4 lifetime, and hence amplify the climatic and chemical impacts of a CH_4 perturbation (Isaksen and Hov, 1987; Berntsen *et al.*, 1992). The delta-CH_4 simulations from six different 2-D and 3-D models show that these chemical feedbacks change the relative loss rate for CH_4 by -0.17% to -0.35% for each 1% increase in CH_4 concentration, as shown in Table 7-6. This range can reflect differences in the modeled roles of CH_4, CO, and NMHC as sinks for OH (Prather, 1994). For example, model M, with the smallest feedback factor, has fixed the concentrations of CO; and model R has shown that calculating CO instead with a flux boundary condition (as most of the other models have done) results in a larger feedback. These differences cannot be resolved with this intercomparison, and this range underestimates our uncertainty in this factor.

Recent theoretical analysis has shown that the feedback factor (FF) defined in Table 7-6 can be used to derive a residence time that accurately describes the time scale for decay of a pulse of CH_4 added to the atmosphere. Effectively, a pulse of CH_4, no matter how small, reduces the global OH levels by a similar amount (*i.e.*, -0.3% per +1%). This leads to the buildup of a corresponding increase in the already-existing atmospheric reservoir of CH_4, that, in net, cannot be distinguished from a longer residence time for the initial pulse. Thus the residence time (RT) is longer than the lifetime (LT) derived from the budget (*i.e.*, total abundance divided by total losses). Prather (1994) has shown that the ratio, RT/LT, is equal to 1/(1 + FF) and that this residence time applies to all CH_4 perturbations, positive or "negative," no matter how small or large, as long as the change in CH_4 concentration is not so large as to change the feedback factor. Based on model results, this assumption should apply at least over a ±30% change in current CH_4 concentrations. Two of the models with results in Table 7-6 have shown that small CH_4 perturbations decay with the predicted residence time.

Based on these limited results, we choose 1.45 as the best guess for the ratio RT/LT, with an uncertainty bracket of 1.20 to 1.70. The budget lifetime of CH_4 is calculated to be about 9.4 yr, using the CH_3CCl_3 lifetime as a standard for OH and including stratospheric and soil losses. Thus, the residence time for any additional emissions of CH_4 is 13.6 yr (11.3-16.0 yr). This enhanced time scale describes the effective duration for all current

emissions of CH_4; it is independent of other emissions as long as current concentrations of CH_4, within ±30%, are maintained. Some of this effect was included in the previous assessment as an "indirect OH" enhancement to the size of the CH_4 perturbations. Here we recognize that the OH chemical feedback gives a residence time for CH_4 emissions that is substantially longer than the lifetime used to derive the global budgets. This effective lengthening of a CH_4 pulse applies also to all induced chemical perturbations such as tropospheric O_3 and stratospheric H_2O.

REFERENCES

Balkanski, Y.J., and D.J. Jacob, Transport of continental air to the subantarctic Indian Ocean, *Tellus, 42B,* 62–75, 1990.

Balkanski, Y.J., D.J. Jacob, R. Arimoto, and M.A. Kritz, Long-range transport of radon-222 over the North Pacific Ocean: Implications for continental influences, *J. Atmos. Chem., 14,* 353–374, 1992.

Balkanski, Y.J., D.J. Jacob, G.M. Gardner, W.M. Graustein, and K.K. Turekian, Transport and residence times of continental aerosols inferred from a global 3-dimensional simulation of ^{210}Pb, *J. Geophys. Res., 98,* 20573–20586, 1993.

Berntsen, T., J.S. Fuglestvedt, and I.S.A. Isaksen, Chemical-dynamical modelling of the atmosphere with emphasis on the methane oxidation, *Ber. Bunsenges. Phys. Chem., 96,* 3, 241–251, 1992.

Berntsen, T.K., and I.S.A. Isaksen, A 3-D photochemistry/transport model of the global troposphere, Report No. 89, Institute for Geophysics, University of Oslo, Norway, 1994.

Brost, R.A., J. Feichter, and M. Heimann, Three-dimensional simulation of ^{7}Be in a global climate model, *J. Geophys. Res., 96,* 22423–22445, 1991.

Brühl, C., and P.J. Crutzen, On the disproportionate role of tropospheric ozone as a filter against solar UV-B radiation, *Geophys. Res. Lett., 17,* 703–706, 1989.

Chameides, W.L., P.S. Kasibhatla, J.J. Yienger, H. Levy II, and W.J. Moxim, The growth of continental-scale metro-agro-plexes, regional ozone pollution, and world food production, *Science, 264,* 74–77, 1994.

Chatfield, R.B., The anomalous HNO_3/NO_x ratio of remote tropospheric air: Is there conversion of nitric acid to formic acid and NO_x?, submitted to *Geophys. Res. Lett.,* 1994.

Chin, M., D.J. Jacob, J.W. Munger, D.D. Parrish, and B.G. Doddridge, Relationship of ozone and carbon monoxide over North America, *J. Geophys. Res., 99,* 14565–14573, 1994.

Crutzen, P.J., and P.H. Zimmermann, The changing photochemistry of the troposphere, *Tellus, 43AB,* 136–151, 1991.

Danielsen, E.F., and V. Mohnen, Project Duststorm: Ozone transport, in situ measurements, and meteorological analysis of tropopause folding, *J. Geophys. Res., 82,* 5867–5877, 1977.

Derwent, R.G., The influence of human activities on the distribution of hydroxyl radicals in the troposphere, submitted to *Philosophical Transactions of the Royal Society,* 1994.

Easter, R.C., R.D. Saylor, and E.G. Chapman, Analysis of mid-tropospheric carbon monoxide data using a three-dimensional global atmospheric chemistry numerical model, in *Proceedings 20th Inter. Tech. Meeting on Air Pollution Modeling and Its Application,* Valencia, Spain, 1993.

Fan, S.-M., D.J. Jacob, D.L. Mauzerall, J.D. Bradshaw, S.T. Sandholm, D.R. Blake, H.B. Singh, R.W. Talbot, G.L. Gregory, and G.W. Sachse, Origin of tropospheric NO_x over subarctic eastern Canada in summer, *J. Geophys. Res., 99,* 16867-16877, 1994.

Feichter, J., and P.J. Crutzen, Parameterization of vertical tracer transport due to deep cumulus convection in a global transport model and its evaluation with $^{222}Radon$ measurements, *Tellus, 42B,* 100–117, 1990.

Feichter, J., R.A. Brost, and M. Heimann, Three-dimensional modeling of the concentration and deposition of ^{210}Pb aerosols, *J. Geophys. Res., 96,* 22447–22460, 1991.

Flatøy, F., *Modelling of Coupled Physical and Chemical Processes in the Troposphere over Europe,* Ph.D. Thesis, Geophysical Institute, University of Bergen, Norway, 1994.

Flatøy, F., Ø. Hov, and H. Smit, 3-D model studies of vertical exchange processes in the troposphere over Europe, submitted to *J. Geophys. Res.,* 1994.

Fuglestvedt, J.S., J.E. Jonson, and I.S.A. Isaksen, Effects of reductions in stratospheric ozone on tropospheric chemistry through changes in photolysis rates, *Tellus, 46B,* 172–192, 1994a.

Fuglestvedt, J.S., J.E. Jonson, W.-C. Wang, and I.S.A. Isaksen, Responses in tropospheric chemistry to changes in UV fluxes, temperatures and water vapour densities, to appear in *Atmospheric Ozone as a Climate Gas*, edited by W.-C. Wang and I.S.A. Isaksen, NASA ASI Series, in press, 1994b.

Fung, I., J. John, J. Lerner, E. Matthews, M. Prather, L.P. Steele, and P.J. Fraser, Three-dimensional model synthesis of the global methane cycle, *J. Geophys. Res., 96,* 13033–13066, 1991.

Gallardo, L., H. Rodhe, and P.J. Crutzen, Evaluation of a global 3-D model of the tropospheric reactive nitrogen cycle, submitted to *J. Geophys. Res.,* 1994.

Galloway, J.N., H. Levy II, and P.S. Kasibhatla, Year 2020: Consequences of population growth and development on deposition of oxidized nitrogen, *Ambio, 23,* 120–123, 1994.

Gidel, L.T., and M.A. Shapiro, General circulation estimates of the net vertical flux of ozone in the lower stratosphere and the implications for the tropospheric ozone budget, *J. Geophys. Res., 85,* 4049–4058, 1980.

Gleason, J.F., P.K. Bhartia, J.R. Herman, R. McPeters, P. Newman, R.S. Stolarski, L. Flynn, G. Labow, D. Larko, C. Seftor, C. Wellemeyer, W.D. Komhyr, A.J. Miller, and W. Planet, Record low global ozone in 1992, *Science, 260,* 523–526, 1993.

Gold, S., H. Barkhau, W. Shleien, and B. Kahn, Measurement of naturally occurring radionuclides in air, in *The Natural Radiation Environment*, edited by J.A.S. Adams and W.M. Lowder, University of Chicago Press, 369–382, 1964.

Hauglustaine, D.A., C. Granier, G.P Brasseur, and G. Mégie, The importance of atmospheric chemistry in the calculation of radiative forcing on the climate system, *J. Geophys. Res., 99,* 1173–1186, 1994.

IPCC, Intergovernmental Panel on Climate Change, *Radiative Forcing of Climate Change,* The 1994 Report of the Scientific Assessment Working Group of IPCC, 1994.

Isaksen, I.S.A., and Ø. Hov, Calculation of trends in the tropospheric concentration of O_3, OH, CH_4, and NO_x, *Tellus, 39B,* 271–285, 1987.

Jacob, D.J., M.J. Prather, S.C. Wofsy, and M.B. McElroy, Atmospheric distribution of ^{85}Kr simulated with a general circulation model, *J. Geophys. Res., 92,* 6614–6626, 1987.

Jacob, D.J., and M.J. Prather, Radon-222 as a test of convection in a general circulation model, *Tellus, 42,* 118–134, 1990.

Jacob, D.J., S.C. Wofsy, P.S. Bakwin, S.-M. Fan, R.C. Harriss, R.W. Talbot, J.D. Bradshaw, S.T. Sandholm, H.B. Singh, E.V. Browell, G.L. Gregory, G.W. Sachse, M.C. Shipham, D.R. Blake, and D.R. Fitzjarrald, Summertime photochemistry of the troposphere at high northern latitudes, *J. Geophys. Res., 97,* 16421–16431, 1992.

Jacob, D.J., J.A. Logan, R.M. Yevich, G.M. Gardner, C.M. Spivakovsky, S.C. Wofsy, J.W. Munger, S. Sillman, M.J. Prather, M.O. Rodgers, H. Westberg, and P.R. Zimmerman, Simulation of summertime ozone over North America, *J. Geophys. Res., 98,* 14797–14816, 1993a.

Jacob, D.J., J.A. Logan, G.M. Gardner, R.M. Yevich, C.M. Spivakovsky, S.C. Wofsy, S. Sillman, and M.J. Prather, Factors regulating ozone over the United States and its export to the global atmosphere, *J. Geophys. Res., 98,* 14817–14826, 1993b.

Johnson, C.E., The sensitivity of a two-dimensional model of global tropospheric chemistry to emissions at different latitudes, *AEA Environment & Energy,* United Kingdom Atomic Energy Authority, AEA-EE-0407, 1993.

Johnson, C., J. Henshaw, and G. McInnes, Impact of aircraft and surface emissions of nitrogen oxides on tropospheric ozone and global warming, *Nature, 355,* 69-71, 1992.

Kanakidou, M., and P.J. Crutzen, Scale problems in global tropospheric chemistry modelling: Comparison of results obtained with a three-dimensional model, adopting longitudinally uniform and varying emissions of NO_x and NMHC, *Chemosphere, 26* (1-4), 787–801, 1993.

Kanakidou, M., H.B. Singh, K.M. Valentin, and P.J. Crutzen, A two-dimensional model study of ethane and propane oxidation in the troposphere, *J. Geophys. Res., 96,* 15395-15413, 1991.

Kanakidou, M., P.J. Crutzen, P.H. Zimmermann, and B. Bonsang, A 3-dimensional global study of the photochemistry of ethane and propane in the troposphere: Production and transport of organic nitrogen compounds, in *Air Pollution Modelling and Its Application IX,* edited by H. van Dop and G. Kallos, Plenum Press, New York, 415–426, 1992.

Kasibhatla, P.S., H. Levy II, W.J. Moxim, and W.L. Chameides, The relative impact of stratospheric photochemical production on tropopsheric NO_y levels: A model study, *J. Geophys. Res., 96,* 18631–18646, 1991.

Kasibhatla, P.S., NO_y from sub-sonic aircraft emissions: A global three-dimensional model study, *Geophys. Res. Lett., 20,* 1707–1710, 1993.

Kasibhatla, P.S., H. Levy II, and W.J. Moxim, Global NO_x, HNO_3, PAN, and NO_y distributions from fossil fuel combustion emissions: A model study, *J. Geophys. Res., 98,* 7165–7180, 1993.

Kaye, J., S. Penkett, and F.M. Ormond (eds.), *Concentrations, Lifetimes and Trends of CFCs, Halons, and Related Species*, National Aeronautics and Space Administration Reference Publication No. 1339, 1994.

Kerr, J.B., and C.T. McElroy, Evidence for large upward trends of ultraviolet-B radiation linked to ozone depletion, *Science, 262,* 1032–1034, 1993.

Kirchhoff, V.W.J.H., I.M.O. da Silva, and E.V. Browell, Ozone measurements in Amazonia: Dry season versus wet season, *J. Geophys. Res., 95,* 16913–16926, 1990.

Law, K.S., and J.A. Pyle, Modelling trace gas budgets in the troposphere 1. Ozone and odd nitrogen, *J. Geophys. Res., 98,* 18377–18400, 1993a.

Law, K.S., and J.A. Pyle, Modelling trace gas budgets in the troposphere 2. CH_4 and CO, *J. Geophys. Res., 98,* 18401–18412, 1993b.

Lelieveld, J., Model simulations of the 1850 and 1990 atmosphere chemical compositions, accepted for publication in *J. Geophys. Res.,* 1994.

Lelieveld, J., and P. Crutzen, Role of deep convection in the ozone budget of the troposphere, *Science, 264,* 1759–1761, 1994.

Liu, S.C., and M. Trainer, Responses of tropospheric ozone and odd hydrogen radicals to column ozone change, *J. Atmos. Chem., 6,* 221–233, 1988.

Liu, S.C., S.A. McKeen, and S. Madronich, Effect of anthropogenic aerosols on biologically active ultraviolet radiation, *Geophys. Res. Lett., 18,* 2265–2268, 1991.

Logan, J.A., Trends in the vertical distribution of ozone: An analysis of ozonesonde data, submitted to *J. Geophys. Res.,* 1994.

Madronich, S., and C. Granier, Impact of recent total ozone changes on tropospheric ozone photodissociation, hydroxyl radicals, and methane trends, *Geophys. Res. Lett., 19,* 465–467, 1992.

Mahlman, J.D., H. Levy II, and W.J. Moxim, Three-dimensional tracer structure and behavior as simulated in two ozone precursor experiments, *J. Atmos. Sci., 37,* 655–685, 1980.

Montzka, S.A., R.C. Myers, J.H. Butler, and J.W. Elkins, Global tropospheric distribution and calibration scale of HCFC-22, *Geophys. Res. Lett., 20,* 703–706, 1993.

Murphy, D.M., D.W. Fahey, M.H. Proffitt, S.C. Liu, K.R. Chan, C.S. Eubank, S.R. Kawa, and K.K. Kelly, Reactive nitrogen and its correlation with ozone in the lower stratosphere and the upper troposphere, *J. Geophys. Res., 98,* 8751–8773, 1993.

Müller, J.-F., and G. Brasseur, IMAGES: A three-dimensional chemical transport model of the troposphere, accepted for publication in *J. Geophys. Res.,* 1994.

Patten, K.O., P.S. Connell, D.E. Kinnison, D.J. Wuebbles, L. Froidevaux, and T.G. Slanger, Effect of vibrationally excited oxygen on ozone production in the stratosphere, *J. Geophys. Res., 99,* 1211–1223, 1994.

Penner, J.E., C.S. Atherton, J. Dignon, S.J. Ghan, J.J. Walton, and S. Hameed, Tropospheric nitrogen: A three-dimensional study of sources, distributions, and deposition, *J. Geophys. Res., 96,* 959–990, 1991.

Penner, J.E., C.S. Atherton, and T.E. Graedel, Global emissions and models of photochemically active compounds, in *Global Atmospheric-Biospheric Chemistry*, edited by R. Prinn, Plenum Publ., New York, 223-248, 1994.

Pickering, K.E., A.M. Thompson, J.R. Scala, W.-K. Tao, and J. Simpson, Ozone production potential following convective redistribution of biomass burning emissions, *J. Atmos. Chem., 14,* 297–313, 1992.

Pickering, K.E., A.M. Thompson, W.-K. Tao, and T.L. Kucsera, Upper tropospheric ozone production following mesoscale convection during STEP/EMEX, *J. Geophys. Res., 98,* 8737–8749, 1993.

Polian, G., G. Lambert, B. Ardouin, and A. Jegou, Long-range transport of radon in sub-Antarctic and Antarctic areas, *Tellus, 38B,* 178–189, 1986.

Prather, M.J., Lifetimes and eigenstates in atmospheric chemistry, *Geophys. Res. Lett., 21,* 801–804, 1994.

Prather, M.J., M. McElroy, S. Wofsy, G. Russell, and D. Rind, Chemistry of the global troposphere: Fluorocarbons as tracers of air motion, *J. Geophys. Res., 92,* 6579–6613, 1987.

Prather, M.J., and E.E. Remsberg (eds.), *The Atmospheric Effects of Stratospheric Aircraft: Report of the 1992 Models and Measurements Workshop*, National Aeronautics and Space Administration Reference Publication No. 1292, 1992.

Prinn, R., D. Cunnold, P. Simmonds, F. Alyea, R. Boldi, A. Crawford, P. Fraser, D. Gutzler, D. Hartley, R. Rosen, and R. Rasmussen, Global average concentration and trend for hydroxyl radicals deduced from ALE/GAGE trichloroethane (methyl chloroform) data for 1978-1990, *J. Geophys. Res., 97,* 2445–2461, 1992.

Roemer, M.G.M., and K.D. van der Hout, Emissions of NMHCs and NO_x and global ozone production, in *Proceedings of the 19th NATO/CCMS International Technical Meeting on Air Pollution Modelling and Its Application,* North Atlantic Treaty Organization/Committee on the Challenges of Modern Society, September 29–October 4, 1991, Crete, Greece, Plenum Press, New York, 1992.

Simpson, D., Photochemical model calculations over Europe for two extended summer periods: 1985 and 1989. Model results and comparison with observations, *Atmos. Environ., 27A,* 921–943, 1993.

Singh, H.B., D. O'Hara, D. Herlth, J.D. Bradshaw, S.T. Sandholm, G.L. Gregory, G.W. Sachse, D.R. Blake, P.J. Crutzen, and M. Kanakidou, Atmospheric measurements of peroxyacetyl nitrate and other organic nitrates at high-latitudes: Possible sources and sinks, *J. Geophys. Res., 97,* 16511–16522, 1992.

Singh, H.B., and M. Kanakidou, An investigation of the atmospheric sources and sinks of methyl bromide, *Geophys. Res. Lett., 20,* 133-136, 1993.

Singh, H.B., D. O'Hara, D. Herlth, W. Sachse, D.R. Blake, J.D. Bradshaw, M. Kanakidou, and P.J. Crutzen, Acetone in the atmosphere: Distribution, sources and sinks, *J. Geophys. Res., 99,* 1805–1820, 1994.

Smith, R.C., B.B. Prézelin, K.S. Baker, R.R. Bidigare, N.P. Boucher, T. Coley, D. Karstenz, S. MacIntyre, H. Matlick, D. Menzies, M. Ondrusek, Z. Wan, and K.J. Waters, Ozone depletion: Ultraviolet radiation and phytoplankton biology in Antarctic waters, *Science, 255,* 952–959, 1992.

Spivakovsky, C.M., R. Yevich, J.A. Logan, S.C. Wofsy, M.B. McElroy, and M.J. Prather, Tropospheric OH in a three-dimensional chemical tracer model: An assessment based on observations of CH_3CCl_3, *J. Geophys. Res., 95,* 18441–18472, 1990a.

Spivakovsky, C.M., S.C. Wofsy, and M.J. Prather, A numerical method for parameterization of atmospheric chemistry: Computation of tropospheric OH, *J. Geophys. Res., 95,* 18433–18440, 1990b.

Spivakovsky, C.M., and Y.J. Balkanski, Tropospheric OH: Constraints imposed by observations of ^{14}CO and methyl chloroform, in *Report of the WMO-Sponsored Meeting of Carbon Monoxide Experts,* edited by P.C. Novelli and R.M. Rosson, Global Atmospheric Watch, World Meteorological Organization, Geneva, in press, 1994.

Strand, A., and Ø. Hov, A two-dimensional zonally averaged transport model including convective motions and a new strategy for the numerical solution, *J. Geophys. Res., 98,* 9023–9037, 1993.

Strand, A., and Ø. Hov, Two-dimensional global study of the tropospheric ozone production, accepted for publication in *J. Geophys. Res.,* 1994.

Tie, X., C.-Y. Kao, E.J. Mroz, R.J. Cicerone, F.N. Alyea, and D.M. Cunnold, Three-dimensional simulations of atmospheric methyl chloroform: Effect of an ocean sink, *J. Geophys. Res., 97,* 20751–20769, 1992.

Thompson, A.M., The oxidizing capacity of the Earth's atmosphere: Probable past and future changes, *Science, 256,* 1157–1165, 1992.

WMO, *Scientific Assessment of Ozone Depletion: 1989,* World Meteorological Organization Global Ozone Research and Monitoring Project – Report No. 20, Geneva, 1990.

WMO, *Scientific Assessment of Ozone Depletion: 1991,* World Meteorological Organization Global Ozone Research and Monitoring Project – Report No. 25, Geneva, 1992.

Wuebbles, D.J., J.S. Tamaresis, and K.O. Patten, *Quantified Estimates of Total GWPs for Greenhouse Gases Taking Into Account Tropospheric Chemistry*, Lawrence Livermore National Laboratory UCRL-115850, 1993.

PART 4

CONSEQUENCES OF OZONE CHANGE

Chapter 8
Radiative Forcing and Temperature Trends

Chapter 9
Surface Ultraviolet Radiation

CHAPTER 8

Radiative Forcing and Temperature Trends

Lead Author:
K.P. Shine

Co-authors:
K. Labitzke
V. Ramaswamy
P.C. Simon
S. Solomon
W.-C. Wang

Contributors:
C. Brühl
J. Christy
C. Granier
A.S. Grossman
J.E. Hansen
D. Hauglustaine
H. Mao
A.J. Miller
S. Pinnock
M.D. Schwarzkopf
R. Van Dorland

SCIENTIFIC SUMMARY

I. Radiative Forcing and Climatic Impact of Ozone Change

- Recent one-dimensional studies support earlier conclusions that between 1980 and 1990 the observed decrease in stratospheric ozone has caused a negative global-mean radiative forcing (*i.e.,* it acts to cool the climate) that is about -0.1 Wm^{-2}; this can be compared to the direct radiative forcing due to changes in CO_2, CH_4, N_2O, and the chlorofluorocarbons (the "well-mixed" gases) of about 0.45 Wm^{-2} over the same period. An accurate assessment of the potential climatic effect of changes in stratospheric ozone is limited by the lack of detailed information on the ozone change, especially in the vicinity of the tropopause. A limited sensitivity study using different assumptions about the vertical profile of ozone loss indicates that, for the same change in total column ozone, the ozone forcing could conceivably be up to a factor of two less negative.

- Model simulations and deductions from limited observations of the increase in tropospheric ozone since pre-industrial times suggest a positive global-mean forcing that may be around 0.5 Wm^{-2}; this can be compared to the direct radiative forcing due to changes in well-mixed gases of about 2.4 Wm^{-2} over the same period. Particular difficulties are the verification of the geographical extent of the tropospheric ozone increases and the problems in accurately specifying the vertical profile of the change.

- On the basis of these estimates, the net global-mean radiative forcing due to ozone changes is likely to have been positive since pre-industrial times. However, Chapter 1 indicates that tropospheric ozone has changed little since 1980 and so, since then, the stratospheric ozone change is likely to have dominated, giving a negative global-mean forcing due to ozone changes.

- An intercomparison of radiation codes used in assessments of the radiative forcing due to ozone changes has shown that, in general, differences between these codes can be explained; the intercomparison highlights the detail with which solar and thermal infrared processes must be represented.

- The only general circulation model (GCM) experiment to investigate the climatic impact of observed lower stratospheric ozone loss between 1970 and 1990 indicates the expected surface cooling in response to the negative radiative forcing.

- Other GCM simulations raise important, but as yet unresolved, issues about the way in which the global mean of a spatially very inhomogeneous radiative forcing, such as that due to ozone change, can be directly compared to the global-mean forcing due to, for example, changes in well-mixed greenhouse gases.

- The previous assessment noted that the negative radiative forcing due to stratospheric ozone loss in the 1980s is of a similar size as, but the opposite sign to, the positive direct radiative forcing due to halocarbons over the same period. Attempts have been made to partition the indirect negative forcing due to ozone loss amongst individual halocarbons. They have emphasized that bromocarbons are, on a per molecule basis, much more efficient at destroying ozone than chlorofluorocarbons (CFCs). One evaluation attributes about 50% of the 1980-1990 negative forcing to the CFCs; since the CFCs dominate the direct forcing, their net effect is reduced by about 50% due to the ozone loss. Carbon tetrachloride and methyl chloroform each contribute about 20%, while bromocarbons contribute about 10% to the indirect forcing; these species contribute relatively little to the direct forcing so their net effect is likely to be negative.

II. Lower Stratospheric Temperature Trends

- The temperature of the lower stratosphere showed a marked rise, of about 1 deg C in the global mean, due to the radiative effects of increases in stratospheric aerosol loading following the eruption of Mt. Pinatubo in June 1991. The maximum warming occurred in the six months following the eruption; temperatures have now returned to near pre-eruption levels. This warming has been successfully simulated by GCMs.

- Data from radiosondes over the past three decades and satellite observations since the late 1970s continue to support the existence of a long-term global-mean cooling of the lower stratosphere of about 0.25 to 0.4 deg C/ decade; there is some indication of an acceleration in this cooling during the 1980s, but the presence of large temperature perturbations induced by volcanic aerosols makes trend analysis difficult.

- Model calculations indicate that ozone depletion is likely to have been the dominant contributor to the temperature trend in the lower stratosphere since 1980 and is much more important than the contribution of well-mixed greenhouse gases. In addition, observed temperature trends since 1979 are found to be significantly negative at the same latitudes and times of year as significant decreases in column ozone, with the exception of the southern midlatitudes in midwinter. However, there are other potential causes of lower stratospheric temperature change (such as changes in stratospheric water vapor or cirrus clouds) whose contributions are difficult to quantify.

III. Radiative Properties of Halocarbon Substitutes

- More laboratory measurements of the infrared absorption cross sections of actual and proposed substitutes to chlorofluorocarbons have become available, including molecules not hitherto reported in assessments. These cross sections have been included in radiative transfer models to provide estimates of the radiative forcing per molecule. The radiative forcing estimates are subjectively estimated to be accurate to within 25%, but not all of the studies have yet been reported in adequate detail in the open literature; this hinders a detailed understanding of differences in existing estimates.

8.1 INTRODUCTION

In recent ozone assessments, changes in the radiation balance have been an issue because (i) the chlorofluorocarbons (CFCs) and their hydrohalocarbon replacements are powerful absorbers of infrared radiation and (ii) changes in stratospheric ozone have been shown to cause a significant radiative forcing of the surface-troposphere system (WMO, 1992). Hence both factors are of potential importance in understanding climate change.

The aim of this Chapter is to provide an update of research in these two areas. In addition, significant changes in stratospheric temperature have been reported in recent assessments (WMO, 1988); it is believed that changes in the radiative properties of the stratosphere are an important part of the cause of the temperature trends. Changes in ozone appear to be of particular significance; in turn, ozone may itself be affected by the temperature changes. This Chapter will update both the observations of temperature changes and our understanding of their causes; we will concentrate on the lower stratosphere because ozone losses are believed to be greatest in this region and also because it is changes in this region that are believed to be of most climatic significance.

It is not our aim to provide an overall assessment of our understanding of the radiative forcing of climate change. Such an assessment will be part of IPCC (1994). Instead we concentrate on the radiative forcing due to halocarbons and ozone change, building on the discussion in IPCC (1994). In common with the rest of this assessment, we will also consider the role of tropospheric ozone changes.

One important discussion in IPCC (1994) concerns the utility of the entire concept of radiative forcing. Radiative forcing is defined as the global-mean change in the net irradiance at the tropopause following a change in the radiative properties of the atmosphere or in the solar energy received from the Sun. As discussed in IPCC (1994), the preferred definition includes the concept of stratospheric adjustment, in which the stratospheric temperatures are allowed to alter such as to re-establish a state of global-mean radiative equilibrium; this process is of particular relevance when considering the forcing due to stratospheric ozone change.

The utility of radiative forcing has been based on model results indicating that the climate response is essentially independent of the forcing mechanism. Thus, a radiative forcing of x Wm^{-2} due to a change in greenhouse gas concentration would give essentially the same climate response as x Wm^{-2} at the tropopause due to, say, a change in solar output; this is despite the fact that the two mechanisms involve rather different partitioning of the irradiance change between the surface and troposphere as well as between different latitudes and seasons.

Recent, and rather preliminary, results from general circulation models (GCMs) indicate that this relationship may not be so well-behaved for radiative forcings due to changes in ozone and tropospheric aerosols, where there are strong vertical, horizontal, and temporal variations in both the concentrations of the species and their changes with time.

If this work were to be confirmed, it would make it more difficult to intercompare the forcings in Wm^{-2} between different climate change mechanisms; in particular it might be difficult to add the forcings from different mechanisms to achieve a meaningful total forcing.

Hence radiative forcing must be used with some caution, although much more work is needed to investigate whether the concept lacks general validity. Radiative forcing remains a useful measure for intercomparing different calculations of ozone forcing and for intercomparing the strength of different halocarbons.

8.2 RADIATIVE FORCING DUE TO OZONE CHANGE

8.2.1 Recent Calculations

8.2.1.1 Stratospheric Ozone Change

The principal features outlined in IPCC (1992) and WMO (1992) concerning the net radiative forcing of the surface-troposphere system due to ozone depletion in the lower stratosphere are:

a) the distinction between the solar component that acts to heat the surface-troposphere system and the longwave component that tends to cool it;

b) the difference between the instantaneous forcing (referred to as "Mode A" in WMO, 1992)

and the forcing calculated using adjusted stratospheric temperatures (referred to as "Mode B" in WMO, 1992); the consequent cooling of the lower stratosphere enhances the longwave radiative effects to give a net negative forcing.

These features have been supported by several model studies (Ramaswamy *et al.*, 1992; Wang *et al.*, 1993; Shine, 1993; Karol and Frolkis, 1994), as well as by an intercomparison exercise to be discussed in Section 8.2.2.

An accurate knowledge of the magnitude of the ozone loss in the lower stratosphere in different regions is crucial in evaluating the global-mean radiative forcing. Chapter 1 indicates the possibility of a small ozone depletion in the tropics. The radiative forcing consequences of such a loss would depend on the vertical profile of the loss profile; it could be significant if it were to be concentrated in the lower stratosphere (Schwarzkopf and Ramaswamy, 1993).

The radiative forcing is strongly governed by the shape of the vertical profile of the ozone loss, particularly in the vicinity of the tropopause (Wang *et al.*, 1980; Lacis *et al.*, 1990). While it is unambiguously clear that a loss of ozone in the lower stratosphere will lead to a negative radiative forcing of the surface-troposphere system, the precise value is dependent on the assumed altitude shape of the ozone change.

Schwarzkopf and Ramaswamy (1993) examine this problem by using 1978-1990 ozone changes at altitudes above 17 km derived from Stratospheric Aerosol and Gas Experiment (SAGE) observations; they make a range of assumptions about how the ozone changes between the tropopause and 17 km. The results can be quoted in terms of the radiative forcing per Dobson unit (DU) change in stratospheric ozone. Their results depend on latitude, mainly because a smaller fraction of the ozone depletion is located near the tropopause at higher latitudes. In the tropics, the estimates range from 0.007 to 0.01 Wm^{-2}/DU; at midlatitudes the relative uncertainty is greater with a range of 0.003 to 0.008 Wm^{-2}/DU. Such values are obviously dependent on the SAGE ozone change profiles used in the calculations.

Wang *et al.* (1993) report instances where the change in stratospheric ozone results in a warming rather than a cooling of the surface-troposphere system; this can be explained by the fact that the position of the tropopause in these calculations is such that some of the ozonesonde-observed increases in tropospheric ozone are attributed to the lower stratosphere. Hauglustaine *et al.* (1994) also find that the decrease in stratospheric ozone causes a warming of the surface-troposphere system. They used a 2-D chemical-dynamical-radiative model to simulate changes in concentration of a number of gases, including ozone, since pre-industrial times; the sign of the stratospheric ozone effect in their model appears to be because, in the Northern Hemisphere at least, their model simulates less ozone depletion in the lower stratosphere than is indicated by recent observations – their fractional ozone loss is found to be highest in the mid- to upper stratosphere, where a decrease in ozone leads to a positive radiative forcing (Lacis *et al.*, 1990). The model of Hauglustaine *et al.* (1994) does include an interactive dynamical response, so they are not dependent on assumptions such as those required when applying fixed dynamical heating.

These recent model studies highlight the need for a detailed consideration to be given to the vertical profile of the depletion and for consistency between the tropopause level chosen to estimate the surface-troposphere forcing and the altitude profile of the ozone change. Model-dependent factors are also significant for the accuracy of the computed forcing, as will be discussed in Section 8.2.2.

The overall effect of observed stratospheric ozone depletion on radiative forcing has not been significantly updated since WMO (1992), which reported a forcing of about -0.1 Wm^{-2} between 1980 and 1990. Hansen *et al.* (1993) compute a global mean change of -0.2 ± 0.1 Wm^{-2} between 1970 and 1990. Such values represent a small but not negligible offset to the greenhouse forcing from changes in CO_2, CH_4, N_2O, and CFCs (the so-called "well-mixed" gases) that result in a forcing of about 0.45 Wm^{-2} between 1980 and 1990. The results of Schwarzkopf and Ramaswamy (1993) show that different assumptions about the vertical profile of ozone change, for the same change in total column ozone, could conceivably result in an ozone forcing up to a factor of two less negative.

8.2.1.2 Tropospheric Ozone Change

Estimates for the global effect of tropospheric ozone increases are scarcer, mainly because of the difficulties in making global estimates of ozone change from

the limited observations that are available. The model study of Hauglustaine *et al.* (1994) found that their simulated tropospheric ozone increases contributed about 0.5 Wm^{-2} to the radiative forcing; this can be compared to the forcing of about 2.4 Wm^{-2} due to the changes in well-mixed gases since pre-industrial times (IPCC, 1990). (See Chapter 7 for an assessment of the ability of current models to represent tropospheric ozone changes.) Marenco *et al.* (1994) have used observations from France in the late nineteenth century, together with recent observations of the meridional distribution of tropospheric ozone, to make a simple radiative forcing estimate; they derive a global-mean radiative forcing since pre-industrial times of 0.6 Wm^{-2}. Fishman (1991), using observed trends, estimates that between 1965 and 1985, a 1%/year trend in tropospheric ozone applied over the entire Northern Hemisphere implies an approximate global-mean forcing of 0.15 Wm^{-2}, or about 20% of the effect of well-mixed gases over this period. Particular difficulties in all studies of the radiative forcing due to tropospheric ozone change are the verification of the geographical extent of the ozone increases and the problems in accurately specifying the vertical profile of ozone change.

8.2.1.3 Net Effect of Ozone Change

While it is clear that a tropospheric ozone increase would lead to a positive radiative forcing, and that this would be opposite to the effect due to the lower stratospheric losses, the sign of the net effect is uncertain (WMO, 1986; Lacis *et al.*, 1990; Karol and Frolkis, 1994; Schwarzkopf and Ramaswamy, 1993; Wang *et al.*, 1993). Wang *et al.* point out that the net forcing due to the total ozone change in the atmosphere at the locations of the sonde measurements could be positive or negative; at Hohenpeissenberg the net forcing due to ozone changes between the 1970s and 1980s was calculated to be positive and comparable to that due to the increases in the well-mixed greenhouse gases over the same period. Lacis *et al.* (1990), on the other hand, found that for the period 1970-1982, the forcing due to the Hohenpeissenberg changes was negative; however the uncertainty, due to uncertainties in the trend estimate, was large. The effects due to the total atmospheric ozone change are extremely sensitive to the vertical profile of the changes (both in the troposphere and the stratosphere), the tropopause level assumed, and the latitude and season.

On the basis of these estimates, the net global-mean radiative forcing due to ozone changes is likely to have been positive since pre-industrial times. However, Chapter 1 indicates that tropospheric ozone has changed little since 1980 and so, since then, the stratospheric ozone change is likely to have dominated, giving a negative global-mean forcing due to ozone changes.

8.2.2 Intercomparison of Models Used to Calculate Radiative Forcing

The recent work described above highlights the need to understand the reported differences in radiative forcing due to ozone change. Whilst the overall features of these differences were attributable to different assumptions about the vertical profile of ozone change, it

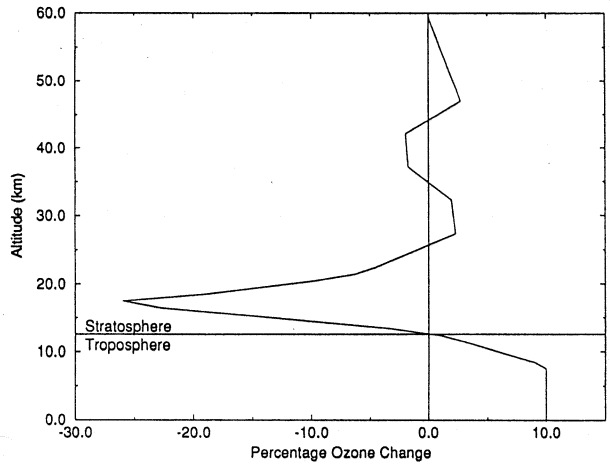

Figure 8-1. Idealized change in ozone as a function of height used solely for the purposes of the intercomparison of radiative codes. The stratospheric change is based on the midlatitude S2 profile of Schwarzkopf and Ramaswamy (1993), which was derived from SAGE/SAGE II measurements during the 1980s above 17 km, then decreasing linearly with altitude to zero at the tropopause at 13 km. The tropospheric increase is an idealized one of 10% up to 8 km, then decreasing linearly with altitude to zero at the tropopause. The stratospheric decrease is 15.5 Dobson units and the tropospheric increase is 3.5 Dobson units. The results shown in Figure 8-2 to 8-4 are calculated using the change in the stratosphere only.

Table 8-1. Participants in Ozone Radiative Forcing Intercomparison and brief description of model type. It is emphasized that the spectral resolution of a radiative transfer scheme is not always a good indication of its accuracy.

Group	Thermal IR scheme	Solar Scheme
GFDL (Geophysical Fluid Dynamics Laboratory)	10 cm^{-1} narrow-band code – Ramaswamy *et al.* (1992)	Wide-band code based on Lacis and Hansen (1974) – two bands in UV and visible
GFDL (2)	Line-by-line code – Schwarzkopf and Fels (1991)	
KNMI (Koninklijk Nederlands Meteorologisch Instituut)	Wide-band scheme amended from Morcrette (1991) to include more trace gases	Wide-band delta-Eddington scheme from Morcrette (1991) – one band in UV and visible
KNMI (2)	As KNMI(1) but including 14 μm band of ozone	As KNMI
LLNL (Lawrence Livermore National Laboratory)	25 cm^{-1} narrow-band scheme – Grossman and Grant (1994)	Narrow-band code with 126 bands between 175-725 nm using adding method for scattering – Grossman *et al.* (1993)
NCAR/CNRS (National Center for Atmospheric Research/ Centre National de la Recherche Scientifique)	Longwave Band Model (LWBM) 100 cm^{-1} resolution – Briegleb (1992)	Wide-band scheme based on Lacis and Hansen (1974) – Kiehl *et al.* (1987)
Reading (University of Reading)	10 cm^{-1} narrow-band scheme – Shine (1991)	Delta-Eddington scheme from Slingo and Schrecker (1982) with 10 bands in UV and visible
Reading (2)	As Reading but excluding 14 μm and microwave bands of ozone	As Reading
SUNY (State University of New York)	Wide-band scheme – Wang *et al.* (1991)	Wide-band scheme based on Lacis and Hansen (1974) – Kiehl *et al.* (1987)

is important to isolate to what extent differences are due to the radiative transfer methods employed in the studies. An intercomparison of results from different radiative codes was initiated to study this issue. The results are reported in more detail in Shine *et al.* (1994); the main conclusions of the study will be described here.

The intercomparison used tightly specified input parameters to ensure that all groups were using the same conditions. A midlatitude summer clear-sky atmosphere was used with a spectrally constant surface albedo of 0.1. The solar forcing was calculated using an effective daylength and mean solar zenith angle appropriate to 15 April at 45°N. The vertical profile of ozone and ozone change was specified; the ozone change is shown in Figure 8-1 and is described in the caption. Groups were asked to provide the change in solar and thermal infrared irradiances at the tropopause for both the instantaneous and adjusted forcings (calculated using the fixed dynamical heating assumption [*e.g.*, WMO, 1992]). Three different cases were considered: (i) stratospheric depletion only, (ii) tropospheric increase only, and (iii) both stratospheric depletion and tropospheric increase. The results from the case with stratospheric depletion only will be concentrated on here.

Six groups participated in at least part of the comparison. They are listed in Table 8-1 along with an

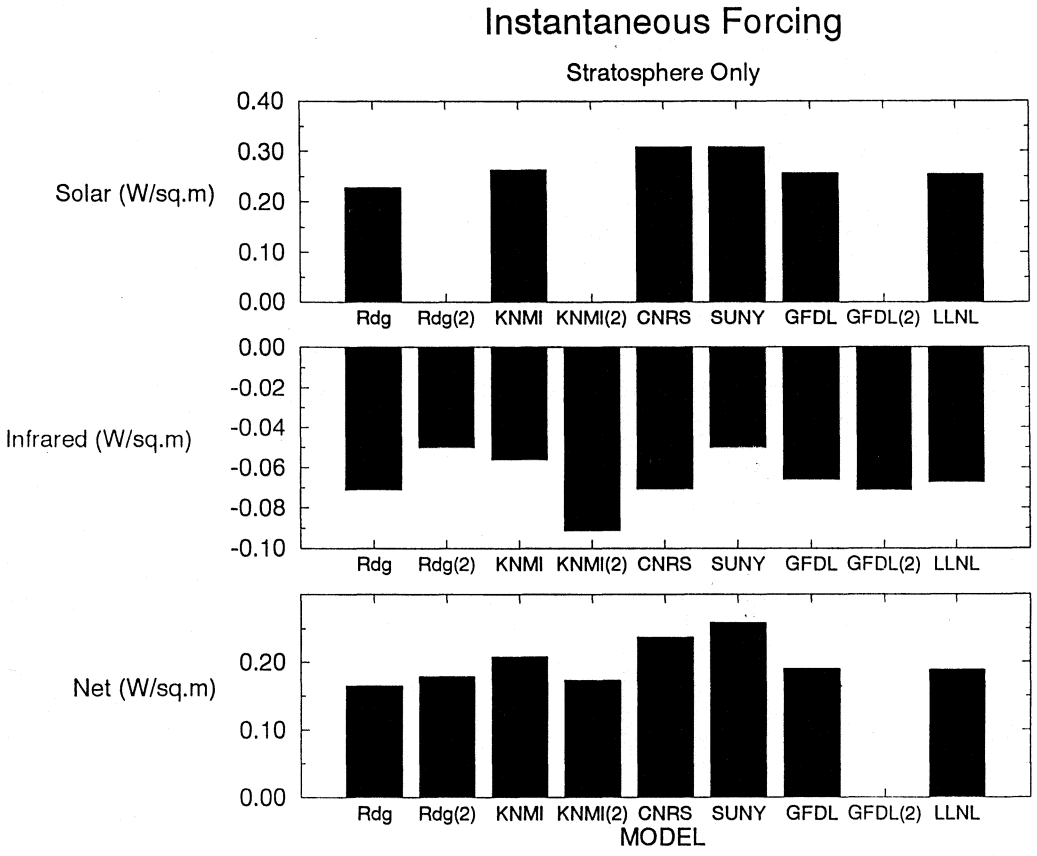

Figure 8-2. Instantaneous changes in solar, thermal infrared, and net (solar minus thermal infrared) irradiances (Wm^{-2}) at the tropopause following a change in ozone in the stratosphere (see Figure 8-1) calculated by the participants in the Ozone Radiative Forcing Intercomparison given in Table 8-1.

indication of the nature of the radiative transfer codes. Some groups contributed results from more than one model configuration.

Figure 8-2 shows the change in solar, thermal infrared, and net irradiance at the tropopause for the instantaneous, stratospheric-depletion case. The spread in solar results is quite marked, ranging from 0.23 to 0.31 Wm^{-2}; these differences will be discussed later. In all cases the net change is positive, indicating a tendency to warm the surface-troposphere system.

The most important conclusions from the instantaneous case concern the thermal infrared. First, the narrow-band calculations are in very good agreement with the Geophysical Fluid Dynamics Laboratory (GFDL) line-by-line calculations. Second, it became apparent that the results were splitting into two classes – those calculations that included the 14 μm band of ozone (which is spectroscopically very weak compared to the 9.6 μm band) obtained a forcing of about -0.07 Wm^{-2}, whilst those without this band reported a value of about -0.05 Wm^{-2}; *i.e.*, the 14 μm band contributes about 30% of the total forcing. The University of Reading calculations were repeated with and without the 14 μm band, and this band was indeed shown to explain the difference. It should be noted that this band is not included in many general circulation model calculations. Further, the 14 μm band contributes only 2% of the change in irradiance for the change in tropospheric ozone only, because in the troposphere this band is more heavily overlapped by pressure-broadened lines of carbon dioxide; this indicates that models that neglect the 14 μm band will give greater relative weight to tropospheric ozone changes compared to stratospheric ozone changes.

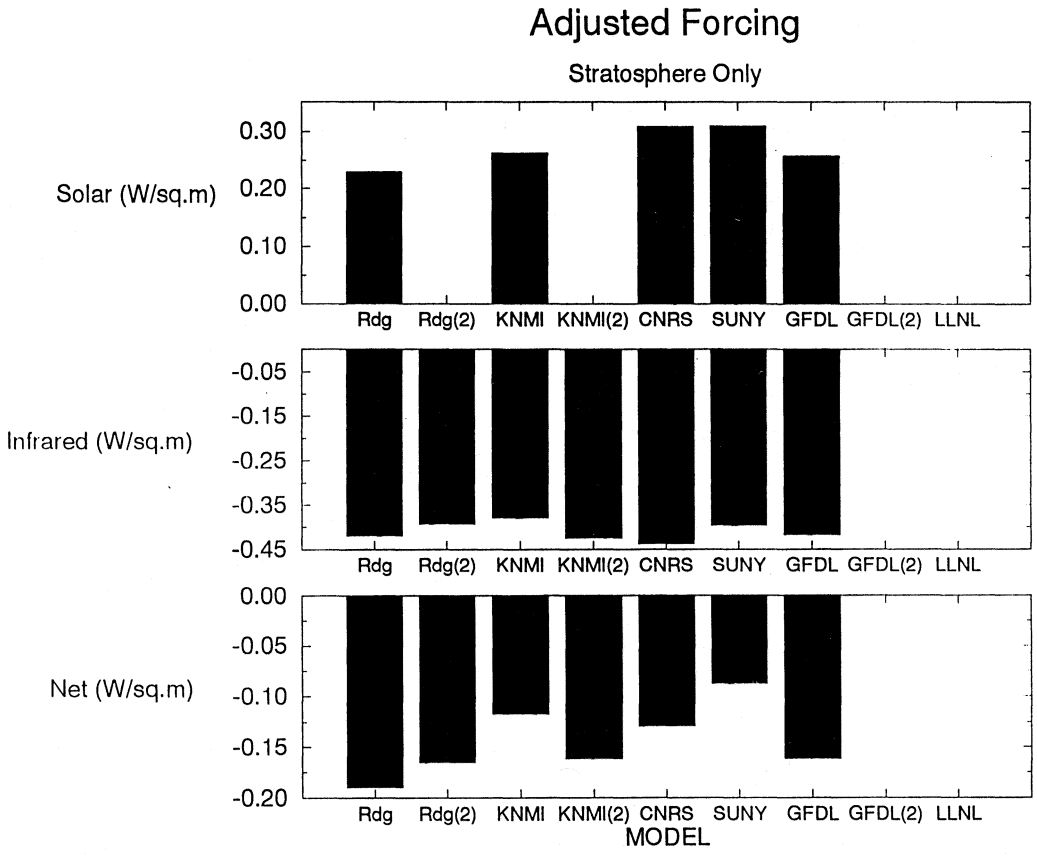

Figure 8-3. As in Figure 8-2, but after allowing for stratospheric temperature changes ("adjusted forcing" using Fixed Dynamical Heating) shown in Figure 8-4.

Figure 8-3 shows the changes in solar, thermal infrared, and net irradiances after allowing for stratospheric adjustment. The solar changes are only very slightly affected by the adjustment process, but the stratospheric cooling decreases the thermal infrared (and hence net) irradiance by typically 0.3 Wm^{-2} compared to the instantaneous case. The relative effect of the 14 μm band is less than in the instantaneous case, but it is more important in an absolute sense and contributes about -0.03 Wm^{-2}. All models now indicate that a decrease in lower stratospheric ozone leads to a cooling tendency for the surface-troposphere system, but the spread in the results is greater than for the instantaneous forcing (Figure 8-2).

Figure 8-4 shows the temperature changes calculated by each of the models; again there is a substantive spread. The effect of the adjustment process can be ascertained by computing the change in the net irradiance between the instantaneous and adjusted calculations; the results agree to within 10%. This agreement is better than might be anticipated from Figure 8-4. However, calculations with the Reading model indicate that most of the change in net irradiance at the tropopause when adjustment was included came from the temperature changes within about 3 km of the tropopause; at these levels the temperature changes predicted by the models are in much better agreement.

The results were interpreted by Shine *et al.* (1994) as follows. About 50% of the modeled temperature change is due to the change in solar heating rates. Altitudes nearest the tropopause are most influenced by the longer wavelength (Chappuis) absorption bands of ozone; the models are in much better agreement about the change in these bands than the changes at shorter

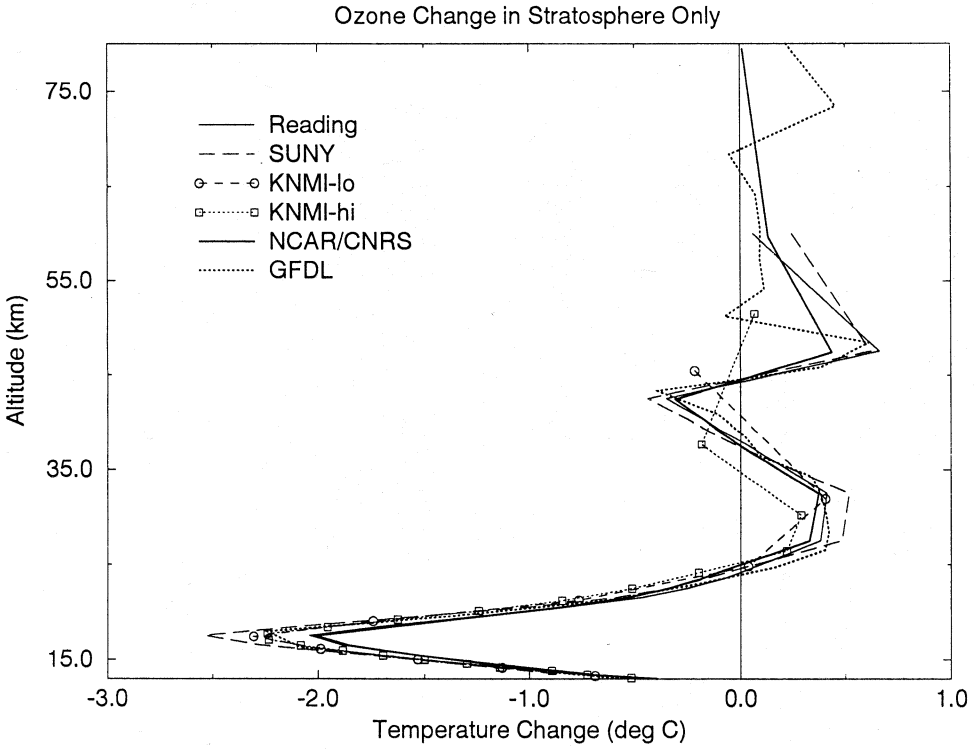

Figure 8-4. Change in stratospheric temperature (deg C) as a function of altitude computed by the participants in the Ozone Radiative Forcing Intercomparison for the change in stratospheric ozone shown in Figure 8-1. The Fixed Dynamical Heating approximation is used. The KNMI results are presented at two vertical resolutions.

wavelengths, so that the effect of adjustment is more similar in the models. The results can be brought into good agreement for the adjusted case by (i) adding the effect of the 14 μm band to those calculations that do not include it and (ii) using a single value of the solar irradiance change, rather than using the solar irradiance change calculated by each model independently. The major conclusion from this is that the main reason for inter-model differences is the way the solar forcing is calculated; it is this aspect of the calculations most in need of scrutiny in each model. As reported by Shine *et al.* (1994), high-resolution calculations of the solar irradiance change appear to be in good agreement; hence, the spread in shortwave results is not believed to represent the actual uncertainty in modeling irradiances, but is more a reflection of the simplifications used in existing parameterizations.

8.2.3 General Circulation Model Calculations

Hansen *et al.* (1992, 1994) have used a general circulation model (GCM) to evaluate the relative effects of changes in the well-mixed greenhouse gases and ozone upon the surface temperature. A sequence of model runs with the 1970-1990 increases in the well-mixed greenhouse gases only is compared with a sequence including observed stratospheric ozone changes; the members of each sequence differ only in their initial conditions. It is estimated that the 1970-1990 modeled surface warming (0.35 deg C) due to greenhouse gases is reduced by 15% due to the ozone changes (see Figure 8-5). There is a considerable spread among the different GCM realizations in the sequence of experiments performed; however, the results indicate that the cooling induced by ozone loss has the potential to reduce the warming effect due to the halocarbon increases over the time period considered. The results from this study are broadly

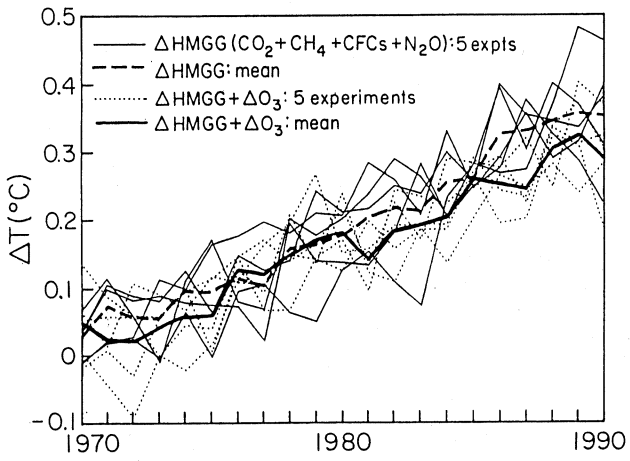

Figure 8-5. Transient global surface temperature change due to changes in greenhouse gases, as simulated by the GISS GCM (Hansen *et al.*, 1992, 1994). Five experiments were run with homogeneously mixed greenhouse gases (HMGG) (CO_2, CH_4, N_2O, and CFCs). Five additional experiments were run with an ozone change inferred from the Total Ozone Mapping Spectrometer (TOMS) and placed entirely in the 70-250 mb layer in addition to the changes in HMGG.

consistent with the expected temperature changes anticipated from the radiative forcing calculations.

Hansen *et al.* (1994) also investigate the climate sensitivity to changes in the vertical profile of ozone using a simplified 3-D model; all previous studies have used 1-D models. Such an investigation of parameter space would be difficult with a full GCM because of the computational cost. Instead, Hansen *et al.* use a sector version of the 9-level Goddard Institute for Space Studies (GISS) GCM they call the "Wonderland" Climate Model (see also Hansen *et al.*, 1993). The surface temperature response is a strong function of the height of the ozone change for two reasons. First, as is well-established (see Section 8.2.1), the radiative forcing is a strong function of the height of the ozone change; in addition, the climate sensitivity (*i.e.*, the surface warming per unit radiative forcing) is found to be a function of the height of the ozone change. This sensitivity is most marked in experiments that allow cloud feedbacks; in experiments with large and idealized perturbations in ozone, the climate sensitivity to changes in tropospheric ozone is substantially modified when cloud feedbacks are included.

The results of Hansen *et al.* (1994) have not yet been reported in detail and must be regarded as preliminary. In addition, the sensitivity to cloud feedbacks is likely to vary considerably amongst different GCMs because of the recognized difficulties in modeling clouds in GCMs (*e.g.*, IPCC, 1990, 1992). However, if confirmed by other studies, the new results could have very significant implications for the way the possible climatic impacts of ozone changes are assessed.

As discussed in IPCC (1994) available GCM simulations raise important, but as yet unresolved, issues about the way in which the global mean of a spatially very inhomogeneous radiative forcing, such as that due to ozone change, can be directly compared to the global-mean forcing due to, for example, changes in well-mixed greenhouse gases.

8.2.4 Attribution of Ozone Radiative Forcing to Particular Halocarbons

As discussed in earlier chapters, the weight of evidence suggests that heterogeneous chemical reactions involving halocarbons are the cause of the observed lower stratospheric ozone depletion. Since several of these compounds, particularly the CFCs, exert a (direct) positive radiative forcing, the (indirect) negative radiative forcing due to the chemically induced ozone loss has the potential to substantially reduce the overall contribution of the halocarbons to the global-mean greenhouse forcing, particularly over the past decade.

Daniel *et al.* (1994) have employed simplified chemical considerations and partitioned the total direct and the total indirect forcing among the various halocarbons (see also the discussion in Chapter 13 and Figure 13-9). The indirect effect is strongly dependent upon the effectiveness of each halocarbon for ozone destruction. On a per-molecule basis, bromine-containing compounds are estimated to contribute more to the indirect effect because they are more effective ozone depletors than chlorine-containing compounds, whilst the chlorinated compounds have a much bigger direct effect because they are stronger absorbers in the infrared. Thus for the total halocarbon forcing up to 1990, Daniel *et al.* estimate that the indirect effect of the CFCs is about 20% of the direct effect but has the opposite sign. For the halons, though, the (indirect) cooling effect is about 3 times larger than the warming due to the direct effect. Nevertheless, because of their greater concentrations,

the CFCs are estimated to have contributed about 50% of the total indirect forcing; the precise value depends on the value used for the effectiveness of bromine, relative to chlorine, at destroying ozone.

For the period 1980 to 1990, Daniel *et al.* attribute about 50% of the negative forcing to the CFCs, about 20% each to carbon tetrachloride and methyl chloroform, and about 10% to the bromocarbons. The net (direct plus indirect) forcing for the CFCs is about 50% of their direct effect, while the net forcing for carbon tetrachloride, methyl chloroform, and the bromocarbons is likely to have been negative.

The analysis suggests that the net forcing by halocarbons was probably quite strong in the 1960s and 1970s (see Figure 8-6); then, when the ozone decrease became more marked, the growth in the net forcing decreased substantially. Using projections for the change in halocarbons over the next century (based on the Copenhagen Amendment to the Montreal Protocol and projections of possible hydrofluorocarbon (HFC) use), Daniel *et al.* estimate that the cooling effect due to ozone depletion will soon begin to decrease; by the latter half of next century, the positive forcing due to HFCs will be the dominant contributor to the radiative forcing due to halocarbons.

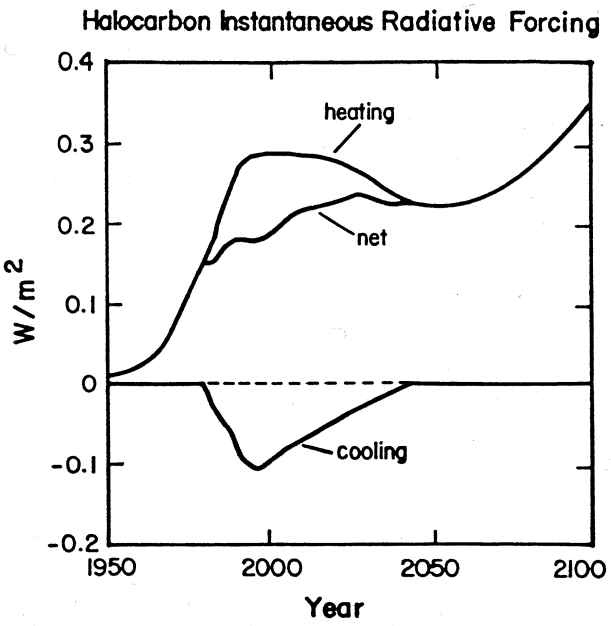

Figure 8-6. Radiative forcing (Wm^{-2}) due to changes in halocarbons (labeled "heating") and an estimate of the associated stratospheric ozone loss (labeled "cooling") and net change using observed halocarbon changes and an "optimistic" scenario based on the Copenhagen Amendment to the Montreal Protocol and assuming bromine is 40 times more effective at destroying ozone than chlorine. From Daniel *et al.* (1994).

8.2.5 Outstanding Issues

Radiative forcing due to a specified ozone change, as a function of the ozone altitude, is qualitatively well understood. However, as revealed by the intercomparison exercise, approximate radiative methods appear to differ in their estimates; it is important that such differences be understood. The principal limitation inhibiting an accurate estimate of the global ozone forcing is the lack of knowledge of the precise vertical profile of change with latitude and season.

In contrast to the well-mixed greenhouse gases, ozone change causes a more complicated radiative forcing – neither the ozone profile nor the change are uniform in the horizontal and vertical domains. The spatial patterns of the radiative forcing differ for changes in ozone and the well-mixed gases. Even the apportionment of the radiative forcing between the surface and the troposphere is different for ozone compared to the well-mixed greenhouse gases (WMO, 1986, 1992). Ozone forcings have not been used for systematic climate studies analogous to those carried out for the well-mixed greenhouse gases. A remaining question is the degree to which the irradiance change at the tropopause is a reasonable indicator of the surface temperature response in the case of ozone changes; it is for the well-mixed greenhouse gases, but preliminary work indicates that it may not be for ozone.

A further complication that needs to be explored is that changes in ozone in the vicinity of the tropopause have the potential to alter tropopause height. Thus, the energy received by the surface-troposphere system may be different in a model that allows changes in the tropopause height than in a model with a fixed tropopause. The vertical resolution of a model in the upper troposphere could then be an important consideration.

As discussed in earlier chapters, there is evidence that heterogeneous chemistry on sulfate aerosol leads to enhanced ozone loss. The observations of unusually low ozone in the northern midlatitudes during the winter of

1992-93 and spring of 1993 suggest a possible link with the Mt. Pinatubo aerosols. Such a volcano-ozone link would imply an enhancement of the transient negative radiative forcing owing to the presence of unusually large volcanic sulfate aerosol concentrations.

Additional complications in the determination of the ozone forcing are uncertainties in the feedbacks related to chemical processes. One example of this is the connection between stratospheric ozone loss, OH, and methane lifetimes. A depletion of stratospheric ozone would lead to an enhancement in tropospheric UV radiation, which in turn increases the rate of production of OH and destruction of methane (see, *e.g.,* Chapter 7 and Madronich and Granier [1992, 1994]). However, it is important to note that photochemical oxidation of methane and other species that react with OH takes place largely in the tropics, where ozone losses are small or not statistically significant. Thus a quantitative assessment of this effect requires consideration not only of tropospheric chemistry but also the latitudinal distribution of ozone depletion (particularly the tropical trends and the sensitivity to them). A cooling of the lower stratosphere due to the ozone loss can affect the water vapor mixing ratios there, with the potential to alter heterogeneous chemical reactions. Also, changes in methane in the stratosphere as a consequence of the altered tropospheric processes could be accompanied by changes in stratospheric water vapor that, in turn, would affect the radiation balance.

8.3 OBSERVED TEMPERATURE CHANGES

A large number of factors can influence stratospheric temperatures (see, *e.g.,* Randel and Cobb, 1994). Natural phenomena can result in a change in the radiative fluxes in the stratosphere, such as changes in solar output or in aerosols resulting from volcanic eruptions. Internal variability of the climate system, such as the quasi-biennial oscillation and the El Niño-Southern Oscillation, can induce dynamical effects that result in temperature change by advection and, if ozone changes as a result, also by radiative processes. Additionally, human activity is resulting in changes in a number of radiatively active constituents, such as ozone and carbon dioxide, and these can perturb the radiation balance and hence the temperature; attempts to detect trends due to human activity require consideration of the natural processes. Most recent work on temperature trends has concentrated on the lower stratosphere, so we will concentrate on this region in this section; the particular emphasis will be on (i) the impact of Mt. Pinatubo and (ii) the detection of long-term trends.

8.3.1 Effects of the Volcanic Eruptions, Especially Mt. Pinatubo

A number of studies have reported the lower stratospheric warming following the eruption of Mt. Pinatubo (Labitzke and McCormick, 1992; Angell, 1993; Spencer and Christy, 1993; Christy and Drouilhet, 1994); this warming is associated with the increased absorption of upwelling thermal infrared radiation and solar radiation by the stratospheric aerosol layer (see, *e.g.*, WMO, 1988).

Angell (1993), from a selection of radiosonde stations, finds that the warming of the lower stratosphere following both Agung and El Chichón was greatest in the equatorial zone and least in the polar zones. The warming following El Chichón was slightly greater than following Agung everywhere except the south polar zone. Preliminary analysis for Mt. Pinatubo indicated that, in the north extratropics and the tropics, the warming following this eruption was comparable to the warming following Agung and El Chichón. However, in south temperate and south polar zones, the warming following Mt. Pinatubo is considerably greater, perhaps due to a contribution from the eruption of Volcán Hudson in Chile. Globally, the warming of the lower stratosphere following Mt. Pinatubo is greater than that following El Chichón and Agung.

Figure 8-7 (updated from Labitzke and Van Loon, 1994) shows the Northern Hemisphere annual area-weighted temperature series from an analysis of radiosonde data. The times of the Agung, El Chichón, and Mt. Pinatubo eruptions are marked, although it should be noted that other, less intense volcanic eruptions during this period probably led to some enhancement of the stratospheric aerosol load (*e.g.,* Robock, 1991; Sato *et al.*, 1993). Whilst the Northern Hemisphere post-Pinatubo warming is clear, particularly at 50 mbar, it is not obviously larger than that due to El Chichón.

More recently, satellite observations from Channel 4 of the Microwave Sounder Unit (MSU) on the NOAA polar-orbiting satellites have been used to monitor lower stratospheric temperatures (*e.g.,* Spencer and Christy,

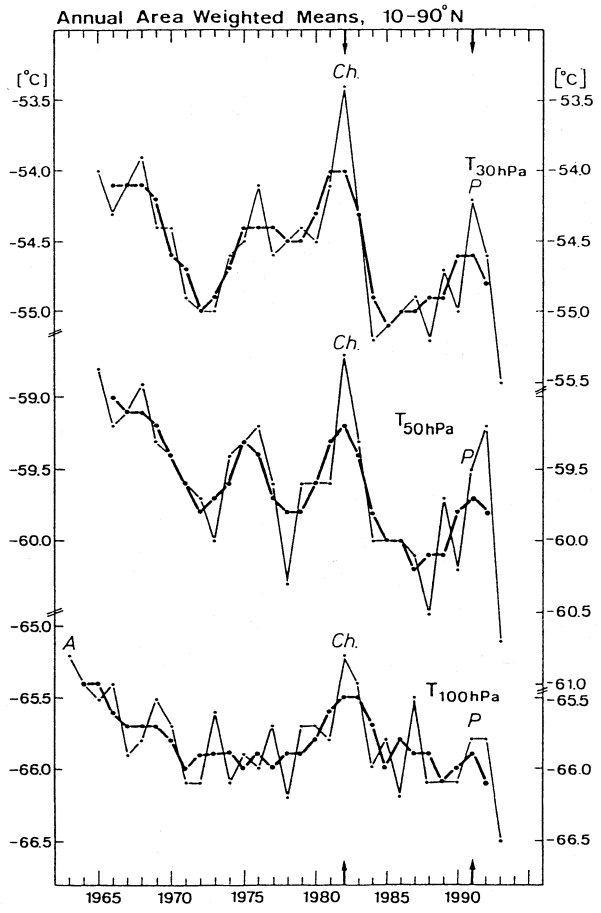

Figure 8-7. Annual mean area-weighted (10°-90°N) temperatures (°C) at 30, 50, and 100 mb. The heavy lines are three-year running means. Based on daily radiosonde analysis by the Free University of Berlin (updated from Labitzke and Van Loon, 1994). A, Ch, and P denote the times of the Agung, El Chichón, and Mt. Pinatubo eruptions, respectively.

1993; Christy and Drouilhet, 1994; Randel and Cobb, 1994). The weighting function for Channel 4 peaks at about 75 mbar with half-power values at 120 and 40 mbar (Christy and Drouilhet, 1994). Figure 8-8 shows the global and hemispheric monthly-mean anomalies from MSU between January 1979 and July 1994 (J. Christy and R. Spencer, personal communication). From the global data set, Mt. Pinatubo gives a slightly greater warming (about 1.1 deg C in 1991/1992) than El Chichón (about 0.7 deg C in 1982/1983) compared to the immediate pre-eruption temperatures.

The Northern Hemisphere MSU Channel 4 data in Figure 8-8 can be compared with the radiosonde data analysis in Figure 8-7, although differences in the vertical resolution of the data sets need to be recognized. Both data sets are in general agreement that the immediate post-eruption warming is similar for both El Chichón and Mt. Pinatubo. The greater warming in the Southern Hemisphere following Mt. Pinatubo is consistent in both the MSU analysis (see Figure 8-8 and Christy and Drouilhet [1994]) and radiosonde analysis (Angell, 1993).

Hansen *et al.* (1993) show that the tropical warming in the lower stratosphere associated with Mt. Pinatubo is very well simulated by the GISS GCM with an imposed idealized volcanic aerosol cloud.

One interesting development in the identification of volcanic signals is the use of temperature and ozone data together (Randel and Cobb, 1994; A.J. Miller, personal communication). Normally, temperatures in the lower stratosphere and total ozone are positively correlated; Randel and Cobb show that this correlation changes sign when the lower stratospheric aerosol layer is enhanced as a result of volcanic eruptions.

8.3.2 Long-Term Trends

Both Figures 8-7 and 8-8 emphasize that the detection of long-term trends in temperatures in the lower stratosphere will be difficult because of the episodic and frequent volcanic eruptions that cause a major perturbation to those temperatures. An additional problem concerns the quality of available radiosonde data (see, *e.g.*, IPCC, 1992; Gaffen, 1994; Parker and Cox, 1994). Changes in instrumentation, ascent times, and reporting practices introduce a number of time-varying biases that have not yet been properly characterized; they indicate the need for some caution when using data primarily intended for weather forecasting for climate trend analysis. Nevertheless, since 1979, comparison of independent MSU Channel 4 data with radiosonde analyses in the lower stratosphere has shown good agreement (Oort and Liu, 1993; Christy and Drouilhet, 1994).

Considering all available radiosonde reports for the period December 1963 through November 1988, Oort and Liu (1993) infer a trend in the global lower stratospheric (100-50 mbar) temperature of -0.4 ± 0.12 deg C/decade; the cooling trend is apparent during all seasons and in both hemispheres. These results were

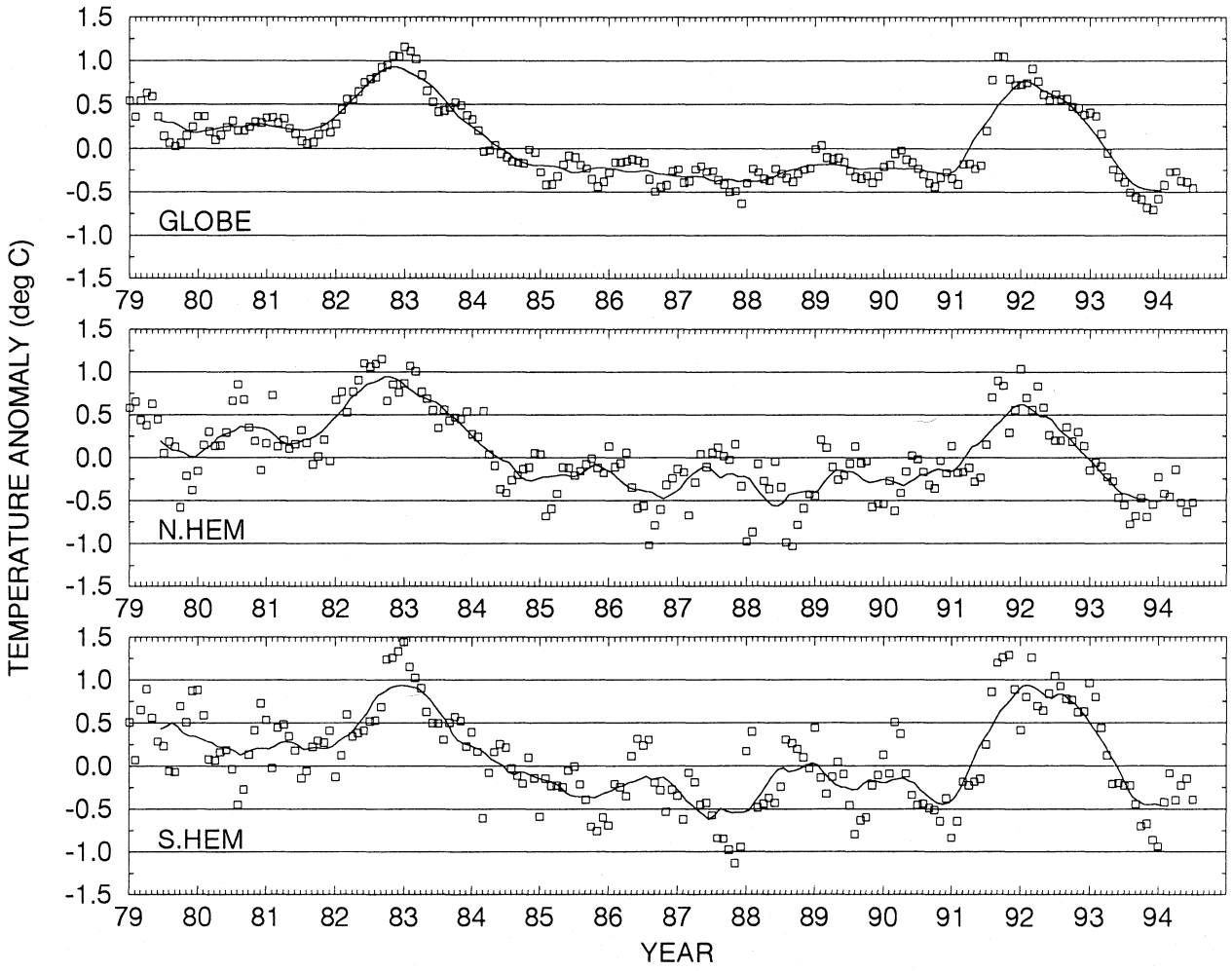

Figure 8-8. Global and hemispheric monthly-mean lower stratospheric temperature anomalies (from 1982-1991 means) from the MSU Channel 4 from January 1989 to July 1994. The solid line indicates the 12-month running mean. (Data from J.R. Christy and R. Spencer. See text for a description of the weighting function of MSU Channel 4.)

compared with earlier estimates by Angell (1988), who used a subset of 63 sonde stations, for the same time period; Oort and Liu find that their global and hemispheric trends agree with Angell's within the error bars, although Angell's larger Southern Hemisphere trends are believed to be associated with undersampling. These trend analyses are also consistent with the findings in Miller *et al.* (1992). IPCC (1992) combines the analysis of Oort and Liu with more recent data from Angell to deduce a global trend of -0.45 deg C/decade between 1964 and 1991 for the 100-50 mbar layer.

A concern expressed in IPCC (1992) was that trend analyses starting in 1964 may be biased by the warming associated with the eruption of Agung in 1963; however, Oort and Liu (1993) extend their own Northern Hemisphere analysis and Angell's global analysis back to December 1958 and find the decadal trends to differ little from those calculated for the period December 1963 to November 1988.

Latitudinal profiles of the estimated trends from Oort and Liu (1993) (see Figure 8-9) show that the cooling of the lower stratosphere has occurred everywhere,

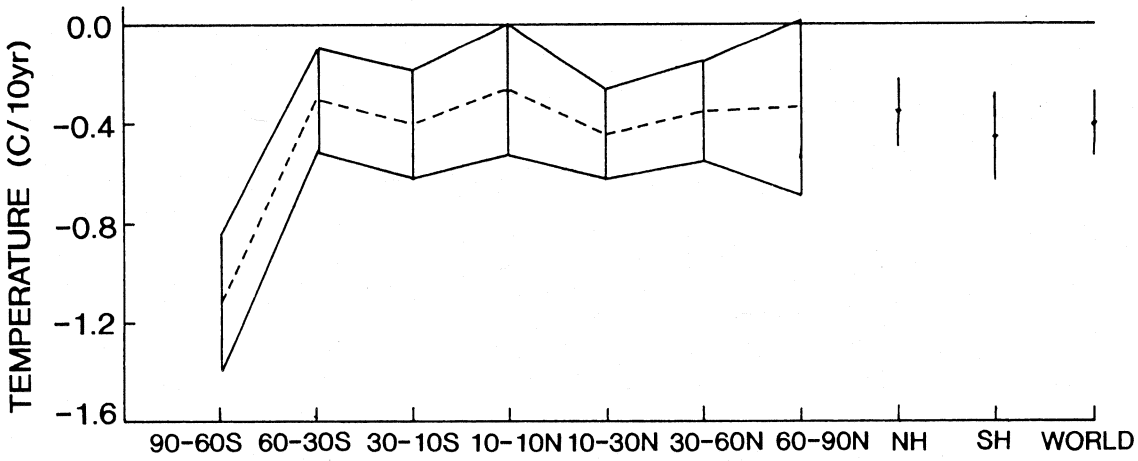

Figure 8-9. Latitudinal profiles of the estimated trends in the annual mean temperatures (in deg C/decade) from the GFDL radiosonde analysis (after Oort and Liu, 1993) for the 100-50 mb layer during the period December 1963 - November 1989. The 95% confidence limits are also shown. The hemispheric and global-mean changes are shown on the right of the figure.

but that the strongest temperature decreases (-1 deg C/decade) have occurred in the Southern Hemisphere extratropics, strongly suggesting an association with the Antarctic ozone hole.

Labitzke's (personal communication) analysis of Northern Hemisphere sonde data indicates an annual mean trend of -0.2 to -0.4 deg C/decade between 1965 and 1992 between 30 and 80 mbar at most latitudes; however, the trend varies greatly from month to month both in size and in sign, and is most difficult to detect in the extratropics during the Northern Hemisphere winter when interannual variability is substantial. This suggests that the winter months are best avoided for long-term trend detection. There is an indication that the trend during springtime is more negative over the period 1979-1993 than over the period 1965-1993. Figure 8-10 shows the analyses for May for these two periods; for substantial regions the trend is almost double for the later period, although it must be noted that the significance level is much lower, as it contains fewer data.

For the shorter period available from MSU Channel 4 observations, trends are clearly sensitive to the period of analysis (Figure 8-8); Christy and Drouilhet (1994) report a trend of -0.26 deg C/decade for the period January 1979 to November 1992, but comment that, because of the effects of the volcanoes, its significance is hard to assess. Downward trends are most marked for the temperatures in the lower stratosphere of the polar cap regions (defined as being 67.5° to 83.5°), being -0.78 deg C/decade for the north polar cap and -0.90 deg C/decade for the south polar caps for the period January 1979 to January 1994 (J.R. Christy, personal communication).

For the period 1979-1991, Randel and Cobb (1994), using MSU data, infer a significant cooling of the lower stratosphere over the Northern Hemisphere midlatitudes in winter-spring (with a peak exceeding -1.5 deg C/decade) and over Antarctica in the Southern Hemisphere spring (peak exceeding -2.5 deg C/decade) (Figure 8-11); the overall space-time patterns are similar to those determined for ozone trends. The Northern Hemisphere trends derived from MSU data are in good agreement with the sonde analysis from the Free University of Berlin (McCormack and Hood, 1994; K. Labitzke, personal communication).

In summary, the available analyses continue to support the conclusions of WMO (1992) that the lower stratosphere has, on a global-mean basis, cooled by about 0.25-0.4 deg C/decade in recent decades, although more work on the quality of the archived data sets is clearly warranted.

In the upper stratosphere and mesosphere there is little new to report beyond the discussion in WMO (1992). Upper stratospheric temperature trends based on

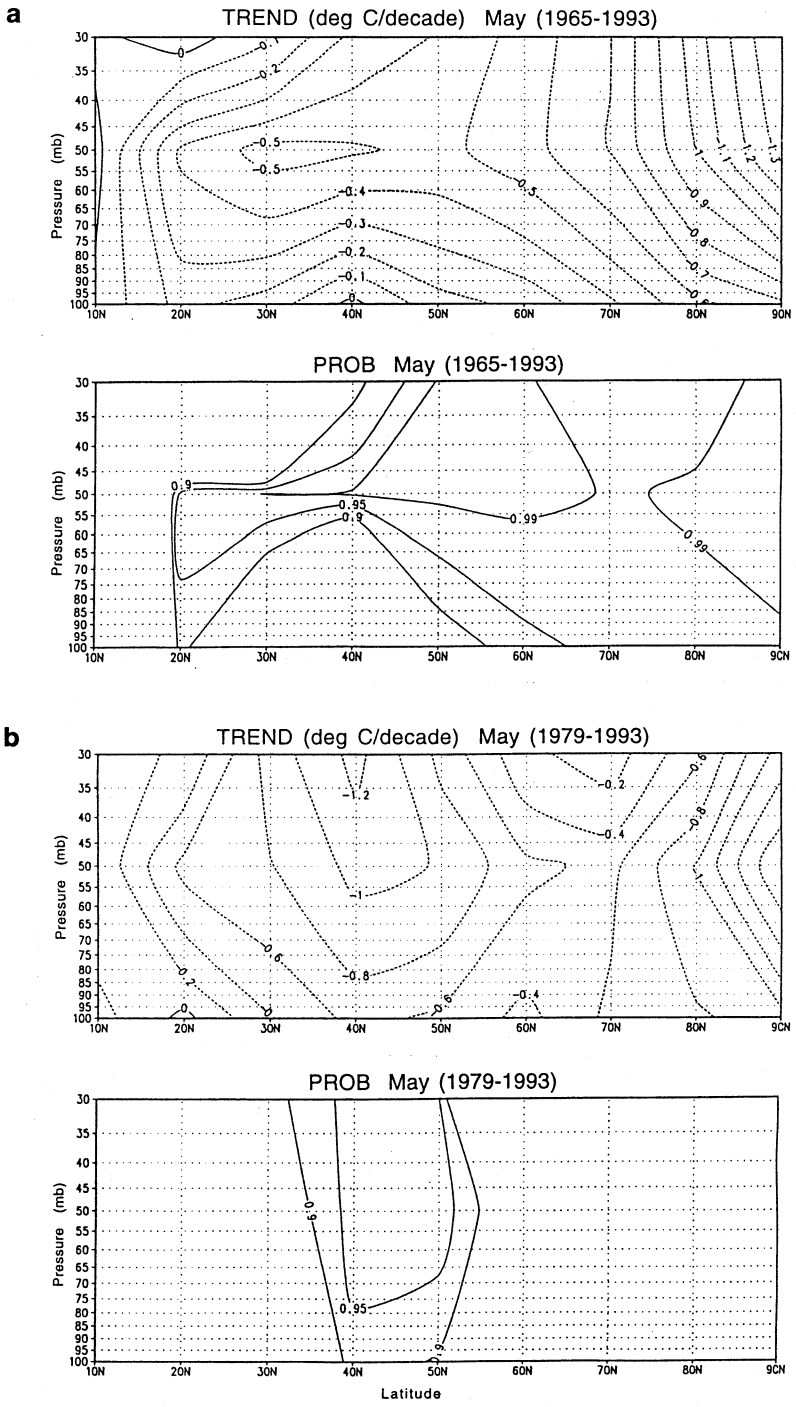

Figure 8-10. (a) Upper Panel—Northern Hemisphere temperature trend derived from radiosonde analyses (deg C/decade) in May for the period 1965-1993 based on data at 100, 50, and 30 mb levels. Lower Panel—lines of 90, 95, and 99% significance. (b) As (a) but for the period 1979-1993. (K. Labitzke, personal communication).

satellite, rocket, and lidar data do not lead to a clear conclusion concerning trends; mesospheric coolings of several deg C per decade in the past decade have been deduced (see also Chanin, 1993; Kokin and Lysenko, 1994).

8.3.3 Interpretation of Trends

Models indicate that the loss of ozone in the lower stratosphere leads to a decrease in the temperature there (WMO, 1992 and Section 8.2.1.1). One-dimensional models, such as the Fixed Dynamical Heating (FDH) and the Radiative-Convective Models, compute significant temperature changes of several tenths of a deg C/ decade in the lower stratosphere due to the ozone changes of the past decade (WMO, 1992; Miller *et al.*, 1992; Shine, 1993; Karol and Frolkis, 1994; Ramaswamy and Bowen, 1994). It is this temperature change in the FDH models that determines, to a substantial extent, the negative forcing due to the ozone losses (see Section 8.2.1.1).

The cooling trends in the lower stratosphere, either from the long-term records or those over the past decade, are too negative to be attributable to increases in the well-mixed greenhouse gases (mainly CO_2) alone (Miller *et al.*, 1992; Hansen *et al.*, 1993; Shine, 1993; Ramaswamy and Bowen, 1994). In contrast, models employing the observed ozone losses yield a global temperature decrease that is broadly consistent with observations. This strongly suggests that, among the trace gases, stratospheric ozone change is the dominant contributor to the observed cooling trends. However, the potential competing effects due to unknown changes in other radiative constituents (*e.g.*, ice clouds, water vapor, tropospheric aerosols, and tropospheric ozone: Hansen *et al.*, 1993; Ramaswamy and Bowen, 1994) make it difficult to rigorously quantify the precise contribution by ozone to the temperature trends.

McCormack and Hood (1994) calculate the temperature decreases using an FDH model employing the ozone changes deduced from Solar Backscatter Ultraviolet (SBUV) observations for the period 1979-1991; the temperature changes are comparable to or slightly less than the decadal change inferred from satellite and radiosonde data in regions where the observed trends are statistically significant. Importantly, the modeled latitudinal and seasonal dependences are in reasonable agreement with the observations.

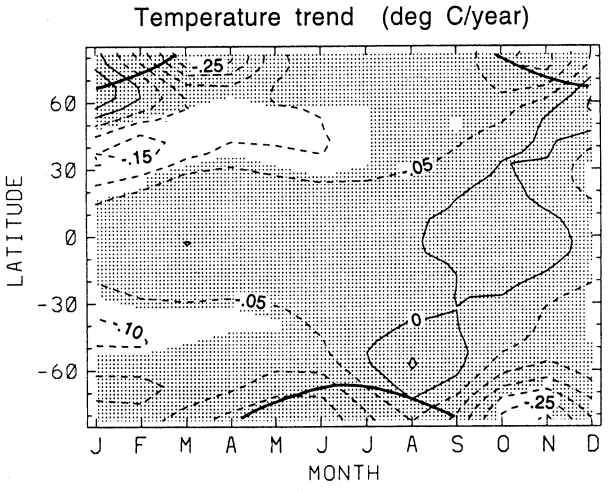

Figure 8-11. Latitude-time sections of zonal-mean lower stratospheric temperature trends in deg C/ year calculated from MSU Channel 4 data (Randel and Cobb, 1994) for the period 1979-1991. Stippling denotes regions where the statistical fits are not different from zero at the 2σ level. (See text for description of the weighting function of MSU Channel 4.)

General circulation model (GCM) studies with imposed ozone losses in the lower stratosphere also obtain a temperature decrease in this region. Hansen *et al.* (1993) obtain a cooling in the lower stratosphere that is qualitatively consistent with and, in the global mean, agrees well with the decadal trend (-0.4 deg C) inferred from radiosonde observations. Another GCM study (V. Ramaswamy, personal communication) finds a similar cooling of the lower stratosphere and shows that the FDH temperature changes exhibit a qualitatively similar zonal pattern to the GCM results.

Mahlman *et al.* (1994) present a three-dimensional chemical-radiative-dynamical investigation of the climatic effects due to the Antarctic ozone losses. The transport of ozone and the ozone losses are handled explicitly, although the modeled Antarctic ozone loss is somewhat less than observed. There is a decrease of the lower stratospheric temperatures in the Southern Hemisphere that is consistent with the observed trends. An important aspect of the GCM calculations is that they simulate a slight cooling in the lower stratosphere at lower latitudes as a dynamical consequence of extratropical ozone depletion; this is in contrast to FDH models which

calculate temperature changes only at latitudes of ozone change. Thus the presence of equatorial cooling in observations (see, *e.g.*, Figure 8-9) cannot be used as a simple discriminator of whether ozone depletion has occurred in the equatorial lower stratosphere (see Chapter 1). In addition, the simulation of Mahlman *et al.* (1994) shows a dynamically induced heating in the Antarctic mid-stratosphere as a consequence of the loss of ozone in the lower stratosphere; such dynamical effects need to be taken into account when attempting to detect temperature trends from other causes, such as the increased concentrations of other greenhouse gases.

It is encouraging that both the FDH models and the GCMs yield a cooling in the lower stratosphere that is consistent with the magnitude inferred from observations. Precise agreement might not be expected as, in all the model studies, the temperature changes in the lower stratosphere are subject to uncertainties related to the assumed vertical and horizontal distribution of the ozone change and there are uncertainties in the observed trends.

8.4 HALOCARBON RADIATIVE FORCING

8.4.1 Comparison of IR Absorption Cross Sections

Since the review in the AFEAS (1989) report (see also Fisher *et al.*, 1990), further work on the absorption cross sections of halocarbons has been reported; this is particularly important for some of the HCFCs (hydrochlorofluorocarbons) and HFCs (hydrofluorocarbons), as some of the data used in earlier assessments were from a single source. Recent comparisons of strengths of many CFCs (chlorofluorocarbons) are presented in McDaniel *et al.* (1991), Cappellani and Restelli (1992), and Clerbaux *et al.* (1993) and are not repeated here. For newer HCFCs and HFCs, measurements are more limited and the available measurements are reviewed. Molecules that are created by the destruction of halocarbons have the potential to cause a radiative forcing, but their lifetimes are believed to be too short for them to be of importance (see Chapter 12); they are therefore not considered here.

Measurements of infrared (IR) cross sections are normally made using Fourier transform IR spectrometers and, sometimes, grating spectrometers; spectral resolutions range from around 0.01 cm^{-1} to 0.1 cm^{-1}. Clerbaux *et al.* (1993) present a detailed error estimate with errors ranging from 1-2% for strong absorption and 3-4% for weak absorption. Cappellani and Restelli (1992) estimate an uncertainty of 2.5% and other workers estimate uncertainties of between 5 and 10%.

Table 8-2 lists the integrated absorption cross sections of measurements of HFCs and HCFCs known to the authors. Measurements for a number of these molecules, as well as a number of halogenated ethers used as anesthetics, are also reported by Brown *et al.* (1990); however, the absorption cross sections are reported for only a limited spectral region (800 - 1200 cm^{-1}) that neglects some important absorption features. Garland *et al.* (1993) report measurements in the region 770-1430 cm^{-1} of the absorption cross sections of HFC-236cb, HFC-236ea, and HFC-236fa, as well as the fluorinated ether E-134. Because the results are presented as relative cross sections, they are not included in Table 8-2; their integrated strengths are reported to be between 1.5 and 2.3 times stronger than CFC-11.

As examples of the degree of agreement in the near-room temperature measurements, for HCFC-123, HCFC-141b, and HCFC-142b the spread of results is more than 25% of the mean cross section; however, the spread between the results from the two published studies (Cappellani and Restelli, 1992; Clerbaux *et al.*, 1993) is generally smaller. For HFC-134a the spread is about 10%. Detailed descriptions, including temperatures and pressures of the measurements, are not available for all the data sets, so it is difficult to comment on the discrepancies. Except for HCFC-22, only Cappellani and Restelli (1992), Clerbaux *et al.* (1993), and Clerbaux and Colin (1994) have published the details of their measurements of HFC/HCFC cross sections and presented measurements for a range of temperatures. In general, the change in integrated cross section over the range of temperatures is less than 10%, although the two groups do not always agree on the sign of the temperature effect. The spread of results puts a limit on our knowledge of the accuracy with which the radiative forcing due to these gases can currently be modeled.

Table 8-2. Integrated absorption cross sections of HFC and HCFCs in units of $x10^{-17}$ $cm^{-1}(molec\ cm^{-2})^{-1}$.

Gas	Clerbaux[1]	Brühl[2]	Gehring[3]	Majid[3]	Hurley[4]	Cappellani[5]	McDaniel[6]
HCFC-22	10.0-10.3		8.9	9.5		10.9-10.3	8.3-9.0
HFC-23					12.7		
HFC-32					6.3		
HFC-41					1.7		
HCFC-123	12.2-12.9	13.6	9.5	10.6	12.5	13.1-12.8	
HCFC-124	14.4	14.8	15.1				
HFC-125	16.1	15.7	14.5				
HFC-134a	12.7-12.6	12.5	11.8	12.2	13.0	14.1-13.2	
HCFC-141b	6.8-7.8	9.0	6.5	7.1	7.6		
HCFC-142b	10.8-11.1	12.1	9.2	9.6	10.3	11.3-10.7	
HFC-143	7.0-6.9						
HFC-143a		11.4	12.7				
HFC-152a	7.1-6.9	5.9		6.1	7.3	7.5-6.9	
HCFC-225a	17.5-17.7						
HCFC-225b	16.5-15.6						
HFC-227ea		21.2					

1. Clerbaux *et al.* 1993; ranges correspond to values at 253 K and 287 K, respectively; where only one value is quoted, it is for 287 K. Measurements in spectral interval 600-1500 cm^{-1} at 0.03 cm^{-1} resolution. HFC-143 is from Clerbaux and Colin (1994).
2. C. Brühl, personal communication of room temperature measurements at Max-Planck Institute–Mainz; measurements over interval 500-1400 cm^{-1} approx. Values supplied in cm^{-1}(atm cm at 296 K)$^{-1}$ – converted by multiplying by $296 \div (273 \times 2.687 \times 10^{19})$.
3. Reported in Fisher *et al.* (1990); measurements made at room temperature. Values reported as cm^{-1} (atm cm at STP)$^{-1}$. Converted by multiplying by $1 \div 2.687 \times 10^{19}$. Some authors (Clerbaux *et al.*, 1993, and Cappellani and Restelli, 1992) convert assuming the gas amounts are atm cm at 296 K; we have been unable to resolve this with D. Fisher. If original units are indeed at 296 K instead of STP, the values in the above table should be multiplied by 1.08.
4. M. Hurley and T.J. Wallington, personal communication of measurements by Ford; integrated cross sections derived by S. Pinnock (University of Reading). Measurements in spectral interval 700-3800 cm^{-1} at 0.12 cm^{-1} resolution at 296 K; estimated uncertainty is 5%. Experimental set-up described in Wallington *et al.* (1989).
5. Cappellani and Restelli, 1992. Range corresponds to values at 233K and 293 K. Measurements in spectral interval 600-1500 cm^{-1} at 0.01 cm^{-1}.
6. McDaniel *et al.*, 1991. Range corresponds to values at 203 K and 296 K. Measurements in spectral interval 600 - 1500 cm^{-1} at 0.03 cm^{-1}.

8.4.2 Comparison of Radiative Forcing Calculations

In IPCC (1990, 1992, 1994) a specific definition of radiative forcing was adopted such that:

> The radiative forcing of the surface-troposphere system (due to a change, for example, in greenhouse gas concentration) is the change in net irradiance (in Wm^{-2}) at the tropopause after allowing for stratospheric temperatures to re-adjust to radiative equilibrium.

The tropopause is chosen because, in simple models at least, it is considered that in a global and annual-mean sense, the surface and troposphere are so closely coupled that they behave as a single thermodynamic system (see, *e.g.*, Rind and Lacis, 1993; IPCC,1994) This follows earlier work (*e.g.,* Ramanathan *et al.*, 1985, Hansen *et al.*, 1981, and references therein). One advantage of allowing for the stratospheric adjustment is that the change in the net irradiance at the top of the atmosphere is then the same as the change at the tropopause; this is not the case when stratospheric temperatures are not adjusted (see Hansen *et al.*, 1981).

In preparing this review some difficulty has been experienced in intercomparing work performed by different authors, because some have applied the term "radiative forcing" to the instantaneous change in tropopause irradiance, not allowing for any change in stratospheric temperature. In other works, it is not clear which definition of radiative forcing has been adopted. It is also emphasized here that the forcing should be calculated as a global mean using appropriate vertical profiles of temperature, trace gas concentrations, and cloud conditions – again, it is not always clear, in published estimates, what conditions are being used for calculations. An added problem is that if perturbations used to calculate the forcings are too small, the results can be affected by computer precision, an effect that will vary between models, depending on their construction. Finally, when results are presented as ratios of forcings to other gases (*e.g.,* CO_2 or CFC-11) rather than as absolute forcings (*e.g.,* as Wm^{-2} $ppbv^{-1}$), it is important to know the absolute forcing of the reference gas to rigorously intercompare different works. Again, such information is not always presented.

The first calculations of the radiative forcing due to a large range of HFCs and HCFCs were reported in Fisher *et al.* (1990). More recent calculations include those of Shi (1992), Brühl (personal communication), Clerbaux *et al.* (1993) and Clerbaux and Colin (1994); C. Granier (personal communication) has updated the Clerbaux *et al.* (1993) calculations to account for the effect of clouds, and these new values are used here. The results from these sources differ in general, because of the use of different radiation schemes, different spectroscopic data, different assumptions about vertical profiles of temperatures, clouds, etc., and whether stratospheric adjustment was included.

The Fisher *et al.* (1990) values for this class of gases were instantaneous forcings. The effect of adjustment can be estimated from the 1-dimensional radiative-convective model values in Fisher *et al.* (1990) (see footnote to Table 8-3). The adjustment leads to the adjusted forcing being up to 10% greater than the instantaneous forcing because an increase in the concentrations of these gases generally leads to a warming of the lower stratosphere, increasing the downwelling thermal infrared irradiance at the tropopause. The values most affected are those for the more heavily fluorinated gases (such as HFC-125 and HFC-134a).

Table 8-3 lists recent estimates of the strengths of the HFC and HCFCs, on a per-molecule basis, relative to CFC-11. The variations of the relative forcings from different studies show little consistency. The same spectral data in different radiation schemes do not always give the same relative forcings amongst the HFCs and HCFCs; and schemes using different spectral data do not always show differences that would be anticipated from the cross sections used. For the majority of gases, Shi (1992) computes a radiative forcing weaker than those given in IPCC (1990), by as much as 30% for HFC-125. The results from Brühl and Clerbaux *et al.* generally show no systematic difference compared with the Atmospheric and Environmental Research, Inc. (AER) values. For only two gases is there a consistent and large deviation from AER values: HFC-125 and HFC-152a.

More systematic work needs to be done to establish the effect of factors such as overlap with other species, stratospheric adjustment, the vertical profile of the absorber, and the dependence of the calculation on the spectral resolution, if the range in the current estimates is to be understood better.

Table 8-4 presents our recommended forcings for a wide range of gases, all relative to CFC-11. We have

Table 8-3. Radiative forcing due to HFC and HCFCs on a per-molecule basis relative to CFC-11 for gases for which more than one assessment is available.

Gas	AER[1]	AER adj[2]	Du Pont[3]	Shi[4]	Brühl[5]	Granier[6]
HCFC-22	0.86	0.92	0.80	0.75	0.79	0.87
HCFC-123	0.80	0.82	0.69	0.67	0.80	0.89
HCFC-124	0.87	0.93	0.81	0.88	0.95	0.93
HFC-125	1.08	1.19	0.89/0.93	0.74	0.91	0.90
HFC-134a	0.77	0.84	0.71	0.65	0.66	0.78
HCFC-141b	0.62	0.64	0.57	0.64	0.68	0.65
HCFC-142b	0.82	0.89	0.76	0.63	0.93	0.81
HFC-143a	0.63	0.68	0.65	0.50	0.58	
HFC-152a	0.53	0.56	0.44/0.46	0.44	0.48	0.49
HFC-227ea			—/1.24		1.09	

1. AER results from Fisher *et al.* (1990). They are instantaneous forcings.
2. AER-adjusted forcings deduced from results in Fisher *et al.* (1990), Tables 3 and 4. These authors wrote the climate sensitivity λ in terms of instantaneous forcing so that the surface temperature change equals λ times the instantaneous forcing. The climate sensitivity is reasonably independent of gas when using the adjusted forcing (*e.g.*, Rind and Lacis, 1993). The adjusted forcing, relative to CFC-11, can be estimated by multiplying the instantaneous forcing relative to CFC-11 by the ratio of the instantaneous sensitivity of a given gas to the instantaneous sensitivity for CFC-11.
3. Du Pont forcings from Fisher *et al.* (1990). They are instantaneous forcings. The adjusted forcings could be deduced as for the AER forcings above. Second values, where quoted, are more recent values from D. Fisher (personal communication).
4. From Shi (1992) and includes overlap with methane and nitrous oxide using spectral data from Fisher *et al.* (1990). The calculations are not believed to include stratospheric adjustment.
5. From C. Brühl (personal communication) using MPI-Mainz absorption cross sections and including overlap with methane and nitrous oxide.
6. From C. Granier (personal communication) using measurements from Clerbaux *et al.* (1993). The results include clouds and do not include stratospheric adjustment; the original Clerbaux *et al.* values were for clear skies.

chosen to retain values used in IPCC (1990) where there was neither a large nor a consistent deviation from more recent calculations. We replace the earlier values for HFC-125 and HFC-152a by those from C. Granier (personal communication). In cases where details of calculations have not been provided, we simply take the means of available estimates. It is subjectively estimated that these values are accurate to within about 25%, but it is anticipated that further revision will be necessary in the future. Another feature of Table 8-4 is that an attempt is made to classify HFC/HCFC species on the basis of likely emissions (using information from A. McCulloch [personal communication]).

Estimates for the forcing due to increased concentrations of HFCs and HCFCs between 1990 and 2100 include 0.15 Wm^{-2} by Daniel *et al.* (1994) and between 0.2 and 0.4 Wm^{-2} by Wigley (1994). For the sets of assumptions used by these authors, the forcing is a small fraction of the estimates of forcing due to increases in the well-mixed greenhouse gases between 1990 and 2100; the various scenarios used in IPCC (1992) give that forcing to lie between 3.4 and 8.5 Wm^{-2}. The actual radiative forcing due to future emissions of the HFCs and HCFCs depends critically on factors such as growth rates in emissions and the precise mix of species used.

Table 8-4. Radiative forcing relative to CFC-11 per unit mass and per molecule change in the atmosphere. The table shows direct forcings only. The absolute radiative forcing due to CFC-11 is taken from IPCC 1990 and is 0.22 dX Wm^{-2}, where dX is the perturbation to the volume mixing ratio of CFC-11 in ppbv.

GAS		Forcing per		
		unit mass	molecule	Source
CFCs and other controlled chlorinated species				
CFC-11	$CFCl_3$	1.00	1.00	IPCC (1990)
CFC-12	CF_2Cl_2	1.45	1.27	IPCC (1990)
CFC-113	$CF_2ClCFCl_2$	0.93	1.27	IPCC (1990)
CFC-114	CF_2ClCF_2Cl	1.18	1.47	IPCC (1990)
CFC-115	CF_3CF_2Cl	1.04	1.17	IPCC (1990)
*Carbon tetrachloride	CCl_4	0.41	0.46	IPCC (1990)
Methyl chloroform	CH_3CCl_3	0.23	0.22	IPCC (1990)
HFC/HCFCs in production now and likely to be widely used				
HCFC-22	CHF_2Cl	1.37	0.86	IPCC (1990)
HCFC-141b	CH_3CFCl_2	0.73	0.62	IPCC (1990)
HCFC-142b	CH_3CF_2Cl	1.12	0.82	IPCC (1990)
HFC-134a	CF_3CH_2F	1.04	0.77	IPCC (1990)
*HFC-32	CH_2F_2	1.06	0.40	Fisher (personal communication)
HFC/HCFCs in production now for specialized end use				
HCFC-123	CF_3CHCl_2	0.72	0.80	IPCC (1990)
HCFC-124	CF_3CHFCl	0.88	0.87	IPCC (1990)
*HFC-125	CF_3CHF_2	1.03	0.90	Granier (personal communication)
HFC-143a	CH_3CF_3	1.03	0.63	IPCC (1990)
*HFC-152a	CH_3CHF_2	1.02	0.49	Granier (personal communication)
*HCFC-225ca	$CF_3CF_2CHCl_2$	0.72	1.07	Granier (personal communication)
*HCFC-225cb	$CClF_2CF_2CHClF$	0.87	1.29	Granier (personal communication)
HFC/HCFCs under consideration for specialized end use				
*HFC-23 (+)	CHF_3	1.59	0.81	Fisher (personal communication)
*HFC-134	CHF_2CHF_2	1.08	0.80	Fisher (personal communication)
*HFC-143	CH_2FCHF_2	0.85	0.52	Clerbaux and Colin (1994)
*HFC-227	CF_3CHFCF_3	0.95	1.17	Mean of Brühl and Fisher (pers. comms.)
*HFC-236	$CF_3CH_2CF_3$	1.06	1.17	Fisher (personal communication)
*HFC-245	$CHF_2CF_2CFH_2$	0.95	0.93	Fisher (personal communication)
*HFC-43-10mee	$C_5H_2F_{10}$	0.86	1.58	Fisher (personal communication)
Fully fluorinated substances				
*CF_4		0.69	0.44	Isaksen *et al.* (1992)
*C_2F_6		1.36	1.37	Isaksen *et al.* (1992)
*C_3F_8		0.77	1.05	Brühl (personal communication)
*perfluorocyclobutane	cC_4F_8	1.00	1.46	Fisher (personal communication)
*C_6F_{14}		0.75	1.84	Mean of Brühl and Ko (pers. comms.)
*SF_6		2.75	2.92	Mean of Ko *et al.* (1993)/Stordal *et al.* (1993)
Other species				
CFC-13	$CClF_3$	1.37	1.04	Mean of Brühl and Fisher (pers. comms.)
$CHCl_3$		0.09	0.078	Fisher (personal communication)
CH_2Cl_2		0.23	0.14	Fisher (personal communication)
halon 1301	CF_3Br	1.19	1.29	IPCC (1990)
*CF_3I		1.20	1.71	Pinnock (personal communication)

\+ Also emitted as a by-product of other halocarbon production

* Indicates value amended from IPCC 1990, or gas not previously listed; the mass factor for CCl_4 has altered due to a typographical error in IPCC 1990.

REFERENCES

AFEAS, Alternative Fluorocarbons Environmental Acceptability Study, *AFEAS Report – Appendix (Volume 2) of Scientific Assessment of Stratospheric Ozone: 1989,* World Meteorological Organization Global Ozone Research and Monitoring Project – Report No. 20, Geneva, 1989.

Angell, J.K., Variations and trends in tropospheric and stratospheric global temperatures, 1958-1987, *J. Climate, 1,* 1296-1313, 1988.

Angell, J.K., Comparison of stratospheric warming following Agung, El Chichón and Pinatubo volcanic eruptions, *Geophys. Res. Lett., 20,* 715-718, 1993.

Briegleb, B.P., Longwave band model for thermal radiation in climate studies, *J. Geophys. Res., 97,* 11475-11485, 1992.

Brown, A.C., C.-E. Canosa-Mas, A.D. Parr, and R.P. Wayne, Laboratory studies of some halogenated ethanes and ethers: Measurements of rates of reaction with OH and of infrared absorption cross sections, *Atmos. Environ., 24A,* 2499-2511, 1990.

Cappellani, F., and G. Restelli, Infrared band strengths and their temperature dependence of the hydrohalocarbons HFC-134a, HFC-152a, HCFC-22, HCFC-123 and HCFC-142b, *Spectrochimica Acta, 48A,* 1127-1131, 1992.

Chanin, M.-L., Long-term trend in the middle atmosphere temperature, in *The Role of the Stratosphere in Global Change,* edited by M.-L. Chanin, NATO-ASI Series, Springer-Verlag, Berlin, 301-317, 1993.

Christy, J.R., and S.J. Drouilhet, Variability in daily, zonal mean lower stratospheric temperatures, *J. Climate, 7,* 106-120, 1994.

Clerbaux, C., R. Colin, P.C. Simon, and C. Granier, Infrared cross sections and global warming potentials of 10 alternative hydrohalocarbons, *J. Geophys. Res., 98,* 10491-10497, 1993.

Clerbaux, C., and R. Colin, Determination of the infrared cross section and global warming potential of 1,1,1-trifluoroethane (HFC-143), *Geophys. Res. Lett., 21,* 2377-2380, 1994.

Daniel, J.S., S. Solomon, and D.L. Albritton, On the evaluation of halocarbon radiative forcing and global warming potentials, *J. Geophys. Res.*, in press, 1994.

Fisher, D.A., C.H. Hales, W.-C. Wang, M.K.W. Ko, and N.-D. Sze, Model calculations of the relative effects of CFCs and their replacements on global warming, *Nature, 344,* 513-516, 1990.

Fishman, J., The global consequences of increasing tropospheric ozone concentrations, *Chemosphere, 22,* 685-695, 1991.

Gaffen, D.J., Temporal inhomogeneities in radiosonde temperature records, *J. Geophys. Res., 99,* 3667-3776, 1994.

Garland, N.L., L.J. Medhurst, and H.H. Nelson, Potential chlorofluorocarbon replacements: OH reaction rate constants between 250 and 315 K and infrared absorption spectra, *J. Geophys. Res., 98,* 23107-23111, 1993.

Grossman, A.S., K.E. Grant, and D.J. Wuebbles, Radiative flux calculations at UV and visible wavelengths, LLNL Report UCRL-ID-115336, Lawrence Livermore National Laboratory, Livermore, California, 1993.

Grossman, A.S., and K.E. Grant, A correlated k-distribution model of the heating rates for atmospheric mixtures of H_2O, CO_2, O_3, CH_4 and N_2O in the 0-2500 cm^{-1} wavenumber region at altitudes between 0-60 km, in *Proceedings of the 8th Conference on Atmospheric Radiation,* American Meteorological Society, Boston, Massachusetts, 97-99, 1994.

Hansen, J., D. Johnson, A. Lacis, S. Lebedeff, P. Lee, D. Rind, and G. Russel, Climate impacts of increasing carbon dioxide, *Science, 213,* 957-966, 1981.

Hansen, J., W. Rossow, and I. Fung, Long-term monitoring of global climate forcing and feedbacks, *NASA Conference Publications 3234*, National Aeronautics and Space Administration, Washington, D.C., 1992.

Hansen, J., A. Lacis, R. Ruedy, M. Sato, and H. Wilson, How sensitive is the world's climate?, *National Geographic Research and Exploration, 9,* 142-158, 1993.

Hansen, J., M. Sato, A. Lacis, and R. Ruedy, The impact on climate of ozone change and aerosols, in *Proceedings of IPCC Hamburg Meeting*, a joint workshop of IPCC Working Group I and the International Ozone Assessment Panel, Hamburg, available from IPCC WGI Technical Support Unit, Hadley Center, Meteorological Office, Bracknell, UK, 1994.

Hauglustaine, D.A., C. Granier, G.P. Brasseur, and G. Mégie, The importance of atmospheric chemistry in the calculation of radiative forcing on the climate system, *J. Geophys. Res., 99,* 1173-1186, 1994.

IPCC, *Climate Change. The IPCC Scientific Assessment,* Intergovernmental Panel on Climate Change, Cambridge University Press, 1990.

IPCC, *Climate Change 1992. The Supplementary Report to the IPCC Scientific Assessment,* Intergovernmental Panel on Climate Change, Cambridge University Press, 1992.

IPCC, *Radiative Forcing of Climate Change. An Interim Scientific Assessment,* Intergovernmental Panel on Climate Change, to be published by Cambridge University Press, 1994.

Isaksen, I.S.A., C. Brühl, M. Molina, H. Schiff, K. Shine, and F. Stordal, An assessment of the role of CF_4 and C_2F_6 as greenhouse gases, Center for International Climate and Research, University of Oslo Policy Note 1992:6, 1992.

Karol, I., and V.A. Frolkis, Model evaluation of the radiative and temperature effects of the ozone content changes in the global atmosphere of the 1980s, in *Proceedings of the Quadrennial Ozone Symposium 1992,* Charlottesville, Virginia, 13 June 1992, NASA Conference Publication CP-3266, 409-412, 1994.

Kiehl, J.T., R.J. Wolski, B.P. Briegleb, and V. Ramanathan, Documentation of radiation and cloud routines in the NCAR Community Climate Model, NCAR Technical Note TN-288+IA, National Center for Atmospheric Research, Boulder, Colorado, 1987.

Ko, M.K.W., N.-D. Sze, W.-C. Wang, G. Shia, A. Goldman, F.J. Murcray, D.G. Murcray, and C.P. Rinsland, Atmospheric sulfur hexafluoride: Sources, sinks and greenhouse warming, *J. Geophys. Res., 98,* 10499-10507, 1993.

Kokin, G.A., and E.V. Lysenko, On temperature trends of the atmosphere from rocket and radiosonde data, *J. Atmos. Terr. Phys., 56,* 1035-1044, 1994.

Labitzke, K., and M.P. McCormick, Stratospheric temperature increases due to Pinatubo aerosols, *Geophys. Res. Lett., 19,* 207-210, 1992.

Labitzke, K., and H. Van Loon, A note on trends in the stratosphere: 1958-1992, *COSPAR Colloquia Series, 5,* Pergamon Press, 537-546, 1994.

Lacis, A.A., and J.E. Hansen, A parameterization for the absorption of solar radiation in the earth's atmosphere, *J. Atmos. Sci., 31,* 118-133, 1974.

Lacis, A.A., D.J. Wuebbles, and J.A. Logan, Radiative forcing of climate by changes in the vertical distribution of ozone, *J. Geophys. Res., 95,* 9971-9981, 1990.

McCormack, J.P., and L.L. Hood, Relationship between ozone and temperature trends in the lower stratosphere: Latitudinal and seasonal dependences, *Geophys. Res. Lett., 21,* 1615-1618, 1994.

McDaniel, A.H., C.A. Cantrell, J.A. Davidson, R.E. Shetter, and J.G. Calvert, The temperature dependent infrared absorption cross sections for chlorofluorocarbons: CFC-11, CFC-12, CFC-13, CFC-14, CFC-22, CFC-113, CFC-114 and CFC-115, *J. Atmos. Chem, 12,* 211-227, 1991.

Madronich, S., and C. Granier, Impact of recent total ozone changes on tropospheric ozone photodissociation, hydroxyl radicals and methane trends, *Geophys. Res. Lett., 19,* 465-467, 1992.

Madronich, S., and C. Granier, Tropospheric chemistry changes due to increased UV-B radiation, in *Stratospheric Ozone Depletion—UV-B Radiation in the Biosphere*, edited by R.H. Biggs and M.E.B. Joyner, Springer-Verlag, Berlin, 3-10, 1994.

Mahlman, J.D., J.P. Pinto, and L.J. Umscheid, Transport, radiative and dynamical effects of the Antarctic ozone hole: A GFDL "SKYHI" model experiment, *J. Atmos. Sci., 51,* 489-509, 1994.

Marenco, A., H. Gouget, P. Nédelec, J-P. Pagés, and F. Karcher, Evidence of a long-term increase in tropospheric ozone from Pic du Midi data series – consequences: Positive radiative forcing, *J. Geophys. Res., 99,* 16617-16632, 1994.

Miller, A.J., R.M. Nagatani, G.C. Tiao, X.F. Niu, G.C. Reinsel, D. Wuebbles, and K. Grant, Comparisons of observed ozone and temperature trends in the lower stratosphere, *Geophys. Res. Lett., 19,* 929-932, 1992.

Morcrette, J.J., Radiation and cloud radiative properties in the ECMWF forecasting system, *J. Geophys. Res., 96,* 9121-9132, 1991.

Oort, A.H., and H. Liu, Upper air temperature trends over the globe, 1958-1989, *J. Climate, 6,* 292-307, 1993.

Parker, D.E., and D.I. Cox, Towards a consistent global climatological rawinsonde data base, *Int. J. Climatology*, in press, 1994.

Ramanathan, V., R.J. Cicerone, H.B. Singh, and J.T. Kiehl, Trace gas trends and their potential role in climate change, *J. Geophys. Res., 90,* 5547-5566, 1985.

Ramaswamy, V., M.D. Schwarzkopf, and K.P. Shine, Radiative forcing of climate from halocarbon-induced global stratospheric ozone loss, *Nature, 355,* 810-812, 1992.

Ramaswamy, V., and M.M. Bowen, Effect of changes in radiatively active species upon the lower stratospheric temperatures, *J. Geophys. Res.,* 18909-18921, 1994.

Randel, W.J., and J.B. Cobb, Coherent variations of monthly mean total ozone and lower stratospheric temperature, *J. Geophys. Res., 99,* 5433-5447, 1994.

Rind, D., and A. Lacis, The role of the stratosphere in climate change, *Surveys in Geophysics, 14,* 133-165, 1993.

Robock, A., The volcanic contribution to climate change of the past 100 years, in *Greenhouse Gas Induced Climatic Change: A Critical Appraisal of Simulations and Observations*, edited by M.E. Schlesinger, Elsevier, Amsterdam, 429-443, 1991.

Sato, M., J.E. Hansen, M.P. McCormick, and J.B. Pollack, Stratospheric aerosol optical depths, 1850-1990, *J. Geophys. Res., 98,* 22987-22994, 1993.

Schwarzkopf, M.D., and S.B. Fels, The simplified exchange method revisited: An accurate, rapid method for computation of infrared cooling rates and fluxes, *J. Geophys. Res., 96,* 9075-9096, 1991.

Schwarzkopf, M.D., and V. Ramaswamy, Radiative forcing due to ozone in the 1980s: Dependence on altitude of ozone change, *Geophys. Res. Lett., 20,* 205-208, 1993.

Shi, G., Global Warming Potential due to chlorofluorocarbons and their substitutes, *Chinese J. Atmos. Sci., 16,* 240-248, 1992.

Shine, K.P., On the cause of the relative greenhouse strength of gases such as the halocarbons, *J. Atmos. Sci., 48,* 1513-1518, 1991.

Shine, K.P., The greenhouse effect and stratospheric change, in *The Role of the Stratosphere in Global Change*, edited by M.-L. Chanin, NATO ASI Series, Springer-Verlag, Berlin, 285-300, 1993.

Shine, K.P., B.P. Briegleb, A.S. Grossman, D. Hauglustaine, H. Mao, V. Ramaswamy, M.D. Schwarzkopf, R. Van Dorland, and W.-C. Wang, Radiative forcing due to changes in ozone – A comparison of different codes, in *Atmospheric Ozone as a Climate Gas,* edited by W.-C. Wang and I.S.A. Isaksen, NATO ASI Series, Springer-Verlag, Berlin, in press, 1994.

Slingo A., and H.M. Schrecker, On the shortwave properties of stratiform water clouds, *Quart. J. Roy. Meteorol. Soc., 108,* 407-426, 1982.

Spencer, R.W., and J.R. Christy, Precision lower stratospheric temperature monitoring with the MSU: Validation and results 1979-1991, *J. Climate, 6,* 1194-1204, 1993.

Stordal, F., B. Innset, A.S. Grossman, and G. Myhre, SF_6 as a greenhouse gas, *Norwegian Institute for Air Research (NILU) Report 0-92102,* 1993.

Wallington, T.J., C.A. Gierczak, J.C. Ball, S.M. Japar, Fourier transform infrared study of the self reaction of $C_2H_5O_2$ radicals in air at 295 K, *Int. J. Chem. Kinet., 21,* 1077-1089, 1989.

Wang, W.-C., J.P. Pinto, and Y.L. Yung, Climatic effects due to halogenated compounds in the Earth's atmosphere, *J. Atmos. Sci., 37,* 333-338, 1980.

Wang W.-C., G.Y. Shi, and J.T. Kiehl, Incorporation of the thermal radiative effect of CH_4, N_2O, CF_2Cl_2 and $CFCl_3$ into the NCAR Community Climate Model, *J. Geophys. Res., 96,* 9097-9103, 1991.

Wang, W.-C., Y.-C. Zhuang, and R.D. Bojkov, Climate implications of observed changes in ozone vertical distributions at middle and high latitudes of the Northern Hemisphere, *Geophys. Res. Lett., 20,* 1567-1570, 1993.

Wigley, T.M.L., The contribution from emissions of different gases to the enhanced greenhouse effect, in *Climate Change and the Agenda for Research*, edited by T. Hanisch, Westview Press, Boulder, Colorado, 1994.

WMO, *Atmospheric Ozone, 1985: Assessment of Our Understanding of the Processes Controlling Its Present Distribution and Change,* World Meteorological Organization Global Ozone Research and Monitoring Project – Report No. 16, Geneva, 1986.

WMO, *Report of the International Ozone Trends Panel,* World Meteorological Organization Global Ozone Research and Monitoring Project – Report No. 18, Geneva, 1988.

WMO, *Scientific Assessment of Ozone Depletion: 1991,* World Meteorological Organization Global Ozone Research and Monitoring Project – Report No. 25, Geneva, 1992.

CHAPTER 9

Surface Ultraviolet Radiation

Lead Author:
R.L. McKenzie

Co-authors:
M. Blumthaler
C.R. Booth
S.B. Diaz
J.E. Frederick
T. Ito
S. Madronich
G. Seckmeyer

Contributors:
S. Cabrera
M. Ilyas
J.B. Kerr
C.E. Roy
P.C. Simon
D.I. Wardle

CHAPTER 9

SURFACE ULTRAVIOLET RADIATION

Contents

SCIENTIFIC SUMMARY

- There is overwhelming experimental evidence that, all other things being equal, decreases in atmospheric ozone result in UV-B increases at the Earth's surface, in quantitative agreement with predictions by radiative transfer models.

- Large UV-B increases have been observed in association with the ozone "hole" at high southern latitudes. Biologically damaging radiation at the South Pole exceeded that in the Arctic by more than a factor of two, for the same solar zenith angle. At Palmer Station, Antarctica (64.5°S), erythemal and DNA-damaging radiation sometimes exceeded summer maxima at San Diego (32°N). These measured differences agree well with model calculations.

- Large increases in UV-B were measured, despite the natural variability in cloudiness, at northern middle and high latitudes in 1992/93 compared with previous years. These are the first reported examples of persistent increases associated with anomalous ozone reductions over densely populated regions.

- Clear-sky UV measurements at midlatitude locations in the Southern Hemisphere are significantly larger than at a midlatitude site in the Northern Hemisphere, in agreement with the expected differences due to ozone column and Sun-Earth separation.

- The increases in UV resulting from ozone reductions measured by satellite from 1979 to early 1994 have been calculated, assuming other factors such as pollution and cloudiness did not change systematically over this period. The calculated increases are largest at short wavelengths and at high latitudes. Poleward of 45°, the increases are significantly greater in the Southern Hemisphere. At 45° (N and S), the calculated increase at 310 nm was approximately 8 to 10 percent over this 15-year period, but there was considerable year-to-year variability.

- Tropospheric ozone and aerosols can reduce global UV-B irradiances appreciably. At some locations, tropospheric pollution may have increased since pre-industrial times, leading to some decreases in surface UV radiation. However, recent trends in tropospheric pollution probably had only minor effects on UV trends relative to the effect of stratospheric ozone reductions.

- Only a few studies have monitored UV-B over time scales of decades, and these have yielded conflicting results on the magnitude and even sign of the trends. Some studies may have been affected by problems with instrument stability and calibration, and local pollution trends. Recently published data from unpolluted locations appear to show the expected increases due to ozone depletion. The baseline UV irradiances present at mid and high latitudes before ozone depletion began are not known.

- Significant improvements have been made in UV instrumentation and its calibration. Intercomparisons between spectro-radiometers show, however, that it is still difficult to achieve absolute calibration accuracies better than ±5 percent in the UV-B region. Therefore, the detection of future trends will require careful measurements at short wavelengths that are more sensitive to changes in ozone.

- Cloud variability causes large temporal changes in UV. Although recent advances have been made, our ability to realistically model cloud effects is still limited.

- Scattering by stratospheric aerosols from the Mt. Pinatubo volcanic eruption did not alter total UV irradiances appreciably, but did increase the ratio of diffuse to direct radiation.

9.1 INTRODUCTION

Although the ultraviolet (UV) region represents only a small component of the total solar spectrum, these wavelengths are important because the photon energies are comparable with molecular bond energies in the biosphere. The UV radiation that reaches the Earth surface can be arbitrarily divided into 2 sub-regions: UV-B (280-315 nm), which is strongly absorbed by ozone; and UV-A (315-400 nm), which is only weakly absorbed by ozone. Less than 2 percent of the extra-terrestrial solar energy falls within the UV-B range, and only a small fraction of this reaches the surface.

Here we review progress in our understanding of UV at the surface since the last assessment (WMO, 1992) and attempt to identify remaining gaps in our knowledge. Impacts of UV increases (*e.g.*, effects on the biosphere, including human health and materials) are outside the scope of this report and are discussed in the UNEP "Effects Panel" reports (1991, 1994). Impacts on tropospheric chemistry that may result from changes in UV radiation fields are also discussed in Chapter 5 of this report. These may lead to either positive or negative feedbacks to stratospheric ozone depletion (UNEP, 1991 and 1994; Madronich and Granier, 1994).

Detailed reviews of our understanding of UV at the surface can also be found in Tevini (1993) and Young *et al.* (1993).

9.2 UPDATE ON TREND OBSERVATIONS

9.2.1 Results Derived from Broad-Band Meters

Analyses of broad-band data have focused on variability in the radiation received in specific geographic regions over time scales of months to years. The much-discussed work of Scotto *et al.* (1988) showed a decline in annually integrated irradiance measured by eight Robertson-Berger (RB) meters in the continental United States between 1974 and 1985. The average trend based on all stations was -0.7 percent per year, while the statistically significant values for individual stations varied from -0.5 to -1.0 percent per year. A careful analysis of the RB meter's operating characteristics was carried out shortly after the publication of Scotto *et al.* (1988). These studies showed that the spectral response functions of selected meters were remarkably stable over time, although small differences between instruments existed (DeLuisi *et al.*, 1992). As part of this evaluation, Kennedy and Sharp (1992) found no obvious problems in the RB meter system apart from a well-documented temperature sensitivity. This does not appear to be a likely explanation for the downward trends found by Scotto *et al.* (1988). However, some of the detailed information required to assess the stability of the RB meter network is no longer in existence. More recent work (DeLuisi, 1993; DeLuisi *et al.*, 1994) has uncovered a potential shift in calibration of the RB meter network in 1980 that could remove the downward trend found by Scotto *et al.* (1988). This issue merits further attention before definitive conclusions are reached.

Frederick and Weatherhead (1992) studied the time series of RB data from two specific sites, Bismarck (46.8°N) and Tallahassee (30.4°N), where Dobson column ozone data were available over the period from 1974 to 1985. They found that the derived trend in clear-sky RB data during the summer months was consistent with that expected from the Dobson data. However, during winter, when the measured broad-band irradiances were very small, a pronounced downward trend near -2 percent per year exists in the RB data. This differs in sign from spectrally weighted irradiance calculations for clear skies based on the Dobson ozone. The winter behavior in the RB data sets at Bismarck and Tallahassee is not readily explained by any known change in the atmosphere above these sites. Although the influences of cloudiness and ozone in the boundary layer can be detected in the output of the RB meter (Frederick *et al.*, 1993a), these influences are not likely to be causes of the winter trends in broad-band irradiance.

Blumthaler and Ambach (1990) reported an upward trend in RB readings made from an unpolluted site in the Swiss Alps at latitude 47°N during the period 1981 through 1989. Readings were expressed as ratios to the total solar irradiance measured by a pyranometer so as to remove the effects of aerosols. These measurements have continued, and the upward trend in the ratios was 0.7 ± 0.3 percent per year to the end of 1991, but results from 1992 were similar to those at start of the period. The analysis did not examine the trend by month of the year.

Recently, Zheng and Basher (1993) reported an upward trend in clear-sky RB data from Invercargill, New Zealand, at 46°S. The observation site is in an un-

polluted region where changes in aerosols were small over the observation period. The deduced trend is anti-correlated in the expected way with column ozone data from the same location.

Temperature coefficients of order 1%/K have been reported for RB meters and their derivatives (Johnsen and Moan, 1991; Blumthaler, 1993; Dichter *et al.*, 1994). Of the trend analyses above, only that by Blumthaler and Ambach (1990) applied corrections for instrument temperature changes. New generation temperature-stabilized instruments are now available and are being tested against spectro-radiometers (Grainger *et al.*, 1993; McKenzie, 1994a).

9.2.2 Multi-Wavelength Measurements

The longest time series of UV irradiance at the ground has been published by Correll *et al.* (1992). A multi-filter instrument was used in Maryland (39°N, 77°W), over the period September 1975 to December 1990. The data show a large increase in UV-B, especially at shorter wavelengths over the period 1980 to 1987. The authors deduce from their measurements that the "RB-weighted" UV (over the interval 295-320 nm, however) would have increased by 35 percent over the period 1977-78 to 1985. This increase is much larger than expected from stratospheric ozone losses. The integral used would, however, show greater sensitivity to ozone loss than a real RB meter, which is more responsive at wavelengths longer than 320 nm in the UV-A region that are unaffected by ozone changes. A decrease in the irradiances after 1987 may be a consequence of changes to the instrument at that time, though the authors speculate that changes in aerosols and cloud conditions may have influenced the results.

9.2.3 Status of Trend Observations

The measurement of trends in UV is challenging from an instrumental point of view, and the availability and deployment of instruments to monitor trends in UV have been far from ideal. Instrument development over the past few years has continued to address the issues of stability, spectral response, spectral resolution, cost, and ease of maintenance in an attempt to meet the varied needs of the community. Short-term process studies have revealed strong anticorrelations between ozone and UV, in agreement with those expected from model calculations (WMO, 1992). Thus there is no doubt that, in the absence of other changes, reductions in stratospheric ozone will result in UV increases. However, the results of long-term studies have been conflicting. The network of RB meters was never designed to measure long-term trends, and questions still remain over the ability of broad-band meters to achieve this aim. Evidence now suggests that changing aerosol (and cloud) conditions can lead to increases or decreases in UV (Justus and Murphey, 1994). Further comparisons between RB measurements and pyranometer data at other sites are warranted. It is significant that at unpolluted sites, the observed increases in UV are comparable with those expected from ozone changes. Even at more polluted sites where UV has apparently not increased, it is reasonable to assert that current UV levels are greater than they would otherwise have been without ozone depletion. Better instruments are now available to monitor changes. These include improved broad-band monitors and sophisticated spectro-radiometers that can distinguish between changes caused by ozone and other effects such as aerosols and clouds. However, if current predictions are correct (see Chapter 13), much of the expected ozone depletion has already occurred. It will therefore be important to maintain careful calibration of these instruments over decadal time scales if trends in UV are to be discerned from natural variability. Although measurements from polluted sites will be of interest to epidemiologists and for process studies, instruments designed to monitor trends due to ozone depletion should generally be located at remote sites where tropospheric changes are minimized.

9.3 SPECTRO-RADIOMETER RESULTS

The observation period from spectro-radiometers is too short to detect trends. However, multi-year data are now available from a network of instruments operated by the National Science Foundation (NSF) (Booth *et al.*, 1994) and from several other groups (Gardiner *et al.*, 1993; McKenzie *et al.*, 1993; Kerr and McElroy, 1993; Ito *et al.*, 1994). Process studies using these data have already provided experimental corroboration of the modeled relationship between ozone and UV (WMO, 1992).

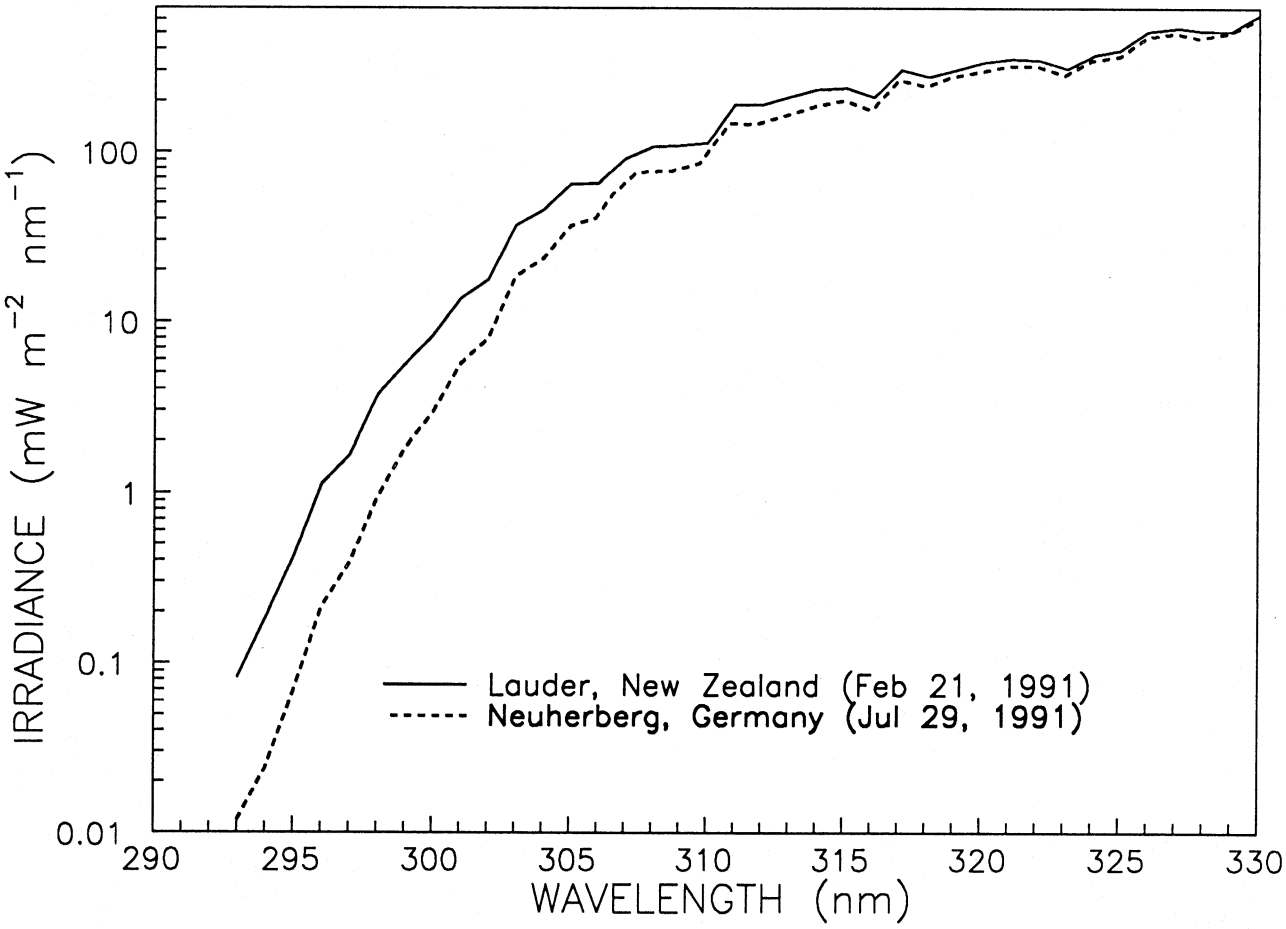

Figure 9-1. Measured clear-sky spectral irradiances in New Zealand and Germany for solar zenith angle 34.3°. The ozone column was 266 Dobson units (DU) in New Zealand and 352 DU in Germany. Note the logarithmic scale on the y-axis (adapted from Seckmeyer and McKenzie, 1992).

9.3.1 Intercomparisons

The measurement of solar UV spectral irradiances is demanding. The steep slope of the solar spectrum in the UV-B region (Figure 9-1) poses specific instrumental problems that must be overcome to cope with the wide dynamic range, the need to reject stray light adequately, and the need to align the wavelength accurately (McKenzie *et al.*, 1992). An additional problem concerns tracing the absolute calibration to a common standard. National standards laboratories themselves disagree by more than ±2 percent in the UV-B region (Walker *et al.*, 1991).

Excellent radiometric stability is required to measure UV trends or geographic differences. However, recent intercomparisons have revealed large calibration differences between some spectro-radiometers. Major sources of uncertainty are instability of sensitivity and cosine errors. Agreement at the ±5 percent level (Figure 9-2) is as good as can be expected at present (Gardiner *et al.*, 1993; McKenzie *et al.*, 1993; Seckmeyer *et al.*, 1994b). Further field and laboratory intercalibrations between instruments are required.

Given these measurement uncertainties, it will probably be necessary to use very short wavelengths in the UV-B that have a high sensitivity to ozone change to detect trends in UV due to the ozone depletions expected over the next decade. As one moves to shorter wavelengths, the sensitivity to ozone reductions increases dramatically. For example, a 1 percent reduction in

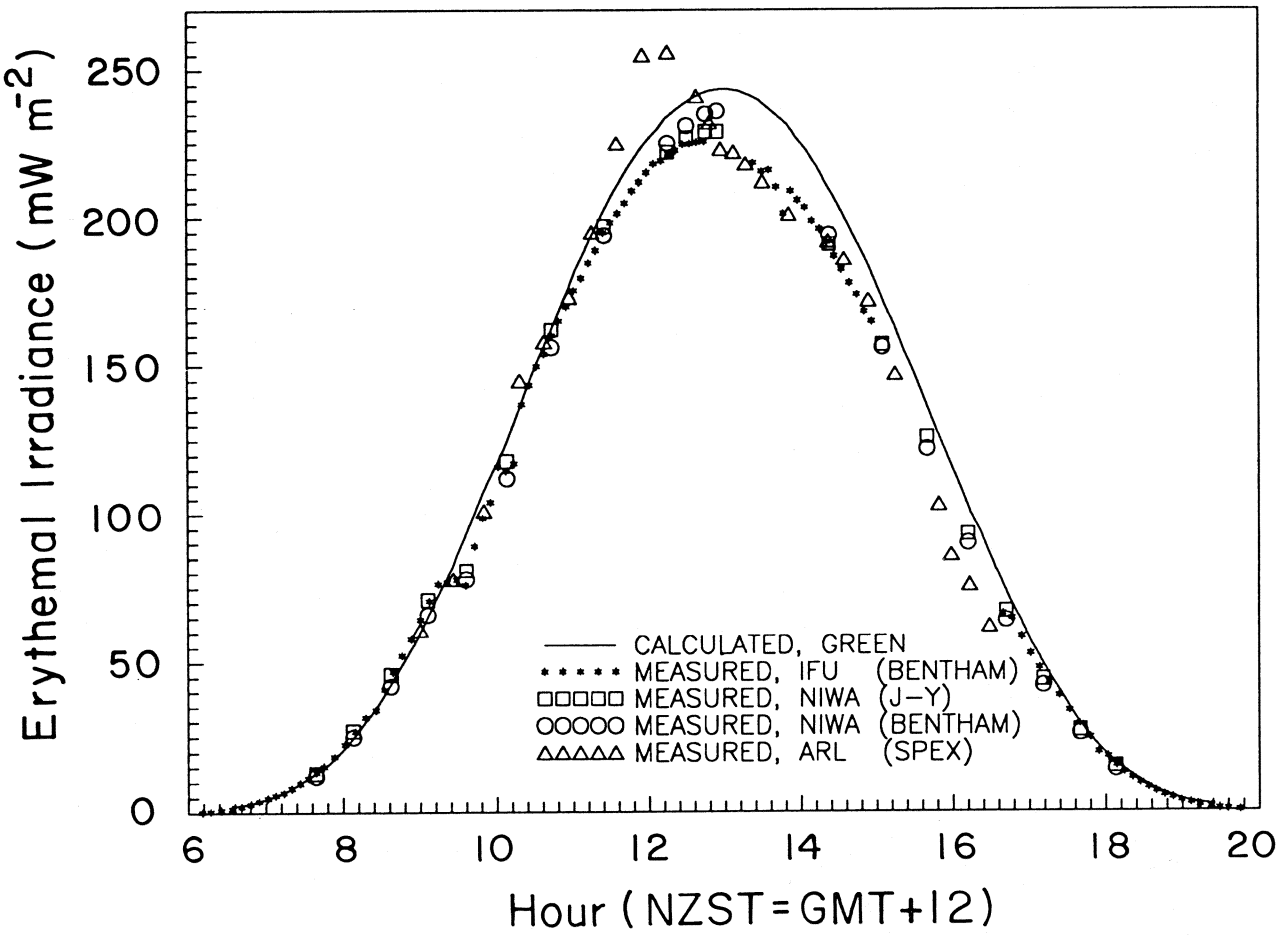

Figure 9-2. Comparison between measurements made with 4 spectro-radiometers at Lauder, New Zealand, on Feb 23, 1993. Instruments included were from National Institute of Water and Atmospheric Research, New Zealand (2), Australian Radiation Laboratory, Australia, and Fraunhofer Institute for Atmospheric Environment, Germany. Clear-sky model results are shown for comparison, although the observation day was not perfectly clear (adapted from McKenzie *et al.,* 1993).

ozone causes an increase of approximately 1 percent in UV at 310 nm, whereas the increase at 300 nm is 3 to 4 times as large (see Figure 9-12).

9.3.2 Geographic Differences

Although large geographical differences in UV-B are expected from theoretical considerations, there have been few published studies demonstrating measured geographic differences in UV-B radiation. A climatology obtained from a network of RB meters in the 1970s (Berger and Urbach, 1982) may be biased by the strong temperature coefficient of these instruments. Although the UV data base is improving, it still remains largely uncoordinated. Large latitudinal gradients have, however, been observed from the NSF network of spectro-radiometers, as discussed in Section 9.3.3 (Booth *et al.,* 1994).

Geographic intercomparisons based on measurements from the same instrument (Seckmeyer and McKenzie, 1992) have shown that for clear-sky observing conditions and similar solar zenith angles, UV irradiances measured in Europe are much less than in New Zealand (Figure 9-1). The differences are larger than expected from calculations using an earlier ozone climatology, though their spectral characteristics indi-

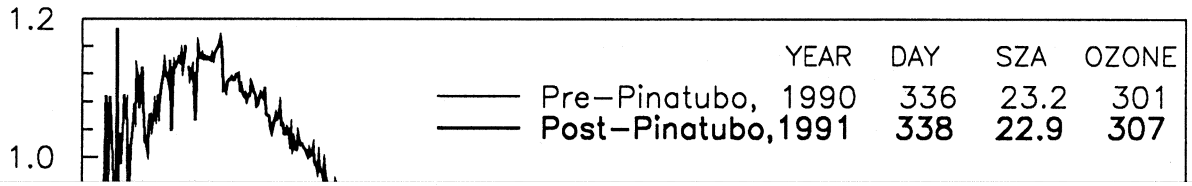

SURFACE UV RADIATION

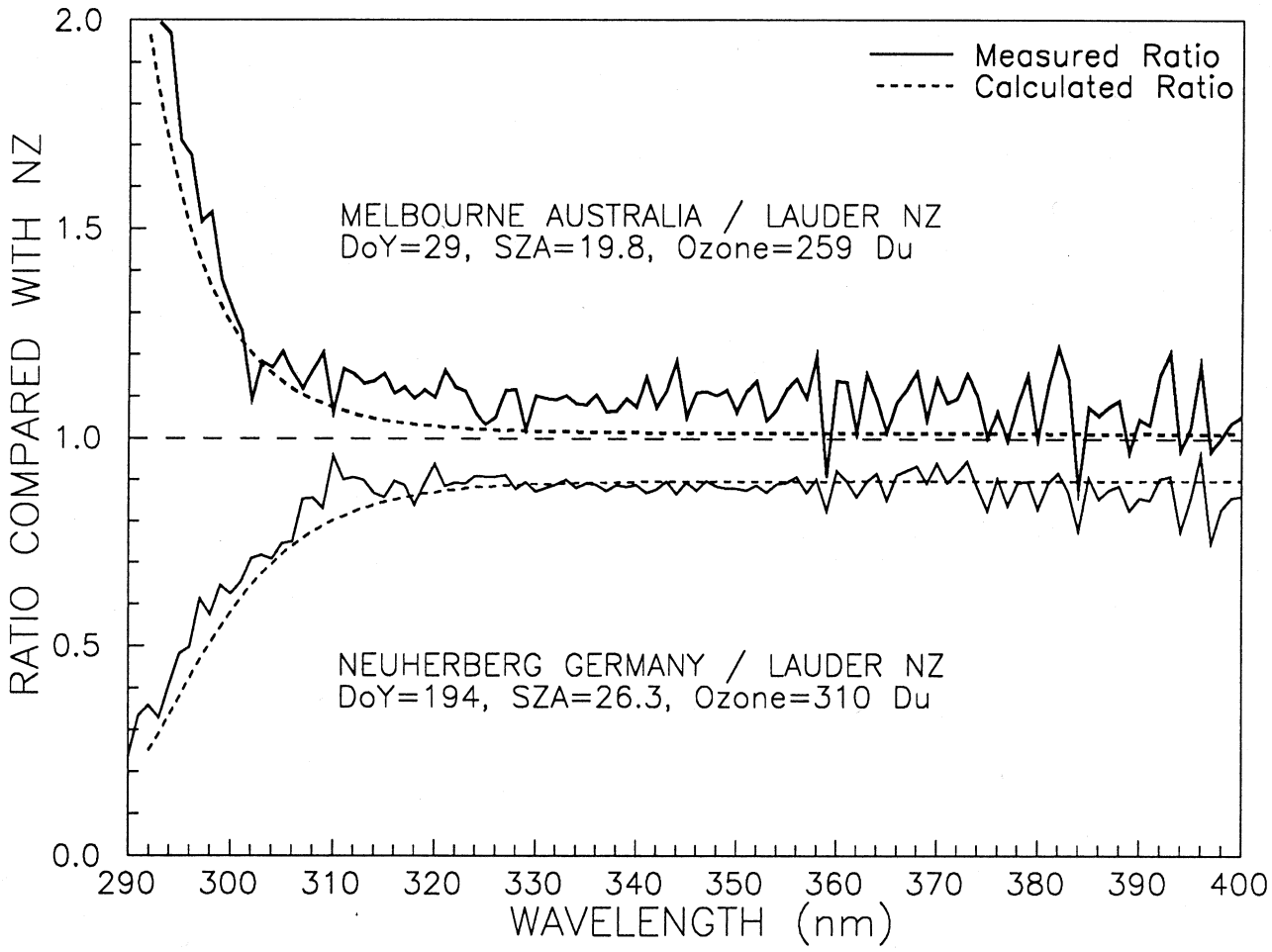

Figure 9-3. Geographic comparison between maximum clear-sky spectra measured in three countries. The ratios are with respect to a spectrum measured at Lauder on Dec. 27, 1992 (Day-of-Year [DoY] =362, sza=21.8°, ozone=278 DU). The smooth curves show calculated ratios assuming similar albedos and aerosol properties (adapted from McKenzie *et al.*, 1993).

cate that they are primarily due to ozone. This illustrates the importance of tropospheric ozone, which has increased in Europe (Staehelin and Schmid, 1991).

Data from cross-calibrated instruments have been used to compare the maximum clear-sky irradiances measured over several summers at three sites (McKenzie *et al.*, 1993). Ratios of these maximum clear-sky spectra

suming no differences in aerosol loading. The calculated differences in UV are due to differences in ozone, sun angle, and Earth-Sun separation. Measured and calculated ratios are in agreement within experimental uncertainties.

9.3.3 High Latitude (North and South)

(Cabrera *et al.*, 1994; Blumthaler *et al.*, 1994b). At 300 nm, increases of 24 ± 4%/km have been measured in Europe for snow-free conditions (Blumthaler *et al.*, 1994b). UV-B increases of 18%/km have also been measured, although this included the effect of snow cover at the high elevation site (Ambach *et al.*, 1993). Larger gradients in UV-B have been observed during the winter near Santiago, Chile (33°S), though the same study reported gradients of only 4-5%/km in less polluted regions (Cabrera *et al.*, 1994). The calculated gradients for clear conditions are typically 5-8%/km (Madronich, 1993). Larger gradients result from increased tropospheric ozone or aerosols.

High concentrations of tropospheric pollutant gases (*e.g.*, SO_2, NO_2, O_3) can also have a significant influence on surface UV irradiances (Bais *et al.*, 1993).

9.4.3 Magnitude of Changes

Recent ozone losses in the Northern Hemisphere have been much larger than expected (Herman and Larko, 1994; Chapter 4), so that UV increases are much larger. For the first time, greatly enhanced UV was seen for extended periods of time in heavily populated latitude bands, and there may be future implications for human health (UNEP, 1994). However, the UV irradiances in 1993 were still less than for comparable southern latitudes where ozone and aerosol concentrations are lower, and where the minimum Sun-Earth separation occurs in summer.

Previously, the Radiation Amplification Factor *(RAF)* for changes in ozone was defined in terms of a linear relationship between incremental changes in ozone (ΔO_3) and UV (ΔE):

$$RAF = -(\Delta E/E)/(\Delta O_3/O_3) \qquad (9\text{-}1)$$

If this definition is (incorrectly) applied to the large depletions in ozone that have occurred recently, the magnitude of the deduced increase in UV is underestimated. To avoid this problem, the radiative change due to ozone depletion has been reformulated in terms of a power law (Madronich, 1993) so that:

$$RAF = \ln(E^*/E)/\ln(O_3/O_3^*), \qquad (9\text{-}2)$$

where E^* and E are two UV irradiances, and O_3^* and O_3 are corresponding ozone amounts. With this definition, previously calculated *RAF* values, which agree well with measurements (*e.g.*, UNEP, 1991), can still be used to deduce the increases in UV caused by the large reductions in ozone that have occurred in Antarctica and more recently at midlatitudes. For example, Booth and Madronich (1994) have used measurements from Antarctica to show that the power relationship works well, even for ozone variations of a factor of two (Figure 9-10).

9.5 UPDATE ON PREDICTIONS

9.5.1 Semi-Empirical Method

No suitable data base exists to directly measure changes in UV that may have already occurred as a result of ozone depletion. Unfortunately, the potential to calculate temporal changes in UV at the surface is also limited by inadequacies in our capability to model the effects of clouds. A semi-empirical technique has been implemented to overcome these difficulties, so that UV-B can be inferred using solar pyranometer data to estimate cloud effects, and ozone data (Ito *et al.*, 1994). Satellite ozone data suitable for these studies are available from the year 1978, when ozone depletions were small.

The relationship between pyranometer data and ozone data to derive UV-B was verified using ground-based measurements of UV spectra at four sites in Japan, and the technique has been applied to infer historical records of UV over an eleven-year period at these sites. Over this period, the long-term changes were found to be small compared with the year-to-year variability. The geographical distribution of UV over Japan has also been deduced (Ito *et al.*, 1994).

Although the technique is imperfect, the historical record and geographical differences derived may provide useful information for users such as epidemiologists. The method will be more useful if it can be successfully applied to biologically weighted UV irradiances (*e.g.*, erythemal irradiance) rather than an unweighted integral (290-315 nm) which is relatively insensitive to ozone changes.

9.5.2 Calculated Changes in Clear-Sky UV Using Global Ozone Measurements

A multi-layer radiative transfer model (Madronich, 1993) was used to calculate UV irradiances (*i.e.*, the flux passing through a horizontal surface) and their

vided by 1989-90). The bottom panel compares the

9.4.2 Tropospheric Pollution

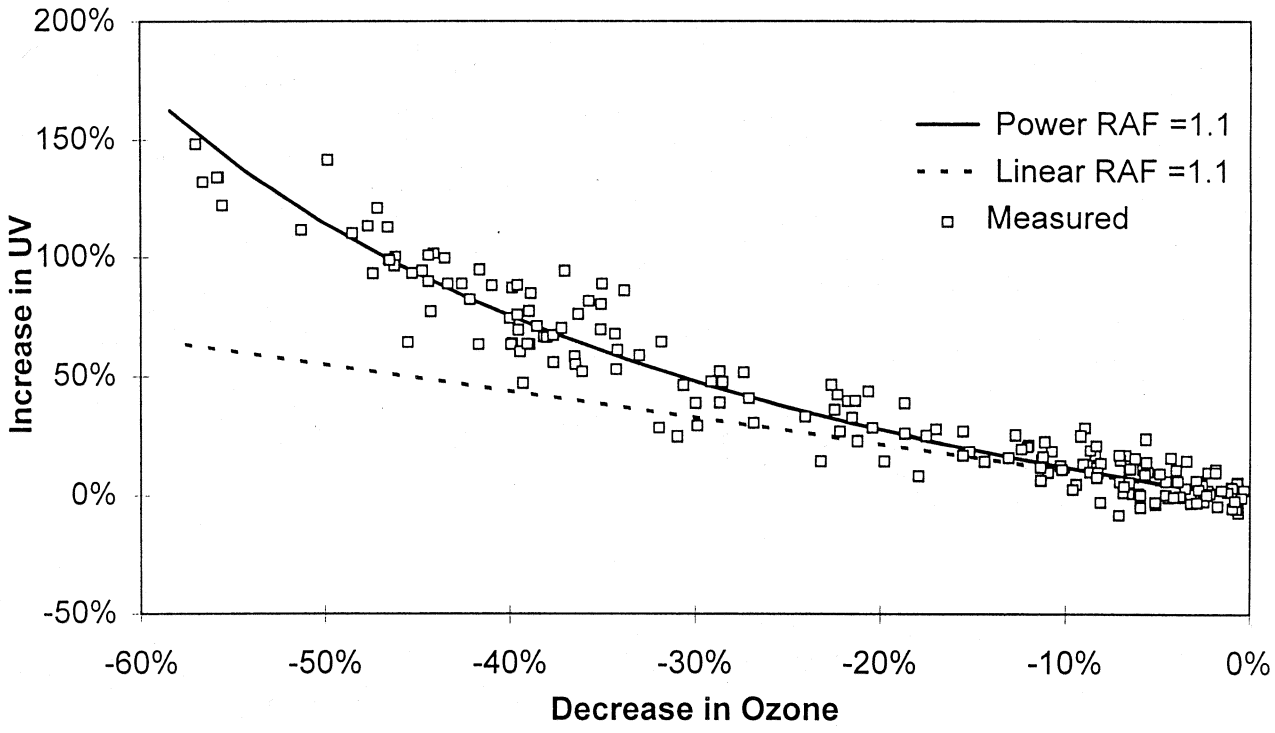

Figure 9-10. Dependence of erythemally weighted UV radiation on ozone column changes. Measurements from South Pole, 1 Feb. 1991 to 12 Dec. 1992 (from Booth and Madronich, 1994).

changes over time as a function of latitude using ozone fields from the Solar Backscatter Ultraviolet spectrometer (SBUV) and SBUV2 satellite instruments (see Chapter 1) over the period late 1978 through early 1994. The calculations presented are for clear-sky aerosol-free conditions, with a constant surface albedo of 0.05. The sensitivity of this model to changes in ozone has been assessed previously and agrees well with measurements (McKenzie *et al.*, 1991; UNEP, 1991). Here, we report calculated irradiances at selected wavelengths in the UV region. Corresponding biologically-weighted irradiances are discussed in the UNEP "Effects Panel" report (1994).

The calculated latitudinal variation in clear-sky UV for selected wavelengths using satellite ozone data over the period 1979 to 1992 is shown in Figure 9-11. The irradiances increase strongly with wavelength (note the logarithmic scale) and have maxima near the equator. Latitudinal gradients and hemispheric asymmetries increase at shorter wavelengths, where ozone absorptions are greatest. The hemispheric differences are most pronounced at latitudes poleward of 45°. At the shortest wavelength shown (300 nm), the daily spectral irradiance at the South Pole is an order of magnitude greater than at the North Pole.

The changes in these quantities over the period 1978 to 1994 (relative to the mean of the period) are shown in Figure 9-12. Changes are largest at latitudes where ozone depletions have been most severe, so that percentage trends increase towards the poles, with largest increases in the Southern Hemisphere. The effects of ozone reduction are much more important at shorter wavelengths.

The calculated time dependence of changes in 310 nm UV at latitudes 45° and 55° (N and S) for the period 1979 to 1994 is illustrated in Figure 9-13. The rate of increase in UV is not constant, but is anticorrelated with ozone changes which include perturbations due to the 11-year solar cycle. Hemispheric differences in the timing of the increases are also apparent. Percentage changes generally lead the absolute changes by a few months, as expected from the timings of greatest ozone

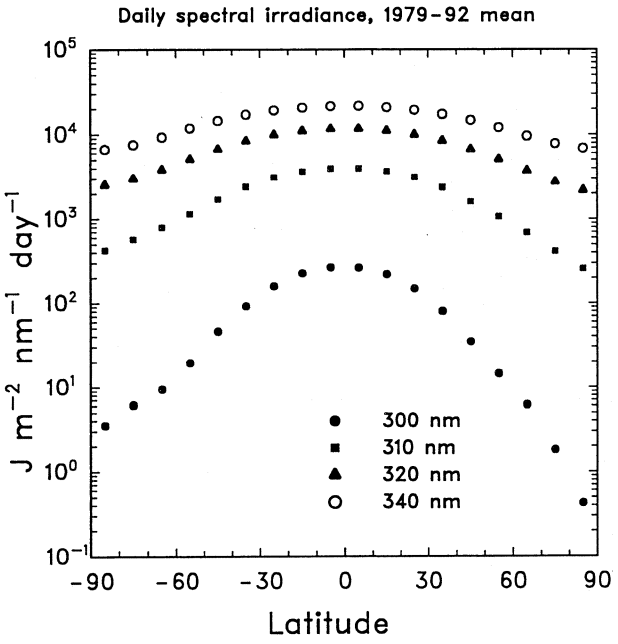

Figure 9-11. Calculated daily spectral irradiance, averaged over all months of 1979-1992, at different wavelengths. Sea level, cloudless and aerosol-free skies.

depletion (winter, spring) compared with the greatest natural UV levels (summer). The absolute changes approach zero in winter, when the UV has a minimum.

At latitude 45° the trend is approximately +0.5 percent per year in both hemispheres. At latitude 55° the trends are significantly larger, particularly in the Southern Hemisphere. Gradients are larger at shorter wavelengths and continue to increase at higher latitudes, where hemispheric differences become more pronounced.

9.5.3 Cloud and Albedo Effects

The analysis in Section 9.5.2 assumes cloud-free conditions. In practice, cloud variability causes large year-to-year changes in UV. The theory of radiative transfer through clouds is well developed, and algorithms for its numerical implementation are available (*e.g.,* Stamnes *et al.,* 1988). However, the practical application of the theory to the atmosphere is still limited because of incomplete cloud characterization.

Cloud cover at most surface observation sites is specified only as the fraction of sky covered by cloud, with little or no information about the optical depth or layering. Further, although cloud optical depth is not a strong function of wavelength, there is a nonlinear relationship between observed cloud cover and its effect in the UV-B region where a much larger fraction of the energy is diffuse (Seckmeyer *et al.,* 1994a). Measured reductions in UV-B are relatively small even for large fractional cloud covers (Ito *et al.,* 1994; Bais *et al.,* 1993).

Satellite measurements of clouds are more quantitative, but stratification of clouds is difficult to measure, and the cloud cover viewed from space is not generally the same as that viewed from the ground (Henderson-Sellers and McGuffie, 1990). Other complications arise from the nonlinear relationship between UV transmission and cloud optical depth, and the fact that cloud effects are modulated by surface albedo (Lubin *et al.,* 1994). Generally, with high surface albedo, the effective optical depth of clouds is reduced by multiple scattering effects between the surface and the cloud base, which

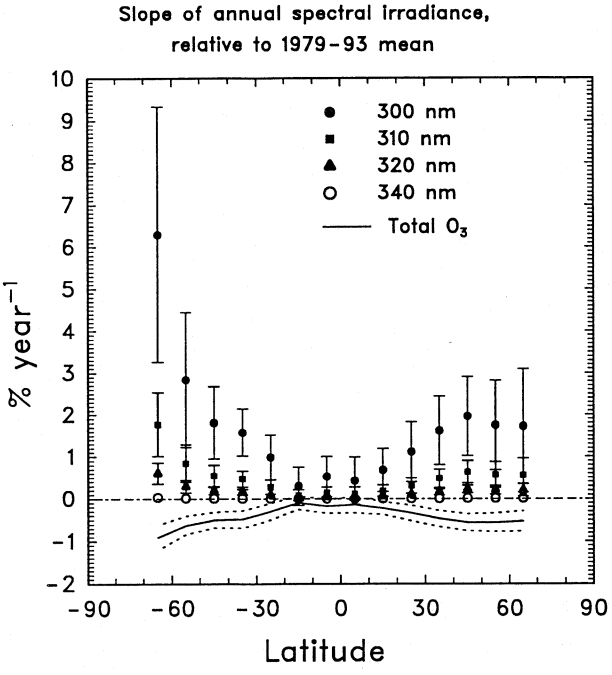

Figure 9-12. Calculated rate of increase of the annual spectral irradiances from 1978 to 1993. For comparison, the negative quadrants give the changes in annually averaged ozone column. Values are least-squares slopes expressed as percent of the 1979-1993 mean. Error bars are 2σ.

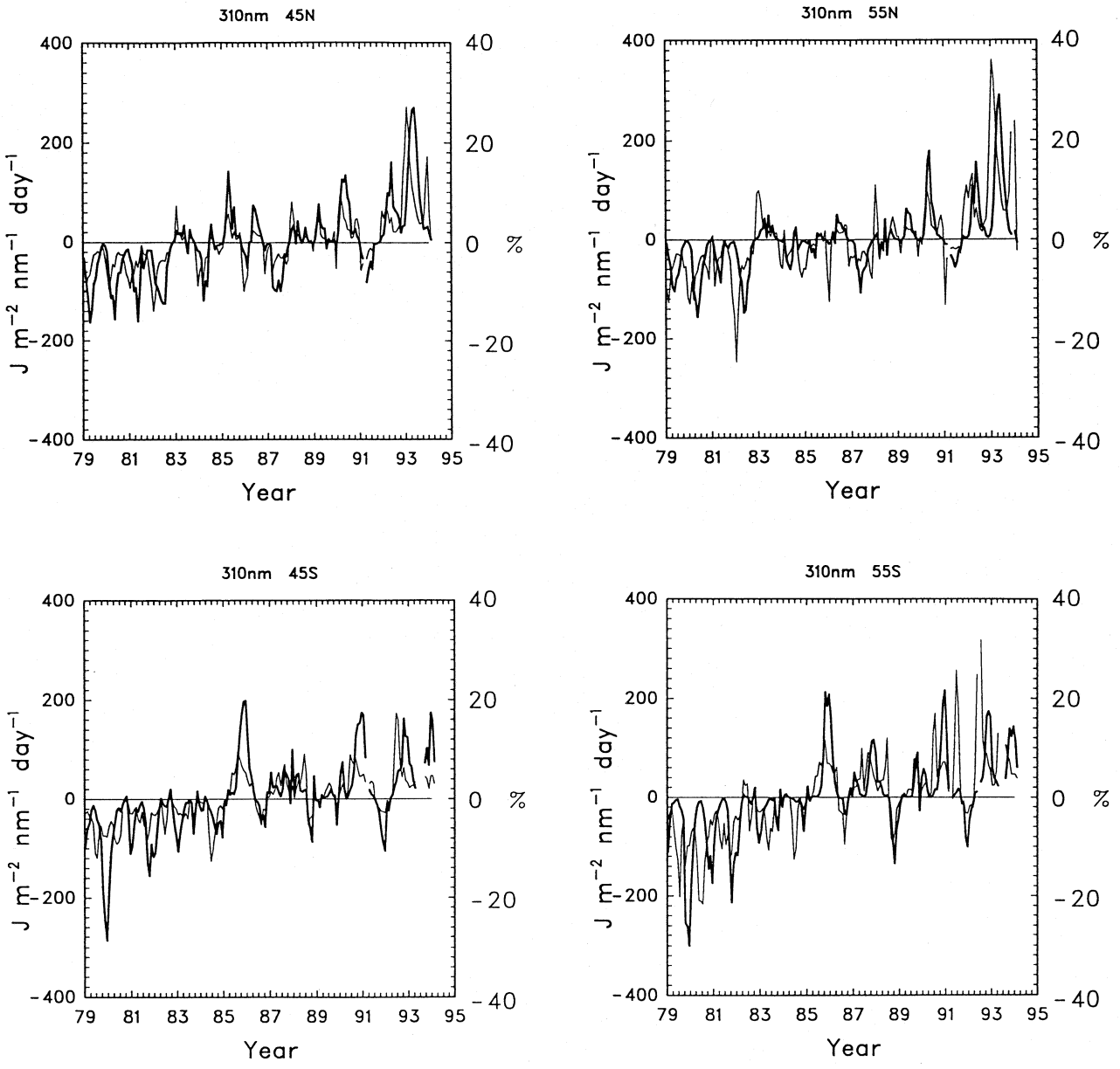

Figure 9-13. Calculated deviations from the 1978-1993 average monthly values of the daily spectral irradiance at 310 nm at latitudes 45° and 55° (N and S). Thick lines and left scales give absolute irradiance changes, thin lines and right scales give percent changes.

enhance the flux. Methods have, however, recently been developed and successfully implemented to map surface UV-B using multi-spectral satellite imagery (Lubin *et al.,* 1994).

9.5.4 UV Forecasts

In recent years, efforts have been made in several countries to educate the public concerning ambient UV-B levels. This information is often reported in the form of a daily UV index delivered with local weather forecasts (*e.g.,* Burrows *et al.,* 1994). Most of the indices in current use are based on erythemally weighted UV and are reported in a variety of forms, including arbitrary scales, weighted energy dose units, "burn times," and others. The information would be more useful if a single index could be agreed upon. The values forecast for these indices can be based on measurements, or models, or a combination of both. To be useful, such forecasts must be capable of assimilating ozone measurements in near real time and predicting changes in ozone fields within a few hours. No operational forecasts currently make realistic allowances for changes due to clouds. Ground-truthing and verifying predictive algorithms will be important in the development of UV indices.

9.6 GAPS IN OUR KNOWLEDGE

High quality extraterrestrial irradiances are required to test models against measurements and to deduce accurately the spectral consequences of changes in aerosol optical depth. New irradiance measurements from instruments on board the Upper Atmosphere Research Satellite (UARS) may fill this need (Lean *et al.,* 1992; Brueckner *et al.,* 1993; Rottman *et al.,* 1993).

Despite the importance of clouds in modulating UV transfer through the atmosphere, our ability to model their effects is poor. The role of aerosols has not been fully determined.

Detailed intercomparisons between measured and modeled UV are now being attempted (Wang and Lenoble, 1994; Zeng *et al.*, 1994). These require a wide range of measured input parameters (*e.g.,* aerosol and ozone profiles, cloud cover) to constrain the models. These measurements are often not available or inadequate. The validity of parameterizations of these quantities is also untested.

The achievable accuracy of UV measurements is limited by the lack of suitable irradiance standards. Robust protocols to maintain secondary standards and to transfer them accurately to field instruments are also lacking.

Detailed instrument intercomparisons and instrument-model comparisons are limited by our understanding of the effects of instrument errors due to imperfections in the cosine response. One approach would be to develop improved detectors for which these errors are small. In addition to cosine-weighted measurements that are already available, measurements of the angular dependence of sky radiances, altitude-dependences, and direct-sun observations may be useful for model validation (Seckmeyer and Bernhard, 1993).

Historical and geographic changes in UV radiation are not adequately understood. The data set produced by a network of broad-band meters would be a valuable source of information for the photobiology and epidemiology communities. All instruments must be characterized and calibrated in the same way. In the past there has been a lack of international coordination. The data from numerous, uncoordinated meters, while not necessarily incorrect, could provide questionable, and sometimes conflicting, information on long-term changes in broad-band solar UV radiation at the ground.

There is a lack of high quality spectral measurements of UV and ancillary measurements from the same site from which photobiological effects can be evaluated, and our understanding of the reasons for changes in UV can be improved. Useful ancillary measurements include ozone, total solar irradiance, aerosols (turbidity), and cloud cover.

REFERENCES

Ambach, W., M. Blumthaler, and T. Schöpf, Increase of biologically effective ultraviolet radiation with altitude, *J. Wilderness Medicine, 4,* 189-197, 1993.

Bais B.A., C.S. Zerefos, C. Meleti, I.C. Ziomas, and K. Tourpali, Spectral measurements of solar UVB radiation and its relations to total ozone, SO_2, and clouds, *J. Geophys. Res., 98, D3,* 5199-5204, 1993.

Berger, D.S., and F. Urbach, A climatology of sunburning ultraviolet radiation, *Photochem. Photobiol., 35,* 187-192, 1982.

Blumthaler, M., Solar UV measurements, in *UV-B Radiation and Ozone Depletion: Effects on Humans, Animals, Plants, Microorganisms, and Materials*, edited by M. Tevini, Lewis Publishers, Boca Raton, Florida, USA, 71-94, 1993.

Blumthaler, M., and W. Ambach, Indication of increasing solar ultraviolet-B radiation in alpine regions, *Science, 248,* 206-208, 1990.

Blumthaler, M., and W. Ambach, Changes in solar radiation fluxes after the Pinatubo eruption, *Tellus, 46B,* 76-78, 1994.

Blumthaler, M., W. Ambach, R. Silbernagl, and J. Staehelin, Erythemal UV-B irradiance (Robertson-Berger sunburn meter data) under ozone deficiencies in winter/spring 1993, *Photochem. Photobiol., 59,* 6, 657-659, 1994a.

Blumthaler, M., M. Huber, and W. Ambach, Measurements of direct and global UV spectra under varying turbidity, in *Proceedings International Symposium on High Latitude Optics,* Tromso, Norway, 28 June-2 July, 1993.

Blumthaler, M., A.R. Webb, G. Seckmeyer, and A.F. Bais, Simultaneous spectral UV measurements applied to the determination of the altitude effect, presented at WMO Meeting of Experts on UV-B Measurements, Les Diablerets, Switzerland, 18-21 July, 1994b.

Booth, C.R., and S. Madronich, Radiation Amplification Factors: Improved formulation accounts for large increases in ultraviolet radiation associated with Antarctic ozone depletion, in *Ultraviolet Radiation in Antarctica: Measurements and Biological Research,* edited by C. S. Weiler and P. A. Penhale, AGU Antarctic Research Series, volume 62, American Geophysical Union, Washington, D.C., 39-42, 1994.

Booth, C.R., T.B. Lucas, J.H. Morrow, C.S. Weiler, and P.A. Penhale, The United States National Science Foundation/Antarctic Program's Network for Monitoring Ultraviolet Radiation, in *Ultraviolet Radiation in Antarctica: Measurements and Biological Research,* edited by C. S. Weiler and P. A. Penhale, AGU Antarctic Research Series, volume 62, American Geophysical Union, Washington, D.C., 17-37, 1994.

Booth, C.R., T.M. Mestechkina, T. Lucas, J. Tusson, and J. Morrow, Contrasts in Southern and Northern Hemisphere high latitude ultraviolet irradiance, in *Proceedings International Symposium on High Latitude Optics,* European Optical Society and International Society for Optical Engineering, Tromso, Norway, 28 June-2 July, 1993.

Brueckner, G.E., K.L. Edlow, L.E. Floyd, J.L. Lean, and M.E. VanHoosier, The Solar Ultraviolet Spectral Irradiance Monitor (SUSIM) experiment on board the Upper Atmosphere Research Satellite (UARS), *J. Geophys. Res., 98, D6,* 10695-10711, 1993.

Burrows, W.R., M. Vallée, D.I. Wardle, J.B. Kerr, L.J. Wilson, and D.W. Tarasick, The Canadian operational procedure for forecasting total ozone and UV radiation, accepted for publication in *Met. Apps.*, 1994.

Cabrera, S., S. Bozzo, and H. Fuenzalida, Latitudinal and altitudinal variations of UV radiation along Chile, submitted to *Photochem. Photobiol.*, 1994.

Correll, D.L., C.O. Clark, B. Goldberg, V.R. Goodrich, D.R. Hayes, W.H. Klein, and W.D. Scherer, Spectral ultraviolet-B radiation fluxes at the Earth's surface: Long-term variations at 39°N, 77°W, *J. Geophys. Res., 97,* 7579-7591, 1992.

Davies, R., Increased transmission of ultraviolet radiation to the surface due to stratospheric scattering, *J. Geophys. Res., 98,* 7251-7253, 1993.

DeLuisi, J.J., Possible calibration shift in the U.S. surface UV network instrumentation 1979 to 1985, paper presented at the U.S. Department of Energy UV-B Critical Issues Workshop, Cocoa Beach, Florida, 24-26 February, 1993.

DeLuisi, J.J., J. Wendell, and F. Kreiner, An examination of the spectral response characteristics of seven Robertson-Berger meters after long-term field use, *Photochem. Photobiol., 56,* 115-122, 1992.

DeLuisi, J.J., J.M. Barnett, and G.F. Cotton, A close examination of the U.S. Robertson-Berger network: Detection of a calibration anomaly, submitted to *Geophys. Res. Lett.,* 1994.

Diaz, S.B., C.R. Booth, T.B. Lucas, and I. Smolskaia, Effects of ozone depletion on irradiances and biological doses over Ushuaia, *Archiev für Hidrologie,* special issue in press, 1994.

Dichter, B.K., D.J. Beaubien, and A.F. Beaubien, Effects of ambient temperature changes on UV-B measurements using thermally regulated and unregulated fluorescent phosphor ultraviolet pyranometers, in *Proceedings Quadrennial Ozone Symposium,* Charlottesville, Virginia, June 1992, NASA Conf. Public. 3266, 766-769, 1994.

Frederick, J.E., and E.C. Weatherhead, Temporal changes in surface ultraviolet radiation: A study of the Robertson-Berger meter and Dobson data records, *Photochem. Photobiol., 56,* 123-131, 1992.

Frederick, J.E., A.E. Koob, A.D. Alberts, and E.C. Weatherhead, Empirical studies of tropospheric transmission in the ultraviolet: Broad band measurements, *J. Appl. Meteorol., 32,* 1883-1892, 1993a.

Frederick, J.E., P.F. Soulen, S.B. Diaz, I. Smolskaia, C.R. Booth, T. Lucas, and D. Neuschuler, Solar ultraviolet irradiance observed from Southern Argentina: September 1990 to March 1991, *J. Geophys. Res., 98, D5,* 8891-8897, 1993b.

Frederick, J.E., S.B. Diaz, I. Smolskaia, W. Esposito, T. Lucas, and C.R. Booth, Ultraviolet solar radiation in the high latitudes of South America, submitted to *Photochem. Photobiol.,* October 1993c.

Gardiner, B.G., A.R. Webb, A.F. Bais, M. Blumthaler, I. Dirmhirn, P. Foster, D. Gillotay, K. Henriksen, M. Huber, P. J. Kirsch, P.C. Simon, T. Svenoe, P. Weihs, and C.S. Zerefos, European intercomparison of ultraviolet spectroradiometers, *Environ. Techn., 14,* 25-43, 1993.

Grainger, R.G., R.E. Basher, and R.L. McKenzie, UV-B Robertson-Berger characterization and field calibration, *Appl. Optics, 32,* 3, 343-349, 1993.

Henderson-Sellers, A., and K. McGuffie, Are cloud amounts estimated from satellite sensor and conventional surface-based observations related?, *Int. J. Remote Sensing, 11,* 3, 543-550, 1990.

Herman, J.R., and D. Larko, Low ozone amounts during 1992-1993 from NIMBUS-7 and METEOR-3/ TOMS, *J. Geophys. Res., 99, D2,* 3483-3496, 1994.

Ito, T., Y. Sakoda, T. Uekubo, H. Naganuma, M. Fukuda, and M. Hayashi, Scientific application of UV-B observations from JMA network, in *Proceedings 13th UOEH International Symposium and the 2nd Pan Pacific Cooperative Symposium on Human Health and Ecosystems,* Kitakyushu, Japan, 13-15 October 1993, in press, 1994.

Johnsen, B., and J. Moan, The temperature sensitivity of the Robertson-Berger sunburn meter, model 500, *J. Photochem. Photobiol. B.: Biol., 11,* 277-284, 1991.

Justus, C.G., and B.B. Murphey, Temporal trends in surface irradiance at ultraviolet wavelengths, *J. Geophys. Res., 99, D1,* 1389-1394, 1994.

Kennedy, B.C., and W.E. Sharp, A validation study of the Robertson-Berger meter, *Photochem. Photobiol., 56,* 133-141, 1992.

Kerr, J.B., and C.T. McElroy, Evidence for large upward trends of ultraviolet-B radiation linked to ozone depletion, *Science, 262,* 1032-1034, 1993.

Kerr, J.B., and C.T. McElroy, Response (to comment by Michaels *et al.*, 1994), *Science, 264,* 1342-1343, 1994.

Lean, J., M. VanHoosier, G. Brueckner, D. Prinz, L. Floyd, and K. Edlow, SUSIM/UARS observations of the 120 to 300 nm flux variations during the maximum of the solar cycle: Inferences for the 11-year cycle, *Geophys. Res. Lett., 19,* 22, 2203-2206, 1992.

Liu, S.C., S.A. McKeen, and S. Madronich, Effect of anthropogenic aerosols on biologically active ultraviolet radiation, *Geophys. Res. Lett., 18,* 12, 2265-2268, 1991.

Lubin, D., P. Ricchiazzi, C. Gautier, and R.H. Whritner, A method for mapping Antarctic surface ultraviolet radiation using multi-spectral satellite imagery, in *Ultraviolet Radiation in Antarctica: Measurements and Biological Research,* edited by C. S. Weiler and P. A. Penhale, AGU Antarctic Research Series, volume 62, American Geophysical Union, Washington, D.C., 53-81, 1994.

Madronich, S., The atmosphere and UV-B radiation at ground level, in *Environmental UV Photobiology,* edited by A. R. Young *et al.*, Plenum Press, New York, 1-39, 1993.

Madronich, S., and C. Granier, Tropospheric chemistry changes due to increased UV-B radiation, in *Stratospheric Ozone Depletion/UV-B Radiation in the Biosphere,* edited by R. H. Biggs and M. E. B. Joyner, NATO ASI Series I, Vol 18, Springer-Verlag, 3-10, 1994.

McKenzie, R.L., UV radiation monitoring in New Zealand, in *Stratospheric Ozone Depletion/UV-B Radiation in the Biosphere,* edited by R.H. Biggs and M.E.B. Joyner, NATO ASI Series I, Vol 18, Springer-Verlag, 239-246, 1994a.

McKenzie, R.L., UV spectral irradiance in New Zealand: Effects of Pinatubo volcanic aerosol, in *Proceedings Quadrennial Ozone Symposium,* Charlottesville, Virginia, June 1992, NASA Conf. Public. 3266, 627-630, 1994b.

McKenzie, R.L., P.V. Johnston, M. Kotkamp, A. Bittar, and J.D. Hamlin, Solar ultraviolet spectroradiometry in New Zealand: Instrumentation and sample results from 1990, *Appl. Optics, 31,* 30, 6501-6509, 1992.

McKenzie, R.L., W.A. Matthews, and P.V. Johnston, The relationship between erythemal UV and ozone, derived from spectral irradiance measurements, *Geophys. Res. Lett., 18,* 12, 2269-2272, 1991.

McKenzie, R.L., M. Kotkamp, G. Seckmeyer, R. Erb, C.R. Roy, H.P. Gies, and S.J. Toomey, First Southern Hemisphere intercomparison of solar UV spectra, *Geophys. Res. Lett., 20,* 20, 2223-2226, 1993.

McKinlay, A.F., and B. L. Diffey, A reference spectrum for ultraviolet induced erythema in human skin, in *Human Exposure to Ultraviolet Radiation: Risks and Regulations*, edited by W. R. Passchler and B. F. M. Bosnajokovic, Elsevier, Amsterdam, 1987.

Michaels, P.J., S.F. Singer, and P.C. Knappenberger, Analysing Ultraviolet-B radiation: Is there a trend? *Science, 264,* 1341-1342, 1994.

Michelangeli D.V., M. Allen, Y.L. Young, R.-L. Shia, D. Crisp, and J. Eluszkiewicz, Enhancement of atmospheric radiation by an atmospheric aerosol layer, *J. Geophys. Res., 97, D1,* 865-874, 1992.

NRC, *Acid Deposition Long-Term Trends*, National Research Council, National Academy Press, Washington, D.C., 1986.

Prezelin, B.B., N.P. Boucher, and R.C. Smith, Marine primary production under the influence of the Antarctic ozone hole: Icecolors '90, in *Ultraviolet Radiation in Antarctica: Measurements and Biological Research,* edited by C. S. Weiler and P. A. Penhale, AGU Antarctic Research Series, volume 62, American Geophysical Union, Washington, D.C., 159-186, 1994.

Rottman, G.J., T.N. Woods, and T.P. Sparn, Solar-Stellar Irradiance Comparison Experiment 1: 1. Instrument design and operation, *J. Geophys. Res., 98, D6,* 10667-10677, 1993.

Scotto, J., G. Cotton, F. Urbach, D. Berger, and T. Fears, Biologically effective ultraviolet radiation: measurements in the United States 1974-1985, *Science, 239,* 762-764, 1988.

Seckmeyer, G., and R.L. McKenzie, Increased ultraviolet radiation in New Zealand (45°S) relative to Germany (48°N), *Nature, 359,* 135-137, 1992.

Seckmeyer, G., and G. Bernhard, Cosine error of spectral UV-irradiances, in *Proceedings International Symposium on High Latitude Optics,* Tromso, Norway, 28 June-2 July, 1993.

Seckmeyer, G., B. Mayer, R. Erb, and G. Bernhard, UVB in Germany higher in 1993 than in 1992, *Geophys. Res. Lett., 21,* 7, 577-580, 1994a.

Seckmeyer, G., S. Thiel, M. Blumthaler, P. Fabian, S. Gerber, A. Gugg-Helminger, D.-P. Hader, M. Huber, C. Kettner, U. Kohler, P. Kopke, H. Maier, J. Schafer, P. Suppan, E. Tamm, and E. Thomalia, First intercomparison of spectral UV radiation measurement systems, *Appl. Optics,* in press, 1994b.

Setlow, R.B., The wavelengths in sunlight effective in producing skin cancer: A theoretical analysis, *Proc. Nat. Acad. Sci. USA., 71(9),* 3363-3366, 1974.

Smith, G.J., M.G. White, and K.G. Ryan, Seasonal trends in erythemal and carcinogenic ultraviolet radiation at mid-Southern latitudes 1989-1991, *Photochem. and Photobiol., 57,* 3, 513-517, 1993.

Smith, R.C., B.B. Prezelin, K.S. Baker, R.R. Bidigare, N.P. Boucher, T. Coley, D. Karentz, S. MacIntyre, H.A. Matlick, D. Menzies, M. Ondrusek, Z. Wan, and K.J. Waters, Ozone depletion: Ultraviolet radiation and phytoplankton biology in Antarctic waters, *Science, 255,* 952-959, 1992.

Staehelin, J., and W. Schmid, Trend analysis of tropospheric ozone concentrations utilizing the 20-year data set of ozone balloon soundings over Payerne (Switzerland), *Atmos. Environ., 25A,* 9, 1739-1749, 1991.

Stamnes, K., S.-C. Tsay, W. Wiscombe, and K. Jayaweera, Numerically stable algorithm for discrete-ordinate-method radiative transfer in multiple scattering and emitting layered media, *Appl. Opt., 27,* 2502-2509, 1988.

Tevini, M., (ed.), *UV-B Radiation and Ozone Depletion: Effects on Humans, Animals, Plants, Microorganisms, and Materials,* Lewis Publishers, Boca Raton, Florida, USA, 1993.

Tsay, S.-C., and K. Stamnes, Ultraviolet radiation in the Arctic: The impact of potential ozone depletions and cloud effects, *J. Geophys. Res., 97,* 7829-7840, 1992.

UNEP, *Environmental Effects of Ozone Depletion: 1991 Update,* United Nations Environment Programme, panel report pursuant to Article 6 of the Montreal Protocol on Substances that Deplete the Ozone Layer, November 1991.

UNEP, *Environmental Effects of Ozone Depletion: 1994 Update,* United Nations Environment Programme, panel report pursuant to Article 6 of the Montreal Protocol on Substances that Deplete the Ozone Layer, in preparation, 1994.

Walker, J.H., R.D. Saunders, J.K. Jackson, and K.D. Mielenz, Results of a CCPR intercomparison of spectral irradiance measurements by National Laboratories, *J. Res. National Institute of Standards and Technology (NIST), 96,* 647-668, 1991.

Wang, P., and J. Lenoble, Comparison between measurements and modeling of UV-B irradiance for clear sky: A case study, *Appl. Optics, 33,* 18, 3964-3971, 1994.

WMO, *Scientific Assessment of Ozone Depletion: 1991,* World Meteorological Organization Global Ozone Research and Monitoring Project—Report No. 25, Geneva, 1992.

Young, A.R., L.O. Björn, J. Moan, and W. Nultsch (eds.), *Environmental UV Photobiology,* Plenum Press, New York, 1993.

Zeng, J., Z. Jin, and K. Stamnes, Impact of stratospheric ozone depletion on UV penetration into the ocean at high latitudes, in *Underwater Light Measurements*, edited by H. Chr. Eilertsen, Proc. SPIE 2048, 1993.

Zeng, J., R.L. McKenzie, K. Stamnes, M. Winleland, and J. Rosen, Measured UV spectra compared with discrete ordinate method simulations, *J. Geophys. Res.,* in press, 1994.

Zheng, X., and R.E. Basher, Homogenisation and trend detection analysis of broken series of solar UV-B data, *Theor. Appl. Climatol., 47,* 4, 189-303, 1993.

PART 5

SCIENTIFIC INFORMATION FOR FUTURE DECISIONS

Chapter 10
Methyl Bromide

Chapter 11
Subsonic and Supersonic Aircraft Emissions

Chapter 12
Atmospheric Degradation of Halocarbon Substitutes

Chapter 13
Ozone Depletion Potentials, Global Warming Potentials, and Future Chlorine/Bromine Loading

CHAPTER 10

Methyl Bromide

Lead Author:
S.A. Penkett

Co-authors:
J.H. Butler
M.J. Kurylo
C.E. Reeves
J.M. Rodriguez
H. Singh
D. Toohey
R. Weiss

Contributors:
M.O. Andreae
N.J. Blake
R.J. Cicerone
T. Duafala
A. Golombek
M.A.K. Khalil
J.S. Levine
M.J. Molina
S.M. Schauffler

CHAPTER 10

METHYL BROMIDE

Contents

SCIENTIFIC SUMMARY

- Four potentially major sources for atmospheric methyl bromide (CH_3Br) have been identified: the ocean, which is a natural source, and three others that are almost entirely anthropogenic; these are agricultural usage, which has been reaffirmed, biomass burning, which is newly recognized, and the exhaust of automobiles using leaded gasoline.

- The estimated uncertainty range for these sources is large, with oceans ranging from 60 to 160 ktonnes/yr, agriculture from 20 to 60 ktonnes/yr, biomass burning from 10 to 50 ktonnes/yr, and automobile exhaust from 0.5 to 22 ktonnes/yr. In the latter case, the range results from two conflicting assessments, which yield 0.5 to 1.5 ktonnes/yr and 9 to 22 ktonnes/yr, respectively.

- There are also two minor anthropogenic sources, structural fumigation (4 ktonnes/yr) and industrial emissions (2 ktonnes/yr), each of which are well quantified.

- Measurements of CH_3Br yield a global average ground-level atmospheric mixing ratio of approximately 11 pptv. These measurements also have confirmed that the concentration in the Northern Hemisphere is higher by about 30% than the concentration in the Southern Hemisphere (interhemispheric ratio of 1.3). Such a ratio requires that the value of sources minus sinks in the Northern Hemisphere exceeds the same term in the Southern Hemisphere.

- There is no clear long-term change in the concentration of CH_3Br during the time period of the systematic continued measurements (1978-1992). One possible explanation is that CH_3Br from automobiles may have declined while, at the same time, emissions from agricultural use may have increased, leading to relatively constant anthropogenic emissions over the last decade.

- The magnitude of the atmospheric sink of CH_3Br due to gas phase chemistry is well known and leads to a lifetime of 2 ± 0.5 yr. The recently postulated oceanic sink leads to a calculated atmospheric lifetime due to oceanic hydrolysis of 3.7 yr, but there are large uncertainties (1.3 to 14 yr). Thus the overall atmospheric lifetime due to both of these processes is 1.3 yr with a range of 0.8 to 1.7 yr.

- Recognizing the quoted uncertainties in the size of the individual sources of CH_3Br, the most likely estimate is that about 40% of the source is anthropogenic. The major uncertainty in this number is the size of the ocean source. Based on the present atmospheric mixing ratio and the current source estimate, a lifetime of less than 0.6 yr would require identification of new major sources and sinks.

- The chemistry of ozone destruction by bromine in the stratosphere is now better understood. A high rate coefficient for the $HO_2 + BrO$ reaction is confirmed and there is no evidence that it produces HBr. A conservative upper limit of 2% can be placed on the reaction channel yielding HBr. Stratospheric measurements confirm that the concentration of HBr is very low (less than 1 pptv) and that it is not a significant bromine reservoir.

- The combined efficiency of the bromine removal cycles for ozone ($HO_2 + BrO$ and $ClO + BrO$) is likely to be about 50 times greater than the efficiency of known chlorine removal cycles on an atom-for-atom basis.

- The calculated Ozone Depletion Potential (ODP) for CH_3Br is currently estimated to be 0.6 based on an atmospheric lifetime of 1.3 years. The range of uncertainties in the parameters associated with the ODP calculation places a lower limit on the ODP of 0.3.

10.1 INTRODUCTION

Bromine atoms are highly effective in removing ozone in the stratosphere through catalytic cycles involving free radicals such as BrO and ClO. In fact the bromine atoms remove ozone more effectively than chlorine atoms on an atom-for-atom basis, because the large majority of the inorganic bromine is in a more labile form capable of taking part in the ozone removal cycles. This is discussed in more detail in Section 10.7.

The role of bromine in the distribution of stratospheric ozone has assumed greater prominence in the past few years due to the re-evaluation upwards in the efficiency of the reaction HO_2 + BrO, which cycles BrO radicals back to bromine atoms, and due to the probability that a sizeable fraction of the main bromine source gas to the stratosphere, methyl bromide (CH_3Br), is of anthropogenic origin. Overall, the impact on ozone of approximately 20 pptv of inorganic bromine in the stratosphere could be equivalent to about 1000 pptv of inorganic chlorine. This compares with a present total of inorganic chlorine in the stratosphere in the range of 3500 pptv.

Bromine is carried into the stratosphere in various forms such as halons and substituted hydrocarbons, of which CH_3Br is the predominant form. The halons are rather stable in the troposphere, and their production for consumption in developed countries ceased on 31 December 1993, under the latest Amendments to the Montreal Protocol. Methyl bromide, on the other hand, is much less stable in the troposphere and limitations to its emission could have a rapid impact on the amount of bromine carried into the stratosphere in this form. At present, CH_3Br production for consumption in developed countries is capped at 1991 levels beginning in 1995 under the terms of the Montreal Protocol. The U.S. Environmental Protection Agency has recently announced a phase-out by 2001 in the U.S. based upon an Ozone Depletion Potential (ODP) of 0.7.

The case of CH_3Br is much more complex than the halons or indeed of any other potential ozone-depleting substance so far considered for regulation, because it is produced by the biosphere and is emitted into the atmosphere by natural processes. The atmospheric science of CH_3Br was reviewed in 1992 (Albritton and Watson, 1992) and many of the uncertainties associated with its atmospheric distribution, sources, sinks, and involvement in the removal of ozone in the stratosphere were discussed. The present chapter is written against this background and the 1992 methyl bromide review will be referred to extensively (UNEP, 1992). A major objective of the present chapter will be to describe more recent progress towards defining a minimum and most likely ODP for CH_3Br and in highlighting the remaining uncertainties in our knowledge of its behavior in the atmosphere.

10.2 MEASUREMENTS, INCLUDING INTERHEMISPHERIC RATIOS

Methyl bromide is a ubiquitous component of the Earth's lower atmosphere. Over the past two decades, sporadic measurements have been made largely in the surface air but also in the free troposphere and stratosphere. These latter measurements have been performed using aircraft and balloon platforms. Here we provide a synthesis of much of the recently available data, with emphasis on the remote global atmosphere. In most cases, air samples are collected in pressurized stainless steel canisters and analyzed after a period of several days or weeks. In some instances, especially on shipboard platforms, this sampling process is omitted and the air sample is directly analyzed.

Many of the measurements have been made with a technique involving sample preconcentration (100-1000 ml), gas chromatographic separation, and electron capture detection. Other measurements have involved mass spectrometric detection; these are more specific and less prone to artifacts. Substantial uncertainties in absolute standards (±30%) probably still exist but no systematic intercomparison studies have been performed to accurately quantify the level of uncertainty that is present in the published measurements. The reported mean concentrations fluctuate between 5-30 pptv, but there appears to be a convergence between 8-15 pptv in publications made since 1985. It is presumed that a large part of the differences in various measurements is due to the uncertainties in calibration standards. However, there is a distinct possibility that other sampling/analysis problems are also present, such as growth and decay in sample containers and co-elution of other substances with CH_3Br that are detected by the electron capture detector.

Table 10-1. Mean CH_3Br mixing ratios (pptv) in the surface air of the Northern and Southern Hemispheres.

NH	SH	NH/SH	Year	Platform (Region)	Latitude Range	Ref. No.
26	20	1.3	1981-1982 (December)	Ship (Pacific)	40°N -32°S	(1)
15	11	1.4	1982-1983 (November)	Ship (Atlantic)	40°N - 75°S	(2)
11	10	1.2*	1985-1987 (Ann. Avg.)	Coastal (Pacific)	71°N - 44°S	(3)
11	8	1.4	1983-1992 (Ann. Avg.)	Coastal (Pacific)	71°N - 42°S	(4)
11	9	1.2	1992 (April/August)	Coastal (Pacific)	90°N - 45°S	(5)
12.0	9.5	1.3	1984-1993 (Spring/Fall)	Ship (Pacific, Atlantic)	60°N - 90°S	(6)

(1) Singh *et al.* (1983) (2) Penkett *et al.* (1985)
(3) Cicerone *et al.* (1988) (4) Khalil *et al.* (1993)
(5) Blake *et al.* (1993) (6) Schauffler *et al.* (1993a); Schauffler, personal communication.
* Note: the value of 1.15 has been corrected to 1.2 (Cicerone, 1994).

A number of campaigns have collected a body of data largely in the surface marine boundary layer in both hemispheres. In Table 10-1 we summarize the mean NH (Northern Hemisphere) and SH (Southern Hemisphere) surface air concentrations of CH_3Br measured by several different investigators.

As stated earlier, most of the recent measurements show global mean concentrations in the vicinity of 8-15 pptv. In all cases a NH/SH gradient, which should be independent of calibration uncertainties, is observed. The higher NH mixing ratios have been ascribed to the domination of anthropogenic CH_3Br sources in the NH (*e.g.*, Singh and Kanakidou, 1993; Reeves and Penkett, 1993). It is pertinent to note that the observed surface NH/SH gradients are by no means uniform and a range of 1.2 to 1.45 has been observed (Albritton and Watson, 1992). Figure 10-1 shows the variability that is inherent in an extensive marine air data set collected by one set of workers at different times and in different locations (Schauffler *et al.*, 1993a) and it probably reflects the spatial and temporal variability in the sources of CH_3Br or, alternatively, it may reflect experimental artifacts. Another factor in the calculation of interhemispheric ratios from various data sets is the latitudinal range of the data. This is sometimes restricted to a Southern Hemispheric limit of 40°S which, as can be seen from the Schauffler *et al.* data, would lead to a smaller ratio than a consideration of the full range of 60°N to 90°S. Overall the most likely value for the interhemispheric gradient is 1.3. This contrasts with the interhemispheric gradient for methyl chloride, which is close to 1 (Singh *et al.*, 1983) and strongly suggests a preponderance of Northern Hemispheric sources of CH_3Br that are very possibly anthropogenic.

The major known removal process for CH_3Br is its reaction with OH, resulting in an atmospheric lifetime of about 2 years. Theoretical studies suggest that such a chemical should show a distinct seasonal cycle larger than that observed for methyl chloroform, which would be expected to have a smaller amplitude. However, in a number of attempts so far, no distinct seasonal cycle has been observed (Singh *et al.*, 1983; Cicerone *et al.*, 1988; Khalil *et al.*, 1993). Figure 10-2 shows an example of this based on data collected in Tasmania and Oregon. Inadequate measurement precision, seasonal variations in the sources of CH_3Br, or unidentified sinks may be responsible for a lack of observed seasonal behavior.

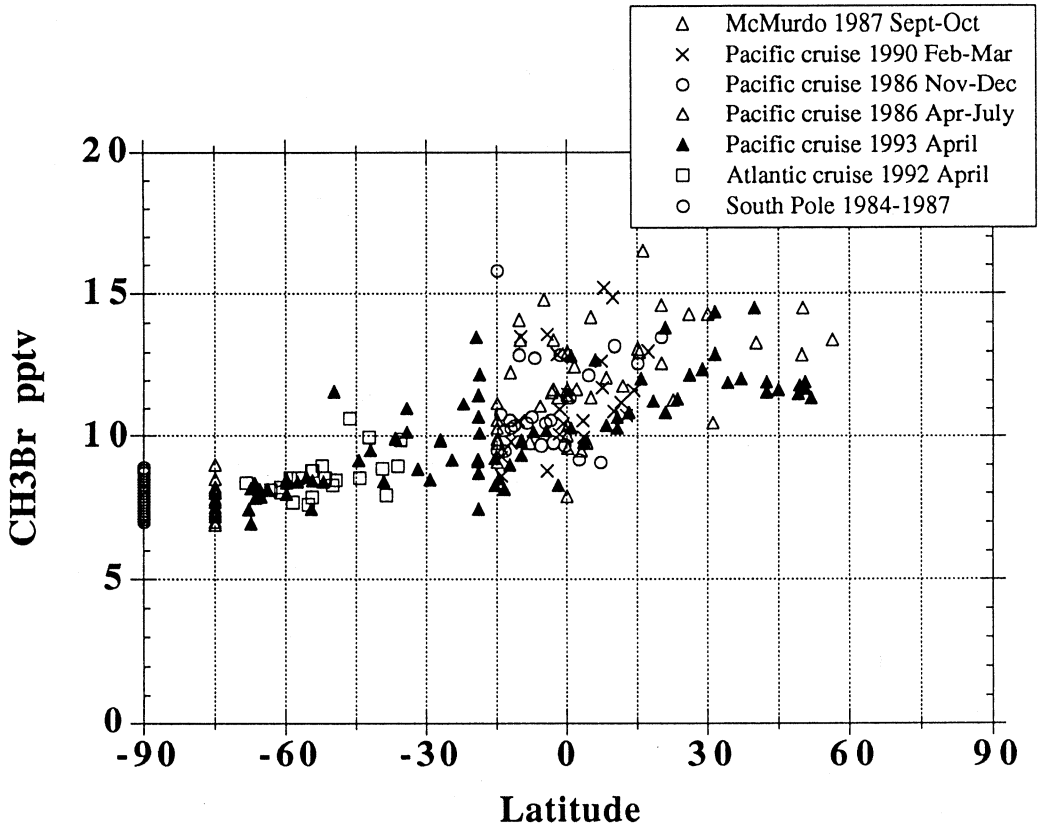

Figure 10-1. Latitudinal transect measurements of methyl bromide in oceanic air (after Schauffler *et al.*, 1993a; Schauffler, personal communication).

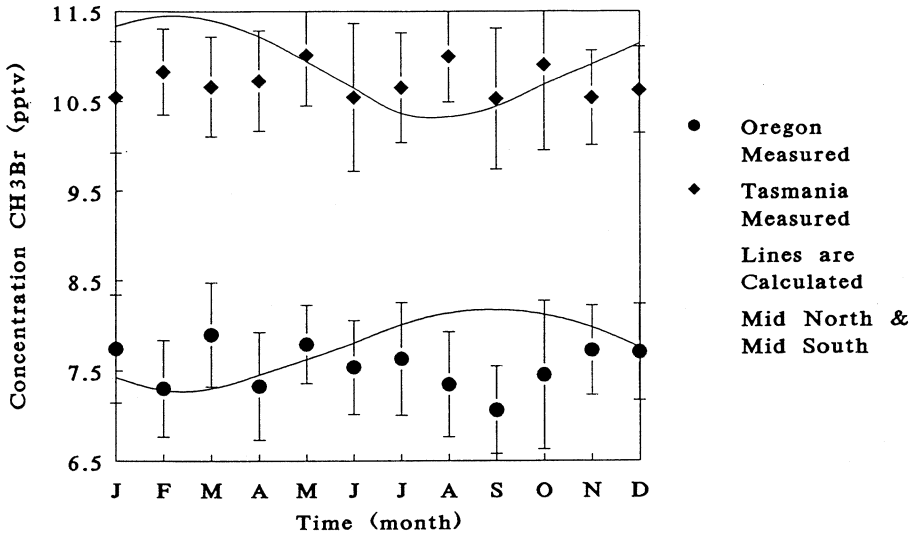

Figure 10-2. Seasonal cycle of methyl bromide in Tasmania (Southern Hemisphere) and Oregon (Northern Hemisphere). (After Khalil *et al.*, 1993.)

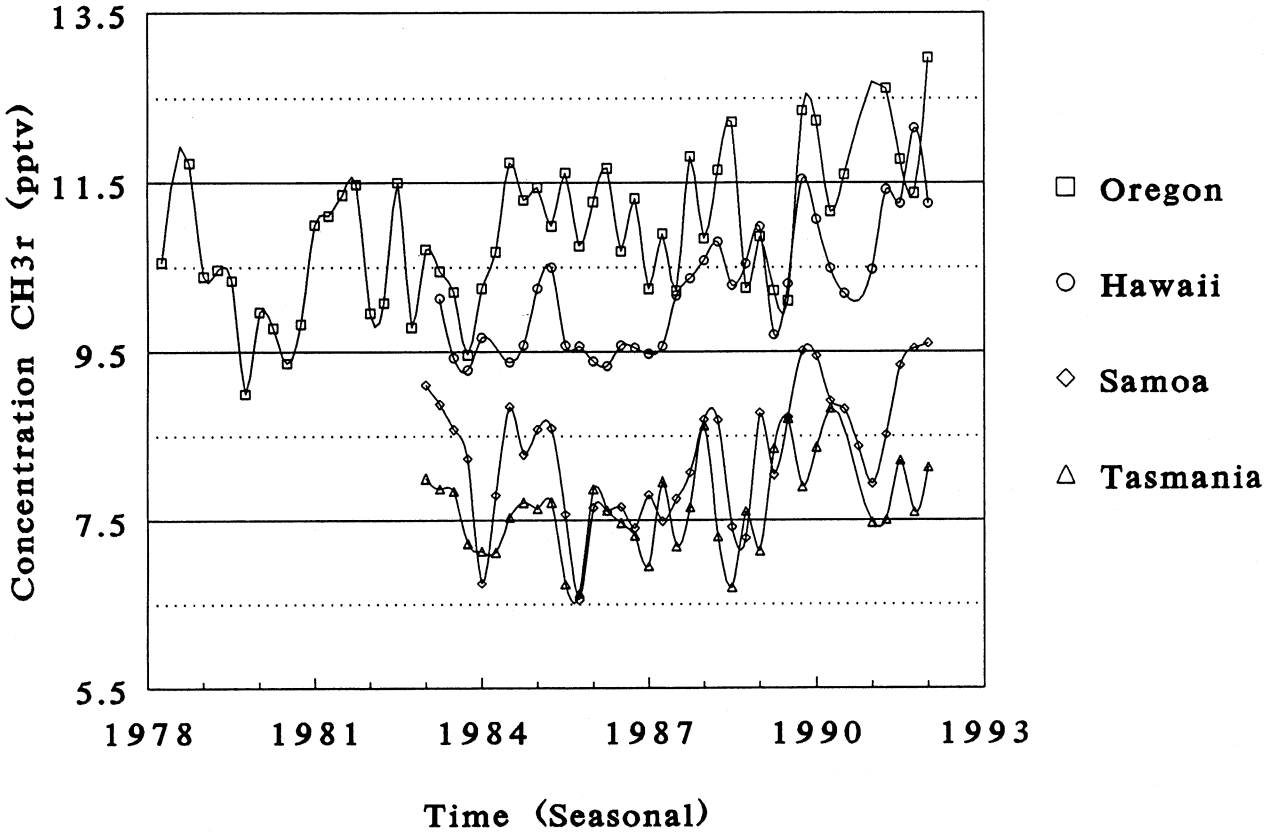

Figure 10-3. Trends in methyl bromide at four locations over the period 1978 to 1992. (After Khalil *et al.*, 1993.)

10.2.1 Vertical Profiles

The salient features of the vertical structure of CH_3Br are that its concentrations decrease with increasing altitude at a slow rate in the troposphere (Blake *et al.*, 1993; Khalil *et al.*, 1993), and then relatively rapidly in the stratosphere (Lal *et al.*, 1994). The slight decrease in the troposphere is largely dictated by the surface source of CH_3Br and a lifetime probably in excess of 1 year. The rapid loss in the lower stratosphere suggests strongly that CH_3Br is a major source of bromine atoms in this region. Co-measurements of CH_3Br and CFC-11 in the stratosphere by Schauffler *et al.* (1993b) will allow an accurate estimate of the stratospheric lifetime of CH_3Br for ODP purposes.

10.2.2 Trends

Only one set of internally consistent data is available to assess atmospheric trends of CH_3Br. Figure 10-3 shows the nature of data reported by Khalil *et al.* (1993) from four island sites in the NH and SH from 1978-1992. An evident feature is the large variability in these measurements that have no discernible seasonal character. Based on these data, Khalil *et al.* calculate a positive global trend of 0.3 (±0.1) pptv/year between 1988 and 1992 (Figure 10-3). It appears that a significant trend may not have existed prior to 1988. The positive trend in later years is not inconsistent with the mean trend of 0.2 pptv per year calculated from a consideration of increased agricultural usage (Singh and Kanakidou, 1993). However, these studies did not take into account changes that may have occurred in the potential source from gasoline consumption and the large biomass contribution. The variability in measured data is sufficiently large, and the data base sufficiently sparse, that a quantitative rate of increase cannot be reliably defined from these measurements alone. It is also likely that experimental artifacts associated with sample or standard storage would make

a small trend impossible to detect. Overall it can be concluded at present that no useful statement can be made from a consideration of the available trend data.

10.2.3 Calibration Issues

At the time of writing there has been no attempt to carry out an intercalibration exercise amongst the various groups making and publishing CH_3Br measurements in the atmosphere. That such an exercise is clearly needed is shown by the data in Table 10-1. Accurate measurements of CH_3Br will allow limits to be set on the source strength for comparison with independent estimates (see Section 10.3). They will also allow a data base to be built up in the future that could detect trends and seasonal variations, etc.

10.3 SOURCES OF METHYL BROMIDE

10.3.1 The Oceanic Source

The oceans are a major natural reservoir of bromine. They have generally also been regarded as a major natural source of atmospheric CH_3Br, based principally on the measurements of Singh *et al.* (1983) that found surface water concentrations in the eastern Pacific Ocean to be 2.5 times the atmospheric equilibrium concentrations (*i.e.*, 150% supersaturation). From this value they calculated a net global oceanic source of about 300 Gg/yr. Singh and Kanakidou (1993) have recently revised this net flux estimate downward to 40-80 Gg/yr by correcting for large differences in calibration and by weighting the calculations according to regional ocean productivity differences. Taking only the correction for calibration differences and using a mean tropospheric mixing ratio of 11 pptv, together with the same air-sea exchange and solubility coefficients used by Butler (1994), yields a global net flux of about 110 Gg/yr for a supersaturation of 150%.

Most recently Khalil *et al.* (1993) have reported the results of CH_3Br measurements from two Pacific Ocean expeditions in 1983 and 1987. They obtained a range of surface water saturations for these expeditions of 1.4 to 1.8 (*i.e.*, 40-80% supersaturation), and calculated a net global flux of 35 Gg/yr (range: 30-40 Gg/yr) by integrating the exchange fluxes as a function of latitude and ocean area, without allowing for latitudinal variations in the exchange coefficient or solubility. For purposes of comparison, if one uses this measured mean supersaturation of 60%, together with the same 11 pptv mean tropospheric mixing ratio and the same air-sea exchange and solubility coefficients used by Butler, the resulting global net flux is 45 Gg/yr.

It is important to stress that these and other measurements of the air-sea disequilibrium of CH_3Br can only be used to calculate net exchange fluxes across the air-sea interface. If, as is discussed below, the oceans are responsible for the chemical destruction of 50 Gg/yr of tropospheric CH_3Br, then the global net oceanic fluxes reported above must be increased by this 50 Gg/yr to obtain gross strengths for the oceanic source. It is also important to stress that there is a very large uncertainty in the magnitude of the gross oceanic source, which is a necessary consequence of the disagreements among measurements of the air-sea disequilibrium and the uncertainties in the air-sea exchange rate and the oceanic chemical destruction rate. These are active research topics at the time of writing.

10.3.2 Agricultural Usage and Emission of CH_3Br

The use of CH_3Br for agricultural purposes was well covered in the UNEP 1992 Report (Albritton and Watson, 1992), and the respective table showing CH_3Br sales over the period 1984-1990 is reproduced here with updated values for 1991 and 1992 provided by Duafala (personal communication, 1994) (Table 10-2). In 1990, 66.6 thousand tonnes were sold, with 3.7 thousand tonnes being used as a chemical intermediate (1 metric ton = 1 tonne = 10^3 kg). The resultant 63 thousand tonnes were used in the environment in some manner, with the amount in the column marked "Structural" referring to fumigation of buildings and containers, etc. All of this will escape to the atmosphere, but the fraction of the bulk of the CH_3Br used for agricultural purposes that escapes is not known with any certainty. A theoretical analysis predicted that between 45 and 53% would do so, resulting in an atmospheric source from agricultural activities in the region of 30 thousand tonnes per year (Albritton and Watson, 1992).

An earlier analysis carried out in 1982 (Rolston and Glauz) compared measured concentrations of CH_3Br in soil after application with those calculated by theory, with and without sheet covering at the time of injection. Theory and measurement agreed well with the

Table 10-2. Methyl bromide sales, in thousands of tonnes.*

Year	Pre-Planting	Post-Harvesting	Structural	Chemical Intermediates**	Total
1984	30.4	9.0	2.2	4.0	45.6
1985	34.0	7.5	2.3	4.5	48.3
1986	36.1	8.3	2.0	4.0	50.4
1987	41.3	8.7	2.9	2.7	55.6
1988	45.1	8.0	3.6	3.8	60.5
1989	47.5	8.9	3.6	2.5	62.5
1990	51.3	8.4	3.2	3.7	66.6
1991	55.1	10.3	1.8	4.1	71.2
1992	57.4	9.6	2.0	2.6	71.6

* production by companies based in Japan, Western Europe, and the U.S.
** not released into the atmosphere

assumption that most of the CH_3Br escaped to the atmosphere, with 27% and 67% of the applied CH_3Br escaping by 1 and 14 days, respectively, after fumigation. The work suggested that plastic barriers were almost totally ineffective in preventing CH_3Br release in the long-term, but Rolston and Glauz appear to have used unusually permeable tarping material.

More recently, an experimental study was carried out by Yagi *et al.* (1993) to compare the flux of CH_3Br released to the atmosphere with the amount applied. They showed that 87% was released to the atmosphere. Lower values have been obtained in unpublished studies conducted recently both by workers at the University of California at Davis and by Cicerone and co-workers, who found that application in wet soil conditions greatly reduced emissions to ~35%. Soil pH and organic matter parameters also influence rates of decomposition of CH_3Br, and thus the fraction that escapes. Further, the depth and technique of injection are likely to exert some influence. To date, these factors have not been investigated thoroughly. Overall it is assumed here that 50% of the CH_3Br used for purposes such as pre-planting and post-harvesting escapes to the atmosphere, leading to an emission in the region of 35 thousand tonnes per year in 1991 and 1992 from a usage of approximately 70 thousand tonnes per year for pre-planting, post-harvesting purposes, and structural purposes.

10.3.3 Biomass Burning

Recent measurements of gaseous emissions from biomass burning in very diverse ecosystems indicate that CH_3Br is a significant combustion product (Manö and Andreae, 1994). In addition, satellite measurements suggest that biomass burning (*i.e.*, the burning of tropical, temperate, and boreal forests, savannas, grasslands, and agricultural lands following the harvest) is much more widespread and extensive than previously believed (Levine, 1991; Cahoon *et al.*, 1992; Andreae, 1993a). Almost all biomass burning is initiated or controlled by human activities, and pyrogenic emissions must therefore be classified as an anthropogenic source. Wildfires probably represent less than 10% of the biomass combusted globally (Andreae, 1993b). About 80% of biomass burning takes place in the tropics, mostly in conjunction with savanna fires, deforestation, and biomass fuel use. The emissions in the Southern Hemisphere, where the largest savanna areas are burned and most deforestation takes place, are about twice as large as those in the Northern Hemisphere (Andreae, 1993b; Hao *et al.*, 1990).

Measurements of CH_3Br emissions were obtained from burning savanna grasslands in southern Africa and boreal forests in Siberia (Manö and Andreae, 1994), and from tropical forests in Brazil (Blake *et al.*, 1993). Manö and Andreae (1994) reported a CH_3Br to CO_2 emission ratio from the south African savanna fires in the range of 4.4×10^{-8} to 7.7×10^{-7}, with an average of 3.7×10^{-7}.

(The emission ratio is the ratio of CH_3Br in smoke minus ambient atmospheric CH_3Br to CO_2 in smoke minus ambient atmospheric CO_2.) The CH_3Br to CO_2 emission ratios from the boreal forest fires in Siberia were higher, ranging from $(1.1\text{-}13) \times 10^{-7}$. The higher value from the boreal forest fire is probably due to the fact that forest fires usually have a lower combustion efficiency than grass fires and, hence, a larger fraction of the smoldering-phase compounds are produced. The emission ratio for CH_3Br to methyl chloride (CH_3Cl) from the south African and boreal forest fires was found to be about 1%, which is similar to the Br/Cl ratios found in plants (0.1-1%). Manö and Andreae (1994) have estimated the global emission of CH_3Br from biomass burning based on the CH_3Br to CO_2 and CH_3Br to CH_3Cl emission ratios. The global emission of CO_2 from biomass burning is in the range of 2.5-4.5 Pg C/yr (1 Petagram = 10^{15} grams) and the global emission of CH_3Cl from biomass burning is in the range of 0.65-2.6 Tg Cl/yr (1 Teragram = 10^{12} grams) (Andreae, 1993b). Using these estimates of pyrogenic CO_2 and CH_3Cl emissions and the corresponding CH_3Br emission factors, Manö and Andreae (1994) estimate that the global production of CH_3Br falls in the range from 9-37, and from 22-50 thousand tonnes CH_3Br/yr, respectively. The range of emission from this source is thus 10-50 thousand tonnes per year, with perhaps a mid-range value of 30 thousand tonnes per year.

10.3.4 Industrial Sources, including Gasoline Engine Exhaust

Methyl bromide is used as an intermediate compound in the manufacture of various industrial chemicals, including pesticides. Assessments for the preparation of the UNEP Methyl Bromide Technology Report, which is proceeding simultaneously with this report, suggest that approximately 2.1 thousand tonnes per year is emitted by inadvertent production and in the course of chemical processing.

Methyl bromide is also formed indirectly in the internal combustion engine from ethylene dibromide added in conjunction with lead tetraethyl to gasoline. According to a study conducted in 1989 (Baumann and Heumann), between 22 and 44% of the bromine in gasoline is emitted in an identified organic form in the exhaust, of which 64-82% is CH_3Br.

Using these factors, an estimate for emissions of CH_3Br from motor vehicle exhaust worldwide has been supplied for the year 1991-92 (M. Speigelstein, personal communication, 1994). In this year about 24 thousand tonnes of ethylene dibromide were used in the U.S. and 37 thousand tonnes in the rest of the world, making a total of 61 thousand tonnes. This would allow a range of between 8.6 and 22 thousand tonnes of CH_3Br to be emitted and a mean of 15 thousand tonnes.

The use of ethylene dibromide as a fuel additive has declined rapidly since the 1970s in the U.S. This is shown in Table 10-3.

In 1971, for instance, the amount of bromine used for gasoline additives in the U.S. was 121 thousand tonnes; this had declined to 100 thousand tonnes in 1978 and very rapidly thereafter down to 24 thousand tonnes in 1991. Obviously much more CH_3Br would have been emitted from this source using the above analysis in the 1970s than in the 1980s, with at least 30 thousand tonnes being emitted from the U.S. alone in 1971. The decline in use of ethylene dibromide, however, has been compensated by the increase in use of bromine for a variety of other purposes, including flame retardants (specified) and most probably agricultural use of CH_3Br, listed under "other," so that the total bromine usage has remained nearly constant (162 thousand tonnes in 1971 and 170 thousand tonnes in 1991). It is not impossible that the growth in emission to the atmosphere from agricultural usage could have compensated for the decline in emission from motor vehicle exhaust. No figures are available for the time dependence of gasoline usage of bromine in the rest of the world at the time of writing. Emission of CH_3Br from this source is thus highly uncertain, but in the past it could have been dominant.

A recent study by the U.S. Environmental Protection Agency (W. Thomas, personal communication) estimates that between 10 and 30 tonnes of CH_3Br were emitted from the 2 billion gallons of leaded gasoline used in 1992 in the United States. The same study estimated that about 100 billion gallons of leaded fuel are used worldwide. Assuming the same ethylene dibromide additive levels (0.04 gm per gallon) as in the United States, and the same emission factors as found by Baumann and Heumann, this would extrapolate to between 500 and 1500 tonnes of CH_3Br emitted globally from this source. These numbers are probably low estimates, though, because the lead levels and hence

Table 10-3. U.S.: Bromine consumption by end-use, 1971 to 1991 (thousand tonnes).

Year	Gasoline Additives	Sanitary Preparations	Flame Retardants	Other	Total
1971	121	11	16	14	162
1972	122	11	17	14	164
1973	115	17	27	6	165
1974	109	17	25	14	165
1975	100	17	22	16	155
1976	109	18	26	25	178
1977	103	18	29	20	170
1978	100	16	32	23	171
1979	91	26	28	35	180
1980	73	21	25	16	135
1981	54	26	35	35	150
1982	45	27	47	46	165
1983	39	16	45	48	148
1984	34	16	45	68	163
1985	35	-	52	85	172
1986	-	-	-	-	-
1987	30	14	41	67	152
1988	-	-	-	-	-
1989	32	24	49	70	175
1990	25	-	50	-	-
1991	24	9	48	89	170

[Source: Roskill Information Services Ltd., *The Economics of Bromine,* Sixth Edition, ISBN: 0 86214 383 7, London, 1992.]

ethylene dibromide levels used in gasoline in many countries are likely to be significantly larger than in the U.S.

To a large extent the discrepancy in emission of CH_3Br from gasoline additives between the estimates is traceable to the quantities of ethylene dibromide assumed to be used in the U.S. Table 10-3, for instance, suggests that 24 thousand tonnes of bromine were being used in 1991, whereas the U.S. EPA Survey (W. Thomas, personal communication) estimated a usage of about 80 tonnes only.

10.3.5 Summary of CH_3Br Emissions from Individual Sources

So far, four major sources and two minor sources have been identified for emission of CH_3Br to the atmosphere. Table 10-4 gives a summary of the most likely contribution made by each source, with ranges, to the atmospheric burden.

The uncertainty ranges in the estimates are also shown in Table 10-4, and they show the very imperfect state of knowledge with respect to sources of atmospheric CH_3Br at the present time. In the case of the ocean, the newer, often unpublished, data indicate that it is an active sink, and thus zero net emission cannot be discounted. Agricultural emission estimates vary widely, mostly in association with the care taken and conditions prevailing at the time of application of the CH_3Br. Biomass burning estimates are also very uncertain, reflecting the recent identification of this source and also current uncertainties in the magnitude of biomass burning sources of many compounds. The uncertainties in emission from structural purposes and those incurred during industrial processing are likely to be small, but the source of CH_3Br associated with the inclusion of

Table 10-4. Emission of CH_3Br in thousand tonnes/year (best estimates).

Source	Strength	Range	Anthropogenic	Natural
Ocean*	90	60 - 160	0	90
Agriculture	35	20 - 60	35	0
Biomass Burning	30	10 - 50	25	5
Gasoline Additives†	1	0.5 - 1.5	1	0
	15	9 - 22	15	0
Structural Purposes	4	4	4	0
Industrial Emissions	2	2	2	0
Totals	**162**	**97 - 278**	**67**	**95**
	176	**105 - 298**	**81**	**95**

* The ocean source of 90 thousand tonnes per year is a gross source and is made up of two very uncertain quantities, as explained in Section 10.3.1, and the most likely value and the range are expected to change markedly as a result of new research.

† The two values given for this source reflect the large difference in the two estimates discussed in the text.

ethylene dibromide in leaded gasoline to prevent the accumulation of lead deposits in car engines could either be large or insignificant. Even given these uncertainties, however, it is very likely that the anthropogenic emissions make up at least 40% of the total. This percentage is heavily biased by the value given to the highly uncertain ocean source.

10.4 SINK MECHANISMS

The residence time of CH_3Br in the Earth's atmosphere is controlled by various removal processes occurring in the atmosphere, in the oceans, and on land. The most quantitative information exists for tropospheric and stratospheric mechanisms involving chemical reaction and photolysis. However, there are several degradation processes that may be operative in oceanic surface waters. This is now an accepted removal process for CH_3CCl_3 (Kaye *et al.*, 1994) and both the hydrolysis rate and the solubility of CH_3Br are higher than those for CH_3CCl_3. Finally, a quantitative assessment of any global significance of the dry deposition of CH_3Br on soils or vegetation is yet to be made.

10.4.1 Atmospheric Removal Processes

The removal of CH_3Br within the atmosphere occurs primarily via its tropospheric reaction with the hydroxyl radical (OH). The consistent body of laboratory data for this reaction (Mellouki *et al.*, 1992; Zhang *et al.*, 1992; Poulet, 1993) points to a tropospheric OH-removal lifetime for CH_3Br of slightly greater than two years. Zhang *et al.* (1992) estimate a tropospheric lifetime with respect to OH of 2.1 years by a comparison with the OH reactivity of CH_3CCl_3 (Talukdar *et al.*, 1992) coupled with the lifetime of the latter deduced from observational data (Prather, 1993). The use of the data from either of the other two kinetic studies yields the same value. Mellouki *et al.* (1992) used a coupled dynamical/chemical two-dimensional (2-D) model to calculate a tropospheric lifetime with respect to OH of 1.83 years. The OH reactive loss process for CH_3Br is thought to dominate over reactions involving NO_3 or Cl. For example, tropospheric concentrations of NO_3 are highly variable, with nighttime values in continental air masses ranging from 20-200 pptv (Wayne *et al.*, 1991). Assuming an average nighttime concentration of 50 pptv over the continents in the lowest 2 km of the troposphere (with negligible concentrations during daytime and over the oceans), the lifetime for the removal of CH_3Br by NO_3 is calculated to be greater than 28 years, using a comparative estimate for the reaction rate constant (Wayne *et al.*, 1991). Given the large uncertainty in this calculation and the small estimated contribution (~5%) to the tropospheric reactive lifetime, the NO_3 reaction will not be considered further in calculations of the over-

Table 10-5. Oceanic loss mechanisms for CH_3Br.

Process	Reaction	Loss Rate, % d^{-1}	References
Neutral Hydrolysis	$CH_3Br + H_2O \rightarrow CH_3OH + HBr$	0.2 - 10	Elliott and Rowland (1993) Elliott (1984) Mabey and Mill (1978) Robertson *et al.* (1959) Laughton and Robertson (1956)
Basic Hydrolysis	$CH_3Br + OH^- \rightarrow CH_3OH + Br^-$	< 1 - 10	Gentile *et al.* (1989) Mabey and Mill (1978) Fells and Moelwyn-Hughes (1959)
Nucleophilic Displacement	$CH_3Br + Cl^- \rightarrow CH_3Cl + Br^-$	1 - 50	Elliott and Rowland (1993) Elliott (1984) Swain and Scott (1953)
UV Photosensitization	$CH_3Br + h\nu \rightarrow (CH_3Br)^{\ddagger}$ $(CH_3Br)^{\ddagger} + H_2O \rightarrow CH_3OH + HBr$	≤ 6 times neutral hydrolysis	Gentile *et al.* (1989) Castro and Belser (1981)
Biological Consumption	Uncertain	Uncertain	Rasche *et al.* (1990)

all lifetime. For the possible removal by atomic chlorine, the lifetime is even more difficult to estimate since there are no direct measurements of Cl in the troposphere and a mechanism for maintaining concentrations sufficient to have a significant impact (~10^5 cm^{-3}) on a global scale is not known. In fact, model calculations support much lower global tropospheric Cl concentrations, on the order of 10^2 - 10^3 cm^{-3}, yielding Cl removal lifetimes for CH_3Br of 750 - 7500 years. A minor, but clearly identified, removal process occurring in the atmosphere involves the transport of CH_3Br to the stratosphere followed by its reaction with OH and photodissociation, with a lifetime of approximately 35 years (Prather, 1993). Therefore, the overall lifetime of CH_3Br associated with identified atmospheric removal processes alone is approximately 2 years with an overall uncertainty of ±25%.

10.4.2 Oceanic Removal Processes

There is growing evidence that CH_3Br is destroyed in seawater by up to five processes of differing efficiencies (Table 10-5). Three of these have been investigated to some extent in pure water and seawater, allowing for rough estimates of the degradation rate of CH_3Br in the surface ocean (Table 10-5).

According to Elliott and Rowland (1993) the predominant reaction in seawater is chloride substitution, which is significantly more effective than hydrolysis. They further suggest that these reactions could be a factor of 10 times faster or slower at the oceanographic extremes of 0°C and 30°C. The other two mechanisms (photosensitization by ultraviolet light and destruction by microorganisms) have not been studied under conditions representative of natural systems, thereby not permitting quantification of these rates at the present time. However, there is a limit to the effect that aquatic degradation can have on the atmospheric flux, since at high loss rates, the flux will be restricted by air-sea exchange, as discussed in Section 10.5. These data can be used to compute an area-weighted removal rate for CH_3Br in seawater of 10% per day (J. Butler, private communication) with a probable range of 3-30% d^{-1}, de-

pending on the actual rates and their dependencies on salinity, temperature, and (in the case of biological losses) oceanic productivity. It must be stressed here, however, that the ocean loss process has not been investigated with the same thoroughness as the homogeneous gas phase loss processes discussed above, and that the absolute magnitude of this process is therefore not well defined at present. The impact of oceanic loss of CH_3Br on the overall atmospheric lifetime is discussed later in Sections 10.5 and 10.8.

10.4.3 Surface Removal Processes

Recent experiments have indicated the potential for degradation of CH_3Br in different environments. Anaerobic degradation in salt marsh sediments (Oremland *et al.*, 1994b), has been attributed to nucleophilic substitution reactions with sulfides of biological origin. Time constants of 2-5 days for CH_3Br consumption were measured. Laboratory and field experiments have also provided evidence for biodegradation by methanotrophic bacteria (Oremland *et al.*, 1994a), with time constants of a day or less. However, the degradation time constant seems to be inversely related to the relative concentrations of CH_4 and CH_3Br in the experiments. Because the smallest initial concentrations of CH_3Br injected in these studies were of the order of ppmv, it is difficult to extrapolate time constants to the pptv levels typical of the atmosphere. Other soil types may also consume CH_3Br; in the soil, CH_3Br will be partitioned between soil gas, liquid, and solid phases. The effectiveness of soil sinks would depend on (a) the rate of consumption by physical and/or biological processes in the soil, and (b) the rate of exchange of soil gas with the overlying atmosphere. Experiments to evaluate these processes should be performed with CH_3Br concentrations as close as possible to those in the ambient atmosphere because, for example, soil microbes may exhibit different activities in different concentration ranges.

Given the lack of information on any of the individual processes involved, further laboratory and field measurements are required to quantify the role of any land uptake and degradation of CH_3Br, and it is not included further in atmospheric lifetime calculations.

10.5 THE ROLE OF THE OCEANS

The oceans represent an important special case in the global tropospheric budget of CH_3Br. As indicated previously, the oceans are not only likely to be the largest natural source of tropospheric CH_3Br, they have at the same time been shown to be an important natural sink of tropospheric CH_3Br through chemical removal processes in the oceanic mixed layer. Because the exchange time of tropospheric CH_3Br with the surface layer of the ocean is of the same order of magnitude as its tropospheric residence time with respect to photochemical destruction, its time-dependent response must be evaluated in the context of a coupled ocean-atmosphere system.

Butler (1994) was the first to draw attention to the relationships between the oceanic production and loss mechanisms for CH_3Br and the tropospheric lifetime of CH_3Br. To illustrate these relationships, we present here a much-simplified tutorial that leans heavily on the work of Butler and qualitatively and quantitatively reproduces the main characteristics of the coupled ocean-atmosphere system. In our subsequent assessment of the effect of the oceans on the atmospheric CH_3Br lifetime and its effect on the Ozone Depletion Potential, we rely on Butler's (1994) published values.

10.5.1 A Simple Ocean-Atmosphere Model

Consider a simple two-box model representing the average square meter of ocean surface (Figure 10-4). Above this surface the equivalent volume of atmosphere, calculated by dividing by the fraction of the Earth's surface that is covered by ocean (0.71), corresponds to a column height of 11.9 km calculated at 20°C and 1 atm. The mean depth of the oceanic mixed layer below this surface is taken as 75 m, but because the volume equilibrium partition coefficient (*i.e.*, the Ostwald solubility coefficient, S) favors the liquid phase by a factor of 3.9 at 20°C (Singh *et al.*, 1983), the equivalent depth of the mixed layer reservoir with respect to atmospheric CH_3Br is 3.9×75 m = 293 m. Here we have used the same mixed layer depth as Butler (1994), but we have done the calculation for a mean solubility at 20°C rather than the value at 25°C used by Butler. The effects of this difference and other minor differences in the calculations are discussed below.

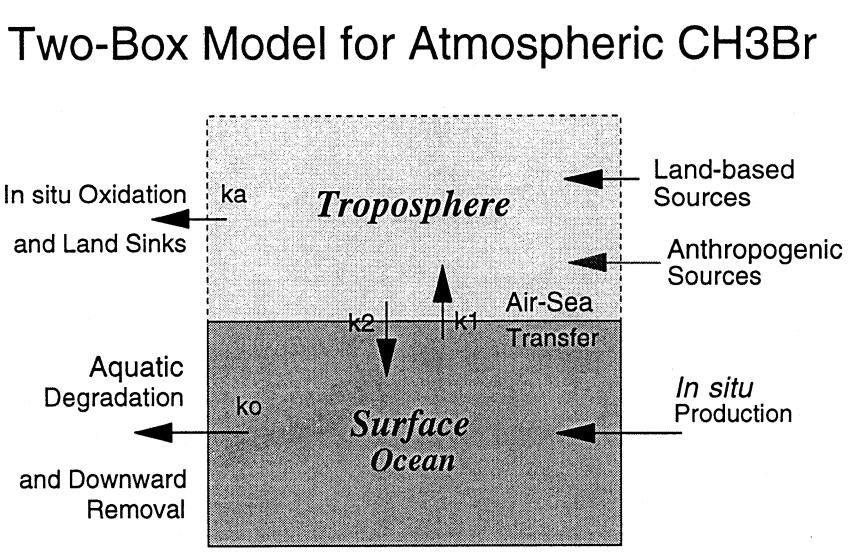

Figure 10-4. A two-box model illustrating methyl bromide coupling between atmosphere and ocean (after Butler, 1994).

In this simple system the effective volumes of the two reservoirs for CH_3Br differ by a ratio of 11,900 ÷ 293 = 41. That is, when the ocean mixed layer is at solubility equilibrium with the atmosphere, only about 2.5% of the atmospheric burden resides in the mixed layer. The magnitude of "buffering" of the atmospheric burden of CH_3Br by the additional CH_3Br in ocean surface waters is therefore realistically limited to only about 2 or 3 percent.

Butler (1994) estimates that the mean atmospheric exchange coefficient, or "piston velocity," for dissolved oceanic CH_3Br is about 4.1 m/d. That is, for a 75 m mixed layer, the CH_3Br mean residence time with respect to atmospheric exchange is (75 m) ÷ (4.1 m/d) = 18.3 d. As the exchange flux must be equal in both directions and the atmospheric reservoir is 41 times larger than the mixed layer reservoir, the residence time of atmospheric CH_3Br with respect to oceanic exchange is 41 × 18.3 d = 750 d, or 2.1 years.

The mean residence time of dissolved CH_3Br in the oceanic mixed layer with respect to the various chemical destruction mechanisms listed in Table 10-5 has been estimated by Butler (1994) at about 10 d. For purposes of illustration, consider first how the simple two-box model would behave if the chemical destruction rate in the surface ocean were infinite. In this case the mixed layer concentration would be zero, and the upward component of the exchange flux would be reduced to zero while the downward component would remain unchanged. Thus, the atmospheric residence time with respect to oceanic exchange of 2.1 years would also be the atmospheric lifetime with respect to oceanic chemical destruction, and the air-sea exchange rate would become the rate-limiting step. In other words, within the uncertainties in the air-sea exchange rate, the atmospheric lifetime with respect to oceanic chemical destruction cannot be less than 2.1 years.

Consider now the balance that is achieved for CH_3Br in the oceanic mixed layer if the mean replacement time by atmospheric exchange is 18.3 d, the mean chemical destruction lifetime is 10 d, and there is no oceanic production. If f is the fraction of the equilibrium atmospheric CH_3Br concentration in the mixed layer at steady state, then the atmospheric replacement rate, which is proportional to (1-f) ÷ 18.3 d, must be equal to the destruction rate, which is similarly proportional to f ÷ 10 d. Solving for f gives a value of 0.35. That is, for the given ratio of the air-sea exchange and chemical destruction rate constants, and no oceanic production, the mixed layer will be 65% undersaturated with respect to atmospheric equilibrium. The corresponding atmospheric CH_3Br lifetime with respect to oceanic chemical destruction then becomes 2.1 y ÷ 0.65, or 3.2 years.

It is important to recognize that this 3.2-year atmospheric lifetime of CH_3Br with respect to oceanic removal does not depend on whether the oceans are a net source or sink for the atmosphere. This is because air-sea exchange and oceanic chemical destruction are both regarded as first-order processes. Any CH_3Br production in the oceans will be partly destroyed *in situ* and partly exchanged with the atmosphere, where it will be subjected to the same combination of atmospheric and oceanic losses as CH_3Br produced elsewhere, either naturally or anthropogenically.

10.5.2 Oceanic Uptake and the Atmospheric Lifetime

Butler (1994) carried out calculations similar to the above tutorial, except that he included a relatively small term for mixing between the oceanic mixed layer and the underlying waters. The greatest difference between the two calculations is that Butler used the mean solubility coefficient at 25°C rather than 20°C, which leads to an increase of about 20% in the calculated atmospheric lifetime with respect to oceanic destruction. Although the mean ocean surface temperature is about 18°C, there is reason to weight the calculation toward the higher temperature solubilities because the chemical removal rates are much greater in warmer waters. Finally, neither calculation takes into account that only the ~85% of the atmosphere that is in the troposphere is able to exchange with the oceans on this time scale. Correction for this effect would shorten the atmospheric lifetime with respect to oceanic destruction by about 15% in both calculations.

Using the results reported by Butler (1994), the best atmospheric mean lifetime for CH_3Br with respect to oceanic destruction is 3.7 years, with a large uncertainty range of 1.3 to 14 years that depends principally on the large uncertainties in the aquatic degradation rate and the air-sea exchange rate. Assuming a mean tropospheric CH_3Br mixing ratio of 11 pptv, this corresponds to an oceanic destruction of about 50 Gg/yr (range: 136 - 13 Gg/yr). If the atmospheric lifetime with respect to atmospheric photochemical destruction alone is 2.0 years, then the corresponding best combined lifetime is 1.3 years (range: 0.8 - 1.7 years).

10.6 MODELED ESTIMATES OF THE GLOBAL BUDGET

10.6.1 Introduction

In recent years, there have been several attempts to determine the strength of the anthropogenic CH_3Br source by constraining model calculations with observed atmospheric concentrations. These model calculations have varied from 3-D and 2-D models to simple 2-box models, but the principle, intrinsic to all these model studies, has been to investigate the latitudinal gradient exhibited in the observations and to account for the magnitude of the average mixing ratio. The results of these studies are summarized in Table 10-6. The atmospheric lifetime of CH_3Br, required for these studies, has largely been estimated by combining modeled OH fields with reaction kinetic data derived from laboratory studies, and the individual lifetimes shown in the table reflect differences in these quantities at the times of publication of the modeling studies. This has the advantage, however, of considering a range of lifetimes including those from gas phase processes alone and including both atmospheric and oceanic removal. None of the modeling studies referred to here explicitly considered sources such as biomass burning and motor vehicle exhausts or a substantial ocean sink. Even so, conclusions concerning the proportions of source type between natural and anthropogenic and the overall annual budget are probably valid.

10.6.2 Budget and the Anthropogenic Contribution

Singh and Kanakidou (1993) used a simple model made up of 2 boxes, each representing a hemisphere, with an interhemispheric exchange rate of 1.1-1.2 years. Assuming a lifetime of 1.7-1.9 years, no natural sources, and injecting 93% of the anthropogenic emissions into the Northern Hemispheric box, an interhemispheric N/S ratio of 1.6-1.8 was calculated. Their 2-D model also produced a similarly high interhemispheric ratio. The 2-D model of Reeves and Penkett (1993), calculates the interhemispheric ratio of the surface concentrations to be 1.69 when no natural sources are assumed and all anthropogenic emissions are injected into the northern midlatitudes (see Figure 10-5 for their relationship between the interhemispheric ratio and anthropogenic

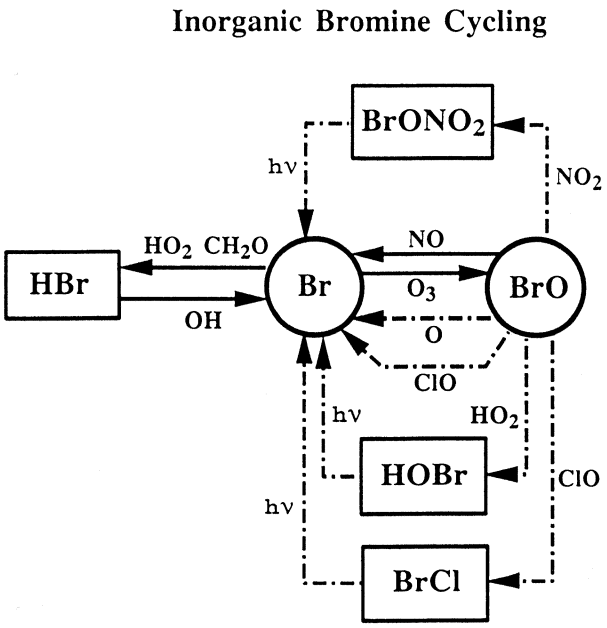

Figure 10-6. Stratospheric gas phase bromine cycle.

10.7 STRATOSPHERIC CHEMISTRY: MEASUREMENTS AND MODELS

The chemistry of bromine in the stratosphere is analogous to that of chlorine and is shown schematically in Figure 10-6. Upon reaching the stratosphere, the organic source gases photolyze or react with OH and $O(^1D)$ rapidly to liberate bromine atoms. Subsequent reactions, predominantly with O_3, OH, HO_2, ClO, NO, and NO_2, partition inorganic bromine between reactive forms (Br and BrO) and reservoir forms ($BrONO_2$, BrCl, HOBr, and HBr). However, unlike chlorine chemistry, where reactive forms are a small fraction of the total inorganic budget (except in the highly perturbed polar regions in wintertime), reactive bromine is about half of the total inorganic bromine budget in the lower stratosphere. Therefore, bromine is more efficient in catalytic destruction of ozone than is chlorine. In addition, the gas phase photochemical partitioning between reactive and reservoir forms of bromine is fairly rapid in sunlight, on the order of an hour or less, such that direct heterogeneous conversion of HBr and $BrONO_2$ to BrO is likely to have little impact on the partitioning of bromine, except perhaps in polar twilight (see later).

Mixing ratios of NO_x, HO_x, and ClO_x increase more strongly with altitude above 20 km than does BrO, and the fractional contribution to ozone loss due to bromine is greatest in the lower stratosphere (Avallone *et al.*, 1993a; Garcia and Solomon, 1994). There, where oxygen atom concentrations are small, the O + BrO reaction is relatively unimportant, and the three reaction cycles listed below are primarily responsible for bromine-catalyzed ozone loss, with Cycle III being of less importance than Cycles I and II:

$$\begin{aligned} &ClO + BrO + h\nu \rightarrow Br + Cl + O_2 \\ &Br + O_3 \rightarrow BrO + O_2 \\ &Cl + O_3 \rightarrow ClO + O_2 \end{aligned} \quad \textbf{(I)}$$

$$\begin{aligned} &BrO + HO_2 \rightarrow HOBr + O_2 \\ &HOBr + h\nu \rightarrow OH + Br \\ &Br + O_3 \rightarrow BrO + O_2 \\ &OH + O_3 \rightarrow HO_2 + O_2 \end{aligned} \quad \textbf{(II)}$$

$$\begin{aligned} &BrO + NO_2 + M \rightarrow BrONO_2 + M \\ &BrONO_2 + M \rightarrow Br + NO_3 \\ &NO_3 + h\nu \rightarrow NO + O_2 \\ &Br + O_3 \rightarrow BrO + O_2 \\ &NO + O_3 \rightarrow NO_2 + O_2 \end{aligned} \quad \textbf{(III)}$$

In the polar regions, where NO_x is reduced and ClO is enhanced by heterogeneous reactions on sulfate aerosols and polar stratospheric clouds, Cycle I dominates the ozone loss due to bromine. At midlatitudes the first two cycles contribute approximately equally to ozone loss at 20 km, and Cycle II is the most important near the tropopause, where the abundance of HO_2 is substantial but where ClO abundances are negligible.

10.7.1 Observations

Measurements of organic bromine across the tropopause indicate that mixing ratios of total bromine in the stratosphere should be about 18 pptv, with CH_3Br providing 54% (Schauffler *et al.*, 1993c). Both remote and *in situ* measurements of BrO indicate mixing ratios are between 4 and 10 pptv, generally increasing with altitude, in the lower stratosphere (Brune *et al.*, 1990; Carroll *et al.*, 1990; Toohey *et al.*, 1990; Wahner *et al.*, 1990; Wahner and Schiller, 1992; Arpag *et al.*, 1994). Results from photochemical models are in good agreement with *in situ* BrO profiles between 16 and 22 km (Garcia and Solomon, 1994). However, profile information above 22 km is limited because all *in situ* data to

date have been obtained with the NASA ER-2 aircraft, a platform with an altitude ceiling of 22 km, and it is difficult to derive profile information above 20 km from column measurements (Arpag *et al.*, 1994).

Attempts to observe HBr directly by far-infrared emission techniques have been hampered by the small anticipated abundances, especially at high altitudes where these techniques are most sensitive (Traub *et al.*, 1992). However, a systematic search of dozens of individual spectra obtained at various altitudes from about 25 km to 35 km revealed a small positive signal that could be attributed to an average HBr mixing ratio of about 1 pptv of HBr (Traub 1993). Within the measurement uncertainties, these observations are broadly consistent with results from photochemical models that include a small HBr branching ratio (less than 5%) for the BrO + HO_2 reaction and show no unexpected features, suggesting that the major sources of HBr have been accounted for adequately in ozone loss calculations. Supporting these observations are results from a 2-D model (Garcia and Solomon, 1994) indicating that an HBr yield of greater than a few percent is also not consistent with the *in situ* observations of the abundances and latitudinal gradient of BrO at midlatitudes. Thus, HBr likely represents a minor reservoir for reactive bromine in the lower stratosphere and is unlikely to exceed 2% of total bromine.

Information about inorganic bromine photochemistry is available from geographic and solar zenith angle variations in BrO. Mixing ratios within the polar vortices are about twice as great as values observed at midlatitudes under background sulfate aerosol conditions, consistent with the differences in NO_x abundances in these regions (Toohey *et al.*, 1990). Higher BrO abundances observed at midlatitudes following the eruption of Mount Pinatubo (Avallone and Toohey, 1993; Arpag *et al.*, 1994) reflected the concurrent decreases in NO_x due to enhanced heterogeneous reaction of N_2O_5 on sulfate aerosols. Similar increases were observed in ClO (Avallone *et al.*, 1993b). The results of ER-2 diurnal studies (Toohey *et al.*, 1990) and remote observations at sunrise and sunset of both BrO and OClO (Solomon *et al.*, 1990; Arpag *et al.*, 1994), the latter a by-product of the ClO and BrO reaction, indicate that reactive bromine is tied up at night into photolytically labile reservoir forms such as $BrONO_2$ and BrCl. These results are consistent with inferences that $BrONO_2$ is a major inorganic bromine reservoir. However, some measurements from the NASA DC-8 aircraft at northern high latitudes reveal non-zero BrO column abundances in darkness that cannot be explained with standard photochemistry (Wahner and Schiller, 1992).

10.7.2 Laboratory Studies

A breakdown of the contributions from the catalytic cycles above indicates that Cycle I and Cycle II account for most of the bromine-catalyzed ozone loss and contribute about equally (Isaksen, 1993). At lower altitudes, where bromine reactions contribute most to ozone loss rates and the alpha factor is greatest (Garcia and Solomon, 1994), temperatures are low (below 220K) and there are some uncertainties in BrO kinetics. The reaction between BrO and ClO is complex, but it has been studied extensively under stratospheric conditions and appears to be well understood (DeMore *et al.*, 1992). Remote observations of BrO and OClO, the latter produced by the side reaction BrO + ClO $\rightarrow$ Br + OClO and itself not affecting ozone, and diurnal studies of BrO *in situ* support the view that our understanding of the coupled photochemistry between BrO and ClO is basically sound at stratospheric pressures and temperatures (Solomon *et al.*, 1990; Wahner and Schiller, 1992).

Recent measurements of the rate constant for the BrO and HO_2 reaction indicate that at room temperature it is about six times larger than previously reported, making Cycle II correspondingly more efficient (Poulet *et al.*, 1992; Bridier *et al.*, 1993; Maguin *et al.*, 1994). Furthermore, it is now clear that the major reaction products are HOBr and O_2. A recent report of the upper limit to the efficiency of the channel yielding HBr + O_3 at room temperature gave a value of less than 0.01% (Mellouki *et al.*, 1994), which was established by investigating the rate of the reverse reaction, namely, HBr + O_3 $\rightarrow$ BrO + HO_2. A direct determination at stratospheric temperatures remains to be carried out.

10.7.3 Ozone Loss Rates

Loss rates of ozone as calculated by a photochemical model that best reproduces observations of ozone, NO_x, ClO, and BrO obtained at midlatitudes at the spring equinox appear in Figure 10-7 (Garcia and Solomon, 1994). Because bromine is released more rapidly with altitude than chlorine, and because a greater

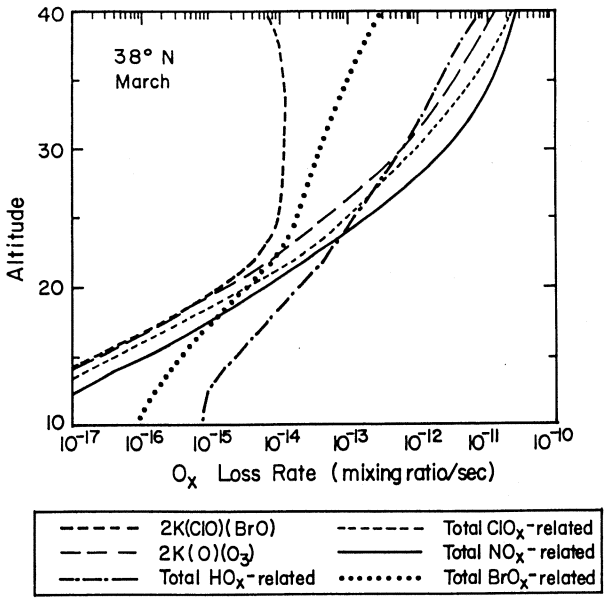

Figure 10-7. Midlatitude ozone loss rates associated with various removal cycles between 15 and 30 km (after Garcia and Solomon, 1994).

fraction of inorganic bromine remains in active forms, catalytic destruction of ozone by bromine is more important than chlorine on a mole-per-mole basis. As a consequence, at about 20 km the bromine contribution to the overall ozone loss rate is nearly as important as the chlorine contribution. However, total ozone losses are a result of continuous photochemical destruction as ozone is transported from the source region in the tropics to lower altitudes at higher latitudes (Rodriguez *et al.*, 1994), so it is difficult to assess the overall contribution to ozone column trends from instantaneous ozone loss rates. However, 2-D model results indicate that at present abundances of bromine and chlorine in the stratosphere, a 5 pptv increase in inorganic bromine results in a column loss of ozone of 0.5% to 1.0%, with the greater losses occurring at higher latitudes (Isaksen, 1993).

The importance of Cycle I in the lower stratosphere has been ascertained directly from simultaneous *in situ* measurements of the abundances of BrO and ClO and concurrent ozone decreases within the Antarctic ozone hole (Anderson *et al.*, 1990). Analyses using *in situ* BrO and ClO data indicate that Cycle I contributed approximately 25% to ozone losses observed over Antarctica in 1987 (Anderson *et al.*, 1990; Murphy, 1991) and could contribute as much as 40% to total ozone loss over the Arctic in winter (Salawitch *et al.*, 1990, 1993).

On the other hand, because HO_2 measurements have a greater uncertainty (approx. 50%) relative to measurements of BrO (approx. 35%) (Toohey *et al.*, 1990) and ClO (approx. 25%) (Anderson *et al.*, 1990), and because the uncertainty in the rate constant for the BrO + HO_2 reaction at low temperatures is greater than that for the ClO + BrO reaction, the importance of the BrO + HO_2 reaction is less certain. Future simultaneous *in situ* measurements of BrO and HO_2 on the ER-2 aircraft, reductions in BrO and HO_2 measurement uncertainties, and low-temperature kinetics studies will all contribute to a better understanding of the importance of this reaction in the atmosphere, leading to a better assessment of ozone losses due to bromine. However, in the perturbed polar regions where Cycle I dominates, uncertainties in HO_x kinetics and measurements are of little consequence to estimates of the importance of bromine to ozone losses.

10.8 THE OZONE DEPLETION POTENTIAL OF METHYL BROMIDE

10.8.1 General Considerations

The concept of Ozone Depletion Potential (ODP) has been extensively discussed in the literature (Wuebbles, 1983; Fisher *et al.*, 1990; WMO, 1990, 1992; Albritton and Watson, 1992; Solomon *et al.*, 1992; Solomon and Albritton, 1992). A single time-independent index has been introduced to quantify the steady-state depletion of ozone by unit mass emission of a given trace species, relative to the same steady-state ozone reduction by unit mass emission of CFC-11. This index, the so-called steady-state ODP, is approximately given by:

$$ODP_{CH_3Br} \cong \left(\frac{1}{3}\frac{M_{CFC-11}}{M_{CH_3Br}}\frac{\tau_{CH_3Br}}{\tau_{CFC-11}}\beta\right)\left(<\frac{F_{CH_3Br}}{F_{CFC-11}}\alpha>\right)$$

$$ODP_{CH_3Br} \equiv [BLP][BEF] \qquad (10\text{-}1)$$

where M_{CH_3Br} and M_{CFC-11} denote the molecular weight of CH_3Br and CFC-11, F_{CH_3Br}/F_{CFC-11} represents the bromine release from CH_3Br relative to that of chlorine release from CFC-11 in the stratosphere, α de-

notes the efficiency of the released bromine in catalytic removal of ozone, relative to chlorine; β is the decrease in the mixing ratio of CH_3Br at the tropical tropopause, relative to the mixing ratio at the surface; and < > denotes the spatial and seasonal averaging of the quantity with the appropriate weighting given by the ozone distribution.

The term in the first bracket represents the amount of bromine delivered to the stratosphere by CH_3Br relative to chlorine in CFC-11, per unit mass emission. This is the so-called Bromine Loading Potential (BLP). The second term, the Bromine Efficiency Factor (BEF), denotes the amount of stratospheric ozone removed per unit mass of CH_3Br delivered to the stratosphere, relative to CFC-11. Values for the parameters in Equation 10-1 can be obtained either from global models of the atmosphere (and the ocean) or estimated from observations (Solomon *et al.*, 1992; Solomon and Albritton, 1992). A fuller discussion of the usefulness of the ODP is given in Chapter 13.

The time constants (lifetimes) $\tau_{CFC\text{-}11}$ and τ_{CH_3Br} relate the change in (steady-state) atmospheric burden (B) to a change in anthropogenic emission (S). This therefore places limits on the range that can be chosen for the atmospheric lifetimes (see Sections 10.3 and 10.6) and in the case of CH_3Br:

$$\Delta B_{CH_3Br}\,(kT) = \Delta S_{CH_3Br}\,(kT/yr)\,\tau_{CH_3Br} \qquad (10\text{-}2)$$

This time constant (lifetime) can be obtained by considering all removal processes for the species in question, both atmospheric and surface:

$$\frac{1}{\tau_{CH_3Br}} = \frac{1}{\tau_{OH}} + \frac{1}{\tau_{strat}} + \frac{1}{\tau_{ocean}} + \frac{1}{\tau_{other}} \qquad (10\text{-}3)$$

where τ_{OH} denotes the time constant for removal by tropospheric OH (2.0 years; see Section 10.4) assuming the rate constants of Mellouki *et al.* (1992), Zhang *et al.* (1992), and Poulet (1993), and scaling to a lifetime of 6.6 years for methyl chloroform removal by OH; τ_{strat} is the time constant for stratospheric removal (35 years; Section 10.4); τ_{ocean} denotes the time constant for ocean removal (about 3.7 years: Butler, 1994; Section 10.5); and τ_{other} denotes time constants for removal by other sink mechanisms, such as reaction with Cl or biodegradation, which are at this point not well established and are therefore given a value of zero. Adopting the above values for τ_{OH}, τ_{strat}, and τ_{ocean}, we obtain a value of:

$$\tau_{CH_3Br} \approx 1.3 \text{ years} \qquad (10\text{-}4)$$

with an uncertainty range of 0.8 to 1.7 years.

Adopting the above value of τ_{CH_3Br} and taking $\tau_{CFC\text{-}11} = 50$ years (Kaye *et al.*, 1994), a Bromine Loading Potential of 0.013 is calculated from the expression in the first brackets of Equation 10-1. A Bromine Efficiency Factor (BEF) of 48 is calculated by the Atmospheric and Environmental Research, Inc. (AER) 2-D model, adopting heterogeneous chemistry on background aerosols and the kinetic recommendations of DeMore *et al.*, 1992. Using this value (48), the present estimate for the ODP of CH_3Br, taking into account uncertainties in ocean removal, etc., is

$$ODP_{CH_3Br} \approx 0.6$$

10.8.2 Steady-State ODP: Uncertainties

The algorithm given by Equation 10-1 provides a useful framework to estimate the uncertainties in the calculated ODP of CH_3Br due to uncertainties in the different input parameters. Uncertainties in the input parameters and their impact on the calculated ODP are listed in Table 10-7. Uncertainties in the Bromine Loading Potentials are directly calculated from Equation 10-1, while the AER 2-D model has been used to calculate the Bromine Efficiency Factor.

The largest uncertainties in ODP are due to the following:

- Uncertainties in the lifetime of CH_3Br. Values of τ_{CH_3Br} smaller than 1 year would be possible if ocean uptake, removal by reactions with atomic chlorine, and/or surface biodegradation were fast enough. The value of β is unlikely to be much less than 1; recent measurements suggest a value of 0.9 (Blake *et al.*, 1993).
- Uncertainties in the kinetics of $BrO + HO_2$. Atmospheric measurements of BrO and (upper limits) for HBr (Section 10.7) indicate that the branching of the $BrO + HO_2$ reaction to the HBr channel is probably much less than 2%. Measurements of HBr below 30 km would further constrain this parameter. There are at present no measurements of either the rate or branching of the above reaction at

Table 10-7. Principal uncertainties in calculated steady-state ODP for CH_3Br.

Parameter	Value-Range	τ_{CH_3Br} (yrs)	BLP	BEF	ODP
τ_{OH}	2.0 yr (± 25%)[a]	1.1 - 1.5	0.011 - 0.015	48	0.52 - 0.76
τ_{ocean}	3.7 yr (± 1.3 - 14)[b]	0.78 - 1.7	0.0078 - 0.017	48	0.37 - 0.80
$\tau_{CFC\text{-}11}$	50 yr (± 10%)[c]		0.012 - 0.014	48	0.55 - 0.67
$F_{CH_3Br}/F_{CFC\text{-}11}$	1.08 (± 15%)[d]			41 - 55	0.52 - 0.70
k_{BrO+HO_2}	6.3 (2.2 - 18) × 10^{-11} cm^3 s^{-1} [e]			32 - 50	0.41 - 0.64
Branching of $BrO+HO_2 \rightarrow HBr+O_3$	0 (< 2%)[f]			30 - 48	0.38 - 0.61

a Kaye *et al.*, 1994; Prather, 1993
b Butler, 1994 (Section 10.5)
c Kaye *et al.*, 1994
d Pollock *et al.*, 1992
e DeMore *et al.*, 1992, evaluated at 215 K
f Section 10.7

Table 10-8. Calculated time-dependent ODPs.

Time Horizon (yr)	TD-ODP (τ_{ocean} = 3.7 yr)	TD-ODP (τ_{ocean} = 1.3 yr)	TD-ODP (τ_{ocean} = 14 yr)
5.0	16	12	18
10	5.3	2.7	7.1
15	3.1	1.5	4.2
20	2.2	1.1	3.0
25	1.8	0.9	2.4
30	1.5	0.7	2.1
Infinite (steady state)	0.6	0.3	0.84

stratospheric temperatures. The uncertainties in the rate of BrO + HO_2 due to the lack of temperature information imply uncertainties in the Bromine Efficiency Factor of the order of 50%.

At the same time, there is no single process whose present estimated uncertainty could reduce the ODP of CH_3Br below 0.3. Smaller values could be possible if two improbable situations occurred simultaneously and several of the parameters were at the extremes of their error limits.

The "semi-empirical" ODPs discussed by Solomon *et al.* (1992) provide a valuable constraint to the model-based results, particularly if we are interested in the ODP for a particular region of the atmosphere. Larger uncertainties are introduced when steady-state ODPs are derived from the semi-empirical approach, since the necessary observations are usually not available for a global coverage. This is particularly true for CH_3Br, where (a) coincidental measurements of the BrO, ClO, and HO_2 are sparse, particularly at midlatitudes, and (b) the existing measurements have uncertainties of 25% for ClO, 35% for BrO, and 50% for HO_2 (see Section 10.7).

Overall, the lower limit for the ODP of CH_3Br is about 0.3 and its most likely value lies between 0.5 and 1.0 (0.6 with BEF = 48).

10.8.3 Time-Dependent ODPs

Previous studies (WMO, 1990, 1992; Albritton and Watson, 1992; Solomon and Albritton, 1992) have shown that species with short atmospheric lifetimes have much larger ODPs over short time horizons than over longer time horizons. Table 10-8 updates previous esti-

mates of the time-dependent ODP of CH_3Br based on the formulation of Solomon and Albritton (1992) with particular respect to changes adopted in the ocean lifetime including a low value (1.3 years) which is outside the limits set by the analysis of ocean sink processes in Section 10.5.1. Uncertainties in the Bromine Efficiency Factor would lead to the same scaling factors for each time horizon as for the steady-state values in Table 10-7. Over the period of any reasonable lifetime for CH_3Br (*i.e.*, less than and up to 5 years), its ODP is in excess of 10, indicating that a cessation of emissions of CH_3Br would have a rapid impact on the extent of stratospheric ozone loss.

10.9 CONCLUSIONS

This review of the atmospheric science of CH_3Br has revealed that many uncertainties still exist in both the sources and sinks for this molecule, although its chemistry in the stratosphere and to a large extent in the troposphere is now mostly resolved. The situation with regard to sources and sinks is complicated by the role of the ocean, which acts both as a source and a sink, with the overall balance still in doubt. The research effort on CH_3Br has been somewhat limited and this is partly responsible for the uncertainties. In spite of this, there is considerable confidence in our best current estimate of 0.6 for the ODP of CH_3Br. Consideration of the existing uncertainties indicates that it is improbable that this value would be less than 0.3 or larger than 0.8. Individual points are addressed in more detail in the scientific summary for this chapter.

REFERENCES

Albritton, D.L., and R.T. Watson, Methyl bromide and the ozone layer: A summary of current understanding, in *Methyl Bromide: Its Atmospheric Science, Technology, and Economics, Montreal Protocol Assessment Supplement,* edited by R.T. Watson, D.L. Albritton, S.O. Anderson, and S. Lee-Bapty, United Nations Environment Programme, Nairobi, Kenya, 3-18, 1992.

Anderson, J.G., W.H. Brune, S.A. Lloyd, D.W. Toohey, S.P. Sander, W.L. Starr, M. Loewenstein, and J.R. Podolske, Kinetics of O_3 destruction by ClO and BrO within the Antarctic vortex: An analysis based on *in situ* ER-2 data, *J. Geophys. Res., 94,* 11480-11520, 1990.

Andreae, M.O., Global distribution of fires seen from space, *EOS Trans. AGU 74,* 129-135, 1993a.

Andreae, M.O., The influence of tropical biomass burning on climate and the atmospheric environment, in *Biogeochemistry of Global Change: Radiatively Active Trace Gases*, edited by R.S. Oremland, Chapman & Hall, New York, NY, 1993b.

Arpag, K.A., P.V. Johnson, H.L. Miller, R.W. Sanders, and S. Solomon, Observations of the stratospheric BrO column over Colorado, 40°N, *J. Geophys. Res., 99,* 8175-8181, 1994.

Avallone, L.M., and D.W. Toohey, ER-2 BrO results from the Airborne Arctic Stratospheric Expedition II, AASE-II CD-ROM, NASA, 1993.

Avallone, L.M., D.W. Toohey, W.H. Brune, R.J. Salawitch, A.E. Dessler, and J.G. Anderson, Balloon-borne *in situ* measurements of ClO and ozone: Implications for heterogeneous chemistry and mid-latitude ozone loss, *Geophys. Res. Lett., 20,* 1795-1798, 1993a.

Avallone, L.M., D.W. Toohey, M.H. Proffitt, J.J. Margitan, K.R. Chan, and J.G. Anderson, *In situ* measurements of ClO at mid latitudes: Is there an effect from Mt. Pinatubo?, *Geophys. Res. Lett., 20,* 2519-2522, 1993b.

Baumann, H., and K.G. Heumann, Analysis of organobromine compounds and HBr in motor car exhaust gases with a GC/microwave plasma system, *Fresenius Z. Anal.*, 186-192, 1989.

Blake, D.R., B. Sive, M. Zondlo, and F.S. Rowland, Estimated methyl bromide emissions from biomass burning, *EOS Trans. AGU 74, (*43), 134, 1993.

Bridier, I., V. Veyret, and R. Lesclaux, Flash photolysis kinetic study of reactions of the BrO radical with BrO and HO_2, *Chem. Phys. Lett., 201,* 563-568, 1993.

Brune, W.H., J.G. Anderson, and K.R. Chan, *In situ* observations of BrO over Antarctica: ER-2 aircraft results from 54°S to 72°S latitude, *J. Geophys. Res., 94,* 16639-16647, 1990.

CHAPTER 11

SUBSONIC AND SUPERSONIC AIRCRAFT EMISSIONS

Contents

SCIENTIFIC SUMMARY

Extensive research and evaluations are underway to assess the atmospheric effects of the present and future subsonic aircraft fleet and of a projected fleet of supersonic transports. Assessment of aircraft effects on the atmosphere involves the following:

i) measuring the characteristics of aircraft engine emissions;
ii) developing three-dimensional (3-D) inventories for emissions as a function of time;
iii) developing plume models to assess the transformations of the aircraft engine emissions to the point where they are governed by ambient atmospheric conditions;
iv) developing atmospheric models to assess aircraft influences on atmospheric composition and climate; and
v) measuring atmospheric trace species and meteorology to test the understanding of photochemistry and transport as well as to test model behavior against that of the atmosphere.

Supersonic and subsonic aircraft fly in atmospheric regions that have quite different dynamical and chemical regimes. Subsonic aircraft fly in the upper troposphere and in the stratosphere near the tropopause, where stratospheric residence times due to exchange with the troposphere are measured in months. Proposed supersonic aircraft will fly in the stratosphere near 20 km, where stratospheric residence times due to exchange with the troposphere increase to years. In the upper troposphere, increases in NO_x typically lead to increases in ozone. In the stratosphere, ozone changes depend on the complex coupling among HO_x, NO_x, and halogen reactions.

- Emission inventories have been developed for the current subsonic and projected supersonic and subsonic aircraft fleets. These provide reasonable bases for inputs to models. Subsonic aircraft flying in the North Atlantic flight corridor emit 56% of their exhaust emissions into the upper troposphere and 44% into the lower stratosphere on an annual basis.

- Plume processing models contain complex chemistry, microphysics, and turbulence parameterizations. Only a few measurements exist to compare to plume processing model results.

- Estimates indicate that present subsonic aircraft operations may have increased NO_x concentrations at upper tropospheric altitudes in the North Atlantic flight corridor by about 10-100%, water vapor concentrations by about 0.1% or less, SO_x by about 10% or less, and soot by about 10% compared with the atmosphere in the absence of aircraft and assuming all aircraft are flying below the tropopause.

- Preliminary model results indicate that the current subsonic fleet produces upper tropospheric ozone increases as much as several percent, maximizing at the latitudes of the North Atlantic flight corridor.

- The results of these rather complex models depend critically on NO_x chemistry. Since there are large uncertainties in the present knowledge of the tropospheric NO_x budget (especially in the upper troposphere), little confidence should be put in these quantitative model results of subsonic aircraft effects on the atmosphere.

- Atmospheric effects of supersonic aircraft depend on the number of aircraft, the altitude of operation, the exhaust emissions, and the background chlorine and aerosol loading. Rough estimates of the impact of future supersonic operations (assuming 500 aircraft flying at Mach 2.4 in the stratosphere and emitting 15 grams of nitrogen oxides per kilogram of fuel) indicate an increase of the North Atlantic flight corridor concentrations of NO_x up to about 250%, water vapor up to about 40%, SO_x up to about 40%, H_2SO_4 up to about 200%, soot up to about 100%, and CO up to about 20%.

- One result of two-dimensional model calculations of the impact of such a projected fleet in a stratosphere with a chlorine loading of 3.7 ppbv (corresponding to the year 2015) implies additional annually averaged ozone column decreases of 0.3-1.8% for the Northern Hemisphere. Although NO_x aircraft emissions have the largest impact on ozone, the effects from H_2O emissions contribute to the calculated ozone change (about 20%).

- Net changes in the column ozone from supersonic aircraft modeling result from ozone mixing ratio enhancements in the upper troposphere and lower stratosphere and depletion at higher stratospheric altitudes.

- There are important uncertainties in supersonic assessments. In particular, these assessment models produce ozone changes that differ among each other, especially in the lower stratosphere below 25 km. When used to calculate ozone trends, these same models predict smaller changes than are observed in the stratosphere below 25 km between 1980 and 1990. Thus, these models may not be properly including mechanisms that are important in this crucial altitude range.

- Increases in ozone at altitudes near the tropopause, such as are thought to result from aircraft emissions, enhance the atmosphere's greenhouse effect. Research to evaluate the climate effects of supersonic and subsonic aircraft operations is just beginning, so reliable quantitative results are not yet available, but some initial estimates indicate that this effect is of the same order as that resulting from the aircraft CO_2 emissions.

11.1 INTRODUCTION

Tremendous growth occurred in the aircraft industry during the last several decades. Figure 11-1 shows the increasing use of aircraft fuel as a function of time. Aircraft fuel consumption has increased by about 75% during the past 20 years and is projected to increase by 100 to 200% over the next 30 years. At the present time, approximately 3% of the worldwide usage of fossil fuels is by aircraft. Ninety-nine percent of this aircraft fuel is burned by subsonic aircraft, of which a large proportion occurs in the upper troposphere. Table 9.2 of the previous assessment (WMO, 1992) demonstrates that subsonic aircraft emit a significant fraction of their exhaust products into the lower stratosphere. This depends on factors such as latitude and season.

Despite the small percentage of the total fossil fuel usage for aviation, the environmental effects of aircraft should be closely examined for several reasons. One reason is the rapid growth that has occurred and is projected to occur in aircraft emissions, and another is that aircraft emit their exhaust products at specific altitudes where significant effects might be expected. For instance, an environmental concern of the 1970s was the effect that large fleets of supersonic aircraft would have on the stratospheric ozone layer. The main concern was then and still is that catalytic cycles involving aircraft-emitted NO_x (NO plus NO_2) enhance the destruction of ozone.

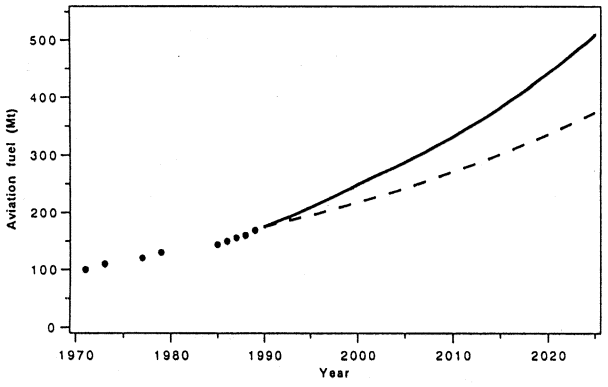

Figure 11-1. Aviation fuel versus time. Data up to 1989 from the International Energy Agency (1990). Extrapolations according Kavanaugh (1988) with 2.2% per year in a low-fuel scenario and with 3.6% up to 2000 and 2.9% thereafter in a high-fuel scenario. (Based on Schumann, 1994.)

Since supersonic aircraft engines may emit significant amounts of NO_x, the fear is that large fleets of supersonic aircraft flying at stratospheric levels, where maximum ozone concentrations exist, might seriously deplete the stratospheric ozone layer, leading to increased ultraviolet radiation flux on the biosphere. Also, climate sensitivity studies have shown that ozone changes in the upper troposphere and lower stratosphere will have greater radiative effects on changing surface and lower tropospheric temperatures than would ozone changes at other levels (see Chapter 8).

Also, in the 1950s, "smog reactions" were discovered that implied the depletion of tropospheric ozone when NO_x concentrations are low and ozone production when NO_x concentrations are high. Thus, there is a concern that new fleets of supersonic aircraft flying in the stratosphere would lead to harmful stratospheric ozone depletion, while present and future subsonic aircraft operations will lead to undesired enhanced levels of ozone in the upper troposphere.

Development of any successful aircraft requires a period of about 25 years, and each aircraft will have a useful lifetime of about 25 years as well. Thus, even if an environmentally motivated decision is made to utilize new aircraft technologies, it will take decades to fully realize the benefits.

One can get some perspective on possible atmospheric effects of aircraft operations by noting the following. Current subsonic aircraft operations in the North Atlantic flight corridor are probably increasing NO_x concentrations at upper tropospheric altitudes by about 10-100%, water vapor concentrations by about 0.1% or less, and SO_x by about 10% or less compared to an atmosphere without aircraft. Future supersonic operations in the stratosphere might increase the North Atlantic flight corridor concentrations of NO_x up to about 250%, water vapor up to about 40%, SO_x up to about 40%, H_2SO_4 up to about 200%, soot up to about 100%, and CO up to about 20%. Thus, present subsonic aircraft perturbations in atmospheric composition are now probably significant, and future large supersonic aircraft fleet operations will also be significant in affecting atmospheric trace gas concentrations.

These and other concerns have led to an increasing amount of research into the atmospheric effects of current and future aircraft operations. In the U.S., NASA's Atmospheric Effects of Aviation Project is composed of

two elements. The Atmospheric Effects of Stratospheric Aircraft (AESA) element was initiated in 1990 to evaluate the possible impact of a proposed fleet of high-speed (*i.e.*, supersonic) civil transport (HSCT) aircraft. A Subsonic Assessment (Wesoky *et al.*, 1994) was begun in 1994 to study the impact of the current commercial aircraft fleet. In Europe, the Commission of the European Communities (CEC) has initiated the Impact of NO_x Emissions from Aircraft upon the Atmosphere (AERONOX) and Measurement of Ozone on Airbus In-service Aircraft (MOZAIC) programs (Aeronautics, 1993) and Pollution from Aircraft Emissions in the North Atlantic Flight Corridor (POLINAT) to investigate effects of the emissions of the present subsonic aircraft fleet in flight traffic corridors. In addition, there are also several national programs in Europe and Japan looking at various aspects of the atmospheric effects of aircraft emissions.

Atmospheric models play a particularly important role in these programs since there does not appear to be any purely experimental approach that can evaluate the global impact of aircraft operations on the atmosphere. The strategy is to construct models of the present atmosphere that compare well with atmospheric measurements and to use these models to try to predict the future atmospheric effects of changed aircraft operations. At the present time, the subsonic and supersonic assessment programs are in quite different stages of maturity and are utilizing different approaches in both modeling and observations. Therefore, in this chapter the subsonic and supersonic evaluations will be considered separately since the chemical and dynamical regimes are quite different. In this context the "lower stratosphere" refers to the region above the local tropopause where there are lines of constant potential temperature that connect the stratosphere and troposphere. In this region, stratosphere-troposphere exchange can occur by horizontal advection with no need to expend energy in overcoming the stable stratification. In the stratosphere near 20 km, where Mach 2.4 HSCT operate, no lines of constant potential temperature connecting the stratosphere and troposphere exist. Therefore residence times of tracers are much larger (about 2 years) in the stratosphere at 20 km than in the lower stratosphere.

In this chapter, we will review what is known about aircraft emissions into the atmosphere and discuss the transformations that take place in the aircraft plume as it adjusts from the physical conditions of the aircraft exhaust leaving the engine tailpipe to those of the ambient atmosphere. Some of the atmospheric effects of the different chemical families that are emitted by aircraft are then considered, and finally, modeling studies of the atmospheric effects of aircraft emissions on ozone are presented, along with a discussion of possible climate effects of aircraft operations. A discussion of the level of uncertainty of these predictions, and some conclusions are presented.

Further details of the NASA effort to assess the atmospheric effects of future supersonic aircraft operations can be found in Albritton *et al.* (1993) and the references therein. An external evaluation of these efforts can be found in NRC (1994). No similar documents exist at this time pertaining to the atmospheric effects of subsonic aircraft operations.

11.2 AIRCRAFT EMISSIONS

The evaluation of the potential impact of emissions from aircraft on atmospheric ozone levels requires a comprehensive understanding of the nature of the emissions produced by all types of aircraft and a knowledge of the operations of the total global aircraft fleet in order to generate a time-dependent, three-dimensional emissions data base for use in chemical/dynamical atmospheric models.

Emissions from the engines, rather than those associated with the airframe, are considered to be dominant (Prather *et al.*, 1992). These are functions of engine technology and the operation of the aircraft on which the engines are installed. Primary engine exhaust products are CO_2 and H_2O, which are directly related to the burned fuel, with minor variations due to the precise carbon-hydrogen ratio of the fuel. Secondary products include NO_x (= NO + NO_2), CO, unburned and partially burnt fuel hydrocarbons (HC), soot particulates/smoke, and SO_x. NO_x is a consequence of the high temperature in the engine combustor; the incomplete combustion products (CO, HC, and soot/smoke) are functions of the engine design and operation and may vary widely between engines. SO_x is directly related to fuel composition. Currently, typical sulfur levels in aviation kerosene are about 0.05% sulfur by weight, compared with an allowed specification limit of 0.3% (ICAO, 1993).

Table 11-1. Emission Index (grams per kilograms of fuel used) of various materials for subsonic and supersonic aircraft for cruise condition. Values in parentheses are ranges for different engines and operating conditions.

Species (gm MW)	Subsonic Aircraft* Short range	Long range	Supersonic Aircraft#
CO_2 (44)	3160	3160	3160
H_2O (18)	1230	1230	1230
CO (28)	5.9 (0.2-14)	3.3 (0.2-14)	1.5 (1.2-3.0)
HC as methane (16)	0.9 (0.12-4.6)	0.56 (0.12-4.6)	0.2 (0.02-0.5)
SO_2 (64)	1.1	1.1	1.0
NO_x as NO_2 (46)	9.3 (6-19)	14.4 (6-19)	depends on design (5-45)

* Mean (fuel-consumption weighted) emission indices for 1987 based on Boeing (1990). The values were calculated from a data base containing emission indices and fuel consumptions by aircraft types. The difference between short range (cruise altitude around 8 km) and long range (cruise altitude between 10 and 11 km) reflects different mixes of aircraft used for different flights.

Based on Boeing (1990) and McDonnell Douglas (1990).

The measure of aircraft emissions traditionally used in the aviation community is the Emissions Index (EI), with units of grams per kilogram of burnt fuel. Typical EI values for subsonic and anticipated values for supersonic aircraft engines are given in Table 11-1 for cruise conditions. By convention, EI(NO_x) is defined in terms of NO_2 (similarly, hydrocarbons are referenced to methane).

Historically, the emissions emphasis has been on limiting NO_x, CO, HC, and smoke, mainly for reasons relating to boundary layer pollution. Standards are in place for control of these over a Landing/Take-Off (LTO) cycle up to 915 m altitude at and around airports (ICAO, 1993). Currently there are no regulations covering other flight regimes, *e.g.* cruise, though ICAO (1991) is considering the need and feasibility of introducing standards.

It is now recognized that the list of chemical species (emitted from engines or possibly produced in the young plume, also by reactions with ambient trace species like hydrocarbons) that may be relevant to ozone and climate change extends well beyond the primary combustion species and NO_x. A more complete set of "odd nitrogen" compounds, known as NO_y—including NO_x, N_2O_5, NO_3, HNO_3—and PAN (peroxyacetylnitrate) should be considered, along with SO_x and soot particles as aerosol-active species. HC and CO may also play an important role in high altitude HO_x chemistry.

11.2.1 Subsonic Aircraft

Engine design is a compromise between many conflicting requirements, among which are safety, economy, and environmental impacts. For subsonic engines, the various manufacturers have resolved these conflicts with different compromises according to their own in-house styles. This has resulted in a spread of emission values for HC, CO, NO_x, and smoke, all meeting the LTO cycle regulatory standards.

Historical trends (1970–1988) in aircraft engine emissions for the typical LTO cycle show that very substantial decreases in HC and CO emissions have been realized over the past two decades due to improvements in fuel-efficient engine design and emissions control technology. A substantial increase in NO_x emissions would have been expected due to the much higher combustion temperatures associated with the more fuel-efficient engine cycles. However, other improvements in engine technology have kept NO_x relatively constant. Combining the increased passenger miles in the period from 1970 to 1988 with that of the technology improvements

would imply that the actual mass output should have decreased by about 77% for HC and 30% for CO, while NO_x mass output should have increased by about 110%. Considerable further reductions of HC and CO will come as older aircraft are phased out, but little change can be expected for NO_x without the introduction of low-NO_x technology engines.

The first steps to develop combustion systems producing significantly lower NO_x levels relative to existing technology were made in the mid-1970s (CIAP 2, 1975). These systems achieve at least a 30% NO_x reduction, and are now being developed into airworthy systems for introduction in medium and high thrust engines.

11.2.2 Supersonic Aircraft

The first generation of civil supersonic aircraft (Concorde, Tupolev TU144) incorporated turbojet engines of a technology level typical of the early 1970s. The second generation, currently being considered by a number of countries and industrial consortia, will have to incorporate technology capable of meeting environmental requirements. A comprehensive study of the scientific issues associated with the Atmospheric Effects of Stratospheric Aircraft (AESA) was initiated in 1990 as part of NASA's High Speed Research Program (HSRP; Prather *et al.*, 1992). No engines or prototypes exist and designs are only at the concept stage. A range of cruise EI(NO_x) levels (45, 15, and 5) has been set as the basis for use in atmospheric model assessments and in developing engine technology. An EI(NO_x) of 45 is approximately what would be obtained if HSCT engines were to be built using today's jet engine technology without putting any emphasis on obtaining lower EI(NO_x) emissions. Jet engine experts have great confidence in their ability to achieve an HSCT engine design with EI(NO_x) no greater than 15 and have set a goal of designing an HSCT engine with EI(NO_x) no greater than 5. Laboratory-scale studies of new engine concepts, which appear to offer the potential of at least 70-80% reduction in NO_x compared with current technology, are being pursued. Early results indicate that these systems seem able to achieve the low target levels of EI(NO_x) = 5 (Albritton *et al.*, 1993).

11.2.3 Military Aircraft

In contrast to the majority of civil aviation, military aircraft do not operate to set flight profiles or frequencies. Also, national authorities are reluctant to disclose this information. Thus it is extremely difficult to make realistic assessments of the contribution of military aircraft in terms of fuel usage or emissions. Earlier estimates (Wuebbles *et al.*, 1993) were that the world's military aircraft used about 19% of the total aviation fuel and emitted 13% of the NO_x, with an average EI(NO_x) of 7.5. With the changes following the breakup of the former Soviet Union, there has been considerable reduction in activity, and an estimate of about 10% fuel usage may be more appropriate (ECAC/ANCAT, 1994).

11.2.4 Emissions at Altitude

As noted above, engines are currently only regulated for some species over an LTO cycle. Internationally accredited emissions data on these are available (ICAO, 1994). However, experimental data for other flight conditions are sparse, since these can only realistically be obtained from tests in flight or in altitude simulation test facilities. Correlations, in particular for NO_x, have been developed from theoretical studies and combustor test programs for prediction of emissions over a range of flight conditions. A review of these is given elsewhere (Prather *et al.*, 1992; Albritton *et al.*, 1993). Engine tests under simulated altitude conditions are being carried out within the AERONOX program (Aeronautics, 1993) and should be useful to check this approach for subsonic engines.

11.2.5 Scenarios and Emissions Data Bases

Air traffic scenarios have been developed as a basis for evaluating global distributions of emissions from aircraft (McInnes and Walker, 1992; Prather *et al.*, 1992; Wuebbles *et al.*, 1993; ECAC/ANCAT, 1994). The first two based their traffic assessment on scheduled commercial flight information from timetables and supplemented these data with information from other sources for non-scheduled charter, general aviation, and military flights. The third is based on worldwide Air Traffic Control data supplemented by timetable information and other data as appropriate.

McInnes and Walker (1992) generated 2-D and 3-D inventories of NO_x emissions from subsonic aircraft, using relatively broad assumptions for numbers of aircraft types, flight profiles/distance bands, and cell sizes. However, the evaluation did not include non-scheduled, military, cargo, or general aviation, and

both inventories accounted for only 51% of the total estimated fuel consumption of 166.5×10^9 kg for the year 1989 (IEA, 1990). The fuel consumption was simply scaled to match the total estimated fuel consumption in order to estimate the total NO_x mass. Their average EI(NO_x) value of 11.6 is within the range quoted elsewhere (Nüßer and Schmitt [1990] 6 - 16.4; Egli [1990] 11-30; and Beck *et al.* [1992] 17.9).

Wuebbles *et al.* (1993) generated for the HSRP/AESA (Prather *et al.*, 1992; Stolarski and Wesoky, 1993a) a comprehensive assessment of all aircraft types to determine fuel, NO_x, CO, and HC for general scenarios comprising the 1990 fleet and projected fleets of subsonic and supersonic aircraft (HSCTs) for the year 2015. A much better match (76%) of the calculated fuel use with the total estimated fuel consumption for 1990 was achieved. The remainder is likely to be mainly attributable to factors such as the non-idealized flight routings and altitudes actually flown by aircraft due to factors such as air traffic control, adverse weather, etc., as well as low-level unplanned delays and ground operations. However, scaling to match the total estimated fuel consumption gave a total annual NO_x mass (1.92 Tg) similar to that of McInnes and Walker. Illustrations of the global NO_x inventories as functions of latitude/longitude, or altitude/latitude for both 1990 and 2015 are given in Figures 11-2 and 11-3.

The European Civil Aviation Conference (ECAC) Abatement of Nuisance Caused by Air Traffic (ANCAT) work, carried out to complement the AERONOX program, has also considered NO_x emissions from subsonic and supersonic fleets for the year 1992. Unlike the other inventories, the traffic data have been compiled for four equally spaced months throughout the year to provide information on the seasonal variation. Preliminary results indicate a higher fuel burn, NO_x annual mass, and EI(NO_x) than those of the other inventories and are likely to represent upper bounds on the aircraft NO_x emission burden. The current grid scale is larger than that of the HSRP/AESA inventory, but this may give a more realistic representation of the NO_x distribution within the heavily traveled air traffic routes, such as the North Atlantic, where there is known to be a significant divergence of actual flight paths from the ideal great circle routes currently assumed by all inventories. Further work is being carried out to produce forecast inventories for the years 2003 and 2015.

Considerable comparative analysis is being undertaken between the ECAC/ANCAT and the HSRP/AESA inventories in order to understand the reasons underlying the differences (EI(NO_x) 10.9 to 16.8; NO_x mass 1.92 to 2.8 Tg) and to refine the inventories. For example, it is already known that there is some double counting of traffic in some geographically important areas of the ECAC/ANCAT inventory. Another significant factor is a large difference in the contribution from military aircraft. A comparison summary of the inventories is given in the table at the bottom of the page.

11.2.6 Emissions Above and Below the Tropopause

In a global perspective, the North Atlantic, apart from North America and Europe, contains the largest specific subsonic traffic load. In 1990 the average daily movements across the Atlantic (both directions) between 45° and 60°N amounted to 595 flights in July and 462 flights in November. One recent study (Hoinka *et al.*, 1993) has assessed the aircraft fleet mix and the resulting emissions for this flight corridor. By correlation of the traffic data with the tropopause height from the European Centre for Medium-Range Weather Forecasts

	McInnes and Walker, 1992	*Wuebbles et al., 1993*	*ECAC/ANCAT, 1994*
Year	1989	1990	1992
Grid size	7.5° × 7.5° × 0.5km	1° × 1° × 1km	2.8° × 2.8° × 1km
Fuel match	51%	76%	99%
EI (NO_x) global	11.6	10.9	16.8
NO_x mass (Tg)#	1.91#	1.92#	2.8#

Note: all data for NO_x mass have been scaled to 100% fuel match.

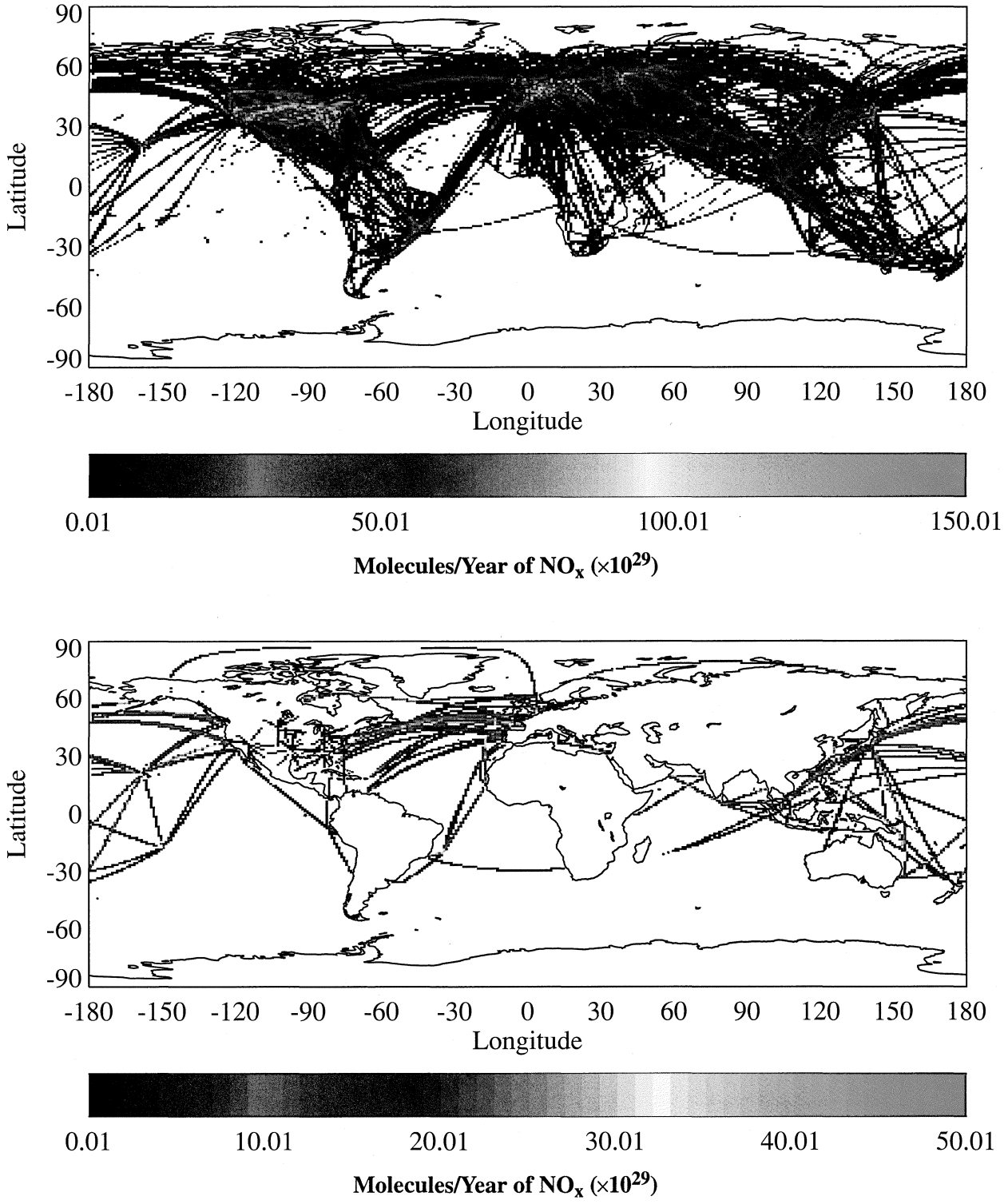

Figure 11-2. Annual NO_x emissions for proposed 2015 subsonic and Mach 2.4 (EI(NO_x)=15) HSCT fleets as function of latitude and longitude. Top panel shows emissions below 13 km (primarily subsonic traffic) while bottom panel shows emissions above 13 km (primarily HSCT traffic). (Albritton *et al.*, 1993)

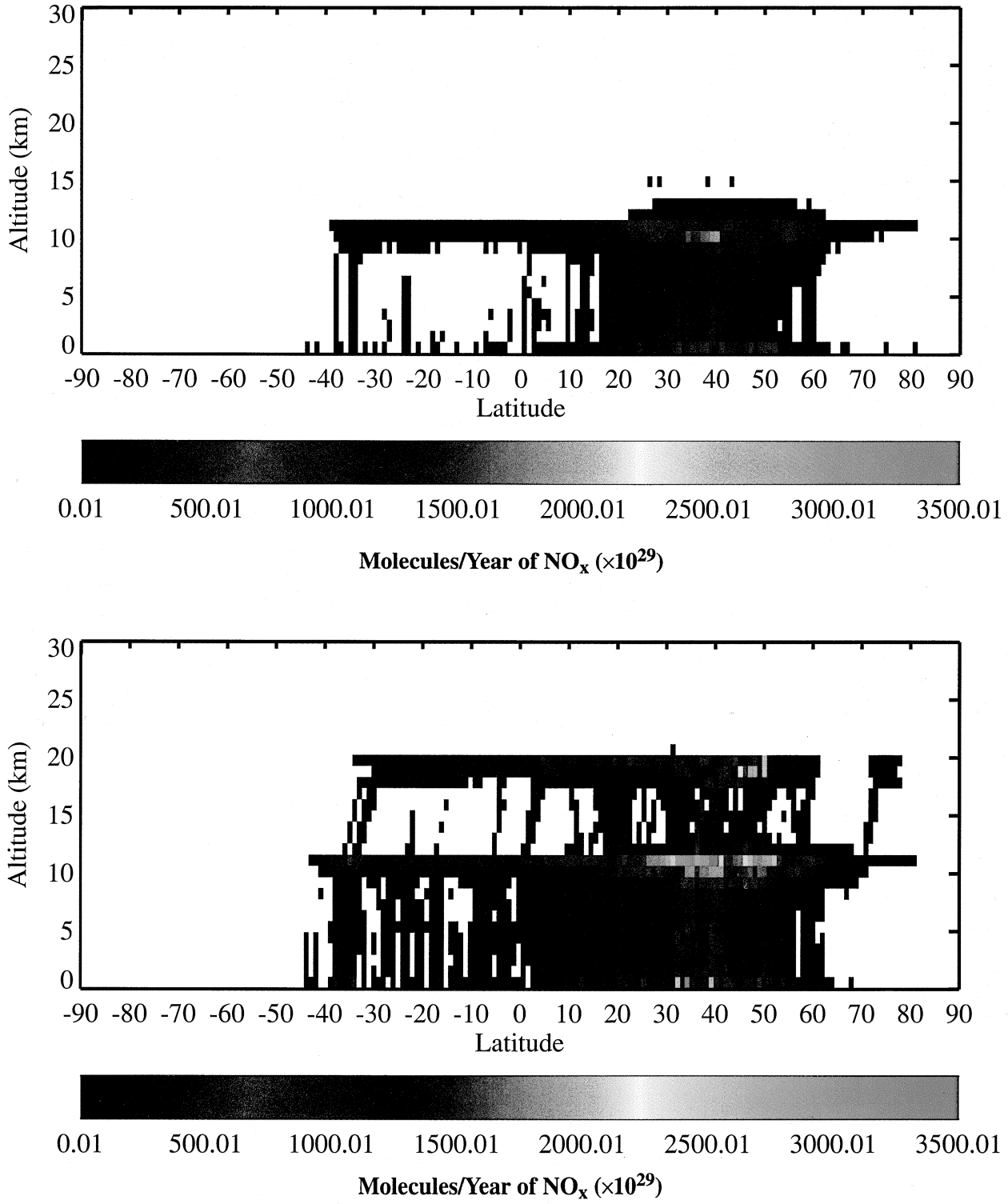

Figure 11-3. Annual NO_x emissions as a function of altitude and latitude for 1990 subsonic fleet (Scenario A, top panel) and for proposed 2015 subsonic and Mach 2.4 ($EI(NO_x)=15$) HSCT fleets (bottom panel). (Albritton *et al.*, 1993)

(ECMWF) data, it is estimated that 44% of the NO_x emissions are injected in the lower stratosphere and 56% are injected in the upper troposphere.

11.3 PLUME PROCESSES

Plume processing involves the dispersion and conversion of aircraft exhausts on their way from the scales of the jet engines to the grid scales of global models. The details of plume mixing and processing can be important for conversion processes that depend nonlinearly on the concentration levels, such as the formation of contrails, the formation of soot, sulfur and nitric acid particles, and nonlinear photochemistry. Also, the vertical motion of the plumes relative to ambient air and sedimentation of particles may change the effective distribution of emitted species at large scales. Contrails may impact the mixing, sedimentation, heterogeneous chemistry, and the formation of cirrus clouds, with climatic consequences.

11.3.1 Mixing

The aircraft wake can be conveniently subdivided into three regimes (Hoshizaki *et al.*, 1975): the jet, the vortex, and the dispersion regimes. The vortex regime persists until the vortices become unstable and break up into a less ordered configuration. Thereafter, the dispersion regime follows, in which further mixing is influenced by atmospheric shear motions and turbulence depending on shear, stratification, and other parameters (Schumann and Gerz, 1993). With respect to mixing models, the jet and vortex regime, including the very early dispersion regime, can be computed with models as described by Miake-Lye *et al.* (1993). The engine plumes grow by turbulent mixing to fill the vortex pair cell. Due to rotation, centripetal acceleration causes inward motions of the relatively warm jet plumes so that the exhaust gases get trapped near the narrow well-mixed core of the vortices. The radial pressure gradient also causes adiabatic cooling and hence increases the formation of contrails. These centripetal forces are much larger for supersonic aircraft than for subsonic aircraft. It should be noted, however, that these model results remain largely untested, observationally.

Details of the plume fluid dynamics depend critically on the aircraft scales. For a Boeing-747, one may estimate that the jet regime lasts for about 10 s and the following vortex regime for about 1 to 3 minutes. The cross-section of the trailing vortex pair represents an upper bound for the mixed area of the plumes. However, measurements of water vapor concentration and temperature in the jet and vortex regime (>2 km behind a DC-9 at cruising altitude) exhibit a spiky concentration field within the double vortex system, indicating that the individual jet plumes may not yet be homogeneously mixed over the vortex cross-section at such distances (Baumann *et al.*, 1993).

The lift of the aircraft induces downward motion of the double vortex structure at about 2.4 ± 0.2 m s^{-1} for a Boeing-747, which decreases when the vortices mix with the environment at altitudes that may be typically 100 m lower than flight level. During this descent, parts of the exhaust gases are found to escape the vortex cores.

In the supersonic case, the vortex pair has more vertical momentum (descent velocity of about 5 m/s), and its vertical motion will continue (possibly in the form of vortex rings) well after the vortex system has broken up. This will lead to exhaust species deposition a few hundred meters below flight altitude (Miake-Lye *et al.*, 1993). Radiation cooling of the exhaust gases may contribute to additional sinking (Rodriguez *et al.*, 1994), in particular when contrails are forming.

Very little is known about the rate of mixing in the dispersion range, and it is this rate of mixing that plays a large role in determining the time evolution of the gas composition of the plume (Karol *et al.*, 1994). In fact, it is yet unknown at what time scales the emissions become indistinguishable from the ambient atmosphere. Table 11-2 shows estimates of the concentration increases due to aircraft emissions in a young exhaust plume (vortex regime) and at the scales of the North Atlantic flight corridor (Schumann, 1994). These are the scales in between which global models will be able to resolve the concentration fields. The background concentration estimates are taken from Penner *et al.* (1991) for NO_x, Möhler and Arnold (1992) for SO_2, and Pueschel *et al.* (1992) for soot. With respect to background, the concentration increases in young plumes are of importance for all aircraft emissions included in Table 11-2. A strong corridor effect is expected for NO_x and, at least in the lower stratosphere, also for SO_x and soot particles.

11.3.2 Homogeneous Processes

Several models have been developed to describe the finite-rate chemical kinetics in the exhaust plumes

Table 11-2. Mean concentration increases in vortex regime (5000 m² cross-section) of a B-747 plume, and mean concentration increase in the North Atlantic flight corridor due to traffic exhaust emissions from 500 aircraft. (Table adopted from Schumann, 1994.)

Species	EI (g/kg)	Background concentration at 8 km	Mean concentration increase in vortex regime	Mean concentration increase in North Atlantic flight corridor
CO_2	3150	358 ppmv	14 ppmv	0.02 ppmv
H_2O	1260	20-400 ppmv	14 ppmv	0.02 ppmv
$NO_x(NO_2)$	18	0.01-0.05 ppbv	78 ppbv	0.1 ppbv
SO_2	1	50-300 pptv	3100 pptv	4 pptv
soot	0.1	3 ng/m³	240 ng/m³	0.3 ng/m³

(Danilin *et al.*, 1992; Miake-Lye *et al.*, 1993; Pleijel *et al.*, 1993; Weibrink and Zellner, 1993). Most models follow a well-mixed air parcel as a function of plume age or distance behind the aircraft. The models are initialized either with an estimate of emissions from the jet exit or a separate model describing the kinetics after the combustion chamber within the engine. Considerable deviations from local equilibrium are predicted at the jet exit, in particular for CO, NO, NO_2, HNO_3, OH, O, and H. In the models, the air parcel grows in size as a prescribed function of mixing with the environment, and the concentrations in the plume change according to mixing with the ambient air and due to internal reactions in the homogeneous mixture. The models differ in the treatment of mixing, in the reaction set used to simulate the exhaust plume finite-rate chemical kinetics, photolysis rates, treatment of heterogeneous processes, and in the prescription of the effective plume cross-section as a function of time or distance. Since most of the NO_x emissions are in the form of NO, a rapid but local destruction of ozone is to be expected.

Besides some incidental measurements in flight corridors or contrails (Hofmann and Rosen 1978; Douglass *et al.*, 1991), very few data exist at this time on the gaseous emissions in aircraft plumes in the atmosphere. Measurements of the gases HNO_2, HNO_3, NO, NO_2, and SO_2 were recently made (Arnold *et al.*, 1992, 1994a) in the young plume of an airliner at cruising altitude (see Figure 11-4). The data imply that not more than about 1% of the emitted odd-nitrogen underwent chemical conversion to longer living HNO_3. Hence, most of the emitted odd nitrogen initially remains in a reactive form, which can catalytically influence ozone.

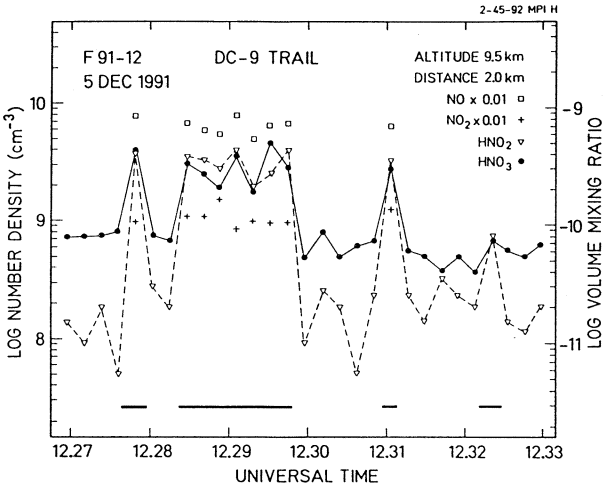

Figure 11-4. Time plot of nitrous acid (HNO_2) and nitric acid abundance measured during chase of a DC-9 airliner at 9.5 km altitude and a distance of 2 km. Periods when the research aircraft was inside the exhaust-trail of the DC-9 are marked by bars. For these periods NO and NO_2 abundance are also given. (Arnold *et al.*, 1992, 1994b; recalibration changed conversion factors shown in figure to: NO × 0.006 and NO_2 × 0.003.)

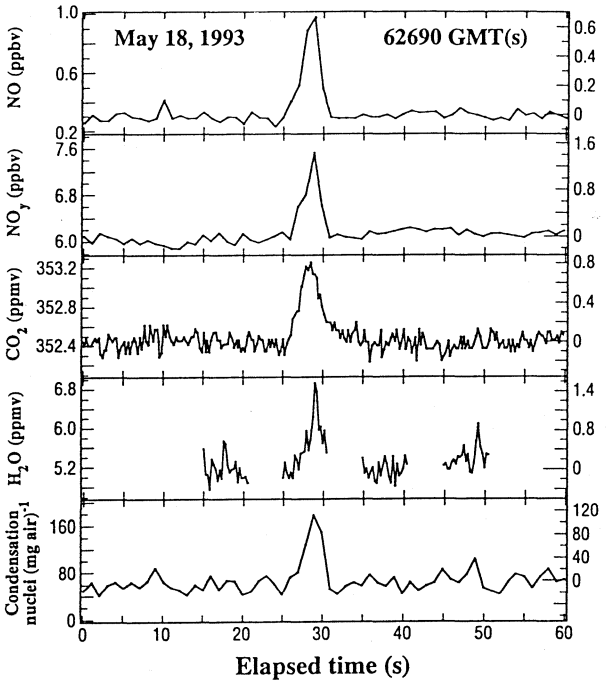

Figure 11-5. Time series for NO, NO_y, CO_2, H_2O, and CN during the plume encounters on May 18, 1993. The approximate Greenwich Mean Time (GMT) is noted in the top panel. The scale on the left side indicates the absolute value of each species. The zero in the right scale is set to the approximate background values of each species. At the ER-2 airspeed of 200 m s^{-1}, the panel width of 60 seconds corresponds to 12 km. (Based on Fahey *et al.*, 1994.)

In situ measurements of NO_y, NO, CO_2, H_2O, condensation nuclei, and meteorological parameters (Figure 11-5) have been used to observe the engine exhaust plume of the NASA ER-2 aircraft approximately 10 minutes after emission operating in the lower stratosphere (Fahey *et al.*, 1994). The obtained EI(NO_x) of 4 is in good agreement with values scaled from limited ground-based tests of the ER-2 engine. Non-NO_x nitrogen species comprise less than about 20% of emitted reactive nitrogen, consistent with model evaluations.

11.3.3 Heterogeneous Processes

New particles form in young exhaust plumes of jet aircraft. This is documented by *in situ* condensation nucleus (CN) measurements made (Hofmann and Rosen, 1978; Pitchford *et al.*, 1991; Hagen *et al.*, 1992; Whitefield *et al.*, 1993) in plumes under flight conditions.

The molecular physics details of nucleation are not well known and the theory of bimolecular nucleation is only in a rudimentary state. For a jet engine exhaust scenario, nucleation takes place in a non-equilibrium mechanism, which further complicates a theoretical description. It seems, however, that jet aircraft may form long-lived contrails composed of $H_2SO_4 \cdot H_2O$ aerosols and soot particles covered with $H_2SO_4 \cdot H_2O$. Under conditions of low ambient temperatures around 10 km altitude, particularly in winter at high latitudes, contrails composed of $HNO_3 \cdot H_2O$ aerosols may also form (Arnold *et al.*, 1992). Even if $HNO_3 \cdot H_2O$ nucleation does not occur, some HNO_3 may become incorporated into condensed-phase $H_2SO_4 \cdot H_2O$ by dissolution at low temperatures.

There are several potential effects of newly formed CN and activated soot. Such CN may trigger water contrail formation, induce heterogeneous chemical reactions, and serve as cloud condensation nuclei (CCN). Thereby, jet aircraft-produced CN may have an impact on trace gas cycles and climate. However, at present this is highly speculative.

Numerical calculations with chemical plume models show that the impact of aircraft emissions on the atmosphere in the wake regime critically depends on heterogeneous processes where considerable uncertainties still exist (Danilin *et al.*, 1992, 1994). Danilin *et al.* (1992) have considered the heterogeneous reaction $N_2O_5 + H_2O \rightarrow 2HNO_3$ on ambient aerosol particles only. They have found that this reaction does not play an important role at time scales of up to one hour in the wake, but may get important at larger time scales. Taking contrail ice (or/and nitric acid trihydrate [NAT]) particle formation into account, Danilin *et al.* (1994) estimate that heterogeneous processes are more important at lower temperatures, but their impact on heterogeneous conversion is small during the first day after emission. In contrast, Karol *et al.* (1994) found noticeable "heterogeneous impact" on the chemistry in the plume taking into account the growth of ice particles.

Around 10 km altitude, there seems to exist a strong CN source, which is not due to aircraft but to H_2SO_4 resulting from sulfur sources at the Earth's surface (Arnold *et al.*, 1994a). Hence, the relative contribution of aircraft to CN production around 10 km

Table 11-3. Estimates of stratospheric perturbations due to aircraft effluents of a fleet of approximately 500 Mach 2.4 HSCTs (NO_x EI=15) relative to background concentrations. (Perturbations are estimated for a broad corridor at northern midlatitudes.) (Expanded from Stolarski and Wesoky, 1993b.)

Species	Perturbation	Background
NO_x	3-5 ppbv	2-16 ppbv
H_2O	0.2-0.8 ppmv	2-6 ppmv
SO_x	10-20 pptv	50-100 pptv
H_2SO_4	350-700 pptm	350-700 pptm
Soot	~7 pptm	~7 pptm
Hydrocarbons	2 ppbv (NMHC)	1600 ppbv (CH4)
CO	~2ppbv	10-50 ppbv
CO_2	~1 ppbv	350 ppmv

altitude needs to be determined. It is uncertain whether CN production around 10 km actually has a significant impact on trace gas cycles and CCN.

11.3.4 Contrails

Miake-Lye *et al.* (1993) have applied the analysis of Appleman (1953) to the standard atmosphere as a function of altitude and latitude. Their result shows that much of the current high-flying air traffic takes place at altitudes where the formation of contrails is very likely, in particular in the northern winter hemisphere. A small reduction of global mean temperature near and above the tropopause, by say 2 K, would strongly increase the region in which contrails have to be expected. Also, a slight change in the threshold temperature below which contrails form has a strong effect on the area of coverage with contrails.

Except for *in situ* measurements by Knollenberg (1972), little is known about the spatial structure and microphysical parameters of contrails. Recent measurements (Gayet *et al.*, 1993) show that contrails contain more and smaller ice particles than natural cirrus, leading to about double the optical thickness in spite of their smaller ice content. Contrail observations from satellite data, Lidar measurements, and climatological observations of cloud cover changes have been described by Schumann and Wendling (1990). Large (1 to 10 km wide and more than 100 km long) contrails are observed regionally on about a quarter of all days within one year, but the average contrail coverage is only about 0.4% in mid-Europe. Lidar observations show that particles from contrails sediment quickly at approximately 10 km altitude (Schumann, 1994).

11.4 NO_x/H_2O/SULFUR IMPACTS ON ATMOSPHERIC CHEMISTRY

11.4.1 Supersonic Aircraft

The impacts of HSCT emissions on chemistry are discussed in detail in Stolarski and Wesoky (1993b). Here we give a short summary. Effects of emissions from HSCTs (see Table 11-3) on ozone are generally predicted to be manifested through gas phase catalytic cycles involving NO_x, HO_x, ClO_x, and BrO_x. The amounts of these radicals are changed by two pathways. First, they are changed by chemistry, either addition of or repartitioning within nitrogen, hydrogen, and halogen chemical families. Predicted changes in ozone from this pathway are initiated primarily by NO_x chemistry. Second, they are changed when HSCT emissions affect the properties of the aerosols and the probability of polar stratospheric cloud (PSC) formation. Changes in ozone from this pathway are determined primarily by ClO_x and BrO_x chemistry, with a contribution from HO_x chemistry (see Chapter 6 for more detail).

Heterogeneous chemistry on sulfate aerosols also has a large impact on the potential ozone loss. Most important is the hydrolysis of N_2O_5: $N_2O_5 + H_2O \rightarrow 2\ HNO_3$. Several observations are consistent with this reaction occurring in the lower stratosphere (*e.g.*, Fahey *et al.*, 1993; Solomon and Keys, 1992). Its most direct

effect is to reduce the amount of NO_x. Indirectly, it increases the amounts of ClO and HO_2 by shifting the balance of ClO and $ClONO_2$ more toward ClO during the day and by reducing the loss of HO_x into HNO_3. As a result, the HO_x catalytic cycle is the largest chemical loss of ozone in the lower stratosphere, with NO_x second, and both the ClO_x and BrO_x catalytic cycles have increased importance compared to gas phase conditions.

The addition of the emissions from HSCTs will affect the partitioning of radicals in the NO_y, HO_y, and ClO_y chemical families, and thus will affect ozone. The NO_x emitted from the HSCTs will be chemically converted to other forms, so that the NO_x/NO_y ratio of these emissions will be almost the same as for the background atmosphere. As a result, the NO_x emissions will tend to decrease ozone, but less than would occur in the absence of sulfate aerosols.

The increase in H_2O will lead to an increase in OH, because the reaction between $O(^1D)$ that comes from ozone photolysis and H_2O is the major source of OH; however, increases in NO_y will act to reduce HO_x through the reactions of OH with HNO_3 and HNO_4. On the other hand, HNO_3, formed in the reaction of OH with NO_2, can be photolyzed in some seasons and latitudes to regenerate OH. When all of these effects are considered, the amount of HO_x is calculated to decrease—HO_2 by up to 30% and OH by up to 10%. Thus, the catalytic destruction of ozone by HO_x, the largest of the catalytic cycles, is decreased.

Finally, ClO_x concentrations decrease with the addition of HSCT emissions for two reasons. First and most important, with the addition of more NO_2, the daytime balance between ClO and $ClONO_2$ is shifted more toward $ClONO_2$. Second, with OH reduced, the conversion of HCl to Cl by reaction with OH is reduced, so that more chlorine stays in the form of HCl. Thus, the catalytic destruction of ozone by ClO_x is decreased.

The addition of HSCT emissions results in increases in the catalytic destruction of ozone by the NO_x cycle that are compensated by decreases in the catalytic destruction by ClO_x and HO_x. Because the magnitudes of the changes in catalytic destruction of ozone are similar for the NO_x, HO_x, and ClO_x cycles, compensation results in a small increase or decrease in ozone. Model calculations indicate a small decrease. The decreases in the catalytic destruction of O_3 by ClO_x and HO_x involve the effects of increased water vapor and HNO_3 on the rates of heterogeneous reactions on sulfate and the probability of PSC formation.

The addition of sulfur to the stratosphere from HSCTs will increase the surface area of the sulfate aerosol layer. This change in aerosol surface area is expected to be small compared to changes from volcanic eruptions, with a possible exception being the immediate vicinity of the aircraft wake. Model calculations by Bekki and Pyle (1993) predict regional increases of the mass of lower stratospheric $H_2SO_4 \cdot H_2O$ aerosols, due to air traffic, by up to about 100%. The importance of sulfur emissions from HSCTs in the presence of this large and variable background needs to be assessed.

11.4.2 Subsonic Aircraft

The emissions from subsonic aircraft take place both in the lower stratosphere and troposphere. The primary chemical effects of aircraft in the troposphere seem to be related to their NO_x emissions. The concentration of ozone in the upper troposphere depends on transport of ozone mainly from the stratosphere and on upper troposphere ozone production or destruction. The impact of subsonic aircraft occurs through the influence of NO_x on the tropospheric HO_x cycle (see Chapter 5 for a fuller discussion of tropospheric ozone chemistry).

The HO_x cycle is initialized by the photolysis of ozone itself, which results in the production of OH radicals and destruction of ozone. OH radicals have two possible reaction pathways: reaction with CO, CH_4, and non-methane hydrocarbons (NMHC) resulting in HO_2 and RO_2 radicals; or reaction with NO_2, removing OH and NO_x from the cycle. The HO_2 radicals that are produced also have two possible pathways: reaction with ozone or reaction with NO. The first one removes ozone from the cycle; the second one (also valid for RO_2 radicals) produces ozone and regains NO. Additionally, both pathways regain OH radicals.

As a consequence, ozone is destroyed photochemically in the absence of NO_x. Only in the presence of NO_x can ozone be produced. The net production/destruction depends on the combination of these processes. Their relative importance is controlled mainly by the NO_x concentration. In a regime of low NO_x, the ozone concentration will be reduced photochemically. At higher NO_x concentrations (on the order of 10 pptv NO_x) NO_x will lead to a net ozone production. In both regimes, additional NO_x will result in higher ozone

concentrations. Only when the concentration of NO_x is so high (over a few hundred pptv NO_x) that the OH concentration starts to decline, will additional NO_x result in a lower ozone production.

The impact of NO_x emitted by aircraft depends, therefore, on the background NO_x concentration and on the increase in NO_x concentration. Measurements show that background NO_x concentrations (including NO_x emitted from subsonic aircraft) are in the range of 10-200 pptv NO_x. Therefore, airplane emissions take place in the regime of increasing ozone production most of the time, where increasing NO_x results in increased local ozone concentrations.

In this regime, the concentration of OH radicals is enhanced also by additional NO_x. First, enhanced ozone means higher production of OH by photolysis of ozone. Second, the partitioning in the HO_x family is shifted towards OH by the reaction of HO_2 with NO. The loss process of OH by reaction with NO_2 is not yet important. This enhancement of the OH concentration reduces the tropospheric lifetime of many trace species like CH_4, NO_x, etc.

The emission of sulfur from aviation is much smaller than from surface emissions and negligible in terms of the resultant acid rain, but may be important if emitted at high altitudes. Hofmann (1991) reported observations that show an increase of non-volcanic stratospheric sulfate aerosol of about 5% per year. He suggests that if about 1/6 of the Northern Hemisphere air traffic takes place directly in the stratosphere and if a small fraction of other emissions above 9 km would enter the stratosphere through dynamical processes, then the jet fleet appears to represent a large enough source to explain the observed increase. On the other hand, Bekki and Pyle (1992) conclude from a model study that although aircraft may represent a substantial source of sulfate below 20 km, the rise in air traffic is insufficient to account for the observed 60% increase in large stratospheric aerosol particles over the 1979-1990 period. Sulfate particles generated from SO_x may also contribute to nucleation particles (Arnold *et al.*, 1994a). Whitefield *et al.* (1993) find a positive correlation between sulfur content and CCN efficiency of particles formed in jet engine combustion.

The possible enhancement of aerosol surface area may affect the nighttime chemistry of the nitrogen oxides. The heterogeneous reaction of N_2O_5 (and possibly NO_3) on aerosol surfaces will reduce the concentration of photochemically active NO_x during the day, giving rise to lower ozone and OH concentrations in the upper troposphere (Dentener and Crutzen, 1993).

11.5 MODEL PREDICTIONS OF AIRCRAFT EFFECTS ON ATMOSPHERIC CHEMISTRY

The first investigations concerning the potential effects of supersonic aircraft on the ozone layer were conducted in the 1970s. Early assessments were obtained using one-dimensional (1-D) photochemical models; more recent assessments rely on 2-D models (*e.g.*, Stolarski and Wesoky, 1993b). In addition, the transport in 2-D models has been compared to 3-D model transport by examining the evolution of the distribution of passive tracers.

11.5.1 Supersonic Aircraft

Evaluations of the effects of the emissions of the HSCT on the lower stratosphere have used two-dimensional (2-D) models. These are zonally averaged (latitude-height) models and are discussed in detail in Chapter 6. For use in such 2-D models, both the source of exhaust and the emission transport (both horizontal and vertical) are zonally averaged. In fact, the source of emissions is not zonally symmetric, as HSCT flight is expected to be restricted to oceanic corridors. Furthermore, the transport processes through which trace species are removed from the stratosphere are not well represented by a zonally averaged model. Stratosphere-troposphere exchange processes (STE) occur preferentially near jet-systems, above frontal perturbations, and during strong convection in tropical regions. The two former processes may transport effluents released by HSCTs irreversibly to lower levels and lead to tropospheric sinks. Effluents may be rapidly advected also to lower latitudes by large-scale motions. Such processes are poorly represented in 2-D models. The horizontal scale for STE is small and can only be represented using 3-D models with high resolution. These small scales are not explicitly resolved in most global 3-D models. Thus, any use of a 3-D model to evaluate the use of a 2-D model for these assessments must include a critical evaluation of the 3-D model STE. 2-D models do have the practical advantage that it is possible to complete many

assessment calculations, using a reasonably complete representation of stratospheric chemistry, and also by considering the sensitivity of the results to model parameters one can take some aspects of feedbacks among atmospheric processes into account.

Current 3-D models, though impractical for full chemical assessments, are practical for calculations that consider the transport of aircraft exhaust, which is treated as a passive tracer. Such calculations have been compared directly with 2-D models (Douglass *et al.*, 1993; Rasch *et al.*, 1993). Their results show that for seasonal simulations, provided that the residual circulation derived from the 3-D fields is the same as used in the 2-D calculation, the tracer is dispersed faster vertically and has similar horizontal spread for 3-D compared with 2-D calculations. Although the tracer is also transported upward more rapidly in 3-D than in 2-D (where vertical upward transport is minimal), the more rapid downward transport is the more pronounced effect. Accumulation of aircraft exhaust in flight corridors is found in regions of low wind speed, but only a small number of typical corridors (North Atlantic, North Pacific, and tropical) have been considered. The effect of such local accumulation would be largest if a threshold chemical process such as particle formation is triggered at high concentration of aircraft exhaust constituents. In 2-D models that use residual mean formulation, transport to the troposphere takes place principally through two mechanisms: advective transport by the residual mean circulation (mostly at middle to high latitudes) and diffusive transport across the tropopause (all latitudes). The latter is largest where the 2-D model's tropopause height is discontinuous (to represent the downward slope of the tropopause from the tropics to middle and polar latitudes) (Shia *et al.*, 1993). The difference in the character of STE in 2-D and 3-D models leads to different sensitivities to the latitude at which exhaust is injected in the models. For the 3-D model, the atmospheric lifetime of a tracer species is relatively insensitive to the latitude of injection. For the 2-D model, the tracer species lifetime is much longer for injection at lower latitudes than at higher latitudes, since transport to higher latitudes must take place before most of the pollutant is removed from the stratosphere.

Treatments of the transport and photochemistry used in 2-D models have been examined through a series of model intercomparisons and comparisons with observations (Jackman *et al.*, 1989b; Prather and Remsberg, 1993). Model results for a "best" simulation, as well as for various applications and constrained calculations, were compared with each other and with observations. There are significant differences in the models that lead to differences in the model assessments as discussed below. In addition, there are some features, such as the very low observed values of N_2O and CH_4 in the upper tropical stratosphere, and the NO_y/O_3 ratio at tropical latitudes, that are not well represented by all 2-D models.

There are also many areas of agreement between models and observations that suggest that an evaluation of the effects of the HSCT may be an appropriate use of these models. For example, the models' total ozone fields show general consistency when compared with observed fields such as Total Ozone Mapping Spectrometer (TOMS) data, the overall vertical and latitudinal distributions of such species as N_2O, CH_4, and HNO_3, and the ozone climatology that is based on Stratospheric Aerosol and Gas Experiment (SAGE) and Solar Backscatter Ultraviolet (SBUV) observations. If the SAGE results for O_3 loss over the past decade at altitudes just above the tropopause are correct (see Chapter 1), however, then the inability of present models to reproduce this O_3 decrease (see Chapter 6) casts doubt on their ability to correctly model aircraft effects in this important region.

At the beginning of the NASA HSRP/AESA program, the assessment models contained only gas phase photochemical reactions. The importance of the heterogeneous reaction (temperature independent) $N_2O_5 + H_2O \rightarrow 2\ HNO_3$ on the surface of stratospheric aerosols was noted by Weisenstein *et al.* (1991) and Bekki *et al.* (1991) and has been further explored by Ramaroson and Louisnard (1994). This process changes the balance between the reactive nitrogen species, NO and NO_2 (NO_x), and the reservoir species, HNO_3. For gas phase evaluations, lower stratospheric ozone was most sensitive to the amount of NO_x from aircraft exhaust injected into the lower stratosphere. For evaluations including this heterogeneous process, the NO_x levels in both the base atmosphere and in the perturbed atmosphere are much lower than in the gas phase evaluations, and the calculated ozone change is greatly reduced (Ko and Douglass, 1993).

2-D models have also been used to examine other processes that are of potential significance. For example,

Table 11-4. Calculated percent change in the averaged column content of ozone between 40°N and 50°N.

Scenarios	AER	GSFC	LLNL	OSLO	CAMED	NCAR
I: Mach 1.6, NO_x EI=5*	-0.04	-0.11	-0.22	+0.04	+0.69	-0.01
II: Mach 1.6, NO_x EI=15*	-0.02	-0.07	-0.57	+0.15	+0.48	-0.60
III: Mach 2.4, NO_x EI=5*	-0.47	-0.29	-0.58	-0.47	+0.38	-0.26
IV: Mach 2.4, NO_x EI=15*	-1.2	-0.86	-2.1	-1.3	-0.45	-1.8
V: Mach 2.4, NO_x EI=15**	-2.0	-1.3	-2.7	-0.42	-1.1	-2.3
VI: Mach 2.4, NO_x EI=45*	-5.5	-4.1	-8.3	-3.5	-2.8	-6.9

Table 11-5. Calculated percent change in the averaged column content of ozone in the Northern Hemisphere.

Scenarios	AER	GSFC	LLNL	OSLO	CAMED	NCAR
I: Mach 1.6, NO_x EI=5*	-0.04	-0.12	-0.18	+0.02	+0.63	-0.04
II: Mach 1.6, NO_x EI=15*	-0.02	-0.14	-0.48	+0.10	+0.63	-0.54
III: Mach 2.4, NO_x EI=5*	-0.42	-0.27	-0.50	-0.39	+0.25	-0.25
IV: Mach 2.4, NO_x EI=15*	-1.0	-0.80	-1.8	-1.0	-0.26	-1.5
V: Mach 2.4, NO_x EI=15**	-1.7	-1.2	-2.3	-0.43	-0.80	-1.9
VI: Mach 2.4, NO_x EI=45*	-4.6	-3.6	-7.0	-3.1	-2.1	-5.1

* Relative to a background atmosphere with chlorine loading of 3.7 ppbv, corresponding to the year 2015

** Relative to a background atmosphere with chlorine loading of 2.0 ppbv, corresponding to the year 2060

if HSCT planes are flown, the lower stratospheric levels of total odd nitrogen and water vapor are expected to rise. In addition to a general increase over background levels throughout the lower stratosphere, there is a possibility for large enhancements in areas of high traffic (air "corridors"). Peter *et al.* (1991) and Considine *et al.* (1993) have considered the possibility that the increases in H_2O and in HNO_3 (a consequence of the heterogeneous conversion of NO_x) will lead to an increase in the amount of nitric acid trihydrate (NAT) cloud formation. They indeed find this to be so.

The evaluation of the effects of a future fleet of supersonic aircraft on stratospheric ozone was made by Johnston *et al.* (1989) and by Ramaroson (1993) using gas phase models. The ozone loss for an injection at a fixed level was found to increase nearly linearly as the amount of NO_x injected was increased. The ozone loss was found to be larger for injection at higher levels because the ozone response time decreases with altitude, and because the pollutant has a longer stratospheric lifetime when injected farther from the model tropopause.

Jackman *et al.* (1989a) used a 2-D model to test the dependence of the supersonic aircraft assessments on model dynamical inputs. As anticipated, the calculated change in ozone is larger (smaller) for a slower (faster) residual circulation because the circulation controls the magnitude of the steady-state stratospheric NO_x perturbation. This paper also showed that the annual cycle of the zonally averaged total ozone is sensitive to the annual cycle in the residual circulation. A similar sensitivity to the residual circulation has been demonstrated for a 3-D calculation using winds from a data assimilation procedure for transport (Weaver *et al.*, 1993).

The supersonic aircraft assessment scenarios discussed here are for Mach numbers 1.6 and 2.4, which correspond to the two aircraft cruise altitudes 16 km and 20 km, respectively, and for three values for EI(NO_x) (see Stolarski and Wesoky [1993b] for specific details). The emission indices are given in Table 11-1. The calculated total ozone changes are given for each participating model in Table 11-4 for the calculated annually averaged column ozone change in the latitude band where the aircraft emissions are largest (40°-50°N), and in Table 11-5 for the Northern Hemisphere average. The model calculations use an aerosol background similar to that observed in 1979 (*e.g.*, before the Mt. Pinatubo eruption). Some similarities and differences are seen among the model results. For all of the models, the ozone change for Mach 2.4 is more negative than that for Mach 1.6. The ozone change at Mach 2.4 is more negative as the EI is increased, but the change is more rapid than a linear change. The complexity of the assessment is capsulated by the change in ozone calculated at Mach 1.6 for the two different EIs in Table 11-4. For all models,

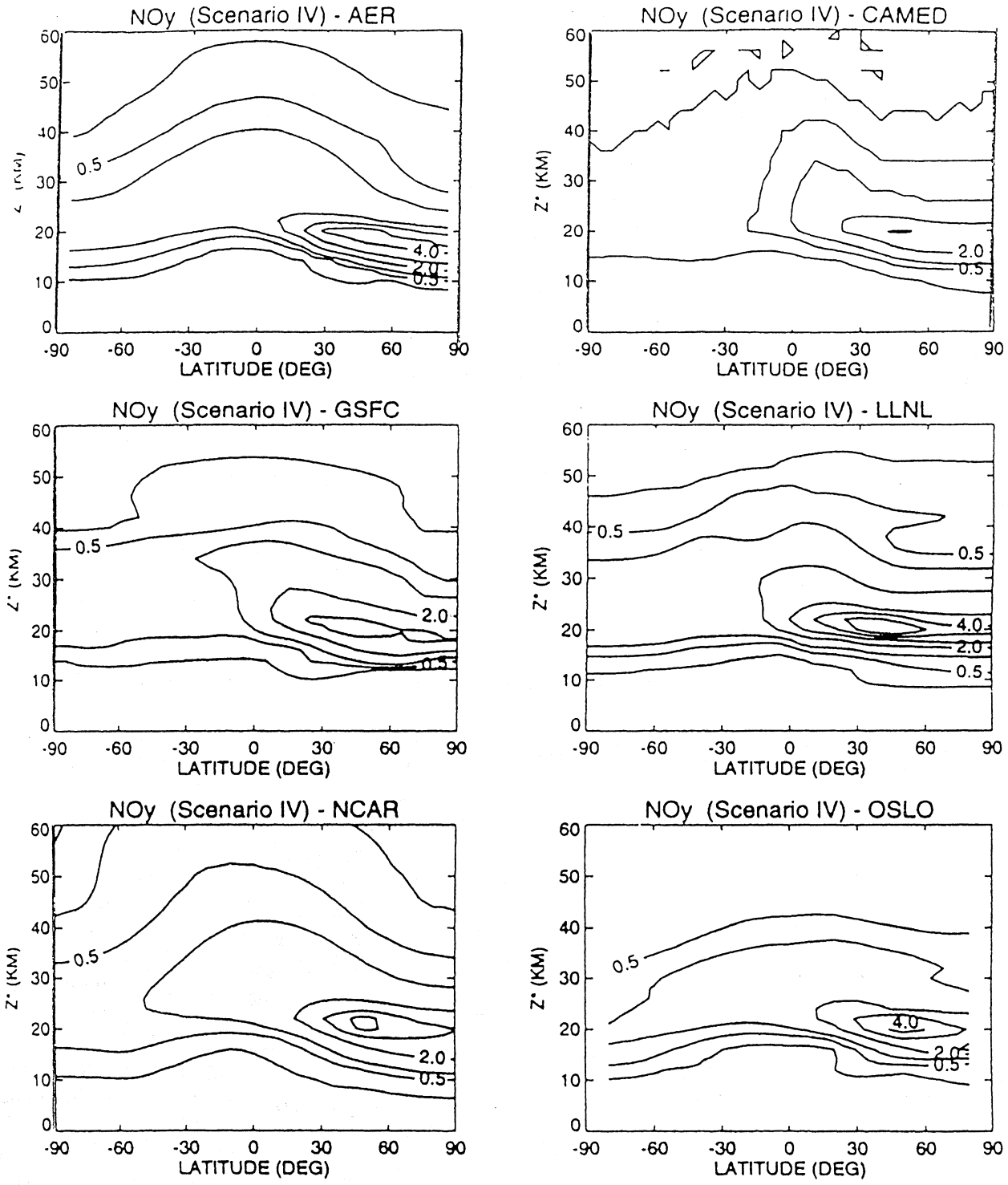

Figure 11-6. Calculated changes in the local concentration of NO_y (ppbv) in June for Mach 2.4 ($EI(NO_x)=15$) case. The contour intervals are 1 ppbv, 2 ppbv, 3 ppbv, 4 ppbv, and 5 ppbv (Stolarski and Wesoky, 1993b).

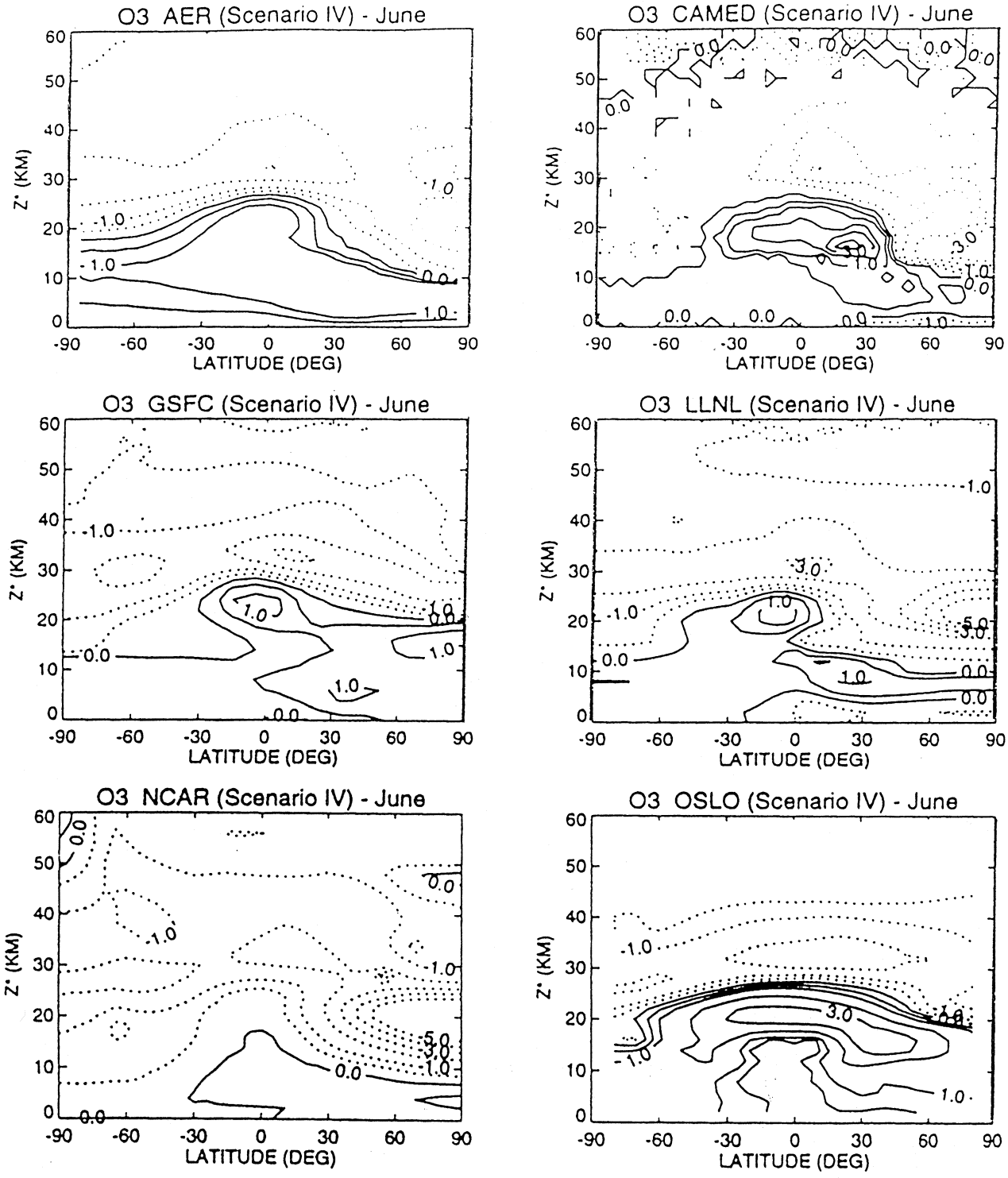

Figure 11-7. Model-calculated percent change in local ozone for June for Mach 2.4 ($EI(NO_x)$=15) fleet in the 2015 atmosphere. The contour intervals are -4%, -3%, -2%, -1%, -0.5%, 0%, 0.5%, 1%, 2%, 3%, 4% (Albritton *et al.*, 1993).

and for both cases at ClO_x mixing ratios of 3.7 ppbv, the changes are less than 1%. For three of the models (Atmospheric and Environmental Research, Inc., AER; Goddard Space Flight Center, GSFC; and the University of Oslo, OSLO), the ozone change is less negative (more positive) for EI = 15 than for EI = 5. For the other three models (Lawrence Livermore National Laboratory, LLNL; the University of Cambridge and the University of Edingburgh, CAMED; and the National Center for Atmospheric Research, NCAR), the ozone change is more negative (less positive) for the larger emission index.

The assessment initiated by the "Comite Avion-Ozone" shows similar results. A 2-D model including heterogeneous reactions on aerosol and PSC surfaces and a similar emission scenario to that for the HSRP assessments shows a global mean decrease of total ozone of 0.3% (Ramaroson and Louisnard, 1994). The results depend upon the prescribed background atmosphere (*e.g.*, aerosol loading) used (see also: Tie *et al.*, 1994; Considine *et al.*, 1994).

The change in NO_y is given in Figure 11-6 for each of the models for a scenario in which the HSCT fleet is assumed to fly at Mach 2.4 with an $EI(NO_x) = 15$ and a background chlorine mixing ratio of 3.7 ppbv. This NO_y change indicates the sensitivity to the different transport. LLNL has the largest change in NO_y, and also the largest global ozone changes in Tables 11-4 and 11-5. However, the calculated global changes are clearly not ordered by the magnitude of the NO_y change. The latitude height change in ozone for each of the models is given in Figure 11-7. There are remarkably large differences in the local ozone changes, particularly in the upper troposphere/lower stratosphere region where the aircraft emissions produce an increase in the ozone production as well as an increase in the ozone loss. Although changes in NO_x have the largest impact on O_3, the effects from H_2O emissions contribute to the calculated O_3 changes (about 20%).

The assessment models' representation of upper tropospheric chemistry was not considered as a part of the Models and Measurements Workshop (Prather and Remsberg, 1993). Further attention must be paid to the upper tropospheric chemistry to understand the spread in the results for these assessments. This subject is discussed in the following section on the evaluation of the impact of the subsonic fleet.

11.5.2 Subsonic Aircraft

The Chapter 7 discussions indicate that tropospheric photochemical-dynamic modeling is much less developed than is this type of stratospheric modeling; however, several types of models have been used to assess the impact of subsonic aircraft emissions. These include global photochemistry and transport models in latitude-height dimensions ignoring the longitudinal variation of emissions. This is an important drawback for species with short lifetimes. Another type of model used is the longitude-height model that addresses a restricted range of latitudes. They neglect the effect of latitudinal transport. Three-dimensional global dynamical models are being developed to study the impact of aircraft emissions, but the results from these models are as yet restricted to NO_x and NO_y species. The published results from two-dimensional models have used a range of estimates to represent present and future aircraft emissions, and consequently, the results are not easily comparable. There have been no organized efforts to intercompare models for subsonic aircraft as there have been for the supersonic aircraft problem.

The sensitivity of modeled ozone concentrations to changes in aircraft NO_x emissions has been found to be much higher than for surface emissions, with around twenty times more ozone being created per unit NO_x emission for aircraft compared to surface sources (Johnson *et al.*, 1992). Several authors have investigated the role of hydrocarbon and carbon monoxide emissions from aircraft on ozone concentrations, but have found small effects (Beck *et al.*, 1992; Johnson and Henshaw, 1991; Wuebbles and Kinnison, 1990). The increase in net ozone production with increasing NO_x is steeper at lower concentrations of NO_x (Liu *et al.*, 1987), and therefore larger ozone sensitivities are expected for emissions to the Southern Hemisphere, where NO_x concentrations are lower (Johnson and Henshaw, 1991). Beck *et al.* (1992) note the influence of lightning production of NO_x in controlling the sensitivity of ozone to aircraft NO_x emissions. These studies indicate the importance of predicting a realistic background NO_x concentration, and underline the importance of measurements in model testing.

Several recent publications (Johnson and Henshaw, 1991; Wuebbles and Kinnison, 1990; Fuglestvedt *et al.*, 1993; Beck *et al.*, 1992; Rohrer *et al.*, 1993) esti-

mate the percentage increases in ozone concentrations due to the impact of aircraft emissions. The results show maximum increases at around 10 km of between 12% and 4% between 30° and 50°N.

NO_x concentrations in the upper troposphere are controlled by the transport of NO_x downwards from the stratosphere, by aircraft and lighting emissions, and by the convection of NO_x from surface sources (Ehhalt *et al.*, 1992). The available measurements of NO_x in the free troposphere are discussed in Chapter 5. There are a number of observations where the vertical NO profile is strongly and unequivocally influenced by one or the other of these sources, *e.g.*, lightning (Chameides *et al.*, 1987; Murphy *et al.*, 1993), aircraft emissions (Arnold *et al.*, 1992), fast vertical transport (Ehhalt *et al.*, 1993), which makes it clear that all these sources can and do make a contribution to the NO_x in the upper troposphere. An example is given in Figure 11-8, which presents the daytime NO distribution across the North Atlantic during the period June 4-6, 1984, of the Stratospheric Ozone (STRATOZ III) campaign (Ehhalt *et al.*, 1993). Large longitudinal gradients of NO mixing ratio up to a factor of 5 were observed at all altitudes in the free troposphere in which the effects of an outflow of polluted air from the European continent are seen. This tongue of high NO over the Eastern Atlantic was accompanied by elevated CO and CH_4 mixing ratios and therefore was probably due to surface sources. Figure 11-8 also illustrates the variance superimposed by longitudinal gradients on average meridional cross sections. However, at present there are not enough data to derive the respective global contributions from atmospheric measurements alone. Independent estimates of the various source strengths are needed. Our lack of knowledge about the NO_x budget in the troposphere, especially in the upper troposphere, makes model predictions for this region questionable. Thus, at present, we can have little confidence in our ability to correctly model subsonic aircraft effects on the atmosphere.

Figure 11-9 shows published comparisons of available NO measurements (Wahner *et al.*, 1994) with predictions from two-dimensional models (Berntsen and Isaksen, 1992). Using a quasi-two dimensional longitude-height model and considering estimates of all important tropospheric sources of NO_x (input from the stratosphere, lightning, fossil fuel combustion, soil emissions and aircraft) for the latitude band of 40°-50°N (see

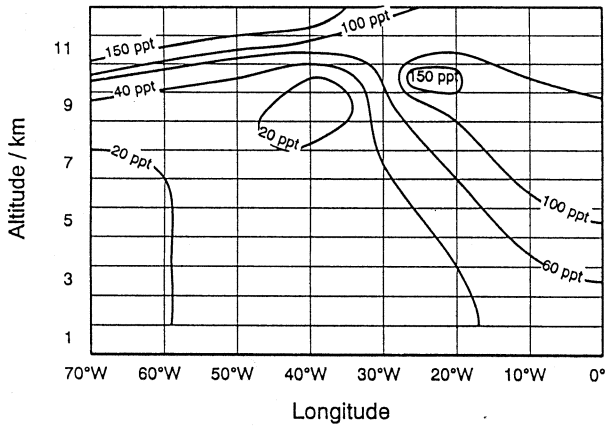

Figure 11-8. Daytime NO mixing ratio distribution (altitude vs. longitude) across the North Atlantic during the period June 4-6, 1984, of the STRATOZ III campaign. (Based on Ehhalt *et al.*, 1993.)

Figure 11-10), Ehhalt *et al.* (1992) could reproduce quite reasonably the measured vertical profiles shown in Figure 11-9. The transport of polluted air masses from the planetary boundary layer to the upper troposphere by fast vertical convection is considered an important process for NO_x by these authors. However, Kasibhatla (1993) suggests that the stratospheric source is a more important source than that arising from rapid vertical convection, but the calculations did not consider lightning, biomass burning, and soil emissions, and the heterogeneous removal of N_2O_5.

Despite considerable differences in model transport characteristics and emission rates, all the studies suggest that aircraft are important contributors to upper tropospheric NO_x and NO_y concentrations. For example Ehhalt *et al.* (1992) suggest that aircraft emissions (estimated for 1984) contribute around 30% to upper tropospheric NO_x (Figure 11-10). Kasibhatla (1993) estimates that about 30% of the NO_x in the upper troposphere between 30° and 60°N are from aircraft. It is clear from the results of Beck *et al.* (1992) and Kasibhatla (1993) that despite large latitudinal variations in the rate of aircraft emissions, the impacts become manifest over the entire zonal band, though not evenly. This behavior is in contrast to the behavior in the lower troposphere, and is due to the slower conversion of NO_x to form HNO_3, and the slower removal rates for HNO_3, which allow for reconversion back to NO_x.

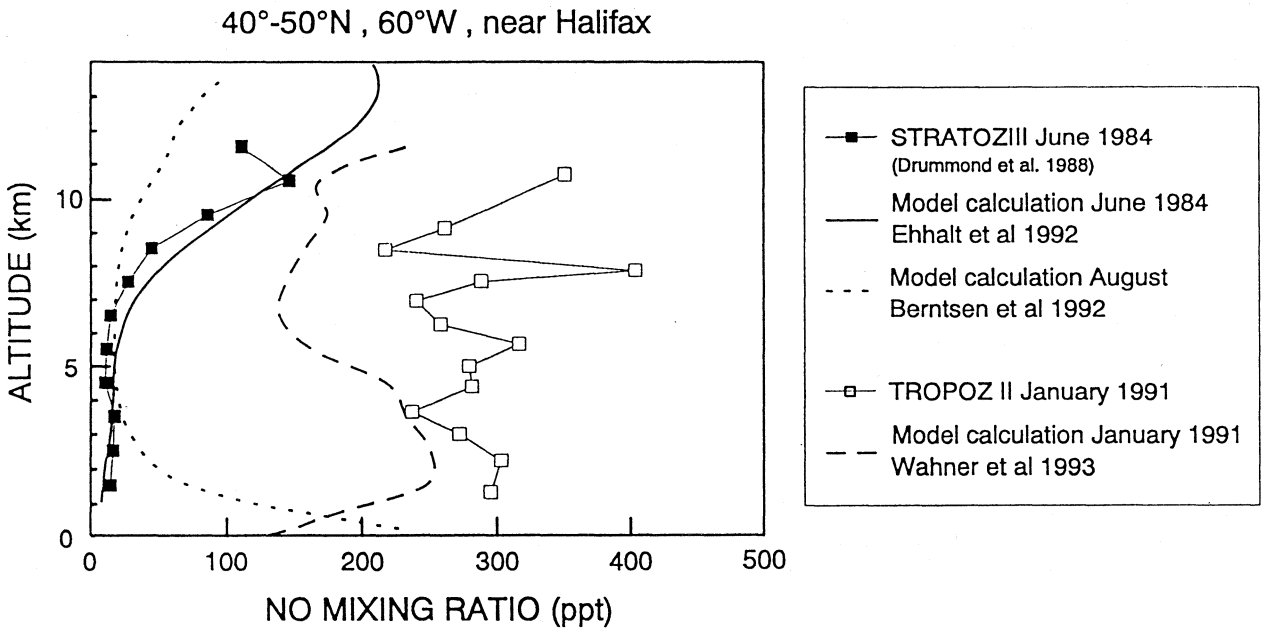

Figure 11-9. Comparisons of measured vertical profiles of NO (June 1984 and January 1991) with calculations from two-dimensional models. (Based on data from: Wahner *et al.*, 1994; Berntsen and Isaksen, 1992; Drummond *et al.*, 1988.)

Several authors discuss the changes to OH concentration consequent to the growth in ozone, and the consequences to methane destruction. Beck *et al.* (1992) predicts OH changes of +10% at around 10 km for the region 30°-60°N. Similar values are suggested by Fuglestvedt and Isaksen (1992) (+20%) and Rohrer *et al.* (1993) (+12%). These subsonic aircraft results should be considered as being preliminary given the complexity of the models, the lack of model intercomparison exercises, as well as the paucity of measurements to test against model results.

11.6 CLIMATE EFFECTS

Both subsonic and supersonic aircraft emissions include constituents with the potential to alter the local and global climate. Species important in this respect include water vapor, NO_x (through its impact on O_3), sulfur, soot, cloud condensation nuclei, and CO_2. However, quantitative assessments of the climate effects of aircraft operations are difficult to make at this time, given the uncertainty in the resulting atmospheric composition changes, as well as uncertainties associated with the climate effects themselves. Therefore, the following discussion will be on possible mechanisms by which aircraft operations might affect climate, along with some estimates of their relative importance.

Increases of CO_2 and water vapor, and alterations of ozone and cirrus clouds have the potential to alter *in situ* and global climate by changing the infrared (greenhouse) opacity of the atmosphere and solar forcing. Sulfuric acid, which results from SO_x emissions, may cool the climate through producing aerosols that give increased scattering of incoming solar radiation, while soot has both longwave and shortwave radiation impacts. The direct radiative impact for the troposphere as a whole is largest for concentration changes in the upper troposphere and lower stratosphere, where the effectiveness is amplified by the colder radiating temperatures. However, the impact (including feedbacks) on surface air temperature may be limited if changes at the tropopause are not effectively transmitted to the surface (see Chapter 8).

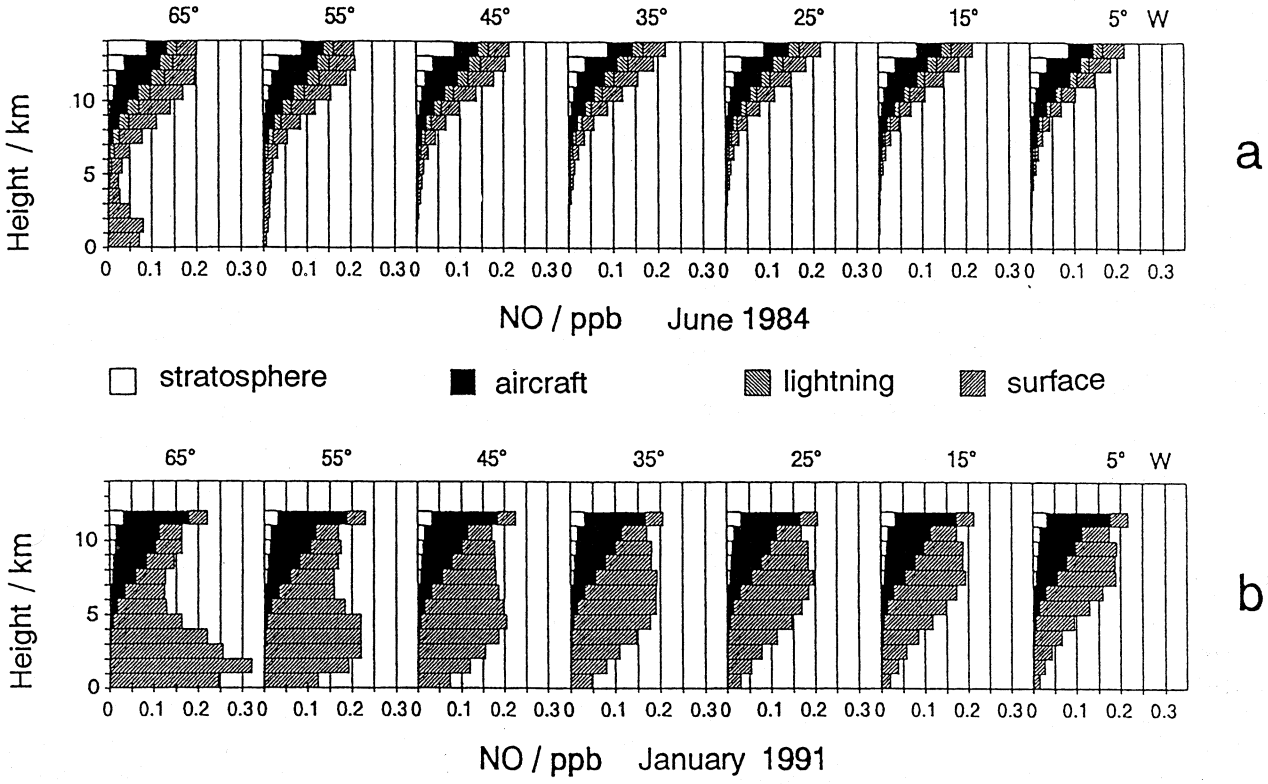

Figure 11-10. Calculations of vertical profiles of NO during summer (June, top panel) and winter (January, bottom panel) using a quasi-two dimensional longitude-height model for the latitude band of 40°-50°N. The different shadings relate to the different sources: stratosphere, lightning, surface (fossil fuel combustion and soil emissions), and aircraft (Ehhalt *et al.*, 1992).

11.6.1 Ozone

As has been discussed in Chapter 8, the impact of ozone changes on the radiation balance of the surface-troposphere system depends on the vertical distribution of the ozone changes. Reduction in tropospheric and lower stratospheric ozone tends to cool the climate, by reducing the atmospheric greenhouse effect. Reduction in middle and upper stratospheric ozone tends to warm the climate, by allowing more shortwave radiation to reach the surface (Lacis *et al.*, 1990).

The preliminary assessments of the HSRP/AESA program are that supersonic aircraft operations could decrease ozone in the lower stratosphere by less than 2 percent for an EI(NO_x) of 15, while increasing it in the upper troposphere by a similar percentage. When these ozone changes were put into the NASA Goddard Institute for Space Studies (GISS) 3-D climate/middle atmosphere model (Rind *et al.*, 1988), the resulting change in global average surface air temperature was approximately -0.03°C. The net result is a consequence of the net effect of varying influences: ozone reduction in the stratosphere at 20 km, and ozone increases in the upper troposphere produce surface warming, while ozone reduction in the lower stratosphere produces surface cooling. The net result provides the small temperature changes found in this experiment.

Assuming a local ozone increase (8 to 12 km, 30° to 50°N) of 4 - 7% due to doubling of the subsonic aircraft NO_x emission and incorporating these changes into the Wang *et al.* (1991) model, the inference can be drawn that a radiative forcing of 0.04 to 0.07 W m^{-2} will result (Mohnen *et al.*, 1993; Fortuin *et al.*, 1994). This radiative forcing is of the same order as that resulting from the aircraft CO_2 emissions (see Chapter 8.2.1). The estimated feedback on radiative forcing from methane

decreases (due to the OH increase from increasing NO_x) has been estimated to be small using two-dimensional models (Johnson, 1994; Fuglestvedt *et al.*, 1994).

11.6.2 Water Vapor

Water vapor is the primary atmospheric greenhouse gas. Increases in water vapor associated with aircraft emissions have the potential to warm the climate at low tropospheric levels, while cooling at altitudes of release, due to greater thermal emission. The effects are largest when water vapor perturbations occur near the tropopause (Graßl, 1990; Rind and Lacis, 1993), as is likely to be the case.

High-speed aircraft may increase stratospheric water vapor by up to 0.8 ppmv for a corridor at Northern Hemisphere midlatitudes, with a Northern Hemispheric effect perhaps 1/4 as large (Albritton *et al.*, 1993). When changes of this magnitude were used as input to the stratosphere, the GISS climate/middle atmosphere model failed to show any appreciable surface warming, as the radiative effect of the negative feedbacks (primarily cloud cover changes) were as important as the stratospheric water forcing. In general, the stratosphere cooled by a few tenths of a degree, associated with the increased thermal emission.

Subsonic tropospheric emissions of water vapor could possibly result in increases on the order of 0.02 ppmv. Shine and Sinha (1991) estimate that a global increase of 1 ppmv for a 50 mbar slab between 400 and 100 mbar would increase surface air temperature by 0.02°C. Therefore the climate effects from subsonic water vapor emission by aircraft seem to be very small.

11.6.3 Sulfuric Acid Aerosols

Subsonic aircraft, flying both in the troposphere and stratosphere, are presently adding significant amounts of sulfur to the atmosphere. Hofmann (1991) has estimated that the current fleet may be contributing about 65% of the background non-volcanic stratospheric aerosol amount, whose optical thickness is approximately $1 - 2 \times 10^{-3}$; note however, that this view is a controversial one as can be seen in Section 3.2.1 of Chapter 6. This added optical thickness would imply a contribution to the equilibrium surface air temperature cooling on the order of 0.03°C due to aircraft sulfur emissions (Pollack *et al.*, 1993).

11.6.4 Soot

Particles containing elemental carbon are the result of incomplete combustion of carbonaceous fuel. Such particles have greater shortwave absorbing characteristics than do sulfuric acid aerosols, and thus a different shortwave/longwave impact on net radiation. Upper tropospheric aircraft emissions of soot presently account for about 0.3% of the background aerosol (Pueschel *et al.*, 1992).

The total soot source for the stratosphere is currently estimated as 0.001 teragrams/year (Stolarski and Wesoky, 1993b), most likely coming primarily from commercial air traffic. This accounts for about 0.01% of the total stratospheric (background) aerosol loading (Pueschel *et al.*, 1992). It is estimated that the proposed HSCT fleet would double stratospheric soot concentrations for the hemisphere as a whole, while increases of up to a factor of ten could occur in flight corridors (Turco, 1992).

11.6.5 Cloud Condensation Nuclei

Contrails in the upper atmosphere act in a manner somewhat similar to cirrus clouds, with the capability of warming the climate by increasing longwave energy absorption in addition to the shortwave cooling effect. Aircraft sulfur emissions in addition to frozen droplets are the most likely contributor to this "indirect" effect of aerosols, but soot might also be important.

The impact of aircraft particle emissions on upper tropospheric cloud amounts and optical processes is not yet known, though it is likely to grow with increased air traffic. Changes in cloud cover and cloud optical thickness resulting from aircraft operations might be the most significant aircraft/climate effect, but quantitative evaluations of this are very uncertain. In a 2-D analysis, increases in cirrus clouds of 5% between 20-70°N produced a warming of 1°C, due to increased thermal absorption (Liou *et al.*, 1990). For 0.4% additional cloud coverage by contrails and mid-European conditions, an increase in surface temperature of about 0.05°C is estimated (Schumann, 1994).

11.6.6 Carbon Dioxide

While aircraft CO_2 emissions are at a different altitude from other anthropogenic emissions, the climate

impact should be qualitatively similar, as CO_2 is a relatively well-mixed gas. Therefore the climate impact from subsonic CO_2 emissions can be estimated to be approximately 3% of the total anthropogenic CO_2 impact, since subsonic aircraft fuel consumption is about 3% of the global fossil fuel consumption.

11.7 UNCERTAINTIES

This chapter deals with the atmospheric effects of both the present subsonic aircraft fleet and an envisioned future supersonic aircraft fleet. The uncertainties in assessing these two atmospheric effects are of a different nature. For instance, there is a real uncertainty in the present emissions data base that results from uncertainties in the aircraft engine characteristics, engine operations, and air traffic data. There are also uncertainties relating to the models being used to examine the atmospheric effects of these subsonic emissions. In the supersonic case, assessments are being made for a hypothetical aircraft fleet, so modeling uncertainties are the main concern. The modeling uncertainties are probably much greater than the emission uncertainties at the present time.

11.7.1 Emissions Uncertainties

As was indicated previously, the evaluation of a time-dependent emissions data base for use in atmospheric chemical-transport models requires a rather complete knowledge of the specific emissions produced by all types of aircraft, as well as a knowledge of the operations and routing of the aircraft fleet.

There has been very limited aircraft engine testing under realistic cruise conditions for the present subsonic aircraft fleet. At the present time, some engine tests are being carried out under simulated altitude conditions to see if the present method of determining NO_x, for example, from a combination of theoretical studies and laboratory combustor testing can be validated.

A disagreement exists between the quantity of fuel produced and predicted fuel usage by the data bases. This discrepancy probably results from uncertainties in emissions for the non-OECD (Organization for Economic Cooperation and Development) countries and for military traffic, and from the uncertain estimates of loading and power settings of the aircraft fleet.

11.7.2 Modeling Uncertainties

There are two types of modeling uncertainties in the aircraft assessment process. One is related to modeling of small-scale plume processes, while the other relates to the global atmospheric modeling.

Plume Modeling

As was indicated earlier in this chapter, considerable modeling is required to characterize the evolution of the aircraft exhaust leaving the engines' tailpipes to flight corridor spatial scales and then to the scales that are treated in the atmospheric models of aircraft effects. These plume models must treat turbulent dynamics and both gas phase and heterogeneous chemistry. Only one such model presently exists that treats the full problem and there exists no measurement program that is aimed at the validation of this model (Miake-Lye *et al.*, 1993). There have been very few actual measurements in airplane exhaust wakes. There are the chemical measurements at altitudes of about 10 km by Arnold *et al.* (1992), and there were turbulence and humidity data taken by Baumann *et al.* (1993) at the same time. Also, there are the SPADE (Stratospheric Photochemistry, Aerosols, and Dynamics Expedition) measurements taken during crossings of the ER-2 exhaust plume (Fahey *et al.*, 1994). These measurements, while valuable, are not sufficient to validate the plume processing model.

Atmospheric Modeling

The upper troposphere and lower stratosphere, the regions of major interest in this chapter, are particularly difficult regions to model. In 2-D models of supersonic aircraft effects, the meridional transport circulation is difficult to obtain since the radiative heating is comprised of a number of small terms of different sign. Thus, small changes in any radiation term can have important consequences for transport. Similarly, the time scales for both transport and chemistry to modify the ozone distribution are generally long and comparable. The complete problem must be solved. The NO_x, HO_x, and ClO_x chemical processes are highly coupled in the stratosphere. Modeling the chemical balance correctly, in regions where few measurements are available, presents formidable difficulties. This situation is even worse in the upper troposphere than in the stratosphere, given that

the chemistry of the upper troposphere is more complex and there are fewer existing observations of this region.

Supersonic aircraft have their cruising altitudes in the middle stratosphere (near 20 km) while subsonic aircraft have cruise altitudes that lie both in the troposphere and lower stratosphere. Supersonic assessment calculations have been done using 2-D models up to the present time, while it is generally appreciated that 3-D models will be necessary for credible subsonic assessments. Thus, separate discussions of modeling uncertainties follow for aircraft perturbations in the stratosphere and in the troposphere.

Transport

Two particular problems relating to atmospheric transport are extremely important for the supersonic aircraft problem. First, stratosphere-troposphere exchange, which cannot be modeled in detail with great confidence in global (2-D or 3-D) models, is clearly of special significance to the chemical distribution in these regions, to the lifetime of emitted species, etc. More work on this topic is essential. Second, the present 2-D assessment models do not model well the details of the polar vortex, although improvements are anticipated when these models include the Garcia (1991) parameterization for breaking planetary waves. If the ideas of the polar vortex as a "flowing processor" are correct (see Chapter 3), then the correct modeling of polar vortex dynamics will have a crucial impact on the distribution of species in the lower stratosphere, and present 2-D models would clearly be performing poorly there. There is also the larger issue that the uncertainty connected with the use of 2-D models to assess the inherently 3-D aircraft emission problem needs to be evaluated further. Even when 3-D models are available to model this problem, however, the question will remain as to how well these 3-D models simulate the actual atmosphere until adequate measurement-model comparisons are done.

For modeling aimed at assessing the atmospheric effects of both subsonic and supersonic aircraft, it is crucial to properly model ambient NO_x distributions in the upper troposphere, and these, in turn, depend on properly modeling transport between the boundary layer and the free troposphere, on proper modeling of the fast upward vertical transport accompanying convection, and on modeling the lightning source for NO_x. Considerable effort is needed to improve our capability in these areas. It is also necessary to model stratospheric-tropospheric transport processes carefully so that NO_x fluxes and concentrations in the region near the tropopause are realistic. This requires a substantial effort to improve our understanding of stratosphere-troposphere exchange processes.

Chemical Changes

The effect of NO_x emitted by subsonic aircraft depends on the amount of NO_x in the free troposphere. The ambient NO_x concentrations are not very well known, and depend on several factors such as surface emission from anthropogenic and natural biogenic sources, the strength of the lightning source for NO_x, and the transport of stratospheric NO_x into the troposphere (see Chapter 2, Table 2-5). The inclusion of wet and dry deposition processes and entrainment in clouds in assessment models is at a very preliminary stage.

Heterogeneous chemistry is another important area of uncertainty for models of the troposphere and lower stratosphere. For example, the hydrolysis of N_2O_5 is important in both the troposphere and stratosphere, but the precise rate for this reaction is not known. Observational studies are needed to elucidate the exact nature and area of the reactive surfaces. Furthermore, at the present time, heterogeneous chemistry is being crudely modeled. Although there do exist models describing the size distribution and composition of stratospheric aerosols, no aircraft assessment model presently exists that incorporates and calculates aerosol chemistry.

In supersonic assessment models, it is important to properly model the switch over (at some altitude) from NO_x-induced net ozone production to net ozone destruction. The precise altitude at which this switch over occurs differs from model to model, and this can lead to very different ozone changes in different models of supersonic aircraft effects. The different responses of the various models used in the HSCT/AESA assessment of the impact of changed EI (see Tables 11-4 and 11-5, for example) point to important, unresolved differences in these models that must be addressed before a satisfactory assessment of the atmospheric effects of supersonic aircraft can be made with confidence. Also, it is clear from examining the modeled O_3 changes in Chapter 6 that the model results at altitudes below about 30 km differ significantly from one another. They also do not give as large O_3 losses as are observed (see Chapter 1). This

problem is particularly acute if one accepts the SAGE results indicating large decreases in ozone concentrations just above the tropopause (see Chapter 1) as being correct. Then, the fact that present stratospheric models do not correctly give this effect casts doubt on present assessment models to correctly simulate that atmospheric region. Since it is in this region where effects from aircraft operations are particularly significant, there is the question of how well we can correctly predict atmospheric effects in this altitude region. It may be that the SAGE ozone trends in this region are in error, or it may be that important effects in this region are not properly included in present models.

11.7.3 Climate Uncertainties

The study of the possible impact of aircraft on climate is now just beginning. One can make some preliminary extrapolations based on existing climate research, but one should appreciate that the complexity of climate research, in general, implies that it will be some time before great confidence can exist in estimates of aircraft impacts on climate.

11.7.4 Surprises

Early assessments of the impact of aircraft on the stratosphere varied enormously with time as understanding slowly improved. Our understanding of the lower stratosphere/upper troposphere region is still far from complete and surprises can still be anticipated, which may either result in greater or lesser aircraft effects on the atmosphere.

ACRONYMS

AER	Atmospheric and Environmental Research, Inc.
AERONOX	The Impact of NO_x Emissions from Aircraft upon the Atmosphere
AESA	Atmospheric Effects of Stratospheric Aircraft
ANCAT	Abatement of Nuisance Caused by Air Traffic
CAMED	University of Cambridge and University of Edingburgh
CEC	Commission of the European Communities
CIAP	Climatic Impact Assessment Program
ECAC	European Civil Aviation Conference
ECMWF	European Centre for Medium-Range Weather Forecasts
EI	Emission Index
GISS	NASA Goddard Institute for Space Studies
GSFC	NASA Goddard Space Flight Center
HSCT	High-Speed Civil Transport
HSRP	High Speed Research Program
ICAO	International Civil Aviation Organization
IEA	International Energy Agency
LLNL	Lawrence Livermore National Laboratory
LTO	Landing/Take-Off cycle
MOZAIC	Measurement of Ozone on Airbus In-service Aircraft
NASA	National Aeronautics and Space Administration
NCAR	National Center for Atmospheric Research
NRC	National Research Council
OECD	Organization for Economic Cooperation and Development
OSLO	University of Oslo
POLINAT	Pollution from Aircraft Emissions in the North Atlantic Flight Corridor
SAGE	Stratospheric Aerosol and Gas Experiment
SBUV	Solar Backscatter Ultraviolet spectrometer
SPADE	Stratospheric Photochemistry, Aerosols, and Dynamics Expedition
WMO	World Meteorological Organization

REFERENCES

Aeronautics, *Synopsis of Current Aeronautics Projects 1993,* Industrial and Materials Technologies Programme—Area 3, Aeronautics, CEC Brussels (ISBN 92-826-6442-2), 1993.

Albritton, D.L., *et al.*, *The Atmospheric Effects of Stratospheric Aircraft: Interim Assessment of the NASA High-Speed Research Program,* NASA Reference Publication 1333, NASA Office of Space Science and Applications, Washington, D.C., June 1993.

Appleman, H., The formation of exhaust condensation trails by jet aircraft, *Bull. Amer. Meteorol. Soc., 34,* 14-20, 1953.

Arnold, F., J. Scheidt, T. Stilp, H. Schlager, and M.E. Reinhardt, Measurements of jet aircraft emissions at cruise altitude I: The odd-nitrogen gases NO, NO_2, HNO_2 and HNO_3, *Geophys. Res. Lett., 19,* 2421-2424, 1992.

Arnold, F., J. Scheidt, T. Stilp, H. Schlager, and M.E. Reinhardt, Sulphuric acid emission by jet aircraft, submitted to *Nature*, 1994a.

Arnold, F., J. Schneider, M. Klemm, J. Scheid, T. Stilp, H. Schlager, P. Schulte, and M.E. Reinhardt, Mass spectrometric measurements of SO_2 and reactive nitrogen gases in exhaust plumes of commercial jet airliners at cruise altitude, in *Impact of Emissions from Aircraft and Spacecraft upon the Atmosphere,* Proc. Intern. Sci. Colloquium, Cologne, Germany, April 18-20, 1994, edited by U. Schumann and D. Wurzel, DLR-Mitt. 94-06, 323-328, 1994b.

Baumann, R., R. Busen, H.P. Fimpel, C. Kiemle, M.E. Reinhardt, and M. Quante, Measurements on contrails of commercial aircraft, in *Proceedings 8th Symp. Meteorol. Obs. and Instrum.*, Amer. Met. Soc., Boston, 484-489, 1993.

Beck, J.P., C.E. Reeves, F.A.A.M. de Leeuw, and S.A. Penkett, The effect of aircraft emissions on tropospheric ozone in the North hemisphere, *Atmos. Environ., 26A,* 17-29, 1992.

Bekki, S., and J.A. Pyle, 2-D assessment of the impact of aircraft sulphur emissions on the stratospheric sulphate aerosol layer, *J. Geophys. Res., 97,* 15839-15847, 1992.

Bekki, S., and J.A. Pyle, Potential impact of combined NO_x and SO_x emissions from future high speed civil transport on stratospheric aerosols and ozone, *Geophys. Res. Lett., 20,* 723-726, 1993.

Bekki, S., R. Toumi, J.A. Pyle, and A.E. Jones, Future aircraft and global ozone, *Nature, 354,* 193-194, 1991.

Berntsen, T., and I.S.A. Isaksen, Chemical-dynamical modelling of the atmosphere with emphasis on the methane oxidation, *Ber. Bunsenges. Phys. Chem., 96,* 241-251, 1992.

Boeing, *HSCT Study, Special Factors,* NASA Contractor Report 181881, 1990.

Chameides, W.L., D.D. Davis, J. Bradshaw, M. Rodgers, S. Sandholm, and D.B. Bai, An estimate of the NO_x production rate in electrified clouds based on NO observations from the GTE/CITE 1 fall 1993 field campaign, *J. Geophys. Res., 92,* 2153-2156, 1987.

CIAP Monograph 2, *Propulsion Effluents in the Stratosphere,* Climate Impact Assessment Program, DOT-TST-75-52, U.S. Department of Transportation, Washington, D.C., 1975.

Considine, D.B., A.R. Douglass, and C.H. Jackman, Effects of a parameterization of nitric acid trihydrate cloud formation on 2D model predictions of stratospheric ozone depletion due to stratospheric aircraft, submitted to *J. Geophys. Res.,* 1993.

Considine, D.B., A.R. Douglass, and C.H. Jackman, Sensitivity of 2D model predictions of ozone response to stratospheric aircraft, submitted to *J. Geophys. Res.,* 1994.

Danilin, M.Y., B.C. Krüger, and A. Ebel, Short-term atmospheric effects of high-altitude aircraft emissions, *Ann. Geophys., 10,* 904-911, 1992.

Danilin, M.Y., A. Ebel, H. Elbern, and H. Petry, Evolution of the concentrations of trace species in an aircraft plume: Trajectory study, *J. Geophys. Res., 99,* 18951-18972, 1994.

Dentener, F.J., and P.J. Crutzen, Reaction of N_2O_5 on tropospheric aerosols: Impact on the global distribution of NO_x, O_3, and OH, *J. Geophys. Res., 98,* 7149-7164, 1993.

Douglass, A.R., M.A. Carroll, W.B. Demore, J.R. Holton, I.S.A. Isaksen, H.S. Johnston, and M.K.W. Ko, The atmospheric effects of stratospheric aircraft: A current consensus, NASA Refer. Publ. 1251, 1991.

Douglass, A.R., R.B. Rood, C.J. Weaver, M.C. Cerniglia, and K.F. Brueske, Implications of three-dimensional tracer studies for two-dimensional assessments of the impact of supersonic aircraft on stratospheric ozone, *J. Geophys. Res., 98,* 8949-8963, 1993.

Drummond, J.W., D.H. Ehhalt, and A. Volz, Measurements of nitric oxide between 0 and 12 km altitude and 67°N-60°S latitude obtained during STRATOZ III, *J. Geophys. Res., 93,* 15831-15849, 1988.

ECAC, European Civil Aviation Committee, Abatement of Nuisance Caused by Air Traffic, Databank, 1994.

Egli, R.A., NO_x emissions from air traffic, *Chimia, 44,* 369-371, 1990.

Ehhalt, D.H., F. Rohrer, and A. Wahner, Sources and distribution of NO_x in the upper troposphere at northern mid-latitudes, *J. Geophys. Res., 97,* 3725-3738, 1992.

Ehhalt, D.H., F. Rohrer, and A. Wahner, The atmospheric distribution of NO, O_3, CO, and CH_4 above the North Atlantic based on the STRATOZ III flight, in *The Tropospheric Chemistry of Ozone in the Polar Regions,* NATO ASI Series, Vol. 17, edited by H. Niki and K.H. Becker, Springer-Verlag, Berlin, Heidelberg, 171-187, 1993.

Fahey, D.W., S.R. Kawa, E.L. Woodbridge, P. Tin, J.C. Wilson, H.H. Jonsson, J.E. Dye, D. Baumgardner, S. Borrmann, D.W. Toohey, L.M. Avallone, M.H. Proffitt, J.J. Margitan, R.J. Salawitch, S.C. Wofsy, M.K.W. Ko, D.E. Anderson, M.R. Schoeberl, and K.R. Chan, In situ measurements constraining the role of nitrogen and sulfate aerosols in mid-latitude ozone depletion, *Nature, 363,* 509-514, 1993.

Fahey, D.W., E.R. Keim, E.L. Woodbridge, R.S. Gao, K.A. Boering, B.C. Daube, S.C. Wofsy, R.P. Lohmann, E.J. Hintsa, A.E. Dessler, C.R. Webster, R.D. May, C.A. Brock, J.C. Wilson, R.C. Miake-Lye, R.C. Brown, J.M. Rodriguez, M. Loewenstein, M.H. Profitt, R.M. Stimpfle, S. Bowen, and K.R. Chan, In situ observations in aircraft exhaust plumes in the lower stratosphere at mid-latitudes, *J. Geophys. Res.*, in press, 1994.

Fortuin, J.P.F., R. van Dorland, W.M.F. Wauben, and H. Kelder, Greenhouse effects of aircraft emissions as calculated by a radiative transfer model, submitted to *Ann. Geophys.*, 1994.

Fuglestvedt, J.S., and I.S.A. Isaksen, in *Regional and Global Air Pollution from Aircraft,* edited by F. Stordal and U. Pedersen, Norsk Institutt for Luftforskning (NILU) Report O-1537, 1992.

Fuglestvedt, J.S., T.K. Berntsen, and I.S.A. Isaksen, *Responses in Tropospheric O_3, OH, and CH_4 to Changed Emissions of Important Trace Gases,* Centre for Climate and Energy Research, Oslo, Report 1993:4, 1993.

Fuglestvedt, J.S., I.S.A. Isaksen, and W.-C. Wang, *Direct and Indirect Global Warming Potentials of Source Gases,* Centre for Climate and Energy Research, Oslo, Report 1994:1, March, 1994.

Garcia, R.R., Parameterization of planetary wave breaking in the middle atmosphere, *J. Atmos. Sci., 48,* 1405-1419, 1991.

Gayet, J.-F., G. Febvre, G. Brogniez, and P. Wendling, Microphysical and optical properties of cirrus and contrails: Cloud field study on 13 October 1989, in *EUCREX-2, Proc. 6th ICE/EUCREX Workshop,* Department of Meteorology, Stockholm Univ., Sweden, 24-26 June 1993, edited by H. Sundquist, 30-39, 1993.

Graßl, H., Possible climatic effects of contrails and additional water vapor, in *Air Traffic and the Environment, Lect. Notes in Engineering, 60,* edited by U. Schumann, Springer-Verlag, Berlin, 124-137, 1990.

Hagen, D.E., M.B. Trueblood, and P.D. Whitefield, A field sampling of jet exhaust aerosols, *Particulate Sci. & Techn., 10,* 53-63, 1992.

Hofmann, D.J., Aircraft sulphur emissions, *Nature, 349,* 659, 1991.

Hofmann, D.J., and J.M. Rosen, Balloon observations of a particle layer injected by a stratospheric aircraft at 23 km, *Geophys. Res. Lett., 5,* 511-514, 1978.

Hoinka, K.P., M.E. Reinhardt, and W. Metz, North Atlantic air traffic within the lower stratosphere: Cruising times and corresponding emissions, *J. Geophys. Res., 98,* 23113-23131, 1993.

Hoshizaki, H., L.B. Anderson, R.J. Conti, N. Farlow, J.W. Meyer, T. Overcamp, K.O. Redler, and V. Watson, Aircraft wake microscale phenomena, Chapter 2 in *CIAP Monograph 3,* Department of Transportation, Washington, D.C., DOT-TST-75-53, 1975.

ICAO, International Civil Aviation Organization, Committee on Aviation Environmental Protection, 2nd Meeting, Montreal, 1991.

ICAO, International Civil Aviation Organization, Aircraft emissions regulations, Annex 16, Vol. II 2nd Edition, 1993.

ICAO, International Civil Aviation Organization, Aircraft engine exhaust emissions databank, 1994.

IEA, International Energy Agency, Oil and Gas Information (1987-89), OECD, 1990.

Jackman, C.H., A.R. Douglass, P.D. Guthrie, and R.S. Stolarski, The sensitivity of total ozone and ozone perturbation scenarios in a two-dimensional model due to dynamical inputs, *J. Geophys. Res., 94,* 9873-9887, 1989a.

Jackman, C.H., R.K. Seals, and M.J. Prather (eds.), *Two-Dimensional Intercomparison of Stratospheric Models,* NASA Conference Publication 3042, Proceedings of a workshop sponsored by the National Aeronautics and Space Administration, Washington, D.C., Upper Atmosphere Theory and Data Analysis Program held Sept. 11- 16, 1988, in Virginia Beach, VA, 1989b.

Johnson, C.E., *The Total Global Warming Impact of Step Changes of NO_x Emissions,* ARA/CS/18358017/003, Harwell Laboratory, U.K., 1994.

Johnson, C.E., and J. Henshaw, *The Impact of NO_x Emissions from Tropospheric Aircraft,* ARA-EE-0127, Harwell Laboratory, U.K., 1991.

Johnson, C.E., J. Henshaw, and G. McInnes, Impact of aircraft and surface emissions of nitrogen oxides on tropospheric ozone and global warming, *Nature, 355,* 69-71, 1992.

Johnston, H.S., D. Kinnison, and D.J. Wuebbles, Nitrogen oxides from high altitude aircraft: An update of the potential effect on ozone, *J. Geophys. Res., 94,* 16351-16363, 1989.

Karol I.L., Y.E. Ozolin, and E.V. Rosanov, Small and medium scale effects of high flying aircraft on the atmospheric composition, accepted for publication in *Ann. Geophysicae*, 1994.

Kasibhatla, P.S., NO_y from subsonic aircraft emissions: A global three-dimensional model study, *Geophys. Res. Lett., 20,* 1707-1710, 1993.

Kavanaugh, M., New estimates of NO_x from aircraft: 1975-2025, in *Proceedings 81st Annual Meeting of APCA (Air Pollution Control Association)*, Dallas, Texas, June 19-24, paper 88-66.10, page 15, 1988.

Knollenberg, R.G., Measurements of the growth of the ice budget in a persisting contrail, *J. Atmos. Sci., 29,* 1367-1374, 1972.

Ko, M., and A.R. Douglass, Update of model simulations for the effects of stratospheric aircraft, Chapter 4 in *Atmospheric Effects on Stratospheric Aircraft: A Third Program Report,* edited by R.S. Stolarski and H.L. Wesoky, 1993.

Lacis, A.A., D.J. Wuebbles, and J.A. Logan, Radiative forcing of climate by changes in the vertical distribution of ozone, *J. Geophys. Res., 95,* 9971-9981, 1990.

Liou, K.-N., S.-C. Ou, and G. Koenig, An investigation of the climatic effect of contrail cirrus, in *Air Traffic and the Environment, Lect. Notes in Engineering, 60,* edited by U. Schumann, Springer-Verlag, Berlin, 154-169, 1990.

Liu, S.C., M. Trainer, F.C. Fehsenfeld, D.D. Parrish, E.J. Williams, D.W. Fahey, G. Huebler, and P.C. Murphy, Ozone production in the rural troposphere and the implications for regional and global ozone distributions, *J. Geophys. Res., 92,* 4191-4207, 1987.

McDonnell Douglas Aircraft Co., *Procedure for Generating Global Atmospheric Emissions Data for Future Supersonic Transport Aircraft,* NASA Contractor Report 181882, 1990.

McInnes, G., and C.T. Walker, *The Global Distribution of Aircraft Air Pollution Emissions,* Warren Spring Lab., Report No. LR872 (AP), 1992.

Miake-Lye, R.C., M. Martinez-Sanchez, R.C. Brown, and C.E. Kolb, Plume and wake dynamics, mixing, and chemistry behind a high speed civil transport aircraft, *J. Aircraft, 30,* 467-479, 1993.

Mohnen, V.A., W. Goldstein, and W.-C. Wang, Tropospheric ozone and climate change, *J. Air & Waste Management Assoc., 43,* 1332-1344, 1993.

Möhler, O., and F. Arnold, Gaseous sulfuric acid and sulfur dioxide measurements in the Arctic troposphere and lower stratosphere: Implications for hydroxyl radical abundance, *Geophys. Res. Lett., 19,* 1763-1766, 1992.

Murphy, D.M., D.W. Fahey, M.H. Proffitt, S.C. Liu, K.R. Chan, C.S. Eubank, S.R. Kawa, and K.K. Kelly, Reactive nitrogen and its correlation with ozone in the lower stratosphere and upper troposphere, *J. Geophys. Res., 98,* 8751-8774, 1993.

NRC, National Research Council, *Atmospheric Effects of Stratospheric Aircraft: An Evaluation of NASA's Interim Assessment,* National Academy Press, Washington, D.C., 1994.

Nüßer, H.G., and A. Schmitt, The global distribution of air traffic at high altitudes, related fuel consumption and trends, in *Air Traffic and the Environment, Lect. Notes in Engineering, 60,* edited by U. Schumann, Springer-Verlag, Berlin, 1-11, 1990.

Penner, J.E., C.S. Atherton, J. Dignon, S.J. Ghan, and J.J. Walton, Tropospheric nitrogen: A three-dimensional study of sources, distributions, and deposition, *J. Geophys. Res., 96,* 959-990, 1991.

Peter, T., C. Brühl, and P.J. Crutzen, Increase in the PSC-formation probability caused by high-flying aircraft, *Geophys. Res. Lett., 18,* 1465-1468, 1991.

Pitchford, M., J.G. Hudson, and J. Hallet, Size and critical supersaturation for condensation of jet engine exhaust particles, *J. Geophys. Res., 96,* 20787-20793, 1991.

Pleijel, K., J. Moldanova, and Y. Anderson-Skold, *Chemical Modelling of an Aeroplane Exhaust Plume in the Free Troposphere,* Swedish Environmental Research Institute, IVL Report B. 1105, 1993.

Pollack, J.B., D. Rind, A. Lacis, J. Hansen, M. Sato, and R. Ruedy, GCM simulations of volcanic aerosol forcing I: Climate changes induced by steady state perturbations, *J. Climate, 7,* 1719-1742, 1993.

Prather, M.J., *et al., The Atmospheric Effects of Stratospheric Aircraft: A First Program Report,* NASA Reference Publication 1272, NASA Office of Space Science and Applications, Washington, D.C., January 1992.

Prather, M.J., and E.E. Remsberg (eds.), *The Atmospheric Effects of Stratospheric Aircraft: Report of the 1992 Models and Measurements Workshop,* NASA reference publication 1292, Vol. I-III, 1993.

Pueschel, R.F., D.F. Blake, K.G. Snetsinger, A.D.A. Hansen, S. Verma, and K. Kato, Black carbon (soot) aerosol in the lower stratosphere and upper troposphere, *Geophys. Res. Lett., 19,* 1659-1662, 1992.

Ramaroson, R., Etude des effets potentiels des futurs avions supersoniques sur la couche d'ozone, *La Recherche Aerospatials,* No. 3, 1993.

Ramaroson, R., and N. Louisnard, Potential effects on ozone of future supersonic aircraft / 2D simulation, *Ann. Geophys.*, in press, 1994.

Rasch, P.J., X.X. Tie, B.A. Boville, and D.L. Williamson, A three-dimensional transport model for the middle atmosphere, *J. Geophys. Res.*, in press, 1993.

Rind, D., and A. Lacis, The role of the stratosphere in climate change, *Surveys in Geophys., 14,* 133-165, 1993.

Rind, D., R. Suozzo, N.K. Balachandran, A. Lacis, and G.L. Russell, The GISS global climate/middle atmosphere model Part I: Model structure and climatology, *J. Atmos. Sci., 45,* 329-370, 1988.

Rodriguez, J.M., R.-L. Shia, M.K.W. Ko, C.W. Heisey, and D.K. Weisenstein, Subsidence of aircraft engine exhaust in the stratosphere: Implications for calculated ozone depletions, *Geophys. Res. Lett., 21,* 69-72, 1994.

Rohrer, F., D.H. Ehhalt, E.S. Grobler, A.B. Kraus, and A. Wahner, Model calculations of the impact of nitrogen oxides emitted by aircraft in the upper troposphere at northern mid-latitudes, in *Proceedings of the 6th European Symposium on Physico-chemical Behaviour of Atmospheric Pollutants,* Varese, in press, Oct., 1993.

Schumann, U., On the effect of emissions from aircraft engines on the state of the atmosphere, *Ann. Geophys., 12,* 365-384, 1994.

Schumann, U., and P. Wendling, Determination of contrails from satellite data and observational results, in *Air Traffic and the Environment, Lect. Notes in Engineering, Vol. 60,* edited by U. Schumann, Springer-Verlag, Berlin, 138-153, 1990.

Schumann, U., and T. Gerz, Turbulent mixing in stably stratified shear flows, submitted to *J. Appl. Met.*, 1993.

Shia, R.-L., M.K. Ko, M. Zou, and V.R. Kotamarthi, Cross-tropopause transport of excess ^{14}C in a two dimensional model, *J. Geophys. Res., 98,* 18599-18606, 1993.

Shine, K.P., and A. Sinha, Sensitivity of the earth's climate to height-dependent changes in the water vapour mixing ratio, *Nature, 354,* 382-384, 1991.

Solomon, S., and J.G. Keys, Seasonal variations in Antarctic NO_x chemistry, *J. Geophys. Res. 97,* 7971-7978, 1992.

Stolarski, R.S., and H.L. Wesoky (eds.), *The Atmospheric Effects of Stratospheric Aircraft: A Second Program Report,* NASA Reference Publication 1293, NASA Office of Space Science and Applications, Washington, D.C., March 1993a.

Stolarski, R.S., and H.L. Wesoky (eds.), *The Atmospheric Effects of Stratospheric Aircraft: A Third Program Report,* NASA Reference Publication 1313, NASA Office of Space Science and Applications, Washington, D.C., November 1993b.

Tie, X.X., G. Brasseur, X. Lin, P. Friedlingstein, C. Granier, and P. Rasch, The impact of high altitude aircraft on the ozone layer in the stratosphere, *J. Atmos. Chem., 18,* 103-128, 1994.

Turco, R., Report of the Stratospheric Aerosol Science Committee (SASC), May 19, 1992, in *Engine Trace Constituent Measurements Recommended for the Assessment of the Atmospheric Effects of Stratospheric Aircraft,* edited by T.C. Miake-Lye, W.J. Dodds, D.W. Fahey, C.E. Kolb, and S.R. Langhoff, Engine Exhaust Trace Chemistry Committee, Atmospheric Effects of Stratospheric Aircraft, NASA High Speed Research Program, Report number ARI-RR-947, August 1992.

Wahner, A., F. Rohrer, D.H. Ehhalt, B. Ridley, and E. Atlas, Global measurements of photochemically active compounds, in *Proceedings of 1st IGAC Scientific Conference: Global Atmospheric-Biospheric Chemistry,* Eilat, Israel, in press, 205-222, 1994.

Wang, W.-C., G.-Y. Shi, and J.T. Kiehl, Incorporation of the thermal radiative effect of CH_4, N_2O, CF_2Cl_2, and $CFCl_3$ into the NCAR Community Climate Model, *J. Geophys. Res., 96,* 9097-9103, 1991.

Weaver, C.J., A.R. Douglass, and R.B. Rood, Thermodynamic balance of three-dimensional stratospheric winds derived from a data assimilation procedure, *J. Atmos. Sci., 50,* 2987-2993, 1993.

Weibrink, G., and R. Zellner, Modelling of plume chemistry of high flying aircraft with H_2 combustion engines, in *Orbital Transport - Technical Meteorological and Chemical Aspects*, edited by H. Oertel and H. Korner, Springer-Verlag, Berlin, 439-448, 1993.

Weisenstein, D.K., M.K.W. Ko, J.M. Rodriguez, and N.-D. Sze, Impact of heterogeneous chemistry on model-calculated ozone change due to high speed civil transport aircraft traffic, *Geophys. Res. Lett., 18,* 1991-1994, 1991.

Wesoky, H.L., A.M. Thompson, and R.S. Stolarski, NASA Atmospheric Effects of Aviation project: Status and plans, *Proceedings of the International Scientific Colloquium on the Impact of Emissions from Aircraft and Spacecraft upon the Atmosphere,* Organized by DLR, Cologne, Germany, April 1994, 20-25, 1994.

Whitefield, P.D., M.B. Trueblood, and D.E. Hagen, Size and hydration characteristics of laboratory stimulated jet engine combustion aerosols, *Particulate Sci. & Techn., 11,* 25ff, 1993.

WMO, *Scientific Assessment of Ozone Depletion: 1991,* World Meteorological Organization Global Ozone Research and Monitoring Project—Report No. 25, Geneva, 1992.

Wuebbles, D.J., and D.E. Kinnison, Sensitivity of stratospheric ozone to present and possible future aircraft emissions, in *Air Traffic and the Environment, Lect. Notes in Engineering, 60,* edited by U. Schumann, Springer-Verlag, Berlin, 107-123, 1990.

Wuebbles, D.J., S.L. Baughcum, M. Metwally, and R.K. Seals, Jr., Emissions scenarios development: Overview and methodology, in *The Atmospheric Effects of Stratospheric Aircraft: A Third Program Report,* edited by R. S. Stolarski and H. L. Wesoky, NASA Reference Publication 1313, NASA Office of Space Science and Applications, Washington, D.C., 1993.

CHAPTER 12

Atmospheric Degradation of Halocarbon Substitutes

Lead Author:
R.A. Cox

Co-authors:
R. Atkinson
G.K. Moortgat
A.R. Ravishankara
H.W. Sidebottom

Contributors:
G.D. Hayman
C. Howard
M. Kanakidou
S.A. Penkett
J. Rodriguez
S. Solomon
O. Wild

CHAPTER 12

ATMOSPHERIC DEGRADATION OF HALOCARBON SUBSTITUTES

Contents

SCIENTIFIC SUMMARY

The substitutes for long-lived halocarbons have been selected on the basis of either their susceptibility to oxidation in the lower part of the atmosphere and minimization of their transport to the stratosphere, or by absence of chlorine or bromine from the molecules. It has been assumed that the atmospheric degradation of the substitutes leads to products that do not cause ozone loss. Further, it is assumed that the degradation products have no other deleterious environmental effects.

These assumptions are examined in this chapter by assessing three aspects of chlorofluorocarbon (CFC) and halon substitutes: the factors that control their atmospheric lifetimes, the processes by which they are degraded in the atmosphere, and the nature of their degradation products. The main findings are:

- If a substance containing Cl , Br, or I decomposes in the stratosphere, it will lead to ozone destruction. Use of hydrochlorofluorocarbons (HCFCs) and other CFC substitutes containing Cl, Br, or I, which have short tropospheric lifetimes, will reduce the input of ozone-destroying substances to the stratosphere, leading to reduced ozone loss.

- None of the proposed CFC substitutes that are degraded in the troposphere will lead to significant ozone loss in the stratosphere via their degradation products.

- It is known that atomic fluorine itself is not an efficient catalyst for ozone loss and it is concluded that the F-containing fragments from the substitutes (such as CF_3O_x) also do not destroy ozone.

- Trifluoroacetic acid, formed in the degradation of certain HCFCs and hydrofluorocarbons (HFCs), will partition into the aqueous environment where biological, rather than physico-chemical, removal processes may be effective.

- The amount of long-lived greenhouse gases formed in the atmospheric degradation of HCFCs and HFCs appears to be insignificant.

- Certain classes of compounds, some of which have already been released to the atmosphere, such as perfluorocarbons, have extremely long atmospheric lifetimes and large global warming potentials.

12.1 BACKGROUND

Chlorofluorocarbons (CFCs) and halons deplete stratospheric ozone because of their long atmospheric lifetimes, allowing them to be transported to the stratosphere where they release chlorine and bromine, resulting in catalytic destruction of ozone. The substitute molecules have been selected on the basis of either their shorter tropospheric lifetime due to their susceptibility to oxidation in the lower part of the atmosphere and minimization of their transport to the stratosphere or, in some cases, by absence of chlorine or bromine from the molecules. It has been assumed that the atmospheric degradation of the substitutes leads to products that have lifetimes shorter than transport times for delivery of chlorine or bromine to the stratosphere. Further, it is assumed that the degradation products have no other deleterious environmental effects.

The purpose of this chapter of the 1994 WMO/UNEP assessment is scientific evaluation of the above assumptions concerning the substitute molecules. The following lead questions will be addressed:

1) Is significant ozone-destroying halogen released in the stratosphere from the substitute molecules themselves?
2) Is significant ozone-destroying halogen transported into the stratosphere from the degradation products formed in the troposphere?
3) Are ozone-depleting catalysts other than Cl or Br released in the stratosphere?
4) Are there any products formed that have other potential environmental impacts?

These questions are answered by examining three aspects of CFC and halon substitutes: the factors that control their atmospheric lifetimes, the processes by which they are degraded in the atmosphere, and the nature and behavior of their degradation products.

The atmospheric lifetime is the critical parameter required for the calculation of the Ozone Depletion Potential (ODP) and Global Warming Potential (GWP) of the substitutes, as discussed in Chapter 13 of this document. For the most part, these lifetimes are calculated from models using laboratory data. The accuracy of the calculated lifetimes, ODPs, and GWPs reflects the uncertainties in the laboratory data and in the models, *i.e.*, the treatment of transport, heterogeneous chemistry, etc. Here, the hydrofluorocarbons (HFCs) and hydrochlorofluorocarbons (HCFCs), the largest classes of replacements proposed to date, are treated first. Then, other replacements, which do not fall into one single category, are discussed.

12.2 ATMOSPHERIC LIFETIMES OF HFCS AND HCFCS

The atmospheric lifetimes of all the HFCs and HCFCs are determined by the sum of their loss rates in the troposphere and in the stratosphere. The processes responsible for their losses in these two regions are slightly different and, hence, are discussed separately.

12.2.1 Tropospheric Loss Processes

The major fraction of the removal of HFCs and HCFCs occurs in the troposphere. Their reactions with the hydroxyl (OH) radical have been identified as the predominant tropospheric loss pathways. Reactions of HFCs and HCFCs, which are saturated hydrocarbons, with tropospheric oxidants such as NO_3 (Haahr *et al.*, 1991) and O_3 (Atkinson and Carter, 1984) are very slow and, hence, unimportant. Physical removal (*i.e.*, dry and wet deposition) of these compounds is negligibly slow (WMO, 1990).

The evaluated rate coefficients for the reaction of OH with the HFCs and HCFCs considered here are those recommended by the National Aeronautics and Space Administration (NASA) Panel (DeMore *et al.*, 1992). This Panel has reviewed the changes in the data base since the last evaluation. None of the changes affects significantly the calculated lifetimes and ODPs. References have been given where new data have been used.

In addition to their reaction with OH, these molecules may be removed from the troposphere via reaction with chlorine atoms (Cl). The rate coefficients for the reactions of Cl with a variety of HFCs and HCFCs have been measured and found to be of the same order of magnitude as the rate coefficients for their OH reactions (DeMore *et al.*, 1992; Atkinson, *et al.*, 1992; Tuazon *et al.*, 1992; Wallington and Hurley, 1992; Sawerysyn *et al.*, 1992; Warren and Ravishankara, 1993; Thompson, 1993). Because the global tropospheric concentration of Cl is likely to be less than 1% of that of OH, the only effect of Cl atom reactions is the small reduction of atmospheric lifetimes; the products of reaction are similar

to those from OH reactions. The contributions of Cl reactions would be at most a few percent of those due to OH reactions. Loss by Cl atom reaction will only reduce the lifetimes in the atmosphere and the products of the reactions are similar to those from the OH reactions.

12.2.2 Stratospheric Loss Processes

In addition to the reactions of OH free radicals, the HFCs may be removed from the stratosphere by their reaction with $O(^1D)$ atoms. In the case of HCFCs and brominated compounds, ultraviolet (UV) photolysis can also be important. The sum of the rates of these three processes, *i.e.*, OH reaction, $O(^1D)$ reaction, and UV photolysis, determines where and how rapidly these molecules release ozone-depleting species in the stratosphere. In addition, the removal in the stratosphere also contributes to the overall lifetimes of these compounds.

The rate coefficients for the reaction of $O(^1D)$ with the HFCs and HCFCs have been evaluated by the NASA and International Union of Pure and Applied Chemistry (IUPAC) Panels (DeMore *et al.*, 1992; Atkinson *et al.*, 1992). Inclusion of these reactions is unlikely to substantially reduce the calculated atmospheric lifetimes of these species. The UV absorption cross sections needed for these calculations have been reviewed previously (WMO, 1990; Kaye *et al.*, 1994) and there are no new data that need to be considered here. In general, HCFCs must have at least two Cl atoms for photolytic removal in the stratosphere to be competitive with OH reaction. The reactions of $O(^1D)$ are important only for species with lifetimes longer than a few decades, *i.e.*, for molecules such as HFC-23.

12.3 ATMOSPHERIC LIFETIMES OF OTHER CFC AND HALON SUBSTITUTES

In addition to the HFCs and HCFCs, many other substitutes for CFCs have been considered for use and evaluated for their environmental acceptability. They include the fluoroethers, perfluorocarbons (PFCs), sulfur hexafluoride (SF_6), and trifluoromethyl iodide (CF_3I). The PFCs and SF_6 are very long-lived species with strong infrared absorption characteristics. Thus they can be efficient greenhouse gases. On the other hand CF_3I is very short-lived. Yet, iodine in the stratosphere can be even more efficient than bromine in destroying ozone and hence is of concern.

The rate coefficients for reactions of OH and $O(^1D)$ reaction with the fluoroethers have not so far been reported. The H-containing fluoroethers are expected to have reactivity with OH comparable to the HFCs, and therefore their lifetimes will be similar due to tropospheric degradation. The ether functional group does not make photolysis an important loss process.

The major loss process for the PFCs, other than CF_4 and C_2F_6, appears to be their photolysis in the upper stratosphere and the mesosphere by the Lyman-α (121.6 nm) radiation (Cicerone, 1979; Ravishankara *et al.*, 1993). The absorption cross sections at this wavelength, needed for this evaluation, are given by Ravishankara *et al.* (1993). Reaction with $O(^1D)$ atoms has been shown to be unimportant as a loss process for the PFCs. In the case of some PFCs, such as the perfluorocyclobutane, their reactions with ions in the ionosphere may also contribute (Morris *et al.*, 1994).

CF_4 and C_2F_6 are already present in the atmosphere as by-products of aluminum production. Their loss processes through reaction with atmospheric ions are slower than the heavier PFCs, giving lifetimes in excess of 300,000 years. The ion-molecule reactions are the only identified loss processes for CF_4 and C_2F_6; however, their breakdown in air used in combustion could shorten the lifetimes of CF_4 and C_2F_6 to 50,000 years and 10,000 years, respectively (Morris *et al.*, 1994).

Another long-lived compound is SF_6, for which the major loss processes appear to be Lyman-α photolysis and electron attachment. Since it is not clear if SF_6 is removed in the latter process, the estimated lifetime of 600 years is a lower limit.

CF_3I has been considered as a substitute for halons and CFCs. The major atmospheric loss process for this molecule, as with all organic-iodine compounds, appears to be photolysis in the troposphere (Solomon *et al.*, 1994). This process leads to an average atmospheric lifetime of only a few days. Other loss processes, such as reaction with OH, are unlikely to compete with the photolytic removal of CF_3I and can only marginally decrease the lifetime, even if they are very rapid.

The chemistry of iodine in the troposphere has been described by Chameides and Davis (1980), Jenkin *et al.* (1985), and more recently by Jenkin (1993), who made use of the expanded kinetic data base that has been evaluated by the IUPAC panel (Atkinson *et al.*, 1992). Recently Solomon *et al.* (1994) have considered the

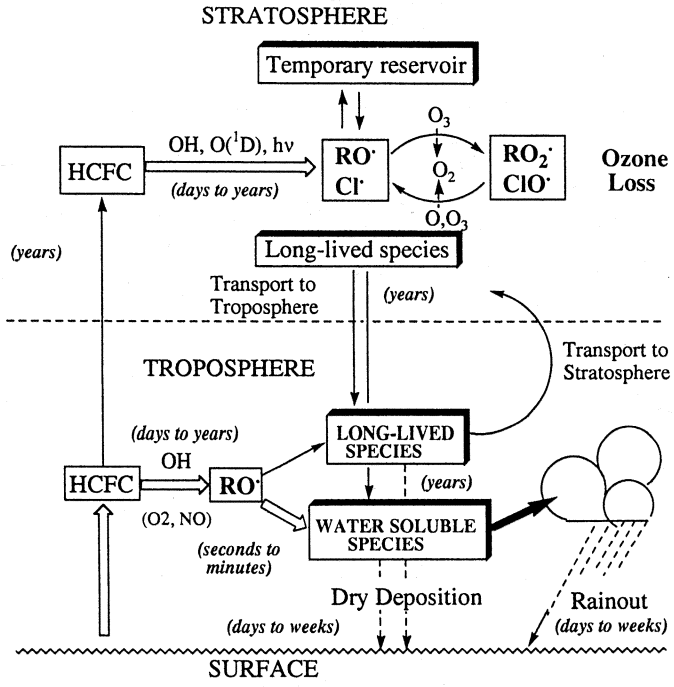

Figure 12-1. Atmospheric degradation of HCFCs, HFCs, and other CFC substitutes. The time scales for the different processes involving transport and chemistry are given in italics.

impact of iodine compared to chlorine and bromine on stratospheric ozone. They show that iodine is likely to be at least as effective as bromine for ozone destruction, and they note that several key chemical processes relating to iodine-catalyzed ozone destruction, notably IO + ClO, IO + BrO and IO + O_3, have not yet been quantified in laboratory studies. These factors are taken into account in calculating the ODP for CF_3I in Chapter 13.

The data base needed for the calculation of the lifetimes of halons and their possible bromine-containing substitutes has been evaluated in the past assessments (WMO, 1990, 1992) and there are no significant changes in this data base.

12.4 ATMOSPHERIC DEGRADATION OF SUBSTITUTES

A general flow diagram of the degradation of the HFCs and HCFCs is shown in Figure 12-1, which shows the approximate time scales for various processes. A key question is: Could the degradation products of the substitutes generate species that can destroy ozone in the stratosphere? If long-lived chlorine-containing species are produced, they can be transported into the stratosphere from the troposphere. In such a case, the assumption that degradation in the troposphere essentially stops transport of chlorine or bromine to the stratosphere would be erroneous. Similarly, if ozone-destroying radicals other than chlorine are released from degradation products, erroneous ODPs will result. If long-lived greenhouse gases are produced, their impact on climate forcing becomes an issue, with potential feedback to the ozone depletion problem.

Laboratory studies to elucidate the atmospheric degradation mechanisms and numerical atmospheric model calculations have been carried out. The laboratory studies include analysis of the end products in air and direct measurements of the rate coefficients and products for some of the key reactions. From these studies, it appears that the slowest step in the conversion of HFCs and HCFCs to their ultimate stable products (such as CO_2, H_2O, HF, HCl, and in some cases, other products such as trifluoroacetic acid) is the initiation by reaction with OH. The time scale for this process ranges from

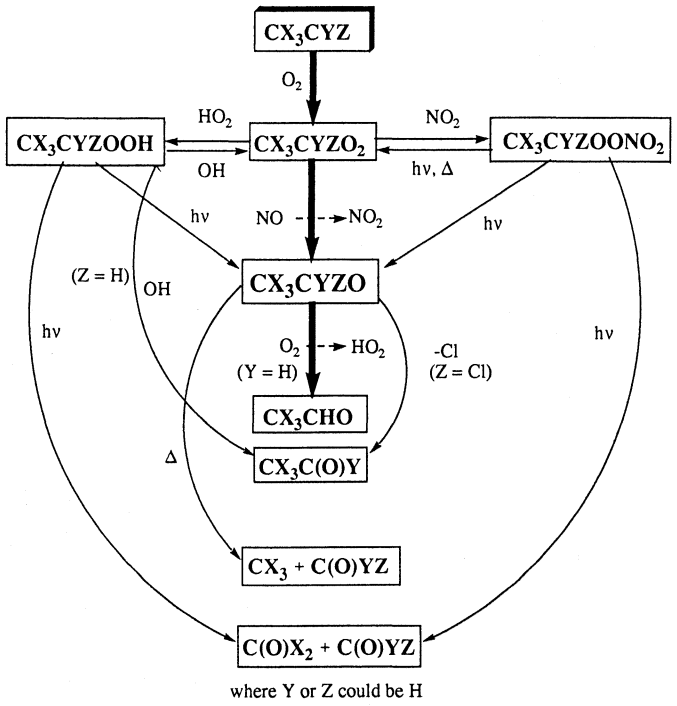

Figure 12-2. Generalized atmospheric degradation scheme for CX_3CYZ radicals. X, Y, and Z may be F, Cl, Br, or H, hν indicates photolysis; Δ indicates thermal decomposition. Reactant species are indicated on arrows.

weeks, for the shortest-lived substitutes, to hundreds of years for the long-lived ones. In some cases, such as with CF_4 and C_2F_6, where the normal degradation processes are inoperative, lifetimes are even longer, while CF_3I is removed by photolysis in a time scale of a few days. The subsequent chemistry that leads to breakdown is very rapid. However, the formation of shorter-lived, but potentially important atmospheric species needs to be considered. The overall degradation of all the HFCs and HCFCs and CF_3I appears to go through the formation of the haloalkoxy (RO) radical. There are two special reasons for the importance of the RO radical formation. It can potentially lead to destruction of ozone in the stratosphere, via reactions of species such as CF_3O and FC(O)O, and in addition RO can lead to the formation of semi-stable species that are sufficiently long-lived to be transported into the stratosphere. If such a species contains an ozone-destroying Cl atom (or CF_3 group), the Ozone Depletion Potentials of the starting HCFCs or HFCs would be larger than that calculated by ignoring this transport. In addition, the reactions of the RO radical lead to the formation of water-soluble end products. Finally, it has been hypothesized that reactions of oxygen with CF_3O and FC(O)O could potentially lead to destruction of O_3 in the stratosphere.

The "broad-brush" picture of the degradation, shown in Figure 12-1, will be discussed in detail in the following sections. This picture shows where in the degradation scheme the above questions arise. Research carried out during the past few years has addressed these issues and is discussed below.

12.5 GAS PHASE DEGRADATION CHEMISTRY OF SUBSTITUTES

In the atmosphere, photolysis or OH radical reaction (H-atom abstraction from a haloalkane, or OH radical addition to a haloalkene) leads to the formation of haloalkyl peroxy radicals (WMO, 1990, 1992). The general degradation scheme, after formation of the haloalkyl radical, is shown in Figure 12-2 and is applicable to both the troposphere and stratosphere, and leads to the

formation of the carbonyls $C(O)X_2$, $C(O)XY$, CX_3CHO, and $CX_3C(O)Y$ from the CX_3CYZ radical. There are differences between the degradation of the carbonyls in the troposphere and stratosphere caused by (a) the importance of physical loss processes of carbonyls in the troposphere and (b) increased intensity of short-wavelength UV radiation in the stratosphere, leading to increased importance of photolysis of carbonyl compounds in the stratosphere.

12.5.1 Reaction with NO

Rate constants for the reactions of a number of haloalkyl peroxy radicals with NO have been measured (Wallington and Nielsen, 1991; Peeters and Pultau, 1994; Atkinson *et al.*, 1992; Sehested *et al.*, 1993). The reactions are expected to produce NO_2 and the haloalkoxy radical, RO:

$$CX_3CYZO_2 + NO \rightarrow CX_3CYZO + NO_2 \quad (12\text{-}1)$$

and, to date, there is no evidence for the formation of the nitrates via the pathway:

$$CX_3CYZO_2 + NO \xrightarrow{M} CX_3CYZONO_2 \quad (12\text{-}2)$$

In any case, photolysis of the haloalkyl nitrates is expected to occur with a close to unit quantum yield by breakage of the $O\text{-}NO_2$ bond (Atkinson *et al.*, 1992) to produce the haloalkoxy radical, RO.

12.5.2 Reaction with NO_2

The reactions of haloalkyl peroxy radicals with NO_2 have been evaluated by Atkinson *et al.*, (1992). These reactions lead to the formation of peroxynitrates $CX_3CYZOONO_2$.

12.5.3 Reaction with HO_2 Radicals

Rate constants for reaction with the HO_2 radical have been measured for $CF_2ClCH_2O_2$ and CF_3CHFO_2 radicals (Hayman, 1993), and a product study has been conducted for the CH_2FO_2 radical reaction (Wallington *et al.*, 1994a). The two measured rate constants are similar to those determined for the methyl and ethyl peroxy radicals. However, Wallington *et al.* (1994a) have shown that the HO_2 radical reaction with CH_2FO_2 proceeds by two channels at room temperature:

$$CH_2FO_2 + HO_2 \xrightarrow{(30\%)} CH_2FOOH + O_2 \quad (12\text{-}3)$$

$$CH_2FO_2 + HO_2 \xrightarrow{(70\%)} HC(O)F + O_2 + H_2O \quad (12\text{-}4)$$

As shown in Figure 12-2, this second reaction channel bypasses the intermediate formation of the haloalkoxy radical, but forms the same carbonyl product.

12.5.4 Hydroperoxides

As discussed in WMO (1992), the hydroperoxides $CX_3CYZOOH$ are expected to undergo photolysis, reaction with the OH radical, and (in the troposphere) wet deposition. Photolysis leads to formation of the alkoxy radical CX_3CZYO plus OH or possibly to $X + CX_2CZYOOH$ for X = Br and I. OH radical reaction will lead to reformation of the haloalkyl peroxy radical CX_3CYZO_2. For hydroperoxides of the structure $CX_3CYZOOH$ with Z = H, OH reaction also yields $CX_3C(O)Y$:

$$OH + CX_3CHYOOH \rightarrow H_2O + CX_3CYOOH \quad (12\text{-}5)$$

$$\downarrow$$

$$CX_3C(O)Y + OH \quad (12\text{-}6)$$

To date, kinetic and photochemical data are only available for methyl hydroperoxide and *tert*-butyl hydroperoxide (OH reaction rate constant only) and, based on these limited data, the haloalkyl hydroperoxides are expected to have tropospheric lifetimes of a few days and hence a very low potential for transporting Cl or Br into the stratosphere.

The fate of $CX_3CYZOOH$ in aqueous solution needs to be investigated. In particular, any transformation to yield a long-lived species (for example CX_3H or CX_3Z), that is desorbed from solution back into the gas phase may be important.

12.5.5 Haloalkyl Peroxynitrates

As discussed in WMO (1992) and the IUPAC evaluation (Atkinson *et al.*, 1992), the haloalkyl peroxynitrates thermally decompose back to the peroxy radical and NO_2 (Figure 12-2). The thermal decomposition rates of

the peroxynitrates $ROONO_2$, where R = CF_2Cl, $CFCl_2$, CCl_3, CF_2ClCH_2, and $CFCl_2CH_2$, have been measured (Köppenkastrop and Zabel, 1991; Kirchner *et al.*, 1991). The lifetimes due to thermal decomposition range from <1 s for the C_2 haloalkyl peroxynitrates and 3-20 s for the C_1 haloalkyl peroxynitrates at 298 K, to approximately 2 days for the C_2 haloalkyl peroxynitrates and 0.1-1 year for the C_1 haloalkyl peroxynitrates in the upper troposphere and lower stratosphere.

By analogy with CH_3OONO_2 (Atkinson *et al.*, 1992), the haloalkyl peroxynitrates are also expected to undergo photolysis in the troposphere, with lifetimes of a few days, and transport of the haloalkyl peroxynitrates to the stratosphere will be insignificant.

Hence, apart from those reaction paths noted above and shown in Figure 12-2, the tropospheric degradation reactions of the HCFCs and HFCs funnel through the formation of the haloalkoxy radical, and the tropospheric reactions of the RO radicals then determine tropospheric degradation products formed from the HCFCs and HFCs (WMO, 1990, 1992).

12.5.6 Reactions of Haloalkoxy Radicals

There are three potential reaction paths for the haloalkoxy radicals formed from the HCFCs, HFCs and halons:

C-Cl or C-Br bond cleavage:

$$CX_3CYClO \rightarrow CX_3C(O)Y + Cl \quad (Z = Cl) \qquad (12\text{-}7)$$

$$CX_3CYBrO \rightarrow CX_3C(O)Y + Br \quad (Z = Br) \qquad (12\text{-}8)$$

C-C bond cleavage:

$$CX_3CYZO \rightarrow CX_3 + C(O)YZ \qquad (12\text{-}9)$$

H-atom abstraction:

$$CX_3CHYO + O_2 \rightarrow CX_3C(O)Y + HO_2 \quad (Z = H) \qquad (12\text{-}10)$$

The actual pathway followed and hence the particular carbonyl product formed depend on the nature of X, Y, and Z.

12.5.7 Halogenated Carbonyl Compounds

Halogenated carbonyl compounds are produced from the atmospheric degradation of all halocarbons, including CFCs, HCFCs, HFCs, halons, and the halogenated aldehyde intermediates. The carbonyls fall into the following categories:

Carbonyl halides	$C(O)X_2$	(X = F or Cl)
Formyl halides	HC(O)X	(X = F, Cl, or Br)
Acetyl halides	$CX_3C(O)Y$	(Y = F or Cl and X = H, F, Cl, or Br)
Organic acids	$CX_3C(O)OH$	(X = H, F, Cl, or Br)
Aldehydes	$CX_3C(O)H$	(X = H, F, Cl, or Br)

The fate of these carbonyl compounds is dependent on whether they are generated in the troposphere or in the stratosphere. Removal in the stratosphere is largely dominated by photolysis, whereas in the troposphere, physical removal and hydrolysis processes may be important relative to photolysis or reaction with the OH radical. Figure 12-2 and Table 12-1 show a summary of the products formed from the tropospheric degradation of HCFCs and HFCs. CF_3 radicals are also formed from several of the HCFCs and HFCs (Table 12-1), and their atmospheric chemistry is considered below.

12.5.8 Aldehydes

In the troposphere, the aldehydes, CX_3CHO, will react with OH radicals and undergo photolysis. The rate constants for the reaction with OH radicals have been determined (Scollard *et al.*, 1993; Atkinson, 1994) and lead to lifetimes in the troposphere of 4-25 days (Scollard *et al.*, 1993). While the absorption cross sections have been measured (Libuda *et al.*, 1991; Rattigan *et al.*, 1991, 1993), the photodissociation quantum yields are not available. Assuming unit quantum yields, the photolysis lifetimes of the halogenated aldehydes and CH_3CHO are calculated to be 1-7 hours. Thus, the aldehydes are likely to have short tropospheric lifetimes, of the order of a few hours to approximately one month, depending on the magnitude of the photodissociation quantum yields.

Assuming a photodissociation quantum yield significantly less than unity, similar to that for CH_3CHO, photolysis of the halogenated aldehydes is still expected to dominate as a tropospheric loss process, leading to C-C bond cleavage.

$$CX_3CHO + h\nu \rightarrow CX_3 + HC(O) \qquad (12\text{-}11)$$

Table 12-1. Carbonyl products formed from the tropospheric degradation reactions of a series of HCFCs and HFCs. (Formation of CF_3 radicals is also noted.)

HCFC or HFC	Chemical Formula	Carbonyl and/or CF_3	(a)
methyl chloroform	CH_3CCl_3	CCl_3CHO	
chloroform	$CHCl_3$	$C(O)Cl_2$	
methylene chloride	CH_2Cl_2	HC(O)Cl	
HCFC-22	CHF_2Cl	$C(O)F_2$	
HCFC-123	CF_3CHCl_2	$CF_3C(O)Cl$	
HCFC-124	CF_3CHFCl	$CF_3C(O)F$	
HCFC-141b	$CFCl_2CH_3$	$CFCl_2CHO$	
HCFC-142b	CF_2ClCH_3	CF_2ClCHO	
HCFC-225ca	$CF_3CF_2CHCl_2$	$CF_3CF_2C(O)Cl$	
HCFC-225cb	CF_2ClCF_2CHFCl	$CF_2ClCF_2C(O)F$	(b)
methyl bromide	CH_3Br	HC(O)Br	
HFC-23	CHF3	CF_3	
HFC-32	CH_2F_2	$C(O)F_2$	
HFC-125	CHF_2CF_3	$C(O)F_2 + CF_3$	
HFC-134	CHF_2CHF_2	$C(O)F_2$	
HFC-134a	CH_2FCF_3	$CF_3C(O)F$	(c)
		$HC(O)F + CF_3$	(c)
HFC-143a	CH_3CF_3	CF_3CHO	
HFC-152a	CH_3CHF_2	CHF_2CHO	
		$C(O)F_2$	
HFC-227ea	CF_3CHFCF_3	$CF_3C(O)F + CF_3$	

(a) From WMO (1990), Edney *et al.* (1991), Sato and Nakamura (1991), Hayman *et al.* (1991), Jemi-Alade *et al.* (1991), Scollard *et al.* (1991), Edney and Driscoll (1992), Wallington *et al.* (1992), Nielsen *et al.* (1992a, b), Tuazon and Atkinson (1993a, b, 1994), Shi *et al.* (1993), Hayman (1993), Meller *et al.* (1991, 1993), Zellner *et al.* (1991, 1993), Rattigan *et al.* (1994).

(b) ~1% yield of C(O)FCl also observed at room temperature and atmospheric pressure of air (Tuazon and Atkinson, 1994); $C(O)F_2$ also presumably formed as co-product with C(O)FCl.

(c) $CF_3C(O)F$ and $HC(O)F + CF_3$ yields are a function of temperature and O_2 concentration (Wallington *et al.*, 1992; Tuazon and Atkinson, 1993a; Rattigan *et al.*, 1994).

The quantum yield for formation of CHF_3 from CF_3CHO via

$$CF_3CHO + h\nu\ (\lambda>290\ nm) \rightarrow CHF_3 + CO \qquad (12\text{-}12)$$

is too low to significantly enhance the GWP of the parent compound (Meller *et al.*, 1993).

The OH radical reactions proceed by H-atom abstraction to initiate a series of reactions such as shown in Figure 12-3.

The initially formed acyl radical, CX_3CO, has been shown to either thermally decompose or react with O_2 to form the acyl peroxy radical, $CX_3C(O)OO$ (Barnes *et al.*, 1993; Tuazon and Atkinson, 1994):

$$CX_3CO \rightarrow CX_3 + CO \qquad (12\text{-}13)$$

$$CX_3CO + O_2 \rightarrow CX_3C(O)OO \qquad (12\text{-}14)$$

There is a monotonic trend towards decomposition, at 298 K and atmospheric pressure of air, with increasing number of Cl atoms in the $CCl_xF_{3-x}CO$ radical (Barnes *et al.*, 1993; Tuazon and Atkinson, 1994). Only for CF_3CO, CF_2ClCO, and $CFCl_2CO$ is the O_2 addition reaction important under atmospheric conditions. This can lead to the formation of the peroxyacylnitrates ($CF_3C(O)OONO_2$ from HCFC-143a, $CF_2ClC(O)OONO_2$ from HCFC-142b, and $CFCl_2C(O)OONO_2$ from HCFC-141b) by adding to NO_2. The alternative reaction pathways with NO or HO_2 lead to loss of the acyl group through formation of RCO_2, which decomposes to $R + CO_2$.

12.5.9 Peroxyacyl Nitrates

By analogy with peroxyacetyl nitrate and methyl peroxynitrate, the thermal decomposition lifetimes of the halogen-containing peroxyacyl nitrates are expected to be significantly longer than those for the haloalkyl peroxynitrates, and this expectation is borne out by the data of Barnes *et al.* (1993). Thermal decomposition rates have been measured by Barnes *et al.* (1993) for $RC(O)OONO_2$, with R = CF_3, CF_2Cl, and $CFCl_2$.

The calculated thermal decomposition lifetimes of these peroxyacyl nitrates range from approximately 2-3 hours at 298 K (ground level) to 6000-7000 years in the upper troposphere (220 K). By analogy with peroxyacetyl nitrate (Atkinson *et al.*, 1992), photolysis is likely

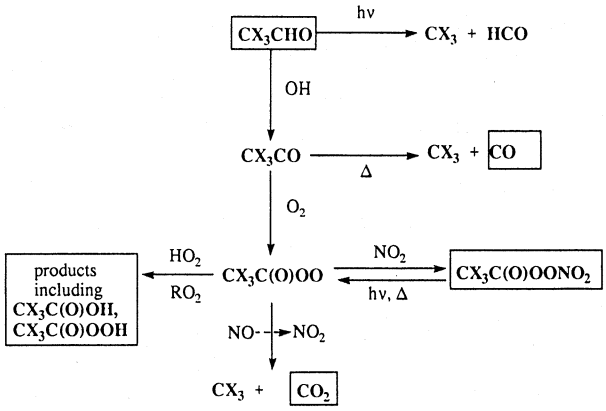

Figure 12-3. Oxidation of aldehydes formed from HCFC and HFC degradation. Stable species are indicated by boxes; x = F or Cl.

to dominate as the loss process in the upper troposphere, while still being slow enough that transport to the stratosphere could be competitive. The potential for transport of chlorine into the stratosphere from $CF_2ClC(O)OONO_2$ and $CFCl_2(O)OONO_2$ is discussed later.

12.5.10 Carbonyl Halides

Carbonyl halides are produced in the stratosphere from degradation of all halocarbons, including CFCs. The photolysis of C(O)FCl and $C(O)F_2$ is slow in the lower stratosphere and significant amounts of these degradation products are present there, as shown from infrared spectroscopic observation from space (Zander *et al.*, 1992) and from the ground (Reisinger *et al.*, 1994). A fraction of these stratospheric carbonyls is transported back to the troposphere, where efficient physical removal takes place; when chlorine is removed from the stratosphere in this way, *e.g.*, as C(O)FCl or $C(O)Cl_2$, the ODP of the precursor halocarbons can be reduced because the assumption of complete Cl release in the stratosphere is not valid.

12.5.11 Acetyl Halides

The acetyl halides released in the stratosphere will behave similarly to the carbonyl halides, being removed mainly by photolysis. The available evidence suggests that the quantum yield for formation of fully halogen-

ated compounds, such as CF_3Cl, from photolysis of $CF_3C(O)Cl$,

$$CF_3C(O)Cl + h\nu \rightarrow CF_3Cl + CO \qquad (12\text{-}15)$$

is sufficiently low (Meller *et al.*, 1993) that the ODP of the parent compounds will be increased by <0.01.

12.6 HETEROGENEOUS REMOVAL OF HALOGENATED CARBONYL COMPOUNDS

The carbonyl halides such as $C(O)F_2$, HC(O)F, and C(O)FCl, and acetyl halides, especially $CF_3C(O)Cl$ and $CF_3C(O)F$, are soluble in water. In aqueous solution they undergo hydrolysis, forming halogenated carboxylic acids or hydrogen halides and carbon dioxide. They are therefore likely to be removed from the troposphere by heterogeneous processes such as rainout or uptake by cloud droplets or surface waters, possibly followed by hydrolysis (Wine and Chameides, 1990).

The rate of these removal processes is governed by the rate of mass transfer of material between the gas and the aqueous phase, the solubility in the liquid phase, which is defined by the Henry's Law constant, H, and the hydrolysis rate constant, k_h.

$$CF_3C(O)X\,(g) \overset{H}{\Longleftrightarrow} CF_3C(O)X\,(aq) \qquad (12\text{-}16)$$

$$CF_3C(O)X\,(aq) + H_2O \overset{k_h}{\rightarrow} CF_3C(O)OH\,(aq) + HX\,(aq) \qquad (12\text{-}17)$$

or

$$C(O)X_2\,(g) \overset{H}{\Longleftrightarrow} COX_2\,(aq) \qquad (12\text{-}18)$$

$$COX_2\,(aq) + H_2O \overset{k_h}{\rightarrow} CO_2\,(aq) + 2HX\,(aq) \qquad (12\text{-}19)$$

Both H and k_h are required to assess their fate. The Henry's Law constant controls aqueous phase uptake, and the hydrolysis constant the rate of aqueous phase destruction. For instance, if k_h is low, then efficient uptake into cloud droplets might not lead to destruction because most cloud droplets are transient and will evaporate on relatively short time scales, vaporizing unreacted absorbed carbonyl or haloacetyl halides back into the atmosphere.

The uptake coefficients, g, reflect a convolution of all processes at the interface that may influence the effective rate of mass transfer between gas and aqueous phases. If the uptake coefficient is greater than $\sim 10^{-3}$, the tropospheric uptake rate will not be determined by the uptake coefficient, and removal time would be ~1 week. Values of less than $g = 5 \times 10^{-3}$ have been obtained for $C(O)Cl_2$, $C(O)F_2$, $CCl_3C(O)Cl$, $CF_3C(O)F$, and $CF_3C(O)Cl$ by Worsnop *et al.* (1989), De Bruyn *et al.* (1992a), Edney and Driscoll (1993), Ibusuki *et al.* (1992), and George *et al.* (1993), and hence the removal time of these compounds can be larger than 1 week. Estimated lifetime values are given in Table 12- 2.

Trifluoroacetic acid (TFA), $CF_3C(O)OH$, is the hydrolysis product of both $CF_3C(O)F$ and $CF_3C(O)Cl$. Currently it is believed that $CF_3C(O)OH$, like other organic acids, is removed from the atmosphere primarily by rainout (Ball and Wallington, 1993; Rodriguez *et al.*, 1993). Other processes, such as gas phase reactions with OH (Carr *et al.*, 1994) or surface photolysis (Meller *et al.*, 1993), are unlikely to lead to significant reduction in the amount of $CF_3C(O)OH$ rained out. Although the environmental fate of TFA cannot be defined yet (Edney *et al.*, 1992; Franklin, 1993), there are indications that many natural organisms are capable of degrading it (Visscher *et al.*, 1994).

The physical removal of carbonyl compounds in the troposphere is the key requirement for the eventual removal of the degradation products from the atmosphere. A comparison of the tropospheric lifetimes of halogenated carbonyl compounds with respect to loss by OH radicals, photolysis, and/or physical removal processes is shown in Table 12-2.

The data in Table 12-2 indicate that the carbonyl compounds $C(O)F_2$, C(O)FCl, HC(O)F, $CF_3C(O)F$, and $CF_3C(O)OH$ have long tropospheric lifetimes with respect to photolysis or OH reaction. Consequently, physical removal will be the most likely loss process that competes with transport into the stratosphere, where the compounds are slowly photolyzed. The other chlorinated and brominated compounds will primarily undergo photolysis in the troposphere. Depending on the location, photolysis of $CF_3C(O)Cl$ will compete with wet deposition.

12.7 RELEASE OF FLUORINE ATOMS IN THE STRATOSPHERE

The atmospheric degradation of HFCs, HCFCs, and PFCs can lead to the release of F atoms. For example, the reaction of CF_3O and FC(O)O with NO leads to FNO, which because of its strong absorption in the 290-340 nm region (Johnston and Bertin, 1959) will rapidly photolyze to F atoms. In fact most CFCs also yield F

Table 12-2. Tropospheric lifetimes of halogenated carbonyl compounds.

	Photolysis [a]	OH [b]	Heterogeneous [c]
Carbonyl halides			
$C(O)Cl_2$	16 years	> 30 years	< a few weeks
$C(O)F_2$	$> 1 \times 10^8$ years	—	< a few weeks
C(O)FCl	$> 1 \times 10^7$ years	—	no data
Formyl halides			
HC(O)F	$> 1 \times 10^8$ years	> 8 years	~ 1 month
HC(O)Cl	3 years	> 36 days	no data
HC(O)Br	4 days	no data	no data
Acetyl halides			
$CF_3C(O)F$	1700 years	—	< a few weeks
$CF_3C(O)Cl$	85 days	—	< a few weeks
$CH_3C(O)F$	24 years	—	no data
$CH_3C(O)Cl$	23 days	3 years	no data
$CCl_3C(O)Cl$	6 days	—	no data
$CClH_2C(O)Cl$	30 days	—	no data
$CCl_2HC(O)Cl$	9 days	—	no data
Organic acids			
$CF_3C(O)OH$	$> 7 \times 10^5$ years	4 months	< a few weeks

(a) Absorption cross sections have been measured by Libuda *et al.*, (1991); Meller *et al.* (1991, 1993); Nölle *et al.* (1992, 1993); Rattigan *et al.*, (1993). Photolysis processes become important in the lower troposphere at wavelengths beyond 295 nm. Unit quantum yields for the dissociation of the molecules have been assumed for the calculation of the approximate tropospheric photolytic lifetimes near the boundary layer (2 km).

(b) An average OH concentration of 1×10^6 molecules cm^{-3} was used for the calculation of the tropospheric lifetimes with respect to OH loss. Rate constant data are for 298 K, since temperature dependencies are not available. The rate coefficients for the OH reactions are from Wallington and Hurley (1993), Nelson *et al.* (1990), and Libuda *et al.* (1990). For compounds with no H atom, it can be assumed that OH loss is negligible.

(c) There are considerable discrepancies in the values of the uptake rate coefficients measured in different laboratories. Therefore, conservative upper limits for the heterogeneous removal rates are quoted. (Behnke *et al.*, 1992; DeBruyn *et al.*, 1992; Exner *et al.*, 1992; Rodriguez *et al.*, 1992; Ugi and Beck, 1961.)

atoms upon degradation in the stratosphere. Hence, the possibility of the involvement of fluorine in catalytic destruction of O_3 needs to be addressed.

The reaction of F atoms with O_3 is much more rapid than the corresponding reaction of Cl atoms (DeMore *et al.*, 1992; Atkinson *et al.*, 1992). Further, the reaction of FO with O is also rapid, so that the catalytic cycle:

$$F + O_3 \rightarrow FO + O_2 \quad (12\text{-}20)$$
$$FO + O \rightarrow F + O_2 \quad (12\text{-}21)$$
$$\text{Net: } O + O_3 \rightarrow 2O_2$$

can occur rapidly. Other catalytic cycles involving F atoms are also possible. However, the reactions of F atoms with CH_4 and H_2O to form HF are also very fast and can compete with the reaction between F and O_3 (DeMore *et al.*, 1992; Atkinson *et al.*, 1992). Therefore, any catalytic cycle involving F atoms that destroys ozone cannot have a large chain length, because F atoms are efficiently removed to form HF.

Unlike the case of HCl, HBr, and HI, which can react with various gas phase free radicals to regenerate the corresponding halogen atoms, HF is inert to attack by stratospheric free radicals, except for very reactive, and hence very low abundance, species such as $O(^1D)$ atoms. Further, HF does not absorb at wavelengths longer than 165 nm and, consequently, is not photolyzed efficiently in the stratosphere (Safary *et al.*, 1951; Nee *et al.*, 1985). Lastly, HF cannot be converted to an active F-containing species via heterogeneous reactions on ice (Hanson and Ravishankara, 1992) and it is expected to be very insoluble in sulfuric acid and unable to take part in heterogeneous reactions. Therefore, release of fluorine into the stratosphere from either CFCs or their substitutes leads to the formation of stable HF and does not lead to catalytic ozone destruction.

12.8 CF_3O_x AND $FC(O)O_x$ RADICAL CHEMISTRY IN THE STRATOSPHERE – DO THESE RADICALS DESTROY OZONE?

12.8.1 CF_3O_x Radical Chemistry

As shown in Figures 12-2 and 12-3 and discussed above, the trifluoromethyl radical is a major intermediate in the atmospheric degradation of HCFCs, HFCs, and halons that contain the CF_3 group. As discussed previously for other haloalkyl radicals, it is expected that the CF_3 radical will be quantitatively converted to CF_3O, by addition to O_2 followed by reaction with NO. Halomethoxy radicals containing hydrogen, bromine, or chlorine atoms are removed under atmospheric conditions either by halogen atom elimination or by H atom abstraction with molecular oxygen to give the corresponding carbonyl or formyl species. In contrast, CF_3O does not undergo unimolecular elimination of a fluorine atom because it is too endothermic, and reaction of CF_3O with O_2 is too slow to be important (Batt and Walsh, 1982, 1983; Schneider and Wallington, 1994; Turnipseed *et al.*, 1994). Hence, further degradation of CF_3O radicals must occur by reaction with atmospheric trace gas species.

There has been speculation that CF_3O_x (CF_3O and CF_3O_2) radicals could participate in catalytic ozone destruction cycles in the stratosphere (Francisco *et al.*, 1987; Biggs *et al.*, 1993). As discussed recently by Ko *et al.* (1994), there are a number of potential catalytic ozone destruction cycles involving CF_3O_x radicals that are analogous to the corresponding HO_x cycles. In the lower stratosphere the cycle:

$$CF_3O + O_3 \rightarrow CF_3O_2 + O_2 \quad (12\text{-}22)$$
$$CF_3O_2 + O_3 \rightarrow CF_3O + 2O_2 \quad (12\text{-}23)$$
$$\text{net: } 2O_3 \rightarrow 3O_2$$

could be important, whereas in the mid-stratosphere the reaction sequence:

$$CF_3O + O_3 \rightarrow CF_3O_2 + O_2 \quad (12\text{-}24)$$
$$CF_3O_2 + O \rightarrow CF_3O + O_2 \quad (12\text{-}25)$$
$$\text{net: } O + O_3 \rightarrow 2O_2$$

may also lead to ozone depletion. The reactions of CF_3O and CF_3O_2 radicals with ozone are chain-propagating steps in the cycles, and the efficiencies of the chain processes depend on the rate of these reactions relative to those for the sink reactions of CF_3O_x radicals.

The kinetics of the reaction of CF_3O radicals with ozone have recently been investigated using a number of different techniques (Biggs *et al.*, 1993; Nielsen and Sehested, 1993; Wallington *et al.*, 1993b; Maricq and Szente, 1993; Fockenberg *et al.*, 1994; Ravishankara *et al.*, 1994; Meller and Moortgat, 1994; O'Reilly *et al.*, 1994; Turnipseed *et al.*, 1994). With the exception of the

data of Biggs *et al.* (1993), the data indicate that $k(CF_3O + O_3) < 5 \times 10^{-14}$ cm^3 molecule s^{-1} at 298 K. For the reaction of CF_3O_2 with O_3, only upper limits for the rate constant have been estimated (Nielsen and Sehested, 1993; Maricq and Szente, 1993; Fockenberg *et al.*, 1994; Ravishankara *et al.*, 1994; Meller and Moortgat, 1994; O'Reilly *et al.*, 1994) and these studies suggest $k(CF_3O_2 + O_3) < 1 \times 10^{-14}$ cm^3 molecule^{-1} s^{-1} at 298 K. The upper limits to the rate constants determined for the reactions of CF_3O and CF_3O_2 with O_3 at 298 K are similar to the measured rate coefficients for the analogous reactions of OH and HO_2 radicals with O_3 (Atkinson *et al.*, 1992; DeMore *et al.*, 1992).

In the stratosphere the main chain terminating processes will be the reactions of CF_3O with NO and CH_4. The reaction of CF_3O radicals with NO over the pressure range 1-760 Torr and at 298 K leads to stoichiometric formation of $C(O)F_2$ and FNO (Chen *et al.*, 1992a, 1993; Bevilacqua *et al.*, 1993; Sehested and Nielsen, 1993):

$$CF_3O + NO \rightarrow C(O)F_2 + FNO \qquad (12\text{-}26)$$

The rate constant for this reaction has been shown to be independent of both pressure and temperature (Fockenberg *et al.*, 1993; Turnipseed *et al.*, 1994). These results suggest that the reaction of CF_3O with NO provides a permanent sink for CF_3O. In contrast, the sink mechanisms for ClO_x and HO_x generate only temporary reservoirs for these O_3-depleting species. The reaction of CF_3O with CH_4 appears to involve a direct hydrogen abstraction process with an activation energy of approximately 3 kcal mol^{-1} (Bednarek *et al.*, 1994; Barone *et al.*, 1994):

$$CF_3O + CH_4 \rightarrow CF_3OH + CH_3 \qquad (12\text{-}27)$$

CF_3OH will be a temporary reservoir for CF_3O only if subsequent reactions in the stratosphere lead to regeneration of CF_3 or CF_3O. The available evidence indicates that photolysis or reaction with OH will be negligible under stratospheric conditions (Wallington and Schneider, 1994) and that circulation back into the troposphere with loss by precipitation is the likely sink for CF_3OH (Ko *et al.*, 1994). From the kinetic parameters and the stratospheric concentrations of trace gas species, the chain length of the catalytic cycles for O_3 loss by reaction with CF_3O_x are estimated to be less than unity. This value, compared with a chain length of around 1000-10,000 for the ClO_x ozone loss cycle, suggests that catalytic cycles involving CF_3O_x will be of negligible importance. The permanency of the sink mechanism further reduces its effectiveness.

In the troposphere the major fate of CF_3O radicals will be by reaction with hydrocarbons (Chen *et al.*, 1992b; Saathoff and Zellner, 1993; Kelly *et al.*, 1993; Sehested and Wallington, 1993; Bevilacqua *et al.*, 1993; Ravishankara *et al.*, 1994; Bednarek *et al.*, 1994; Barone *et al.*, 1994), H_2O (Wallington *et al.*, 1993a), CO (Saathoff and Zellner, 1992; Ravishankara, private communication, 1994), and NO (Chen *et al.*, 1992a; Saathoff and Zellner, 1992; Fockenberg *et al.*, 1993; Sehested and Nielsen, 1993; Ravishankara *et al.*, 1994). As was the case in the stratosphere, the ultimate fate of CF_3O in the troposphere is the formation of either CF_3OH or CF_2O. Under tropospheric conditions, the most probable fate of both CF_3OH and CF_2O is uptake by cloud, rain, or ocean water to yield CO_2 and HF (Franklin, 1993).

12.8.2 $FC(O)O_x$ Radical Chemistry

Atmospheric degradation of HCFCs and HFCs gives rise to formation of HC(O)FCOFCl and $C(O)F_2$. In the stratosphere, photolysis of HC(O)F and $C(O)F_2$ may be a minor source of FC(O) radicals. Reaction of FC(O) with O_2 is rapid and leads to formation of $FC(O)O_2$ (Maricq *et al.*, 1993; Wallington *et al.*, 1994b). It has been suggested that $FC(O)O_x$ radicals could participate in a catalytic ozone destruction cycle (Francisco *et al.*, 1990) similar to that described for CF_3O_x,

$$FC(O)O_2 + O_3 \rightarrow FC(O)O + 2O_2 \qquad (12\text{-}28)$$

$$FC(O)O + O_3 \rightarrow FC(O)O_2 + O_2 \qquad (12\text{-}29)$$

$$\text{net:} \quad 2O_3 \rightarrow 3O_2$$

Wallington *et al.* (1994b) have recently shown that $FC(O)O_2$ and FC(O)O both react rapidly with NO, whereas the rate constant for reaction of FC(O)O with O_3 has an upper limit of 6×10^{-14} cm^3 molecule^{-1} s^{-1}. Reaction of FC(O)O with NO gives FNO and CO_2 and is hence a permanent sink for FC(O)O. Use of these rate parameters, together with the concentrations of NO and O_3 in the stratosphere, shows that the contribution to ozone destruction for cycles involving $FC(O)O_x$ radicals can have no significance.

12.9 MODEL CALCULATIONS OF THE ATMOSPHERIC BEHAVIOR OF HCFCS AND HFCS

The aim of this section is to review the state of knowledge of the atmospheric behavior of the CFC substitutes as determined by calculations using 2- and 3-dimensional numerical models, which are formulated on the basis of knowledge of atmospheric motions and solar radiation, and on laboratory data related to atmospheric chemistry. These models have been formulated using global transport, validated against atmospheric observations of chemically inert tracers such as CFCs, ^{85}Kr, etc. Chemical schemes have been incorporated to provide time-dependent fields of oxidizing species such as OH, which allow the atmospheric loss by photochemical oxidation of reactive substitutes and their oxidation products to be calculated. This allows the evolving distribution and concentration levels of a particular substitute molecule and its degradation products to be calculated for a given emission scenario. Physical removal in the precipitation and at the Earth's surface has been incorporated in a parameterized way so that rainout and hydrolysis of degradation products can be assessed, and the distribution and fate of the degradation products determined.

Some models include transport to and from the stratosphere and allow a detailed treatment of stratospheric loss of these substitutes. This allows a treatment of the delivery of halogen to the stratosphere, either directly by the halocarbon itself or by its degradation products. This information has relevance for assessment of the ODP of the substitutes, but the evaluation of these comparative indices is dealt with in a later chapter in this assessment. It is unlikely that observations of the C_2 carbonyls, peroxynitrates, or acids expected as degradation products of HCFCs and HFCs will help validation of the models, since the abundance of these molecules in the troposphere will be extremely small; even with the future anticipated buildup in the emission rates of the substitutes, the abundance of these molecules will be too small to detect with foreseeable technology. Analysis of the model results allows determination of the atmospheric lifetime of the various chemical species; assessment of atmospheric lifetimes is dealt with in Chapter 13. In this chapter the principal focus is the behavior of the degradation products.

12.9.1 The Models

Three 2-dimensional models—from Harwell (Hayman and Johnson, 1992), AER (Rodriguez *et al.*, 1993, 1994) and Cambridge (Rattigan *et al.*, 1992)—and the Max-Planck-Institute 3-D MOGUNTIA model (Kanakidou *et al.*, 1993) have been employed for the assessment of the atmospheric behavior of the degradation products of HCFCs and HFCs. There are some differences in model domain; for example, only the AER and Cambridge models provide full treatment of the stratosphere. All models have detailed schemes for tropospheric chemistry and degradation schemes for a range of substitutes are included in all models except for the AER model, which is restricted to HFC-134a, and HCFC-123, and -124. The models all use different emission scenarios, and so calculated concentration fields cannot be compared directly. However, the conclusions drawn from analysis of model output can be compared.

Model calculations of the degradation of the proposed CFC substitutes have been carried out using the mechanisms and photochemical kinetic data described in the previous sections. The main questions addressed by the modeling studies of the degradation of the proposed CFC substitute molecules are:

- To what extent do any long-lived degradation products of the substitutes transport chlorine and bromine to the stratosphere, thereby enhancing ozone depletion?
- To what extent can the reactions of CF_3O_x radicals lead to ozone destruction in the stratosphere?
- To what extent does the atmospheric degradation of the substitutes lead to products that have other environmental concerns, *e.g.*, toxicity, enhanced GWPs?

12.9.2 Transport of Chlorine and Bromine from the Troposphere to the Stratosphere

The classes of degradation product that could potentially carry Cl and Br to the stratosphere are the formyl, carbonyl, and acetyl halides; the fully halogenated peroxynitrates, especially the acylperoxynitrates, formed in the degradation of compounds of general formula CH_3CX_3; and halocarbons formed by photochemical decomposition of carbonyl compounds, *e.g.*, CX_3Y from $CX_3C(O)Y$.

The effectiveness of the formyl, carbonyl, and acetyl halides as chlorine and/or bromine carriers is reduced essentially to zero by their removal through hydrolysis and removal in precipitation. The model calculations of Rodriguez *et al.* (1993), Kanakidou *et al.* (1993), and Rattigan *et al.* (1992) show that the lifetimes of these molecules is of the order of a few days, resulting from removal at the surface, rainout, and loss in clouds.

In the upper troposphere the halogenated peroxyacetylnitrates $CX_3C(O)O_2NO_2$ are relatively unreactive. The oxidation of HCFC-141b and 142b in the troposphere produces the aldehydes CCl_2FCHO and $CClF_2CHO$, which, following OH attack (in competition with the photolysis of the aldehydes), may sometimes form $CCl_2FC(O)O_2NO_2$ and $CClF_2C(O)O_2NO_2$. Rodriguez *et al.* (1994) and Kanakidou *et al.* (1993) have modeled the degradation of HCFC-141b (and 142b) using a variety of assumptions regarding the rate parameters for the relevant photochemical reactions. Even when the assumptions maximized the formation of peroxyacetylnitrates, the calculated tropospheric concentrations of $CFCl_2C(O)O_2NO_2$ and $CClF_2C(O)O_2NO_2$ were well below the 1×10^{-12} (pptv) level and comprised only a small fraction (~1-2%) of the corresponding concentrations of HFC-141b and 142b at the steady state. Thus it can be concluded that transfer of Cl to the stratosphere in these product molecules is insignificant.

The only other long-lived product containing chlorine is the halocarbon CF_3Cl, possibly formed by photolysis of $CF_3C(O)Cl$. Model studies of this process in the atmosphere have not been performed, but the very low quantum yields of CF_3Cl observed in laboratory studies imply that it is of negligible importance in conveying Cl to the stratosphere.

12.9.3 Transfer of Cl to the Stratosphere by HCFC Molecules

Although the HCFCs are removed predominantly in the troposphere, there is some degradation and release of Cl in the stratosphere by reaction with OH and by photolysis. For example, Kanakidou *et al.* (1993) find that stratospheric loss accounts for 7% for HCFC-22 and 10% for HCFC-141b. Except for CF_2HCl (F22), these are the most important potential chlorine carriers; the other HCFCs are a factor of 3-10 less effective in terms of the fraction of their chlorine delivered to the stratosphere. These factors are taken into account in the ODP calculations discussed further in Chapter 13.

12.9.4 Modeling of Ozone Loss Due to CF_3O Chemistry

The influence of additional O_3 loss mechanisms involving the CF_3O reactions on the Ozone Depletion Potentials of HCFCs and HFCs has been investigated in model calculations (Ko *et al.*, 1994; Ravishankara *et al.*, 1994).

In both studies the efficiency of CF_3O_x as a catalyst for ozone depletion was calculated relative to the efficiency of chlorine release from CFCs. Ravishankara *et al.* (1994) showed that the new kinetics measurements for the key reactions of CF_3O lead to negligibly small ODPs. For example, the best estimate of the ODP for the key substitute HFC-134a is only $(1\text{-}2) \times 10^{-5}$. The results of Ko *et al.* (1994), which were based on estimates for the relevant kinetic parameters, are consistent with this conclusion.

12.9.5 Degradation Products That Have Other Potential Environmental Impacts

Trifluoroacetic acid, formyl, and fluoride formed from the degradation of HCFCs and HFCs have been identified as a potential environmental concern because of their toxicity.

Trifluoroacetic acid (TFA) is produced by hydrolysis of $CF_3C(O)F$ formed in the degradation of HFC-134a and HCFC-124 and hydrolysis of $CF_3C(O)Cl$ from degradation of HCFC-123. The yield of $CF_3C(O)F$ from HCFC-124 is almost 100%, but the competitive pathway forming HC(O)F reduces the yield from HFC-134a. Tropospheric photolysis of $CF_3C(O)Cl$ competes with hydrolysis and consequently reduces the yield of TFA from HFC-123.

Most interest has focused on the production of TFA from HFC-134a (Rodriguez *et al.*, 1993; Rattigan *et al.*, 1994; Kanakidou *et al.*, 1993; Ball and Wallington, 1993). Using the most recent laboratory data, cloud hydrolysis of atmospheric $CF_3C(O)F$ is sufficiently rapid so that TFA production is equal to the rate of $CF_3C(O)F$ production, and is therefore controlled by the local rate of HFC-134a reaction with OH and by the branching ratio for the competing reactions of CF_3CHFO:

$$CF_3CHFO + O_2 \rightarrow CF_3C(O)F + HO_2 \quad (12\text{-}30)$$

$$CF_3CHFO \rightarrow CF_3 + HCOF \quad (12\text{-}31)$$

Because of the temperature, total pressure, and O_2 partial pressure dependence of this branching ratio, there is significant latitude and altitude dependence in the fraction of HFC-134a producing $CF_3C(O)F$. For average atmospheric conditions, about 40% of HFC-134a is degraded to TFA.

Rodriguez *et al.* (1993) have calculated the zonally averaged concentrations of TFA in rainwater, making various assumptions regarding the extent to which the gaseous acid is dry deposited at the surface after evaporation from clouds. The results show considerable latitudinal and seasonal variation in rainfall TFA, the pattern depending on the assumptions made. The key results of this study are:

- Predicted global average concentrations of TFA in rain are of the order of 1 mg/l for a 1 Tg $year^{-1}$ source of HFC-134a in the Northern Hemisphere. These concentrations are relatively insensitive to the parameters adopted for uptake of $CF_3C(O)F$ in cloud droplets.
- The concentrations of TFA in rain are primarily determined by the source strength of HFC-134a, the relative yields of $CF_3C(O)F$ from the CF_3CHFO radical, and the loss processes for gas phase TFA.
- Calculated local concentrations of TFA in rain could be very sensitive to other loss processes of $CF_3C(O)F$, as well as to rainfall patterns.

Calculations in the same study indicate a 50-100% yield of TFA in rain from degradation of HCFC-124 and HCFC-123. The smaller values for HCFC-123 reflect the removal of $CF_3C(O)Cl$ by photolysis in the troposphere. The results from the other model studies of HFC-134a oxidation are in broad agreement with these conclusions concerning the formation of TFA. There are differences in quantitative detail that may be a result of different model formulation as well as uncertainties in the input data.

No laboratory data are available for the uptake and hydrolysis rates of HC(O)F in aqueous solution. Its gas phase loss processes are extremely slow in the troposphere and, if the hydrolysis and uptake rates are also low, this molecule could build up in the troposphere and be transported to the stratosphere (Kanakidou *et al.*, 1993). Stratospheric photolysis leads to $FC(O)O_x$ but, as discussed above, this will not lead to ozone depletion.

REFERENCES

Atkinson, R., and W.P.L. Carter, Kinetics and mechanisms of the gas-phase reactions of ozone with organic compounds under atmospheric conditions, *Chem. Rev., 84*, 437-470, 1984.

Atkinson, R., D.L. Baulch, R.A. Cox, R.F. Hampson, Jr., J.A. Kerr, and J. Troe, Evaluated kinetic and photochemical data for atmospheric chemistry, Supplement IV, IUPAC subcommittee on gas kinetic data evaluation for atmospheric chemistry, *J. Phys. Chem. Ref. Data, 21*, 1125-1568, 1992.

Atkinson, R., Gas-phase tropospheric chemistry of organic compounds, *J. Phys. Chem. Ref. Data, Monograph 2*, 1-216, 1994.

Ball, J.C., and T.J. Wallington, Formation of trifluoroacetic acid from the atmospheric degradation of hydrofluorocarbon 134a: A human health concern?, *J. Air Waste Manage. Assoc., 43*, 1260-1262, 1993.

Barnes, I., K.H. Becker, F. Kirchner, F. Zabel, H. Richer, and J. Sodeau, Formation and thermal decomposition of $CCl_3C(O)O_2NO_2$ and $CF_3C(O)O_2NO_2$, in *Kinetics and Mechanisms for the Reactions of Halogenated Organic Compounds in the Troposphere,* STEP-HALOCSIDE/AFEAS Workshop, March 23-25, Dublin, 1993.

Barone, S., A.A. Turnipseed, and A.R. Ravishankara, Kinetics of the reactions of the CF_3O radical with alkanes, *J. Phys. Chem.*, in press, 1994.

Batt, L., and R. Walsh, A reexamination of the pyrolysis of bis trifluromethyl peroxide, *Int. J. Chem. Kinet., 14*, 933-944 (1982) and *15*, 605-607, (1983).

Bednarek, G., J.P. Kohlmann, H. Saathoff, and R. Zellner, Temperature dependence and product distribution for the reaction of CF_3O radicals with methane, *J. Phys. Chem.*, in press, 1994.

Behnke, W., M. Elend, H.-U. Krüger, and C. Zetzsch, An aerosol chamber technique for the determination of mass accommodation coefficients on submicron aqueous solution droplets of carbonyl halides: Phosgene, in *Atmospheric Wet and Dry Deposition of Carbonyl and Haloacetyl Halides*, Alternative Fluorocarbons Environmental Acceptability Study (AFEAS) Workshop Proceedings, 22 September 1992, Brussels, 68-75, 1992.

Bevilacqua, T.J., D.R. Hanson, and C.J. Howard, Chemical ionization mass spectrometric studies of the gas-phase reactions CF_3O_2 + NO, CF_3O + NO and CF_3O + RH, *J. Phys. Chem., 97,* 3750-3757, 1993.

Biggs, P., C.E. Canosa-Mas, D.E. Shallcross, R.P. Wayne, C. Kelly, and H.W. Sidebottom, The possible atmospheric importance of the reaction of CF_3O radicals with ozone, in *Kinetics and Mechanisms for the Reactions of Halogenated Organic Compounds in the Troposphere*, STEP-HALOCSIDE/AFEAS Workshop, March 23-25, Dublin, 177-181, 1993.

Carr, S., J.J. Treacy, H.W. Sidebottom, R.K. Connel, C.E. Canosa-Mas, R.P. Wayne, and J. Franklin, Kinetics and mechanism for the reaction of hydroxyl radicals with TFA under atmospheric conditions, *Chem. Phys. Lett.*, in press, 1994.

Chameides, W.L., and D.D. Davis, Iodine: Its possible role in tropospheric photochemistry, *J. Geophys. Res., 85,* 7383-7398, 1980.

Chen, J., T. Zhu, and H. Niki, FTIR product study of the reaction of CF_3O with NO: Evidence for CF_3O + NO $\rightarrow$ CF_2O + FNO, *J. Phys. Chem., 96,* 6115-6117, 1992a.

Chen, J., T. Zhu, H. Niki, and G.J. Mains, Long path FTIR spectroscopic study of the reactions of CF_3O radicals with ethane and propane, *Geophys. Res. Lett., 19,* 2215-2218, 1992b.

Chen, J., V. Young, T. Zhu, and H. Niki, Long path FTIR spectroscopic study of the reactions of CF_3OO and CF_3O radicals with NO_2, in *Kinetics and Mechanisms for the Reactions of Halogenated Organic Compounds in the Troposphere,* STEP-HALOCSIDE/AFEAS Workshop, March 23-25, Dublin, 150-162, 1993.

Cicerone, R.J., Atmospheric carbon tetrafluoride: A nearly inert gas, *Science, 206,* 59-61, 1979.

DeMore, W.B., S.P. Sander, D.M. Golden, R.F. Hampson, M.J. Kurylo, C.J. Howard, A.R. Ravishankara, C.E. Kolb, and M. Molina, *Chemical Kinetics and Photochemical Data for Use in Stratospheric Modeling,* NASA/Jet Propulsion Laboratory Pub. No. 92-20, 1992.

De Bruyn, W.J., S.X. Duan, X.Q. Shi, P. Davidovits, D.R. Worsnop, M.S. Zahnizer, and C.E. Kolb, Tropospheric heterogeneous chemistry of carbonyl halides, *Geophys. Res. Lett., 19,* 1939-1942, 1992a.

De Bruyn, W.J., J.A. Shorter, P. Davidovits, D.R. Worsnop, M.S. Zahnizer, and C.E. Kolb, The heterogeneous chemistry of carbonyl and haloacetyl halides, in *Atmospheric Wet and Dry Deposition of Carbonyl and Haloacetyl Halides,* Alternative Fluorocarbons Environmental Acceptability Study (AFEAS) Workshop Proceedings, 22 September 1992, Brussels, 12-17, 1992b.

Edney, E.O., and D.J. Driscoll, Chlorine initiated photooxidation studies of hydrochlorofluorocarbons (HCFCs) and hydrofluorocarbons (HFCs): Results for HCFC-22 ($CHClF_2$); HFC-41 (CH_3F); HCFC-124 ($CClFHCF_3$); HFC-125 (CF_3CHF_2); HFC-134a (CF_3CH_2F); HCFC-142b ($CClF_2CH_3$); and HFC-152a (CHF_2CH_3), *Int. J. Chem. Kinet., 24,* 1067-1081, 1992.

Edney, E.O., and D.J. Driscoll, Laboratory investigations of the deposition of oxidation products of hydrochlorofluorocarbons (HCFCs) and hydrofluorocarbons (HFCs) to aqueous solutions, *Water, Air and Soil Poll., 66,* 97-110, 1993.

Edney, E.O., D.J. Driscoll, E.W. Corse, and F.T. Blanchard, Atmospheric fate of trifluoroacetate during evaporation of complex aqueous solutions, in *Atmospheric Wet and Dry Deposition of Carbonyl and Haloacetyl Halides*, Alternative Fluorocarbons Environmental Acceptability Study (AFEAS) Workshop Proceedings, 22 September 1992, Brussels, 86-90, 1992.

Edney, E.O., B.W. Gay, Jr., and D.J. Driscoll, Chlorine initiated oxidation studies of hydrochlorofluorocarbons: Results for HCFC-123 (CF_3CHCl_2) and HCFC-141b ($CFCl_2CH_3$), *J. Atmos. Chem., 12,* 105-120, 1991.

Exner, M., H. Herrmann, J. Michel, and R. Zellner, Hydrolysis rate of CF_3COF and the decarboxylation of CF_3COO^- anions, in *Atmospheric Wet and Dry Deposition of Carbonyl and Haloacetyl Halides,* Alternative Fluorocarbons Environmental Acceptability Study (AFEAS) Workshop Proceedings, 22 September 1992, Brussels, 50-56, 1992.

Fockenberg, Ch., H. Saathoff, and R. Zellner, Paper presented at NOAA/NASA/AFEAS Workshop, Boulder, Colorado, November 16-19, 1993.

Fockenberg, Ch., H. Saathoff, and R. Zellner, A laser photolysis/LIF study of the rate constant for the reaction $CF_3O + O_3 \rightarrow$ products, *Chem. Phys. Lett.*, in press, 1994.

Francisco, J.S., Z. Li, and I.H. Williams, Dissociation dynamics of the trifluoromethoxy radical, *Chem. Phys. Lett.*, *140*, 531-536, 1987.

Francisco, J.S., A.N. Goldstein, Z. Li, Y. Zhao, and I.H. Williams, Theoretical investigation of chlorofluorocarbon degradation processes: Structures and energetics of $XC(O)O_x$ intermediates (X = F, Cl), *J. Phys. Chem.*, *94*, 4791-4795, 1990.

Franklin, J., The atmospheric degradation and impact of 1,1,1,2-tetrafluoroethane (hydrofluorocarbon 134a), *Chemosphere, 27*, 1565-1601, 1993.

George, C., J.L. Ponche, and P. Mirabel, Experimental determination of uptake coefficient for acid halides, in *Kinetics and Mechanisms for the Reactions of Halogenated Organic Compounds in the Troposphere*, STEP-HALOCSIDE/AFEAS Workshop, March 23-25, Dublin, 196-202, 1993.

Haahr, N., J. Hjorth, and G. Ottobrini, An FTIR study of the gas-phase reactions between NO_3 radicals and some HCFs and HCFCs and of the degradation of halogenated PAN-type species in air, in *Kinetics and Mechanisms for the Reactions of Halogenated Organic Compounds in the Troposphere*, STEP-HALOCSIDE/AFEAS Workshop, May 14-16, Dublin, 27-30, 1991.

Hanson, D.R., and A.R. Ravishankara, The heterogeneous chemistry of HBr and HF, *J. Phys.Chem.*, *96*, 9441-9446, 1992.

Hayman, G.D., M.E. Jenkin, T.P. Murrels, and S.J. Shalliker, Kinetics and mechanistic studies associated with the atmospheric degradation of HCFC-123, in *Kinetics and Mechanisms for the Reactions of Halogenated Organic Compounds in the Troposphere*, STEP-HALOCSIDE/AFEAS Workshop, May 14-16, Dublin, 79-87, 1991.

Hayman, G.D., and C.E. Johnson, Tropospheric modeling studies related to the degradation of the replacement compounds, in *Atmospheric Wet and Dry Deposition of Carbonyl and Haloacetyl Halides,* AFEAS Workshop Proceedings, 22 September 1992, Brussels, 76-85, 1992.

Hayman, G.D., The kinetics and mechanisms of processes involved in the atmospheric degradation of hydrochlorofluorocarbons and hydrofluorocarbons, in *Kinetics and Mechanisms for the Reactions of Halogenated Organic Compounds in the Troposphere*, STEP-HALOCSIDE/AFEAS Workshop, March 23-25, Dublin, 1993.

Ibusuki, T., K. Takeuchi, and S. Kutsuna, Determination of mass transfer coefficients of carbonyl and halocarbonyl halides into water, in *Atmospheric Wet and Dry Deposition of Carbonyl and Haloacetyl Halides*, AFEAS Workshop Proceedings, 22 September 1992, Brussels, 62-67, 1992.

Jemi-Alade, A.A., P.D. Lightfoot, and R. Lesclaux, UV absorption spectra of peroxy radical derivatives of hydrohalocarbons, in *Kinetics and Mechanisms for the Reactions of Halogenated Organic Compounds in the Troposphere*, STEP-HALOCSIDE/AFEAS Workshop, May 14-16, Dublin, 67-72, 1991.

Jenkin, M.E., R.A. Cox, and D.E. Candeland, Photochemical aspects of tropospheric iodine behaviour, *J. Atm. Chem., 2,* 359-375, 1985.

Jenkin, M. E., A comparative assessment of the role of iodine photochemistry in tropospheric ozone depletion, in *The Tropospheric Chemistry of Ozone in the Polar Regions,* edited by H. Niki and K.-H. Becker, NATO ASI Series, Vol 17, 405-416, 1993.

Johnston, H.S., and H.J. Bertin, Absorption and emission spectra of nitrosyl fluoride, *J. Mol. Spectrosc., 3,* 683-696, 1959.

Kanakidou, M., F.J. Dentener, and P.J. Crutzen, A global 3-dimensional study of the degradation of HCFCs and HFC-134a in the troposphere, in *Kinetics and Mechanisms for the Reactions of Halogenated Organic Compounds in the Troposphere*, STEP-HALOCSIDE/AFEAS Workshop, March 23-25, Dublin, 113-130, 1993.

Kaye, J., S.A. Penkett, and F.M. Ormond (eds.), *Report on Concentrations, Lifetimes and Trends of CFCs, Halons and Related Species,* NASA Reference Publication No. 1339, 1994.

Kelly, C., J. Treacy, H.W. Sidebottom, and O.J. Nielsen, *Chem. Phys. Lett., 207,* 498-502, 1993.

Kirchner, F., F. Zabel, and K.H. Becker, Thermal stability of $CClF_2CH_2O_2NO_2$, $CCl_2FCH_2O_2NO_2$ and $CClF_2C(O)O_2NO_2$, in *Kinetics and Mechanisms for the Reactions of Halogenated Organic Compounds in the Troposphere*, STEP-HALOCSIDE/AFEAS Workshop, May 14-16, Dublin, 73-78, 1991.

Ko, M.K.W., N.-D. Sze, J.M. Rodriguez, D.K. Weisenstein, C.W. Heisey, R.P. Wayne, P. Biggs, C.E. Canosa-Mas, H.W. Sidebottom, and J. Treacy, CF_3 chemistry: Potential implications for stratospheric ozone, *Geophys. Res. Lett.*, *21*, 101-104, 1994.

Köppenkastrop, D., and F. Zabel, Thermal decomposition of chlorofluoromethyl peroxynitrates, *Int. J. Chem. Kinet., 23,* 1-15, 1991.

Libuda, H.G., F. Zabel, E.H. Fink, and K.H. Becker, Formyl chloride: UV absorption cross sections and rate constants for the reactions with Cl and OH, *J. Phys. Chem.*, *94*, 5860-5865, 1990.

Libuda, H.G., F. Zabel, and K.H. Becker, UV spectra of some organic chlorine and bromine compounds of atmospheric interest, in *Kinetics and Mechanisms for the Reactions of Halogenated Organic Compounds in the Troposphere,* STEP-HALOCSIDE/AFEAS Workshop, May 14-16, Dublin, 126-131, 1991.

Maricq, M.M., and J.J. Szente, Upper limits for the rate constants of the reactions $CF_3O + O_3 \rightarrow CF_3O_2 + O_2$ and $CF_3O_2 + O_3 \rightarrow CF_3O + 2O_2$, *Chem. Phys. Lett., 213*, 449-456, 1993.

Maricq, M.M., J.J. Szente, G.A. Khitrov, and J.S. Francisco, Temperature dependent kinetics of the formation and self reactions of $FC(O)O_2$ and FC(O)O radicals, *J. Chem. Phys.*, *98*, 9522-9531, 1993.

Meller, R., D. Boglu, and G.K. Moortgat, UV spectra of several halogenated carbonyl compounds and FTIR studies on the degradation of CF_3COCl, HCFC-123 and HFC-134a, in *Kinetics and Mechanisms for the Reactions of Halogenated Organic Compounds in the Troposphere*, STEP-HALOCSIDE/AFEAS Workshop, May 14-16, Dublin, 110-115, 1991.

Meller, R., D. Boglu, and G.K. Moortgat, Absorption cross-sections and photolysis studies of halogenated carbonyl compounds. Photo-oxidation studies on CF_3-containing CFC-substitutes, in *Kinetics and Mechanisms for the Reactions of Halogenated Organic Compounds in the Troposphere*, STEP-HALOCSIDE/AFEAS Workshop, March 23-25, Dublin, 1993.

Meller, R., and G.K. Moortgat, Photolysis of $CF_3O_2CF_3$ in the presence of O_3 in oxygen: Kinetic study of the reaction of CF_3O and CF_3O_2 radicals with O_3, submitted to *J. Photochem. Photobiol.*, 1994.

Morris, R.A., T.M. Miller, A.A. Viggiano, J.F. Paulson, S. Solomon, and G. Reid, Effect of electron and ion reactions on atmospheric lifetimes of fully fluorinated compounds, *J. Geophys. Res.,* in press, 1994.

Nee, J.B., M. Suto, and L.C. Lee, Photoabsorption cross section of HF at 107-145 nm, *J. Phys. B: Mol. Phys., 18,* L293-L294, 1985.

Nelson, L., I. Shanahan, H.W. Sidebottom, J. Treacy, and O.J. Nielsen, Kinetics and mechanism for the oxidation of 1,1,1-trichloroethane, *Int. J. Chem. Kinet., 22,* 577-590, 1990.

Nielsen, O.J., and J. Sehested, Upper limits for the rate constants of the reactions of CF_3O_2 and CF_3O radicals with ozone at 295 K, *Chem. Phys. Lett., 213,* 433-441, 1993.

Nielsen, O.J., T. Ellermann, E. Bartkiewicz, T.J. Wallington, and M.D. Hurley, UV absorption spectra, kinetics and mechanisms of the self-reaction of CHF_2O_2 radicals in the gas phase at 298 K, *Chem. Phys. Lett., 192*, 82-88, 1992a.

Nielsen, O.J., T. Ellermann, J. Sehested, and T.J. Wallington, Ultraviolet absorption spectrum and kinetics and mechanism of the self-reaction of $CHF_2CF_2O_2$ radicals in the gas phase at 298 K, *J. Phys. Chem., 96*, 10875-10879, 1992b.

Nölle, A., H. Heydtmann, R. Meller, W. Schneider, and G.K. Moortgat, UV absorption spectrum and cross-section of COF_2 at 296 K in the range 200-230 nm, *Geophys. Res. Lett., 19,* 281-284, 1992.

Nölle, A., H. Heydtmann, R. Meller, and G.K. Moortgat, Temperature dependent UV absorption spectra of carbonyl chloro-fluoride, *Geophys. Res. Lett., 20,* 707-710, 1993.

O'Reilly, J., H.W. Sidebottom, M. Buck, C.E. Canosa-Mas, and R.P. Wayne, The reaction of O_3 with CF_3O and CF_3O_2, submitted to *Chem. Phys. Lett.,* 1994.

Peeters, J., and V. Pultau, Reactions of hydrofluorocarbon- and hydrochlorofluorocarbon-derived peroxy radicals with nitric oxide: Results for CF_3CH_2F (HFC-134a), CF_3CH_3 (HFC-143a), CF_2ClCH_3 (HCFC-142b), CF_3CCl_2H (HFC-123) and CF_3CFHCl (HCFC-124), in *Physico-Chemical Behaviour of Atmospheric Pollutants, Vol. 1,* Comm. Eur. Communities, Rep. no. 15609, 372-378, 1994.

Rattigan, O.V., R.A. Cox, and R.L. Jones, The UV absorption cross-sections of CF_3COCl, CF_3COF, CH_3COF and CCl_3CHO, in *Kinetics and Mechanisms for the Reactions of Halogenated Organic Compounds in the Troposphere*, STEP-HALOCSIDE/AFEAS Workshop, May 14-16, Dublin, 116-125, 1991.

Rattigan, O.V., O. Wild, K. Law, R.L. Jones, J. Pyle, and R.A. Cox, Two-dimensional modeling studies of HCFCs, HFCs and their degradation products, in *Atmospheric Wet and Dry Deposition of Carbonyl and Haloacetyl Halides*, AFEAS Workshop Proceedings, 22 September 1992, Brussels, 92-102, 1992.

Rattigan, O.V., O. Wild, R.L. Jones, and R.A. Cox, Temperature-dependent absorption cross-sections of CF3COCl, CF3COF, CH3COF, CCl3CHO and CF3COOH, *J. Photochem. Photobiol. A: Chem., 73,* 1-9, 1993.

Rattigan, O.V., D.M. Rowley, O. Wild, R.L. Jones, and R.A. Cox, Mechanism of the atmospheric oxidation of 1,1,1,2 tetrafluoroethane (HFC 134a), accepted for publication in *J. Chem. Soc. Faraday Trans.,* 1994.

Ravishankara, A.R., S. Solomon, A.A. Turnipseed, and R.F. Warren, Atmospheric lifetimes of long-lived halogenated species, *Science, 259,* 194-199, 1993.

Ravishankara, A.R., A.A. Turnipseed, N.R. Jensen, S. Barone, M. Mills, C.J. Howard, and S. Solomon, Do hydrofluorocarbons destroy stratospheric ozone?, *Science, 263,* 71-75, 1994.

Reisinger, A.R., N.B. Jones, W.A. Matthews, and C.P. Rinsland, Southern Hemisphere ground based measurements of carbonyl fluoride (COF_2) and hydrogen fluoride(HF): Partitioning between fluorine reservoir species, *Geophys. Res. Lett., 21,* 797-800, 1994.

Rodriguez, J.M., M.K.W. Ko, N.-D. Sze, and C.W. Heisey, Model assessment of the impact of wet and dry deposition on the tropospheric abundance of acetyl halides and trifluoroacetic acid, in *Atmospheric Wet and Dry Deposition of Carbonyl and Haloacetyl Halides*, AFEAS Workshop Proceedings, 22 September 1992, Brussels, 25-32, 1992.

Rodriguez, J.M., M.K.W. Ko, N.-D. Sze, and C.W. Heisey, Two-dimensional assessment of the degradation of HFC-134a: Tropospheric accumulations and deposition of trifluoroacetic acid, in *Kinetics and Mechanisms for the Reactions of Halogenated Organic Compounds in the Troposphere*, STEP-HALOCSIDE/AFEAS Workshop, March 23-25, Dublin, 104-112, 1993.

Rodriguez, J.M., M.K.W. Ko, N.-D. Sze, and C.W. Heisey, Three-dimensional assessment of the degradation of HCFCs and HFCs: Tropospheric distributions and stratospheric inputs, in *Atmospheric Degradation of HCFCs and HFCs,* Proceedings NASA/NOAA/AFEAS Workshop, Boulder, Colorado, 17-19 November 1993, 1994.

Saathoff, H., and R. Zellner, Spectroscopic identification and kinetics of the CF_3O (X^2E) radical, abstract of paper presented at the 12th Int. Symp. on Gas Kinetics, Reading, U.K., July, 1992.

Saathoff, H., and R. Zellner, LIF detection of the CF_3O radical and kinetics of its reactions with CH_4 and C_2H_6, *Chem. Phys. Lett., 206,* 349-354, 1993.

Safary, E., J. Romand, and B. Vodar, Ultraviolet absorption spectrum of gaseous hydrogen fluoride, *J. Chem. Phys., 19,* 379-380, 1951.

Sato, H., and T. Nakamura, The degradation of hydrochlorofluorocarbons by reaction with Cl atoms and O_2, *Nippon Kagaku Kaishi,* 548-551, 1991.

Sawerysyn, J.P., A. Talhaoui, B. Meriaux, and P. Devolder, Absolute rate constants for elementary reactions between chlorine atoms and CHF_2Cl, CH_3CFCl_2, CH_3CF_2Cl, and CH_2FCF_3 at 297 ± 2 K, *Chem. Phys. Lett., 198,* 197-201, 1992.

Scollard, D., M. Corrigan, J. Treacy, and H. Sidebottom, Kinetics and mechanisms for the oxidation of halogenated aldehydes, in *Kinetics and Mechanisms for the Reactions of Halogenated Organic Compounds in the Troposphere*, STEP-HALOCSIDE/ AFEAS Workshop, May 14-16, Dublin, 40-51, 1991.

Scollard, D.J., J.J. Treacy, H.W. Sidebottom. C. Balestra-Garcia, G. Laverdet, G. LeBras, H. MacLeod, and S. Teton, Rate constants for the reactions of hydroxyl radicals and chlorine atoms with halogenated aldehydes, *J. Phys. Chem., 97,* 4683-4688, 1993.

Schneider, W.F., and T.J. Wallington, Ab initio investigation of the heats of formation of several trifluoromethyl compounds, submitted to *J. Phys. Chem.,* 1994.

Sehested, J. and O.J. Nielsen, Absolute rate constants for the reaction of CF_3O_2 and CF_3O radicals with NO at 295 K, *Chem. Phys. Lett., 206,* 369-375, 1993.

Sehested, J., O.J. Nielsen, and T.J. Wallington, Absolute rate constants for the reaction of NO with a series of peroxy radicals in the gas phase at 295 K, *Chem. Phys. Lett., 213,* 457-464, 1993.

Sehested, J., and T.J. Wallington, Atmospheric chemistry of hydrofluorocarbon 134a: Fate of the alkoxy radical CF_3O, *Environ. Sci. Technol., 27,* 146-152, 1993.

Shi, J., T.J. Wallington, and E.W. Kaiser, FTIR study of the Cl-initiated oxidation of C_2H_5Cl: Reactions of the alkoxy radical CH_3CHClO, *J. Phys. Chem., 97,* 6184-6192, 1993.

Solomon, S., J.B. Burkholder, A.R. Ravishankara, and R.R. Garcia, On the ozone depletion and global warming potentials of CF_3I, *J. Geophys. Res., 99,* 20929-20935, 1994.

Thompson, J.E., *Kinetics of $O(^1D)$ and $Cl(^2P)$ Reactions with Halogenated Compounds of Atmospheric Interest,* M.S. thesis, University of Colorado at Boulder, Boulder, Colorado, 1993.

Tuazon, E.C., R. Atkinson, and S.B. Corchnoy, Rate constants of the gas-phase reactions of Cl atoms with a series of hydrofluorocarbons and hydrochlorofluorocarbons at 298 ± 2 K, *Int. J. Chem. Kinet., 24,* 639-648, 1992.

Tuazon, E.C., and R. Atkinson, Tropospheric degradation products of CH_2FCF_3 (HFC-134a), *J. Atmos. Chem., 16,* 301-312, 1993a.

Tuazon, E.C., and R. Atkinson, Tropospheric transformation products of a series of hydrofluorocarbons and hydrochlorofluorocarbons, *J. Atmos. Chem., 17,* 179-199, 1993b.

Tuazon, E.C., and R. Atkinson, Products of the tropospheric reactions of hydrochlorofluorocarbons (HCFCs) -225ca, -225cb, -141b and -142b, submitted to *Environ. Sci. Technol.*, 1994.

Turnipseed, A.A., S. Barone, and A.R. Ravishankara, Kinetics of the reactions of CF_3O_x radicals with NO, O_3, and O_2, *J. Phys. Chem.*, in press, 1994.

Ugi, I., and F. Beck, Reaktion von Carbonsäurehalogeniden mit Wasser und Aminen, *Chem. Ber., 94,* 1839-1850, 1961.

Visscher, P.T., C.W. Culbertson, and R.S. Oremland, Degradation of trifluoroacetate in oxic and anoxic sediments, *Nature, 369,* 729-731, 1994.

Wallington, T.J., and O.J. Nielsen, Pulse radiolysis study of CF_3CHFO_2 radicals in the gas phase at 298 K, *Chem. Phys. Lett., 187,* 33-39, 1991.

Wallington, T.J., and M.D. Hurley, A kinetic study of the reaction of chlorine atoms with CF_3CHCl_2, CF_3CH_2F, $CFCl_2CH_3$, CF_2ClCH_3, CHF_2CH_3, CH_3D, CH_2D_2, CHD_3, CD_4, and CD_3Cl at 295 ± 2 K, *Chem. Phys. Lett., 189,* 437-442, 1992.

Wallington, T.J., M.D. Hurley, J.C. Ball, and E.W. Kaiser, Atmospheric chemistry of hydrofluorocarbon 134a: Fate of the alkoxy radical CF_3CFHO, *Environ. Sci. Technol., 26,* 1318-1324, 1992.

Wallington, T.J., and M.D. Hurley, Atmospheric chemistry of HC(O)F: Reaction with OH radicals, *Environ. Sci. Technol., 27,* 1448-1452, 1993.

Wallington, T.J., M.D. Hurley, W.F. Schneider, J. Sehested, and O.J. Nielsen, Atmospheric chemistry of CF_3O radicals: Reaction with H_2O, *J. Phys. Chem.*, *97*, 7606-7611, 1993a.

Wallington, T.J., M.D. Hurley, and W.F. Schneider, Kinetic study of the reaction $CF_3O + O_3 \rightarrow CF_3O_2 + O_2$, *Chem. Phys. Lett.*, *213*, 442-448, 1993b.

Wallington, T.J., M.D. Hurley, W.F. Schneider, J. Sehested, and O.J. Nielsen, Mechanistic study of the gas phase reaction of CH_2FO_2 radicals with HO_2, submitted to *Chem. Phys. Lett.*, 1994a.

Wallington, T.J., T. Ellerman, O.J. Nielsen, and J. Sehested, Atmospheric chemistry of FCO_x radicals: UV spectra and self reaction kinetics of FCO and $FC(O)O_2$, and kinetics of some reactions of FCO_x with O_2, O_3 and NO at 296 K, *J. Phys. Chem.*, in press, 1994b.

Wallington, T.J., and W.F. Schneider, The stratospheric fate of CF_3OH, *Geophys. Res. Lett.*, in press, 1994.

Warren, R.F., and A.R. Ravishankara, Kinetics of $Cl(^2P)$ reactions with a few hydrochlorofluorocarbons (HCFCs), *Int. J. Chem. Kinet.*, *25*, 833-844, 1993.

Wine, P.H., and W.L. Chameides, Possible atmospheric lifetimes and chemical reaction mechanisms for selected HCFCs, HFCs, CH_3CCl_3 and their degradation products against dissolution and/or degradation in sea water and cloud water, in *Scientific Assessment of Stratospheric Ozone: 1989,* Volume II, Appendix: AFEAS Report, World Meteorological Organization Global Ozone Research and Monitoring Project – Report No. 20, Geneva, 271-295, 1990.

WMO, *Scientific Assessment of Stratospheric Ozone; 1989,* World Meteorological Organization Global Ozone Research and Monitoring Project – Report No. 20, Volume II, Appendix: AFEAS Report, Geneva, 1990.

WMO, *Scientific Assessment of Ozone Depletion: 1991,* World Meteorological Organization Global Ozone Research and Monitoring Project – Report No. 25, Geneva, 1992.

Worsnop, D.R., M.S. Zahnizer, and C.E. Kolb, J.A.. Gardner, J.T. Jayne, L.R. Watson, J.M. VanDoren, and P. Davidovits, Temperature dependence of mass accommodation of SO_2 and H_2O_2 on aqueous surfaces, *J. Phys. Chem., 93,* 1159-1172, 1989.

Zander, R., M.R. Gunson, C.B. Farmer, C.P. Rinsland, F.W. Irion, and E. Mahieu, The 1985 chlorine and fluorine inventories in the stratosphere based on ATMOS observations at 30°N latitude, *J. Atmos. Chem., 15,* 171-186, 1992.

Zellner, R., A. Hoffmann, D. Bingemann, V. Mors, and J.P. Kohlmann, Time resolved product studies in the oxidation of HCFC-22 and HFC-134a under simulated tropospheric conditions, in *Kinetics and Mechanisms for the Reactions of Halogenated Organic Compounds in the Troposphere*, STEP-HALOCSIDE/AFEAS Workshop, May 14-16, Dublin, 94-103, 1991.

Zellner, R., A. Hoffmann, V. Mors, and W. Malms, Time resolved studies of intermediate products in the oxidation of HCFC's and HFC's, in *Kinetics and Mechanisms for the Reactions of Halogenated Organic Compounds in the Troposphere*, STEP-HALOCSIDE/AFEAS Workshop, March 23-25, Dublin, 1993.

CHAPTER 13

Ozone Depletion Potentials, Global Warming Potentials, and Future Chlorine/Bromine Loading

Lead Authors:
S. Solomon
D. Wuebbles

Co-authors:
I. Isaksen
J. Kiehl
M. Lal
P. Simon
N.-D. Sze

Contributors:
D. Albritton
C. Brühl
P. Connell
J.S. Daniel
D. Fisher
D. Hufford
C. Granier
S.C. Liu
K. Patten
V. Ramaswamy
K. Shine
S. Pinnock
G. Visconti
D. Weisenstein
T.M.L. Wigley

CHAPTER 13

OZONE DEPLETION POTENTIALS, GLOBAL WARMING POTENTIALS, AND FUTURE CHLORINE/BROMINE LOADING

Contents

SCIENTIFIC SUMMARY

Scientific indices representing the relative effects of different gases upon ozone depletion and climate forcing are presented. Several scenarios for future chlorine/bromine loading are described that are aimed at implementation of the Copenhagen Amendments of the Montreal Protocol and the consideration of possible further options. Ozone Depletion Potentials (ODPs) and Global Warming Potentials (GWPs) are evaluated with improved models and input data, and their sensitivities to uncertainties are considered in greater detail than in previous assessments. Major new findings are as follows:

- *Peak levels of ozone-depleting compounds are expected at stratospheric altitudes in the late 1990s.* Because current emission estimates suggest that the tropospheric chlorine/bromine loading will peak in 1994, further reductions in emissions would not significantly affect the timing or magnitude of the peak stratospheric halogen loading expected later this decade (*i.e.*, about 3-5 years after the tropospheric peak).

- *Approaches to lowering stratospheric chlorine and bromine abundances are limited.* Further controls on ozone-depleting substances would be unlikely to change the timing or the magnitude of the peak stratospheric halocarbon abundances and hence peak ozone loss. However, there are four approaches that would steepen the initial fall from the peak halocarbon levels in the early decades of the next century:

  (i) If emissions of methyl bromide from agricultural, structural, and industrial activities were to be eliminated in the year 2001, then the integrated effective future chlorine loading above the 1980 level (which is related to the cumulative future loss of ozone) is predicted to be 13% less over the next 50 years relative to full compliance with the Amendments and Adjustments to the Protocol.

  (ii) If emissions of hydrochlorofluorocarbons (HCFCs) were to be totally eliminated by the year 2004, then the integrated effective future chlorine loading above the 1980 level is predicted to be 5% less over the next 50 years relative to full compliance with the Amendments and Adjustments to the Protocol.

  (iii) If halons presently contained in existing equipment were never released to the atmosphere, then the integrated effective future chlorine loading above the 1980 level is predicted to be 10% less over the next 50 years relative to full compliance with the Amendments and Adjustments to the Protocol.

  (iv) If chlorofluorocarbons (CFCs) presently contained in existing equipment were never released to the atmosphere, then the integrated effective future chlorine loading above the 1980 level is predicted to be 3% less over the next 50 years relative to full compliance with the Amendments and Adjustments to the Protocol.

- *Failure to adhere to the international agreements will delay recovery of the ozone layer.* If there were to be additional production of CFCs at, for example, 20% of 1992 levels for each year through 2002 and ramped to zero by 2005 (beyond that allowed for countries operating under Article 5 of the Montreal Protocol), then the integrated effective future chlorine loading above the 1980 level is predicted to be 9% more over the next 50 years relative to full compliance with the Amendments and Adjustments to the Protocol.

- *Production of CF_3 from dissociation of CFCs, HCFCs, and hydrofluorocarbons (HFCs) is highly unlikely to affect ozone.* ODPs of HFCs containing the CF_3 group (such as HFC-134a, HFC-23, and HFC-125) are highly likely to be less than 0.001, and the contribution of the CF_3 group to the ODPs of HCFCs (*e.g.*, from HCFC-123) and CFCs is believed to be negligible.

ODPs, GWPs and Cl-Br LOADING

- *ODPs for several new compounds such as HCFC-225ca, HCFC-225cb, and CF_3I have been evaluated using both semi-empirical and modeling approaches,* and estimated to be 0.03 or less.

- *Both the direct and indirect components of the GWP of methane have been estimated using model calculations.* Methane's influence on the hydroxyl radical and the resulting effect on the methane response time lead to substantially longer response times for decay of emissions than OH removal alone, thereby increasing the GWP. In addition, indirect effects including production of tropospheric ozone and stratospheric water vapor were considered and are estimated to range from about 15 to 45% of the total GWP (direct plus indirect) for methane.

- *GWPs including indirect effects of ozone depletion have been estimated for a variety of halocarbons (CFCs, halons, HCFCs, etc.), clarifying the relative radiative roles of different classes of ozone-depleting compounds.* The net GWPs of halocarbons depend strongly upon the effectiveness of each compound for ozone destruction; the halons are highly likely to have negative net GWPs, while those of the CFCs are likely to be positive over both 20- and 100-year time horizons.

- *GWPs are not very sensitive to likely future changes in CO_2 abundances or major climate variables.* Increasing CO_2 abundances (from about 360 ppmv currently to 650 ppmv by the end of the 22nd century) could produce 20% larger GWPs for time horizons of the order of centuries. Future changes in clouds and water vapor are unlikely to significantly affect GWPs for most species.

- *GWPs for 16 new chemical species have been calculated, bringing the number now available to 38.* The new species are largely HFCs, which are being manufactured as substitutes for the CFCs, and the very long-lived fully fluorinated compounds, SF_6 and the perfluorocarbons.

13.1 INTRODUCTION

Numerical indices representing the relative impacts of emissions of various chemical compounds upon ozone depletion or global radiative forcing can be useful for both scientific and policy analyses. Prominent among these are the concepts of Chlorine/Bromine Loading, steady-state and time-dependent Ozone Depletion Potentials (ODPs), and Global Warming Potentials (GWPs), which form the focus of this chapter. Detailed descriptions of the formulations of these indices are provided later. Here we briefly review the broad definitions of these concepts and cite some of their uses and limitations:

Chlorine/Bromine Loading

Chlorine/bromine loading represents the amount of total chlorine and bromine in the troposphere or stratosphere. Stratospheric chlorine/bromine loading depends upon the surface emissions of gases such as chlorofluorocarbons (CFCs), hydrochlorofluorocarbons (HCFCs), and halons (which are based in large part upon industrial estimates of usage) and upon knowledge of the reactivity and hence the atmospheric lifetimes and chemical roles of those and related compounds. Recent depletions in stratospheric ozone in Antarctica and in the Arctic have been linked to anthropogenic halocarbon emissions (see Chapter 3), and the weight of evidence suggests that ozone depletions in midlatitudes are also related to the emissions of these compounds (see WMO, 1992 and Chapter 4 of this document). Thus, the chlorine/bromine loading is a key indicator of past and future changes in ozone. However, it should be recognized that chlorine/bromine loading is a measure only of changes in halogen content. It does not account for additional factors that could also affect the time-dependent changes in atmospheric ozone or the linearity of their relationship to chlorine/bromine loading (*e.g.*, carbon dioxide trends that can also affect stratospheric temperatures).

Ozone Depletion Potentials

Ozone Depletion Potentials (ODPs) provide a relative measure of the expected impact on ozone per unit mass emission of a gas as compared to that expected from the same mass emission of CFC-11 integrated over time (Wuebbles, 1983; WMO, 1990, 1992; Solomon *et al.*, 1992). Their primary purpose is for comparison of relative impacts of different gases upon ozone (*e.g.*, for evaluating the relative effects of choices among different CFC substitutes upon ozone). As in prior analyses, the ODP for each substance presented herein is based on the mass emitted into the atmosphere, and not on the total amount used. In some cases (such as emissions of CH_3Br in soil fumigant applications) not all of the compound used may be emitted into the global atmosphere (see Chapter 10). Steady-state ODPs represent the cumulative effect on ozone over an infinite time scale (also referred to here as "time horizon"). Time-dependent ODPs describe the temporal evolution of this ozone impact over specific time horizons (WMO, 1990, 1992; Solomon and Albritton, 1992; see Section 13.4.5). Atmospheric models and semi-empirical methods have been used in combination to best quantify these relative indices (Solomon *et al.*, 1992; WMO, 1992). As a relative measure, ODPs are subject to fewer uncertainties than estimates of the absolute percentage ozone depletion, particularly when only the ODP differences among various chlorinated gases are considered. Models used to evaluate ODPs now include better representations of midlatitude and polar vortex heterogeneous chemistry processes than those used earlier. Comparisons of model and semi-empirical methods reduce the uncertainties in ODPs. However, evaluations of ODPs are still subject to uncertainties in atmospheric lifetimes and in the understanding of stratospheric chemical and dynamical processes. The recent re-evaluation of the chemical rate and products for the reaction of $BrO + HO_2$ and resulting effects on ODPs for bromocarbons provide a graphic example of potential impacts of such uncertainties (see Section 13.4). Like chlorine/bromine loading, ODPs do not include other processes (such as changes in CO_2 and hence stratospheric temperatures) that could affect the future impacts of different gases upon ozone.

Global Warming Potentials

Global Warming Potentials provide a simple representation of the relative radiative forcing resulting from a unit mass emission of a greenhouse gas compared to a reference compound. Because of its central role in concerns about climate change, carbon dioxide has generally been used as the reference gas. However, because of the complexities and uncertainties associated with the

carbon cycle, extensive effort has been put into evaluating the effects on GWPs from uncertainties in the time-dependent uptake of carbon dioxide emissions. As described in Chapter 4 of IPCC (1994), calculations made with climate models indicate that, for well-mixed greenhouse gases at least, the relationship between changes in the globally integrated adjusted radiative forcing at the tropopause and global-mean surface temperature changes is independent of the gas causing the forcing. Furthermore, similar studies indicate that, to first order, this "climate sensitivity" is relatively insensitive to the type of forcing agent (*e.g.*, changes in the atmospheric concentration of a well-mixed greenhouse gas such as CO_2, or changes in the solar radiation reaching the atmosphere). GWPs have a number of important limitations. The GWP concept is difficult to apply to gases that are very unevenly distributed and to aerosols (see, *e.g.*, Wang *et al.*, 1991, 1993). For example, relatively short-lived pollutants such as the nitrogen oxides and the volatile organic compounds (precursors of ozone, which is a greenhouse gas) vary markedly from region to region within a hemisphere and their chemical impacts are highly variable and nonlinearly dependent upon concentrations. Further, the indices and the estimated uncertainties are intended to reflect global averages only, and do not account for regional effects. They do not include climatic or biospheric feedbacks, nor do they consider any environmental impacts other than those related to climate. The direct GWPs for a number of infrared-absorbing greenhouse gases have been analyzed in this report, with a particular emphasis on a wide range of possible substitutes for halocarbons. The evaluation of effects on other greenhouse gases resulting from chemical interactions (termed indirect effects) has been more controversial. Underlying assumptions and uncertainties associated with both direct and indirect GWPs are discussed briefly in Section 13.5.

13.2 ATMOSPHERIC LIFETIMES AND RESPONSE TIMES

Atmospheric lifetimes or response times are used in the calculation of both ODPs and GWPs. The list of compounds considered in this assessment is an extension of those in WMO (1992), primarily reflecting the consideration of additional possible replacements for CFCs and halons. Additional compounds, such as the unusually long-lived perfluorocarbons and SF_6, are also included because of their potential roles as greenhouse gases and because some have been suggested as CFC and halon replacements.

After emission into the current or projected atmosphere, the time scale for removal (*i.e.*, the time interval required for a pulse emission to decay to 1/e of its initial perturbed value) of most ozone-depleting and greenhouse gases reflects the ratio of total atmospheric burden to integrated global loss rate. As such, the total lifetime must take into account all of the processes determining the removal of a gas from the atmosphere, including photochemical losses within the troposphere and stratosphere (typically due to photodissociation or reaction with OH), heterogeneous removal processes, and permanent removal following uptake by the land or ocean. In a few cases, the time scale for removal of a gas from the atmosphere cannot be simply characterized or is dependent upon the perturbation and/or the background atmosphere and other sources; in those cases (chiefly CO_2 and CH_4) we refer to removal of a pulse as the response time or decay response.

Alternatively, atmospheric lifetimes can be defined by knowledge of global source strengths together with the corresponding mean atmospheric concentrations and trends, but these are usually more difficult to define accurately. The atmospheric lifetime may be a function of time, due to changing photochemistry associated, for example, with ozone depletion or temperature trends, but these effects are likely to be small for at least the next several decades and will not be considered here.

The total lifetimes of two major industrially produced halocarbons, CFC-11 and CH_3CCl_3, have been reviewed and re-evaluated in a recent assessment (Kaye *et al.*, 1994). The empirically derived lifetime for CFC-11 determined in that study is 50 (±5) years (as compared to 55 years in the previous WMO [1992] assessment). As in previous assessments, the lifetimes presented here are not based solely upon model calculations, but use information from measurements to better constrain the lifetimes of these and other gases. The lifetime of CFC-11 is used here to normalize lifetimes for other gases destroyed by photolysis in the stratosphere (based upon scaling to the ratios of the lifetimes of each gas compared to that of CFC-11 obtained in the models discussed in Kaye *et al.*, 1994). This approach could be limited by the fact that different gases are destroyed in

different regions of the stratosphere depending upon the wavelength dependence of their absorption cross sections (weakening the linearity of their comparison to CFC-11), particularly if stratospheric mixing is not rapid (see Plumb and Ko, 1992). Depending on absolute calibration factors used by different research groups, Kaye *et al.* (1994) derived a total lifetime for CH_3CCl_3 of either 5.7 (±0.3) years for 1990 or 5.1 (±0.3) years, respectively (see Prinn *et al.*, 1992), compared to 6.1 years in the earlier WMO (1992) assessment. Because of the current uncertainties in absolute calibration, we use a lifetime for CH_3CCl_3 of 5.4 years with an uncertainty range of 0.6 years in this report. From this total atmospheric lifetime, together with the evaluated loss lifetimes of CH_3CCl_3 due to the ocean (about 85 years, with an uncertainty range from 50 years to infinity; see Butler *et al.*, 1991) and stratospheric processes (40 ± 10 years), a tropospheric lifetime for reaction with OH of 6.6 years can be inferred (±25%). The lifetimes of other key gases destroyed by OH (*i.e.*, CH_4, HCFCs, and hydrofluorocarbons [HFCs]) can then be inferred relative to that of methyl chloroform (see, *e.g.*, Prather and Spivakovsky, 1990) with far greater accuracy than would be possible from a priori calculations of the complete tropospheric OH distribution. We note that a few of the newest CFC substitutes (namely, the HFCs -236fa, -245ca, and -43-10mee) have larger uncertainties in lifetimes since fewer kinetic studies of their chemistry have been reported to date. It is likely that methane is also destroyed in part by uptake to soil (IPCC, 1992), but this process is believed to be relatively slow and makes a small contribution to the total lifetime. Possible soil sinks are not considered for any other species.

The special aspects of the lifetime of methane and the response time of a pulse added to the atmosphere were defined in Chapter 2 of IPCC (1994), based largely upon Prather (1994). Those definitions are also employed here. Small changes in CH_4 concentrations can significantly affect the atmospheric OH concentration, rendering the response time for the decay of the added gas substantially longer than that of the ensemble (*i.e.*, longer than the nominal 10-yr lifetime for the bulk concentration of atmospheric CH_4 in the current atmosphere). This is due to the nonlinear chemistry associated with relaxation of the coupled OH-CO-CH_4 system (see Prather, 1994; Lelieveld *et al.*, 1993; and Chapter 2 of IPCC [1994] for further details). This effect was also discussed in IPCC (1990) and IPCC (1992) as an indirect effect on OH concentrations, and thus is not new. It arises through the fact that small changes in OH due to addition of a small pulse of CH_4 slightly affect the rate of decay of the much larger amount of CH_4 in the background atmosphere, thereby influencing the net removal of the added pulse. It is critical to note that the exact value of the CH_4 pulse response time depends upon a number of key factors, including the absolute amount of CH_4, size of the pulse, etc., making its interpretation complex and case-dependent. Here we consider small perturbations to the present atmosphere, and base the definition of the methane pulse response time to be used in calculation of the GWP upon the detailed explanation of the effect as presented in Prather (1994) and in Chapter 2 of IPCC (1994).

Table 13-1 shows the recommended total atmospheric lifetimes for all of the compounds considered here except methyl bromide (the reader is referred to Chapter 10 for a detailed discussion of the lifetime of this important gas). The response time of methane is also indicated. The lifetimes for many compounds have been modified relative to values used in WMO (1992; Table 6-2). The estimates for the lifetimes of many of the gases destroyed primarily by reaction with tropospheric OH (*e.g.*, HCFC-22, HCFC-141b, HCFC-142b, etc.) are about 15% shorter than in WMO (1992), due mainly to recent studies suggesting a shorter lifetime for CH_3CCl_3 based upon improved calibration methods and upon an oceanic sink (Butler *et al.*, 1991). Similarly, the estimates for the lifetimes of gases destroyed mainly by photolysis in the stratosphere (*e.g.*, CFC-12, CFC-113, H-1301) are about 10% shorter than in IPCC (1992) due to a shorter estimated lifetime for CFC-11 and related species. Lifetime estimates of a few other gases have also changed due to improvements in the understanding of their specific photochemistry (*e.g.*, note that the lifetime for CFC-115 is now estimated to be about 1700 years, as compared to about 500 years in earlier assessments). Fully fluorinated species such as SF_6, CF_4, and C_2F_6 have extremely long atmospheric lifetimes, suggesting that significant production and emissions of these greenhouse gases could have substantial effects on radiative forcing over long time scales. In contrast, CF_3I, which is being considered for use as a fire extinguishant and other applications, has an atmospheric lifetime of less than 2 days.

Table 13-1. Lifetimes and response times recommended for ODP and GWP calculations.

Gas	Lifetime or Response Time (yrs)	Reference
CFC-11	50 (±5)	2
CFC-12	102	3
CFC-13	640	1
CFC-113	85	3
CFC-114	300	1
CFC-115	1700	1
CCl_4	42	3
CH_3CCl_3	5.4 (±0.4)	2
$CHCl_3$	0.55	4
CH_2Cl_2	0.41	4
HCFC-22	13.3	4
HCFC-123	1.4	4
HCFC-124	5.9	4
HCFC-141b	9.4	4
HCFC-142b	19.5	4
HCFC-225ca	2.5	4
HCFC-225cb	6.6	4
CH_3Br	1.3	Chapter 10
CF_3Br (H-1301)	65	3
CF_2ClBr (H-1211)	20	3
HFC-23	250	10
HFC-32	6.0	4
HFC-125	36	4
HFC-134	11.9	5
HFC-134a	14	4
HFC-143	3.5	11
HFC-143a	55	4
HFC-152a	1.5	4
HFC-227ea	41	9
HFC-236fa	250	7
HFC-245ca	7	6
HFC-43-10mee	20.8	7
HFOC-125E	82	6
HFOC-134E	8	6
SF_6	3200	1
CF_4	50000	1
C_2F_6	10000	1
C_6F_{14}	3200	1
C_5F_{12}	4100	1
c-C_4F_8	3200	1
CF_3I	< 0.005	8
N_2O	120	3
CH_4 (pulse response)	14.5 ± 2.5	12

Table 13-1. Notes.

1. Ravishankara *et al.* (1993).
2. Prather, private communication 1993, based on NASA CFC report (Kaye *et al.*, 1994) and other considerations as described in text.
3. Average of reporting models in NASA CFC report (Kaye *et al.*, 1994). Scaled to CFC-11 lifetime.
4. Average of JPL 92-20 and IUPAC (1992) with 277 K rate constants for OH+halocarbon scaled against OH+CH_3CCl_3 and lifetime of tropospheric CH_3CCl_3 of 6.6 yr. Stratospheric lifetime from WMO (1992).
5. DeMore *et al.* (1993). Used 277 K OH rate constant ratios with respect to CH_3CCl_3, scaled to tropospheric lifetime of 6.6 yr for CH_3CCl_3.
6. Cooper *et al.* (1992). Lifetime values are estimates.
7. W. DeMore (personal communication, 1994) with 277 K rate constants for OH+halocarbon scaled against OH+CH_3CCl_3 and lifetime of tropospheric CH_3CCl_3 of 6.6 yr.
8. Solomon *et al.* (1994).
9. Brühl, personal communication based on data for the reaction rate constant with OH provided by Hoescht Chemicals, 1993; Zhang *et al.* (1994) and Nelson *et al.* (1993) with 277 K rate constants for OH+halocarbon scaled against OH + CH_3CCl_3 and lifetime of tropospheric CH_3CCl_3 of 6.6 yr.
10. Schmoltner *et al.* (1993) with 277 K rate constants for OH+halocarbon scaled against OH+CH_3CCl_3 and lifetime of tropospheric CH_3CCl_3 of 6.6 yr.
11. Barry *et al.* (1994) with 277 K rate constants for OH+halocarbon scaled against OH+CH_3CCl_3 and lifetime of tropospheric CH_3CCl_3 of 6.6 yr.
12. Prather (1994) and Chapter 2 of IPCC (1994).

The basis for the recommended lifetimes is described within the Table and its footnotes. These values are used for all calculations presented in this chapter.

13.3 CHLORINE/BROMINE LOADING AND SCENARIOS FOR CFC SUBSTITUTES

13.3.1 Equivalent Tropospheric Chlorine Loading

For the purposes of this report, a detailed assessment of those sources of tropospheric chlorine and bromine loading relevant to stratospheric ozone destruction was carried out. The approach taken is similar to that of Prather and Watson (1990) and previous assessment reports (WMO, 1992). This analysis is more complete in that it includes a description of the time delay between consumption and emission of the ozone-depleting substances. The time delays are based upon uses (*e.g.*, refrigeration, solvents, etc.). The procedure is also discussed in Daniel *et al.* (1994). The best understanding of the past history of emissions of fourteen of the most important halocarbons, together with current estimates of the lifetimes of these gases (Table 13-1) provides the input needed to evaluate past trends. The longest and most complete record of CFC emissions is contained in the industry-sponsored "Production, Sales and Atmospheric Release of Fluorocarbons" report (AFEAS, 1993). This report contains estimates of production in countries not covered in the industry survey. Recently, with declining global production in response to the Montreal Protocol, the fractional contribution to the total of this "unreported" production, a portion of which is in developing (Article 5) countries, has amounted to about 25%. Estimates of unreported production based on matching observed and calculated trends in the relevant trace gases are consistent with AFEAS estimates (see, *e.g.*, the detailed analysis in Cunnold *et al.*, 1994).

Expected uses and the corresponding release times for each of the gases are considered, in order to more accurately determine yearly emission amounts (AFEAS, 1993; Fisher and Midgley, 1993; Gamlen *et al.*, 1986; McCarthy *et al.*, 1977; McCulloch, 1992; Midgley, 1989; Midgley and Fisher, 1993). Possible time-dependent changes in release times (*e.g.*, for improved technologies) are not considered. For methyl bromide, a budget of natural and anthropogenic sources based upon

Chapter 10 is adopted. Anthropogenic sources of methyl bromide are assumed to be zero before 1931. A constant anthropogenic emission is assumed from 1931 to 1994 of 73 ktonnes/year (see Chapter 10). As noted in Chapter 10, it is possible that decreases in methyl bromide emissions associated with the declining use of gasoline additives could have offset some of the known increases in agricultural use of this compound during the 1970s and 1980s. However, precise information is not available. Although this assumption will affect the calculated historical contribution of methyl bromide to equivalent chlorine loading, because of the short lifetime of methyl bromide, it has very little effect on projected contributions. Anthropogenic emission of methyl bromide does not equal production, and this difference is explicitly considered in all calculations of methyl bromide's atmospheric loading and their impacts presented in this chapter.

The calculated contributions of methyl bromide and other bromocarbons to equivalent chlorine loading are more uncertain than that of other compounds. For the purpose of comparing the roles of chlorine- and bromine-containing gases once they reach the stratosphere, it is assumed that each bromine atom is 40 times more damaging to ozone than chlorine (see Section 13.4), allowing evaluation of an "equivalent tropospheric chlorine" that includes an estimate of the net ozone impact of bromocarbons. The enhanced effectiveness of bromine (hereafter referred to as α) depends in principle upon the amount of active chlorine present, making it a time-dependent quantity. However, in the next few decades (*i.e.*, until about 2020), the chlorine content of the stratosphere is expected to change relatively little, making α essentially constant during this period. Towards the middle and latter parts of the twenty-first century, decreases in chlorine abundances will likely lead to increases in the value of α, at least in polar regions. This follows from the fact that the reaction of ClO with itself represents an important ozone loss process in the Antarctic (and Arctic) that is dependent upon the square of the stratospheric chlorine abundance, while the reaction of ClO with BrO is linearly dependent upon the stratospheric chlorine abundance. Thus, as chlorine abundances decline, the reaction of ClO with BrO will become more important relative to ClO + ClO. This and other considerations discussed in Section 13.4 (particularly the role of the HO_2 + BrO reaction in the lower stratosphere) suggest that the adopted value of α of 40 is likely to be a low estimate. A higher value of α would increase the contributions of methyl bromide and the halons. The adopted methyl bromide lifetime of 1.3 years includes an ocean sink. If loss to the ocean were to be slower, the lifetime would be longer and the anthropogenic methyl bromide contribution would be larger. On the other hand, a faster ocean sink would decrease the contribution. Similarly, a decrease (increase) in the fractional emission of methyl bromide used for agricultural purposes would decrease (increase) the calculated contribution from that source. The budget of methyl bromide and its uncertainties are discussed in detail in Chapter 10 of this assessment.

Chlorinated solvents such as CH_2Cl_2, C_2Cl_4, and C_2HCl_3 were not explicitly considered in this analysis. Based upon emission estimates, WMO (1992) suggests that these species are present at about the 35, 32, and 1 pptv levels, respectively, within the current troposphere. Wang *et al.* (1994) present observations of C_2Cl_4 showing average abundances of only 7 pptv. The lifetimes of these gases may be long enough to allow a fraction to reach the stratosphere and thereby contribute to stratospheric chlorine loading. Schauffler *et al.* (1993) report tropospheric measurements of CH_2Cl_2 of about 30 pptv in 1992 and report direct measurements of this gas near the tropical tropopause of about 15 pptv, suggesting substantial transport to the stratosphere. While the abundances of these gases are presently small, increasing use would increase the abundances. At a growth rate of, for example, 3%/year, CH_2Cl_2 and C_2HCl_3 could reach abundances of 0.1 ppbv in 36 and 156 years, respectively. Thus, while these relatively short-lived gases probably contribute little to contemporary stratospheric chlorine loading, there is observational evidence of significant transport to the stratosphere for some species, and continued growth would lead to a greater contribution to stratospheric chlorine loading. On the other hand, a recent survey (P. Midgley, personal communication) indicates that industrial emissions of these gases in the U.S., Europe, and Japan have steadily decreased since 1984, so that current emissions are more likely to be decreasing than increasing.

Water-soluble emissions such as sea salt or volcanic HCl are effectively removed in clouds and rain (see, *e.g.*, Tabazadeh and Turco, 1993) and do not represent significant sources of stratospheric chlorine. Short-lived

bromocarbons such as bromoform were also not considered here.

Equivalent chlorine loading was evaluated for eight cases to demonstrate impacts of various assumptions for future use of ozone-depleting substances. A complete description of the scenarios is provided in Table 13-2. Global compliance to the Copenhagen agreements is represented by case A. Estimates of future emissions of hydrochlorofluorocarbons (HCFCs) and hydrofluorocarbons (HFCs) are based on a detailed analysis of projected global demand for each gas carried out by the U.S. Environmental Protection Agency (EPA) to 2030 (D. Hufford, personal communication, 1993). Estimates beyond 2030 will depend on agreements for HCFC use in developing countries; no attempt is made to account for potential use and emissions beyond 2030. Such use would increase the HCFC equivalent chlorine loading. Figure 13-1 shows calculated tropospheric concentrations of HCFCs and HFC-134a based on the EPA analysis.

A complete phase-out of HCFCs after 2030 is assumed, after which time a 2.5%/year increase in HFC-134a is adopted (intended to represent not only HFC-134a itself but the combined impact of a class of hydrofluorocarbons that could be used as HCFC substitutes after 2030). These are important only insofar as their radiative forcing is concerned, since they do not significantly deplete stratospheric ozone (see Section 13.4). The use of shorter-lived or less infrared active gases could reduce the estimated radiative forcing from such compounds. Figure 13-1 shows a steep increase in the projected HFC concentrations in the latter part of the twenty-first century; the effect of such increases on radiative forcing is discussed further in Chapter 8.

Cases B through G demonstrate impacts relative to case A of continued CFC production outside international agreements, an accelerated HCFC phaseout, a methyl bromide phaseout or a 2%/year increase in industrial methyl bromide use, and complete recapture (as opposed to recycling) of halons, CFCs-11, -12, and -113 banked in existing equipment (*i.e.*, refrigeration, air-conditioning, fire extinguishants). Recapture illustrates the impact of potential use of non-ozone depleting substitutes that could reduce future emissions of these compounds. Case H is presented in order to compare the current (Copenhagen) agreements to the earlier London Amendments.

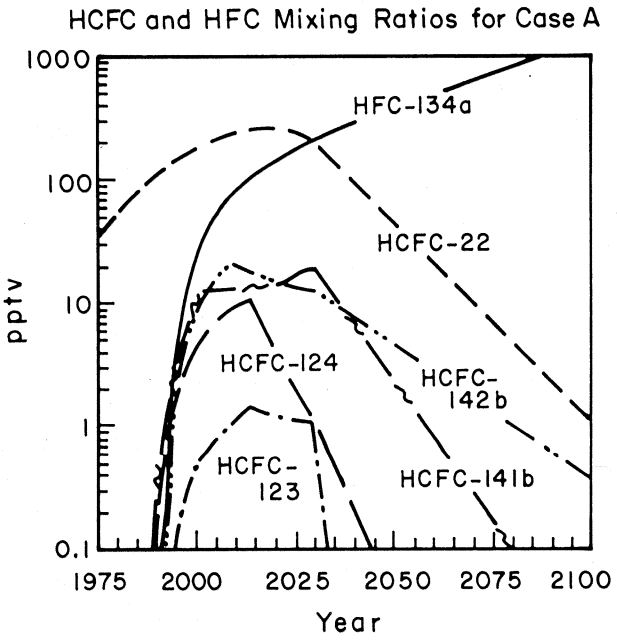

Figure 13-1. Calculated abundances of hydrofluorocarbons and hydrochlorofluorocarbons for case A.

The bottom panel of Figure 13-2 shows the contributions of the various gases considered here to the equivalent tropospheric chlorine versus time for case A. It shows that anthropogenic sources of chlorine and bromine are believed to have contributed much of the equivalent chlorine in today's troposphere. Direct measurements of chlorinated and brominated source gases have been obtained near the inflow region at the tropical tropopause on recent aircraft missions (Schauffler *et al.*, 1993). These reveal abundances of halocarbon source gases very close to those shown in Figure 13-2 for 1992. Further, concurrent measurements on-board the same aircraft confirm that HCl emitted at low altitudes from volcanoes, oceans, and other sources makes a very small contribution to the total chlorine injected in the tropical stratospheric inflow region (less than 0.1 ppbv; Schauffler *et al.*, 1993). Figure 13-2 also shows that equivalent chlorine is expected to maximize in the troposphere in 1994 under current agreements, and would return to levels near those believed to be present when Antarctic ozone depletion first became statistically significant compared to variability (*i.e.*, near 1980) around the middle of the twenty-first century if the emissions corresponding to case A are adopted. Since equivalent

Table 13-2. Scenarios for future chlorine and bromine loading.

Case	Description
Case A	Global Compliance to Montreal Protocol as Amended and Adjusted in Copenhagen (Protocol): CFCs, carbon tetrachloride, and methyl chloroform phased out in developed countries by 1996. Consumption in 1992 for Article 5 countries is assumed to be 5% of 1992 global production, growing to 10% of 1992 global production by 1996, constant to 2002, and a linear decline to zero by 2006. HCFC emissions based on U.S. EPA analysis as described in the test, and are consistent with limits under the Protocol. The halons in existing equipment (the "bank") as derived from McCulloch, 1992, are emitted in equal amounts over the period 1993 - 2000 for halon-1211 and the period 1993-2010 for halon-1301. Methyl bromide emissions are assumed constant over the period 1994 - 2100.
Case B	Production and Consumption Outside Protocol: Assumes continued production of CFC and carbon tetrachloride production at a rate equal to about 20% of 1992 global production through 2002 and then a linear decrease to zero by 2006. All other emissions as in case A.
Case C	Destruction of Halon Bank: Assumes all halons contained in existing equipment are completely recovered after 1994. All other emissions as in case A.
Case D	HCFC Early Phase-Out: Assumes that HCFC emissions cease on a global basis in 2004. All other emissions as in case A.
Case E	Methyl Bromide Increase: Assumes a 2%/year increase in agricultural emissions of methyl bromide until global agricultural emissions reach a maximum value three times that of the present. All other emissions as in case A.
Case F	Methyl Bromide Phase-Out: Assumes a 100% phase-out in all anthropogenic sources of methyl bromide emission except biomass burning (see Chapter 10) by 2001. All other emissions as in case A.
Case G	Destruction of CFC Bank: Assumes that all banked CFC-11 and CFC-12 in hermetically sealed and non-hermetically sealed refrigeration categories are completely recovered in 1995 and hence never released to the atmosphere. All banked CFC-113 is also assumed to be completely recovered. All other emissions as in case A.
Case H	London Amendments: Global compliance with the 1990 London Amendments to the Montreal Protocol rather than the 1992 Copenhagen Amendments.

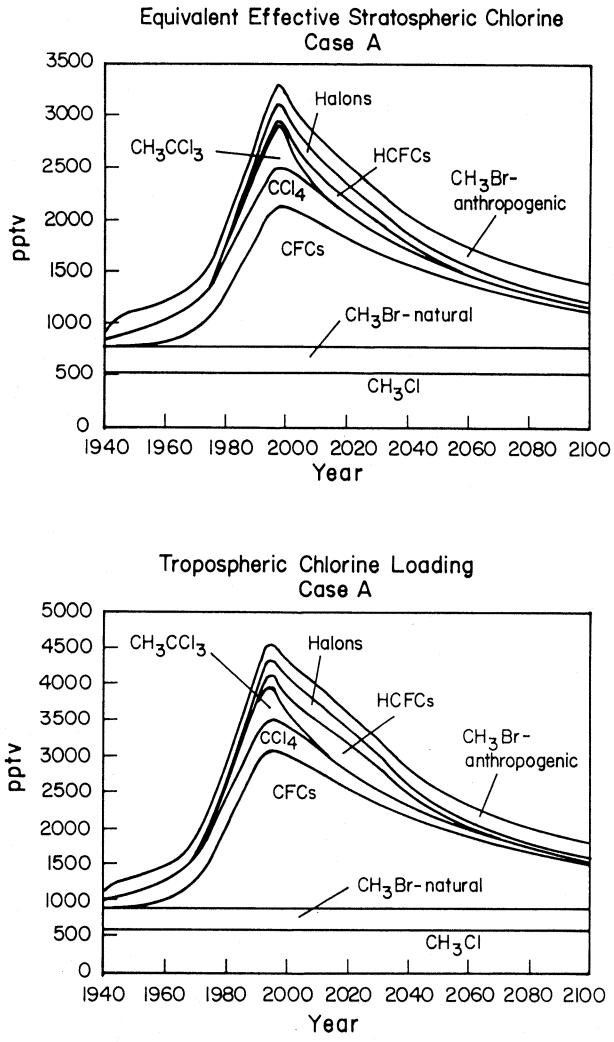

Figure 13-2. Contributions of various gases to the equivalent tropospheric (bottom) and stratospheric (top) chlorine versus time for case A.

tropospheric chlorine loading is expected to maximize in 1994, further controls would not reduce peak concentrations provided that global emissions continue to follow the requirements of the Protocol and its Amendments. However, consumption outside current Protocol agreements could increase the concentration.

13.3.2 Equivalent Effective Stratospheric Chlorine

Tropospheric chlorine loading alone does not determine the impact of a compound upon ozone loss, especially in the key region below about 25 km. Compounds that dissociate less readily within the stratosphere than others deliver less reactive chlorine, thereby decreasing their effectiveness from that indicated by their tropospheric loading. Examples of this behavior include HCFC-22 and HCFC-142b. Observations show that about 65% of the input of these gases to the stratosphere remains undissociated by the time they exit the stratosphere (see Solomon *et al.*, 1992), substantially reducing their impact on stratospheric ozone as compared to gases such as CCl_4, which undergo nearly complete dissociation while in the stratosphere. Here we evaluate the chlorine release in the lower stratosphere (below 25 km), since this is the region where most of the column-integrated ozone loss in the present atmosphere is observed to take place (WMO, 1992 and Chapter 1 of this document). The dissociation of many key compounds relative to a reference gas (CFC-11) in the lower stratosphere has been evaluated by Solomon *et al.* (1992) and by Daniel *et al.* (1994) using both observations and model calculations and is used here to define the equivalent effective stratospheric chlorine (EESC). In addition, a 3-year lag between tropospheric emission of halocarbons and stratospheric ozone impact is assumed, based in part on tracer studies (*e.g.*, Pollock *et al.*, 1992). Using these factors together with the estimate of α of 40 as discussed above, we define an "equivalent effective stratospheric chlorine" abundance that characterizes the impact of each source gas upon lower stratospheric ozone (similar to the "free halogen" defined in WMO, 1992). This definition is the same as that used for time-dependent ODPs discussed in Section 13.4.5.

The top panel of Figure 13-2 displays cumulative equivalent effective stratospheric chlorine for case A. Curves are lowered compared to tropospheric chlorine loading due to incomplete dissociation of the compounds. Peak chlorine loading occurs in 1997 as determined by the peak tropospheric loading that occurred three years earlier (bottom panel), suggesting that the maximum risk of ozone depletion has been determined by emissions occurring prior to 1995, assuming case A emissions.

Figure 13-3 shows the equivalent effective stratospheric chlorine represented by case A (Copenhagen Amendments) compared to the provisions of the original 1987 Montreal Protocol. The figure also illustrates what could have happened with no international agreements

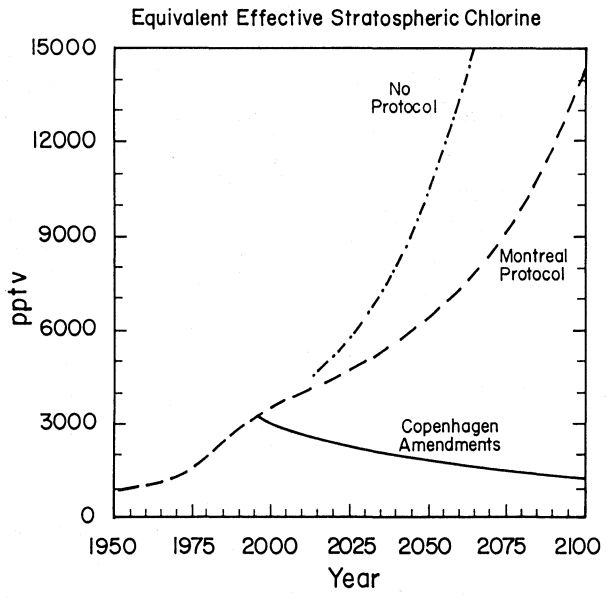

Figure 13-3. Estimated equivalent effective stratospheric chlorine represented by case A (Copenhagen Amendments) compared to the provisions of the original 1987 Montreal Protocol, and a case with no international agreements on ozone-depleting gases (where a 3%/year increase in global emissions of CFCs and methyl chloroform was assumed, less than known trends up to that time).

on ozone-depleting gases (where a 3%/year increase in global emissions of CFCs and methyl chloroform was assumed, less than known trends up to that time). The figure shows that without international agreements, equivalent effective stratospheric chlorine would likely reach values about twice as large as today's levels by 2030 and about three times today's levels by about 2050. Even with the provisions of the original Montreal Protocol, equivalent effective stratospheric chlorine would be likely to double by about the year 2060. Instead, under the current provisions, the stratospheric abundances of ozone-depleting gases are expected to begin to decrease within a few years.

One important measure of future ozone loss is the time integrated equivalent effective chlorine (pptv-year) to be expected from January 1, 1995, through the time when ozone depletion is likely to cease (*i.e.*, the integrated future ozone loss). Ozone depletion first became observable in a statistically significant sense in about 1980, making the return to equivalent effective chlorine for that year a reasonable proxy for the point where, all other things being equal, ozone depletion is likely to cease. For case A, for example, that point in time (referred to here as x) is expected to be reached in 2045. Table 13-3 presents the corresponding years for the other scenarios considered here. For evaluating cumulative long-term ecological impacts due to ozone depletion, it may also be useful to consider a similar integral beginning not in 1995 but in 1980 (thus integrating over the entire period when ozone depletion has been observed). A similar definition was used in WMO (1992), except that tropospheric values in 1985 were chosen as the reference point below which ozone depletion was assumed to cease, and the integral was performed from that point onwards rather than from 1995 onwards. Table 13-3 compares the percent differences from the base case A for each scenario for the following quantities: a) integrated equivalent effective stratospheric chlorine loading from 1995 until year x (the point when EESC drops below 1980 levels) and b) integrated equivalent effective stratospheric chlorine loading from 1980 until year x. Positive values denote integrated EESC levels that exceed the base case, while negative values indicate integrated EESC levels below the base Copenhagen scenario. The magnitudes of natural sources of chlorine and bromine (*e.g.*, from CH_3Cl and CH_3Br) do not influence these calculations, provided that they are not changing with time.

13.4 OZONE DEPLETION POTENTIALS

13.4.1 Introduction

Understanding of atmospheric chemical processes and the representation of these processes in models of global atmospheric chemistry and physics have improved since the WMO (1992) assessment. In particular, prior modeling analyses of ODPs were based largely on calculations including only gas phase chemistry, although a few calculations were carried out that included some of the chemistry occurring on background sulfuric acid aerosols. Some of the models used in the analysis presented here include representations of polar vortex processes (albeit in highly parameterized fashions) as well as most effects of heterogeneous chemistry on background sulfuric acid (but not volcanic) aerosols. The models still tend to underestimate the absolute

Table 13-3. Results of scenario calculations: integrated EESC differences (from case A) and the year when EESC drops below 1980 levels.

Scenario	Year (x) when EESC is expected to drop below 1980 value	Percent difference in $\int_{1995}^{x} EESC\,dt$ from case A.	Percent difference in $\int_{1980}^{x} EESC\,dt$ from case A.
A - Copenhagen	2045	0.0	0.0
B - Production outside of Protocol	2048	+9	+7
C - Destruction of halon bank	2043	-10	-7
D - HCFC early phase-out	2044	-5	-4
E - Methyl bromide increase	2057	+11	+9
F - Methyl bromide phase-out	2040	-13	-10
G - Destruction of CFC bank	2044	-3	-2
H - London Amendments	2055	+38	+30

ozone losses in the lowest part of the stratosphere (see Chapter 6); these limitations can affect ODPs, especially those for bromocarbons. The semi-empirical approach developed by Solomon *et al.* (1992) implicitly accounts for observed ozone destruction profiles both inside and outside of the polar vortices that are believed to reflect heterogeneous processes. While the semi-empirical approach is based upon limited data at low latitudes and high altitudes (above about 25 km), these limitations occur in regions that are believed to make relatively small contributions to the globally averaged ozone loss and hence to the ODP. Based upon these improvements in understanding, we did not explicitly evaluate chlorine loading potentials (a simpler but less complete index) in this report (see WMO, 1992).

13.4.2 Relative Effectiveness of Halogens in Ozone Destruction

A range of molecules are being considered as substitutes for the chlorofluorocarbons and halons. Some of these are non-halogenated compounds that result in no ozone loss, but others contain iodine or fluorine and could in principle deplete stratospheric ozone. It is also of interest to review the effectiveness of bromine relative to chlorine for ozone loss, which is critical for the ODPs of the halons and CH_3Br.

13.4.2.1 Fluorine

It has long been assumed that atomic fluorine released from chlorofluorocarbons would be tied up in the form of HF and therefore unable to participate in catalytic cycles that significantly deplete ozone. For example, Stolarski and Rundel (1975) concluded that the catalytic efficiency for ozone depletion by fluorine atoms is less than 10^{-4} that of chlorine in the altitude range from 25 to 50 km. While recent estimates of the equilibrium constant, K_{eq}, for $F + O_2 \Leftrightarrow FO_2$ published in JPL (1992) suggest that FO_2 could have an appreciable thermal dissociation lifetime of the order of 1 day or longer in the stratosphere, it is unlikely that FO_x compounds can lead to significant ozone loss, as discussed in Chapter 12. Direct observations of HF and fluorine source gases (*e.g.*, Zander *et al.*, 1992) support the view that there are no large unrecognized reservoirs for fluorine. As in previous reports, we assume here that atomic fluorine and related species do not cause significant ozone depletion.

In contrast to atomic fluorine, FO, and FO_2, it has, however, recently been suggested (Li and Francisco,

1991; Biggs *et al.*, 1993) that the CF_3O_x group could be stable enough to undergo catalytic cycles that deplete ozone at a significant rate before being decomposed to less stable products that form HF. It has also been suggested that the $FC(O)O_x$ group could undergo similar chemistry (see Chapter 12). These free radical groups are produced upon decomposition of a number of HFCs and HCFCs, and even a few CFCs. Notably, it was suggested that such processes could compromise the use of HFC-134a as a substitute that does not damage the ozone layer. Briefly, the key chemical reactions are:

$$CF_3CFH_2 \text{ (HFC-134a)} + OH \text{ (multi-step)} \rightarrow CF_3 + \text{other products} \quad (13\text{-}1)$$

$$CF_3 + O_2 + M \rightarrow CF_3O_2 \quad (13\text{-}2)$$

$$CF_3O_2 + O_3 \rightarrow CF_3O + 2\,O_2 \quad (13\text{-}3)$$

$$CF_3O + O_3 \rightarrow CF_3O_2 + O_2 \quad (13\text{-}4)$$

The last two reactions constitute a catalytic cycle analogous to the OH and HO_2 reactions with ozone, and could in principle be an effective ozone loss cycle in the lower stratosphere. The key factors in terminating this catalytic chain are reactions that can break down the CF_3 group, forming either stable products or products that rapidly decompose to produce HF. Two such reactions have been identified:

$$CF_3O + NO \rightarrow CF_2O + FNO \quad (13\text{-}5)$$

$$CF_3O + CH_4 \rightarrow CF_3OH + CH_3 \quad (13\text{-}6)$$

Chapter 12 discusses recent measurements of these and other relevant kinetic rate constants in considerable detail. Direct laboratory measurements coupled with model calculations have shown that the chain-terminating reactions above are sufficiently fast, and the chain-propagating reactions sufficiently slow, that the Ozone Depletion Potentials relating to the presence of a CF_3 group are essentially negligible. Recently, Ravishankara *et al.* (1994) and Ko *et al.* (1994a) have examined the implications of these processes for the effectiveness of CF_3 radical groups for ozone loss relative to chlorine. Figure 13-4 shows the calculated efficiency of CF_3 as compared to chlorine from the Garcia-Solomon model used in the study of Ravishankara *et al.* for midlatitudes in winter. The figure illustrates that current laboratory measurements imply that the CF_3 group is at most about

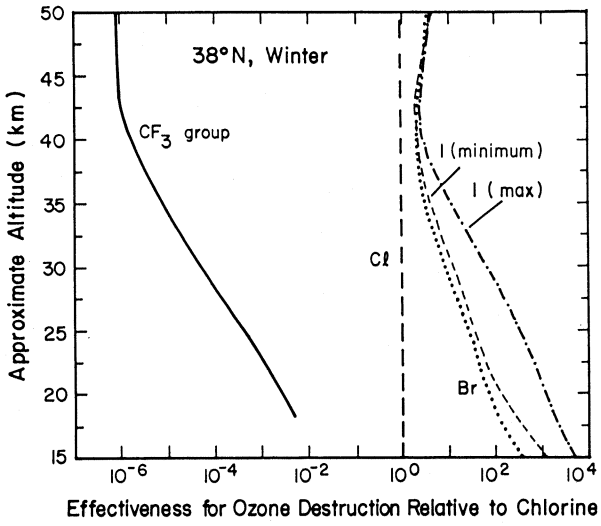

Figure 13-4. Calculated effectiveness of CF_3, bromine, and iodine in ozone destruction at midlatitudes relative to chlorine (based on results from Garcia-Solomon model as discussed in text).

1000 times less effective than chlorine for ozone destruction at 20 km in midlatitudes. While higher local values might be obtained in polar winter (where NO abundances are very small), the impacts of CF_3-related reactions on the globally averaged ODPs of CF_3-containing chlorofluorocarbons (such as CF_3Cl) and hydrochlorofluorocarbons (such as CF_3CHCl_2) are believed to be negligible, and the ODPs of HFCs such as HFC-134a and HFC-23 are highly likely to be less than 1×10^{-3} based upon current kinetic data (Ravishankara *et al.*, 1994).

13.4.2.2 Bromine

The chemistry of atmospheric bromine is discussed further in Chapter 10. The understanding of the relative roles of bromine and chlorine in depleting ozone was discussed by Solomon *et al.* (1992), who noted that *in situ* and remote sensing measurements of ClO, BrO, and OClO strongly suggest that bromine is about 40 times more efficient than chlorine for Antarctic ozone loss. Assuming that the rate-limiting steps for ozone loss in the Antarctic are the reactions ClO + ClO and ClO + BrO, the value of α for Antarctic ozone loss can be derived as follows:

$$\alpha \approx \frac{2k(BrO)(ClO)/(Br_y)}{2k(ClO)(ClO)+2k(BrO)(ClO)/(Cl_y)} \quad (13\text{-}7)$$

where the denominator represents the rate of ozone loss due to chlorine compounds per atom of chlorine available (*i.e.*, Cl released from all source gases, denoted here as Cl_y) and the numerator represents the rate of ozone loss due to bromine compounds per atom of bromine available (Br_y). Since the reaction ClO + ClO is believed to account for about 75% of the Antarctic ozone loss while ClO + BrO accounts for about 25% (see Solomon *et al.*, 1992 and references therein) and Cl_y is about 2.5 ppbv while Br_y is about 15 pptv in this region, the value of α for Antarctic ozone loss is about 40. Salawitch *et al.* (1990, 1993) pointed out that the lower absolute abundances of ClO observed in the Arctic as compared to Antarctica implies that bromine will be more effective for ozone loss there (*i.e.*, ClO + BrO will be more important compared to ClO + ClO).

Recent laboratory studies have confirmed and expanded understanding of the important role of bromine. Poulet *et al.* (1992) have shown that the kinetic rate constant for the reaction of BrO + HO_2 is about six times faster than previously believed at room temperature; this has been confirmed by the measurements of Bridier *et al.* (1993). As noted in WMO (1992), the importance of bromine for ozone loss could be substantially diminished if as much as 10% of the reaction between BrO + HO_2 were to yield HBr at the rate indicated by Poulet *et al.* (1992), while it would be *enhanced* if less than a few percent HBr is produced. The latter appears to be true based upon the study of Mellouki *et al.* (1994), who showed that the yield of HBr from this reaction is likely to be below 0.1% even at stratospheric temperatures based on new measurements and thermochemical data, a result consistent with modeling studies of the BrO gradient (Garcia and Solomon, 1994). Figure 13-4 shows the calculated effectiveness of bromine for ozone destruction relative to chlorine based upon the above photochemistry from the model of Garcia and Solomon (1994). The figure suggests that bromine is roughly 100 times more effective in the region of peak observed ozone loss (near 20 km). Very similar results have also been calculated with the Lawrence Livermore National Laboratory (LLNL) two-dimensional model. The figure illustrates that model calculations of the ODP for bromine-bearing compounds are likely to be quite sensitive to the altitude profile of ozone destruction. Since present models tend to underestimate the observed ozone losses in the lowest part of the stratosphere (see Chapter 6), where bromine is particularly efficient for ozone loss, this figure implies that the model-derived globally averaged values of α (weighted by the ozone loss distribution) will also be underestimates assuming present photochemical schemes.

Bromine's effectiveness for ozone loss in the lower stratosphere is related to the fact that a large fraction of the available Br_y resides in the ozone-depleting forms of Br and BrO. In contrast, only a very small fraction of available Cl_y resides in Cl and ClO except in the special case of polar regions. Thus, since all halogen atoms are very reactive (*e.g.*, with atomic oxygen, HO_2, and each other), bromine chemistry's effectiveness relative to chlorine will generally be driven by the fact that the BrO/Br_y ratio is on the order of 50-100 times larger than the ClO/Cl_y ratio in the lower stratosphere outside of polar regions. This in turn implies that the value of α is not very sensitive to which reactions are the dominant rate-limiting steps in ozone destruction, at least for current photochemical schemes (*e.g.*, ClO + BrO, HO_2 + BrO, HO_2 + ClO, etc.).

13.4.2.3 Iodine

The ability of reservoir molecules to sequester halogen radicals and thereby reduce their impact on ozone is inversely related to the size of the halogen atom. Thus fluorine rapidly forms HF, while chlorine forms HCl and $ClONO_2$. The bromine reservoirs (HBr and $BrONO_2$) are weakly bound, making BrO and Br effective ozone-destroying species as shown above. Iodine reservoirs such as HI, $IONO_2$, and others are known to be very readily dissociated by photolysis or reaction with OH, rendering any iodine that reaches the stratosphere at least as effective as bromine for ozone loss and very probably much more so. However, iodine source gases are very short-lived because of the relatively weak carbon-iodine bond. If the iodine source gases are short-lived enough, then anthropogenic releases (particularly at the surface at midlatitudes) may not reach the stratosphere in abundances sufficient to result in significant ozone loss. In this case, compounds such as CF_3I could represent useful substitutes for the halons.

effectiveness of bromine relative to chlorine for ozone loss in this analysis was assumed to be 40; as indicated in Section 13.4, this value is likely to be too low in the region where bromine emissions are most effective in destroying ozone at midlatitudes, suggesting that the semi-empirical ODPs for CH_3Br and the halons may be underestimated. A value of α of 80 is plausible in the lower stratosphere (see Chapter 10 and Garcia and Solomon, 1994), and would approximately double the ODPs of these compounds.

13.4.5 Time-Dependent Effects

While steady-state Ozone Depletion Potentials describe the integrated impact of emission of a halocarbon upon the ozone layer compared to CFC-11, it is also of interest to consider the time dependence of these effects (WMO, 1990, 1992; Solomon and Albritton, 1992). Time-dependent ODPs can be used to provide insight into the effect of a mix of compounds upon the short-term future of the ozone layer (*e.g.*, the next few decades, when peak chlorine and bromine loading are expected to occur), while steady-state ODPs indicate integrated effects over longer time scales. We describe below in more detail than in previous reports the physical processes that control the expected time dependence of ODPs for various chemicals. We then present updated time-dependent Ozone Depletion Potentials for several molecules of interest based upon new kinetic information and lifetimes as discussed in this report.

A simple semi-empirical framework for understanding the physical reasons for time-dependence of ODPs was presented by Solomon and Albritton (1992), who showed that the following equation can be used to approximate the time-dependent ODP at any point in the stratosphere:

$$ODP_X(t) = \left\{\frac{F_X}{F_{CFC-11}}\right\} \cdot \frac{M_{CFC-11}}{M_X} \cdot \frac{n_X}{3} \cdot \alpha \cdot \frac{\int_{t_s}^{t} e^{-(t-t_s)/\tau_X}\, dt}{\int_{t_s}^{t} e^{-(t-t_s)/\tau_{CFC-11}}\, dt} \qquad (13\text{-}8)$$

The term in brackets, $\{F_X/F_{CFC-11}\}$, denotes the fraction of the halocarbon species, x, injected into the stratosphere that has been dissociated compared to that of CFC-11 (obtained from measurements of both). M_X, M_{CFC-11}, τ_X, and τ_{CFC-11} indicate the molecular weights and atmospheric lifetimes of species x and CFC-11, respectively, while n_X is the number of chlorine or bromine atoms in the molecule (and note that CFC-11 contains 3 chlorine atoms per molecule). Also, t_s is the time required for a molecule to be transported from the surface to the region of the stratosphere in question, and t is time. In the following figures, the time refers to the time since reaching the lower stratosphere at middle-to-high latitudes (which is believed to be on the order of three years). In principle, the above equation should be integrated over the entire stratosphere in order to derive the globally averaged time-dependent ODP. In practice, however, the ozone column depletion observed in the current atmosphere is dominated by the region below 25 km. Further, mixing processes imply compact linear correlations between many of the long-lived halocarbon source gases in this region (Plumb and Ko, 1992), making the term in brackets, $\{F_X/F_{CFC-11}\}$, very nearly a constant over broad regions of the lower stratosphere (see Daniel *et al.*, 1994).

Using the above equation, together with the revised lifetimes of Table 13-1, updated values of $\{F_X/F_{CFC-11}\}$ where available from Daniel *et al.* (1994), and a value of α of 40 for bromocarbons and 2000 for iodocarbons, semi-empirical time-dependent ODPs were deduced. In addition, the instantaneous (*i.e.*, not integrated) relative ozone loss was also considered. Figure 13-5 shows instantaneous time-dependent relative ozone loss rates (compared to CFC-11) for several molecules of interest here. The time axis on the figure refers to the time since reaching the stratosphere, not the total time (which is about 3-5 years longer; see Pollock *et al.*, 1992). The instantaneous ozone loss rates relative to CFC-11 for the first few years are determined largely by the values of α for bromocarbons or iodocarbons and by the values of $\{F_X/F_{CFC-11}\}$ and n_X for chlorocarbons. Over longer time scales, the short-lived compounds are removed from the atmosphere, and the slope of their decay depends upon the relative values of τ_X and τ_{CFC-11}. Note, for example, that HCFC-141b (which contains 2 chlorine atoms) initially destroys roughly 2/3 as much ozone as CFC-11. It has a lifetime of about 10 years, and therefore its instantaneous ozone loss drops to very small values within a few decades. The ozone-depleting effects of pulsed injections of compounds with shorter lifetimes (such as HCFC-123) decay much faster. A

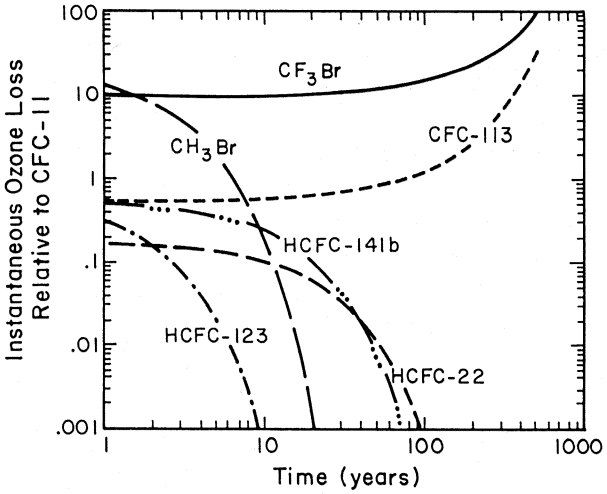

Figure 13-5. Instantaneous time-dependent relative ozone loss rates (compared to CFC-11) for several compounds of interest. Note that the x-axis refers to the time since reaching the stratosphere, not the total time.

compound with a lifetime longer than that of CFC-11 (such as CFC-113) has an impact on the ozone layer relative to CFC-11 that grows for time scales longer than the 50-year lifetime of CFC-11, because of the decay of the reference gas. The behavior of CH_3Br is qualitatively similar to that of HCFC-123, but it has a very large initial ozone impact because of the value of α, making its relative ozone loss in the first few years close to 10 times that of CFC-11 (approximately $\alpha/3$).

The time-dependent Ozone Depletion Potentials are simply the time integrals of the instantaneous relative ozone loss rates shown in Figure 13-5. These are illustrated in Figure 13-6. Note, for example, the growth of the ODP for CFC-113 for time scales longer than about 100 years, at which time more CFC-113 remains to destroy ozone than the reference gas, CFC-11. The time-dependent ODP for a very short-lived gas such as HCFC-123 has large values for the first five years. However, by the end of the first five years, HCFC-123 is destroying very little ozone (Figure 13-5), because it has been nearly completely removed from the atmosphere. The reference gas, CFC-11, is continuing to destroy ozone, so that the cumulative value of the denominator in Equation 13-8 continues to increase. It is this slow increase in the denominator that controls when the ODPs for short-lived gases such as HCFC-123 reach their steady-state values. The steady-state ODP for HCFC-123 therefore asymptotes to a value below 0.02 in about 100 years. A calculation of the time-dependent ODPs for CH_3Br using the Oslo model gave values of 5.6, 2.3, and 1.5 for time scales of 10, 20, and 30 years, respectively, very similar to the semi-empirical values shown in Figure 13-6. In the above calculations, a lifetime of 2.0 years was used for CH_3Br. The ODPs for this gas would be about 30% smaller over long time scales if a lifetime of 1.3 years was employed.

Figure 13-6 includes an upper-limit estimate of the time-dependent ODP for surface releases of CF_3I, based on the framework described in Solomon *et al.* (1994a). The calculated upper limit to the ODP for this gas is about 0.08 in the first five years and asymptotes to a value below 0.01 in about 100 years.

Although the ODP concept has primarily been applied to the relative effects of halocarbons on stratospheric ozone, there have also been several recent attempts to determine ODPs for emissions of other gases. For example, Ko *et al.* (1994b) have evaluated an ODP for chlorine emitted directly into the stratosphere from launch of the U.S. Space Shuttle. They derive a time-dependent ODP that is quite large initially (but is also dependent on the definition of what constitutes a mass emission, the choice being emission of HCl only or

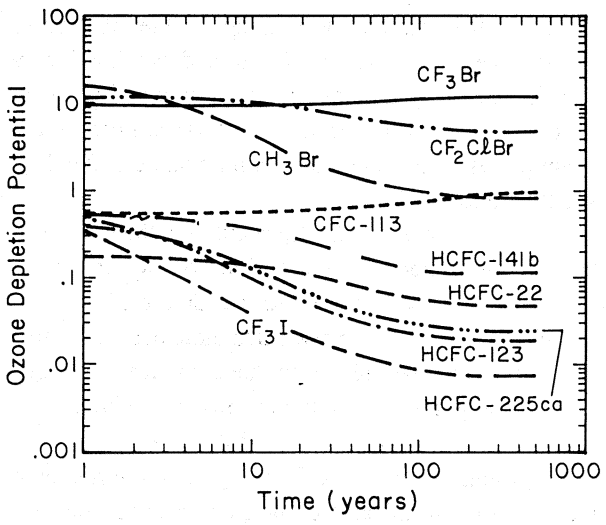

Figure 13-6. Time-dependent Ozone Depletion Potentials for several compounds of interest. Note that the x-axis refers to the time since reaching the stratosphere, not the total time.

the total fuel load). The effect from the Space Shuttle decays quite rapidly due to removal of the emitted HCl from the stratosphere.

Since the ozone layer is believed to respond relatively rapidly to changes in chlorine and/or bromine loading (time scale of about 3-5 years or less), time-dependent Ozone Depletion Potentials provide an appropriate measure of the expected ozone response to changing inputs of source gases relative to the reference molecule. On the other hand, steady-state Ozone Depletion Potentials may be applicable to evaluation of associated long-term biological impacts, where the ecosystem response may take place over many decades of exposure to changes in ultraviolet radiation resulting from ozone changes.

13.5 GLOBAL WARMING POTENTIALS

13.5.1 Introduction

This section addresses the numerical indices that can be used to provide a simple representation of the relative contribution of an atmospheric trace gas to greenhouse warming, drawing heavily on the information in the earlier ozone assessments (WMO, 1990, 1992), the climate-system reports of the Intergovernmental Panel on Climate Change (IPCC, 1990, 1992, 1994), and recent journal publications. The major objective of the text that follows is to update the information on radiative forcing indices. To this end, we describe the calculations of the indices contained herein, discuss the sensitivity of the results to some of the specifications and assumptions, and present the resulting numerical indices and their uncertainties.

As in the case of ODPs, calculating the relative alteration in radiative forcing due to the change in greenhouse gas A compared to that due to a change in greenhouse gas B can be evaluated more accurately than the absolute climate response due a change in a single greenhouse gas alone. In the following, we briefly discuss some key factors that contribute to GWPs.

Common to all greenhouse gases are three major factors – two technical and one user-oriented – that determine the relative contribution of a greenhouse gas to radiative forcing and hence are the primary input in the formulation, calculation, and use of radiative forcing indices:

Factor 1: The strength with which a given species absorbs longwave radiation and the spectral location of its absorbing wavelengths. Chemical species differ markedly in their abilities to absorb longwave radiation. Overlaps of the absorption spectra of various chemical species with one another (especially H_2O, CO_2, and, to a lesser extent, O_3) are important factors. In addition, while the absorption of infrared radiation by many greenhouse gases varies linearly with their concentration, a few important ones display nonlinear behavior (*e.g.*, CO_2, CH_4, and N_2O). For those gases, the relative radiative forcing will depend upon concentration and hence upon the scenario adopted for the future trace-gas atmospheric abundances. A key factor in the greenhouse role of a given species is the location of its absorption spectrum relative to the region in the absorption of atmospheric water vapor through which most outgoing planetary thermal radiation escapes to space. Consequently, *other things being equal*, chemical species that have strong absorption band strengths in the relatively weak water-vapor "window" are more important greenhouse gases than those that do not. This is illustrated in Figure 13-7, which shows how the instantaneous radia-

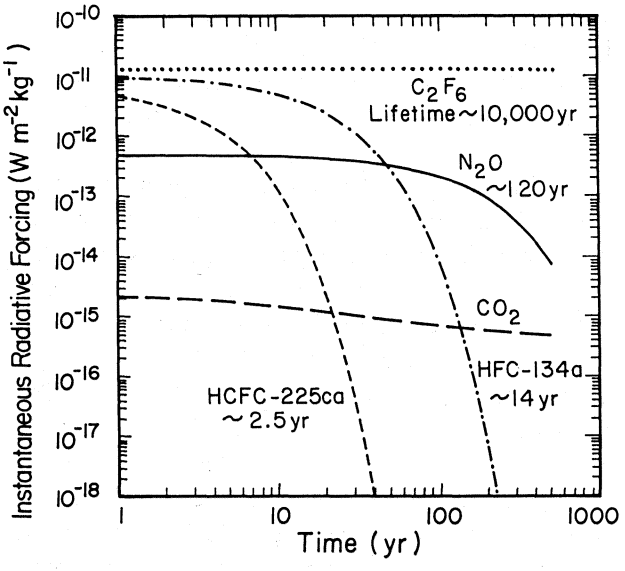

Figure 13-7. Instantaneous radiative forcing (W m^{-2} kg^{-1}) versus time after release for several different greenhouse gases. The CO_2 decay response function is based upon the Bern carbon cycle model with fixed CO_2 concentrations.

tive forcings due to the pulse emission of one kilogram of various long-lived gases with differing absorption properties change as the concentrations decay away in time after they have become well mixed (*e.g.*, about a year after injection into the atmosphere). The relevant point here is on the left-hand scale at t = 1, namely, that the radiative forcing of an equal emission of the various gases can differ by as much as four orders of magnitude. Laboratory studies of molecular radiative properties are a key source of the basic information needed in the calculation of radiative forcing indices. The status of such spectroscopic data of greenhouse gases is discussed in detail in Chapter 8 and in Chapter 4 of IPCC (1994).

Factor 2. The lifetime of the given species in the atmosphere. Greenhouse gases differ markedly in how long they reside in the atmosphere once emitted. Clearly, greenhouse gases that persist in the atmosphere for a long time are more important, other things being equal, in radiative forcing than those that are shorter-lived. This point is also illustrated in Figure 13-8. As shown, the initial dominance of the radiative forcing at early times can be overwhelmed by the lifetime factor at later times.

The relative roles of the strength of radiative absorption and lifetimes on GWPs, as shown in Figures 13-7 and 13-8, parallel those of chemical effectiveness and lifetimes on ODPs, as illustrated in Figures 13-5 and 13-6.

Factor 3. The time period over which the radiative effects of the species are to be considered. Since many of the responses of the Earth's climate to changes in radiative forcing are long (*e.g.*, the centennial-scale warming of the oceans), it is the *cumulative* radiative forcing of a greenhouse gas, rather than its instantaneous value, that is of primary importance to crafting a relevant radiative forcing index. As a consequence, such indices involve an integral over time. Rodhe (1990) has noted that the choice of time interval can be compared to cumulative-dosage effects in radiology. IPCC (1990, 1992) used integration *time horizons* of 20, 100, and 500 years in calculating the indices. Figure 13-8 shows the integrals of the decay functions in Figure 13-7 for a wide range of time horizons. It illustrates the need for the user of the radiative forcing indices to select the time period of consideration. A strongly absorbing, but short-lived, gas like HCFC-225ca will contribute more radiative forcing in the short term than a weaker-absorbing, but longer-lived, gas like N_2O; however, in the longer term, the reverse is true. Methane is a key greenhouse gas discussed extensively below; its integrated radiative forcing would lie below that of N_2O and reach a plateau more quickly because of its shorter lifetime.

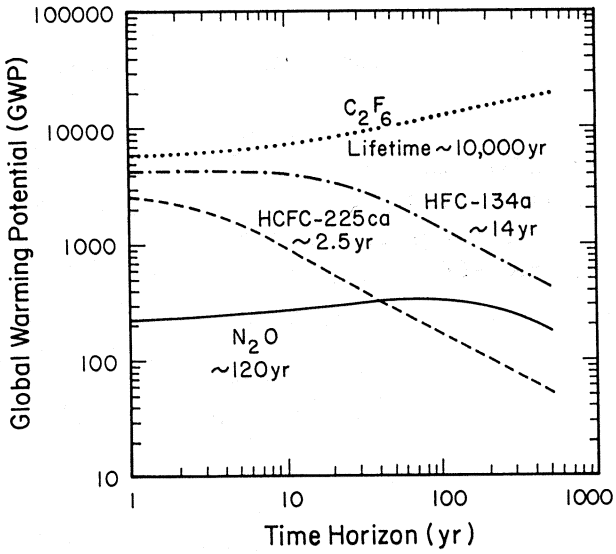

Figure 13-8. Global Warming Potentials (GWPs) for a range of greenhouse gases with differing lifetimes, using CO_2 as the reference gas.

The spread of numerical values of the radiative forcing indices reported in Section 13.5.2 below largely reflects the influence of these three major factors. In addition to these direct radiative effects, some chemical species also have indirect effects on radiative forcing that arise largely from atmospheric chemical processes. For example, important products of the oxidative removal of CH_4 are water vapor in the stratosphere and ozone in the troposphere, both of which are greenhouse gases. These are discussed in Section 13.5.4.

13.5.2 Radiative Forcing Indices

13.5.2.1 Formulation

The primary radiative forcing indices used in scientific and policy assessments are the Global Warming Potential (GWP) and Absolute Global Warming Potential (AGWP). Other possible formulations are described and contrasted with those in IPCC (1994).

Global Warming Potential

Based on the major factors summarized above, the relative potential of a specified emission of a greenhouse gas to contribute to a change in future radiative forcing, *i.e.*, its GWP, has been expressed as the time-integrated radiative forcing from the instantaneous release of 1 kg of a trace gas expressed relative to that of 1 kg of a reference gas (IPCC, 1990):

$$GWP(x) = \frac{\int_0^{TH} a_x \cdot [x(t)]dt}{\int_0^{TH} a_r \cdot [r(t)]dt} \qquad (13\text{-}9)$$

where TH is the time horizon over which the calculation is considered; a_x is the climate-related radiative forcing due to a unit increase in atmospheric concentration of the gas in question; [x(t)] is the time-decaying abundance of a pulse of injected gas; and the corresponding quantities for the reference gas are in the denominator. The adjusted radiative forcings per kg, a, are derived from infrared radiative transfer models and are assumed to be independent of time. The sensitivity of these factors to some climate variables (H_2O, clouds) is discussed later. As noted above, a_r is a function of time when future changes in CO_2 are considered. Time-dependent changes in a_x or lifetimes are not explicitly considered here. The trace gas amounts, [x(t)] and [r(t)], remaining after time t are based upon the atmospheric lifetime or response time of the gas in question and the reference gas, respectively.

The reference gas has been taken generally to be CO_2, since this allows a comparison of the radiative forcing role of the emission of the gas in question to that of the dominant greenhouse gas that is emitted as a result of human activities, hence of the broadest interest to policy considerations. However, the atmospheric residence time of CO_2 is among the most uncertain of the major greenhouse gases. Carbon dioxide added to the atmosphere decays in a highly complex fashion, showing an initial fast decay over the first 10 years or so, followed by a more gradual decay over the next 100 years or so, and a very slow decline over the thousand-year time scale, mainly reflecting transfer processes in the biosphere, ocean, and deep ocean sediments, respectively. Because of these different time constants, the removal of CO_2 from the atmosphere is quite different from that of other trace gases and is not well described by a single lifetime (Moore and Braswell, 1994). Wuebbles *et al.* (1994b) and Wigley (1993) have also noted the importance of uncertainties in the carbon cycle for calculations of GWPs when CO_2 is used as the reference. Furthermore, CO_2 is also recirculated among these reservoirs at an exchange rate that is poorly known at present, and it appears that the budget of CO_2 is difficult to balance with current information. As a result, when CO_2 is used as the reference gas, the numerical values of the GWPs of all greenhouse gases are apt to change in the future (perhaps substantially) simply because research will improve the understanding of the removal processes of CO_2. While recognizing these issues, Caldeira and Kasting (1993) discuss feedback mechanisms that tend to offset some of these uncertainties for GWP calculations.

Absolute Global Warming Potential

Wigley (1993; 1994a, b) has emphasized the uncertainty in accurately defining the denominator for GWP calculations if CO_2 is used as the reference molecule, and suggested the use of "Absolute" or AGWPs given simply by the integrated radiative forcing of the gas in question:

$$AGWP(x) = \int_0^T a_x \cdot [x(t)]\, dt \quad W \cdot yr \cdot kg^{-1} \cdot m^{-2} \qquad (13\text{-}10)$$

The advantage of this formulation is that the index is specific only to the gas in question. An important disadvantage is that the absolute value of radiative forcing depends upon many factors that are poorly known, such as the distributions and radiative properties of clouds (*e.g.*, Cess *et al.*, 1993).

Based upon the recommendation of the co-authors of Chapter 1 from IPCC (1994), we use the results from the carbon cycle model of Siegenthaler and co-workers ("Bern" model) for the decay response of CO_2 for the GWP calculations presented here. The fast initial (first several decades) decay of added CO_2 calculated in current carbon cycle models reflects rapid uptake by the biosphere and is believed to be an important improvement compared to that used in IPCC (1990, 1992). This change in decay decreases the integrated radiative forc-

ing of CO_2 and thereby acts to increase the estimated GWPs of all gases (see IPCC, 1994). We present AGWPs for CO_2 needed for conversion of the results to other units and other CO_2 decay functions (*e.g.*, to show the impact of the choice of the denominator on GWP values).

13.5.2.2 Sensitivity to the State of the Atmosphere

To provide realistic evaluations of GWPs for specified time horizons and estimate their uncertainties, future changes in the radiative properties of the atmosphere must be considered. Some of these changes to the present state can be estimated based upon scenarios (*e.g.*, CO_2 concentrations), while others are dependent upon the evolution of the entire climate system and are poorly known (*e.g.*, clouds and water vapor). In IPCC (1990), the composition of the background atmosphere used in the GWP calculations was the present-day abundances of CO_2, CH_4, and nitrous oxide (N_2O), which were assumed constant into the future. However, likely changes in CO_2, CH_4, or N_2O concentrations will lead to future changes in the radiative forcing per molecule of those gases (and perhaps others whose spectral bands overlap with them), as noted previously. The radiative properties of CO_2 are particularly sensitive to changes in concentration, since the large optical depth of CO_2 in the current atmosphere makes its radiative forcing depend logarithmically on concentration (see WMO, 1992 and Chapter 8 of this document). Thus, the forcing for a particular incremental change of CO_2 will become smaller in the future, when the atmosphere is expected to contain a larger concentration of the gas. In the case of CH_4 and N_2O, there is a square-root dependence of the forcing on their respective concentrations (IPCC, 1990); hence, just as for CO_2, the forcings due to a specified increment in either gas are expected to become smaller for future scenarios. For the other trace gases considered here, the present and likely future values are such that the direct radiative forcing is linear with respect to their concentrations and hence is independent of the scenario.

IPCC (1994) showed in detail that the dependence of the AGWP of CO_2 upon choice of future atmospheric CO_2 concentrations is not a highly sensitive one. A constant atmosphere at pre-industrial values (280 ppmv) would yield values different by less than about 20% for all time horizons. Similarly, the increasing CO_2 concentrations in a future scenario stabilizing at 650 ppmv would yield GWP values that are smaller by 15% or less. The decreases in the radiative forcing per molecule due to the increasing CO_2 atmospheric abundance appear to be opposite in sign to those due to the changed CO_2 decay response (see Caldeira and Kasting, 1993, and Wigley, 1994a).

IPCC (1994) and this report also considered the possible evolution of the radiative forcing of CH_4 and N_2O and the interplay between the spectral overlap of these two gases using the IS92a scenario published in the Annex of IPCC (1992). If the calculations were made with the IS92a CH_4 and N_2O scenarios rather than with the constant current values, the direct GWPs of CH_4 would decrease by 2 to 3%, and the 20-, 100-, and 500-yr GWPs of N_2O would decrease by 5, 10, and 15%, respectively. The impact of the adopted future scenarios for CO_2, CH_4, and N_2O on the radiative forcing of other trace species was not considered.

Water Vapor

While it is likely that water vapor will change in a future climate state, the effect of such changes upon the direct GWPs of the great majority of molecules of interest here is expected to be quite small. For example, the model of Clerbaux *et al.* (1993) was used to test the sensitivity of the direct GWP for CH_4 to changes in water vapor. Even for changes as large as 30% in water vapor concentration, the calculated GWP of CH_4 changed by only a few percent (C. Granier, personal communication, 1993). For many other gases whose radiative impact occurs largely in the region where water vapor's absorption is relatively weak, similar or smaller effects are likely.

Clouds

Clouds composed of water drops or ice crystals possess absorption bands in virtually the entire terrestrial infrared spectrum. By virtue of this property, they modulate considerably the infrared radiation escaping to space from the Earth's surface and atmosphere. Since cloud tops generally have lower temperatures than the Earth's surface and the lower part of the atmosphere, they reduce the outgoing infrared radiation. This reduction depends mainly on cloud height and optical depth. The higher the cloud, the lower is its temperature and the greater its reduction in infrared emission. On the other hand, higher clouds (in particular, high ice clouds) tend

to have low water content and limited optical depths. Such clouds are partially transparent, which reduces the infrared trapping effect.

The absorption bands of several trace gases overlap significantly with the spectral features of water drops and ice crystals, particularly in the "window" region. Owing to the relatively strong absorption properties of clouds, the absolute radiative forcing of many trace molecules is diminished in the presence of clouds. However, it is important to note that the impact of changes in clouds upon GWPs depends upon the difference between the change in radiative forcing of the gas considered and that of the reference gas, not the absolute change in radiative forcing of the gas alone. IPCC (1994) shows that the model calculations of Granier and co-workers suggest that the presence or absence of clouds results in changes of the relative radiative forcings of the molecules considered here of at most about 12%. Thus, uncertainties in future cloud cover due to climate change are unlikely to substantially impact GWP calculations.

13.5.3 Direct GWPs

New direct GWPs of many gases were calculated for IPCC (1994) and for this report with the radiative transfer models developed at the National Center for Atmospheric Research – NCAR (Briegleb, 1992; Clerbaux *et al.*, 1993), Lawrence Livermore National Laboratory – LLNL (Wuebbles *et al.*, 1994a, b), the Max Planck Institut für Chemie – Mainz (C. Brühl *et al.*, 1993; Roehl *et al.*, 1994), the Indian Institute of Technology (Lal and Holt, 1991, updated in 1993), and the University of Oslo (Fuglestvedt *et al.*, 1994). The radiative forcing a-factors adopted are those given in Chapter 8 of this report and in IPCC (1994). Some of these values are apt to be amended in the near future (see Chapter 4 of IPCC, 1994). Table 13-5 presents a composite summary of those results. In addition, it presents results from the studies of Ko *et al.* (1993) and Stordal *et al.* (personal communication, 1994) for SF_6, and from Solomon *et al.* (1994a) for CF_3I. With the exception of CF_3I, all of the molecules considered have lifetimes in excess of several months and thus can be considered reasonably well-mixed; only an upper limit rather than a value is presented for CF_3I. For those species addressed in IPCC (1992), a majority of the GWP values are larger, typically by 10-30%. These changes are largely due to (i) changes in the CO_2 reference noted above and (ii) improved values for atmospheric lifetimes.

Several new gases proposed as CFC and halon substitutes are considered here for the first time, such as HCFC-225ca, HCFC-225cb, HFC-227ea, and CF_3I. Table 13-5 also includes for the first time a full evaluation of the GWPs of several fully fluorinated species, namely SF_6, CF_4, C_2F_6, and C_6F_{14}. SF_6 is used mainly as a heat transfer fluid for electrical equipment (Ko *et al.*, 1993), while CF_4 and C_2F_6 are believed to be produced mainly as accidental by-products of aluminum manufacture. C_6F_{14} and other perfluoroalkanes have been proposed as potential CFC substitutes. The very long lifetimes of the perfluorinated gases (Ravishankara *et al.*, 1993) lead to large GWPs over long time scales.

The uncertainty in the GWP of any trace gas other than CO_2 depends upon the uncertainties in the AGWP of CO_2 and the AGWP of the gas itself. The uncertainties in the relative values of AGWPs for various gases depends upon the uncertainty in relative radiative forcing per molecule (estimated to be about 25% for most gases, as shown in Chapter 8) and on the uncertainty in the lifetimes of the trace gas considered (which are likely to be accurate to about 10% for CFC-11 and CH_3CCl_3 and perhaps 20-30% for other gases derived from them). Combining these dominant uncertainties (in quadrature) suggests uncertainties in the direct AGWPs for nearly all of the trace gases considered in Table 13-5 of less than ±35%. Uncertainties in the AGWPs for CO_2 depend upon uncertainties in the carbon cycle (see Chapter 1 of IPCC, 1994) and on the future scenario for CO_2. The effect of the latter uncertainty is likely to be relatively small, as shown in Chapter 5 of IPCC (1994).

The reference gas for the GWPs in Table 13-5 is the CO_2 decay response from the "Bern" carbon cycle model (Chapter 1 of IPCC, 1994). The GWPs calculations were carried out with background atmospheric trace gas concentrations held fixed at 354 ppmv.

The direct GWPs given in Table 13-5 can be readily converted to other frameworks such as AGWPs, GWPs for a changing atmosphere, and GWPs using as reference either a specific carbon cycle model or the three-parameter fit employed in IPCC (1990, 1992). Table 13-6 presents the relevant factors to carry out such conversions:

- To convert to AGWP units, the numbers in Table 13-5 should be multiplied by the AGWP for the

Table 13-5. Global Warming Potentials (mass basis), referenced to the AGWP for the adopted carbon cycle model CO_2 decay response and future CO_2 atmospheric concentrations held constant at current levels. Only direct effects are considered, except for methane.

Species	Chemical Formula	Global Warming Potential (Time Horizon) 20 years	100 years	500 years
CFCs				
CFC-11	$CFCl_3$	5000	4000	1400
CFC-12	CF_2Cl_2	7900	8500	4200
CFC-13	$CClF_3$	8100	11700	13600
CFC-113	$C_2F_3Cl_3$	5000	5000	2300
CFC-114	$C_2F_4Cl_2$	6900	9300	8300
CFC-115	C_2F_5Cl	6200	9300	13000
HCFCs, etc.				
Carbon tetrachloride	CCl_4	2000	1400	500
Methyl chloroform	CH_3CCl_3	360	110	35
HCFC-22 (†††)	CF_2HCl	4300	1700	520
HCFC-141b (†††)	$C_2FH_3Cl_2$	1800	630	200
HCFC-142b (†††)	$C_2F_2H_3Cl$	4200	2000	630
HCFC-123 (††)	$C_2F_3HCl_2$	300	93	29
HCFC-124 (††)	C_2F_4HCl	1500	480	150
HCFC-225ca (††)	$C_3F_5HCl_2$	550	170	52
HCFC-225cb (††)	$C_3F_5HCl_2$	1700	530	170
Bromocarbons				
H-1301	CF_3Br	6200	5600	2200
Other				
HFC-23 (†)	CHF_3	9200	12100	9900
HFC-32 (†††)	CH_2F_2	1800	580	180
HFC-43-10mee (†)	$C_4H_2F_{10}$	3300	1600	520
HFC-125 (††)	C_2HF_5	4800	3200	1100
HFC-134 (†)	CHF_2CHF_2	3100	1200	370
HFC-134a (†††)	CH_2FCF_3	3300	1300	420
HFC-152a (††)	$C_2H_4F_2$	460	140	44
HFC-143 (†)	CHF_2CH_2F	950	290	90
HFC-143a (††)	CF_3CH_3	5200	4400	1600
HFC-227ea (†)	C_3HF_7	4500	3300	1100
HFC-236fa (†)	$C_3H_2F_6$	6100	8000	6600
HFC-245ca (†)	$C_3H_3F_5$	1900	610	190
Chloroform (††)	$CHCl_3$	15	5	1
Methylene chloride (††)	CH_2Cl_2	28	9	3
Sulfur hexafluoride	SF_6	16500	24900	36500
Perfluoromethane	CF_4	4100	6300	9800
Perfluoroethane	C_2F_6	8200	12500	19100
Perfluorocyclo-butane	$c\text{-}C_4F_8$	6000	9100	13300
Perfluorohexane	C_6F_{14}	4500	6800	9900
Methane*	CH_4	62 ± 20	24.5 ± 7.5	7.5 ± 2.5
Nitrous oxide	N_2O	290	320	180
Trifluoroiodo-methane	CF_3I	< 5	<< 1	<<< 1

* Includes direct and indirect components (see Section 13.5.4.2).
(†††) Indicates HFC/HCFCs in production now and likely to be widely used (see Chapter 4 of IPCC, 1994).
(††) Indicates HFC/HCFCs in production now for specialized end use (see Chapter 4 of IPCC, 1994).
(†) Indicates HFC/HCFCs under consideration for specialized end use (see Chapter 4 of IPCC, 1994).

Table 13-6. Absolute GWPs (AGWPs) (W m^{-2} yr $ppmv^{-1}$).*

Case	Time Horizon		
	20 year	100 year	500 year
CO_2, Bern Carbon Cycle Model, fixed CO_2 (354 ppmv)	0.235	0.768	2.459
CO_2, Bern Carbon Cycle Model, S650 scenario	0.225	0.702	2.179
CO_2, Wigley Carbon Cycle Model, S650 scenario	0.248	0.722	1.957
CO_2, Enting Carbon Cycle Model, S650 scenario	0.228	0.693	2.288
CO_2, LLNL Carbon Cycle Model, S450 scenario	0.247	0.821	2.823
CO_2, LLNL Carbon Cycle Model, S650 scenario	0.246	0.790	2.477
CO_2, LLNL Carbon Cycle Model, S750 scenario	0.247	0.784	2.472
CO_2-like gas, IPCC (1990) decay function, fixed CO_2 (354 ppmv)	0.267	0.964	2.848

*Multiply these numbers by 1.291×10^{-13} to convert from per ppmv to per kg.

adopted Bern carbon cycle model, fixed CO_2 (354 ppmv) scenario (*i.e.*, Line 1 in Table 13-6) and multiplied by 1.291×10^{-13} to convert the AGWP of CO_2 from per ppmv to per kg.

- To convert to GWP units using one of the other indicated carbon cycle models and/or trace-gas future scenarios, the numbers in Table 13-5 should be multiplied by the AGWP for the adopted Bern carbon cycle model, fixed CO_2 (354 ppmv) scenario (Line 1) and divided by the AGWP value in Table 13-6 for the carbon cycle model and/or scenario in question.
- To convert to GWPs that are based on the same reference as was used in IPCC (1990,1992), the numbers in Table 13-5 should be multiplied by the AGWP for the adopted Bern carbon cycle model, fixed CO_2 (354 ppmv) scenario (Line 1) and divided by the AGWP value in Table 13-6 for the CO_2-like gas, IPCC (1990) decay function, fixed CO_2 (354 ppmv) (*i.e.*, last line in Table 13-6).

13.5.4 Indirect Effects

13.5.4.1 General Characteristics

In addition to the direct forcing caused by injection of infrared-absorbing gases to the atmosphere, some compounds can also modify the radiative balance through indirect effects relating to chemical transformations. When the full interactive chemistry of the atmosphere is considered, a very large number of possible indirect effects can be identified (ranging from the production of stratospheric water vapor as an indirect effect of H_2 injections to changes in the HCl/ClO ratio and hence in ozone depletion resulting from CH_4 injections).

The effects arising from such processes are difficult to quantify in detail (see Chapter 2 of IPCC, 1994), but many are highly likely to represent only small perturbations to the direct GWP and to global radiative forcing. As noted above for ODPs, recent work has shown that the production of products such as fluoro- and chlorophosgene and organic nitrates from the breakdown of CFCs and HCFCs is unlikely to represent a substantial indirect effect on the GWPs of those species, due to the rapid removal of these water-soluble products in clouds and rain (see Chapter 12 and Kindler *et al.*, 1994). Similarly, the addition of HCFCs and HFCs to the atmosphere can, in principle, affect the oxidizing capacity of the lower atmosphere and hence their lifetimes, but the effect is completely negligible for reasonable abundances of these trace gases.

Table 13-7 summarizes some key stratospheric and tropospheric chemical processes that do represent important indirect effects for GWP estimates. The current state of understanding of these processes is examined in detail in Chapters 2 and 5 of IPCC (1994). It is particularly difficult to calculate GWPs of short-

Table 13-7. Important indirect effects on GWPs.

Species	Indirect Effect	Sign of Effect on GWP
CH_4	Changes in response times due to changes in tropospheric OH	+
	Production of tropospheric O_3	+
	Production of stratospheric H_2O	+
	Production of CO_2 (for certain sources)	+
CFCs, HCFCs, Bromocarbons	Depletion of stratospheric O_3	-
	Increase in tropospheric OH due to enhanced UV	-
CO	Production of tropospheric O_3	+
	Changes in response times due to changes in tropospheric OH	+
	Production of tropospheric CO_2	+
NO_x	Production of tropospheric O_3	+
NMHCs	Production of tropospheric O_3	+
	Production of tropospheric CO_2	+

lived gases with localized sources, such as NO_x and non-methane hydrocarbons. Further, lack of detailed knowledge of the distributions of these and other key tropospheric gases complicates calculations of indirect effects relating to tropospheric ozone production (see Chapters 5 and 7). It is, however, important to recognize that ozone processes in the upper troposphere are more effective for radiative forcing than those near the surface (see Chapter 8), emphasizing chemical processes occurring in the free troposphere.

We present here the indirect GWP effect of tropospheric ozone production only for CH_4. Additional GWP quantification (*e.g.*, for tropospheric ozone precursors such as CO, non-methane hydrocarbons (NMHCs), and NO_x) must await further study of the model intercomparisons described in Chapter 2 of IPCC (1994) and improved field, laboratory, and theoretical characterization of the processes involved in tropospheric ozone production. Reliable radiative forcing indices for gases that form atmospheric aerosols (*e.g.*, sulfur dioxide, SO_2) cannot currently be formulated meaningfully, chiefly because of the lack of understanding of many of the processes involved (*e.g.*, composition of the aerosols, radiative properties, etc.) and because of uncertainties regarding the climate response to the inhomogeneous spatial distributions of the aerosols (see Chapter 3 of IPCC, 1994). For the first time, an estimate of the effects from depletion of ozone on halocarbon GWPs is also presented in this chapter, drawing upon (i) the extensive discussion on ODPs and photochemical considerations behind them in Section 13.4, (ii) the discussion of the relationship between radiative forcing due to ozone change and climate sensitivity in Chapter 8, and (iii) the available scientific literature.

13.5.4.2 Indirect Effects upon the GWP of CH_4

Recent research studies of the indirect effects on the GWP of methane include those of Hauglustaine *et al.* (1994a, b), Lelieveld and Crutzen (1992), Lelieveld *et al.*, (1993), and Brühl (1993). In this report, we consider those results together with inputs from Chapters 2 and 4 of IPCC (1994). The relative radiative forcing for methane itself compared to CO_2 on a per-molecule basis is given in Table 4.2a of IPCC (1994) and is used here. Eight multi-dimensional models were used to study the chemical response of the atmosphere to a 20% increase in methane, as discussed in Section 2.9 of IPCC (1994). The calculated range of ozone increases from the full set of tropospheric models considered in that study provides insight regarding the likely range in ozone production.

Uncertainties in these calculations include those related to the NO_x distributions employed in the various models, formulation of transport processes, and other factors discussed in detail in Chapter 2 of IPCC (1994). The estimated uncertainty in the indirect GWP for CH_4 from tropospheric ozone production given below is based upon the calculated mid-to-upper tropospheric ozone response of the models to the prescribed methane perturbation at northern midlatitudes and consideration of the current inadequacies in the understanding of many relevant atmospheric processes. The calculated ozone changes from the model simulations derived for a 20% increase in methane imply an indirect effect that is about $25 \pm 15\%$ of the direct effect of methane (or $19 \pm 12\%$ of the total), using the infrared radiative code of the LLNL model. A similar number is estimated in Chapter 4 of IPCC (1994). This upper end of this range is close to that presented in IPCC (1990).

Release of CH_4 leads to increased stratospheric water vapor through photochemical oxidation; estimates of this indirect effect range are on the order of 5% or less of the direct effect of methane (4% of the total) based on the discussion in Chapter 4 of IPCC (1994); current results from the LLNL, NCAR, and Mainz radiative/photochemical two-dimensional models; and the published literature (*e.g.*, Lelieveld and Crutzen, 1992; Lelieveld *et al.*, 1993; Brühl, 1993; Hauglustaine *et al.*, 1994a, b). We adopt 5% of the direct effect in the table below, which is smaller than the value quoted in IPCC (1990).

Each injected molecule of CH_4 ultimately forms CO_2, representing an additional indirect effect that would increase the GWPs by approximately 3 for all time horizons (see IPCC, 1990). However, as noted by Lelieveld and Crutzen (1992), this indirect effect is unlikely to apply to biogenic production of CH_4 from most sources (*e.g.*, from rice paddies), since the ultimate source of the carbon emitted as CH_4 in this case is CO_2, implying no net gain of carbon dioxide. While non-biogenic methane sources such as mining operations do lead indirectly to a net production of CO_2, this methane is often included in national carbon production inventories. In this case, consideration of CO_2 production in the GWP could lead to "double-counting," depending upon how the GWPs and inventories are combined. As shown in IPCC (1994), most human sources of methane are biogenic, with another large fraction being due to coal mines and natural gas. Thus, the indirect effect of CO_2 production does not apply to much of the CH_4 inventory, and is not included in the table below (in contrast to IPCC (1990), where this effect was included).

As in Table 13-5, the GWPs were calculated relative to the CO_2 decay response of the Bern carbon cycle model with a constant current CO_2 and CH_4 atmosphere. Table 13-8 summarizes the composite result for methane GWPs, its uncertainty, and considers the breakdown of the effects among various contributing factors. The ranges in CH_4 GWPs shown in Table 13-8 reflect the uncertainties in response time, lifetime, and indirect effects, as discussed below. We assume a lifetime of methane in the background atmosphere of 10 ± 2 years (which is consistent with the budget given in IPCC, 1994). However, the response time of an added pulse is assumed to be much longer (12-17 years based upon Chapter 2 of IPCC, 1994). The total GWPs reported in IPCC (1990) including indirect effects are within the ranges shown in Table 13-8. The longer response time adopted here for methane perturbations is responsible for a large part of the change in methane GWP values compared to the nominal values including direct effects only in the IPCC (1992) report (although the fact that indirect effects were likely to be comparable to the direct effect was noted). This change is based entirely on the analysis presented in Chapter 2 of IPCC (1994) used to define the methane response time for this report (see Prather, 1994). The decay response has been thoroughly tested only for small perturbations around a background state and continuing input flux approximately representative of today's atmosphere. It would be different if, for example, large changes in methane emissions were to occur in the near future. It is also believed to be sensitive to other chemical factors such as the sources of carbon monoxide. The GWP determined in this manner is similarly valid for relatively small perturbations, *e.g.*, those that would be required to stabilize concentrations at current levels rather than continuing the small trend (order 1%/year) observed in the past decade (see Chapter 2). However, the GWP shown in Table 13-8 cannot be used to estimate the radiative forcing that occurred since pre-industrial times, when methane concentrations more than doubled.

Table 13-8. Total GWP for CH_4, including indirect effects, referenced to the AGWP computed for the CO_2 decay response of the Bern carbon cycle model and future CO_2 atmospheric concentrations held constant at current levels.

GWP	Time Horizon		
	20 year	100 year	500 year
Total CH_4 GWP, including indirect effects and 12-17 year response time	42-82	17-32	5-10
Fraction of total GWP due to tropospheric O_3 change	19 ± 12%	19 ± 12%	19 ± 12%
Fraction of total GWP due to stratospheric H_2O change	4%	4%	4%

13.5.4.3 Net Global Warming Potentials for Halocarbons

Chlorofluorocarbons effectively absorb infrared radiation and have been estimated to have accounted for as much as about 25% of the anthropogenic direct radiative forcing of the Earth's climate system over the period from 1980 to 1990 (IPCC, 1990). Improved understanding of the impact of ozone depletion on global radiative forcing has, however, markedly altered this picture (WMO, 1992; IPCC, 1992). It is now clear that the large ozone depletions observed in the lower stratosphere are likely to influence temperatures near the tropopause (Lacis *et al.*, 1990; Ramaswamy *et al.*, 1992), implying that in addition to their *direct* greenhouse warming, the *indirect* effect of ozone depletion is significant for estimating the GWPs of ozone-destroying gases. Ramaswamy *et al.* (1992) and WMO (1992) concluded that the globally averaged *decrease* in radiative forcing at the tropopause due to ozone depletion approximately balanced the globally averaged *increase* in direct radiative warming in the troposphere related to the direct forcing due to halocarbons during the decade of the 1980s. While changes in ozone have been reported in the upper troposphere (see Chapter 1), these are probably due to factors other than halocarbon increases (*e.g.*, changes of CO, NO_y, etc.) and do not affect the inference of halocarbon GWPs so long as the vertical profile of ozone depletion can be characterized. If such changes were to mask the vertical extent of halocarbon-induced ozone loss, then the cooling tendency ascribed to halocarbons could be underestimated. Updated estimates of halocarbon radiative forcing are provided in Chapter 8 of this report, IPCC (1994), and Schwarzkopf and Ramaswamy (1993). Daniel *et al.* (1994) have considered the indirect effects of ozone depletion in analyses of the GWPs for halocarbons. They concluded that the indirect effect varies greatly for different kinds of halocarbons (*e.g.*, halons, CFCs, HCFCs), a result that will be discussed further below.

Several recent studies have addressed the degree to which the radiative heating due to additions of a quasi-uniformly distributed tropospheric gas such as a CFC may be equated with the spatially inhomogeneous cooling at the tropopause due to ozone depletion for the purposes of evaluating a net climate response (*e.g.*, Molnar *et al.*, 1994). Some studies suggest that ozone depletion may result in important dynamical changes that modulate the realized climate response (Molnar *et al.*, 1994). For the purposes of the present analysis, it will be assumed that the indirect and direct radiative effects of halocarbons can be compared to one another in a globally averaged sense, an assumption that is currently being tested with detailed three-dimensional models (see Chapter 8 and IPCC, 1994).

Model calculations show that radiative cooling is a strong function of the vertical profile of the ozone loss (Schwarzkopf and Ramaswamy, 1993; Wang *et al.*, 1993). This implies that it will be difficult to calculate these effects using a fully interactive two-dimensional chemistry-dynamics model, since these tend to underestimate the ozone losses observed in the critical lowest part of the stratosphere (see, *e.g.*, Hauglustaine *et al.*, 1994a). Satellite and ozonesonde observations (see Chapter 1) can, however, be used to characterize the shape of the ozone loss profile fairly well. It has been shown by Schwarzkopf and Ramaswamy (1993) that the uncertainty in the globally averaged ozone cooling is on

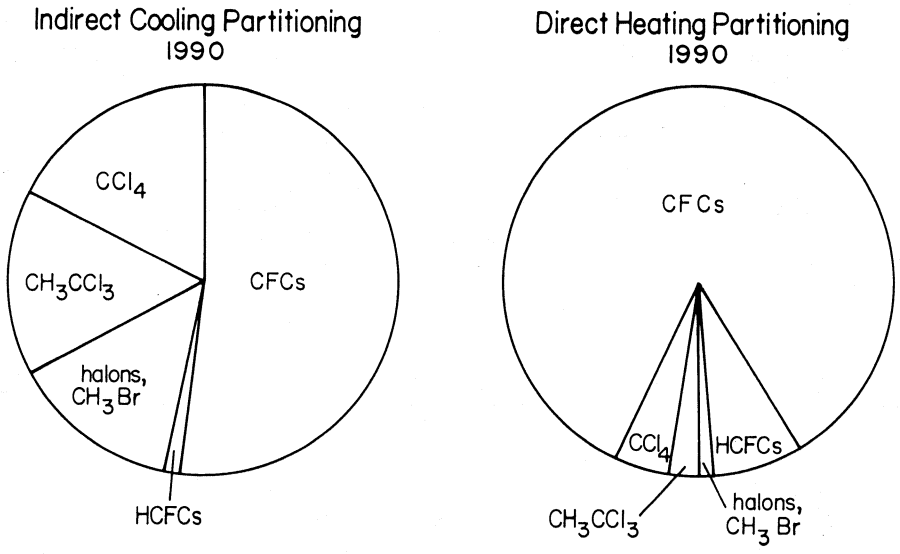

Figure 13-9. Contributions of various gases to the total estimated radiative cooling (indirect) and heating (direct) due to halocarbons in 1990 (Adapted from Daniel *et al.*, 1994). The adopted value of α for these calculations is 40.

the order of ±30% for a broad range of assumptions regarding the magnitude of the ozone depletion observed during the 1980s in the lowest part of the stratosphere (*i.e.*, below the region where satellite data exist). This estimate does not, however, include the enhanced ozone depletions that have been obtained in 1992 and 1993, nor does it consider the large changes in ozone observed by the Stratospheric Aerosol and Gas Experiment (SAGE) near the tropical tropopause (see Chapter 1). Insofar as these may be halocarbon-induced, these effects would tend to increase the global cooling and hence decrease the GWPs of ozone-depleting gases shown below.

Daniel *et al.* (1994) combined estimates of radiative cooling for the 1980s and their uncertainties (from the work of Schwarzkopf and Ramaswamy, 1993) with the detailed evaluation of past and future equivalent effective stratospheric chlorine for each halocarbon described in Section 13.3 to examine the net radiative forcing that can be attributed to each halocarbon. They emphasized that both Antarctic and midlatitude total ozone depletions appear to be quite small prior to about 1980, but to increase rapidly after that time, suggesting that a "threshold" for ozone destruction may have been reached. They assumed that the indirect radiative cooling for each halocarbon depends linearly upon its contribution to the total equivalent effective stratospheric chlorine whenever the latter lies above this threshold value. Possible nonlinearities associated, for example, with temperature feedbacks between ozone depletion and polar stratospheric cloud frequencies have therefore been neglected in this study. The impact of changing UV radiation due to ozone depletion upon OH and hence tropospheric chemistry has also not been considered here.

Insofar as significant ozone loss likely occurs only for total equivalent effective stratospheric chlorine levels above a certain threshold, the total indirect radiative cooling caused by any halocarbon depends upon the abundances of others and cannot be specified independent of scenario. This implies that GWPs for halocarbons based upon the indirect effects estimated for injection of an infinitesimally small amount of added gas can no longer be used to directly calculate the net radiative impact of the true amount of that gas in the Earth's atmosphere; this limitation is similar to that for methane discussed above.

Figure 13-9 shows an estimate of the contributions of various gases to the total estimated radiative cooling (indirect) and heating (direct) due to halocarbons in 1990 (Daniel *et al.*, 1994). A key point noted by Daniel *et al.* (1994) is that the CFCs are likely to be responsible for a much larger fraction of the estimated heating than

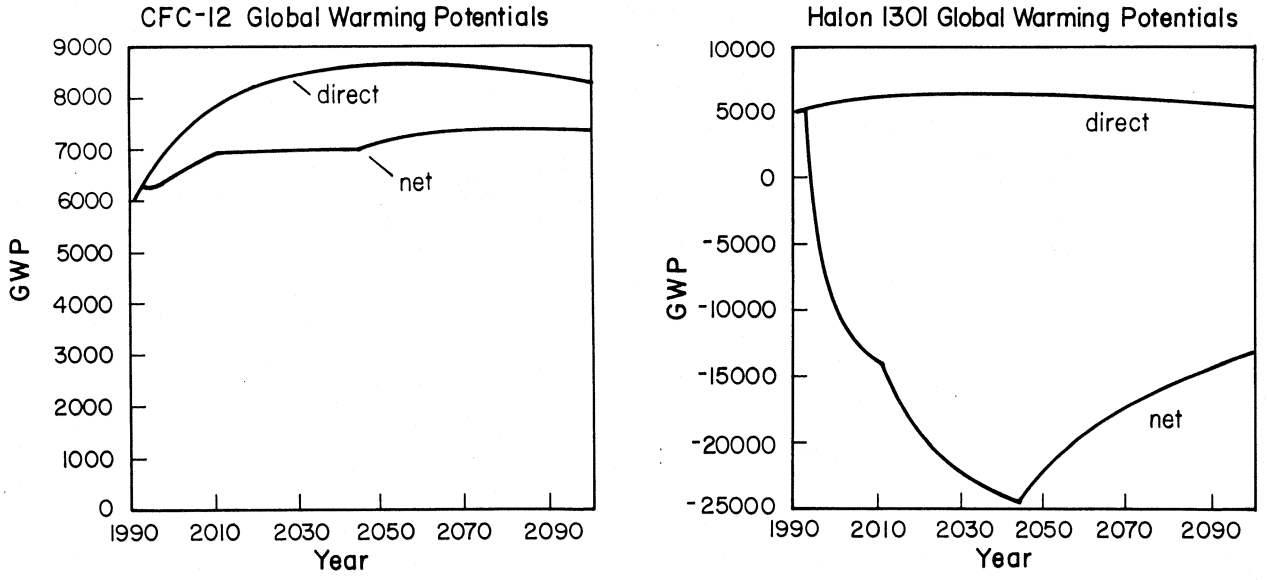

Figure 13-10. Calculated time-dependent GWPs for CFC-12 and halon-1301, adapted from the study of Daniel *et al.* (1994), for the basic Copenhagen scenario described in Section 13.3 (case A) and assuming a value of α of 40. The denominator used in these calculations is based upon the carbon cycle model as discussed in the text.

of the cooling, while for compounds such as the halons and anthropogenic CH_3Br, the situation is reversed. This is due to the enhanced effectiveness of brominated compounds compared to chlorinated species for ozone loss (see Section 13.4.2), by about a factor of 40. CCl_4 and CH_3CCl_3, while not as effective as the bromocarbons for ozone destruction, contain several chlorine atoms per molecule and release them readily in the stratosphere, making them relatively effective ozone destroyers (and hence cooling agents) as well. This introduces a new factor that would have to be dealt with in the use of such indices in policy decisions, underscoring the difficulty of considering gases with multiple, and very different, environmental impacts using a single simple index. Multiple impacts could require more sophisticated policy tools.

Figure 13-10 shows calculated GWPs for CFC-12 and halon-1301 as a function of time horizon adapted from the study of Daniel *et al.* (1994), for the base Copenhagen scenario (case A) described in Section 13.3, assuming a value of α of 40, and using the Bern *et al.* carbon cycle model results for the denominator as in IPCC (1994). As suggested by Figure 13-10, the net GWP of CFC-12 remains positive while that of halon-1301 becomes large and negative when indirect effects are considered in this framework. Daniel *et al.* (1994) considered the following key uncertainties in deriving the GWPs for halocarbons: (i) variations in the scenario for future concentrations of ozone-depleting gases, as in the scenarios of Section 13.3, (ii) uncertainties in the globally-averaged relative efficiency of bromine for ozone loss as compared to chlorine (α, assumed to lie between 40 and 200), and (iii) uncertainties in the magnitude of the cooling in the lower stratosphere due to uncertainties in the ozone loss profile (estimated to be about ±30% as noted above). They found that the GWPs were not as sensitive to the adopted range of possible scenarios for future concentrations of halocarbons nor to the exact values of the thresholds or scenarios assumed as to the uncertainties in the absolute value of the cooling and the value of α. This is consistent with the rather small differences in key aspects of the various scenarios shown in Table 13-3. The GWPs for bromocarbons were found to be extremely sensitive to the chosen value of α, while those for CFCs were quite sensitive to the adopted uncertainty in the total absolute radiative cooling in the 1980s. Table 13-9 shows the range of 20- and 100-year net GWPs derived for the halocarbons including indirect

Table 13-9. Net GWPs per unit mass emission for halocarbons including indirect effects (adapted from Daniel et al., 1994). Relative to CO_2 using Bern model for decay function (as in IPCC, 1994).

	Time Horizon = 2010					Time Horizon = 2090				
	Uncertainty in scenario, α		Uncertainty in cooling		Direct	Uncertainty in scenario, α		Uncertainty in cooling		Direct
compound	min	max	min	max		min	max	min	max	
CFC-11	1900	2900	1300	3000	5000	1400	1800	640	2200	4000
CFC-12	6300	6900	6100	6900	7900	6900	7100	6500	7400	8500
CFC-113	3200	3800	2800	3800	5000	3300	3500	2800	3800	5000
HCFC-22	3900	4000	3800	4000	4300	1500	1500	1500	1600	1700
HCFC-142b	3800	3900	3700	4000	4200	1800	1800	1700	1800	2000
CH_3Br	-18600	-4900	-6400	-3300		-5700	-1500	-2000	-1000	
H-1301	-97200	-22400	-31000	-13800	6200	-87300	-21600	-31200	-14200	5600
H-1211	-92400	-21500	-29600	-13400		-50600	-13600	-18800	-8900	
HCFC-141b	910	1200	690	1200	1800	270	370	180	390	630
CH_3CCl_3	-780	-450	-1100	-420	360	-260	-150	-360	-140	110
CCl_4	-1800	-520	-2500	-430	2000	-1500	-1100	-2400	-630	1400
HCFC-123	120	170	67	180	300	37	52	20	54	93
HCFC-124	1300	1400	1300	1370	1500	410	430	390	430	480
HFC-134a	3300	3300	3300	3300	3300	1300	1300	1300	1300	1300

effects from these sensitivity studies and compares them to GWPs for the direct effect only (adapted from Daniel *et al.*, 1994 for the denominator used here).

The range of values in the table underscores the uncertain nature of these estimates due to uncertainties in α and in the total absolute radiative cooling (*i.e.*, ozone loss distribution), but also illustrates systematic differences between various broad classes of compounds that are more robust. In particular, the CFCs and HCFCs are highly likely to be net warming agents. CCl_4 and CH_3CCl_3 are likely to be nearly "climate neutral," while halons and methyl bromide are believed to be net cooling agents. The impact of the implementation of the Copenhagen Amendments on radiative forcing and hence on climate change will depend upon the time-dependent mix of these gases and their substitutes in the future (see Chapter 8).

REFERENCES

AFEAS, Alternative Fluorocarbons Environmental Acceptability Study, *Production, Sales and Atmospheric Release of Fluorocarbons through 1992,* Grant Thornton Company, Washington, D.C., 1993.

Atkinson, R., D.L. Baulch, R.A. Cox, R.F. Hampson, J.A. Kerr, and J. Troe, Evaluated kinetic and photochemical data for atmospheric chemistry, supplement IV, IUPAC subcommittee on gas kinetic data evaluation for atmospheric chemistry, *J. Phys. Chem. Ref. Data, 21,* 1125-1568, 1992.

Barry, J., H.W. Sidebottom, J. Treacy, and J. Franklin, Kinetics and mechanism for the atmospheric oxidation of 1,1,2-trifluoroethane, *Int. J. Chem. Kin.*, in press, 1994.

Biggs, P., *et al.*, paper presented at STEP-HALOCIDE AFEAS workshop, University College, Dublin, Ireland, 23 to 25 March, 1993.

Bridier, I., B. Veyret, and R. Lesclaux, Flash photolysis kinetic study of reactions of the BrO radical with BrO and HO_2, *Chem. Phys. Lett., 201,* 563-568, 1993.

Briegleb, B., Longwave band model for thermal radiation in climate studies, *J. Geophys. Res., 97,* 11475-11486, 1992.

Brühl, C., The impact of the future scenarios for methane and other chemically active gases on the GWP of methane, *Chemosphere, 26,* 731-738, 1993.

Butler, J.H., J.W. Elkins, T.M. Thompson, B.D. Hall, T.H. Swanson, and V. Koropalov, Oceanic consumption of CH_3CCl_3: Implications for tropospheric OH, *J. Geophys. Res., 96,* 22347-22355, 1991.

Caldeira, K., and J.F. Kasting, Global warming on the margin, *Nature, 366,* 251-253, 1993.

Cess, R.D., *et al.*, Uncertainties in carbon dioxide radiative forcing in atmospheric general circulation models, *Science, 262,* 1252-1255, 1993.

Chameides, W.L., and D.D. Davis, Iodine: Its possible role in tropospheric photochemistry, *J. Geophys. Res., 85,* 7383-7398, 1980.

Clerbaux, C., R. Colin, P.C. Simon, and C. Granier, Infrared cross sections and global warming potentials of 10 alternative hydrohalocarbons, *J. Geophys. Res., 98,* 10491-10497, 1993.

Cooper, D.L., T.P. Cunningham, N.L. Allen, and A. McCulloch, Tropospheric lifetimes of potential CFC replacements: Rate coefficients for reaction with the hydroxyl radical, *Atmos. Env., 26A,* 1331-1334, 1992.

Cunnold, D., P. Fraser, R. Weiss, R. Prinn, P. Simmonds, B. Miller, F. Alyea, and A. Crawford, Global trends and annual releases of $CFCl_3$ and CF_2Cl_2 estimated from ALE/GAGE and other measurements from July 1978 to June 1991, *J. Geophys. Res., 99,* 1107-1126, 1994.

Daniel, J.S., S. Solomon, and D.L. Albritton, On the evaluation of halocarbon radiative forcing and global warming potentials, accepted for publication in *J. Geophys. Res.*, 1994.

DeMore, W.B., Rate constants for the reactions of OH with HFC-134a and HFC-134, *Geophys. Res. Lett., 20,* 1359-1362, 1993.

Fisher, D.A., and P.M. Midgley, The production and release to the atmosphere of CFCs 113, 114 and 115, *Atmospheric Environment, 27A,* 271-276, 1993.

Fuglestvedt, J.S., J.E. Jonson, and I.S.A. Isaksen, Effects of reduction in stratospheric ozone on tropospheric chemistry through changes in photolysis rates, accepted for publication in *Tellus*, 1994.

Gamlen, P.H., B.C. Lane, P.M. Midgley, and J.M. Steed, The production and release to the atmosphere of CCl_3F and CCl_2F_2 (chlorofluorocarbons CFC 11 and CFC 12), *Atmospheric Environment, 20,* 1077-1085, 1986.

Garcia, R.R., and S. Solomon, A new numerical model of the middle atmosphere 2. Ozone and related species, *J. Geophys. Res., 99,* 12937-12951, 1994.

Hauglustaine, D.A., C. Granier, G.P. Brasseur, and G. Mégie, The importance of atmospheric chemistry in the calculation of radiative forcing on the climate system, *J. Geophys. Res., 99,* 1173-1186, 1994a.

Hauglustaine, D.A., C. Granier, and G.P. Brasseur, Impact of increased methane emissions on the atmospheric composition and related radiative forcing of the climate system, submitted to *Environ. Monitor. Assoc.*, 1994b.

IPCC, Intergovernmental Panel on Climate Change, *Climate Change: The Scientific Assessment*, edited by J.T. Houghton, G.J. Jenkins, and J.J. Ephraums, Cambridge University Press, Cambridge, U.K., 1990.

IPCC, Intergovernmental Panel on Climate Change, *Climate Change: The Supplementary Report to the IPCC Scientific Assessment*, edited by J.T. Houghton, B.A. Callander, and S.K. Varney, Cambridge University Press, Cambridge, U.K., 1992.

IPCC, Intergovernmental Panel on Climate Change, *Climate Change: The Scientific Assessment,* in preparation, 1994.

IUPAC, International Union of Pure and Applied Chemistry, Evaluated kinetic and photochemical data for atmospheric chemistry, *J. Phys. Chem. Ref. Data, 21,* 6, 1992.

Johnson, C., J. Henshaw, and G. McInnes, Impact of aircraft and surface emissions of nitrogen oxides on tropospheric ozone and global warming, *Nature, 355,* 69-71, 1992.

JPL, Jet Propulsion Laboratory, *Chemical Kinetics and Photochemical Data for Use in Stratospheric Modelling,* JPL report number 92-20, 1992.

Kaye, J., S. Penkett and F.M. Ormond, *Report on Concentrations, Lifetimes and Trends of CFCs, Halons, and Related Species,* NASA office of Mission to Planet Earth, NASA Reference Publication 1339, 1994.

Kindler, T.P., W.L. Chameides, P.H. Wine, D.M. Cunnold, F.N. Alyea, and J.A. Franklin, The fate of atmospheric phosgene and the ozone depletion potentials of its parent compounds: CCl_4, C_2Cl_4, C_2HCl_3, CH_3CCl_3, $CHCl_3$, submitted to *J. Geophys. Res.*, 1994.

Ko, M.K.W., N.-D. Sze, W.-C. Wang, G. Shia, A. Goldman, F.J. Murcray, D.G. Murcray, and C.P. Rinsland, Atmospheric sulfur hexafluoride: Sources, sinks, and greenhouse warming, *J. Geophys. Res., 98,* 10499-10507, 1993.

Ko, M.K.W., N.-D. Sze, J.M. Rodriguez, D.K. Weisenstein, C.W. Heisey, R.P. Wayne, P. Biggs, C.E. Canosa-Mas, H.W. Sidebottom, and J. Treacy, CF_3 chemistry: Potential implications for stratospheric ozone, *Geophys. Res. Lett., 21,* 101-104, 1994a.

Ko, M.K.W., N.-D. Sze, and M.J. Prather, Protection of the ozone layer: Adequacy of existing controls, *Nature, 367,* 545-548, 1994b.

Lacis, A.A., D.J. Wuebbles, and J.A. Logan, Radiative forcing by changes in the vertical distribution of ozone, *J. Geophys. Res., 95,* 9971-9981, 1990.

Lal, M., and T. Holt, Ozone depletion due to increasing anthropogenic trace gas emissions: Role of stratospheric chemistry and implications for future climate, *Clim. Res., 1,* 85-95, 1991.

Lelieveld, J., and P.J. Crutzen, Indirect chemical effects of methane on climate warming, *Nature, 355,* 339-342, 1992.

Lelieveld, J., P.J. Crutzen, and C. Brühl, Climate effects of atmospheric methane, *Chemosphere, 26,* 739-768, 1993.

Li, Z., and J.S. Francisco, Laser-induced fluorescence spectroscopic study of the $^2A_1$-^2E transition of trifluoromethoxy radical, *Chem. Phys. Lett., 186,* 336, 1991.

McCarthy, R.L., F.A. Bower, and J.P. Jesson, The fluorocarbon-ozone theory—I. Production and release: World production and release of CCl_3F and CCl_2F_2 (fluorocarbons 11 and 12) through 1975, *Atmospheric Environment, 11,* 491-497, 1977.

McCulloch, A., Global production and emissions of bromochlorodifluoromethane and bromotrifluoromethane (halons 1211 and 1301), *Atmospheric Environment, 26A,* 1325-1329, 1992.

Mellouki, A., R.K. Talukdar, and C.J. Howard, Kinetics of the reactions of HBr with O_3 and HO_2: The yield of HBr from HO_2 + BrO, *J. Geophys. Res., 99,* 22949-22954, 1994.

Midgley, P.M., The production and release to the atmosphere of 1,1,1-trichloroethane (methyl chloroform), *Atmospheric Environment, 23,* 2663-2665, 1989.

Midgley, P.M., and D.A. Fisher, The production and release to the atmosphere of chlorodifluoromethane (HCFC 22), *Atmospheric Environment, 27A,* 271-279, 1993.

Molnar, G.I., M.K.W. Ko, S. Zhou, and N.-D. Sze, Climatic consequences of the observed 1980s ozone loss: Relevance to the greenhouse problem, *J. Geophys. Res.*, in press, 1994.

Moore, B., III, and B.H. Braswell, Jr., The lifetime of excess atmospheric carbon dioxide, *Global Biogeochem. Cycles, 8,* 23-28, 1994.

Nelson, D.D., M.S. Zahniser, and C.E. Kolb, OH reaction kinetics and atmospheric lifetimes of $CF_3CFCHCF_3$ and CF_3CH_2Br, *Geophys. Res. Lett., 20,* 197-200, 1993.

Plumb, R.A., and M.K.W. Ko, Interrelationships between mixing ratios of long-lived stratospheric constituents, *J. Geophys. Res., 97,* 10145-10156, 1992.

Pollock, W.H., L.E. Heidt, R.A. Lueb, J.F. Vedder, M.J. Mills, and S. Solomon, On the age of stratospheric air and ozone depletion potentials in polar regions, *J. Geophys. Res., 97,* 12993-12999, 1992.

Poulet, G.M., M. Pirre, F. Magain, R. Ramaroson, and G. Le Bras, Role of the BrO + HO_2 reaction in the stratospheric chemistry of bromine, *Geophys. Res. Lett., 23,* 2305-2308, 1992.

Prather, M.J., and R.T. Watson, Stratospheric ozone depletion and future levels of atmospheric chlorine and bromine, *Nature, 344,* 729-734, 1990.

Prather, M.J., and C.M. Spivakovsky, Tropospheric OH and the lifetimes of hydrochlorofluorocarbons (HCFCs), *J. Geophys. Res., 95,* 18723-18729, 1990.

Prather, M.J., Lifetimes and Eigenstates in atmospheric chemistry, *Geophys. Res. Lett., 21,* 801-804, 1994.

Prinn, R., D. Cunnold, P. Simmonds, F. Alyea, R. Boldi, A. Crawford, P. Fraser, D. Gutzler, D. Hartley, R. Rosen, and R. Rasmussen, Global averaged concentration and trend for hydroxyl radicals deduced from ALE/GAGE trichloroethane (methyl chloroform) data for 1978-1990, *J. Geophys. Res., 97,* 2445-2462, 1992.

Ramaswamy, V., M.D. Schwarzkopf, and K.P. Shine, Radiative forcing of climate from halocarbon-induced global stratospheric ozone loss, *Nature, 355,* 810-812, 1992.

Ravishankara, A.R., A.A. Turnipseed, N.R. Jensen, S. Barone, M. Mills, C.J. Howard, and S. Solomon, Do hydrofluorocarbons destroy stratospheric ozone?, *Science, 263,* 71-75, 1994.

Ravishankara, A.R., S. Solomon, A A. Turnipseed, and R.F. Warren, Atmospheric lifetimes of long-lived species, *Science, 259,* 194-199, 1993.

Rodhe, H., A comparison of the contributions of various gases to the greenhouse effect, *Science, 248,* 1217-1219, 1990.

Roehl, C.M., D. Boglu, C. Brühl, and G.K. Moortgat, Infrared band intensities and global warming potentials of CF_4, C_2F_6, C_3F_8, C_4F_{10}, C_5F_{12}, and C_6F_{14}, submitted to *Geophys. Res. Lett.,* 1994.

Salawitch, R.J., *et al.*, Loss of ozone in the Arctic vortex for the winter of 1989, *Geophys. Res. Lett., 17,* 561-564, 1990.

Salawitch, R.J., *et al.*, Chemical loss of ozone in the Arctic polar vortex in the winter of 1991-1992, *Science, 261,* 1146-1149, 1993.

Schauffler, S.M., L.E. Heidt, W.H. Pollock, T.M. Gilpin, J. Vedder, S. Solomon, R.A. Lueb, and E.L. Atlas, Measurements of halogenated organic compounds near the tropical tropopause, *Geophys. Res. Lett., 20,* 2567-2570, 1993.

Schwarzkopf, M.D., and V. Ramaswamy, Radiative forcing due to ozone in the 1980s: Dependence on altitude of ozone change, *Geophys. Res. Lett., 20,* 205-208, 1993.

Schmoltner, A.M., R.K. Talukdar, R.F. Warren, A. Mellouki, L. Goldfarb, T. Gierczak, S.A. McKeen, and A.R. Ravishankara, Rate coefficients for reactions of several hydrofluorocarbons with OH and $O(^1D)$ and their atmospheric lifetimes, *J. Phys. Chem., 97,* 8976-8982, 1993.

Solomon, S., J. Burkholder, A.R. Ravishankara, and R.R. Garcia, Ozone depletion and global warming potentials for CF_3I, *J. Geophys. Res., 99,* 20929-20935, 1994a.

Solomon, S., R.R. Garcia, and A.R. Ravishankara, On the role of iodine in ozone depletion, *J. Geophys. Res., 99,* 20491-20499, 1994b.

Solomon, S., M.J. Mills, L.E. Heidt, W.H. Pollock, and A.F. Tuck, On the evaluation of ozone depletion potentials, *J. Geophys. Res., 97,* 825-842, 1992.

Solomon, S., and D.L. Albritton, A new analysis of time-dependent ozone depletion potentials, *Nature, 357,* 33, 1992.

Stolarski, R.S., and R.D. Rundel, Fluorine photochemistry in the stratosphere, *Geophys. Res. Lett., 2,* 443-445, 1975.

Tabazadeh, A., and R.P. Turco, Stratospheric chlorine injection by volcanic eruptions: HCl scavenging and implications for ozone, *Science, 260,* 1082-1086, 1993.

Wang, W.C., M.P. Dudek, X.Z. Liang, and J.T. Kiehl, Inadequacy of effective CO_2 as a proxy in simulating the greenhouse effect of other radiative active gases, *Nature, 350,* 573-577, 1991.

Wang, W.C., Y.C. Zhuang, and R.D. Bojkov, Climate implications of observed changes in ozone vertical distributions in middle and high latitudes of the Northern Hemisphere, *Geophys. Res. Lett., 20,* 1567-1570, 1993.

Wang, C.J.L., D.R. Blake, and F.S. Rowland, Seasonal variations in the atmospheric distribution in remote surface locations of reactive chlorine compounds, tetrachloroethylene (C_2Cl_4), submitted to *Geophys. Res. Lett.,* 1994.

Wigley, T.M.L., Balancing the carbon budget: Implications for projections of future carbon dioxide concentration changes, *Tellus, 45B,* 409-425, 1993.

APPENDIX A

LIST OF INTERNATIONAL AUTHORS, CONTRIBUTORS, AND REVIEWERS

CO-CHAIRS

Daniel L. Albritton	National Oceanic and Atmospheric Administration, Boulder, Colorado	US
Robert T. Watson	Office of Science and Technology Policy, Washington, D.C.	US
Piet J. Aucamp	Department of National Health, Pretoria	South Africa

AUTHORS AND CONTRIBUTORS

COMMON QUESTIONS ABOUT OZONE

Coordinators

Susan Solomon	NOAA Aeronomy Laboratory	US
F. Sherwood Rowland	University of California at Irvine	US

PART 1. OBSERVED CHANGES IN OZONE AND SOURCE GASES

CHAPTER 1: OZONE MEASUREMENTS

Chapter Lead Author

Neil R.P. Harris	European Ozone Research Coordinating Unit	UK

Co-authors

Gerard Ancellet	Centre National de la Recherche Scientifique	France
Lane Bishop	Allied Signal, Inc.	US
David J. Hofmann	NOAA Climate Monitoring and Diagnostics Laboratory	US
James B. Kerr	Atmospheric Environment Service	Canada
Richard D. McPeters	NASA Goddard Space Flight Center	US
M. Margarita Préndez	Universidad de Chile	Chile
William J. Randel	National Center for Atmospheric Research	US
Johannes Staehelin	Eidgenössische Technische Hochschule Zürich	Switzerland
B.H. Subbaraya	Physical Research Laboratory	India
Andreas Volz-Thomas	Forschungszentrum Jülich	Germany
Joseph M. Zawodny	NASA Langley Research Center	US
Christos S. Zerefos	Aristotle University of Thessaloniki	Greece

Contributors

Marc Allaart	Koninklijk Nederlands Meteorologisch Instituut	The Netherlands
James K. Angell	NOAA Air Resources Laboratory	US

AUTHORS, CONTRIBUTORS, AND REVIEWERS

Rumen D. Bojkov	World Meteorological Organization	Switzerland
Kenneth P. Bowman	Texas A&M University	US
G.J.R. Coetzee	Weather Bureau	South Africa
Malgorzata Degórska	Polish Academy of Sciences	Poland
John J. DeLuisi	NOAA Air Resources Laboratory	US
Dirk De Muer	Institut Royal Météorologique de Belgique	Belgium
Terry Deshler	University of Wyoming	US
Lucien Froidevaux	California Institute of Technology/Jet Propulsion Laboratory	US
Reinhard Furrer	Freie Universität Berlin	Germany
Brian G. Gardiner	British Antarctic Survey	UK
Hartwig Gernandt	Alfred Wegener Institut	Germany
James F. Gleason	NASA Goddard Space Flight Center	US
Ulrich Görsdorf	Deutscher Wetterdienst	Germany
Kjell Henriksen	University of Tromsø	Norway
Ernest Hilsenrath	NASA Goddard Space Flight Center	US
Stacey M. Hollandsworth	Applied Research Corporation	US
Øystein Hov	Universitetet I Bergen	Norway
Hennie Kelder	Koninklijk Nederlands Meteorologisch Instituut	The Netherlands
Volker Kirchhoff	Instituto Nacional de Pesquisas Espaciais	Brazil
Ulf Köhler	Deutscher Wetterdienst	Germany
Walter D. Komhyr	NOAA Climate Monitoring and Diagnostics Laboratory	US
Janusz W. Krzyścin	Polish Academy of Sciences	Poland
Zenobia Lityńska	Centre of Aerology	Poland
Jennifer A. Logan	Harvard University	US
Pak Sum Low	United Nations Environment Programme Ozone Secretariat	Kenya
W. Andrew Matthews	National Institute of Water and Atmospheric Research	New Zealand
A.J. Miller	NOAA National Meteorological Center	US
Samuel J. Oltmans	NOAA Climate Monitoring and Diagnostics Laboratory	US
Walter G. Planet	National Oceanic and Atmospheric Administration, NESDIS	US
J.-P. Pommereau	Centre National de la Recherche Scientifique	France
Hans-Eckhart Scheel	Fraunhofer Institut für Atmosphärische Umweltforschung	Germany
Jonathan D. Shanklin	British Antarctic Survey	UK
Paula Skřivánková	Czech Hydrometeorological Institute	Czech Republic
Herman Smit	Forschungszentrum Jülich	Germany
Joe W. Waters	California Institute of Technology/Jet Propulsion Laboratory	US
Peter Winkler	Deutscher Wetterdienst	Germany

CHAPTER 2: SOURCE GASES: TRENDS AND BUDGETS

Chapter Lead Author

Eugenio Sanhueza	Instituto Venezolano de Investigaciones Cientificas	Venezuela

Co-authors

Paul J. Fraser	CSIRO Division of Atmospheric Research	Australia
Rudi J. Zander	University of Liege	Belgium

Contributors

Fred N. Alyea	Georgia Institute of Technology	US
Meinrat O. Andreae	Max-Planck-Institut für Chemie	Germany
James H. Butler	NOAA Climate Monitoring and Diagnostics Laboratory	US
Derek N. Cunnold	Georgia Institute of Technology	US
J. Dignon	Lawrence Livermore National Laboratory	US
Ed Dlugokencky	NOAA Climate Monitoring and Diagnostics Laboratory	US
Dieter H. Ehhalt	Forschungszentrum Jülich	Germany
James W. Elkins	NOAA Climate Monitoring and Diagnostics Laboratory	US
D. Etheridge	CSIRO Division of Atmospheric Research	Australia
David W. Fahey	NOAA Aeronomy Laboratory	US
Donald A. Fisher	E.I. DuPont de Nemours and Company	US
Jack A. Kaye	NASA Goddard Space Flight Center	US
M.A.K. Khalil	Oregon Graduate Institute of Science and Technology	US
Paulette Middleton	Science and Policy Associates, Inc.	US
Paul C. Novelli	University of Colorado	US
Joyce Penner	Lawrence Livermore National Laboratory	US
Michael J. Prather	University of California at Irvine	US
Ronald G. Prinn	Massachusetts Institute of Technology	US
William S. Reeburgh	University of California at Irvine	US
J. Rudolph	Forschungszentrum Jülich	Germany
P. Simmonds	University of Bristol	UK
L. Paul Steele	CSIRO Division of Atmospheric Research	Australia
Michael Trainer	NOAA Aeronomy Laboratory	US
Ray F. Weiss	Scripps Institution of Oceanography	US
Donald J. Wuebbles	University of Illinois	US

PART 2. ATMOSPHERIC PROCESSES RESPONSIBLE FOR THE OBSERVED CHANGES IN OZONE

CHAPTER 3: POLAR OZONE

Chapter Lead Author

David W. Fahey	NOAA Aeronomy Laboratory	US

Co-authors

Geir Braathen	Norsk Institutt for Luftforskning	Norway
Daniel Cariolle	Météo-France, Centre National de Recherches Météorologiques	France
Yutaka Kondo	Nagoya University	Japan
W. Andrew Matthews	National Institute of Water and Atmospheric Research	New Zealand
Mario J. Molina	Massachusetts Institute of Technology	US
John A. Pyle	University of Cambridge	UK
Richard B. Rood	NASA Goddard Space Flight Center	US
James M. Russell III	NASA Langley Research Center	US
Ulrich Schmidt	Forschungszentrum Jülich	Germany
Darin W. Toohey	University of California at Irvine	US

PART 5. SCIENTIFIC INFORMATION FOR FUTURE DECISIONS

CHAPTER 10: METHYL BROMIDE

Chapter Lead Author

Stuart A. Penkett	University of East Anglia	UK

Co-authors

James H. Butler	NOAA Climate Monitoring and Diagnostics Laboratory	US
Michael J. Kurylo	NASA Headquarters/NIST	US
C.E. Reeves	University of East Anglia	UK
Jose M. Rodriguez	Atmospheric and Environmental Research, Inc.	US
Hanwant B. Singh	NASA Ames Research Center	US
Darin W. Toohey	University of California at Irvine	US
Ray F. Weiss	Scripps Institution of Oceanography	US

Contributors

Meinrat O. Andreae	Max-Planck-Institut für Chemie	Germany
N.J. Blake	University of California at Irvine	US
Ralph J. Cicerone	University of California at Irvine	US
Tom Duafala	Methyl Bromide Global Coalition	US
Amram Golombek	Israel Institute for Biological Research	Israel
M.A.K. Khalil	Oregon Graduate Institute of Science and Technology	US
Joel S. Levine	NASA Langley Research Center	US
Mario J. Molina	Massachusetts Institute of Technology	US
Sue M. Schauffler	National Center for Atmospheric Research	US

CHAPTER 11: SUBSONIC AND SUPERSONIC AIRCRAFT EMISSIONS

Chapter Lead Authors

Andreas Wahner	Forschungszentrum Jülich	Germany
Marvin A. Geller	State University of New York at Stony Brook	US

Co-authors

Frank Arnold	Max-Planck-Institut für Kernphysik	Germany
William H. Brune	Pennsylvania State University	US
Daniel A. Cariolle	Météo-France, Centre National de Recherches Météorologiques	France
Anne R. Douglass	NASA Goddard Space Flight Center	US
Colin E. Johnson	UK Meteorological Office/AEA Technology	UK
Dave H. Lister	Defence Research Agency/Aerospace and Propulsion Department	UK
John A. Pyle	University of Cambridge	UK
Richard Ramaroson	Office National d'Etudes et de Recherches Aérospatiales	France
David Rind	NASA Goddard Institute for Space Studies	US
Franz Rohrer	Forschungszentrum Jülich	Germany
Ulrich Schumann	DLR Institut für Physik der Atmosphäre	Germany
Anne M. Thompson	NASA Goddard Space Flight Center	US

CHAPTER 12: ATMOSPHERIC DEGRADATION OF HALOCARBON SUBSTITUTES

Chapter Lead Author

R.A. Cox	National Environmental Research Council Headquarters	UK

Co-authors

Roger Atkinson	University of California at Riverside	US
Geert K. Moortgat	Max-Planck-Institut für Chemie	Germany
A.R. Ravishankara	NOAA Aeronomy Laboratory	US
H.W. Sidebottom	University College, Dublin	Ireland

Contributors

G.D. Hayman	Harwell Laboratory/AEA Environment and Energy	UK
Carleton J. Howard	NOAA Aeronomy Laboratory	US
Maria Kanakidou	Centre National de la Recherche Scientifique	France
Stuart A. Penkett	University of East Anglia	UK
Jose M. Rodriguez	Atmospheric and Environmental Research, Inc.	US
Susan Solomon	NOAA Aeronomy Laboratory	US
Oliver Wild	University of Cambridge	UK

CHAPTER 13: OZONE DEPLETION POTENTIALS, GLOBAL WARMING POTENTIALS, AND FUTURE CHLORINE/BROMINE LOADING

Chapter Lead Authors

Susan Solomon	NOAA Aeronomy Laboratory	US
Donald J. Wuebbles	University of Illinois	US

Co-authors

Ivar S.A. Isaksen	Universitetet I Oslo	Norway
Jeffrey T. Kiehl	National Center for Atmospheric Research	US
Murari Lal	Indian Institute of Technology	India
Paul C. Simon	Institut d'Aeronomie Spatiale de Belgique	Belgium
Nien-Dak Sze	Atmospheric and Environmental Research, Inc.	US

Contributors

Daniel L. Albritton	NOAA Aeronomy Laboratory	US
Christoph Brühl	Max-Planck-Institut für Chemie	Germany
Peter S. Connell	Lawrence Livermore National Laboratory	US
John S. Daniel	NOAA Aeronomy Laboratory/CIRES	US
Donald A. Fisher	E.I. DuPont de Nemours and Company	US
D. Hufford	U.S. Environmental Protection Agency	US
Claire Granier	National Center for Atmospheric Research	US
Shaw C. Liu	NOAA Aeronomy Laboratory	US
Ken Patten	Lawrence Livermore National Laboratory	US
S. Pinnock	University of Reading	UK

V. Ramaswamy	NOAA Geophysical Fluid Dynamics Laboratory/Princeton University	US
Keith P. Shine	University of Reading	UK
Guido Visconti	Universita' degli Studi-l'Aquila	Italy
D. Weisenstein	Atmospheric and Environmental Research, Inc.	US
Tom M.L. Wigley	University Corporation for Atmospheric Research	US

REVIEWERS

Daniel L. Albritton	NOAA Aeronomy Laboratory	US
Gerard Ancellet	Centre National de la Recherche Scientifique	France
Meinrat O. Andreae	Max-Planck-Institut für Chemie	Germany
Roger Atkinson	University of California at Riverside	US
Piet J. Aucamp	Department of National Health	South Africa
Helmuth Bauer	Forschungszentrum für Umwelt und Gesundheit	Germany
Slimane Bekki	University of Cambridge	UK
Tibor Bérces	Hungarian Academy of Sciences	Hungary
Lane Bishop	Allied Signal, Inc.	US
Donald R. Blake	University of California at Irvine	US
G. Bodeker	University of Natal/NIWA	South Africa
Rumen D. Bojkov	World Meteorological Organization	Switzerland
Byron Boville	National Center for Atmospheric Research	US
Guy P. Brasseur	National Center for Atmospheric Research	US
Christoph Brühl	Max-Planck-Institut für Chemie	Germany
William H. Brune	Pennsylvania State University	US
James H. Butler	NOAA Climate Monitoring and Diagnostics Laboratory	US
Sergio Cabrera	Universidad de Chile	Chile
Bruce A. Callander	UK Meteorological Office	UK
Daniel A. Cariolle	Météo-France, Centre National de Recherches Météorologiques	France
William L. Chameides	Georgia Institute of Technology	US
Marie-Lise Chanin	Centre National de la Recherche Scientifique	France
Ralph J. Cicerone	University of California at Irvine	US
R. A. Cox	National Environmental Research Council Headquarters	UK
Paul J. Crutzen	Max-Planck-Institut für Chemie	Germany
John S. Daniel	NOAA Aeronomy Laboratory/CIRES	US
Frank Dentener	Wageningen Agricultural University	The Netherlands
Susana B. Diaz	Austral Center of Scientific Research (CADIC/CONICET)	Argentina
Russell Dickerson	University of Maryland	US
Tom Duafala	Methyl Bromide Global Coalition	US
Christine A. Ennis	NOAA Aeronomy Laboratory/CIRES	US
David W. Fahey	NOAA Aeronomy Laboratory	US
Jack Fishman	NASA Langley Research Center	US
P.M. de F. Forster	University of Reading	UK
James Franklin	Solvay S.A.	Belgium
Paul J. Fraser	CSIRO Division of Atmospheric Research	Australia
Lucien Froidevaux	California Institute of Technology/Jet Propulsion Laboratory	US

Brian G. Gardiner	British Antarctic Survey	UK
Marvin A. Geller	State University of New York at Stony Brook	US
Amram Golombek	Israel Institute for Biological Research	Israel
Thomas E. Graedel	AT&T Bell Laboratories	US
Claire Granier	National Center for Atmospheric Research	US
William B. Grant	NASA Langley Research Center	US
Alexander Gruzdev	Russian Academy of Sciences	Russia
James E. Hansen	NASA Goddard Institute for Space Studies	US
Neil R.P. Harris	European Ozone Research Coordinating Unit	UK
Shiro Hatekeyama	National Institute for the Environment	Japan
Sachiko Hayashida	Nara Women's University	Japan
David J. Hofmann	NOAA Climate Monitoring and Diagnostics Laboratory	US
James R. Holton	University of Washington	US
Lon L. Hood	University of Arizona	US
Robert D. Hudson	University of Maryland	US
Abdel M. Ibrahim	Egyptian Meteorological Authority	Egypt
Mohammad Ilyas	University of Science Malaysia	Malaysia
Ivar S.A. Isaksen	Universitetet I Oslo	Norway
Tomoyuki Ito	Japan Meteorological Agency	Japan
Charles H. Jackman	NASA Goddard Space Flight Center	US
Daniel J. Jacob	Harvard University	US
Harold S. Johnston	University of California at Berkeley	US
P.V. Johnston	National Institute of Water and Atmospheric Research	New Zealand
Roderic L. Jones	University of Cambridge	UK
Torben S. Jørgensen	Danish Meteorological Institute	Denmark
Igor L. Karol	A.I. Voeikov Main Geophysical Observatory	Russia
Prasad Kasibhatla	Georgia Institute of Technology	US
Jack A. Kaye	NASA Goddard Space Flight Center	US
Hennie Kelder	Koninklijk Nederlands Meteorologisch Instituut	The Netherlands
James B. Kerr	Atmospheric Environment Service	Canada
M.A.K. Khalil	Oregon Graduate Institute of Science and Technology	US
Vyacheslav Khattatov	Central Aerological Observatory	Russia
Volker Kirchhoff	Instituto Nacional de Pesquisas Espaciais	Brazil
Malcolm K.W. Ko	Atmospheric and Environmental Research, Inc.	US
Antti Kulmala	World Meteorological Organization	Switzerland
Michael J. Kurylo	NASA Headquarters/NIST	US
Murari Lal	Indian Institute of Technology	India
G. LeBras	Centre National de la Recherche Scientifique	France
Yuan-Pern Lee	National Tsing Hua University	Taiwan
Jos Lelieveld	Wageningen University	The Netherlands
Robert Lesclaux	Université de Bordeaux 1	France
Joel Levy	NOAA Office of Global Programs	US
J.B. Liley	National Institute of Water and Atmospheric Research	New Zealand
Peter Liss	University of East Anglia	UK
Nicole Louisnard	Office National d'Etudes et de Recherches Aérospatiales	France
Pak Sum Low	United Nations Environment Programme Ozone Secretariat	Kenya
Daniel Lubin	University of California at San Diego	US

AUTHORS, CONTRIBUTORS, AND REVIEWERS

Sasha Madronich	National Center for Atmospheric Research	US
Jerry Mahlman	NOAA Geophysical Fluid Dynamics Laboratory	US
W. Andrew Matthews	National Institute of Water and Atmospheric Research	New Zealand
Konrad Mauersberger	Max-Planck-Institut für Kernphysik	Germany
Archie McCulloch	ICI Chemicals and Polymers Limited	UK
Mack McFarland	E.I. DuPont de Nemours and Company	US
Richard L. McKenzie	National Institute of Water and Atmospheric Research	New Zealand
Gérard Mégie	Centre National de la Recherche Scientifique	France
A.J. Miller	NOAA National Meteorological Center	US
Igor Mokhov	Institute of Atmospheric Physics	Russia
Hideaki Nakane	National Institute for Environmental Studies	Japan
Samuel J. Oltmans	NOAA Climate Monitoring and Diagnostics Laboratory	US
Alan R. O'Neill	University of Reading	UK
Michael Oppenheimer	Environmental Defense Fund	US
Juan Carlos Pelaez	Instituto de Meteorologia	Cuba
Stuart A. Penkett	University of East Anglia	UK
Thomas Peter	Max-Planck-Institut für Chemie	Germany
Leon F. Phillips	University of Canterbury	New Zealand
Ken Pickering	NASA Goddard Space Flight Center	US
Michel Pirre	Centre National de la Recherche Scientifique	France
Giovanni Pitari	Universita' degli Studi-l'Aquila	Italy
Michael J. Prather	University of California at Irvine	US
M. Margarita Préndez	Universidad de Chile	Chile
John A. Pyle	University of Cambridge	UK
Lian Xiong Qiu	Academia Sinica	China
V. Ramaswamy	NOAA Geophysical Fluid Dynamics Laboratory/Princeton University	US
William J. Randel	National Center for Atmospheric Research	US
A.R. Ravishankara	NOAA Aeronomy Laboratory	US
Curtis P. Rinsland	NASA Langley Research Center	US
Henning Rodhe	Stockholm University	Sweden
Jose M. Rodriguez	Atmospheric and Environmental Research, Inc.	US
F. Sherwood Rowland	University of California at Irvine	US
Jochen Rudolph	Forschungszentrum Jülich	Germany
Nelson Sabogal	United Nations Environment Programme	Kenya
Ross Salawitch	Harvard University	US
Eugenio Sanhueza	Instituto Venezolano de Investigaciones Cientificas	Venezuela
Ulrich Schmidt	Forschungszentrum Jülich	Germany
Keith P. Shine	University of Reading	UK
Paul C. Simon	Institut d'Aeronomie Spatiale de Belgique	Belgium
Susan Solomon	NOAA Aeronomy Laboratory	US
Johannes Staehelin	Eidgenössische Technische Hochschule Zürich	Switzerland
Knut Stamnes	University of Alaska	US
Leopoldo Stefanutti	Istituto di Riccrea sulle Onde Elettromagnetiche del CNR	Italy
Richard S. Stolarski	NASA Goddard Space Flight Center	US
Frode Stordal	Norsk Institutt for Luftforskning	Norway
B.H. Subbaraya	Physical Research Laboratory	India
Anne M. Thompson	NASA Goddard Space Flight Center	US

Margaret A. Tolbert	University of Colorado	US
Ralf Toumi	University of Cambridge	UK
Karel Vanicek	Czech Hydrometeorological Institute	Czech Republic
Andreas Volz-Thomas	Forschungszentrum Jülich	Germany
Andreas Wahner	Forschungszentrum Jülich	Germany
David A. Warrilow	UK Department of the Environment	UK
Robert T. Watson	Office of Science and Technology Policy	US
E.C. Weatherhead	NOAA Air Resources Laboratory	US
Ray F. Weiss	Scripps Institution of Oceanography	US
Howard Wesoky	National Aeronautics and Space Administration	US
Paul H. Wine	Georgia Institute of Technology	US
Donald J. Wuebbles	University of Illinois	US
Vladimir Yushkov	Central Aerological Observatory	Russia
Ahmed Zand	Tehran University	Iran
Reinhard Zellner	Universität Gesamthochschule Essen	Germany
Christos Zerefos	Aristotle University of Thessaloniki	Greece

OZONE PEER-REVIEW MEETING

Les Diablerets, Switzerland
July 18-22, 1994

Daniel L. Albritton	NOAA Aeronomy Laboratory	US
Meinrat O. Andreae	Max-Planck-Institut für Chemie	Germany
Piet J. Aucamp	Department of National Health	South Africa
Helmuth Bauer	Forschungszentrum für Umwelt und Gesundheit	Germany
Lane Bishop	Allied Signal, Inc.	US
Rumen D. Bojkov	World Meteorological Organization	Switzerland
Byron Boville	National Center for Atmospheric Research	US
Guy P. Brasseur	National Center for Atmospheric Research	US
William H. Brune	Pennsylvania State University	US
Bruce A. Callander	UK Meteorological Office	UK
Marie-Lise Chanin	Centre National de la Recherche Scientifique	France
Ralph J. Cicerone	University of California at Irvine	US
R. A. Cox	National Environmental Research Council Headquarters	UK
Paul J. Crutzen	Max-Planck-Institut für Chemie	Germany
John S. Daniel	NOAA Aeronomy Laboratory/CIRES	US
Susana B. Diaz	Austral Center of Scientific Research (CADIC/CONICET)	Argentina
Tom Duafala	Methyl Bromide Global Coalition	US
Christine A. Ennis	NOAA Aeronomy Laboratory/CIRES	US
David W. Fahey	NOAA Aeronomy Laboratory	US
Paul J. Fraser	CSIRO Division of Atmospheric Research	Australia
Marvin A. Geller	State University of New York at Stony Brook	US
Amram Golombek	Israel Institute for Biological Research	Israel
Neil R.P. Harris	European Ozone Research Coordinating Unit	UK
Sachiko Hayashida	Nara Women's University	Japan

AUTHORS, CONTRIBUTORS, AND REVIEWERS

David J. Hofmann	NOAA Climate Monitoring and Diagnostics Laboratory	US
James R. Holton	University of Washington	US
Abdel M. Ibrahim	Egyptian Meteorological Authority	Egypt
Mohammad Ilyas	University of Science Malaysia	Malaysia
Ivar S.A. Isaksen	Universitetet I Oslo	Norway
Tomoyuki Ito	Japan Meteorological Agency	Japan
Charles H. Jackman	NASA Goddard Space Flight Center	US
Daniel J. Jacob	Harvard University	US
Roderic L. Jones	University of Cambridge	UK
Igor L. Karol	A.I. Voeikov Main Geophysical Observatory	Russia
Hennie Kelder	Koninklijk Nederlands Meteorologisch Instituut	The Netherlands
James B. Kerr	Atmospheric Environment Service	Canada
M.A.K. Khalil	Oregon Graduate Institute of Science and Technology	US
Malcolm K.W. Ko	Atmospheric and Environmental Research, Inc.	US
Antti Kulmala	World Meteorological Organization	Switzerland
Michael J. Kurylo	NASA Headquarters/NIST	US
Murari Lal	Indian Institute of Technology	India
Joel Levy	NOAA Office of Global Programs	US
Pak Sum Low	United Nations Environment Programme Ozone Secretariat	Kenya
Sasha Madronich	National Center for Atmospheric Research	US
W. Andrew Matthews	National Institute of Water and Atmospheric Research	New Zealand
Konrad Mauersberger	Max-Planck-Institut für Kernphysik	Germany
Mack McFarland	E.I. DuPont de Nemours and Company	US
Richard L. McKenzie	National Institute of Water and Atmospheric Research	New Zealand
Gérard Mégie	Centre National de la Recherche Scientifique	France
Hideaki Nakane	National Institute for Environmental Studies	Japan
Samuel J. Oltmans	NOAA Climate Monitoring and Diagnostics Laboratory	US
Alan R. O'Neill	University of Reading	UK
Michael Oppenheimer	Environmental Defense Fund	US
Juan Carlos Pelaez	Instituto de Meteorologia	Cuba
Stuart A. Penkett	University of East Anglia	UK
Michael J. Prather	University of California at Irvine	US
M. Margarita Préndez	Universidad de Chile	Chile
Lian Xiong Qiu	Academia Sinica	China
V. Ramaswamy	NOAA Geophysical Fluid Dynamics Laboratory/Princeton University	US
A.R. Ravishankara	NOAA Aeronomy Laboratory	US
F. Sherwood Rowland	University of California at Irvine	US
Nelson Sabogal	United Nations Environment Programme	Kenya
Eugenio Sanhueza	Instituto Venezolano de Investigaciones Cientificas	Venezuela
Keith P. Shine	University of Reading	UK
Paul C. Simon	Institut d'Aeronomie Spatiale de Belgique	Belgium
Susan Solomon	NOAA Aeronomy Laboratory	US
Johannes Staehelin	Eidgenössische Technische Hochschule Zürich	Switzerland
Richard S. Stolarski	NASA Goddard Space Flight Center	US
Frode Stordal	Norsk Institutt for Luftforskning	Norway
B.H. Subbaraya	Physical Research Laboratory	India
Margaret A. Tolbert	University of Colorado	US

Andreas Volz-Thomas	Forschungszentrum Jülich	Germany
Andreas Wahner	Forschungszentrum Jülich	Germany
David A. Warrilow	UK Department of the Environment	UK
Robert T. Watson	Office of Science and Technology Policy	US
Ray F. Weiss	Scripps Institution of Oceanography	US
Donald J. Wuebbles	University of Illinois	US
Vladimir Yushkov	Central Aerological Observatory	Russia
Ahmed Zand	Tehran University	Iran
Christos Zerefos	Aristotle University of Thessaloniki	Greece

Sponsoring Organizations Liaisons

Rumen D. Bojkov World Meteorological Organization Switzerland
K.M. Sarma United Nations Environment Programme Kenya
Daniel L. Albritton National Oceanic and Atmospheric Administration US
Michael J. Kurylo National Aeronautics and Space Administration US

Coordinating Editor

Christine A. Ennis NOAA Aeronomy Laboratory/CIRES US

Editorial Staff

Jeanne S. Waters NOAA Aeronomy Laboratory US

Publication Design and Layout

University of Colorado at Boulder Publications Service:
Elizabeth C. Johnston
Patricia L. Jensen
Andrew S. Knoedler

Conference Coordination and Documentation

Rumen D. Bojkov World Meteorological Organization Switzerland
Marie-Christine Charriére World Meteorological Organization France
Christine A. Ennis NOAA Aeronomy Laboratory/CIRES US
Jeanne S. Waters NOAA Aeronomy Laboratory US

Conference Support

Flo M. Ormond Birch and Davis Associates, Inc. US
Kathy A. Wolfe Computer Sciences Corporation US

APPENDIX B

MAJOR ACRONYMS AND ABBREVIATIONS

AAOE	Airborne Antarctic Ozone Experiment
AASE	Airborne Arctic Stratospheric Expedition
ABLE 2A	Amazon Boundary Layer Experiment 2A
ABLE 3B	Arctic Boundary Layer Expedition 3B
AEA	Atomic Energy Authority (United Kingdom)
AER	Atmospheric and Environmental Research, Inc. (United States)
AERONOX	Impact of NO_X Emissions from Aircraft upon the Atmosphere
AESA	Atmospheric Effects of Stratospheric Aircraft
AFEAS	Alternative Fluorocarbons Environmental Acceptability Study
AGU	American Geophysical Union
AGWP	Absolute Global Warming Potential
AL	Aeronomy Laboratory (NOAA)
ALE/GAGE	Atmospheric Lifetime Experiment/Global Atmospheric Gases Experiment
ANCAT	Abatement of Nuisance Caused by Air Traffic
ASL	above sea level
ATLAS	Atmospheric Laboratory for Applications and Science
ATMOS	Atmospheric Trace Molecule Spectroscopy
BEF	Bromine Efficiency Factor
BLP	Bromine Loading Potential
BM	Brewer-Mast (ozonesonde)
CADIC/COCINET	Austral Center of Scientific Research/National Council of Scientific and Technological Research (Argentina)
CCMS	Committee on the Challenges of Modern Society
CCN	cloud condensation nuclei
CEC	Commission of the European Communities
CHEMRAWN	Chemical Research Applied to World Needs
CFC	chlorofluorocarbon
CIAB	Coal Industry Advisory Board
CIAP	Climatic Impact Assessment Program
CIRES	Cooperative Institute for Research in Environmental Sciences (United States)
CITE	Chemical Instrumentation Test and Evaluation
CLAES	Cryogenic Limb Array Etalon Spectrometer
CLP	Chlorine Loading Potential
CMDL	Climate Monitoring and Diagnostics Laboratory (NOAA)
CN	condensation nuclei
CNRM	Centre National de Recherches Météorologiques (France)
CNRS	Centre National de la Recherche Scientifique (France)
CSIRO	Commonwealth Scientific and Industrial Research Organization (Australia)
CTM	chemistry transport model

ACRONYMS

DIAL	Differential Absorption Laser
DNA	deoxyribonucleic acid
DoY	Day-of-Year
DU	Dobson unit
EASOE	European Arctic Stratospheric Ozone Expedition
ECAC	European Civil Aviation Conference
ECC	electrochemical concentration cell (ozonesonde)
ECMWF	European Centre for Medium-Range Weather Forecasts (United Kingdom)
EESC	equivalent effective stratospheric chlorine
EI	Emissions Index
EMEP MSC-W	European Monitoring and Evaluation Programme, Meteorological Synthesizing Centre — West
EMEX	Equatorial Mesoscale Experiment
ENSO	El Niño-Southern Oscillation
EPA	Environmental Protection Agency (United States)
ESA	European Space Agency
ETBL	equivalent tropospheric bromine loading
ETCL	equivalent tropospheric chlorine loading
FDH	Fixed Dynamical Heating
FTIR	Fourier transform infrared spectrometer
GAGE	Global Atmospheric Gases Experiment
GCM	general circulation model
GFDL	Geophysical Fluid Dynamics Laboratory (NOAA)
GISS	Goddard Institute for Space Studies (United States)
GIT	Georgia Institute of Technology (United States)
GMT	Greenwich Mean Time
GSFC	Goddard Space Flight Center (NASA)
GWP	Global Warming Potential
HALOE	Halogen Occultation Experiment
HC	hydrocarbon
HCFC	hydrochlorofluorocarbon
HFC	hydrofluorocarbon
HSCT	High Speed Civil Transport
HSRP	High Speed Research Program
ICAO	International Civil Aviation Organization
IEA	International Energy Agency
IIT	Indian Institute of Technology
INPE	Instituto Nacional de Pesquisas Espaciais (Brazil)
IOTP	International Ozone Trends Panel
IPCC	Intergovernmental Panel on Climate Change
IR	infrared
ISAMS	Improved Stratospheric and Mesospheric Sounder
IUPAC	International Union of Pure and Applied Chemistry
IVIC	Instituto Venezolano de Investigaciones Cientificas (Venezuela)

JPL	Jet Propulsion Laboratory (California Institute of Technology; United States)
KNMI	Koninklijk Nederlands Meteorologisch Instituut
LIMS	Limb Infrared Monitor of the Stratosphere
LLNL	Lawrence Livermore National Laboratory (United States)
LRC	Langley Research Center (NASA)
LTO	Landing/Take-Off cycle
MIPAS	Michelson Interferometric Passive Atmosphere Sounder
MLOPEX	Mauna Loa Observatory Photochemistry Experiment
MLS	Microwave Limb Sounder
MOZAIC	Measurement of Ozone on Airbus In-service Aircraft
MPI	Max-Planck-Institute (Germany)
MPIA	Max-Planck-Institute for Aeronomy (Germany)
MPIC	Max-Planck-Institute for Chemistry (Germany)
MRI	Meteorological Research Institute (Japan)
MSU	Microwave Sounder Unit
NACNEMS	North American Cooperative Network of Enhanced Measurement Sites
NAD	nitric acid dihydrate
NASA	National Aeronautics and Space Administration (United States)
NAT	nitric acid trihydrate
NCAR	National Center for Atmospheric Research (United States)
NCSU	North Carolina State University (United States)
NESDIS	National Environmental Satellite, Data, and Information Service (NOAA)
NH	Northern Hemisphere
NILU	Norsk Institutt for Luftforskning (Oslo)
NIR	near infrared
NIST	National Institute of Standards and Technology (formerly NBS; United States)
NIWA	National Institute of Water and Atmospheric Research, Ltd. (New Zealand)
NMC	National Meteorological Center (United States)
NMHC	non-methane hydrocarbon
NOAA	National Oceanic and Atmospheric Administration (United States)
NPP	net primary productivity
NRC	National Research Council (United States)
NSF	National Science Foundation (United States)
NYU	New York University (United States)
ODP	Ozone Depletion Potential
ODW	Ozone Data for the World
OECD	Organization for Economic Cooperation and Development (Paris)
OSE	ozonesonde instrument used in former East Germany; similar to Brewer-Mast
OTP	Ozone Trends Panel

ACRONYMS

PAN	peroxyacetyl nitrate
PBL	planetary boundary layer
PFCs	perfluorocarbons
POLINAT	Pollution from Aircraft Emissions in the North Atlantic Flight Corridor
ppbm	parts per billion by mass
ppbv	parts per billion by volume
ppmv	parts per million by volume
pptv	parts per trillion by volume
PSCs	polar stratospheric clouds
PV	potential vorticity
QBO	quasi-biennial oscillation
RAF	Radiation Amplification Factor
RB	Robertson-Berger (UV irradiance meter)
SAGE	Stratospheric Aerosol and Gas Experiment
SAM II	Stratospheric Aerosol Measurement
SAMS	Stratospheric and Mesospheric Sounder
SAOZ	Système d'Analyse par Observation Zénithale
SAT	sulfuric acid tetrahydrate
SBUV	Solar Backscatter Ultraviolet spectrometer
SH	Southern Hemisphere
SOS/SONIA	Southern Oxidants Study/Southeast Oxidant and Nitrogen Intensive Analysis
SPADE	Stratospheric Photochemistry, Aerosols and Dynamics Expedition
SPEs	solar proton events
SSA	stratospheric sulfuric acid aerosol
SSBUV	Shuttle Solar Backscatter Ultraviolet spectrometer
STE	stratosphere-troposphere exchange
STEP	Stratosphere-Troposphere Exchange Project
STP	standard temperature and pressure
STRATOZ	Stratospheric Ozone expedition
SUNY	State University of New York (United States)
SUSIM	Solar Ultraviolet Spectral Irradiance Monitor
SZA	solar zenith angle
TFA	trifluoroacetic acid
TIROS	Television and Infrared Observation Satellite
TNO	Netherlands Organization for Applied Scientific Research
TOMS	Total Ozone Mapping Spectrometer
TOR	Tropospheric Ozone Research
TOVS	TIROS Operational Vertical Sounder
TROPOZ II	Tropospheric Ozone II expedition

UARS	Upper Atmosphere Research Satellite
UCI	University of California at Irvine (United States)
UEA	University of East Anglia (United Kingdom)
UKMO	United Kingdom Meteorological Office
UNEP	United Nations Environment Programme
UV	ultraviolet
UV-A	ultraviolet-A
UV-B	ultraviolet-B
VOC	volatile organic compound
WCRP	World Climate Research Programme
WMO	World Meteorological Organization
WODC	World Ozone Data Center

APPENDIX C

CHEMICAL FORMULAE AND NOMENCLATURE

HALOGEN-CONTAINING SPECIES

Cl	atomic chlorine	Br	atomic bromine
ClO	chlorine monoxide	BrO	bromine monoxide
OClO	chlorine dioxide		
Cl_2O_2	dichlorine peroxide (ClO dimer)		
ClONO	chlorine nitrite	$BrNO_2$	bromine nitrite
$ClONO_2$	chlorine nitrate	$BrONO_2$	bromine nitrate
HCl	hydrogen chloride (hydrochloric acid)	HBr	hydrogen bromide
HOCl	hypochlorous acid	HOBr	hypobromous acid
F	atomic fluorine	I	atomic iodine
FO	fluorine monoxide	IO	iodine monoxide
HF	hydrogen fluoride (hydrofluoric acid)	HI	hydrogen iodide
SF_6	sulfur hexafluoride	$IONO_2$	iodine nitrate

HALOCARBONS

Chlorofluorocarbons (CFCs)

CFC-10	CCl_4
CFC-11	CCl_3F
CFC-12	CCl_2F_2
CFC-13	$CClF_3$
CFC-14	CF_4
CFC-113	CCl_2FCClF_2
CFC-114	$CClF_2CClF_2$
CFC-115	$CClF_2CF_3$
CFC-116	CF_3CF_3

Hydrochlorofluorocarbons (HCFCs)

HCFC-21	$CHCl_2F$
HCFC-22	CHF_2Cl
HCFC-30	CH_2Cl_2
HCFC-40	CH_3Cl
HCFC-123	CF_3CHCl_2
HCFC-124	CF_3CHFCl
HCFC-141b	$CFCl_2CH_3$
HCFC-142b	CF_2ClCH_3
HCFC-225ca	$CF_3CF_2CHCl_2$
HCFC-225cb	CF_2ClCF_2CHFCl

Hydrofluorocarbons (HFCs)

HFC-23	CHF_3	HFC-152a	CH_3CHF_2
HFC-32	CH_2F_2	HFC-227ea	CF_3CHFCF_3
HFC-41	CH_3F	HFC-236cb	$CF_3CF_2CH_2F$
HFC-125	CHF_2CF_3	HFC-236ea	$CF_3CHFCHF_2$
HFC-134	CHF_2CHF_2	HFC-236fa	$CF_3CH_2CF_3$
HFC-134a	CH_2FCF_3	HFC-245ca	$CHF_2CF_2CFH_2$
HFC-143	CHF_2CH_2F	HFC-43-10mee	$CF_3CHFCHFCF_2CF_3$
HFC-143a	CH_3CF_3		

CHEMICAL FORMULAE

Halons

halon-1211	CF_2ClBr
halon-1301	CF_3Br
halon-2402	$C_2F_4Br_2$

Others

CH_3Cl	methyl chloride	CH_3Br	methyl bromide
CH_2Cl_2	methylene chloride, dichloromethane	CH_2Br_2	methylene bromide, dibromomethane
$CHCl_3$	chloroform, trichloromethane	$CHBr_3$	bromoform, tribromomethane
CCl_4	carbon tetrachloride	$C_2H_4Br_2$	ethylene dibromide; 1,2 dibromoethane
CH_3CCl_3	methyl chloroform		
C_2HCl_3	trichloroethylene		
C_2Cl_4	tetrachloroethylene		
$COCl_2$	phosgene, carbonyl chloride		
CF_4	perfluoromethane	CH_3I	methyl iodide
C_2F_6	perfluoroethane		
C_3F_8	perfluoropropane		
c-C_4F_8	perfluorocyclobutane		
C_6F_{14}	perfluorohexane		
CHF_3	fluoroform, trifluoromethane		
TFA	trifluoroacetic acid ($CF_3C(O)OH$)		
$CHClBr_2$	dibromochloromethane	COFCl	fluorophosgene
CF_3Br	trifluorobromomethane (halon-1301)		
CH_2ClI	chloroiodomethane		
CF_3I	trifluoromethyl iodide		
C_2F_5I	iodopentafluoroethane		

OTHER CHEMICAL SPECIES

O	atomic oxygen	H	atomic hydrogen
O_2	molecular oxygen	H_2	molecular hydrogen
O_3	ozone	OH	hydroxyl radical
$O(^1D)$	atomic oxygen (first excited state)	HO_2	hydroperoxyl radical
O_x	odd oxygen (O, $O(^1D)$, O_3)	H_2O	water
		H_2O_2	hydrogen peroxide
		HO_x	odd hydrogen (H, OH, HO_2, H_2O_2)

N	atomic nitrogen	HO_2NO_2	peroxynitric acid
N_2	molecular nitrogen	$ROONO_2$	peroxynitrates
N_2O	nitrous oxide	PAN	peroxyacetylnitrate ($CH_3C(O)OONO_2$)
NO	nitric oxide		
NO_2	nitrogen dioxide	NO_y	odd nitrogen (usually including NO, NO_2, NO_3, N_2O_5, $ClONO_2$, HNO_4, HNO_3)
NO_3	nitrogen trioxide, nitrate radical		
N_2O_5	dinitrogen pentoxide		
$ClONO_2$	chlorine nitrate	NO_x	oxides of nitrogen (NO + NO_2)
HNO_2, HONO	nitrous acid	NAD	nitric acid dihydrate ($HNO_3 \cdot 2H_2O$)
HNO_3	nitric acid		
$RONO_2$	alkyl nitrates	NAT	nitric acid trihydrate ($HNO_3 \cdot 3H_2O$)
NO_3^-	nitrate ion		
S	atomic sulfur	SF_6	sulfur hexafluoride
SO_2	sulfur dioxide	CS_2	carbon disulfide
SO_x	sulfur oxides	COS, OCS	carbonyl sulfide
H_2SO_4	sulfuric acid		
SAT	sulfuric acid tetrahydrate ($H_2SO_4 \cdot 4H_2O$)		
$SO_4^=$	sulfate ion		
Be	beryllium	Kr	krypton
Pb	lead	Rn	radon
Sr	strontium		
C	carbon		
CO	carbon monoxide		
CO_2	carbon dioxide		
HC	hydrocarbon	CH_2O	formaldehyde
NMHC	non-methane hydrocarbon	CH_3OH	methanol
VOC	volatile organic compound	RO	alkoxy radicals
CH_4	methane	CH_3OOH	methyl hydroperoxide
C_2H_6	ethane	CH_3COO	methyl peroxy radical
C_3H_8	propane	RO_2	organic peroxy radical
C_2H_4	ethylene, ethene	$CH_3C(O)OO$	acetyl peroxy radical
C_2H_2	acetylene, ethyne		
C_5H_8	isoprene (2-methyl 1,3 butadiene)		
C_6H_6	benzene		
CFCs	chlorofluorocarbons*		
HCFCs	hydrochlorofluorocarbons*		
HFCs	hydrofluorocarbons*		

* Family of compounds; see above for individual species

☆ U.S. GOVERNMENT PRINTING OFFICE: 1995 - 674-332 / M 3194 REGION NO. 8